INTERNATIONAL JOURNAL OF MODERN ENGINEERING RESEARCH (IJMER)

ISSN : 2249-6645

Volume 3 - Issue 4

Web : www.ijmer.com
Email : ijmer.editor@gmail.com

International Journal of Modern Engineering Research (IJMER)

Editorial Board

International Journal of Modern Engineering Research (IJMER)
www.ijmer.com Vol.3, Issue.4, Jul - Aug. 2013 pp-1857-1860 ISSN: 2249-6645

Optical and Impedance Spectroscopy Study of ZnS Nanoparticles

Ramna Tripathi[1] & Akhilesh Kumar[2]
[1]*Department of Physics, THDC-Institute of Hydropower Engineering & Technology, Tehri, Uttarakhand, India*
[2]*Department of Physics, Government Post Graduate College, Rishikesh, Uttarakhand, India*

Abstract: *Zinc Sulphide particle in the nanometer size regime has been synthesized using chemical routes. The particles were capped using 2-mercaptoethanol to achieve the stability and avoid the coalescence. The as-obtained particles were characterized by X-ray diffraction (XRD), Transmission electron microscopy (TEM), UV–VIS absorption and photoluminescence (PL) spectra. The dielectric measurements of the ceramic were carried out as a function of frequency (100 Hz–1 MHz) and temperature (298–373 K) by impedance spectroscopy. Impedance spectroscopy was employed to determine the electrical parameters (resistance, capacitance and relaxation time) of the grain and the grain boundary. The grain boundary conduction, total grain (grain plus grain boundary) and the frequency max of grain boundary followed an Arrhenius law associated with activation energies of 0.27eV, 0.28 eV and 0.3 eV respectively.*

Keywords- *Chemical synthesis, Impedance spectroscopy, Optical properties, Zinc Sulphide*

I. INTRODUCTION

Zinc Sulphide is a semi-conducting material, with a wide band gap of 3.70 eV [1]. Among the wide band gap materials, luminescent semi-conducting nanocrystals, also termed as nanophosphors, have been paid much attention particularly for their life time shortening and enhanced emission efficiencies [2, 3]. There have been extensive reports in the past few years demonstrating the systematic exploration of growing ZnS nanoparticles in the surfactant system to control the particle size. Tang et al. [4] for example have studied the luminescence and photo physical properties of ZnS nanoparticles prepared by reverse micelle method. During the recent years, various properties of ZnS have been investigated by researchers [5-10].

It is to be mentioned that the impedance spectroscopy is one of the powerful tools for the characterization of electrical properties of semiconducting nanomaterials. AC impedance spectroscopy allows measurement of the capacitance and loss tangent (tan δ) and/or conductance over a frequency range at various temperatures. From the measured capacitance and tan δ, four complex dielectric functions can be computed: impedance (Z*), electric modulus (M*), permittivity (ε*), and admittance (Y*).

II. EXPERIMENTS

Although various methods are available for the synthesis of ZnS nanoparticles, chemical precipitation is widely being used for the preparation of colloidal nanoparticles as the possibility of cluster formation is very less in this method when compared to the other methods. Here, 0.27 g of $ZnCl_2$ (1/10 M, 20ml) solution and 0.1M Na_2S solution were prepared in distilled water and were first refluxed for an hour separately. 50 ml Na_2S solution was then added to the mercaptoethanol solution of 0.25 ml (10^{-2} M) and then 20 ml $ZnCl_2$, which was continuously refluxed to get a colloidal form of ZnS. The colloidal sample was refluxed for another 20 min at 80°C for uniform distribution of the particles. Then this was filtered out and washed with distilled water and ethanol for removing the additional impurities formed during the preparation process. The filtrate was dried at room temperature, which yields high-quality ZnS nanocrystals.

The X-ray diffraction of the sample at room temperature is taken by a powder X-ray diffratometer (Rigaku Miniflex-II). The transmission electron micrograph of the sample is taken by a transmission electron microscope (Jeol JEM-100cx). The absorption and luminescence spectra for ZnS nanoparticles were recorded using UV-Visible spectrophotometer (Shimadzu UV-2450) and spectrofluorometer (Shimadzu RF-5310) respectively.

The dielectric measurement of the sample of thickness 2.06 mm and diameter 10.41 mm was carried out using gold electrodes by an LCR meter (Hioki) in the frequency range from 100 Hz to 1 MHz and in the temperature range from 298 K to 373 K. The temperature was controlled with a programmable oven. All the dielectric data were collected while heating at a rate of 1^0C min^{-1}. The complex electric modulus M^* ($=1/\varepsilon^*$) and impedance Z^* ($=M^*/j\omega C_o$) are obtained from the temperature dependence of the real (ε') and imaginary (ε") components of the dielectric permittivity ε^* ($= \varepsilon'-j\varepsilon''$) and $\varepsilon''= \varepsilon' \tan\delta$.

III. RESULTS AND DISCUSSION

Fig. 1 shows the X-ray diffraction pattern of the sample taken at room temperature. The broadening of the diffraction peaks is primarily due to the finite size of the nanocrystallites and is quantitatively analyzed by the Debye–Scherrer formula

$$L = \frac{0.94\lambda}{B\cos\theta} \qquad (1)$$

where L is the average size of the particle, λ is the wavelength of X-ray radiation, B is the full width at half maximum (FWHM) and θ is the diffraction angle. According to the data in Fig. 1 and given formula, the average particle size of the material is found to be 45 nm. The transmission electron micrograph of the ZnS is shown in the inset of Fig. 1. The average grain size of the nanoclusters of ZnS is found to be 50 nm. Particle size analyzed by XRD and TEM are in good agreement.

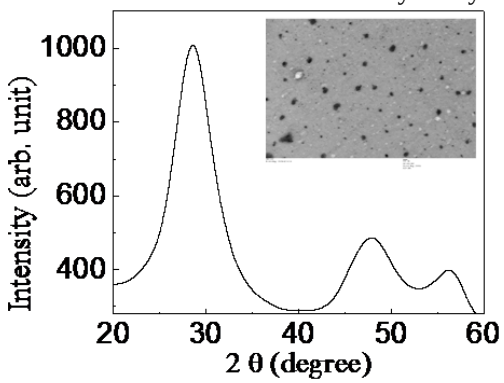

Fig. 1. The XRD (TEM micrograph shown in the inset) for ZnS.

The inset of Fig. 2 shows the UV – visible spectra of ZnS nanoparticles in the absorbance range of 200-350 nm. The absorbance peak at 277 nm is blue shifted compared to the bulk ZnS for which absorption peak is at 345 nm. The blue-shifted absorption edge is due to the quantum confinement of the excitons present in the sample, resulting in a more discrete energy spectrum of the individual nanoparticles. The broadening of the absorption spectrum is mainly due to the quantum confinement of the ZnS nanoparticles. The effect of the quantum confinement on impurity critically depends on the size of the host crystal. As the host decreases, the degree of confinement and its effect increases. The band gap energy is increased (~4.1 eV) compared to that (~3.6 eV) of bulk ZnS shown in the Fig. 2, the enlargement of the band gap can be attributed to the quantum confinement effect of the ZnS nanoparticles.

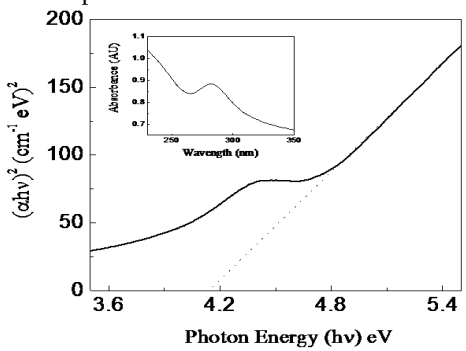

Fig. 2. Energy band gap determination of ZnS nanoparticles. The UV-visible absorption spectra of the ZnS nanoparticles shown in the inset.

Fig. 3 shows the PL emission (a) and excitation (b) spectra of ZnS nanoparticles. It shows strong blue-luminescence with peak maximum around 335 nm and a side band at 352 nm. The corresponding excitation spectra with peak maximum at 420 nm indicate energy-transfer from the band-to-band electronic excitation of the quantum confined ZnS [11].

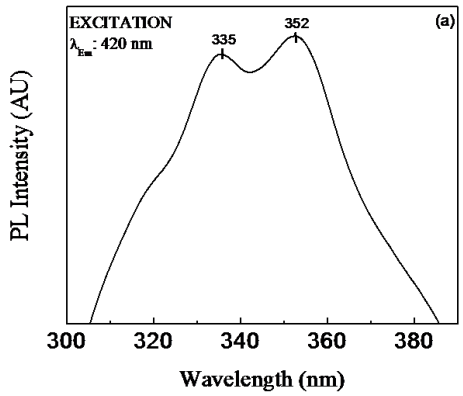

Fig.3. Photoluminescence emission spectra of ZnS nanoparticles.

With the self-aggregation of nanoparticles, the excitation spectra also show reduction in the intensity but more significantly, a gradual red-shift in the peak maximum with larger line broadening. The origin of the blue-luminescence of ZnS nanoparticles has been studied by different groups [11, 12]. Highly asymmetric and broadened emission band with multiple

peak maxima indicate the involvement of different luminescence centers in the radiative process. The nanoparticles prepared under sulphur deficient synthetic condition of S^{2-}/Zn^{2+} will have larger concentration of sulphur vacancies (VS).

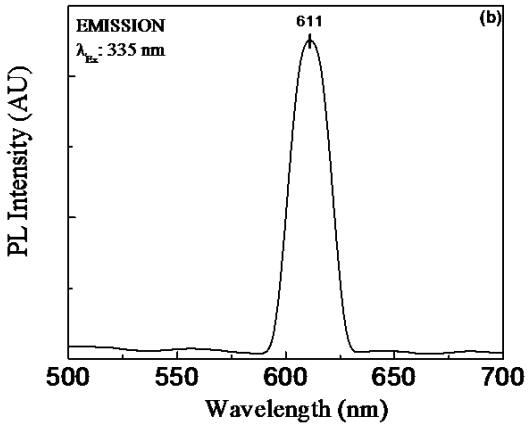

Fig.3. Photoluminescence excitation spectra of ZnS nanoparticles.

It is reported that sulphur vacancies can act as doubly ionized electron trap centers and facilitate VS/VB (valence band) and/or VS/SS (surface states, including interstitial defects and impurities) [11]. Though the lattice vacancies are point defects, due to the large surface-to-volume ratio of nanoparticles, the concentration of these defects will be more at the surface regions than the interiors. Therefore, in the ZnS nanoparticles with unmodified surfaces, the effect of surface states will be dominant as seen by the strong blue luminescence. However, the observed quenching of these emission bands with the self-assembly of nanoparticles suggests that the vacancy centers are annihilated during the particle-to-particle attachment/interface precipitation by way of incorporation of more and more crystal growth units at the nanoparticles surfaces.

Fig. 4 shows a complex-plane impedance plot (Z^*) of ZnS, plotting the imaginary part Z'' against the real part Z'. In general, for a perfect crystal, the values of resistance R and capacitance C can be analyzed by an equivalent circuit of one parallel resistance-capacitance (RC) element. This RC element give rise to one semicircular arc on the complex plane and has intercepts on the Z' axis of zero and R. Thus, C can be calculated with the relation $\omega_m RC=1$, where $\omega_m=2\pi\nu_m$ and ν_m is the frequency at the arc maxima.

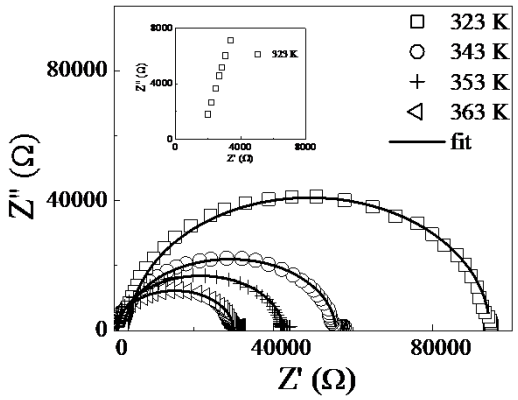

Fig.4. The complex–plane impedance plot with the corresponding equivalent circuit is shown for ZnS at various temperatures. The solid line is the best fit for ZnS. The inset shows expanded views of the high-frequency data near the origin at 323 K.

For a nano crystal containing interfacial boundary layers, the equivalent circuit may be considered as two parallel RC elements connected in serial and giving rise to two arcs in complex plane: one for the nano crystal (grain) and the other for the interfacial boundary (grain-boundary) response. The relative position of the two arcs in the complex plane can be identified by the frequency. Based on the equivalent circuit consisting of two parallel RC elements in series, the nonzero intercept on the Z'-axis (at 323 K) indicates the presence of an arc with ω_{max} higher than the maximum frequency measured (1 MHz).

Dielectric relaxation observed in electroceramics are better analysed using the simplified equivalent circuits consisting of two parallel RC circuits connected in series, one RC element, R_g C_g, representing the grain, and the other $R_{gb}C_{gb}$, representing the grain boundary [13, 14], as shown in the inset of Fig. 4. Here, R_g, C_g and R_{gb}, C_{gb} are the resistance and capacitance associated with the grain and the grain boundary, respectively. Each parallel RC element results in a semicircle in the impedance plots. Fig. 4 shows a complex impedance Z* (Z" versus Z') plot for ZnS nanoceramics, obtained by plotting the imaginary part (Z") against the real part (Z') in the 323 K–363 K temperature range. The high frequency impedance response of the sample in the 323 K–363 K temperature range has been highlighted in Fig. 5 to show the evolution of the high frequency semicircle.

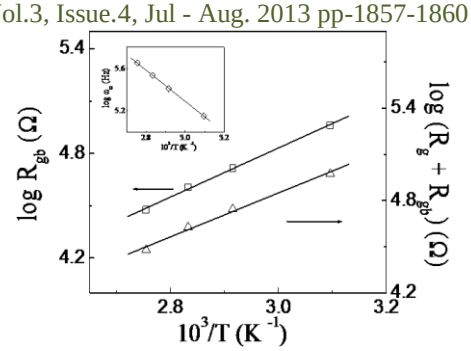

Fig.5. Arrhenius plot for the grain boundary resistance (*R*gb) and total grain. The insetshows grain boundary relaxation frequency (ω_{gb}) for ZnS nanoceramics. The solid line is the best fit for the Arrhenius equations.

The equivalent electrical equation can be represented by

$$Z' = \frac{R_g}{1+(\omega R_g C_g)^2} + \frac{R_{gb}}{1+(\omega R_{gb} C_{gb})^2} \quad (2)$$

$$Z'' = R_g\left(\frac{\omega R_g C_g}{1+(\omega R_g C_g)^2}\right) + R_{gb}\left(\frac{\omega R_{gb} C_{gb}}{1+(\omega R_{gb} C_{gb})^2}\right) \quad (3)$$

The best fitting of RC equivalent circuit by solid line for 323 K, 343 K and 363 K with two semicircular arc of R_g and R_{gb} is shown in the table 1.

The resistance values of the grains and the grain boundaries are obtained from the intercepts of the corresponding semicircles with the real axis (Z') (diameter of each semicircle) which gives R_g and R_{gb}, respectively. The resistance obtained for the total resistance or dc resistance of the sample log $(R_g + R_{gb})$ and log R_{gb} is plotted in the Arrhenius format in the Fig. 5, obey the Arrhenius law with activation energy of 0.28 eV and 0.27 eV respectively. Plot of log (ω_{gb}) (relaxation frequency of grain boundary) (inset of Fig. 5) reveal that ω_{gb} follow an Arrhenius law associated with activation energies of 0.28 eV. Furthermore, as it is clear from Fig. 5, $R_{gb} + R_g$ are only slightly higher than R_{gb} in the entire temperature range under study. Hence, it could be concluded that $R_{gb} >> R_g$, so that in the entire temperature range $C_{gb} >> C_g$.

IV. CONCLUSIONS

The frequency-dependent dielectric dispersion of ZnS nanoparticles synthesized by soft chemical method is investigated in the temperature range from 298 K to 373 K for the first time. The increasing dielectric constant with increasing temperature is attributed to the conductivity which is directly related to an increase in mobility of localized charge carriers. Analyses of the real and imaginary part of complex permittivity with frequency were performed assuming a distribution of relaxation times as confirmed by Cole-Cole plot as well as the scaling behavior of impedance spectra. The scaling behavior of the imaginary part of impedance spectra suggests that the relaxation describes the same mechanism at various temperatures. The frequency-dependent electrical data are also analyzed in the framework of conductivity and modulus formalisms.

ACKNOWLEDGMENT

R. Tripathi and A. Kumar are thankful to Uttarakhand state council of science and technology (U-COST) for its financial support, SAIF, Bose Institute, Kolkata for instrument facility and Gajendra Saini, AIRF, Jawaharlal Nehru University (JNU), New Delhi for TEM measurement.

References

[1] B. S. Zou, R. B. Little, J. P. Wang, M. A. Sayed, Int . J. Quantum Chem. *72* (1999) 439.
[2] R. N. Bhargava, D. Gallangher, Phys.Rev.Lett. *72* (1994) 416.
[3] T. Igarashi, T. Isobe, M. Senna, Phys.Rev.B. *56* (1995) 6444.
[4] H. Tang, G. Y. Xu, L. Q. Weng, L. J. Pan, L. Wang, Acta Mater. *52* (2004) 1489.
[5] M.Y. Nadeem, Waqas Ahmad**,** Turk J Phy, *24* (2000), 651.
[6] R. P. Vijayalakshmi, R. Venugopal, D. R. Reddy, B. Reddy, Physica Scripta. *53* (1996) 123.
[7] K. S. Rathorea, D. Patidara, Y. Janub, N.S. Saxenaa, K. Sharmaa, T. P. Sharmaa, Chalcogenide Lett. 5 (2008) 105.
[8] J. P. Borah, J. Barman, K.C. Sarma, Chalcogenide Lett. *5* (2008) 201.
[9] D. Denzler, M. Olschewski, K. Sattler, J. Appl. Phys. *84* (1998) 2841.
[10] J. Nanda, Sameer Sapra, D. D. Sarma, Chem. Mater. *12* (2000) 1018.
[11] K. Manzoor, S.R. Vadera, N. Kumar, T.R.N. Kutty, Mater. Chem. Phys. *82* (2003) 718.
[12] D. C. Sinclair, A. R. West, J. Appl. Phys. *66* (1989) 3850.
[13] A. M. Macdonald, Impedance Spectroscopy (New York: Wiley), 1987.
[14] A.K. Jonscher, Dielectric Relaxation in Solids, Chelsea Dielectrics Press, London, 1983.
[15] A.K. Jonscher, Universal Relaxation Law, Chelsea Dielectrics Press, London, 1996.
[16] K. S. Cole, R. H. Cole, J. Chem. Phys. *9* (1941) 341.

International Journal of Modern Engineering Research (IJMER)
www.ijmer.com Vol.3, Issue.4, Jul - Aug. 2013 pp-1861-1871 ISSN: 2249-6645

Hortizontal Aggregation in SQL for Data Mining Analysis to Prepare Data Sets

B. Susrutha[1], J. Vamsi Nath[2], T. Bharath Manohar[3], I. Shalini[4]

[1,4]*M. Tech 2ndyr,Dept of CSE,PBRVITS(Affiliated to JNTU Kakinada), Kavali,Nellore.Andhra Pradesh.India.*
[2]*Associate Professor, Dept of CSE, PBRVITS(Affiliated to JNTU Kakinada), Kavali, Nellore, Andhra Pradesh. India.*
[3] *Asst. Professor,Dept of CSE, CMR College of Engineering &Technology,(Affiliated to JNTU Hyderabad) Hyderabad. Andhra Pradesh. India.*

Abstract*: Preparing a data set for analysis is generally the most time consuming task in a data mining project, requiring many complex SQL queries, joining tables and aggregating columns. Existing SQL aggregations have limitations to prepare data sets because they return one column per aggregated group. In general, a significant manual effort is required to build data sets, where a horizontal layout is required. We propose simple, yet powerful, methods to generate SQL code to return aggregated columns in a horizontal tabular layout, returning a set of numbers instead of one number per row. This new class of functions is called horizontal aggregations. Horizontal aggregations build data sets with a horizontal denormalized layout (e.g. point-dimension, observation-variable, instance-feature), which is the standard layout required by most data mining algorithms. We propose three fundamental methods to evaluate horizontal aggregations: CASE: Exploiting the programming CASE construct; SPJ: Based on standard relational algebra operators (SPJ queries); PIVOT: Using the PIVOT operator, which is offered by some DBMSs. Experiments with large tables compare the proposed query evaluation methods. Our CASE method has similar speed to the PIVOT operator and it is much faster than the SPJ method. In general, the CASE and PIVOT methods exhibit linear scalability, where as the SPJ method does not.*

Keywords: *Aggregation, Data Preparation, Pivoting, SQL.*

I. INTRODUCTION

In a relational database, especially with normalized tables, a significant effort is required to prepare a summary data set that can be used as input for a data mining or statistical algorithm. Most algorithms require as input a data set with a horizontal layout, with several Records and one variable or dimension per column. That is the case with models like clustering, classification, regression and PCA; consult. Each research discipline uses different terminology to describe the data set. In data mining the common terms are point-dimension. Statistics literature generally uses observation-variable. Machine learning research uses instance-feature. This article introduces a new class of aggregate functions that can be used to build data sets in a horizontal layout (denormalized with aggregations), automating SQL query writing and extending SQL capabilities. We show evaluating horizontal aggregations is a challenging and interesting problem and we introduced alternative methods and optimizations for their efficient evaluation.

II. MOTIVATION

As mentioned above, building a suitable data set for data mining purposes is a time- consuming task. This task generally requires writing long SQL statements or customizing SQL Code if it is automatically generated by some tool. There are two main ingredients in such SQL code: joins and aggregations; we focus on the second one. The most widely-known aggregation is the sum of a column over groups of rows. Some other aggregations return the average, maximum, minimum or row count over groups of rows. There exist many aggregations functions and operators in SQL. Unfortunately, all these aggregations have limitations to build data sets for data mining purposes.

The main reason is that, in general, data sets that are stored in a relational database (or a data warehouse) come from On-Line Transaction Processing (OLTP) systems where database schemas are highly normalized. But data mining, statistical or machine learning algorithms generally require aggregated data in summarized form. Based on current available functions and clauses in SQL, a significant effort is required to compute aggregations when they are desired in a cross tabular (Horizontal) form, suitable to be used by a data mining algorithm. Such effort is due to the amount and complexity of SQL code that needs to be written, optimized and tested. There are further practical reasons to return aggregation results in a horizontal (cross-tabular) layout. Standard aggregations are hard to interpret when there are many result rows, especially when grouping attributes have high cardinalities. To perform analysis of exported tables into spreadsheets it may be more convenient to have aggregations on the same group in one row (e.g. to produce graphs or to compare data sets with repetitive information).

OLAP tools generate SQL code to transpose results (sometimes called PIVOT). Transposition can be more efficient if there are mechanisms combining aggregation and transposition together. With such limitations in mind, we propose a new class of aggregate functions that aggregate numeric expressions and transpose results to produce a data set with a horizontal layout. Functions belonging to this class are called horizontal aggregations. Horizontal aggregations represent an extended form of traditional SQL aggregations, which return a set of values in a horizontal layout (somewhat similar to a multidimensional vector), instead of a single value per row. This article explains how to evaluate and optimize horizontal aggregations generating standard SQL code.

III. LITERATURE SURVEY

We have to analysis the DATA MINING Outline Survey:

Data Mining

Generally, data mining (sometimes called data or knowledge discovery) is the process of analyzing data from different perspectives and summarizing it into useful information - information that can be used to increase revenue, cuts costs, or both. Data mining software is one of a number of analytical tools for analyzing data. It allows users to analyze data from many different dimensions or angles, categorize it, and summarize the relationships identified. Technically, data mining is the process of finding correlations or patterns among dozens of fields in large relational databases.

The Scope of Data Mining

Data mining derives its name from the similarities between searching for valuable business information in a large database — for example, finding linked products in gigabytes of store scanner data — and mining a mountain for a vein of valuable ore. Both processes require either sifting through an immense amount of material, or intelligently probing it to find exactly where the value resides. Given databases of sufficient size and quality, data mining technology can generate new business opportunities by providing these capabilities:

- Automated prediction of trends and behaviors. Data mining automates the process of finding predictive information in large databases. Questions that traditionally required extensive hands-on analysis can now be answered directly from the data — quickly. A typical example of a predictive problem is targeted marketing. Data mining uses data on past promotional mailings to identify the targets most likely to maximize return on investment in future mailings. Other predictive problems include forecasting bankruptcy and other forms of default, and identifying segments of a population likely to respond similarly to given events.
- Automated discovery of previously unknown patterns. Data mining tools sweep through databases and identify previously hidden patterns in one step. An example of pattern discovery is the analysis of retail sales data to identify seemingly unrelated products that are often purchased together. Other pattern discovery problems include detecting fraudulent credit card transactions and identifying anomalous data that could represent data entry keying errors.

The most commonly used techniques in data mining are:

- Artificial neural networks: Non-linear predictive models that learn through training and resemble biological neural networks in structure.
- Decision trees: Tree-shaped structures that represent sets of decisions. These decisions generate rules for the classification of a dataset. Specific decision tree methods include Classification and Regression Trees (CART) and Chi Square Automatic Interaction Detection (CHAID) .
- Genetic algorithms: Optimization techniques that use processes such as genetic combination, mutation, and natural selection in a design based on the concepts of evolution.
- Nearest neighbor method: A technique that classifies each record in a dataset based on a combination of the classes of the k record(s) most similar to it in a historical dataset (where k ³ 1). Sometimes called the k-nearest neighbor technique.
- Rule induction: The extraction of useful if-then rules from data based on statistical significance.

An Architecture for Data Mining

To best apply these advanced techniques, they must be fully integrated with a data warehouse as well as flexible interactive business analysis tools. Many data mining tools currently operate outside of the warehouse, requiring extra steps for extracting, importing, and analyzing the data. Furthermore, when new insights require operational implementation, integration with the warehouse simplifies the application of results from data mining. The resulting analytic data warehouse can be applied to improve business processes throughout the organization, in areas such as promotional campaign management, fraud detection, new product rollout, and so on.

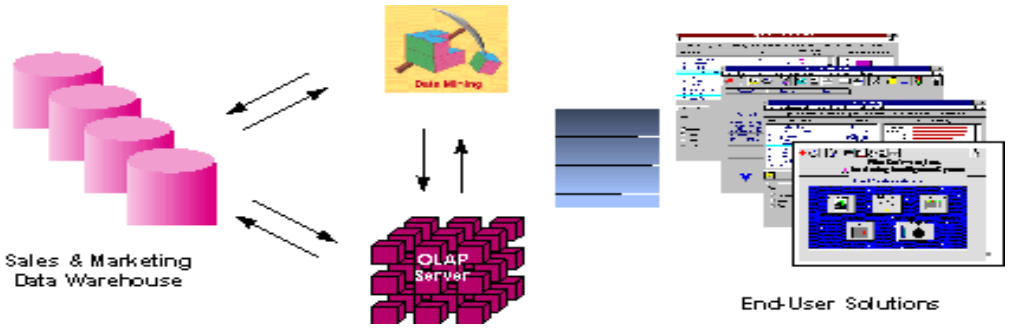

Figure 1: Integrated Data Mining Architecture

The Ideal starting point is a data warehouse containing a combination of internal data tracking all customer contact coupled with external market data about competitor activity. Background information on potential customers also provides an excellent basis for prospecting. This warehouse can be implemented in a variety of relational database systems: Sybase, Oracle, Redbrick, and so on, and should be optimized for flexible and fast data access.

Data Mining Products:

Data mining products are taking the industry by storm. The major database vendors have already taken steps to ensure that their platforms incorporate data mining techniques. Oracle's Data Mining Suite (Darwin) implements classification and regression trees, neural networks, k-nearest neighbors, regression analysis and clustering algorithms. Microsoft's SQL Server also offers data mining functionality through the use of classification trees and clustering algorithms. If you're already working in a statistics environment, you're probably familiar with the data mining algorithm implementations offered by the advanced statistical packages SPSS, SAS, and S-Plus.

Conclusion

Comprehensive data warehouses that integrate operational data with customer, supplier, and market information have resulted in an explosion of information. Competition requires timely and sophisticated analysis on an integrated view of the data. However, there is a growing gap between more powerful storage and retrieval systems and the users' ability to effectively analyze and act on the information they contain. Both relational and OLAP technologies have tremendous capabilities for navigating massive data warehouses, but brute force navigation of data is not enough. A new technological leap is needed to structure and prioritize information for specific end-user problems. The data mining tools can make this leap. Quantifiable business benefits have been proven through the integration of data mining with current information systems, and new products are on the horizon that will bring this integration to an even wider audience of users.

IV. SYSTEM ANALYSIS

Existing System:

An existing to preparing a data set for analysis is generally the most time consuming task in a data mining project, requiring many complex SQL queries, joining tables and aggregating columns. Existing SQL aggregations have limitations to prepare data sets because they return one column per aggregated group.

Disadvantage:

1)Existing SQL aggregations have limitations to prepare data sets.
2)To return one column per aggregated group

Previous Process Flow:

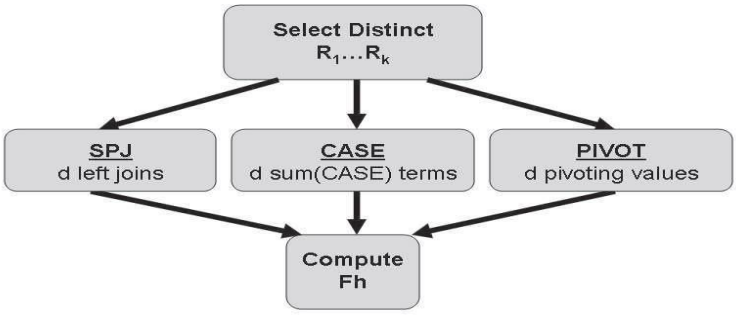

Fig: Previous Process Flow

Proposed System:

Our proposed horizontal aggregations provide several unique features and advantages. First, they represent a template to generate SQL code from a data mining tool. Such SQL code automates writing SQL queries, optimizing them and testing them for correctness.

Advantage:

1) The SQL code reduces manual work in the data preparation phase in a data mining project.
2) The SQL code is automatically generated it is likely to be more efficient than SQL code written by an end user.
3) The data sets can be created in less time.
4) The data set can be created entirely inside the DBMS.

Proposed Process Flow:

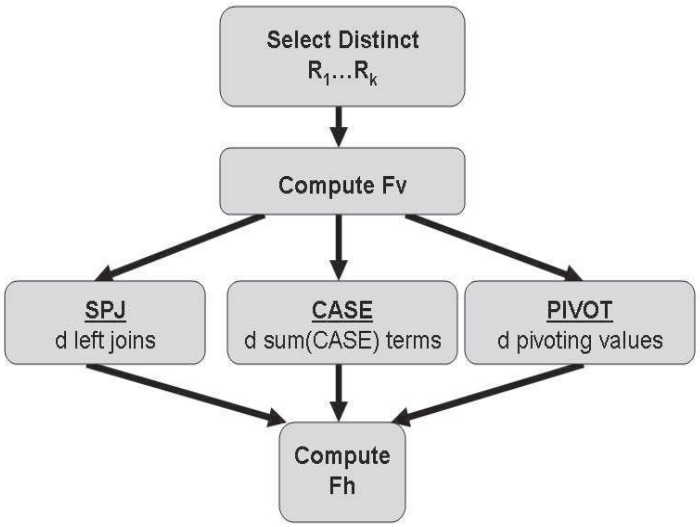

Fig: Proposed Process Flow

Modules Description:

1. Admin Module
2. User Module
3. View Module
4. Download Module

Module 1 : Admin Module

Admin will upload new connection form based on regulations in various states. Admin will be able upload various details regarding user bills like a new connection to a new user, amount paid or payable by user. In case of payment various details regarding payment will be entered and separate username and password will be provided to users in large.

Module 2 : User Module

User will be able to view his bill details on any date may be after a month or after months or years and also he can to view the our bill details in a various ways for instance, The year wise bills, Month wise bills, totally paid to bill in EB. This will reduce the cost of transaction. If user thinks that his password is insecure, he has option to change it. He also can view the registration details and allowed to change or edit and save it.

Module 3 : View Module

Admin has three ways to view the user bill details, the 3 ways are

i) SPJ
ii) PIVOT
iii) CASE

i) SPJ : While using SPJ the viewing and processing time of user bills is reduced.

ii) PIVOT : This is used to draw the user details in a customized table. This table will elaborate us on the various bill details regarding the user on monthly basis.

iii) CASE : using CASE query we can customize the present table and column based on the conditions. This will help us to reduce enormous amount of space used by various user bill details. It can be viewed in two difference ways namely Horizontal and Vertical.

In case of vertical the number of rows will be reduced to such an extent it is needed and column will remain the same on other hand the Horizontal will reduce rows as same as vertical and will also increase the columnar format.

Module 4 : Download Module

User will be able to download the various details regarding bills. If he/she is a new user, he/she can download the new connection form, subscription details etc. then he/she can download his /her previous bill details in hands so as to ensure it.

V. SYSTEM DESIGN & ARCHITECTURE DIAGRAMS

Data Flow Diagram / Use Case Diagram / Flow Diagram

The DFD is also called as bubble chart. It is a simple graphical formalism that can be used to represent a system in terms of the input data to the system, various processing carried out on these data, and the output data is generated by the system.

Class Diagram:

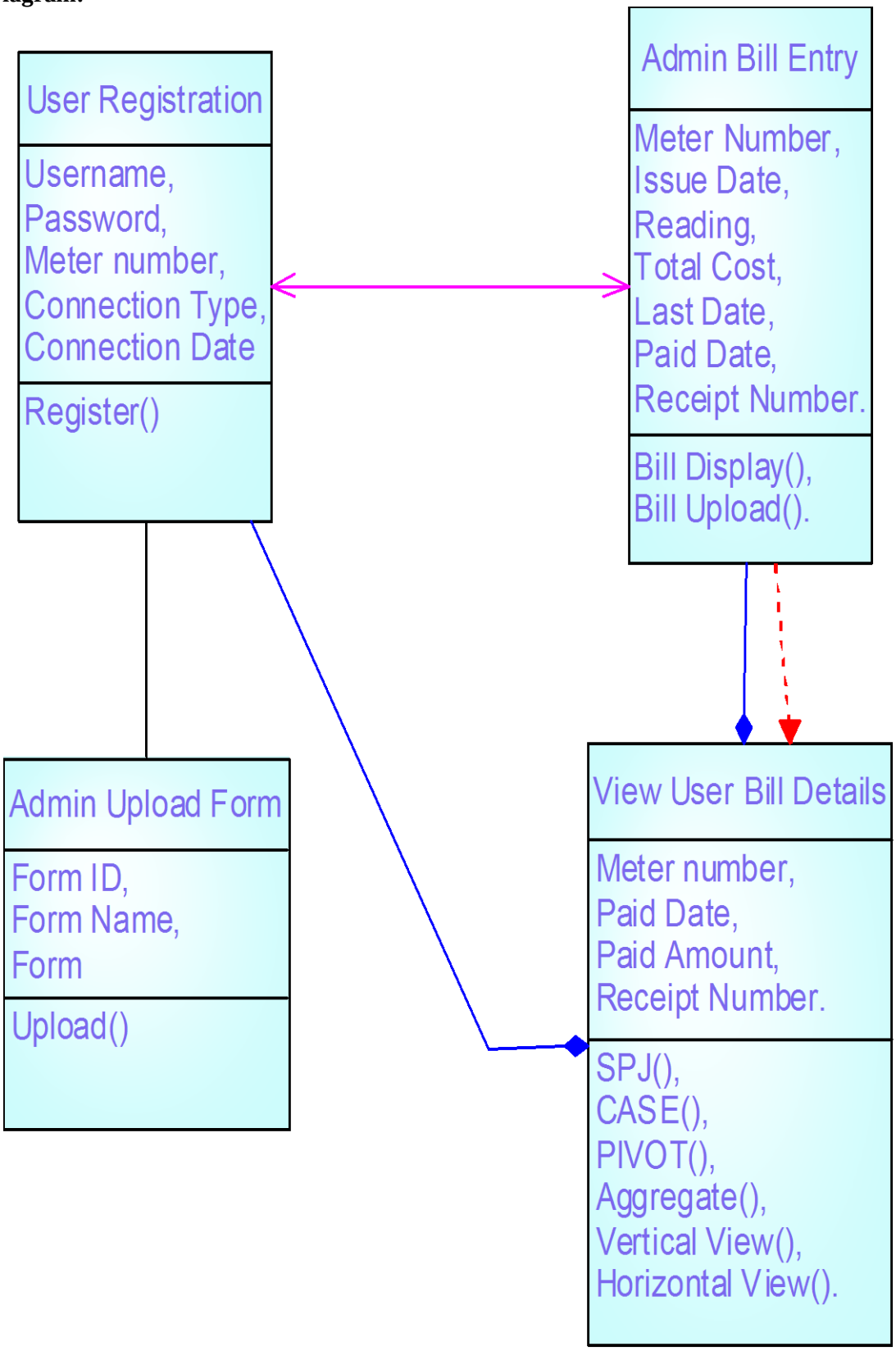

Data Flow Diagram:

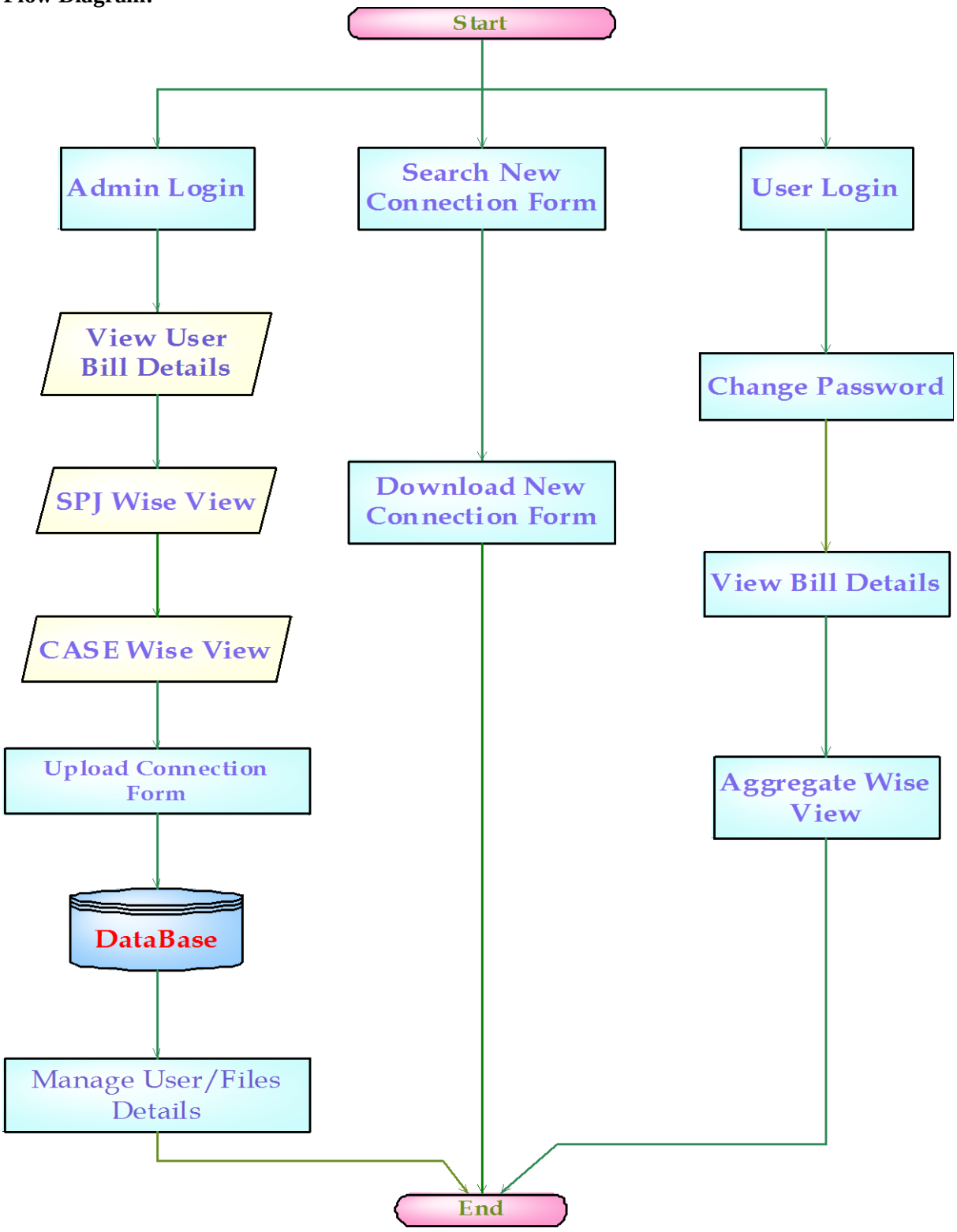

Activity Diagram:

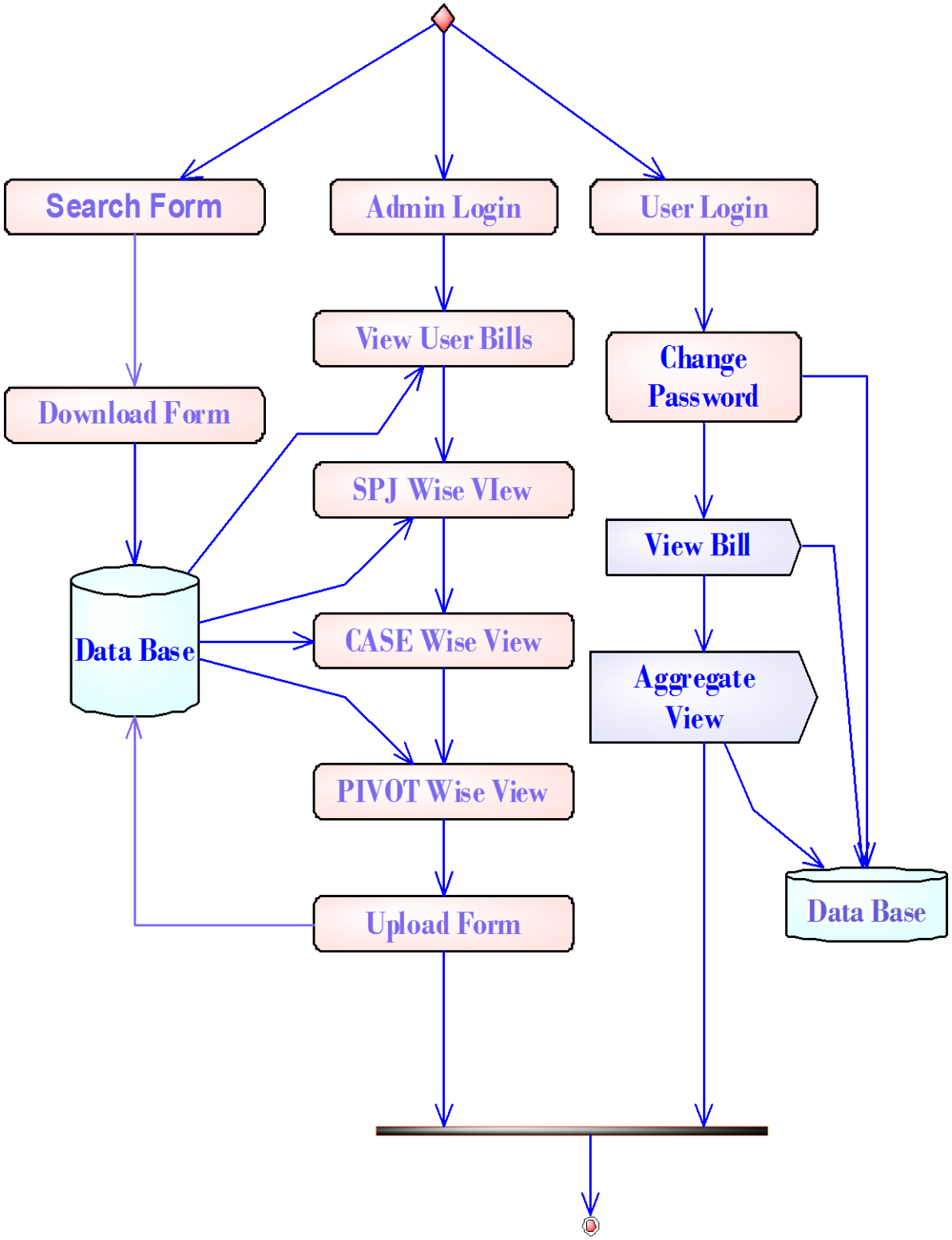

Use case Diagram:

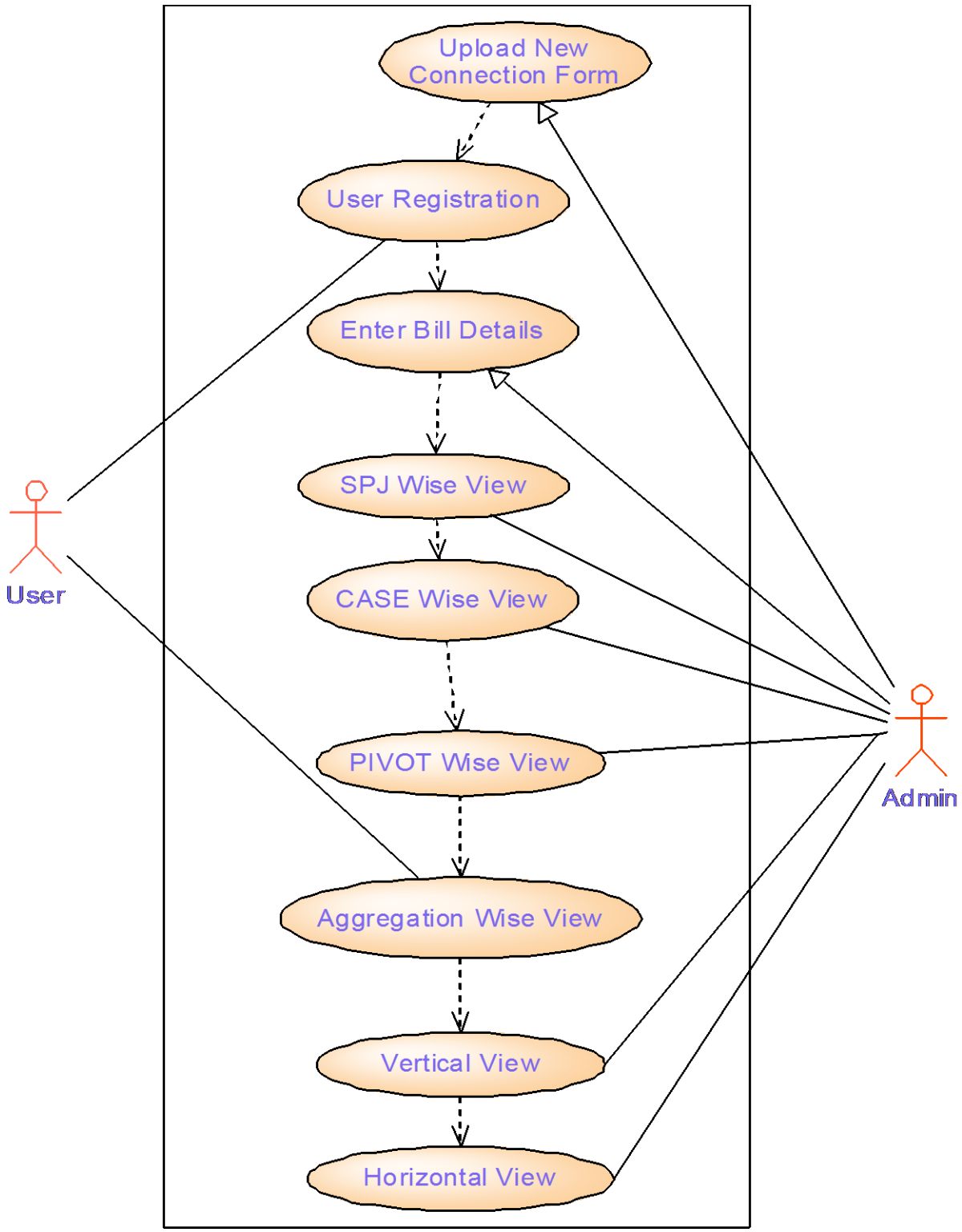

Sequence Diagram:

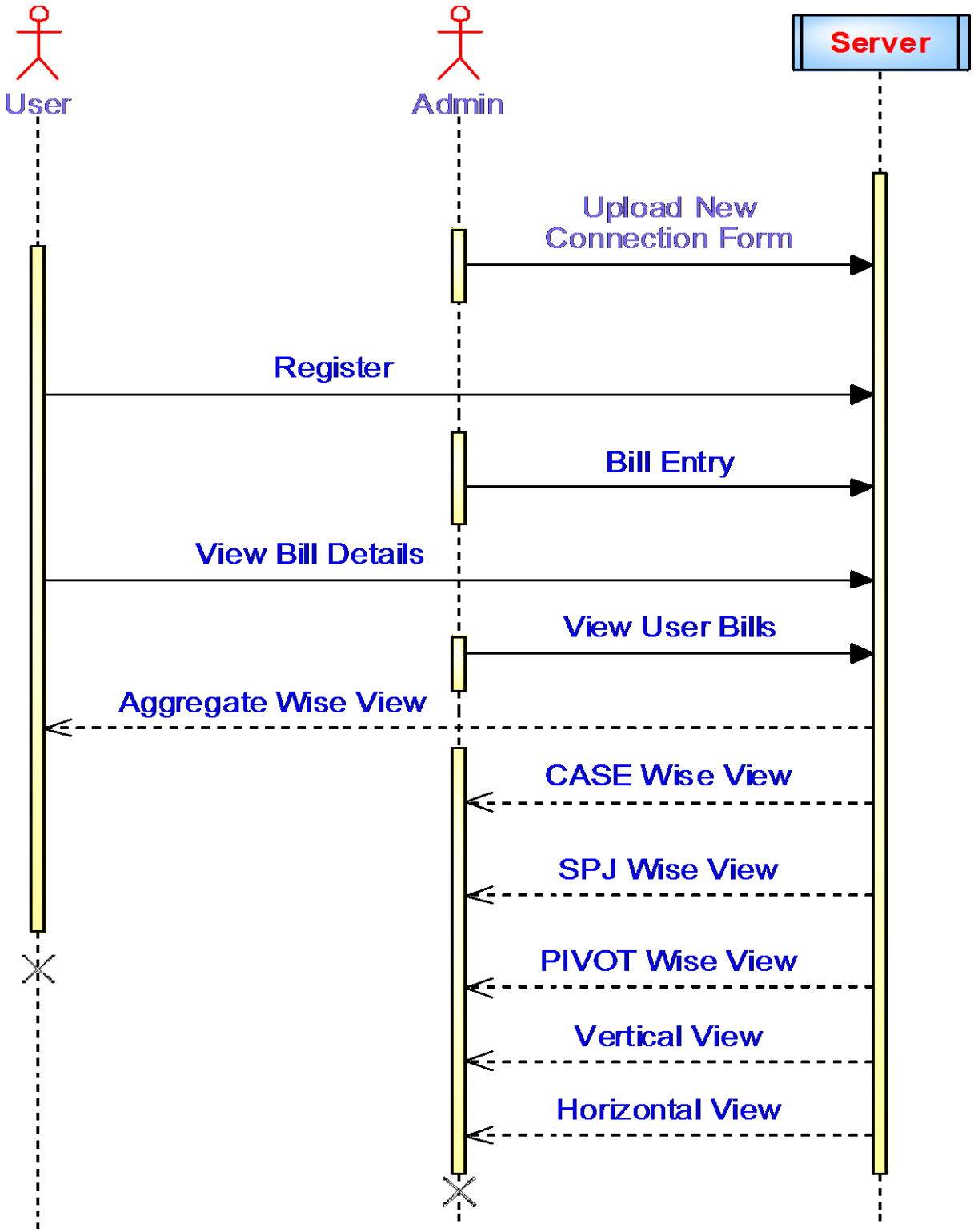

VI. EXPERIMENT & RESULT

We performed several experiments to test the proposed algorithm and evaluate its performance against different attacks and experienced various results as follows:

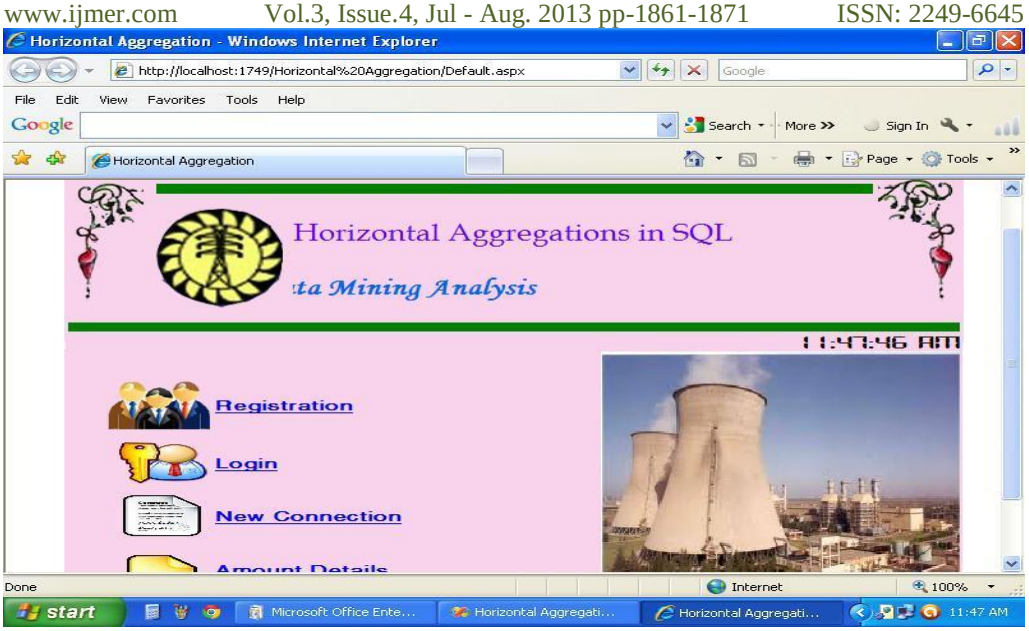

Fig: Horizontal Aggregations in SQL

Fig: Horizontal view results

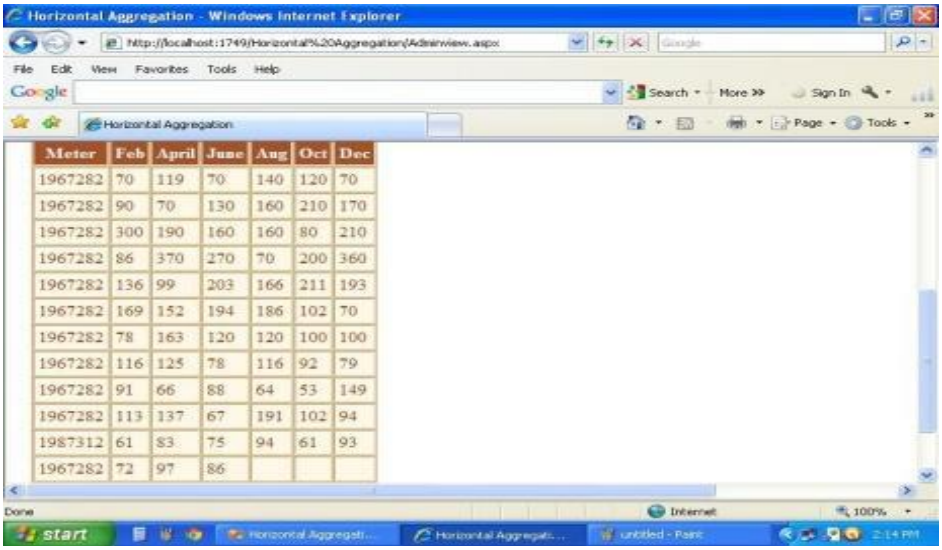

Fig: Results obtained processing the records in Database

VII. CONCLUSION

We introduced a new class of extended aggregate functions, called horizontal aggregations which help preparing data sets for data mining and OLAP cube exploration. Specifically, horizontal aggregations are useful to create data sets with a horizontal layout, as commonly required by data mining algorithms and OLAP cross-tabulation. Basically, a horizontal aggregation returns a set of numbers instead of a single number for each group, resembling a multi-dimensional vector.

We proposed an abstract, but minimal, extension to SQL standard aggregate functions to compute horizontal aggregations which just requires specifying subgrouping columns inside the aggregation function call. From a query optimization perspective, we proposed three query evaluation methods. The first one (SPJ) relies on standard relational operators. The second one (CASE) relies on the SQL CASE construct. The third (PIVOT) uses a built-in operator in a commercial DBMS that is not widely available. The SPJ method is important from a theoretical point of view because it is based on select, project and join (SPJ) queries. The CASE method is our most important contribution. It is in general the most efficient evaluation method and it has wide applicability since it can be programmed combining GROUP-BY and CASE statements. We proved the three methods produce the same result.

We have explained it is not possible to evaluate horizontal aggregations using standard SQL without either joins or ”case” constructs using standard SQL operators. Our proposed horizontal aggregations can be used as a database method to automatically generate efficient SQL queries with three sets of parameters: grouping columns, subgrouping columns and aggregated column. The fact that the output horizontal columns are not available when the query is parsed (when the query plan is explored and chosen) makes its evaluation through standard SQL mechanisms infeasible. Our experiments with large tables show our proposed horizontal aggregations evaluated with the CASE method have similar performance to the built-in PIVOT operator. We believe this is remarkable since our proposal is based on generating SQL code and not on internally modifying the query optimizer. Both CASE and PIVOT evaluation methods are significantly faster than the SPJ method. Precomputing a cube on selected dimensions produced acceleration on all methods.

ACKNOWLEDGMENT

I would like to express my sincere thanks to my Guide and my Co-Authors for their consistence support and valuable suggestions.

REFERENCES

[1] G. Bhargava, P. Goel, and B.R. Iyer. Hypergraph based reordering of outer join queries with complex predicates. In ACM SIGMOD Conference, pages 304–315, 1995.
[2] J.A. Blakeley, V. Rao, I. Kunen, A. Prout, M. Henaire, and C. Kleinerman. .NET database programmability and extensibility in Microsoft SQL Server. In Proc. ACM SIGMOD Conference, pages 1087–1098, 2008.
[3] J. Clear, D. Dunn, B. Harvey, M.L. Heytens, and P. Lohman. Non-stop SQL/MX primitives for knowledge discovery. In ACM KDD Conference, pages 425–429, 1999.
[4] E.F. Codd. Extending the database relational model to capture more meaning. ACM TODS, 4(4):397–434, 1979.
[5] C. Cunningham, G. Graefe, and C.A. Galindo-Legaria. PIVOT and UNPIVOT: Optimization and execution strategies in an RDBMS. In Proc. VLDB Conference, pages 998–1009, 2004.
[6] C. Galindo-Legaria and A. Rosenthal. Outer join simplification and reordering for query optimization. ACM TODS, 22(1):43–73, 1997.
[7] H. Garcia-Molina, J.D. Ullman, and J. Widom. Database Systems: The Complete Book. Prentice Hall, 1st edition, 2001.
[8] G. Graefe, U. Fayyad, and S. Chaudhuri. On the efficient gathering of sufficient statistics for classification from large SQL databases. In Proc. ACM KDD Conference, pages 204–208, 1998.
[9] J. Gray, A. Bosworth, A. Layman, and H. Pirahesh. Data cube: A relational aggregation operator generalizing group-by, cross-tab and subtotal. In ICDE Conference, pages 152–159, 1996.
[10] J. Han and M. Kamber. Data Mining: Concepts and Techniques. Morgan Kaufmann, San Francisco, 1st edition, 2001.
[11] G. Luo, J.F. Naughton, C.J. Ellmann, and M. Watzke. Locking protocols for materialized aggregate join views. IEEE Transactions on Knowledge and Data Engineering (TKDE), 17(6):796–807, 2005.
[12] C. Ordonez. Horizontal aggregations for building tabular data sets. In Proc. ACM SIGMOD Data Mining and Knowledge Discovery Workshop, pages 35–42, 2004.
[13] C. Ordonez. Statistical model computation with UDFs. IEEE Transactions on Knowledge and Data Engineering (TKDE), 22, 2010.
[14] C. Ordonez. Data set preprocessing and transformation in a database system. Intelligent Data Analysis (IDA), 15(4), 2011.
[15] C. Ordonez and S. Pitchaimalai.Bayesian classifiers programmed in SQL. IEEE Transactions on Knowledge and Data Engineering (TKDE), 22(1):139–144, 2010.

International Journal of Modern Engineering Research (IJMER)
www.ijmer.com Vol.3, Issue.4, Jul - Aug. 2013 pp-1885-1889 ISSN: 2249-6645

Iris Segmentation: a survey

Adegoke, B. O.[1*], Omidiora, E. O[1], Falohun, S. A. [1] and Ojo, J.A.[2]
[1]*Department of Computer Science and Engineering,*
[2]*Department of Electrical and Electronics Engineering, Ladoke Akintola University of Technology, Ogbomoso, Nigeria.*

Abstract: *The use of biometric systems has been increasingly encouraged by both government and private entities in order to replace or improve traditional security systems. Iris recognition biometric systems have proved to be efficient at personal recognition with highest recognition accuracy. This paper presents an up-to-date survey of iris segmentation algorithms that had been developed in literatures. It discusses the centrality of segmentation stage to effectiveness of iris recognition system. It identifies the methods used in the segmentation algorithms, database(s) on which the algorithms were used, the accuracy of the method and some noticed limitation(s) of the reviewed algorithms. Through this, it is able to identify the gaps for further researches in the field of application of iris recognition system in computer security. It was discovered that much work has not been done on black iris segmentation.Researchers are hereby encouraged to develop iris segmentation algorithm that can effectively localise black iris.*

Key words: *computer security, iris, iris database, iris recognition, iris segmentation, noise.*

I. Introduction

With increase in emphasis on security nowadays, biometric technologies are becoming much more important than ever [1]. In particular, iris recognition in recent years receives growing interests. Iris pattern recognition is unique to each subject,remain stable throughout life and offers several distinct advantages[2; 3; 1]. Especially, it is protected by the body's own mechanisms and impossible to be modified without risk. Thus, iris is reputed to be the most accurate and reliable for person's identification [5] and has received extensive attentions over the last decades.The degree of freedom of iris textures is extremely high, the probability of finding two identical irises is close to zero therefore, iris recognition systems are very reliable and could be used in most secure places.

Iris segmentation is to locate the valid part of the iris for iris biometrics [7], including finding the pupillary and limbic boundaries of the iris, localizing its upper and lower eyelids if they occlude and detecting and excluding any superimposed occlusions of eyelashes, shadows or reflections. The centrality of segmentation to effectiveness of any iris recognition system cannot be overemphasized[4]. It determines effectiveness of the system [8].Two well-known iris segmentation approaches are attributed to Daugman and Wildes. Daugman developed integro-differential operator to find circular pupil and limbus boundaries. It can be interpreted as a circular edge detector, which searches, in a smoothed image by Gaussian filter, the parameters of a circular boundary along which the integra derivative is maximal [2]. Wildes proposed a two-stage iris segmentation method: a gradient based intensity image, and next the inner and outer boundaries are detected using Hough transform [9]. It is reported that most failures to match in iris recognition system result from inaccurate segmentation [10].

The contents of this paper are thus arranged: section 2 elucidates on available iris segmentation techniques. Section 3 identifies some available public iris databases that can be used for iris system validation. Section 4 gives an exhaustive literature review of iris segmentation methods discussed in literatures/researches while 5 and 6 discuss some limitations and areas of future researches respectively.

II. Existing iris segmentation techniques.

The review of iris segmentation in literatures reveals two major approaches: Daugman'sintegro-differential operator and Hough's transform-based. Nearly all existing methodologies use one of these two or their variants for segmentation.

2.1 Daugman's method

Daugman presented the first approach to computational iris recognition, including iris localization [2]. An integro-differential operator is proposed for locating the inner and outer boundaries of an iris. The operator assumes that pupil and limbus are circular contours and performs as a circular edge detector. Detecting the upper and lower eyelids is also performed using the Integro-differential operator by adjusting the contour search from circular to a designed accurate [2]. Integro-differential operator is defined as:

$$\max_{(r,x_0,y_0)} \left| G_\sigma(r) * \frac{\partial}{\partial r} \oint_{r,x_0,y_0} \frac{I(x,y)}{2\pi r}\, ds \right| \qquad (1)$$

where $I(x,y)$is an image containing an eye. The integro-differential operator searches over the image domain (x,y) for the maximum in the blurred partial derivative with respect to increasing radius r of the normalized contour integral of $I(x,y)$along a circular arc ds of radius r and center co-ordinate (x_0,y_0). The symbol * denotes convolution and $G_\sigma(r)$ is a smoothing function such as a Gaussian of scale (σ) and is defined as:

$$G_\sigma(r) = \frac{1}{\sqrt{2\pi r}} e^{-\frac{(r-r_0)^2}{2\sigma^2}} \qquad (2)$$

The integro-differential operator behaves as a circular edge detector. It searches for the gradient maxima over a 3D parameter space, so there are no threshold parameters required as in the Canny edge detector. Daugman simply excludes the upper and lower most portions of the image where eyelid occlusion is expected to occur.

2.2 Wilde's method

Wildes had proposed an iris recognition system in which iris localization is completed by detecting edges in iris images followed by use of a circular Hough transform to localize iris boundaries [9]. In a circular Hough transform, images are analyzed to estimate the three parameters of one circle (x, y, r) using the equations:

$$H(x_0, y_0, r) = \sum_i h(x_i, y_i, x_0, y_0, r) \qquad (3)$$

where(x_i, y_i) is an edge pixel and *i* is the index of the edge pixel

$$h(x_i, y_i, x_0, y_0, r) = \begin{cases} 1 & if\ g(x_i, y_i, x_0, y_0, r) = 0 \\ 0 & otherwise \end{cases}$$

where

$$g(x_i, y_i, x_0, y_0, r) = (x_i - x_0)^2 + (y_i - y_0)^2 - r^2 \qquad (4)$$

The location (x_0, y_0, r) with the maximum value of $H(x_0, y_0, r)$ is chosen as the parameter vector for the strongest circular boundary. Wildes' system models the eyelids as parabolic arcs. The upper and lower eyelids are detected by using a Hough transform based approach. The only difference is that it votes for parabolic arcs instead of circles. One weak point of the edge detection and Hough transform approach is the use of thresholds in edge detection. Different settings of threshold values may result in different edges that in turn affect the Hough transform result significantly.

2.3 Camus and Wildes' method

Camus and Wildes (2004) described an algorithm for finding a subject's iris in a closed-up image. In a way similar to Daugman's methodology, their algorithm searches in anspace for the three circumference parameters (center(x, y), radius (r)) by maximizing the function

$$C = \sum_{\theta=1}^{n} \left((n-1)\|g_{\theta,r}\| - \sum_{\emptyset=\theta+1}^{n} \|g_{\theta,r} - g_{\theta,r}\| - \frac{I_{\theta,r}}{n} \right) \qquad (5)$$

The method is very accurate on images where the pupil and iris regions' intensities are clearly separated from the sclera ones and on images that contain no reflections or other noise factors. When dealing with noisy data, the algorithm's accuracy deteriorates significantly [11].

2.4 Martin-Roche methods

This methodology, proposed by Martin in a way similar to Daugman's. it receives a grey-scale image, applies the histogram stretch and tries to maximise the average intensity differences of the five consecutive circumferences, defined as

$$D = \sum_m \left(\sum_{K=1}^{5} (I_{n,m} - I_{n-k,m}) \right) \qquad (6)$$

where$I_{i,j} = I(x_0 + i\Delta_r \cos(j\Delta_\theta), y_0 + I\Delta_r \sin(j\Delta_\theta)).\Delta_r$ and$\Delta_\theta$are the increments of radius and angle, respectively, and is the image intensity[12]. In practical sense, this method find three N^3circumference parameters (center(x, y), radius (r)), where the intensity difference between five successive circumferences is maximal.

III. Various Public Iris Databases and their limitations

There are many various public databases available for verification of performance of iris recognition systems. It include: *CASIA:* this is the most widely used iris image database, having different distinct versions (up to version 4.) the first version has one major advantage: the authors pre-processed the images such that the pupil region is identified and filled with black pixels. The database is not captured under varied light intensity. *BATH:*images from this database are quite similar to the one contained in MMU they have very similar characteristics and few noise factors, almost exclusively related with small eyelid or eyelashes obstructions.*MMU:* images from this database present few noise factors and their characteristics are also very homogenous. A fixed image-capture process must have been followed, clearly simulating a cooperative environment.*ICE:UPOL:WVU:UBRIS:Lions institute:* this is the most heterogeneous iris database images: thus it is useful for heterogeneous iris recognition system. All images were captured with optometric framework resulting in optimal images with extremely similar characteristics (Dobes and Machala,).

IV. Literature review on iris segmentation

Daugman proposed an integro-differential operator for localizing iris regions along with removing the possible eyelids noises [2]. From the publication, we cannot judge whether pupil and eyelash noises are considered in his method.
Kong developed a noise detection model for iris segmentation. Whereas pupil noises have not been considered in the model, secondly noise regions were directly segmented from original iris an image, which is time-consuming, and thirdly, it has not been tested based on the prevailing recognition algorithm on a large iris dataset [13].

Daugman proposed an Integro-differential operator for locating the inner and outer boundaries of iris, as well as the upper and lower eyelids. The operator computes the partial derivative of the average intensity of circle points, with respect to

increasing radius, *r*. After convolving the operator with Gaussian kernel, the maximum difference between inner and outer circle will define the centre and radius of the iris boundaries. For upper and lower eyelids detection, the path of contour integration is modified from circular to parabolic curve [2;3].

Wildes used edge detection and Hough transform to localize the iris. Edge detector is applied to a grey scale iris image to generate the edge map. Gaussian filter is applied to smooth the image to select the proper scale of edge analysis. The voting procedure is realized using Hough transform in order to search for the desired contour from the edge map. The center coordinate co-ordinate and radius of the circle with maximum number of edge points is defined as the contour of interest. For eyelids detection, the contour is defined using parabolic curve parameter instead of the circle parameter [9].

Kong *et al.*,proposed Gabor filter and variance of intensity approaches for eyelash detection. The eyelashes were categorized into separable eyelashes and multiple eyelashes. Separable eyelashes are detected using 1D Gabor filters and multiple eyelashes were detected using variance of intensity. Connective criterion was used in their model. A low output value was obtained from the convolution of the separable eyelashes with the Gabor filter. For multiple eyelashes, the variance of intensity in a window is smaller is smaller than a threshold, the center of the window was considered as the eyelashes [13].

Boles and Boashah, Lim and his associates, and Noh mainly focused on the iris image representing and feature matching, and did not introduce the information about segmentation [14;15;16].

In 2002, Tisse*et al.* proposed a segmentation method based on integro-differential operators with a Hough Transform. This reduced the computation time and excluded potential centers outside of the eye image. Eyelash and pupil noises were also not considered in his method [17].

Ma, in their algorithm processed iris segmentation by simple filtering, edge detection and Hough Transform. This made the overall method very efficient and reliable. There was no method proposed for processing eyelash and pupil noises. Their algorithm was able to detect noise due to pupils and eyelashes [18].

Cui *et al.*,(2004)decomposed the iris image using Haar wavelet before pupil localization. Modified Hough's algorithm was used to obtain the centre and radius of pupil. Iris outer boundary was localized using an integral differential operator. Texture segmentation was adopted to detect upper and lower eyelids. The energy of high spectrum at each region is computed to segment the eyelashes. The region with high frequency is considered as the eyelashes area. The upper eyelashes are fit with parabolic arc. The parabolic arc shows the position of the upper eyelid. For lower eyelid detection, the histogram of the original image is used. The lower eyelid area is segmented to compute the edge point of the lower eyelid and the lower eyelid is fit with edge points [19]. The same year, Huang *et al.*, published an iris segmentation method which fussed edge and region information for noise detection. Edge information was obtained based on phase congruency by a bank of Log-Gabor filers whose kernels are suitable for noise detection [20]. Threshold method was used to exclude noise due to pupil and eyelashes because they both have high intensity values.

Black hole search method was proposed by Teo and Ewe to compute the center and area of a pupil. Since the pupil is the darkest region in the image, this approach applies threshold segmentation method to find the dark areas in the iris image. The dark areas are called "black holes" [21]. The center of mass of these black holes is computed from the global image. The area of the pupil is the total number of those black holes within the region. The radius of the pupil can be calculated from the formula of a circle, (2005).

Proenca and Alexandreproposed an iris segmentation method which aimed at detecting noise due to eyelashes and pupils. Their algorithm aims at proper segmentation of iris captured under non-cooperating condition from the subject. The method proposed a pre-processing method which applies the fuzzy-k-means clustering algorithm on the position and intensity feature vector of the iris image followed by Hough transform.Tuceryan textural method (Tuceryan, 1994) was employed on UBIRIS database and then modified it to appropriately segment iris images. Representing the images as 3D ((x,y),z) (pixel position + intensity), information about the spatial relations in the image as well as about the individual properties of each pixel were preserved [22]. The moments f_{20} andf_{02}proved to identify the iris border but also produced considerable noise regarding the eyelid region.

Richard *et al.*, developed an iris segmentation approach which was able compensate all four types of noises in order to achieve higher accuracy rate [23]. It consists of four parts: firstly, the pupil is localized using threshold and Circular Hough Transform methods. Secondly, two search regions including the outer iris boundaries are defined to locate the outer iris. Next, two search regions are selected based on pupil position to detect the upper and lower eyelids and finally, threshold is implemented to remove eyelashes, reflection and pupil noises. The method's performance on CASIA iris database was found to perform as high as 98.62% accuracy.

Peihua and Xiaomin presented an incremental method for accurate iris segmentation. The algorithm works in two stages: first roughly locate a square region that contain pupil, followed by Canny edge detection plus Hough transform for accurate pupillary boundary localization; secondly roughly localizing two annulus sectors in which limbic boundary is finely positioned. The proposed method is not without limitations. Some limitations of the approach include: closure (complete or almost) of the eye; poor quality of the images due to variation of illumination, bad focus or noise; finally, inaccurate rough localization of pupillary boundary [1]. Nakissa and Mohammed developed a stepwise level set approach for iris segmentation of an iris recognition system [8]. Though it has many advantages on all existing methods, the lack of point correspondence is one of its important drawbacks.Yahyah and Nordin proposed iris segmentation by direct least squares fitting of ellipses [24].

Donida and his research group developed agent-based pupil localization (MAPL) and multiple views iris boundaries iris refining (MVBR) method for iris localization [25]. The present method was advancementon their previous work [26] method which employed an ANN method to locate pupil area. Donida and Scotti identified the iris boundaries by searching the peculiar pattern transitions in the radial gradient image around an observation point.In the present work, they used a set

of *N* observation points and properly fused the extracted information in order to better interpolate the inner and outer iris boundaries. The algorithm was applied on two major public iris databases (CASIA and UBIRIS version 2). The segmentation algorithm error rate was 2.9% and it did not have eyelash location and reflection removal algorithm.
Kheirolahy*et al.,* (2009) used optimized color mapping to make pupil region clear and easy to segment and they achieved 98% recognition accuracy by applying optimized color mapping [27]. The algorithm worked well in most of the eye models.
Abdulsamad and Nordin employed Chan-Vese active contour method to extract the iris from the surrounding structures [28]. The proposed algorithm is such that the image is loaded, reflections are identified using inpainting technique, adaptive boosting (AdaBoost)-Cascade Detector is adopted to detect iris region and finally Chan-Vese active contour method is applied to find the boundaries of the iris.When employed on UBIRIS iris database against some other iris segmentation methods [3; 9], it was discovered that it performed better with error rejection rate (ERR) of 5.5068. (Daugma [16.8635];Wildes [33.8226]).

Puhan and Kaushalramdeveloped an efficient segmentation algorithm using Fourier spectral density [29]. The Fourier spectral density computed for a pixel indicates the energy level in its neighbourhood. In an iris image, the energy level at pixels in sclera region is higher than the iris pixels due to the white sclera region. Thus making it possible to discriminate the sclera region from the iris. The specular reflections were removed by performing connected component labelling and threshold on the image.

Mahmoud and Ali proposed an iris segmentation algorithm which was able to localise an iris image in an unconstrained environment [30]. After pre-processing stage, circular Hough's transform was utilised for localizing circular area of iris inner and outer boundaries. Linear Hough transform was used to localise the boundaries between upper and lower eyelids occluding the iris. The algorithm was applied on CASIA iris database and gave an accuracy of 97.5%. Efficiency of the algorithm is not too good with varied illumination as we have in BATH database.

Sastr and Durga, developed an enhanced iris segmentation method that allows real-time iris recognition system [31]. This reduced iris segmentation time further allows high resolution iris images to be used thereby enhancing recognition accuracy of the system. His main target was to reduce the segmentation time.All occlusion were removed using Sobel filter both in vertical and horizontal directions. The inner and the outer boundaries were assumed to be a circle. Its recognition accuracy was found to be 99%.

V. Limitations of identified algorithms

Daugman, identified the following facts about human iris which must be bore in mind while developing iris recognition system [7]. The inner and outer boundaries are not perfect circle, active contour can be used for appropriate boundary determination. Secondly much greater demands are coming as nations are thinking of biometric based security system. The presence of outlier members of the populate who for various reasons may have non-standard eye appearance (e.g., non-round iris, coloboma, oddly shaped pupil, drooping eyelids, or much eyelash occlusion) or who simply have difficulty presenting to the camera (e.g., nystagmus or deviated gaze).
From all the aforementioned works, several interesting points can be concluded as follows:

- All these methods including Kong's detected all possible noise regions directly from original iris images. It would be more time-consuming if one want to accurately detect all possible noises;
- Although Kong's model has introduced how to accurately detect eyelash and reflection noises, it has not been tested based on the prevailing recognition algorithm on a large iris database;
- No method considered how to accurately segment the iris regions and the pupil regions when the shape of the pupil boundary cannot be approximated as circles;
- No method has been proposed to detect all four kinds of noises, namely eyelashes, eyelids, reflections and pupil in a single algorithm;
- Inner and outer boundaries, eyelashes and eyelid are detected in different steps, causing a considerable increase in processing time of the system;
- Usually, the inner and outer boundaries are detected by circle fitting techniques. This is a source of error, since the iris boundaries are not exactly circles.
- The results of the circle fitting method are sensitive to the image rotation, particularly if the angular rotation of the input image is more than 10^0.
- In noisy situations, the outer boundary of iris does not have sharp edges.
- After detecting iris boundaries, the resulted iris area is mapped into a size independent rectangular shape area. The rectangular normalization is having its disadvantages (Mahboubeh and Abdolreza, 2011).
- Critical examination of African iris reveals an improperly differentiated boundaries which will require a modification of some of the existing segmentation algorithm(s) for their proper recognition.

VI. Conclusion

Advancement of iris segmentation algorithm for black iris is needed urgently as world globalization and inter/intra boarder movement increases in this century. Development of public black iris database will also be of great importance to enhance development in iris biometric researches.

References

[1] Peihua L. and Xiaomin L., (2008). An incremental method for accurate iris segmentation. *Proceedings of IEEE.*
[2] Daugman J., (1993). High confidence visual recognition of person' by a test of statistical independence.*IEEE Transaction, PAMI,* 15(11), pp. 1148-1161.
[3] Daugman J., (2003). The importance of being random: statistical principles of iris recognition. *Pattern recognition.* 36(2), pp 279-291.
[4] Peihua Li and Xiaomin Liu, (2008). An incremental method for accurate iris segmentation *IEEE transactions.*
[5] Jain A., Bolle R., and Pankani S., (1999). Biometrics: Personal identification in a networked society.
[6] Camus, T. and R. Wildes, (2004). Reliable and fast eye inding in close-up images. Proceeding of the 16th International conference on pattern recognition, Aug. 11-15, IEEE Computer Society, Washington DC, USA., pp. 389-394.
[7] Lim S., Lee K., Byeon O. and Kim J., (2001). Efficient iris recognition through improvement of feature vector and classifier.*ETRI Journal,* 23(2), pp. 61-70.
[8] Nakissa B. and Mohammad S.M., (2008). A new approach for iris localization in iris recognition systems.*IEEE Transaction,* 5(8), pp. 516-523.
[9] Wildes, R.P., (1997). Iris recognition: an emerging biometric technology. Proceeding ofIEEE, 85(9), pp. 1348-1364.
[10] Ma, L., T. Tan, Y. Wang and D. Zhang, (2004). Efficient iris recognition by characterizing key local variations. IEEE Trans., Image Processing, 13: 739-750.
[11] Wildes, R. J., Asmuth, G. G. and Hsu, H., (2004). A system for automated iris recognition.*SecondIEEE workshop on applications of computer vision.*
[12] Martin-Roche, D., Sanchez-Avila, C., and Sanchez-Reillo, R., (2002). Iris recognition system for biometric identification using dyadic wavelet transform zero-crossing.*IEEE Aerospace Electron System Magazine,* 17(10), pp. 3-6.
[13] Kong W. and Zhang D., (2001). Accurate iris segmentation based on novel reflection and eyelash detection model. *In proceedings of ISIMVP,* pp. 263-266.
[14] Boles W. and Boashash B., (1998). A human identification techniques using images of the iris and wavelet transform. *IEEE Transaction, Signal processing,* 46(4): pp.1185-1188.
[15] Lim S., Lee K., Byeon O. and Kim J., (2001). Efficient iris recognition through improvement of feature vector and classifier.*ETRI Journal,* 23(2), pp. 61-70.
[16] Noh S. Pae K. Lee C. and Kim K., (2002). Multi-resolution independent component analysis for iris identification.*In proceedings of itc-CSCC'02,* pp. 1674-1678.
[17] Tisse C., Martin L., Torres L. and Robert M., (2002). Person identification technique using human iris recognition.*In proceedings of ICVI' 02,* pp. 294-299.
[18] Ma L., Tan T., Wang Y. and Zhang D., (2003). Personal Recognition based on iris Texture Analysis. *IEEE Transaction, PAMI,* 25(12), pp. 1519 – 1533.
[19] Cui, J, Wang, T., Tan, L.M and Sun, Z., (2004). A fast and robust iris localizationmethod based on texture segmentation. *Proceedings of the SPIE.,*vol. 5404, pp. 401-408.
[20] Huang Junzhou, Wang Yunhong, Tan Tieniu and Cui Jiali, (2004).A new iris segmentation method for recognition.*Proceedings of the 17th international conference on pattern recognition.* pp. 1051 – 4651.
[21] Teo, C.C. and Ewe, H.T., (2005). An efficient one-dimesional fractal analysis for iris recognition. *Proceedings of the 13th WSCG International Conference in Central Europe on Computer Graphics, Visualization and Computer Vision, pp. 157-160.*
[22] Proenca H. and Alexandre L. A., (2006). Iris segmentation methodology for non-cooperative recognition.*IEE proceedings: visual image signal process,* (153) 2, pp. 199- 205.
[23] Richard, Yew Fatt Ng, Yong, Haur Tay and Kai Ming Mok, (2007). An effective segmentation method for iris recognition system.
[24] Yahyah,A. E. and Nordin M. J., (2008). Accurate iris segmentation method for non- cooperative iris recognition system.*Journal of Computer Science,* 6(5), pp. 527-532.
[25] Donida R. L. and Scotti F., (2009). Agent-based image iris segmentation and multiple views boundary refining.
[26] Donida R. L. and Scotti F., (2008). Noisy iris segmentation with boundary regularization and reflection removal. *Image and vision computing,* vol.
[27] Kheirolahy, R; Masmoudi, D.S.; Derbel, N., (2009). Robust pupil boundary detection by optimized colour mapping for iris recognition. 14th International Computer Conference proceeding (CSICC, 2009). pp. 170-175.
[28] Abdulsamad E. Y. and Nordin M. J., (2010). Accurate iris segmentation method for non- cooperative iris recognition system.*Journal of Computer Science,* 6(5), pp. 527-532.
[29] Puhan, N.B. and Kaushalram, A.S., (2011). Efficient segmentation technique for noisy frontial view iris images using Fourier spectral density. SIViP, Springer, pp.105-119.
[30] Mahmoud M. and Ali N., (2012). Human iris segmentation for iris recognition in unconstrained environments.*International journal of Computer Science issues.* vol. 9 issue 1, no 3, pp. 149- 155.
[31] Sastry, A. V. G.S. and Durga, B.S., (2013). Enhanced segmentation method for iris recogni tion.*International journal of computer trends and technology.* Vol. 4, issue 2, pp. 68-71.

International Journal of Modern Engineering Research (IJMER)
www.ijmer.com Vol.3, Issue.4, Jul - Aug. 2013 pp-1890-1893 ISSN: 2249-6645

A Total Ergonomics Model for integration of health, safety and work to improve productivity of thermal Power Plants

Vijay Kumar Agnihotri[1], Devendra S.Dandotiya[2], S. K. Agrawal[3]
[1]*M. Tech Student SRCEMBanmoremorenaM.P.india*
[2, 3] *Assistance professor Mechanical engg. Dept. SRCEM morena india*

Abstract: *This paper presents a outline for development of integrated health, safety and work in complex critical systems of thermal power plant. In this paper operation and maintenance department of a thermal power plant was chosen as the case of our study. First, to achieve objectives, an integrated approach based on total ergonomics factors was developed. Second, it was applied to the thermal power plant and the advantages of total ergonomics approach were discussed. Third, the impacts of total ergonomics factors on local factors were examined through non-parametric statistical analysis. It is shown that total ergonomics model is much more beneficial than conventional approach. It should be noted that the traditional ergonomics methodology is not capable of locating the findings of total ergonomics model. The aspect of this study is the employment of a total system approach based on integration of the conventional ergonomics factors with factors.*

Key word: *Safety. Total system design, Environmental protection, Power plants, Human performance, Ergonomic, Macro ergonomics*

I. Introduction

The systematic process of designing for human use purpose is to provide a systematic and deliberate method for solving human factors issues in the most cost effective way. Analyses are conducted, solutions are implemented, Results are measured and follow-up actions taken, and Systems are affected. Productivity improvements for thermal power plants using Ergonomic point of view is categorized in as noise, Temperature, Lighting, Working Postures, Safety, Workers Productivity and Occupational Health, Equipment Design[1]. A design process can be described as a systematic series of actions that are under taken design a system or project [2].

The industrial challenge is to create an national interface among human operators, machine and managerial structures. In reality, managerial errors are often the basis causes of human errors and man-machine failures (3). Hence, the interface systems must be matched with operators' capabilities (4,5). In addition, there is a need for an integrated design between operators, machines, management and organization (6,7).

The need for productivity improvement arises due to the intimate link between productivity and economic growth; Economic growth has implications for resource use in general and for use of technology in particulars [8]. Productivity growth is critical for ensuring sustained increase in the production and services [9].

II. Methodologies

The systematic procedure for ergonomic point is to perform productivity needs analysis which gives an overview of current working condition of the company identifies the key productivity measures for the plant and forms the basis for the detailed work of production efficiency. Working need analysis which is constructed followed a plant tour and interviews/workshops with senior management to ascertain the current level of adoption of lean tools within the processes. Technological factor which gives perception and control philosophy (manual and automation), type of technology, system safely, market maintainability, national tradition and resource etc. and Anthropological factors which gives environmental and physiological characteristics, body sizes, level of skills education and knowledge attitudes and preferences. Training needs analysis (TNA) assesses the level of understanding and application of the same tools by the workforce. Idea generation and concept developments that are scenario, driven discussion design decision group focus groups

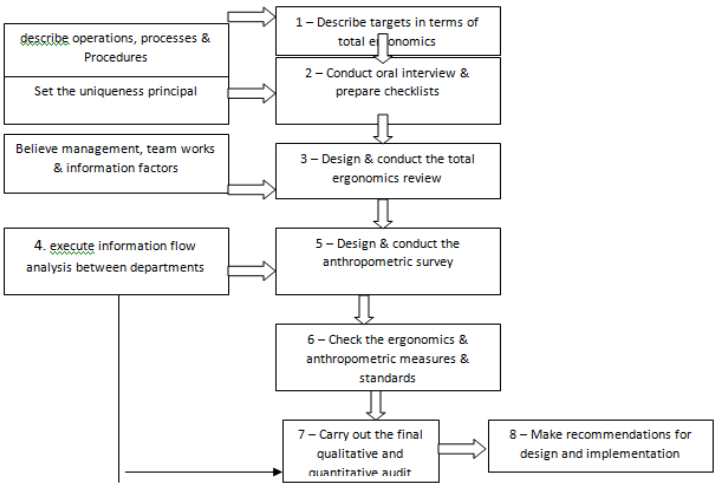

Fig. 1: The general steps required to achieve a total ergonomics model.

2.1Posture of employee during work

Calculated for each In this study work all the employees doing this operations were in the age group of 20 to 25 years with minimum tow year experience including training period and 450 people's interviews were conducted with a sample of plant's engineers and designers of which 417 completed and returned and obtain their description of the design process and use of ergonomics information. Risk priority numbers (RPN) were work elements based on posture and force for each major muscle group and the average was taken as the RPN for the effort intensity for the work. The major muscle groups considered were Back, Knees & ankles neck, Shoulders, Arms & wrists, Fingers and thumbs. The duration of continuous effort was recorded for each steps and RPN calculated based on the period of continuous effort. In calculating the total RNs for each work,. Weight age was given to the three parameters, based on their potential as risk factors for CTDs. Prioritization of works is carried out according to the total RPNs scored. The process of thermal power plant is identified as the work with maximum risk for cumulative Trauma Disorders according to the hazard rating scale-and RPNs of 8 & above, improvements to be taken up.

2.2Safety in Thermal Power Plants:

In this work 150 people were asked to fill out a structure questionnaire in connection with an accident investigation of thermal power plant. 125 subject returned the questionnaire for a response rate of 77%. The non responses percentage was 33%. The subject consists of 40 accident victim, 35 eyewitness, 10 worker's safety representative, 15 foreman, 05 manager, 15 safety officer, 05 groups neglected to mention groups to which they belongs, total number was 125. The subject estimated the effect of 24 measures on both productivity and safety. They rated each measure on a five-point scale so that values – 2 and 1 described a negative effect of a measure and value+1and + 2 a positive effect. The subjects chose the value zero if they felt that the measure had neither a positive nor a negative effect.

2.3Workers Productivity, Occupational Health

The work was conducted in 10 thermal power plant representing in urban, suburban and rural area. The number of thermal power plants in urban, suburban and rural area are 03(30%). 04(40%), 03 (30%) respectively. Investigate ergonomics, worker productivity and OHS in industries involved development of a checklist that included questions regarding: 91) demography of the company, (i) productivity and safety issues, (ii) ergonomic issues, (iii) environmental factors, and (iv) organizational and management issues. The demography of the companies included 10 questions such as number of workers, type of industry, if targets are set and percentage of targets achieved. Regarding productivity and safety issues, managers were asked 10 questions about worker productivity, quality of work, absenteeism and number of injuries. The ergonomic issues included 10 questions regarding worker's complaints on health and safety such as back pain, upper-body pain, fatigue, stress, manual material handling and motivation and training.

In this work 150 people were asked to fill out a structure questionnaire in connection with an accident investigation of thermal power plant. 120 subjects returned the questionnaire for a response rate of 80%. The non response percentage was 20%. The subject consist of 60 worker's safety representative, 20 foreman, 10 manager, 30 safety officer, total number was 120. The subjects estimated the effect of 10 measures on both productivity and safety. They rated each measure on a five-point scale so that values -2 and -1 described a negative effect of a measure and values + 1and + 2 a positive effect. The subjects chose the value zero if they felt that the measure had neither a positive nor a negative effect.

2.4 Noise in Thermal Power Plant

This work is conducted in three thermal power plants representing suburban locality. Noise is measure at selected stations in the different departments of the three plants using a precision sound level meter. Noise is measure with meter set on a network as well as the different octave bands. Noise data is recorded in brief. A random sample of 1050 male workers was selected from the different departments in the three surveyed plants of which 900 completed and returned. Out of 80 questionnaires about 20% were not returned and the rest incomplete. These (80) questionnaires were almost equally diapered within the 21 surveyed location. The questionnaire was designed to assess the socioeconomic characteristics of the individuals (age, marital status, occupation, education, and income) and individual's attitudes towards noise pollution.

2.5 Temperature Experimental Procedures

Temperature is measured at selected stations in the different departments of the three plants using a precision thermometer. Fifty healthy men participated in the research. The physical characteristic is summarized. The exposure time of each experiment was 3 hours. Firs, all subjects were exposed in climates with equal air, globe and radiant temperature. The subjects are examined at 7 "reference climates", where the temperature ranged from 27 to 55^{o}C. In subsequent experiments, minimum air temperature was 27^{o}C. Each step was combined with stepwise elevated radiant temperatures until the physiological reactions were at least equal or greater than those at the corresponding reference climate. Similar experiments were performed with variations of air velocity, physical work load and cloth is. The workers seemed to be related to the work environment (i.e. Plant Climate) due to high heat and high air ambient temperature, excessive noise dusts, dusts and noise level seeded to the worker. Heat load due to summer climate (Outside factory = 42^{o}C) and working near the boiler furnace (45^{o}C to 50^{o}C) affected operators by allowing less ability to work for a specific time. Additional heat was radiated by sunshine into the factory environment through tin roofed sheds

III. Results And Discussion:

3.1Working Posture: Intensity of Effort:

Risk priority numbers or RPNs were calculated for each work element, based on posture and force for each major muscle group of thermal power plants and the average was taken as the RPN for the effort intensity for the work in table 3.9. The major muscle groups considered were Back, Knees & ankles, neck, Shoulders, Arms & wrists, figures and thumbs the work, Using the Rodger's risk rating scale for each work step, prioritization of the work steps was done (risk scores or RPN of 8 & above) and improvement to be taken up, were finalized in consultation of engineers and team leaders as shown in table 3.10.

Table 3.9 Risk Priority Number of Each Work

SN	Activity	Risk Rating
1	Read the actual metal temperature of HP casing	4
2	Check the operational mode of HP & LP bypass value manual and auto.	6
3	Check the temperature control loop of the HP bypass station.	8
4	Ensure that the evacuating valves CR/105 & CR/106 and valves across NRVS in reheat lines are closed.	5
5	Check HP bypass valve and raise the steam pressure of boiler to design value.	9
6	Check the bypass valve of MSV & ESV.	4
7	Check steam pressure	5
8	Check drain system	6
9	Note down various metal temperatures	6
10	Bring the control of LP bypass valve on manual mode.	4
11	Manually closed the HP bypass valve.	7
12	Check that the eccentricity and different expansion system.	4
13	Check ESV inlet valve and CV of HP & IP turbine	4
14	Check bypass valve of MSV	4
15	Listen the turbine rubbing at 500m. Check the vibration of various bearing.	4
16	Check the speed to 300 rpm and hold the turbine for 5 minutes with a view to carry out inspection and listening soaking.	4
17	Ensure that the main centrifugal oil pumps are in ready position.	9
18	Synchronize the set load.	4
19	The raising of steam parameter and loading.	4

Table 3.10 Work Requiring Attention and improvements

SN	Work requiring attention	Improvement suggested
1	Office work station	Office workstation in adjustable height
2	Check drain system and note down various metal temperature	Height of adjustable platform to reduced twisting and bending and twisting can be avoided
3	Check the operation mode of H.P. Value	Redesign so that bending and twisting can be avoided
4	Pick up more than 3 kg weight from the rack above the shoulder level	Redesign the rack so that above shoulder operations are eliminated.
5	Operation mode of HP & LP valve manual and auto.	Redesign the height to avoid twisting and bending.
6	Temperature & Pressure measurement of HP bypass station.	Redesign of height to avoid twisting and bending.
7	Centrifugal oil ump reading	Redesign the height of pressure and temperature & soil level to reduced bending and back pain.

References

[1]. Saksvik P. Nytr, K. Implementation of internal control (IC) of health, environment and safety (HES) in Norwegian enterprises. Safety Science. 1996; **23(1):** 53–61.
[2]. Jensen PL. Risk assessment- a regulatory Strategy for stimulating working environment activities. Human Factorsand Ergonomics in Manufacturing. 2001; **11(2):**101-16
[3]. Reason J. Human Error. Cambridge University Press, England, 1992: pp. 132-47.
[4]. Eklund J. Development work for quality and ergonomics. Applied Ergonomics. 2000; **31:**641-48.
[5]. Lajunen T, Parker D, Summala H. The Manchester driving behavior questionnaire:
[6]. a cross-cultural study. Acci Anal Prevent. 2004: **36(2):**231-38.
[7]. Hendrick H.W. Macro Ergonomics: A Concept Who's Time Has Come. Bulletinof Human Factors Society. 1987; **30(2):**1-2.
[8]. Hart RA, Whitaker JM, Hughes DH HP. Templet. Team Concept to Mitigate an MIC Failure in a Petrochemical Plant Cooling System. Material Performance. 1990; **29:**40-44.
[9]. Harmon J. Social Judgment Analysis and Small Group Decision Making. OrganizationalBehavior and Human DecisionBehavior. 1990; **46:**34-54.
[10]. Bailey RW. Human Performance Engineering. Prentice Hall, New York, 1989: pp.66-81.

[11]. Kannapin O, Pawlik K, Zinn F. The pattern of variables predicting self-reported environmental behavior. Journal for Experimental Psychology. 1998; **45(4):**365-377.
[12]. Beevis D, Slade IM. Ergonomics-costs and benefits. Applied Ergonomics. 2005; 34(5**):**413–18.
[13]. Kleiner BM, d Drury CG. Large-scale regional economic development: macro ergonomic in theory and practice. Hum Factors Ergon Manuf. 1999; **9(2):** 151-63.
[14]. Drucker PE. Emerging Theory of Manufacturing. Harvard Business Review. 1990: b pp.94-101.
[15]. Deependra Kumar Jha, Naoto Yorino and Yoshifumi Zoka , Benchmarking Results of Electricity Generating Plants in Nepal Using Modified DEA Models , Osaka, Japan ,2007

International Journal of Modern Engineering Research (IJMER)
www.ijmer.com Vol.3, Issue.4, Jul - Aug. 2013 pp-1894-1899 ISSN: 2249-6645

HMM-Based Speech Synthesis

Smita Chopde[#], Pushpa U. S.[*]
[#]*EXTC Dept. Mumbai University, Mumbai*

Abstract: *This paper describes a approach to text-to-speech synthesis (TTS) based on HMM. In the proposing approach, speech spectral parameter sequences are generated from HMMs directly based on maximum likelihood criterion. By considering relationship between static and dynamic features during parameter generation, smooth spectral sequences are generated according to the statistics of static and dynamic parameters modelled by HMMs, resulting in natural sounding speech. In this paper, first, the algorithm for parameter generation is derived, and then the basic structure of an HMM based TTS system is described. Results of subjective experiments show the effectiveness of dynamic feature.*

Keywords: *Include at least 5 keywords or phrases*

I. INTRODUCTION

A Hidden Markov Model (HMM) is finite state machine which generates a sequence of discrete time observation. At each time unit (frame) the HMM changes state according to state transition probability distribution, and then generates an observation o_t at time t according to output probability distribution of the current state .Hence the HMM is doubly stochastic random process model.

An N state HMM is defined by state transition probability distribution $A=\{aij\}N\ i,j=0$and output probability $B=\{b_j(o)\}^N_{j=0}$ and initial state probability distribution $\pi=\{\pi_i\}^N_{i=0}$. For convenience the compact notation.

$$\lambda = (A,B,\pi)$$

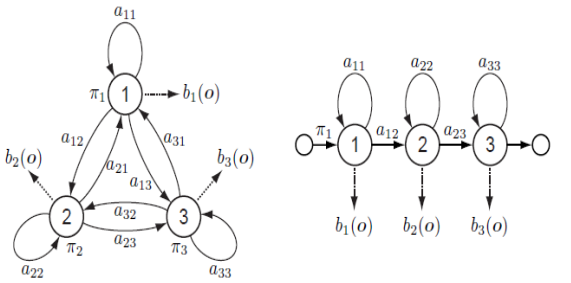

(a) A 3-state ergodic model (b) A 3-state left-to-right model

Figure 1. Examples of HMM parameter is used to indicate parameter set of the model

Figure 1 shows the HMM model Figure 1 (a) shows the 3 state ergodic state ,in every state of model could be reached from every other state of the model in single step figure 1(b) shows the a 3 state left to right model in which the state index increases or stays same as time increase. Generally left to right HMMs are used to model speech parameter sequence since they can appropriate model signal whose property changes in successive manner. The output probability distribution $b_j(o_t)$ can be discrete or continuous depending on the observation. Usually in continuous distribution HMM (CDHMM) an output probability distribution is modelled by mixture of multivariate Gaussian distribution which as follows

$$b_j(o)=\sum_{m=1}^{M} w_{jm} N(o|\mu_{jm},,U_{jm})$$

Where M= number of mixture component w_{jm}, $\boldsymbol{\mu}_{jm}$, $\boldsymbol{U}_{jm}$ are weight, a mean vector, and covariance matrix component m of state j, respectively. A Gaussian distribution $N(o|\mu_{jm},,U_{jm})$ is defined by

$$N(o|\mu_{jm},,U_{jm}) = (1/(\sqrt{2\pi})^d |U|) \exp[-1/2(o-\mu\mu_{jm})^T U_{jm}^{-1}(o - \mu_{jm})$$

Where d is dimensionality of o. mixture weight w_{jm} satisfies the stochastic constraint

$\sum w_{jm} = 1 \quad 1 \le j \le N$

$W_{jm} \ge 0 \quad 1 \le j \le N, \quad 1 \le m \le M$

So that $b_j(o)$ are properly normalized .

$\int bj(o)do = 1 \quad 1 \le j \le N$

When the observation vector o is divided into S independent data stream i.e. $o = [o_1^T, o_2^T, o_3^T, \ldots\ldots\ldots\ldots o_S^T]^T$ bj(o) is formulated by product of Gaussian mixture densities.

$$\mathbf{b_j(o)=\prod_{s=1}^{S} b_s(o_s)}$$

$$b_j(o) = \sum_{s=1}^{S} \{ \sum_{m=1}^{M_s} w_{jsm} N(o_s | \mu_{jsm}, U_{jsm}) \}$$

Likelihood calculation

When the state sequence is determined as Q= (q_1 q_2 q_3 q $_4$….q_T), the likelihood of generating an observation sequence O=(o_1, o_2, o_3, o_4,….o_T) is calculated by multiplying the state transition probabilities and output probabilities for each state

$$P\left(O, \frac{Q}{\lambda}\right) = \sum_{t=1}^{T} \boldsymbol{Aqt-1, Aqt, Bqt, O(t)}$$

Where A_{q0j} denote π_j. The likelihood of generating O from HMM $\boldsymbol{\lambda}$ is calculated by summing P(O,Q/$\boldsymbol{\lambda}$) for all possible sequences

$$P\left(\frac{O}{\boldsymbol{\lambda}}\right) = \sum_{Qall} \prod_{t=1}^{T} \boldsymbol{Aqt-1, Aqt, Bqt, O(t)}$$

The likelihood of above equation is sufficiently calculated using forward and/or backward procedure .

The forward and backward variables are

$\alpha_t(i)=P(o_1,o_2,.....o_T,q_t=i/\lambda)$

$\beta_t(i)=P(o_{t+1},o_{t+2}, ...o_T,q=i,\lambda)$

can be calculated individually as

1. Initialization
   $\alpha_1(i)=\Pi\, b_i(o_1)$ 1<i<N
   $\beta_T(i) = 1$ 1<i<N`
2. Recursion
   $\alpha_{T+1}(i)=\left[\sum_{j=1}^{N} \alpha t(j) aji\right] b_i(t+1)$ 1 <i<N
   t=2,.....T
3. Termination
   $P^* = \max[(\delta_T(i)]$
   $q^* = argmax[(\delta_T(i)]$
4. Path back tracking
   $q_t^* = \Psi_{t+1}(q^*_{t+1})$

Maximum Likelihood Estimation of HMM parameter

There is no known method to analytically obtain the model parameter set based on maximum likelihood based on maximum likelihood (ML) criterion ., that is to obtain which maximises likelihood P(O/λ) for a given observation sequence O , in a closed form. Since this problem is a high dimensional nonlinear optimization problem, and there will be number of local maxima . , it is difficult to obtain λ which globally maximizes P(O/λ) and can be obtained using an iterative procedure such as the expectation –maximization (EM) algorithm (which is often referred to as Baum-Weich algorithm), and the obtained parameter set will be a good estimate if a good initial estimate is provided .

In the following , the EM algorithm for the CD-HMM are described . The algorithm for the HMM with discrete output distribution can also be derived in the straight forward manner

Q-Function

In the E M algorithm , an auxiliary function Q(λ',λ) of current parameter set λ' and new parameter set λ is defined as follows

$$Q(\lambda',\lambda) = \frac{1}{P(\frac{O}{\lambda})} \sum P(O, Q|\lambda') \log P(O, Q\backslash\lambda).$$

Here , each mixture component is decomposed into a substrate and Q is redefined as a substrate sequence i.e.

Q=((q_1 ,s_1) ,(q_2 ,s_2), ...(q_T,s_T)

Where (q_T,s_T) represents the being substrate s_t of state q_t at time t.

At each iteration of procedure current parameter set λ' is replace by new parameter set which maximises Q(λ',λ). This iterative procedure can be provided to increase likelihood P(O|λ) monotonically and converge to a certain critical point since it can provide that Q- function satisfies the following theorem

Theorem 1

Q(λ',λ)≥ Q(λ',λ') i.e. P(O|λ)≥P(O|λ')

Theorem 2

The auxiliary function Q(λ',λ) has a unique global maximum as a function of λ and this is the one and the critical point.

Theorem 3

A parameter set λ is the critical point of the likelihood P(O|λ) if and only if it is a critical point of the Q- function.

Maximization of the Q-Function

logP(O, O|λ) can be written as

$\log P(O, O|\lambda) = \sum_{t=1}^{T} aqt-1qt + \sum_{t=1}^{T} wqtst + \sum \log \mathcal{N}(ot|\mu qt\, st$,Uqt st),

where a_{q0q1} denotes Π_{q1}. Hence the Q function can be written as

$Q(\lambda',\lambda)=\sum_{i=1}^{N} P(O,q1=i|\lambda')log\Pi i$
$+\sum_{i=1}^{N}\sum_{j=1}^{N}\sum_{t=1}^{T-1} P(O,qt=i,qt+1=j|\lambda')logaij+\sum_{i=1}^{N}\sum_{j=1}^{N}\sum_{t=1}^{T} P(O,qt=i,st=k|\lambda')logwqtst+$
$\sum_{i=1}^{N}\sum_{k=1}^{M}\sum_{t=1}^{T} P(O,qt=1,st=k|\lambda)log\mathcal{N}(ot|\mu qtst,Uqtst)$

$$\sum_{i=1}^{N} \Pi i = 1$$

$\sum_{J=1}^{N} aij = 1$ 1≤i≤N

$\sum_{k=1}^{M} wik = 1$ 1≤i≤N

can be derived from lagaranges or differential calculs.

$\Pi_i = \gamma_1(i)$, $aij=\frac{\sum_{t=1}^{T-1}\xi' t(i,j)}{\sum_{t=1}^{T-1}\gamma t(i)}$; $wik = \frac{\sum_{t-1}^{T}\gamma t(i,k)}{\sum_{t-1}^{T}\gamma t(i)}$; $\mu ik = \frac{\sum_{t-1}^{T}\gamma t(i,k).Ot}{\sum_{t=1}^{T}\gamma t(i,k)}$; $Uik = \frac{\sum_{t-1}^{T}\gamma t(i,k).(ot-\mu ik).(ot-\mu ik)}{\sum_{t-1}^{T}\gamma t(i,k)}$

Probability of state i being at t and probability of state i being at t+1 are

$\gamma t(i) = P(O,qt=i|\lambda) = \frac{\alpha i(t)\beta t(i)}{\sum_{j=1}^{N}\alpha t(j)\beta t(j)}$; γt(i,k)=P(O,qt=1,st=k|λ)= $\frac{\alpha t(i)\beta t(i)}{\sum_{j=1}^{N}\alpha t(j)\beta t(j)}\cdot\frac{wjk\mathcal{N}(ot|\mu jk,Ujk)}{\sum_{m=1}^{M}wjm\mathcal{N}(ot|\mu j m' Ujm)}$

ξt(i,j)=P(O,qt=i,qt+1=j|λ)=$\frac{\alpha t(i)bj(ot+1)\beta t+1(j)}{\sum_{t=1}^{N}\sum_{n=1}^{N}\alpha t(l)\alpha lnbn(ot+1)\beta t+1(n)}$

II. METHOD

The system consists of two stages : the training stage and the synthesis stage.First in training stage mel-cepstrumm coffecient are obtained from the speech signal by delta –delta mel-cepstral coefficient.Then phoneme HMM are trained using mel-cepstral coefficient and their deltas and deltas-deltas .

In the synthesis stage an arbitrary given text to be synthesized is transformed into phoneme sequence . According to phoneme sequence , a sentence HMM which represents the whole text to be synthesized is constructed by concatening phoneme HMMs. From the sentence HMM ,a speech parameter is generated using the algorithm for speech parameter generation for HMM By using Mel-Log spectral Approximation speech is synthesized from the generated mel-spectral coefficient.

Speech data base

HMM are trained using 503 phonetically balance sentences uttered by male speaker . Speech signal is sampled at 20KHz and downsampled to 10KHz and re-labelled using 60 phonemes and silence given in table 1. Unvoiced vowles with previous consonants are treated as individual phonemes e.g shi is composed of unvoiced i with previous sh.

Vowels a , i, u,e,o
Consonants N, m , n ,y,w,r,p,pp,t,tt,k,kk,b,d,dd, g, ch cch ts tts s ss sh, ssh, h,f ,ff,z j, my ny ry by gyp y ppy ky kky hy
Unvoiced vowels with previous consonants pi, pu,ppi,ki,ku,kku,chi,cchi,tsu,su,shi, shu, sshi,sshu, hi, fu

Table :1 Phoenems used in system

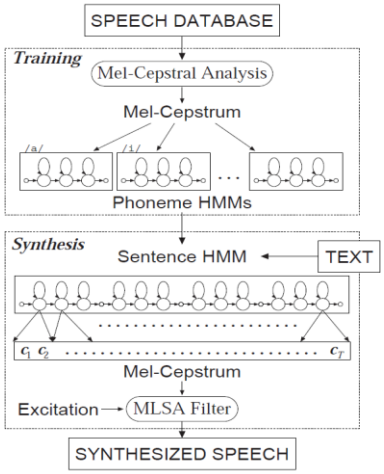

Figure:2 Block diagram of HMM based speech synthesis system.

Speech Analysis

Speech signal are windowed by 25.6ms Blackman window with 5ms shift , then mel cepstral coefficients are obtained by 15 th order mel-cepstral analysis. The dynamic feature Δc_t and $\Delta\Delta c_t$ i.e. delta and delta –delta mel-cepstral coefficient at frame t are calculated as

$\Delta c_t = \frac{1}{2}(c_{t+1} - c_{t-1})$, $\Delta^2 c_t = \frac{1}{2}(\Delta c_{t+1} - \Delta c_{t-1})$

The feature vector is composed of 16 mel- cepstral coefficient including the zeroth coefficient and their delta and delta-delta coefficient .

Training of HMM

All HMM used in system were left- to – right model with no skip . each state has single Gaussian distribution with diagonal convergence . Initially a set of microphone models were trained . These models were cloned to produce a triphone model for all distinct triphones in the training data. The triphone models were reestimated with the embedded version of Bauman Welch version algorithm. All the states at same position of the triphone HMM derived from same microphone HMM were clustered using further neighbourhood hierarchical clustering algorithm. The output distribution in the same cluster were tied to reduce the number of parameters and to balance the complexity against the available data .Tied triphone models were re estimated with embedded training again.

Finally the data was aligned to the models via viterbi algorithm to obtain state duration densities . each of the state duration densities was modelled by single Gaussian distribution .

Speech Synthesis

An aritbitrary given text to be synthesized is converted in phoneme sequence Then triphone HMM corresponding to the phoneme sequence are concatenated to obtain HMM sentence which represents the whole text to be synthesized . Instead of triphones which did not exist in the training data , monophone models are used .. From the sentence HMM , a speech parameter sequence is generated using algorithm. By using MLSA filter speech is synthesized from the generated mel cepstral coefficient directly .

Subjective Experiments

Subjective test were conducted to evaluate the effect of including dynamic feature and to investigate the relationship between the number of states of tied triphone HMMs and the quality of speech synthesized .The test sentence consisted of twelve sentences which were not included in training sentences. Fundamental frequency contours were extracted from natural utterances, and used for speech synthesis using linear time warping within each phoneme to adjust phoneme duration of extracted fundamental frequency contours to generated parameter sequence . In the test sentences set, there exist 619 distinct triphonens in which 38(5.8%) triphones where not included in training data and replaced by monophones. The test sentence set where divided into three set and each set was evaluated by individual subjects . Subjects were presented with a pair of synthesized set at each trial, and asked to judge which of two speech samples sounded better .

Effect of dynamic features

To investigate the effect of dynamic features , a pared compression test was conducted . Speech samples used in the test were synthesized using (1) speech spectral sequence generated without dynamic feature from model stringed using static features

(2) spectral sequence generated using only static features and then linearly interpolated between the centers of state duration.

(3) Spectral sequence generated using static and delta parameters from the models trained using static and dynamic parameter

(4) Spectral parameters generated using static , delta and delta –delta from the models trained using static, delta and delts-delta parameters. All the models were triphone models without sate tying.

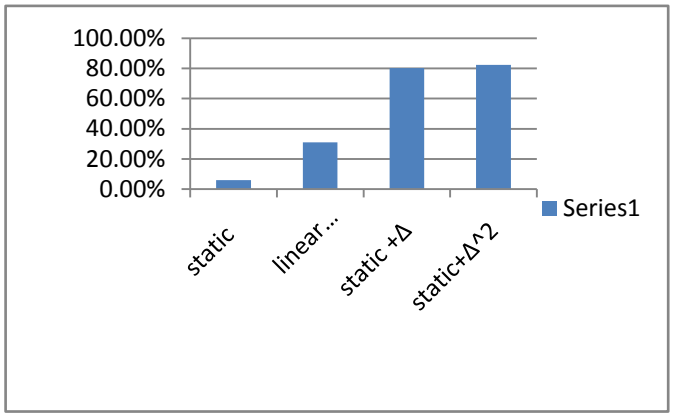

Figure:3 Effects of dynamic features

Figure:3 shows the results of the paired comparison test. Vertical axis denotes the preference score . From the result it can be seen that the score for synthetic speech generated using dynamic feature are much higher than those synthetics speech generated using static features with and without linear interpolation. This is due that by exploiting statics of dynamic features for speech parameter generation, generated spectral sequence can reflect not only shapes spectra but also transition appropriately comparing to spectral sequence generated using static features only with linear interpolation.

State tying

To investigate the relationship between total number of state of tied tri phone HMMs and quality of speech synthesized speech, paired comparison test were conducted using 3 and 5 tied triphone HMMs .By modifying stop character for state clustering several sets of HMMs which had different numbers of states were prepared for test. For 3-stse HMMs comparison were performed using triphone model without state tying(totally 10,544 states) tied triphone models with totally 1,961and 1,222 states and monophone models (183 states) and for 5 state HMMs triphone models without state tying

(totally 17,590 states), tied triphone models with totaly 2,040 and 1,199 states and monophone models (305 states). It is noted that sate duration distribution of triphone models were also used for monophone models to avoid of phoneme duration on speech quality.

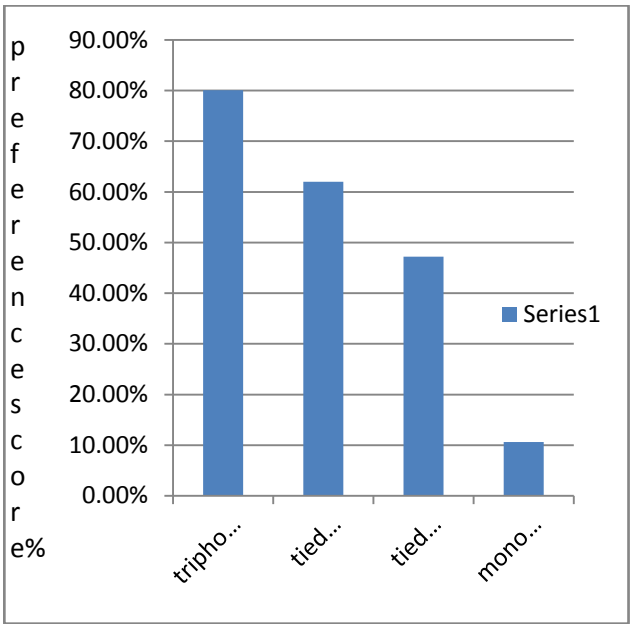

Figure: 4a 3 state HMMs

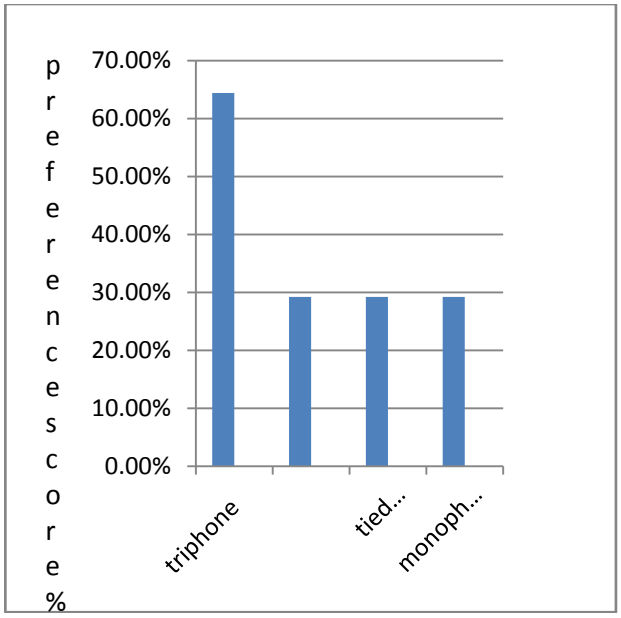

Figure:4b 5 state model

Figure: 4a and Figure:4b shows the result for 3 state and 5 state HMM. From the result , it can be seen that the quality of synthetic speech degrade as the number of states decrease .From informal listening test and investigation of generated spectra , it was observed that shapes of spectra were getting flatten as the number of state decreases and this cause degrading of in intelligibility . It was observed that that the audible discontinuity in synthetic speech increased as the number of state increased , meanwhile the generated spectra varied smoothly when the number of states were small. The discontinuity caused in the lower score for 5 state triphone models compared to 3 – state triphone models. It is noted that significant degradation in communicability was not observed even if the mono phone models were used for speech synthesis .

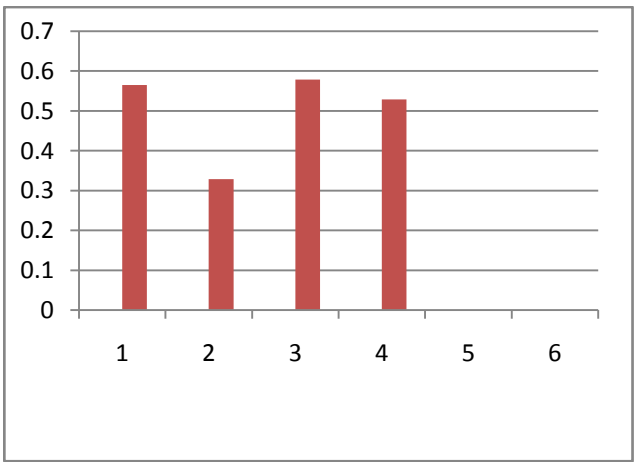

Figure: 5 Comparison of 3-state and 5- state HMMs

Along x-axis
1 3-state HMM (1961 states)
2 3-state HMM (1222 states)
3 5-state HMM (2040 states)
4 5-state HMM (1199 states)

From the above figure it can be seen that scores for 3-state and 5-state models were almost equivalent when number of states were almost 2000, the score of 5-state models was better when the number states were 1200. When the total number of tied states were almost the same , 5- sate model has higher resolution in time than 3- sate model reversely, 3-sate model has better resolution in parameter space than 5-state model .From the result if total number of state state is limited, models with higher resolution in time can synthesize more naturally sounding speech than model with higher parameter resolution in space .

III. CONCLUSION

In parameter generation algorithm a speech generation sequence is obtained so that likelyhood of HMM for generated parameter sequence is maximized. By exploiting the constraints between static and dynamic features the generated parameter sequence results not only for static of shapes of spectra but also transition obtained from training data appropriately, resulting in smooth and realistic spectral sequence .In parameter generation algorithm a problem of generating parameter speech was simplified assuming that parameter sequence was generated along single path. The extended parameter algorithm using multi-mixture HMMs model has more ability to generate natural soundings speech, however extended algorithm has more computational complexity since it is based on expectation- maximization algorithm ,which results in iteration of forward –backward algorithm and parameter generation algorithm.

References

[1]. R . E. Donowan and E.M.Eide,"The IBM Trainable Speech Synthesis System," Proc . ICSLP-98 , 5,pp,1703 1706 , Dec 1998.
[2]. F.A.Falaschi ,M. Giustiniani and M. Verola , " A Hidden Markov Model approach to speech synthesis , " Proc. EUROSPEECH-89, pp.187-190.sep.1989.
[3]. A. Gustiniani and P.Pierucci, "Phonetic ergodic HMM for speech synthesis," Proc.EUROSPEECH-91,pp.349-352,sep1991.
[4]. M. Tonomura, T.Kosakaand S. Matsunaga, "Speaker adaptation based on transfer vector field smoothing using maximum a posterior probability estimation," Computer speech and Language , vol.10.n0.2pp.117-132,Apr.1996.

International Journal of Modern Engineering Research (IJMER)
www.ijmer.com Vol. 3, Issue. 4, Jul - Aug. 2013 pp-1900-1905 ISSN: 2249-6645

Profile modification of adhesively bonded cylindrical joint for maximum torque transmission capability

Walame M. V.[1], Ahuja B. B.[2]
[12]*Department of Production Engineering, College of Engineering, Pune-411005*

ABSTRACT: *The increasing demand for light weight, high quality and more cost effective product has led adhesive bonding to emerge as one of the primary ways of fastening structural members. Adhesive joints have previously been designed empirically but now a day's data is available to design adhesive joints in an optimum way. The fixing of cylindrical components subjected to torque is a common requirement in industrial manufacture and there is a need to design and optimize the adhesively bonded cylindrical joint for maximum torque transmission capability facilitating keyless fastening. Some typical examples of adhesively bonded cylindrical joints are shaft to shaft, gear to shaft, rotor to shaft, fan to shaft, pulley to shaft etc. The present paper aims at the development of analytical model for adhesively bonded cylindrical joint subjected to torsion loading for determination of the joint profile geometry for maximum torque transmission capability. The analysis is based on classical torsion theory and constitutive, equilibrium and compatibility equations of theory of elasticity are used to obtain stress field in the adhesive layer and optimize joint profile. The analytical model developed is used to determine profile of adherends of bonded cylindrical joint for maximum torque transmission capability and with minimum weight.*

Keywords: *Bonded joint, Torsion, Analytical solution, Stress distribution, Optimization*

I. INTRODUCTION

As compared to former times, today's products are designed and optimized under completely different rules, with the main focus being on vital questions such as shortages of raw materials, total energy content and the environment-friendly disposal or reuse of a product. The increasing demand for light weight, high quality and more cost effective product has led adhesive bonding to emerge as one of the primary ways of fastening structural members.

The fixing of cylindrical components which are subjected to different kinds of loads like axial tensile, axial compressive, bending, torque, pressure etc. is a common requirement in industrial manufacture. In recent years, adhesives, especially anaerobic adhesives, have found many applications that range across many industries replacing traditional methods. Some typical cylindrical joints are Shaft to Shaft, Gear to Shaft, Rotor to Shaft, Bearing into Housing, Tube into Casting, Cylinder Liner into Engine Block, Pulley to Shaft, Fan to Shaft, Trunnions into Rollers and Bushings into Housings etc.

Adhesive joints have previously been designed empirically. For optimum design of adhesively bonded cylindrical joint, complete knowledge of stress distribution and the parameters affecting stress distribution in adhesive joint is necessary. Also for maximum torque transmission capability of the joint the stress distribution should be uniform.

The increased application of adhesive bonding was accompanied by development of mathematical and numerical methods to analyse and predict the behaviour of joints each with different assumptions and simplifications but at present also this is still an open problem.

II. LITERATURE SURVEY

The stress distribution in adhesive bonded tubular lap joints subjected to torsion was analysed by D. Chen and S. Cheng [1]. The analysis was based on the elasticity theory in conjunction with variational principle of complimentary energy, with two adherends may be having different materials and different thickness. The closed form solution so obtained was used to determine the stress intensities in adhesive layer and stress concentration factor.

A closed form solution for stress distribution of tubular lap joint in torsion whose adherends were of composite materials was obtained by Choon T. Chon [2]. The stress concentrations at and near the end was studied as function of various parameters such as wrap angles, overlap length and thickness of adhesive layer.

N. Pugno and G. Surace [3] analysed problem of torsion in adhesive bonded tubular joint and the stress field in the adhesive layer was obtained based on the elasticity theory and pure torsion theory. A special type of tubular joint was proposed by optimizing the tubular joint for torsional strength.

Zhenyu Ouyang , Guoqiang Li [4] obtained Cohesive Zone Model (CZM) based analytical solutions for the bonded pipe joints under torsion. The concept of the minimum interfacial cohesive shear slip is introduced and used in the fundamental expression of the external torsion load. The results obtained from Cohesive Zone Model were in good agreement with finite element analysis (FEA) results.

The experimental investigations for effect of different surface roughness values on bonding strength for both static and dynamic loading conditions was performed by Tezcan Sekercioglu, Alper Gulsoz, Hikmat Rende [5]. For the experimentation adherends of structural steel and anaerobic adhesive Loctite 638 were used.

Tezcan Sekercioglu [6] investigated experimentally the effect of parameters namely interference fit, bonding clearance, surface roughness, adherend materials and temperature on bonding strength of adhesive. For shear strength estimation of adhesively bonded tubular joints the nonlinear models (GASSEM) were developed using Genetic Algorithm (GA) approach.

Present paper aims at the development of analytical model for adhesively bonded cylindrical joint subjected to torsion loading for profile modification of the joint for maximum torque transmission capability and minimum weight.

III. ANALYTICAL SOLUTION

The following assumptions are made in the current study-

- Two shafts and adhesive layer forming the cylindrical joint are governed by an isotropic linear elastic law.
- Deformations considered are very small and Classical Torsion theory is used.
- The variation of stress across the thickness of adhesive layer is neglected as the thickness of adhesive layer is very very small and torsion load carried by thin adhesive layer is ignored [10].

Consider two shafts bonded adhesively by a thin adhesive layer with 2*c* as bond length, as shown in fig.(1) subjected to torsion moment T.

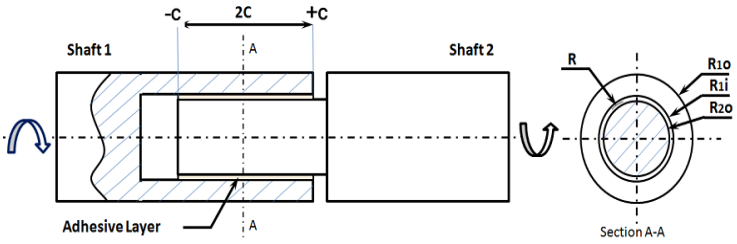

Figure 1: Two shafts bonded adhesively by thin adhesive layer

Torque transfer takes place gradually from shaft 1 to shaft 2 and at any cross section torque $T1$ and torque $T2$ are produced in shaft 1 and shaft 2 respectively. The external torsion load is assumed to be resisted by shafts only and hence the sum of the moments absorbed by the two shafts must be equivalent to the applied torsional moment T for every cross section. Here torsion load carried by thin adhesive layer is ignored.

$$T = T_1(z) + T_2(z) \quad [1]$$

The torsional moment T_i (z) at any section z of shaft *i* can be expressed as function of z.

$$T_1(z) = T * f(z) \quad [2]$$

$$T_2(z) = T * (1 - f(z)) \quad [3]$$

With Boundary conditions

$$T_1(-c) = T \quad , \quad T_1(+c) = 0 \quad [4]$$

$$T_2(-c) = 0 \quad , \quad T_2(+c) = T$$

Consider an differential element of length *dz* $(-c \le z \le +c)$ belonging to the shaft 1 as shown in fig.(2) and imposing rotational equilibrium the stress field in the adhesive layer equivalent to applied torsional moment can be written as –

$$\tau(z) = \frac{-1}{2\pi R^2} \frac{dT_1(z)}{dz} \quad [5]$$

Where R is the mean radius of adhesive surface and $T_1(z)$ is torsional moment in shaft 1 at section 'z'.

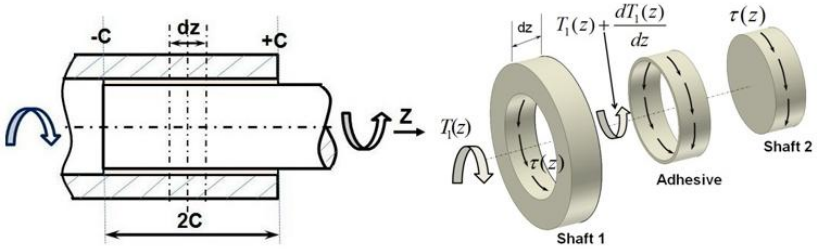

Figure 2: Bonded cylindrical joint under torsion

From equation (5) it can be seen that the shear stress in adhesive layer depends on rate of change of torque in bonded shafts. Now if the joint profile is modified in such a way that the rate of change of torque in the shafts along bond length remains constant then the shear stress in adhesive layer will be constant along bond length as shown in fig.(3).

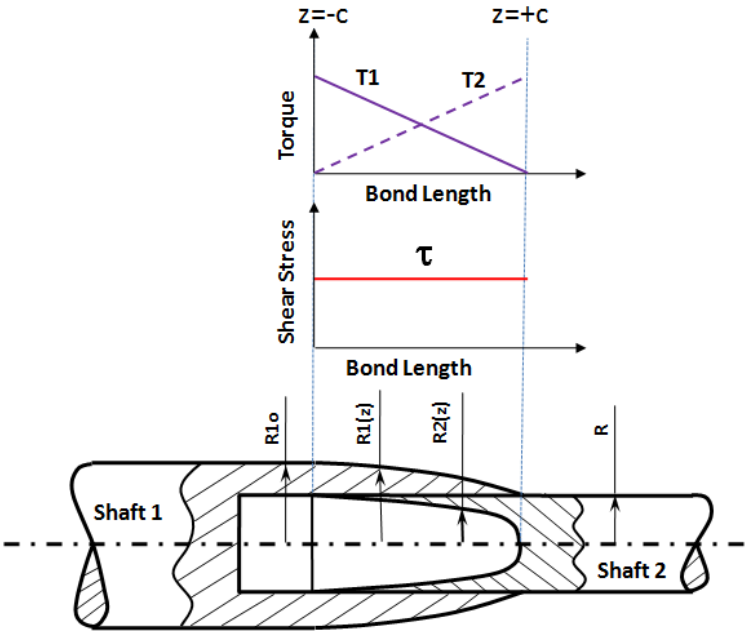

Figure 3 : Profile modification of Cylindrical Joint for uniform strength

The boundary conditions mentioned in equation (4) and linear rate of change of torque is satisfied by the following function.

$$f(z) = \left(\frac{c - z}{2c}\right) \qquad [6]$$

At any cross section if the rotations of shaft 1 and shaft 2 are identical then there is no relative displacement between them at that cross section. But if at any cross section if the rotations of shaft 1 and shaft 2 are different from each other, a relative rotation occurs resulting in circumferential relative displacement θ(z) at the bond layer which can be written as

$$\theta(z) = \theta_2(z) - \theta_1(z) \qquad [7]$$

From the Torsional moments absorbed by the two shafts at the joint, the rotations $\theta_1(z)$ and $\theta_2(z)$ of the cross sections of shaft 1 and shaft 2 respectively can be obtained from the compatibility and the circumferential relative displacements at the bond layer and θ(z) can be written as –

$$\theta(z) = \int_{-c}^{z} \frac{T_2(z)}{G_2 J_2}\, dz - \int_{-c}^{z} \frac{T_1(z)}{G_1 J_1}\, dz + \Delta\theta_i \qquad [8]$$

Where G_i = Shear modulus of material of shaft i , J_i = polar moment of inertia of shaft i and $\Delta\theta_i$ is the difference in the absolute rotations of shaft 1 and shaft 2 at the initial section $(z = -c)$.

The strain field γ (z) in the adhesive layer can be obtained from the stress field equation (5) and deformed geometry of adhesive layer as shown in fig.(4).

$$\gamma(z) = \frac{-1}{2\pi R^2 G_a} \frac{dT_1(z)}{dz} = \frac{R\ \theta(z)}{t_a} \qquad [9]$$

Where t_a is adhesive layer thickness and G_a Shear modulus of adhesive.

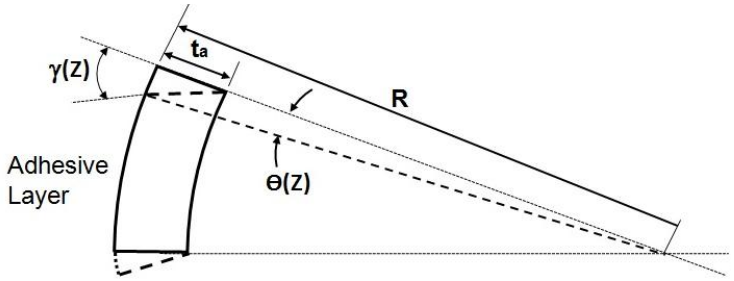

Figure 4: Shearing strain in adhesive layer

The rate of change of torque in shaft 1 along bond length can be obtained by substituting values of $\theta(z)$, $\tau(z)$ from equations (8) and (5) in equation (9).

$$\frac{dT_1(z)}{dz} = \frac{-2\pi R^3 G_a}{t_a}\left(\int_{-c}^{z} \frac{T_2(z)}{G_2 J_2}\, dz - \int_{-c}^{z} \frac{T_1(z)}{G_1 J_1}\, dz + \Delta\theta_i \right) \quad [10]$$

The following condition is obtained after differentiating equation (10) w.r.t. z and substituting values of $T_1(z)$, $T_2(z)$, f(z) from equations (2), (3), (6).

$$\frac{G_2 J_2(z)}{G_1 J_1(z)} = \frac{(c+z)}{(c-z)} \quad [11]$$

For unique solution of optimized geometry profile an additional condition must be considered of symmetric torsional stiffness of shafts section by section which can be written as-

$$G_1 J_1(z) = G_2 J_2(-z) \quad [12]$$

From the geometry of shaft 1 the following equations can be written for the torsional stiffness of shaft at different locations along the bond length.

$$At \quad z = -c \qquad G_1 J_1 = G_1\left(\frac{\pi}{2}\right)\left(R^4 1o - R^4\right) \quad [13]$$

$$z = +c \qquad G_1 J_1 = 0 \quad [14]$$

$$at \quad any \quad z \qquad G_1 J_1 = G_1\left(\frac{\pi}{2}\right)\left(R^4{}_1(z) - R^4\right) = G_1\left(\frac{c-z}{2c}\right)\left(\frac{\pi}{2}\right)\left(R^4 1o - R^4\right) \quad [15]$$

Rearranging equation (15) for $R_1(z)$ the following equation can be obtained

$$R_1(z) = \sqrt[4]{R^4 + \frac{c-z}{2c}\left(R_{1o}^4 - R^4\right)} \quad [16]$$

Now applying symmetric torsional stiffness condition (12) for shafts, the inner radius of shaft 2, $R_2(+z)$ can be obtained as-

$$R_2(+z) = \sqrt[4]{\left(R^4 - \frac{G_1}{G_2}\left(\frac{c+z}{2c}\right)\left(R_{1o}^4 - R^4\right)\right)} \quad [17]$$

The equations (16) and (17) obtained are for the geometry of shaft 1 and shaft 2 as shown in fig.(3) in the bond region and which satisfies both the conditions as mentioned in equations (11) and (12).

The mean radius of adhesive surface (R) can be obtained from equation (12) that the torsional stiffness of shaft 1 at z=-c is equal to torsional stiffness of shaft 2 at z=+c.

$$G_1\left(\frac{\pi}{2}\right)\left(R^4{}_{1o} - R^4\right) = G_2\left(\frac{\pi}{2}\right)\left(R^4 - R_{2i}^4\right) \quad [18]$$

Limits of inner radius (R_{2i}) of shaft 2 will be $0 \le R_{2i} < R$ and which can be written as –

$$R_{2i} = \eta R \text{ where } 0 \le \eta < 1 \quad [19]$$

Inserting value of R_{2i} in terms of R from equation (19) in to equation (18) and after rearrangement the outer radius (R_{1o}) of shaft 1 can be written as-

$$R_{10} = \xi R \quad [20]$$

$$where \quad \xi = \sqrt[4]{\frac{G_1 + G_2 - G_2\eta^4}{G_1}}$$

The maximum torsional shear stress in the shafts due to applied torque occurs at the external radius (R_{1o}) of shaft 1. This maximum shear stress should be less than the allowable shear stress (τ_a) for the material of shaft 1.

$$\tau_{\max} = \frac{T}{\left(\frac{\pi}{2}\right)\left(\frac{R_{1o}^4 - R^4}{R_{10}}\right)} \le \tau_a \quad [21]$$

Inserting value R_{1o} in terms of R from equation (20) in to the equation (21) , the mean radius of adhesive surface can be obtained as –

$$R \ge \sqrt[3]{\left(\frac{2T}{\pi\,\tau_a}\right)\left(\frac{\xi}{\psi}\right)} \quad [22]$$

$$where \quad \psi = \left(\frac{G_2(1-\eta^4)}{G_1}\right)$$

The external radius (R_{1o}) of shaft 1 can be obtained from equations (19) and (20) as –

$$R_{1o} \ge \sqrt[3]{\left(\frac{2T}{\pi\,\tau_a}\right)\left(\frac{\xi^4}{\psi}\right)} \quad [23]$$

From the joint profile obtained the weight of joint is proportional to –

$$\text{Joint Weight} \quad \alpha \quad \xi^2 - \eta^2 \quad [24]$$

The torsional shear stress in adhesive layer can be obtained by inserting equations (2) and (6) into (5)

$$\tau(z) = \frac{T}{4\pi R^2 c} \quad [25]$$

From the above equation it can be seen that the shear stress in adhesive layer is constant and do not vary along the bond length and hence the joint is of uniform strength.

IV. CONCLUSION

i. Varying torsional stiffness profile for shaft 1 and shaft 2 as determined by the equations (16), (17) gives joint of uniform torsional strength and shear stress in adhesive layer remains constant (i.e. independent of z) equal to the average shear stress in adhesive layer.

ii. For cylindrical joint with uniform torsional strength the torque transmission capability increases as compared to the constant diameter shaft profile. The torque transmission capability increases by the ratio of maximum value of shear stress with constant diameter profile to the mean or average value of shear stress.

iii. When shaft 2 is solid (i.e. R_{2i}=0 or η=0) the outer radius of shaft 1 is minimum but the joint weight is maximum. For minimum weight hollow shafts are preferred and hence when shaft 2 is made hollow (i.e. η→1) the outer radius of shaft 1 increases but joint weight decreases.

REFERENCES

[1] N.Pugno and G. Surace. "Tubular bonded joint under torsion: theoretical analysis and optimization for uniform torsional strength". *Journal of Strain Analysis*, 36(1), 2001.

[2] Choon T Chon. "Analysis of tubular joint in torsion". *Journal of Composite Materials*, 16:268, 1982.

[3] D. Chen and S. Cheng. " Torsional Stress in Tubular Lap Joint". *Journal of Solids Structures, 29(7):*845–853, 1992.

[4] Zhenyu Ouyang and Guoqiang Li. "Interfacial debonding of pipe joints under torsion loads:a model for arbitrary nonlinear cohesive laws". *International Journal of Fracture*,(155):19–31, 2009.

[5] Tezcan Sekercioglu, Hikmat Rende, Alper Gulsoz, Cemal Meran "The effects of surface roughness on the strength of adhesively bonded cylindrical components". *Journal of Materials Processing Technology* (142) :82–86, 2003.

[6] Tezcan Sekercioglu. "Shear strength estimation of adhesively bonded cylindrical components under static loading using the genetic algorithm approach". *International Journal of Adhesion and Adhesives*, (25):352–357, 2005.

[7] M.M. Abdel Wahab "Fatigue in Adhesively Bonded Joints: A Review". *International Scholarly Research Network , ISRN Material science, Article ID* 746308, 2012

[8] Kozo Ikegami. "Tensile and torsional strength of metal shaft joint connected adhesively with cylindrical coupling". *22nd DANUBIA-ADRIA Symposium on Experimental Methods in Solid Mechanics*, 2005

[9] Hiroshi Kawamuraa and Toshiyuki Sawab. "Effect of fitted position on stress distribution and strength of a bonded shrink fitted joint subjected to torsion". *International Journal of Adhesion and Adhesives*, (23):131–140, 2003

[10] O. Nemes and F.Lachaud. "Contribution to the study of cylindrical adhesive joining*". International Journal of Adhesion and Adhesives*, 26:474–480, 2006.

[11] Je Hoon Oh. "Nonlinear analysis of adhesively bonded tubular single-lap joints for composites in torsion". *Composites Science and Technology*, 2006

[12] Avinash Parashar, Pierre Mertiny. "Adhesively bonded composite tubular joints: Review". *International Journal of Adhesion & Adhesives* (38): 58–68, 2012.

International Journal of Modern Engineering Research (IJMER)
www.ijmer.com Vol.3, Issue.4, Jul - Aug. 2013 pp-1906-1909 ISSN: 2249-6645

A Novel Multi- Viewpoint based Similarity Measure for Document Clustering

S. Neelima[1], A. Veerabhadra Rao[2]
[1]*M. Tech(CSE), Sri Sai Madhavi Institute of Science & Technology, A.P., India.*
[2]*Asst. Professor, Dept.of CSE, Sri Sai Madhavi Institute of Science & Technology, A.P., India.*

Abstract: *Data mining is a process of analyzing data in order to bring about patterns or trends from the data. Many techniques are part of data mining techniques. Other mining techniques such as text mining and web mining also exists. Clustering is one of the most important data mining or text mining algorithm that is used to group similar objects together. In other words, it is used to organize the given objects into some meaningful sub groups that make further analysis on data easier. Clustered groups make search mechanisms easy and reduce the bulk of operations and the computational cost. Clustering methods are classified into data partitioning, hierarchical clustering, data grouping. The aim of this paper is to develop a new method that is used to cluster text documents that have sparse and high dimensional data objects. Like k-means algorithm, the proposed algorithm work faster and provide consistent, high quality performance in the process of clustering text documents. The proposed similarity measure is based on the multi-viewpoint.*

Keywords: *Clustering, Euclidean distance, HTML, Similarity measure.*

I. INTRODUCTION

Clustering is a process of grouping a set of objects into classes of similar objects and is the most interesting concept of data mining in which it is defined as a collection of data objects that are similar to one another. Purpose of Clustering is to group fundamental structures in data and classify them into a meaningful subgroup for additional analysis. Many clustering algorithms have been published every year and can be proposed for developing several techniques and approaches. The k-means algorithm has been one of the top most data mining algorithms that is presently used. Even though it is a top most algorithm, it has a few basic drawbacks when clusters are of various sizes. Irrespective of the drawbacks is understandability, simplicity, and scalability is the main reasons that made the algorithm popular. K-means is fast and easy to combine with the other methods in larger systems.

A common approach to the clustering problem is to treat it as the optimization process. An optimal partition is found by optimizing the particular function of similarity among data. Basically, there is an implicit assumption that the true intrinsic structure of the data could be correctly described by the similarity formula defined and embedded in the clustering criterion function. An algorithm with an adequate performance and usability in most of application scenarios could be preferable to one with better performance in some cases but limited usage due to high complexity. While offering reasonable results, k-means is fast and easy to combine with the other methods in larger systems. The original k-means has sum-of-squared-error objective function that uses the Euclidean distance. In a very sparse and high-dimensional domain like text documents, spherical k- means, which uses cosine similarity (CS) instead of the Euclidean distance as the measure, is deemed to be more suitable [1], [2]. The nature of similarity measure plays a very important role in the success or failure of the clustering methods. Our objective is to derive a novel method for multi viewpoint similarity between data objects in the sparse and high-dimensional domain, particularly text documents. From the proposed method, we then formulate new clustering criterion functions and introduce their respective clustering algorithms, which are fast and scalable like k-means.

II. RELATED WORK

Document clustering is one of the important text mining techniques. It has been around since the inception of the text mining domain. It is the process of grouping objects into some categories or groups in such a way that there is maximization of intra cluster object similarity and inter-cluster dissimilarity. Here an object does mean the document and term refers to a word in the document. Each document considered for clustering is represented as an ***m*** – dimensional vector "**d**". The "m" represents the total number of terms present in the given document. Document vectors are the result of some sort of the weighting schemes like TF-IDF (Term Frequency –Inverse Document Frequency). Many approaches came into existence for the document clustering. They include the information theoretic co-clustering [3], non – negative matrix factorization, probabilistic model based method [4] and so on. However, these approaches did not use specific measure in finding the document similarity. In this paper we consider methods that specifically use the certain measurement. From the literature it is found that one of the popular measures is the Eucludian distance:

$$\text{Dist}\,(d_i, d_j) = \|d_i - d_j\| \quad \text{---- (1)}$$

K-means is one of the important clustering algorithms in the world. It is in the list of top 10 clustering algorithms. Due to its simplicity and ease of use it is still being used in the data mining domain. Euclidian distance measure is used in k-means algorithm. The main purpose of the k-means algorithm is to minimize the distance, as per the Euclidian measurement, between objects in clusters. The centroid of such clusters is represented as follows:

$$\text{Min} \sum^{k}\sum_{r=1\ d_i \in S_r} \|d_i - C_r\|^2 \quad \text{---------- (2)}$$

In text mining domain, the cosine similarity measure is also widely used measurement for finding document similarity, especially for hi-dimensional and sparse document clustering . The cosine similarity measure is also used in one of the variants of ***k***-means known as the spherical ***k***-means. It is mainly used to maximize the cosine similairity between the cluster's centroid and the documents in the cluster. The difference between k-means that uses the Euclidian distance and the k-means that make use of cosine similarity is that the former focuses on vector magnitudes while the latter focuses on vector directions. Another popular approach is known as the graph partitioning approach. In this approach the document corpus is considered as the graph. Min – max cut algorithm is the one that makes use of this approach and it focuses on minimizing the centroid function:

$$\text{Min} \sum_{r=1}^{k} \frac{D_r^t D}{\|Dr\|^2} \quad \text{----- (3)}$$

CLUTO [1] software package is a method of document clustering based on graph partitioning is implemented. It builds a nearest neighbor graph first and then makes clusters. In this approach for given non-unit vectors of document, the extend Jaccard coefficient is:

$$Sim_{eJacc}\ (u_i,u_j) = \frac{ui\ uj}{||ui||2 + ||uj||2 - uti\ uj} \quad \text{-- (4)}$$

Both direction and magnitude are considered in the Jaccard coefficients when compared with cosine similarity and Euclidean distance. When the documents in the clusters are represented as unit vectors, the approach is very much similar to cosine similarity. All measures such as the cosine, Euclidean, Jaccard, and Pearson correlation are compared . The conclusion made here is that the Eucldean and the Jaccard are best for web document clustering. In [1], the authors research has been made on categorical data. They both selected related attributes for a given subject and calculated distance between two values. Document similarities can also be found using the approaches that are concept and phrase based. In [1], tree similarity measure is used conceptually while proposed phrase-based approach. Both of them used an algorithm known as the Hierarchical Agglomerative Clustering in order to perform the clustering. For XML documents also measures are found to know the structural similarity [5]. However, they are different from the normal text document clustering.

III. PROPOSED WORK

The main work is to develop a novel multi viewpoint based algorithm for document clustering which provides maximum efficiency and performance. It is particularly focused in studying and making the use of cluster overlapping phenomenon to design cluster merging criteria. Proposing a new way to compute the overlap rate in order to improve the time efficiency and ―the veracity is mainly concentrated. Based on the Hierarchical Clustering Method, the usage of the Expectation-Maximization (EM) algorithm in the Gaussian Mixture Model to count the parameters and make the two sub-clusters combined when their overlap is the largest is narrated. In the simplest case, an optimization problem consists of maximizing or minimizing a real function by systematically choosing the input values from within an allowed set and computing the value of the function. The generalization of optimization theory and the techniques to other formulations comprises a large area of applied mathematics.

The cosine similarity can be expressed be expressed as follows:

$$Sim(d_i, d_j) = \cos(d_i - 0, d_j - 0) = (d_i - 0)^t (d_j - 0) \quad \text{---- (5)}$$

where "0" is vector 0 that represents the origin point. According to this formula, the measure takes "0" as one and only reference point.

The similarity between the two documents is defined as follows :

$$\underset{d_i, d_j \in S_r}{sim(d_i, d_j)} = \frac{1}{n - n_r} \sum_{d_h \in S \setminus S_r} sim(d_i - d_h, d_j - d_h) \quad \text{---- (6)}$$

The multi view based similarity in equ. (6) depends on particular formulation of the individual similarities within the sum. If the relative similarity is defined by the dot product of the difference vectors, we have:

$$\mathrm{MVS}(d_i, d_j \mid d_i, d_j \in S_r)$$

$$= \frac{1}{n - n_r} \sum_{d_h} \cos(\ d_i - \ d_h, d_j - d_h) \| d_i - \ d_h \| \ \| d_j - d_h \| \qquad \text{---- (7)}$$

The similarity between the two points di and dj inside cluster Sr, viewed from a point dh outside this cluster, is equal to the product of the cosine of the angle between di and dj looking from dh and the Euclidean distances from dh to these two points.

Now we have to carry out a validity test for the cosine similarity and multi view based similarity as follows. For each type of similarity measure, a similarity matrix called A = {aij}n×n is created. For CS, this is simple, as aij = dti dj . The procedure for building MVS matrix is described in Procedure 1.

procedure BUILDMVSMATRIX(*A*)
Step 1: for r ← 1 : c do
Step 2: DS \Sr ← $\sum_{d_i \notin S_r} d_i$
Step 3: nS \Sr←|S \ Sr|
Step 4: end for
Step 5: for i ← 1 : n do
Step 6: r ← class of di
Step 7: for j ← 1 : n do
Step 8: if dj ∈ Sr then
Step 9: $a_{ij} \leftarrow d_i^t d_j - d_i^t \frac{D_{S\setminus S_r}}{n_{S\setminus S_r}} - d_j^t \frac{D_{S\setminus S_r}}{n_{S\setminus S_r}} + 1$
Step 10: else
Step 11: $a_{ij} \leftarrow d_i^t d_j - d_i^t \frac{D_{S\setminus S_r} - d_j}{n_{S\setminus S_r} - 1} - d_j^t \frac{D_{S\setminus S_r} - d_j}{n_{S\setminus S_r} - 1} + 1$
Step 12: end if
Step 13: end for
Step 14: end for
Step 15: return A = {aij}n×n

Firstly, the outer composite with respect to each class is determined. Then, for each row **a**i of A, i = 1, . . . , n, if the pair of documents di and dj, j = 1, . . . , n are in the same class, aij is calculated as in line 9. Otherwise, dj is assumed to be in di's class, and aij is calculated as in line 11.

After matrix A is formed, the code in Procedure 2 is used to get its validity score:

procedure GETVALIDITY(*validity,A, percentage*)
Step 1: for r ← 1 : c do
Step 2: qr ← floor(percentage × nr)
Step 3: if qr = 0 then
Step 4: qr ← 1
Step 5: end if
Step 6: end for
Step 7: for i ← 1 : n do
Step 8: {aiv[1], . . . , aiv[n] } ←Sort {ai1, . . . , ain}
Step 9: s.t. aiv[1] ≥ aiv[2] ≥ . . . ≥ aiv[n]
{v[1], . . . , v[n]} ← permute {1, . . . , n}
Step 10: r ← class of di
Step 11: $validity(d_i) \leftarrow \frac{|\{d_{v[1]}, \ldots, d_{v[q_r]}\} \cap S_r|}{q_r}$
Step 12: end for
Step 13: $validity \leftarrow \frac{\sum_{i \leftarrow 1}^{n} validity(d_i)}{n}$

Step 14: return validity

For each document di corresponding to row **a**i of A, we select qr documents closest to point di. The value of qr is chosen relatively as the percentage of the size of the class r that contains di, where percentage $\in$ (0, 1]. Then, validity with respect to di is calculated by the fraction of these qr documents having the same class label with di, as in line 11. The final validity is determined by averaging the over all the rows of A, as in line 13. It is clear that the validity score is bounded within 0 and 1. The higher validity score a similarity measure has, the more suitable it should be for the clustering process.

IV. CONCLUSION

Clustering is one of the data mining and text mining techniques used to analyze datasets by dividing it into various meaningful groups. The objects in the given dataset can have certain relationships among them. All the clustering algorithms assume this before they are applied to datasets. The existing algorithms for the text mining make use of a single viewpoint for measuring similarity between objects. Their drawback is that the clusters cannot exhibit the complete set of relationships among objects. To overcome this drawback, we propose a new similarity measure known as the multi-viewpoint based similarity measure to ensure the clusters show all relationships among objects. This approach makes use of different viewpoints from different objects of the multiple clusters and more useful assessment of similarity could be achieved.

REFERENCES

[1] A. Ahmad and L. Dey, "A Method to Compute Distance Between Two Categorical Values of Same Attribute in Unsupervised Learning for Categorical Data Set," Pattern Recognition Letters, vol. 28, no. 1, pp. 110-118, 2007

[2] S. Zhong, "Efficient Online Spherical K-means Clustering," Proc. IEEE Int'l Joint Conf. Neural Networks (IJCNN), pp. 3180-3185, 2005

[3] I. S. Dhillon, S. Mallela, and D. S. Modha, "Information-theoretic co-clustering," in KDD, 2003, pp. 89–98.

[4] A. Banerjee, I. Dhillon, J. Ghosh, and S. Sra, "Clustering on the unit hypersphere using von Mises-Fisher distributions," J. Mach. Learn. Res., vol. 6, pp. 1345–1382, Sep 2005.

[5] S. Flesca, G. Manco, E. Masciari, L. Pontieri, and A. Pugliese, "Fast detection of xml structural similarity," IEEE Trans. On Knowl. And Data Eng., vol. 17, no. 2, pp. 160–175, 2005.

.

International Journal of Modern Engineering Research (IJMER)
www.ijmer.com Vol.3, Issue.4, Jul - Aug. 2013 pp-1910-1915 ISSN: 2249-6645

Neural Network Based Optimal Switching Pattern Generation for Multiple Pulse Width Modulated Inverter

K. Tamilarasi[1], C. Suganthini[2]
[1, 2] *Dept of CSE, Velammal Institute of Technology, Anna University, Chennai, India*

Abstract: *A novel concept of application of neural networks for generation of optimal switching patterns in voltage-controlled inverter is presented. In multiple pulse width modulated inverter (PWM) proper selection notch angles can eliminate the specific harmonics. In this work 8 notches per half cycle is assumed. This gives a choice of seven switching angles in a quarter cycle. It is proposed to eliminate all possible lower order harmonics by proper selection of switching angles for different modulation index. A neural network is trained to generate the switching angles and patterns for different modulation index. Simulation results confirm that neural network based switching pattern generation can eliminate all lower order harmonics up to the order 22nd. The switching patterns for different modulation index, training of neural network and the simulated performance of the inverter are presented.*

Key words: *Feed forward Neural Network, Inverter, Selective Harmonic Elimination Pulse Width modulation***.**

I. INTRODUCTION

An inverter is an electronic circuit that converts DC to AC power by switching the DC input voltage (or current) in a pre-determined sequence to generate AC voltage (or current) output. The topology used here consists of three phase bridge inverter. The conversion from DC to AC using the power electronic device introduces harmonics in the output voltage. In conventional methods, large sized filters are used to filter the lower order harmonics (5^{th}, 7^{th} etc). These lower order harmonics cause serious voltage distortion. In the proposed method, selective harmonic elimination technique is used to eliminate the lower order harmonics.

The Optimal Switching Pattern (OSP) Pulse Width Modulation (PWM) strategies constitute the best choice for high power, three-phase voltage controlled inverter with low allowable level of switching frequency. The proposed project is presented in the following phases namely,

1. Elimination of lower order harmonics 2.Training of neural network 3.Gate pulse generation of inverter circuit.

Selective harmonic elimination pulse width modulation (SHE-PWM) techniques offer a tight control of the harmonic spectrum of a given voltage waveform generated by a power electronic converter along with a low number of switching transitions. These optimal switching transitions can be calculated through Fourier series theory, and quarter-wave and half-wave symmetries have been assumed when formulating the problem. In the selective harmonics elimination PWM, the undesirable lower order harmonics can be eliminated. And the fundamental voltage can be controlled by SHEPWM technique for the required value of modulation index, the necessary switching angles are calculated. This switching angles are used for generation of gating pulses for the inverter switches.

Neural network (NN) has been employed in many applications in recent years. An NN is an interconnection of a number of artificial neurons that simulates a biological brain system. NN have been successfully introduced into power electronics circuits to generate the optimal switching angles of a PWM inverter for a given modulation index.

The PWM generator generates the switching signals to the full-bridge inverter. For linear load, the output voltage is pure Sinusoidal. The schematic block diagram representation as shown in figure1.

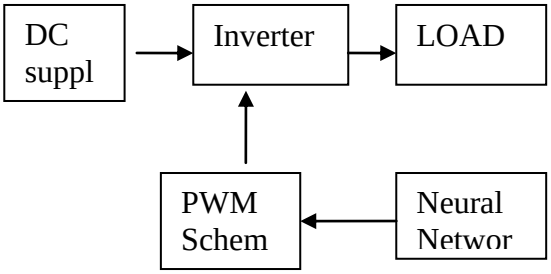

Fig.1 Basic Block diagrams.

II. HARMONICS ELIMINATION STRATEGY

By placing notch in the output waveform at proper locations, certain harmonics can be eliminated. This allows lower switching frequencies to be used. Normally, a look-up table is prepared in microcomputer memory and the angles, as functions of modulation index value, are retrieved for digital implementation. After training, as the commanded modulation index m* is impressed at the input, all the correct 'α' angles are retrieved at the output. The advantages of an ANN in this case, are avoiding the need of a large precision look-up table memory.

Harmonics elimination technique for single phase and three phases are presented below:

For Single-phase Inverter, with 7 values of α, the 3^{th}, 5^{th}, 7th, 9th, 11th and 13^{th} harmonics can be eliminated. Using MathCAD program, these transcendental equations can be solved numerically for the notch angles α_1, α_2, α_3, α_4, α_5, α_6 and

α_7 and for specified fundamental amplitude. For example, at m=0.9 the values are α1=7, α2= 17.263, α3=21.195, α4=34.879, α5=35.879, α6=50.908, α7=51.288.

For the three-phase inverter with 7 values of α, the 5^{th},7^{th},11^{th},13^{th},17^{th} and 19^{th} harmonics and the 3rd order harmonics can be eliminated. Thus n=7 and the equations can be written as:

To reduce harmonics, we have to solve the following equations

$$\cos\alpha1-\cos\alpha2+\cos\alpha3-\cos\alpha4+\cos\alpha5-\cos\alpha6+\cos\alpha7 = m+0.5$$
$$\cos5\alpha1-\cos5\alpha2+\cos5\alpha3-\cos5\alpha4+\cos5\alpha5-\cos5\alpha6+\cos5\alpha7 = 0.5$$
$$\cos7\alpha1-\cos7\alpha2+\cos7\alpha3-\cos7\alpha4+\cos7\alpha5-\cos7\alpha6+\cos7\alpha7 = 0.5$$
$$\cos11\alpha1-\cos11\alpha2+\cos11\alpha3-\cos11\alpha4+\cos11\alpha5-\cos11\alpha6+\cos11\alpha7 = 0.5$$
$$\cos13\alpha1-\cos13\alpha2+\cos13\alpha3-\cos13\alpha4+\cos13\alpha5-\cos13\alpha6+\cos13\alpha7 = 0.5$$
$$\cos17\alpha1-\cos17\alpha2+\cos17\alpha3-\cos17\alpha4+\cos17\alpha5-\cos17\alpha6+\cos17\alpha7 = 0.5$$
$$\cos19\alpha1-\cos19\alpha2+\cos19\alpha3-\cos19\alpha4+\cos19\alpha5-\cos19\alpha6+\cos19\alpha7 = 0.5$$
$$\alpha1 < \alpha2 < \alpha3 < \alpha4 < \alpha5 < \alpha6 < \alpha7 < 90$$

M varies from 0.01 to 0.99

Using MathCAD program, these transcendental equations can be solved numerically for the notch angles α_1, α_2, α_3,α_4 , α_5 , α_6 and α_7 for specified fundamental amplitude. For example, At m=0.9 the alpha values are a1=6.313, α2=16.41, α3=19.921, α4=31.586, α5=33.347,α6=71.833, α7=72.335.

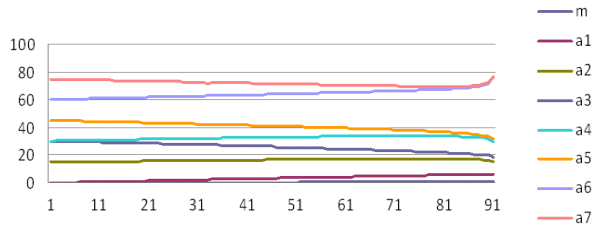

For obtaining the above values of a1 to a7, an analytical Approach of MathCAD software is employed.Various objective functions can be used in the optimal control of an inverter. In the method, notches are created on the square wave at predetermined angles, as shown in fig.2, positive half – cycle output is show with quarter-wave symmetry. It can be shown that the seven notch angles α1, α*2*, α*3*, α*4*, α*5*, α*6*, *and* α*7* can be controlled to eliminate significant harmonic components. The full-cycle switching pattern must possess the half-wave and quarter-wave symmetry in order to eliminate even harmonics; hence, the resultant optimal switching pattern yields a fundamental voltage that corresponds to a given value of the modulation index, where as (n – 1) low-order, odd harmonics are absent in the output voltage.

At even significant deviations from the optimal switching pattern, barely affect the magnitude of the output voltage. This is an advantageous feature, because as seen in Fig. 1 α1, α*2*, α*3*, α*4*, α*5* and α*6*, as well as α*7*, tend to converge at M > 0.95. Therefore, the neural network converter should be made to accurately reproduce the optimal switching angles only within the 0 to 0.95 range of the modulation index.

III. OPTIMAL SWITCHING ANGLES GENERATION USING NEURAL NETWORK.

An Artificial Neural Network (ANN) is an information-processing paradigm that is inspired by the way biological nervous system, such as brain, process information. The key element of this paradigm is the novel structure of the information processing system. It is composed of large number of highly interconnected processing elements (neurons) working in unison to solve problems.

Neural network deals with Mathematical information about processing of a system with input and output. A neural network used for generation of optimal switching angles has a single input for the reference value of the modulation index and N outputs that provide the values of the switching angles. The neurons are trained using the Neural Network toolbox of MATLAB.

3.1 Feed-forward Neural Network:

Individual processing units are organized in three types of layer namely input, hidden and output layer. All neurons within the same layer operate simultaneously.

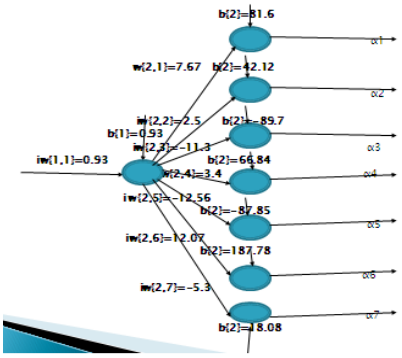

Fig.3 Train neural network representation diagram.

3.1 TRAINING OF FEED-FORWARD NEURAL NETWORK:

- Input encoding
- Output encoding
- Number of hidden units
- Learning rate
- Momentum

Feed-Forward back propagation algorithm is used to train the neural network and input data are given for modulation index m from 0.01 to 0.95, and the training function TRAINLM is employed.

Hidden layer activation function (tangent sigmoid transfer function) TANSIG (N)

Output layer activation function (tangent sigmoid transfer function) TANSIG (N)

Offline training is adopted to ensure the inverter will have fast transient response and low cost. In order to obtain good example patterns for NN off-line training, we need a simulation model that can perform well in the inverter.

The following codes show the neural network equations used for generation of firing pulse to the inverter circuit.

v01=u*1.007-0.45;
α1=v01*7.05+3.3;
α2=v01*2.3+16.5;
α3=v01*(-10.4) +25.8;
α4=v01*3.13+32.1;
α5=v01*(-11.6) +40.5;
α6=v01*11.11+64.3;
α7=v01*(-4.9) +72.2;

As shown, this information is sufficient for generation of the full-cycle switching pattern for all the three phases of the inverter.

IV. NEURAL NETWORK PULSE WIDTH MODULATOR

Since the DC bus voltage is always constant, the inverter has to be controlled to vary the magnitude and frequency of AC output voltage .This is normally accomplished by PWM technique.

The general principle of SHEPWM is the comparison of two voltage waveforms:(1) a variable voltage of the same frequency as the inverter, which is called as the reference voltage ,and a high frequency voltage, which has a triangular waveform, which is called as the carrier voltage. The triangular carrier waveform has fixed amplitude. The amplitude of the reference constant value is adjustable.

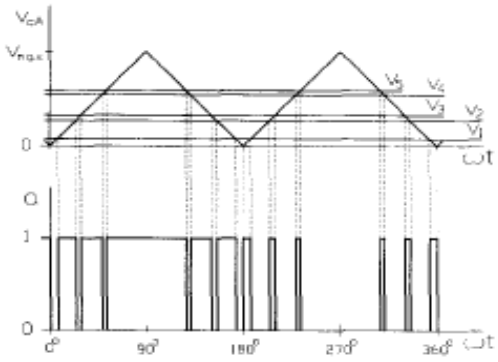

Fig.4 Pictorial representation of selective harmonics elimination technique.

The inverter output frequency is the same as the reference square wave; the inverter output frequency is adjustable by adjustment of the reference wave frequency. In an SHEPWM wave form the total harmonic content is still very significant. The order of harmonics in the SHEPWM waveform depends on the number of pulses per half cycle employed. SPWM offers greater functionality in terms of the minimization of the total harmonic distortion, reductions in size and price, and in additional inverter functional capabilities such as active filtering and reactive power support.

V. DESIGN SPECIFICATIONS

The Inverter based PWM technique is designed based upon the following steps are needed before the experimental setup. (1) To perform the simulation and the gating signal are generated and given to an inverter circuit. (2).Select a Neural Network structure that is simple and yet sufficient to model the simulated and based on the pattern database. (3) Train the Neural Network using MATLAB with Neural Network Toolbox. (4) The gating pulse generated by using the coding written in the c language and in- turn embedded in the microcontroller.

TABLE 1

SINGLE PHASE INVERTER PARAMETERS

PARAMETER	VALUE	UNIT
Switching frequency, f_s	750	Hz
DC source voltage, V_{dc}	100	V
Rated Output Voltage	83	V_{rms}
Rated Output Frequency	50	Hz
Resistive load	10	Ω

TABLE 2

THREE PHASE INVERTER PARAMETERS

PARAMETER	VALUE	UNIT
Switching frequency, f_s	750	Hz
DC source voltage, V_{dc}	220	V
Rated Output Voltage	173	V_{rms}
Rated Output Frequency	50	Hz
Resistive load	10	Ω

VI. SIMULATION RESULTS

Fig 4.Shows the PWM signal to generate the gating signals to the inverter switches and its resulting waveform. The simulation results are obtained using MATLAB - Simulink package. Fig 4 is the subsystem in which the input marked is the carrier triangular wave, which is compare to the reference constant value to generate gate pulses. P1 is use to trigger the switches in the positive half cycle and P2 is used to trigger the inverter switches in the negative half cycle Fig5.2. Show is the output voltage waveform obtained for the linear loads. Here resistive load of 10Ω is used. The result shows that for linear load the output voltage waveform is found to be square wave.

Total harmonic Distortion (THD) is define as

$$THD = \frac{\sqrt{V_3{}^2 + V_5{}^2 + V_7^2 + \ldots\ldots V_{21}^2}}{V_1}$$

Where, terms 2...N is the power levels of the harmonics and term 1 is the power level of the fundamental (the pure tone).

The MATLAB function block includes the programs for triangular wave generation. The results so obtained are shown fig 6.5. The program was written in MATLAB M-file. Fig 6.1 & Fig 6.5. shows the complete simulation of single phase and three-phase inverter using Neural Network.

The simulated results are shown in Fig 5 for single-phase inverter and in Fig 6.for three-phase inverter. For single phase inverter the lower order harmonics are removed by adjusting the switching angles (i.e.) 3^{rd},5^{th},7^{th},9^{th},11^{th} and 13^{th} order harmonics are completely eliminated.

TABLE 3

COMPARISON OF THD for SINGLE PHASE INVERTER

Order of harmonics	3^{rd}	5^{th}	7^{th}	9^{th}	11^{th}	13^{th}
Sine PWM THD	8.14	6.92	6.56	6.15	5.91	5.21
Proposed THD	6.55	6.12	5.81	5.63	5.21	4.97

COMPARISON OF THD for THREE PHASE INVERTER

Order of harmonics	3^{rd}	5^{th}	7^{th}	9^{th}	11^{th}	13^{th}
Sine PWM THD	14.32	13.7	13.2	12.91	12.5	11.5
Proposed THD	7.14	6.91	6.52	6.3	6.51	5.22

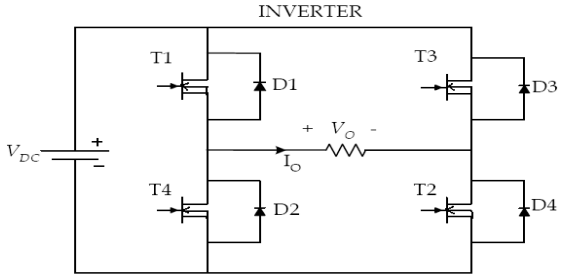

Fig6.1 for single-phase inverter

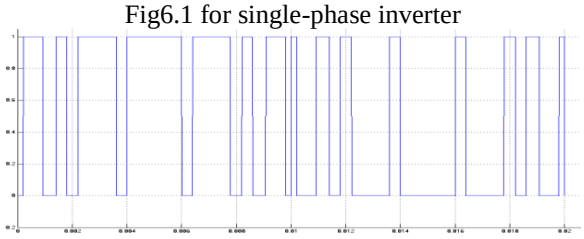

Fig.6.2 for single-phase inverter gating pulse

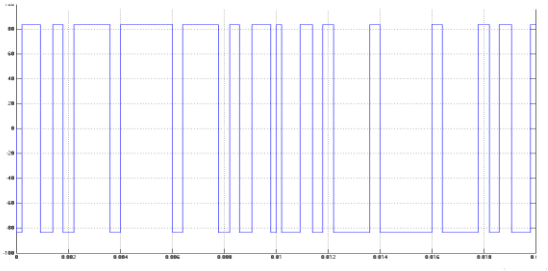

Fig.6.3 for single-phase inverter output voltage waveform result.

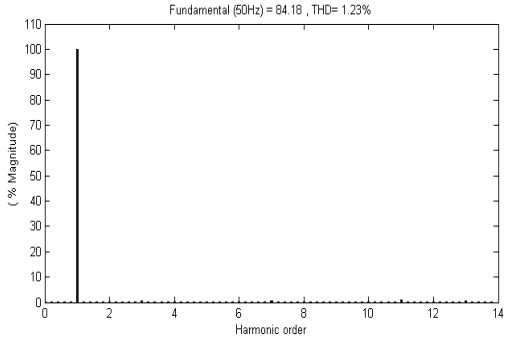

Fig.6.4 simulated harmonic spectrum for single-phase inverter.

And for three phase inverter the lower order harmonics are removed by adjusting the switching angles (i.e.) 5^{rd},7^{th},11^{th},13^{th},17^{th} and 19^{th} order harmonics are completely Eliminated.

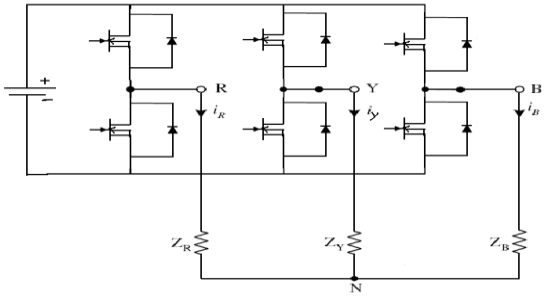

Fig.6.5 three-phase inverter

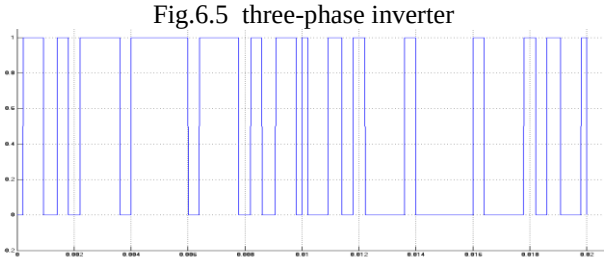

Fig.6.6 for three-phase inverter gating pulse

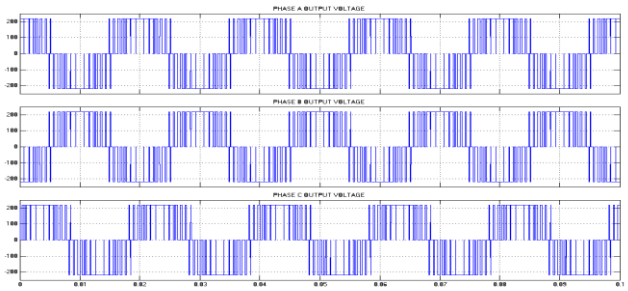

Fig.6.7 for three phase inverter output voltage waveform result.

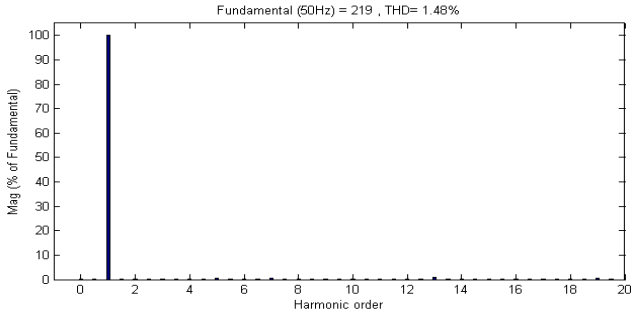

Fig.6.8 simulated harmonic spectrum for three-phase inverter.

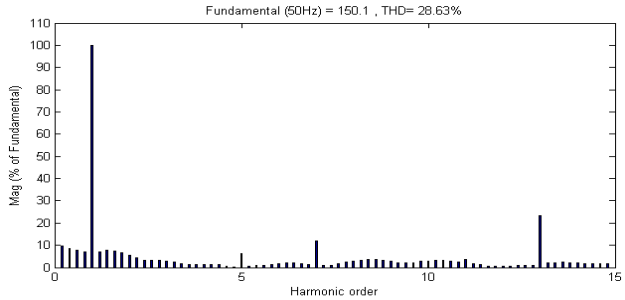

Fig.6.9 simulated harmonic spectrum for three-phase inverter by sinusoidal pulse width modulation.

VII. CONCLUSION

The optimal switching pattern-pulse width modulation strategy constitutes the best choice for high power voltage controlled inverters with low allowable level of switching frequency. The neural network used for elimination of lower order harmonics can be used as optimal technique for non-linear loads. The proposed multiple PWM technique improves the fundamental voltage. In future power factor correction can also been implemented.

REFERENCES

[1]. José R. Espinoza, Géza Joós, Johan I. Guzmán, Luis A. Moran, and Rolando P. Burgos" Selective Harmonic Elimination and Current/Voltage control in Current/Voltage- Source Topologies: A Unified Approach" IEEE transactions On industrial electronics, vol. 48, no. 1, February 2001.

[2]. Li Li, Dariusz Czarkowski, Yaguang Liu, and Pragasen Pillay, *Senior Member, IEEE "*Multilevel Selective Harmonic Elimination PWM Technique in Series-Connected Voltage Inverter", IEEE transactions on industry Applications, vol. 36, no. 1, January/February 2000.

[3]. Vassilios G. Agelidis, Anastasios Balouktsis, Ioannis Balouktsis, and Calum Cossar, *"*Multiple Sets of Solutions for Harmonic Elimination PWM Bipolar Waveforms: Analysis and Experimental Verification", IEEE transactions on power electronics, vol. 21, no. 2, march 2006.

[4] O.Bouhali,M.Berkouk,B.Francois,Saudemont,S.Labiod, "Solving Harmonics Elimination Problem in Three-Phase Voltage controlled Inverter Using Artificial Neural Networks". J. Electrical Systems 1-1 (2005): 39-51

[5]. S. sirisukprasert, J. S. Lai and T. H. Liu, "Optimum Harmonic Reduction with a Wide Range of Modulation indexes for Multilevel Converters", *IEEE Transactions on Industrial Electronics*,Vol.49,No.4,Aug2002, pp.875-881.

[6]. K.W.E.Cheng, H.Y.Wang and D.Sutanto, "Adaptive directive neural network control for three phase AC/DC PWM converter" *IEE Proc-Electr. Power Appl. Vol. 148, No. 5, September 2001.*

[7]. John N.Chiasson, Leon M. olbert, Keith J.McKenzie, and Zhong Du, "A Unified Approach to Solving the Harmonic Elimination Equations in Multilevel Converters", *IEEE* Transactions on power electronics,vol.19,no.2,march- 2004

International Journal of Modern Engineering Research (IJMER)
www.ijmer.com Vol.3, Issue.4, Jul - Aug. 2013 pp-1916-1918 ISSN: 2249-6645

Implementation of Monitoring System for Cloud Computing

Soon-kak Kwon[1], Jeong-hyun Noh[2]
[12]*Department of Computer Software Engineering, Dongeui University, Korea*

Abstract: *As the benefits of cloud computing have increased, its utilization has been higher, but it has caused overload problems for virtual server. This paper implements the monitoring dashboard of cloud computing in order to prevent the failure of virtual servers and desktops in the cloud computing environment.*

Keywords: *Cloud computing, Dashboard, Monitoring*

I. INTRODUCTION

Recently as the benefits of cloud computing has been magnified, the utilization of cloud computing is increasing. However, the increased utilization makes virtual servers and desktops increase, then the unexpected problems are caused by failure.

Examples of failure are with a virtual server hypervisor[1,2] and a virtual desktop. The performance of virtual servers and desktops eventually is affected by the server's physical resource. If CPU, memory, and storage are under an overload, then the virtual desktops running on the server is running will not be able to perform their normal function. Therefore the number of working desktops is higher, the loss of expenses is larger.

In order to prevent the problems, the monitoring system is required to check the virtual server's physical resource in the real time and notice the status to administrator .

In this paper, we show the real-time resource utilization of XenServer[3], and implement the monitoring dashboard that can respond instantly in the event of a failure of the server and virtual machine (VM).

II. DESIGN OF MONITORING SYSTEM

The proposed monitoring system for cloud computing is shown in Fig. 1. Xensever Broker performs the ability to get information about CPU, RAM, Storage of XenServer and then transfer to the Cloud Manager.

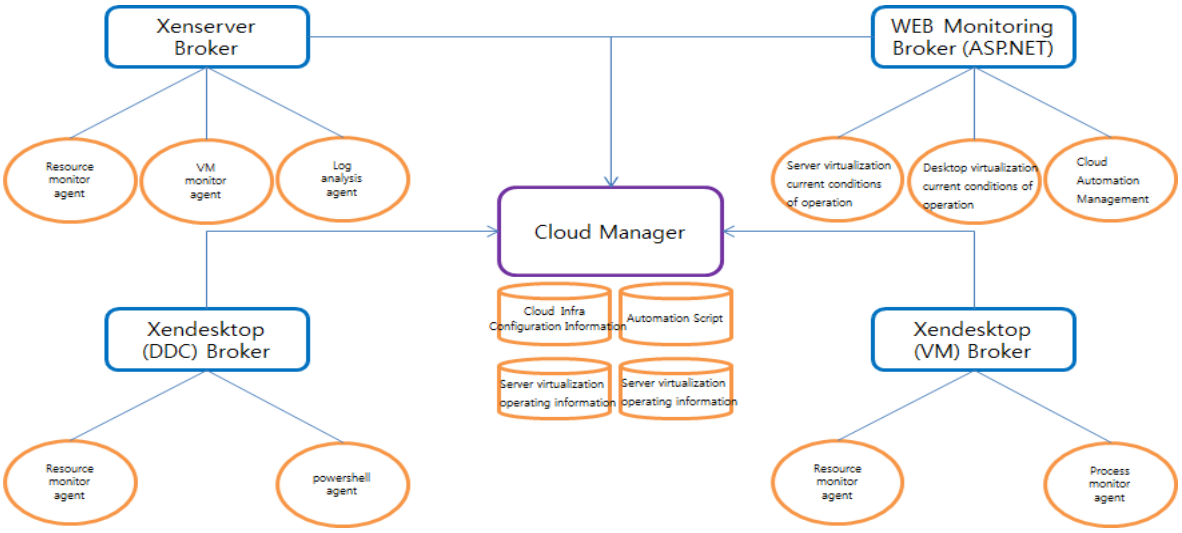

Fig. 1. System Architecture

Xendesktop DDC(Desktop Delivery Controller) Broker performs the Powershell Script through DDC's VM management tool and transfer the information of VM obtained by DDC to Cloud Manager. WEB Monitoring Broker gets the information of CPU, RAM, storage of Xensever and Xendesktop, then outputs the information to user in order to see. Xendesktop VM Broker performs the function to obtain the information about CPU, RAM, storage of Xendesktop VM, and then transfer to the Cloud Manager. Cloud Manager saves in memory the information from Xenserver Broker, Xendesktop DDC Broker, Xendesktop VM Broker, and transfer the data of memory to WEB Monitoring Broker.

III. IMPLEMENTATION OF MONITORING SYSTEM

We implement the monitoring system for cloud computing. Implemented system is classified four parts; Xenserver agent, Xendesktop agent, Cloud Manager, and Web monitoring page.

Xenserver agent is developed to be collected the server's real-time information such as CPU, memory, storage.

- Design of Linux-based agent compatible with Xenserver
- Gathering UUID (Universally Unique Identifiers) information required to identify the server
- Gathering information of Xenserver Version

- Check of connection status with Cloud Manager if agent is executed
- Transmission to Cloud Manager the total amount of resources of CPU, MEMORY, DISK, actual usage, remaining usage
- Performance testing and feedback through Q, A

Xendesktop agent is developed to be collected PC name, state, OS type, CPU, memory, storage of VM.

- Similar with Xenserver agent, but transmission detailed information of VM to Cloud Manager as VM customized agent
- Check of connection status with Cloud Manager if agent is executed
- Performance testing and feedback through Q, A

Cloud Manager is developed.

- Save in memory the information sent by agents, response when the Web Monitoring Page requests the information
- Calculation the value of the normal / fault depending on the connection state of the VM agent and Server agent
- Performance testing and feedback through Q, A

Web Monitoring page is finally developed.

- User authentication through Login page.
- Graph representation by using MS chart of numerical value for Xenserver and VM's resource usage
- Display of warning when the utilization of CPU, memory, storage is reached to the defined values of utilization. Fig. 2 shows that a warning is displayed when the memory utilization of the server DongEuiXen01exceeds 90%.
- Graph representation of VD's PC name, OS version, corresponding resource utilization, information of the IP as shown in Fig. 3 when a certain VD is clicked from the VD list.
- Turning active VD list as shown in Fig. 4 when each server box is clicked from the main screen
- Display of normal / fault of Xenserver & VM state as shown in Fig. 4, by determining the status of each VD from Cloud Manager

Fig. 2. Web Monitoring Main

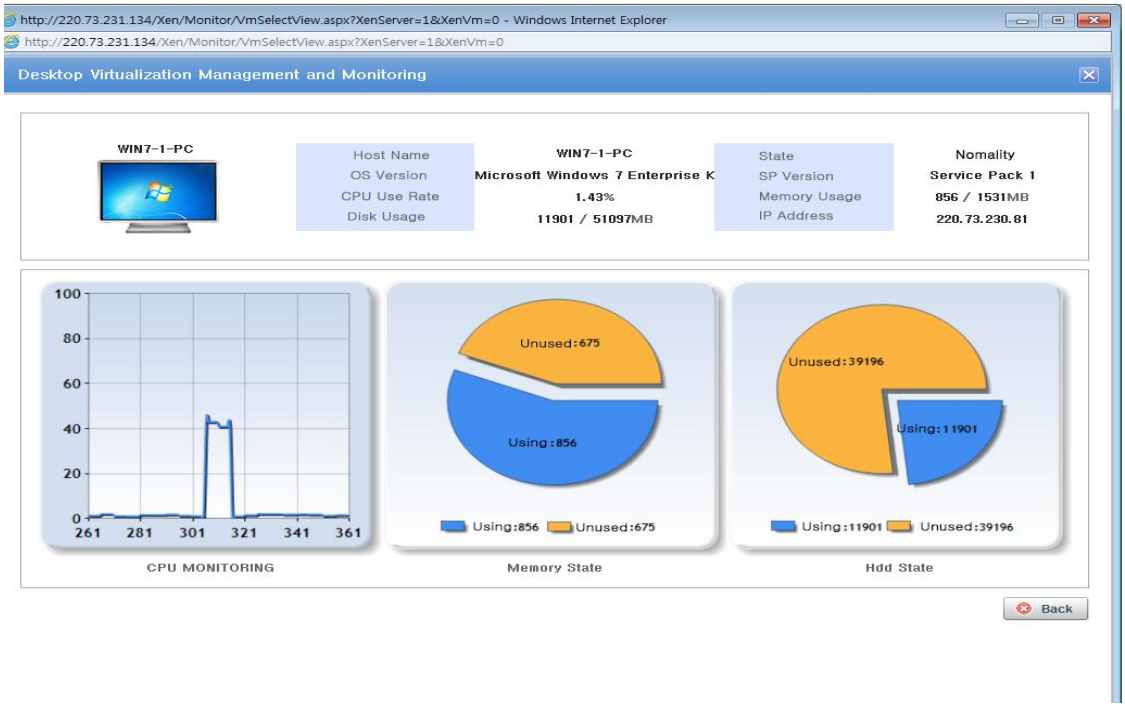

Fig. 3. VD Monitoring page

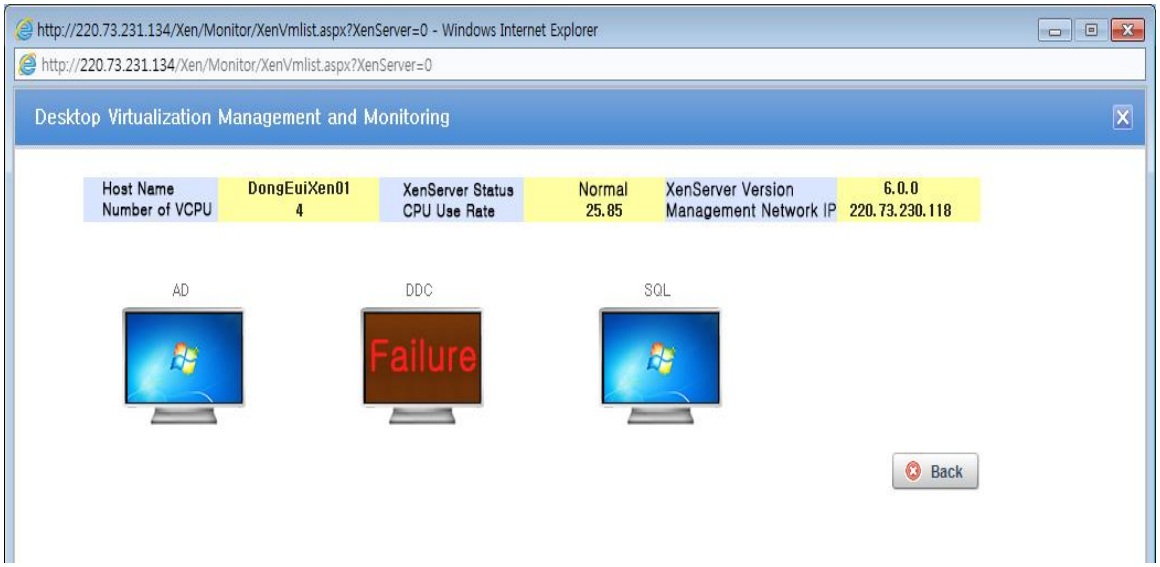

Fig. 4. Hypervisor's VD list

IV. CONCLUSION

In this paper, in order to solve the problem of a failure for clouding computing, the current states of resources are checked on the real-time detection, then the information are monitored when a failure occurs. Using the data processing of the non-cumulative resource usage, the data are immediately processed quickly on memory.

ACKNOWLEDGEMENTS

The authors would like to thank Namu Tech Co., Ltd for developing this system. Corresponding author: Soon-kak Kwon (skkwon@deu.ac.kr).

REFERENCES

[1] J. Szefer, R. B. Lee, "Architectural Support for Hypervisor-Secure Virtualization," in Proceedings of the International Conference on Architectural Support for Programming Languages and Operating Systems (ASPLOS), March 2012.
[2] A. Vasudevan, J. M. McCune, N. Qu, L. v. Doorn, A. Perrig, "Requirements for an Iintegrity-Protected Hypervisor on the x86 Hardware Virtualized Architecture," In Proc. of the 3rd international conference on Trust and Trustworthy Computing, June 2010.
[3] R. Sailer, T. Jaeger, E. Valdez, R. Caceres, R. Perez, S. Berger, J. L. Griffin, and L. v. Doorn, "Building a MAC-Based Security Architecture for the Xen Open-Source Hypervisor," In Proc. of ACSAC '05, 2005.

International Journal of Modern Engineering Research (IJMER)
www.ijmer.com Vol. 3, Issue. 4, Jul - Aug. 2013 pp-1919-1922 ISSN: 2249-6645

Face expression recognition using Scaled-conjugate gradient Back-Propagation algorithm

Harish Kumar Dogra[1], Zohaib Hasan[2], Ashish Kumar Dogra[3]
[1,2](Department of ECE, G.G.I.T.S, Jabalpur, India)
[3] (Department of ECE, Lovely Professional University, India

ABSTRACT: *Since decades, face recognition has become an active area of research in computer vision and psychology. The rapid developments of face recognition are being fueled by numerous advances in computer vision. An ongoing challenge in this field is to design an effective human-computer interaction (HCII). In this paper we will study the latest work done that has been done in the field of facial expression recognition and analysis. In our work we have recognized six different expressions using Cohn-kanade database and system is trained using scaled conjugate gradient back-propagation algorithm. In proposed methodology we have used MATLAB's computer vision toolbox for face detection & cropping the images and neural network toolbox. In our work we have achieved 100% training accuracy and 87.2% overall testing accuracy of six different expressions.*

Keywords: *FACS (Face action coding system), neural network, Action units (AU), SVM (Support vector machines).*

I. INTRODUCTION

Human-computer interaction such as voice, gesture, and force-feedback are emerging. Despite important advances, one necessary ingredient for natural interaction is still missing that is emotions. Emotions play an important role in human-to-human communication and interaction, allowing people to express themselves beyond the verbal domain. The ability to understand human emotions is desirable for the computer in several applications. The facial expressions are one of the most powerful channels of non-verbal Communication. Facial expression provides information about emotional response, regulates interpersonal behavior, and communicates aspects of psychopathology. Facial expressions can reveal what people are thinking and feeling, it is only recently that the face has been studied scientifically and has the great potential for human-computer interaction.

Several approaches have been used for automatic facial emotions recognition from static images or video sequences. In all these approaches, the first step is to detect the face and once the face is detected the next step is to extract the features from the detected face that are relevant to display of emotions and classified into a predefined set of facial actions or furthermore to emotion related expressions. Most of the facial emotion or expression analyzers recognize expressions corresponding to the basic emotions, i.e happiness, anger, fear, surprise, disgust and sadness. Fig. 1 explains basic steps that are used for facial expression analysis system.

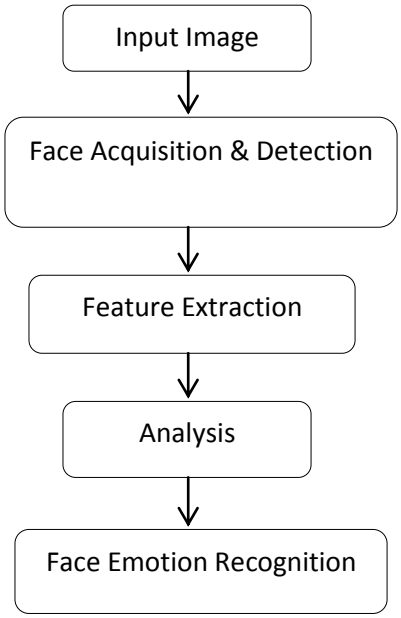

Fig 1:- Basic Face expression analysis system

First step is the input image with different expressions play an important role in the facial expression analysis. Properties of the image like its resolution, sizes etc are important and usually, the facial image in the frontal or near frontal view is used to recognize facial expression. Once we have the image the next step is to cut and crop the image and detect face using the face detector. Now after second step we got the balanced image whose feature should be fed to the system.

The facial features are mainly of two types: geometric and appearances features [3]. Geometric features measures the variation in shape, location, distance of facial components in different expressions. The appearance features can be extracted on either whole face or specific regions in a facial image. The last and most critical step is the expression classification. The classification systems classify the emotions into different categories according to the mood.

In the next section we will study about the related work that has been done in the field of face expression recognition and analysis.

II. LITERATURE REVIEW

Research on human perception and cognition has been conducted for many years, but it is still unclear how humans recognize facial expressions. Which types of parameters are used by humans, and how are they processed? By comparing human and automatic facial expression recognition we may be able advance our understanding of each and discover new ways of improving automatic facial expression recognition. Although it is often assumed that more fine-grained recognition is preferable, the answer depends on both the quality of the face images and the type of application. Ideally, an automatic face expression system should recognize all action units and their combinations. In high quality images, this goal seems achievable; emotion-specified expressions then can be identified based on emotion prototypes identified in the psychology literature. For each emotion, prototypic action units have been identified. In lower quality image data, only a subset of action units and emotion specified expression may be recognized. Recognition of emotion-specified expressions directly may be needed. We seek systems that become 'self-aware' about the degree of recognition that is possible based on the information of given images and adjust processing and outputs accordingly. Recognition from coarse-to-fine, for example from emotion-specified expressions to subtle action units, depends on image quality and the type of application.

Two main streams in the current research on automatic analysis of facial expressions consider facial effect (emotion) interference from facial expressions and facial muscle action detection [1]. In this section, we also evaluate the various frameworks for emotion detection. The objective is to assess the relevance of different framework to deal with a different kind of data.

2.1 Facial Action Coding System (FACS)

The Facial Action Coding System (FACS) is a comprehensive, anatomically based system for measuring nearly all visually discernible facial movements [4]. FACS describes facial activity on the basis of action units (AU), as well as several categories of head and eye positions and movements. Action Units (AU) are the fundamental actions of individual muscles or groups of muscles. FACS is recognized as the most comprehensive and objective means for measuring facial movement currently available, and it has become the standard for facial measurement in behavioral research in psychology and related fields. Since FACS deals with the movement, not with other visible facial signs, it limits a full understanding of the psychology of facial behavior. Thus the person performing the classification has to be trained to interpret the expression from the action units obtained.

2.2 Neural network based analysis

Neural network learning methods provide a robust approach to approximating real-valued, discrete-valued, and vector-valued target functions. For certain types of problems such as learning to interpret complex real-world sensor data, artificial neural networks are among the most effective learning methods currently known. For example, the BACKPROPAGATION has proven surprisingly successful in many practical problems such as learning to recognize handwritten characters (Lecunn et al. 1989), learning to recognize spoken words (Lang et al 1990) and learning to recognize faces (Cottrell 1990).

Padgent [5], Hara and Kobayashi [6, 7], Zhang [8] and Zhao [7] used neural network approach for expression classification. They classified images into six or seven emotional categories. Padgett et al., [5] trained neural networks from the data of 11 subjects and tested with the data from one subject. The training and testing dataset was interchanged and new networks were trained and tested. A classification accuracy of 86% was achieved in this study. Hara and Kobayashi [6, 7] also used neural networks approach. The training dataset consisted of from data of 15 subjects (90 images) and these networks were tested using data from another 15 subjects. The classification accuracy achieved was 85 %. Zhang et al., [8] used the JAFFE data base which consists of 10 Japanese female subjects. Although an accuracy of 90.1% was achieved; same data was used for training and testing.

2.3 EMG based methods

Facial EMG measures the electrical activity of the facial muscles [9]. Facial expression analysis using EMG based techniques requires invasive insertion of electrodes into the facial muscle fiber for accurate result. The major disadvantage of using EMG based methods is that it may alter the normal behavior of the subjects due to attachment of electrodes and confuse the subject.

Various teams have worked on the face expression recognition and analysis systems using FACS AU.

The results analysis work is done in two categories:

A) Person Independent:- Person independent category means in such systems, during training few images are not shown to the system and we will use those images to check how many images the system identify based on the mood correctly.

B) Person Specific: - Person specific category means the faces that we have trained or shown to the system and testing is done on the same faces.

Teams	Emotion Detection		Overall
	Person Independent	Person Specific	
ANU [16]	0.649	0.838	0.734
KIT [1]	0.658	0.944	0.773
MIT-Cambridge [1]	0.448	0.433	0.44
Montreal [1]	0.579	0.870	0.700
NUS [21]	0.636	0.730	0.672
Riverside [2]	0.752	0.962	0.838

Table 2:- Emotion recognition using SVM and their accuracies by different teams.

III. EXPERIMENTATION

In this section we will explain the implementation of our proposed work. Our proposed work is divided into four main steps explained below:

Step 1:-Collection of different face expression images

First step is to collect different images of different facial expressions. So for that we have used cohn-kanade database. It consists of six basic emotions that we need to classify.

Step 2:- Creation of dataset

Step 3:- Selection of neural network

Once the dataset is created the next step is to select the neural network. It means we need to decide about input layer, hidden layer and output layer. For our work, we have used 50*50 images it means our input layer consist of 2500 features. We have used 200 hidden layer and since we want to classify six different emotions hence our output layer consist of 6 classes.

Fig: Neural network used

Step 4:- Training the system using Scale conjugate gradient back propagation algorithm.

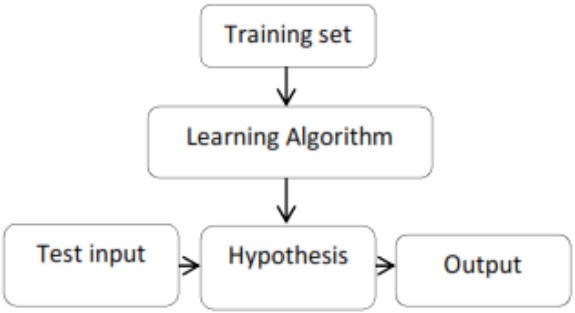

Once the network architecture is decided the next step is to train this network. For that we have used scale conjugate gradient back-propagation as learning algorithm

Step 5: Testing the system using unseen images.

Once the system is trained, Test input i.e. unseen images that are not shown to the system is provided to the system and according to hypothesis the image is classified accordingly.

IV. RESULTS

In this section, we will evaluate the proposed method. We have implemented our face recognition system using MATLAB. We have used Cohn-Kanade database for emotion recognition which contains six different emotions. Classification rates [1] by the baseline method for the emotion detection sub-challenge are shown in Table V. After simulating, we have got good training and testing accuracies as shown in table 3.

Training accuracy	100%
Testing Accuracy	87.2%

Table 3: - Overall Training and testing accuracy

We have also measure performance of our system by estimating mean square error and % Error.

Mean squared error is the average squared difference between outputs and targets. Lower values are better. Zero means no error.

Percent Error indicates the fraction of samples which are misclassified. A value of 0 means no misclassification, 100 indicates maximum misclassification.

	Mean square error	Error(%)
Training	1.16455e-5	0
Testing	4.04047e-2	12.76595e-0

Table 4:- Mean square error and Error (%)

In addition, we have provided confusion matrices for the for emotion recognition of the overall test dataset. Rows are predicted results, columns the ground truth.

	Angry	Disgust	Fear	Happy	Sad	Surprise
Angry	**3**	0	0	0	0	0
Disgust	0	**5**	1	0	0	0
Fear	0	0	**7**	0	1	0
Happy	0	2	0	**12**	0	0
Sad	2	2	1	0	**5**	0
Surprise	0	0	0	0	0	**9**

Table 5:- Confusion Matrix for emotion recognition of the overall test dataset.

V. CONCLUSION

This paper describes the different techniques that are employed in face expression recognition and analysis. With respect to machine learning techniques, we noticed a strong trend to use SVMs. Most of the teams result that we have already shown in Table 2 used SVM, such techniques have proven very popular in recent literature. But in our work we have used scale conjugate gradient back propagation algorithm and we are getting overall testing accuracy up to 87.2% which is better than the as compared to the work done using SVM explained in table 2.

In our future work, we can improve our recognition rate by using LBP histogram, equalization techniques & PCA techniques before training the system.

REFERENCES

[1] Michel F. Valstar , Marc Mehu, Bihan Jiang, Maja Pantic and Klaus Scherer "Meta-Analysis of the first facial expression recognition Challenge" IEEE transactions on systems, man and cybernetics-part B, Vol 42 N0. 4, August 2012.

[2] Z Zeng, M Pantic, G. I Roisman and T.S Huang, "A survey of affect recognition methods : audio, visual and spontaneous expressions" IEEE transaction patternanal. Mach. Intell. Vol. 31, no. 1, Jan 2009.

[3] Stan Z. Li, Anil K. Jain "Handbook of Face Recognition" Springer edition 2005.

[4] Ekman P., Friesen W.V., "The Facial Action Coding System: A Technique for the Measurement of Facial Movement," San Francisco, Consulting Psychologists Press, 1978.

[5] Padgett C., Cottrell G.W., "Representing Face Images for Emotion Classification," Proceedings of Conference on Advances in Neural Information Processing Systems, 1996, 894-900.

[6] Kobayashi H., Hara F., "Facial Interaction between Animated 3D Face Robot and Human Beings," Proceedings of International Conference on Systems, Man, Cybernetics, 1997, 3, 732-737.

[7] Kobayashi, H., Hara, F., "The Recognition of Basic Facial Expressions by Neural Network," Proceedings of International Joint Conference on Neural Network, 1991, 460-466.

[8] Zhang Z., Lyons M., Schuster M., Akamatsu S., "Comparison between Geometry- Based and Gabor Wavelets-Based Facial Expression Recognition Using Multi-Layer Perceptron," Proceedings of International Conference on Automatic Face and Gesture Recognition, 1998, 454-459.

[9] Zhao J., Kearney G., "Classifying Facial Emotions by Back-propagation Neural Networks with Fuzzy Inputs," Proceedings of Conference on Neural Information Processing, 1996, 1, 454-457.

International Journal of Modern Engineering Research (IJMER)
www.ijmer.com Vol.3, Issue.4, Jul - Aug. 2013 pp-1923-1934 ISSN: 2249-6645

Upgrading of Low Temperature Solar Heat with Cascade Vapor Compression and Absorption Heat Pump

Nattaporn Chaiyat[1]
School of Renewable Energy, Maejo University, Chiang Mai, Thailand

Abstract: *The objective of this project is to study a method to upgrade a low temperature heat form solar energy by cascaded vapor compression heat pump/absorption heat pump. The modified system could be used to produce high temperature heat such as high temperature hot water with full replacement or partial support for boiler in hotel, hospital and other related industries. The input energy comes from solar energy which is clean and friendly to environment.*
In this study, a solar water heating system was designed and constructed. The unit had 10 units of flat-plate solar collectors (1 unit = 2.3 m^2) each generated hot water at a temperature range of 40-60 oC and a storage tank of 1,500 liter. After that these hot water temperature was upgraded by 2 units of R-123 vapor compression heat pumps each having a heating capacity of 10 kW. Hot water at a higher temperature of around 60-80 ^oC was produced and kept in a 200 liter hot water tank. Then a 10 kW water-Libr absorption heat pump upgraded the final hot water temperature to be around 90-110 ^oC kept in a 200 liter tank. Since the water temperature might be over the boiling point then glycol was mixed in the water with a concentration of around 40%,
Mathematical correlations of the related parameters from the experimental data could be set up and these could be used to predict outputs of the studied system under various operating conditions. The final outputs such as the system COP and the final hot water temperature simulated by the models were found to be close with those of the experimental results.
From the economic results, the modified system was used to partially support a boiler for generating hot water at 5 Ton/d compared up to fully support at 35 Ton/d. For the partially support, the energy saving and the payback period for the modified system were around 2,675,434 Baht/y (1 USD = 30.6535 Baht) and 1 year 2 months, respectively. The payback was longer with the higher load of the system.

Keywords: *Absorption heat transformer; Vapor compression heat pump; Solar collector; Boiler, Economical analysis*

I. INTRODUCTION

In tropical area, even solar radiation level is rather high but diffuse solar radiation component is also very significant thus only solar flat-pate solar collector could be competitive with conventional energy for heat generation. Normally, the flat-plate one will not supply heat with a temperature over 60 ^oC, otherwise its thermal efficiency is very low, therefor, a technique to boost-up the temperature is needed.

Absorption heat transformer (AHT) and vapor compression heat pump (VCHP) are a method for upgrading heat to a higher temperature level. For the VCHP, this technology is used to upgrade a low temperature heat (around 40-60 ^oC) to a medium temperature level (around 60-80 ^oC). In a conventional AHT, the absorption system is used to upgrade a medium temperature heat (around 70-80 ^oC) to a high temperature level (around 90-120 ^oC). In a conventional AHT, low temperature heat is absorbed at the AHT generator and the AHT evaporator while high temperature heat is delivered at the AHT absorber and there is waste heat rejected at the AHT condenser. Theoretical and experimental studies of the AHT have been reported by various literatures. Kiatsiriroat et al. [1] reported thermal performance of a water-LiBr AHT for upgrading low temperature heat such as waste heat from industrial processes or solar heat. The coefficient of performance (COP) did not exceed 0.5 because there was a high heat rejection at the AHT condenser. Florides et al. [2] modeled and simulated an absorption solar cooling system in Cyprus which used 3 types of solar collectors, flat plate solar collectors, compound parabolic collectors (CPC) and evacuated tube collectors for comparison by the TRNSYS simulation program. It could be seen that the compound parabolic collector was appropriate for solar absorption cooling in a house during the whole year. The final optimized system consisted of a 15 m^2 compound parabolic collector tilted 30^o from the horizontal plane and a 600 L hot water storage tank. Xuehu et al. [3] also reported the test results of an industrial-scale water-LiBr AHT in China which was used to recover waste heat released from organic vapor at 98 ^oC in a synthetic rubber plant. The recovered heat was used to heat hot water from 95~110 ^oC. The AHT system was operating with a heat rate of 5,000 kW with a mean COP of 0.47. Chaiyat et al. [4] reported a concept of a single-stage H_2O-LiBr absorption heat transformer (AHT) when it was coupled with a vapor compression heat pump (VCHP) for upgrading low temperature heat (CAHT). Heat rejected at the AHT condenser was recovered by the VCHP and transferred to the AHT evaporator. It could be seen that a simulation results of the modified system could be increased around 0.8 compared with 0.5 of the normal AHT. Moreover, Chaiyat et al. [5] also reported a simulation result of a H_2O-LiBr absorption heat transformer performance having an R-123 vapor compression heat pump (CAHT). The CAHT unit was used to upgrade heat from a set of flat-plate solar collectors. It could be found the number of the solar collectors could be decreased 30 units which is about 50 % of that without the VCHP. Moreover, the COP of the modified AHT is about 0.8 compared with 0.5 of the conventional AHT. But this technique could be upgraded the maximum temperature around 90 ^oC.

The objective of this study is to study a method to upgrade a low temperature heat form solar energy by the vapor compression heat pump cascaded with the absorption heat pump to generate a high temperature level at over 100 ^oC. The modified system could be used to produce high temperature heat such as high temperature hot water with full replacement or

partial support for boiler in hotel, hospital and other related industries. The input energy comes from solar energy which is clean and friendly to environment. For the VCHP, an appropriate working fluid has been selected. The seven parameters for evaluating the thermal performance of the VCHP will be considered and compared with those of the common VCHP.

II. SYSTEM DESCRIPTION

Fig.1 shows a schematic sketch of a general solar-absorption heat transformer (Solar-AHT). Solar heat is supplied to the AHT generator and the AHT evaporator at a medium temperature (around 60-80 $^{\circ}$C). At the AHT generator, binary liquid mixture consists of a volatile component (absorbate) and a less volatile component (absorbent) is heated at a medium temperature. Part of the absorbate boils at a low pressure (P_C) and a generator temperature (T_G) at state 1. The vapor condenses in the AHT condenser at a condenser temperature (T_C) to be liquid at state 2 and rejected heat at a lower temperature (around 35-45 $^{\circ}$C). After that the absorbate in liquid phase is pumped to the AHT evaporator at state 3 of which the pressure (P_E) is higher than that of the AHT condenser. The AHT evaporator is heated at the medium temperature (T_E) and the absorbate in a form of vapor enters the AHT absorber which has the same pressure as the AHT evaporator at state 4. Meanwhile liquid mixture from the AHT generator, at state 5 is pumped through a heat exchanger (state 6) into the AHT absorber to a high pressure at state 7. In the AHT absorber, the strong solution absorbs the absorbate vapor and the weak solution leaves the absorber at state 8. During absorption process, heat is released at a high temperature (T_A) which is higher than those at the generator and the evaporator (around 80-110 $^{\circ}$C). This liberated heat is the useful output of the AHT. The weak solution at state 8 from the AHT absorber is then throttled to a low pressure through the AHT heat exchanger at state 9 into the AHT generator again at state 10 and new cycle restarts.

At the AHT condenser, high amount of heat rate is rejected to the environment thus the coefficient of performance (COP) of the normal AHT system is rather low. Moreover, when the solar collectors generates the high water temperature which results to its higher heat loss too.

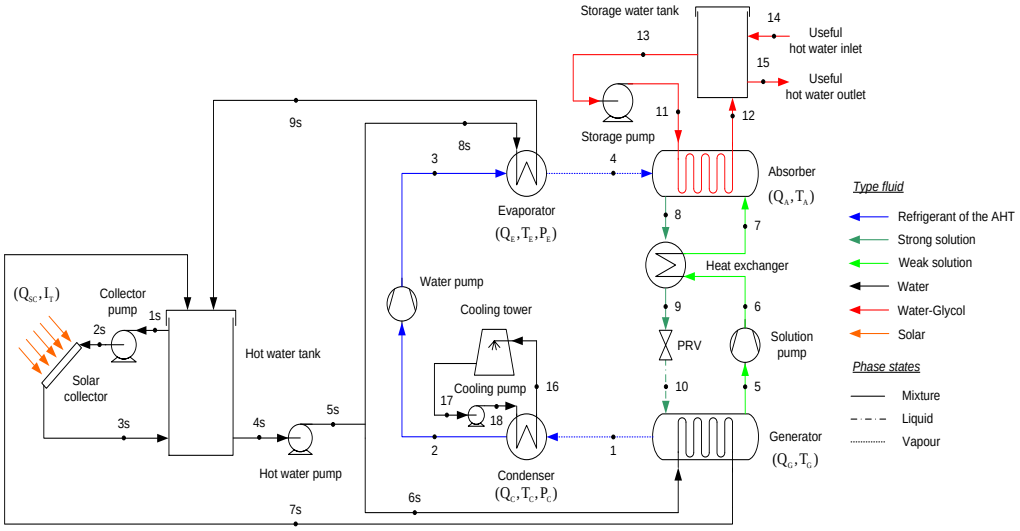

Figure 1. Schematic diagram of a solar-absorption heat transformer.

Fig.2 shows a schematic sketch of a solar water heating system (SWHS) combined with a vapor compression heat pump (VCH) cascaded an absorption heat transformer (AHT). Solar heat is supplied to the VCHP evaporator at a low temperature (around 40-60 ^{o}C) and upgraded heat at a medium temperature (around 60-80 ^{o}C) at the VCHP condenser. After that, a medium temperature heat is obtained at the AHT generator and evaporator for boosting heat to a high temperature level (around 100-120 ^{o}C) at the AHT absorber. Besides, the solar collector will supply heat at a low temperature level compared with the normal system since the solar collector operates at a higher efficiency.

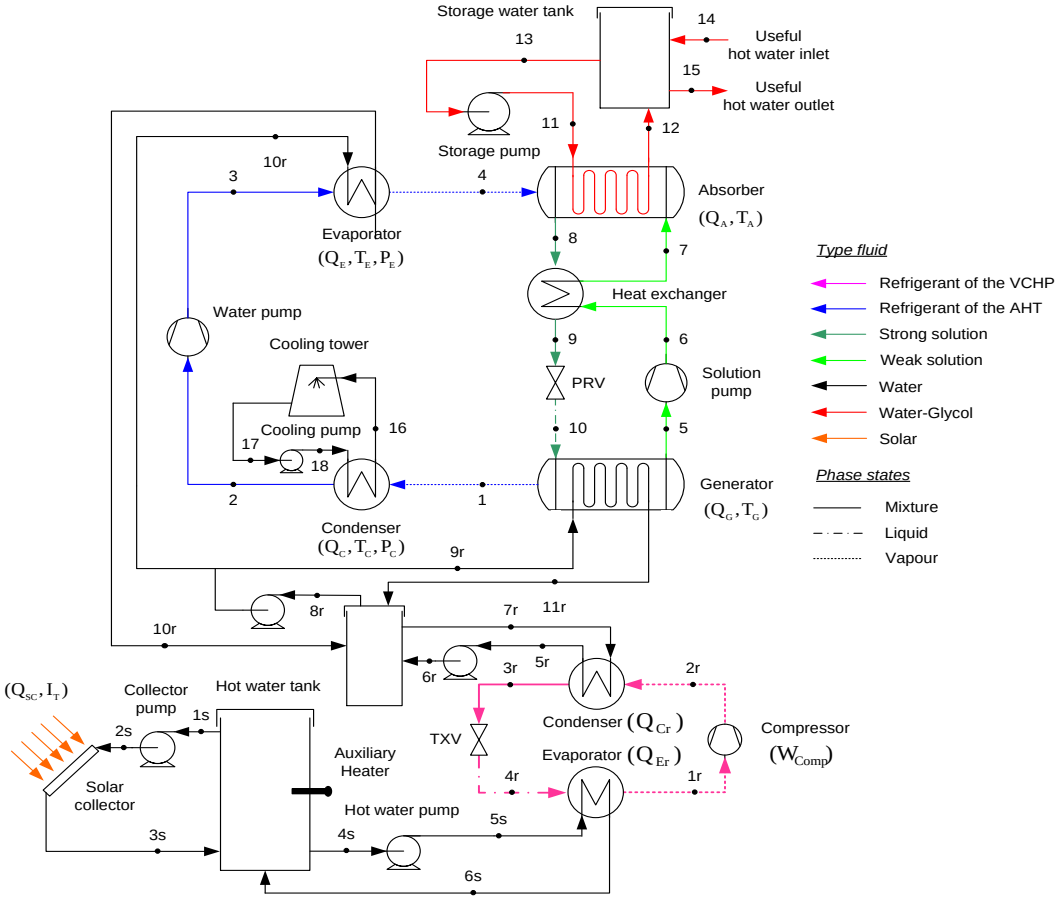

Figure 2. Schematic diagram of a solar absorption heat transformer.

III. SELECTION WORKING FLUID OF THE VCHP

For the method to select the suitable working fluid of the VCHP, the mathematical simulation has been used [6]. For the VCHP, the main components are compressor, condenser, evaporator and expansion valve as shown in Fig.2. At the VCHP evaporator, the working fluid in liquid phase is boiled at a low pressure and temperature to be vapor at state 1r. After that, the fluid in vapor phase is compressed in the compressor to state 2r and the vapor condenses in the VCHP condenser at a high pressure and temperature to be liquid at state 3r. The liquid is then throttled to a low pressure at state 4r and the temperature drops down thus the fluid could absorbed low temperature heat at the VCHP evaporator again and the new cycle restarts. The basic equations for using to simulate the behavior of each component in the VCHP cycle are as follows:

- Evaporator$_r$

$$Q_{Er} = \dot{m}_r (h_{1r} - h_{4r}), \quad (1)$$

$$\dot{m}_r = \dot{m}_{1r} = \dot{m}_{2r} = \dot{m}_{3r} = \dot{m}_{4r}. \quad (2)$$

- Compressor$_r$

$$W_{Comp} = \dot{m}_r (h_{2r} - h_{1r}), \quad (3)$$

$$s_{1r} = s_{2r} \text{ (Isentropic process)}, \quad (4)$$

$$\eta_{Comp} = \frac{h'_{2r} - h_{1r}}{h_{2r} - h_{1r}}. \quad (5)$$

- Condenser$_r$

$$Q_{Cr} = \dot{m}_r (h_{2r} - h_{3r}). \quad (6)$$

- Expansion valve$_r$

$$h_{3r} = h_{4r} \text{ (Throttling process)}. \quad (7)$$

- Coefficient of performance (COP)

$$COP_{VCHP} = \frac{Q_{Cr}}{W_{Comp}}. \quad (8)$$

Table 1. Physical properties of working fluids.

Working Fluid	R-22	R-290	R-134a	R-717	R-123
Chemical formulae	$CHClF_2$	C_3H_8	CF_3CH_2F	NH_3	$CHCl_2CF_3$
Molecular mass (kg/kmol)	86.46	44.10	102.03	17.03	152.93
Critical temperature (^oC)	96.14	96.68	101.06	132.25	183.68
Critical pressure (MPa)	4.99	4.25	4.06	11.33	3.66
Critical density (kg/m^3)	523.84	218.50	511.90	225.00	550.00
Boiling point (^oC)	-40.81	-42.09	-26.07	-33.33	27.82
Latent heat of vaporization at 40 ^oC (kJ/kg)	164.24	302.30	160.88	1089.82	164.04
Flammability	NO	YES	NO	YES	NO
Toxicity	NO	NO	NO	YES	YES
ALT (Year, Atmosphere Life Time)	13.3	< 1	14	< 1	1.4
ODP (CO_2-related, Ozone Depletion Potential)	0.034	~0	0.0015	~0	0.02
GWP (100 Years, Global Warming Potential)	1780	0	1320	0	76

Five working fluids, R-22 (Chlorodifluoromethane), R-290 (Propane), R-134a (1,1,1,2-Tetrafluoroethane), R-717 (Ammonia) and R-123 (2,2-Dichloro-1,1,1-trifluoroethane) have been considered as working fluid in the VCHP. Table 1 shows physical properties of the working fluids [6]. The working conditions for the evaluation are:

1. The VCHP evaporator temperature (T_{Er}) is at 40 ^oC.
2. Total cooling capacity (Q_{Er}) is 10 kW.
3. The VCHP condenser temperature (T_{Cr}) is at 90 ^oC
4. No pressure drops at the VCHP condenser and the VCHP evaporator.
5. Isentropic efficiency of compressor (η_{Comp}) is 80%.
6. Degree of superheating (SH) is 5 ^oC.
7. Degree of subcooling (SC) is 5 ^oC.
8. The properties of working fluids are based upon REFPROP [6].

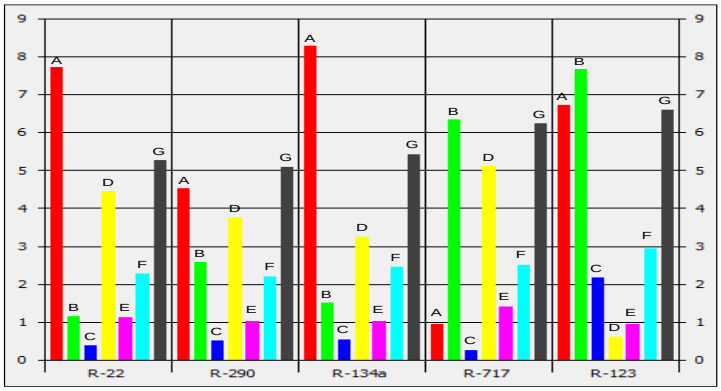

A) Mass of refrigerant per unit heat output, (g/kJ)
B) Vapor volume flow rate, (10^{-2} m3/kg)
C) Displacement volume, (10 m^3/h)
D) Discharge pressure, (10 bar)
E) Discharge temperature, (10^2 ^oC)
F) Pressure ratio, (-)
G) COP_{hp}, (-).

Figure 3. The results for the selected refrigerants.

The indicators used to identify the appropriate working fluid are mass of refrigerant per unit heat output, volume flow rate of refrigerant, high-side pressure, refrigerant temperature at the compressor outlet, pressure ratio and heating COP. Fig.3 shows the results of the selected refrigerants.

Form the simulation results, it could be seen that R-123 gives the suitable refrigerant in terms of energy consumption for the heat pump for generating heat at about 70-80 ^oC due to its low maximum pressure for the heat pump compressor, the cycle pressure ratio is not high and highest COP is obtained.

IV. EXPERIMENTAL PROCEDURES AND SIMPLIFIED MODEL

For the experimental procedures, the constructed of solar water heating system combined with the vapor compression heat pump cascaded with the absorption heat pump AHT is tested its thermal performances to upgrade heat from the installed flat-plate solar collector. The objective of this experiment is to find out a simplified model which is the

correlation between the input parameters and the thermal efficiency of the VCHP and the AHT. For the correlation model, thermal performance could be predicted under various operating conditions and decreased the complicated simulation compared with the old procedure too.

For the solar water heating system, a set of 10 unit solar collectors each in parallel connection and an auxiliary heater of 10 kW were integrated with a 1,500 liter of hot water tank for supplying heat to the absorption system at temperature around 40-60 ^{o}C. The description of each components of the solar water heating system are shown in Table 2.

Table 2. The description of the main components of the solar water heating system.

Component	Type	Specification
1. Solar collector	Flat-plate solar collector	• Area 2.3 m^2/unit • 10 units • $F_R(\tau\alpha)$ = 0.802 • F_RU_L= 10.37 W/m^2.K
2. Hot water tank	Vertical tank	• Capacity 1,500 liter • Thickness of insulator 1 in
3. Double tube heater	Water heater	• Double tube heat exchanger • Capacity 10 kW • Thickness of insulator 0.5 in

For the VCHP system, hot water temperature form solar water heating system is upgraded by 2 units of R-123 vapor compression heat pumps each having a heating capacity of 10 kW. Hot water at a higher temperature of around 60-80 ^{o}C (system could be increased hot water temperature around 20 ^{o}C) is produced and kept in a 200 liter hot water tank. The descriptions of the heat pump components are given in Table 2 and Fig.4 also shows the R-123 heat pump.

Table 3. The descriptions of the 10 kW heat pump components.

Component	Type	Specification
Compressor	Scroll compressor	Power input 1.50 A Displacement volume 12.7 m^3/h
Evaporator	Plate heat exchanger	Capacity 8.00 kW Area 1.64 m^2
Condenser	Plate heat exchanger	Capacity 10.00 kW Area 1.64 m^2
Expansion valve	Thermo static orifice 02	Capacity 10.00 kW Pressure ratio 3.00

Figure 4. 10 kW of R-123 vapor compression heat pump.

For the AHT system, a 10 kW water-Libr absorption heat pump upgrades the final hot water temperature form the VCHP system to be around 90-110 ^{o}C (system could be increased temperature around 20-30 ^{o}C) and keeps in a 200 liter tank. Since the water temperature might be over the boiling point then glycol is mixed in the water with a concentration of around 40%. The descriptions of the absorption heat transformer components are shown in Table 4 and Fig.5 shows the assembly of the absorption system.

Table 4. The description of the 10 kW absorption heat transformer.

Component	Type	Specification
1. Generator	Flooded shell and tube heat exchanger	• Capacity 10.3 kW • Weak solution 50 %LiBr • Strong solution 55 %LiBr • Generator temperature 85 ^{o}C • Tube diameter 4/8 in

Component	Type	Specification
		• Number of Tube passes 4 • Length 1.24 m • Area 1.02 m^2
2. Condenser	Shell and tube heat exchanger	• Capacity 10.6 kW • Condenser temperature 55 ^oC • Tube diameter 4/8 in • Number of Tube passes 2 • Length 1.01 m • Area 0.42 m^2
3. Absorber	Flooded shell and tube heat exchanger	• Capacity 10 kW • Weak solution 50 %LiBr • Strong solution 55 %LiBr • Absorber temperature 115 ^oC • Tube diameter 3/4 in • Number of Tube passes 6 • Length 1.1 m • Area 1.44 m^2
4. Evaporator	Shell and tube heat exchanger	• Capacity 10.8 kW • Evaporator temperature 85 ^oC • Tube diameter 4/8 in • Number of Tube passes 9 • Length 0.94 m • Area 1.16 m^2
5. Pressure relief device	Orifice type	• Capacity 10 kW • Pressure ratio 6.00
6. Lithium bromide	-	• Main content 50-55% • Light yellow transparent liquid • Chloride = 0.05% max • Sulphate = 0.05% max • Bromate = Non reaction • Ca = 0.0001% max • Mg = 0.0001% max • Na = 0.03% max • PH = 9.0-10.5 • Lithium chromate = 0.2-0.3%
7. Solution pump	Inline pump	• Flow rate 0.6-3.7 m^3/h • Maximum head 6 m • Maximum temperature 110 ^oC • Maximum pressure 10 bar • Capacity 78 W • Current 0.34 A • Voltage 230 V

Figure 5. The prototype of absorption heat transformer.

Mathematical correlations of the related parameters from the experimental data is set up and used to predict the thermal performance under various operating conditions.
For the VCHP system, the mathematical model shows the related data between an energy efficiency ratio (EER_{VCHP}) and the different temperature of the entering water temperature at the VCHP condenser and the VCHP evaporator. This correlation is called performance curve and used to predict the thermal performance of the VCHP as shown in Fig.6.

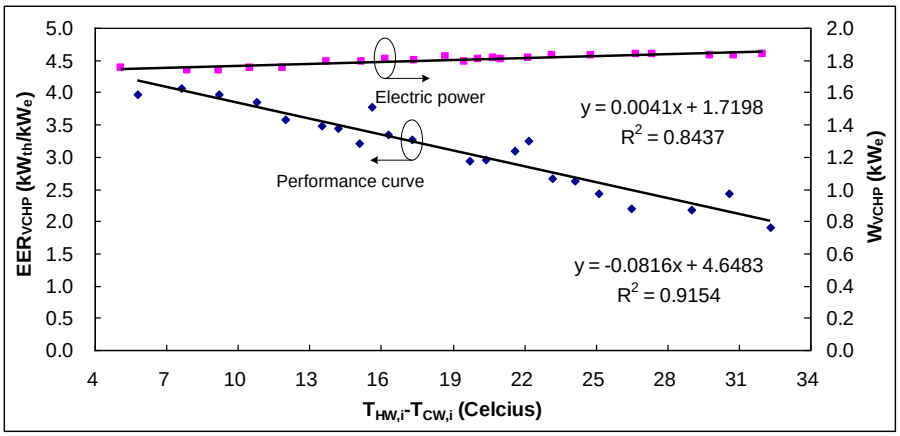

Figure 6. Performance curve of the 10 kW of R-123 vapor compression heat pump.

Fig.6 shows the correlations between thermal efficiency in term of EER_{VCHP} and the entering hot water temperature at the VCHP and the VCHP condenser. It could be found that when increased the hot water temperature different effects the EER_{VCHP} reduced because the electrical power consumption of the compressor is increased at nearly constants of heating capacity at the VCHP condenser. The mathematical model of the heat pump performances are shown as follow:

$$EER_{VCHP} = -0.0816(T_{HW,i} - T_{CW,i}) + 4.6483, (kW_{th}/kW_e), \quad (9)$$
$$W_{VCHP} = 0.0041(T_{HW,i} - T_{CW,i}) + 1.7193, (kW_e). \quad (10)$$

Fig.7 shows EER_{AHT} with $(T_{A,i} - T_E)/(T_{G,i} - T_C)$ when water in the storage tank (AHT side) is used and non-used. In both cases, use and non-use of hot water, when the value of $(T_{A,i} - T_E)/(T_{G,i} - T_C)$ increases the COP_{AHT} and the EER_{AHT} decreased due to lower extracted heat at the absorber. When hot water is used, the COP_{AHT} and EER_{AHT} are higher than those of another case since the hot water temperature in the storage tank is lower thus the absorption could supply more heat. The empirical correlations of the COP_{AHT} with $(T_{A,i} - T_E)/(T_{G,i} - T_C)$ for both cases could be:

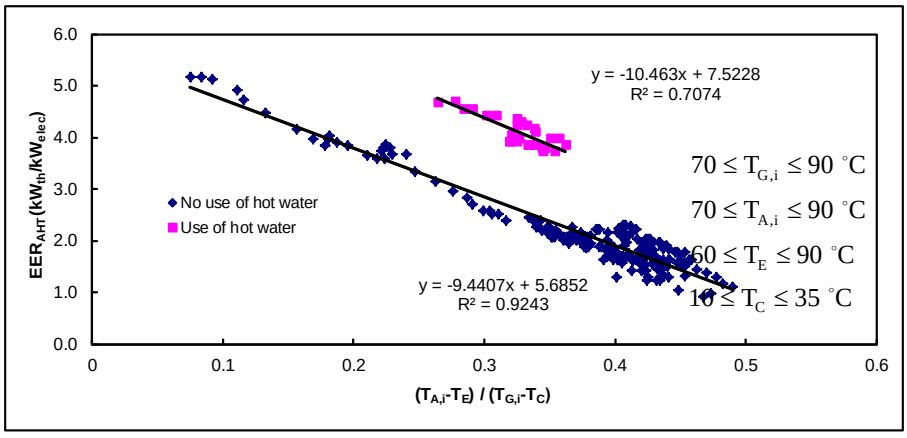

Figure 7. Effect of $(T_{A,i} - T_E)/(T_{G,i} - T_C)$ on COP_{AHT} of the CAHT at hot water temperature leaving the AHT around 100 ˚C from the experimental results.

For used hot water condition:

$$EER_{AHT} = -10.463(T_{A,i}-T_E)/(T_{G,i}-T_C) + 7.5228. \quad (11)$$

For non-used hot water condition:

$$EER_{AHT} = -12.577(T_{A,i}-T_E)/(T_{G,i}-T_C) + 6.7079. \quad (12)$$

These equations are valid for the following criteria:

$$70 \le T_{G,i} \le 90\ ^{\circ}C,\ 70 \le T_{G,i} \le 90\ ^{\circ}C,$$
$$60 \le T_E \le 90\ ^{\circ}C,\ 10 \le T_C \le 35\ ^{\circ}C. \quad (13)$$

Fig.8 and Fig.9 show steps of calculation for the analyses of the VCHP and the AHT cycles with the simplified models. Performance correlations of the EER and the electrical power consumption with the operating temperatures are given. With the input data which are the operating conditions, the upgraded temperature leaving the VCHP condenser and that leaving the AHT absorber are the outputs of the calculations, respectively.

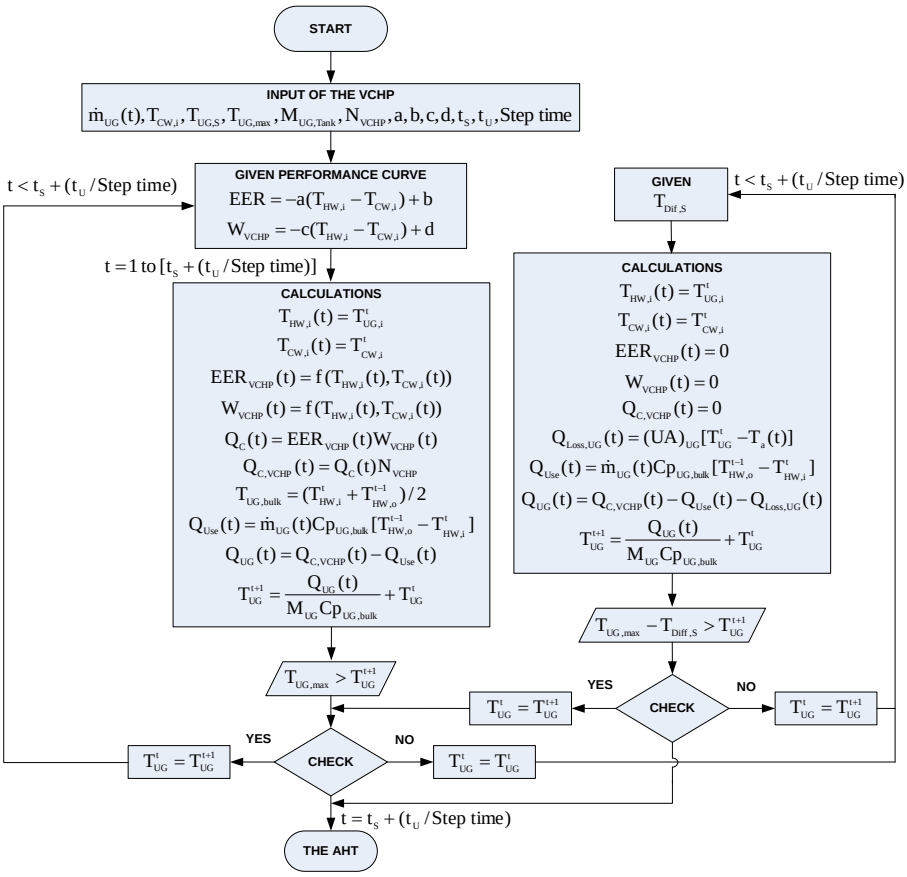

Figure 8. Flow chart for simulation of the vapor compression heat pump by using performance curve.

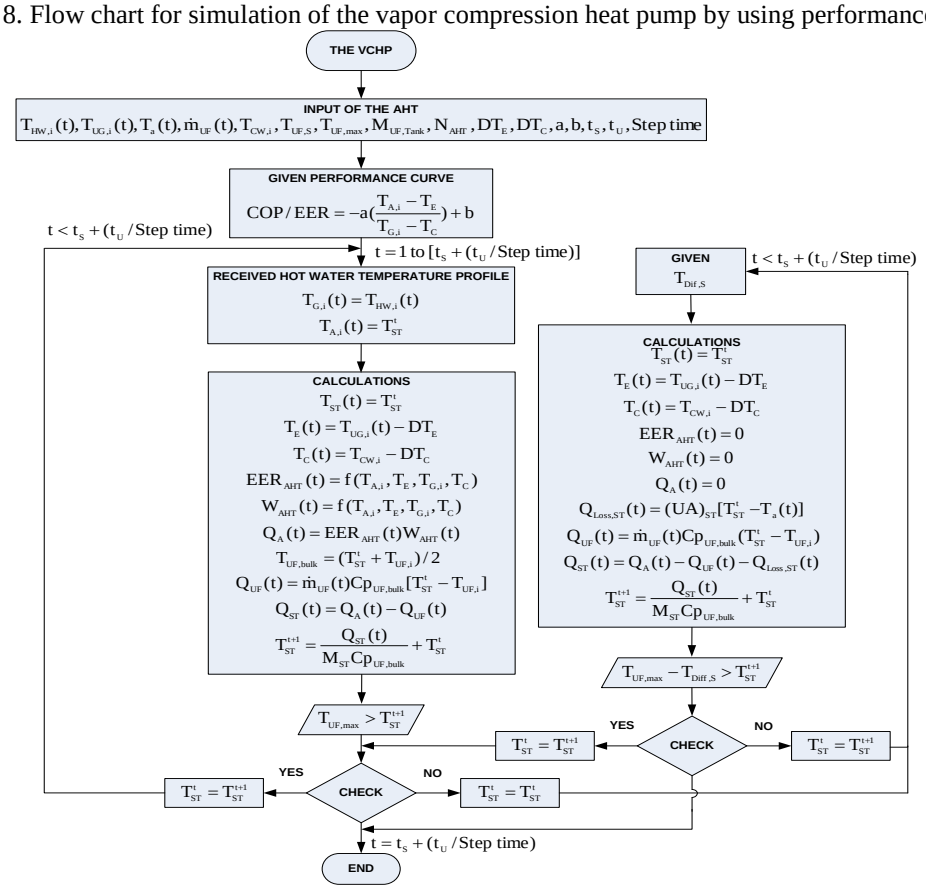

Figure 9. Flow chart for simulation of the absorption heat transformer by using performance curve.

V. RESULTS AND DISCUSSIONS

The modified system of the solar water heating system combined with the VCHP system cascade with the AHT system as described above was tested. The EER of its VCHP was evaluated when the hot water of 200 liter at the AHT absorber was used at a heating capacity around 10 kW_{th}. The result was shown in Fig.10. It could be seen that the simulation results agreed well with those of the experimental data. Fig.10 also showed the water temperatures leaving the VCHP condenser and EER_{VCHP}. In this figure, hot water temperature and the EER_{VCHP} were nearly constant around 60 ^{o}C and 3.1, respectively.

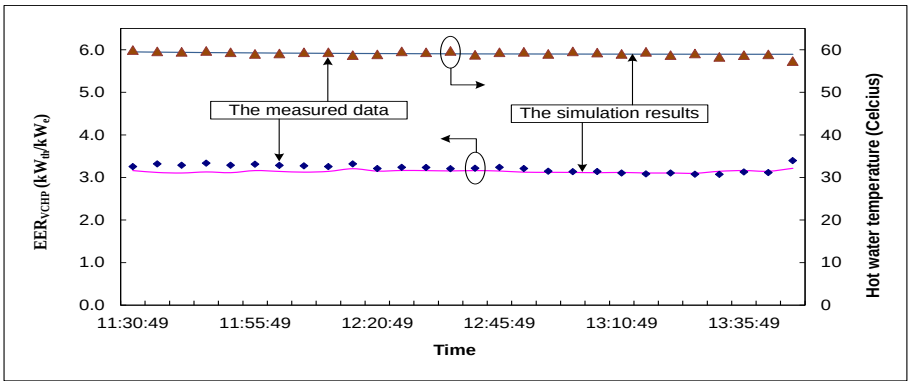

Figure 10. Comparison results of the measured data and the simulation results of hot water temperature from the R-123 VCHP system at flow rate 0.031 l/s (hot water is used at tank 200 liter)

Fig.11 shows the simulated results of the EER_{AHT} when the R-123 VCHP system is coupled with the AHT system. Since the water temperature might be over the boiling point then glycol was mixed in the water with a concentration of around 40% by mass. In this case, the generated hot water was non-used. It could be seen that the simulated results agreed well with the measured data. The hot water temperature also affected the EER_{AHT} which as the temperature increased the EER decreased. Fig.12 also shows the EER_{AHT} when the generated hot water is used at a flow rate of 0.024 l/s. It could be seen that when the hot water was used, the EER_{AHT} was higher than that of the non-used hot water because the water temperature in the storage tank was lower than the system could supply more heat rate. In this Figure, the hot water temperature in the storage tank was nearly constant at 90 $^{\circ}$C and the EER_{AHT} was nearly constant at around 4.1. The simulated results agreed well with the measured data.

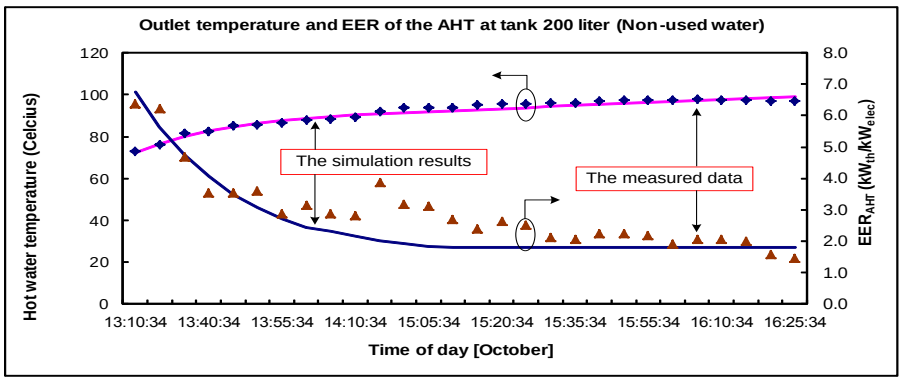

Figure 11. Comparison results of the measured data and the simulation results of the water-glycol solution temperature from the AHT system (hot water is not used at tank 200 liter)

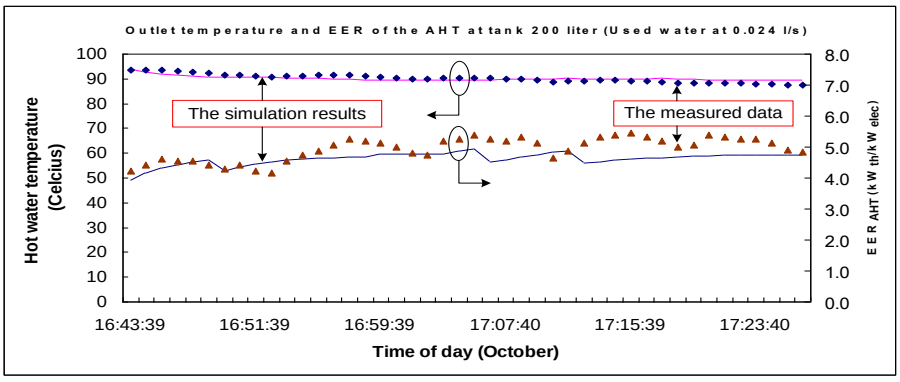

Figure 12. Comparison results of the measured data and the simulation results of water-glycol solution temperature from the AHT system at flow rate 0.024 l/s (hot water is used at tank 200 liter)

For the economic results, the modified system is used to partial support a boiler for generating hot water in a hospital. For the hospital, the boiler is normally used to generate heat in a form of steam at temperature higher 120 °C. For the some processes, the using steam temperature does not exceed 90 °C such as a drying process. Thus the modified is used to support the boiler for reducing the fossil fuel and the green house emission form fossil combustion.

The flue rate of the hospital in Chiang Mai, Thailand is selected for the simulation. A boiler using diesel and heavy oil at around 326 l/d and 2,523 l/d, respectively, is taken to generate steam at temperature around 150 °C. The conditions for the simulation are as follow:

- Operating period 15 h/d.
- Profile of hot water consumption as in **Error! Reference source not found.**
- Initial temperature of hot water ($T_{HW,S}$) in a storage tank is at 30 °C and the maximum temperature is at 85 °C.
- The rate of hot water consumption is around 35,000 l/d.
- Fill-in water temperature ($T_{Sup,i}$) is at 27 °C.

Table 5. The fuel rate of the hospital in Chiang Mai, Thailand [7].

Data	Diesel (liter)	Heavy oil (liter)
Average (l/d)	326	2,523
Total (l/d)	2,848	
Fraction of fuel (Diesel/Heavy oil)	13.08%	
Average (l/m)	10,100	78,200
Total (l/m)	88,300	

In this study, the modified unit is conducted to work with the boiler as described above to reduce the fossil fuel. Fig.13 shows the schematic skate of the boiler to generate steam 35 m^3/d. Fig.14 shows the schematic skate of the modified system operating with the boiler to produce steam and hot water at 30 m^3/d and 5 m^3/d, respectively. The economic results of the modified system shows in Table 6.

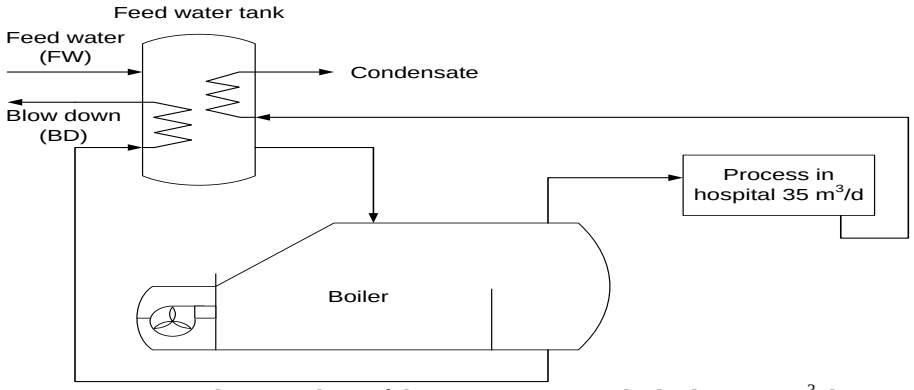

Figure 13. Schematic skate of the steam generation by boiler at 35 m^3/d.

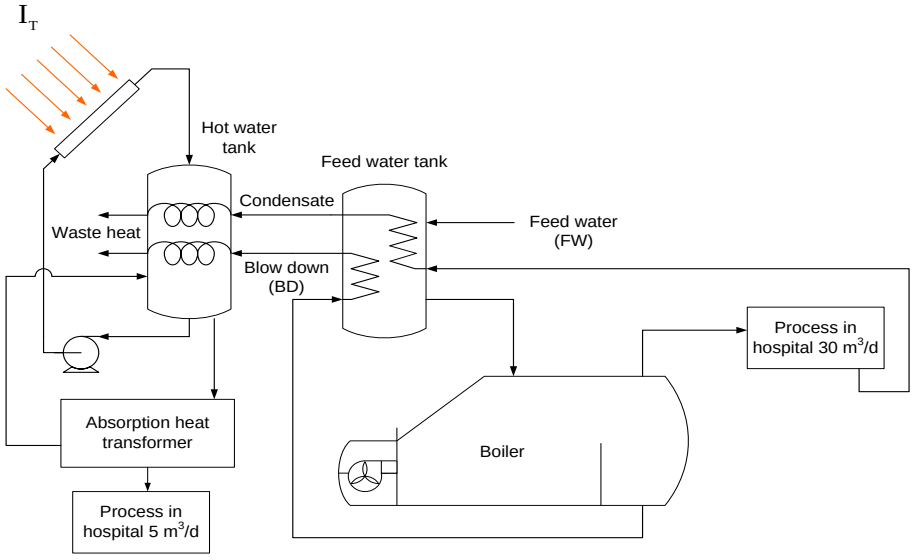

Figure 14. Schematic skate of the steam and hot water generation by boiler and the modified system at 30 m^3/h and 5 m^3/h, respectively.

Table 6. The economics results

Descriptions	The normal unit	The modified unit
Working time (h/d)	15	15
• On-peak period (9.00 - 22.00, h/d)	8	8
• Off-peak period (22.00 - 9.00, h/d)	4	4
Fuel type		
• Diesel (l/d)	373	316
• Heavy oil (l/d)	2,475	2,097
• Total (l/d)	2,848	2,413
Cost of fuel (Baht/y)	11,306,123	8,288,9906
The electrical cost [8] (Baht/y)	38,477.33	380,176.09
Cost of solar collector at 2 m^2/unit (36 units, Baht)	-	900,000
Cost of the VCHP system 20 kW (2 units, Baht)	-	1,000,000
Cost of the AHT system 10 kW (2 units, Baht)	-	1,000,000
Payback period (y)	1.12	

Note: 1 USD = 30.6535 Baht

Table 6 shows the economic results of the method to upgrade a low temperature heat form solar energy by the VCHP system cascade with the AHT system to generate heat partial the boiler. It could be seen that payback period of the modified system is around 1 y 2 m. For increasing the load form 10,000-35,000 l/d at temperature around 85 °C, it could be found that the payback is longer with the higher load because the saving cost at the high load is less than the investment cost compared with the lower load as shown in Fig.15.

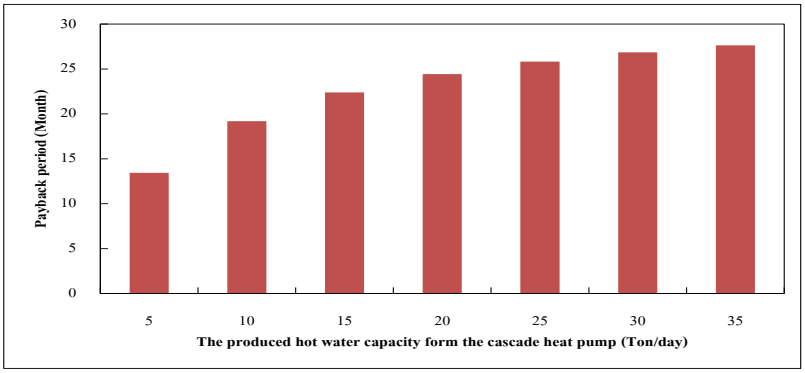

Figure 15. Comparison results of the payback period of the modified system for varying the hot water load at 10,000-35,000 l/d

VI. CONCLUSION

From this study, the conclusions are as follows:

1. The modified system could be upgraded hot water temperature around 50 °C which increases solar heat form 40-60 °C to be around 90-110 °C of the final hot water temperature.
2. The prediction results from performance curve of the modified system could be simulated the system performance such as the system EER and the final hot water temperature of the models to be close with those of the experimental results.
3. From the economic results, the modified system was used to partially support a boiler for generating hot water at 5 Ton/d compared up to fully support at 35 Ton/d. For the partially support, the energy saving and the payback period for the modified system were around 2,675,434 Baht/y and 1 year 2 months, respectively. The payback was longer with the higher load of the system.

ACKNOWLEDGEMENTS

The authors would like to thank School of Renewable Energy, Maejo University and Thermal System Research Unit, Chiang Mai University for supporting testing facilities.

NOMENCLATURE

A	Area, (m^2)
C_p	Heat capacity, (kJ/kg·K)
COP	Coefficient of performance
EER	Energy efficiency ratio, (kW_{th}/kW_e)
h	Enthalpy, (kJ/kg)
I_T	Solar radiation, (W/m^2)
m	Mass flow rate, (kg/s)

P	Pressure, (bar)
Q	Heat rate, (kW)
s	Entropy, (kJ/kg·K)
SC	Subcooling, (°C)
SH	Superheating, (°C)
t	Time, (s)
T	Temperature, (°C)
U	Overall heat transfer coefficient, ($W/m^2 \cdot K$)
W	Work, (kW)
X	Concentrate, (%LiBr)

Greek Symbol

η	Efficiency, (%)
ε	Effectiveness, (%)
ρ	Density, (kg/m^3)

Subscript

A	Absorber
Aux	Auxiliary heat
act	Actual
amb	Ambient
bulk	Bulk temperature
C	Condenser
Coll	Solar collector
Comp	Compressor
CW	Cooling water
e	Electric
E	Evaporator
G	Generator
H	High
HS	Heat source
HW	Hot water
HX	Heat exchanger
i	Inlet
L	Low
max	Maximum
min	Minimum
o	Outlet
r	Refrigerant
S	Start
SC	Solar collector
ST	Storage tank
Sup	Supply
th	Thermal
U	Stop using time
UF	Useful
UG	Upgraded

REFERENCES

[1] Kiatsiriroat, T, Bhattacharya, S.C., Wibulswas, P. Upgrading Heat by a Reversed Absorption Heat Pump. *Applied Thermal Engineering, 25*, 1986, 175-186.

[2] Florides, GA, Kalogirou, SA, Tassou, SA,Wrobel, LC. Modeling and Simulation of an Absorption Solar Cooling System for Cyprus. *Solar Energy, 72*, 2002, 43-51.

[3] Xuehu, Ma, Jiabin, C, Songping Li, Qingyun, Sha, Aiming, L, Wei, Li, Jiayan, Z, Guojun, Z, Zhihao, F. Application of absorption heat transformer to recover waste heat from a synthetic rubber plant. *Apply Thermal Energy, 25*, 2002, 797-806.

[4] Chaiyat, N, and Kiatsiriroat, T. Improvement of an Absorption Heat Transformer Performance for Upgrading Low Temperature Heat by Coupling with a Vapor Compression Heat Pump, *Chiang Mai University Journal of Natural Sciences, 10(2)*, 2011, pp.315-333.

[5] Chaiyat, N, and Kiatsiriroat, T. Upgrading of Low Temperature Solar Heat for Medium Temperature Applications by a Solar-Absorption Heat Transformer Assisting with a Vapor Compression Heat Pump, *Proc. 1st Conf. on International Symposium on Low Carbon & Renewable Energy Technology (ISLCT2010)*, Korea, 15-18 November 2010, 150.

[6] Chaiyat, N. and Chaichana, C. Drying Room from Geothermal Energy, *Proc. 8th Conf. on Heat and Mass Transfer in Thermal Equipments*, Thailand, 12-14 March 2008, 87-91

[7] Maharaj Nakorn Chiang Mai Hospital. The fuel rate of boiler, Chiang Mai University, Thailand, 2013.

[8] Provincial Electricity Authority. The rate of electricity cost. Online, http://www.pea.co.th, 2013.

International Journal of Modern Engineering Research (IJMER)
www.ijmer.com Vol.3, Issue.4, Jul - Aug. 2013 pp-1935-1938 ISSN: 2249-6645

Sender Authentication with Transmission Power Adjustment Method Using RSSI in Wireless Sensor Network

Archana Arudkar[1], Prof. Vimla Jethani[2]
*(Computer Department, RAIT / Mumbai University, India)
** (Computer Department, RAIT / Mumbai University, India)

Abstract: *With the advent of powerful and efficient wireless sensor nodes, the usage of wireless sensor networks (WSN) has been increased greatly. Sensor networks consist of a network of autonomous sensors that can reconfigure themselves so as to sense the environment in the most efficient manner. These nodes are having low power and limited range. Low power implies limited battery life. In WSN, to perform the task successfully low energy consumption is the major concern. Wide use of WSN in practical application makes it necessary to maintain the network security.IP or MAC addresses are used for sender authentication which can be spoofed easily. This makes these types of networks vulnerable to many identity-based attacks. To protect wireless network from such type of attacks, Received Signal Strength Indicator (RSSI) value called 'Signalprint' can be used for sender authentication, which is harder to spoof. However in WSN battery discharge causes received signal characteristics to vary. This may give false alarm in sender authentication. Low energy consumption is one way to mitigate this problem.*

Keyword: *Received Signal Strength Indicator, Signalprint, Sender Authentication, Transmission Power, Wireless Sensor Network.*

I. INTRODUCTION

A wireless sensor network consists of spatially distributed autonomous sensors to cooperatively monitor physical or environmental conditions, such as temperature, sound, vibration, pressure, motion. The development of wireless sensor networks (WSN) was motivated by military applications such as battlefield surveillance. It is now used in many industrial and civilian application areas, including industrial process monitoring and control, machine health monitoring, environment and habitat monitoring, healthcare applications, home automation and traffic control.

A sensor node, also known as a mote is a node in a WSN that is capable of performing some processing, gathering sensory information and communicating with other connected nodes in the network. Therefore the success of WSN depends on the ability of the member nodes of the network to co-operate among them. Due to this high level of co-operation required, WSNs are susceptible to many security attacks from intruders. In the absence of security mechanism, attackers are getting success to degrade the performance of the network and even bring down the network. To provide the security to WSN needs to separate the nodes of the intruders from the member nodes. To separate the intruder's node from legal member nodes needs to identify the member nodes in the network. Presently IP or MAC addresses are used to identify the node, which is vulnerable to spoofing. [1] proposes a method that uses the sent data characteristics called Received Signal Strength Indicator (RSSI) to identify the sender. The characteristic of the signal at the receiver depends on factors such as attenuation, atmospheric conditions and intervening obstacles. This makes it hard for the receiver to alter the transmitted signal characteristics so as to masquerade as another node. RSSI value captured at several different nodes is aggregated and a signalprint is generated for the sender. This provides security from the identity based attacks like Masquerading and Resource Depletion attacks. RSSI value proves very good identifying characteristics for a node in WSN, where little or no mobility of the node occurs. A node in a WSN has limited battery life. As the battery discharges the intensity of the transmitted signal also reduces. The transmission power of the sensor node reduces with the supply voltage of the battery [4].This affects the RSSI values which may raise a false alarm. To overcome from this problem, in WSNs, transmission power adjustment using RSSI is one way to minimize energy consumption and prolong the battery life and thus the network lifetime.

II. ATTACKS ON WSN

2.1Resource Depletion Attacks

This is essentially a Daniel of Service (DoS) attack. The attacker floods the network with unnecessary requests, thereby consuming large amount of network bandwidth, computational power and memory. The attacker goes one step ahead and attempts to mask its identity by spoofing its IP or MAC address. So it is difficult to detect. However, as signalprints are hard to spoof, a mechanism based on signalprints can detect such an attack.

2.2Masquerade Attacks

In a masquerade attack, the attacker poses as a valid member node. Most techniques involve spoofing IP or MAC address, so as to acquire the privileges of another valid member node. This allows the attacker to enter and access a network to which he is not authorized. Identity-based security mechanisms that use IP or MAC address – or any information that the sender sends as a part of data – cannot detect such security violations. The properties of signalprint makes it possible to detect this attack[1].

III. SIGNALPRINT

RSSI value is used to identify the sender. But the single value of RSSI is not sufficient to identify a sender. Multiple RSSI values are used for the sender's identity.

3.1 Received Signal Strength Indicator (RSSI)

RSSI is an indication of the power level being received by the antenna. Generally, the higher the RSSI level, the stronger is the signal. We can say that RSSI is used to indicate strength of the incoming signal in a receiver. (The signal strength indicator on a cell phone display is a common example.).RSSI is defined as ten times the logarithm of the ratio of power of the received signal and a reference power (e.g. 1mW) i.e., RSSI α 10 log P/Pref.This means RSSI α log P [5].It is a known fact that power dissipates from a point as it moves further out. So the relationship between power and distance is that power is inversely proportional to the square of the distance travelled. In other words:

$$RSSI \alpha \log (1/distance^2) \quad \ldots\ldots\ldots\ldots\ldots(1)$$

The RSSI values are highly dependent on environment phenomena. This dependence of RSSI values on the environmental phenomena makes it extremely difficult for the intruder to spoof RSSI values.

3.2 Signalprint Properties

Following are the properties of signalprint

- Signalprints are hard to spoof- The transmitted signal attenuation depends on the distance ,environmental factors and obstacles such as walls,furnitures.As the transmitter has no control on the environmental factor and thus unable to change the produced signalprint.
- Signalprint are strongly correlated with the physical location of the client.
- RSSI value from particular sender will not show a large difference from the initial RSSI value received [2].

3.3 Signal print Representation

-50	**-78**	**-36**	**-65**	**-46**

Fig1. Signal print Representation

Figure 1 shows the typical signalprint representation. A signal print is a vector of RSSI values received at different nodes for the same message transmitted for the same sender. The vector contains one entry for each receiver.

3.4 Signalprint Generation

The RSSI measured at a single receiver is not enough to uniquely identify the sender. However, a set of RSSI values taken at multiple receivers can uniquely and accurately identify the sender. Therefore, it is required to aggregate the individual RSSI values from multiple locations into a single signalprint vector. In [2], RSSI values measured at multiple 802.11 access points were sent to a central wireless appliance. The wireless appliance then acted as a central authority to generate and compare the signalprints. In a WSN, however, there is no natural centralized node. Therefore, a distributed approach is used. Each node in the network can obtain the RSSI values measured at the other nodes and generate the complete signalprint from these. When a signalprint generation is requested, all the nodes in the range of the sender measure the RSSI value corresponding to a transmission by the sender. These RSSI values are then passed on to all the neighbours along with a signature of the received message, so as to match the RSSI values with the received message. When a node receives the RSSI values from the other nodes, it places each RSSI value in its corresponding location in the signalprint vector .The greater the number of receivers collaborating to generate the signalprints, the greater is the number of RSSI values captured and, hence, the greater is the accuracy of the signalprint in identifying the receiver. Therefore, it is important to have as many receivers as possible. It is also observed that as the distance between the transmitter and the receiver increases, the sensitivity of the RSSI to changes in distance reduces. Hence, we would like the receiver to be close to the sender.

3.5 Differential Values

In order to identify the sender, we need to compare the generated signalprint with the previously stored signalprint for the vector. However, before comparing the signalprints ,convert each signalprint into differential values.Signalprints are either written with absolute or differential values: for example, a signalprint S1: (-50,-62,-76) written using differrential signal strength becomes S1: (0,-12,-26).The use of differential values increase the robustness of signalprint operations against devices that vary their transmission power levels between frames. With absolute values, changes in transmission power create similar changes in the detected RSSI, which could cause the system to attribute multiple packets sent by single client to multiple devices. Using differential values, transmissions performed by a stationary transmitter generate similar signalprints, increasing chances of attack detection [1].

IV. TRANSMISSION POWER ADJUSTMENT METHOD

To avoid identity based attacks on WSN [1] suggest the signalprint method using RSSI for sender authentication which is hard to spoof. There is a variation in RSSI value because of environmental condition, obstacles found in propagation, transmission power used and the discharge of battery. This work considers the battery drainage problem. The

variation in RSSI value occurs because of low battery power, gives false alarm in sender authentication. So this work compares the signalprint method for sender authentication with and without Transmission Power Adjustment which reduces false alarm by low energy consumption and hence better sender authentication.
In WSN, due to power limitations, transmission power adjustment using RSSI is way to minimize energy consumption and extend the battery life of sensor nodes. To minimize the power consumption, a node of should transmit each packet with the minimum power required for successful transmission.

All nodes are not pre-configured. Therefore, self-configuration is useful and practical way to gain useful information such as neighbour nodes. When a node is power on, its neighbour table is empty. So each node must send a wireless query to detect its neighbouring node so that it can communicate with it directly. This is called Neighbour Discovery process. To discovery of a neighbouring node, instead of sending many messages send only one message with maximum transmission power. Run this neighbor discovery process periodically to note down the updated RSSI value. To dynamically adjust the transmission power such that it will reduce the energy consumption without packet loss.
The minimum transmission power for sending a message from node x to node y is calculated using RSSI is:

We know that,

$$\text{RSSI (dBm)} = A - n \log d \quad \ldots\ldots\ldots\ldots\ldots\ldots\ldots\ldots\ldots\ldots.. (2)$$

Where A – transmission power
n – Propagation constant
d – Distance between sender and receiver node

If $P(x)$ – transmission power of x
$P_{max}(x)$ - maximum transmission power of node x
$P_{min}(x, y)$ - minimum transmission power required for node x to communicate with node y.

Put $A= P_{max}(x)$ in (2)
Therefore,

$$RSSI_{max}(x, y) = P_{max}(x) – 10n\log d\ldots\ldots\ldots\ldots\ldots\ldots\ldots\ldots\ldots\ldots (3)$$

Put A = Pmin(x,y) for minimum transmission power

$$RSSI_{min}(x, y) = P_{min}(x, y) – 10n\log d\ldots\ldots\ldots\ldots\ldots\ldots\ldots\ldots.. (4)$$

(5) is calculated by performing (4)-(3)

$$P_{min}(x, y) = RSSI_{max}(x, y) – RSSI_{min}(x, y) + P_{max}(x)\ldots\ldots.\ (5)$$

Here values of $RSSI_{min}(x, y)$ and $P_{max}(x)$ obtained from device datasheet for CC2431 their values are -92dBm and 0 respectively.
To find the value of $RSSI_{max}(x, y)$, x sends a message using node’s maximum transmission power to y and y will send back the message of $RSSI_{max}(x, y)$ value.
The variation in RSSI value is calculated as $RSSI_{delta}$ and included in (6) for error adjustment.

$RSSI_{delta}$ is calculated by using the difference between the maximum, Max ($RSSI_{max}(x,y)$) and minimum, Min($RSSI_{min}(x,y)$)

$$RSSI_{delta} = Max (RSSI_{max}(x, y)) – Min (RSSI_{min}(x, y))\ldots\ldots\ldots\ldots... (6)$$

Therefore,

$$P_{min}(x, y) = RSSI_{max}(x, y) – RSSI_{min}(x, y) + P_{max}(x) + RSSI_{delta} \ldots\ldots. .(7)$$

Suppose sender node is x and receiver node is y.Sender x broadcast a hello packet with maximum transmission power to receiver node y.Then receiver y replies a unicast message with $RSSI_{max}$ (x,y) to x. After that, x adds y and $RSSI_{max}$ (x, y) in its neighbour table. This process will be repeated periodically for updating $RSSI_{max}$ value during packet transmission. As mentioned in (7), minimum transmission power for sending messages from x to y is computed and adjusted to the closest transmission power level which is greater than or equal to the computed one.
By using the above transmission power, it was found that

- Packet loss rate of sending with power adjustment does not to be significantly different from sending with maximum power.
- Energy consumption for sending packet is reduced around 50% for all distances [6].

V. CONCLUSION

Signalprint using RSSI technique for sender authentication helps to detect Identity based attacks. As RSSI is hard to spoof and strongly associated with the location of the node, it is good option for sender authentication where less or no mobility occurs.

In WSN energy consumption is the major concern. More the energy consumption less is the battery life and hence the network life .Low battery power affects the RSSI value which may give false alarm. Transmission power adjustment is one method to improve the result. It is a known fact that most of the energy is consumed during neighbour discovery process.

Neighbour discovery is very important in wireless sensor networks. Many processes, such as topology-control, medium access control, and routing, rely on the information provided by the ND process. The RSSI value is one of the useful information for transmission power adjustment. This testbed uses RSSI value to estimate minimum transmission power for sending each packet to a neighbour node. Since reducing transmission power may raise the unsuccessful sending and receiving messages, dynamic adjustments of output power control is done by periodically sending a hello message to the neighbour and then receiving the current feedback RSSI value from that neighbour. Comparing to transmission with the maximum power, the testbed results show that the energy consumption in transmission process is significantly decreased, while the packet loss rate is not significantly different.

References

[1] Sudip Misra,Ashim Ghosh,A.P.Sagar P.,Mohammad S.Obaidat**,** Detection of Identity-Based Attacks in Wireless Sensor Networks Using Signalprints**,***2010 IEEE/ACM International Conference on Green Computing and Communication & 2010 IEEE/ACM International Conference on Cyber, Physical and Social Computing.*

[2] D.B. Faria and D.R. Cheriton,Detecting Identity Based Attacks In Wireless Networks using Signalprint**,** *Proceedings of the 5th ACM workshop on wireless security, Los Angeles, California, Sept 29, 2006.*

[3] K.Srinivasan and P. Levis, RSSI Is Under Appreciated**,** *in Proceedings of the 3th ACM workshop on Embedded Networked Sensors, May 2006.*

[4] S.Hussain and M.S. Rahman, Using Received Signal Strength Indicator to Detect Node Replacement and Replication Attacks in Wireless Sensor Networks, *in SPIE Proceedings on Data Mining, Intrusion Detection, Information Assurance and Data Networks.*

[5] Ambili Thottam Parameswaran,Mohammad I.Husain,Shambhu Upadhyaya, Is RSSI a Reliable Parameter in Sensor Localization Algorithms-An Experimental Study**,** *in field failure data analysis workshop, Niagara Falls,USA, September 2009*

[6] Wilawan Rukpakavong,Iain Phillips,Lin Guan, Neighbour Discovery for Transmit Power Adjustment in IEEE 802.15.4 using RSSI, New Technologies, Mobility and Security(NTMS),2011 4th IFIP International Conference on Feb-2011.

International Journal of Modern Engineering Research (IJMER)
www.ijmer.com Vol.3, Issue.4, Jul - Aug. 2013 pp-1939-1941 ISSN: 2249-6645

Conservation of Energy: a Case Study on Energy Conservation in Campus Lighting in an Institution

Biswajit Biswas[1], Sujoy Mukherjee[2] , Aritra Ghosh[3]
[12]*Department of AEIE, Murshidabad College of Engineering & Technology, India*
[3]*Department of EE, Murshidabad College of Engineering & Technology, India*

ABSTRACT : *Fossil fuel reserve in India is depleting in a rapid way with development of the country. To meet the energy crisis, end user efficiency has an important role. This paper deals with the energy conservation in lighting system with the replacement of illumination scheme as there is an increasing demand of energy in all sectors in India. A number of commonly used lighting source and their comparison in terms of luminous efficacy was discussed. The campus lighting system comprising of T12 fluorescent light fixture for vigilance purpose of residential and institutional area of an existing institution can be replaced with proposed LED light fixture of equivalent output but of higher efficiency to reduce consumption of lighting energy. This improvement of end user efficiency will reduce the peak and average demand of electricity and hence reduce burden on electric network. The savings of annual energy with the proposed scheme is around 65% compared to the existing expense which is a significant achievement through energy conservation technique. Payback period of installation of proposed illumination scheme is slightly over three years. The initial investment for short term assessment is little higher but, in long term assessment the initial investment for the proposed scheme is will reduced by 50% as the operating life span of the proposed scheme is around five times the existing scheme.*

Keywords: *Energy conservation, End User, LEDs, Luminous Efficacy, Payback Period*

I. INTRODUCTION

India has over 17 percent of the world's population and hence a significant consumer of energy resources. India consumes its maximum energy in Residential, commercial and agricultural purposes in comparison to China, Japan, Russia, EU-27 and US [1]. It is found that the share of energy consumption in India and China has also been on the raise due to sharp urbanization, population explosion, and intensive growth of IT and related business [2]. Development of the society highly depends on availability of energy. Hence meeting energy demand for the nation is an important task for sustainable development of the country. In all five year planning in India, energy sector has received significant priority. It is found that requirement of electricity during year 2010-11 was 861,591 million units and availability was 788,355 million units, i.e. a shortage of 73,236 million units (8.5%). In the year 2011-12, the requirement was 933,741 million units and the availability was 837,374 million units, again resulting in shortage of 96,367 million units (10.3%) [3]. It is seen that there exist a considerable gap demand and supply of power. It is very much essential to minimize the gap between generation and demand. From 1991 to 2007 a number of reforms have been introduced by the government to improve the power system in India. It in turn revolutionized the growth in power capacity, reliability in supply, growth in the revenue collection [4].

The conservation of energy is an important means to reduce peak and average demand of energy. It is observed that investment in energy efficiency and energy conservation is highly cost effective [5]. End user efficiency can considerably be improved by Energy conservation technology. It is possible to save energy with the implementation of energy conservation technology which means increasing generation of energy with available source [6]. The improvement of end user efficiency is a part of demand side management which reduces the amount of energy consumption by the end users. It in turn reduces the burden from the existing power supply system which also reduces in unit cost of the energy [7] [8].

In domestic, commercial and industrial sector, lighting system consumes significant amount of energy. It consumes 50% of total energy consumption in commercial buildings and 10% in industries. A number of places are found having inefficient lighting design for a particular task [9]. In all the sectors both indoor and outdoor lighting efficiency can be improved with higher efficient lighting sources which will help to reduce the gap between demand and supply.

II. SECTOR WISE ENERGY DEMAND IN INDIA

India is the one of the most populated country in the world and one of the most growing countries in the world. In order to have sustainable growth rate, energy in the usable form plays an important role. From the time of independence, India has raised the power generation capacity from 1362 MW to many folds at present [10]. In every five year planning, energy got significant importance. But the gap between generation and the demand is increasing day by day. The fossil fuel reserve in India is not very vast and may be depleted totally by the middle of the century which indicates an alarm situation of near future. Energy consumption pattern of different sectors in India in the year 2007 are given in the table I. Hence to keep up the growth rate of every sector, meeting required energy demand is essential.

Table I: Sector wise energy consumption

Areas	***Consumption (Year-2007)***
Domestic	21%
Commercial	18.0%
Industrial	32%
Transportation	29%

III. ENERGY CONSERVATION AT THE END USER

It is seen that there always exist a gap between generation of energy and energy demand of energy. It is quite impossible to bridge this gap by increasing the generation capacity as it is a very capital intensive process. At the same time most of the fossil fuel reserve will be depleted by next few decades. From the survey conducted by ministry of power in 1992 it is found that the improvement in efficiency of end users is essential. End user sector is a major area of conservation of energy to bridge the short fall between generation and demand [10]. In all the areas, conservation of energy is possible. Through demand side management it is possible to maximizing the end use efficiency [11]. Around 15,000 MW of energy can be saved through end-use energy efficiency [10]. One of the most significant areas of energy conservation is lighting energy. Lighting load shares a significant portion in all sectors namely domestic, commercial, industrial etc. It is found that in most of the cases indoor lighting get priority as far as energy efficiency is concern but campus lighting in commercial, domestic building get less importance. There is huge possibility to conserve energy if the inefficient light fittings are replaced by efficient one. Basically it is a demand side management which helps to reduce load on the electrical network. Consumption of energy can be reduced by conservation of energy.

IV. LIGHTING SOURCES AND THEIR EFFICIENCY

In all sectors there are some commonly used light fittings such as incandescent light, fluorescent light, sodium vapour, mercury vapour, metal halide etc. for particular application. Luminous efficacy i.e. lumen per watt for these light sources are different. Among these a number of areas found with incandescent light as a source of lighting which very inefficient from the point of view of energy efficiency. It is obvious that higher efficiency of lighting source will definitely reduce the energy consumption. Luminous efficacy of different light sources is listed in table II.

Table II: luminous efficacy of different light sources

Light source	***Luminous efficacy (lumen/watt)***
Incandescent light	18-20
Fluorescent light	60-70
Sodium Vapour	40-120
Mercury Vapour	50-60
Metal Halide	80-125
CFLs	50-80
LEDs	20-60

It is seen that the luminous efficacy of the LED and CFL are at per but LED is much energy efficient due to low power consumption at the driving circuit and negligible loss of power in terms of heat generation. Hence LED for lighting purpose is a good alternative of commonly used light sources. More over research is going on to develop more efficient LEDs. It is true that the initial cost of LEDs is high but its life span is extremely high compared to other light sources. So LEDs can be good alternative to replace the existing less efficient lighting source in all sectors of application.

V. A CASE STUDY OF REPLACING EXISTING LIGHTING SYSTEM (T12 FLUORESCENT) BY LED LIGHT IN THE CAMPUS OF AN INSTITUTIONAL AREA

A survey was conducted to an Engineering College and its residential complex and found that 40 number of fluorescent lamp (T12) fixture is connected to the entire campus for vigilance purpose. It is observed that all the lights remain in operation for around 12 hours at the night (6 p.m. to 6 am) for every day. The duration of operation may slightly vary depending on the seasonal change of day length. It is also observed that the lights remain in operation throughout the year irrespective of holydays and vacation as it operates for vigilance purpose of the campus. All of the lights fixtures are having electromagnetic ballast which consumes around 12 to 14 watt of additional power while in operation. So the power consumption of a single fluorescent light fixture considering minimum ballast loss is 40+12=52 watts. The light output of the fluorescent light fixtures is around 2400 lumen. Hence a significant amount of energy can be saved with improvement of end user i.e. replacing the existing light fittings with high efficient light fittings. For this purpose high efficient LED street light fixture of SHAH ELECTRONICS model no. SESTL-LED-1811was proposed. It consumes 18 watt with luminous efficacy of around 120-140 lm/w. This LED Street light provides average luminous output of around 2340 lumen and dedicated for outdoor application. The comparative study between existing lighting fittings and proposed light fittings will provide very close output with much less energy consumption. Taking 12 hours of operation in a day, total energy consumption of a single existing light i.e. fluorescent light in a day is given by:

52*12 watts-hour = 624 watt-hour.

So, annual energy consumption of a single existing light is given by:

624*365 watt-hour =227760 watt-hour or 227.76 units.

Hence annual energy consumption of total existing light i.e. 40 fluorescent light is given by:

40*227.76 unit = 9110.4 units.

Annual energy cost for campus lighting with existing light fixture is given by:

5*9110.4 = Rs. 45,552/- (Considering unit cost as Rs. 5/-)

If all existing light fittings are replaced by proposed 18 watt LED Street light which gives output of around 2340 lumen which is very close to the light output of existing fluorescent light fixture. Taking same hours of operation i.e. 12 hours day, energy consumption in a day of a LED Street light fixture is given by:
18*12 = 216 watt-hour
So, annual energy consumption of a single LED Street light fixture is given by:
216*365 = 78840 watt-hour or 78.84 units
Hence annual energy consumption of total LED Street light fixture i.e. 40 is given by:
40*78.84 = 3153.6 units
Annual energy cost for campus lighting with LED Street light fixture is given by:
5*3153.6 = Rs. 15,768/- (Considering unit cost as Rs. 5/-)
Hence annual energy savings is (9110.4 – 3153.6) = 5956.8 units.
Percentage savings in annual energy consumption is 65.38%.
Annual savings in energy cost is (45552 - 15768) = Rs. 29,784/-
Now the cost of proposed LED light fittings is Rs. 2500/- per unit.
Cost of installation of proposed LED light fittings is = 2500*40 = Rs. 100,000/-
Payback period = 100000/29784 = 3.35 years = 3 years 4 months.
It is fact that the initial investment and payback period of the proposed lighting system is high. But the savings in long term is of very significance. Minimum life span of a LED is 50000 hours whereas the life span of fluorescent light is around 10000 hours. Taking 12 hours of operation LED light fixture will last for 2 years and 3 months. For the same hours of operation per day, LED light fixture will last around 11 years. So the onetime investment in LED light is bound for around 11 years whereas the investment of fluorescent light fitting is bound only around 2 years 3 months. Hence for the period of 11 years the existing fittings needs to replace five times.

Now the cost of one light fitting of with T12 fluorescent light fixture for outdoor use is around Rs. 1,000/-. Hence total investment in 40 number is 1000*40 = Rs. 40,000/-. For the period of 11 years, the investment for light fitting of with T12 fluorescent light fixture is five times i.e. 5*40000 = Rs. 200,000/- whereas the investment for LED light fixture is Rs.100,000 only. In long term assessment the initial investment in LED light fixture is 50% less than that of fitting of with T12 fluorescent light fixture. Moreover annual savings in energy cost is around 65%. This savings through end user efficiency is of very significant for conservation of energy.

VI. CONCLUSION

It is found that the improvement of end user efficiency with proposed higher efficient LED light fixture provide significant result for campus lighting system. It is also found that the initial investment is high and the payback period is slightly above 3 years. It is also found that in spite of higher initial investment, the operating life of the LED system is reasonably high which results 50% savings on initial investment on long term basis as compared to existing fluorescent lamp (T12) fixture. It is also found that around 65% of annual energy consumption can be reduced with the proposed scheme.

REFERENCES

[1] M. Lalwani, M. Singh, Conventional and Renewable Energy Scenario of India: Present and Future, *Canadian Journal on Electrical and Electronics Engineering, Vol. 1, No. 6*, October 2010, 122-140
[2] S. P. Ramesh, M Emran Khan, Energy efficiency in green buildings – Indian concept, *International Journal of Emerging Technology and Advanced Engineering*, Volume 3, Special Issue 3, Feb 2013, 329-336
[3] Government of India, 'Load Generation Balance Report 2011-12', A report by Central ElectricityAuthority (CEA), Ministry of Power, available at http://www.cea.nic.in/reports/yearly/lgbr_report.pdf
[4] V. Kumar Yadav, N.P. Padhy and H.O. Gupta, Assessment of Indian Power Sector Reforms Through Productivity Analysis: Pre and Post Electricity Act, 2003, *IEEE PES Transmission and Distribution Conference*, 2010, 1-8
[5] V. S. Verma, 'Energy Efficient Technologies use in India – An Overview 2004', *Bureau of EnergyEfficiency (BEE)*, 20 August 2004
[6] N. V.Vader, R.U.Patil, Energy Conservation In Electrical System, *National conference on recent trends in Engineering & Technology Organized by Agnel Polytechnic, Vashi in association with IIE ZENITH – 2009*, 30 - 31st OCT –09
[7] S. Mukhopadhyay, and A.K. Rajput, Demand side management and load control—an Indian experience, *IEEE power and Energy Society General meeting*, 2010, pp-1-5,
[8] C.C.A Rajan, Demand side management using expert system, *IEEE Conference on Convergent Technologies for Asia-Pacific Region TENCON 2003*.
[9] P. Dabur, G. Singh, N. K. Yadav, Electricity Demand Side Management: Various Concept and Prospects, *International Journal of Recent Technology and Engineering (IJRTE)*, Volume-1, Issue-1, April 2012, ISSN: 2277-3878
[10] A. N. Singh, J. Sharma, Energy Conservation in India: Challenges & Achievements, *International Journal of Mechanical and Industrial Engineering (IJMIE)*, Volume-1, Issue-3, 2012, ISSN No. 2231 –6477
[11] F.Boshell, O.P.Veloza, Review of developed demand side management programs including different concepts and their results, *IEEE/PES trans. On Transmission and Distribution conference and Exposition, Latin America, 2008*.

International Journal of Modern Engineering Research (IJMER)
www.ijmer.com Vol.3, Issue.4, Jul - Aug. 2013 pp-1942-1946 ISSN: 2249-6645

Analysis and Performance evaluation of Traditional and Hierarchal Sensor Network

Uma Narayanan[1], Arun Soman[2]
*(Information Technology, Rajagiri College of Engineering & Technology / M.G University, India)
** (Assistant Professor, Department of Information Technology,Rrajagiri College of Engineering & Technology/ M.G University, Kerala, India)

ABSTRACT: *The paper deals with the working of wireless sensor network. In which it compare the different working of wireless sensor network. Basically there are two types of wireless sensor network, Traditional sensor network and the Hierarchical sensor network. Traditional sensor network is the already available network which uses more battery. But hierarchical sensor network introduces two level of nodes i.e., low end and high end. This will increase the overall lifetime of network. After considerable research it is found out that performance of hierarchical network is more than traditional and it increases the lifetime of network.*

Keywords: *WSN, High-end, Low-end, energy –contraint, Hybrid.*

I. INTRODUCTION

As the technology of wireless networks become increasingly matured and supported by small, micro-mobile devices fully, wireless sensor network has gradually become a research hotspot. A wireless sensor network (WSN) consists of a number of sensor nodes (few tens to thousands) with the capability of storing, processing and relaying the sensed data, and often has a base station called Sink for further computation. It has very broad application prospects and great potential value in many areas, such as in the military and national defense, environmental monitoring, and biomedical, smart homes, remote monitoring dangerous areas, and so no.

However, in wireless sensor networks, because sensor nodes are energy-constrained, efficient use of energy is the key issues of wireless sensor networks. In addition to using energy efficiently, according to the requirements of different applications, wireless sensor networks need to meet the different performance, such as the delay of network pockets, the reliability of data transmission and the connectivity of Network.

II. THE ARCHITECTURE FOR TRADITIONAL WIRELESS SENSOR NETWORK

The architecture of traditional wireless sensor network generally adapts flat structure (i.e. single-layer planar structure). We also call this kind network flat wireless sensor network [1]. A large number of sensor nodes with the same hardware structure, and poor the sensing, processing, and communicating capabilities are deployed in the monitoring area, and transmit and forward information gathered by the other sensor nodes to sink node using the form of multi-hop under the help of other nodes within wireless sensor network. And then wireless sensor network is connected with other types of networks by sink node, finally the user can remotely access, queries and manage the wireless sensor network [2]. Most study of wireless sensor networks aim for flat wireless sensor network, such as single-hop wireless sensor networks [3], the traditional multi-hop wireless sensor networks, and so on. A typical architecture of traditional wireless sensor network is shown as Figure 1.

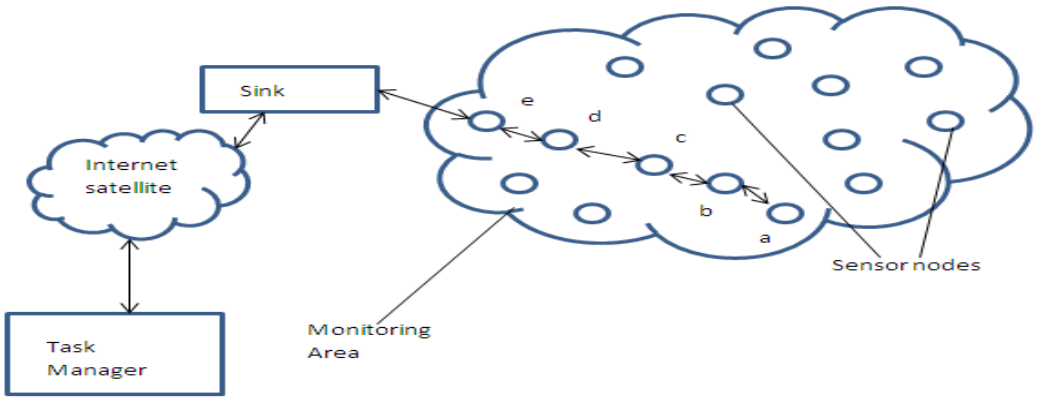

Fig 1: A typical architecture of traditional wireless sensor network

.

In flat wireless sensor network, the larger network size is, the more data lost in communication path, and the worse the network performance is. At the same time, the large flat wireless sensor network also lead to intermediate nodes for forwarding data more energy consumption and energy heterogeneous problems arise. Therefore, there are a large number of practical applications where a hierarchical wireless sensor network is more appropriate, such as IPv6 wireless sensor networks [4], hybrid wireless sensor networks [5-6], multiple sinks wireless sensor networks [7] and wireless sensor networks with mobile sinks [8] and so on. Hierarchical wireless sensor network is usually composed of some kinds of

heterogeneous devices which mainly act as sinks that are responsible for gathering and forwarding data from underlying sensor nodes. Some of them are energy-rich or rechargeable, some have better capability of communication than that of sensor nodes, and some even are able to move randomly. These features can not only improve the network performance such as energy-efficiency, throughput, reliability and scalability, but also extend the potential applications and make commercial implementation easy [9].

In traditional wireless sensor networks, the sink nodes and the sensor nodes are generally assumed to be static. We usually ignore the impact of the mobility coming from sensor nodes on the network. In some scenarios which need the sensor nodes are mobile, the traditional network architecture is no longer applicable [10], such as in the field of medical care, the prevention of infectious diseases in airport immigration, and so on. In these areas, the tiny sensor nodes can be worn on the patient's body, and randomly move with the movement of patients in the monitoring region, and patients can enter and leave the care area at any time, so the number and density of network nodes are quite different at different network moments. At the same time, we need to ensure the real-time of network and energy efficiency of sensor nodes. The flat wireless sensor network is difficult to meet these requirements. On the one hand, when the sensor nodes randomly move in the region, they may be unconnected with other sensor nodes and then become isolated nodes, which will result in significant network delay; on the other hand, with the growth of the network size, the hop number between the source sensor node and the sink node will increase significantly, which will cause intermediate sensor nodes to increase the energy consumption and prolong data delay; besides, because the sensor nodes are mobile, the collision probability of sensing data will rapidly increase in the process of transmission, which will also grow the network delay and energy loss of sensor nodes.

III. HIERARCHICAL NETWORK ARCHITECTURE

To design a low-power, low-delay wireless sensor networks with mobile sensor nodes is a very difficult task. On the one hand, the topology of such wireless sensor network has very high dynamics and mobility; on the other hand, the mobile sensor nodes have very poor sensing, processing, and transmitting capabilities. With the expansion of network scale, flat wireless mobile networks are difficult to achieve the dynamic extension of the mobile sensor nodes and to adapt to network topology changes. At the same time, it also cannot meet the requirements of energy consumption and data delay caused by the dynamic extension of the network sensor nodes. Therefore, the flat network architecture is not suitable for mobile wireless sensor networks [11]. And then, designing multiple layer network architecture for mobile wireless sensor network is necessary, which can meet the energy efficiency of sensor nodes and the real-time of data transmission.

A. Network Structure

In order to make energy consumption and pocket delay achieve an ideal state, we present hierarchical mobile wireless sensor network architecture which has a large of mobile sensor nodes. In the network architecture, we will increase a small number of high-end routing nodes in flat mobile wireless sensor networks and these high-end routing nodes keep connection each and are responsible for collecting and forwarding the sensing data from sensor nodes. Simultaneously, they have abundant resources, and their position remain unchanged; while relative to the high-end routing nodes, the sensor nodes, namely low-end nodes, are only responsible for sensing data and reporting of the data to the high-end routing nodes, and they cannot communicate with the other sensor nodes. The hierarchical mobile wireless sensor network architecture is divided into two layers, shown in Figure 2:

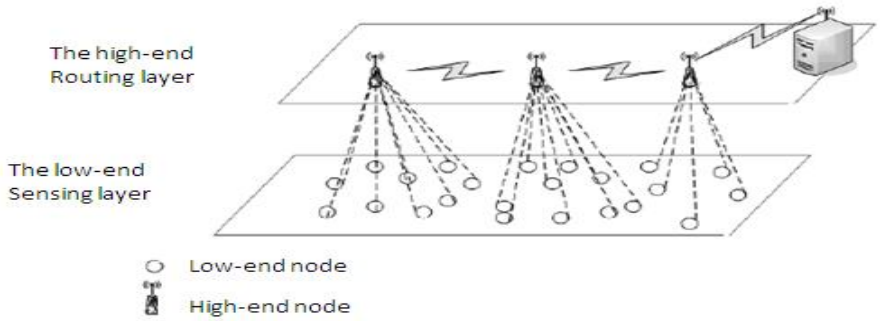

Fig 2: Architecture of hierarchical mobile wireless sensor network

a) The low-end sensing layer: A large number of sensor nodes with poor resource are randomly deployed in the specified region and can randomly change its location; they are responsible for sensing interesting data in the monitoring region, and send the sensing data to the static high-end routing nodes in single-hop form, after the sensor nodes obtain the interesting data. Then the high-end routing nodes route the sensing data to sink by muti-hops in the high-end routing layer after collecting data from sensor nodes.

b) The high-end routing layer: This routing layer consists of a small number of static high-end routing nodes, and plays the role of gathering and forwarding the sensing data obtained by sensor nodes, and their processing, communication, storage capabilities are stronger than the mobile sensor nodes, even they can get continuous power supply. The data will be transmitted in multi-hop form between the high-end routing nodes until it do not arrive sink

B. Network Features

Hierarchical mobile wireless sensor network with mobile sensor nodes belongs to heterogeneous wireless sensor network and adapts the hierarchical means to organize mobile wireless sensor network. It combines the relative stability model and the absolute mobility model.

a) Static relative stability model: Static high-end routing nodes constitute a relatively stable high-layer sub-network. This sub-network follows mesh structure and its location is relatively stable, which inherited the relatively static features of traditional wireless sensor network. In addition, the high-layer sub-network has a small number of high-end routing nodes so that the average transmission hops of the sensing data obtained by sensor nodes in the network will decrease, which effectively reduce the transmission delay of network. At the same time, in order to ensure the reliability of data transmission, the high-end routing nodes can have rich resources.

b) The absolute mobility model: A large number of sensor nodes, namely low-end sensing nodes, and high-end routing nodes constitute many low-layer mobile sub-networks which belong to single-hop mobile wireless sensor network. Sensor nodes within such single-hop mobile wireless sensor network can randomly move in monitoring region and do not directly communicate with each other. Multiple sensor nodes and a high-end routing node form a single-hop wireless sensor network which shows star topology, and single-hop network adapt media access time-division multiplexing technology to avoid large amounts of data collision when the sensor nodes compete to use wireless channel, which reduce pocket delay of network's and energy consumption of mobile sensor node's. Moreover, it can ensure the expansion of the network. A hierarchical mobile wireless sensor network with mobile sensor nodes is composed of many such single-hop mobile wireless sensor networks.

C. Node Work Process

a) The work process of sensor nodes: In the hierarchical mobile wireless sensor network with mobile sensor nodes, the sensor nodes can freely move and change their positions. Since there exist many high-end routing nodes in network, the routing nodes around the sensor nodes may be more than one, so the sensor node wanted to report sensing data should select one routing node which has smallest distance and apply to it for registration. The sensor node can collect the environmental data and send it to the routing node after successfully registers, then the sensor nodes into sleep and wait for the next task. The work process of sensor nodes is shown as Figure 3.

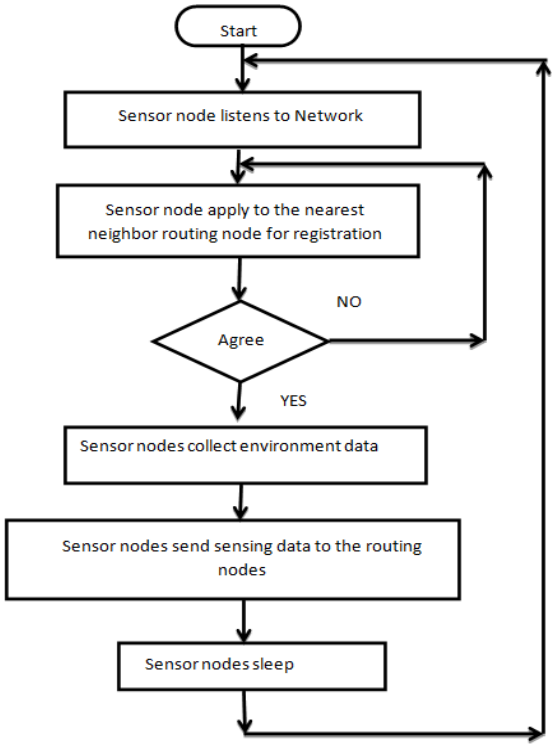

Fig 3: Flow Chart for the working of sensor nodes

b) The work process of routing nodes: In the hierarchical mobile wireless sensor network with mobile sensor nodes, the high-end routing nodes are responsible for the collection and forwarding of sensing data. When the high-end nodes work, they always listen to the state of wireless sensor network and determine whether there are registrations in the network. If the routing nodes find there are some nodes to register, then they obtain the relevant information of registrations and judge the type of registered nodes. If they are sensor nodes, the routing nodes add them to the set of sensor nodes, or add them to the set of neighbor nodes. When the routing nodes need to transmit data, they firstly determine the data will be transmitted to whom, sensor nodes or neighbor routing nodes. If target is sensor nodes, then the routing nodes directly send the data to sensor nodes, otherwise to neighbor routing nodes. The work process of routing nodes is shown as Figure 4.

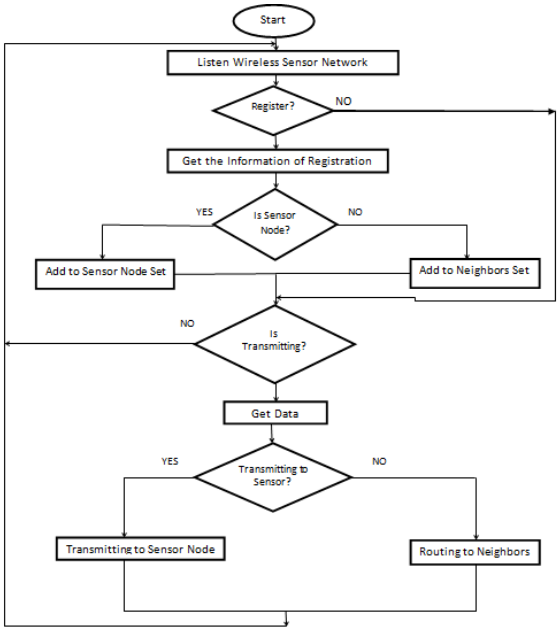

Fig 4: The work process of routing node

IV. SIMULATION

We evaluate two different performance metrics which are crucial to prolong the lifetime of wireless sensor network and improve the quality of delay. The data delivery delay is referred to the duration from data generation to data reception by sink. For evaluating the lifetime of the network, we observe the total remaining energy of mobile sensor nodes.

In this paper, we make simulation using ns2 in the Linux environment, the simulation region is set to 50 × 50 rectangle, and the scenarios of the movement and cbr traffic are generate by the corresponding tools of ns2. The moving speeds of sensor nodes are set from 1 to 5m per second, the communication range is set as 15m, and the size of packets is 1024 byte. Simulation time is set to 100s, the initial energy of sensor nodes are 100. The sending and receiving energy of node is set as 1, idle listening energy is 0.5, and dormant energy is 0.1. It generates 4 trace file after 4 groups of Simulation, and we process the 4 trace file and display the consequence by gnuplot tool which is Linux native tool.

Energy Analysis

In this section, we will analyze the energy consumption of the network by the simulations. Our approach is to calculate the corresponding total remaining energy of every moment using the trace files for both kinds of mobile wireless sensor network with the same number of mobile sensor nodes—one is flat mobile wireless sensor network, another is hierarchical mobile wireless sensor network, and then to compare total remaining energies of both kinds of mobile wireless sensor network in the same moment. In a certain moment, if one of two kind mobile wireless sensor networks has a large total remaining energy, it must have small energy consumption. On the contrary, we could also say that if one mobile wireless sensor network has larger energy consumption than another one, it must have smaller total remaining energy when the two mobile wireless sensor networks have the same total initial energy. In this paper, the four experiments have been made. The flat mobile wireless sensor network which have 30 mobile sensor nodes, and the hierarchical mobile wireless sensor network which have also 30 mobile sensor nodes. We have compared the total remaining energy of tow kind mobile wireless sensor networks which have the same number of mobile sensor nodes at different moment. The results of experiments are shown in Figure 5. Finally, we can conclude by the experiment results that the hierarchical mobile wireless senor network has better energy efficiency than flat mobile wireless sensor network.

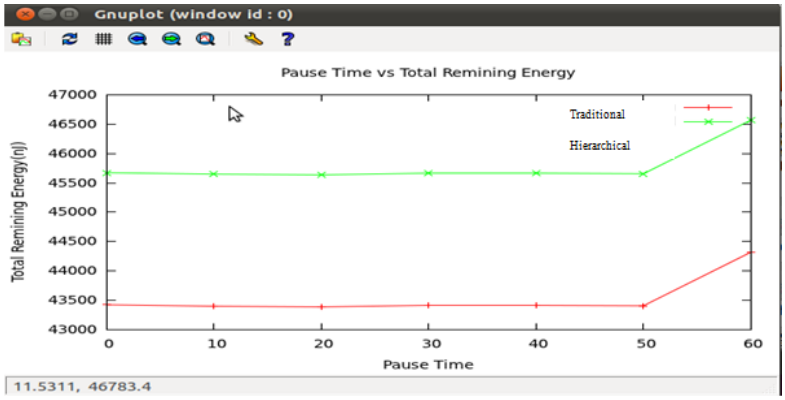

Fig 5: Remaining energy for traditional and hierarchical

V. CONCLUSION

We can conclude that the total energy consumption and pocket delay of flat mobile wireless sensor network are increasing with the growth of network size, and the loss rate of the mobile sensor nodes' data is higher, which makes the weak stability of network. When we adapt the hierarchical network architecture, the total energy consumption and pocket delay can be effectively reduced. Sensing data can be reliably transmitted, and network is connectivity at all moments in the state. Hierarchical wireless sensor network can be applied to the scenarios with mobile sensor nodes effectively.

REFERENCES

[1] F.G. Nakamura, F.P. Quintao, G.C. Menezes, and G.R. Mateus. An Optimal Node Scheduling for flat Wireless Sensor Networks. In Proceedings of the IEEE InternationalConference on Networking (ICN05), volume 3420, pages 475–483, 2005.
[2] LI Ying-chun, ZHU Shi-bing, CHEN Gang. Research on Wireless Sensor Network Architecture [J]. Shanxi Electronic Technology. 2009. (4):71-73.
[3] Singh M, Prasanna V K. Energy optimal and energy balanced sorting in a single hop sensor network[A].IEEE Conference on Pervasive Computing and Communications (PERCOM) [C] .Washington, DC, USA:IEEE ComputeSociety, 2003.50—59.
[4] WANG Xiao-nan, QIANHuan-yan, TANG Zhen-min. Routing protocol for wireless sensor networks based on 6LoWPAN [J]. Application Research of Computer.2009.26 (10).3881-3887.
[5] Ren,B.,Ma,J.,and Chen,C.The hybrid mobile wireless sensor networks for data gathering.In Proceeding of the international Conference on Communications and Mobile Computing,2006
[6] R. S. Marin-Perianu, J. Scholten, P. J. M. Havinga, and P. H. Hartel. Cluster-based service discovery for heterogeneous wireless sensor networks. International Journal of Parallel, Emergent and Distributed Systems, 23(4):325–346, August 2008.
[7] Wenning, B.-L., Lukosius, A., Timm-Giel, A., G? rg, C., Tomic, S. Opportunistic Distance-aware Routing in Multi-Sink Mobile Wireless Sensor Networks. Proc. ICT Mobile Summit 2008.
[8] Hiren K, Deva S, Avijit K, Rajib M. Energy Efficient Communication Protocol for a Mobile Wireless Sensor Network System[C]. International Journal of Computer Science and Network Security (IJCSNS), 2009.2(9):386-394
[9] Ren,B.,Ma,J.,and Chen,C.The hybrid mobile wireless sensor networks for data gathering.In Proceeding of the international Conference on Communications and Mobile Computing,2006
[10] CHEN Chen, XIE Wei-guang, PEI Qing-qi. Research on Mobility Support in Wireless Sensor Networks [J].Computer Scienc.2009. 29 (10):27-31.
[11] GUO Jiang, FENG Bin. Design of Adaptive Architecture for Mobile Wireless Sensor Networks [J]. Micronanoelectronic Fechnolo, 2007. (7/8):480-482.

International Journal of Modern Engineering Research (IJMER)
www.ijmer.com Vol. 3, Issue. 4, Jul - Aug. 2013 pp-1947-1457 ISSN: 2249-6645

Composite Analysis of Phase Resolved Partial Discharge Patterns using Statistical Techniques

Yogesh R. Chaudhari[1], Namrata R. Bhosale[2], Priyanka M. Kothoke[3]
[1]*School of Engineering and Technology, Navrachana University, India*
[2,3]*Department of Electrical Engineering, Veermata Jijabai Technological Institute, University of Mumbai, India)*

ABSTRACT : *Partial discharges (PDs) in high-voltage (HV) insulating systems originate from various local defects, which further results in degradation of insulation and reduction in life span of equipment. One of the most widely used representations is phase-resolved PD (PRPD) patterns. For reliable operation of HV equipment, it is important to observe statistical characteristics of PDs and identify the properties of defect to ultimately determine the type of the defect. In this work, we have obtained and analysed combined use of PRPD patterns (φ-q), (φ-n) and (n-q) using statistical parameters such as skewness and kurtosis for (φ-q) and (φ-n),and mean, standard deviation, variance, skewness and kurtosis for (n-q).*

Keywords: *Kurtosis, Partial Discharge, Phase- Resolved, Skewness and Statistical Techniques*

I. INTRODUCTION

PD is an incomplete electrical discharge that occurs between insulation or insulation and a conductor. Partial discharges occur wherever the electrical field is higher than the breakdown field of an insulating medium. There are two necessary conditions for a partial discharge to occur in a cavity: first, presence of a starting electron to initiate an avalanche and second, the electrical field must be higher than the ionization inception field of the insulating medium [1]. In general, PDs are concerned with dielectric materials used, and partially bridging the electrodes between which the voltage is applied. The insulation may consist of solid, liquid, or gaseous materials, or any combination of them. PD is the main reason for the electrical ageing and insulation breakdown of high voltage electrical apparatus. Different sources of PD give different effect on insulation performance. The occurrence of sparks, arcs and electrical discharges is a sure indication that insulation problems exist. Therefore, PD classification is important in order to evaluate the harmfulness of the discharge [11].
PD classification aims at the recognition of discharges of unknown origin. For many years, the process was performed by investigating the pattern of the discharge using the well known ellipse on an oscilloscope screen, which was observed crudely by eye. Nowadays, there has been extensive published research to identify PD sources by using intelligent technique like artificial neural networks, fuzzy logic, and acoustic emission [11].

There seems to be an expectation that, with sufficiently sophisticated digital processing techniques, it should be possible not only to gain new insight into the physical and chemical basis of PD phenomena, but also to define PD 'patterns' that can be used for identifying the characteristics of the insulation 'defects' at which the observed PD occur [2].

Broadly, there are three different categories of PD pulse data patterns gathered from the digital PD detectors during the experiments. They are: phase-resolved data, time-resolved data and data having neither phase nor time information. The phase-resolved data consist of three-dimensional discharge epoch, φ charge transfer, q discharge rate, n patterns (φ~q, q~n and φ~n patterns) at some specific test voltage. The time-resolved data constitute the individual discharge pulse magnitudes over some interval of time, i.e., q~t data pattern. The third category of data consists of variations in discharge pulse magnitudes against the amplitude of the test voltage, V (for both increasing and decreasing levels), i.e., q~V data [3].

There are many types of patterns that can be used for PD source identification. If these differences can be presented in terms of statistical parameters, identification of the defect type from the observed PD pattern may be possible [4]. As each defect has its own particular degradation mechanism, it is important to know the correlation between discharge patterns and the kind of defect. Therefore, progress in the recognition of internal discharge and their correlation with the kind of defect is becoming increasingly important in the quality control in insulating systems [5]. Researches have been carried out in recognition of partial discharge sources using statistical techniques and neural network. In our study, we have tested various internal and external discharges like void, surface and corona using statistical parameters such as skewness and kurtosis for (φ-q) and (φ-n) and mean, standard deviation, variance, skewness and kurtosis for (n-q).

II. STATISTICAL PARAMETERS

The important parameters to characterize PDs are phase angle φ, PD charge magnitude q and PD number of pulses n. PD distribution patterns are composed of these three parameters. Statistical parameters are obtained for phase resolved patterns (φ-q), (φ-n) and (n-q).

2.1 Processing of data

The data to be processed obtained from generator includes *φ, q, n* and voltage *V*. From this data, phase resolved patterns are obtained.

2.1.1. *Analysis of Phase-Resolved (φ-q) and (φ-n) using Statistical Techniques*

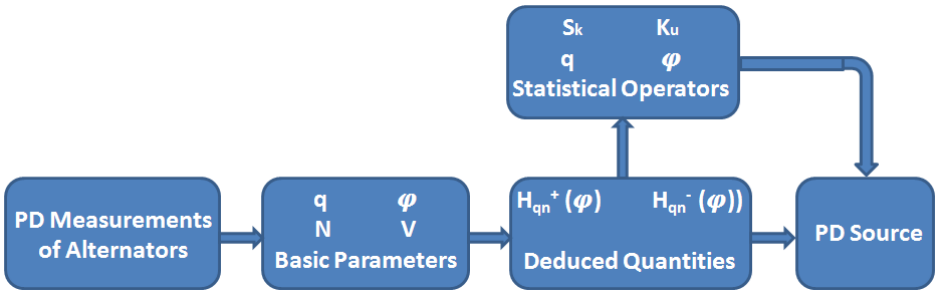

Fig.1 (a) Block diagram of discharge analysis for (φ-q)

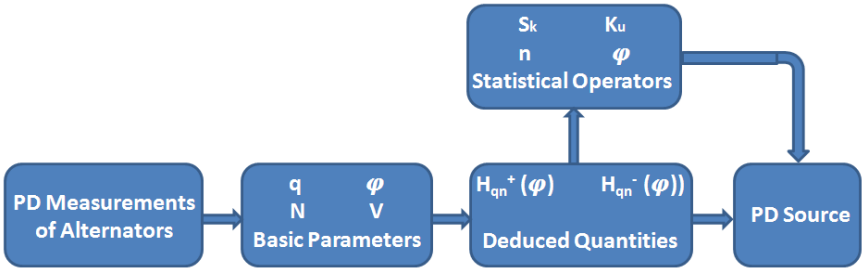

Fig.1 (b) Block diagram of discharge analysis for (φ-n)

PD pulses are grouped by their phase angle with respect to 50 (± 5) Hz sine wave. Consequently, the voltage cycle is divided into phase windows representing the phase angle axis (0 to 360'). If the observations are made for several voltage cycles, the statistical distribution of individual PD events can be determined in each phase window. The mean values of these statistical distributions results in two dimensional patterns of the observed PD patterns throughout the whole phase angle axis [6]. A two-dimensional (2D) distribution φ-q and φ-n represents PD charge magnitude 'q' and PD number of pulses 'n' as a function of the phase angle 'φ' [3].

The mean pulse height distribution H_{qn} (φ) is the average PD charge magnitude in each window as a function of the phase angle φ. The pulse count distribution H_n (φ) is the number of PD pulses in each window as a function of phase angle φ. These two quantity are further divided into two separate distributions of the negative and positive half cycle resulting in four different distributions to appear: for the positive half of the voltage cycle H_{qn}^+ (φ) and H_n^+ (φ) and for the negative half of the voltage cycle H_{qn}^- (φ) and H_n^- (φ) [5]. For a single defect, PD quantities can be described by the normal distribution. The distribution profiles of H_{qn} (φ) and H_n (φ) have been modeled by the moments of the normal distribution: skewness and kurtosis.

$$\text{Skewness } (S_k) = \frac{\sum_{i=1}^{N}(x_i - \mu)^3 f(x_i)}{\sigma^3 \sum_{i=1}^{N} f(x_i)} \qquad \dots\dots\dots (1)$$

$$\text{Kurtosis: } (K_u) = \frac{\sum_{i=1}^{N}(x_i - \mu)^4 f(x_i)}{\sigma^4 \sum_{i=1}^{N} f(x_i)} - 3 \qquad \dots\dots\dots (2)$$

where,

f(x) = PD charge magnitude q,
μ = average mean value of q,
σ = variance of q.

Skewness and Kurtosis are evaluated with respect to a reference normal distribution. Skewness is a measure of asymmetry or degree of tilt of the data with respect to normal distribution. If the distribution is symmetric, Sk=0; if it is asymmetric to the left, Sk>0; and if it is asymmetric to the right, Sk<0. Kurtosis is an indicator of sharpness of distribution. If the distribution has same sharpness as a normal distribution, then Ku=0. If it is sharper than normal, Ku>0, and if it is flatter, Ku<0 [3] [7].

2.1.2. *Analysis of Phase-Resolved (q-n) using Statistical Techniques*

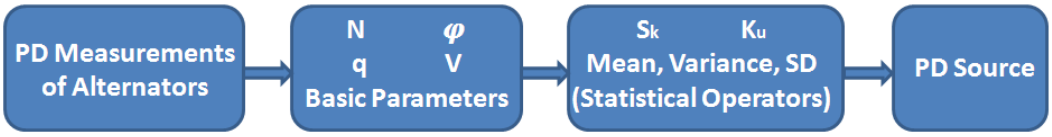

Fig. 2 Block diagram of discharge analysis for (n-q)

Where,
S.D = standard deviation
Sk = skewness

Ku = kurtosis

Statistical analysis is applied for the computation of several statistical operators. The definitions of most of these statistical operators are described below. The profile of all these discrete distribution functions can be put in a general function, i.e., $y_i=f(x_i)$. The statistical operators can be computed as follows:

$$\text{Mean Value: } (\mu) = \frac{\sum_{i=1}^{N}(x_i)\, f(x_i)}{\sum_{i=1}^{N} f(x_i)} \quad \ldots\ldots\ldots (3)$$

$$\text{Variance: } (\sigma^2) = \frac{\sum_{i=1}^{N}(x_i-\mu)^2\, f(x_i)}{\sum_{i=1}^{N} f(x_i)} \quad \ldots\ldots\ldots (4)$$

$$\text{Standard Deviation} = \sqrt{Variance} \quad \ldots\ldots\ldots (5)$$

where,

x = number of pulses n,
f(x) = PD charge magnitude q,
μ = average mean value of PD charge magnitude q,
σ = variance of PD charge magnitude q

Skewness and Kurtosis are evaluated with respect to a reference normal distribution as described in section 2.1.1.

III. RESULTS AND DISCUSSIONS

Analysis involves determining unknown PD patterns by comparing those with known PD patterns such as void, surface and corona. The comparison is done with respect to their statistical parameters [9] [10].

3.1. Analysis for (φ-q)

The phase resolved patterns are divided into two types: (φ-q) and (φ-n). The phase resolved patterns (φ-q) are obtained for three known PD patterns: void, surface and corona (as discussed in 3.1.1) and three unknown PD patterns: data1, data2 and data3 (as discussed in 3.1.3) [9]

3.1.1. 2D distribution of (□-q) for known PD patterns

We have obtained the results from known PD parameters so as to plot the graphs showing below in Fig.3 (a), Fig.3 (b) and Fig.3 (c). These graphs are the phase φ vs. charge q plot for void, surface and corona discharges respectively.

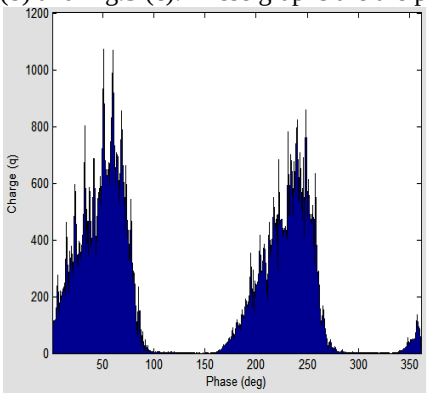

Fig.3(a).Phase plot (φ-q) of void discharge

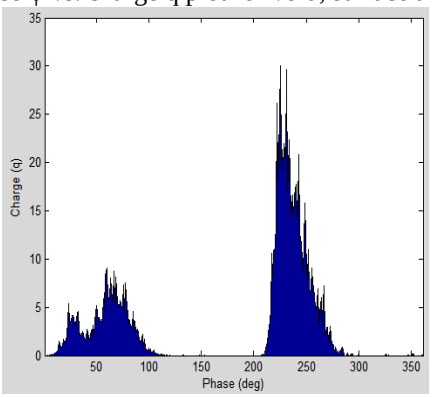

Fig.3(b). Phase plot (φ-q) of surface discharge

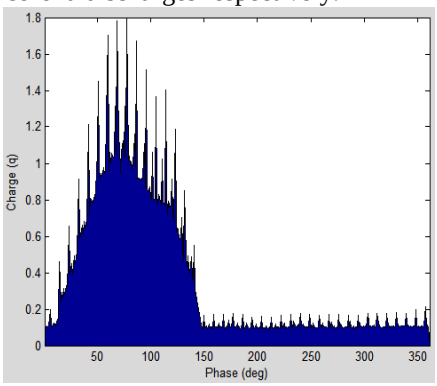

Fig.3(c). Phase plot (φ-q) of corona discharge

3.1.2. Parameters of known PD patterns

The table I below is the average value of skewness and kurtosis where values for H_{qn}^{+} (φ) are obtained over 0^0 to 180^0 on the other hand values for H_{qn}^{-} (φ) are obtained over $181^0$to 360^0, representing the phase. These values are obtained for known PD parameters.

TABLE I. PARAMETERS OF KNOWN PD PATTERNS

Parameter	void	surface	corona
Skewness H_{qn}^{+} (φ)	1.0013	1.2134	0.3555
Skewness H_{qn}^{-} (φ)	0.9901	1.8219	1.3659
Kurtosis H_{qn}^{+} (φ)	2.9046	3.6064	2.4354
Kurtosis H_{qn}^{-} (φ)	2.7872	5.4506	7.5947

3.1.3. 2D distribution of (□-q) for unknown PD patterns

We have obtained the results from unknown PD parameters so as to plot the graphs showing below in Fig.4 (a), Fig.4 (b) and Fig.4 (c) which are the phase φ vs. charge q plot for data1, data2 and data3 respectively.

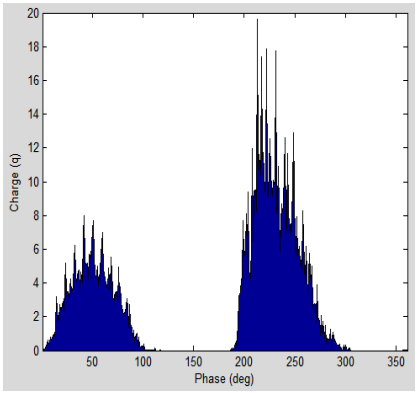

Fig.4 (a) Phase plot (φ-q) of data1

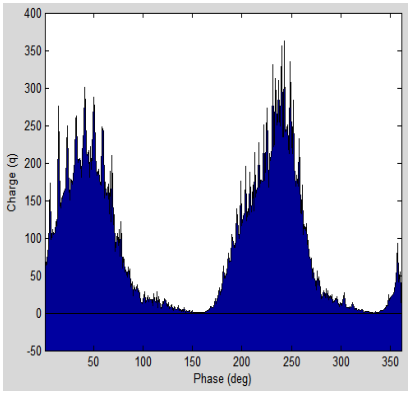

Fig.4 (b) Phase plot (φ-q) of data2

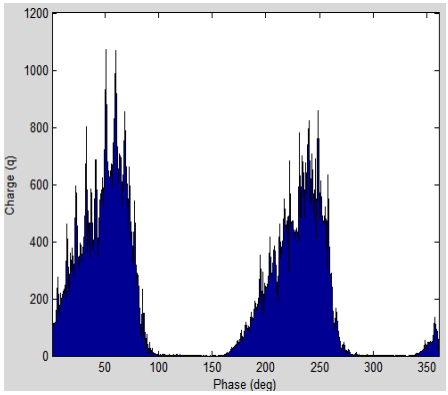

Fig.4 (c) Phase plot (φ-q) of data3

From Fig.4 (a), it is seen that the following plot is similar to void and surface discharge. Fig.4 (b), is also similar to void and surface discharge and Fig.4(c), is similar to void discharge.

3.1.4. Parameters of unknown PD Patterns

The table II below is the average value of skewness and kurtosis where values for H_{qn}^{+} (φ) are obtained over 0^0 to 180^0 on the other hand values for H_{qn}^{-} (φ) are obtained over $181^0$to 360^0, representing the phase. These values are obtained for unknown PD parameters.

TABLE II. PARAMETERS OF UNKNOWN PD PATTERNS

Parameter	data1	data2	data3
Skewness H_{qn}^{+} (φ)	0.8991	0.7456	1.0013
Skewness H_{qn}^{-} (φ)	1.1833	0.8509	0.9901
Kurtosis H_{qn}^{+} (φ)	2.5719	2.1814	2.9046
Kurtosis H_{qn}^{-} (φ)	3.7467	2.6512	2.7872

3.2. Analysis for (φ-n)

The phase resolved (φ-n) patterns consist of three known PD patterns: void, surface and corona (as discussed in 3.2.1) and three unknown PD patterns: data1, data2 and data3 (as discussed in 3.2.3) [9]. The plots are discussed below:

3.2.1 Phase resolved plot (□-n) of known PD patterns

We have obtained the results from known PD parameters so as to plot the graphs showing below Fig.5 (a), Fig.5 (b) and Fig.5 (c) are the phase φ vs. number of pulses n for void, surface and corona discharges respectively.

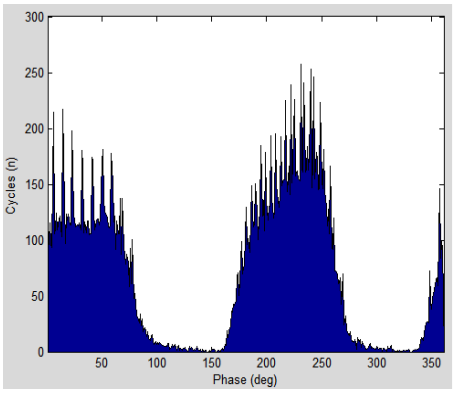

Fig.5(a). Phase plot (φ-n) of void discharge

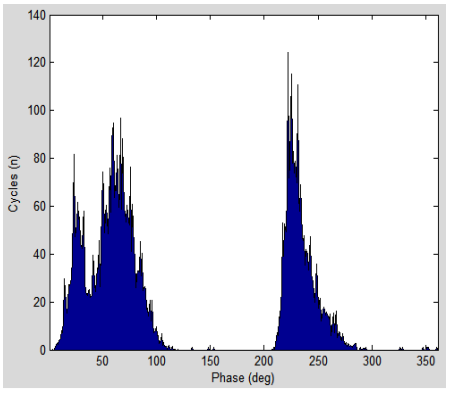

Fig.5(b). Phase plot (φ-n) of surface discharge

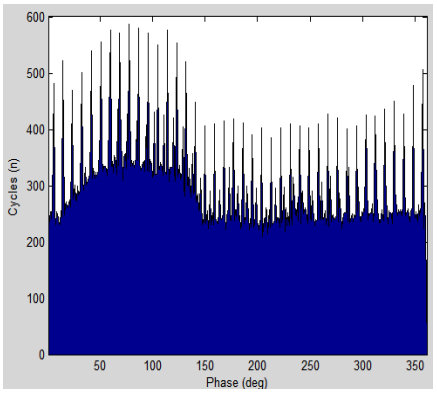

Fig.5(c). Phase plot (φ-n) of corona discharge

3.2.2. Parameters of known PD Patterns

The table III below is the average value of skewness and kurtosis where values for H_n^{+} (φ) are obtained over 0^0 to 180^0 on the other hand values for H_n^{-} (φ) are obtained over $181^0$to 360^0, representing the phase. These values are obtained for known PD parameters.

TABLE III. PARAMETERS OF KNOWN PD PATTERNS

Parameter	void	surface	corona
Skewness $H_n^+(\varphi)$	0.4954	1.0082	1.3942
Skewness $H_n^-(\varphi)$	0.4329	2.3686	1.3798
Kurtosis $H_n^+(\varphi)$	2.0535	2.871	4.8337
Kurtosis $H_n^-(\varphi)$	1.9137	8.4788	7.3215

3.2.3. Phase resolved plot (□-n) of unknown PD patterns

We have obtained the results from unknown PD parameters so as to plot the graphs showing below Fig.6(a), Fig.6(b) and Fig.6 (c) are the phase φ vs. number of pulses n for void, surface and corona discharges respectively.

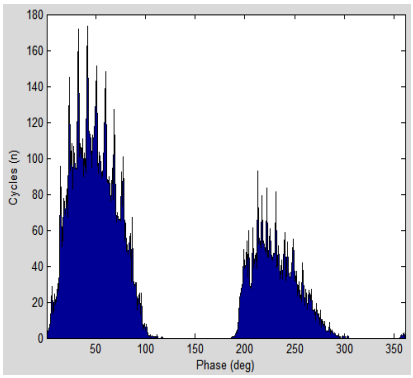

Fig.6(a). Phase plot (φ-n) of data1

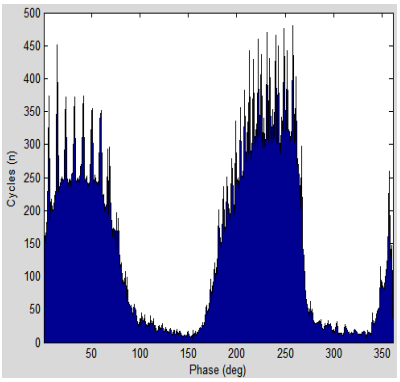

Fig.6(b). Phase plot (φ-n) of data2

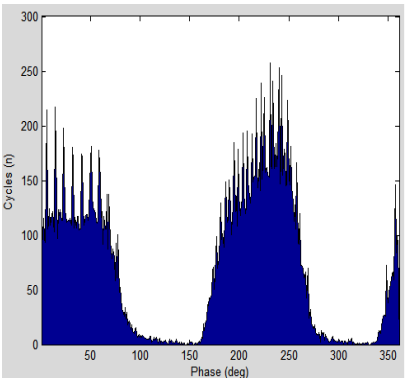

Fig.6(c). Phase plot (φ-n) of data3

From Fig.6 (a), it is seen that the following plot is similar to void and surface discharge. Fig.6 (b), is similar to void discharge and Fig.6 (c), is also similar to void discharge

3.2.4. Parameters of unknown PD patterns

The table IV below is the average value of skewness and kurtosis where values for $H_n^+(\varphi)$ are obtained over 0^0 to 180^0 on the other hand values for $H_n^-(\varphi)$ are obtained over $181^0$to 360^0, representing the phase. These values are obtained for unknown PD parameters.

TABLE IV. PARAMETERS OF UNKNOWN PD PATTERNS

Parameter	data1	data2	data3
Skewness $H_n^+(\varphi)$	0.8016	0.574	0.4954
Skewness $H_n^-(\varphi)$	1.0169	0.42	0.4329
Kurtosis $H_n^+(\varphi)$	2.3724	2.1091	2.0535
Kurtosis $H_n^-(\varphi)$	3.2011	1.8003	1.9137

3.3. Analysis for (n-q)

The phase resolved patterns n-q are obtained for three known PD patterns: void, surface and corona (as discussed in 3.3.1) and three unknown PD patterns: data1, data2 and data3 (as discussed in 3.3.3) [10].

3.3.1. 2D distribution of n-q for known PD patterns

We have obtained the results from known PD parameters so as to plot the graphs showing below Fig. 7(a), Fig. 7(b), Fig. 7(c), Fig. 7(d) and Fig. 7(e) are the n-q plot of mean, standard deviation, variance, skewness and kurtosis for void discharge respectively.

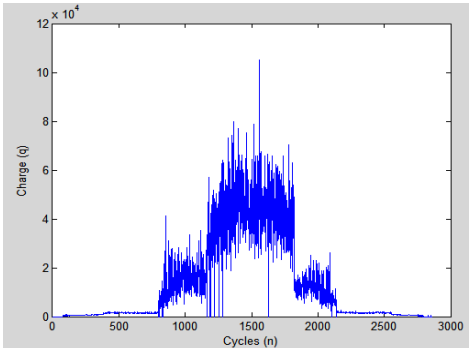

Fig.7(a). Mean plot (n-q) of void discharge

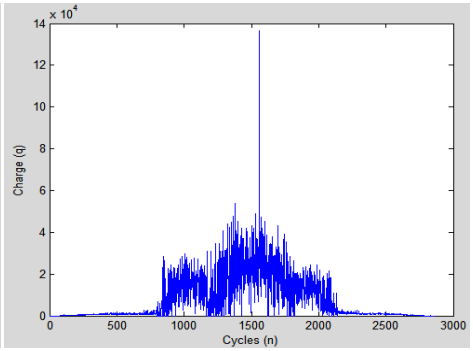

Fig.7(b). Standard deviation plot (n-q) of void discharge

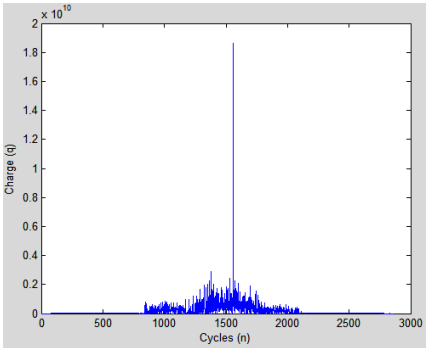

Fig.7(c). Variance plot (n-q) of void discharge

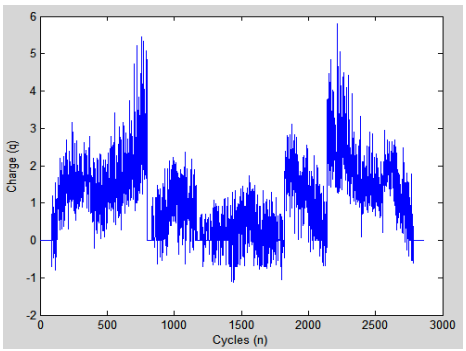

Fig.7 (d) Skewness plot (n-q) of void discharge

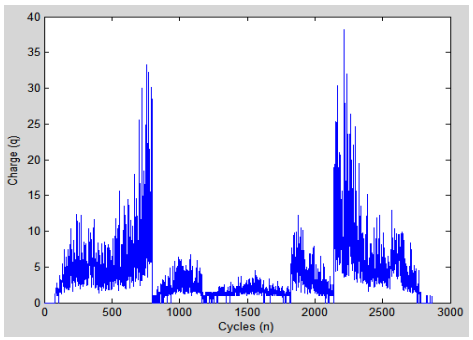

Fig.7 (e) Kurtosis plot (n-q) of void discharge

Referring to Fig. 7 (a), Fig. 7 (b) and Fig. 7 (c) of void discharge, it can be seen there is a peak occurring somewhere after 1500 cycle, which is a void discharge and in Fig. 7 (d) and Fig. 7 (e) of skewness and kurtosis, the value decreases at that cycle where peak occurs.

We have obtained the results from unknown PD parameters so as to plot the graphs showing below Fig. 8(a), Fig. 8(b), Fig. 8(c), Fig. 8(d) and Fig. 8(e) are the n-q plot of mean, standard deviation, variance, skewness and kurtosis for surface discharge respectively.

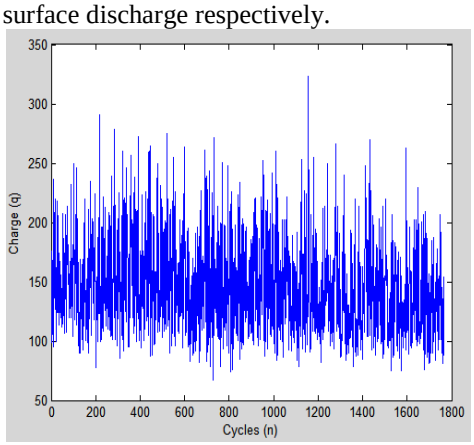

Fig.8 (a) Mean plot (n-q) of surface discharge

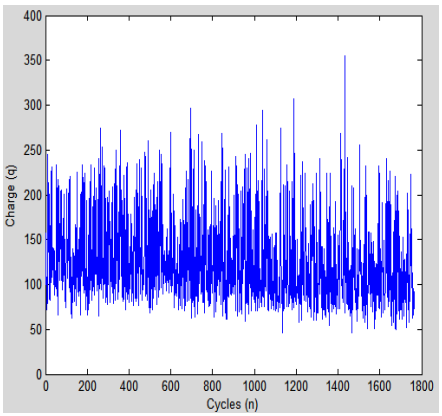

Fig.8 (b) Standard deviation plot (n-q) of surface discharge

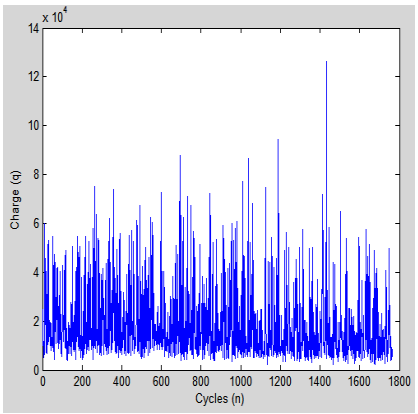

Fig.8 (c) Variance plot (n-q) of surface discharge

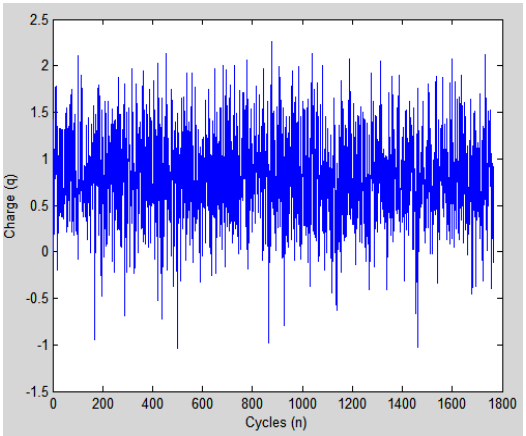

Fig.8 (d) Skewness plot (n-q) of surface discharge

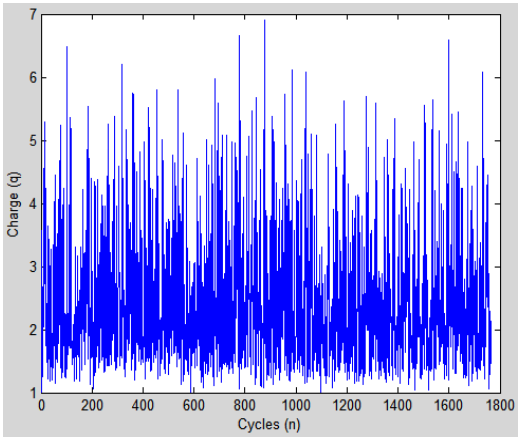

Fig.8 (e) Kurtosis plot (n-q) of surface discharge

In surface discharge, charges are distributed uniformly over all cycles for mean, standard deviation, variance, skewness and kurtosis as shown in Fig. 8(a), Fig. 8(b), Fig. 8(c), Fig. 8(d) and Fig. 8(e). Fig. 9(a), Fig. 9(b), Fig. 9(c), Fig. 9(d) and Fig. 9(e) are the n-q plot of mean, standard deviation, variance, skewness and kurtosis for corona discharge respectively.

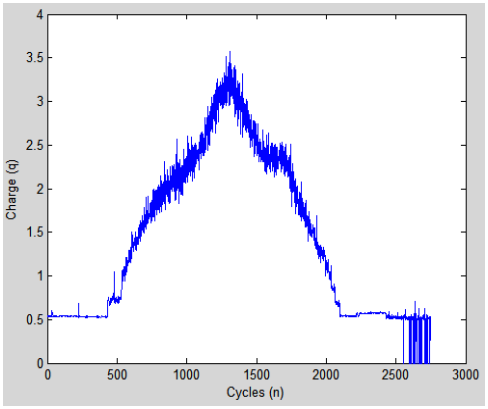

Fig.9 (a) Mean plot (n-q) of corona discharge

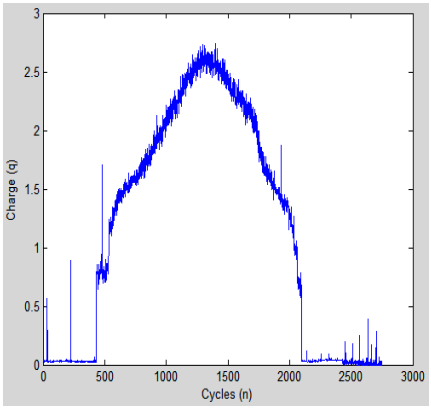

Fig.9 (b) Standard deviation (n-q) of corona discharge

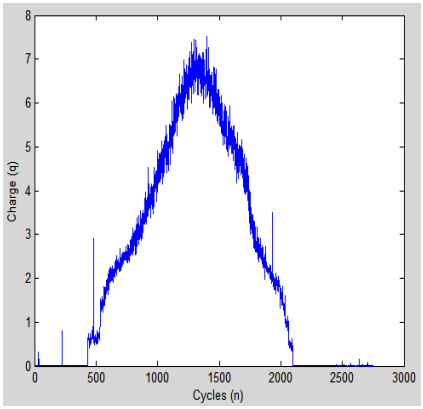

Fig.9 (c) Variance plot (n-q) of corona discharge

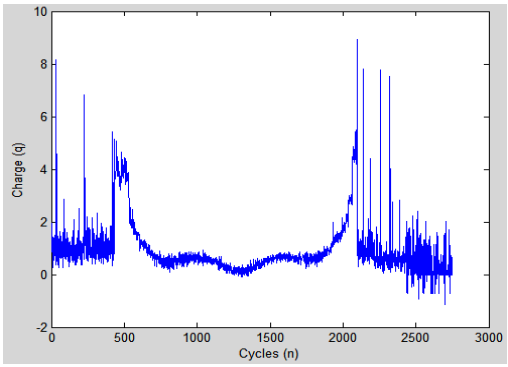

Fig.9 (d) Skewness plot (n-q) of corona discharge

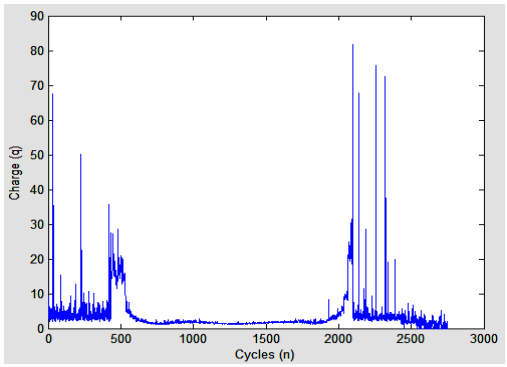

Fig.9 (e) Kurtosis plot (n-q) of corona discharge

Referring to Fig. 9(a), Fig. 9(b) and Fig. 9(c) of corona discharge, it can be seen the charges starts occurring after 500 cycle increasing somewhere upto 1200 cycle and then decreasing after 2000 cycle, and in Fig. 9(d) and Fig. 9(e) of skewness and kurtosis, the value decreases from 500 cycle till 2000 cycle.

3.3.2. Parameters of known PD patterns

The table V below is the average value of mean, standard deviation, variance, skewness and kurtosis for void, surface and corona discharges respectively . These values are obtained for known PD parameters.

TABLE V. PARAMETERS OF KNOWN PD PATTERNS

Parameters	Void	Surface	Corona
Mean	13320.32	145.706	1.426
Standard deviation	7553.716	126.009	1.139
Variance	$1.64*10^{8}$	17921.01	2.279
Skewness	$3.66*10^{-17}$	0.809	0.26
Kurtosis	0.04878	2.442	0.966

3.3.3. 2D distribution of (n-q) for unknown PD patterns

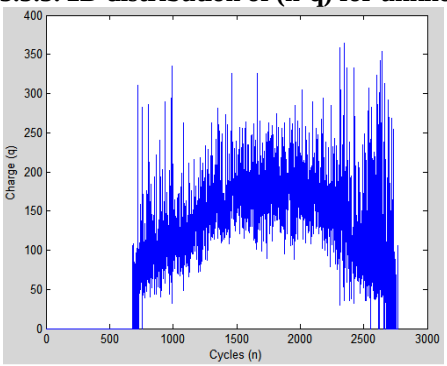

Fig.10 (a) Mean plot (n-q) of data1

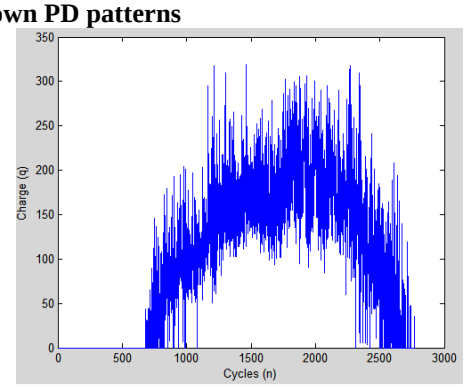

Fig.10 (b) Standard deviation plot (n-q) of data1

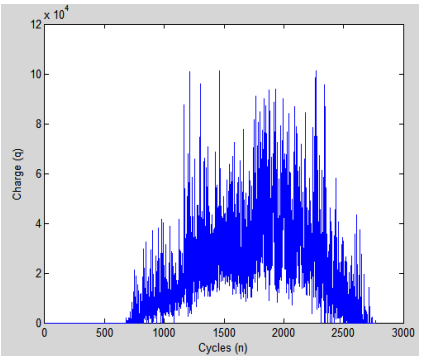

Fig.10 (c) Variance plot (n-q) of data1

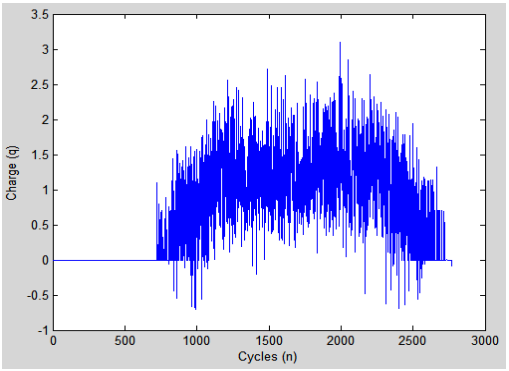

Fig.10 (d) Skewness plot (n-q) of data1

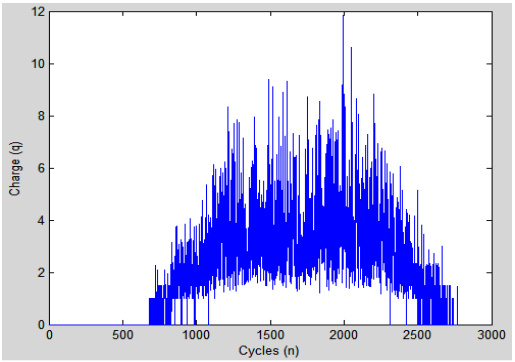

Fig.10 (e) Kurtosis plot (n-q) of data1

We have obtained the results from known PD parameters so as to plot the graphs shown above Fig. 10(a), Fig. 10(b), Fig. 10(c), Fig. 10(d) and Fig. 10(e) are the n-q plot of mean, standard deviation, variance, skewness and kurtosis for data1 respectively.

In Fig. 10(a), Fig. 10(b), Fig. 10(c), Fig. 10(d) and Fig. 10(e), the charges are uniformly distributed similar to surface discharge. Hence, it can be concluded that data1 is having surface discharge.Fig. 11(a), Fig.11(b), Fig. 11(c), Fig. 11(d) and Fig. 11(e) are the n-q plot of mean, standard deviation, variance, skewness and kurtosis for data2 respectively.

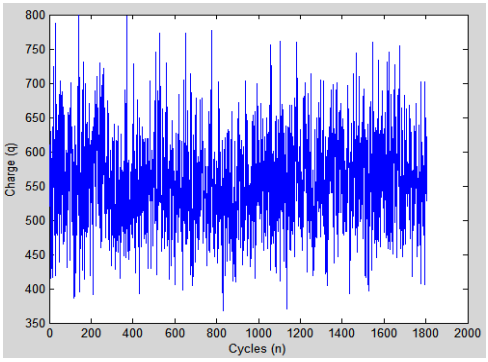

Fig.11 (a) Mean plot (n-q) of data2

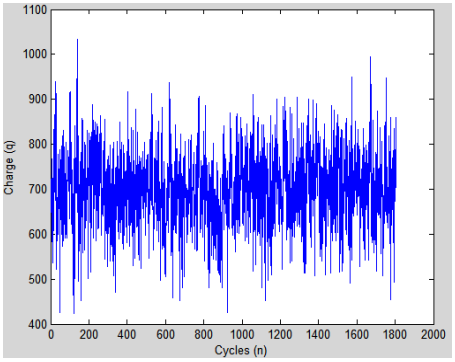

Fig.11 (b) Standard deviation plot (n-q) of data2

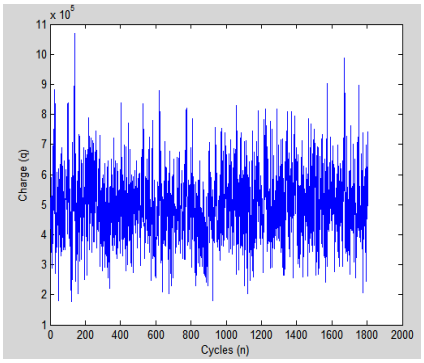

Fig.11 (c) Variance plot (n-q) of data2

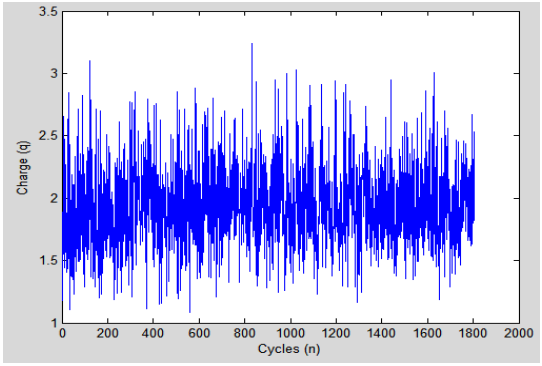

Fig.11 (d) Skewness plot (n-q) of data2

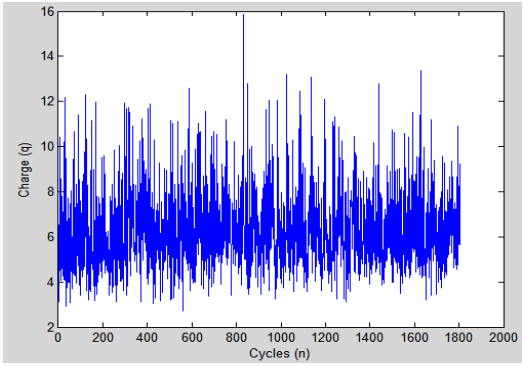

Fig.11 (e) Kurtosis plot (n-q) of data2

In Fig. 11(a), Fig. 11(b), Fig. 11(c), Fig. 11(d) and Fig. 11(e), the charges are uniformly distributed similar to surface discharge. Hence, it can be concluded that data2 is having surface discharge.

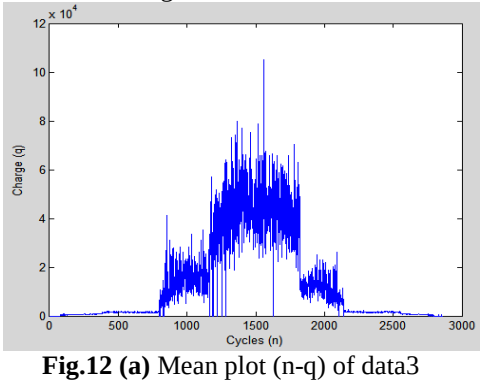

Fig.12 (a) Mean plot (n-q) of data3

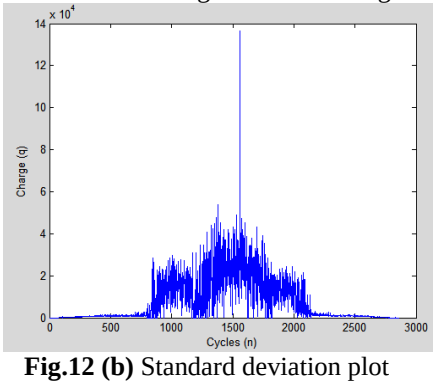

Fig.12 (b) Standard deviation plot (n-q) of data3

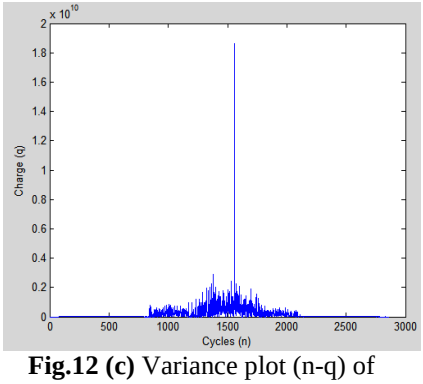

Fig.12 (c) Variance plot (n-q) of data3

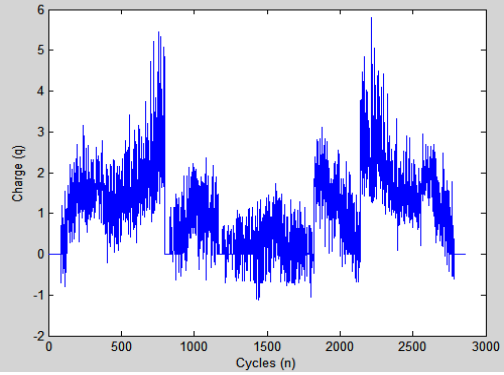

Fig.12 (d) Skewness plot (n-q) of data3

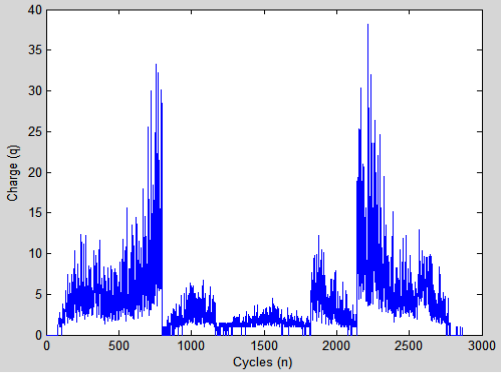

Fig.12(e). Kurtosis plot (n-q) of data3

Fig. 12(a), Fig. 12(b), Fig. 12(c), Fig. 12(d) and Fig. 12(e) are the n-q plot of mean, standard deviation, variance, skewness and kurtosis for data3 respectively. In Fig. 12(a), Fig. 12(b) and Fig. 12(c), there is a occurrence of peak after 1500 cycle and in Fig. 12(d) and Fig. 12(e), the skewness and kurtosis value decreases at that peak which is similar to void discharge. Hence, it can be concluded that data3 is void discharge.

3.3.4. Parameters of unknown PD patterns

The table VI below is the average value of mean, standard deviation, variance, skewness and kurtosis for void, surface and corona discharges respectively . These values are obtained for unknown PD parameters

TABLE VI. PARAMETERS OF UNKNOWN PD PATTERNS

Parameters	data1	data2	data3
Mean	105.119	553.93	13320.32
Standard deviation	97.966	698.3	7553.716
Variance	16714.23	$4.94*10^{5}$	$1.64* 10^{8}$
Skewness	0.692	1.939	$-3.7*10^{-17}$
Kurtosis	2.004	6.31	0.04878

IV. OBSERVATIONS

From the above results, following observations are made:

- Fig. 13(a), Fig. 13(b) and Fig. 13(c) are the characteristics of skewness and kurtosis ($H_{qn}^{+}(\varphi)$ and $H_{qn}^{-}(\varphi)$) of data 1, data2 and data3 against void., surface and corona discharges respectively.
- From Fig. 13(a), it is observed that data3 characteristics overlaps void discharge characteristics, it can be concluded that data3 is void discharge. Data2 characteristics approximately fits against void, it can be concluded that data2 is also void discharge
- From Fig. 13(b), it is observed that data 1 characteristics is similar to surface discharge characteristics, it can be concluded that data 1 is surface discharge.
- From Fig. 13(c), it is observed that none of the data characteristics is similar to corona discharge characteristics, it can be concluded that none of the data has corona discharge.

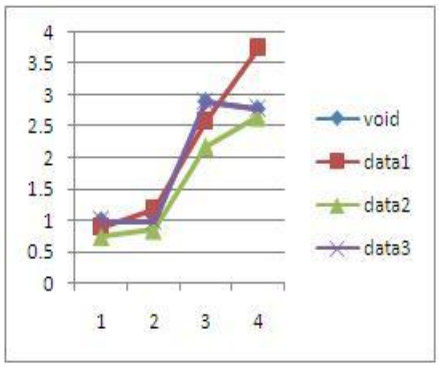

Fig.13 (a) Characteristics of skewness and kurtosis($H_{qn}^{+}(\varphi)$ and $H_{qn}^{-}(\varphi)$) of data1, data2, and data3 against void

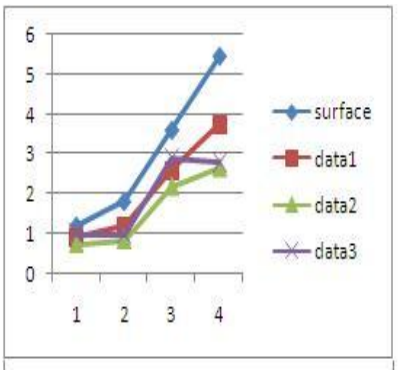

Fig.13 (b) Characteristics of skewness and kurtosis($H_{qn}^{+}(\varphi)$ and $H_{qn}^{-}(\varphi)$) of data1, data2, and data3 against surface

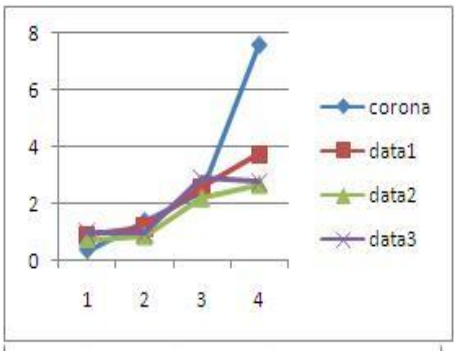

Fig.13 (c) Characteristics of skewness and kurtosis($H_{qn}^{+}(\varphi)$ and $H_{qn}^{-}(\varphi)$) of data1, data2, and data3 against corona

Fig. 14(a), Fig. 14(b) and Fig. 14(c) are the characteristics of skewness and kurtosis ($H_n^+(\varphi)$ and $H_n^-(\varphi)$) of data 1, data2 and data3 against void., surface and corona discharges respectively. These results are obtained over 0^0 to 180^0 for $H_n^+(\varphi)$ on the other hand values for $H_n^-(\varphi)$ are obtained over $181^0$to 360^0, representing the phase. These values are obtained for unknown PD parameters.

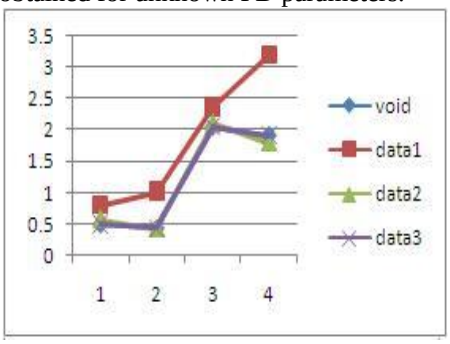

Fig.14 (a) Characteristics of skewness and kurtosis($H_n^+(\varphi)$ and $H_n^-(\varphi)$) of data1, data2, and data3 against void

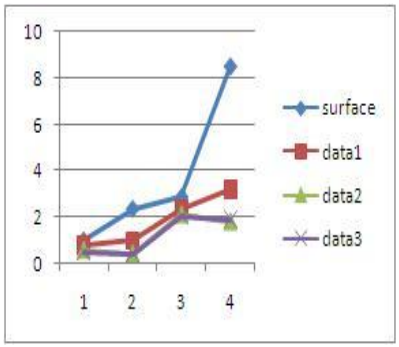

Fig.14 (b) Characteristics of skewness and kurtosis($H_n^+(\varphi)$ and $H_n^-(\varphi)$) of data1, data2, and data3 against surface

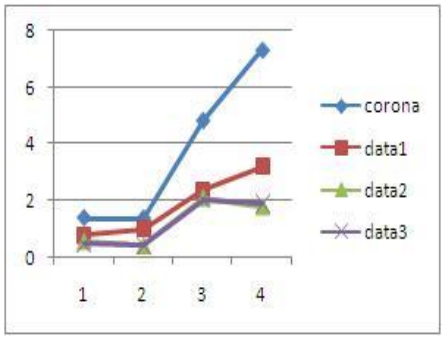

Fig.14 (c) Characteristics of skewness and kurtosis($H_n^+(\varphi)$ and $H_n^-(\varphi)$) of data1, data2, and data3 against corona

From Fig. 14(a), it is observed that data3 characteristics overlaps void discharge characteristics, it can be concluded that data3 is void discharge. Data2 characteristics approximately fits against void, it can be concluded that data2 is also void discharge. From Fig. 14(b), it is observed that data1 characteristics are close to surface discharge characteristics, it can be concluded that data 1 is surface discharge. From Fig. 14(c), it is observed that none of the data characteristics is similar to corona discharge characteristics, it can be concluded that none of the data has corona discharge.

In below figures, Fig. 15(a) represents the statistical characteristics of mean, standard deviation, variance, skewness and kurtosis of void discharge against data3. Fig. 15(b), Fig. 15(c) are the statistical characteristics of mean, standard deviation, variance, skewness and kurtosis of surface discharge against data1 and data2 respectively.

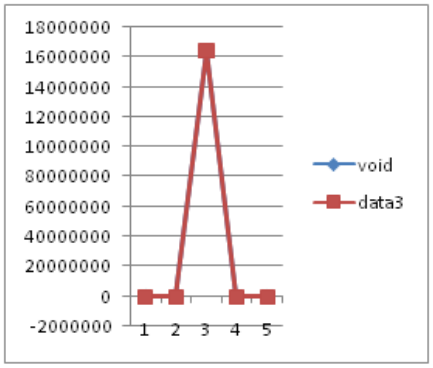

Fig.15 (a) Statistical Characteristics of data3 against void discharge

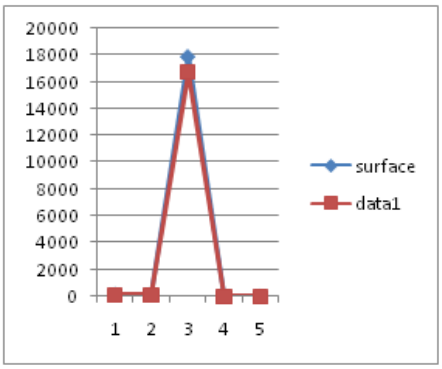

Fig.15 (b) Statistical characteristics of data1 against surface discharge

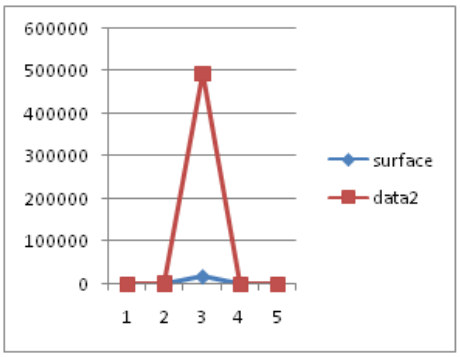

Fig.15 (c) Statistical characteristics of data2 against surface discharge

Plotting statistical parameters of void discharge against data3 in Fig. 15(a) shows data3 characteristics overlaps void characteristics, it can be concluded that data3 is void discharge. Similarly, for surface discharge, data1 and data2 characteristics (Fig. 15(b) and Fig. 15(c)) approximately fit surface discharge characteristics, it can be concluded that data1 and data2 is surface discharge

V. CONCLUSION

From all the above observations using all the three phase-resolved patterns(φ-q), (φ-n) and (n-q), it can be concluded that, data1 is surface discharge in all the three phase-resolved patterns, data2 is surface discharge in (n-q) pattern and void discharge in (φ-q) and (φ-n), hence data2 is both void and surface discharge and data3 is void discharge in all the three phase-resolved patterns.

REFERENCES

[1] MICAMAXX^{TM} plus – Partial Discharge Basics
[2] M. G. Danikas, "The Definitions Used for Partial Discharge Phenomena," IEEE Trans. Elec. Insul., Vol. 28, pp. 1075-1081, 1993.
[3] N.C. Sahoo, M. M. A. Salama, R. Bartnikas, "Trends in Partial Discharge Pattern Classification: A Survey", IEEE Transactions on Dielectrics and Electrical Insulation, Vol. 12, No. 2; April 2005.
[4] E. Gulski, J. Smith, R. Brooks, "Partial Discharge Databases for Diagnosis Support of HV Components", IEEE Symposium on Electrical Insulation, pp. 424-427, 1998
[5] E. Gulski and F. H. Kreuger, "Computer-aided recognition of Discharge Sources," IEEE Transactions on Electrical Insulation, Vol. 27 No. 1, February 1002.
[6] E. Gulski and A. Krivda, "Neural Networks as a Tool for Recognition of Partial Discharges", IEEE Transactions on Electrical Insulation, Vol. 28 No.8, December 1993.
[7] F. H. Kreuger, E. Gulski and A. Krivda, "Classification of Partial Discharges", IEEE Transactions on Electrical Insulation, Vol. 28 No. 6, December1993.
[8] C. Chang and Q. Su, "Statistical Characteristics of Partial Discharges from a Rod-Plane Arrangement"
[9] Namrata Bhosale, Priyanka Kothoke Amol Deshpande, Dr. Alice Cheeran, "Analysis of Partial Discharge using Phase-Resolved(φ-q) and (φ-n) Statistical Techniques", International Journal of Engineering Research and Technology, Vol. 2 (05), 2013,ISSN2278-0181.
[10] Priyanka Kothoke, Namrata Bhosale, Amol Deshpande, Dr. Alice Cheeran, "Analysis of Partial Discharge using Phase-Resolved (n-q) Statistical Techniques", International Journal of Engineering Research and Applications.

Proceedings papers:

[11] Nur Fadilah Ab Aziz, L. Hao, P. L. Lewin, "Analysis of Partial Discharge Measurement Data Using a Support Vector Machine," The 5th Student Conference on Research and Development, 11-12 December 2007, Malaysia.

International Journal of Modern Engineering Research (IJMER)
www.ijmer.com Vol.3, Issue.4, Jul - Aug. 2013 pp-1958-1964 ISSN: 2249-6645

Performance Analysis of DV-Hop Localization Using Voronoi Approach

Mrs. P. D.Patil[1], Dr. (Smt). R. S. Patil[2]
*(Department of Electronics and Telecommunication, DYPatil college of Engg& Technology, India)

ABSTRACT : *Localization that is to be aware of position of the node in the network is an essential issue in wireless sensor network (WSN). Localization algorithm in WSN can be divided into rangebased and range-free algorithm. In this paper, we present the analysis of DV-Hop using Voronoi diagrams in order to scale a DV-Hop localization algorithm while maintaining or even reducing its localization error. With this we tried to analyze the efficiency of the DV-Hop localization algorithm by changing various parameters.We show how the proposed algorithm can scale in different aspects such as communication and processing costs when increasing the number of nodes and beacons.*

Keywords: *Localization, DV-Hop, Range free algorithms, WSN*

I. INTRODUCTION

Wireless Sensor Network is composed of large number of low cost sensor nodes which are limited in power, computational capacity and memory. Sensor nodes are capable of sensing and communicating with each other. The WSN can deploy these low cost sensors in variety of different settings. WSN can supply many applications, such as weather sensing, environment monitoring, building and structure monitoring, military sensing. Localization is to determine the location and it coordinates of the sensor nodes that are deployed randomly in the sensor network. It is the important issue in location dependent applications of WSN. Global Positioning System GPS is straightforward solution to this problem but due to its large equipment and high cost it is not feasible [1]. Localization algorithms in WSN are divided into range based and range free algorithms. Range based algorithm finds the location of the sensor node using point to point distances [2] for this it requires hardware support but provide more accurate localization result than range free approaches. It includes algorithms such as Time of Arrival (TOA), Time Difference of Arrival (TDOA), Angle of Arrival (AOA), and Received Signal Strength Indicator (RSSI) [3]. Whereas range free algorithm depends on connectivity and hop information such as Centroid, APIT, Amorphous, DV-Hop, etc. It provides low accuracy, but it is preferred over range based because it is easier to implement with less hardware which is suitable for low power, low cost WSN.

DV-Hop [4] range free localization algorithm finds the distance using hop information and then calculates the location. This algorithm is simple, feasible, provides high coverage quality, and is useful and does not require localization devices. The other important advantage of DV-Hop is the fact that it does not depend on measurement error. But the position accuracy obtained through this algorithm is low. In this paper we analyze DV-Hop approach of range free localization algorithm by varying different parameters. A DV-Hop localization system works by transforming the distance to all beacons (nodes that know their position) from hops to units of length measurement (e.g., meters, feet) using the average size of a hop as a correction factor. A typical example of this technique is the Ad Hoc Positioning System (APS) [5]. Some of the advantages of the DV-Hop technique are: first, it is suitable for sparse networks; second,it is immune to RSSI inaccuracies; and third, it requires a small number of beacons. However, the DV-Hop technique has also a few disadvantages: first, it has a large communication cost of O(bn) — where b is the number of beacons and n the number of nodes — that compromises the algorithm scalability; and second, by mapping hops into distance units, the DV-Hop technique introduces errors that are propagated to the computation of a node location.. The rest of this paper is organized as follows. Section II presents the DV-Hop algorithm. In section III The Distributed Voronoi Localization System – DV-Loc and simulation results are shown in section IV and localization performances are discussed. Finally, we present our conclusions and future scope in Section V.

II. PROBLEM STATEMENT

In this work, we consider a WSN as composed of n nodes, with a communication range of r units, and distributed in a two-dimensional squared sensor field Q = [0, s] × [0, s]. For the sake of simplification, we consider symmetric communication links, i.e., for any two nodes u and v, u reaches v ifand only if, v reaches u. Thus, we represent the network by a graph G = (V,E) with the following properties:

- V = {v1, v2. . . vn} is the set of sensor nodes;
- {i, j} ∈ E iff vi reaches vj , i.e., the distance between vi and vj is less than r;
- ω(e) ≤ r is the weight of edge e = {i, j}, i.e., the distance between vi and vj .

In an Euclidean graph, each node has a coordinate (xi, yi) ∈ R2 in a 2-dimensional space, which represents the location of the node i in Q. For the sake of simplicity, we will only consider two dimensions in this work, but the methods here explained can be easily extended to provide position information in three dimensions.

Some terms can be used to designate the current state of a node:

(Unknown Nodes – U): Also known as free or dumb nodes, these are the nodes of the network that do not know their position. The position estimation of these nodes is the main goal of the localization systems.

(Settled Nodes – S): These nodes are initially unknown nodes, but manage to estimate their positions by using a localization system. The number of settled nodes and the estimated position error of these nodes are the main parameters of the quality of a localization system.

(Beacon Nodes – B): These nodes, also known as landmarks or anchors, do not need the localization system to estimate their physical positions. Their position is obtained by manual placement or by external means such as a GPS. These nodes form the base for most localization systems for WSNs.

The localization problem can then be stated as follows.

Given a network that uses a multi-hop communication represented by a graph G = (V,E), and a set of beacon nodes B and their positions (xb, yb), for all b ∈ B, we want to find the position (xu, yu) of as many unknown nodes u ∈ U as possible, transforming these unknown nodes into settled nodes.

In a DV-Hop localization system, as proposed by Niculescu and Nath in APS [5], the beacon nodes start by propagating their position information (Fig. 1(a)). Working as an extension of the distance vector algorithm, all nodes receive the position information from every beacon as well as the number of hops to these beacons. When a beacon node receives a position information from the other beacon nodes, it has enough information to compute the average size of one hop based on its own position, the position of the other beacon nodes, and the number of hops among them (Fig. 1(b)). This last value is then flooded in a controlled manner into the network as a correction factor. When an unknown node receives the correction, it is able to convert its distance to the beacon nodes from hops to units of length measurement (Fig. 1(c)). The complexity of message exchange of this algorithm is determined by the total number of beacon and regular nodes, which is O(n(b + 1)), where n is the number of nodes and b is the number of beacon nodes.

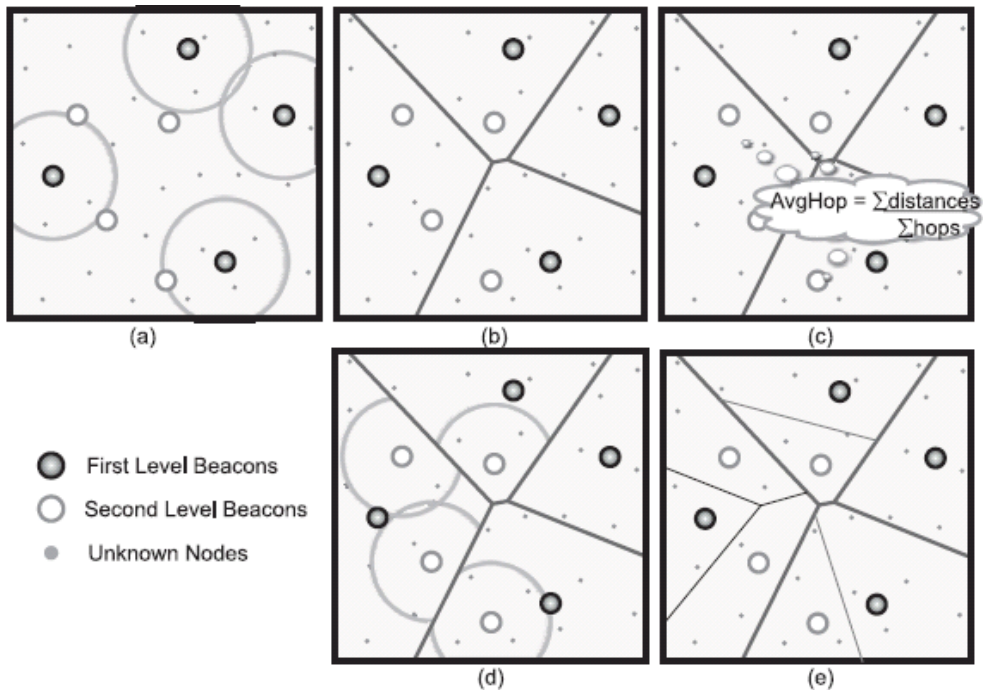

Figure 1: Example and phases of the DV-Loc algorithm

III. THE DISTRIBUTED VORONOI LOCALIZATION SYSTEM – DV-LOC

As mentioned in the previous section (1) the complexity of message exchange in the APS DV-Hop algorithm limits its applicability. In this section, Here propose and explain the Distributed Voronoi Localization (DV-Loc), a new DV-Hop localization solution[6].

A. The Localization Algorithm

The main idea of DV-Loc is to use the Voronoi diagram to limit the scope of the flooding in a DV-Hop localization system. DV-Loc is a scalable solution that uses the Voronoi cell of a node to limit the region when computing its position in order to reduce its localization error.

Algorithm 1 shows the pseudo-code of the DV-Loc algorithm. Initially, b beacon nodes (set B) are deployed in the sensor field with the u unknown nodes (set U). These beacon nodes are previously divided into levels. For example, four beacons are first level beacons, other four beacons are second level, other eight or less are third level, and so on. It is important to note that besides we are considering the use of four nodes as the first level beacon nodes, any other number greater than three could be used. The same applies to the other levels. The DV-Loc works in four steps:

1) The four beacon nodes of the first level start the algorithm by flooding its position information. Each node that forwards the packets saves the position and the number of hops to each one of the beacon nodes—Fig. 1
2) Upon receiving the packets, the nodes are capable of building a Voronoi diagram based on the position information of the first level beacon nodes — Fig. 1(b).Each node is also capable of estimating the Voronoi cell it belongs to; based on the number of hops (the beacon with the lowest number of hops is the cell of a node).When the distance towards two or

more beacons are the same, the node can use the sum of the RSSI as a tiebreaker The beacons of second level compute the average size of a hop (like in the APS algorithm) based on the position information of the first level beacon nodes—Fig. 1(c) Steps are repeated for the beacons of the other levels with a few differences:

3) When no beacon packet is received after a timeout, a node transforms the distances to the beacon nodes from hops to distance units based on the average size of a hop received by one or more beacon nodes. The position is then computed by using multilateration. The node checks if the computed position is inside or outside its estimated Voronoi cell. If the computed position is outside the Voronoi cell, the node changes its computed position to the nearest point inside the Voronoi cell. This characteristic is responsible for decreasing the localization error computed by the nodes.

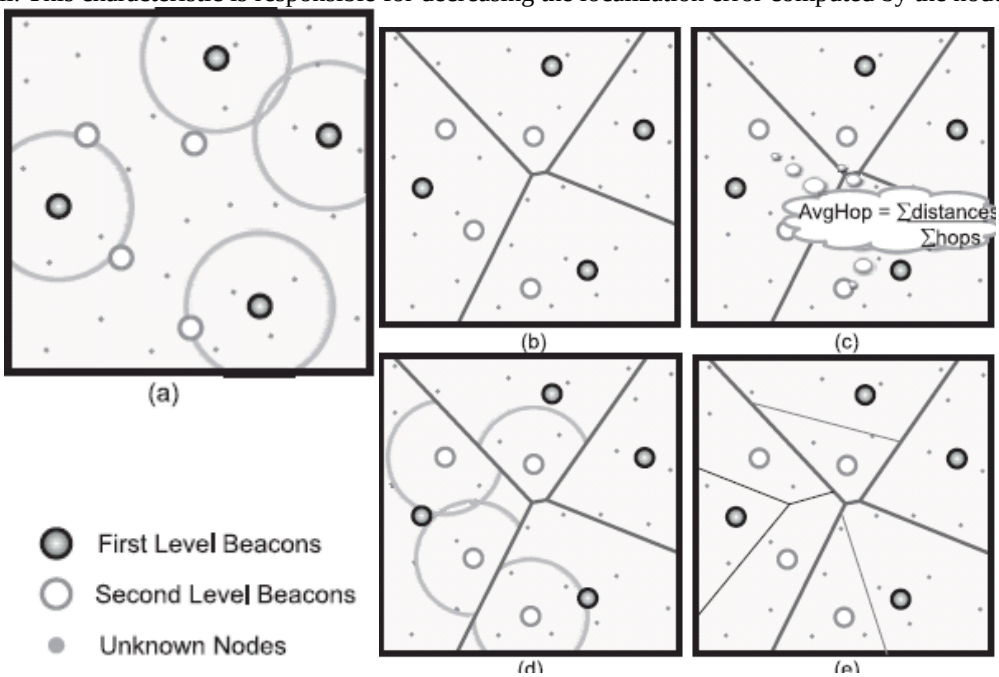

Figure 2: Example and phases of the DV-Loc algorithm

B. Flowchart of DV-Loc Algorithm.

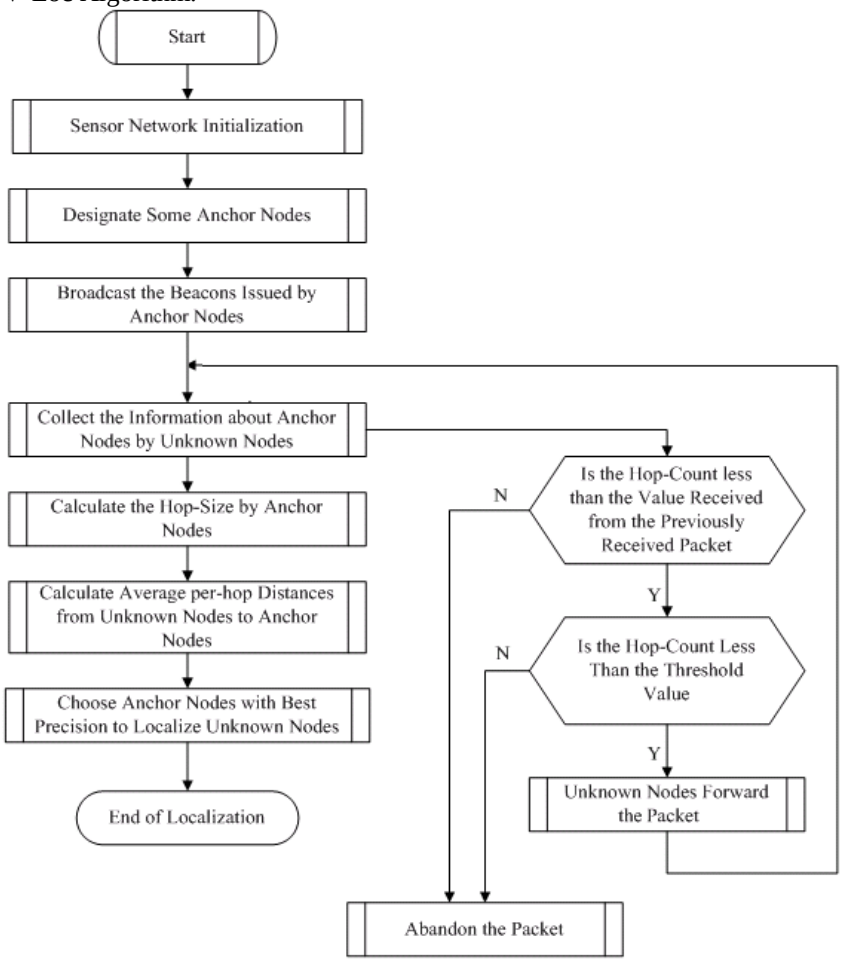

IV. SIMULATION RESULTS

In this section, the proposed scheme, DV-Loc algorithm is evaluated and compared it with the APS algorithm, a similar DV-Hop algorithm that uses the position information of all beacons to compute its position.

The Impact of the Network Scale –

Scalability is evaluated by varying the network size from 50 to 150 nodes with a constant density of 0.03 nodes/m2.Thus, the sensor field is resized according to the number of sensor nodes. The number of beacons in both algorithms is fixed i.e. 4. The comparison of the localization error obtained by the APS algorithm and DV-Loc algorithm is shown in Fig. 6. In both the cases, localization error increases with network size, but in DV-Loc algorithm less error occurs in large networks. Number of sent packets increase when the size of network increases. As the previous section shows, localization errors can increase with the number of nodes. The first solution to this problem would be the deployment of additional beacon nodes in the network to decrease localization errors. Hence, the communication cost also increases with the number of beacons. The number of sent packets by the DV-Loc is not only smaller than in APS but it also increases with a logarithmic factor (b' = 4+log(b−4), which shows how the DV-Loc can also scale in the number of beacons[6]. The number of correctly estimated cells increases when the number of beacons increases.

As shown in experimental results, the DV-Loc algorithm can maintain a high level of correct cell estimations even when the number of beacons and, consequently, number of cells, increases. Here n=no. of nodes.

Figure 3 (a) Average Delay Graph for n=50 nodes

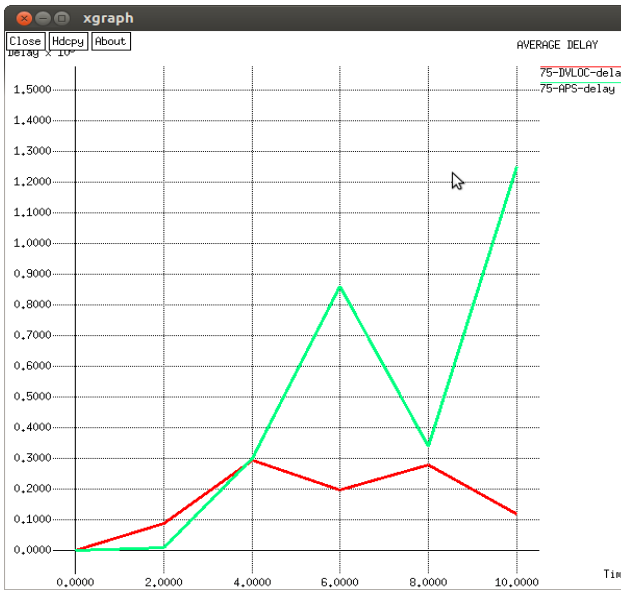

Figure 4(b)Average Delay Graph for n=75 nodes

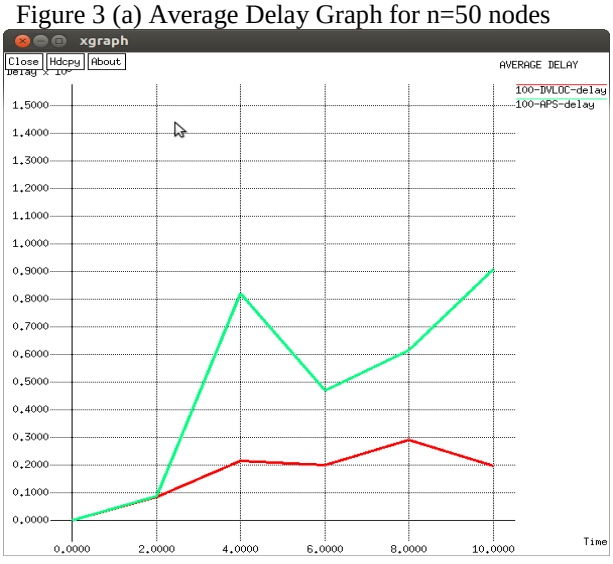

Figure 5(c) Average Delay Graph for n=100 nodes

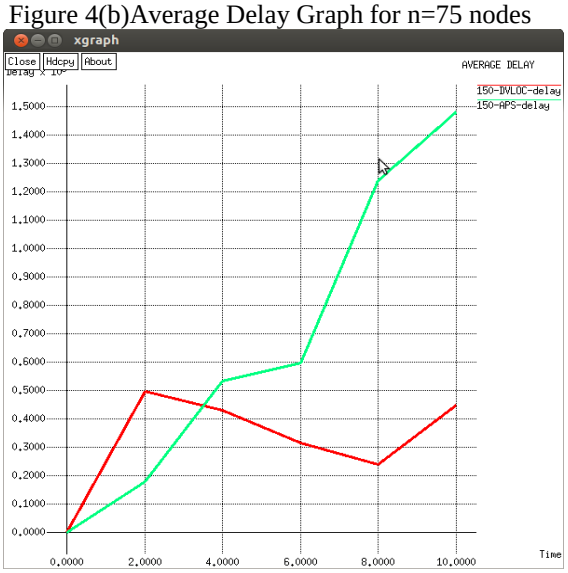

Figure 6(d) Average Delay Graph for n=150 nodes

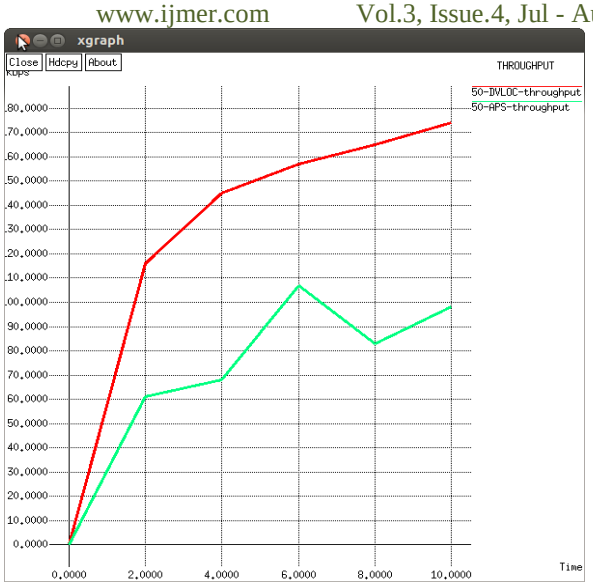

Figure 7 (a) Throughput for n=50

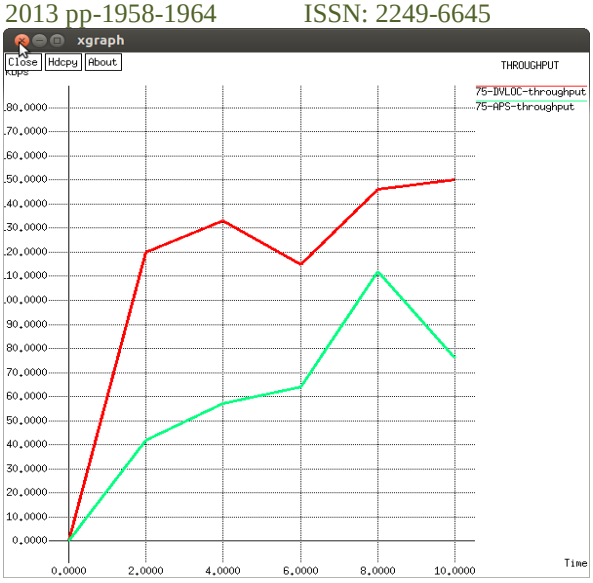

Figure 8 (b) Throughput for n=75

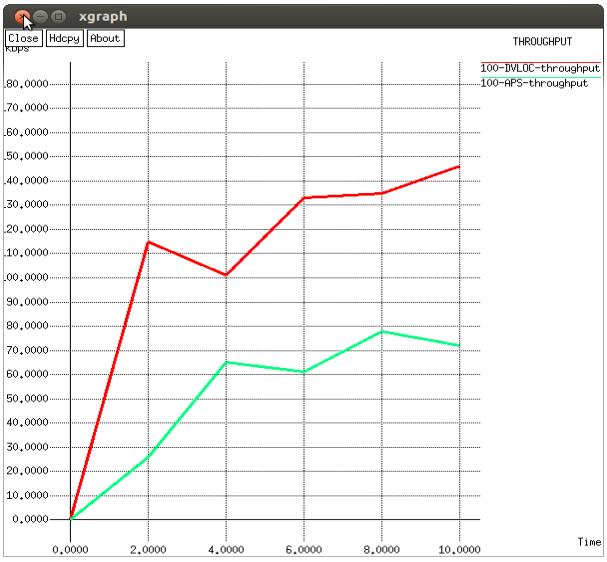

Figure 9 (c) Throughput for n=100

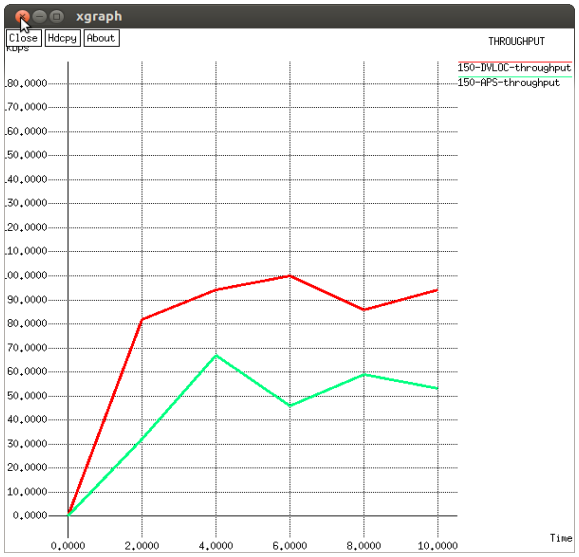

Figure 10 (d) Throughput for n=150

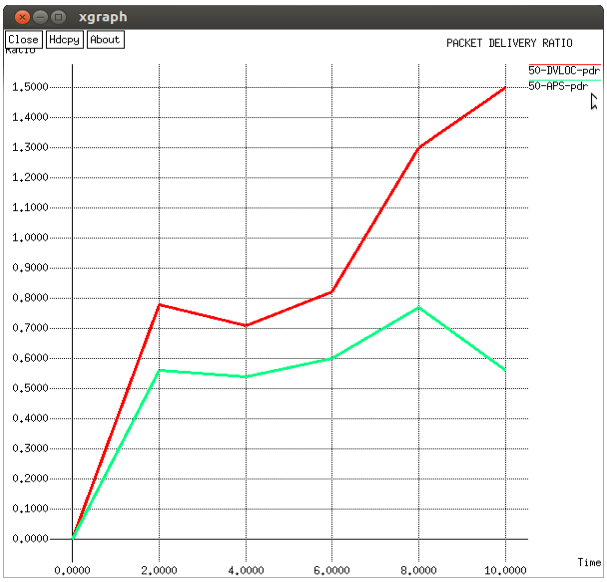

Figure 11 (a) Packet Delivery Ratio for n=50

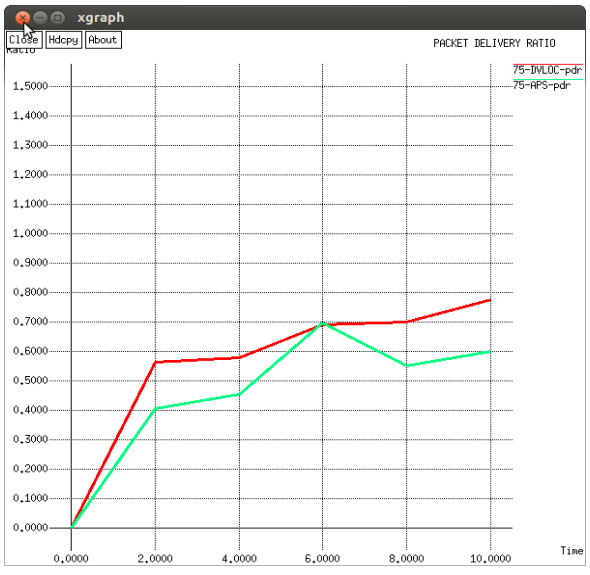

Figure 12 (b) Packet Delivery Ratio for n=75

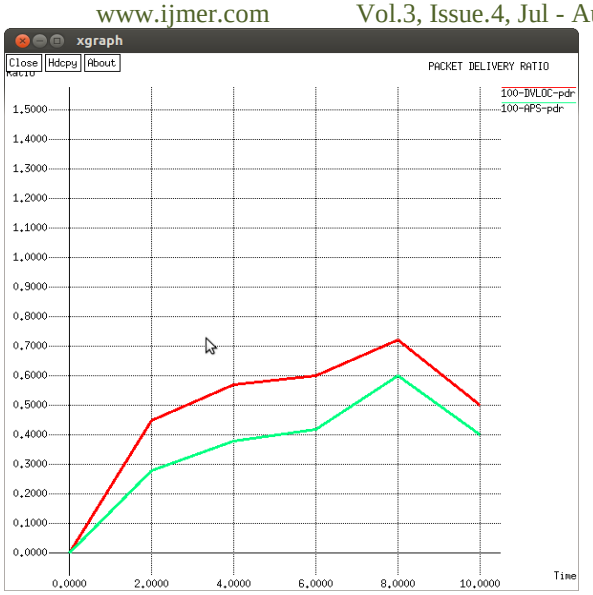

Figure 13 (c) Packet Delivery Ratio for n=100

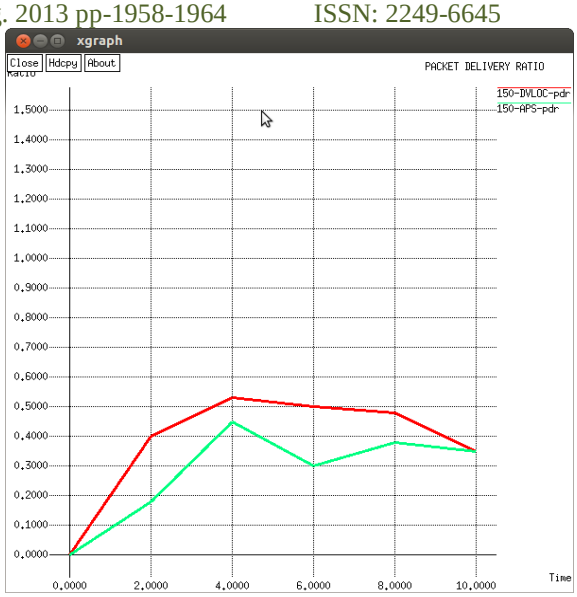

Figure 14 (d) Packet Delivery Ratio for n=150

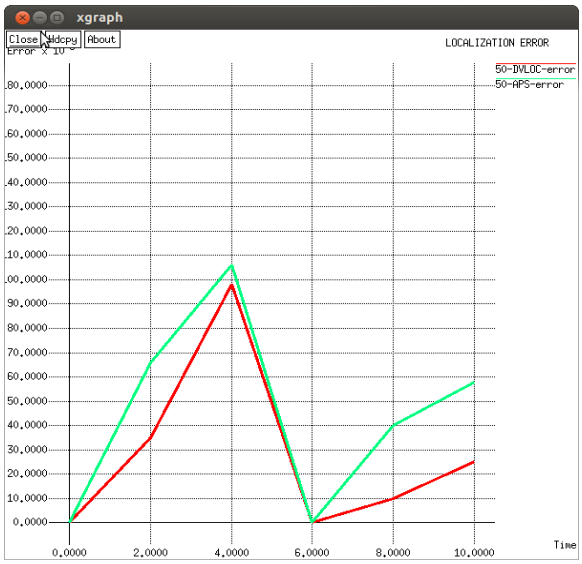

Figure 15(a) Localization Error for n=50

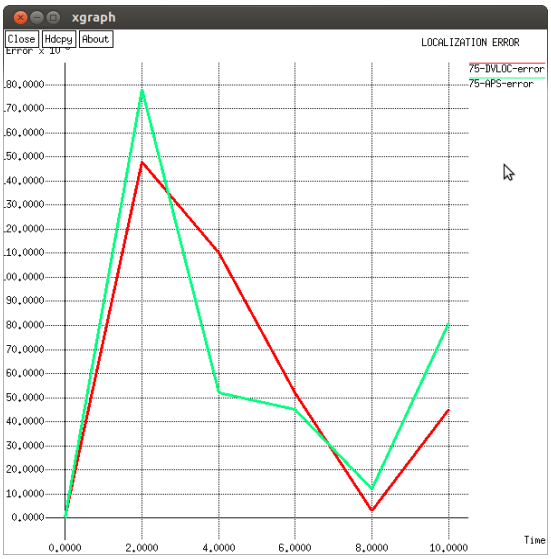

Figure 16(b) Localization Error for n=75

Figure 17(c) Localization Error for n=100

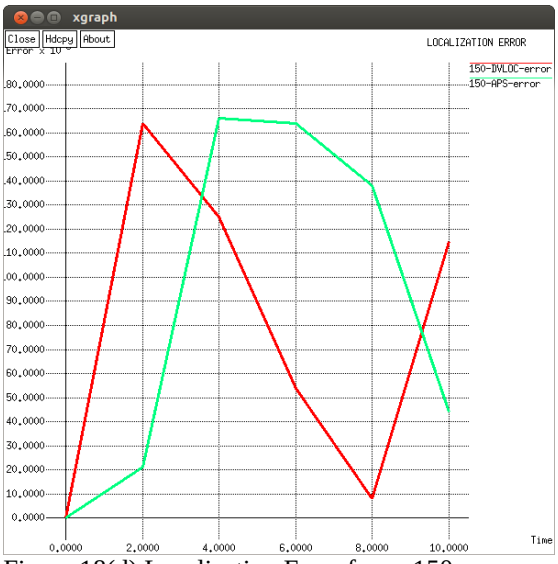

Figure 18(d) Localization Error for n=150

We can see that the best results (Fig.6) are achieved by the DV-Loc algorithm because it limits the position errors to the node's Voronoi cell. Also, to better understand and compare the error behavior of these algorithms, the localization error of both algorithms decreases as the number of beacon nodes increases.

In the DV-Loc algorithm, although the network size increases, the localization error decreases effectively as compared to APS algorithm. Finally, it is important to evaluate the number of nodes that correctly estimated their Voronoi cell, since those cells can be used not only to reduce localization errors but can also be used by routing and clustering algorithms. The DV-Loc maintains a high level of correct cell estimations even when the network size increases.

Table IV.1 Average Values for Different Parameters in APS-Algorithm

PARAMETERS	NUMBER OF NODES 'n'			
	n=50	n=75	n=100	n=150
DELAY(ms)	535.01	584.41	556.1	805.75
ERROR	0.061	0.0734	0.105	0.106
PDR	0.5516	0.462	0.339	0.0606
THROUGHPUT	83.6	70.08	60.314	51.34

Table IV.2 Average Values for Different Parameters in DV-Loc Algorithm

PARAMETERS	NUMBER OF NODES 'n'			
	n=50	n=75	n=100	n=150
DELAY(ms)	182.13	190.65	194.91	385.49
ERROR	0.038	0.0714	0.0922	0.0934
PDR	1.022	0.6640	0.598	0.4752
THROUGHPUT	151.68	132.53	99.01	91.18

As noted in the above Tables IV.1 and IV.2, the delay deteriorates for number of nodes =150. Thus both the algorithms perform better for number of nodes <150 in the network

V. CONCLUSION

The main contribution in this paper is a distributed algorithm for localization of nodes in a wireless ad hoc communication network and its error estimation. There are many possible improvements of the algorithm. For example, an unknown node could only query some of its neighbors and use correlation coding. This would reduce communication costs but increase computations. The algorithm can also be iterated to exploit the newly obtained position estimates of unknown nodes.

In DV-Loc (Distributed Voronoi Localization) algorithm, a DV-Hop localization system takes advantage of Voronoi diagrams to produce a scalable and robust WSN localization algorithm. The proposed localization system provides a way of localizing the nodes by their Voronoi cell. This leads naturally to a novel routing algorithm capable of taking full advantage of node information and the resulted Voronoi cells can be used by clustering algorithms.

REFERENCES

Journal Papers:

[1] YousiZheng, Lei Wan, Zhi Sun and Shunliang Mei, *"A Long Range DV-Hop Localization Algorithm With Placement Strategy in Wireless Sensor Networks." 2010 IEEE*.

[2] Guo Qing GAO and Lin LEI, *"An Improved DV-Hop Localization Algorithm in WSN." University of Electronic Science and Technology of china, IEEE, October 2010*.

[3] MertBal, Min Liu, WeimingShen, Hamada Ghenniwa, *"Localization in coorperative Wireless Sensor Networks:A Review". 2009 IEEE.*

[4] Hongyang Chen, Kaoru Sezaki, Ping Deng, Hing Cheung So, *"An Improved DV-Hop Localization Algorithm in Wireless Sensor Networks." 2008 IEEE.*

[5] D. Niculescu and B. Nath, *"Ad hoc positioning system (aps)," in IEEEGlobal Communications Conference (GlobeCom '01),* San Antonio, TX,USA, November 2001, pp. 2926–2931.

[6] AzzedineBoukerche, Horacio A.B.F. Oliveira*"A Voronoi Approach for Scalable and Robust DV-Hop Localization System for Sensor Networks" 1-4244-1251-X/07/$25.00 ©2007 IEEE*.

International Journal of Modern Engineering Research (IJMER)
www.ijmer.com Vol. 3, Issue. 4, Jul - Aug. 2013 pp-1965-1979 ISSN: 2249-6645

Report on Technology Transfer of Solar Charkha in Khadi Sector

Mr. Ravi Kandasamy[1], Mr. Deep Varma[2], Mr. Sachin Raut[3], Mr. Ganesh There[4]

The Report: The present report deals with the field trial project funded by the KVIC "Technology Transfer of Solar Charkha in Khadi Sector". The basic concept of this technology is to operate the manual NM Charkha used in khadi sector through solar energy in a viable way.

I. Background

1.1 Bapu and the Spinning Revolution:

"I have no doubt in my mind that the wheel can serve as the instrument of earning one's livelihood and, at the same time, enable the worker to render useful service to his neighbor. In order to ply the wheel intelligently, he should know all the processes that precede and succeed spinning" (H,17-3-1946, p. 42).

"Revival of the cottage industry, and not cottage industries, will remove the growing poverty. When once we have revived the one industry, all the other industries will follow…. I would make the spinning-wheel the foundation on which to build a sound village life. I would make the wheel the centre round which all other activities will revolve" (YI, 21-5-1925, pp. 176, 177).

The above statements of Mahatma Gandhi reflect not only his confidence on the spinning-wheel as an effective tool for eradication of poverty and unemployment in the country but also his confidence that the success of this decentralized cottage industry will enable all the others to follow. He also indicates the need for revival of existing systems. The KVIC has kept alive the production of khadi on the principles of Gandhiji, where it is essential that the spinning on charkha and weaving on handloom has to be performed manually.

1.2 The position of manual spinning in the new millennium:

Though the manual spinning operation on charkha was most appropriate during the freedom struggle movement, the situation is different today. During Gandhiji's time there were not many alternative job avenues and therefore the manual spinning on charkha was readily accepted by the masses particularly in rural India. However, the situation has drastically changed in the case of spinning and weaving. Mainly ladies are involved in spinning. Because of hard labor and poor wages the attraction of manual spinning on charkha is decreasing day by day with the result of decrease in employment in khadi sector. (as see in the table below):

Year	1997-98	1998-99	1999-00	2000-01	2001-02	2002-03	2003-04	2004-05	2005-06	2006-07	2007-08
Production (Rs in crores)	624	636	552	432	444	457	460	464	468	491	543

The invention of MGIRI's solar charkha has opened up a new approach to reverse this trend. With a number of job opportunities including NREGA providing employment to the rural masses the manual spinning on charkha is not able to continue its role as a source of employment. Hence an effective intervention like solarisation of charkha because the need of the hour since otherwise many lakhs charkhas will have to be abandoned besides leaving the dependants on them in the lurch.

1.3 Solar energy operated charkha as an alternative

"A scientific study of the spinning-wheel will lead on to Sociology. The spinning-wheel will not become a power for the liberation of India in our hands unless we have made a deep study of the various sciences related to it. It will then not only make India free, but point the way to the whole world". (H, 31-3-1946, p. 59)

It is very clear from the above statements of Gandhiji that he never objected to the introduction of new technology in the khadi sector. Announcement of the prize of Rs 1 lakh way back in 1929 for the development of improved charkha is a unique example of the importance given by him for technological innovations and scientific studies. His main objection was that technology which should not replace the human being and technology should not become a source of exploitation of the poor by the rich.

It is possible to eliminate altogether the hardship/drudgery involved in the manual operation of charkha and also increase the wage earning capacity by increasing its productivity by operating the charkha by means solar energy. Since charkhas are being mainly operated in rural areas and since rural areas have no assured electric supply only the use of solar energy could be thought of. The use of solar energy can usher in a new era of khadi spinning. The principle of conversion of solar light into electric energy is well established and solar panels of various capacities are now readily available. Since the

NMC charkha is a small machine, it is feasible to operate the charkha using solar energy. A commercially viable solar system for the operation of 8 spindle NMC charkha is now developed at MGIRI. The technology is now well proven through nationwide field trials and technology demonstration workshops.

To revive the large numbers of charkhas going out of operation in villages solar energy could be easily harnessed. For the operation of MGIRI Solar charkha we need only 30 watts motor and 60wp solar photovoltaic panel. A specifically designed solar charkha kit attachment has also been developed to operate the existing 8-10 spindle charkha which is normally used for manual operation in practice.

Mr. Patel former Governor, Reserve bank of India quoted that - Gandhiji was against capitalism if the means of production was concentrated in a few hands. ''He wanted everyone to own his means of production — a concept much wider than the current notion of empowerment through education and the like. He was against socialism as it concentrated all means of production in the hands of the state, which led to the enslavement of everyone. If everyone could have access to machinery, he was for it. Where large-scale production was inescapable as in the case of steel, he was for public ownership,'' he says.

''Decentralisation of production may not be easy. But something needs to be done to prevent the relentless march to urban slums. With today's technology and with rural electrification and technical training, it should be possible to carry jobs where people live and not vice versa,'' says Patel.

1.4 The aim of solarisation project:

- To bring a revolution in the khadi sector particularly through enhanced wage earnings of the spinners.
- To eliminate the drudgery of the spinner.
- To effect of an increase in the number of spinner- particularly through the 'cotton-to-garment' clusters in the cotton growing regions like Vidarbha.
- To provide lighting, fan and radio operating system with the use of solar panel in rural areas that have been deprived of such opportunities for ages.

II. Earlier Research Background:

The First Solar Motor: The earliest known record of the direct conversion of solar radiation into mechanical power belongs to Auguste Mouchout, a mathematics instructor at the Lyce de Tours. Mouchout began his solar work in 1860 after expressing grave concerns about his country's dependence on coal.

The First Commercial Venture: Boston resident Aubrey Eneas began his solar motor experimentation in 1892, formed the first solar power company (The Solar Motor Co.) in 1900, and continued his work until 1905. One of his first efforts resulted in a reflector much like Ericsson's early parabolic trough.

Solar charkha: For the past few years several attempts in bringing out a solar charkha were made by various institutions and research organizations. Some institutions in Gujarat and other places tried to operate a 2-spindle charkha on solar but could only succeed to operate it with more power giving an impression that the cost of photovoltaic panel will be prohibitive. One such feasible model was established in Uttaranchal in the context of a silk reeling unit. The Ministry of New and Renewable Energy had taken the initiative to develop Solar Powered Motorized cum Pedal Operated Spinning Machine or Solar Charkha (originally it is a reeling machine). This was approved by Central Silk Board (CSTRI) to produce fine yarn from silk and wool waste.

Unlike the traditional Spinning Machine, this Solar Charkha (reeling machine) is equipped with an electric motor powered by Solar Energy and battery bank capable of running the machine 5-6 hours a day.

More than 250 such Solar Charkhas have been installed and are running successfully in various parts of Uttaranchal. The project was however not taken to commercial level and its lateral expansion in the broader field of textile was not thought of.

(Ref:http://daskumars.com/yahoo_site_admin/assets/docs/solar_charkha_features.227190953.pdf)

III. Design details of MGIRI Solar Charkha

3.1 Design objectives

In designing the MGIRI's solar charka the following objectives were kept in mind:

1. Cost effectiveness in providing the solar energy support to the charkha such that the investment for the system should be justifiable with the output.
2. Standardized technology for the operation of charkha on solar energy.

3. Assurance of significantly higher wages compared to manual spinning. For example Rs. 100 per charkha per 8 hr. and more wages by operating more charkha more spindle or over longer periods.
4. Enhancement of productivity
5. Improvement in yarn quality
6. Overall reduction in yarn price.

3.2 Details of solar powering of NM Charkha

Charkha:

These are 8-10 spindle manually operated New Model Charkha (NMC) presently used in khadi sector. A large number of such charkhas are available in hundred of khadi institutions –particularly the ones recognized as a part of the SFURTI program of KVIC.

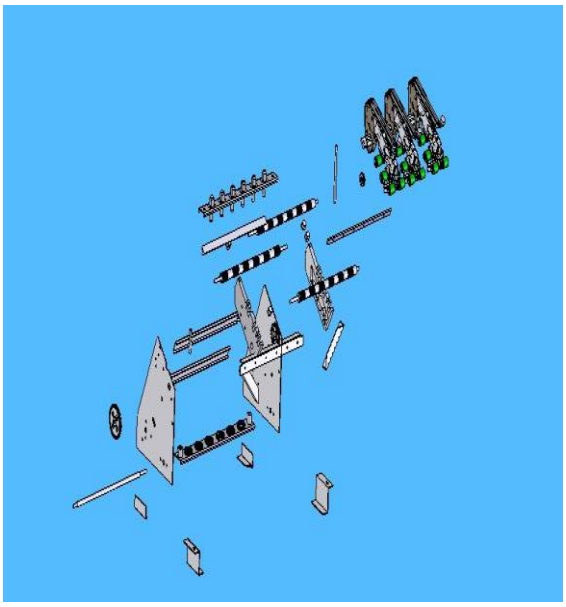

A conventional yarn spinning device (charkha) operates by drawing a sliver from the feed roll and stretching it over one or more rollers. The rollers are usually set to operate at serially faster speeds.. The drawn sliver is then wound around a spool attached to a spindle. The spool revolves at a calibrated speed, facilitating further drawing of the sliver and twisting the same to form yarn.

The required power input in this device is at three places:

a) The operation of the rollers which draw the sliver,
b) The rotation of the spindle which twists and winds the sliver into usable yarn and
c) The CAM which bobs the spindle mounted bobbin up and down while winding the twisted yarn around it.

The power input is provided through the driver shaft. The driver shaft is connected by three independent gear tread systems to the roller shaft, the pulley system driving the spindles and the CAM. There can be one or more spindles, each with corresponding rollers operating in parallel in a given assembly. The power input required to operate the driver shaft is directly proportional to the number of spindles. In a hand operated charkha, the driver shaft is manually rotated by a handle attached to the driver shaft. The torque requirement on these conventional charkhas with 6 to 8 spindles is about 1.5 kg.

The manual charkha suffers two limitations, the manual operations limit the output possible from the machine since the torque requirement is about 1.5 kg for an assembly of 8-10 spindles and quality of the yarn obtained may be uneven due to reasons like human fatigue.

A motor was attached to one such hand spinning device (charkha) and it was found that the eight spindle charkha required not less than 50 watts. When the motor was connected to solar power source a panel of over 60-75 watts was required.

The power requirement for operating the charkha is brought down by attaching a specially designed D.C. motor. This leads to a lower wattage solar panel requirement and thereby to an lower affordable system cost.

The human fatigue could be certainly reduced by brining in the best possible bearing and other mechanism; but the torque needed for the functional requirements like drawing, twisting etc. cannot be done away with. Now when the increase of productivity is needed the functional torque requirements also Internationally accepted health convention do not permit the human being to be made to put in more than certain watts of power. Thus a vible means of motorization at some stage is necessary. In the mean time the effirt to reduce the torque need through best mechanical subsystem should also continue for obvious reason.

The present invention reduces the power requirement for a spinning device uniform supply of power from solar with a battery backup provided to the motor ensures the consistent quality of yarn.

The present invention maintains all the essential constructional features of the conventional charkha namely one or more feed roll pony from which a sliver is drawn and the series of rollers over which the sliver is stretched, such roller series operating at serially faster speeds. The drawn sliver is then wound around spindles spool attached correspondingly to one spindles. The spool revolves at a calibrated speed, facilitating drawing of the sliver and twisting the same to form yarn.
In the motorized version of this charkha, the torque requirement is further reduced by a motor connected to the pulley shaft instead of the driver shaft through a separate pulley system, with calibrated differences in diameter of the pulleys in this system, causing a negative gearing effect, thereby reducing the rpm with which the pulley shaft rotates. This increases the life of the yarn spinning device, as well as reduces the maintenance cost of the device. The reduced wattage motor can be powered by relatively inexpensive solar panels of 50 to 75 watts peak.
A motorized mechanism ensures an even power supply, which in turn ensures a better quality of yarn.

3.4 Solar kit to power the NM Charkha:
The solar kit to be fitted to the charkha comprises of two major subsystems. They are,

i. The motor

A specially designed 12 volt PMDC (permanent magnet direct current) motor and pulleys which can be directly mounted on the charkha. This motor requires about 30-35 watts of power to operate the charkha. The motor is fitted to the charkha's back channel with the help of two metal clamps. The driver pulley of the motor transmits power through a rubber belt to the driven pulley mounted on the spindle driving shaft. The ratio of the driver and the driven pulley is calibrated to get about 70-75 handle RPMs. The motor, pulley and clamps are designed for quick mounting on the existing charkha frame. The motor's main cord is fitted with the male part of the electrical socket at its end which fits into the female part of the socket of the control unit.

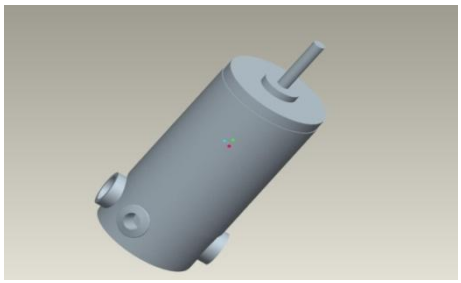

ii. The Control Unit

The control unit is a robust box made of steel with digital display, electrical sockets, switches and a handle. The charge controller and a battery is fitted in this properly ventilated box. A 12 volt 26 AH Exide battery is used in this system. The charge controller is specially designed to suit the ongoing process of operating the charkha as well as charging the battery. The charge controller has a current over charge, deep discharge and a cut-off protection circuit. The digital LCD display on the unit displays the solar in-voltage, battery voltage, charging status and load on/off status. The front panel also consists of a main switch for total on/off of the system, fuse, and sockets for various connections. The electrical sockets are for solar input, motor output and for additional accessories like lamps, fan, FM etc. The sockets are different for different connections such that one application socket does not fit in for other application, thus avoiding confusion.

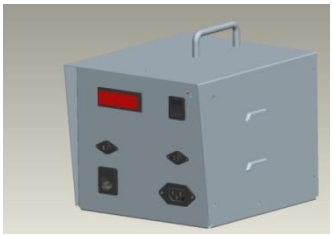

iii. Solar panel:

The solar panel of 60/74 Wp are suitable for proper functioning of the system. The PV modules fitted to the system is from the reputed suppliers. The SPV panel are placed in the open and connected to the control unit through cables.

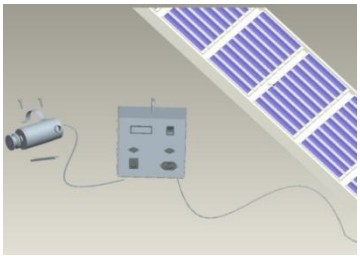

iv. Summary of specifications and other features

Specifications:
- 8-10 spindle NM charkha
- Solar PV module – 60 - 80 Wp
- Motor Drive - 12 V DC, 30 W
- Production capacity - 800 – 1000 gms /8hrs (40counts or more)
- Battery - 12 V, 26 Ah, SMF

Other features:
- Battery back-up available
- Fine quality yarn production
- Low yarn breakages
- Low fatigue
- Can also be operated manually
- User friendly system design

IV. Lab studies and Field trials

4.1 Objectives of Lab studies / Field trials

4.1.1 Lab trials

MGIRI has installed 18 solar charkhas in the institute and has been recording performance since May 2008. It has also been corroborating its results with the observations in other centres also in cities like Wardha, Indore, Surendranagar, Etah etc.
MGIRI's efforts were also to carry out test with a view to compare the yarns that come out of solar charkha with that of traditional NM Charkhas. It has also pursued a search for the best parameters achievable with the solar charkha.
The tables in 4.2 highlight some of the most important results.

4.1.2 Field trials on all India basis

a. Number of hours in a day that the solar charkha could be operated continuously.
b. Number of hanks prepared i.e productivity
c. Comparison of the operation of solar charkha with that of manual charkha
d. Standardizing the parameters for various stations in India.
e. Problems faced during the operation of solar charkha
f. Other observations.

4.2 Results of lab trials

The lab trials proved that

- yarn from a solar charkha are stronger compared to the manually operated charkha. In fact yarns of desired strength could be achieved by proper choice of the drive.
- yarn are more uniform compared to a manually operated. This is because of the incorporation of a battery which helps to give uniform power even in the variable climatic conditions.
- yarn are nearly free from knots. This is because of the absence of jolts and jerks in the charkha which are there when a human being cranks it throwing more or less a significant fraction of the body weight on it – thus resulting in fewer breakage of yarn, less down-time and greater productivity.

The following table indicates the test results carried out in MGIRI

Comparative report on Yarn produced by Solar Charkha Vs NMC Charkha

Aspect	Solar Charkha	NMC Charkha
Thin & Thick places/km	• Thin places /km= 254 • Thick places/km = 996	• Thin places /km=368 • Thick places/km=1156
Unevenness(%)	17.02	17.6
Breakages	Less	More
Strength of Yarn (CSP)	1830	1805

Also the results were confirmed by the tests conducted in The R.S.R Mohota Spg.& Wvg. Mills Ltd, Hinganghat, Maharashtra (See Annexure –II).

4.3 National level field trials

The KVIC funded a project for field trial of MGIRI's solar charkha in six SFURTI clusters across the country. The experiments were carried out during April-June 2010 and have proved that a spinner can earn more than Rs 100 in 8 hrs and more than Rs 150 in the case of silk reeling. If the battery is used to work during another 4 to 8 hrs the earning could be

increased by 50% to 100%. Further since one person can supervise 2 to 4 charkhas the earnings could be further multiplied depending on the investments in additional charkhas thus enabling the spinner to reach the expectations of the minimum wages act of the land.

- **Project: Technology Transfer of Solar Charkha In Khadi sector**
- **Principal Investigator: Deep Varma (PSO, E&I)**
- **Solar charkha installation in the following centers were completed in April itself:**

Sr. No.	Name of Cluster	Date of completion of Installation
1	Karakudi Khadi Cluster, Tamilnadu	**08-April-2010**
2	Khadi Cluster, Bassi, Rajasthan	**10-April-2010**
3	Raibareli Khadi Cluster, UP	**15-April-2010**
4	Surendranagar Khadi Cluster, Gujrat	**20-April-2010**
5	Berampur Jangipur Cotton Khadi Cluster, West Bengal	**23-April-2010**
6	Nagaland Khadi Cluster, Dimapur	**24-April-2010**

Solar Charkha at Karaikudi, TN

Solar Charkha at Bassi, Rajasthan and Raibarely U.P.

Solar charkha at Limbdi, Gujrat

Solar charkha at Murshidabad (W.B.)and Dimapur (Nagaland) Cluster

V. Data analysis

The stations conducting the field trial of MGIRI solar charkha were asked to collect data to finally fill up the following table:

Date	Solar Charkha Identification no.	Count of Yarn	Production (Hanks)	Total Time (Working hrs)

A feedback report on the performance of solar charkha was submitted to KVIC on June 2010 and it was found that there was huge variation in the outputs. The chief reason was that the set standards were not followed. (see annexure - I) In fact the charkhas that were employed where from many sources each are having different gear setting etc. thus creating large variations in torque requirement.

A rigorous retuning was carried out to minimize variations. Further a decision was taken by the KVIC (No.SFURTI/Solar Charkha/2011 dated 26th May 2010) to carry out a rigorous combined field trial monitoring of one week through a committee consisting of responsible officer from KVIC & MGIRI. Thus the daily data were recorded for further analysis.

The segment of the data from this controlled experiment is presented in tables – I, II, III, IV and V below.

The table related to Dimapur (Nagaland) is not presented here since the voluminous data in this station was free from problems right from the beginning. Further this station used the solar technology for the silk yarn spinning and since the rates of raw material and wages were incomparable to the case of cotton yarn spinning there is not presented below. However reports and data from Dimapur were sent to KVIC and as per the analysis and conclusion by the KVIC they had one of the best performances. It is reported that Dimapur attained the earning of Rs. 150/person per day whereas it was Rs 60-Rs70 per person per day before the introduction of solar charkha.

Table I Data recorded during the combined field trials
Solar Charkha Report of Paho Kahdi Cluster, Raibarely (U. P)

SN	Date and Solar Charkha		Hank (Count) Number	Production (Hank)	Total Time (Working hrs)
1	11/05/10	Solar Charkha- I	35	31	6:30 Hr.
		Solar Charkha – II	35	36	6:45 Hr.
		Solar Charkha- III	35	34	7:00 Hr.
		Solar Charkha IV	35	22	5:30 Hr.
2	12/05/10	Solar Charkha- I	35	39	7:00 Hr.
		Solar Charkha – II	35	41	8:00 Hr.
		Solar Charkha- III	35	47	8:00 Hr.

		Solar Charkha IV	35	43	8:00 Hr.
3	13/05/10	Solar Charkha- I	35	34	6:45Hr.
		Solar Charkha – II	35	37	7:35Hr.
		Solar Charkha- III	35	40	8:00Hr.
		Solar Charkha IV	35	36	7:15Hr.
4	14/05/10	Solar Charkha- I	35	34	7:00 Hr.
		Solar Charkha – II	35	34	7:00Hr.
		Solar Charkha- III	35	30	6:15Hr.
		Solar Charkha IV	35	32	6:30Hr.
5	16/05/10	Solar Charkha- I	35	41	8:00 Hr.
		Solar Charkha – II	35	35	6:40Hr.
		Solar Charkha- III	35	32	6:15Hr.
		Solar Charkha IV	35	33	6:25Hr.
6	17/05/10	Solar Charkha- I	35	33	7:00 Hr.
		Solar Charkha – II	35	33	6:35Hr.
		Solar Charkha- III	35	35	6:25Hr.
		Solar Charkha IV	35	34	6:35Hr.

*** Low quality Rowing

Table – II Solar Charkha Report of Limbdi Kahdi Cluster, Rajkot (Raj) I

Sr. No.	Date and Solar Charkha		Hank (Count) Number	Production (Hank)	Total Time (Working hrs)
1	10/06/10	Solar Charkha- I	40	27	5:45Hr.
		Solar Charkha – II	40	30	6:15Hr.
		Solar Charkha- III	40	17	4:15Hr.
		Solar Charkha IV	40	13	3:30Hr.
2	11/06/10	Solar Charkha- I	40	11	4:15Hr.
		Solar Charkha – II	40	22	4:45Hr
		Solar Charkha- III	40	18	4:15Hr.
		Solar Charkha IV	40	17	4:15Hr.
3	12/06/10	Solar Charkha- I	40	30	5:45Hr.
		Solar Charkha – II	40	28	6:15Hr.
		Solar Charkha- III	40	16	3:45Hr.
		Solar Charkha IV	40	18	5:00Hr.
4	14/05/10	Solar Charkha- I	40	17	5:00Hr.
		Solar Charkha – II	40	35	6:00Hr.
		Solar Charkha- III	40	22	6:30Hr.
		Solar Charkha IV	40	22	6:45Hr.
5	15/05/10	Solar Charkha- I, I, III, IV	No Production due to Rain		
6	16/06/10	Solar Charkha- I	40	13	3:00Hr.
		Solar Charkha – II	40	28	5:00Hr.
		Solar Charkha- III	40	21	5:00Hr.
		Solar Charkha IV	40	18	5:00Hr.
7	17/06/10	Solar Charkha- I, iI, III, IV	Hon. Minister Programme at Surendranagar (Raj.)		
8	18/06/10	Solar Charkha- I	40	30	6:30Hr.
		Solar Charkha – II	40	35	6:30Hr.
		Solar Charkha- III	40	30	6:30Hr.
		Solar Charkha IV	40	22	4:30Hr.
9	19/06/10	Solar Charkha- I	40	32	6:30Hr.
		Solar Charkha – II	40	34	6:30Hr.
		Solar Charkha- III	40	30	6:30Hr.
		Solar Charkha IV	40	22	4:30Hr.

*** Solar Charkha No. 3 and 4 are very poor in quality

Table – III Solar Charkha Report of Beharmpur Khadi Cluster, Murshidabad (WB)

Sr. No.	Date and Solar Charkha		Hank (Count) Number	Production (Hank)	Total Time (Working hrs)
1	21/06/10	Solar Charkha- I	70	30	6:30 Hr.

		Solar Charkha - II	70	30	6:35 Hr.
		Solar Charkha- III	70	33	7:30 Hr.
		Solar Charkha IV	70	34	7:30 Hr.
2	22/06/10	Solar Charkha- I	70	30	6:30 Hr.
		Solar Charkha - II	70	31	6:45 Hr.
		Solar Charkha- III	70	32	7:00 Hr.
		Solar Charkha IV	70	30	6:30 Hr.
3	23/06/10	Solar Charkha- I	70	26	6:00Hr.
		Solar Charkha - II	70	30	7:00Hr.
		Solar Charkha- III	70	30	7:00Hr.
		Solar Charkha IV	70	30	7:00Hr.
4	24/06/10	Solar Charkha- I	70	18	4:30 Hr.
		Solar Charkha - II	70	27	6:00Hr.
		Solar Charkha- III	70	30	6:30Hr.
		Solar Charkha IV	70	34	7:30Hr.
5	25/06/10	Solar Charkha- I	70	31	7:00 Hr.
		Solar Charkha - II	70	31	7:00Hr.
		Solar Charkha- III	70	29	7:00Hr.
		Solar Charkha IV	70	30	7:00Hr.
6	26/06/10	Solar Charkha- I	70	17*	4:00 Hr.
		Solar Charkha - II	70	07*	2:00Hr.
		Solar Charkha- III	70	07*	2:00Hr.
		Solar Charkha IV	70	18*	4:00Hr.

** Production less due to low working hours out of climatic conditions

Table – IV Solar Charkha Report of Karaikudi Khadi Cluster, Kandanur (TN)

SN	Date and Solar Charkha		Hank (Count) Number	Production (Hank)	Total Time (Working hrs)
1**	22/06/10	Solar Charkha- I	30	30	6:00 Hr.
		Solar Charkha - II	30	30	6:00 Hr.
		Solar Charkha- III	30	20	6:00 Hr.
		Solar Charkha IV	30	30	6:00 Hr.
		Solar Charkha - V	30	14	4:00Hr.
2**	23/06/10	Solar Charkha- I	30	26	4:50 Hr.
		Solar Charkha - II	30	30	4:50 Hr.
		Solar Charkha- III	30	25	5:00 Hr.
		Solar Charkha IV	30	30	4:50 Hr.
		Solar Charkha - V	30	Nil	Nil
3**	24/06/10	Solar Charkha- I	30	10	1:50Hr.
		Solar Charkha - II	30	35	5:45Hr.
		Solar Charkha- III	30	20	4:50Hr.
		Solar Charkha IV	30	35	6:00Hr.
		Solar Charkha - V	30	25	4:15Hr
4**	24/06/10	Solar Charkha- I	30	18	4:30 Hr.
		Solar Charkha - II	30	27	6:00Hr.
		Solar Charkha- III	30	30	6:30Hr.
		Solar Charkha IV	30	34	7:30Hr.
		Solar Charkha -V	30	25	4:15Hr
5	25/06/10	Solar Charkha- I	30	35	6:15 Hr
		Solar Charkha - II	30	35	5:45Hr.
		Solar Charkha- III	30	30	5:45Hr.
		Solar Charkha IV	30	39	6:30Hr.
		Solar Charkha -V	**30**	**39**	**6:20Hr**
6	26/06/10	Solar Charkha- I	30	31	5:45 Hr.
		Solar Charkha - II	30	30	5:20Hr.
		Solar Charkha- III	30	30	5:35Hr.
		Solar Charkha IV	30	35	5:25Hr.
		Solar Charkha -V	30	30	5:20Hr.

** Due to Cloudy weather & lesser working hours production is low

Table – V Solar Charkha Report of Bassi, Rajasthan

SN	Date and Solar Charkha		Hank (Count) Number	Production (Hank)	Total Time (Working hrs)
1	08/06/10	Solar Charkha- I	40	27	5:00 Hr.
		Solar Charkha - II	40	20	5:00 Hr.
		Solar Charkha- III	40	23	5:00 Hr.
		Solar Charkha IV	40	31	7:00 Hr.
2	09/06/10	Solar Charkha- I	40	35	7.00 Hr.
		Solar Charkha - II	40	32	7.00 Hr.
		Solar Charkha- III	40	36	7.00 Hr.
		Solar Charkha IV	40	36	7.00 Hr.
3	10/06/10	Solar Charkha- I	40	35	7.00 Hr.
		Solar Charkha - II	40	33	7.00 Hr.
		Solar Charkha- III	40	32	7.00 Hr.
		Solar Charkha IV	40	35	7.00 Hr.
4	11/06/10	Solar Charkha- I	40	35	7.00 Hr.
		Solar Charkha - II	40	35	7:00Hr.
		Solar Charkha- III	40	38	8.00Hr.
		Solar Charkha IV	40	43	8.00Hr.
5	12/06/10	Solar Charkha- I	40	35	7.00 Hr.
		Solar Charkha - II	40	36	7.00 Hr.
		Solar Charkha- III	40	31	7.00 Hr.
		Solar Charkha IV	40	36	7.00 Hr.
6	14/06/10	Solar Charkha- I	40	40	7.00 Hr.
		Solar Charkha - II	40	36	7.00 Hr.
		Solar Charkha- III	40	42	7.00 Hr.
		Solar Charkha IV	40	28	5.30 Hr.

VI. Conclusions

Interim results of field trials:

Hanks produced / 8 hrs on MGIRI's solar charkha as per reports from SFURTI clusters

Khadi cluster	Count	Ave production of hanks		Hanks / 8hrs	Wages / day in Rs
		per day	of hrs		
Paho, Raibereli (UP)	35	35	6.84	41	107
Limbidi, Rajkot (GJ)	40	23	5.01	37	103
Behrampur, Murshidabad (WB)	70	27	6.00	36	107
Kandanur,Karaikudi (TN)	30	28	5.07	44	132
Banskho, Bassi (RJ)	40	35	6.60	42	124
Dimapur, Nagaland (Muga Silk)	45	21	6.00	28	153

A review of the interim results took place in KVIC, Mumbai on 8-9 July 2010 in which Commission members, relevant khadi institutions, manufacturers of khadi implements and representatives from MGIRI participated. It is clear from the above results that the spinner can earn more than 100 Rs./day per solar charkha.

The KVIC, during this two day convention confirmed the interest of KVIC institutions, manufacturers and Khadi Mission members in the solar charkha project.

The Chairperson of KVIC also announced to the press that the field trials have proved that **MGIRI solar charkha is technically and economically viable** for the spinner and weavers.

KVIC institutions, Commission members, manufactures, respectively, in the Mumbai meet on 8-9 July 2010.

Warm reception from the artisans, Khadi institutions, Khadi Mission and state governments:

There was exceptionally high response from the artisans and khadi enthusiasts in a dozen national level exhibitions and *karigar sammelans.*

President of India watches the Solar Charkha at Amravati during a visit on 7-1-2010. Mr Deep Varma (Designer of Solar Charkha) is explaining the system.

Solar Charkha in Khadi Utsav-2010 at Allahabad attracted large crowds.

The reaction from khadi mission is clear from the encouragement/ guidance they gave when the solar charkha was demonstrated in their annual meeting at Wardha on 17- 07- 2008. Further, the Khadi Mission in their March 2010 meeting at Wardha took a historic decision that the yarn from the solar charkha should be linked to the handlooms so that the later could be liberated from the government system of 'hank yarn obligation' which places the weavers at the mercy of spinning mills.
It didn't take much time for the state governments to understand that the above development has enormous implications to energy management, rural development, social welfare, textile and many other contexts and that spinning could emerge as a decentralized 'home industry' following the case of weaving. The fact that the Chief Minister of Karnataka chose solar charka as a major symbol on the occasion of October 2, 2009 is an indication of the above. Similarly the interest of the Tamilnadu Government to work out a solar alternative to the energy starved spinning mills is an interesting example.

Chief Minister of Karnataka Shri B S Yadyurappaji inaugurated the Solar Charkha at Gandhi Bhavan, Bangalore on the auspicious occasion of 2nd Oct 2009, Gandhi Jayanti.

A note about the working of MGIRI solar charkha in all parts of India during all the seasons:

A question may be raised that although the solar charkhas were found to perform uniformly well in all the six stations spread across the country only because the trial was conducted during April-June which are summer months; and that the performance could vastly differ had the trial been conducted during the winter.

The above observation/criticism is well founded; and its implication to the solar technology project could also be easily explained if one takes a systemic point of view. In fact the solar energy is an input and in the cases where relation between input and output are linear the experiments need not be conducted for all the ranges of input.

In fact the solar insolation (average energy received from sun's rays during a particular day) for various locations of India have been measured and documented by the scientists and the relevant charts are available in the website of MNRE for every month. A perusal of this chart indicate that indeed there are two zones of India – namely Kashmir and a pocket of North-east where the insolation drops by almost 40% during a few months of the year. From this data a systems approach helps us to conclude that the solar charkha could be used to get the same output in these zones even during low insolation period provided we are willing to invest a proportionately higher area of photo voltaic panel. There will be a few other issues like the effect of cloud, snow fall etc. But these questions will also encountered in other areas as well. Certainly a few days in a year are lost in every economic activity due to exigencies like flood, cyclone etc.

Annexure -I

Report on the documentation and field problems rectification

In the recently completed Solar Charkha installations at various Khadi institutions SFURTI clusters, variation in the yarn production of the Solar Charkha's was noted in the feedback report. Every institute is given a feedback report format to be filled on daily basis. For the purpose of documentation and to indentify the problem of the variation in the yarn production, an urgent visit to every cluster was planned. It was decided to complete the visit program within a week's time. Persons visiting at these places were,

- Deep Varma (PI) and Sachin Raut (SSO, E&I) to Paho, Raibarelly U.P; Bassi, Rajasthan; Murshidabad, West Bengal, Dimapur, Ngaland.
- Dr. T. Karunakaran (Director, MGIRI) to Limbdi, Gujrat.
- Mr. Ravikumar Kandasamy (Deputy Director, E&I) to Karaikudi Tamilnadu.

1) Raibarelly (Paho) U.P.

Deep Varma (PI) and Sachin Raut (SSO, E&I)

Highlights:

Starting time: 9:30AM
Lunch time: 1:00 to 1:30 PM
Stop time: 5 PM
Effective average working period: @ 7 hours
Hank number: 35-40 count
Maximum production achieved in a day: 44 hanks

Reported problems:

- Large variation in yarn production, like in one Solar Charkha with a maximum production of 44 hanks/day and the other with a minimum production of 20 hanks/day.
- Some Solar Charkha production was declining day by day.
- One Solar Charkha stops in the evening.

Problems Identified:

- The Solar Charkha with minimum production had a very high pressure of Top Arms.
- The Motor was jammed with the roving and yarn tightly wound in between the shaft pulley and the bearing.
- Shafts, Bushes etc. were blocked by threads and filaments.
- Gearing was not proper.
- Some new Charkhas had alignment problems.
- The Solar PV panels are placed on the terrace of the CFC and the boundary wall and pillars are of more than 6 feet high, hence sun light falling on the SPV was restricted during morning and evening time. A design of fabrication structure for the mounting of SPV panel was given to them during the installation phase and was suggested to implement as early as possible.
- The Solar Charkha was consuming more than double the wattage and running at half the speeds because of the above stated problems. Hence, the production of some Solar Charkha was deteriorating day by day.
- One SPV panel was getting in early shadow of the pillar and the Solar Control Unit attached to it, was used for other purposes also, hence the unit was stopping during evening time.
- The spinners keep their own Charkha very neat and clean but not the Solar Charkha, as they think that they are not responsible for these Charkha's. One single Master has to take care of the all Charkhas in that area.

Action Taken:

- Overhauling of the Solar Charkha was fully conducted including cleaning, oiling of parts, optimizing top arm pressures etc.
- Proper gearing set fitting and proper alignment of the Solar Charkha was done.
- SPV panel stand of 7 feet height was fabricated. The panels were mounted on the stand and then fitted on the terrace.
- All the above stated problems where conveyed to the people concerned there and were instructed to take actions accordingly.

Result:

- The production came back to normal as it was at the initial stage (ie. 35 – 40 hanks/day/Solar Charkha).
- People understood the importance of the project and agreed to take due care of the system.

2) Bassi (Banskho) Rajasthan:

Deep Varma (PI) and Sachin Raut (SSO, E&I)

Highlights:
Starting time: 9:30 AM
Lunch time: 12:00 to 1:00 PM
Stop time: 5 PM
Effective average working period: 7 hours
Hank number: 35-40 count
Solar Charkhas are in good condition and proper care is taken.

Reported problems:
- Some Solar Charkha speed was declining in the evening time in between days.
- The Solar Charkha production is consistent but a little less as compared to other clusters.

Problems Identified:
- The Solar PV panels are placed on the tin roof of the CFC and the cluster is located at a foot hill. The hill is on the western side adjacent to this cluster hence, the sun light falling on the SPV is restricted during evening time.
- Two motors were consuming a little more wattage.
- Gearing of the Charkha are not as required.

Action Taken:
- Rearrangement of working time schedule is suggested such that the lunch time can be illuminated and the spinners can stop work one hour early in the evening.
- Motors were changed as a precautionary measure.

Result:
- The production has enhanced and expected to be much better after altering the gearing ratio.

3) Mushidabad, West Bengal:
Deep Varma (PI) and Sachin Raut (SSO, E&I)

Highlights:
Starting time: 9:30AM
Lunch time: 12:00 to 1:00 PM
Stop time: 5:00 PM
Effective average working period: less than 7 hours
Hank number: 70 count

Reported problems:
- Variation in yarn production, like in one Solar Charkha with a maximum production of 31-32 hanks/day and the other with a minimum production of 20 hanks/day.

Problems Identified:
- Gearing set in this Charkha is different from that used in lower count hanks.
- The Charkha with high production of hanks was having altogether a different gearing set as compared to Charkha's with lower hank production.
- Know-how about these Charkhas was lacking.
- The Solar PV panels were placed on the terrace of the CFC. But the panels were placed in the fabricated guarding wires, this obstructs the sunlight falling on the panels.

Action Taken:
- Gearing ratios were corrected with reference to higher producing Charkha.
- They are told to remove the SPV panels from the fabricated frame and to place them over this frame.
- All the above stated problems where conveyed to the people concerned.

Result:
- The average hank production of each Solar Charkha is now similar (ie. 31 – 33 hanks/day/Solar Charkha).

4) Rajkot (Limbdi), Gujrat:
Dr. T. Karunakaran (Director MGIRI)

Highlights:
Starting time: 9:00 AM
Lunch time: 12:00 to 2:00 PM
Stop time: 5 PM
Effective average working period: less than 6 hours

Hank number: 35-40 count

Reported problems:
- The daily Solar Charkha production is consistent but lesser as compared to other clusters.

Problems Identified:
- Working time is lesser.
- Gearing of the Charkha are not as required.
- Spinners operating more than one Solar Charkha and are inexperienced.

Action Taken:
- Rearrangement of working time schedule is suggested such that the lunch time can be reduced which also is the peak period of Sunlight.
- Gearing ratio change and induction of compatible spinners is suggested.

Result:
- The hank production has enhanced after the gearing change.
- The other results are still awaited.

5) Karaikudi, Tamilnadu:
Ravikumar Kandasamy (Deputy Director E&I, MGIRI)

Highlights:
Starting time: 9:00 AM
Lunch time: 12:00 to 1:00 PM
Stop time: 5 PM
Effective average working period: less than 7 hours
Hank number: 35-40 count

Reported problems:
- The daily Solar Charkha production is consistent but lesser as compared to other clusters.
- One Solar Charkha is not working from soon after installation.

Problems Identified:
- Gearing of the Charkha are not as required.
- The fuse was blown out in one unit.
- Technical staff is not available on regular basis.
- The Charkas maintenance is poor.

Action Taken:
- The stopped control unit is changed.
- Gearing ratio change and proper maintenance of the system was suggested.

Result:
- The hank production has enhanced after the gearing change.
- The other results are still awaited.

6) Dimapur, Ngaland:

Highlights:
Starting time: 9:00 AM
Lunch time: 12:00 to 1:00 PM
Stop time: 5 PM
Effective average working period: less than 7 hours
Mooga Silk production unit
Production of silk from Solar Charkha is 500 – 600 grams/day that is almost double than hand spinning

Reported problems:
The daily Solar Charkha production is consistent and not much problem is reported.

ANNEXURE II

The Rai Saheb Rekhchand Mohota Spg. & Wvg. Mills Ltd.
Corporate Office : Post Box. No. 1, Hinganghat, Dist. Wardha, Maharashtra - 442 301
Ph. : 07153-244282, 244545 Fax : 244753 Gram - MOHTAMILL E-mail info@rsmm.com

ISO 9001 - 2008 CERTIFIED QUALITY SYSTEM

QUALITY CERTIFICATE

Sample Result of 20s K (100%) Cotton

Solar Charkha Yarn & Yarn from manual operation

Supplier : M/S Mahatma Gandhi Institute for Rural Industrialisation Wardha

Date of Receipt : 31.08.2010

Standards Dept. Date of Testing : 31.08.2010

Sr.No.	Properties	Results			
	Product	20s K			
	Blend %	100% Cotton			
	Count & Test Parameter	**Solar Charkha Yarn**		**Yarn from Manual Operation**	
	Teeth (Gear)	**20 Teeth**	**18 Teeth**	**20 Teeth**	**18 Teeth**
1	Avg. Count	20.67s	20.39s	20.78s	20.66s
2	Avg. Test in Lbs.	106.64	113.73	110.28	106.66
3	C.S.P.	2204	2319	2292	2204
	Uster & Imperfection Value				
6	Yarn U %	16.11	17.78	16.3	17.97
7	Thin Places / Km	328	799	406	825
8	Thick Places / Km	770	872	675	934
9	Neps / Km	964	1099	921	1290
10	Total / Km	2062	2770	2002	3049
	Twist Results				
11	T.P.I.	18.22	21.03	17.41	18.68
12	ASTM Grade	C	D	C	C

Manager Q C G.M.(Tech.) C.E.O.

International Journal of Modern Engineering Research (IJMER)
www.ijmer.com Vol.3, Issue.4, Jul - Aug. 2013 pp-1980-1987 ISSN: 2249-6645

Indirect Vector Control of Induction Motor Using Pi Speed Controller and Neural Networks

C. Mohan Krishna M. Tech[1], G. Meerimatha M.Tech[2], U. Kamal Kumar M. Tech[3]
[1]*Assistant Professor, EEE Department SVIT Engineering College ANANTAPUR*
[2]*Associate Professor, EEE Department SRIT Engineering College ANANTAPUR.*
[3]*Assistant Professor SRIT Engineering College ANANTAPUR.*

Abstract: *In this paper, an implementation of intelligent controller for speed control of an induction motor (IM) using indirect vector control method has been developed and analyzed in detail. The indirect vector controlled induction motor drive involve decoupling of the stator current in to torque and flux producing components. The comparative performance of Proportional integral (PI) and Artificial Neural Networks (NN). control techniques have been presented and analyzed in this work.*

Keywords: *indirect vector controller (IVC), Proportional integral (PI), Artificial Neural Networks (NN).*

I. INTRODUCTION

A three-phase induction motor is a singly excited a.c machine in the sense that is supplied from a single source. Its stator winding is directly connected to a.c source, whereas stator winding receives its energy from stator by means of induction. Balanced three phase currents in three phase windings produce at constant amplitude rotating m.m.f wave. The stator produced m.m.f wave and rotor produced m.m.f wave, both rotate in the air gap in the same direction at synchronous speed. These two m.m.f wave are thus stationary [1] with respect to each other, consequently the development of steady electromagnetic torque is possible at all speeds but not at synchronous speed. The vector control or field oriented control (FOC) theory is the base of a special control method for induction motor drives [2]. The most commonly used controller for the speed control of Induction motor is Proportional plus Integral (PI) controller [1]. However, the PI controller has some demerits such as: the high starting overshoot, sensitivity to controller gains and sluggish response due to sudden disturbance. To overcome these problems, replacement of PI controller by an intelligent controller based on neural networks is proposed and compared with the PI controller using simulation results

II. PI CONTROLLER BACKGROUND

A PI controller responds to an error signal in a closed control loop and attempts to adjust the controlled quantity to achieve the desired system response. The controlled parameter can be any measurable system quantity such as speed, torque, or flux. The benefit of the PI controller is that it can be adjusted empirically by adjusting one or more gain values and observing the change in system response[4]. It is assumed that the controller is executed frequently enough so that the system can be properly controlled. The error signal is formed by subtracting the desired setting of the parameter to be controlled from the actual measured value of that parameter. The sign of the error indicates the direction of change required by the control input Result is a small remaining steady state error. The Integral (I) term of the controller is used to eliminate small steady state errors. The I term calculates a continuous running total of the error signal. Therefore, a small steady state error accumulates into a large error value over time. This accumulated error signal is multiplied by an I gain factor and becomes the I output term of the PI controller.

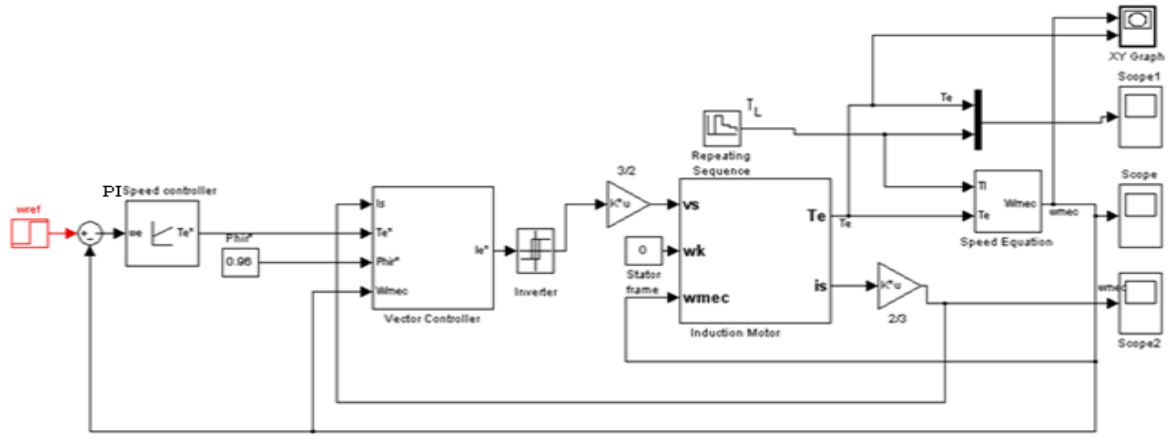

Fig-2.1 PI BASED CONTROLLER

2.1.1 Tuning of pi controllers

Proportional-integral (PI) controllers have been introduced in process control industries. Hence various techniques using PI controllers to achieve certain performance index for system response are presented[5] . The technique to be adapted

for determining the proportional integral constants of the controller, called *Tuning*, depends upon the dynamic response of the plant.

In presenting the various tuning techniques we shall assume the basic control configuration wherein the controller input is the error between the desired output (command set point input) and the actual output. This error is manipulated by the controller (PI) to produce a command signal for the plant according to the relationship.

$U(s) = K_p (1+1/\tau_i s)$ ——————(1)

Or in time domain

$U(t) = K_p [e(t) + (1/\tau_i) \int edt]$ ———(2)

Where K_p = proportional gain

τ_i = integral time constant

If this response is *S*-shaped as in, Ziegler-Nichols tuning method is applicable**.**

2.1.2 Zeigler- Nichols Rules for tuning PI controllers:

First Rule:

The *S*-shaped response is characterized by two constants, the dead time *L* and the time constant *T* as shown. These constants can be determined by drawing a tangent to the *S*-shaped curve at the inflection point and state value of the output. From the response of this nature the plant can be mathematically modeled as first order system with a time constant *T* and delay time *L* as shown in block diagram[6] . The gain *K* corresponds to the steady state value of the output C_{ss}. The value of K_p,T_i and T_d of the controllers can then be calculated as below:

$Kp=1.2(T/L)$ ---------- (3)

$\tau_i = 2L$ ----------(4)

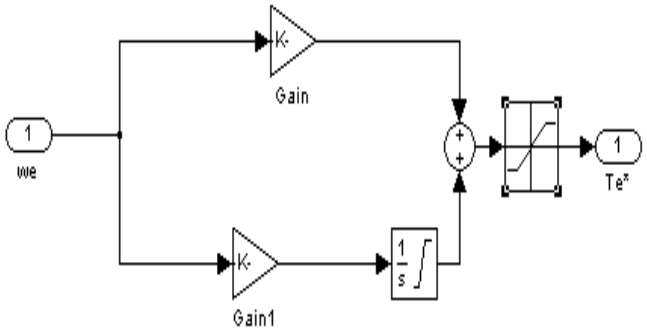

Fig 2.3 PI Controller 1st order system block diagram

III. NEURAL NETWORKS BASED CONTROLLER:

Neural networks are simply a class of mathematical algorithms, since a network can be regarded as a graphic notation for a large class of algorithms. An Artificial Neural Network (ANN) is an information processing paradigm that is inspired by the way biological nervous systems, such as the brain, process information. It is composed of a large number of highly interconnected processing elements (neurons) working in unison to solve specific problems. An ANN is configured for a specific application, speed control or energy saver, through a learning process. Neural network key part is a feed forward NN with two inputs and one output. NN is divided into three layers, named the input layer with 2 neurons, the hidden layer with 10 neurons, and the output layer with 1 neuron [6]. The activation function of the input neurons is linear while that of the output layer and hidden layer is sigmoid, Neural networks can perform massively parallel operations. The exhibit fault tolerance since the information is distributed in the connections throughout the network [7]. By using neural controller the peak overshoot is reduced and the system reaches the steady state quickly when compared to a conventional PI controller [8].

3.1 Program for creating the neural network:

```
Load n
k1=max (i');
k2=max (o1');
P=i'/k1;
T=o1'/K2;
n=157128;
Net = newff (minmax (P), [5 1], {'tansig' 'purelin'});
 net.trainParam.epochs = 200;
Net = train (net, P, T);
Y = Sim (net);
Plot (P, T, P, Y,' ô') gensim (net,-1)
```

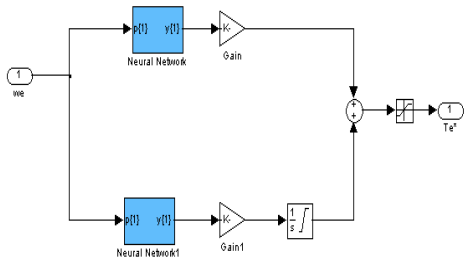

Fig 3.1 NN Controller 1st order system block diagram

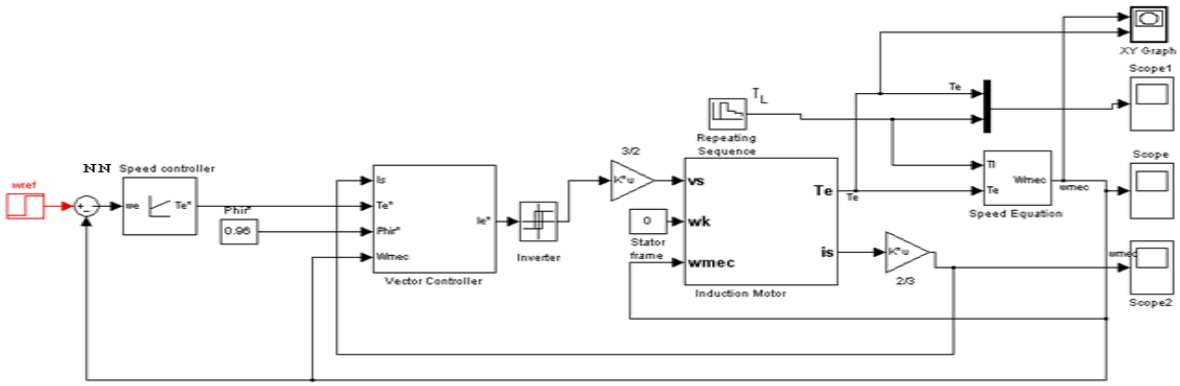

Fig-3.2 NN BASED CONTROLLER

IV. Simulation Results and discussion:

The simulation was done using the Matlab/Simulink package.

4.1 Case 1: No-Load :(for Speed =120rad/s, torque Te= 0, 0,0,0,0 N-m)

4.1.1 PI Controller:

Speed (rad/s) Vs Time(s):

Speed (rad/s)

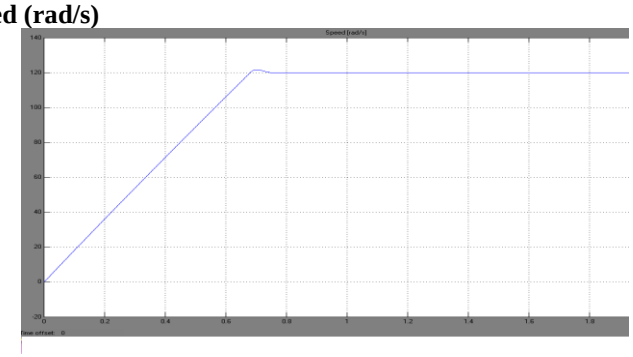

Time(s)

Fig: 4.1

Torque (N-m) Vs Time(s)

Torque (N-m)

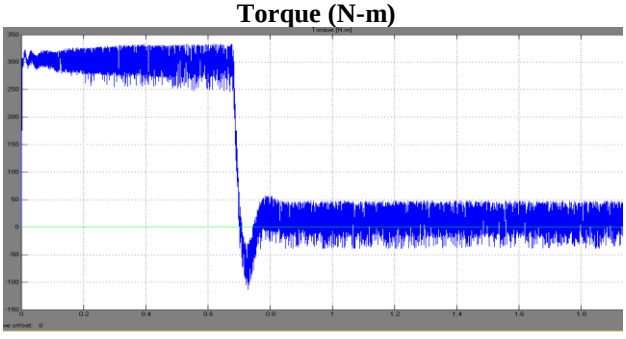

Time(s)

Fig: 4.2

Current (A) Vs Time(s)

Current (A)

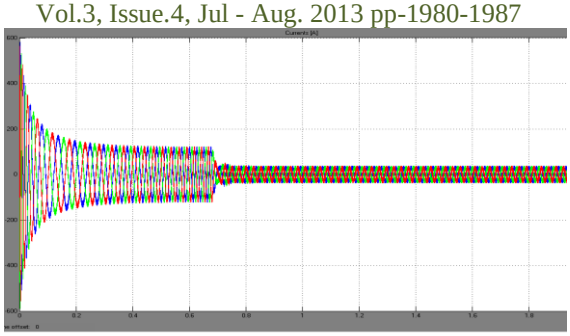

Time(s)
Fig: 4.3

4.1.2 NN Controller:
Speed (rad/s) Vs Time(s):

Speed (rad/s)

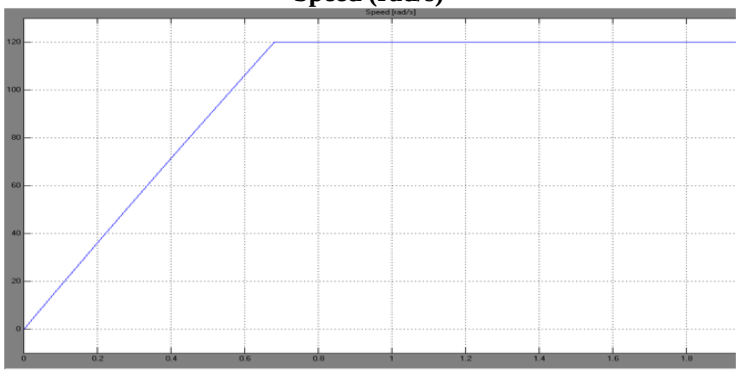

Time(s)
Fig: 4.4

Torque (N-m) Vs Time(s)

Torque (N-m)

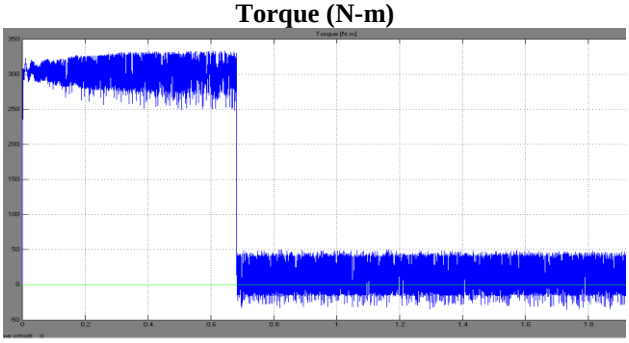

Time(s)
Fig: 4.5

Current (A) Vs Time(s)

Current (A)

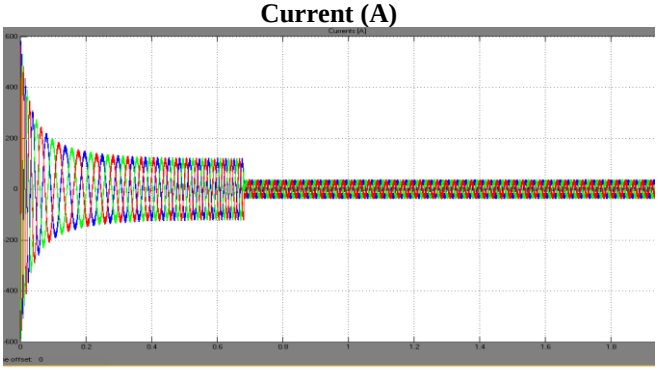

Time(s)
Fig: 4.6

4.2 Case 2: Step Change in –Load :(for Speed =120rad/s Torque Te=0, 50, 200, 100, 50 N-m)
4.2.1 PI Controller:

Speed (red/s) Vs Time(s):

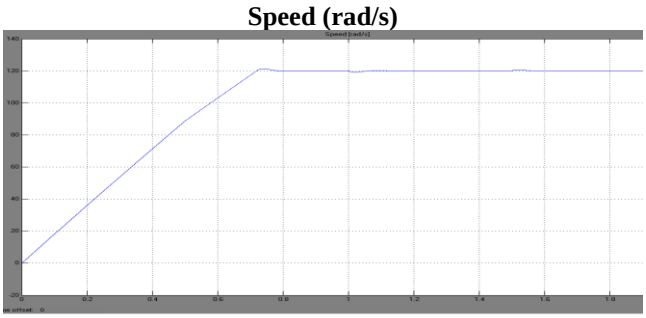

Fig: 4.7

Torque (N-m) Vs Time(s)

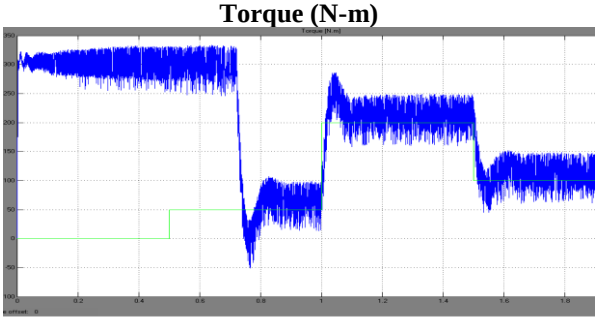

Fig: 4.8

Current (A) Vs Time(s)

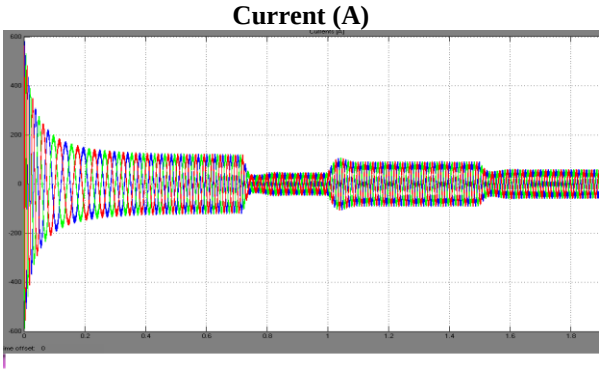

Fig: 4.9

4.2.2 <u>NN Controller</u>:

Speed (rad/s) Vs Time(s):

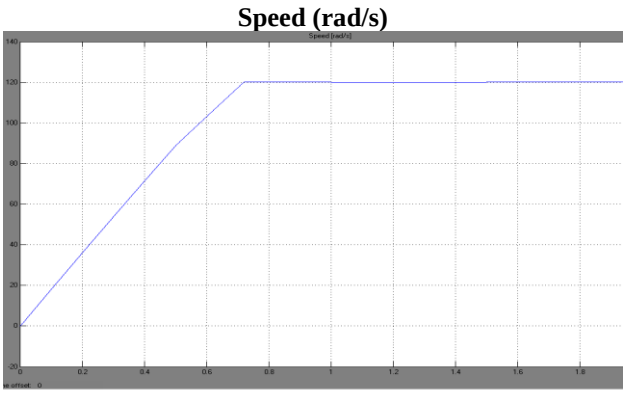

Fig: 4.10

Torque (N-m) Vs Time(s)

Torque (N-m)

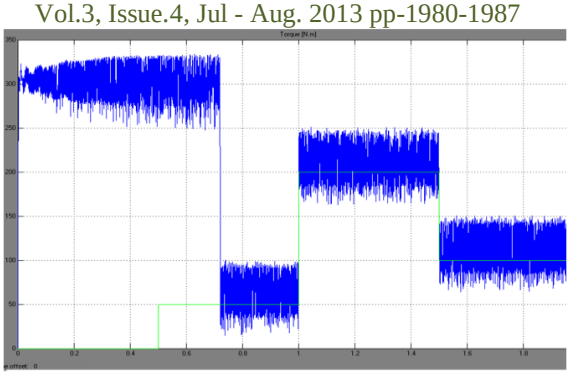

Time(s)
Fig: 4.11

Current (A) Vs Time(s)

Current (A)

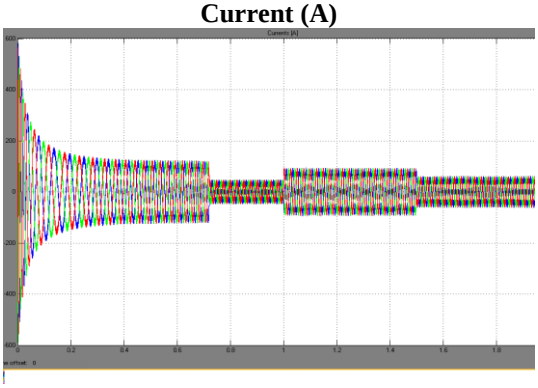

Time(s)
Fig: 4.12

4.3 Case 3: Speed Reversal: (For Speed □ =120 to 120 rad/s, Torque Te=0, 50,200,100,50N-m)

4.3.1 PI Controller:

Speed (rad/s) Vs Time(s):

Speed (rad/s)

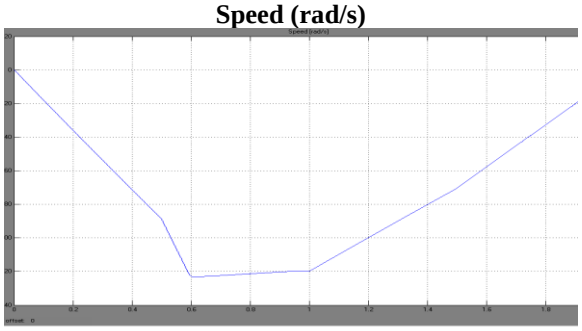

Time(s)
Fig: 4.13

Torque (N-m) Vs Time(s)

Torque (N-m)

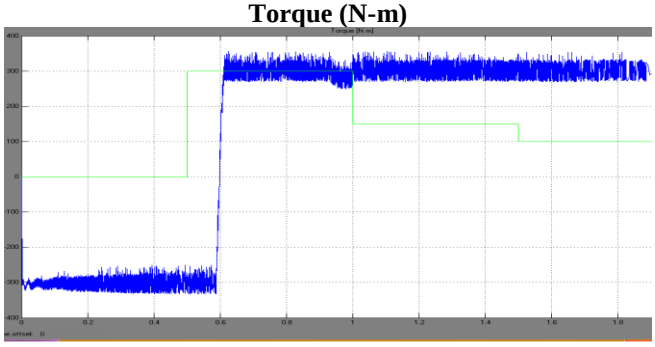

Time(s)
Fig: 4.14

Current (A) Vs Time(s)

Current (A)

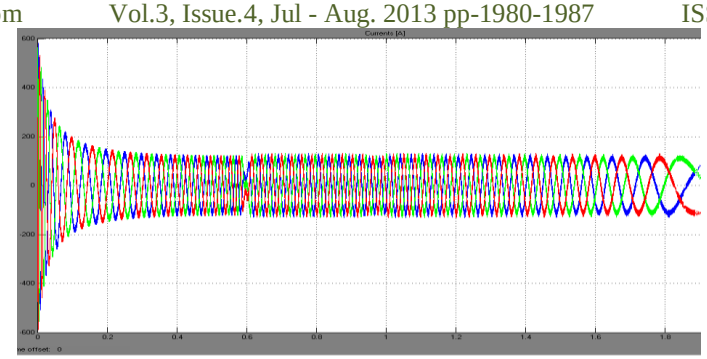

Time(s)
Fig 4.16

4.3.2 NN Controller:
Speed (rad/s) Vs Time(s):

Speed (rad/s)

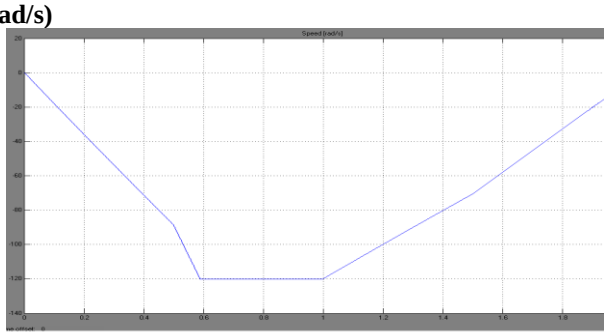

Time(s)
Fig: 4.18

Torque (N-m) Vs Time(s)

Torque (N-m)

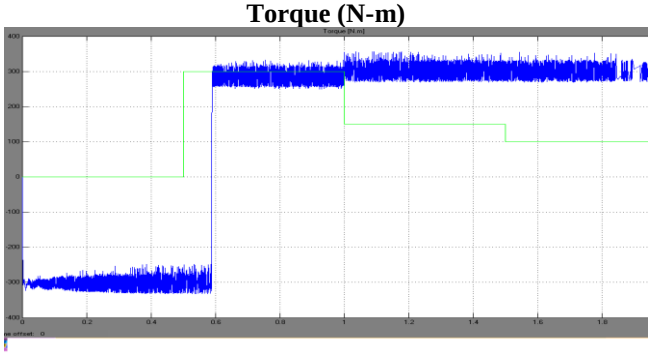

Time(s)
Fig 4.17

Current (A) Vs Time(s)

Current (A)

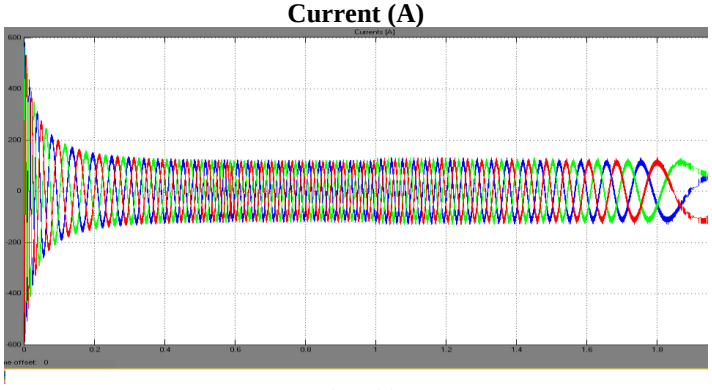

Time(s)
Fig: 4.18

From the simulation results it is clear that, at no-load using PI based controller with speed 120 rad/s, torque Te=0, 0,0,0,0 N-m the characteristics obtained from PI based controller are shown in fig 4.1, 4.2, and 4.3, from the characteristics

Speed Vs Time it is observed that overshoot appeared at 0.7sec. From Torque Vs time characteristics, it is observed that under shoots appeared at 0.75 sec and from Current Vs time characteristics it is observed that disturbances occurred at 0.75 sec because of mismatching of op-amps used in speed controller. Using neural network based speed controller, over shoots at 0.7 sec in Speed Vs Time characteristics are eliminated, under shoots at 0.75 sec in Torque Vs Time characteristics are eliminated and disturbances at 0.75 sec in Current Vs Time characteristics are eliminated. These characteristics are shown in fig 4.4, 4.5, 4.6.

At step change using PI based controller with speed 120 rad/s, torque Te=0,50,200,100,50 N-m the characteristics obtained from PI based controller are shown in fig 4.7,4.8,and 4.9, from the characteristics Speed Vs Time it is observed that overshoot appeared at 0.7,1,1.5 sec . From Torque Vs time characteristics, it is observed that under shoots appeared at 0.75, 1, 1.5 sec. and from Current Vs time characteristics it is observed that disturbances occurred at 0.75, 1, 1.5 sec. Using neural network based speed controller, over shoots at 0.7, 1, 1.5 sec in Speed Vs Time characteristics are eliminated, under shoots at 0.75, 1, 1.5 sec in Torque Vs Time characteristics are eliminated and disturbances at 0.75, 1, 1.5 sec in Current Vs Time characteristics are eliminated . These characteristics are shown in fig 4.10, 4.11, and 4.12.At speed reversal using PI based controller with speed -120 to 120 rad/s, torque Te=0,50,200,100,50 N-m the characteristics obtained from PI based controller are shown in fig 4.13,4.14,and 4.15, from the characteristics Speed Vs Time it is observed that overshoot appeared at 0.5,1,1.5 sec. From Torque Vs time characteristics, it is observed that under shoots appeared at 0.95 sec and from Current Vs time characteristics it is observed that disturbances occurred at 0.6 sec. Using neural network based speed controller, over shoots at 0.5, 1, 1.5 sec in Speed Vs Time characteristics are eliminated, under shoots at 0.95 sec in Torque Vs Time characteristics are eliminated and disturbances at 0.6 sec in Current Vs Time characteristics are eliminated. These characteristics are shown in fig 4.16, 4.17, and 4.18.

V. CONCLUSION

Challenging and excelling the human brain is one of our long cherished dreams. Intelligent controllers reflect human thinking, human perception and human way of reasoning. Simulation studies show that the Neural Networks based controller provides better results for an induction motor when compared to a conventional PI controller. So, Neural Networks controller is an attractive technique when the plant model is complex.

REFERENCES

[1]. B. K. Bose. Modern Power Electronics and AC Drives. Prentice-Hill PTR Companies, Inc. Upper Saddle River, NJ07458, 2002.
[2]. C.M.Liaw.Y.S.Kung and C.M.Wu Design and implementation of a high performance field oriented induction motor drive. IEEE Tran Ind.Applicat. Vol.38.pp.275-282, 1991.
[3]. R. Krishnan. Electric motor drives modeling, analysis and Control. PHI Pvt. Ltd, New Delhi, 2003.
[4] Y miloud and A.Draou." Application of a Three Level GTO Voltage Source PWM Inverter to feed AC Motors for Variable-Speed Drive with a PI- Controller". International Conference on Electronics, ICEL' 2000. Vol. 1, November 13-15. pp 223-227. Oran, Algeria
[5] Woodley, K.M., Li, H., Foo, S.Y.: Neural Network modeling of Torque Estimation and d-q Transformation for Induction Machine. Eng. Appl. of Artif. In tell. 18(1), 57–63 (2005)
[6]. C.M.Liaw.Y.S.Kung and M.S.Ouyang Identification and control of induction machines using artificial neural networks. IEEE Trans Ind.Applicat. Vol.31.pp.612-619, 1995.
[7]. H.A.Al-Rashidi, A.Gastli, A.Al-Badi, "Optimization of Variable Speed Induction Motor Efficiency Using Artificial Neural Network".
[8] Howard Demuth, Mark Beal, "Neural Network Toolbox for Use with Matlab", User Guide, the Math Work Inc. June 1992

AUTHORS

Mohan Krishna M.Tech Assistant Professor SriVenkateshwaraInstitute of Technology Engineering College ANANTAPUR.

G.Meerimatha M.Tech Associate Professor, EEE Department SriRamanujan Institute of Technology Engineering College ANANTAPUR.

U.Kamal Kumar M.Tech Assistant Professor SriRamanujan Institute of Technology Engineering College ANANTAPUR.
.

International Journal of Modern Engineering Research (IJMER)
www.ijmer.com Vol.3, Issue.4, Jul - Aug. 2013 pp-1988-1993 ISSN: 2249-6645

"Comparison of Maximum Stress distribution of Long & Short Side Column due to Blast Loading"

[1]Prof. M. R.Wakchaure, [2]Seema T. Borole
[1, 2] *Department of Civil Engineering*
Amrutvahini College of Engineering, Amrutnagar Tal-Sangamner, Dist-Ahmednagar (M.S.) India – 422608

Abstract: *A bomb explosion within or immediately nearby a building can cause catastrophic damage on the building's external and internal structural frames like RC column, slab, beam, collapsing of walls, blowing out of large expanses of windows, and shutting down of critical life-safety systems. The Study conducted on the behavior of structural concrete subjected to blast loads. These studies gradually enhanced the understanding of the role that structural details play in affecting the behavior. The comparison between long side & short side column is made & further result is presented. In final result Percentage of Stress of Reinforced concrete column for long & short side column are presented in this paper. An extensive parametric study was carried out on a series of 8 columns at long & short side to investigate the effect of transverse reinforcement, longitudinal reinforcement due to blast loading. The finite element package ANSYS is used to analysis of RC Column subjected to blast loading.*

Key words: *RC Column, Stress, Blast loading, structure, collapse, ANSYS*

I. INTRODUCTION

In the past few decades considerable emphasis has been given to problems of blast and earthquake. The earthquake problem is rather old, but most of the knowledge on this subject has been accumulated during the past fifty years. The blast problem is rather new; information about the development in this field is made available mostly through publication of the Army Corps of Engineers, Department of Defense, U.S. Air Force and other governmental office and public institutes. Much of the work is done by the Massachusetts Institute of Technology, The University of Illinois, and other leading educational institutions and engineering firms. Due to different accidental or intentional events, the behavior of structural components subjected to blast loading has been the subject of considerable research effort in recent years.

Disasters such as the terrorist bombings of the Taj Mahal Hotel in India in 26 Nov. 2008 U.S. embassies in Nairobi, Kenya and Dares Salaam, Tanzania in 1998, the Khobar Towers military barracks in Dhahran, Saudi Arabia in 1996, the Murrah Federal Building in Oklahoma City in 1995, and the World Trade Center in New York in 2001 have demonstrated the need for a thorough examination of the behavior of columns subjected to blast loads. To provide adequate protection against explosions, the design and construction of public buildings are receiving renewed attention of structural engineers. These models span the full range of sophistication from single degree of freedom systems to general purpose finite element programs such as ABAQUS, ANSYS, and ADINA etc.

II. METHODS FOR PREDICTING BLAST LOADS

The following methods are available for prediction of blast effects on building structures:

- Empirical (or analytical) methods
- Semi-empirical methods
- Numerical (or first-principle) methods.

Empirical methods are essentially correlations with experimental data. Most of these approaches are limited by the extent of the underlying experimental database. The accuracy of all empirical equations diminishes as the explosive event becomes increasingly near field.

Semi-empirical methods are based on simplified models of physical phenomena. They attempt to model the underlying important physical processes in a simplified way. These methods rely on extensive data and case study. Their predictive accuracy is generally better than that provided by the empirical methods.

Numerical (or first-principle) methods are based on mathematical equations that describe the basic laws of physics governing a problem. These principles include conservation of mass, momentum, and energy. In addition, the physical behavior of materials is described by constitutive relationships. These models are commonly termed computational fluid dynamics (CFD) models.

2.1 Empirical Methods

Over the years, as a result of research coupled with test programs, a number of analytical methods for predicting blast loading were developed. These analytical procedures are presented in several technical design manuals and reports, are described below.

Technical Manual(TM) 5-1300 (US Department of the Army, 1990) this manual is one of the most widely used publications available to both military and civilian sectors for designing structures to provide protection against the blast effects of an explosion. It contains step-by-step analysis and design procedures, including information on (i) blast loading; (ii) principles of non-linear dynamic analysis; and (iii) reinforced concrete and structural steel design.

The design curves presented in the manual give the blast wave parameters as a function of scaled distance for three burst environments: (i) free air burst; (ii) air burst; and (iii) surface burst.

III. FINITE ELEMENT ANALYSIS

With the advent of digital computers and powerful methods of analysis, such as the finite element method many efforts to develop analytical solutions which would obviate the need for experiments have been undertaken by investigators. The finite element method has thus become a powerful computational tool, which allows complex analyses RC structures to be carried out in a routine fashion.FEM is useful for obtaining the load deflection behavior and its crack patterns in various loading.

3.1 Element Type

There are few assumptions that will be made with this model due to the SOLID65 concrete element capabilities. One assumption is that the base of the column will be fixed due to the rigid foundation on the existing column. The model in this analysis will not be used to accurately depict the results of the displacement or applied forces to the existing column. This is a consequence of not having any concept of the placement, size, and number of reinforcing members of steel being used. The reason we cannot predict the longitudinal or transverse steel orientation is due to the smeared reinforcement associated with the SOLID65 element.

3.2 Modeling Properties

The specimen will be modeled using the SOLID65 concrete element, which is used for modeling three dimensional solid models with or without rebar. The element is capable of cracking, crushing, plastic deformation, and creep in tension and compression using material properties. The material properties (Table I) are as follows:

Table I: Material Properties

Structural	
Young's Modulus	2.e+005 MPa
Poisson's Ratio	0.3
Density	7.85e-006 kg/mm³
Thermal Expansion	1.2e-005 1/°C
Tensile Yield Strength	250. MPa
Compressive Yield Strength	250. MPa
Tensile Ultimate Strength	460. MPa
Compressive Ultimate Strength	0. MPa
Thermal	
Thermal Conductivity	6.05e-002 W/mm·°C
Specific Heat	434. J/kg·°C
Electromagnetic	
Relative Permeability	10000
Resistivity	1.7e-004 Ohm·mm

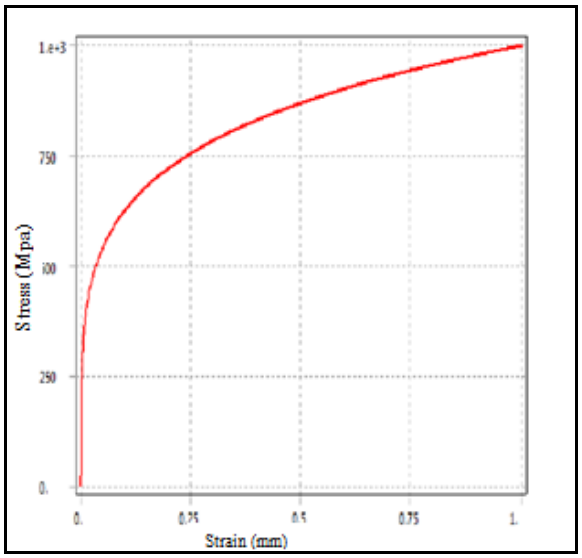

Figure 1: Stress-Strain Graph

3.3 Column Geometry

Using the finite element models discussed above extensive parametric study was carried out with the following cases considered for each columns for which the spacing of the transverse reinforcement is determined in accordance with the requirement in the IS 456-2000 code.

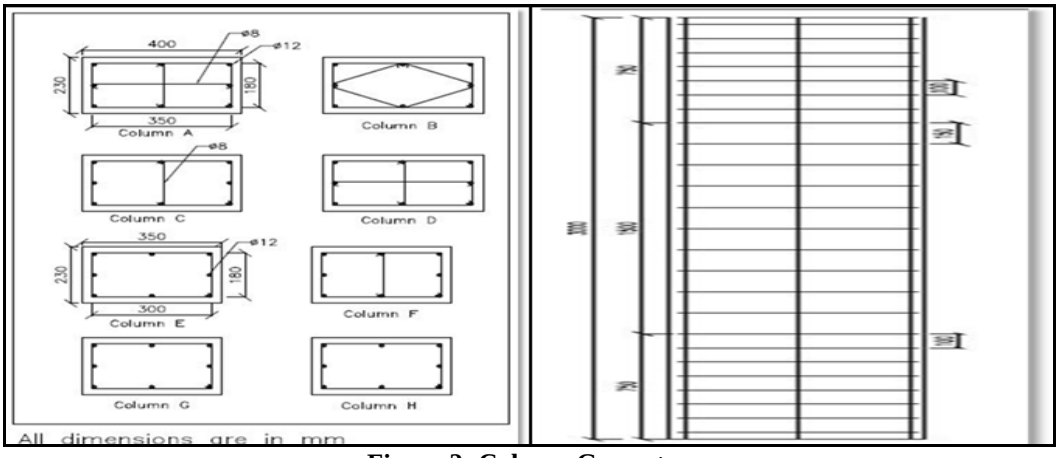

Figure 2: Column Geometry

3.4 Blast Loading

A scaling chart that gives the positive phase blast wave parameters for a surface burst of a hemispherical TNT charge is presented in Figure 2-13. Such scaling charts provide blast load data at a distance R (called the standoff distance) along the ground from a specific explosive. The following step-by-step procedure for determining blast wave parameters for a surface blast is outlined in TM5-1300:

Step 1.Determine the charge weight, W, as TNT equivalent, and ground distance R_G from the charge to the surface of a structure.

Step 2.Calculate scaled ground distance, Z_G:

$$Z_G = R_G / W^{1/3}$$

Step 3.Read the blast wave parameters from Manual TM5-1300 on Page No. 2-13 & Clause No 2-13-3 for corresponding scaled ground distance, Z_G. To obtain the absolute values of the blast wave parameters, multiply the scaled values by a factor $W^{1/3}$.

An extensive parametric study was carried out on a series of 8 columns at long & short side to investigate the effect of transverse reinforcement, longitudinal reinforcement subjected by same blast load. Consider Third-storey building having height 12.5m is analyzed in this study. Standoff distance is considered as 6m, & Charge weight 500 kg which is the closest point to the building as shown in figure.

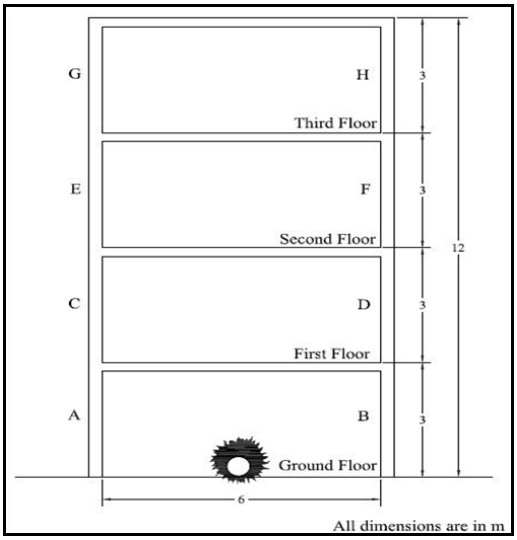

Figure 3: Location of explosion on building

Required: Free field blast wave parameters P_{so}, P_r, U, t_o, t_A for a surface burst of W =500kg at a distance of R_h = 6m.

Table II: Blast Load Parameter

Sr.No.	Floor	Column	Column Size(mm)	P_r (Mpa)	P_{so} (Mpa)	U (M/ms)	t_o (Ms)
1	Ground	A-B	230x400	14.5	2.06	1.46	08.22
2	First	C-D	230x400	8.27	1.31	1.16	16.44
3	Second	E-F	230x350	4.31	0.91	0.97	19.73
4	Third	G-H	230x300	2.06	0.48	0.85	20.83

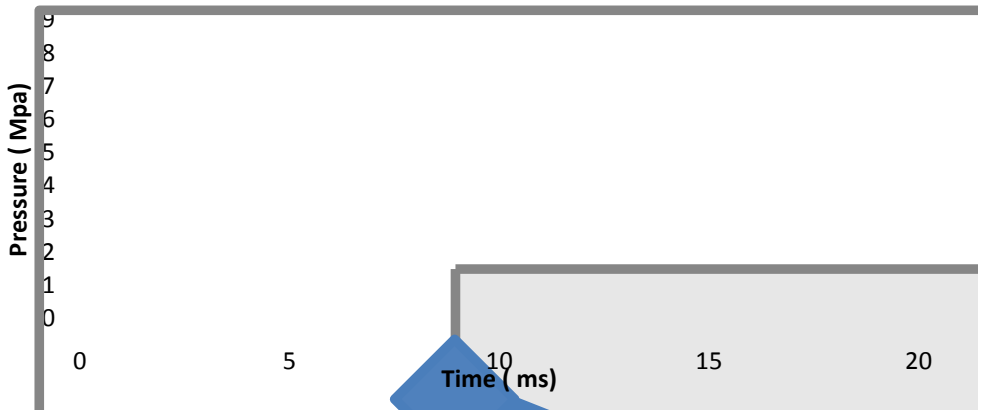

Figure 4: Blast loading of column C & D

IV. RESULT & DISCUSSION

According to the results, the system affects significantly, the actual charge weight of explosive used by the terrorist, the efficiency of the chemical reaction and the source location are not reliably predictable. The stand-off distance is the key parameter that determines the blast pressure so for protecting a structure is to keep the bomb as far away as possible by maximizing the stand-off distance. Blast has a characteristic of high amplitude. The results showed that if the member subjected to high pressure, they could cause big deformation on the element and cause to be exceed the support rotation so the elements which are close to explosion are damaged.

4.1 RC Column Responses to Blast Loading

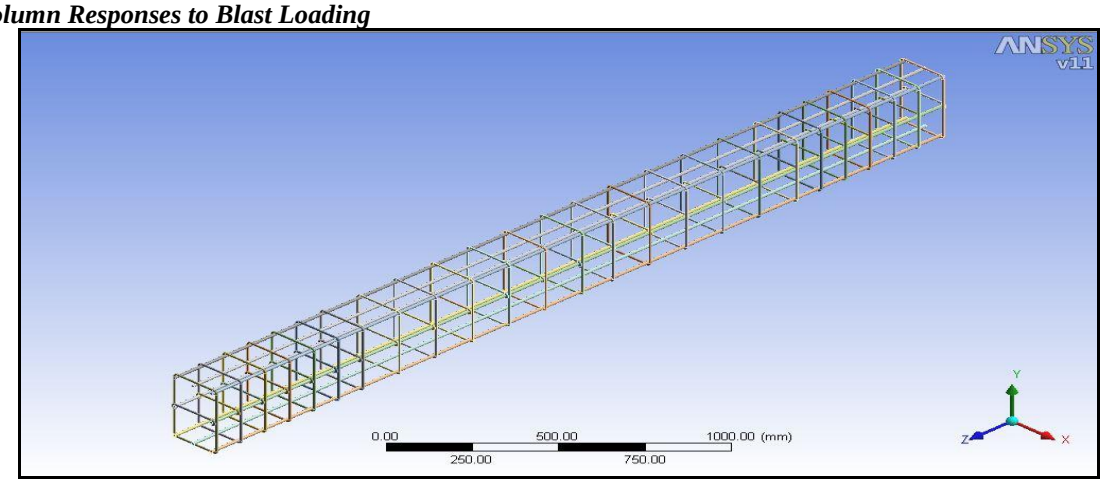

Figure 5: Rebar Structure of column in ANSYS Software

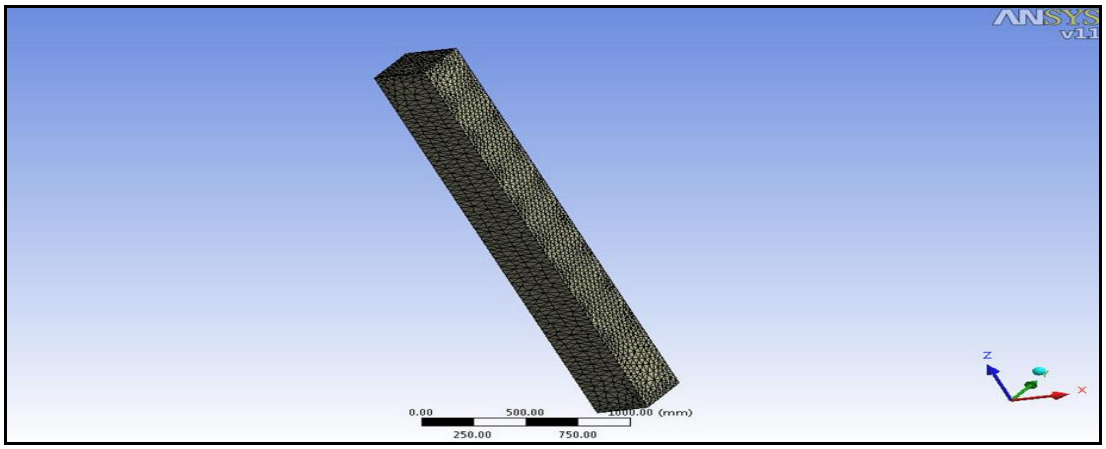

Figure 6: Meshing of Column

.

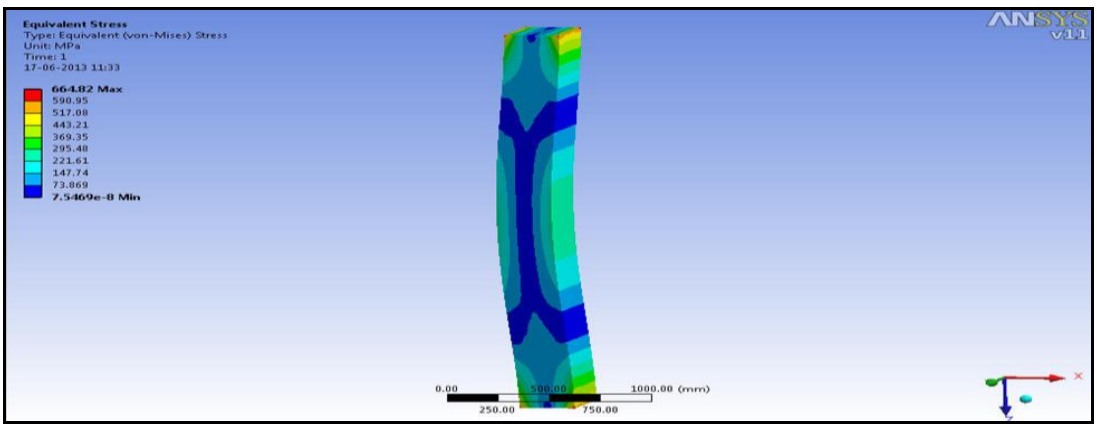

Figure 7: Max. Stress of Long Side Column C

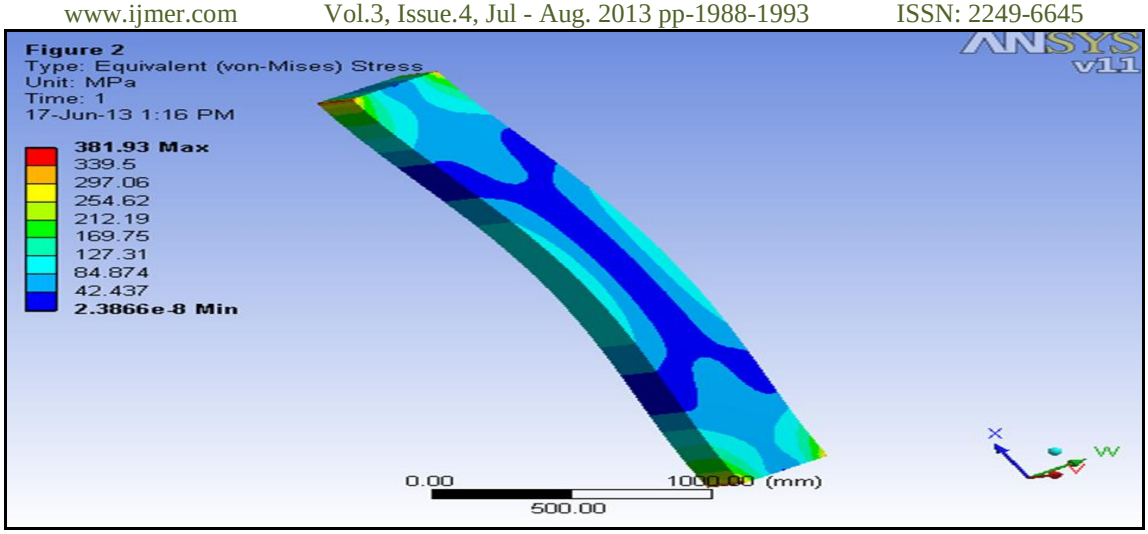

Figure 8: Max. Stress of Short Side Column C

4.2 *Comparison of Pressure Vs Stress of long side & Short side Column C & D*

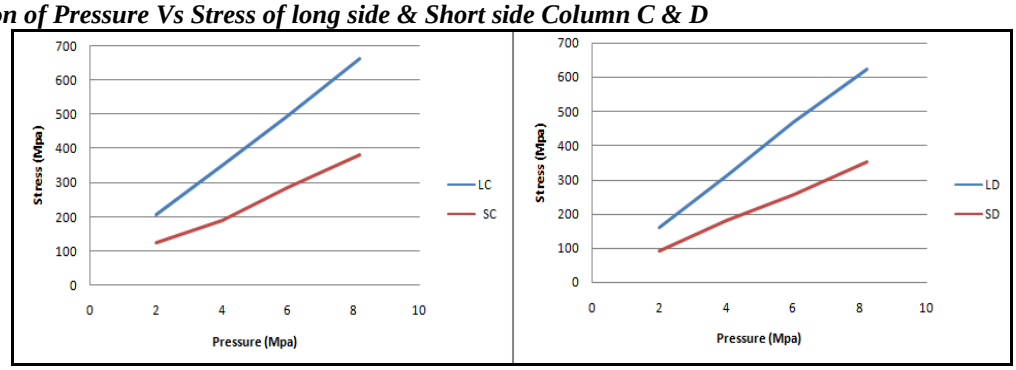

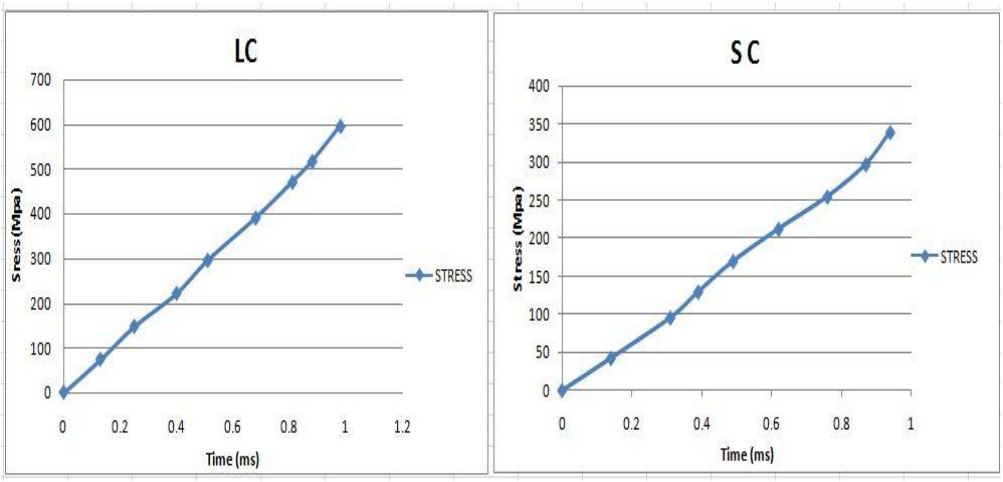

Figure 9: Comparison of Time Vs Stress for Long &Short side Column C

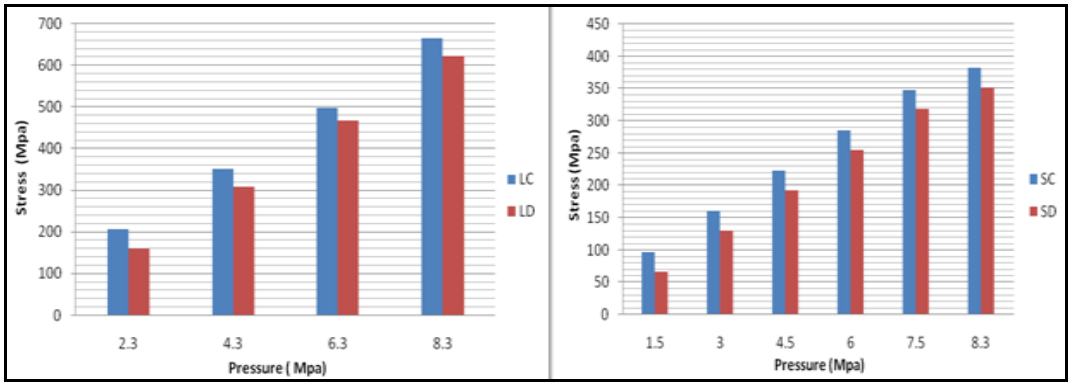

(i) Long column C & D **(ii) Short column C & D**

Figure 10: Graph of Pressure Vs Stress

Table III: Comparison of the Maximum Stress Distribution of Long & Short side columns,

Sr. No.	Floor	Element	Stress (Mpa)
1	GF	LA	841.06
2	GF	SA	661.63
3	GF	LB	701.06
4	GF	SB	434.30
5	FF	LC	664.82
6	FF	SC	381.93
7	FF	LD	622.50
8	FF	SD	351.63
9	SF	LE	540.26
10	SF	SE	262.77
11	SF	LF	512.44
12	SF	SF	238.79
13	TF	LG	401.35
14	TF	SG	131.60
15	TF	LH	390.11
16	TF	SH	170.90

V. CONCLUSION

Based on the results of the parametric study, the following main conclusions can be drawn. The ultimate objective is to make available the Procedure for calculating the blast loads on the structures. The comparison between the Long side column and short side column showed that the critical impulse for the long column case is significantly higher. From result shows Maximum stress distribution ratios of short side to long side for the Column A, B, C, D, E, F, G, and H are 0.78, 0.61, 0.57, 0.56, 0.48, 0.46, 0.32, and 0.30 respectively. The effect of blast load is more critical in the case of columns with a low transverse reinforcement ratio.

ACKNOWLEDGMENT

The study acknowledges the contribution of Ms. Kavita D. Shelar and Ms. Prachi P. More and also the contribution of ANSYS inc. for the wonderful analysis software developed.

REFERENCES

[1]. A. Khadid et al. (2007), "Blast loaded stiffened plates" Journal of Engineering and Applied Sciences, Vol. 2(2) pp. 456-461.
[2]. A.K. Pandey et al. (2006) "Non-linear response of reinforced concrete containment structure under blast loading" Nuclear Engineering and design 236. pp.993-1002.
[3]. Alexander M. Remennikov, (2003) "A review of methods for predicting bomb blast effects on buildings", Journal of battlefield technology, vol 6, no 3. pp 155-161.
[4]. American Society for Civil Engineers 7-02 (1997), "Combination of Loads", pp 239-244.
[5]. ANSYS Theory manual, version 5.6, 2000.
[6]. Biggs, J.M. (1964), "Introduction to Structural Dynamics", McGraw-Hill, New York.
[7]. Dannis M. McCann, Steven J. Smith (2007), "Resistance Design of Reinforced Concrete Structures", STRUCTURE magazine, pp 22-27, April issue.
[8]. Demeter G. Fertis (1973), "Dynamics and Vibration of Structures", A Wiley-Interscience publication, pp. 343-434.
[9]. D.L. Grote et al. (2001), "Dynamic behavior of concrete at high strain rates and pressures", Journal of Impact Engineering, Vol. 25, Pergamon Press, NewYork, pp. 869-886,
[10]. IS 456:2000 Indian Standard Plain and Reinforced Concrete Code of Practice.
[11]. J.M. Dewey (1971), "The Properties of Blast Waves Obtained from an analysis of the particle trajectories", Proc. R. Soc. Lond. A.314, pp. 275-299.
[12]. J.M. Gere and S.P. Timoshenko (1997.), "Mechanics of materials", PWS publishing company, Buston.

International Journal of Modern Engineering Research (IJMER)
www.ijmer.com Vol. 3, Issue. 4, Jul - Aug. 2013 pp-1994-1998 ISSN: 2249-6645

Complex test pattern generation for high speed fault diagnosis in Embedded SRAM

[1]Prasanna Kumari P., [2]Satyanarayana S. V. V., [3]Nagireddy S.
[1, 3] *Associate professor,* [2]*Master of Engineering, Teegala Krishna Reddy Engineering college, Meerpet, Faculty of Electronics and Communication Engineering, Jawaharlal Nehru Technological University, Hyderabad, India.*

Abstract: *The memory blocks testing is a separate testing procedure followed in VLSI testing. The memory blocks testing involve writing a specific bit sequences in the memory locations and reading them again. This type of test is called March test. A particular March test consists of a sequence of writes followed by reads with increasing or decreasing address. For example the March B test has the following test pattern. ↕(W0)↑(R0,W1,R1,W0,R0,W1)↑(R1,W0,W1)↓(R1,W0,W1,W0)↓(R0,W1,W0) There are several test circuits available for testing the memory chips. However no test setup is developed so far for testing the memory blocks inside the FPGA. The SRAM blocks of FPGA are designed to work at much higher frequency than the FPGA core logic. Hence testing the SRAMs at higher speed is essential. The conventional memory test circuits cannot be used for this purpose. Hence the proposed work develops a memory testing tool based on March tests for FPGA based SRAM (Block RAM testing). The code modules for March test generator shall be developed in VHDL and shall be synthesized for Xilinx Spartan 3 Family device. A PC based GUI tool shall send command to FPGA using serial port for selecting the type of test. The FPGA core gets the command through UART and performs the appropriate and sends the test report back to PC. The results shall be verified in simulation with Xilinx ISE simulator and also in hardware by using Chip scope. Xilinx Spartan 3 family FPGA board shall be used for hardware verification of the developed March test generator.*

Key words: *SRAM block, FPGA, VLSI-very large scale integration.*

I. INTRODUCTION

Nowadays, the area occupied by embedded memories in System-on-Chip (soc) is over 90 %, and expected to rise up to 94% by 2014 [1]. Thus, the performance and yield of embedded memories will dominate that of SOCs. However, memory fabrication yield is limited largely by random defects, random oxide pinholes, and random leakage defects. Gross processing and assembly faults, specific processing faults, misalignments, gross photo defects and other faults and defects [2].

This paper aims to propose a new solution for researchers and engineers to find a efficient test and diagnosis algorithm in shorter time. A combinational march-based test algorithm will be implemented for this purpose. Universities and industry involved in memory Built-in-Self test, Built-in-self diagnose will benefit by saving a few years on research and development developed in this work is compatible and expandable for SRAM memory due to fact the manual and automatic test procedure testing.

In this article, we present an original memory test frame work: an SRAM memory test bench, roaming and programmable. This test bench allows not only to employ different commercial SRAM memories but also to apply various algorithms for test. With this new test bench, students can concertize the memories testing's lectures and enlightened the inherent properties of the various applied algorithms as well as the difference between the memory architectures and technologies.

II. MARCH TEST GENERATOR

The memory blocks testing involve writing a specific bit sequences in the memory locations and reading them again [3]. This type of test is called March test. A March test consists of a sequence of March elements. A March elements has a certain number of operations (or March primitives) that must be applied to all memory cells of an arrays. Thus, ↑ (r0; w1) is a March element and r0 and w1 are March primitives. The addressing order of a March element can be done in an up (↑), down (↓) way or (↕) if the order is not significant .A March primitive can be a write 1 (w1), write 0 (w0), read 0 (r0) that can be performed ina memory cell. There are many March tests such as March SR, March C-, March B, and so on. March B chosen in this paper because it has better fault coverage Than March SR and March C- . March B is an efficient and economical memory test should provide best fault coverage in the shortest time [4].

March **B algorithm** has following steps :
↕ (W0) ↑(R0,W1,R1,W0,R0,W1)↑(R1,W0,W1)
↓(R1,W0,W1,W0)↓(R0,W1,W0)

In the above steps, "up" represent executing SRAM address in ascending order while "down" in descending order. This well-know March test allows to detect all the stuck @ and transition fault of a memory cell array, as well as all address decoder faults and coupling (interaction between two cells) faults.

The following figure shows the sequences of March tests to be applied to the SRAMs of FPGA.

March C-	↕(W0) ↑(R0,W1) ↑(R1,W0) ↓(R0,W1) ↓(R1,W0) ↕(R0)
March SR	↓(W0) ↑(R0,W1,R1,W0) ↓(R0,R0) ↑(W1) ↓(R1,W0,R0,W1) ↑(R1,R1)
March B	↕ (W0) ↑(R0,W1,R1,W0,R0,W1) ↑(R1,W0,W1) ↓(R1,W0,W1,W0) ↓(R0,W1,W0)

Fig 2.1: March Test Sequence

III. TEST BENCH ARCHITECTURE

Our test bench architecture for memories is composed of one computer, a March test generator, a serial interface (for communication between the programmable generator and the computer) and SRAMs on FPGA.

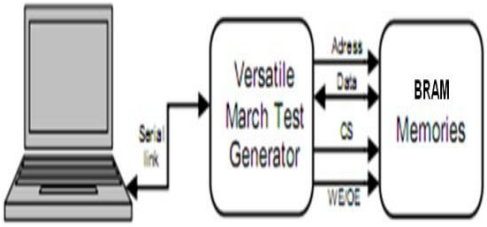

Fig 3.1: Test Bench Architecture

A user interface allows us to choose or set a specific March test. The chosen March test is uploaded through the serial connection to the Programmable test generator and then applied to SRAMs of FPGA.

If no fault is detected, the programmable generator returns a positive acknowledgement on the SRAM. Whether the opposite case occurs, i.e; when a reading operation (r0 or r1) does not return the expected data: the failing memory, the failing address, the failing march element and operation. Only the knowledge of physical defects beside the observed fault, or at least to make reasonable suppositions.

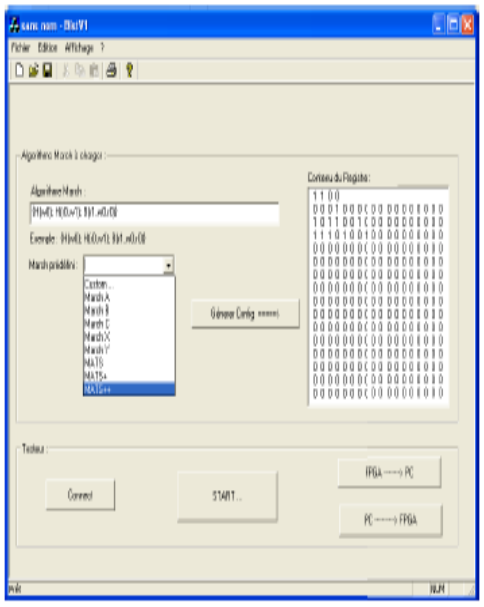

Fig 3.2: User Interface

IV. EXPERIMENTAL RESULTS

The following chapter consists of all the software and hardware results observed in the project. The results include snapshots of each and every module individually with all the inputs, outputs and intermediate waveforms.

4.1 Simulation results

Figure 4.1: Data output of SRAM using March C

- The written input values into SRAM with expected values. are read
- Here the contents of SRAM are read without any failure.
- Hence March test C- is Successful and SRAM is fault Free.

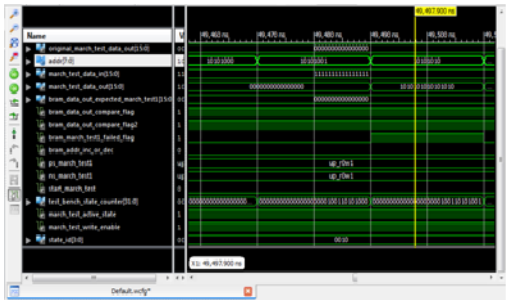

Figure 4.2: Data output of SRAM using March C- with Fault insertion

- The written input values into SRAM are read with expected values except at address "aa".
- Here the contents of SRAM are read with fault.
- Hence March test C- is Successful and SRAM is faulty.

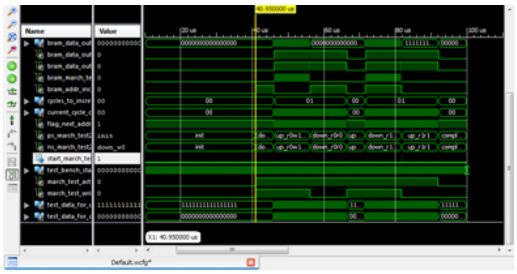

Figure 4.3: Data output of SRAM Using March SR

- The written input values into SRAM are read with expected values.
- Here the contents of SRAM are read without any failure.
- Hence March SR test is Successful and SRAM is fault Free.

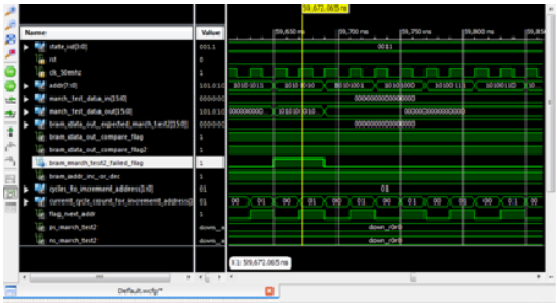

Figure 4.4: Data output of SRAM using March SR with Fault insertion

- The written input values into SRAM are read with expected values except at address "aa".
- Here the contents of SRAM are read with fault.
- Hence March SR test is Successful and SRAM is faulty.

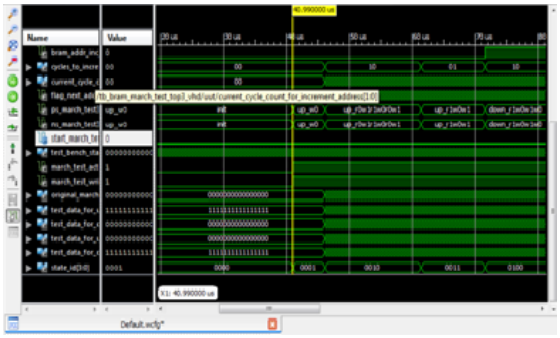

Figure 4.5: Data output of SRAM using March B

- The written input values into SRAM are read with expected values.
- Here the contents of SRAM are read without any failure.
- Hence March B test is Successful and SRAM is fault Free.

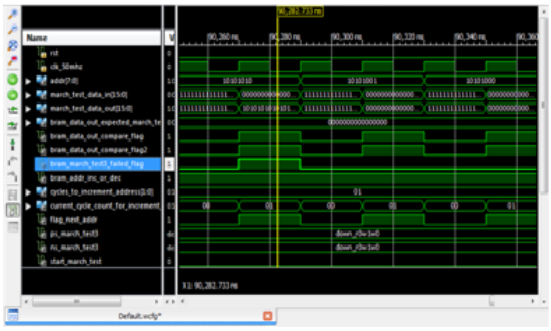

Figure 4.6: Data output of SRAM using March B with fault insertion

- The written input values into SRAM are read with expected values except at address "aa".
- Here the contents of SRAM are read with fault.
- Hence March B test is Successful and SRAM is faulty.

4.2 CHIP SCOPE RESULTS

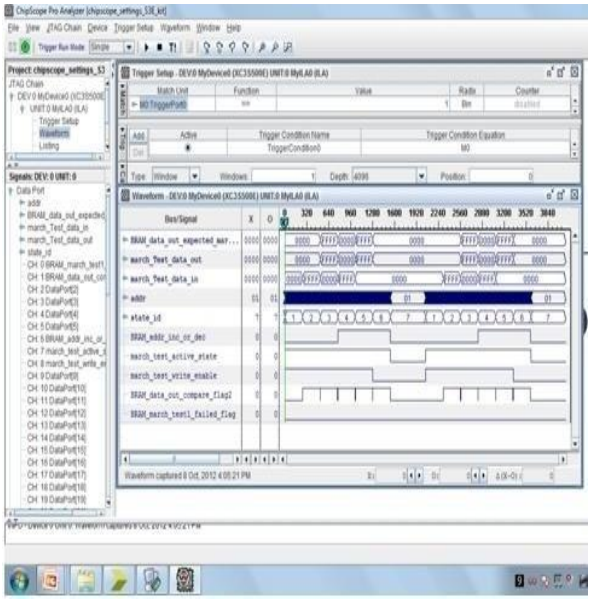

Figure 4.7: Data output of SRAM using March B

V. CONCLUSION

The generation and refinement of this teaching frame work come from the observation that the teaching of the test of the integrated circuits is too often approach in theoretical or virtual ways. We believe that, for our engineering

students, it would be important to have the opportunity to develop theoretical and practical skills to generate adequate test solution for actual electronic device .Although this platform has still to be improved the early feedback of our students is very encouraging. In all cases, they have affirmed to have clearly understood the way March test sequences are applied to have clearly understood the way March test sequence are applied to memories as well as the sensitization and observation process of the various fault models. Moreover, they also showed to have highly perfected their knowledge of the memory architecture and function.

REFERENCES

[1] Semiconductor Industry Association, "International technology roadmap for semiconductors (TTRS), 2003 edition," Hsinchu, Taiwan, Dec.2003.
[2] C. Stapper, A Mclaren, and M Dreckman, "Yield model for productivity optimization of VLSI Memory Chips with redundancy and partially good product," IBM Journal of Research and Development, Vol 24, No. 23, pp.398-409, May 1980.
[3] A.J Van de Goor, "Testing Semiconductor Memories: Theory and Practice, "John Wiley & Sons, ISBN 0-471-92586-1, 1991
[4] Pavlov. Andrei and Sachedev. Manoj, CMOS SRAM Circuit Design and parametric Test in Nano-Scaled Technologies, CA: Springer, 2008, pp.85-86.

Author's Profile

Associate Professor, Department of electronics and communication Engg, Teegala Krishna Reddy Engineering College, Meerpet, Andhra Pradesh, India.

Master Of Scholar, Teegala Krishna Reddy Engineering college, Meerpet, Andhra Pradesh, India

Assistance Professor, Department of electronics and communication Engg, Teegala Krishna Reddy Engineering College, Meerpet, Andhra Pradesh, India.

International Journal of Modern Engineering Research (IJMER)
www.ijmer.com Vol.3, Issue.4, Jul - Aug. 2013 pp-1999-2006 ISSN: 2249-6645

Parametric Optimization of Electrochemical Machining Using Signal-To-Noise (S/N) Ratio

Bhawna Bisht *, Jyoti Vimal**, Vedansh Chaturvedi**
M. Tech Student, Assistant Professor, Department of Mechanical Engineering Madhav Institute of Technology & Science, Gwalior***

Abstract: *Mild steel and aluminium are used as the work piece material for carrying out the experimentation to optimize the Material Removal Rate and surface roughness. There are four machining parameters i.e. Voltage, Electrolyte flow rate, Tool feed rate and Current. Taguchi orthogonal array is designed with three levels of machining parameters with the help of software Minitab 15. Nine experiments are performed and material removal rate (MRR) and surface roughness is calculated. Metal removal rate and surface roughness are the most important output parameters, which decide the cutting performance. Taguchi method stresses the importance of studying the response variation using the signal–to–noise (S/N) ratio, resulting in minimization of quality characteristic variation due to uncontrollable parameter. The metal removal rate was considered as the quality characteristic with the concept of "the larger-the-better" and surface roughness was considered with the concept of "the smaller-the-better". The S/N ratio values are calculated by taking into consideration with the help of software Minitab 15. The MRR and surface roughness values measured from the experiments and their optimum value for maximum material removal rate and minimum surface roughness.*

Keywords: *Taguchi Method, Machining Parameters, Mild Steel, Aluminium alloy, signal to noise ratio.*

I. INTRODUCTION OF ECM

Electrochemical machining (ECM) is a method of removing metal by an electrochemical process. It is normally used for mass production and is used for working extremely hard materials or materials that are difficult to machine using conventional methods. In the ECM process, a cathode (tool) is advanced into an anode (work piece). The pressurized electrolyte is injected at a set temperature to the area being cut. The feed rate is the same as the rate of "liquefication" of the material. Electrochemical machining is one of the widely used non-traditional machining processes to machine complicated shapes for electrically conducting but difficult-to-machine materials such as super alloys, Ti-alloys, alloy steel, tool steel, stainless steel, etc. Use of optimal ECM process parameters can significantly reduce the ECM operating, tooling, and maintenance cost and will produce components of higher accuracy. Its use is limited to electrically conductive materials. Both external and internal geometries can be machined. High metal removal rates are possible with ECM, with no thermal or mechanical stresses being transferred to the part, and mirror surface finishes can be achieved. At high concentration of electrolyte, electrolytes do not behave ideally and resistance of the solution increases which may cause deviation from Faraday's law and Ohm's law. Further, it has been assumed that the process of ECM to be ideal in nature till it obeys Ohm's law and Faraday's law. But there have been no report on the applicability of these laws for electrochemical machining. In the ECM process, a cathode (tool) is advanced into an anode (work piece). The pressurized electrolyte is injected at a set temperature to the area being cut. As electrons across the gap, material from the work piece is dissolved, as the tool forms the desired shape of the work piece. The electrolytic fluid carries away the metal hydroxide formed in the process. In this process, a low voltage (5-15V) is applied across two electrodes with a small gap size (0.2 mm – 0.5 mm) and with a current of (20 – 100A). The Taguchi method is a well-known technique that provides a systematic and efficient methodology for process optimization and this is a powerful tool for the design of high quality systems. Taguchi approach to design of experiments in easy to adopt and apply for users with limited knowledge of statistics, hence gained wide popularity in the engineering and scientific community. This is an engineering methodology for obtaining product and process condition, which are minimally sensitive to the various causes of variation, and which produce high-quality products with low development and manufacturing costs. Signal to noise ratio and orthogonal array are two major tools used in robust design.

Electrochemical machining is one of the widely used non-traditional machining processes to machine complicated shapes for electrically conducting but difficult-to-machine materials such as super alloys, Ti-alloys, alloy steel, tool steel, stainless steel, etc. Use of optimal ECM process parameters can significantly reduce the ECM operating, tooling, and maintenance cost and will produce components of higher accuracy. Its use is limited to electrically conductive materials. Both external and internal geometries can be machined. High metal removal rates are possible with ECM, with no thermal or mechanical stresses being transferred to the part, and mirror surface finishes can be achieved. Electrochemical Machining (ECM) is good for steel and super alloys and most often used when machining either shaped holes or cavities into electrically conductive materials. At high concentration of electrolyte, electrolytes do not behave ideally and resistance of the solution increases which may cause deviation from Faraday's law and Ohm's law. Further, it has been assumed that the process of ECM to be ideal in nature till it obeys Ohm's law and Faraday's law. But there have been no report on the applicability of these laws for electrochemical machining. In the ECM process, a cathode (tool) is advanced into an anode (work piece). The pressurized electrolyte is injected at a set temperature to the area being cut. As electrons across the gap, material from the work piece is dissolved, as the tool forms the desired shape of the work piece. The electrolytic fluid carries

away the metal hydroxide formed in the process. In this process, a low voltage (5-15V) is applied across two electrodes with a small gap size (0.2 mm – 0.5 mm) and with a current of (20 – 100A).
The influence of each control factor can be more clearly presented with response graphs. Optimal cutting conditions of control factors can be very easily determined from S/N response graphs, too. Parameters design is the key step in Taguchi method to achieve reliable results without increasing the experimental costs. Mild steel and aluminium are most suitable for the manufacture of parts such as heavy-duty axles and shafts, gears, bolts and studs. The parameters were used in this experiments are voltage, electrolyte flow rate, tool feed rate and current.

II. METHODOLOGY

• Analysis of Variance (ANOVA)

Analysis of variance (ANOVA) and F-test (standard analysis) are used to analysis the experimental data as given follows

NOTATION

Following Notation are used for calculation of ANOVA method
C.F. = Correction factor
T = Total of all result
n = Total no. of experiments
ST = Total sum of squares to total variation.
Xi = Value of results of each experiments (i = 1 to 27)
SY = Sum of the squares of due to parameter Y (Y = P, S, A, T)
NY1, NY2, NY3 = Repeating number of each level (1, 2, 3) of parameter Y
XY1, XY2, XY3 = Values of result of each level (1, 2, 3) of parameter Y
FY= Degree of freedom (D.O.F.) of parameter of Y
fT = Total degree of freedom (D.O.F.)
fe = Degree of freedom (D.O.F.) of error terms
VY = Variance of parameter Y
Se = Sum of square of error terms
Ve = Variance of error terms
FY = F-ratio of parameter of Y
SY' = Pure sum of square
CY= Percentage of contribution of parameter Y
Ce = Percentage of contribution of error CF = T2/n
ST = Σi=1 to 27 Xi2 – CF
SY = (XY12/NY1 + XY22/NY2 + XY32/NY3) – CF
fY = (number of levels of parameter Y) – 1
fT = (total number of results)-1
fe = fT - ΣfY
VY = SY/fY
Se = ST - ΣSY
Ve = Se/fe
FY = VY/Ve
SY' = SY – (Ve*fz)
CY = SY'/ST * 100%
Ce = (1- ΣPY)*100%

• Signal to Noise Ratio Calculation

Quality Characteristics:

S/N characteristics formulated for three different categories are as follows:

Larger is best characteristic:

Data sequence for MRR (Material Removal Rate), which are higher-the-better performance characteristic are pre-processed as per Eq.1

$$S/N = -10 \log ((1/n) ((1/y2)) \quad \text{.....1}$$

Nominal and Smaller are Best Characteristics:

Data sequences for SR, which are lower-the-better performance characteristic, are pre-processed as per Eq.2 &3

$$S/N = -10 \log (y/s2y) \quad \text{.....2}$$

$$S/N = -10 \log ((1/n) (\Sigma (y2)) \quad \text{.....3}$$

Where y^ is average of observed data y, sy2 is variance of y, and n is number of observations.

III. EXPERIMENTAL SET UP AND WORK PROCEDURE

Material Mild Steel

Mild steel is a type of steel that contains only a small amount of carbon and other elements. It is softer and can be shaped more easily than higher carbon steels. It also bends a long way instead of breaking because it is ductile. It is used on nails and some types of wire; it can be used to make bottle openers, chairs, staplers, staples, railings and most common metal products. Its name comes from the fact it only has less carbon than steel. Mild steel is used in almost all forms of industrial applications and industrial manufacturing. It is a cheaper alternative to steel, but still better than iron.

Aluminium Alloy

Aluminium alloys are alloys in which aluminium (Al) is the predominant metal. The typical alloying elements are copper, magnesium, manganese, silicon and zinc. There are two principal classifications, namely casting alloys and wrought alloys, both of which are further subdivided into the categories heat-treatable and non-heat-treatable. About 85% of aluminium is used for wrought products, for example rolled plate, foils and extrusions. Cast aluminium alloys yield cost-effective products due to the low melting point, although they generally have lower tensile strengths than wrought alloys. The most important cast aluminium alloy system is Al-Si, where the high levels of silicon (4.0% to 13%) contribute to give good casting characteristics. Aluminium alloys are widely used in engineering structures and components where light weight or corrosion resistance is required. Alloys composed mostly of aluminium have been very important in aerospace manufacturing since the introduction of metal skinned aircraft. Aluminium-magnesium alloys are both lighter than other aluminium alloys and much less flammable than alloys that contain a very high percentage of magnesium.

Properties of mild steel

Mild steel has a maximum limit of 0.2% carbon. The proportions of manganese (1.65%), copper (0.6%) and silicon (0.6%) are approximately fixed, while the proportions of cobalt, chromium, niobium, molybdenum, titanium, nickel, tungsten, vanadium and zirconium are not. A higher amount of carbon makes steels different from low carbon mild-type steels. A greater amount of carbon makes steel stronger, harder and very slightly stiffer than low carbon steel. However, the strength and hardness come at the price of a decrease in the ductility of this alloy. Carbon atoms get trapped in the interstitial sites of the iron lattice and make it stronger. What is known as mildest grade of carbon steel or 'mild steel' is typically low carbon steel with a comparatively low amount of carbon (0.16% to 0.2%). It has ferromagnetic properties, which make it ideal for the manufacture of many products. The calculated average industry grade mild steel density is 7.85 gm/cm3. Its Young's modulus, which is a measure of its stiffness, is around 210,000 MPa. Mild steel is the cheapest and most versatile forms of steel and serves every application which requires a bulk amount of steel. The low amount of alloying elements also makes mild steel vulnerable to rust. Naturally, people prefer stainless steel over mild steel, when they want a rust free material. Mild steel is also used in construction as structural steel. It is also widely used in the car manufacturing industry.

Properties of aluminium alloy

Good toughness
Good surface finish
Excellent corrosion resistance to atmospheric conditions
Good corrosion resistance to sea water
Can be anodized
Good weldability and brazability
Good workability

Equipment

After the test, the samples were cleaned and final weight was measured using a digital analytical balance precisa. Three measurements for each sample were taken. The weight loss per unit time for each specimen is calculated and considered as Material Removal Rate (MRR). Similarly the surface roughness was measured using a digital surface roughness tester. This process involves number variables.

Material Removal Rate (MRR) Measurement From the initial and final weight of job MRR is calculated and the relation is given below:

MRR = (Initial Wt - Final Wt)/Time Taken MRR is calculated for both set of experiment. Considering one set correct S/N ratio is calculated from MINITAB 15 software.

IV. EXPERIMENTAL DESIGN

The experimental layout for the machining parameters using the L9 orthogonal array was used in this study. This array consists of four control parameters and three level, as shown in table In the Taguchi method, most all of the observed values are calculated based on ‘the higher the better’ and ‘the smaller the better’. Thus in this study, the observed values of MRR, and SR were set to maximum, and minimum respectively. Next experimental trial was performed with three simple replications at each set value. Next, the optimization of the observed values was determined by comparing the standard analysis and analysis of variance (ANOVA) and SN ratio which was based on the Taguchi method.

Table I: Design Scheme of Experiment of Parameters and Levels

Notation	**Process parameter**	**Level 1**	**Level 2**	**Level 3**
A	Voltage (V)	05	10	15
B	Electrolyte flow rate(L/min)	20	25	30
C	Tool feed rate (mm/min)	0.10	0.20	0.30
D	Current(A)	20	60	100

Table II: Observed Values of MRR and SR for Mild Steel

Trial No.	**Control Parameter (level)**				**Result /Observed value**	
	Voltage	Electrolyte Flow rate	Tool feed rate	Current	MRR (g/min.)	SR (μm)
1	05	20	0.1	20	0.135	0.257
2	05	25	0.2	60	0.268	0.285
3	05	30	0.3	100	0.573	0.431
4	10	20	0.2	100	0.321	0.397
5	10	25	0.3	20	0.409	0.401
6	10	30	0.1	60	0.287	0.376
7	15	20	0.3	60	0.337	0.312
8	15	25	0.1	100	0.286	0.213
9	15	30	0.2	20	0.319	0.413

Table III: Observed Values of MRR and SR for Aluminum Alloy

Parameter (Y)	**DOF (fY)**	**Sum of squares (SY)**	**Mean variance (VY)**	**F-ratio (FY)**	**Pure sum (SY)**	**Contribution (%) (CY)**
A	2	0.0112	0.0056	0.0056	0.0112	18.30
B	2	0.0263	0.0131	0.0131	0.0263	**42.97**
C	2	0.0020	0.0010	0.0010	0.0020	3.27
D	2	0.0217	0.0108	0.0108	0.0217	35.46
Error	0					
Total	8	0.0612	0.0305			100.00

Table IV: Analysis of Variance (ANOVA) and F-Test for Mild Steel

Trial No.	**Control Parameter (level)**				**Result /Observed value**	
	Voltage	Electrolyte Flow rate	Tool feed rate	Current	MRR (g/min)	Surface Roughness (μm)
1	05	20	0.1	20	0.356	0.216
2	05	25	0.2	60	0.463	0.213
3	05	30	0.3	100	0.563	0.312
4	10	20	0.2	100	0.433	0.364
5	10	25	0.3	20	0.376	0.381
6	10	30	0.1	60	0.389	0.282
7	15	20	0.3	60	0.407	0.227
8	15	25	0.1	100	0.368	0.231
9	15	30	0.2	20	0.312	0.254

Table V: Analysis of Variance (ANOVA) and F-Test for Aluminum Alloy

Parameter (Y)	**DOF (fY)**	**Sum of squares (SY)**	**Mean variance (VY)**	**F-ratio (FY)**	**Pure sum (SY)**	**Contribution (%) (CY)**
A	2	0.0744	0.0372	0.0372	0.0744	47.11
B	2	0.0011	0.0005	0.0005	0.0011	0.70
C	2	0.0046	0.0023	0.0023	0.0046	2.91
D	2	0.0778	0.0389	0.0389	0.0778	**49.28**
Error	0					
Total	8					100.00

For Mild Steel

Table VI: S/N Ratio for MRR (Larger Is Better)

Experiment No.	A Voltage(V)	B Electrolyte flow rate (L/min)	C Tool feed (mm/min)	D Current(A)	MRR(g/min)	S/N Ratio
1	1	1	1	1	0.135	-17.393
2	1	2	2	2	0.268	-11.437
3	1	3	3	3	0.573	-4.8369
4	2	1	2	3	0.321	-9.8699
5	2	2	3	1	0.409	-7.7655
6	2	3	1	2	0.287	-10.8424
7	3	1	3	2	0.337	-9.4474
8	3	2	1	3	0.286	-10.8727
9	3	3	2	1	0.319	-9.9242

Table VII: S/N Ratio for Surface Rough (Smaller Is Better)

Experiment No.	A Voltage(V)	B Electrolyte flow rate (L/min)	C Tool feed (mm/min)	D Current(A)	SRF(□ m)	S/N Ratio
1	1	1	1	1	0.257	11.8013
2	1	2	2	2	0.285	10.9031
3	1	3	3	3	0.431	7.3105
4	2	1	2	3	0.397	8.0242
5	2	2	3	1	0.401	7.9371
6	2	3	1	2	0.376	8.4962
7	3	1	3	2	0.312	10.1169
8	3	2	1	3	0.213	13.4324
9	3	3	2	1	0.413	7.6810

Taguchi Analysis: MRR (g/min) versus A, B, C, D

Response Table for Signal to Noise Ratios,
Larger is better

Level	Voltage(A)	Electrolyte flow rate(B)	Tool feed rate(C)	Current(D)
1	-11.223	-12.237	-13.036	-11.694
2	-9.493	10.025	-10.410	-10.576
3	-10.081	-8.534	-7.350	-8.526
Delta	1.730	3.702	5.686	3.168
Rank	4	2	1	3

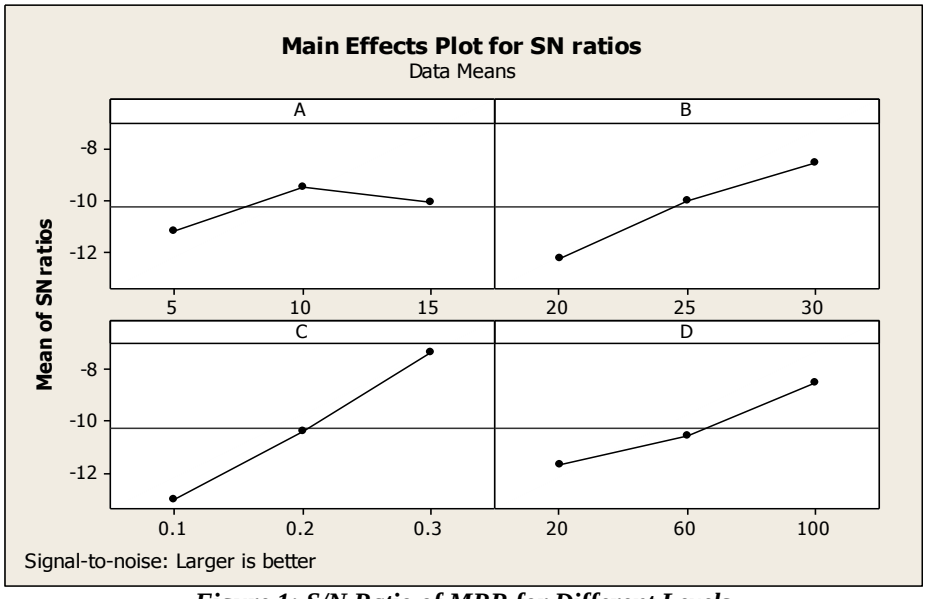

Figure 1: S/N Ratio of MRR for Different Levels

Taguchi Analysis: SR (m) versus A, B, C, D

Response Table for Signal to Noise Ratios

Smaller is better

Level	Voltage(A)	Electrolyte flow rate(B)	Tool feed rate(C)	Current(D)
1	10.005	9.981	11.243	9.140
2	8.153	10.758	8.869	9.839
3	10.410	7.829	8.455	9.589
Delta	2.258	2.928	2.789	0.699
Rank	3	1	2	4

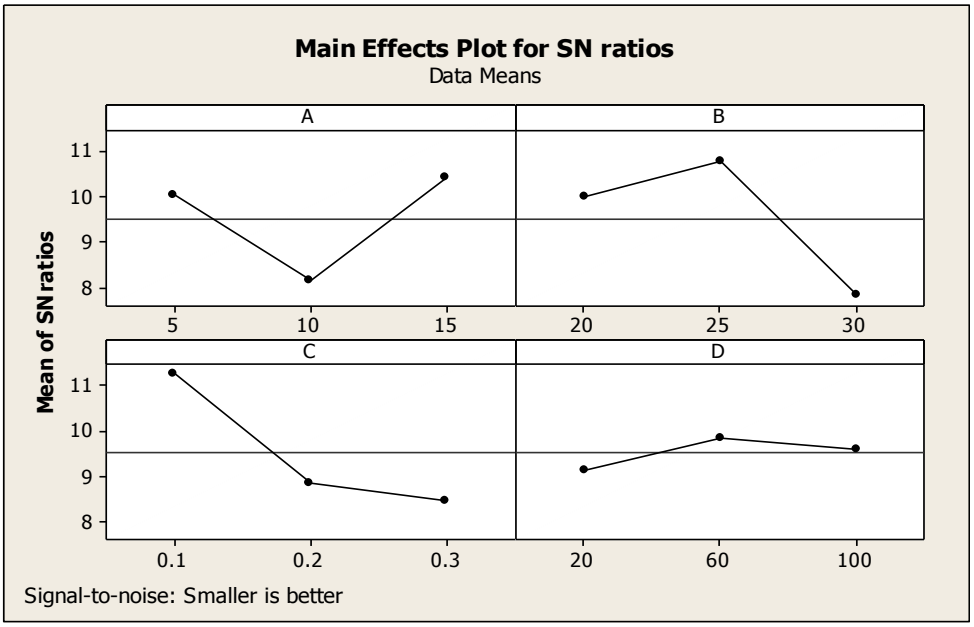

Figure 2: S/N Ratio of SR for Different Levels

For Aluminium Alloy

Table VIII: S/N Ratio for MRR (Larger Is Better)

Experiment No.	A Voltage(V)	B Electrolyte flow rate (L/min)	C Tool feed (mm/min)	D Current(A)	MRR(g/min)	S/N Ratio
1	1	1	1	1	0.356	-8.9710
2	1	2	2	2	0.463	-6.6884
3	1	3	3	3	0.563	-4.9898
4	2	1	2	3	0.433	-7.2702
5	2	2	3	1	0.376	-8.4962
6	2	3	1	2	0.389	-8.2010
7	3	1	3	2	0.407	-7.8081
8	3	2	1	3	0.368	-8.6830
9	3	3	2	1	0.312	-10.1169

Table IX: S/N Ratio for Surface Roughness (Smaller Is Better)

Experiment No.	A Voltage(V)	B Electrolyte flow rate (L/min)	C Tool feed (mm/min)	D Current(A)	SRF(m)	S/N Ratio
1	1	1	1	1	0.216	13.3109
2	1	2	2	2	0.213	13.4324
3	1	3	3	3	0.312	10.1169
4	2	1	2	3	0.364	8.7780
5	2	2	3	1	0.381	8.3815
6	2	3	1	2	0.282	10.9950
7	3	1	3	2	0.227	12.8795
8	3	2	1	3	0.231	12.7278
9	3	3	2	1	0.254	11.9033

Taguchi Analysis: MRR (g/min) versus A, B, C, D

Response Table for Signal to Noise Ratios

Larger is better

Level	Voltage(A)	Electrolyte flow rate(B)	Tool feed rate(C)	Current(D)
1	-6.883	-8.016	-8.618	-9.195
2	-7.989	-7.956	-8.025	-7.566
3	-8.869	-7.769	-7.098	-6.981
Delta	1.986	0.247	1.520	2.214
Rank	2	4	3	1

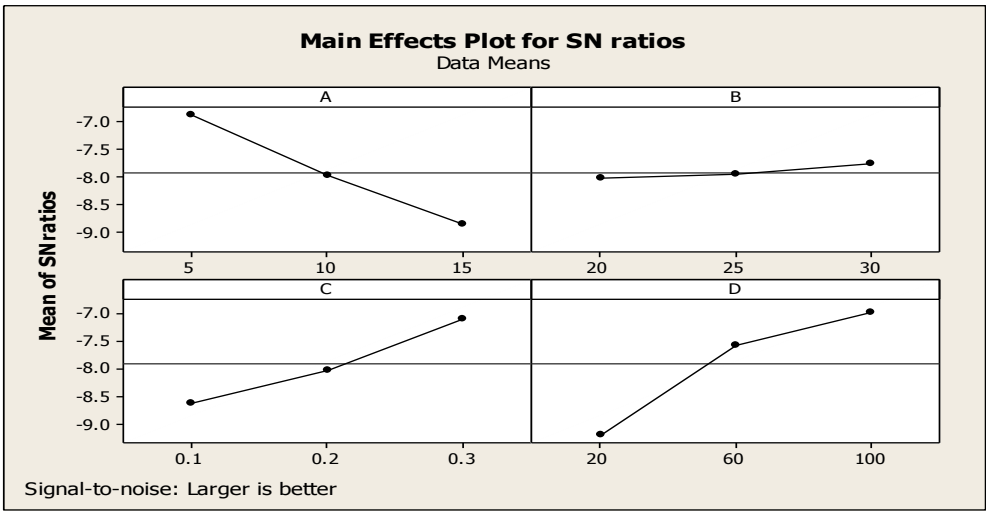

Figure 3: S/N Ratio of MRR for Different Levels

Taguchi Analysis: SR (□ m) versus A, B, C, D

Response Table for Signal to Noise Ratios

Smaller is better

Level	Voltage(A)	Electrolyte flow rate(B)	Tool feed rate(C)	Current(D)
1	12.287	11.656	12.345	11.199
2	9.385	11.514	11.371	12.436
3	12.504	11.005	10.459	10.541
Delta	3.119	0.651	1.885	1.895
Rank	1	4	3	2

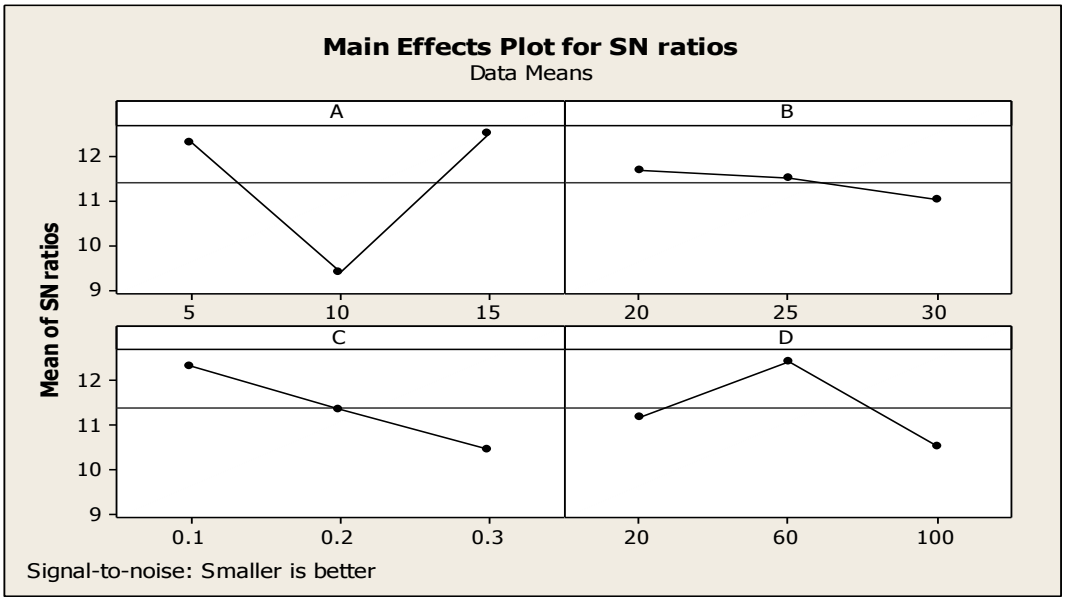

Figure 4: S/N Ratio of SR for Different Level

V. RESULT AND DISCUSSION

The following discussion focuses on the different of process parameters to the observed values (MRR and SR) based on the Taguchi methodology.

Material Removal Rate (MRR)

Main effects of MRR of each factor for various level conditions are shown in figure1. According to figure 1 the MRR increases with four major parameter A, B, C, and D. MRR is maximum in the case of **Voltage (A)** at level 2 (10), in the case of **Electrolyte flow rate (B)** at level 3 (30), in the case of **Tool feed rate (C)** MRR will be maximum at level 3 (0.3), and in the case of Current **(D)** at the level 3 (100). So the optimal parameter setting for the MRR found **A2B3C3D3**

Surface Roughness (SR)

Figure 2 evaluates the main effects of each factor for various level conditions. According to the figure 2 the surface Roughness decreases with four major parameter A, B, C, and D. SR will be minimum in the case of **Voltage (A)** at level 3 (15), in the case of **Electrolyte flow rate (B)** at level 2 (25), in the case of **Tool feed rate (C)** at level 1(0.1) and in the case of **Current (D)** condition surface Roughness will be minimum at level 2 (60). So the optimal parameter setting for minimum surface roughness is **A3B2C1D2.**

VI. CONCLUSIONS

This paper presents analysis of various parameters and on the basis of experimental results, analysis of variance (ANOVA), F-test and SN Ratio the following conclusions can be drawn for effective machining of mild steel and aluminium alloy by ECM process as follows:

- Electrolyte flow rate (B) is the most significant factor for mild steel machining in ECM. Meanwhile Voltage, Tool feed rate, and Current are sub significant in influencing. The recommended parametric combination for optimum material removal rate is **A2B3C3D3.**
- In case of Aluminium Alloy Current is most significant control factor and hence the optimum recommended parametric combination for optimum surface Roughness is **A3B2C1D2.**

REFERENCES

[1] Krishankant, Jatin Taneja, Mohit Bector, Rajesh Kumar, Application of Taguchi Method for Optimizing Turning Process by the effects of Machining Parameters, International Journal of Engineering and Advanced Technology (IJEAT) ISSN: 2249 – 8958, Volume-2, Issue-1, October 2012 263.

[2] Yigit et al. (2011), "Multi-Objective Optimization of the Cutting Forces in Turning Operations Using the Grey-Based Taguchi Method" ISSN 1580-2949.

[3] Rama Rao. S, Padmanabhan. G ," Application of Taguchi methods and ANOVA in optimization of process parameters for metal removal rate in electrochemical machining of Al/5%SiC composites ," International Journal of Engineering Research and Applications (IJERA) ISSN: 2248-9622 www.ijera.com Vol. 2, Issue 3, May-Jun 2012, pp. 192-197**.**

[4] Experimental investigations into the influencing parameters of electrochemical machining of AISI. T. SEKAR Faculty of Mechanical Engineering Advanced Manufacturing Laboratory, Government College of Engineering, Salem – 636011, India.

[5] Dhavamani and Alwarsamy, "Optimization of Cutting Parameters of Composite Materials using Genetic Algorithm" European Journal of Scientific Research ISSN 1450-216X Vol.63 No.2 (2011), pp.279-285.oct-2011

[6] Aggarwal and Parmar (2008) estimated the surface roughness and material removal rate of mild steel using Taguchi method Anova techniques.

[7] Kamal, Anish and M.P.Garg (2012), "Experimental investigation of Material removal rate in CNC turning using Taguchi method"International Journal of Engineering Research and Applications (IJERA) Vol. 2, Issue 2,Mar-Apr 2012, pp.1581-1590

[8] Ballal, Inamdar and Patil P.V. (2012), "Application Of Taguchi Method For Design Of Experiments In Turning Gray Cast Iron " International Journal of Engineering Research and Applications (IJERA) Vol. 2, Issue 3, May-Jun 2012, pp.1391-1397 36

[9] Ashish Yadav, Ajay Bangar, Rajan Sharma, Deepak Pal ," Optimization of Turning Process Parameters for Their Effect on En 8 Material Work piece Hardness by Using Taguchi Parametric Optimization Method," International Journal of Mechanical and Industrial Engineering (IJMIE), ISSN No. 2231 –6477, Volume-1, Issue-3, 2012.

International Journal of Modern Engineering Research (IJMER)
www.ijmer.com Vol. 3, Issue. 4, Jul - Aug. 2013 pp-2007-2010 ISSN: 2249-6645

Properties of Glass Fibre Reinforced Geopolymer Concrete

Dr. Mrs. S. A. Bhalchandra[1], Mrs. A. Y. Bhosle[2]
Department of Applied Mechanics Government College of Engineering, Aurangabad Maharashtra

ABSTRACT: *This paper presents results of an experimental program to determine mechanical properties of Glass fibre reinforced Geopolymer Concrete which contains fly ash, alkaline liquids, fine & course aggregates & glass fibres. The effects of inclusion of glass fibers on density, compressive strength & flexural strength of hardened geopolymer concrete composite (GPCC) was studied. Alkaline liquids to fly ash ratio were fixed as 0.35 with 100% replacement of ordinary Portland cement by fly ash. For alkaline liquid combination ratio of Sodium hydroxide solution to Sodium silicate solution was fixed as 1.00. Glass fibers were added to the mix in 0.01%, 0.02%, 0.03% & 0.04% by volume of concrete. Based on the test results it was observed that the glass fibers reinforced geopolymer concrete have relatively higher strength in short curing time (3 days) than geopolymer concrete & Ordinary Portland cement concrete.*

Keywords*: alkaline liquids, compressive strength, density, flexural strength, fly ash, glass fibers.*

I. INTRODUCTION

With infrastructure development growing, demand for concrete as construction material is on increase worldwide, which ultimately increase the demand for cement. Production of Ordinary Portland cement is highly energy intensive, consume significant amount of non renewable natural resources such as lime stone deposition, coal etc. & about 1.0 ton of carbon dioxide (Co_2) is liberated during production of one ton of Portland cement [4 -11]. The environmental effects associated with production of Portland cement, created an urgent need to develop alternative binder to make concrete. The development of fly ash based geopolymer concrete is in response for the need of greener concrete. The abundant availability of fly ash worldwide create an opportunity to utilize this byproduct of burnt coal as substitute for Portland cement to manufacture concrete.[5]

Davidovits (1988) proposed that an alkaline liquids could be used to react with the Silicon (Si) & Aluminium (Al) in source material of geological origin or in byproduct material such as Fly ash, Metacolin, Ground granulated blast furnace slag (GGBS) Rice husk ash (RHA) etc. to produce binders. [2]

Geopolymer concrete does not utilize any Portland cement in it, however the binder is produced by the reaction of an alkaline liquids with a source material which is rich in Silica & Alumina.[3]. The geopolymer paste binds the loose course & fine aggregates & other un reacted materials together to form geopolymer concrete.The manufacture of geopolymer concrete is carried out using the usual concrete technology methods [1].

High early strength, low shrinkage, freeze thaw resistance, sulphate resistance, & corrosion resistance are the properties of geopolymer concrete.[3] Geopolymer concrete composites are good candidate material of construction from strength & durability considerations. Also bond strength of Geopolymer concrete with rebars is higher than cement concrete.[5]

The water absorption of fly ash geopolymer is less than 5% which is low & Apparent Volume of Permeable Voids is less than 12% (which is classified as good). [10] Water to geopolymer solid ratio is the most influential parameter to increase strength, & to decrease the water absorption / Apparent Volume of Permeable Voids & water permeability.[10]

Fibre reinforced concrete is relatively new composite material in which fibres are introduced in matrics as micro reinforcement so as to improve the tensile cracking & other properties of concrete.[7] Some type of fibres produce greater impact abrasion & shatter resistance in concrete .Addition of glass & polypropylene fibres to concrete increase the splitting tensile strength & compressive strength of concrete by approximately 20-50% [6]. The compressive, split tensile, flexural & bond strength of geopolymer concrete with 100% replacement of cement by fly ash have increase as the fibre content increased. The maximum value of all these strengths obtained at 0.03% of fibre content.

II. EXPERIMENTAL INVESTIGATIONS

2.1 Materials

The materials used for making glass fibres reinforced geopolymer concrete are Low calcium dry fly ash as source material, alkaline liquids, course & fine aggregates, glass fibres & water.

Fly ash

Fly ash is a residue from the combustion of pulverized coal collected by mechanical or electrostatic separators from the flue gases of thermal power plants. The spherical form of fly ash particles improves the flow ability & reduces the water demand. In this experimental work low calcium dry fly ash (Pozzocrete-83) procured from Dirk India limited Nashik obtained from Ekalahare (Nashik) thermal power station was used as source material Fineness of fly ash particles in terms of Specific surface was 430 m^2/Kg .

Alkaline liquids

A combination of Sodium hydroxide solution & Sodium silicate solution was used as alkaline activators for geopolymerization. Sodium hydroxide is available commercially in falkes & pellets form. For this experimental program Sodium hydroxide flakes with 98% purity were dissolved in distilled water to make NaOH solution.

Sodium silicate is available commercially in solution form which was used as such. The chemical composition of Sodium silicate is Na_2O=16.37%, SiO_2=34.35% (total solids=50.72%.), water=49.28%

Aggregates

Course aggregates comprising of max size 20mm having fineness modulus of 6.60, bulk density of 1603 Kg/m^3 , & specific gravity of 2.603 were used.

Fine aggregates (sand) is clean dry river sand was sieved through 4.75mm sieve to remove pebbles, confirming to grading zone I as per IS 383-1970 having specific gravity 2.576, bulk density of 1793 kg/m3, & fineness modulus of 3.35 was used. Both aggregates were in saturated surface dry condition.

Glass Fibres

Glass fibres are made of silicon oxide with addition of small amount of other oxides Glass fibres are characteristic for their high strength, good temperature resistance, corrosion resistance & available at low price. In this investigation alkali resistance glass fibres of 12mm length & 14 microns nominal diameter having density of 2680Kg/m^3 were used.

2.2 Mix design for Glass fibre reinforced Geopolymer concrete

The basic mixtures proportions used for the trial mixtures was based upon previous research on geopolymer mixture proportions [9,12]. In this investigation mix design procedure developed by Shri S. V. Patankar [8] for their PhD thesis work was adopted. Alkaline liquids to fly ash ratio by mass was fixed as 0.35. For alkaline liquid combination ratio of Sodium hydroxide solution to Sodium silicate solution was fixed as 1.00 . Mix proportions for characteristic strength of 30Mpa are described in table 1

Table1: Mix proportions for geopolymer concrete with & without glass fibres

Mix ID	Fly Ash in Kg/m^3	Fine aggregates in Kg/m^3	Course aggregates in Kg/m^3	NaOH Solution inKg/m^3	Na2SiO3 Solution in Kg/m^3	Extra water in Kg/m^3	Glass fibers in gm/m^3
GPC 0.00% fibres	360.00	692.53	1287.78	63.00	63.00	73.68	0.00
GPCC1 0.01% fibres	360.00	692.53	1287.78	63.00	63.00	73.68	268.00
GPCC2 0.02% fibres	360.00	692.53	1287.78	63.00	63.00	73.68	536.00
GPCC3 0.03% fibres	360.00	692.53	1287.78	63.00	63.00	73.68	804.00
GPCC4 0.04% fibres	360.00	692.53	1287.78	63.00	63.00	73.68	1072.00

2.3 Preparation of Geopolymer concrete composites

To prepare 13 molarity concentration of Sodium hydroxide solution 520gm of Sodium hydroxide flakes was dissolved in distilled water & make up to one liter . The mass of NaOH solids was measured as 38.5%. The Sodium hydroxide solution was prepared 24 hours prior to use, because after dissolving flakes of NaOH in water, temperature of solution goes up to $70^0$to 80^0C, hence it is necessary to cool it at room temperature & then it can be used. The Sodium hydroxide solution thus prepared was mixed together with Sodium silicate solution to get desired alkaline solution. The solid constituents of geopolymer concrete mix i.e. fly ash, fine & course aggragates, were dry mixed in drum mixer for about three minutes. The extra water was added to alkaline solution prior to mixing of concrete. Then alkaline solution along with extra water added to dry mix thoroughly for four minutes to get homogeneous mix. For glass fibres reinforced geopolymer concrete mixes, fibres were added to dry mix in four different proportions such as 0.01%.0.02%, 0.03%, & 0.04%by volume of concrete. In this experimental work, 100 X 100 X 100mm size cubes, & 100 X 100 X 500mm size prisms were cast for testing of compressive & flexural strength. After 24 hours of casting all specimens were demoulded & then placed in an oven for thermal curing (heating) at specified temperature of 90^0C for eight hours duration. Then specimens were removed from oven & kept at room temperature. After 3 days, weight of specimens was taken to determine density & tests for compressive strength & Flexural strength were conducted

III. RESULTS & DISCUSSIONS

3.1 Density

Average density values of geopolymer concrete with & without glass fibers was 2650 kg/m^3 which is nearly equal to that of conventional concrete.

3.2 Compressive strength test

The average compressive strength of geopolymer concrete with & without glass fibres at the age of 3 days & 28 days with heat curing of eight hours at 90^0C are described in Table 2 & figure 1

Table 2: Compressive strength of Geopolymer concrete

Mix ID	Age of concrete	Av. Comp load in KN	Av. Comp strength in Mpa	% increase in strength
GPC	3 days	336.67	33.67	-
GPCC- 1	3 days	363.33	36.33	7.9 %
GPCC- 2	3 days	390.00	39.00	15.83 %
GPCC- 3	3 days	423.33	42.33	25.72 %
GPCC- 4	3 days	360.00	36.00	6.98 %
GPC	28 days	363.33	36.33	-
GPCC- 1	28 days	383.33	38.33	5.5 %
GPCC- 2	28 days	400.00	40.00	10.10 %
GPCC- 3	28 days	436.67	43.67	20.20 %
GPCC- 4	28 days	403.33	40.33	11.01 %

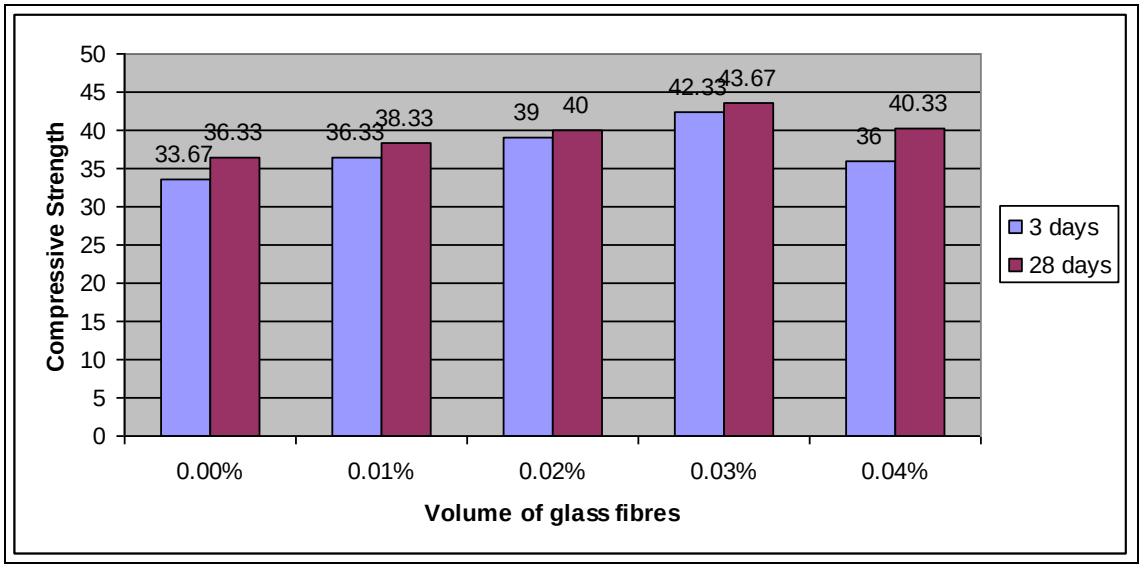

Figure 1: Compressive strength of GPCC

Compressive strength of GPCC was increased with respect to increase in percentage volume fraction of glass fibres Addition of 0.03% volume fraction of glass fibres shows maximum increase in compressive strength i.e. 20.2%with respect to GPC mix without fibres

3.3 Flexural strength

The flexural strength of Geopolymer concrete with & without glass fibres at 3 days & 28 days for heat curing of eight hours are represented in Table 4 & figure 2

Table: 4 Flexural Strength for geopolymer concrete with & without glass fibres.

Mix ID	Age of concrete	Av. Flexural load in kgf	Av. Flexural strength in Mpa	% increase in Flexural strength
GPC	3 days	970	3.81	0.0 %
GPCC- 1	3 days	1320	5.17	35.69 %
GPCC- 2	3 days	1480	5.81	52.49 %
GPCC- 3	3 days	1520	5.96	56.43 %
GPCC- 4	3 days	1300	5.10	33.85 %
GPC	28 days	1020	4.00	0.00%
GPCC- 1	28 days	1380	5.41	35.25%
GPCC- 2	28 days	1520	5.96	49.00%
GPCC- 3	28 days	1600	6.28	57.00%
GPCC- 4	28 days	1400	5.49	37.25%

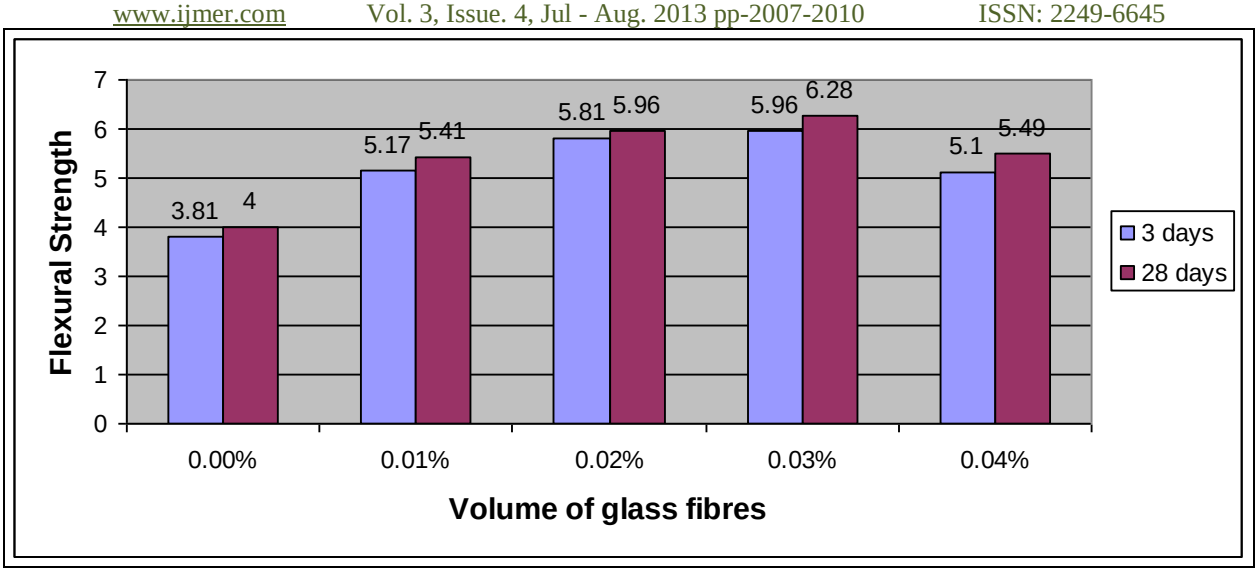

Figure 2 : Flexural strength of GPCC

From test results it can be observed that flexural strength of geopolymer concrete was increased as the volume fraction of glass fibre is increased. Addition of glass fibres increased flexural strength by 57 % with respect to GPC mix without fibre. Flexural strength was highest at 0.03% of glass fibres.

IV. Conclusions

1) Geopolymer concrete is an excellent alternative to Portland cement concrete.
2) Density of Geopolymer concrete is similar to that of ordinary Portland cement concrete.
3) Low calcium fly ash based Geopolymer concrete has excellent compressive strength within short period (3 days) & suitable for structural applications. Inclusion of glass fibres in Geopolymer concrete shows considerable increase in compressive, & flexural strength of GPCC with respect to GPC without fibres.
4) Compressive strength & Flexural strength of glass fibre reinforced geopolymer concrete increases with respect to increase in percentage volume fraction of glass fibres from 0.01%,0.02%,0.03% &0.04%.
5) Addition of 0.03% volume fraction of glass fibres shows maximum increase in Compressive strength & Flexural strength by 20.2%, & 57% respectively with respect to GPC mix without fibres.

References

[1]. D.Hardjito,, S.E.Wallah, D.M.J. Sumajouw, B.V.Rangan, "Introducing fly ash based geopolymer concrete manufacturing & engineering properties 3", 30th conference on OUR WORLD IN CONCRETE & STRUCTURES: 23-24 August 2005 Singapore pp 271 to 278
[2]. N. A. Lloyd & B. V. Rangan" Geopolymer concrete with Fly ash", Second International conference on Sustainable construction materials & Technologies,28-30 June 2010
[3]. N. A. Lloyd & B. V. Rangan, " Geopolymer concrete: A review of development &opportunities", 35th conference on OUR WORLD IN CONCRETE & STRUCTURES: 25-27 August 2010 Singapore
[4]. K.Vijai, R.Kumutha & B.V.Rangan , " Effect of types of curing on strength of geopolymer concrete", International Journal of the Physical Sciences, vol 5(9), 18 August 2010, pp 1419 to 1423.
[5]. N.P. rajmane, M.C. Nataraja & N. Lakshmanan " An introduction to geopolymer concrete ", The Indian Concrete Journal November 11 vol 85, No 11, pp 25 to 28.
[6]. K.Vijai, R.Kumutha & B.G.Vishnuram , "Proporties of glass fiber reinforced geopolymer concrete composites", ASIAN Journal of Civil Engineering (Building & Housing) Vol.13, No.4 , 2012 pp 511 to 520.
[7]. Sathish Kumar.V. Blessen Skariah Thomas, Alex Christopher, " An Experimental Study on Proporties of Glass Fibre Reinforced Geopolumer Concrete", International Journal of Engineering Research & Applications (IJERA)Vol.2, Issue 6, November-December 2012, pp.722-726
[8]. S. V.Patankar, "Mix proportioning of fly ash based geopolymer concrete",Synopsis for PhD.
[9]. R.Anuradha, V.Shreevidya, R.Venkatasubramani, B.V.Rangan, " Modified guidelines for Geopolymer concrete mix design using Indian Standard", ASIAN Journal of Civil Engineering (Building & Housing) Vol.13, No.3 , 2012 pp 353-364.
[10]. Monita Olivia & Hamid R. Nikraz, " Strength & Water Penetrability of fly ash based geopolymer concrete", ARPAN Journal of Engineering & Applied Sciences, vol 6 ,No 7, July 2011,pp70 to 78.
[11]. Rajamane N. P., Nataraja M.C., Lakshmanan N, & Ambily P.S, " Literature Survey on Geopolymer concrete & Research Plan in Indian Context", 148 The Masterbuilder- April 2012.www.masterbuilder.co.in
[12]. M.I. Abdul Aleem & P. D. Arumairaj, "Optimum mix for the geopolymer concrete", Indian Journal of Science & Technology, vol 5, No3, March 2012.

International Journal of Modern Engineering Research (IJMER)
www.ijmer.com Vol. 3, Issue. 4, Jul - Aug. 2013 pp-2011-2013 ISSN: 2249-6645

A survey on Inverse ECG (electrocardiogram) based approaches

Gaddam.Chandra Mohan1, DrSwapna Devi2
[1, 2] *Electonics&communication Engineering department, NITTTR, Chandigarh, India*

ABSRACT: *Analysis of Electrocardiogram signal involves variety of orientations .This paper investigates some of the important areas. Conventional methods are not in a position to deal with the heart related problems. Hence signal reconstruction oriented strategies like inverse problem oriented approaches are gaining momentum in nowadays. Early detection of arrhythmia is necessary to rectify the heart problem.Bruoga syndrome, atrial flutter, ventricular fibrillation, myocardial ischemia are some of the arrhythmias to be detected at an early stage.*
Optimized techniques can be useful to minimize the difference between the predicted potentials and recorded potentials of body surface.
Keywords: *Electrocardiogram, arrhythmia, inverse problem, body surface potentials.*

I. INTRODUCTION

ECG is the electrical activity of the heart measured through the heart potentials generated within the heart functioning like a electrical generator. Basically ECG signal is non stationary. The Reflection may occur at random in the time scale. The disease symptoms which are related to the heart may not show all the time but at certain intervals during the day. Small localized heart muscle damage may not be visible in the routine clinical ECG.All these limitations of ECG are to be rectified .Hence, comprehensive information may be obtained by using some methods like imaging, inverse problem, regularization for obtaining the desired solutions.

Early detection of arrhythmia will save a human life. Arrhythmia detection may not be possible alone using commercially available ECG equipment. Some computing techniques like optimization, imaging is useful for getting the desired properties of the signal. Inverse problem in electrocardiogram is to reconstruct epicardial potentials from body surface potential maps. In this method generally the source parameter that generates the measurements are reconstructed. The most common feature of many inverse problems is their ill posedness. This means that the solution of this problem is not unique. Even small disturbances in the measurements lead to unbounded errors in the solution. In order to stabilize the solution of the problem additional assumptions have to be introduced into the formulation. In other words, a procedure called regularization where priority constants are used to make less sensitive to perturbations.

Arrhythmia detection: Burga syndrome is one type of arrhythmia which causes sudden death in young adults .Analysis of the electrical activity by recording epicardial or endocardial electro grams (EGM) is a valuable for understanding pathological conditions. However recording of EGMs is an inverse procedure only performed in patients already diagnosed with this syndrome. Computing EGMs by non-invasive recordings by solving inverse problem has been presented in [1]. This inverse computed EMGs were compared to those of control subjects in terms of activation times and duration.

A leading cause of death in the western world, myocardial ischemia occurs when cardiac myocates are damaged for lack of oxygen.ECG diagnostics of a myocardial ischemia relies on detecting the elevation of the normally isoelectric ST segment.

This is caused by the injury contents resulting from the transmembrane voltage diifference between healthy and ischemic tissues. A constrained optimization framework for solving has been propose in[2].Here the attempt has been made to localize ischemia by inversely computing the transmembrane potentials(TMP)s through the myocardium from the voltage measured at the body surface. This method does not compute the lead field matrix hence it has lower computational cost. Secondly as it allows flexible discretization resolution for the TMPs and other state variables.

Computational models of the heart have evolved to become an important tool for understanding several types of arrhythmias like AF (atrial flutter) or ventricular fibrillations. Various genetic diseases like long QT or short syndrome can be simulated successfully. A framework has been suggested in order to adopt a generalized model of the human atria to the heart of an individual in[3].In this framework a method is applied that allows for the detection of the local direction of a wavefront and the conduction velocity (CV) of a circular multi electrode catheter. For the validation of the segmentation algorithm the standard methods of medical imaging have been used.

Spatial patterns of body surface potential maps(BSPM) recorded during ballon inflatory percutoneous translurinalcoronary angioplasty(PTCA) in patients with single vessel coronary artery disease have been examined in[4].It is also investigated how well these patterns can be predicted in just 8 independent leads of the 12 lead ECG.Further ,by using inverse solution it also estimated heart surface potential maps from both 120 lead BSMPs and from those derived from 12 lead ECG s by comparing solution. A boundary element torso model was used to estimate the heart surface potential s from body surface potential maps (BSMP) obtained from 12 lead ECG via transformation developed from a designer set of 120 lead ECGs by a least square solution to the linear regression problems. This study shows that for patients with acute myocardial ischemia both the body surface and potential surface maps estimated from the 12 lead ECGs correlate well with those constructed from the 12 lead ECGs.This approach is very much useful in ischemia detection.

Real time oriented approach: Development of tele cardiology systems is a very low cost and realistic system.

The first step in this regard is to build up an automatic ECG analysis system. An efficient algorithm which performs pattern recognition to extract the time plane features of an ECG wave presented in [5].This approach is also further evaluates

clinically required parameters. Any cardiac disease diagnosis can be made on the knowledge basis of abnormal parameters. The basic software package here detects patterns, delianates time plane features and calculates clinical measurements of ECG wave. Hence it can be extended further a cardiac disease inference engine by just configuring different conditions to diagnose generation (3G) cellular network rollout.

Hence uploading the digital image of ECG strip will almost take notime.Nowadays the processing capability of the mobile phones increases in the future the entire process could be assimilated in the mobile phone. Thus the entire concept may be fruitful for remote telemedicine as an application.

Optimization: Finding activation times on the heart non invasively from body surface potential s in inverse ECG problem is known as nonlinear least square optimization problem. A mathematical framework for the original NLLS optimization problem and reformulate it as an equivalent non constrained optimization. Based on this framework isolate the non convexity of the problem to a single constraint on the domain of the optimization variables has been propose in [6].This method has been formulated is a convex relaxation to the original problem by removing the isolated nonconvex content. This method is based in the context of potentially based formulation for the inverse problem that is with the unknowns being free transmembrane potential value at each point on the heart surface at each time instant.

The objective function of an optimization problem used to rank the suitability of a candidate solution. But sometimes there is a mismatch between the objectives of activation based inverse ECG and the objectives of activation based inverse ECG and the objective function of the corresponding optimization problem. This approach suggests that the optimization criteria for the problem need to be carefully reviewed and modified, if necessary to achieve the intended goals. A procedure for activation based inverse ECG as applied to data measured from a patient with wolff-parkinson white(WPW) syndrome has been presented in[7].In this experiments ,number of optimization problems like fastest route algorithm(FRA) initialized non linear square(NLLS) ,a convex relaxation of the NLLS problem and a sequence of NLLS problem. A method based on a convex optimization frame work to explore the solution space used and whether the optimization criteria target and their intended objective FRA also has been analysed.

Inverse problem approach: Basically, Inverse problem constitutes a particularly demanding task as for as computational resources are concerned. The use of proper orthogonal decomposition (POD) for the very fast solution of the forward problem in the form of a selected Eigen function has been proposed in [8].This approach yields a very efficient solution of the inverse problem as it involves multiple forward problem solution at each iteration. The proposed method in the context of current effort adopts a combined utilization of POD along with finite element method (FEM) on a realistic human torso model for rapid solutions of the inverse ECG problem.

This algorithm was tested on multi channel available online. In this procedure the body surface potentials were measured from 128 electrodes positioned equidistantly over the body surface. Inverse problem of ECG can be described as the estimation of cardiac electric sources like the epicardial potential distributions using the body surface potential measurements (BSP).The cardiac electrical source distribution provides useful information about the functioning of the heart. However the inverse ECG problem is illposed.Even a small amount of noise causes unbounded errors. To overcome this drawback various regularization methods were applied in the published literature.Tikhanov regularization is one of the most widely used approach. This method tries to reach a trade off between a good fit to the measurements and a priori information about the solution. This trade off is achieved using a regularization parameter which is usually found using the L curve approach. A method by using Genetic algorithm to estimate the regularization parameters proposed in[9].Here the inverse ECG problem has been by using multiple constraints approach. The genetic algorithm (GA) has been used to estimate the regularization parameters, hence the number of unknowns decreases significantly.

There is a notable gap in the literature regarding the impact of resolution on the practical forward and inverse problems for the finite element method. A study has been focussed on to develop refinement strategies involving hybrid shaped finite elements so as to minimize approximation errors for the ECG inverse problem in[10].This approach examines both the ill posedness of the mathematical inverse problem and the ill conditioning of the problem. The aim of this study was to investigate optimal discretization strategies for the optimizing for the existing regularization schemes. It is observed that refinement strategies developed only for optimizing the forward problem may be inappropriate for the corresponding inverse problem. Resolution strategies include determining the resolution on the heart surface, volume conductor and decomposing the resolution in the tangential and normal direction near the heart surface. The results obtained from the annulus model and the realistic torso model indicated that discretization refinement itself is one form of regularization and can be combined with other classical regularization techniques to further improve the inverse solution.

Regularization is the technique to stabilize the solution in inverse problem. In the published literature tikhanov regularization, truncated singular value decomposition (TSVD) etc.are some of the popular methods. These regularization methods need a certain parameters to solve the inverse problem. L curve method can be used to obtain these parameters. Distribution of electric potentials over the surface of the heart, also called epicardial distributions is a valuable tool to understand the defects in the heart functioning.Diret measurements of these potentials is a highly invasive procedure. Alternatively to reconstruct the epicardial potentials noninvasively from the body surface potential maps is known as inverse problem of ECG.The study to solve the inverse ECG by using by using several regularization methods and comparing their performance has been presented in[11].The performance of regularization methods for solving the inverse ECG was also evaluated on a realistic torso model simulation protocol. It is also investigated the use of genetic algorithm for regularizing the ill posed inverse ECG problem .The results show that GA is an efficient optimization technique for improving the solution of the illposed inverse problem.

An indirect iterative method for solving the inverse problem in the terms of multiple moving dipoles has been proposed in [12].This method based on muti polar representations of the heart electrical activity. Surface potentials generated by multiple

dipoles are iteratively combined to maximize similarity between computed and recorded potentials. The performance of algorithm tested by localizing electrical dipoles from simulated surface potentials in an eccentric spheres model of human torso. Limitations of iterative search strategies are more evident when two simulation dipoles are searched. The accuracy in this indirect method will be dependent on the amount of surface potentials stored for comparison which limits the spatial resolution used for the construction of the database.

One main form of the inverse problem in ECG constitutes the reconstruction of epicardial distributions (EP) from the measured body surface potentials(BSP).As inverse problem is ill posed regularization process has to be applied to get the physiolocally meaningful EPs.In the regularization process the regularization parameter is the key step. Two new regularization parameter selection methods cross validation procedure(CVG) and L curve in the context of total least squares(TLS) are presented in[13].These new methods consider both sides of noise in the linear system equation ax=b using the realistic heart lung torso model. The CVG method seems to be more suitable for parameter selection to the clinical inverse ECG problem because of existing measurement and geometric errors which are inherently prevailing.

Conclusion: Inverse problems are basically seeking the Source from obtained potentials. Body surface potentialsbe calculated from the torso models by using forward problem approach. Source potential estimation by inverse problem is useful for the source from the available body surface potentials. Regularization approach will smoothify the ill posed problem into acceptable solution. Arrhythmia detection methods ill be useful to rectify the problems at an early stage.

Future orientation: Extending the study of realistic ECG problem i n three dimensions is the challenging issue. Properly defining the heart spatial frequency spectrum on the 3D surface and to assess the epicardial information on the heart surface are the issues for further investigation.Computional resources also major constraints in practical simulations.

References

[1] J. Pedrentorciila, Climent, M. Andreu, Millet, Jose, Berne, Paola, Brugada, Josep, Brugada, Ramon, Guillem, Maria S., Characterstics of inverse –computed epicardial electro grams of Brugada Syndrome patients"IEEE Annual International conference of the Engineering n Medicine and Biology Society,EMBC2011,pp:235-238.

[2] 2.Dafang Wang;R.M.Kirbey,R.S Macleod,C.R.Johanson,"An optimization framework for inversely estimating myocardial transmembrane potentials and localizing ischemia "Annual international conference of Engineering in Medicine and biological society,EMBC,2011 pp:1680-1683.

[3] O. Dossel, M. W. Kroeger, F. M. Weber, C. Schillong. W. H. W. Schulze, G. Seemann, "A frame work for personalization of computational models of human atria", Annual international conference of the IEEE Engineering in Medicine and Biology Society,EMBC,2011,PP:4324-4328.

[4] B. M. Horacek, J.W.Waren, J.Y.Wang,"Heart-surface potentials estimated from 12-lead electrocardiograms "Computing in cardiology, 2010, pp: 37-40.

[5] S. Pramanik. S. Mitra, R. N. mitra, B. B. Chaudari, "A Novel approach for delineation and feature extraction in QRS Complex of ECG signal" International conference on image information processing (ICIIP).2011,PP:1-6.

[6] B.E rem. P. M. Van Dam, D. H. Brooks, "A convex relaxation frame work for initialization of activation based inverse electrocardiography Non invasive Functional Source Imaging of the Brain and Heart"8th international conference on bioelectromagnetism(NFSI&ICBEM),2011,PP:12-17.

[7] B. Erem, P. M. van Dam, D. H. Brooks, "Analysis of the criteria of activation based inverse electrocardiography using convex optimization "Annual International Conference of the IEEE Engineering in Medicine and Biology Society, EMBC, 2011, PP:3913-3916.

[8] I. Aitidis E. Gogou, P. Bonovas, H. Panagiotidis, G. Kyriacou. "Equivalent cardiac dipole localization from ECG data using proper orthogonal decomposition"10th international workshop on biomedical engineering, 2011.pp:1-4.

[9] Gavgani, Alireza Mazloumi; Dogrusoz, Yesim Serinagaoglu: Use of genetic algorithm for selection of regularization parameters in multiple constraint inverse ECG problem Engineering and Medicine and Biological society ,EMBC,2011 Annual International conference of the IEEE publication year;2011,pp:985-988.

[10] Dafang wang, R. M. kirby, C. R. Johnson, "Resolution strategies for the Finite Element Based solution of the ECG inverse problem"IEEE Transactions on Biomedical Engineering :vol:57,Issue:2,2010,pp:220-237.

[11] S. Sarikaya, G. W. Weber, Y. S. Dogrusoz: "Combination of conventional regularization methods and genetic algorithm for solving the inverse problem of electrocardiogrphy"5th International symposium on Health Informatics and Bioinformatics (HIBIT), 2010, pp: 13-20.

[12] J. Pedron A. M. Climent, J. Millet, M. S. Guillem, J. Pedron. "An iterative method for indirectly solving the inverse problem of electrocardiography "computing in cardiology, 2010, pp: 89-92.

[13] Guofa Shou, Dongdong Deng, Ling Xia, Mingfeng Jiang,"Choosing Near optimal Regularization parameter for the Inverse problem in Electrocardiography "Fifth International Conference on Natural Computation, 2009, vol, 2009, pp: 172-176.

International Journal of Modern Engineering Research (IJMER)
www.ijmer.com Vol. 3, Issue. 4, Jul - Aug. 2013 pp-2014-2018 ISSN: 2249-6645

Double guard: Detecting Interruptions in N- Tier Web Applications

P. Krishna Reddy[1], T. Manjula[2], D. Srujan Chandra Reddy[3], T. Dayakar Reddy[4]
[1]*M. Tech (CSE), VITS, Kavali*
[2, 3, 4]*Associate Professor, CSE, VITS, Kavali*

Abstract: *Internet services and applications contain develop into an inextricable part of daily life and make possible communication between the management of personal information from anywhere. To put up this increase in application and data complexity, web services have moved to a multi-tiered design wherein the web server runs the application front-end logic and data is outsourced to a database or file server. Double Guard is an IDS system that models the network behavior of user sessions across both the front-end web server and the back-end database. By monitoring both web and succeeding database requests, we are able to search out attacks that an independent IDS would not be able to identify. In addition, we compute the limitations of any multitier IDS in terms of training sessions and functionality coverage. Then we collected and processed real-world traffic over a system deployment in both dynamic and static web applications.*

Index Terms: *Web services, Multi-Tier web application, Virtualization, SQL Injection, Vulnerable*

I. INTRODUCTION

WEB-DELIVERED services and applications have enlarged in both popularity and complexity over the past few years. Everyday tasks, like banking, social networking, are all done through the web. Such services typically employ a web server front end that runs the application user interface logic as a back-end server that consists of a database or file server. The attacks have recently become more different, as attention has shifted from attacking the front end to exploiting vulnerabilities of the web applications in order to corrupt the back-end database system (e.g., SQL injection attacks). A surplus of Intrusion Detection Systems (IDSs) currently examine network packets individually within both the web server and the database system In multitier architectures, the back-end database server is often protected at the back a firewall while the web servers are remotely accessible over the Internet. The IDSs cannot detect cases where in normal traffic is used to attack the web server and the database server. Unluckily, within the current multithreaded web server architecture, it is not possible to detect or profile such causal mapping between web server traffic and DB server traffic since traffic cannot be clearly attributed to user sessions.

In this paper, we present DoubleGuard, a system used to detect attacks in multitier web services. Our approach can create customariness models of isolated user sessions that include both the web front-end (HTTP) and back-end (File or SQL) network transactions. To achieve that, we use a lightweight virtualization technique to assign each user's web session to a dedicated container, an isolated virtual computing environment. We use the container ID to accurately associate the web request with the subsequent data base queries. Thus, DoubleGuard can build a fundamental mapping profile by taking both the web server and data base traffic into account. We have implemented our DoubleGuard container architecture using OpenVZ and performance testing shows that it has reasonable performance overhead and is practical for most web applications. When the request rate is moderate (e.g., under 110 requests per second), there is almost no overhead in comparison to an unprotected vanilla system. The container-based web architecture not only fosters the profiling of causal mapping, but it also provides an isolation that prevents future session-hijacking attacks. Within a lightweight virtualization environment, we ran many copies of the web server instances in different containers so that each one was isolated from the rest. As ephemeral containers can be easily instantiated and destroyed, we assigned each client session a dedicated container so that, even when an attacker may be able to compromise a single session, the damage is confined to the compromised session; other user sessions remain unaffected by it. Using our prototype, we show that, for websites that do not permit content modification rom users, there is a direct causal relationship between the requests received by the front-end web server and those generated for the database back end. Our experimental evaluation, using real-world network traffic obtained from the web and database requests of a large center, showed that we were able to extract 100 percent of functionality mapping by using as few as 35 sessions in the training phase. it does not depend on content changes if those changes can be performed through a controlled environment and retrofitted into the training model. We refer to such sites as "static" because, though they do change over time, they do so in a controlled fashion that allows the changes to propagate to the sites' normality models. In addition to this static website case, there are web services that permit persistent back-end data modifications. These services, which we call dynamic, allow HTTP requests to include parameters that are variable and depend on user input. Sometimes, the same application's primitive functionality (i.e., accessing a table) can be triggered by many different web pages. To address this challenge while building a mapping model for dynamic web pages, we first generated an individual training model for the basic operations provided by the web services. We demonstrate that this approach works well in practice by using traffic from a live blog where we
progressively modeled nine operations. Our results show that we were able to identify all attacks, covering more than 99 percent of the normal traffic as the training model is refined.

II. THREAT MODEL & SYSTEM ARCHITECTURE

We initially set up our threat model to include our assumptions and the types of attacks we are aiming to defend against. The attackers can avoid the web server to directly attack the database server. We assume that the attacks can neither be detected nor prevented by the nearby web server IDS, those attackers may take over the web server after the attack, and that afterward they can obtain full control of the web server to start on succeeding attacks. In addition, we are analyzing only network traffic that reaches the web server and database. We imagine that no attack would occur during the training phase and model building.

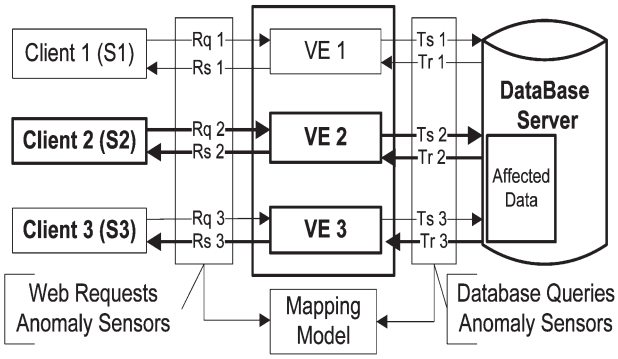

Fig 1: Classic three-tier model

3.1 Building the Normality Model

This container-based and session-separated web server architecture not only enhances the security performances but also provides us with the isolated information flows that are separated in each container session. It allows us to identify the mapping between the web server requests and the subsequent DB queries, and to utilize such a mapping model to detect abnormal behaviors on a session/client level. Our sensors will not be attacked at the database server too, as we assume that the attacker cannot completely take control of the database server. Once we build the mapping model, it can be used to detect abnormal behaviors. Both the web request and the database queries within each session should be in accordance with the model. If there exist any request or query that violates the normality model within a session, then the session will be treated as a possible attack.

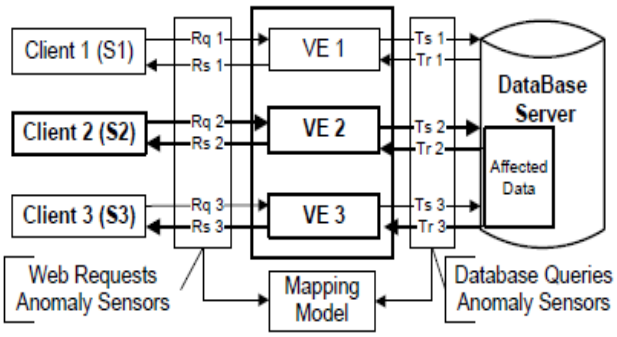

Fig. 2: Web server instances running in containers

Once we build the mapping model, it can be used to detect abnormal behaviors. Both the web request and the database queries within each session should be in accordance with the model. If there is any request or query that violates the normality model within a session, then the session will be treated as a possible attack.

3.2 Attack Scenarios

Our approach is effective at capturing the following type of attacks.

3.2.1 Privilege Escalation Attack

Let's assume that the website serves both regular users and administrators. For a regular user, the web request ru will trigger the set of SQL queries Qu; for an administrator, the request ra will trigger the set of admin level queries Qa. Now suppose that an attacker logs into the web server as a normal user, upgrades his/her privileges, and triggers admin queries so as to obtain an administrator's data. This attack can never be detected by either the web server IDS or the database IDS since both ru and Qa are legitimate requests and queries. Our approach, however, can detect this type of attack since the DB query Qa does not match the request ru, according to our mapping model.

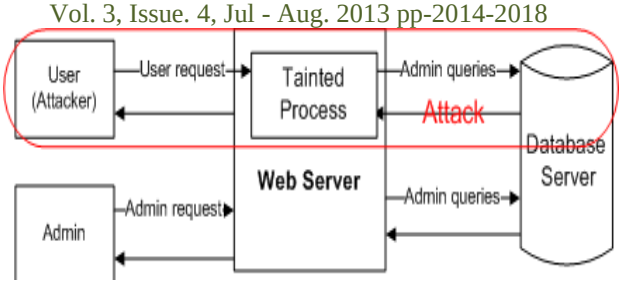

Fig. 3: Privilege Escalation Attack

3.2.2. Hijack Future Session Attack

This type of attacks is mainly aimed at the web server side. An attacker usually takes over the web server and therefore hijacks all subsequent legitimate user sessions to launch attacks. For instance, by hijacking other user sessions, the attacker can eavesdrop, send spoofed replies, and/or drop user requests. A session hijacking attack can be further categorized as a Spoofing/Man-in-the-Middle attack, an Exfiltration Attack, a Denial-of-Service/Packet Drop attack, or a Replay attack. According to the mapping model, the web request should invoke some database queries (e.g., a Deterministic Mapping), then the abnormal situation can be detected.

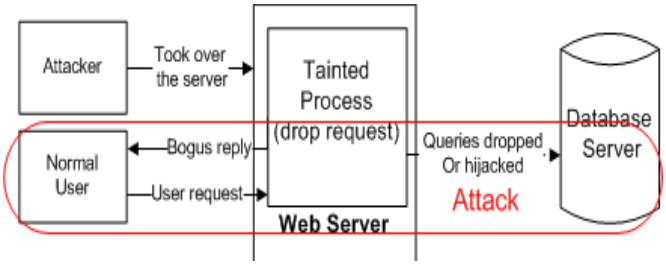

Fig. 4: Hijack Future Session Attack.

3.2.3. Injection Attack

Attacks such as SQL injection do not require compromising the web server. Attackers can use existing vulnerabilities in the web server logic to inject the data or string content that contains the exploits and then use the web server to relay these exploits to attack the back-end database.

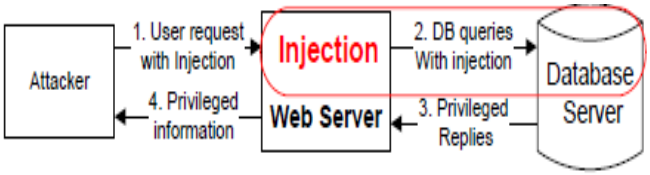

Fig. 5: Injection Attack

.

3.2.4. Direct DB Attack

It is possible for an attacker to bypass the web server or firewalls and connect directly to the database. An attacker could also have already taken over the web server and be submitting such queries from the web server without sending web requests. Without matched web requests for such queries, a web server IDS could detect.

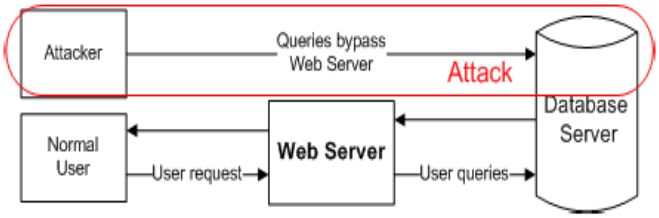

Fig.6: DB Query without causing Web requests.

III. MODELLING MAPPING PATTERNS

Due to their diverse functionality, different web applications exhibit different characteristics. Many websites serve only static content, which is updated and often managed by a Content Management System (CMS).This creates tremendous challenges for IDS system training because the HTTP requests can contain variables in the past parameters. The variable values in both HTTP requests and database queries, preserving the structures of the requests and queries.

4.1 Deterministic Mapping
4.2 Empty Query Set
4.3 No Matched Request
4.4 Nondeterministic Mapping

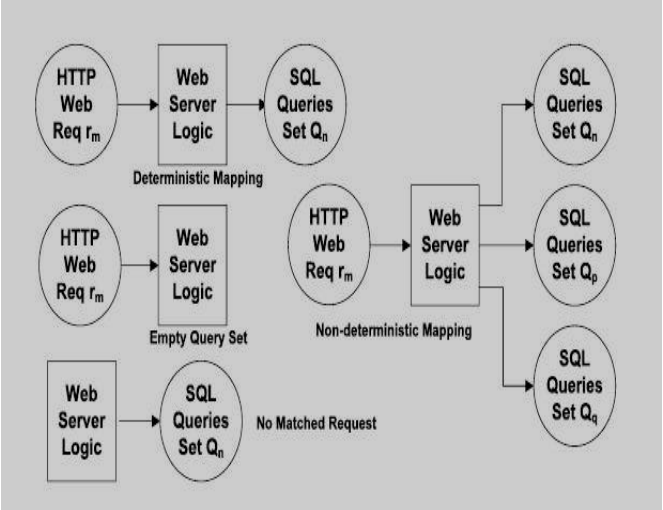

Fig.6: Overall representation of mapping patterns.

IV. MODELING FOR STATIC AND DYNAMIC

In the case of a static website, the nondeterministic mapping does not exist as there are no available input variables or states for static content. We can easily classify the traffic collected by sensors into three patterns in order to build the mapping model. As the traffic is already separated by session, we begin by iterating all of the sessions from 1 to N. For each r_m ЄREQ We maintain a set AR_m to record the IDs of sessions in which r_m appears. The same holds for the database queries.

In contrast to static webpages, dynamic webpages allow users to generate the same web query with different parameters. Additionally, dynamic pages often use POST rather than GET methods to commit user inputs. Based on the webserver' application logic, different inputs would cause different database queries. By placing each rm, or the set requests Rm, in different sessions with many different possible inputs, we obtain as many candidate query sets {Qn, Qp, Qq….} as possible. This mapping model includes both deterministic and nondeterministic mappings, and the set EQS is still hold static file requests.

V. PERFORMANCE EVALUTION

We obtained 329 real user traffic sessions from the blog under daily workloads. During this seven-day phase, we made our website available only to internal users to ensure that no attacks would occur then generated 20 attack traffic sessions mixed with these legitimate sessions, and the mixed traffic was used for detection.

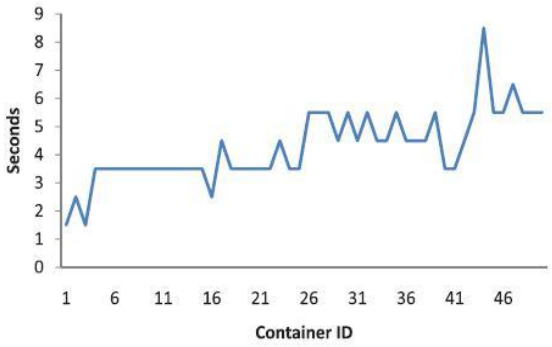

Fig. 7: Time for starting a new container.

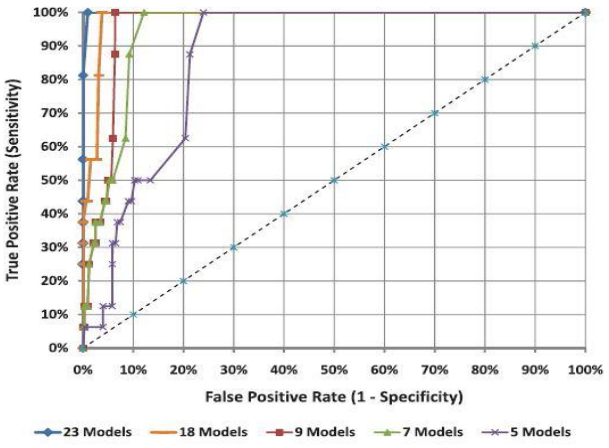

Fig.8. ROC curves for dynamic models.

We model nine basic operations; we can reach 100 percent Sensitivity with six percent False Positive rate. In the case of 23 basic operations, we achieve the False Positive rate of 0.6 percent. By Using Double guard approach we also avoid the following attacks. Privilege Escalation Attack, Hijack Future Session Attack (Webserver-Aimed Attack), Injection Attack.

VI. CONCLUSION

We presented an Intrusion Detection System that builds models of normal behavior for multitier web applications from both front-end web (HTTP) requests and back-end database (SQL) queries. It forms container based IDS with multiple input streams to produce alerts. We have shown that such correlation of input streams provides a better characterization of the system for anomaly detection because the intrusion sensor has a more precise normality model that detects a wider range of threats. We achieved this by isolating the flow of information from each web server session with a lightweight

virtualization. Furthermore, we quantified the detection accuracy of our approach when we attempted to model static and dynamic web requests with the back-end file system and database queries.

REFERENCES

[1] U. Shankar and V. Paxson, "Active Mapping: Resisting NIDS Evasion Without Altering Traffic," Proc. IEEE Symp. Security and Privacy, 2003.
[2] T.H. Ptacek and T.N. Newsham. Insertion, Evasion and Denial of Service: Eluding Network Intrusion Detection Technical report, Secure Networks, January 1998.
[3] M. Roesch. Snort - Lightweight Intrusion Detection for Networks. In *Proceedings of the USENIX LISA '99 Conference*, November 1999.
[4] K. Kendall, "A Database of Computer Attacks for the Evaluation of Intrusion Detection Systems," master's thesis, MIT, June 1999.
[5] G.H. Kim and E.H. Spafford, "The Design and Implementation of Tripwire: A File System Integrity Checker," technical report, Purdue Univ.,

International Journal of Modern Engineering Research (IJMER)
www.ijmer.com Vol. 3, Issue. 4, Jul - Aug. 2013 pp-2019-2022 ISSN: 2249-6645

Design & Optimization of Equipment for Insertion of Tube Bundle of Heat Exchanger

Kantilal P. Patil[1], Sachin S. Barve[2]
*(Department of Mechanical Engineering, V.J.T.I College, Mumbai University, India)
** (Department of Mechanical Engineering, V.J.T.I College, Mumbai University, India)

ABSTRACT : *Presently pressure vessel industries, manufacturing screw plug heat exchanger implements manual way for inserting tube bundle against shell. This manual way of inserting tube bundle inside shell involves challenges such as centre alignment of shell & tube bundle, manual pushing of tube bundle inside shell. This method of insertion may either leads to damage of inner cladding of shell or baffle of tube bundle. Rather than this, manual method of tube bundle insertion needs more labors & more time is needed to complete the entire activity. This article proposes semi-automatic equipment which makes tube bundle insertion process more safe & reliable. Using this equipment around 90% time saving can be achieved for tube bundle insertion activity with reduced numbers of labors as well.*

Keywords: *Cradle, Overhead crane, Profile linear slides, Tube bundle.*

I. INTRODUCTION

Many pressure vessel industries (manufacturer of screw plug heat exchanger) in today's date, still uses manual way for inserting tube bundle inside shell. This manual way for inserting tube bundle inside shell makes use of cradle, overhead crane, locking boom & chain pulley blocks. Cradle is a semi-circular structure made from thick sheet of steel. Cradle is used to support baffles of tube bundle. After placing tube bundle on to cradle, it is lifted to desired height using overhead crane & located against shell such that centre of shell should match with centre of tube bundle. At the end of tube bundle, tubes are welded to thick circular sheet called tube sheet. Locking boom is mounted on tube sheet so that it can serve reaction to pair of chain pulleys. After locating tube bundle against shell, chain pulleys on either side are pulled so that tube bundle starts inserting in to shell. The entire activity takes time of 15-16 hrs with 6 workmen needed to do this job.

Fig.1-Pictures showing manual tube bundle insertion activity

Taking this scenario in to account this article proposes a semi-automatic equipment which facilitate all critical activities involved in manual process such as

- Handling tube bundle using Tube sheet trolley & Baffle Trolley
- Centre alignment of tube bundle using screw jack synchronization & profile linear slides
- Pushing the tube bundle using motor controlled push mechanism

The CAD model of proposed equipment with above mentioned features is depicted below

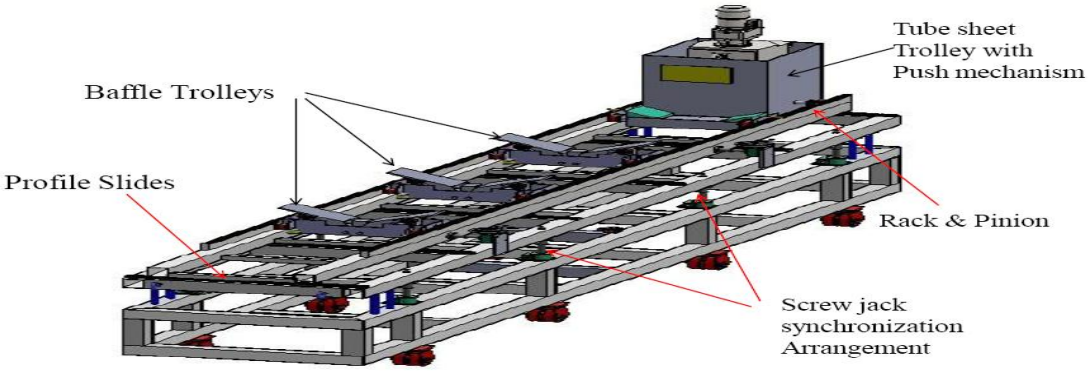

Fig.2- CAD model of tube bundle equipment

The technical specifications of equipment are as below

Heat exchanger type = screw plug
Tube bundle diameter = 1500 mm
Length of tube bundle = 7500 mm
Weight of tube bundle = 25000 Kg
Working range of bundle diameters = 1200 to 1800 mm
Feed velocity for insertion = 1500 mm/min

II. Baffle Trolley Design

Requirements from baffle trolley are

- Baffle trolley must be movable & should have provision to support baffle
- Wings of baffle trolley must be detachable

II.1 Mechanism

Considering above requirements in to account baffle trolley is designed which is movable & has mechanism to attach & detach the movable wings. The mechanism used is called as movable block & lead screw mechanism. By rotating the lead screw angle between wings can be adjusted to desired level (which is usually 130 deg) & can be detached from baffle of tube bundle as soon as baffle is about to enter in to shell. These movable wings swivel about swivel rods located at bottom.

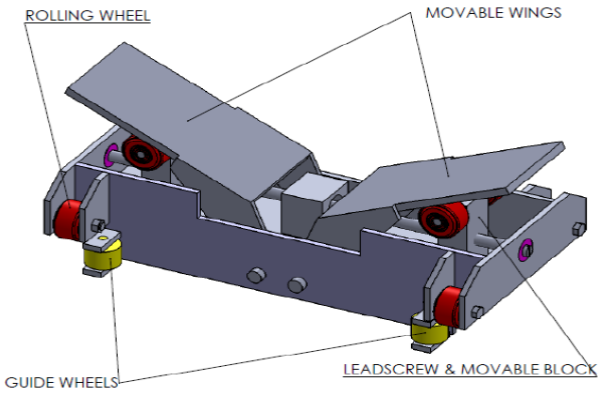

Fig.3- Baffle Trolley

Mechanism contains block which supports wheel on it to rest them against lower surface of movable wings & threading is present inside block in order to engage with corresponding threading with lead screw. Lead screw of baffle trolley are of opposite hands i.e. first half is having left handed threads & second half is having right handed threads so that by rotating lead screw from either side swiveling movement of wings can be obtained. Rolling wheels provide motion to baffle trolley & guiding wheels restricts path of baffle trolley from deviating.

2.1 Structural analysis of baffle trolley

Baffle trolley is checked for sustainability for carrying the load of tube bundle. Approximately 5000 kg of load comes on each baffle trolley (since there are 3 baffle trolleys) for tube bundle weighing 25 tones. The load of tube bundle is applied on certain area of movable wing since baffle is only rested on wing. The material for baffle trolley is plane carbon steel & analysis is carried out in solidworks which gives following results

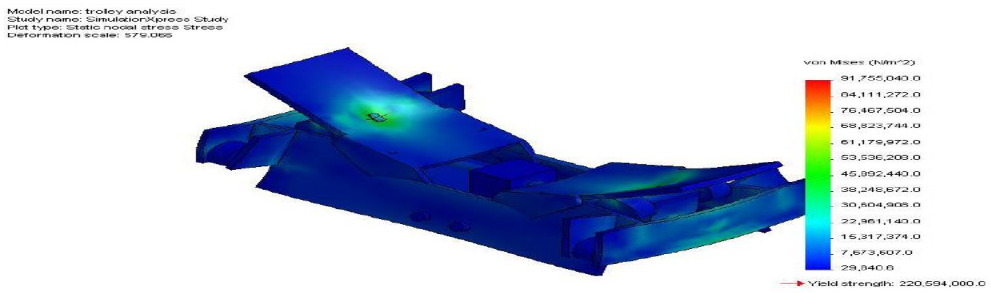

Fig.4-Von Mises Stresses

Maximum von-mises stresses occurred is 91 MPa & Y.S. is 220 MPa i.e. F.S. is more than 2. Hence baffle trolley is safe under applied load.

III. Tube sheet trolley design

Requirements from tube sheet trolley are

- Tube sheet trolley must be movable & should have provision to support tube sheet
- Movable block of tube sheet trolley must be detachable

III.1 Mechanism

Considering above requirements in account tube sheet trolley is designed which has provision to support tube sheet of tube bundle. Mechanism used here in this trolley is movable block & screw. The screw is located against the movable block on either side using plate. Plate has threaded provision to guide screw & adjust location of block as per need. The angle between faces of movable blocks is maintained 130 deg since this particular angle of seating provides maximum stability to the tube bundle.

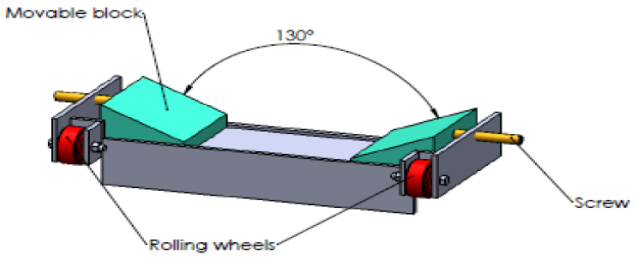

Fig.5- Tube sheet trolley

Rolling wheels provides motion to tube sheet trolley & Tube sheet trolley is firmly attached to the unit carrying push mechanism arrangement.

III.2 Structural analysis of tube sheet trolley

Tube sheet trolley is checked for sustainability for carrying the load of tube sheet of tube bundle. Approximately 10000 kg of load comes on tube sheet trolley for tube bundle weighing 25 tones. The material for tube sheet trolley is plane carbon steel & analysis is carried out in solidworks with its own solver & automatic meshing, which gives following results

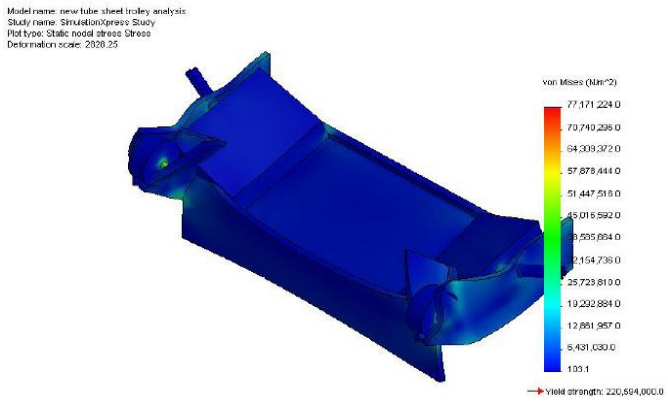

Fig.6- Von-mises stress distribution

Maximum von-mises stresses occurred is 77 MPa & Y.S. is 220 MPa i.e. F.S. is more than 2. Hence tube sheet trolley is safe under applied load.

IV. Push mechanism design

In order to insert tube bundle inside the shell, the necessary push is provided through a mechanism of geared motor & bevel gearbox. The power of geared motor is spitted in two perpendicular directions using 3-way bevel gearbox & transferred to the pinions on rack gear. Thus reaction force needed to push tube bundle inside shell is obtained using rack & pinion gear arrangement.

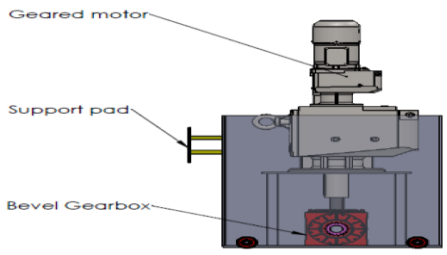

Fig.7- Push mechanism arrangement

Motor power (P) is calculated using,

$P = F \times V$

Where,

F = load to be pushed inside the shell

V = feed velocity of insertion in $\frac{m}{min}$

V. Centre alignment technique using screw jack synchronization & profile linear slides

Before starting tube bundle insertion process it is necessary to locate tube bundle against shell so that centre line of tube bundle should coincide with centre line of shell. For that purpose it is mandatory that tube bundle inserting equipment should have provision to provide bi-axial movement to the tube bundle. The two necessary movements needed are vertical motion & lateral motion.

V.1 Vertical motion using screw jack synchronization

Group of ball screw jacks interconnected using shafts & centrally connected to servo motor using bevel gearbox is an arrangement to provide vertical motion to tube bundle.

V.2 Lateral motion using profile linear slides

A platform on which tube bundle is located is provided a lateral motion using series of profile linear slides with dual shoes. These profile linear slides are located under the platform carrying tube bundle.

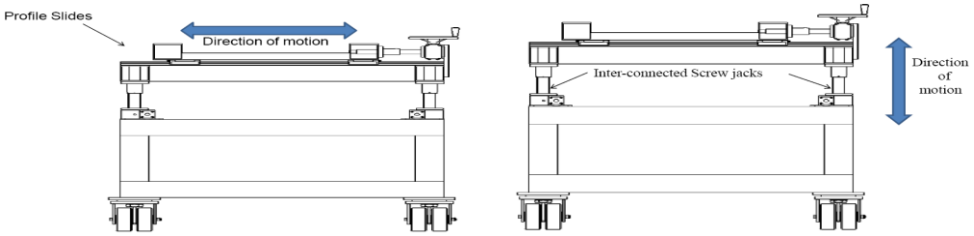

Fig.8- Figures showing lateral & vertical motion provided to tube bundle

VI. Operating procedure of tube bundle equipment

Baffles of tube bundle are rested on baffle trolley & tube sheet of tube bundle is rested on tube sheet trolley making angle between resting surfaces as 130 deg. Since equipment is provided with lockable swivel castors thus it can be easily located at desired location of shell on shop floor & its motion can be locked using lock pad provided on swivel castor. Then centre alignment of shell & tube bundle is made using vertical & lateral motion of screw jack synchronization & profile linear slides respectively. After completion of alignment, tube bundle is pushed inside shell using push mechanism provided on to equipment. As tube bundle starts inserting in to shell, baffle trolleys are detached by rotating lead screw & in this way entire tube bundle is inserted in to shell.

VII. Conclusion

1. Von-mises stress analysis of baffle trolley & tube sheet trolley shows shaft of rolling wheels is critically stressed component. Hence, shafts of wheel must be rigid enough. However, both trolleys are safe under operating load.
2. The equipment gives benefit in terms of time saving since manual operation needs 15-16 hrs & tube bundle equipment makes it in maximum 1 hr. Thus more than 90% of time consumption is reduced.
3. Manual handling may leads to damage of baffle or inner cladding of shell & risk of human life whereas; this equipment ensures complete safety by proper handling provision & motor controlled pushing mechanism thereby ensuring safety & reliability.

VIII. ACKNOLEDGEMENT

I am very grateful to M/S Larsen and Toubro Ltd. Powai, for giving me opportunity to learn and innovate the idea and for letting the industrial exposure to me. I am indebted to the production department and the staff for their help.
I am also thankful to my institute V.J.T.I. Mumbai and my professors for their support and motivation.

REFERANCES

❖ **Books**

V. B. Bhandari, "Design of Machine Elements", New York, McGraw-Hill, pp. 698, 601, 93 (1998).

❖ **Patent**

Bobby J. Travis (1977),"*Tube bundle extractor for use with heat exchanger*", United States Patent, Appl. No.617076.

❖ **Internet**

- ✓ www.**nord**.com
- ✓ www.**powermaster**.in
- ✓ www.rino.co.uk
- ✓ www.**tente**.in
- ✓ www.**nookindustries**.com

International Journal of Modern Engineering Research (IJMER)
www.ijmer.com Vol. 3, Issue. 4, Jul - Aug. 2013 pp-2023-2026 ISSN: 2249-6645

The Adaptation of Clay-Bath and hydro-cyclones in Palm Nut Cracked-Mixture Separation to Small–Scale Oil Palm Processing Industry

[1]Okoronkwo, C. A., [2]Ngozi-Olehi, L. C.,[1]Nwufo, O. C.
[1]*Mechanical Engineering Department, Federal University of Technology, Owerri. Imo State*
[2]*Department of Chemistry, AlvanIkoku Federal College of Education, Owerri. Imo State*

ABSTRACT: *Oil palm is now accepted as one of the most important oil-producing crops in the world. The bid to ensure efficient and quality production has resulted in the invention of machines that have greatly reduced human labour in the production process. Separation of cracked mixture to recover the kernels is one of the most important activities in Palm Kernel oil (PKO) production process. Research has led to the invention of the clay-bath and hydro-cyclones for the recovery of kernels from the cracked mixture. However, these machines are very costly to install and operate and as well require skilled labour. This research work is intended to examine these innovations and recommend suitable adaptations of these machines for use by the small scale mill operators who cannot afford the modern machines and the technical know-how needed to operate them. The clay-bath has been recommended for local mill operators for cracked mixture separation due to its ease of use and scalability.*

KEY WORD: *adaptability, clay bath, hydro-cyclones, palm-nut, cracked mixture*

I. INTRODUCTION

Palm kernel processing industry is very popular in the third world countries because of the dependency of many companies on palm kernel and palm oil as raw material (Hartley, 1987),(Oke,2007). The processing of the palm kernel entails cracking the shell to produce the nut for industrial use. Cracked kernel produced must be separated from its shell to makes it convenient for further processing in the industries. Separation of cracked mixture which results from the nut cracking stage and consists of kernels, broken shells, unbroken nuts and dusts requires the recovery of each of these constituents of the mixture. It is a very important activity in the kernel recovery process of palm mills. In the developing countries, small scale palm mills make use of manual labour for the separation of the kernels. The kernels are handpicked from the mixture and at the same time the unbroken nuts are recovered and taking back to the mill for cracking. This method is slow, laborious and unsuitable for large scale mills. But modern methods of cracked mixture separation have been devised which are classified into two namely: systems based on density and systems based on shape.The principle involved in the system based on density employs the difference in density between the kernels and the shells to chart paths for their independent recovery. The relative density of palm kernel is about 1.07 and that of the shell ranges from 1.15 to 1.20. Clay-bath and hydro-cyclones are two methods devised for cracked mixture separations based on density.These methods of separation are usually known as wet processes since water is always involved and the kernels have to be dried at the end of the separation.(Amoah et al 2007)

Over the years, there have been a lot of innovations geared towards improving the efficiency of these activities by way of reducing energy consumption, water usage, and minimizing damage or rupture of the kernels, noise generation, and generation of palm oil mill effluent (POME). Separation of cracked mixture is a challenging process especially to the small-scale mill owners. Large-scale mills have automated hydro-cyclone machines with high separation efficiency, however, clay-baths and hydro cyclones are known for their high energy and water consumption making their application in small-scale mills difficult(Poku, 2002). On the other hand, inefficient separation process could cause shells to be carried together with kernel to palm kernel expellers which could damage the crushing mechanisms. Therefore, the need to study these processes becomes imperative as a means of investigating the operations of the machines and their suitability in small-scale, medium-scale and large-scale palm mills.

In this paper, the authors aimed at narrowing the information gap by revealing how to adapt the clay-bath and hydro-cyclones in palm nut cracked-mixture separation to small–scale oil palm processing industry especially in the rural areas where grid electricity is absent. Specifically, this study sets out to:

- Critically analyze the innovations already available for the separation of cracked mixture containing shells and kernels.
- Suggest possible ways these innovations could be adapted for use, especially, by small-scale palm mills.

This study will help indigenous small scale industries adopt modern techniques in the cracked mixture to obtain palm kernel and shells.

II. THE CLAY-BATH

The clay-bath uses a clay solution that is maintained within a relative density of 1.12. When the cracked mixture is admitted into the clay-bath, the denser shells will sink to the bottom while the less dense kernels will float (Oguoma et al, 1993).

III. GENERAL DESCRIPTION/OPERATION OF THE CLAY-BATH

The clay-bath is made up of the bottom tank which is of cylindrical shape with portions of sloping rectangular section for the returning clay solution, the top conical chamber which is of inverted cone shape with inlet and outlet side openings for the clay solution, the cylindrical shaped expansion chamber which has a small inlet connected to the pump outlet pipe and large outlet connected to the top conical chamber inlet opening, the vibrating screen made of rectangular single deck type and supported by two steel leaf spring located at both side of the screen, an eccentric shaft driven byelectric motor via flexible rubber coupling used to create the vibrating motion, the stirrer connected with gear motor that is mounted on the bottom tank and extends right to the bottom of the tank, a gear motor used to reduce the speed of the stirrer to about 28rpm through a bevel gear arrangement, the circulating pump connected with electric motor which is of the centrifugal end suction type, a mechanical seal used in place of the gland packing with the pump that is driven by an electric motor via a v-belt drive. The electric motors are 1.5KW, 2.2KWand 7.5KW all 4 pole squirrel cage, 3 phase induction motor suitable for 230/415V, 50Hz electric supply for vibrating screen, circulating pump and the stirrer gear motor respectively.

In this separator (clay-bath), the clay solution is circulated through the system by means of a pump. This pump draws solution from the bottom tank and pushes it to the top conical chamber through the expansion chamber. During operation, the cracked mixture enters the system from the top of the top conical chamber and flows along the solution. Kernel being lighter floats to the top of the solution and shells heavier than the solution sinks to the bottom of the chamber. They are carried along by the solution to the respective outlets and then to the vibrating screen which is partitioned to receive the kernel and the shell in separate compartments thus allowing the solution to flow through the stainless steel mesh and back to the bottom tank while kernel and shell are being screened and exit from the end of the screen, hence the clay solution is circulated and re-used. An inbuilt stirrer is used to homogenize the solution.

It is necessary to top up the solution to make for the losses because little amount of the solution is usually carried away with the kernel and shell. Washing of the kernel ex-separator is possible by installing a clean water pipe to the end of the vibrating screen where small jets of water can be sprayed onto the kernel and wash them before exit from the screen. The clay-bath could be used domestically. A small cemented pit or a ground tank could be used for the clay-bath separator. The tank or pit will be filled with water and the clay will be added in the right proportion so that the density of the suspension is maintained. Manual stirring could be used to keep the clay in suspension, while the cracked mixture is poured into the pit or tank. The density difference will make the shells to sink and the kernels to float. The kernels can easily be skimmed off the surface of the suspension while the shells are evacuated later. Drying of the shells and nuts could be done under the sun on concrete floors or roofing sheets. This will increase the desiccation rate significantly.

IV. PROBLEMS OF CLAY-BATH

One of the problems associated with the clay-bath is that of maintaining the solution within the appropriate density range. Therefore, a solution of common saltof suitable density may be substituted for the clay suspension. This brine has the advantage that it does not settle out which ensures that the density results much steadier but must be topped up from time to time Maycock, (1990). Another problem that may likely arise from the use of this system is the disposal of water after using the clay bath.

V. THE HYDROCYCLONE SEPARATOR

A hydro cyclone assembly consists of two bottom cylindrical tanks with a conical base called baths, two overhead hydro cyclones called the kernel and shell hydro cyclones, two pumps, and two pairs of exit and overflow pipes. The size of the apertures at the bottom of the hydro cyclones is critical to their operation. The heights of the overflow pipes are adjustable as it is used to control the purity of the kernels.

The cracked mixture from the cracker is admitted into cracked mixture bath which is already filled with water. The pump powered by an electric motor is used to pump the cracked mixture together with water into the kernel hydro cyclone.

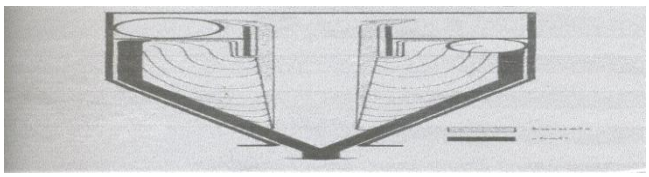

Figure 1: A diagram showing the cyclone action of a hydrocyclone.

At the entry of the cracked mixture into the hydrocyclone, a helical motion is initiated by the tangential entry of the cracked mixture which causes the heavy particles to be thrown by centrifugal force to the wall of the cylinder and after tracing a helical path exits through the bottom of the cyclone.

By choosing the dimensions of the hydrocyclone and the pressure of the pump correctly, most of the shell pieces pass downwards and out through the bottom cone with small proportion of water flow. The larger part of the water together with most of the kernel after taking part in an initial downward circular movement gradually move towards the centre of the cylinder and start moving upwards leaving the hydrocyclone via the overflow tube and exit pipe. In the kernel hydrocyclone, the high overflow pipe is used to ensure that the kernels entering are sufficiently pure and ready for bagging. This high setting also causes some kernels to move downwards and exit with the shells through the exit pipes. The mixture (containing

shells and little proportion of kernels) leaving the exit pipe of the kernel hydrocyclone is passed to another bath called the shell bath where a second pump is used to push the mixture to another hydrocyclone known as the shell hydrocyclone. The two baths are adjacent to each other with a perforated partition between them which allows the water levels to equalize. It is important to prevent the perforations from becoming so worn out that kernels can pass through into the shell fraction.

In the shell hydrocyclone, the overflow pipe is lowered sufficiently so that kernels together with some shells are evacuated and sent back to the cracked mixture bath. The lower overflow pipe ensures that the down flow is cleaner hence only shells move through the exit pipe of the shell hydrocyclone.

VI. SYSTEM BASED ON SHAPE

Other method of nut/kernel separations are based on the shape of the shells and kernels. These include the winnowing column and the vibrating table. These methods are collectively called dry processes since they used either air or no fluid at all.

VII. WINNOWING COLUMN OR PNEUMATIC SEPARATORS

The winnowing column uses air as the fluid for separation;the column consists of tall cylindrical or rectangular steel duct that is connected to a blower or suction fan. The winnowing column is used in conjunction with either of the wet methods of separations- claybath or hydrocyclone. The commercial winnowingsystem uses force or induced draught (Halim, et al, 2009).

Cracked mixture from the cracker is conveyed by a screw conveyor to some height along the winnowing column. As the mixture is poured inside the column, the air draught maintained by a suction pump sucks the fibres, dust and some shell pieces up the duct while the kernels, un-cracked nuts, and the remaining shells fall and are captured in another duct through the use of an air lock. In this way, up to about 30% to 40% of the shell present in the cracked mixture is removed without causing a loss exceeding 1% of the total kernel. This winnowed mixture is now dust free and can then be sent to the claybath or hydrocyclone separator.

According to (Maycock,1990), it is necessary to adjust the air velocity in the separating column to a suitable value to ensure removal of light shell without losing kernel and this is usually found to be in the range of 12.5m/s to 15m/s.
Recently, the four stage winnowing column has been invented and developed by the Malaysian Palm Oil Board (MPOB) in collaboration with Hur Far Engineering Works SdnBhd (HF) and FELDA Palm Industries SdnBhd (FPISB). These separation systems consist of a series of equipment: a four stage winnowing column, a cyclone, a blower fan, an air lock and an auger. Each column was designed with different parameters (e.g. air velocity, fan speed, column height, inlet outlet levels, feeding ratio, etc.) in order to achieve the desired shell and kernel ratio separation at each outlet point (Halim et al,2009).

VIII. THE VIBRATING TABLE

The vibrating table is a dry separation process. The table is supported by two steel leaf springs located at both sides of the table. An eccentric shaft driven by electric motor via flexible rubber coupling is used to create the vibrating motion. The cracked mixture from the cracker is poured on top of the table and as the table vibrates, the kernels are moved to one side of the table, while the shells move to the other side.

IX. WAYS TO ADAPT THESE INNOVATION TO SUIT SMALL SCALE INDUSTRIES

The small scale oil processing industries in the third world countries are mostly situated in the rural areas of the developing countries where grid electricity is mostly nonexistent or irregular. The cost of generating an alternative energy using diesel powered generators can be very enormous and will adversely affect the profit of such industries. Most industries have collapsed in Nigeria due to high running cost of using diesel generating power plants to run the machineries. Recall that the main source of energy to the clay- bath and the hydro cyclone separators is electricity generated using diesel powered generators. The cost of diesel in Nigeria is about $1.00 per litre. In a day, depending on the fuel economy of the generator, an average four cylinder engine consumes about 200litres of fuel in twelve hours. Since an average clay bath motor generatesabout 1.5-7.5kW of power a solar powered generator can replace the diesel powered generator and still produce the same amount of power. To adapt the claybath palm kernel separator to suit the small scale industries, solar powered generators can be used which will drastically reduce the energy cost for the processing of the palm kernel. Another way to reduce operational cost is to replace the bevel gear powered stirrer in the clay bath with a manual stirrer. Though the average stirring speed for the mechanical stirrer is 28rpm, a manual stirrer can produce this speed conveniently. When the stirrer is removed, the cost of installing the stirring system is drastically reduced because it will eliminate the gears used for speed reduction. The ground tank should be constructed in such a way that as to provide a draining chamber where spent water can be channeled into a confined chamber to avoid the degradation of the environment.

X. CONCLUSION AND RECOMMENDATION

Most families in south-east and south-south geographical regions of the Nigeria earn their income from the sales of palm oil and palm kernels. Some individuals and villages already have small- scale palm mills where modern machines are used for the stripping, digesting, pressing and cracking processes. However, the separation of cracked mixture to recover kernels from the cracked mixture still remains the main problem faced by small scale operators.The standard claybath requires enormous power due to electric motor used to power the pumps. However, the technology is easily understood even by local operators and can be easily adopted to suit them even domestically. The hydrocyclone requires more water and power than the claybath and the technology that is associated with hydrocyclone is more complex than that of the claybath,

hence its use by the rural dwellers will be difficulty. It is however recommended that small-scale palm industries adopt the use of clay-bath for crack mixture separation to reduce the laborioustask of handpicking and as well increase the speed of the process

XI. APPENDIX

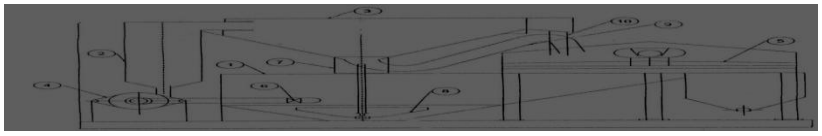

1. BOTTOM TANK
2. EXPANSION CHAMBER
3. TOP CONICAL CHAMBER
4. CIRCULATING PUMP
5. VIBRATING SCREEN
6. PUMP INLET VALVE
7. GEAR DRIVE
8. STIRRER
9. SHELL DISCHARGE PIPE
10. KERNEL DISCHARGE PIPE

Figure 2: A schematic of the claybath

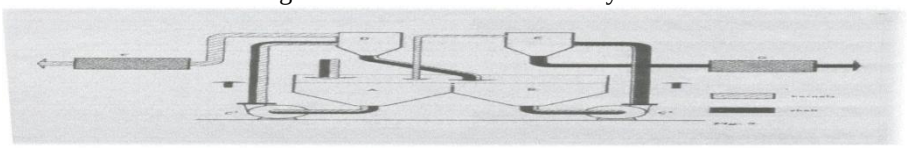

A. CRACKED MIXTURE BATH
B. SHELL BATH
C. PUMP
D. KERNEL HYDROCYCLONE
E. SHELL HYDROCYCLONE
F. KERNEL SCREEN AND DRYER
G. SHELL SCREEN

Figure 3: A schematic of the hydrocyclone

Figure 4: Web shots of a hydrocyclone assembly.

REFERENCES

[1]. Amoah, J. y., Aggey, M., and Annumu, S. (2007): Cracked- Mixture Sieving Rates and Efficiencies In Small Scale Palm Nut Processing In Ghana. Ghana Journal of Science.
[2]. Halim, R M; Bakar, N. A; Wahid, M B.; May C. Y; Ramli, Ridzuan; Ngan, Ma Ah; M, R(2009): Maximizing the Recovery of Dry Kernel and Shell via a Four Stage Winnowing Column. MPOB Information Series (MPOB TT No. 427).
[3]. Hartley, C.W.S , (1987) The Project Of Oil Palm And The Extraction In The Oil Palm, Longman London
[4]. Maycock, J. H., & Symposium on New Developments in Palm Oil.(1990). *Innovations in palm oil mill processing and refining*. Kuala Lumpur: Palm Oil Research Institute of Malaysia.
[5]. Oguoma ,O.N,C.COnwuzuruigbo and Nnamadim(1993) Design of Palm kernel/shell separation for developing countries.Nig.J.Tech.Edu,10:1-2
[6]. OkeP.K(2007) "Development And Performance Evaluation Of Indigenous Palm Kernel Dual Processing Machine", Journal Of Engineering And Applied Sciences, Medwell Journals
[7]. Poku, K.:(2002) Traditional Techniques and Innovations in Small Scale Palm Oil Processing.Retrieved Oct 03, 2010, From FAO Agricultural Services Bulletin.

International Journal of Modern Engineering Research (IJMER)
www.ijmer.com Vol. 3, Issue. 4, Jul - Aug. 2013 pp-2027-2034 ISSN: 2249-6645

The Method of Repeated Application of a Quadrature Formula of Trapezoids and Rectangles to Determine the Values of Multiple Integrals

Nazirov Sh. A.
Tashkent University of Information Technologies, Tashkent, Uzbekistan

Abstract: *The work deals with the construction of multi-dimensional quadrature formulas based on the method of repeated application of the quadrature formulas of rectangles and trapezoids, to calculate the multiple integrals' values. We've proved the correctness of the quadrature formulas.*

Keywords: *multi-dimensional integrals, cubature formulas, re-use method.*

I. INTRODUCNION

The paper is devoted to developing the multiple cubature formulas for the values of n-fold integrals calculation by means of methods of repeated application of, quadrature formulas of trapezoid and rectangles.

According to mathematical analysis multiple integrals can be calculated by recalculating single integrals.

The essence of this approach is the following. Let the domain of integration is limited to single-valued continuous curves [1]

$y = \varphi(x),\ \ y = \psi(x)\ \ (\varphi(x) \le \varphi(x))$

and two vertical lines $x = a,\ \ x = b$ (Fig.1).

Placing the known rules in the double integral

$$I = \iint_{(D)} f(x,y)dxdy \qquad (1)$$

limits of integration, we obtain

$$\iint_{(D)} f(x,y)dxdy = \int_a^b dx \int_{\varphi(x)}^{\psi(x)} f(x,y)dy.$$

Let

$$F(x) = \int_{\varphi(x)}^{\psi(x)} f(x,y)dy. \qquad (2)$$

Then

$$\iint_{(D)} f(x,y)dxdy = \int_a^b F(x)dx. \qquad (3)$$

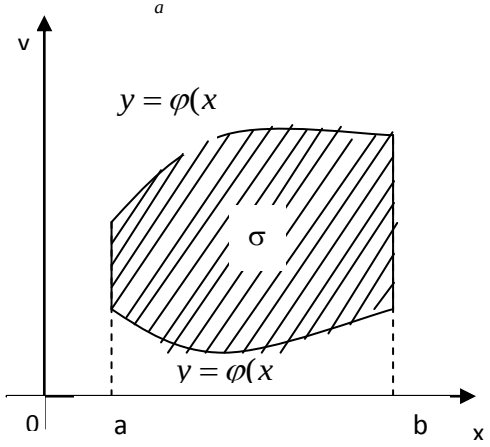

Fig.1

Applying to a single integral in the right-hand side of (3), one of the quadrature formulas, we have

$$\iint_{(\sigma)} f(x,y)dxdy = \sum_{i=1}^{n} A_i F(x_i), \qquad (4)$$

where - $x_i \in [a,b]\ \ (i = 1,2,...,n)$ and A_i are some constant coefficients. In turn, the value

$$F(x_i)=\int_{\varphi(x_i)}^{\psi(x_i)} f(x_i,y)dy$$

can also be found on some quadrature formulas

$$F(x_i)=\sum_{j=1}^{m_i} B_{ij} f(x_i,y_j),$$

where B_{ij} iy - appropriate constants.

From (4) we obtain

$$\iint_{(D)} f(x,y)dxdy=\sum_{i=1}^{n}\sum_{j=1}^{m_i} A_i B_{ij} f(x_i,y_j), \qquad (5)$$

where A_i and B_{ij} iy - are known constants.

Geometrically, this method is equivalent to the calculation of the volume I, given by the integral (2) by means of cross-sections.

For cubature formulas of the type (3), the general comments, relating to the computation of simple integrals, are valid with appropriate modifications.

In three dimensions (3) has the form

$$\iiint_{(D)} f(x,y,z)dxdydz=\sum_{i=1}^{n}\sum_{j=1}^{m_i}\sum_{k=1}^{t_i} A_i B_{ij} C_{ij,k} f(x_i,y_j,z_k).$$

Now these results are generalized to compute the values of multiple integrals

$$\iint\limits_{(D)}\!\!\ldots\!\int f(x_1,x_2,x_k)dx_1dx_2\ldots dx_k =$$

$$=\sum_{i_1=1}^{n_1}\sum_{i_2=1}^{n_2}\ldots\sum_{i_n=1}^{n_k} A_{i_1}^{(1)} A_{i_1 i_2 i_3}^{(2)} A_{i_1 i_2 i_3}^{(3)}\ldots A_{i_1 i_2 i_k}^{(k)} f(x_{1_i},x_{2_i},\ldots,x_{k_i}),$$

Where $A_{i_1}^{(1)}, A_{i_1 i_2}^{(2)},\ldots, A_{i_1 i_2\ldots i_k}^{(k)}$ - are known constants.

This approach can be applied to calculate the approximate value of multiple integrals using appropriate quadrature formulas. In this case, we apply the quadrature formula of trapezoid.

II. ALGORITHM DISCRIPTION

Theorem 1. Let the function

$$y=f(x_1,x_2,\ldots,x_n)$$

Is continuous in a bounded domain D. Then the formula for the approximate values of the n-fold integral calculating

$$J_n=\iint\limits_{(D)}\!\!\ldots\!\int f(x_1,\ldots,x_n)dx_1dx_2,\ldots,dx_n, \qquad (6)$$ based on the trapezoidal rule has the form

$$J_n=\prod_{i=1} h_i \sum_{p_1=0}^{n_1-1}\sum_{p_2=0}^{n_2-}\sum_{p_3=0}^{n_3-1}\ldots\sum_{p_n=0}^{n_n-1}\sum_{i_1=0}^{1}\sum_{i_2=0}^{1}\ldots\sum_{i_n=0}^{1} f_{p_1+i_1,p_2+i_2,\ldots,p_n+i_n}$$

Here D is n-dimensional domain of integration of the form

$$a_i\le x_i\le A_i,\qquad i=\overline{1,n}; \qquad (7)$$

$$h_i=\frac{A_i-a_i}{2}$$

and it is believed that each interval (5), is respectively, divided into $n_1,n_2,\ldots,n_n$ parts.

Proof. Approximate formula for calculating the values of the one-dimensional integral in this case is

$$J_1=\int_{x_0}^{x_1} f(x)dx=\frac{h_x}{2}\left[f(x_0)+f(x_1)\right]=\frac{h_x}{2}\sum_{i=0}^{1} f_i, \qquad (8)$$

where, $h_x=\frac{b-a}{n}$, n - the number of the interval divisions into n parts. In (4) n = 1 .

Now we define the approximate calculation formula for double integrals

$$J_2=\iint\limits_{(D)} f(x,y)dxdy \qquad (9)$$

where D is the two-dimensional area of integration.
It is generally believed that the region of integration in this case is within the rectangle, that is,
$a \le x \le b,\ c \le y \le d$.
Then we rewrite the integral (7) in the form

$$J_2 = \int_a^b dx \int_c^d f(x,y)dy. \qquad (10)$$

Using the trapezoidal rule to calculate the inner integral, we obtain

$$J_2 = \frac{h_y}{2}\left[\int_a^b f(x,y)dx + \int_a^b f(x,y)dx\right]. \qquad (11)$$

Now to each integral we use the trapezoid formulas and the result is

$$J_2 = \frac{h_y}{2}\left\{\frac{h_x}{2}\left[f(x_0,y_0)+f(x_1,y_0)\right]+\frac{h_x}{2}\left[f(x_0,y_1)+f(x_1,y_1)\right]\right\} =$$
$$\frac{h_x h_y}{4}\left[f(x_0,y_0)+f(x_1,y_0)+f(x_0,y_1)+f(x_1,y_1)\right]=\frac{h_x h_y}{4}\sum_{i=0}^{1}\sum_{j=0}^{1} f(x_i,y_j), \qquad (12)$$

where $h_y = \frac{d-c}{m}$.
Similarly, for the approximate calculation of the values of the triple integral we obtain the following formula:

$$J_3 = \int_a^A \int_b^B \int_c^C f(x,y,z)dxdydz = \frac{h_x h_y h_z}{8}\left[f(x_0,y_0,z_0)+f(x_0,y_0,z_1)+f(x_0,y_1,z_0)+\right.$$
$$\left.+f(x_0,y_1,z_1)+f(x_1,y_0,z_0)+f(x_1,y_0,z_1)+f(x_1,y_1z_0)+f(x_1,y_1z_0)+f(x_1,y_1,z_1)\right]= \qquad (13)$$
$$\frac{h_x h_y h_z}{8}\sum_{i=0}^{1}\sum_{j=0}^{1}\sum_{k=0}^{1} f(x_i,y_j,z_k),$$

where $h_z = \frac{C-c}{p}$.
The four-dimensional integral is defined with 16 members:

$$J_4 = \int_a^A \int_b^B \int_c^C \int_d^D f(x,y,z,u)dxdydzdu = \frac{h_x h_y h_z h_u}{16}\left[f(x_0,y_0,z_0,u_0)+f(x_0,y_0,z_0,u_1)+f(x_0,y_0,z_1,u_0)+\right.$$
$$+f(x_0,y_0,z_1,u_1)+f(x_0,y_1,z_0,u_0)+f(x_0,y_1,z_0,u_1)+f(x_0,y_1,z_1,u_0)+f(x_0,y_1,z_1,u_1)+ \qquad (14)$$
$$+f(x_1,y_0,z_0,u_0)+f(x_1,y_0,z_0,u_1)+f(x_1,y_0,z_1,u_0)+f(x_1,y_0,z_1,u_1)+f(x_1,y_1,z_0,u_0)+$$
$$\left.+f(x_1,y_1,z_0,u_1)+f(x_1,y_1,z_1,u_1)\right]=\frac{h_x h_y h_z h_u}{16}\sum_{i=0}^{1}\sum_{j=0}^{1}\sum_{k=0}^{1}\sum_{l=0}^{1} f(x_i,y_j,z_k,u_l);$$

Here $h_u = \frac{D-d}{t}$.
Considering (8.10), we present formulas for the approximate calculation of the n-fold integral on the trapezoidal:

$$J_n = \int_{a_1}^{A_1}\int_{a_2}^{A_2}\int_{a_3}^{A_3}\ldots\int_{a_n}^{A_n} f(x_1,x_2,\ldots,x_n)dx_1dx_2dx_3\ldots dx_n = \frac{1}{2^n}\prod_{i=1}^{n} h_i \sum_{i_1=0}^{1}\sum_{i_2=0}^{1}\sum_{i_3=0}^{1}\ldots\sum_{i_n=0}^{1} f(x_{1i_2},x_{2i_2},\ldots,x_{ni_n}) \qquad (15)$$

Then for the formulas (6) and (8) - (11) we derive the general trapezoid formula. For this purpose, one-dimensional integral for integral intervals [a, b] is divided by n equal parts: $[x_0,x_1],\ldots,[x_{n-1},x_n]$, $x_i = x_0 + ih_x$.
The two-dimensional integral of the $[a,b]\times[c,d]$ region of integration is divided, respectively, by n and m parts:
$[x_0,x_1],\ldots,[x_{n-1},x_n]$; $[y_0,y_1],\ldots,[y_{m-1},y_m]$

$$x_i = x_0 + ih_x,$$
$$y_j = y_0 + jh_y. \qquad (16)$$

In the same way ,the three-, four-, etc. n-dimensional integration region is divided by the corresponding parts.
In this approach, the formula (6) takes the form

$$J_1 = \int_a^b f(x)dx = \frac{h}{2}\sum_{i=0}^{n-1}(y_i + y_{i+1}) = \frac{h}{2}\sum_{i=0}^{n-1}(f_i + f_{i+1}) = \frac{h}{2}\sum_{i=1}^{n}(f_{i-1} + f_i) = \tag{17}$$
$$= \frac{f_0 + f_n}{2} + \sum_{i=0}^{n-1} f_i.$$

The general trapezoid formula for double integrals calculating has the form

$$J_2 = \frac{h_x h_y}{4}\sum_{i=0}^{n-1}\sum_{j=0}^{m-1}\left[f_{i,j} + f_{i,j+1} + f_{i+1,j} + f_{i+1,j+1}\right] = \tag{18}$$
$$= \frac{h_x h_y}{4}\sum_{i=0}^{n-1}\sum_{j=0}^{m-1}\sum_{i_1=0}^{1}\sum_{i_2=0}^{1} f_{i+i_1 j+i_2}.$$

The following is a general formula for the trapezoidal three-and four-fold integrals calculating

$$J_3 = \int_a^A\int_b^B\int_c^C f(x,y,z)dxdydz = \frac{h_x h_y h_z}{8}\sum_{i=0}^{n-1}\sum_{j=0}^{m-1}\sum_{k=0}^{p-1}\left[f_{i,j,k} + f_{i,j,k+1} + f_{i,j+1,k} + \right. \tag{19}$$
$$\left. + f_{i,j+1,k+1} + f_{i+1,j,k} + f_{i+1,j,k+1} + f_{i+1,j+1,k} + f_{i+1,j+1,k} + f_{i+1,j+1,k+1}\right] =$$
$$= \frac{h_x h_y h_z}{8}\sum_{i=0}^{n-1}\sum_{j=0}^{m-1}\sum_{k=0}^{p-1}\sum_{i_1=0}^{1}\sum_{i_2=0}^{1}\sum_{i_3=0}^{1} f_{i+i_1,j+i_2,k+i_3},$$

$$J_4 = \int_a^A\int_b^B\int_c^C\int_d^D f(x,y,z,u)dxdydzdu = \frac{h_x h_y h_z h_u}{16}\left[f_{i,j,k,l} + f_{i,j,k,l+1} + f_{i,j,k+1,l} + \right.$$
$$+ f_{i,j,k+1,l+1} + f_{i,j+1,k,l} + f_{i,j+1,k,l+1} + f_{i,j+1,k+1,l} + f_{i,j+1,k+1,l+1} + f_{i+1,j,k,l} + f_{i+1,j,k,l} + \tag{20}$$
$$\left. + f_{i+1,j,k+1,l} + f_{i+1,j,k+1,l+1} + f_{i+1,j+1,k,l} + f_{i+1,j+1,k,l+1} + f_{i+1,j+1,k+1,l} + + f_{i+1,j+1,k+1,l+1}\right] =$$
$$= \frac{h_x h_y h_z h_u}{16}\sum_{i=0}^{n-1}\sum_{j=0}^{m-1}\sum_{k=0}^{p-1}\sum_{l=0}^{t-1}\sum_{i_1=0}^{1}\sum_{i_2=0}^{1}\sum_{i_3=0}^{1}\sum_{i_4=0}^{1} f_{i+i_1,j+i_2,k+i_3,l+i_4}.$$

Based on the above formula, the approximate calculation of n-fold integral, using the formula (D), takes the form

$$J_n = \frac{1}{2^n}\prod_{i=1}^{n}(A_i - a_i)\sum_{p_1=0}^{n_1-1}\sum_{p_2=0}^{n_2-1}\sum_{p_3=0}^{n_3-1}\ldots\sum_{p_n=0}^{n_n-1}\sum_{i_1=0}^{1}\sum_{i_2=0}^{1}\ldots\sum_{i_n=0}^{1} f_{p_1+i_1,p_2+i_2,\ldots,p_n+i_n}. \tag{21}$$

Thus the theorem is completely proved.

Theorem 2. Approximation formulas for determining the values of the double integral, obtained by the repeated use of the trapezoid quadrature formula is calculated as follows:

$$\iint_{(D)} f(x,y)dxdy = \frac{h_x h_y}{4}\sum_{i=1}^{n}\sum_{j=1}^{m}\lambda_{ij} f_{ij}, \tag{22}$$

where

$$\lambda_{ij} = \begin{bmatrix} 1_* & 2 & 4 & \ldots & 2 & 1 \\ 2 & 4 & 4 & \ldots & 4 & 2 \\ 2 & 4 & 4 & \ldots & 4 & 2 \\ \ldots & \ldots & \ldots & \ldots & \ldots & \ldots \\ 2 & 4 & 4 & \ldots & 4 & 2 \\ 1 & 2 & 2 & \ldots & 2 & 1 \end{bmatrix}. \tag{23}$$

Proof. Let's use the formula (12). Revealing this amount and similar terms, we obtain the following formula:

$$\frac{h_x h_y}{4}\sum_{i=0}^{n-1}\sum_{j=0}^{m-1}\left[f_{ij} + f_{ij+1} + f_{i+1,j} + f_{i+1,j+1}\right] =$$
$$= \frac{h_x h_y}{4}\left[f_{11} + 2f_{12} + 2f_{13} + \ldots + 2f_{1n-1} + f_{1,n}\right. \tag{24}$$
$$2f_{21} + 4f_{22} + 4f_{23} + \ldots + 4f_{2,n-1} + 4f_{2,n}$$
$$\ldots\ldots\ldots\ldots\ldots\ldots\ldots\ldots\ldots\ldots\ldots\ldots\ldots\ldots\ldots\ldots$$
$$4f_{n-1,1} + 4f_{n-1,2} + 4f_{n-1,3} + \ldots + 4f_{n-1,n-1} + 4f_{n-1,n}.$$
$$\left. f_{n,1} + 2f_{n,2} + f_{n,3} + \ldots + 2f_{n,n-1} + f_{n,n}\right]$$

The (17) can form the matrix elements - λ_{ij} in the form (16) and the result (15), indicating the proof of the theorem.

Theorem 3. Approximate formula for calculating the value of triple integrals, obtained by the repeated use of the trapezoid quadrature formula, is calculated as follows:

$$\iiint\limits_{(D)} f(x,y,z)dxdydz = \frac{h_x h_y h_z}{8} \sum_{i=1}^{n} \sum_{j=1}^{m} \sum_{k=1}^{S} \lambda_{ijk} f_{ijk} , \qquad (25)$$

where

$$\lambda_{ijk} = \begin{pmatrix} 1 & 2 & 2 & 2 & \dots & 2 & 1 \\ 2 & 4 & 4 & 4 & \dots & 4 & 2 \\ 2 & 4 & 4 & 4 & \dots & 4 & 2 \\ \dots & & & & & & \\ 2 & 4 & 4 & 4 & \dots & 4 & 2 \\ 1 & 2 & 2 & 2 & \dots & 2 & 1 \end{pmatrix}, \qquad i = 1; n,$$

$$\lambda_{ijk} = \begin{pmatrix} 2 & 4 & 4 & \dots & 4 & 4 & 2 \\ 4 & 8 & 8 & \dots & 8 & 4 & 2 \\ \dots & & & & & & \\ 4 & 8 & 8 & \dots & 8 & 4 & 2 \\ 2 & 4 & 4 & \dots & 4 & 4 & 2 \end{pmatrix}, \qquad i = \overline{2, n-1}. \qquad (26)$$

Proof. Let's use (13). Revealing this amount and similar terms, we obtain

$$\begin{array}{l}
f_{1,1,1} + 2f_{1,1,2} + 2f_{1,1,3} + 2f_{1,1,4} + \dots + 2f_{1,1,n-1} + f_{1,1,n} \\
2f_{1,2,1} + 4f_{1,2,2} + 4f_{1,2,3} + 4f_{1,2,4} + \dots + 4f_{1,1,n-1} + 2f_{1,2,n} \\
\dots \\
2f_{1,n-1,1} + 4f_{1,n-1,2} + 4f_{1,n-1,3} + 4f_{1,n-1,4} + \dots + 4f_{1,n-1,n-1} + 2f_{1,n-1,n} \\
f_{1,n,1} + 2f_{1,n,2} + 2f_{1,n,3} + 2f_{1,n,4} + \dots + 2f_{1,n,n-1} + f_{1,n,n} \\
2f_{2,1,1} + 4f_{2,1,2} + 4f_{2,1,3} + 4f_{2,1,4} + \dots + 4f_{2,1,n-1} + 2f_{2,1,n} \\
4f_{2,2,1} + 8f_{2,2,2} + 8f_{2,2,3} + 8f_{2,2,4} + \dots + 8f_{2,2,n-1} + 4f_{2,2,n} \\
\dots \\
4f_{2,10^{-1},1} + 8f_{2,10^{n-1},2} + 8f_{2,10,3} + 8f_{2,10^{n-1},4} + \dots + 8f_{2,10^{n-1},n-1} + 4f_{2,10^{n-1},n} \\
2f_{2,11,1} + 4f_{2,11,2} + 4f_{2,11,3} + 4f_{2,11,4} + \dots + 4f_{2,11,n-1} + 2f_{2,11,n} \\
\dots \\
2f_{n-1,1,1} + 4f_{n-1,1,2} + 4f_{n-1,1,3} + 4f_{n-1,1,4} + \dots + 4f_{n-1,1,n-1} + 2f_{n-1,1,n} \\
4f_{n-1,2,1} + 8f_{n-1,2,2} + 8f_{n-1,2,3} + 8f_{n-1,2,4} + \dots + 8f_{n-1,2,n-1} + 4f_{n-1,2,n} \\
\dots \\
4f_{n-1,n-1,1} + 8f_{n-1,n-1,2} + 8f_{n-1,n-1,3} + 8f_{n-1,n-1,4} + \dots + 8f_{n-1,n-1,n-1} + 4f_{n-1,n-1,n} \\
2f_{nn,n,1} + 4f_{n-1,n,2} + 4f_{n-1,n,n} + 4f_{n-1,n,n} + \dots + 4f_{n-1,n,n-1} + 2f_{n-1,n,n} \\
f_{n,1,1} + 2f_{n,1,2} + 2f_{n,1,3} + 2f_{n,1,4} + \dots + 2f_{n,1,n-1} + f_{n,1,n} \\
2f_{n,2,1} + 4f_{n,2,2} + 4f_{n,2,3} + 4f_{n,2,4} + \dots + 4f_{n,2,n-1} + 2f_{n,2,n} \\
\dots \\
2f_{n,n-1,1} + 4f_{n,n-1,2} + 4f_{n,n-1,3} + 4f_{n,n-1,4} + \dots + 4f_{n,n-1,n-1} + \dots + 2f_{n,n-1,n} \\
f_{n,n,1} + 2f_{n,n,2} + 2f_{n,n,3} + 2f_{n,n,4} + \dots + 4f_{n,n,n-1} + f_{n,n,n} .
\end{array} \qquad (27)$$

From (19) we form the λ_{ijk} elements, resulting in the relation (18), which shows the proof of the theorem.

Theorem 4. Approximation formulas for the values determining of the quadruple integrals, obtained by the repeated use of the trapezoid quadrature formula, is calculated as follows:

$$\iiint\limits_{(D)}\int f(x,y,z,u)dxdydzdu = \frac{h_x h_y h_z h_u}{16} \sum_{i=0}^{n-1} \sum_{j=0}^{m-1} \sum_{k=0}^{l-1} \sum_{l=0}^{s-1} \lambda_{ijkl} f_{ijkl} , \qquad (28)$$

$$\Lambda\begin{bmatrix} A_{11} & A_{12} & \dots & A_{1,n-1} & A_{1n} \\ A_{21} & A_{22} & \dots & A_{2,n-1} & A_{2n} \\ . & . & \dots & . & . \\ A_{n-1,1} & A_{n-1,2} & \dots & A_{n-1,n-1} & A_{n-1,n} \\ A_{n,1} & A_{n,2} & \dots & A_{n,n-1} & A_{nn} \end{bmatrix},$$

$$A_{n1}=A_{nn}=A_{1n}=\begin{bmatrix} 1 & 2 & 2 & 2 & \dots & 2 & 1 \\ 2 & 4 & 4 & 4 & \dots & 4 & 2 \\ . & . & . & . & \dots & . & . \\ 2 & 4 & 4 & 4 & \dots & 4 & 2 \\ 1 & 2 & 2 & 2 & \dots & 2 & 1 \end{bmatrix},$$

$$A_{n,j}=A_{1,j}\begin{bmatrix} 2 & 4 & 4 & \dots & 4 & 2 \\ 4 & 8 & 8 & \dots & 8 & 4 \\ . & . & . & . & \dots & . \\ 4 & 8 & 8 & \dots & 8 & 4 \\ 2 & 4 & 4 & \dots & 4 & 1 \end{bmatrix}, \quad j=\overline{1,n}-1'$$

$$A_{i1}=A_{in}=\begin{bmatrix} 2 & 4 & \dots & 4 & 2 \\ 4 & 8 & \dots & 8 & 4 \\ . & . & \dots & . & . \\ 4 & 8 & \dots & 8 & 4 \\ 2 & 4 & \dots & 4 & 2 \end{bmatrix}, \quad i=\overline{2,n-1}, \quad A_{ij}=\begin{bmatrix} 4 & 8 & \dots & 8 & 4 \\ 8 & 16 & \dots & 16 & 8 \\ . & . & \dots & . & . \\ 8 & 16 & \dots & 16 & 8 \\ 4 & 8 & \dots & 8 & 4 \end{bmatrix}, \quad \begin{matrix} i=2,3,\dots,n-1, \\ j=2,3,\dots,n-1 \end{matrix}$$

Proof. Disclose the amount (14) and obtain the following relations:

$$f_{1111}+2f_{1112}+2f_{1113}+2f_{1114}+\dots+2f_{111n-1}+f_{111,n}$$
$$2f_{1121}+4f_{1122}+4f_{1123}+4f_{1124}+\dots+4f_{112,n-1}+2f_{112,n}$$
$$2f_{1131}+4f_{1132}+4f_{1133}+4f_{1134}+\dots+4f_{113,n-1}+2f_{113,n}$$

....

$$2f_{11,n-1,1}+4f_{11,n-1,2}+4f_{11,n-1,3}+4f_{11,n-1,4}+\dots+4f_{11,n-1,n-1}+2f_{11,n-1,n}$$
$$f_{11n1}+2f_{11n2}+2f_{11n3}+2f_{11n4}+\dots+2f_{11n,n-1}+f_{111,n}$$
$$2f_{1211}+4f_{1212}+4f_{1213}+4f_{1214}+\dots+4f_{121,n-1}+2f_{121,n}$$
$$4f_{1221}+8f_{1222}+8f_{1223}+8f_{1224}+\dots+8f_{122,n-1}+4f_{122,n}$$
$$4f_{1231}+8f_{1232}+8f_{1233}+8f_{1234}+\dots+8f_{123,n-1}+4f_{123,n}$$

....

$$4f_{12n-1,1}+8f_{12n-1,2}+8f_{12n-1,3}+8f_{12n-1,4}+\dots+8f_{12n-1,n-1}+4f_{12n-1,n}$$
$$2f_{12n1}+4f_{12n2}+4f_{12n3}+4f_{12n4}+\dots+4f_{12n,n-1}+2f_{12n,n}$$

....

$$f_{1n11}+2f_{1n12}+\dots+2f_{1n-1,n-1}+f_{1n,n}$$
$$2f_{1n21}+4f_{1n22}+\dots+4f_{1n-1,2n-1}+2f_{1n,2n}$$

....

$$2f_{1n,n-1,1}+4f_{1nn-1,2}+\dots+4f_{1n,n-1,n-1}+2f_{1nn-1,n}$$
$$f_{1nn1}+2f_{1nn2}+\dots+2f_{1nnn-1}+f_{1nn,n}$$

$$f_{2111}+4f_{2112}+4f_{2113}+\dots+4f_{211,n-1}+2f_{211,n}$$
$$4f_{2121}+8f_{2122}+8f_{2123}+\dots+8f_{212,n-1}+4f_{212,n}$$

....

$$4f_{21n-1,1}+8f_{21n-1,2}+8f_{21n-1,3}+\dots+8f_{21n-1,n-1}+4f_{21n-1,n}$$
$$2f_{21n1}+4f_{21n2}+4f_{21n3}+\dots+4f_{21n,n-1}+2f_{21n,n}$$

$$4f_{2211}+8f_{2212}+8f_{2213}+...+8f_{221,n-1}+4f_{221,n}$$
$$8f_{2221}+16f_{2222}+16f_{2223}+...+16f_{222,n-1}+8f_{222,n}$$
$$8f_{2231}+16f_{2232}+16f_{2233}+...+16f_{223,n-1}+8f_{223,n}$$
.....
$$8f_{22n-1,1}+16f_{22n-1,2}+16f_{22n-1,3}+...+16f_{22n-1,n-1}+8f_{22n-1,n}$$
$$4f_{22n1}+8f_{22n2}+8f_{22n3}+...+8f_{22n,n-1}+4f_{22n,n}$$
.....

$$4f_{n-1,n11}+8f_{n-1,n12}+8f_{n-1,n13}+...+8f_{n-1,n,1,n-1}+4f_{n-1,n,1,n}$$
$$8f_{n-1,n21}+16f_{n-1,n22}+16f_{n-1,n23}+...+16f_{n-1,n,2,n-1}+8f_{n-1,n,2,n}$$
.....

$$2f_{n,n-1,11}+4f_{n,n-1,12}+4f_{n,n-1,13}+...+4f_{n,n-1,1,n-1}+2f_{n,n-1,1,n}$$
$$4f_{n,n-1,21}+8f_{n,n-1,22}+8f_{n,n-1,23}+...+8f_{n,n-1,2,n-1}+4f_{n,n-1,2,n}$$
.....
$$4f_{n,n-1,n-1,1}+8f_{n,n-1,n-1,2}+8f_{n,n-1,n-1,3}+...+8f_{n,n-1,n-1,n-1}+4f_{n,n-1,n-1,n}$$
$$2f_{n,n-1,n,1}+4f_{n,n-1,n,2}+4f_{n,n-1,n,3}+...+4f_{n,n-1,n,n-1}+2f_{n,n-1,n,n}$$

$$8f_{n-1,n,n-1,1}+16f_{n-1,n,n-1,2}+16f_{n-1,n,n-1,3}+...+16f_{n-1,n,n-1,n-1}+8f_{n-1,n,n-1,n}$$
$$4f_{n-1,n,n,1}+8f_{n-1,n,n,2}+8f_{n-1,n,n,3}+...+8f_{n-1,n,n,n-1}+8f_{n-1,n,n,n}$$

$$f_{nn11}+2f_{nn12}+2f_{nn13}+...+2f_{nn1,n-1}+f_{nn1n}$$
$$2f_{nn21}+4f_{nn22}+4f_{nn23}+...+4f_{nn2,n-1}+4f_{nn2,n}$$
.....
$$2f_{nnn-1,1}+4f_{nnn-1,2}+4f_{nnn-1,3}+...+4f_{nn,n-1,n-1}+4f_{nn,n-1,n}$$
$$f_{nnn1}+2f_{nnn2}+2f_{nnn3}+...+2f_{nnnn-1}+f_{nnn,n}$$

From these relations the formula (20) is formed, which fully demonstrates the proof of the theorem.

Now, we calculate the values of integrals by repeated application of quadrature formulas, based on the formula of rectangles.

The rectangle formula to calculate the values of the integrals is quite simple. In fact, here ξ_i is taken as $[x_{i-1}, x_i]$ midpoints. For a uniform grid $(h_i = h, \quad i = \overline{1,n})$ we obtained formulas of the form

$$J_1 = \int_a^b f(x)dx \approx \frac{b-a}{n}\sum_{i=1}^{n} f_{i-1/2}\,, \qquad (29)$$

where $f_{i-1/2} = f(x_i - \frac{h}{2}), \quad x_0 = a, \quad x_n = b$.

Double integral in this case is calculated by the formula

$$J_2 \equiv \int_a^A\int_b^B f(x,y)dxdy = \int_a^A dx\int_b^B f(x,y)dy =$$
$$= \int_a^A\left[\frac{B-b}{n_2}\sum_{j=1}^{n_2} f\left(x, y_{j-1/2}\right)\right]dx = \frac{A-a}{n_1}\frac{B-b}{n_2}\sum_{i=1}^{n_1}\sum_{j=1}^{n_2} f\left(x_{i-1/2}, y_{j-1/2}\right) = \qquad (30)$$
$$= \frac{A-a}{n_1}\frac{B-b}{n_2}\sum_{i=1}^{n_1}\sum_{j=1}^{n_2} f_{i-1/2,\,j-1/2},$$

where $f_{i-1/2,\,j-1/2} = f\left(x_i - \frac{h_x}{n}y_j - \frac{h_y}{2}\right), \qquad n_1 = \frac{A-a}{h_x}, \quad n_2 = \frac{B-b}{h_y};$

h_x - Step on the OX axis, h_y y - a step on the OY axis.

In the same way we define cubature formulas for calculating the values of the three-and four-fold integrals

$$J_3 = \int_a^A \int_b^B \int_c^C f(x,y,z)dxdydz \approx \frac{A-a}{n_1}\frac{B-b}{n_2}\frac{C-c}{n_3}\sum_{i=1}^{n_1}\sum_{j=1}^{n_2}\sum_{k=1}^{n_3} f_{i-1/2,j-1/2,k-1/2}, \quad (31)$$

Where $$f_{i-1/2,j-1/2,k-1/2} = f\left(x_i - \frac{h_x}{2}, y_j - \frac{h_y}{2}, z_k - \frac{h_z}{2}\right),$$

$$J_4 \equiv \int_a^A \int_b^B \int_c^C \int_d^D f(x,y,z,u)dxdydzdu \approx \frac{A-a}{n_1}\frac{B-b}{n_2}\frac{C-c}{n_3}\frac{D-d}{n_4}\sum_{i=1}^{n_1}\sum_{j=1}^{n_2}\sum_{k=1}^{n_3}\sum_{l=1}^{n_4} f_{i-1/2,j-1/2,k-1/2,l-1/2}; \quad (32)$$

Here $$f_{i-1/2,j-1/2,k-1/2,l-1/2} = f\left(x_i - \frac{h_x}{2}, y_j - \frac{h_y}{2}, z_k - \frac{h_z}{2}, u_l - \frac{h_u}{2}\right).$$

On the basis of approximate formulas for calculating the values of one-, two-, three-and four-fold integrals, respectively, expressed by (21) - (24), the formula for calculating the values of n-fold integrals is given .

Theorem 5. Let the $y = f(x_1, x_2, ..., x_n)$ function is defined and continuous in a n-dimensional bounded Ω_n integration domain. Then the cubature formula, obtained by repeated application of the rectangles' formula, has the form

$$\int\int\int\ldots\int_D f(x_1, x_2, ..., x_n)dx_1dx_2...dx_n = \prod_{i=1}^{n}\frac{A_i - a_i}{n_i}\sum_{i_1=1}^{n_1}\sum_{i_2=1}^{n_2}\ldots\sum_{i_n=1}^{n_n} f_{i_1-1/2,i_2-1/2,...i_n-1/2}, \quad (33)$$

where $$x_i \in [a_i, A_i], \quad i = \overline{1,n},$$

$$f_{i_1-1/2,i_2-1/2,...i_n-1/2} = f\left(x_{i_1} - \frac{h_1}{2}, x_{i_2} - \frac{h_2}{2}, ..., x_{i_n} - \frac{h_n}{2}\right).$$

Proof. The proof is given by induction.

From (21) - (24) we see that (25) holds for $n = 1;2;3;4$. We assume that (25) is valid for $n = k$:

$$\int\int\ldots\int_D f(x_1, x_2, ..., x_k)dx_1dx_2...dx_k = \prod_{i=1}^{k}\frac{A_i - a_i}{k_i}\sum_{i_1=1}^{k_1}\sum_{i_2=1}^{k_2}\ldots\sum_{i_k=1}^{k_k} f_{i_1-1/2,i_2-1/2,...i_k-1/2}.$$

Now we show fairness at $n = k+1$:

$$\int\int\underset{(D)}{\ldots}\int f(x_1, x_2, ..., x_k, x_{k+1})dx_1dx_2...dx_kdx_{k+1} \approx$$

$$\approx \int_a^A \prod_{i=1}^{k}\frac{A_i - a_i}{n_i}\sum_{i_1=1}^{n_1}\sum_{i_2=1}^{n_2}\ldots\sum_{i_k=1}^{n_k} f\left(x_{i_1} - \frac{h_1}{2}, x_{i_2} - \frac{h_2}{2}, ..., x_{i_k} - \frac{h_k}{2}, x_{k+1}\right)dx_{k+1} \approx$$

$$\approx \frac{A_{k+1} - a_{k+1}}{n_{k+1}}\prod_{i=1}^{k}\frac{A_i - a_i}{n_i}\sum_{i_1=1}^{n_1}\sum_{i_2=1}^{n_2}\ldots\sum_{i_k=1}^{n_k}\sum_{i_{k+1}=1}^{n_{k+1}} f\left(x_{i_1} - \frac{h_1}{2}, x_{i_2} - \frac{h_2}{2}, ..., x_{i_k} - \frac{h_k}{2}, x_{k+1} - \frac{h_{k+1}}{2}\right) =$$

$$= \prod_{i=1}^{k+1}\frac{A_i - a_i}{n_i}\sum_{i_1=1}^{n_1}\sum_{i_2=1}^{n_2}\ldots\sum_{i_k=1}^{n_k}\sum_{i_{k+1}=1}^{n_{k+1}} f_{i_1-1/2,i_2-1/2,...i_k-1/2,i_{k+1}-1/2}.$$

The obtained result proofs the theory completely.

III. CONCLUSIONS

Thus we have constructed the multi-dimensional cubature formulas to approximate the value of multiple integrals by repeated application of the quadrature formula of trapezoids and rectangles to determine the values of multiple integrals, which are easy to implement on a computer.

REFERENCES

[1]. Demidovich B.L, Maron I.A. "Foundations of Computational Mathematics". - Moscow: Nauka, 1960. - 664 p.
[2]. Rvachev V.L. "Theory of R-functions and some of its applications". - Naukova. Dumka, 1982. - 552 p.
[3]. Rvachev V.L. "An analytical description of some geometric objects". Dokl. Kiev, 1963. - 153, № 4. 765-767pp.
[4]. Nazirov S.A. "Constructive definition of algorithmic tools for solving three-dimensional problems of mathematical physics in the areas of complex configuration" / Iss. Comput. and glue. Mathematics. Tashkent .Scientific works set. IMIT Uzbek Academy of Sciences, 2009. - No. 121. - 15-44pp.
[5]. Kabulov V.K., Faizullaev A., Nazirov S.A. "Al-Khorazmiy algorithm, algorithmization". - Tashkent: FAN, 2006. -664 p.
[6]. Gmurman V.E. "Guide to solving problems in the theory of probability and mathematical statistics". Manual. book for students of technical colleges. - 3rd ed., Rev. and add. - M.: Higher. School, 1979.
[7]. Ermakov S.M. "Monte Carlo methods and related issues". - Moscow: Nauka, 1971.
[8]. Sevastyanov B.A. "The course in the theory of probability and mathematical statistics". - Moscow: Nauka, 1982.
[9]. Mathematics. Great Encyclopedic Dictionary/ Ch. Ed. V. Prokhorov. - Moscow: Great Russian Encyclopedia, 1999.
[10]. Gmurman E. "Probability theory and mathematical statistics." Textbook for technical colleges. 5th ed., revised. and add. - M., Higher. School, 1977.

International Journal of Modern Engineering Research (IJMER)
www.ijmer.com Vol. 3, Issue. 4, Jul - Aug. 2013 pp-2035-2041 ISSN: 2249-6645

Online Bus Arrival Time Prediction Using Hybrid Neural Network and Kalman filter Techniques

M. Zaki[1], I. Ashour[2], M. Zorkany[2], B. Hesham[2]
*(Computer Department, Al Azhar University, Egypt)
*(Electronic Department, National Telecommunication Institute, Egypt)

ABSTRACT : *The ability to obtain accurate predictions of bus arrival time on a real time basis is vital to both bus operations control and passenger information systems. Several studies have been devoted to this arrival time prediction problem in many countries; however, few resulted in completely satisfactory algorithms. This paper presents an effective method that can be used to predict the expected bus arrival time at individual bus stops along a service route. This method is a hybrid scheme that combines a neural network (NN) that infers decision rules from historical data with Kalman filter (KF) that fuses prediction calculations with current GPS measurements. The proposed algorithm relies on real-time location data and takes into account historical travel times as well as temporal and spatial variations of traffic conditions. A case study on a real bus route is conducted to evaluate the performance of the proposed algorithm in terms of prediction accuracy. The results indicate that the system is capable of achieving satisfactory performance and accuracy in predicting bus arrival times for Egyptian environments.*

Keywords: *Intelligent transportation system, Neural network, Kalman filter, Arrival time prediction About five*

I. INTRODUCTION

Traffic plays an important role in modern urban society. Because of the limitation of the traffic resources, those increments will lead to urban traffic congestion. In order to relieve the congestion, the governments all around the world provide funding and support to develop public traffic systems and build traffic applications, such as subway system, signal control systems, traffic information management system, electronic toll collection systems, etc. which fall under intelligent transportation system.

This paper concern is the part of research project called Transportation Management and User Awareness (TMUA) that research project is financially supported by NTRA to interconnect public transportation vehicles and bus stations with a central office to monitor the underlying vehicles. Based on the collected data and by analyzing road condition, accurate arrival times could be computed and transmitted to all relevant stations. Waiting time for the next bus(s) to arrive will be announced on screens and via audio speakers (in Arabic) to commuters on the bus station. Passengers in buses will be notified of the next bus stop using visual and audio announcements. Achieving these main features will cause major improvement in public transport convenience and safety.

It will also allow the central offices to manage effectively their resources (mainly busses) through better route planning in relation to peak hours and congested zones. In the proposed system, virtually all data that are collected and stored are multi-dimensional. Typically, ranges of features are measured at a particular time or condition and stored as a complex data object. The data come in the form of a vector of real values. Different approaches use the spread of the data to suggest a new basis by choosing the directions that maximize the variance of the observations. If there are significant correlations between the different features, the number of features required to capture the data will be decreased.

Arrival-time calculation depends on vehicle speed, traffic flow and occupancy, which are highly sensitive to weather conditions and traffic incidents. These features make travel-time predictions very complex and difficult to reach optimal accuracy. Nonetheless, daily, weekly and seasonal patterns can still be observed at a large scale. For instance, daily patterns distinguish rush hour and late night traffic, weekly patterns distinguish weekday and weekend traffic, while seasonal patterns distinguish winter and summer traffic. The time-varying feature germane to traffic behavior is the key to travel-time modeling.

This research will assess what traffic, transit and freight data are available today from various sources, and consider how to integrate data from busses acting as "probes" in the system. Some obvious information is obtained easily though traditional query operation from traffic database, but deeper information that hides in the traffic database is difficult to be discovered. Deep level information usually contains characteristics of data and forecast information of data development tendency.

Therefore, we are concerned with how to develop a powerful data-mining algorithm and apply it on the available data. In addition, a model-based predictor based on implementing a Kalman filter could be employed when the data-mining algorithm might be failed. In this paper, we propose hybrid Neural Network and Kalman filter Techniques to predict the bus arrival time. This paper is organized as follows. literature review presented in Section 2. Bus arrival time prediction methods are illustrated in Section 3. The proposed scheme for time prediction is presented in Section 4. Simulation results and discussions are given in Section 5 and finally conclusions are drawn in Section 6.

II. LITERATURE REVIEWS

In this section, some relative previous works related with bus travel time prediction are summarized. The main idea of the time prediction is based on the fact that traffic behaviors possess both partially deterministic and partially chaotic properties. Forecasting results can be obtained by reconstructing the deterministic traffic motion and predicting the random behaviors caused by unanticipated factors. Suppose that currently it is time t. Given the historical data f(t-1), f(t-2),…, and f(t-n) at time t-1, t-2,…, t-n, we can predict the future value of f(t+1), f(t+2), … by analyzing historical data set. Hence, future values can be forecasted based on the correlation between the time-variant historical data set and its outcomes. The bus arrival time prediction models can be classified into the following three main items: mathematical algorithms (Historical Approach, Real-Time Approach and Statistical Models), Kalman Filter model with historical data, and Artificial Neural Network(ANN) model which will discussed in the next section.

In 1999, Lin and Zeng developed a mathematical algorithm to provide real-time bus arrival information [1]. They considered schedule information, bus location data, the difference between scheduled and actual arrival time, and waiting time at time-check stops in their algorithm. Their algorithm could not consider traffic congestion and dwell time at bus stops. At the same year, Ojili developed a bus arrival time notification system in College Station [2]. The model breaks the bus route into one-minute time zones. The bus arrival time at a given stop was predicted by counting the estimated number of the one-minute time zones between current location and the given stop. The model had the same issues as Lin and Zeng's. Also, it does not consider the traffic congestion and dwell time at bus stops.

Wall and Dailey are the first authors who use Kalman Filter model to predict bus arrival time [3]. In their algorithm, they used a combination of both global position system(GPS) data and historical data, they used a Kalman filter model to track a vehicle location and used a statistical estimation technique to predict travel time. It was found that they could predict bus arrival time with less than 12% error. However, they did not explicitly deal with dwell time as an independent variable. In 2003, Shalaby and Farhan proposed another bus travel time prediction model by using Kalman filtering technique [4].
In the model, they considered the passenger information at each bus stop. However they predicted dwell time only at time check points, not at every bus stop. Due to the capability to solve complex non-linear relationships, artificial neural network model (ANN) had been used to model the transportation problems. The models had shown better results than those of existing. In 2002, Chien et al developed an artificial neural network model to predict dynamic bus arrival time in New Jersey. Considering the back-propagation algorithm is unsuitable for on-line application, the authors developed an adjustment factor to modify their travel time prediction by using recent observed real-time data. However the dwell time and scheduled data were not considered in their model [5].

In 2004, Jeong and Rilett provided a historical data based model, regression models and Artificial Neural Network (ANN) models to predict bus travel time by considering traffic congestion, schedule adherence and dwell times at stops [6]. In 2006, Ramakrishna et al proposed a multiple linear regression and an ANN model to predict bus travel times. In their model they considered real time GPS data of bus locations [7].

In 2009, Suwardo et al. proposed a statistical neural network model to predict the bus travel time in mixed traffic, while considering bus travel time, distance, average speed, number of bus stop, and traffic conditions. In their paper, they assessed those factors and studied the relationship mode between the factors and bus travel time [8].
In 2011, Feng Li et al. proposed a statistical model to predict the bus arrival time based on proposed linear [9]. In their paper, they had considered all of evaluated factors, such as departure time, driver characteristics, dwell time, intersections, traffic conditions etc.

Among the above models, artificial neural network model and statistical neural network model have shown advantage than other models, such as Kalman Filter model, historical average model, auto-regressive integrated moving average (ARIMA) model and exponential smoothing model. However the parameters for those models are hard to determine because it need more historical data and will cost us more time. Although the models can provide relative bus arrival prediction time, but it is hard for us to explain the mechanism for them. Because of those reasons, in this paper we will provide a Hybrid Kalman filter with Neural network approach to forecast bus arrival time.

III. Bus Arrival Time Prediction methods:

Bus arrival time prediction has been studied by many in recent years, different approaches where studied for time prediction such as:

Historical Approach: Predicts the travel time at a particular time as the average travel time for the same period over different days.

Real-Time Approach: Predicts the travel time at the next time interval to be the same as that in the present time interval, this approach assumes that the bus travel time trend fluctuate within a narrow range which is impossible for actual traffic trend, such as incidents, congestion and other unpredictable traffic conditions.

Statistical Models: Predict the bus arrival time based on a function formed by a set of independent variables.

Model-Based Approaches: The Kalman Filter algorithm outperformed all other developed models in terms of accuracy, demonstrating the dynamic ability to update itself based on new data that reflected the changing characteristics of the transit-operating environment. So that algorithm was used to update the state variable (travel time) continuously as new observations became available.

Machine Learning Techniques: Artificial neural network (ANN) is one of the most commonly reported techniques for traffic prediction mainly because of their ability to solve complex non-linear relationships [10]. Table 1 shows a comparison between different time prediction techniques and summarizes the approaches of estimating the bus travel time.

Table 1: Comparison between different time prediction techniques

Technique	Remarks	Delay considered
Historical approach	Predict the travel time at particular time as the average travel time for the same period historically	no
Real-time approach	Assume the future travel time to be the same as the present one	no
Time series analysis approach	Assume the historical patterns will remain same in the future	no
Statistical models	Predict the dependent variable based on a function formed by a set of independent variables	Yes,
Machine learning techniques	Prediction based on example data .Need large database for an accurate prediction	no
Model-based approaches (Kalman filter)	Establish relationships between the variables and then corroborates using field observation .Not site specific or data specific	yes

IV. The Proposed Prediction Time Method

In the proposed system, two models are suggested for bus arrival time prediction:
1- Machine Learning technique (ANN) for off line estimation using previously collected data from traffic database.
2- Model- based approach (Kalman filter) for online calculations in case of wide deviation between offline estimation and real time data (special cases). Figure 1 shows the preliminary flowchart of the proposed algorithm.
In what follows the basic steps of the underlying algorithm are explained:

V. Data Collection

In the proposed system, virtually all data that are collected and stored are multi-dimensional. Typically, a range of features is measured at a particular time or condition and stored as a complex data object. The data comes in the form of a vector of real values.

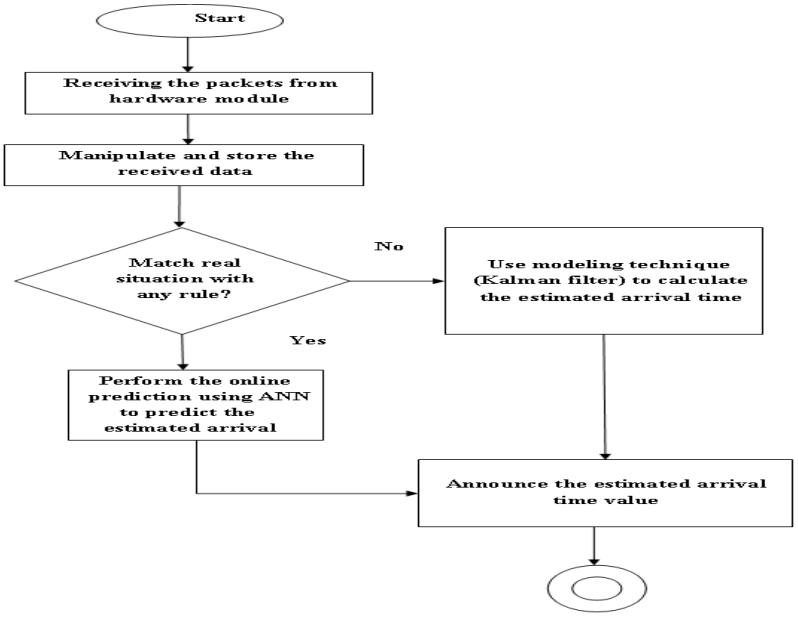

Figure 1: Flowchart of the proposed prediction time algorithm

VI. Proposed Neural Network

Neural networks are statistical models of real world systems, which are built by tuning a set of parameters. These parameters are seen as inputs to an associated set of values: the outputs. The process of tuning the weights to the correct values – training – is carried out by passing a set of examples of input-output pairs through the model and adjusting the weights in order to minimize the error between the answer the network gives and the desired output. Once the weights have been set, the model is able to produce answers for input values, which were not included in the training data [11, 12]. The used neural network, Figure 2, consist of four layers: input, two hidden, and output layer. The Input Layer of the proposed neural network has seven nodes. In this configuration, a double hidden layer is used. The first hidden layer has 10 nodes and the second hidden layer has 3 nodes while the output layer has only one node.

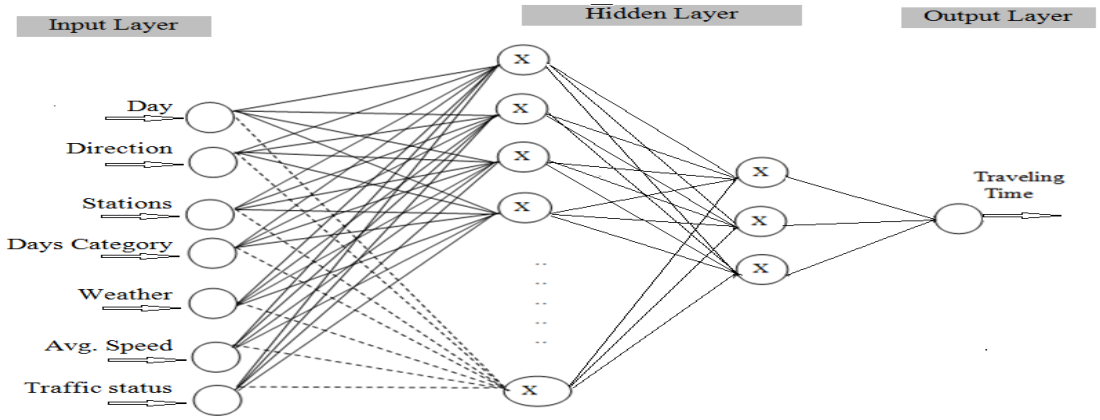

Figure 2: Proposed neural network structure

VII. PROPOSED KALMAN FILTER PREDICTOR

The Kalman filter, also known as linear quadratic estimation (LQE), is an algorithm which uses a series of measurements observed over time, containing noise (random variations) and other inaccuracies, and produces estimates of unknown variables that tend to be more precise than those that would be based on a single measurement alone. More formally, the Kalman filter operates recursively on streams of noisy input data to produce a statistically optimal estimate of the underlying state. The Kalman filter uses a system's dynamics model (e.g., physical laws of motion), known control inputs to that system, and multiple sequential measurements (such as from sensors) to form an estimate of the system's varying quantities (its state) that is better than the estimate obtained by using any one measurement alone.

The Kalman filter estimates a process by using a form of feedback control: the filter estimates the process state at some time and then obtains feedback in the form of (noisy) measurements. As such, the equations for the Kalman filter fall into two groups: time update equations and measurement update equations. The time update equations are responsible for projecting forward (in time) the current state and error covariance. Figure 3 illustrate Kalman filter operations.

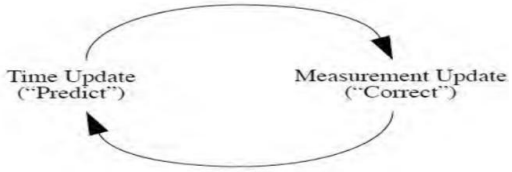

Figure 3: Proposed Kalman Filter structure

The modified Kalman Filter algorithm used in the current research project, the last three similar days in the last three weeks historical data of actual running times between links at the instant k+1 and the last running time observation at the instant (k) on the last day are used to predict the bus running time at the instant (k+1).

The Kalman Filter equations that are used for time prediction are:

$$g(k+1) = \frac{e(k) + VAR[local_{data}]}{e(k) + 2 \cdot VAR[local_{data}]}$$

$$a(k+1) = 1 - g(k+1)$$

$$e(k+1) = VAR[local_{data}] \cdot g(k+1)$$

$$P(k+1) = a(k+1) \cdot art(k) + g(k+1) \cdot art_1(k+1) \quad \text{----------(1)}$$

Where:

g = filter gain, a = loop gain, e = filter error, p = prediction,

art (k) = running time at the instant (k) on the last day at instant (k)

art1 (k+1) = actual running time of the similar day at instant (k+1)

VAR [local data] = prediction variance, and

VAR [local data] = last three similar days in the last three weeks "art3 (k+1), art2 (k+1) and art1 (k+1)" variance.

$$VAR[local_{data}] = VAR[art_1(k+1), art_2(k+1), art_3(k+1)] \quad \text{----------(2)}$$

The variance VAR [local data] is calculated at each instant k + 1 using the actual running time values for last three similar days in the last three weeks: art1 (k + 1), art2 (k + 1) and art3 (k + 1).

Where:

art1 (k+1): actual running time of the bus at instant (k+1) at the similar day on the previous week.

art2 (k+1): actual running time of the bus at instant (k+1) at the similar on two weeks ago.
art3 (k+1): actual running time of the bus at instant (k+1) at the similar on three weeks ago.
The definition of the variance for a random variable is:

$$VAR[X] = E[(X - E[X])^2]$$

$$E(X) = Avg(art) = \frac{art_1(k+1) + art_2(k+1) + art_3(k+1)}{3}$$

----------(4)

Now the variance can be calculated as given in the following equations:

$$\Delta_1 = [art_1(k+1) - avg(art)]^2$$
$$\Delta_2 = [art_2(k+1) - avg(art)]^2$$
$$\Delta_1 = [art_3(k+1) - avg(art)]^2$$

----------(5)

$$VAR\ [local_{data}\ ] = \frac{\Delta_1 + \Delta_2 + \Delta_3}{3}$$

VIII. SIMULATION RESULT

To determine the prediction times of a moving bus to the downstream bus stations, the GPS readings of each equipped bus need to be projected onto the underlying transit network. In a digital transit network model, bus routes are represented by a sequence of line features as an approximation to their true geographical composition.
Such straight line approximations are usually not accurate enough for tracking purposes. To ensure representation accuracy. The end points of each link, also called nodes, are specified by their longitudes and latitudes. All links and nodes are numbered according to the sequence in which the bus passed, and then they are recorded into a file for later use.
The neural network is learned through the creation of a set of random data for one route consisting of 6 stations from S0 to S5. Table 2 shows the ranges that were used for creating the random data, where "Sn, n=0,1,2,…,5" refers to station number.

Table 2: The ranges used to create random data

Day		s0-s1	s1-s2	s2-s3	s3-s4	s4-s5
Sunday	M	5-->7	5-->7	8-->12	4-->6	3-->5
	A	7-->10	7-->10	15-->18	5-->8	4-->7
Monday	M	5-->7	5-->7	8-->12	4-->6	3-->5
	A	7-->10	7-->10	15-->18	5-->8	4-->7
Tuesday	M	7-->11	7-->11	10-->14	6-->8	5-->7
	A	9-->13	9-->13	17-->20	7-->10	6-->9
Wednesday	M	7-->11	7-->11	10-->14	6-->8	5-->7
	A	9-->13	9-->13	17-->20	7-->10	6-->9
Thursday	M	5-->7	5-->7	8-->12	4-->6	3-->5
	A	9-->14	9-->14	18-->21	8-->11	7-->10

The simulation was performed using Matlab, Figure 6 shows the result of the proposed route. The simulation results give acceptable mean square error in the range of 1.2 minute on the whole route (max. 37min) .

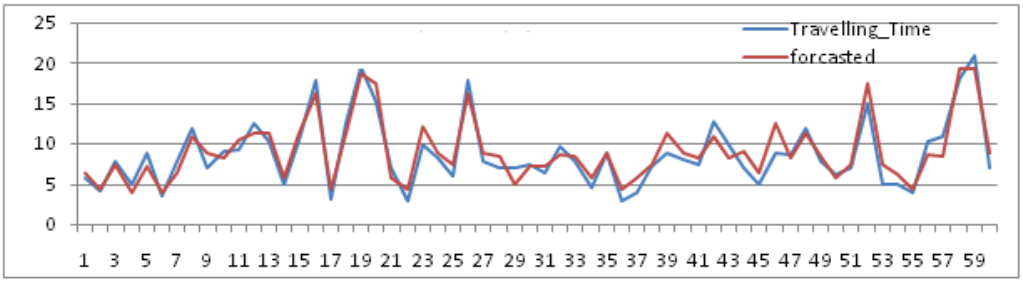

Figure 6: Neural network results

For Kalman filter testing, The example previously used to test the ANN is also applied to test the Kalman filter algorithm. Figure 7 shows the Kalman performance versus the actual running time. The simulation results give acceptable mean square error in the range of 1 minute on the whole route .

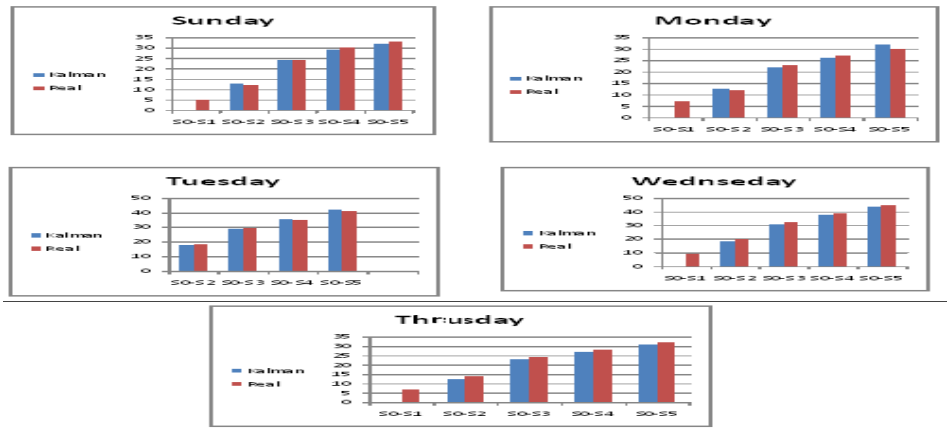

Figure 7 Kalman filter algorithm vs. real arrival time

The comparison between the actual, neural, and Kalman filter results are shown in figure 8.

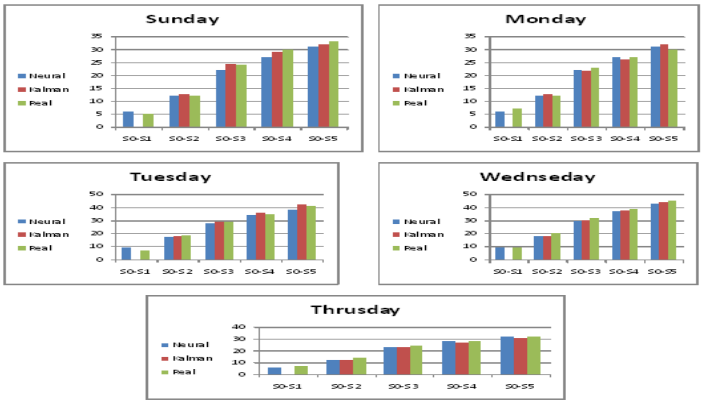

Figure 8 : Comparison between the actual, neural, and Kalman filter results

Figure 8 shows the predicted arrival times at individual bus stations for different time periods and days using neural and proposed Kalman filter techniques. As shown in the figure, there is a variation in prediction accuracy with respect to time period and stations due to the effect of traffic time along the route segment. In the test scenario the firmware switch between two different modes of operation to test the different arrival time calculation algorithms.

Normal mode operation: In this mode, the expected arrival time of station are selected within acceptable deviations from that calculated using ANN algorithm. The firmware loops among the bus stations using the estimated arrival time previously selected. The sever sends the estimated arrival time to the stations using the ANN calculated values.

Congestion mode: In this mode, the expected arrival time of station are selected with wide deviations from that calculated using ANN algorithm. The firmware loops among the bus stations using the estimated arrival time previously selected. In this case, the server will calculate the estimated arrival time using Kalman filter algorithm.

IX. CONCLUSIONS

In this paper, a model-based technique is proposed to predict the expected bus arrival times at individual bus stops along a service route. The proposed prediction algorithm combines real-time location data from GPS receivers which built in buses with average travel speeds of individual route segments, taking into account historical travel speed as well as temporal and spatial variations of traffic conditions. The proposed method is a hybrid scheme that combines the robustness of neural network with the reliability of Kalman filter. A case study on a real bus route is conducted to evaluate the performance of the proposed algorithm in terms of prediction accuracy. The results indicate that the proposed system is capable of achieving satisfactory accuracy in predicting bus arrival times.

REFERENCE

[1]. W. Lin and J. Zeng, "An Experimental Study on Real Time Bus Arrival Time Prediction with GPS Data", in 78th Annual Meeting of the Transportation Research Board, National Research Council, Washington D.C., January 1999.

[2]. S. R. OJ iii, "A Prototype of a Bus Arrival Time Notification System Using Automatic Vehicle Location Data", Master's thesis, Texas A&M University, College Station, June 1999.

[3]. Z. Wall and D. 1. Dailey, "An Algorithm for Predicting the Arrival Time of Mass Transit Vehicles Using Automatic Vehicle Location Data", in 78th Annual Meeting of the Transportation Research Board, National Research Council, Washington D.C., January 1999.

[4]. Shalaby and A. Farhan, "Bus Travel Time Prediction for Dynamic Operations Control and Passenger Information Systems", in 82nd Annual Meeting of the Transportation Research Board, National Research Council, Washington D.C., January 2003.

[5]. S.I.1. Chien, Y.Q. Ding and C.H. Wei, "Dynamic Bus Arrival Time Prediction with Artificial Neural Networks", Journal of Transportation Engineering, vo1.128, no.5, pp. 429-438, 2002.
[6]. R. Jeong and L. Rilett, "The Prediction of Bus Arrival Time using AVL Data", in 83rd Annual General MeetingofTransportation Research Board, National Research Council, Washington D.C., USA, 2004.
[7]. Y. Ramakrishna, P. Ramakrishna, V. Lakshmanan and R. Sivanandan, "Bus Travel Time Prediction Using GPS Data", in Proceedings Map India, 2006, http://www.gisdevelopment.net/proceedings/mapindia/2006/ studentorallmi06stu_84.htm.
[8]. S. Suwardo, M. Napiah, I. Kamaruddin and O. Wahyunggoro, "Bus travel time prediction in the mixed traffic by using statical neural network," in Workshop dan Simposium XII Forum Studi Transportasi antar Perguruan TInggi (FSTP T), Universitas Kristen Petra, November 13-14, 2009.
[9]. Feng Li, Yuan Yu, HongBin Lin and WanLi Min, " Public Bus Arrival Time Prediction Based on Traffic Information Management System", 978-1-4577-0574-8/111$26.00 ©2011 IEEE.
[10]. R.P.S. Padmanaban1 K. Divakar1 L. Vanajakshi1 S.C. Subramanian2, "Development of a real-time bus arrival prediction system for Indian traffic conditions," India, 2009.
[11]. Rocco Zito, Hong-En Lin, "a review of travel-time prediction in transport and logistices," Proceedings of the Eastern Asia Society for Transportation Studies, vol. 5, 2005.
[12]. B. Karlik and A. Vehbi, "Performance analysis of various activation functions in generalized mlp architectures of neural networks," International Journal of Artificial Intelligence and Expert Systems (IJAE), vol. 1, no. 4, p. 111, 2011.

International Journal of Modern Engineering Research (IJMER)
www.ijmer.com Vol. 3, Issue. 4, Jul - Aug. 2013 pp-2042-2047 ISSN: 2249-6645

Effect of rotation on the onset of Rayleigh-Bénard convection in a layer of Ferrofluid

Ramesh Chand[1], Ankuj Bala[2]
[1]Department of Mathematics, Government College Dhaliara, Himachal Pradesh, INDIA
[2]Department of Mathematics, Himachal Institute of Engineering and Technology, Shahpur, Himachal Pradesh, INDIA

ABSTRACT: *The effect of rotation on the Rayleigh-Bénard convection in a horizontal layer of ferrofluid is investigated by using Galerkin weighted residuals method. Linear stability theory based upon normal mode analysis and perturbation method is used to find expressions for Rayleigh number for free-free boundary layer of fluid. It is observed that the system is more stable in the rotating fluid than non-rotating fluid layer. 'Principle of exchange of stabilities' not valid and the oscillatory convection is possible only for certain conditions. The effect of rotation and magnetic parameters on the stationary convection is investigated analytically.*

KEY WORDS: *Ferro fluid, Convection, rotation, Galerkin method, Prandtl number.*

Nomenclature

a	wave number
B	magnetic induction
g	acceleration due to gravity
H	magnetic field Intensity
k	thermal conductivity
K_1	pyomagnetic coefficient
M	magnetization
M_1	buoyancy magnetization
M_3	magnetic parameter
N	magnetic thermal Rayleigh number
n	growth rate of disturbances
p	pressure (Pa)
P_r	Prandtl number
q	fluid velocity
R	Rayleigh number
t	time
T	temperature
Ta	average temperature
T_A	Taylor number
u, v, w	fluid velocity components
(X, y, z)	space co-ordinates

Greek symbols

α	thermal expansion coefficient
β	uniform temperature gradient
μ_o	magnetic permeability
μ	viscosity
ρ	density of the fluid
(ρ c)	heat capacity of fluid
κ	thermal diffusivity
Φ'	perturbed magnetic potential
ω	dimensional frequency
χ	magnetic susceptibility

Superscripts

'	non dimensional variables
' '	perturbed quantity

Subscripts

0	lower boundary
1	upper boundary
H	horizontal plane

I. INTRODUCTION

Ferromagnetic fluid has wide ranges of applications in instrumentation, lubrication, printing, vacuum technology, vibration damping, metals recovery, acoustics and medicine, its commercial usage includes vacuum feed through for semiconductor manufacturing in liquid-cooled loudspeakers and computer disk drives etc. Owing the applications of the ferrofluid its study is important to the researchers. A detailed account on the stability of ferrofluid has been given by Rosensweig (1985) in his monograph. This monograph reviews several applications of heat transfer through ferrofluid. One such phenomenon is enhanced convective cooling having a temperature-dependent magnetic moment due to magnetization of the fluid. This magnetization, in general, is a function of the magnetic field, temperature, salinity and density of the fluid.

In our analysis, we assume that the magnetization is aligned with the magnetic field. Convective instability of a ferromagnetic fluid for a fluid layer heated from below in the presence of uniform vertical magnetic field has been considered by Finlayson (1970). He explained the concept of thermo-mechanical interaction in ferromagnetic fluids.

Thermo convective stability of ferromagnetic fluids without considering buoyancy effects has been investigated by Lalas and Carmi (1971). Linear and nonlinear convective instability of a ferromagnetic fluid for a fluid layer heated from below under various assumptions is studied by many authors Shliomis (2002), Blennerhassett et.al.(1991), Gupta and Gupta (1979), Stiles and Kagan (1990), Sunil et.al. (2005, 2006), Sunil, Mahajan (2008), Venkatasubramanian and Kaloni (1994), Zebib (1996), Mahajan (2010). Rotation also play important role in the thermal instability of fluid layer and has applications in rotating machineries such as nuclear reactors, petroleum industry bio mechanics etc. Owing to the various applications of ferrofluid an attempt has been made to investigate the thermal instability of a ferromagnetic fluid in the presence of rotation in a fluid layer heated from below using Galerkin weighted residuals method.

II. MATHEMATICAL FORMULATION OF THE PROBLEM

Consider an infinite, horizontal layer of an electrically non-conducting incompressible ferromagnetic fluid of thickness 'd', bounded by plane z = 0 and z = d. Fluid layer is acted upon by gravity force **g** (0, 0, -g) and a uniform magnetic field $\mathbf{H} = \mathrm{H}_0^{\mathrm{ext}}\hat{\mathrm{k}}$ acts outside the fluid layer. The layer is heated from below such that a uniform temperature gradient $\beta\left(=\left|\frac{\mathrm{dT}}{\mathrm{dz}}\right|\right)$ is to be maintained. The temperature T at z = 0 taken to be T_0 and T_1 at z = d, ($T_0 > T_1$ as shown in Fig.1.

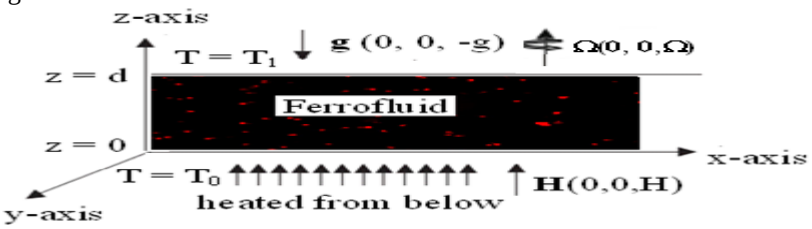

Fig.1 Geometrical configuration of the problem

The governing equations under Boussinesq approximation for the above model (Finlayson (1970), Resenweig (1997), and Mahajan (2010) are:

$$\nabla.\mathbf{q} = 0, \tag{1}$$

$$\rho_0 \frac{\mathrm{d}\mathbf{q}}{\mathrm{dt}} = -\nabla \mathrm{p} + \rho_0 \mathbf{g} + \mu\nabla^2\mathbf{q} + \mu_0(\mathbf{M}.\nabla)\mathbf{H} + 2\rho_0(\mathbf{q}\times\Omega), \tag{2}$$

$$(\rho_\circ C_0)_\mathrm{f} \frac{\mathrm{dT}}{\mathrm{dt}} + (\rho_\circ C_0)_\mathrm{f}\, \mathrm{q}.\nabla \mathrm{T} = \mathrm{k}\nabla^2\mathrm{T}, \tag{3}$$

Maxwell's equations, in magnetostatic limit:

$$\nabla.\mathbf{B} = 0,\ \nabla\times\mathbf{H} = 0,\quad \mathrm{B} = \mu_0(\mathbf{H}+\mathbf{M}). \tag{4}$$

The magnetization has the relationship

$$\mathbf{M} = \frac{\mathbf{H}}{\mathrm{H}}\left[\mathrm{M}_0 + \chi(\mathrm{H}-\mathrm{H}_0) - \mathrm{K}_1(\mathrm{T}-\mathrm{T}_\mathrm{a})\right]. \tag{5}$$

The density equation of state is taken as

$$\rho = \rho_\circ\left[1-\alpha(\mathrm{T}-\mathrm{T}_\mathrm{a})\right]. \tag{6}$$

Here ρ, ρ_0, **q**, t, p, μ, μ_0, **H**, **B**, C_0, T, M, K_1, and α are the fluid density, reference density, velocity, time, pressure, dynamic viscosity (constant), magnetic permeability, magnetic field, magnetic induction, specific heat at constant pressure, temperature, magnetization, thermal conductivity and thermal expansion coefficient, T_a is the average temperature given by,

$T_a = \left(\frac{T_0 + T_1}{2}\right)$ $H = |\mathbf{H}|, M = |\mathbf{M}|$ and $M_0 = M(H_0, T_a)$. The magnetic susceptibility and pyomagnetic coefficient are defined by $\chi = \left(\frac{\partial M}{\partial H}\right)_{H_\circ, T_a}$ and $K_1 = \left(\frac{\partial M}{\partial T}\right)_{H_\circ, T_a}$ respectively.

Since the fluid under consideration is confined between two horizontal planes z = 0 and z = d, on these two planes certain boundary conditions must be satisfied. We take case of free-free surface and assume the temperature and volumetric fraction of the nanoparticles are constant and the boundary conditions [Chandrasekhar (1961)] are

$$w = 0, \quad T = T_0 \quad \text{at} \quad z = 0, \text{ and } \quad w = 0, \quad T = T_1 \quad \text{at} \quad z = d. \tag{7}$$

II.1 Basic Solutions

The basic state is assumed to be a quiescent state and is given by

$$q(u,v,w) = q_b(u,v,w) = 0, \; p = p_b(z), \; T = T_b(z) = -\beta z + T_a, \; H_b = \left[H_\circ + \frac{K_1(T_b - T_a)}{1+\chi}\right]\hat{k},$$

$$M_b = \left[M_\circ - \frac{K_2(T_b - T_a)}{1+\chi}\right]\hat{k} \;\Big], \; H_\circ + M_\circ = H_\circ ext. \tag{8}$$

II.2 The Perturbation Equations

We shall analyze the stability of the basic state by introducing the following perturbations:

$$q = q_b + q', \; p = p_b(z) + \delta p, T = T_b(z) + \theta, \; H = H_b(z) + H' \; M = M_b(z) + M'. \tag{9}$$

where q′(u,v,w), δp, θ, H′(H′$_1$,H′$_2$,H′$_3$) and M′(M′$_1$,M′$_2$,M′$_3$) are perturbations in velocity, pressure, temperature, magnetic field and magnetization. These perturbations are assumed to be small and then the linearized perturbation equations are

$$\nabla.\mathbf{q}' = 0, \tag{10}$$

$$\rho_\circ \frac{\partial \mathbf{q}'}{\partial t} = -\nabla \delta p + \mu \nabla^2 \mathbf{q}' + \rho_0 \alpha g \theta \hat{k} - \frac{\mu_\circ K_1 \beta}{1+\chi}\left((1+\chi)\frac{\partial \varphi_1'}{\partial z}\hat{k} - K_1 \theta \hat{k}\right) + 2\rho_0(\mathbf{q} \times \Omega), \tag{11}$$

$$\frac{\partial \theta}{\partial t} = \kappa \nabla^2 \theta + \beta w, \tag{12}$$

$$\left(1 + \frac{M_0}{H_0}\right)\nabla^2 \phi_1' - \left(\frac{M_0}{H_0} - \chi\right)\frac{\partial^2 \phi_1'}{\partial z^2} = K_1 \frac{\partial \theta}{\partial z}. \tag{13}$$

Where $\mathbf{H}' = \nabla \varphi_1'$ and φ' is the perturbed magnetic potential and $\kappa = \frac{k}{(\rho_0 c_0)_f}$ is thermal diffusivity of the fluid.

And boundary conditions are

$$w = 0, \quad T = T_0, D\varphi = 0 \quad \text{at} \quad z = 0 \text{ and } \quad w = 0, \quad T = T_1, D\varphi = 0 \text{ at } \quad z = d. \tag{14}$$

We introduce non-dimensional variables as

$$(x'', y'', z'') = \left(\frac{x', y', z'}{d}\right), \; \mathbf{q}'' = \mathbf{q}'\frac{d}{\kappa}, \; t' = \frac{\kappa}{d^2}t, \; \delta p' = \frac{d^2}{\mu\kappa}\delta p, \; \theta' = \frac{\theta}{\beta d}, \; \varphi_1'' = \frac{(1+\chi)}{K_1 \beta d^2}\varphi_1'.$$

There after dropping the dashes (") for simplicity.

Equations (10) - (14), in non dimensional form can be written as

$$\nabla.\mathbf{q} = 0, \tag{15}$$

$$\frac{1}{Pr}\frac{\partial \mathbf{q}}{\partial t} = -\nabla \delta p + \nabla^2 \mathbf{q} + R(1 + M_1)\theta \hat{k} - RM_1 \frac{\partial \varphi_1}{\partial z}\hat{k} + \sqrt{T_A}(ve_x - ue_y), \tag{16}$$

$$\frac{\partial \theta}{\partial t} = \nabla^2 \theta + w, \tag{17}$$

$$M_3 \nabla^2 \phi_1 - (M_3 - 1)\frac{\partial^2 \phi_1}{\partial z^2} = \frac{\partial \theta}{\partial z}. \tag{18}$$

Where non-dimensional parameters are:

$P_r = \frac{\mu}{\rho\kappa}$ is Prandtl number; $R = \frac{\rho_0 g\alpha\beta d^4}{\mu\kappa}$ is Rayleigh number; $M_1 = \frac{\mu_0 K_1^2 \beta}{\alpha\rho_0 g(1+\chi)}$ measure the ratio of magnetic to gravitational forces, $T_A = \left(\frac{2\Omega d^2}{\nu}\right)^2$ is the Taylor number, $N = RM_1 = \frac{\mu_0 K_1^2 \beta^2 d^4}{\mu\kappa(1+\chi)}$ is magnetic thermal Rayleigh number; $M_3 = \frac{\left(1+\frac{M_0}{H_0}\right)}{(1+\chi)}$ measure the departure of linearity in the magnetic equation of state and values from one $(M_0 = \chi H_0)$ higher values are possible for the usual equation of state.

The dimensionless boundary conditions are

$$w = 0, \quad T = 1, D\varphi = 0 \text{ at } z = 0 \text{ and } w = 0, \quad T = 0, D\varphi = 0 \text{ at } z = 1. \tag{19}$$

Eliminating p from equation (16) we get

$$\left(\nabla^2 - \frac{1}{Pr}\frac{\partial}{\partial t}\right)\nabla^2 w + R(1+M_1)\nabla_H^2\theta - RM_1\nabla_H^2 D\varphi_1 + \sqrt{T_A}\frac{\partial\xi}{\partial z} = 0, \tag{20}$$

and

$$\left(\nabla^2 - \frac{1}{Pr}\frac{\partial}{\partial t}\right)\xi = -\sqrt{T_A}\frac{\partial w}{\partial z}. \tag{21}$$

Where stands for z- component of the vorticity ∇_H^2, is two-dimensional Laplacian operator on horizontal plane.

Eliminating ξ from equations (20) and (21), we get

$$\left(\nabla^2 - \frac{1}{Pr}\frac{\partial}{\partial t}\right)^2\nabla^2 w + T_A D^2 w + R(1+M_1)\nabla_H^2\left(\nabla^2 - \frac{1}{Pr}\frac{\partial}{\partial t}\right)\theta - RM_1\nabla_H^2\left(\nabla^2 - \frac{1}{Pr}\frac{\partial}{\partial t}\right)D\varphi_1 = 0. \tag{22}$$

III. NORMAL MODE ANALYSIS

Analyzing the disturbances of normal modes and assume that the perturbation quantities are of the form

$$[w, \theta, \varphi_1] = [W(z), \Theta(z), \Phi(z)]\exp(ik_x x + ik_y y + nt), \tag{23}$$

where, k_x, k_y are wave numbers in x- and y- direction and n is growth rate of disturbances.

Using equation (21), equations (20) and (17) - (18) becomes

$$\left(\left(D^2 - a^2 - \frac{n}{Pr}\right)\left(D^2 - a^2\right) + T_A D^2\right)W - a^2 R(1+M_1)\left(D^2 - a^2 - \frac{n}{Pr}\right)\Theta + a^2 RM_1\left(D^2 - a^2 - \frac{n}{Pr}\right)D\Phi = 0, \tag{24}$$

$$W + \left(D^2 - a^2 - n\right)\Theta = 0, \tag{25}$$

$$D\Theta - \left(D^2 - a^2 M_3\right)\Phi = 0. \tag{26}$$

where $D = \frac{d}{dz}$ and $a^2 = k^2_x + k^2_y$ is dimensionless the resultant wave number.

The boundary conditions of the problem in view of normal mode analysis are

$$W = 0, D^2 W = 0, \ \Theta = 0, \ D\Phi = 0 \ \text{ at } \ z = 0,1. \tag{27}$$

IV. METHOD OF SOLUTION

The Galerkin weighted residuals method is used to obtain an approximate solute on to the system of equations (24) – (26) with the corresponding boundary conditions (27). In this method, the test functions are the same as the base (trial) functions. Accordingly W, Θ and Φ are taken as

$$W = \sum_{p=1}^{n} A_p W_p, \Theta = \sum_{p=1}^{n} B_p \Theta_p, D\Phi = \sum_{p=1}^{n} C_p D\Phi_p. \tag{28}$$

Where A_p, B_p and C_p are unknown coefficients, p =1, 2, 3...N and the base functions W_p, Θ_p and $D\Phi_p$ are assumed in the following form for free-free boundaries are:

$$W_p = \text{Cosp}\pi z, \Theta_p = \text{Cosp}\,\pi z, D\Phi_p = \text{Cosp}\pi z, \tag{29}$$

Such that W_p, Θ_p and Φ_p satisfy the corresponding boundary conditions. Using expression for W, Θ and DΦ in equations (24) – (26) and multiplying first equation by W_p second equation by Θ_p and third by $D\Phi_p$ and integrating in the limits from zero to unity, we obtain a set of 3N linear homogeneous equations in 3N unknown A_p, B_p and C_p; p =1,2,3,...N. For existing

of non trivial solution, the vanishing of the determinant of coefficients produces the characteristics equation of the system in term of Rayleigh number R.

V. LINEAR STABILITY ANALYSIS

We confined our analysis to the one term Galerkin approximation; for one term Galerkin approximation, we take N=1, we get the expression for Rayleigh number R as:

$$R = \frac{\left(\pi^2 + a^2 M_3\right)\left(\pi^2 + a^2\right)\left(\pi^2 + a^2 + \frac{n}{Pr}\right)^2 + T_A \pi^2}{a^2\left(\pi^2 + a^2 M_3 + a^2 M_1 M_3\right)\left(\pi^2 + a^2 + \frac{n}{Pr}\right)}. \tag{30}$$

For neutral stability, the real part of n is zero. Hence we put n = iω, in equation (30), where ω is real and is dimensionless frequency, we get

$$R = \frac{\left(\pi^2 + a^2 M_3\right)\left(\pi^2 + a^2\right)\left(\pi^2 + a^2 + \frac{i\omega}{Pr}\right)^2 + T_A \pi^2}{a^2\left(\pi^2 + a^2 M_3 + a^2 M_1 M_3\right)\left(\pi^2 + a^2 + \frac{i\omega}{Pr}\right)}. \tag{31}$$

Equating real and imaginary parts of equation (31), we get

$$\frac{a^2 R\left(\pi^2 + a^2 M_3 + a^2 M_1 M_3\right)\left(\pi^2 + a^2\right)}{\left(\pi^2 + a^2 M_3\right)} = \left(\pi^2 + a^2\right)^4 + T_A \pi^2 - \omega^2\left(\frac{J^2}{Pr^2} + \frac{2J^2}{Pr}\right), \tag{32}$$

and

$$\omega\left(\frac{a^2 R\left(\pi^2 + a^2 M_3 + a^2 M_1 M_3\right)}{Pr\left(\pi^2 + a^2 M_3\right)} - \left(\left(\pi^2 + a^2\right)^2 + \frac{2\left(\pi^2 + a^2\right)^2}{Pr} - \frac{\omega^2}{Pr^2}\right)\right) = 0. \tag{33}$$

From equation (36) it follows that ω is real it is necessary that

$$\frac{a^2 R\left(\pi^2 + a^2 M_3 + a^2 M_1 M_3\right)\left(\pi^2 + a^2\right)}{\left(\pi^2 + a^2 M_3\right)} \le \left(\pi^2 + a^2\right)^4 + T_A \pi^2. \tag{34}$$

Hence equation (32) gives the oscillatory stability provided that inequalities (34) hold.

(a) Stationary Convection

Consider the case of stationary convection i.e., ω = 0, from equation (30), we have

$$R = \frac{\left(\pi^2 + a^2 M_3\right)\left(\pi^2 + a^2\right)^3 + T_A \pi^2}{a^2\left(\pi^2 + a^2 M_3 + a^2 M_1 M_3\right)}. \tag{35}$$

From equation (35) we have

$$\frac{\partial R}{\partial T_A} > 0, \frac{\partial R}{\partial M_3} < 0 \text{ and } \frac{\partial R}{\partial M_1} < 0.$$

Thus rotation has stabilizing effect while magnetization parameters have destabilizing effect on fluid layer.

In the absence of rotation T_A=0, the Rayleigh number R for steady onset is given by

$$R = \frac{\left(\pi^2 + a^2 M_3\right)\left(\pi^2 + a^2\right)^3}{a^2\left(\pi^2 + a^2 M_3 + a^2 M_1 M_3\right)}.$$

This is the good agreement of the result as obtained by Finlayson (1970).

In the absence of rotation T_A=0 and magnetic parameters M_1=M_3=0, the Rayleigh number R for steady onset is given by

$$R = \frac{\left(\pi^2 + a^2\right)^3}{a^2}.$$

Consequently critical Rayleigh number is given by $Rc = \frac{27\pi^2}{4}$.

This is exactly the same the result as obtained by Chandrasekhar (1961) in the classical Bénard problem.

VI. CONCLUSIONS

A linear stability analysis of thermal instability for ferrofluid in the presence of rotation is investigated for free-free boundary layer. Galerkin-type weighted residuals method is used for the stability analysis. The behavior of rotation and magnetization on the onset of convection analyzed.

The main conclusions are as follows:

a. Rotation stabilizes the fluid layer while magnetization parameters destabilize the fluid in case of stationary convection.
b. The 'principle of exchange of stabilities' is not valid for the problem.
c. The oscillatory convection is possible if

$$\frac{a^2R\left(\pi^2+a^2M_3+a^2M_1M_3\right)\left(\pi^2+a^2\right)}{\left(\pi^2+a^2M_3\right)} \le \left(\pi^2+a^2\right)^4+T_A\pi^2 .$$

REFERENCES

[1]. Blennerhassett, P. J., Lin, F. & Stiles, P. J.: Heat transfer through strongly magnetized ferrofluids, Proc. R. Soc. A 433, 165-177, (1991).
[2]. Chandrasekhar, S.: *Hydrodynamic and hydromagnetic stability,* Dover, New York (1981)
[3]. Finlayson, B.A.: Convective instability of ferromagnetic fluids. J. Fluid Mech. **40**, 753-767 (1970).
[4]. Gupta, M.D., Gupta, A.S.: Convective instability of a layer of ferromagnetic fluid rotating about a vertical axis, Int. J. Eng. Sci. **17**, 271-277, (1979).
[5]. Lalas, D. P. & Carmi, S.: Thermo convective stability of ferrofluids. Phys. Fluids 14, 436-437, (1971).
[6]. Mahajan A.: *Stability of ferrofluids: Linear and Nonlinear*, Lambert Academic Publishing, Germany, (2010).
[7]. Rosensweig, R.E.: *Ferro hydrodynamics*, Cambridge University Press, Cambridge (1985).
[8]. Shliomisa, M.I and Smorodinb, B.L.: Convective instability of magnetized ferrofluids, Journal of Magnetism and Magnetic Materials, 252,197-202, (2002).
[9]. Stiles, P. J. & Kagan, M. J.: Thermo-convective instability of a horizontal layer of ferrofluid in a strong vertical magnetic field, J. Magn. Magn. Mater, 85, 196-198, (1990).
[10]. Sunil, Sharma, D. and Sharma, R. C.: Effect of dust particles on thermal convection in ferromagnetic fluid saturating a porous medium, J. Magn. Magn. Mater. 288, 183-195, (2005).
[11]. Sunil, Sharma, A. and Sharma, R. C.: Effect of dust particles on ferrofluid heated and soluted From below, Int. J. Therm. Sci. 45, 347-358, (2006).
[12]. Sunil, Mahajan, A.: A nonlinear stability analysis for magnetized ferrofluid heated from below. Proc. R. Soc. A 464, 83-98 (2008).
[13]. Venkatasubramanian, S., Kaloni, P.N.: Effects of rotation on the thermo convective instability of a horizontal layer of ferrofluids. Int. J. Eng. Sci. **32**, 237–256 (1994).
[14]. Zebib, A: Thermal convection in a magnetic fluid, J. Fluid Mech., 32, 121-136, (1996).

International Journal of Modern Engineering Research (IJMER)
www.ijmer.com Vol. 3, Issue. 4, Jul - Aug. 2013 pp-2048-2055 ISSN: 2249-6645

WAP- Mobile Personal Assistant Application

Adnan Affandi[1], Abdullah Dobaie[2], Mubashshir Husain[3]
Electrical and Computer Engineering Department, King Abdul Aziz University P.O. BOX: 80204, Jeddah 21589

ABSTRACT: *Wireless Application Protocol (WAP) is a result of continuous work to define an industry-wide specification for developing applications that operate over wireless communication networks. The scope for the WAP Forum is to define a set of specifications to be used by service applications.*

Not everybody has a computer, but most of the people have mobiles. And not everybody knows how to use the internet, but most of the people have the ability to use the mobiles. This paper exploits this point and produced a unique novel service that gives everyone the access to the internet using their mobiles, which can be used in many applications such as:

- *Checking train table information*
- *Ticket purchase*
- *Flight check in*
- *Viewing traffic information*
- *Checking weather conditions*
- *Looking up stock values*
- *Looking up phone numbers*
- *Looking up addresses*
- *Looking up sport results*

And much more in these aspects. The Mobile Personal Assistant Application which has been developed by using WAP was the first of its kind here, where software has been developed.

I. INTRODUCTION

You and millions of other people around the world use the Internet every day -- to communicate with others, follow the stock market, keep up with the news, check the weather, make travel plans, conduct business, shop, entertain yourself and learn. Staying connected has become so important that it's hard to get away from your computer and your Internet connection because you might miss an e-mail message, an update on your stock or some news you need to know. With your business or your personal life growing more dependent on electronic communication over the Internet, you might be ready to take the next step and get a device that allows you to access the Internet on the go. That's where **wireless Internet** comes in. You've probably seen news or advertising about cell phones and PDAs that let you receive and send e-mail.

1.2 WML (Wireless Markup Language)

WAP uses Wireless Markup Language (WML), which includes the Handheld Device Markup Language (HDML) developed by Phone.com. WML can also trace its roots to eXtensible Markup Language (XML). A markup language is a way of adding information to your content that tells the device receiving the content what to do with it. The best known markup language is Hypertext Markup Language (HTML). Unlike HTML, WML is considered a meta language. Basically, this means that in addition to providing predefined tags, WML lets you design your own markup language components. WAP also allows the use of standard Internet protocols such as UDP, IP and XML.

There are three main reasons why wireless Internet needs the Wireless Application Protocol:

- Transfer speed
- Size and readability
- Navigation

Most cell phones and Web-enabled PDAs have data transfer rates of 14.4 Kbps or less. Compare this to a typical 56 Kbps modem, a cable modem or a DSL connection. Most Web pages today are full of graphics that would take an unbearably long time to download at 14.4 Kbps. Wireless Internet content is typically text-based in order to solve this problem.

The relatively small size of the LCD on a cell phone or PDA presents another challenge. Most Web pages are designed for a resolution of 640x480 pixels, which is fine if you are reading on a desktop or a laptop. The page simply does not fit on a wireless device's display, which might be 150x150 pixels. Also, the majority of wireless devices use monochrome screens. Pages are harder to read when font and background colors become similar shades of gray.

Navigation is another issue. You make your way through a Web page with points and clicks using a mouse; but if you are using a wireless device, you often use one hand to scroll keys.

WAP takes each of these limitations into account and provides a way to work with a typical wireless device.

1.3 Wireless Application Protocol

Here's what happens when you access a Web site using a WAP-enabled device:

- You turn on the device and open the minibrowser.
- The device sends out a radio signal, searching for service.

- A connection is made with your service provider.
- You select a Web site that you wish to view.
- A request is sent to a gateway server using WAP.
- The gateway server retrieves the information via HTTP from the Web site.
- The gateway server encodes the HTTP data as WML.
- The WML-encoded data is sent to your device.
- You see the wireless Internet version of the Web page you selected.

To create wireless Internet content, a Web site creates special text-only or low-graphics versions of the site. The data is sent in HTTP form by a Web server to a **WAP gateway**. This system includes the WAP encoder, script compiler and protocol adapters to convert the HTTP information to WML. The gateway then sends the converted data to the WAP client on your wireless device.

What happens between the gateway and the client relies on features of different parts of the **WAP protocol stack**. Let's take a look at each part of the stack:

- **WAE** - The Wireless Application Environment holds the tools that wireless Internet content developers use. These include WML and WMLScript, which is a scripting language used in conjunction with WML. It functions much like Javascript.
- **WSP** - The Wireless Session Protocol determines whether a session between the device and the network will be **connection-oriented** or **connectionless**. What this is basically talking about is whether or not the device needs to talk back and forth with the network during a session. In a connection-oriented session, data is passed both ways between the device and the network; WSP then sends the packet to the Wireless Transaction Protocol layer (see below). If the session is connectionless, commonly used when information is being broadcast or **streamed** from the network to the device, then WSP redirects the packet to the Wireless Datagram Protocol layer (see below).
- **WTP** - The Wireless Transaction Protocol acts like a traffic cop, keeping the data flowing in a logical and smooth manner. It also determines how to classify each transaction request: Reliable two-way Reliable one-way Unreliable one-way The WSP and WTP layers correspond to Hypertext Transfer Protocol (HTTP) in the TCP/IP protocol suite.
- **WTLS** - Wireless Transport Layer Security provides many of the same security features found in the Transport Layer Security (TLS) part of TCP/IP. It checks data integrity, provides encryption and performs client and server authentication.
- **WDP** - The Wireless Datagram Protocol works in conjunction with the network carrier layer (see below). WDP makes it easy to adapt WAP to a variety of bearers because all that needs to change is the information maintained at this level.
- **Network carriers** - Also called **bearers**, these can be any of the existing technologies that wireless providers use, as long as information is provided at the WDP level to interface WAP with the bearer.

Once the information is received by the WAP client, it is passed to the **minibrowser**. This is a tiny application built into the wireless device that provides the interface between the user and the wireless Internet.
The minibrowser does not offer anything more than basic navigation. Wireless Internet is still a long way from being a true alternative to the normal Internet. It is really positioned right now for people who need the ability to connect no matter where they are. The WAP Forum is continually working on the specifications of the WAP standard to ensure that it evolves in a timely and useful manner.

II. CREATING A DYNAMIC WAP APPLICATION USING ASP

Microsoft Active Server Pages (ASP) is a viable technology for developing dynamic web content. Its popularity can be seen from the many web sites sporting documents with the .asp extension. Because ASP is a server-side technology, it is well suited to creating dynamic WAP applications, especially in the area of database access.

2.1.1 The MPA Application

The sample application that we will be building in this session is a Mobile Personal Assistant (MPA). The aim of this is to allow users to have a mobile time scheduler that enables them to check on their plans wherever they are.

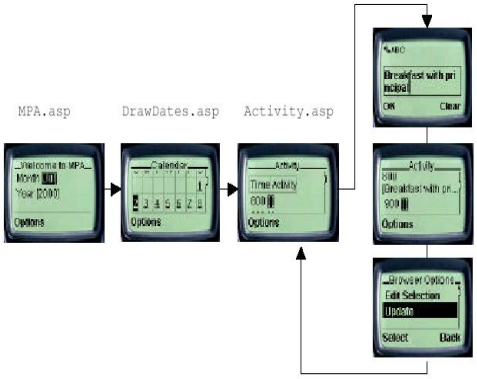

Fig1. Application Overview

As can be seen from the above diagram, there are three decks involved in this application. They are:

- ✓ MPA.asp
- ✓ DrawDates.asp
- ✓ Activity.asp

In implementing this application, the technologies used are ASP and ActiveX Data Objects (ADO). Let's first take a look at the database:

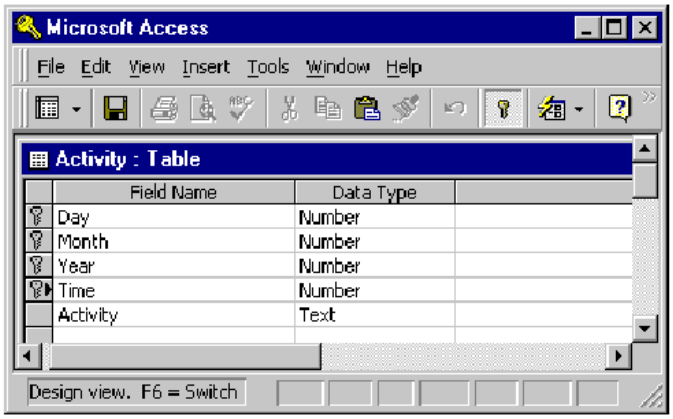

Fig.2 Microsoft Access Database

This Microsoft Access database (PIM.mdb) contains a single table for storing the activities of the user. A typical schedule looks like this:

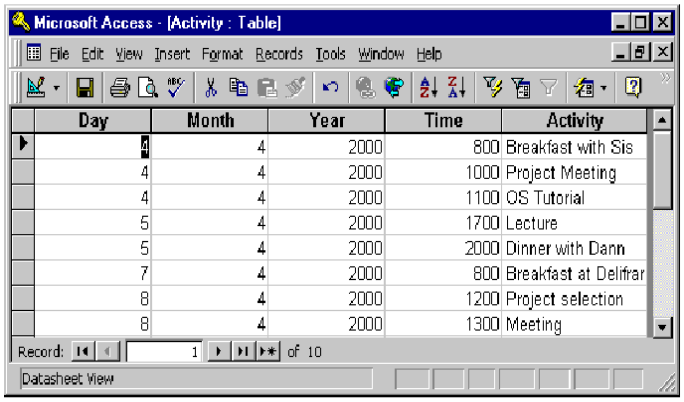

Fig.3. MicroSoft Access Database

2.1.1.1 Creating a Calendar

To enable the user to locate a day and month in their schedule easily, its needed to create a calendar on screen. This is achieved by the code in MPA.asp.

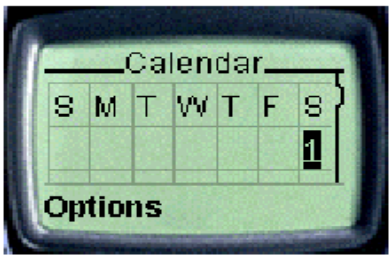

Fig.4. Calendar Created

2.1.1.2 The DrawDates.asp Document

To draw the calendar on the user's screen, so that they can select the day in which to enter their schedule. The generateDate() function is used to generate a table containing all the days in a particular month and year:

Once the month and the year have been selected, they are sent to the DrawDates.asp document using the GET method. A <postfield> element is used to accomplish this:

The DrawDates.asp Document

I need to draw the calendar on the user's screen, so that they can select the day in which to enter their schedule. The generate Date () function is used to generate a table containing all the days in a particular month and year:

2.1.2.2The Activity.asp Document

Once the user has selected a day, they can click on the Follow Link option to retrieve the activity page:

Fig.5 Showing Browser Options & Activity page

Here we have generated all the different time intervals from 8am to 10pm. The time interval is one hour. We use an <input> element to let users modify their activities, and at the same time retrieve the previously saved activity from the database

Notice that in our case we have thirteen different time intervals, and each <input> element has a different name. The first one has the name TimeActivity800, the second one is TimeActivity900, and so on.

Once the user has keyed in their activities, they can proceed to save the activity into the database:

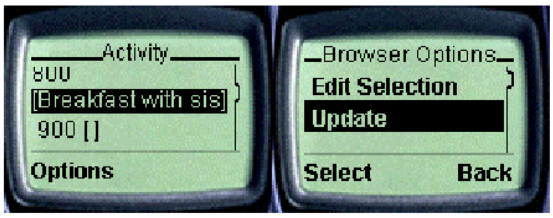

Fig.6 User can save the activity into the Database

2.1.2 Developing Dynamic WAP Applications

Some issues involving in developing dynamic WAP applications:

- ✓ Redirecting pages
- ✓ Caching on WAP devices
- ✓ Cookie support on WAP devices, and maintaining state using the ASP Session object
- ✓ Maintaining state without cookie support
- ✓ Detecting WAP devices
- ✓ Passing values from ASP server-side variables to WML client-side variables, and vice versa.
- ✓ Tips for using ASP to generate WML content
- ✓ Common errors

2.1.2.1 Redirecting Pages

In web application development, it's not unusual to see a browser being redirected to another web page. This may happen, for example, because you don't have the permissions required to view a page, and you must therefore log in before you can do so.

In ASP, you can use the Response.Redirect() method to perform page redirection.

Buffering is disabled by default in ASP 2.0 but enabled by default in ASP 3.0.

If a page is not buffered, the web server will send the HTTP headers to the client before the ASP parser has finished parsing the ASP document. In the case of page redirection, this will cause an error. Try setting the Response.Buffer property to False, and you'll see the error message:

The error message is:

The HTTP headers are already written to the client browser. Any HTTP header modifications must be made before writing page content.

2.1.2.2 Caching on WAP Devices

WAP devices generally cache WML decks. This is to reduce the time that is wasted in trying to reload a page that has been loaded earlier. However, for dynamic content, this is not a good feature — the user may be reading some stale information from the cache.

There are two issues to consider when we talk about caching. They are:

- ✓ Caching by proxy servers
- ✓ Caching by WAP devices

2.1.2.3 Caching by Proxy Servers

Proxy servers help to reduce the time needed to fetch a document from the origin server. In a network, a proxy server may be set up to act as a halfway house between the Internet and the web clients in the various departments. The

proxy server will cache all documents requested by the network, so that it may fulfill subsequent requests for a document retrieved earlier. The trip to the origin server is reduced to making a trip to the proxy server, as the following diagram explains. Proxy servers should not cache ASP documents, as this defeats the purpose of using ASP in the first place. To turn off caching by proxy servers, use the Response.CacheControl property:

<% Response.CacheControl="private" %>

If for any reason you wish to enable caching by the proxy server, you can set the cache control property to public.

<% Response.CacheControl="public" %>

What about caching by a WAP gateway? The WAP Caching Model specification states that a WAP gateway must faithfully implement the role of an HTTP/1.1 proxy with respect to caching and cache header transmission.

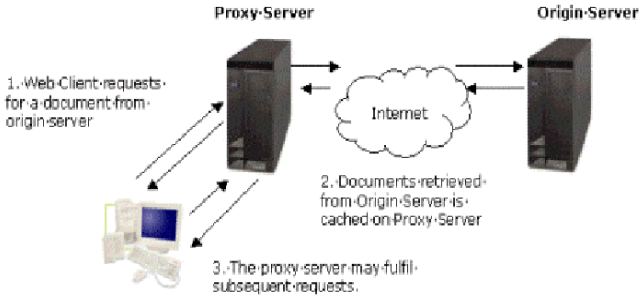

2.1.2.4 Caching by WAP Devices

Just as a proxy server caches pages, WAP devices generally come with some memory to act as a cache. Remember that bandwidth is still a limitation for current WAP devices, so caching WML pages can generally led to improved performance.

While a cache memory helps to load a page that has been loaded previously without making a connection to the origin server, it is a nuisance where timesensitive pages are concerned. Pages like stock information, weather reports, and online ticketing systems are highly time-sensitive.

By default, WML pages are cached. To force a WML deck to expire immediately after it has been received, I use the Response

The Cache-Control <meta> element allows you to set the caching characteristics of the target WAP device. The content attribute can contain the following values:

- ✓ max–age=time_in_seconds
- ✓ must-revalidate
- ✓ no–cache

When the value of content is set to "max–age=0", it expires immediately after it has been loaded. It is equivalent to "no–cache".

We have looked at the two methods for controlling caching on WAP devices, but which is better? In general, controlling the HTTP headers is a better option than using the <meta> element. This is because some WAP gateways may not pass caching-related headers to the WAP device, especially the <meta> elements. Also, <meta> elements are not supported by all WAP devices.

2.1.2.5 Cookie Support on WAP Devices

At the time of writing, WAP 1.1 devices have very limited support for cookies. If you're planning to make use of ASP's Session object, you have to be aware of this and make appropriate allowances.

The Session Object and Cookies

The ASP Session object requires the use of cookies in order to work correctly. Provided that's the case, using it is straightforward.

2.1.2.6 Detecting WAP Devices

To detect what WAP browser the user is using, you can use the Request.ServerVariables collection, as I do in Useragent.asp:

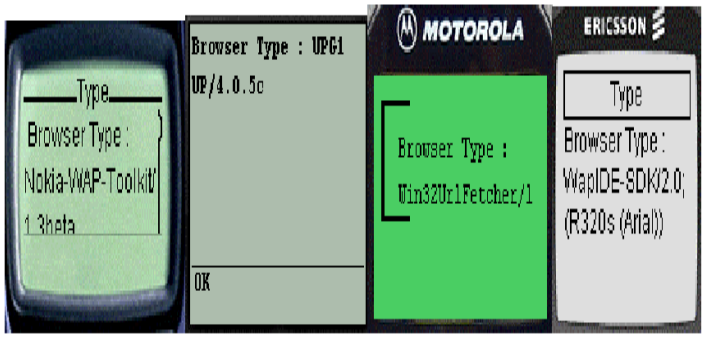

It's up to the developer to decide on the level of compatibility that they want to achieve for a particular application. For a list of user agents, point your browser at http://amaro.g-art.nl/useragent/.

If the user agent contains the word "Mozilla", then the user is using a web browser and I need to redirect them to another HTML page using the Response.Redirect() method.

2.1.2.7 Passing Values from ASP to WML

A common question asked by developers new to WML is how can they pass values between WML client-side variables and ASP server-side variables.

Tips for Using ASP to Generate WML Content

When generating WML content using ASP, bear in mind that a deck can contain multiple cards. If your content for each card is generated dynamically, it may have an impact on the efficiency of your web server.

When the ASP parser parses the above deck, both cards will be 'given' the same time. When the user moves from card1 to card2, they will see the same time on both cards. This may not be what we intended — we might want the cards to contain the different times that they were displayed on the WAP device. To solve this problem, I need to make sure that caching is turned off on the WAP device. For this, I can use the Response.Expires property, as described earlier in the paper. However, this causes the deck to be parsed twice by the ASP parser, as the WAP device will have to reload the same deck from the origin server to display the second card.

Remember: caching is at deck level. When a user moves from a card to another within a deck, using a Response.Expires property will not cause a reload of the deck from the origin server.

Hence, when you have dynamic content on multiple cards within a deck, it is important that these cards be separated into different decks. The diagram showing the request and response between the WAP device and origin server is valid provided caching can be done at the card level.

As can be seen, every time the WAP device requests the same deck, the ASP server spends time parsing it. If the deck contained a lot of cards, the time needed would be substantial: this is inefficient. Instead, by breaking the cards down into multiple decks, the time spent parsing individual decks is reduced.

2.1.2.8 Common Errors

Finally, let's briefly examine some of the common errors that developers may encounter when using ASP to generate WML content.

- **Not setting the correct MIME type**

The WML MIME type must be set using the Response.ContentType property, like this:

```
<% Response.ContentType = "text/vnd.wap.wml" %>
```

- **Cookies are not supported**

When using cookies or the Session object, always ensure that the target platform is capable of supporting cookies.

The POST method may not work correctly on some WAP devices

When using a <postfield> element, be aware that some WAP devices (the Nokia 7110, for instance) have problems in supporting the POST method.

You need a web server to run ASP!

Very often, people just run ASP documents straight from their local hard disk. ASP documents require a web server (in particular, the ASP parser) to process them, so that the resulting page can be sent to the client. Also important point to note is that you need to use the http:// syntax, and not the physical filename.

III. PHP/WML

In this paper we have done three integrated PHP/WML examples, showing you:

- **How to insert dynamic content into WML:** Illustrates how PHP can be integrated directly within a WML deck, so that you can feaure dynamic content for the user (in our example, a date).
- **How to send email to a WAP-enabled Device:** Introduces user interactivity by providing a mechanism in which a user can send email.
- **How to interact with a MySQL Database:** Introduces database interaction to enable the display of information in the Web browser, such as a current soccer score.

3.1 How to Insert Dynamic Content into WML

Consider a simple example where a message is generated along with a current date. The example produces the following output:

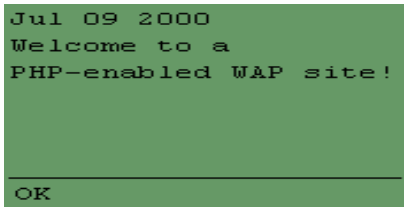

Code Flow

- Send the proper header to the WAP browser.
- Use PHP's date() function to output the current date
- Use PHP to print out a simple message

PHP's date function offers a very flexible way in which to display the current date.

3.2 How to Send Email to a WAP-Enabled Device

Let's apply what we've learned thus far by building a basic WML/PHP application to send email to a wireless device. Two decks are involved, the first consisting of three cards, and the second consisting of one card:

- The first deck prompts the user for various pieces of information, namely the destination email address, the message subject, and the message itself.
- The second deck actually sends the message to the destination address and outputs an appropriate message to the user.

Note: This script will not peform any error checking. However, error checking can easily be scripted. For example, a few extra lines of code can be inserted to ensure that the user enters a valid email address, defines a subject, and inserts a message

Code Flow

Deck 1 (email1.wml):

- Send the proper header to the WAP browser.
- Prompt user for Email recipient.
- Prompt user for message subject.
- Prompt user for message.
- Pass information to second deck, entitled email2.wml

Deck 2 (email2.wml):

- Send message to the recipient.
- Inform user as to whether message has been sent.

3.3 How to Interact with a MySQL Database

The final example involves the extraction of data from a MySQL database for display within a WML card. Suppose you wanted to display the outcomes of a series of soccer matches.

The following MySQL table could be defined:

```
mysql>create table soccer_scores (
   >team1 char(20),
   >score1 int,
   >team2 char(20),
   >score2 int );
```

The following could be stored within the table:

Team1	score1	team2	score2
France	2	Holland	3
England	2	Romania	3
Italy	2	Sweden	1
Yugoslavia	3	Spain	4

We can create a simple script capable of retrieving this data and then displaying it within a WAP browser, as shown below:

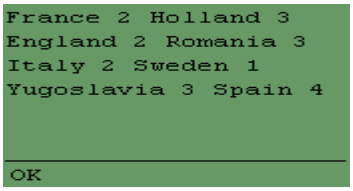

Code Flow

- Send the proper header to the WAP browser.
- Begin a new WML deck.
- Connect to the MySQL server ("www.zend.com")
- Select a MySQL database ("sports")
- Select information from the MySQL table "soccer_scores"
- If data exists within the table, output it using the format: team1 team1_score team2 team2_score
- If data does not exist, output appropriate message.

IV. WAP SECURITY

Security of applications and computer systems is an issue that, quite rightly, many of IT professionals are concerned about. As corporations have utilized technologies, such as remote access, Java and component technologies, and infrastructural advances like the Internet, to facilitate new ways of working, new ways of doing business with clients, partners and suppliers, and even to create entirely new products, services and business models, the need for mechanisms to secure applications, networks and systems has become more and more important.

- WAP is another technology that extends the reach of communication networks, provides new opportunities for innovative corporations, and adds to the complexity of the environment within which applications need to be designed, built and deployed. There is a set of concerns over how secure WAP is as a technology, and whether it is robust enough to implement mobile commerce applications, and other applications with stringent security requirements.
- Before beginning this investigation of WAP security, it is worth noting that there is no such thing as a secure system. The phrase 'secure system' means one that cannot be compromised or accessed without authorization. Considering that hackers who set out to compromise or penetrate systems are resourceful and always target unexpected aspects of the systems, it would be a brave fool who declared a system to be immune to attack. What can be said is that a particular system meets certain predefined security criteria in that it can withstand attacks of a known type, and is therefore considered secure enough for its intended purpose.
- If your interest in this project is to come out with a definitive statement as to whether WAP is 'secure' or not, you will be disappointed. It is only feasible to make the assertion that WAP is or is not 'secure enough' for a particular application when you understand the security requirements of that application, the environment in which that application is to be deployed, the likelihood that the application will be subject to attempts to compromise its security, and the nature of the attempts that are likely to be made. Even then the statement is only valid until something changes in the environment, or someone discovers a new security exposure in the network, the environment, the technologies used or the platform on which the application is deployed.

V. CONCLUSION

In this paper, a Mobile Personal Assistant (MPA) Application using WAP has been developed.
XML (and friends) is at the moment the best possibility to handle the problems occuring with the many combinations of possible mobile devices, their browser versions and the WAP-gateways they are using. Almost every combination has its effects on the user-interface style. The weak commitment to WAP-standards of some vendors makes difficult for developers of mobile services. Nevertheless XML is powerful enough to handle such difficulties and also showed its power in this prototype implementation.

REFERENCES

[1] Lee,W.M. and Foo,S.M. and Watsom K. and Wugofski T., Beginning WAP, WML, & WMLScript, UK, Wrox Press, 2000.
[2] Arehart C. and Chidambaram N. and Guruprasad S. and Homer A. and Howell R. and Kasippillai S. and Machin R. and Myers T. and Nakhimovsky A. and Passani L. and Pedley C. and Taylor R. and Toschi M., Professional WAP, UK, Wrox Press,2000.
[3] The WAP forumat http://www.wapforum.com. At this site the current WAP specifications can be found, together with suggested future specifications
[4] The WAP group at http://www.wireless3.com. Here you can gain access to a network of professionals, all working towards the widespread dispersal of knowledge and the debeloplemt of WAP technique
[5] The site at http://www.wirelessdevnet.com/ is useful for industry news and other information resources.
[6] The site at http://www.w3schools.com/wap/wap_intro.asp is contain WAP tutrial and WAP resources.
[7] UP.SDK Release 4.1, WML Language Reference, Openwave Systems Inc., 2000 http://www.geek.com/menu_databases.htm
[9] Robin Beaumont 28/03/00 Tel: 0191 2731150.
[10] Wei Meng Lee, Ngee Ann Polytechnic, Singapore W.J. Gilmore August 3, 2000
[11] The site at http://www.stc.com.sa is Saudi Telecom Company web site.

International Journal of Modern Engineering Research (IJMER)
www.ijmer.com Vol. 3, Issue. 4, Jul - Aug. 2013 pp-2056-2061 ISSN: 2249-6645

Performance Analysis of the Constructed Updraft Biomass Gasifier for Three Different Biomass Fuels

Prince Yadav[1], Amit Dutta[2], Dr. Bhupendra Gupta[3], Dr. Mukesh Pandey[4]
[1]*Student Master of Engineering, Heat Power, JEC, Jabalpur*
[2]*Assistant Professor, GRKIST, Jabalpur, M.P.*
[3]*Assistant Professor, Jabalpur Engineering College, Jabalpur, India*
[4]*Proffesor, School of Energy and Environment, UIT, RGPV Bhopal, India*

Abstract: *Gasification is the process in which a solid carbonaceous fuel is converted into combustible gas using partial amount of air. The gases which evolve are known as "producer gas". This gas is more suitable than the direct combustion of biomass. In this paper an updraft gasifier is constructed and is used to carry out the experiment. The waste material like bagasse (sugarcane waste), coconut shells and wood particles are used for the generation of producer gas. The sense of this paper is to study the effect of waste products in form of biomass. The performance of the gasifier is evaluated in terms of zone temperature with different air velocity. By taking the different fuels and varying the air flow rate the temperature of the zones are analyzed. The gas composition is not considered. The arrangement of tar is also seen in this apparatus. After analysis it is found that the coconut shell having maximum temperature for all three zones as compare to other two so coconut shell is the best suitable material for this gasifier.*

Keywords: *Biomass gasification, construction, updraft gasifier, temperature analysis.*

I. Introduction

Biomass is an organic material, including plant matter from trees, grasses, and agricultural crops. The chemical composition of biomass varies among species, but basically consists of high, but variable moisture content, a fibrous structure consisting of lignin, carbohydrates or sugars, and ash. Biomass is very heterogeneous in its natural state and possesses a heating value lower than that of coal.

Gasification is a more than century old technology, which flourished before and during the Second World War. The technology disappeared soon after the Second World War, when liquid fuel (petroleum based) became easily available. During the 20th century, the gasification technology roused intermittent and fluctuating interest among the researchers. However, today with rising prices of fossil fuel and increasing environmental concern, this technology has regained interest and has been developed as a more modern and sophisticated technology. A process of conversion of solid carbon fuels into combustible gas by partial combustion known as gasification. The resulting gas known as producer gas (with the composition of CO 15-20%, H_2 10-15%, CH_4upto4%, N_2 45-55%, CO_2 8-12%), is more versatile in its use then the original solid biomass. The equipment used for this gasification process is known as gasifier. Gasification is primarily a thermo-chemical conversion of organic materials at elevated temperature with partial oxidation. In gasification, the energy in biomass or any other organic matter is converted to combustible gases (mixture of CO, CH_4 and H_2), with char, water, and condensable as minor products. Initially, in the first step called pyrolysis, the organic matter is decomposed by heat into gaseous and liquid volatile materials and char (which is mainly a nonvolatile material, containing high carbon content). In the second step, the hot char reacts with the gases (mainly CO_2 and H_2O), leading to product gases namely, CO, H_2 and CH_4. The producer gas leaves the reactor with pollutants and therefore, requires cleaning to satisfy requirements for engines. Mixed with air, the cleaned producer gas can be used in gas turbines (in large scale plants), gas engines, gasoline or diesel engine.

1.1 Processes of Gasification: Four distinct processes in the gasifier -

1. *Drying*:- In this stage, the moisture content of biomass is typically reduced to be 5-35%.In drying zone the temperature is about 100-200°C.
2. *Pyrolysis*:-It is the first step in the combustion or gasification of biomass. When biomass heated in the absence of air to about 350-600°C,it form charcoal, gases and tar vapors.
   Biomass + heat → solid, liquid, gases products (H_2 , H_2O, CO , CO_2)
3. *Combustion*: - In this process the reaction between solid carbonized biomass and oxygen in the air, resulting in formation of CO_2. Hydrogen present in the biomass is also oxidized to generate water. Large amount of heat is released with the oxidation of carbon and hydrogen.
   $C+ O_2 \rightarrow CO_2$
4. *Reduction*: - In absence of oxygen, several reduction reactions occur in the temperature range of 600-1000ºC. These reactions are mostly endothermic. The major in this category are as follows:
   $C+H_2O \rightarrow CO+H_2$
   $C+CO_2 \leftrightarrow 2CO$
   $CO_2+H_2 \leftrightarrow CO+H_2O$
   $C+2H_2 \leftrightarrow CH_4$

1.2 Classification of biomass gasifier: They are classified according to the way air or oxygen is introduced in it. There are three types of gasifier-

1.3.1) **Downdraft:** Biomass is introduced from the top and moves downward. Oxidizer (air) is introduced at the top and flows downward. Producer gas is extracted at the bottom at grate level.

1.3.2) **Updraft:** Biomass is introduced from the top and moves downward. Oxidizer is introduced at the bottom and flows upward. Some drying occurs. Producer gas is extracted at the top.

1.3.3) **Cross draft:** Biomass is introduced from the top and moves downward. Oxidizer is introduced at the bottom and flows across the bed. Producer gas is extracted opposite the air nozzle at the grate.

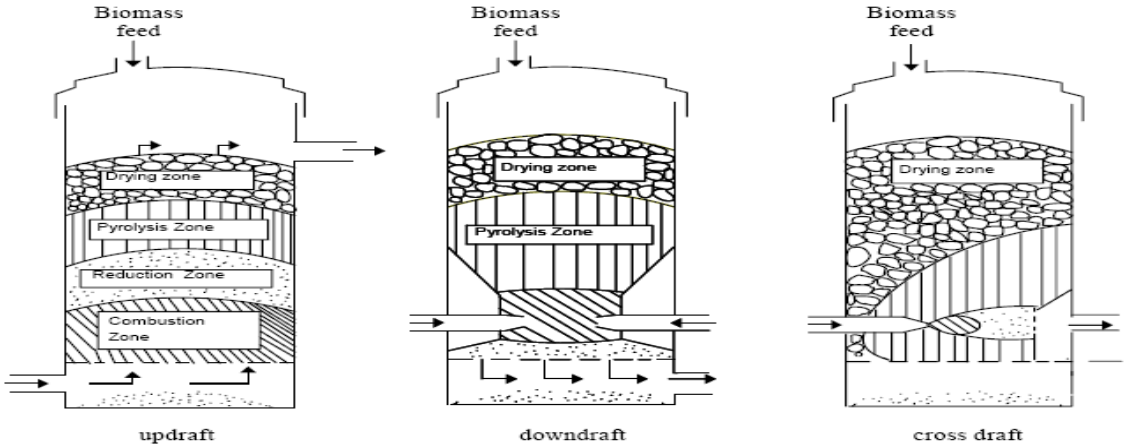

Fig. 1.1- Types of biomass gasifier

Our current work focused on the construction of updraft gasifier and performance analysis of the updraft gasifier. There are various biomass materials are available in the countries. Where in the following three bio mass materials which are commonly available and reliable were taken for performance analysis of the updraft gasifier – wood chips, sugarcane waste, and coconut shells.

II. Construction of Updraft Biomass Gasifier

The original aim with this gasifier project, were to build a compact and simple gasifier, that used inexpensive feedstock (like wood chips or mulch that is available very inexpensively, or even free), and produced high-quality gas. The research showed that the updraft gasifier design generally produced the best quality gas. Some gasifier designs are quite complex and difficult to fabricate, others much simpler. So naturally,we gravitated toward the simpler design. Thework originally aimed to building a simple open core design.

The basic structure of the gasifier is built around 13 inches inside diameter, 2.5mm thickness, and 21 inches long air tank of trucks, and a steel tube 5 inches in inside diameter, 3mm thickness, and 22 inches long. These dimensions are not really critical. The tube could be a little longer or shorter, and a little wider or narrower in diameter. The air tank (fig. 2.1 &fig 2.2) and steel tube brought from a scrap market. The purpose of the drum is to be the main body of the gasifier unit. It contains everything and collects all the gas, ash and char the unit will produce. The steel tube serve as a flame tube where the gasification processes takes place.

Fig.2.1-Air Tank (Top View)

Fig.2.2-Air Tank (Front View)

The work has been started by cutting a large hole in the top of the drum so the stainless steel flame tube can be inserted (figure2.4). The hole was made very oversize, a fortuitous decision as it turned out. The hole is offset to the side of the drum opposite the small bung. The large bung was sacrificed, since I wasn't planning on using it. Next I cut a flange from a piece of 1/8 in steel for mounting the flame tube into the drum. I installed clip nuts on the corners of the hole in the top of the drum, and drilled mating holes in the above flange. This would allow me to bolt the flange down to the top of the drum. Next, I made some angle brackets out of aluminum and bolted the flame tube to the flange. I left 6.5 inches of the flame tube

sticking up above the flange. The rest protrudes down into the drum. Here the unit is being test fit on top of the drum. The holes in the ends of the angle brackets are over the clip nuts in the top of the drum.The high temperature silicone gasket material (figure2.5) is used to seal every crack, crevasse, joint and bolt hole in the gasifier.


Fig.2.3-Cutting of the air tank


Fig.2.4-Cutting flange for tank

Fig.2.5- Silicon gasket


Fig.2.6- Six numbers of j type copper tubes

Here I have installed the six j-tubes (figure 2.6). They are made of 1cm inside diameter, 0.5mm thickness, and 1foot length copper tubing. They are called j-tubes because they are shaped like the letter J. I used a large hose clamp cinched down tight to hold the tubes in place. The opening in the top of the drum needed to have a few notches cut in it to accommodate a couple of the j-tubes that stuck out too far.

The constrictor plate (figure 2.7) installed in the bottom of the flame tube. To make the plate I cut a circle out of a11 inch sheet steel that would fit in the bottom of the flame tube. Then I cut a 1.6 inch diameter hole in the center of the circle. To mount the constrictor in the flame tube, I welded three 1/4-20 nuts to the plate, and drilled passage holes in the flame tube for three 1/4-20 bolts. The manifold I made to cover the inlets of all six j-tubes. It was cut from a 6 in to 4 in steel AC duct reduction fitting. It slips down over the flame tube and covered all six j-tubes. A single air inlet fitting will be installed on the side of the manifold.


Fig.2.7-Constrictor plate


Fig.2.8- Updraft gasifier

After this, the gasifier is ready to use. But before starting the gasifier, it has been equipped with all the measuring instruments to take the readings.

III. Experimental Setup and Procedure

In this setup, the updraft biomass gasifier installed with the blower of different speeds, Anemometer, k-type thermo couples and digital temperature reader. First of all, the pulverized coal is heated with direct burning and this coal is used for the initial combustion of biomass fuel. This burn coal placed to the grate. Firstly, I used wood chips as a biomass fuel and filled the flame tube and closed the upper portion of the flame tube with the special type cap. The cap has two outlet valves for the producer gas. One is going to the burner and another to the nozzle.

Fig.3.1- Experimental setup of updraft biomass gasifier

Fig. 3.2- Experimental setup and burning flame in the burner

Further, blower is started with minimum speed of air inlet and the gasifier has been started. When the velocity of inlet air increases, the combustion presses of the gasifier become faster.This time the temperature of the three different zones of the gasifier increase greatly. The readings of different air velocity have been taken from the Anemometer and temperatures of three different zones taken from the Digital Temperature reader. This process continues with the other two fuels, sugarcane wastes and coconut shells.

IV. Results and Discussion

The gasification experiments were performed in the heat engine laboratory of the JEC, Jabalpur for three different biomass materials for the performance analysis of the constructed updraft biomass gasifier. The different velocity of air was measured with an Anemometer. The pyrolysis, reduction and oxidation zone temperature were also monitored with the aid of K type thermocouples.

The temperatures of the three different zones at different air velocities of the producer gas for these three materials were found out (Table 4.1, Table 4.2, and Table 4.3).

The comparison of Temperatures for these biomass materialswith respect to the air velocity are shown in the graph given below:

Table1: Different zone temperatures at different air velocities for wood chips.

Air velocities (m/sec.)	Temperature of Pyrolysis zone (˚C)	Temperature of Reduction zone (˚C)	Temperature of Combustion zone (˚C)
0.8	380	405	420
1.2	470	520	535
1.8	495	542	578
2.2	585	610	635

Table2: Different zone temperatures at different air velocities for Sugarcane waste.

Air velocities (m/sec.)	Temperature of Pyrolysis zone (˚C)	Temperature of Reduction zone (˚C)	Temperature of Combustion zone (˚C)
0.8	315	356	380
1.2	460	485	510
1.8	625	658	683
2.2	542	558	576

Table3: Different zone temperatures at different air velocities for Coconut shells.

Air velocities (m/sec.)	Temperature of Pyrolysis zone (˚C)	Temperature of Reduction zone (˚C)	Temperature of Combustion zone (˚C)
0.8	535	558	610
1.2	595	638	796
1.8	705	780	835
2.2	785	810	880

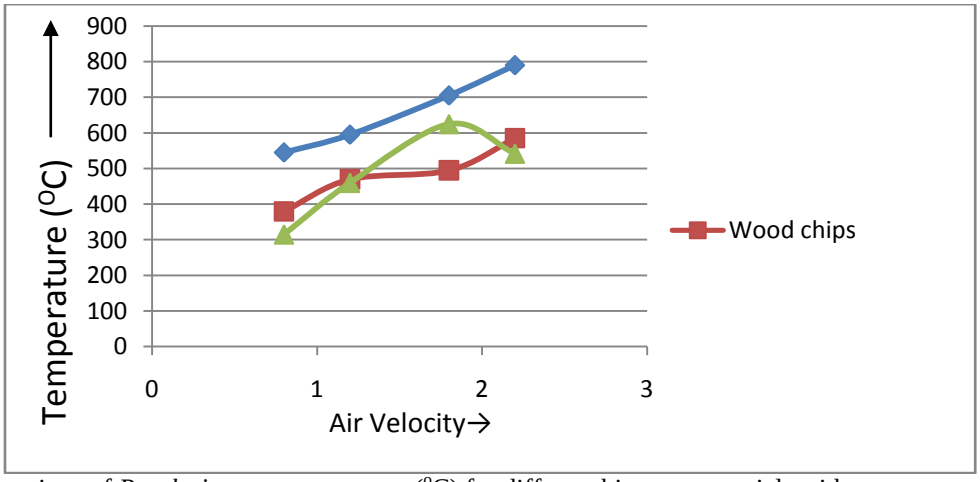

Fig 4.1: Comparison of *Pyrolysis zone* temperature (^{o}C) for different biomass materials with constant variations of air velocity (m/s).

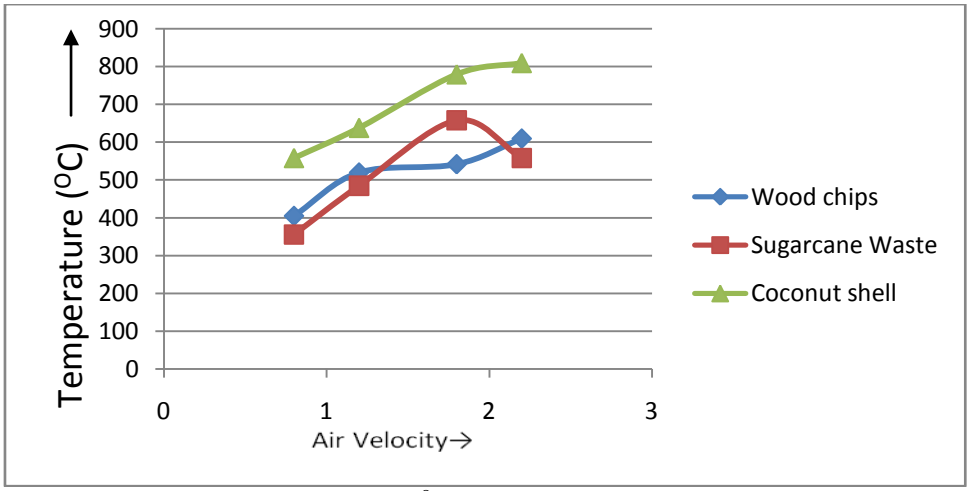

Fig 4.2: Comparison of *Reduction zone* temperature (^{o}C) for different biomass materials with constant variations of air velocity (m/s).

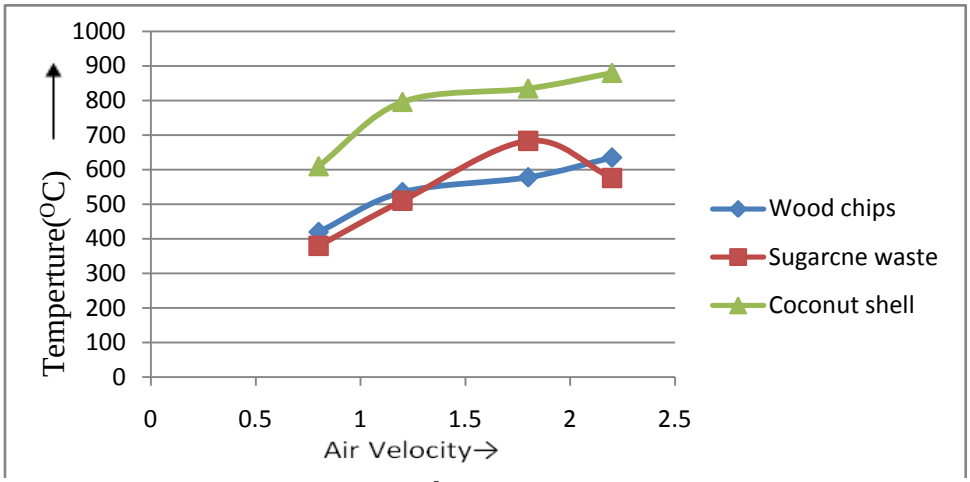

Fig 4.3: Comparison of *Combustion zone* temperature (^{o}C) for different biomass materials with constant variations of air velocity (m/s).

By analyzing the graph, it is found that, when the air velocity increases from 0.8m/sec. to 2.2 m/sec, the pyrolysis, Reduction, and combustion zone temperatures also increases gradually. The temperature of the pyrolysis zone varies from 315˚C to 785˚C at the constant variation of the air velocity. The Temperature of combustion zone varies from 380˚C to 880˚C at the similar variation of the air velocity. The Temperature of Reduction zone varies from 356˚C to 810˚C at the similar variation of the air velocity.

The combustion zone temperature depends upon the heat released due to the biomass combustion and air flow rate. The increasing in combustion zone temperature means that there is greater amount of oxygen takes provides by increasing air velocity but also brings inert N_2, which acts as a heat barrier and reduces the temperature of the combustion and pyrolysis zone. The maximum value of temperature in pyrolysis and combustion zone represents the optimum amount of biomass consumption rate. From the analysis of previous papers, it is assumed that, at the optimum amount of biomass combustion, the amount of carbon monoxide and hydrogen produced are maximum and the fraction of carbon dioxide is minimum.

V. Conclusion

The experimental analysis for different biomass materials clearly show that the coconut shell having the greater temperature for all the zones as compare to the other two, when the air velocity increases. Maximum temperature of the different zones for coconut shell represents the optimum amount of combustion. The energy released will increase the rate of drying and pyrolysis. Optimum amount of biomass consumption rate is not only due to a higher combustion rate, but also due to the enhanced pyrolysis and drying rate. So, the coconut shell is best suitable material for the above constructed updraft biomass gasifier as compare to the other two. The coconut shell is one of the waste biomass and easily available material.

References

[1] Pratik N. Sheth et al. (2009) -Experimental studies on producer gas generation from wood waste in a downdraft biomass gasifier. Bioresource Technology 100 (2009) 3127–3133.
[2] J.K. Ratnadhariya et al. (2010) - Experimental studies on molar distribution of CO/CO2 and CO/H2 along the length of downdraft wood gasifier. Energy Conversion and Management 51 (2010) 452–458.
[3] K. Sivakumar et al. (2010) - Performance analysis of downdraft gasifier for agriwaste biomass materials. Indian Journal of Science and Technology (Jan 2010) ISSN: 0974- 6846.
[4] Sarah Rowland et al. (2009) - Updraft Gasification of Salmon Processing Waste.Journal of food science E427.
[5] J.J. hernández et al. (2012) - Combustion characterization of producer gas from biomass gasification. Global NEST Journal, Vol 14, No 2, pp 125-132, 2012.
[6] Jeng-ChyanMutiLin (2006) -Development of an updraft fixed bed gasifier with an embedded combustor fed by solid biomass. Journal of the Chinese Institute of Engineers, Vol. 29, No. 3, pp. 557-562 (2006).
[7] V. N. Raibhole- Syngas Production By Updraft Biomass Gasifer And Its Parametric Analysis. IOSR Journal of Mechanical and Civil Engineering (IOSR-JMCE) ISSN (e): 2278-1684, ISSN (p): 2320–334X, PP: 56-62.
[8] Adnan Midilli, Murat Dogru, Colin R, Howarth Mike, Ling J and Teoman Ayhan (2001)-Combustible gasproduction from sewage sludge with a down draft gasifier. Energy Conservation & Management; 42, 157-172.
[9] Avdhesh K and Sharma R (2009) - Experimental studyon 75 KW the downdraft (biomass) gasifier system.
[10] Renewable Energy. 34, 1726-1733.
[11] Dogru M, Howarth CR, Akay G, Keskinler B and MalikAA (2002) - Gasification of hazelnut shells in a downdraft gasifier. Energy. 27, 415-427.
[12] Khater EMH, El-Ibiary NN, Khattab IA and Hamad MA(1992) Gasification of rice hulls. Biomass &Bioenergy. 3, 329-333.
[13] Pattarporn Chairprasert and Tharapong Vitidsant (2009)-Promotion of coconut shell gasification by Steam reforming on nickle-dolomite. Am. J. Appl. Sci.6 (2), 332-336.
[14] Paulo R. Wander and Carlos R (2004) - Assessment of a small saw dust gasification unit. Bio mass & Bio Energy. 27, 467-476.

International Journal of Modern Engineering Research (IJMER)
www.ijmer.com Vol. 3, Issue. 4, Jul. - Aug. 2013 pp-2062-2065 ISSN: 2249-6645

Acquisition of Long Pseudo Code in Dsss Signal

I. Anusha M. Tech[1], T. Sarath Babu., M. Tech[2]
Communication & Signal Processing G. Pulla Reddy College Of Engineering & Technology
Kurnool, A.P., India

ABSTRACT: *Rapid pseudo-code is widely used in spread spectrum communication system, because it has a large data rate and a strong anti-jamming property. But it brings us large of difficulty to acquire it as its long period. A new method is proposed to solve this problem in this paper, which is based on the excellent correlation characteristics of the long pseudo-code. The new method divides the local pn sequence into four subsequences, and then each of the sequence is overlapped and accumulated to form four new sequences. Through simple operation of addition, the four new sequences produce two combined sequences as the new reference sequences. At the same time, the received spread spectrum signal's sample rate is reduced to a quarter of the chip rate. Use the results to do correlation with the two new reference sequences to capture the synchronous pseudo-code. This method not only rapids the acquisition speed, but also improves the precision of frequency offset compensation.*

I. INTRODUCTION

Direct Sequence Spread Spectrum (DSSS) is the most typical spread spectrum communication style in military and civilian mobile communications system. One of the primary functions of DSSS receiver is to despread the received pseudo-code. This is accomplished by generating a local replica of the pseudo-code in the receiver and then synchronizing this local pseudo- code signal to the one which is superimposed on the received waveform.

The carrier of the direct-sequence radio stays at a fixed frequency. Narrowband information is spread out into a much larger (at least 10 times) bandwidth by using a pseudo-random chip sequence. The generation of the direct sequence spread spectrum signal (spreading) is shown.

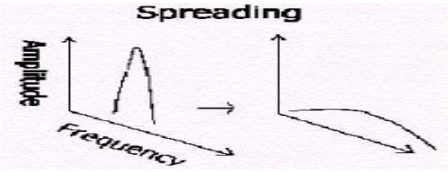

The narrowband signal and the spread-spectrum signal both use the same amount of transmit power and carry the same information. Synchronization of pseudo-code is unique in spread spectrum system, which includes two stages: acquisition and tracking.

At the receiving end of a direct-sequence system, the spread spectrum signal is de-spread to generate the original narrowband signal. **Figure** shows the de-spreading process.

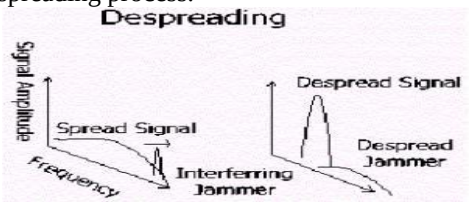

II. LINEAR FEEDBACK SHIFT REGISTER-TO GENERATE PN CODE

A *Linear Feedback Shift Register* (LFSR) is a mechanism for generating a sequence of binary bits. The register consists of a series of cells that are set by an initialization vector that is, most often, the secret key. The behavior of the register is regulated by a counter (in hardware this counter is often referred to as a ``clock''). At each instant, the contents of the cells of the register are shifted right by one position, and the XOR of a subset of the cell contents is placed in the leftmost cell.

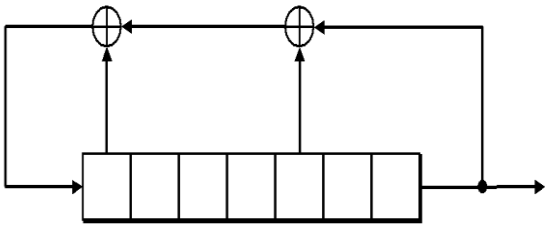

Figure : Linear Feedback Shift Register

III. RAPID ACQUISITION OF PSEUDO-CODE

To enhance the acquisition speed of pseudo-code and improve the precision of frequency offset compensation, algorithm is presented. Sample the input signal at a quarter of chip rate, divide the local pseudo-code into four subsequences, overlap and accumulate each subsequence to form a new sequence, and then use them to form two combined reference sequences. Do correlation of the two combined reference sequences with the input signal sequence to capture the synchronous pseudo-code. Fig. 1 gives the block diagram of this algorithm.

IV. ALGORITHM

In this paper, the rapid acquisition algorithm includes the following three parts

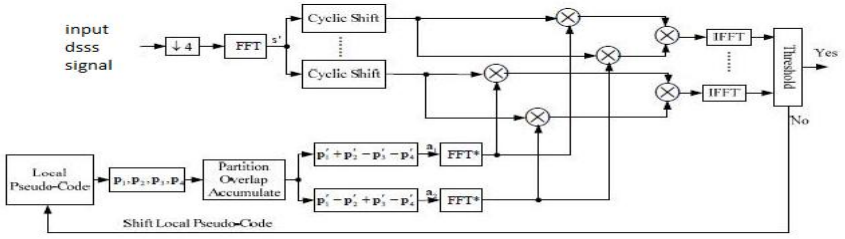

Figure 1. Block diagram of the algorithm

1) Input Signal Processing:

a) Do down-conversion of the input signal and sample it at a quarter of the chip rate.

b) Pick up *L* points of the sampled sequence, and define as $s = (s_1, s_2, s_3, s_4, \ldots\ldots\ldots s_{L-1}, s_L)$

c) Calculate *L* -point FFT for sequence s to get s' .

d) According to the scope of frequency offset, do 2*n* times cyclic shift of the sequence s' , *n (=10)*times to the left and *n(=10)* times to the right respectively, and get 2*n* +1 frequency offset compensation sequences

2) Local Pseudo-Code Processing:

a) Pick up 4*ML* points local pseudo-code, define as

$p = (p_1, p_2, p_3, p_4, \ldots\ldots\ldots, P_{4Ml-3}, P_{4Ml-2}P_{4Ml-1}P_{4Ml})$, and divide it into four subsequences as follows:

$p_1 = (p_1, p_5, p_9, p_{13}, \ldots\ldots, p_{4ML-3}).$

$p_2 = (p_2, p_6, p_{10}, p_{14}, \ldots\ldots, p_{4ML-2}).$

$p_3 = (p_3, p_7, p_{11}, p_{15}, \ldots\ldots, p_{4ML-1}).$

$p_4 = (p_4, p_8, p_{12}, p_{16}, \ldots\ldots, p_{4ML}).$

b) Respectively partition the subsequences p_1, p_2, p_3, p_4 into *M* segments, and each of segments has length *L* . Overlap and accumulate the *M* segments, and get p_1', p_2', p_3', p_4'

c) Do the simple operation $a_1 = p_1', p_2', p_3', p_4',\ a_2 = p_1' - p_2' + p_3' - p_4',$

and get two combined reference sequences.

d) Calculate the conjugate of *L* -point FFT for a_1, a_2 and get sequences a_1', a_2'

3) Judgment:

a) Multiply the results a_1', a_2' by each frequency offset compensation sequence, and then do *L* -point IFFT to get $2(2n+1)$ correlation results sequences.

b) Detect the correlation peaks of the correlation results sequences, and compare the maximum peak of them with the threshold.

c) If the maximum correlation peak is above the threshold, decide that the synchronous pseudo-code is in the searching scope this time. Record the corresponding frequency offset compensation sequence's number *l* , here we name the sequence s_l' optimum frequency offset compensation sequence, and s_l s is the IFFT of s_l' .

d) Multiply s_l' by a_1', a_2', denote the IFFT of the results as b_1, b_2 , mark the two peaks in them as c_1, c_2 . Find out the subsequences according to the product of c_1, c_2

e) If $c_1, c_2 > 0$ the synchronous pseudo-code is in sequences p_1', p' , p_1, p_4 do correlation with s_l respectively to find out the matched sequence, and make the *M* segment in it do correlation with s_l further. Detect the correlation peak and find out the matched segment according to it, record the location of the peak. Contrarily, if $c_1, c_2 < 0$, the synchronous pseudo-code is in sequences p_2', p_3' .

f) However, if a correlation peak above the threshold not be detected, shift $(4M-1)L$ chips of the local code orderly, repeat the above process. When the optimum frequency offset compensation sequence's number is l , the frequency offset compensation value will be $f_1 = lf_s / 4L$. Supposing that the peak is in the j -the segment the k -the point of subsequence p_i , we can decide the synchronous point in p_i is $I = (M-j)L + (L-k) + 2.$ Consequently, the synchronous point in the local code is $J = (I-1)\times 4 + i = [(M-j)L + (L-k) + 1] + i.$ This means the code delay is J-1 .

B. Acquisition Speed and Precision of Frequency Offset Compensation Analysis

From the acquisition process above we can find out the two subsequences in which the synchronous pseudo-code exists according to the value of c_1, c_2 . If $c_1, c_2 > 0$, the synchronous pseudo-code is in the sequences p_1, p_4 . On the Contrary, if $c_1, c_2 < 0$, the synchronous pseudo-code is in the sequences p_2, p_3 . Therefore, the searching scope of the subsequences from four reduces to two, and the precision of frequency offset compensation increases four times.

V. SIMULATION AND RESULTS

In this paper, we use the MATLAB simulation to verify and discuss the acquisition performance of the new algorithm.Select a pseudo-code sequence whose period is 16384, and assume the frequency offset f_d is 800Hz and pseudo-code delay τ is 650 chips. After do analog down-conversion of the input signal, sample it at a quarter of chip rate which equates to 1MHz. Select 1000 points of the sampled sequence. Pick up 8000 chips of local pseudo-code, divide them into four subsequences according to the acquisition process 2 and then divide each subsequence into 2 segments. After that, the length of each segment L is 1000 points, the precision of frequency offset compensation f_{prec} is 250Hz, and the searching scope of local pseudo-code is 8000 chips a time.

A. Optimum Frequency Offset Compensation Sequence

Do cyclic shift of the sequence s' . The number of shift to left and to right is both ten. The frequency offset compensation value is negative when shifting to the left, while the value is positive when shifting to the right. Multiply each of the frequency offset compensation sequences by a_1', a_2' respectively, and then get the correlation results sequences by IFFT, detect the correlation peak in each of them, find out the largest correlation peak above threshold and the optimum frequency offset sequence.

Spectrums of all the signals On x-axis-amplitude &y-axis-index

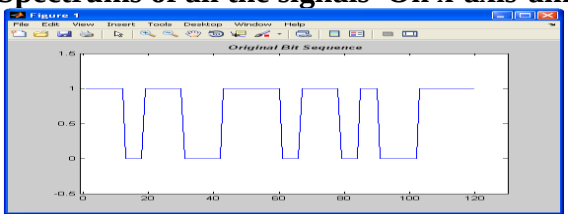

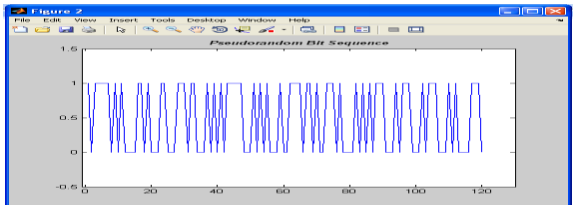

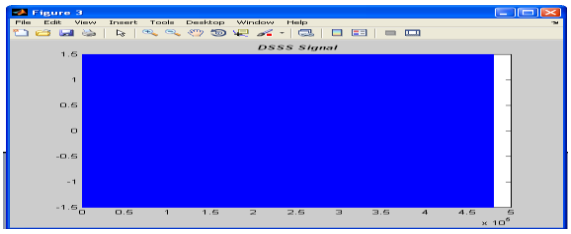

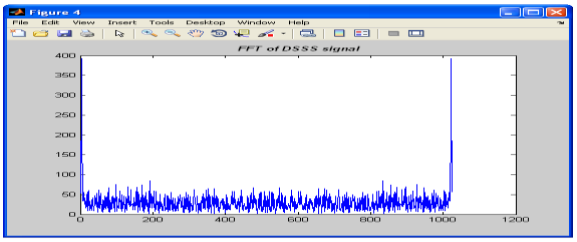

The peak, mentioned here and below, is the absolute value of the real part of complex correlation value. As is evidence from it we can know that the largest peak corresponds to the sequence -3, so the optimum frequency offset sequence is s'_{-3} , the frequency offset compensation value f_l and the residual frequency offset d | $f_d - | f_l \|$ is 50Hz.

B. Detect the Synchronous Pseudo-Code.

Multiply sequence s_{-3} by a_1', a_2' separately. And then through IFFT get the correlation results sequences of s_{-3} with a_1, a_2 . Fig. 3 shows the correlation results of s_{-3} with a_1 , and Fig. 4 is the results of s_{-3} with a_2 .

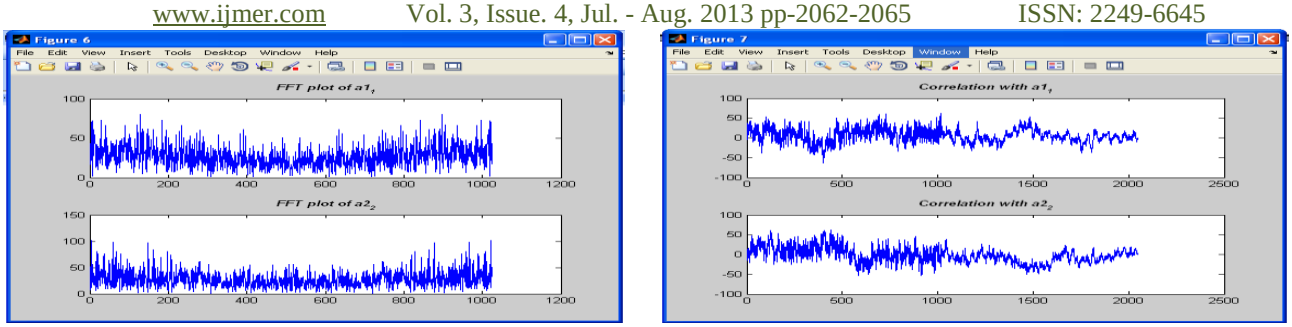

Figure Correlation results of s_{-3} with a1 anda2.

From the figures we can know that the peaks appear at the point of P(=839), and the product of the two peaks is negative. Therefore, according to the acquisition process 3), we can know that the synchronous pseudo-code is in the sequences of p_2', p_3'. Make the sequence s_{-3} s do correlation with p_2', p_3' respectively. Find that the peak appears in sequence p_3'. Then make the 2 segments in p_3 do correlation with s_{-3} separately. Find that the synchronous pseudo-code appears at the first segment. So the synchronous spseudo-code in p_3 is at the point $i=(M-1)L+(L-839)+2=163$ the synchronous point in the local code is $j=(i-1)\times 4+3=651.$ This means the delay in local code is 650 chips, so the results are agree with what we have designed.

VI. CONCLUSION

This paper proposes a new method to rapidly capture the long period pseudo-code in DSSS communication systems.Through reducing the sample rate to a quarter of the chip rate, the precision of frequency offset compensation improves At the same time, doing partition overlapping accumulation to the four subsequences of local pseudo-code, not only extends the searching scope, but also rapids the acquisition speed fast Computer simulation proves that this method has a good acquisition property.

VII. ACKNOWLEDGMENTS

This work is supported by the NSAF Foundation (No.10776040) of National Natural Science Foundation of China, the National Natural Science Foundation of China (No.60602057),the Project of Key Laboratory of Signal and Information Processing of Chongqing (No.CSTC 2009CA 2003), the Natural Science Foun-dation of Chongqing Science and Technology Commission (No.CSTC2009BB2287), the Natural Science Foundation of Chongqing Municipal Education Commission (No.KJ060509, KJ080517), and the Natural Science Foundation of Chongqing University of Posts and Tele-communications (CQUPT) (A2006-04,A2006-86).

REFERENCES

[1]. Yang C, Vasquez J, and Chaffee J. "Fast Direct P(Y)-Code Acquistion Using XFAST"[C], Proceedings.of ION GPS-99.Nashville, Sept.1999. pp. 317-324.
[2]. Jing Pang, Frank Van Graas, Janusz Starzyk, and Zhen Zhu. "Fast direct GPS P-Code acquisition"[C]. GPS Solutions. Vol. 7, Dec. 2003. pp.168- 175.
[3]. Minghao Tian, Yongxin Feng, and Chengsheng Pan. "Research of a Method of Diret Acquisition Based on P Code in Frequency Domine"[J].Acta Electronica Sinica. Vol. 35,No.3, Mar. 2007. pp. 549-552.
[4]. Tianqi Zhang, Zhengzhong Zhou, Xiaokang Ling, and Zengshan Tia "Approach to Blind Estimation of Lower SNR Long Code DS Signal"[J]. Signal processing. Vol. 24, No. 3, Jul. 2008. pp. 370-376.
[5]. Na Wang, Bangning Zhang, and Guomin Zhang. "Direct Acquisition Technique for GPS P(Y)-code"[C]. Wireless Communications,Networking and Mobile Computing , WiCom. Sept. 2007. pp.2985-2987.
[6].] Yaan Ren, Peng Wang, Weidong Xu, and Xinmei Wang. "Research development of the technique of direct P(Y)-code acquisition in GPS"[C]. GNSS world of China. Vol. 8, No.2, 2003. pp. 2-9.

International Journal of Modern Engineering Research (IJMER)
www.ijmer.com Vol. 3, Issue. 4, Jul - Aug. 2013 pp-2066-2072 ISSN: 2249-6645

CFD Simulation on Gas turbine blade and Effect of Hole Shape on leading edge Film Cooling Effectiveness

Shridhar Paregouda[1], Prof. Dr. T. Nageswara Rao
[1] *M. Tech Student, Oxford College of Engineering,Bangalore – 560068, Karnataka*
[2] *Professors, Department Of Mechanical Engineering, Oxford College of Engineering, Bangalore– 560068, Karnataka*

ABSTRACT: *In order to raise thermal efficiency of a gas turbine, higher turbine inlet temperature (TIT) is needed. However, higher TIT increases thermal load to its hot-section components and reducing their life span. Therefore, very complicated cooling technology such as film cooling and internal cooling is required especially for HP turbine blades. In film cooling, relatively cool air is injected onto the blade surface to form a protective layer between the surface and hot mainstream gas. The highest thermal load usually occurs at the leading edge of the airfoil, and failure is likely to happen in this region. Film cooling is typically applied to the leading edge through an array of hole rows called showerhead. In this project initially benchmarks study the current state of heat transfer prediction for commonly used CFD software ANSYS Fluent. The predictions Reynolds-Averaged Navier-Stokes solutions for a baseline Flat film cooling geometry will be analyzed and compared with experimental data. The Fluent finite volume code will be used to perform the computations with the realizable k-ε turbulence model. The film hole is angled at 30° to the crossflow with a Reynolds number of 17,400. The focus of this investigation is to investigate advanced cooling hole geometries on film cooling effectiveness over flat surface. Three film-cooling holes with different hole geometries including a standard cylindrical hole and two holes with a diffuser shaped exit portion (i.e. a fanshaped and a laidback fanshaped hole) will be studied. Finally optimized shape of the hole configuration is included in NASA Mark II vane turbine geometry to study heat transfer characteristics of blade.*

I. INTRODUCTION

The continuous improvement in the performance of air-breathing propulsion systems necessitates a continuous increase in the turbine inlet temperatures. This, coupled with the demands of reduced size of the combustors, has put a significant burden on turbine technology. Since the inlet temperatures of present generation gas turbines are much higher than the melting temperatures of the available alloys used to make the turbine blades, cooling of the blades is a critical issue in turbine technology. The development of turbine inlet temperatures is shown in Fig 1. Improvements in blade materials have allowed an increase of melting point around 200° and use of turbine cooling has allowed an increase of approximately another 250°, which allow turbine inlet gas temperature above the melting points of the materials used [1-2].

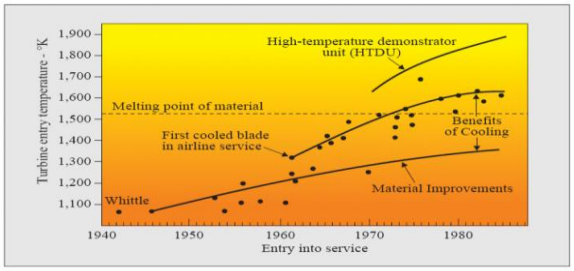

Fig.1 Development of Turbine Inlet Temperature [2]

Various internal and external cooling techniques are employed to bring down the temperature of the blade material below its melting point. As shown in Fig. 2 in internal cooling, relatively cold air is bypassed from the compressor and passed through the hollow passages inside the turbine blade. In external cooling, the bypassed air is exited out through small holes at discrete locations of the turbine blade. This relatively cold air creates a protective blanket that saves the turbine blade from the harsh environment. This type of cooling is called film cooling.

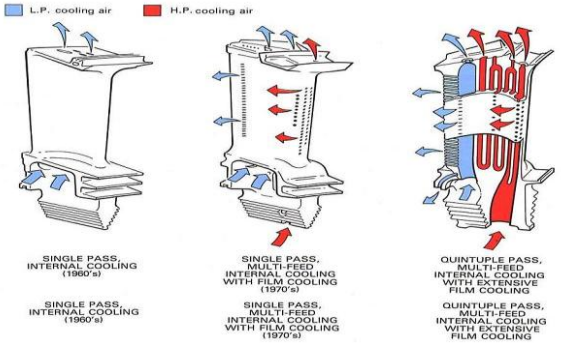

Fig.2 Cooling concepts of a modern multi-pass turbine blade [3]

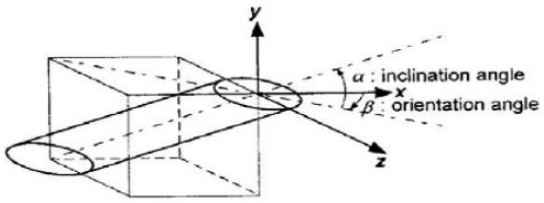

Fig.3 Compound Hole Configuration [6]

Flat surface models can be used to study the effects of individual parameters with relative ease and are less expensive. Early studies have proved that the results obtained on simple flat-surface models can be applied to real engine design with slight corrections. The effects of geometrical parameters (hole geometry, shape, size, spacing) and flow parameters (coolant-to-mainstream mass flux, temperature ratio, mainstream Reynolds number, velocity, etc.) have been studied on flat surface. Also, the effects of pressure gradient and curved surface have also been studied. Some studies have focused only on the heat transfer coefficient enhancement and others have presented only film effectiveness results. Heat transfer coefficient downstream of the film injection is enhanced due to increased turbulence produced by mixing if the coolant jets with the mainstream boundary layer. This increased turbulence locally enhances the heat transfer coefficients. The effect of the coolant jet decreases downstream of injection as the jet structure dissipates and the mainstream dominates the coolant film completely. The high heat transfer coefficient in the near injection region is due to the three-dimensional nature of the jet, and far downstream (x/D>15), the jet structure is completely absent and is two-dimensional in nature. The heat transfer coefficient ratio decreases with increasing axial distance from the injection hole. About 15-hole diameters downstream of injection, the film cooling effect disappears. The heat transfer coefficient ratio is almost equal to unity.

There is a large body of existing literature on film cooling efficiency with the effect of hole geometry. Some of these studies compared simple angle holes with compound angle holes. The compound angle injection hole has two injection angles, as shown in Fig 1.6. The inclination angle (α) is defined as the angle between the injection vector and its projection on the x–z plane, whereas the orientation angle (β) is defined as the angle between the streamwise direction and the projection of the injection vector on the x–z plane. In the compound angle orientation system, the coolant is injected with a spanwise momentum, which provides more uniform film coverage and shows higher heat transfer coefficient enhancement.
The motivation behind this study is to develop and test innovative film cooling hole geometries on film cooling heat transfer and cooling effectiveness over flat and turbine airfoil surfaces. The basic aim of these proposed geometries is to alter the mainstream to directly contact the test surface. Simulations will be conducted to study the effect of hole embedded in transverse slots and hole exit area. Several variations of geometry will be investigated to assist in future design changes. Also, the numerical prediction using FLUENT was performed to determine the jet mainstream interactions to better understand the interaction between the ejected coolant and the second flow and also the surface film effectiveness distributions.

Schmidt et al. [11] measured the film cooling effectiveness using a single row of inclined holes, which injected high-density, cryogenically cooled air. They reported that 60 deg orientation angle injection at a high momentum flux ratio results in higher effectiveness values than streamwise-directed holes. The forward expansion hole with compound angle orientation showed significantly improved effectiveness.

Ekkad et al. [12] provided effectiveness results for two different density ratios. The adopted orientation angles were 0, 45, and 90 deg. using the transient liquid crystal technique, they reported that compound angle injection produces higher film effectiveness than simple angle injection for both density ratios. They concluded that the highest effectiveness was obtained at a mass flux ratio of 1.0 for compound angle injection.

Ammari et al. [13] also presented the effect of density ratio on heat transfer coefficient contours downstream of a film hole inclined 35° along the streamwise direction for two different coolant-to-mainstream density ratios of 1.0 and 1.52 for a coolant blowing ratio of M=1.46. Differences of 10% occurred when coolant densities were changed. It was observed that lower-density injectant provides higher heat transfer coefficient at the same blowing ratio due to higher momentum.

Bons et al.[14] studied the effect of high stream turbulence on film cooling effectiveness. At high free stream turbulence, heat transfer coefficients with film cooling are not as significantly as the film effectiveness. Film injection by itself produces high heat transfer coefficient enhancement due to high turbulent mixing between jet mainstream. Several investigators have studied the slot film cooling. Blair [15] investigated the slot film cooling at the entry of a vane cascade endwall. Chyu [16] et al. provided film effectiveness measurements downstream of 2-D slots modeled as gasp leakages, both aligned and misaligned. Bunker [17] investigated film effectiveness for geometries wherein the coolant from discrete holes enters a slot before mixing with the mainstream. Basically, the angled holes are entrenched in a shallow trench. The holes embedded in the trench provided higher film effectiveness distributions than the ones on the plane surface. However, Bunker [17] provided only film effectiveness distributions and also the hole had a compound angle (radial injection) in the lateral direction. Bunker [17] based their study on an earlier study by Wang et al. [18]. Lu et al.[19] studied the effect of trench exit area and edge shape on film cooling performance using an IR thermography method. Their results showed that the film cooling holes provide higher film effectiveness when embedded in a trench. However, in some geometries when the trench began at the upstream edge of the hole, the film effectiveness diminished. The heat transfer coefficient enhancement due to the embedding was not significantly higher compared to the typical unembedded cylindrical hole. The overall heat flux ratio

comparing film cooling with embedded holes to unembedded holes shows that the full trench and downstream trench spacing after the hole exit produce the highest heat flux reduction.

II. CFD SIMULATION OF FLAT PLATE FILM COOLING

In order to obtain better design in CFD, The mixing of a 3D cooling hole in a turbulent flow is more complicated to analyze than in the 2D slot. Downstream of the hole, the air flow usually form circular motions or vortices when a jet enters at high angle or when the jet velocity is higher the than main stream velocity. Figure below shows a schematic of this phenomenon. Note there are wake vortices between the jet and wall top surface that would affect heat transfer between them.

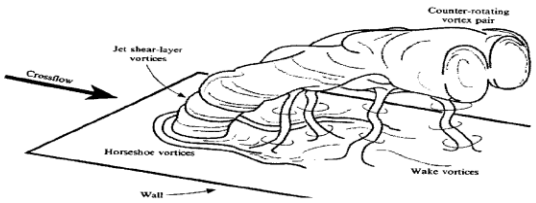

Fig.4 Flat plate Film cooling

There are many factors involved when designing an optimized cooling hole pattern such that the expense of provide cooling air flow to these holes is minimized while providing adequate reduction in metal temperature. The diameter, length, surface angle, and arrangement of holes against the hot gas flow direction are important geometric parameters in designing these holes. Besides, the clearance to internal cooling passage walls and practical manufacturing methods are also important considerations. However, this project will only study on the effect of the geometric parameters on the cooling holes effectiveness.

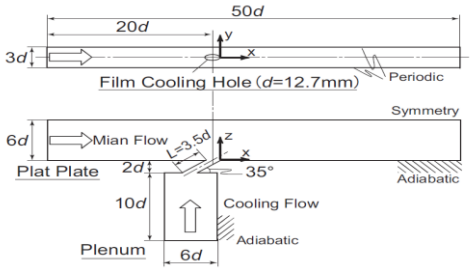

Fig.5 Computational domain

The geometry for the annulus is created in ANSYS Design Modeler and meshing is done in ANSYS Meshing, with grid size 150x150 as shown in Fig 1.4. The mesh nearby to walls is fine meshed to cope-up the thermal and velocity boundary layer formation and at the centre it is coursed meshed.

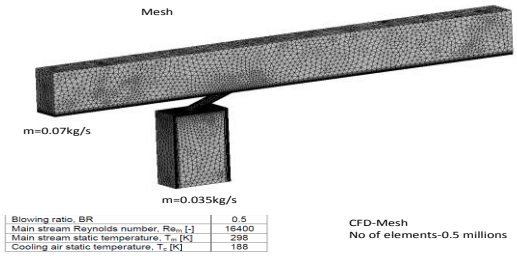

Fig.6 Boundary conditions and CFD Meshing

A tetrahedral grid is used in this study to allow the highest quality in all regions with the prism boundary layers. In this way, the computational domain can be partitioned into several subsections. Jet Cooling hole, mainstream flow duct and other three in the channel. Each section is meshed with appropriate topology. In order to resolve the mean velocity, mean temperature, heat flux and turbulent quantities in the viscosity-affected near wall region (Rey <200) accurately, the near wall turbulence model requests that y+ value at the wall-adjacent cell should be the order of one and there are at least 4 ten cells in this region. So in the hole and the region near the test wall the density of cells is identified to satisfy this requirement. After a series of tests and adjustments the final adopted grid for calculations is obtained. Total no of elements is 0.5 millions.

III. RESULTS AND DISCUSSIONS

Figure 7 shows the jet at the hole exit by means of contours of velocity at XY-plane going through the first row hole. Indeed, they are utilized to illustrate how the jet will interact with freestream flow for 0.5 blowing ratio. At the hole exit there is also strong recirculation zone for low BR. By increasing the coolant mass flow this zone starts to be dissipated, see recirculation zones. Below this zone higher temperature compared with the temperature of recirculation can be seen, which can be seen from contours of temperature, figure 9 at the hole exit. In addition, as BR raises and the jet will become stronger, the lift is increased and the coolant will be detached from the surface. As a result at this region, close to the hole for high BR higher temperature can be seen increase further. Fig. 6 shows the Temperature contours at 45 and 90 min. Fig 7, 8

and 9 shows the velocity vectors in evaporator, adiabatic and condenser section. It shows the in adiabatic section the velocity constant and compared to other section.

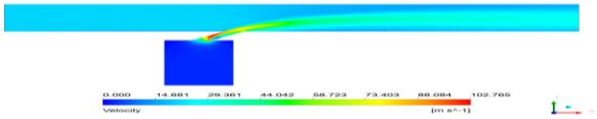

Fig. 7 Pressure contours of film cooling

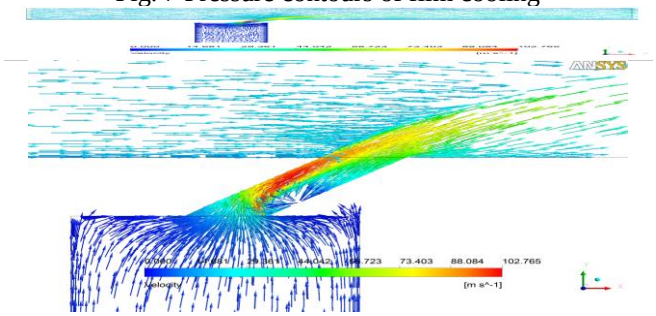

Fig.8 Velocity vectors contours of film cooling

Fig.8 velocity vector map at the slot exit is indicates. After the jet leaves the slot, air particles have high velocity and are projected deep into the main stream, especially those near the right wall of the slot. This band of high velocity sub-stream creates a boundary between the hot main stream and the cooling jet stream. Below this boundary, the mixing air moves relatively slow and circulates around creating a stagnation region.

Fig. 9 Velocity vectors at adiabatic section

Figure 9 shows the temperature contours for the 35 degree slot model with refined mesh. Due to it vertical entrance, the cooling jet disturbs the hot stream strongly and creates a large mixing region high above the alloy surface. So the cooling effect is contained in the air and leaves the heat transfer into the alloy to a minimal level. The cooling jet doesn't create a film after it exits the slot so the effective cooling film length is zero. However, the temperature contours show that the jet does reduce the alloy top surface temperature in some amount, about 100K after a distance 1D.

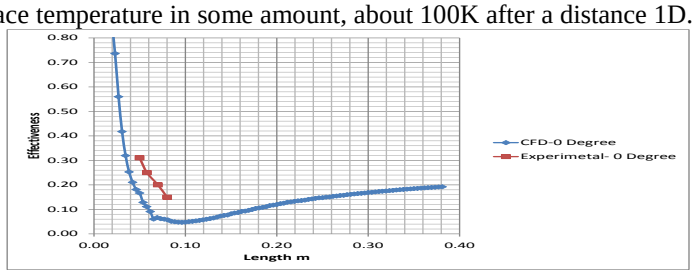

Fig. 10 Comparison of film cooling effectiveness

Averaged film cooling effectiveness at BR=0.5. The k-ω SST model was adopted in the RANS simulations Fig.5.7. The results of previous experiments [39] are also plotted in the figure. Experimental conditions of the reference [39] are almost identical to the present computation. Good agreement is shown among the numerical results except just downstream of film cooling hole.

IV. OPTIMIZATION OF ANGLE

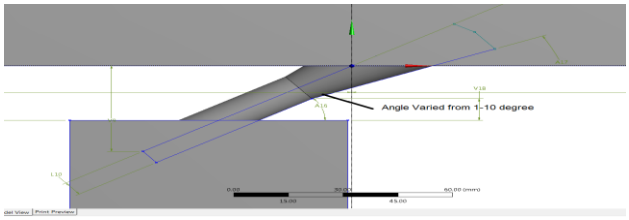

Fig. 11 Optimization of Angle

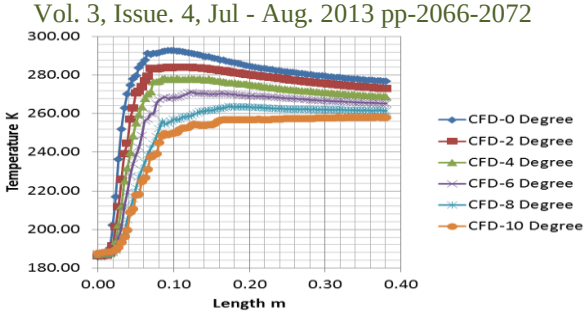

Fig.12 Comparison of Temperature contours of film cooling-0-10^0

The Tw is evaluated by taking the average of all temperature values at nodes along the top surface of the alloy after the slot exit, 0.381m downstream, the same for all models to get a consistent comparison. Table 3 lists the alloy surface average temperature reduction. This temperature reduction is the difference between the Tw and the averaged temperature values along the top the alloy top surface before the slot. And finally, the average cooling film effectiveness or □is calculated per the formula above. The higher □means the cooling film is more effective, with the ideal max value of 1. As expected, the model with 10 degree exit angle gives the best film effectiveness. Also, the table shows the difference in results between coarse and fine meshes. In general, fine mesh produces slightly lower values except the case of 10 degree exit angle. The 10 degree exit angle, in practice, has been used widely in practical applications, such as turbine airfoils. Figure 18 shows temperature contours for the 10 degree exit angle. The cooling film is thin and attaches right after the jet exits the slot, producing a long cooling thermal layer above the alloy surface. The film length where the cooling jet effectively maintains its coolant temperature, shown in dark blue, is approximately 7D. In the case of 8 degree exit angle, this length is 4.5D while the 0 degree exit angle produces no length because the cooling jet detaches from the alloy surface as soon as it leaves the slot. The temperature contours in the alloy shows most of the alloy benefits from the temperature reduction due to the cooling film, with the average temperature reduction of 249K on top surface

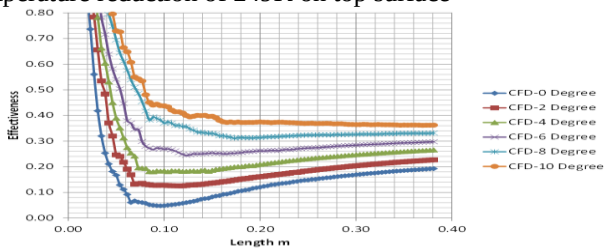

Fig. 13 Comparison of Effectiveness contours of film cooling-0-10^0

V. CFD ANALYSIS OF C3X VANE

The experimental data for validation of the conjugate simulation of flow and heat conduction need to provide clear boundary conditions and cooling air flow rates of high accuracy. The C3X transonic turbine guide vane was selected as the test case, for this work provides detailed measurement of the external and internal convection and the metal surface temperature. The experimental facility consisted of a linear cascade of three C3X turbine vanes.

The computational domain included one vane in the middle of the flow field, with periodic boundary conditions employed to simulate cascade flow as shown in Fig.14. The computational domain inlet is located one chord length upstream of the leading edge, where the turbulence level was measured in the experiments. The outlet is located one chord length downstream of the trailing edge. Meshes are created for the hot gas path and the solid vane. Geometry is created in DM create computational domain. The Extracted fluid domain of C3X vane as shown in Fig.14

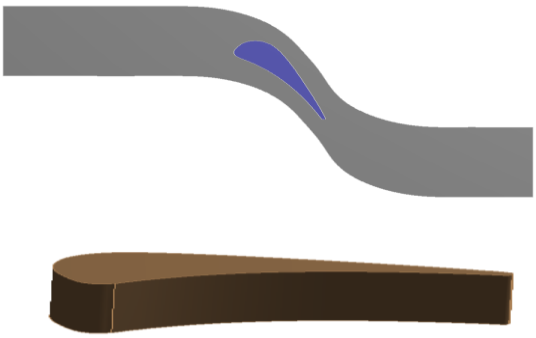

Fig. 14 C3X Turbine Vane

Fig.15 Turbine Blade Meshing

The 3D simulation used unstructured grid (shown in figure 15), increasing the grid density around wall in the fluid domain and the solid domain. Total number of elements was 0.6. Total number of elements in the fluid domain was 3121480 and total number of elements in the solid domain was 2laks. The boundary conditions were shown in table 3. The boundary conditions of cooling channel were given cooling temperature and total pressure boundary conditions.

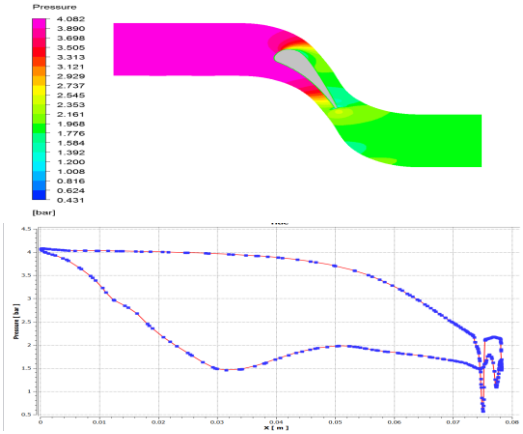

Fig.16 Contours of static Pressure at mid plane

Fig 16 shows the pressure distribution on mid plane of Gas turbine vane. On the suction side (SS), the gas flow accelerates rapidly from the stagnation point toward the throat, reaching the maximum speed around 500m/s. The flow then decelerates until the location around 65 % chord, before resuming a mild acceleration toward the trailing edge (TE). The flow is under a favorable pressure gradient on the entire pressure side (PS). The pressure stays almost constant near P0 from the LE to about 50% chord. and then falls off with further distance toward the TE as shown in Fig.16.

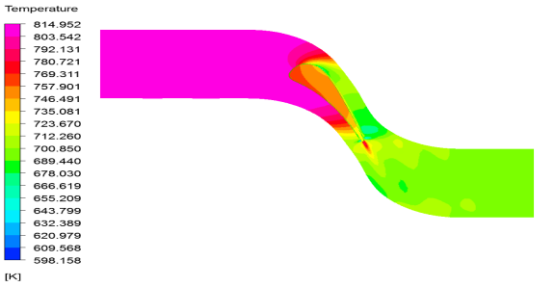

Fig.16 Contours of Temperature at mid plane

7. Shower head cooling

In the drive to increase cycle efficiency, gas turbine designers have increased turbine inlet temperatures well beyond the metallurgical limits of engine components. In order to prevent failure and meet life requirements, turbine components must be cooled well below these hot gas temperatures. Film cooling is a widely employed cooling technique whereby air is extracted from the compressor and ejected through discrete holes drilled in the surface of turbine airfoils, tips, and end walls. The air leaving these holes forms a film of cool air on the component surface which protects the part from hot gases exiting the combustor.

The showerhead-cooled vane used in this study had five rows of staggered cylindrical holes. The center row was placed at the geometric stagnation point while the remaining rows were spaced at four and eight hole diameters on either side. A cylindrical plenum supplied air to all five rows, and each row was spaced three hole diameters apart within the plenum as seen in Figure.17. The analysis is carried out for below conditions. The colling hole mass flow rate

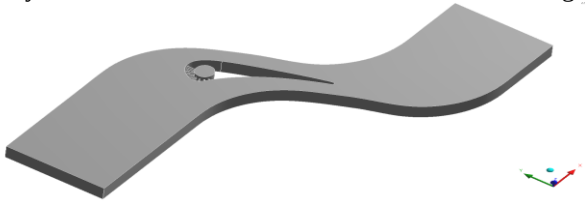

Fig.17 C3X vane with shower head cooling Hole

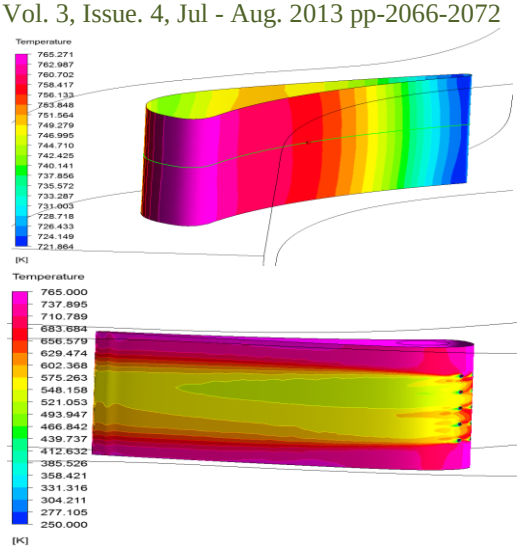

Fig.18 Temperature contours-With and without showerhead cooling holes

VI. CONCLUSIONS

Turbine blade edge regions, including blade tip, leading edge and the platform, experience a high heat load. The earliest film-cooling correlations were made for continuous slot cooling configurations. The slot correlations were then extrapolated to discrete hole film-cooling with cylindrical holes. Advances in film-cooling technology have led to the extensive use of shaped non-cylindrical exit holes in turbine applications. Numerical investigations have been applied on the flow and film cooling for these critical regions. The compressible Navier-Stokes equations, K-epsilon turbulence model together have been solved by Fluent in these studies. . The film hole is angled at 30° to the cross-flow with a Reynolds number of 17,400. It shows the film cooling effectiveness tends to be under-predicted in the value. 3D CFD models of the film cooling processes have shown that by increasing the exit angle of the cooling hole would increase the film effectiveness and in turn reduce the alloy surface temperature. Outside this study, many research and experiment papers analyzed a 30 degree angle with possible lateral compound angle to optimize film coverage. The main interest in other experiments has been the flow field of the cooling jet mixing with main stream while heat transfer is secondary. However, many results of this study are in good agreement with published work.

In all models studied, the 35 degree exit angle in 2D slot model reduced the alloy surface temperature by 15% while in 3D discrete hole model the film coverage length is 9D for 100K (6%) temperature reduction. In reality, the machine used for hole drilling (usually laser) and complex 3D surfaces of the part are the factors limiting the exit angle to be around 30 degrees. For additional heat transfer benefits, a lateral angle in combination with incline (exit) angle and a diffuser at hole exit should be used to give more film coverage.

Then the the showerhead-cooled vane used in this study had five rows of staggered cylindrical holes. The center row was placed at the geometric stagnation point while the remaining rows were spaced at four and eight hole diameters on either side. A cylindrical plenum supplied air to all five rows, and each row was spaced three hole diameters apart within the plenum. This shows 200K reduction in temperature compared to without cooling hole model.

REFERENCES

[1]. http://www.andrew.cmu.edu/
[2]. Friedrichs, S. “Endwall Film-Cooling in Axial Flow Turbines” Cambridge University Dissertation, 1997
[3]. Han, J.C., Park, J.S., and Lie, C.K., 1984. “Heat Transfer and Pressure Drop in Blade Cooling Channels with Turbulence Promoters.” Texas A&M University (prepared for
[4]. NASA CR-3837)
[5]. Hay, N. and Lampard, D., 1996, “Discharge Coefficient of Turbine Cooling Holes: A Review.” ASME paper 96-GT-492
[6]. Goldstein, R.J., 1971. “Film Cooling” In *Advancement in Heat Transfer.* Academic Press, New York, Vol.7, pp321-379
[7]. Lin, Y.Z., Song, B., 2006, “Measured Film Cooling Effectiveness of Three Multihole Patterns”, *Journal of Heat Transfer*, Vol. 128, pp.192-197
[8]. Jung, I.S., Lee, J.S., 2000, “Effects of Orientation Angles on Film Cooling Over a Flat Plate: Boundary Layer Temperature Distributions and Adiabatic Film Cooling Effectiveness”, *Journal of Turbo machinery*, Vol.122, pp. 153-160
[9]. Goldstein, R. J., Eckert, E. R. G., Eriksen, V. L., and Ramsey, J. W., 1970, “Film Cooling Following Injection Through Inclined Circular Tubes,” *Israel Journal of Technology*, Vol.8, No. 1–2, pp. 145–154.
[10]. Mehendale, A.B., Han, J.C. and Ou, S., “Influence of High Mainstream Turbulence on Leading Edge Heat Transfer,” *ASME Journal of Heat Transfer*, Vol. 113, November 1991,pp. 843-850.
[11]. Honami, S., Shizawa, T., and Uchiyama, A., 1994, “Behavior of the Laterally Injected Jet in Film Cooling: Measurements of Surface Temperature and Velocity/ Temperature Field Within the Jet,” *ASME Journal of Turbo machinery*, Vol. 116, pp. 106–112.
[12]. Schmidt, D. L., Sen., B., 1996, “Film Cooling With Compound Angle Holes: Adiabatic Effectiveness,” *ASME Journal of Turbo machinery*, Vol.118, pp. 807–813.
[13]. Ekkad, S. V., Zapata, D., and Han, J. C., 1997, “Film Effectiveness Over a Flat Surface With Air and CO2 Injection Through Compound Angle Holes Using a Transient Liquid Crystal Image Method,” *ASME Journal of Turbo machinery*, Vol.119, pp. 587–593.103.

International Journal of Modern Engineering Research (IJMER)
www.ijmer.com Vol. 3, Issue. 4, Jul - Aug. 2013 pp-2073-2078 ISSN: 2249-6645

Visual Quality for both Images and Display of Systems by Visual Enhancement under Low-Backlight

[1]M. Padma Sailaja, [2]M. Sirisha
[1, 2,] *M. Tech Student, Assistant Professor Dept. Of ECE, DVR&DHS MIC College of Technology, Kanchikacherla, A.P, India*

ABSTRACT: *Visual enhancement techniques provide different approaches for improving visual quality of displays under Low backlight conditions for saving the battery. The existing techniques provide the visual quality may be for noise free images only. This method proposes an algorithm that provides the visual quality for both images and display of systems even the images are corrupted with the noise under low backlight.*

This method first proposes a median filter for removing the impulse noise which is the salt and pepper noise. Then using dilation method of morphological operations for providing better growth or thickness of images so that if any breaks in a image it will be repaired. Then designing a linear spatial filter which is the laplacian operator for sharpening of the image used to enhance the details of an image that has been blurred. After that constrained L0 gradient image decomposition is used for separation of base layer and detail layer, and also median-preserving gamma correction is used to alter the output levels of a monitor and a JND-based Boosting for detail enhancement. Experimental results show that this approach performs better than the existing methods.

KEYWORDS: *Median filter, Dilation operation, Laplacian operator, Constrained L0 gradient image decomposition, Median-preserving gamma correction, Low backlight display, Just-Noticeable Difference (JND).*

I. INTRODUCTION

DISPLAYS are known to be among the largest power consuming components on a modern mobile device like Touch screens and pad-like devices. Now a days the needs of displays increases. The battery life of displays on the handheld devices is hard to save.So for saving the battery life, this method proposed the concept of Backlight Scaling and also enhancing the image signals for better visual quality of displays and images. In this using only 40% backlight more battery power will be saved.

Maintaining image quality under various lighting conditions is critical to portable multimedia devices. This paper proposes a technique to maintain the visual quality for both images and also display of systems while the images are corrupted with noise also under low back-light.The first step in the proposed algorithm is for removing the impulse noise which is the salt and pepper noise by using median filter. Then for providing better growth or thickness of images a dilation method of morphological operations is used. So that if any breaks in an image it will be repaired. Then the linear spatial filter which is the laplacian operator is used for sharpening of the image and to enhance the details of an image that has been blurred.Now after using laplacian operator, based on L0 gradient the image is separated into base layer and detail layer. Then this method proposes a median-preserving gamma correction for controlling the brightness of an image. Meanwhile boost the detail layer using our JND profile.

In this method visual enhancement work for all types of backlight-scaled displays with better image quality is proposed.

II. PROPOSED SYSTEM

Based on the Human visual system (HVS) this method proposes the algorithm of image quality enhancement that preserves the perceptual quality of images displayed under extremely low back-light conditions. In this system the brightness of a pixel on the display is the product of transmittance and backlight illumination. The figure:1 shows the system pipeline. First in this method convert the RGB image to HSV image. The image is separated in to H (hue), S (saturation) and V (illumination). The H and S given directly to the output block. The V is having the illumination signal V(x,y) is taken for our system .

A. Median Filter

The V(x,y) which is taken is given to the median filter to remove the noise (salt & pepper) when the illumination signal is corrupted by impulse noise (salt &pepper) which is caused while taking the image itself. This noise can be caused by sharp & sudden disturbances in the image signal. An effective noise reduction method for this type of noise is the usage of a median filter. The median filter is a technique, often used to remove noise. Median filtering is very widely used in digital image processing because it preserves edges while removing noise.It replaces the value of the center pixel with the median of the intensity values in the neighborhood of that pixel. So here the illumination signal V(x,y) is given to the median filter and the filtered output is represented as Vm(x,y).

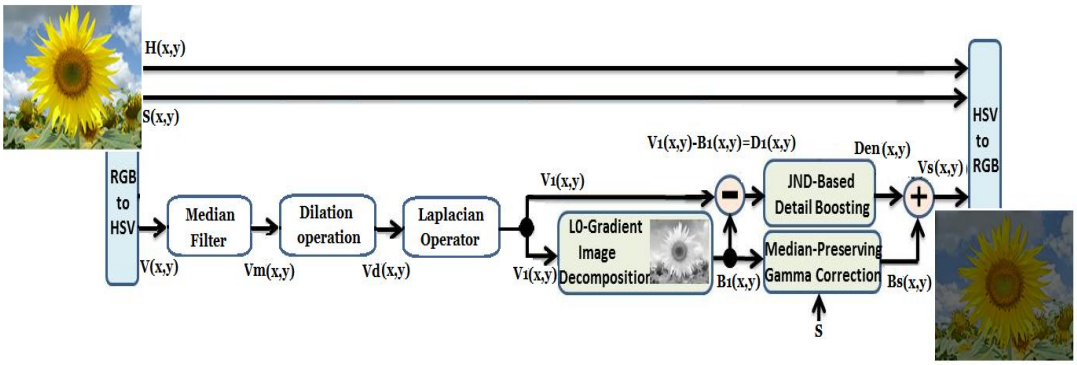

Fig.1: system pipeline

B. Dilation operation

Dilation is the operation that "grows" or "thickness" objects in an image thickening are controlled by a shape referred to structuring element. The structuring element is moved across every pixel in the original image to give a pixel in a new processed image. The value of this new pixel depends on the operation performed.

1. If the origin of the structuring element coincides with a 'white' pixel in the image, there is no change; move to the next pixel.
2. If the origin of the structuring element coincides with a 'black' in the image, make black all pixels from the image covered by the structuring element.

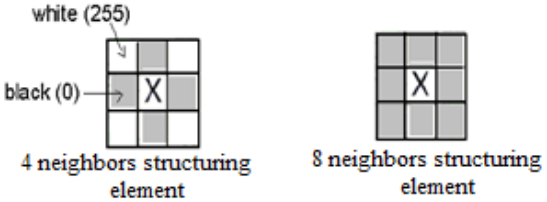

Fig: 2 Structuring element shapes

The structuring element can have any shape. Typical shapes are presented in figure:2.Dilation of image f by structuring element s is given by $f \oplus s$.The structuring element s is positioned with its origin at (x,y).The new pixel value is determined using the rule:

$$g(x,y) = \begin{cases} 1 \text{ if } s \text{ hits } f \\ 0 \text{ otherwise} \end{cases} \qquad (1)$$

Hit: Any on pixel in the structuring element covers an on pixel in the image.So Vd(x,y) is the signal after dilation operation, this signal is given to laplacian operator.

C. Laplacian operation

It can be beneficial to obtain several enhanced images with variety of approaches.Here the approach after dilation operation, image enhancement is done for sharpness of the details using linear spatial filter of laplacian operator. Sharpening in spatial filter is to highlight fine detail in an image and to enhance detail that has been blurred, either in error or as a natural effect of a particular method of image acquisition. In Spatial Filtering Process Simply move the filter mask from point to point in an image. Many spatial filters are implemented with convolution masks. Since the operations performed in the convolution are linear, these types of filters are called linear filters. So here we are using the linear spatial filter of laplacian operator (linear operator) denoted as:

$$\nabla^2 f = \frac{\partial^2 f(x,y)}{\partial x^2} + \frac{\partial^2 f(x,y)}{\partial y^2} \qquad (2)$$

We have different laplacian operators in that here this method uses a laplacian operator having the center coefficient 8 for better sharpening. The mask shows in the figure.3.

1	1	1
1	−8	1
1	1	1

Fig.3: Laplacian operator 8

So move the filter mask from point to point in an image. Equation (3) is used depending on the center coefficient.

$$g(x,y)=\begin{cases} f(x,y)-\Delta^2 f(x,y) \\ f(x,y)+\Delta^2 f(x,y) \end{cases} \quad (3)$$

If center coefficient is negative

If center coefficient is positive

So finally after applying the laplacian operation to the illumination signal of Vd(x,y) it will get the V1(x,y) which is used for further process.

D. Constrained L0 gradient image decomposition

Now V1(x,y) is the signal after laplacian operation. So first this method Decompose the illumination signal V1(x,y) in to base layer B1(x,y) and detail layer D1(x,y) using the constrained L0 gradient minimization. The original L0 gradient minimization is represented as follows:

$$\min_{B(x,y)} \sum_{(x,y)} |V_1(x,y)-B_1(x,y)|^2 + \lambda.C(x,y) \quad (4)$$

In this L0-gradient minimization C(x,y) represents number of non-zero gradient. Where $C(x,y)=\#\{(x,y)||\nabla B_1(x,y)|\neq 0\}$ where # denotes the numbers of pixels while ∇ denotes the difference operator. Since the L0-norm of gradient represents the numbers of non-zero gradient, it is generally counted on the positions containing strong edges. Based on this observation multiplying the Edge (x,y) to the C(x,y) [1]

$$C(x,y)=\#\{(x,y)|Edge\ (x,y).|\nabla B_1(x,y).|\neq 0\} \quad (5)$$

Here Edge (x,y) obtained by adopting the first order Gaussian (FDOG) edge detection on V1(x,y) with a threshold. The thresholds of FDOG and edge map are set to 0.75 and 0.2, respectively. Introducing Edge(x,y) in to minimization can eliminate some inappropriate and speed up the whole process. In this gauss gradient is used. Gradient using first order derivative of Gaussian for edge detection. This function outputs the gradient image using 2-D Gaussian kernel. Determining the size of the kernel and generating 2-D Gaussian kernel along both x and y directions. Applying 2-D filtering by introducing Edge(x,y) process can eliminate in appropriate things. So by taking the absolute values of x and y in a gauss gradient this method can detect the edges or boundaries of a signal. As it is tough to calculate the (4) referring [2] to approximate the L0-norm of gradient by introducing the two auxiliary variables of ax(x,y) and ay(x,y) corresponding to the two variables shown here $(\partial B_1(x,y))/(\partial x)\ and\ (\partial B_1(x,y))/(\partial y)$ Now the L0 gradient minimization is represented as:

$$\min_{B_1,a_x,a_y} \sum_{(x,y)} |V_1(x,y)-B_1(x,y)|^2 + \lambda.C(x,y)+\beta.\left(\left|\frac{\partial B_1(x,y)}{\partial x}-a_x(x,y)\right|^2+\left|\frac{\partial B_1(x,y)}{\partial y}-a_y(x,y)\right|^2\right) \quad (6)$$

Where C(x,y) is represented in equation (5) and β is an automatic tuning parameter to control the similarity between variables a_x (x,y) and a_y (x,y) and their corresponding gradients. The parameters when doing the L0 smoothing while getting the base layer the smoothing weight λ is set to 0.01, while β is set to 0.02 and is multiplied by 2 during iterations, kappa Parameter that controls the rate, kappa = 2 is suggested for natural images.βmax has the fixed value of 1e5 [2].Equation (6) is solved by alternatively minimizing B1, a_x, a_y. We fix one set of variables while obtain another set of variables.

Finding B1:

Fixing a_x (x,y) and a_y (x,y) to obtain B_1(x,y). This is by solving the quadratic cost function in a linear system:

$$\min_{B_1} \frac{1}{\beta}\sum_{(x,y)} |V(x,y)-B_1(x,y)|^2+\left|\frac{\partial B_1(x,y)}{\partial x}-a_x(x,y)\right|^2+\left|\frac{\partial B_1(x,y)}{\partial y}a_y(x,y)\right|^2 \quad (7)$$

Finding a_x and a_y:

In this iteration, fixing B1(x,y) to obtain new ax (x,y) and ay (x,y) by solving the cost function:

$$\min_{a_x,a_y} \frac{\lambda}{\beta}C(x,y)+\left|\frac{\partial B_1(x,y)}{\partial x}-a_x(x,y)\right|^2+\left|\frac{\partial B_1(x,y)}{\partial y}-a_y(x,y)\right|^2 \quad (8)$$

Where the L0-norm of gradient can be modeled as: $C(x,y)=Edge(x,y).H\left(|a_x(x,y)|+|a_y(x,y)|\right)$ (9)

Where H (|ax(x,y)|+ |ay(x,y)|) is the binary function.Returning 1 when (|ax(x,y)|+|ay(x,y)|) ≠0 and returning 0 otherwise. By calculating (7) and (8) final Base layer B1(x,y) is obtained from the L0-gradient minimization. The illumination signal is V1(x,y) from the laplacian operator. So the detail layer is obtained by the difference between illumination signal V1(x,y) and the base layer B1(x,y). i.e. D1(x,y) = V1(x,y) – B1(x,y) (10)

The detail layer which is useful for the JND for extracting the details and boosting the low intensity regions of the image.

E. Median-Preserving Gamma Correction

Since this method compress the range of illumination to simulate low backlight that is applying the 40 % scaling. This method uses only 40% backlight. So this method adopt a Gamma Correction - controls the overall brightness of an image. In other words to enhance the contrast of the displayed images. It is a setting that determines how bright the output of the display will be.

Therefore, "gamma correction" is used to alter the output levels of a monitor. The gamma setting affects both the brightness and the contrast of the display. The reason gamma correction is used is because the input signal, or voltage, sent to a monitor is not high enough to create a bright image. Therefore, if the gamma is not altered, the images on the screen would be dark and difficult to see. By applying gamma correction, the brightness and contrast of the display are enhanced, making the images appear brighter and more natural looking. Here in this system it uses the gamma correction to alter the output levels of the signals when applying the scaling to the input signal. The concept of gamma can be applied to any nonlinear relationship. For the power law relationship $V_{out} = V_{in}^{\gamma}$, the curve on a log–log plot is a straight line, with slope everywhere equal to gamma.(slope is represented here by the derivative operator):

$$\gamma = \frac{d\log(v_{out})}{d\log(v_{in})} \tag{11}$$

Based on this the gamma is represented in the median preserving gamma correction is:

$$\gamma = \frac{\log\left(median\left(B_1(x,y)\right)\right)}{\log\left(median\left(s.B_1(x,y)\right)\right)} \tag{12}$$

This method adopt gamma correction and let the median of the scaled brightness approximate to the median of the original brightness this design forces the final scaled base layer to maintain the brightness of the original full backlight. Suppose if the $\gamma < 1$ the image is weighted toward higher (brighter) output values. If $\gamma > 1$ the image is weighted toward lower (darker) output values. If $\gamma = 1$ the transformation has no effect on the image.An underexposed photograph can be corrected using gamma correction with $\gamma < 1$. An overexposed photograph can be corrected using gamma correction with $\gamma > 1$. Using eq (12) the value of γ=0.25 is obtained. By this if the $\gamma < 1$ the image is weighted toward higher (brighter) output values. The final scaled base layer will come out after applying scaling of 40% backlight which is denoted as denoted as Bs(x,y).
The final scaled base layer can be obtained:

$$B_s(x,y) = s.W.\left(\frac{B_1(x,y) - J_{\max}}{W}\right)^{\gamma} \tag{13}$$

Where W is the white value (equal to 255 in 8-bits image or 1 in normalized images) and J max is the maximum value of human JND. Referring to [3] and have J max=$\mu+\sigma$. W.Here μ and σ are constants.

F. JND-Based Detail Boosting

Just noticeable difference (JND) is the smallest difference in a specified modality of sensory input that is detectable by a human being.Just-noticeable-difference (JND) is the smallest stimulus for human vision to perceive the difference between the operating pixel intensity and its background intensity. Since the flowers are salient as compared to the rest regions, the flowers are enhanced more strongly by using our JND-Based detail boosting.The idea of using this JND is to keep the detail content of the image in the visible luminance range. In addition to the new scaled Bs(x,y).It also enhance the detail layer D1(x,y) to ease human perception. This method proposes a detail boosting method based on JND.

Two-layer image decomposition architecture based on the just noticeable difference (JND) theory is proposed for extracting the details, and a boosting scheme is applied to the details that are in the low intensity regions of the image.
Modifying J max=$\mu+\sigma$. W for the purpose of obtaining the JND is:

$$JND(x,y) = \mu + \sigma.\ B_s(x,y) \tag{14}$$

The parameters of JND are μ is set to 4 and σ is set to 0.015 and Jmax is 0.02. The enhanced detail layer $D_{EN}(x,y)$ is obtained from the JND-Based detail Boosting by using

$$D_{EN}(x,y) = D_1(x,y).\left(\frac{W + JND(x,y)}{W}\right) \tag{15}$$

The final enhanced V-signal can be obtained by combining the Enhanced detail layer DEN(x,y) from the JND-Based detail boosting and scaled base layer B(x,y) from median-preserving gamma correction.

$$\text{i.e } VS(x,y) = B_s(x,y) + D_{EN}(x,y) \tag{16}$$

Now the final enhanced V-Signal is denoted as Vs(x,y) and the original Hue signal H(x,y) and saturation signal S(x,y) of the input HSV image will combined in the output block in order to get the output in the form of HSV. Now finally the system converts the HSV output in to RGB image.

III. RESULTS

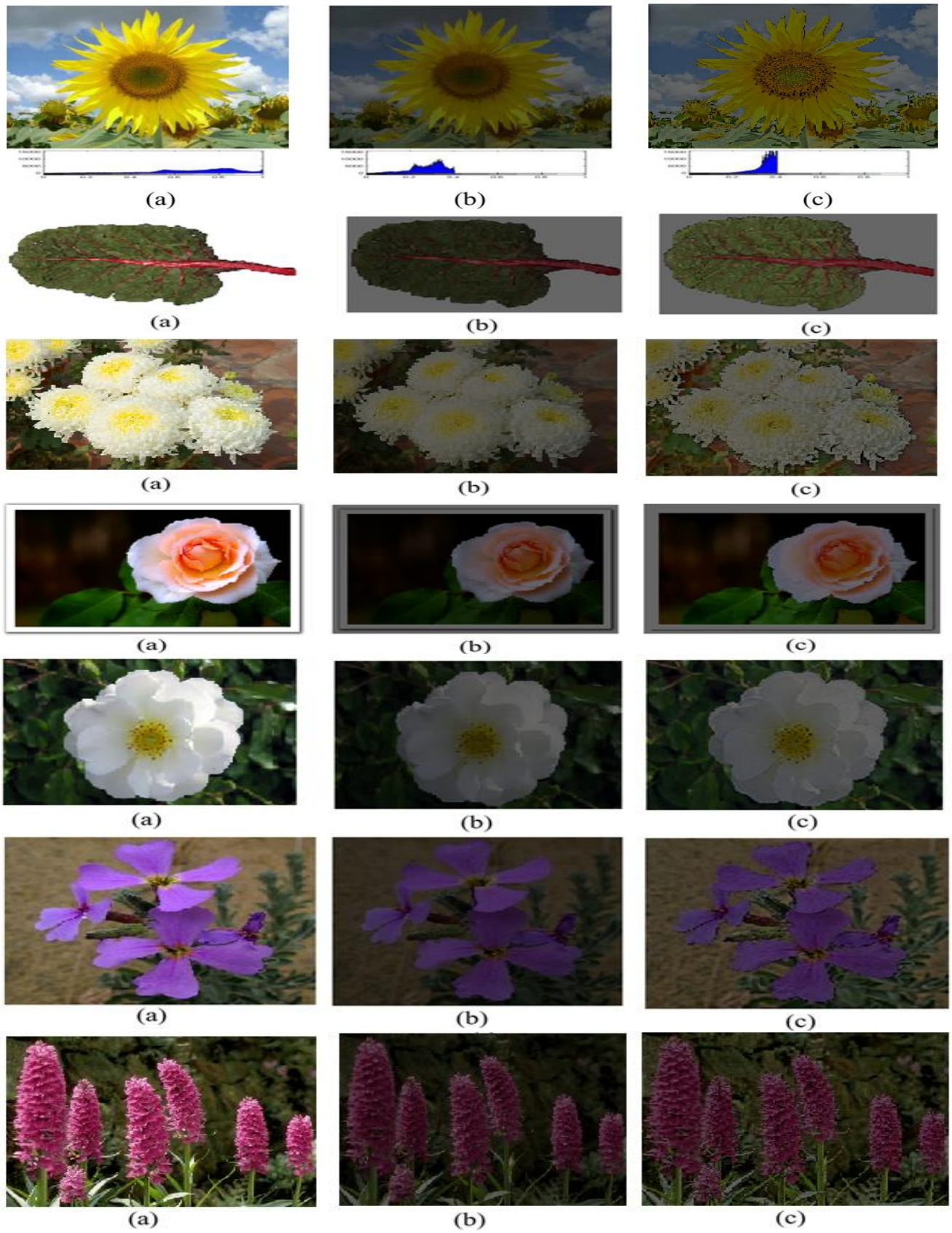

Fig. 4: The results: (a) original image, full 100% backlight: s=1, (b) original image, linear-scaled to 40% backlight: s=0.4, (c) our result using 40% backlight: s=0.4 with improved visual quality of image and also display.

IV. CONCLUSION

This method propose a system which provides the visual quality for both images and display of systems by visual enhancement under low back-light conditions even though the images are corrupted with the noise under low backlight.

So for saving the battery life, this method proposed the concept of Backlight Scaling and also enhancing the image signals for better visual quality of displays and images. If using only 40% backlight then more battery power is saved. This system can not only prolong the battery life but also enhance visual quality. In this work, visual enhancement framework for all kinds of backlight-scaled displays with better image quality is proposed.

The Experimental result shows that the proposed system performs better than the many existing systems.

REFERENCES

[1]. Soo-Chang Pei, Fellow, IEEE, Chih-Tsung Shen, and Tzu-Yen Lee "Visual Enhancement Using Constrained L0 Gradient Image Decomposition for Low Backlight Displays" IEEE *Signal Processing Letters*, VOL. 19, NO. 12, December 2012.
[2]. L. Xu, C. Lu, Y. Xu, and J. Jia, "Image smoothing via l0 gradient minimization,"ACM Trans Graph., vol. 30, no. 6, 2011.
[3]. D. Choi, I. Jang, M. Kim, and N. Kim, "Color image enhancement based on single-scale retinex with a JND-based nonlinear filter," in *IEEE Symp. Circuit and Syst.*, 2007, pp. 3948–3951.
[4]. T.-H. Huang, C.-K. Liang, S.-L. Yeh, and H. H. Chen, "JND-based enhancement of perceptibility for dim images," in IEEE Conf. Image Process., 2008, pp. 1752–1755
[5]. P.-S. Tsai, C.-K. Liang, T.-H.Huang, and H. H. Chen,"Image enhancement for backlight-scaled TFT-LCD displays," *IEEE Trans. Circuits Syst. Video Technol.*, vol. 19, no. 4, pp. 574–583, 2009.
[6]. C. Lee, C. Lee, Y.-Y. Lee, and C.-S.Kim,"Power-constrained contrast enhancement for emissive displays based on histogram equalization,"*IEEE Trans. Image Process.*, vol. 21, no. 1, pp. 80–93, Jan. 2012.
[7]. http://www.mathworks.in

International Journal of Modern Engineering Research (IJMER)
www.ijmer.com Vol.3, Issue.4, Jul - Aug. 2013 pp-2079-2082 ISSN: 2249-6645

Performance Assessment of IPFC with IDVR for Two Feeder Transmission systems

Arumugom S.[1], Dr. M. Rajaram[2]
[1](Assistant Professor, Department of EEE, Udaya School of Engineering, INDIA)
[2] (Vice Chancellor, Anna University, India)

Abstract: The *dynamic voltage restorer (DVR) is one of the modern devices used in transmission systems to protect power flow against sudden changes in voltage amplitude. The proposed algorithm is applied to some disturbances in load voltage caused by induction motors starting, and a three-phase short circuit fault. Also, the capability of the proposed DVR has been tested to limit the downstream fault current. This paper originates a comprehensive evaluation strategy among the Interlined Power Flow Controller (IPFC) and Interline Dynamic Voltage Restorer (IDVR). The fundamental opearation of IDVR and IPFC has compared. The two feeders IDVR connected transmission line performance is presented in a strategic approach and result analysis made for further comparison with IPFC. The MATLAB/Simulink based model developed for IDVR and IPFC; the output response of the system has compared and an remarkable conclusion proposed.*

Keywords: *Interline Dynamic Voltae Restorer, Interline Power Flow Controller, Voltage Sag*

I. INTRODUCTION

Voltage sag is one of the most important power-quality problems that encompass almost 80% of the transmission system PQ problems. According to the IEEE 1959–1995 standard, voltage sag is the decrease of 0.1 to 0.9 p.u. in the rms voltage level at system frequency and with the duration of half a cycle to 1 min . Short circuits, starting large motors, sudden changes of load, and energization of transformers are the main causes of voltage sags

Nowadays Flexible AC Transmission Systems (FACTS) controllers are playing a vital role in terms of power flow control, transient stability and oscillation damping enhancement as reported in [1-3]. Researchers have presented design of FACTS-based stabilizers for SVC, TCSC, TCPS, and Unified Power Flow Controller (UPFC) in [5].

Interline Power Flow Controller (IPFC) is an advanced voltage sourced Converter based FACTS controller [2] which employs a number of dc to ac converters each providing a series compensation for a different lines.
VSC-based FACTS controllers include the Static Synchronous Compensator (STATCOM) for shunt reactive power compensation, the Static Synchronous Series Compensator (SSSC) for series reactive power compensation, the Unified Power Flow Controller (UPFC) with the unique capability of independently controlling both the active and reactive power flow in the line.

Generally speaking, the IPFC employs a number of VSCs linked at the same DC terminal, each of which can provide series compensation for its own line. It can also be regarded as several SSSCs sharing a common DC link.
In this way, the power optimization of the overall system can be realized in the form of appropriate power transfer through the common DC link from over-loaded lines to under-loaded lines [7].

An IDVR, which is two DVRs installed in two feeders with common dc bus, has the capability of active power exchange between two DVRs, and thus the energy storage device is not an issue. Therefore, the design criteria for the Selection of rating of an individual DVR are not applicable in IDVR structure.

These Voltage sag disturbances, mainly due to faults and start-up of large loads [9], are normally Characterized by the number of occurrences, the amplitude and the duration of sag [10].

IDVR consists of several DVRs on different distribution lines sharing a common DC link.References [11 12] discuss the two-line IDVR system. The system utilizes the pre-sag compensation method to mitigate the voltage sag problem in one feeder provided that the voltage of the other is normal.

A novel minimal energy consumption strategy for the IDVR is proposed in [12] where two different voltage distribution systems are protected using two DVRs. The first is a low voltage DVR operating in voltage sag mitigation mode injecting active power from the DC link capacitor. Simultaneously, the other medium voltage DVR keeps the voltage of the DC link capacitor constant. In [13], the optimum rating for two DVRs when used for IDVR system is designed

An IDVR is similar to the inter line power flow controller (IPFC) in transmission systems [11] but to distribution systems. In this paper a performance comparison among interline power flow control and interline dynamic voltage restorer has presented. The approach carried out with application of performance of the system with IPFC and IDVR made and result analysis presented in the system.

1.1 Operational behavior of Interline Power Flow controller (IPFC)

The interline power flow controller shown in fig (1) consist of two VSCs, each of which located series in the lines with their DC sides connected via a common capacitor. For the purpose of modeling the IPFC, it is considered in the form of several VSCs which have common DC connections.

In IPFC design, assuming that it has two VSCs, one line is always selected as the main line and another line which is connected to the IPFC is considered as the dependent or lower line. In the main line, the active and reactive powers are both

manageable entirely, and can adjust them to the desired value, but in the dependent or lower line, only one of the active or reactive powers is controllable, and the other is released.

The important property of IPFC that can transmit power from overloaded lines to under loaded lines. It can be easily indicated that in the main lines, the active and reactive powers are completely controllable, and the control strategy can be achieved by changing the amplitude and angle of series converter voltage.

1.2 Operational behavior of Interline Dynamic Voltage Restorer (IDVR)

The IDVR system consists of several DVRs in different feeders, sharing a common DC-link. A two-line IDVR system shown in Figure 3 employs two DVRs are connected to two different feeders where one of the DVRs compensates for voltage sag or swell produced, the other DVR in IDVR system operates in power-flow control mode.

Firstly, unlike individual DVRs, the duration of compensation in an IDVR is not usually restricted. The reason is that the required energy for compensation comes from another feeder, which is supposed to be healthy. However, energy absorption from the healthy feeder via dc link may cause overload and unacceptable sag in the healthy feeder. Therefore, some inherent limitations always exist which depends on feeder parameters and the depth of sags,but not on the duration of sags. Based on this reasoning, minimum energy strategy is not necessarily applicable in compensation, and it may lead to larger rating and over-size DVR.

II. VOLTAGE SAG COMPENSATION IN A TWO FEEDER IDVR SYSTEM

The voltage sag in a two-feeder IDVR system is caused due to sudden increase of the load across a feeder. Consider the condition when the DVR in the IDVR system operates in Voltage-sag compensating mode while the DVR operates in power-flow control mode to keep the DC-link voltage at a desired level. When there is no voltage disturbance, the load voltage of Feeder is equal to the bus voltage V during Voltage sag, the DVR should be operated to meet this condition while supplying real power to the common DC-link.

The harmonic elimination in any system is one of the important requirements nowadays. The total harmonic distortion in the response obtained can be reduced abruptly with interline dynamic voltage restorer.

III. RESULT ANALYSIS OF IDVR AND IPFC

From the simulink model proposed(fig 1); the interline power flow controller designed with two transmission lines of 50 KM each ; phase to phase RMS voltage (Vrms) = 10 KV

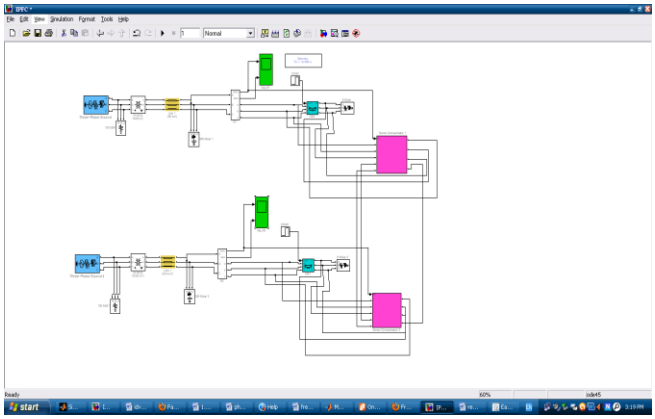

Fig. 1 The IPFC with two series compensators

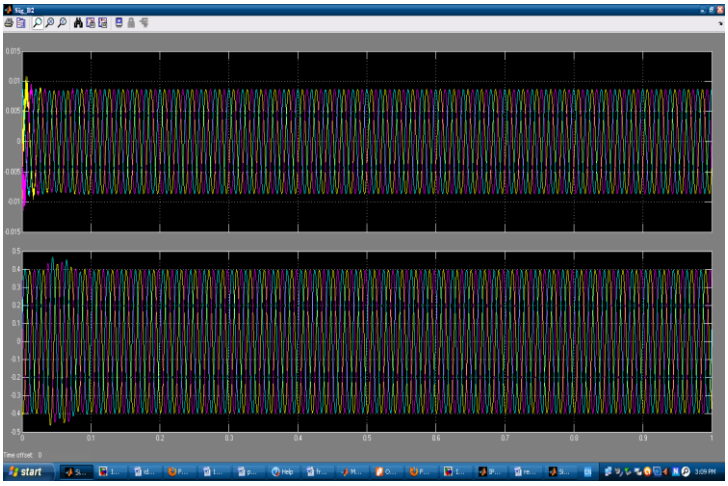

Fig. 2 The IPFC with two series compensators output waveform

The partially controlled three phase voltage and current (V load; I load) response of system when ipfc is applied has given in fig.2. An IDVR model is presented with a line length 300 kilo meters; a three phase rms voltage of13.8 KV; Three phase transformer with 6*350 MVA, 13.8/735 kv in fig.3.The distorted condition of load voltage and current appear when the IDVR is not added as in fig.4 and the fault mitigated voltage and currents are shown in fig 5 with the application of IDVR.

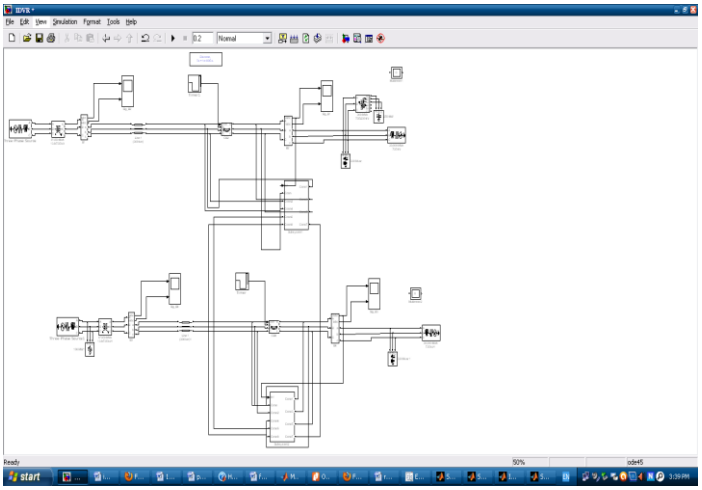

Fig. 3 Interline Dynamic Voltage Restorer (IDVR) with two DVR s in the line

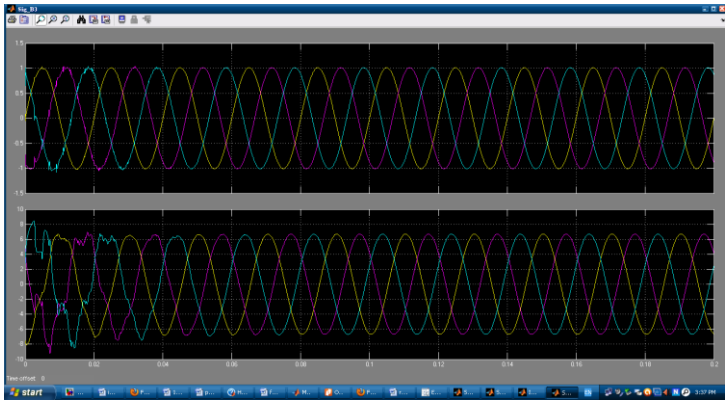

Fig. 4 The output response (V load; I load) of the model when the IDVR is not added

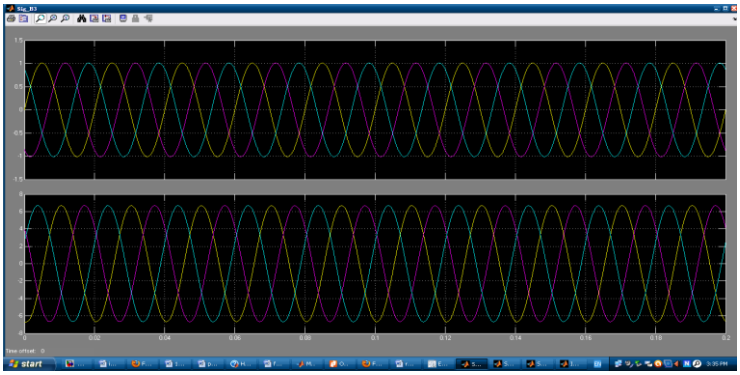

Fig. 5 The stabilized output response (V load; I load) when IDVR add in the model

IV. CONCLUSION

This paper evaluates comprehensive performance among interline dynamic voltage restorer and interline power flow controller presented. The operation behavior of the IDVR and IPFC starting from fundamental structure has carried out in an effective manner. The feasibility of proposed method was verified through computer simulations and observation of the load response presented in order to give effective comparison between IDVR and IPFC Matlab/simulink models. The DVR with proposed method can effectively compensate the voltage sag or interruption for sensitive loads and limiting the downstream fault currents.

REFERENCES

[1]. R. Sadikovic, P. Korba and G. Andersson, "Application of FACTS Devices for Damping of Power System Oscillations,"
[2]. IEEE PowerTech 2005, Russia, June 2005.
[3]. P.K.Dash, S.MishraA, G.Panda, "Damping Multimodal Power System Oscillation Using a Hybrid Fuzzy Controller for Series Connected FACTS Devices," IEEE Transactions on Power Systems, Vol. 15, No. 4, November 2000, pp. 1360 _ 1366.
[4]. H.F. Hang, "Design of SSSC Damping Controller to Improve Power System Oscillation Stability," IEEE 1999.
[5]. N.Tambey and M.L.Kothari, "Damping of Power System Oscillation with Unified Power Flow Controller," IEE Proc. Gener. Trans. Distib. Vol. 150, No. 2, March 2003, pp. 129 – 140.
[6]. N.G. Hingorami, L.Gyugyi, Understanding FACTS: Concepts and Technology of Flexible AC Transmission system, IEEE Press, 1999 6[7] Y.H. Song and A.T. Johns, Flexible AC Transmission systems,IEE Power and Energy series 30, 1999.
[7]. L.Gyugyi, K.K.Sen, C.D.Schauder, "The Interline Power FlowController Concept: A New Approach to Power Flow Management in Transmission Systems," IEEE Transactions on Power Delivery, Vol. 14, No. 3, July 1999, pp. 1115 – 1123.
[8]. J. Chen, T.T. Lie, D.M. Vilathgamuwa, N.G.Hingorani, L.Gyugyi, "Understanding FACTS: concepts and technology of flexible AC transmission systm", IEEE PRESS, 2000.
[9]. Y.H. Song and A.T. Johns, "Flexible AC Transmission System", IEE R Book Series on Power Engineering, December 1999.
[10]. L.Gyugyi, "Application Characteristics of Converter-Based FACTS Controllers", International Conference on PowerCon 2000, Vol.1.
[11]. L.Gyugyi, K.K.Sen, C.D.Schauder, "The Interline Power Flow Controller Concept: A New Approach to Power Flow Management in Transmission Systems", IEEE/PES Summer Meeting, Paper No. PE316-PWRD-0-07-1998,
[12]. L.Gyugyi, K.K.Sen, C.D.Schauder, "The Interline Power Flow Controller Concept: A New Approach to Power Flow Management in Transmission Systems", *IEEE Transactions on Power Delivery*, Vol. 14, No. 3, pp.1115~1123, July 1999.
[13]. Math H. J. Bollen, Understanding Power Quality Problems: Voltage Sags and Interruptions, Wiley, 1999.

International Journal of Modern Engineering Research (IJMER)
www.ijmer.com Vol. 3, Issue. 4, Jul - Aug. 2013 pp-2083-2088 ISSN: 2249-6645

Development of a New Formula for a Clear Water Scour around Groynes

Prof. Dr. Saleh I. Khassaf, Alaa Mhseen Dawood
Kufa University, Iraq, Najaf,

ABSTRACT: *This study based on laboratory experiments for computing depth of local scour around groyne when a different spacing between the groynes using as a countermeasure. This study is conducted using a physical hydraulic model for groyne operated under clear-water condition and using uniform cohesionless sand as bed material.*
A different types of spacing (1, 1.5, and 2) from length of groynes is investigated with different water depths and flow intensities. It is developed a new formula to calculate a local scour around groynes included many parameter. Also, it has been observed that increasing the distance between the groynes leads to increase the depth of the scour about (20)%.

KEY-WORDS: *groynes, Local Scour, Deposition.*

I. INTRODUCTION

The problem of scour around any obstruction placed in alluvial channel is of great importance to hydraulic engineers. In practice, a channel is often obstructed by a means or another, such as groynes, bridge piers, abutment, and so on. Groynes are hydraulic structures that project from the bank of a stream at some angle to the main flow direction. They are used for two purposes, namely river training and erosion protection of the riverbank. With respect to river training, the primary objective is to improve the navigability of a river by providing a sufficient depth of flow and a desirable channel alignment. Groynes also serve to increase the sediment transport rate through the groyne reach, which decreases channel dredging costs. With respect to erosion protection, groynes can be designed to protect both straight reaches and channel bends. Compared with other methods, such as revetments, groynes are among the most economical structures that may be used for riverbank erosion protection (Shields, 1995).

It is important herein to state that the obstruction caused by the groyne generates a complicated system of vortices which are believed to be the main cause of scour.

The primary horseshoe vortex impinges on the sand bed immediately in front of the groyne and throws up the eroded material which is transported downstream by the main flow. See figure (1).

Development of scouring with time depends on flow condition. If shear stress on bed is less than the threshold of sediment motion (clear water), scour develops first very rapidly and then approaches equilibrium asymptotically, whereas in live bed scour develops rapidly and its depth fluctuates in response to the passage of bed features, (Chabert and Engeldinger, 1956) (Figure 2). Maximum scour depth occurs at the threshold of sediment motion (Breusers and Raudkivi, 1991).

The goal of the present work is to show the effectiveness of number of groyne as a counter measure against local scour which formed around groyne located at a specified location.

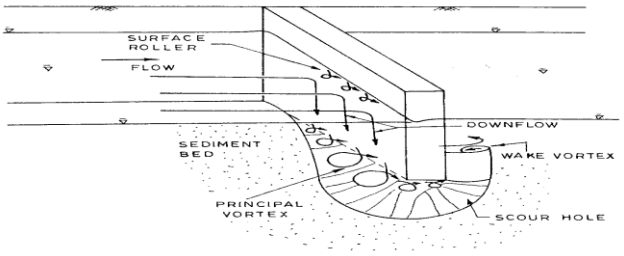

Figure (1): Flow pattern around groyne (Kwan, 1984)

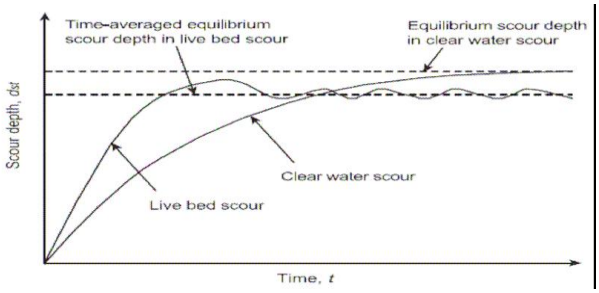

Figure (2): Scouring in clear water and live bed (Raudkivi and Ettema (1983)

II. SCOUR PARAMETERS

Factors which affect the magnitude of the local scour depth at groyne as given by Raudkivi and Ettema (1983) , Richardson and Davies (1995) and Lagasse et al. (2001) are (1) approach flow velocity, (2) flow depth, (3) groyne shape, (4) gravitational acceleration, (5) groyne length if skewed to the main flow direction, (6) size and gradation of the bed material, (7) angle of attack of the approach flow to the groyne, (8) bed configuration, and (9) ice or debris jams. According to Breusers et al. (1977) and Ansari et al. (2002), the parameters that are listed above can be grouped into four major headings, viz.

- ***Approaching Stream Flow Parameters****:* Flow intensity, flow depth, shear velocity, mean velocity, velocity distribution, and bed roughness.
- ***Groyne Parameters***: Lenght, geometry, spacing, number, and orientation of the groyne with respect to the main flow direction (i.e., angle of attack).
- ***Bed sediment parameters****:* Grain size distribution, mass density, particle shape, angle of repose, and cohesiveness of the soil.

• ***Fluid Parameters***: Mass density, acceleration due to gravity, and kinematic viscosity.

III. LABORATORY FLUME

The laboratory flume used in this study is shown in figure (3) .The main flume structure is a glass fiber moulded in steel stiffeners which has a 6.6 m length, 0.4 m wide and 0.4 m depth.

The flume consists of an inlet tank 1.0 m length in upstream, a working section 5.6 m is divided into three parts, in the middle layer of sand with depth and the length 0.1m and 2m respectively, it is filled with erodible uniform sediment. The upstream and downstream portion each have 1.25m length and the bed is raised 0.1m with compressed, coated and non swelling wood to obtain more stable water surface. This tank consists of three screens to avoid entering of any unwanted particles and debris into the working section of the flume. The flume has closed system water. Water is supplied from the reservoir under the ground by a centrifugal pump that is situated on a fabricated steel base plate. The centrifugal pump lies beside the flume at upstream.

The depth of flow is controlled by an adjustable tail gate at the downstream of trap basin. For flow discharge measurement a sharp crested rectangular weir is fabricated which have width of 0.4m and the height of 0.25 and it is mounted at the upstream section of flume.

All depth measurements are carried out using a point gauge with accuracy ±1mm mounted on a carriage which can move to any position above the working area transversely and longitudinally. The scour hole is obtained by performing 4-hours continuous run under clear water condition.

At the end of each experiments, the flume is carefully drained and sand bed level is straightened for next experiments with a scraper, and for more accuracy in bed straightening two thin woods with the same depth and length of the working section on the both sides of working section .this enabled the scraper to slide from beginning to the end of working section over woods, which were mounted on the glass side walls

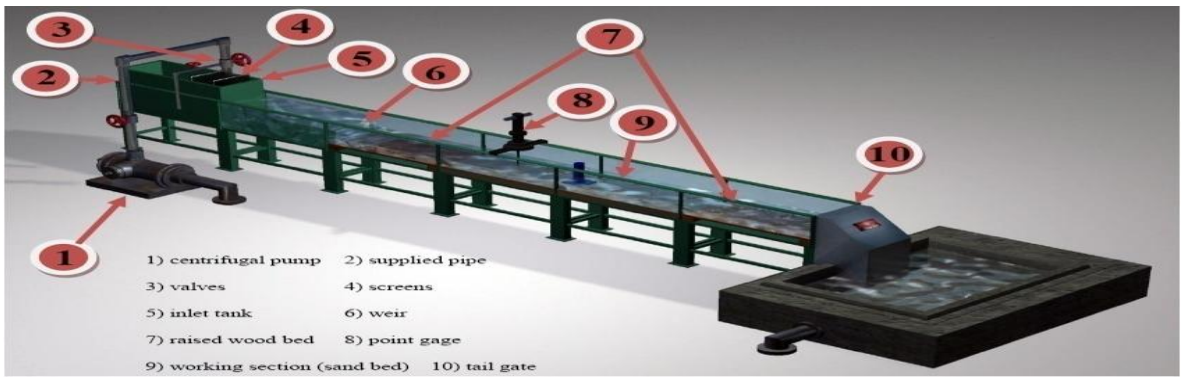

Figure (3): Laboratory Flume

IV. GROYNE MODELS

The groyne models used in the experiments were made of plywood having a thickness of (10) mm and height (20) cm and length (13) cm . Three different spacing between the groynes (1, 1.5, and 2) from length of groynes are used in the experimental works to cover the aims of this work, where more economical design and reliable practical application can be used with new relationship. These models were smoothly finished and painted to prevent any roughness or changes in dimensions resulting from swelling when they are immersed in water for a long period of time.

The groyne locations were chosen to be within the second third of flume to achieve a well established flow. The groynes were fixed vertically in the sand bed.

Groynes were fixed firmly to the side wall of the flume by using silicon adhesive which was fixed on the external wall of the flume. A tape was used to seal the space between the end of groynes and wall of the flume. As shown in plate (1) found groynes before the completion of the experiments.

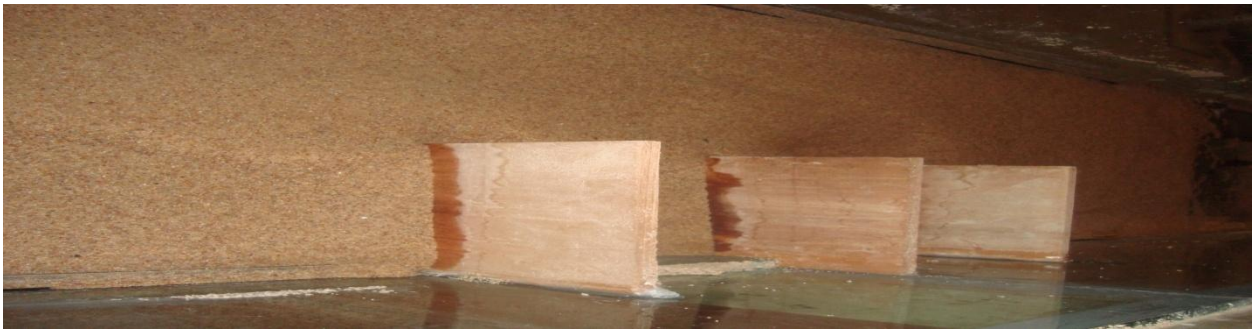

Plate (1): Front view of the groynes

V. SEDIMENT

The result of test showed that the bed material consists of cohesionless sand with a median particle size (d_{50}) equal to 0.71mm. The geometric standard deviation of the sand size (σ_g) equal to 1.31, which is implies that the sand is of uniform size distribution. See figure (4).

The sediments used in this study were well uniform, so that the results do not include the effect of sediment no uniformity in order to eliminate the reduction of local scour that would be expected to occur in no uniform sand due to armoring effect.

If the ratio of the abstraction width to the grain size exceeds a value about 25, the effect of sediment size can be negligible (Melville, 1997). The groyne length is chosen in which the effect of sediment size on the local scour can be negligible.

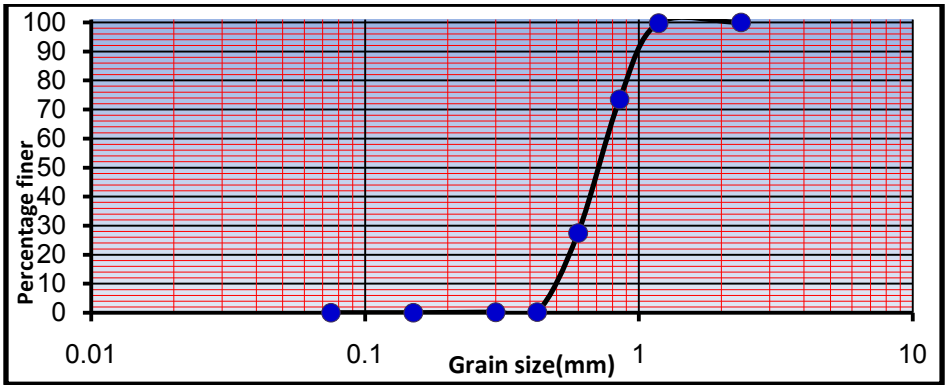

Figure (4): Grain size distribution curve for bed material

VI. THE EXPERIMENTAL WORK AND ITS PURPOSE

All experiments were performed for steady subcritical flow, clear water condition with plain bed.
Different sets of experiments (24 runs) were conducted to deduce the effect of the following parameters on the maximum depth of scour:

(a) Prolonged running time;
(b) Flow rate;
(c) Upstream water depth;
(d) Froude number upstream of the groyne; and
(e) Spacing between the groynes (1, 1.5, and 2) from length of groyne.

Summary of all experimental series are given in table (1)

Table (1) Experimental range of influence parameter for the groynes.

Run	y (mm)	v (m/sec)	v_c (m/se)	b (mm)	Fr	v / vc	b / y	d_s (mm)	d_s / y
1	20	0.233	0.245	260	0.526	0.95	13	49	2.45
2	20	0.208	0.245	260	0.47	0.85	13	48	2.4
3	20	0.184	0.245	260	0.415	0.75	13	35	1.75
4	20	0.159	0.245	260	0.359	0.65	13	26	1.3
5	45	0.192	0.285	260	0.293	0.674	5.78	74	1.644
6	35	0.192	0.273	260	0.328	0.705	7.43	52	1.486
7	25	0.192	0.256	260	0.388	0.75	10.4	40	1.6
8	15	0.192	0.231	260	0.5	0.831	17.33	28	1.867
9	20	0.233	0.245	195	0.526	0.95	9.75	42	2.05
10	20	0.208	0.245	195	0.47	0.85	9.75	40	2.0
11	20	0.184	0.245	195	0.415	0.75	9.75	33	1.65

Table (1):Cont.

12	20	0.159	0.245	195	0.359	0.65	9.75	27	1.35
13	45	0.192	0.285	195	0.293	0.674	4.33	71	1.578
14	35	0.192	0.273	195	0.328	0.705	5.57	50	1.429
15	25	0.192	0.256	195	0.388	0.75	7.8	35	1.4
16	15	0.192	0.231	195	0.5	0.831	13	27	1.8
17	20	0.233	0.245	130	0.526	0.95	6.5	39	1.95
18	20	0.208	0.245	130	0.47	0.85	6.5	35	1.75
19	20	0.184	0.245	130	0.415	0.75	6.5	30	1.5
20	20	0.159	0.245	130	0.359	0.65	6.5	26	1.3
21	45	0.192	0.285	130	0.293	0.674	2.89	63	1.4

22	**35**	**0.192**	**0.273**	**130**	**0.328**	**0.705**	**3.71**	**48**	**1.371**
23	**25**	**0.192**	**0.256**	**130**	**0.388**	**0.75**	**5.2**	**32**	**1.28**
24	**15**	**0.192**	**0.231**	**130**	**0.5**	**0.831**	**8.67**	**26**	**1.733**

Plate (2): After run (1)

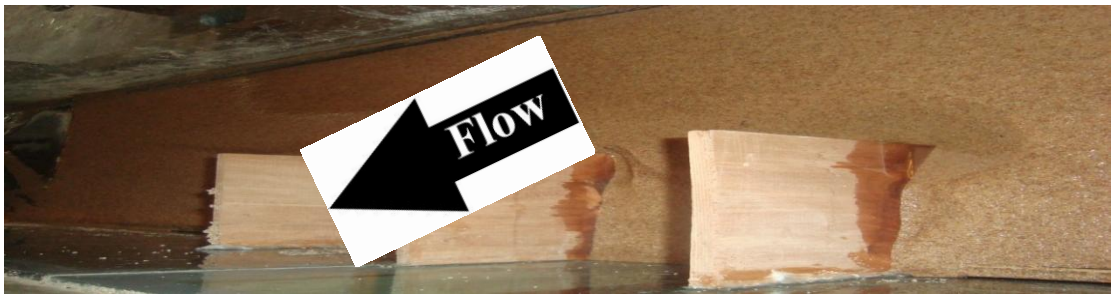

Plate (3): After run (9)

Plate (4): Before run (17)

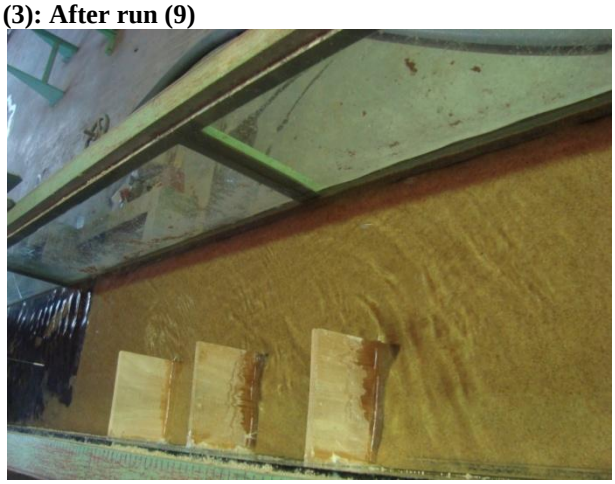

Plate (5): During run (17)

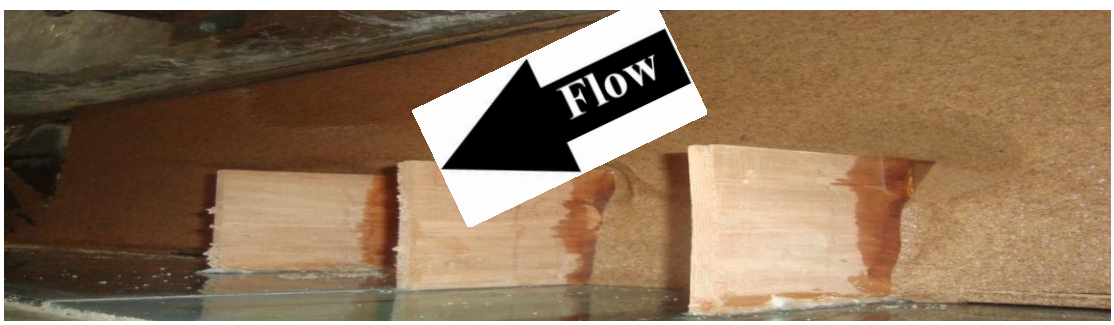

Plate (6): After run (17)

VII. DEVELOPMENT OF A NEW FORMULA

The scour depth is a function of some variables. The non dimensional formula is presented:

$d_s/y = F$ (v/ vc, *F*r, b) ……..(1)

The computer package (STATISTICA) was used to make analysis for the equation through a non- linear regression analysis.

$d_s/y = C_1 \times \{ (v/vc)^{C2} \times (Fr)^{C3} \times (b)^{C4} \}$……..(2)

C_1= 7.590216 C_2= 0.751151 C_3= 0.764262 C_4= 0.178201

R^2 = 0.952

The coefficient of determination (R^2) for this formula is (0.952).

After simplifying and rearranging the above formula becomes:

d_s/y= 7.590 { (v/vc)$^{0.751}$ $Fr^{0.764}$ $b^{0.178}$ } ……(3)

Another data is used to testing the equation, a statistical comparison of equation is used to show the convergence of the predicted to observed records, the value of (R^2= 0.922) are given a good agreement for all data as shown in figure (5).

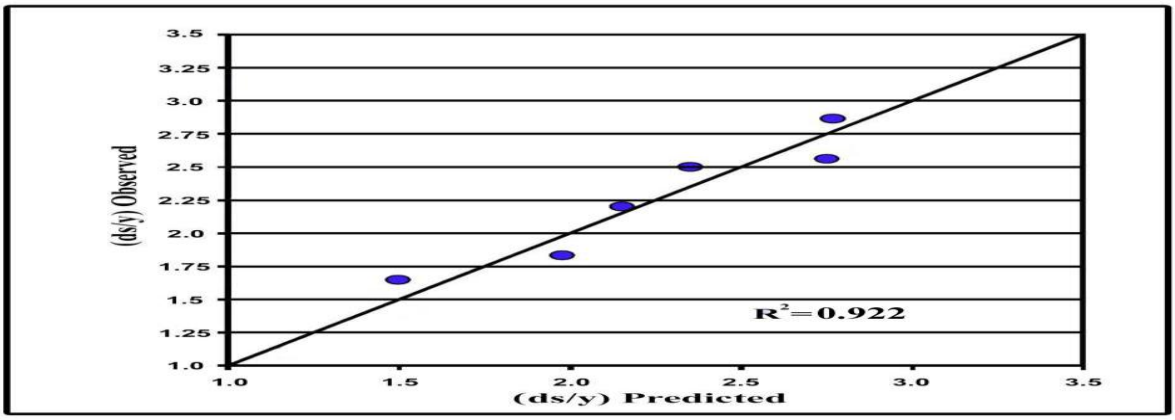

Figure (5): Comparison of equation (3) with experimental data

VIII. ANALYSIS AND DISCUSSION OF RESULTS

Estimating of maximum possible scour depth around groynes is an important step in the design of groyne foundation. To examine such a phenomenon, sets of experiments are performed using straight models to represent the main shape used for groyne.

Flow Depth

The scour process is directly proportional to flow depth. Many investigators showed that the propagation of scour occurs with increasing flow depth and the rate of this propagation decelerates up to a limiting value of flow depth at which its influence is absent.

Flow Velocity

The intensity of flow has direct influence on the scour depth regardless of flow depth. A linear increase of scour depth with velocity is observed for velocities below the threshold value. This finding is in agreement with these of previous investigation for clear water condition.

Spacing between the groyns

A set of experiments are conducting for evaluating the relationship between scour depth and spacing between the groynes. These experiments are shown in the Figure (6).

For b=length of groyne totally excludes the wake vortex system from the scour volume around the groyne and alters the flow field, which is probably influencing on the horse shoe vortex. For b=1.5 from the length of groyne, the spacing between seems to act less on the horse shoe vortex, more on the lower part of the wake vortex system.

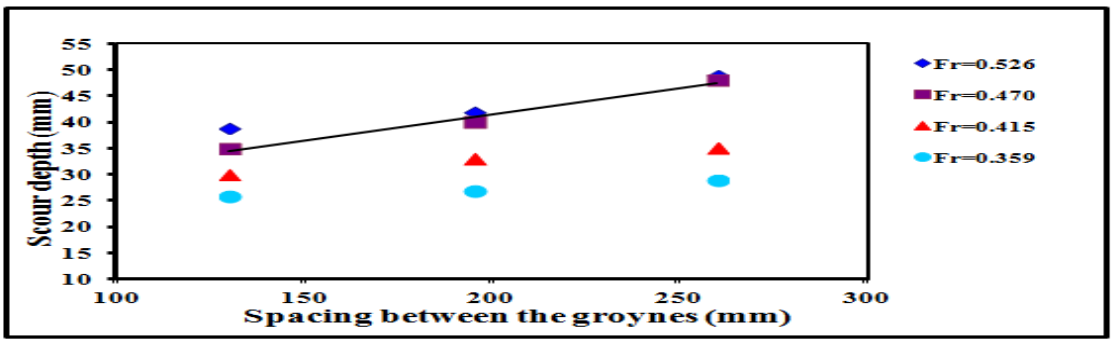

Figure (6): Development of scour depth with spacing between the groynes

IX. CONCLUSIONS

The problem of local scour around the groyne has been studied experimentally.

Under the limitations imposed on this investigation the following conclusions can be drawn.

a) The maximum scour depth was observed at the nose of groyne at the upstream.
b) For a constant spacing between the groynes, the scour depth increases due to increasing the Froude number, flow velocity, and flow depth.
c) The deepest scour occurs at the head of the first groyne because of its objection to the flow.
d) The scour depth is increased about (20)% by increasing the spacing between the groynes about (0.5) from the length.

List of symbols

b Spacing between the groyne
ds Depth of scour around the groyne
d_{50} Median size of the sediment particle
Fr Froude number ($Fr = V/\sqrt{gD}$)
g Acceleration due to gravity
ρ Water density
Re Reynolds number
V Mean approach flow velocity
V_c Critical velocity
y Flow depth
μ Dynamic viscosity

REFERENCES

[1]. Ansari, S.A., Kothyari, U.C. and Rangaraju, K. G. (2002), "*Influence of cohesion on scour around bridge piers*", Journal of Hydraulic Research, Vol. 40, 2002, No. 6, pp.717-729, Dept. Of Civil Engineering, Aligarh Muslim University, Aligarh, INDIA.
[2]. Breusers, H.N.C., Nicollet, G. and Shen, H.W. (1977), "*Local scour around cylindrical piers*", Journal of Hydraulic Research, Vol. 15, No. 3, pp.211-252.
[3]. Chabert, J and P. Engeldinger, (1956), "*Etude des afouillements autour des piles des ponts*" Laboratoire National d'Hydraulique, Chatou, France.
[4]. Clopper, P.E., Lagasse, P.F. and Zevenbergen, L.w. (2007), "*Bridge pier scour countermeasures*", paper presented to World Environmental and Water Resources Congress 2007: Restoring our Natural Habitat.
[5]. Dargahi, B., (1990), "*Controlling Mechanism of Local Scouring*", Journal of Hydraulic. Engineering, ASCE, Vol.116, No. 10, pp. 1197-1214.
[6]. Dey, S. and Raikar, R. V. (2007), "*Characteristics of horseshoe vortex in developing scour holes at piers*", Journal of Hydraulic. Engineering, 133 4, 399–413.
[7]. Ernest F. Brater, Horace Williams King, James E. Lindell, C.Y.Wei (1996), "*Hand book of hydraulics. seventh edition*", McGraw-Hill Book Company N.Y, ISBN 0-07007247-7.
[8]. Ettema, R. Melville, B.W. and Barkdoll, B. (1998), "*Scale effect in pier scour experiments*", Journal of Hydraulic Engineering, Vol. 124, No. 6, PP.42-639.
[9]. Hjorth, P., (1975), "*Studies on the Nature of Local Scour*", Dept. Water Res. Eng., Lund Inst. of Technology, Bulletin Series A, No. 46.
[10]. Johnson, P. A. (1991), "*Advancing bridge-pier scour engineering*", Journal of Professional Issues in Engineering Education and Practice, Vol. 117, No. 1, PP.48-55.
[11]. Kwan, R. T. F., (1984), " *Study of Aabutment Scour*", Rep. No. 328, School of Engineering, The University of Auckland, New Zealand.
[12]. Lagasse, P. F., and Richardson, E. V., (2001). "*ASCE compendium of stream stability and bridge scour papers*", Journal of Hydraulic Engineering, ASCE, Vol. 127, No. 7, pp.531-533.
[13]. Melville, B.W. (1997), "*Pier and abutment scour: integrated approach*", Journal of Hydraulic Engineering, ASCE, Vol.123, No.2, February, 1997, pp.125-136.
[14]. Raudkivi, A. J., and Ettema, R., (1983). "*Clear-water scour at cylindrical piers*", Journal of Hydraulic Engineering, ASCE, Vol. 109, No. 3, pp. 50-338.
[15]. Shields, F. D., (1995). "*Fate of Lower Mississippi River habitats associated with river training dikes*", Journal of Aquatic Conservation - Marine and Freshwater Conservation, 5(2): 97- 108.

International Journal of Modern Engineering Research (IJMER)
www.ijmer.com Vol. 3, Issue. 4, Jul - Aug. 2013 pp-2089-2097 ISSN: 2249-6645

Effect of Chemical Reaction and Radiation Absorption on Unsteady Convective Heat and Mass Transfer Flow in a Vertical Channel with Oscillatory Wall Temperature and Concentration

J. Deepthi[1], Prof. D. R. V. Prasada Rao[2]
[1] *Lecturer, Department of Mathematics, Ragiv Gandhi University of KnowledgeTechnologies, APIIIT, R.K.Valley,A.P,India.*
[2]*Professor, Department of Mathematics, S. K. University, Anantapur, A. P., India.*

Abstract: *We investigate the combined influence of chemical reaction and radiation absorption on mixed convective flow in a vertical channel with oscillatory wall temperature and concentration .The non-linear coupled partial differential equations governing the flow heat and mass transfer are solved by a perturbation technique. The effect of various forces acting on the fluid system is analyzed by graphical representation of the velocity, temperature and concentration.*

Keywords: *chemical reaction, heat and mass transfer, radiation absorption, variable temperature and concentration, vertical channel.*

I. INTRODUCTION

Combined heat and mass transfer problems with chemical reaction are of importance in many processes and have, therefore, received a considerable amount attention in recent years. In processes such as drying, evaporation at the surface of a water body, energy transfer in a wet cooling tower and the flow in a desert cooler, heat and mass transfer occur simultaneously.

We are particularly interested in cases in which diffusion and chemical reaction occur at roughly the same speed. When diffusion is much faster than chemical reaction, then only chemical factors influence the chemical reaction rate; when diffusion is not much faster than reaction, the diffusion and kinetics interact to produce very different effects. The study of heat generation or absorption effects in moving fluids is important in view of several physical problems, such as fluids undergoing exothermic or endothermic chemical reaction. Due to the fast growth of electronic technology, effective cooling of electronic equipment has become warranted and cooling of electronic equipment ranges from individual transistors to main frame computers and from energy suppliers to telephone switch boards and thermal diffusion effect has been utilized for isotopes separation in the mixture between gases with very light molecular weight (hydrogen and helium) and medium molecular weight.

Muthucumaraswamy and Ganesan (12) studied effect of the chemical reaction and injection on flow characteristics in an unsteady upward motion of an unsteady upward motion of an isothermal plate. Deka et at. (4) studied the effect of the first order homogeneous chemical reaction on the process of an unsteady flow past an infinite vertical plate with a constant beat and mass transfer. Chamkha (3) studies the MHD flow of a numerical of uniformly stretched vertical permeable surface in the presence of heat generation/absorption and a chemical reaction. The effect of foreign mass on the free-convection flow past a semi-infinite vertical plate were studied (5) Chamkha (3) assumed that the plate is embedded in a uniform porous medium and moves with a constant velocity in the flow direction in the presence of a transverse magnetic field. Raptis and Perdikis (19) studied the unsteady free convection flow of water near 4 C in the laminar boundary layer over a vertical moving porous plate.

In spite of all these studies, the unsteady MHD free convection heat and mass transfer for a heat generating fluid with radiation absorption has received little attention. Hence, the main objective of the present investigation is to study the effects of radiation absorption, mass diffusion, chemical reaction and hear source parameter of hear generating fluid.The process of free convection as a mode of heat transfer has wide applications in the fields of Chemical Engineering, Aeronautical and Nuclear power generation. It was shown by Gill and Casal (6) that the buoyancy significantly affects the flow of low Prandtl number fluids which is highly sensitive to gravitational force and the extent to which the buoyancy force influences a forced flow is a topic of interest. Free convection flows between two long vertical plates have been studied for many years because of their engineering applications in the fields of nuclear reactors, heat exchangers, cooling appliances in electronic instruments. These flows were studied by assuming the plates at two different constant temperatures or temperature of the plates varying linearly along the plates etc. The study of fully developed free convection flow between two parallel plates at constant temperature was initiated by Ostrach (16). Combined natural and forced convection laminar flow with linear wall temperature profile was also studied by Ostrach (17). The first exact solution for free convection in a vertical parallel plate channel with asymmetric heating for a fluid of constant properties was presented by Anug (1). Many of the early works on free convection flows in open channels have been reviewed by Manca et al. (11). Recently, Campo et al.

(2) considered natural convection for heated iso-flux boundaries of the channel containing a low-Prandtl number fluid. Pantokratoras (18) studied the fully developed free convection flow between two asymmetrically heated vertical parallel plates for a fluid of varying thermophysical properties. However, all the above studies are restricted to fully developed steady state flows. Very few papers deal with unsteady flow situations in vertical parallel plate channels.

Transient free convection flow between two long vertical parallel plates maintained at constant but unequal temperatures was studied by Singh et al.(20). Jha et al. (9) extended the problem to consider symmetric heating of the channel walls. Narahari et al. (15) analyzed the transient free convection flow between two long vertical parallel plates with

constant heat flux at one boundary, the other being maintained at a constant temperature. Singh and Paul (20) presented an analysis of the transient free convective flow of a viscous incompressible fluid between two parallel vertical walls occurring as a result of asymmetric heating / cooling of the walls. Narahari (14) presented an exact solution to the problem of unsteady free convective flow of a viscous incompressible fluid between two long vertical parallel plates with the plate temperature linearly varying with time at one boundary, the other boundary being held at constant. There are many reasons for the flow to become unsteady. When the current is periodic due to on-off control mechanisms or due to partially rectified a-c voltage, there exist periodic heat inputs. Hence, it is important to study the effects of periodic heat flux on the unsteady natural convection, imposed on one of the plates of a channel formed by two long vertical parallel plates, the other being held at a constant initial fluid temperature. Recently Narahari(15) has discussed the unsteady free convection flow of dissipative viscous incompressible fluid between two long vertical parallel plates in which the temperature of one of the plates is oscillatory whereas that of the other plate is uniform. Haritha (7) has analysed unsteady convective heat transfer of dissipative viscous fluid through a porous medium confined in a vertical channel on whose walls an oscillatory temperature is prescribed. Ibrahim et al. (8) have studied the effect of chemical reaction and radiation absorption on the unsteady MHD free convection flow past a semi infinite vertical permeable moving plate with heat source and suction Kesavaiah et al (10) have studied the effect of the chemical reaction and radiation absorption on an unsteady MHD convective Heat and Mass Transfer flow past a semi-infinite vertical permeable moving plate embedded in a porous medium with heat source and suction

In this paper we analyse the effect of chemical reaction and radiation absorption on unsteady convective Heat and Mass Transfer flow of a viscous fluid in a Vertical channel on whose walls an oscillatory temperature is prescribed. Approximate solutions to coupled non-linear partial differential equations governing the flow, heat and mass transfer are solved by a perturbation technique. The velocity, temperature, skin friction, concentration and rate of heat and mass transfer are discussed for different variations of Sc, N, K, Q_1, γ.

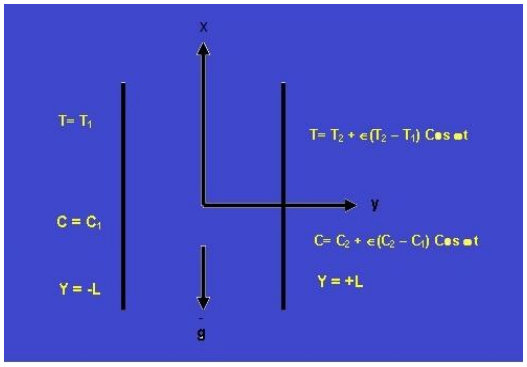

II. FORMULATION OF THE PROBLEM

We consider the flow of a viscous incompressible chemically reacting fluid in a vertical channel bounded by flat walls in the presence of constant heat sources. We choose a Cartesian coordinate system 0(x y) with walls at y = ± 1 by using Boussinesq approximation we consider the density variation only on the buoyancy term. The equation governing the flow to heat and mass transfer are

Equation of Linear Momentum

$$\frac{\partial u}{\partial t} = \frac{\mu}{\rho_0}\frac{\partial^2 u}{\partial y^2} - \rho\bar{g} - (\frac{\mu}{k})u \qquad (1)$$

Equation of Energy

$$\rho_0 C_p\left(\left[\frac{\partial T}{\partial t}\right] = k_f \frac{\partial^2 T}{\partial y^2} + Q + Q_1'(C - C_0)\right. \qquad (2)$$

Equation of Diffusion

$$\frac{\partial C}{\partial t} = D_1\frac{\partial^2 C}{\partial^2 y} - K'C \qquad (3)$$

Equation of State

$$\rho - \rho_0 = -\beta_0(T - T_0) - \beta^*(C - C_0) \qquad (4)$$

where u is the velocity component in x-direction, T is the temperature, p is the pressure, ρ is the density, σ is the electrically conductivity, μ_e is the magnetic permeability, k is the coefficient of porous permeability, μ is dynamic viscocity, k_f is coefficient of thermal conductivity β is the coefficient of volume expansion, Q is the strength of heat source, β* is the volumetric coefficient of expansion with mass fraction, D_1 is the chemical molecular diffusivity and K′ is the coefficient of chemical reaction. Q_1 is radiation absorption parameter.

The boundary conditions are

u = 0,T = T_1 ,C=C1at y = -L

$u = 0,\ T = T_1 + \in(T_2 - T_1)\cos(\omega t),\ C = C_1 + \in(C_2 - C_1)\cos(\omega t)$ at $y = +L$ (5)

On introducing the non-dimensional variables.

$$u' = \frac{u}{\nu / L}, \quad y' = y/L,\ \theta = \frac{T - T_1}{T_2 - T_1}, \quad t' = \omega t, \quad \phi = \frac{(c - c_1)}{(c_2 - c_1)}$$

Equations (2.1) – (2.3) reduce to (dropping the dashes)

$$\gamma^2 \frac{\partial u}{\partial t} = G[\theta + N\phi] + \frac{\partial^2 u}{\partial y^2} - D^{-1}u \quad (6)$$

$$P\gamma^2 \frac{\partial \theta}{\partial t} = \frac{\partial^2 \theta}{\partial y^2} + \alpha + Q_1\phi \quad (7)$$

$$S_c\gamma^2 \frac{\partial C}{\partial t} = C_{yy} - KC \quad (8)$$

where

$G = \beta g L^3 \frac{(T_2 - T_1)}{\gamma^2}$ (Grashoff number)

$P = \frac{\mu C_P}{K_f}$ (Prandtl number)

$\alpha = \frac{\theta L^2}{(T_2 - T_1)K_f}$ (Heat source parameter)

$S_c = \frac{\gamma^2}{D_1}$ (Schmidt number)

$\gamma = \frac{\omega L^2}{\gamma}$ (Wormsly number)

$N = \frac{\beta^*(C_L - C_0)}{\beta(T_L - T_0)}$ (Buoyancy ratio)

$K = \frac{K'L^2}{D}$ (Chemical reaction parameter)

$Q_1 = \frac{Q_1 \Delta C L^2}{\Delta + K_f}$ (radiation absorption parameter)

The transformed boundary conditions are

$u = 0, \quad \theta = 0, \quad \phi = 0$ at $y = -1$

$u = 0, \quad \theta = 1 + \varepsilon\cos(\omega t),\ c = 1 + \varepsilon\cos(\omega t)$ at $y = +1$ (9)

III. METHOD OF SOLUTION

In view of the boundary conditions (5) we assume

$$u = u_0 + \in e^{it} u_1$$
$$\theta = \theta_0 + \in e^{it} \theta_1 \quad (10)$$
$$\phi = \phi_0 + \in e^{it} \phi_1$$

substituting (10) in the equations6-8 and comparing harmonic & Non harmonic terms we get

$$\frac{\partial^2 u_0}{\partial y^2} - D^{-1}u_0 = G(\theta + N\phi_0) \quad (11)$$

$$\frac{\partial^2 u_1}{\partial y^2} - (D^{-1} + i\gamma^2)u_1 = -G(\theta_1 + N\phi_1) \quad (12)$$

$$\frac{\partial^2 \theta_0}{\partial y^2} + \alpha + Q_1\phi_0 = 0 \quad (13)$$

$$\frac{\partial^2\theta_1}{\partial y^2} - iP\gamma^2\theta_1 + Q_1\phi_1 = 0 \quad (14)$$

$$\frac{d^2\phi_0}{dy^2} - K_1\phi_0 = 0 \quad (15)$$

$$\frac{d^2\phi_1}{dy^2} - (K + i\,Sc\,\gamma^2)\phi_1 = 0 \quad (16)$$

III. SOLUTIONS OF THE PROBLEM

The solutions of (11)- (16) subject to the boundary conditions are

$$\phi_0 = \frac{Ch\beta_1 y}{2Ch\beta_1} + \frac{Sh\beta_1 y}{2Sh\beta_1}$$

$\theta_0 = b_1 y^2 + b_2 \text{ Ch } \beta_1 y + b_3 \text{ Sh } \beta_1 y + a_3 y + a_4$

$u_0 = b_4 y^4 + b_7 y^3 + b_8 y^2 + a_5 y + a_6 + (b_5 + b_9) \text{ Ch } \beta_1 y) + (b_6 + b_{10}) \text{ Sh } \beta_1 y.$

$$\phi_1 = \frac{Ch\beta_3 y}{2Ch\beta_3} + \frac{Sh\beta_3 y}{2Sh\beta_3}$$

$\theta_1 = k_{49} \text{ Ch}\beta_3 y + k_{50} \text{ Sh } \beta_3 y + k_{51} \text{ Ch } \beta_2 y + k_{52} \text{ Sh } \beta_2 y$

$u_1 = k_{55} \text{ Ch } \beta_3 y + k_{56} \text{ Sh } \beta_3 y + k_{57} \text{ Ch}\beta_2 y + k_{58} \text{ Sh}\beta_2 y + k_{59} \text{ Ch } \beta_4 y + k_{60} \text{ Sh } \beta_4 y.$

Where $\beta_1^2 = \alpha$ $\beta_2^2 = K$ $\beta_3^2 = i\gamma^2 P$ $\beta_4^2 = i\gamma^2 Sc$

IV. NUSSELT NUMBER and SHERWOOD NUMBER

The rate of heat transfer (Nusselt number) at the walls y = ±1 is given by

$$(Nu)_{y=\pm1} = \left(\frac{d\theta}{dy}\right)_{y=\pm1}$$

and the corresponding expressions are

$$(Nu)_{y=-1} = a_{27} + Ec[a_{28} + a_{29} + a_{30}Sh\beta_1 + a_{31}Ch\beta_1] + (0.01).E_{33}.a_{32}$$

$$(Nu)_{y=+1} = a_{21} + Ec[a_{22} + a_{23} + a_{24}Sh\beta_1 + a_{25}Ch\beta_1] + (0.01).E_{33}.a_{26}$$

The rate of mass transfer (Sherwood number) at the walls y = ±1 is given by

$$(Sh)_{y=\pm1} = \left(\frac{dc}{dy}\right)_{y=\pm1}$$

And the corresponding expressions are

$$(Sh)_{y=-1} = a_{35} + (0.01)E_{33}.a_{36}$$

$$(Sh)_{y=+1} = a_{33} + (0.01)E_{33}.a_{34}$$

where $a_1, a_2, \ldots\ldots a_{36}$ are constants shown in appendix.

V. RESULTS AND DISCUSSION

In this analysis we investigate the effect of chemical reaction on mixed convection heat and mass transfer flow of a viscous fluid through a porous medium in a vertical channel on whose walls oscillatory temperature and concentration are prescribed.

The velocity (u) is shown in figures 1-4 for different values of N,Sc , K, Q_1. The variation of u with buoyancy ratio N shows that when the molecular buoyancy force dominates over the thermal buoyancy force, the velocity enhances in the left half and reduces in the right half when the buoyancy forces act in the same direction and for the forces acting in opposite directions u reduces in the left half and enhances in the right half(fig.1). Fig 2 represents the variation of 'u' with Sc.Lesser the molecular diffusivity smaller 'u' in the flow region, and for further lowering of the diffusivity the velocity enhances in the left half and reduces in the right half and for still lowering of the molecular diffusivity the velocity enhances in the entire flow region. The effect of chemical reaction on u is shown in fig 3. It is found that an increase in $k < 1.5$ enhances |u| in entire region and for higher $k \geq 2.5$, |u| enhances in the left half and reduces in the right half. The variation of 'u' with radiation absorption parameter 'Q_1' is shown in fig 4. Fixing the other parameters. It is found that an increase in Q_1

≤ 2 leads to an enhancement in |u| and for further higher $Q_1 = 4$, |u| reduces in the flow region and for still higher $Q_1 \geq 6$, |u| reduces in the left half and enhances in the right half.

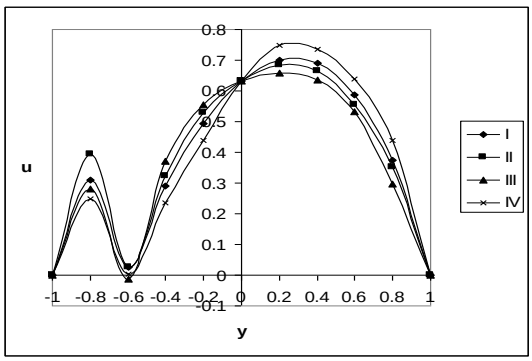

Fig. 1 : Variation of u with N

	I	II	III	IV
N	1	2	-0.5	-0.8

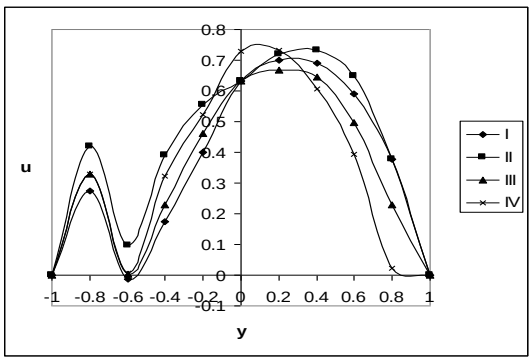

Fig. 2 : Variation of u with Sc

	I	II	III	IV
Sc	0.24	0.6	1.3	2.01

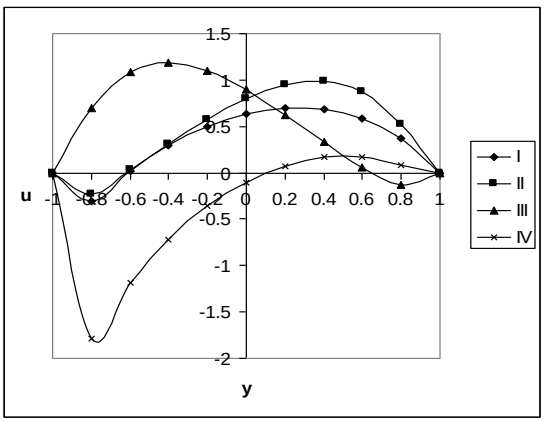

Fig. 3: Variation of u with K

	I	II	III	IV
K	0.5	1.5	2.5	3.5

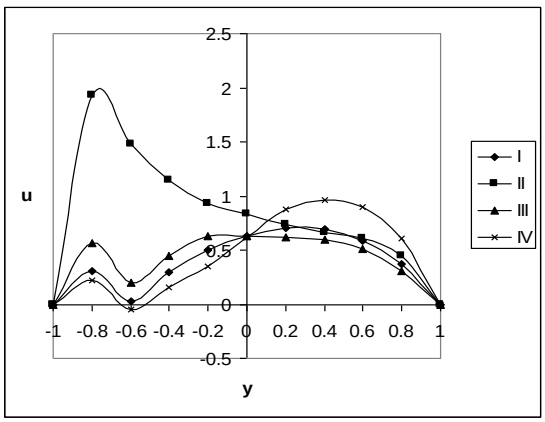

Fig. 4 : Variation of u with Q_1

	I	II	III	IV
Q_1	1	2	4	6

The Non-dimensional temperature distribution (θ) is shown in fig 5- 8 for different parametric values N,Sc , K, Q_1 . The variation of θ with the buoyancy ratio N shows that the actual temperature experiences a depreciation with increasing in |N| irrespective of the directions of the buoyancy forces(fig.5). The variation of 'θ' with Schmidt number Sc shows that lesser the molecular diffusivity larger the actual temperature in the left half and smaller in the right half, and for further lowering of the molecular diffusivity smaller the actual temperature in the entire flow region and for still lowering of the molecular diffusivity smaller the actual temperature in the left half and larger in the right half (fig 6). From fig 7 we notice that for smaller and larger values of the chemical reaction parameter K, the actual temperature depreciates in the flow region and for any intermediate value of K = 2.5, the actual temperature experiences an enhancement in the flow region. The variation of 'θ' with radiation absorption; parameter Q_1 shows that the actual temperature depreciates appreciabelly with increase in Q_1 in the entire flow region (fig.8).

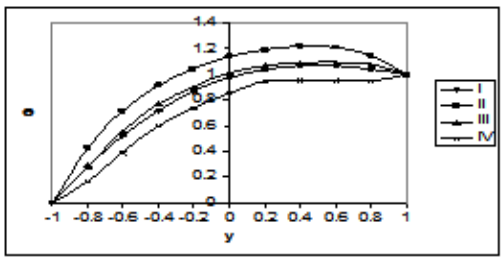

Fig. 5 : Variation of θ with N

	I	II	III	IV
N	1	2	-0.5	-0.8

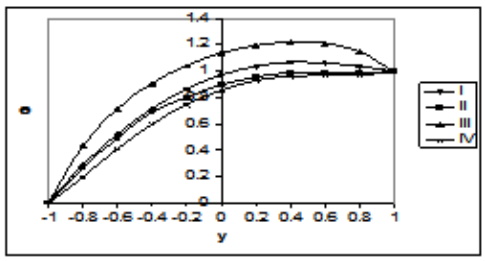

Fig. 6 : Variation of θ with Sc

	I	II	III	IV
Sc	0.24	0.6	1.3	2.01

I

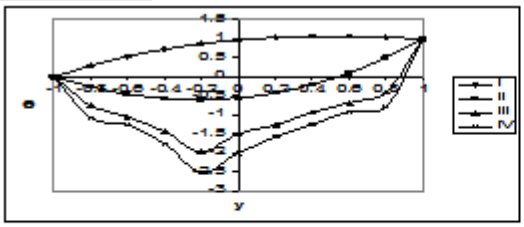

Fig. 7 : Variation of θ with K

	I	II	III	IV
K	0.5	1.5	2.5	3.5

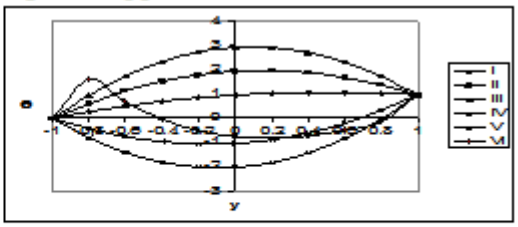

Fig. 8 : Variation of θ with Q_1

	I	II	III	IV
Q_1	1	2	4	6

The non-dimensional concentration 'C' is shown in fig 9-11 for different values of Sc, K and γ. From fig 9 we notice that lesser the molecular diffusivity larger the actual concentration in the flow region. An increase in the chemical reaction parameter 'K' results in a depreciation in the concentration in the entire flow region (fig. 10). An increase in the Wormsely number (γ) leads to an enhancement in the actual concentration in the flow field(fig.11).

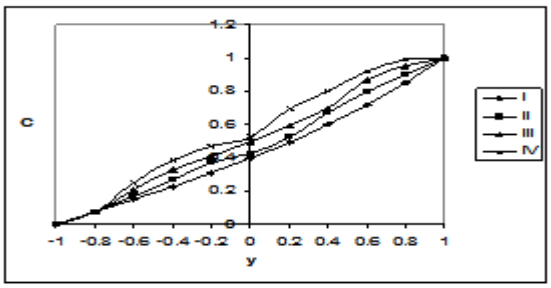

Fig 9 : Variation of C with Sc

	I	II	III	IV
Sc	0.24	0.6	1.3	2.01

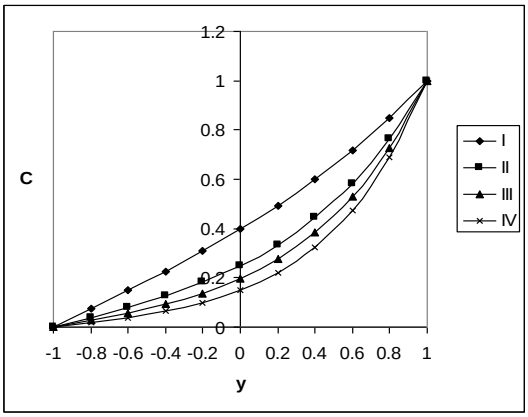

Fig.10 : Variation of C with K

	I	II	III	IV
K	0.5	1.75	2.5	3.5

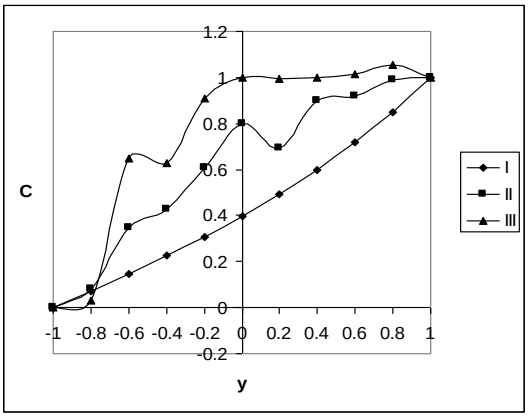

Fig 11 : Variation of C with γ

	I	II	III
γ	2	4	6

The rate of heat transfer at y = ±1 are exhibited in tables 1-4 for different parametric values. It is found that the rate of heat transfer increases with increase in |G| (or) M (or) K, thus higher the Lorentz force larger the Nusselt number at both the walls. An increase in the radiation absorption parameter Q_1 enhances |Nu| at y=+1 and reduces at y = -1 (tables 1 and 3).

From tables 2 and 4 we find that the rate of heat transfer depreciates at y = +1 and enhances at y = -1. The variation of Nu with heat source parameter α shows that the rate of heat transfer reduces at y = +1 and enhances at y = -1 with increase in $\alpha > 0$, while an increase in $\alpha < 0$ reduces |Nu| at y = ±1.

The rate of mass transfer at y = ±1 is shown tables 5-6 for different Sc, K and γ. The rate of mass transfer enhances with Schmidt number Sc.Thus higher the molecular diffusivity larger |Sh| at y = ±1. The variation of Sh with chemical reaction parameter K shows that the rate of mass transfer enhances with K at y = +1 while at y = -1 it enhances with $K \leq 1.5$ and reduces with higher $K \geq 2.5$. With reference to variation of Sh with Wormsely number (γ) exhibits that |Sh| reduces with increase in $\gamma \leq 4$ and enhances with $\gamma \geq 6$, while at y = -1 it experiences an enhancement with γ(tables.5-7).

Table 1

Nusselt Number (Nu) at y = + 1

G	I	II	III	IV	V	VI	VII	VIII	IX	X	XI
10	2.09075	10.62459	53.76271	4.41728	8.59022	125.20120	2.29075	2.19075	1.99075	3.23336	-7.03273
30	21.04668	97.73100	485.93610	40.50675	76.52689	1124.36	22.04668	21.94668	20.64668	6.64833	-151.193701
-10	2.15887	10.65264	53.77809	4.45838	8.63823	125.4219	2.25887	2.20887	20.00887	4.18804	7.70093
-30	21.25105	97.81516	485.9823	40.63005	76.67091	1125.023	22.25105	21.95105	20.65105	9.51236	-106.9927
M	2	3	4	2	2	2	2	2	2	2	2
K	0.5	0.5	0.5	1.5	2.5	3.75	0.5	0.5	0.5	0.5	0.5
Sc	1.3	1.3	1.3	1.3	1.3	1.3	0.24	0.6	2.01	1.3	1.3
Q_1	1	1	1	1	1	1	1	1	1	2	4

Table 2

Nusselt Number (Nu) at y = + 1

G	I	II	III	IV	V	VI
10	-79.46017	2.09075	0.30845	-1.60624	5.25822	6.64338
30	-801.2485	21.04668	21.00595	19.77381	17.55389	14.02036
-10	-5.37833	2.15887	0.37657	-1.53811	5.32634	6.7115
-30	-579.0029	21.25105	21.21033	19.97817	17.75823	14.22473
γ	2	4	2	2	2	2
N	1	1	1	1	1	1
α	2	2	4	6	-2	-4

Table 3

Nusselt Number (Nu) at y = – 1

G	I	II	III	IV	V	VI	VII	VIII
10	23.43691	307.9708	531.3494	44.84242	54.50365	64.98	2.84563	7.1667
30	22.9964	42.5871	68.611	64.8271	76.9875	84.125	3.53735	2.4623
-10	24.12496	38.2541	53.5047	45.25756	54.98854	65.209	2.48786	1.35672
-30	35.0605	43.4371	19.077	66.0725	77.4422	86.156	6.46406	2.63609
M	2	3	4	2	2	2	2	2
K	0.5	0.5	0.5	1.5	2.5	3.75	0.5	0.5
Sc	1.3	1.3	1.3	1.3	1.3	1.3	1.3	1.3
Q_1	1	1	1	1	1	1	2	4

Table 4

Nusselt Number (Nu) at y = – 1

G	I	II	III	IV	V	VI
10	23.4361	23.49691	25.82237	26.95587	14.91011	8.76877
30	32.9964	35.1064	34.4655	44.667	36.2552	10.98309
-10	24.1248	24.42496	26.51042	27.64391	15.59815	9.45681
-30	35.0605	36.0805	36.5296	46.7311	38.3193	13.04721
γ	2	4	2	2	2	2
α	2	2	4	6	-2	-4

Table 5

Sherwood Number (Sh) at y = + 1

S_c	I	II	III	IV	V	VI
0.24	0.8105	1.25841	1.59727	1.88134	0.80996	0.82081
0.6	0.81312	1.25999	1.59842	1.88212	0.81490	0.82832
1.3	0.81583	1.26198	1.60002	1.8834	0.82010	0.83622
2.01	0.81758	1.26341	1.60125	1.88433	0.82353	0.84140
K	0.5	1.5	2.5	3.5	0.5	0.5
γ	2	2	2	2	4	6

Table 6

S_c	I	II	III	IV	V	VI
0.24	1.44945	1.52393	1.05223	0.85282	1.50818	2.49153
0.6	1.71269	1.68234	1.16664	0.93067	1.90167	3.24322
-101.3	1.98342	1.88206	1.32729	1.05200	2.42227	4.03263
2.01	2.15846	2.02504	1.44943	1.15108	2.76520	4.55103
K	0.5	1.5	2.5	3.5	0.5	0.5
γ	2	2	2	2	4	6

VI. CONCLUSION

An attempt has been made to investigate the combined influence of chemical reaction and radiation absorption on the unsteady convective heat and mass transfer flow in a vertical channel technique using a regular perturbation technique the non-linear coupled equations has been solved. The important conclusions of this analysis are

1. Lesser the molecular diffusivity smaller 'u' in the flow region, and for further lowering of the diffusivity the velocity enhances in the left half and reduces in the right half and for still lowering of the molecular diffusivity the velocity enhances in the entire flow region. An increase in $k < 1.5$ enhances $|u|$ in entire region and for higher $k \geq 2.5$, $|u|$ enhances in the left half and reduces in the right half.An increase in $Q_1 \leq 2$ leads to an enhancement in $|u|$ and for further higher $Q_1 = 4$, $|u|$ reduces in the flow region and for still higher $Q_1 \geq 6$, $|u|$ reduces in the left half and enhances in the right half.
2. The actual temperature experiences a depreciation with increasing in $|N|$ irrespective of the directions of the buoyancy forces.Lesser the molecular diffusivity larger the actual temperature in the left half and smaller in the right half, and for further lowering of the molecular diffusivity smaller the actual temperature in the entire flow region and for still lowering of the molecular diffusivity smaller the actual temperature in the left half and larger in the right half.
3. For smaller and larger values of the chemical reaction parameter K, the actual temperature depreciates in the flow region and for any intermediate value of K = 2.5, the actual temperature experiences an enhancement in the flow region.The actual temperature depreciates appreciabelly with increase in Q_1 in the entire flow region.
4. Lesser the molecular diffusivity larger the actual concentration in the flow region. An increase in the chemical reaction parameter 'K' results in a depreciation in the concentration in the entire flow region.
5. Higher the Lorentz force larger the Nusselt number at both the walls. An increase in the radiation absorption parameter Q_1 enhances $|Nu|$ at $y=+1$ and reduces at $y = -1$.
6. The rate of mass transfer enhances with Schmidt number Sc.The rate of mass transfer enhances with K at $y = +1$ while at $y = -1$ it enhances with $K \leq 1.5$ and reduces with higher $K \geq 2.5$.

REFERENCES

[1] Anug .W , Fully developed laminar free convection between vertical plates heated asymmetrically. Int. J. Heat and Mass Transfer, Vol 15, pp.1577-1580, (1972).
[2] Campo. A, Manca O, and Marrone B , Numerical investigation of the natural convection flows for low-Prandtl fluid in vertical parallel-plates channels. ASME Journal of Applied Mechanics, Vol 73, pp. 6-107 (2006).
[3] Chamka A.J, MHD flow of a numerical of uniformly stretched vertical permeable surface in the presence of heat generation/absorption and a chemical reaction. Int Comm Heat and Mass transfer,Vol 30, pp.413-22 (2003).
[4] Deka R. Das U.N, Soundalgekar V.M , Effects of mass transfer on flow past an impulsively started infinite vertical plate with constant heat flux and chemical reaction. Forschung in Ingenieurwesen,Vol60,pp.284-287 (1994).
[5] Gebhart .B, Pera. L ,The nature of vertical natural convection flow resulting from the combined buoyancy effects of thermal and mass diffusion. J. Heat Mass Transfer Vol 14, pp.2025-2050(1971).
[6] Gill W.M and Casal,A.D, A theoretical investigation of natural convection effects in forced horizontal flows, Amer. Inst. Chem. Engg. Jour., V.8,pp.513-520(1962).
[7] Haritha. A , Transient free convective Heat transfer of a viscous fluid in channels/circular ducts with heat sources and radiation effects, Ph.D. Thesis, S.P. Mahila University, Tirupathi (2010).
[8] Ibrahim F.S., Elaiw A.M., Bakr A.A , Effect of chemical reaction and radiation absorption on the unsteady MHD free convection flow past a semi infinite vertical permeable moving plate with heat source and suction. Communications in Nonlinear Science and Numerical Simulation Vol .13, pp.1056-1066 (2008).
[9] Jha B.K, Singh A.K, and Takhar H.S , Transient free convection flow in a vertical channel due to symmetric heating. International Journal of Applied Mechanics and Engineering, 8(3), pp.497-502 (2003).
[10] Kesavaiah DC.h, Satyanarayana P.V and Venkataramana .S, Effects of the Chemical Reaction and Radiation absorption on an unsteady MHD convective Heat and Mass transfer flow past a semi-infinite vertical permeable moving plate embedded in a porous medium with heat source and suction. Int.J. of Appl. Math and Mech.7(1), pp.52-69 (2011).
[11] Manca .O, Marrone. B, Nardini .S, and Naso. V , Natural convection in open channels. In: Sunden B, Comini G. Computational Analysis of Convection Heat Transfer. WIT press, Southempton, pp.235-278 (2000).
[12] Muthucumaraswamy .R, Ganesan .P, Effect of the chemical reaction and injection on flow characteristics in an unsteady upward motion of an isothermal plate, J.Appl.Mech Tech Phys, 42, pp.665-671 (2001).
[13] Narahari M, Free convection flow between two long vertical parallel plates with variable temperature at one boundary. Proceedings of International Conference on Mechanical & Manufacturing Engineering (ICME 2008), Johor Bahru, Malaysia (2008).
[14] Narahari. M, Oscillatory plate temperature effects of free convection flow of dissipative fluid between long vertical parallel plates. Int. J. of Appl. Math. And Mech. 5(3), pp. 30-46 (2009).

[15] Narahari .M, Sreenadh. S, and Soundalgekar V.M , Transient free convection flow between long vertical parallel plates with constant heat flux at one boundary. Thermophysics and Aeromechanics, 9(2), pp.287-293 (2002).
[16] Ostrach .S , Laminar natural-convection flow and heat transfer of fluids with and without heat sources in channels with constant wall temperatures. Technical Report 2863, NASA, USA (1952).
[17] Ostrach.S , Combined natural and forced convection laminar flow and heat transfer of fluids with and without heat sources in channels with linearly varying wall temperature. Technical Report 3141, NASA, USA (1954).
[18] Pantokratoras.A, Fully developed laminar free convection with variable thermo physical properties between two open-ended vertical parallel plates heated asymmetrically with large temperature differences. ASME Journal of Heat Transfer, 128, pp.405-408 (2006).
[19] Raptis .A, Perdikis.C ,Free convection flow of water near 4 C past a moving plate. Forschung Im Ingenieurwesen; Vol. 67, pp.206-208 (2002).
[20] Singh A.K and Paul. T , Transient natural convection between two vertical walls heated/cooled asymmetrically. International Journal of Applied Mechanics and Engineering, 11(1), pp.143-154 (2006).

International Journal of Modern Engineering Research (IJMER)
www.ijmer.com Vol. 3, Issue. 4, Jul - Aug. 2013 pp-2098-2101 ISSN: 2249-6645

A Unique Approach for Data Hiding Using Audio Steganography

Tanmaiy G. Verma[1], Zohaib Hasan[2], Dr. Girish Verma[3]
[1]*Deptt. of Electronics and Communication, Gyan Ganga Institute of Technology Jabalpur-482001, (M.P.), INDIA*
[2]*Asst. Professors, Deptt. Of Electronics and Communication, Gyan Ganga Institute of Technology, Jabalpur -482001(M.P.), INDIA*
[3]*Professor, Deptt. Of Physics, Govt. Home Science College Jabalpur-482001(M.P.), INDIA*

ABSTRACT: *The rapid development of multimedia and internet allows for wide distribution of digital media data. It becomes much easier to edit, modify and duplicate digital information. Besides that, digital documents are also easy to copy and distribute, therefore it will be faced by many threats. It is a big security and privacy issue, it become necessary to find appropriate rotation because of the significance, accuracy and sensitivity of the information. Steganography and Cryptography are considered as one of the techniques which are used to protect the important information, but both techniques have their pro's and con's. This paper aims to conquer their respective drawbacks and to achieve this we are using a double layer protection technique which is cryptography cum steganography approach.*

I. INTRODUCTION

Information security is essential for confidential data transfer. Steganography is one of the ways used for secure transmission of confidential information. Hiding information in a photograph is less suspicious than communicating an encrypted file.

The main purpose of steganography is to convey the information secretly by concealing the very existence of information in some other medium such as image, audio or video.

I.1. Cryptography: Cryptography scrambles messages so it can't be understood.
Modulo encryption is a popular data hiding technique in mobile devices.
Pro's: - secure data, variable bit key for data hiding, fast and flexible easy to implement.
Con's:- limited for mobile devices only, complex hardware, easy to detect cipher patterns.
I.2 Steganography: It is an ancient art of hiding information. It hides information in digital images.
Pro's: Steganography methods reduce the chance of a message being detected.
Con's: Transmitting same images again and again may arouse suspicious-ness to the intruder, easy to decipher ones detected.

II. PROPOSED METHOD

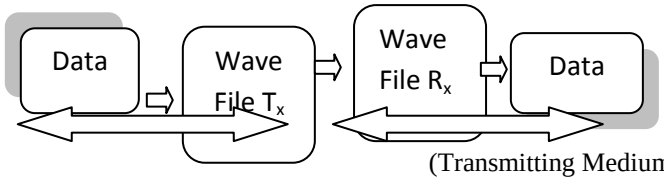

(Transmitting Medium) (Receiving Medium)
Fig 1.1

As shown above, the data is converted in stegano-object (in this case audio file) and is being transmitted and on the receiving terminal the stegano-object is processed and is converted back into the original data.

1.3 Process flow of transmitter

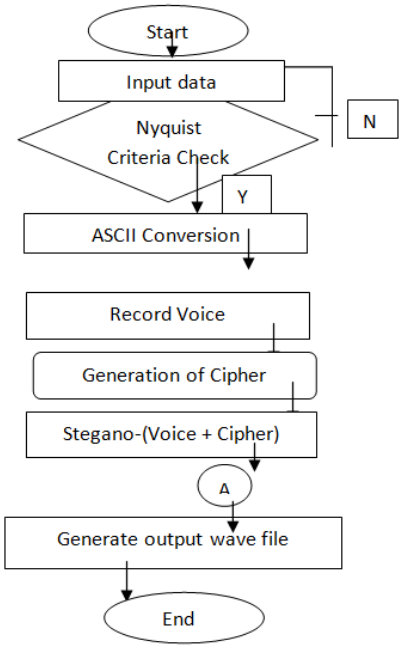

Fig. 1.2

In the above fig. it can be depicted that the data is entered by the user. Then the sampling rate is being entered by the user. Now the sampling rate entered by the user is being compared with the Nyquist rate. If the sampling rate entered by the user is greater than Nyquist rate then next step is followed else previous step is repeated. Then this step is followed by ASCII conversion in which the data is converted in ASCII format. Now the input is given by the user which is in the form of voice. This step is followed by generation of cipher. In the following step stegano-object (i.e. voice generated by the user) and the cipher so generated are combined and the output wave is being generated.

1.4 Process flow of receiver

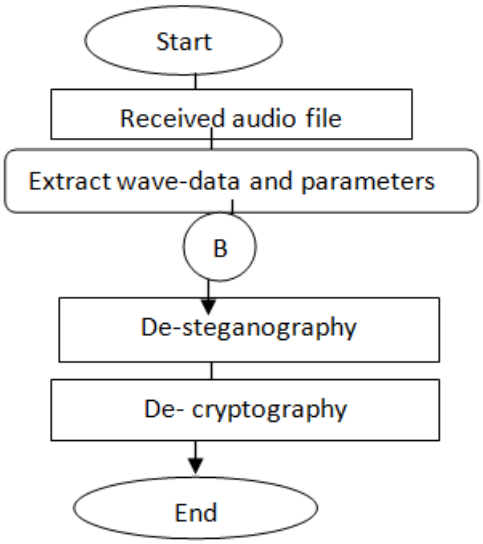

Fig. 1.3

Fig. 1.3 represents data flow of the receiver. At the receiving terminal audio file is received. Then wave-data and parameters are extracted. These parameters include length of data , frequency and step size. As shown in the next step De-steganography is performed in which voice and data cipher are being extracted. Now to convert cipher into data , de-cryptography is performed in which data is obtained in its original form.

Algorithm used for cryptography:

1. Get the data from the user(Data)
2. Transpose the given data to obtain a transposed matrix(Tdata)
   Tdata = transpose(data)

3. Divide the Tdata by any numerical value say '200'
   M = Tdata / 200
4. The 'Cipher' so generated can be obtained by calculating the modulo
   Cipher = M % 256

Algorithm used for steganography:

1. 'X' represents ciphered data
2. 'W' represents wave signal
3. 'Y' represents wave sound stegano-object
4. Then
   Y = [W_0(----),x(0), W_1(----),x(1), W_2(----),x(2), W_3(----),x(3),----------]
5. The range of block of 'W' is decided at run time as per size of 'X'

III. SIMULATION RESULTS

The fig. 1.4 illustrated below represents the pictorial view on the data being transmitted (Transmitter section).

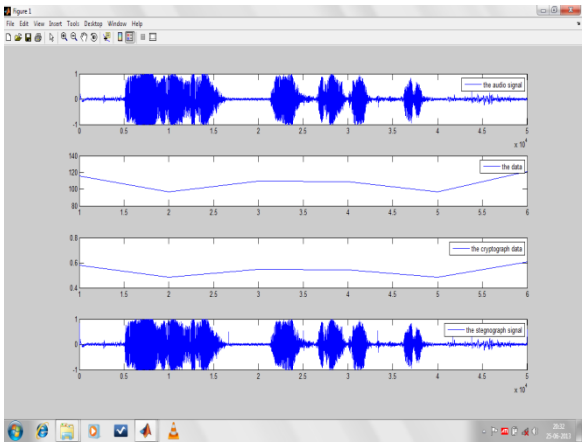

Fig. 1.4

The first part of the fig.1.4 represents the audio signal which has been taken into consideration for the transmission.
The second part of the fig.1.4 represents the data which has to be transmitted over the given channel.
The third part of the fig.1.4 represents the encrypted data or the so called 'cipher' which has been generated by the algorithm used for cryptography.
The fourth part of the fig.1.4 represents the combination of the audio signal and the cipher and the combination of the above is called stegano-object.
The fig. 1.5 illustrated below represents the pictorial view on the data being received (Receiver section).

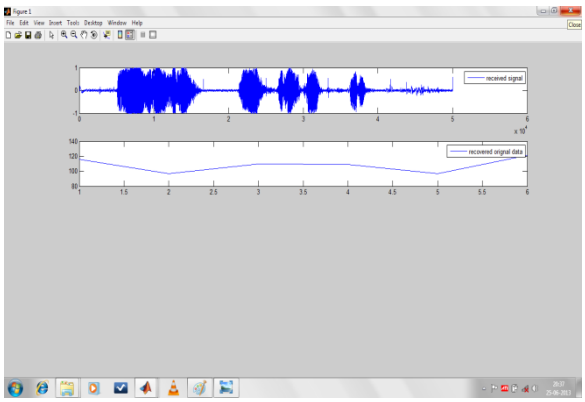

Fig. 1.5

First part of the fig 1.5 displays the received signal which has been received from the transmitter.
The second part of the fig.1.5 represents the original recovered data received by the receiver.
From fig 1.4 and fig. 1.5 it can be seen that both in transmitter and receiver recovered data is same.

IV. CONCLUSIONS

Both the cryptography and steganography have their own respective pros and cons, but the combination of both the model provides better protection of the data from the intruders.

REFERENCES

[1] Debnath Bhattacharyya, Poulami Das, Samir Kumar Bandyopadhyay and Tai-hoon Kim, Text Steganography: A Novel Approach, Research paper , International Journal of Advanced Science and Technology, Vol. 3, February, 2009.
[2] Arvind Kumar, Km. Pooja, Steganography- A Data Hiding Technique, Research paper , International Journal of Computer Applications (0975 – 8887) Volume 9– No.7, November 2010.
[3] Zaidoon Kh. AL-Ani , A.A.Zaidan, B.B.Zaidan and Hamdan.O.Alanazi, Overview: Main Fundamentals for Steganography, JOURNAL OF COMPUTING, VOLUME 2, ISSUE 3, MARCH 2010.
[4] Ross J. Anderson, Fabien A.P. Petitcolas, On The Limits of Steganography, IEEE Journal, May 1998.
[5] Miroslav Dobs´cek, Modern Steganography, Czech Technical University in Prague.

International Journal of Modern Engineering Research (IJMER)
www.ijmer.com Vol. 3, Issue. 4, Jul - Aug. 2013 pp-2102-2107 ISSN: 2249-6645

Testing of web services Based on Ontology Management Service

J. Mahesh Babu[1], P. Rajarajeswari[2], Dr. A. Ramamohan Reddy[3]
[1](M. Tech, Computer Science and Engineering, Madanapalle Institute of Technology & Sciences, Madanapalle, A.P,India)
[2](M. Tech[Ph.d], Asst. Prof., Deptt. of CSE, Madanapalle Institute of Technology & Sciences, Madanapalle, A.P, India)
[3](M. Tech, Ph.d, Professor and Head, S. V. University, Tirupathi, A.P, India)

***Abstract*:** *Web services are emerging technologies that can be considered as the result of the continuous improvement of Internet services due to the tremendous increase in demand that is being placed on them. They are quickly developing and are expected to change the paradigms of both software development and use, by promote software reusability over the Internet, by facilitate the covering of underlying computing models with XML, and by providing various and complicated functionality fast and flexibly in the form of composite service offerings. In this paper, create one web application and Framework for Web services (WS). Web application side any link fault means Web services to display fault link in background side. But proposed work each and every communication link to be checking process using JUnit tool. JUnit tool is net working tool that process is testing for Framework Web Services (WS).*

***Key Words*:** *JUnit Testing Tool, JUnit Test case, distributed/internet based software engineering tools and techniques, testing tools, web services.*

I. INTRODUCTION

Web Services (W3C, 2004b) are considered a new paradigm in building software applications; this paradigm is based on open standards and the Internet. Web Services facilitate the interconnection between heterogeneous applications since it is based on XML open standards that may be used to call remote services or exchange data.Web Services are considered an implementation or realization of the Service-Oriented Architecture (SOA) (Singh & Huhns, 2005), which consists of three roles: *Service Requester* (Consumer), *Service Provider*, and *Service Publisher*(*Broker*). To implement SOA, Web Services depend on a group of XML-based standards such as Simple Object Access Protocol (SOAP), Web Service Description Language (WSDL) and Universal Description, Discovery and Integration(UDDI). A problem that limits the growth of Web Services is the lack of trust worthiness by the requesters of Web Services because they can only see the WSDL document of a Web Service, but not how this service was implement by the provider. An example of using a Web Service is when building an application that needs to get information about a book (e.g., price and author) given the book's ISBN. Amazon provide a Web Service (see Cornelius, 2003) to fulfill this requirement and using the approach in this chapter it can assess how robust the service is before using it. Software Testing is mainly used to assess the quality attributes and detect faults in a software system and demonstrate that the actual program behaviour will conform to the expected behaviour. Testing techniques can be divided into black box and white box depending on the availability of the source code; if test data are generated depending on the source code, then a testing technique belong to white box, while if the source code is unavailable, then a testing technique belongs to black box.

This chapter's approach of Web Services testing assumes that the tester only have the WSDL document of the Web Service under test and not the source code, for this reason black box testing techniques will be used. It will also help the requesters to choose between Web Services doing the same task. However, Web Services testing still face many problems like unavailability of the source code to the requesters and that the traditional testing techniques do not cope with the new characteristics introduced by Web Services standards (Zhang & Zhang, 2005). This chapter introduces an approach to solve part of these problems, which is based on analyzing WSDL documents in order to generate test cases to test the robustness quality attribute of Web Services.

1.1 Generation of testbed. A service often relies on other services to perform its function. However, in service unit testing and also in progressive service integration testing, the service under test wants to be divorced from other services that it depends on. Techniques have been developed to produce service stubs or mock services to replace the other services for testing.

1.2 Checking the correctness of test outputs.

Research work has been reported in the literature to check the correctness of service output against formal specifications, such as using metamorphic relations, or voting mechanism to compare the output from multiple equivalent services etc.

II. Web services architecture

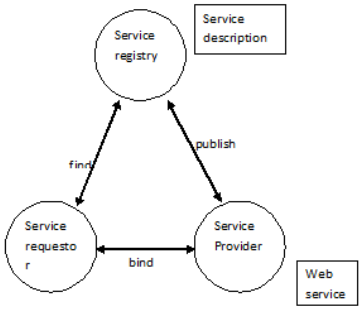

Fig-2: Web services architecture

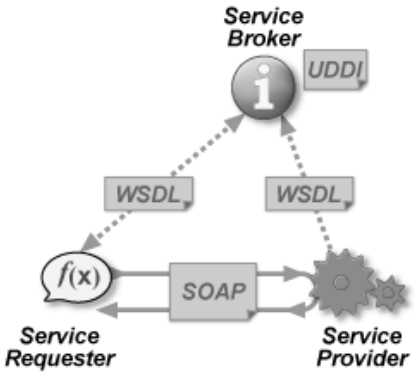

Fig-2.1: Architecture

Fig-2.1Although it is important, the centralized service registry is not the only model for Web service discovery. The simplest form of service discovery is to request a copy of the service description from the service contributor. After delivery the request, the service contributor can simply e-mail the service description as an attachment or provide it to the service requestor on a transferable media, such as a diskette. Between these two extremes, there is a need for a distributed service discovery method that provides references to service descriptions at the service provider's point-of-offering.

2.1WS-Inspection overview

The WS-Inspection specification does not define a service description language. Within a WS-Inspection article a single service can have more than individual reference to a service description. References to these two service descriptions should be put into a WS-Inspection document. If many references are available, it is useful to put all of them in the WS-Inspection document so that the document consumer can select the type of service description that they are capable of understanding and want to use. Fig-2.2 provides an overview of how WS-Inspection documents are used.

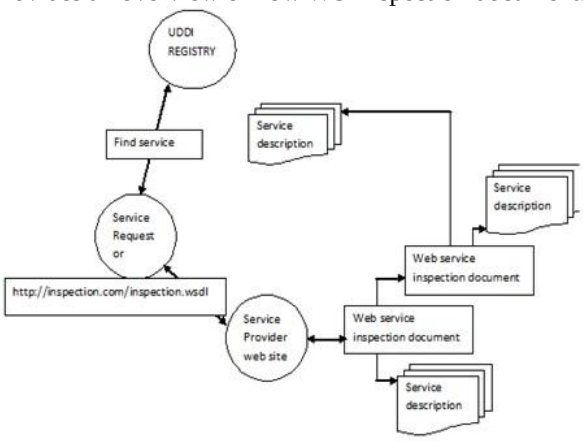

Figure 2.2: WS-Inspection overview

The WS-Inspection specification contains two primary functions, which are discussed in more detail in the next two sections.

2.2 The Architectural Models: The Service Oriented Model focuses on aspects of service, action and so on. Fig2.3 While clearly, in any distributed system, services cannot be sufficiently realized without some means of messaging, the converse is not the case: messages do not need to relate to services.

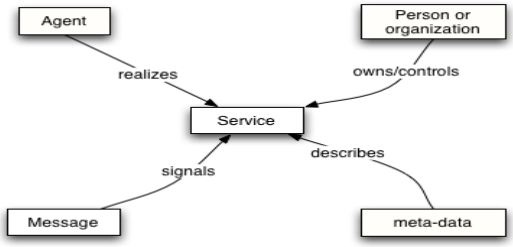

Figure 2.3. Simplified Service Oriented Model

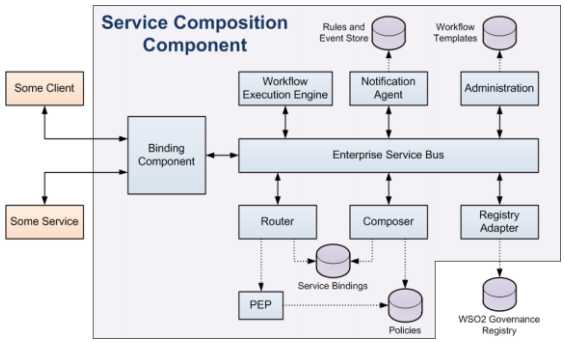

The software infrastructure consists of an **Enterprise Service Bus** (Apache Service Mix), a BPEL Workflow Execution Engine (a customised version of Apache ODE), a Resource Registry (based on the WSO2 Governance Registry and accessed via a registry adapter) and a set of custom built centre components. These are:

- The Workflow Composer selects the concrete services provided by the Resource/Service Registry at runtime. In particular, it equipment a ranking mechanism to support this local selection step.
- It is the Router's responsibility to forward messages to the appropriate endpoints. For outbound messages, which address an endpoint just by semantic information, the router handles the service compulsory in addition to ensures the accessibility of suitable, dynamically created endpoints. For inbound messages it can be configured to route them via a policy enforcement point. It can also apply fault handling strategy in the case of message faults.
- The Notification Agent collects notifications and events from various components and produces higher level notifications according to a set of rules.

III. JUnit Testing Tool

It is important in the test driven development, and is one of a family of unit testing frameworks collectively known as xUnit. JUnit is a unit testing framework for the Java Programming Language.
JUnit promotes the idea of "first testing then coding", which importance on setting up the test data for a piece of code which can be tested first and then can be implemented. This approach is like "test a little, code a little" which increases programmer productivity and stability of program code that reduces programmer stress and the time spent on debugging.

JUnit Test Case:

A Unit Test Case is a part of code which ensures that the another part of code (method) works as expected. To achieve those required results quickly, test framework is required .JUnit is perfect unit test framework for java programming language.

A formal written unit test case is characterized by a known input and by an normal output, which is worked out before the test is executed. The known input should test a condition and the expected output should test a post condition.

There must be at least two unit test cases for each requirement: one positive test and one negative test. If a requirement has sub-requirements, each sub-requirement must have at least two test cases as positive and negative.

Find defects. This is the classic objective of testing. A test is run in order to activate failures that expose defects. Generally, we look for defect in all exciting parts of the product.

Maximize bug count. The distinction between this and "find defects" is that total number of bugs is more important than coverage. We might focus narrowly, on only a few high risk features, if this is the way to find the most bugs in the time available.

Block premature product releases. This tester stops untimely delivery by finding bugs so serious that no one would ship the product until they are fixed. For every release result meeting, the tester's goal is to have new show stopper bugs.

Help managers make ship / no-ship decisions. Managers are typically concerned with risk in the field. They want to know about coverage (maybe not the simplistic code coverage data, but some indicator of how much of the product has been

addressed and how much is left), and how important the known problems are. Problems that show important on paper but will not lead to customer dissatisfaction are probably not relevant to the ship decision.

Minimize technical support costs. Working in combination with a technical support or help desk group, the test team identify the issue that lead to calls for support. These are frequently peripherally related to the product under test--for example, getting the product to work with a specific printer or to import data successfully from a third party database might prevent more calls than a low-frequency, data-damaging crash.
Assess conformance to specification. Any declare made in the specification is checked.

Conform to regulations. If a regulation specifies a certain type of coverage (such as, at least one test for every claim made about the product), the test group creates the suitable tests. If the regulation specifies a style for the specifications or other Documentation, the test group probably checks the style. In general, the test group is focusing on anything covered by regulation and (in the context of *this objective*) nothing that is not covered by regulation.

Minimize safety-related claim risk. Any error that could lead to mistake or injury is of primary interest. Errors that lead to loss of time or data or damage data, but that don't carry a risk of harm or damage to physical things are out of scope.

Find safe scenarios for use of the product (find ways to get it to work, in spite of the bugs). Sometimes, all that you're looking for is one way to do a task that will consistently work--one set of instructions that someone else can follow that will reliably deliver the benefit they are supposed to direct to. In this case, the tester is not looking for bugs.

Assess quality. This is a tricky objective because quality is multi-dimensional. The nature of excellence depends on the nature of the product. For example, a computer game that is rock solid but not entertaining is a lousy game. For example, *reliability* is not just about the number of bugs in the product. It is (or is often defined as being) about the number of reliability-related failures that can be expected in a period of time or a period of use. (*Reliability-related?* In measuring reliability, an association might not care, for example, about misspellings in error messages.) To make this prediction, you need a mathematically and empirically sound model that links test results to dependability. Testing involves meeting the data needed by the model. This strength involve extensive work in areas of the product believed to be stable as well as some work in weaker areas. Visualize a reliability model based on counting bugs found (perhaps weighted by some type of severity) per N lines of code or per K hours of testing.

Troubleshooting to make the bug report easier to understand and more likely to fix is (*in the context of assessment)* out of scope.

Verify correctness of the product. It is not possible to do this by testing. You can prove that the product is *not* correct or you can demonstrate that you didn't find any errors in a given period of time using a given testing strategy. However, you can't test exhaustively, and the product capacities fail under situation that you did not test. The best you can do is assessment--test-based estimation of the probability of errors.

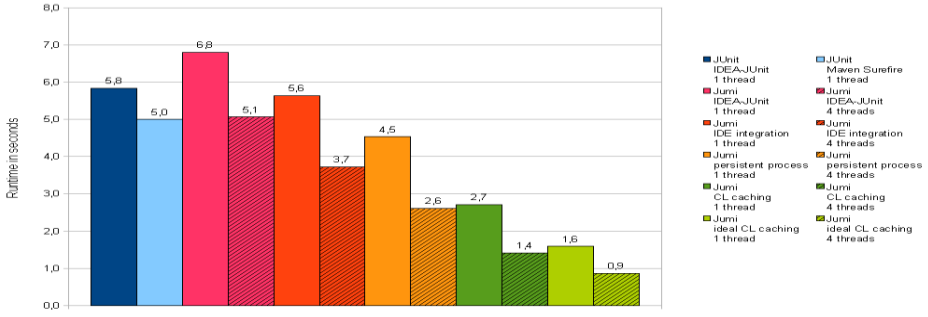

The time spent on 3.b only depends on the performance of the tester (s). It is irrelevant to the efficiency of the broker. Therefore, it is misplaced in our experiment. shows the average lengths of execution times on different tasks with the number of different types of subtasks ranging from 1 to 5. A quadratic polynomial figure fits the curve very well with R2 ¼ 0:9984.In summary, the experiments show that the broker is capable of dealing with test problems of practical sizes with respect to the number of testers registered, the size of the knowledge base, and the difficulty of test tasks.

IV. Testing Modulus:

4.1Test/Functional Service Generation:

F-service should be accompanied with a special T-service so that test executions of the F-service can be performed by the consequent T-service. Thus, the normal operation of the original F-service is not disturbed by test requests and the cost of testing are not charged as real invocations of the F-service. The F-service provider can differentiate real requests from

the test requests so that no real world effect is caused by test requests. F-service should also provide additional support to other test activities.

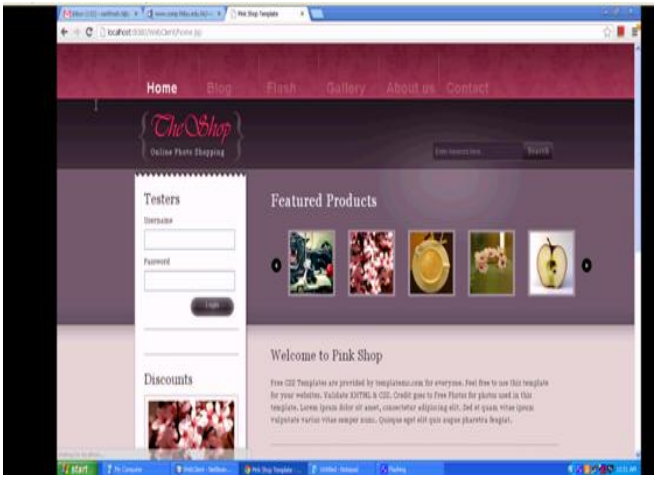

4.2Test case generation:

Besides the service specific T-service that accompanies an F-service, a test service can also be a general function test tool that performs various test activities, such as test planning, test case generation, and test result checking, etc. A general purpose T-service can be focused in certain testing techniques or methods such as the generation of test cases from WSDL. The test broker TB decomposes the test task into a sequence of subtasks and searches for appropriate testers for each subtask by submitting search requests to the registry.

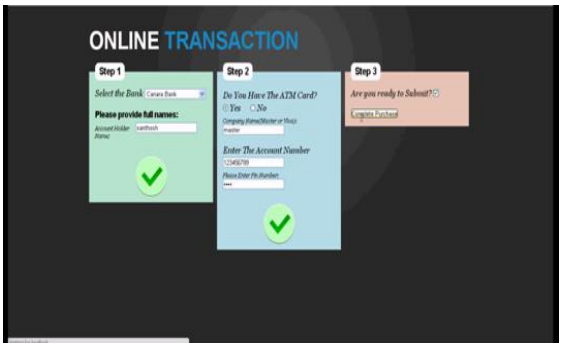

4.3Result Checking:

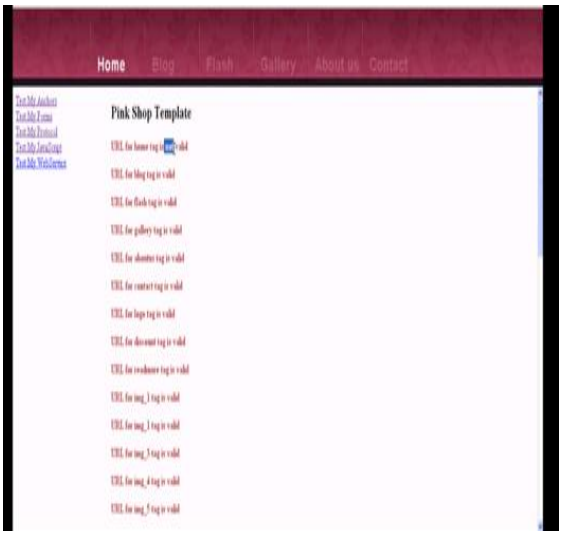

After checking the trustworthy of tester TG, the insurer A's T-service releases its design model to TG. After effectively obtain the design model, TG produce a set of test cases and returns a test suite to the test broker TB. The test broker then pass the test cases to TE, requests for the test summons of the insurer A's services using the test cases and requests it to check the output correctness and to measure the test coverage. TE performs these tasks by association with the insurer A's T-services. The test results are then returned to the test broker TB.

4.4 Report Preparation:

Finally, TB assembles a test report containing information about test output correctness and test sufficiency. The test report is sent to TB, which is used to decide whether the dynamic link will take place.

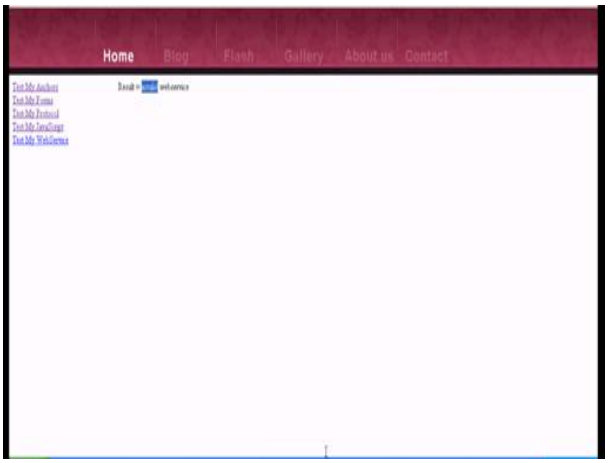

V. Conclusion

we presented a service oriented architecture for testing Web Services. In this architecture, various T-services collaborate with each other to complete the test tasks. We employ the ontology of software testing STOWS to describe the capabilities of T-services and test tasks for the discovery, registration and invocation of T-services. The knowledge of intensive composition of T-services has realized by the development and employment of the test brokers, which are also called T-services. We have implemented the architecture in Semantic WS technology. Here Errors can be identified in particular location. In background side web services to display fault links. By using JUnit tool we can checking the each and every communication links.

References

[1] F. McCabe, E. Newcomer, M. Champion, C. Ferris, and D. Orchard, Web Services Architecture, W3C Working Group Note, http://www.w3.org/TR/ws-arch,2004.
[2] L.F. de Almeida and S.R. Vergilio, “Exploring Perturbation Based Testing for Web Services,” Proc. IEEE Int’l Conf. Web Services (ICWS ’06), pp. 717-726, Sept. 2006.
[3] J.B. Li and J. Miller, “Testing the Semantics of W3C XML Schema,”Proc. 29th Ann. Int’l Computer Software and Applications Conf. (COMPSAC ’05), pp. 443-448, July 2005.
[4] W. Tsai, R. Paul, W. Song, and Z. Cao, “Coyote: An XML-Based Framework for Web Services Testing,” Proc. IEEE Int’l Symp. High Assurance Systems Eng. (HASE ’02), pp. 173-174, Oct. 2002.
[5] X. Bai, W. Dong, W. Tsai, and Y. Chen, “WSDL-Based AutomaticTest Case Generation for Web Services Testing,” Proc. IEEE Int’l Workshop Service Oriented System Eng. (SOSE ’05), pp. 215-220, Oct.2005.
[6] N. Looker, M. Munro, and J. Xu, “WS-FIT: A Tool for Dependability Analysis of Web Services,” Proc. 28th Ann. Int’l Computer Software and Applications Conf. (COMPSAC ’04), pp. 120-123, Sept.2004.
[7] A. Bertolino, J. Gao, and E. Marchetti, “XML Every-FlavorTesting,” Proc. Second Int’l Conf. Web Information Systems and Technologies (WEBIST ’06), pp. 268-273, Apr. 2006.
[8] W. Xu, J. Offutt, and J. Luo, “Testing Web Services by XMLPerturbation,” Proc. IEEE 16th Int’l Symp. Software Reliability Eng.(ISSRE ’05), pp. 257-266, Nov. 2005.
[9] S.C. Lee and J. Offutt, “Generating Test Cases for XML-Based Web Component Interactions Using Mutation Analysis,” Proc. 12th Int’l Symp. Software Reliability Eng. (ISSRE ’01), pp. 200-209, Nov. 2001.

International Journal of Modern Engineering Research (IJMER)
www.ijmer.com Vol. 3, Issue. 4, Jul - Aug. 2013 pp-2108-2110 ISSN: 2249-6645

Enhancement in viscosity of diesel by adding vegetable oil

Shailesh N. Gadhvi[1], Dr. Ajit V. Pandya[2]
Department of Biochemistry, C.U. Shah Science College, Ahmedabad, Gujarat, India

ABSTRACT: *Some time due to improper blending of different refinery distillate stream and variation in distillation range as well as cause of using different crude we are getting resulting diesel having various range of viscosity. When viscosity falling below specification value it is necessary to enhance this value for proper use of this diesel in engine. Enhancement of this viscosity was done by using some vegetable oil in this paper. Soya bin methyl ester and yellow grease methyl ester are two vegetable oil studied among this soya bin methyl ester is most efficient vegetable oil to raise the viscosity of diesel.*

KEYWORDS: *Viscosity, distillate, stream, SME (soya bin methyl ester), YGME (Yellow grease methyl ester.)*

I. INTRODUCTION

The primary role of engine oil is the lubrication of moving engine parts and reducing friction and wear of metal surfaces which provides the good engine performance and its long life. In order to provide a defined quality of engine oils during production and for final products to meet the product specifications we need to know the physical chemical characteristics of engine oils. Certain physical-chemical characteristics which are significant for the quality of engine oils are achieved by adding additives to base oils. The most frequent additives are for: Improving of viscosity index-improvers
Reducing pour point-depressants
Maintaining engine cleanness-detergents and dispersants
Preventing oxidation-antioxidants
Preventing corrosion-corrosion inhibitors

The most important engine oils characteristic is the viscosity defined as a measure of inner friction which works as a resistance to the change of molecule positions in fluid flows when they are under the impact of shear force, or in other words, it is the resistance of fluid particles to shear. When fluids flow, there are friction forces between their particles and also between fluid particles and the adjoining surface, caused by the resistance of fluid to particle shear and also of surface roughness. The viscosity is a changeable category and it depends on the change of temperature and pressure. A higher temperature reduces the viscosity and makes a fluid thinner. The viscosity index is an empirical number which shows how the viscosity of some oils changes by increasing or reducing the temperature. High viscosity index shows relatively small tendency of viscosity to change upon influence of certain temperature, as oppose of low viscosity index which shows greater viscosity change with temperature. The calculation is based on viscosity values determined by ASTM D 445 method at 40 and 100 °C.

II. MATERIALS AND METHODS

Petroleum diesel of refinery grade purchased directly from city petrol pump and different additive added to this diesel were purchased from Shree Padma Bio Fuels is Soya Methyl Ester which is derived from Esterrification of Soya oil with Methanol and yellow grease were make available from Biomass Energy Conversion Center of the Iowa Energy Center in Nevada, Iowa. The methods used in this work are the ASTM standard methods.

III. EXPERIMENTAL

Diesel fuel is composed of a variety of blending components of different hydrocarbon types. Refiners use blending components to balance the viscosity specifications that produce the optimum diesel fuel for specific applications and operating environments.

Petroleum-derived diesel is composed of about 75% saturated hydrocarbons (primarily paraffin including n, iso, and cycloparaffins), and 25% aromatic hydrocarbons (including naphthalene and alkyl benzenes). The average chemical formula for common diesel fuel is C12H23, ranging approximately from C10H20 to C15H28. Some of the blending components are straight-run streams that come directly from the crude oil in the primary distillation process. Other blending components are hydrocracker streams produced from heavy gas oils, thermally cracked distillates typically produced from the delayed coking of refinery residual streams, and light-cycle oils produced from fluid catalytic cracker (FCC) units. Depending on the sulfur content of the crude oil, the straight-run and processed streams may require desulfurization before addition into the final diesel-fuel blend. refinery stream that contribute for saturated hydrocarbon is LGO,HGO,VD,LK,HK,STRAIGHT RUN HEAVY NAPHTHA, while stream that contribute for aromatic are cracked stream like LCO,HEAVY GASOLINE and AGO. Viscosity of diesel is increases with increasing molecular weight of diesel as well as increasing naphthenic and paraffinic compound in diesel. Among all stream that use for diesel HGO having highest concentration of naphthenic and paraffinic compounds as well higher molecular weight. Considering this basic concept generally refiner are used to increase blending ratio of HGO hence we get desired value of viscosity of final blended diesel product but this concept is not always advisable because of cost of HGO as well as direct contribution of HGO on other key parameter of diesel.

Table No. 01 Base diesel blending stream proportion and distillation property

Volume percentage	**28%**	**15%**	**12%**	**2%**	**21%**	**20%**	**0.8%**	**1.2%**	**TOTL= 100%**
Stream	LGO	HGO	VD	LK CDU	HK CDU	LCO	HEAVY GASOLINE FCCU	AGO VBU	RAW DIESEL
IBP	207	268	254	160	189	166	137	175	156
5%	245	294	281	171	215	191	143	195	171
10%	260	312	287	173	222	199	145	202	179
30%	282	332	311	178	236	227	150	229	207
50%	296	345	329	186.0	244	255	156	259	240
70%	312	350	347	198	251	290	164	291	279
85%	328	377	364	210	257	320	172	314	314
90%	336	389	373	216	260	331	177	323	330
95%	348	393	390	225	265	342	183	336	352
FBP	360	399	397	232	269	346	195	342	361
VISCOSITY@ 40^0C	3.934	9.668	6.798	1.551	2.0235	2.665		2.330	1.946

To overcome this problem we have choose to use two different type of bio oil that can enhance viscosity of diesel without measure deviation in other key parameter of diesel .The yellow grease methyl ester (YGME) and the soybean oil methyl ester (SME) were tested as pure fuels and as 20% blends with as such diesel fuel. Diesel fuel was purchased from a local commercial supplier. The SME purchased from Shree Padma Bio Fuels and YGME purchased were prepared in the pilot plant located at the Biomass Energy Conversion Center of the Iowa Energy Center in Nevada, Iowa. Effect of SME blending on viscosity and other parameter is as shown below presented in tables 2

Table No. 02 Properties of diesel fuel and various blends of SME

Property	Diesel 0%	SME 20%	SME 40%	SME 60%	SME 80%	SME 100%
Sulphur fraction in the fuel	0.025	0.00105	0.00208	0.00308	0.00405	0.005
Cetane number	48	48.69	49.37	50.03	50.67	51.3
Fuel density (kg/m3)	830	841	852	863	874	883
Kynemetic viscosity (Cst)	1.946	3.971	4.319	4.635	4.943	5.285

Similarly effect of Yellow grease methyl ester blending on viscosity and other parameter is as shown below presented in tables 3

Table No. 03 Properties of diesel fuel and various blends of YGME

Property	Diesel 0%	YGME 20%	YGME 40%	YGME 60%	YGME 80%	YGME 100%
Sulphur fraction in the fuel	0.025	0.00145	0.00278	0.00388	0.00465	0.002
Cetane number	48	49.85	50.37	51.53	52.17	57.3
Fuel density (kg/m3)	830	841	852	863	874	876
Kinematic viscosity (Cst)	1.946	2.471	2.985	3.585	4.046	4.000

From above two experiments it is merely seen that both the additive having tendency to raise the viscosity of base diesel in addition to this there is no other adverse effect on other key parameter of base diesel.

One more experiment were carry out by adding 1:1 ratio of SME :YGME to diesel in 20% volume the result obtained of this experiment and complete test report of pure SME and YGME are as bellowing shown in Table No. 04

Table No. 04 Fuel Properties of petroleum diesel, yellow grease methyl ester, Soy methyl ester, and B20

Fuel Property	**Test Method**	**Diesel Fuel**	**YGME**	**SME**	**B20 (80%petroleum diesel+10%SME+10%YGME)**
Flash Pt. (oC)	ASTM D93	59	130	160	74
Heating value (BTU/lb.)	ASTM D240	18110	15781	15873	17828
Kinematic Viscosity (cSt @ 40oC)	ASTM D445	1.946	4.0	5.285	2.981
Ash (mass %)	ASTM D482	0	0	0	0
Cetane Number	ASTM D613	48.0	57.3	51.3	49.8
Fuel density (kg/m3)	ASTM D1298	830	876	0.883	0.858
Aromatics (vol. %)	ASTM D1319	27.6	0	0	0
Sulfur (mass %)	ASTM D2622, ASTM D 4294	0.025	0.002	0.005	0.023
Water & Sediment (vol. %)	ASTM D2709	0	0	0	0
HFRR Lubricity (@ 60oC, WSD um)	ASTM D6079	448	376	377	375
Distillation Analysis	ASTM D86				
oF IBP		156	613.8	626.5	358.4
oF 10% Recovered		179	629.7	634.2	432.2
oF 50% Recovered		240	636.6	638.5	534.4
oF 90% Recovered		330	656.9	652.9	638.1
oF Final Boiling Point		361	661.5	651.9	667.6
Vol.% Recovered		97.7	96.2	94.5	98.0
Vol. % Residue		1.6	2.1	5.2	1.3
Vol. % Loss		1.0	1.7	0.3	0.7

IV. RESULTS AND DISCUSSION

Yellow grease methyl ester and soya methyl ester both having ability to enhance viscosity of diesel but out of this both soya methyl ester is most efficient to raise viscosity because of its own higher viscosity value compare to yellow grease methyl ester. Soya Methyl ester having higher value of sulfur and lower value of cetane number compare to yellow grease methyl ester hence it gives reducing effect on other key parameter of diesel with respect to yellow grease methyl ester. Although before using it as additive further study of fuel emission in engine required.

REFERENCES

[1]. Blackie Academic &Professional, London Mortier R.M., Orszulik S.T.: Chemistry and Technology of Lubricants, 1997.
[2]. Maziva ipodmazivanje, JUGOMA, Zagreb, 1986.
[3]. Technische Akademie Esslingen, Dardin A.: Chemistry and Application of Viscosity Index Improvers, Proceedings of the 12th International Colloquium of Tribology, Ostfildern: Technische Akademie Esslingen, (2000) 631.
[4]. ACEA European Oil Sequences 2007, Brussels, Belgium, 2007
[5]. ASTM D 7109-04 Standard Test Method for Shear Stability of Polymer Containing Fluids Using a European Diesel Injector Apparatus at 30 and 90 Cycles
[6]. ASTM D 6278-06 Standard Test Method for Shear Stability of Polymer Containing Fluids Using a European Diesel Injector Apparatus
[7]. Classifications and Specifications Handbook –Chevron Oronite Company LLC Automotive Engine Lubricants 2005,
[8]. Denis J., Briant J.Hipeaux J.C.: Lubricant properties analysis & Testing, EditionTechnip,Paris, 2000.

International Journal of Modern Engineering Research (IJMER)
www.ijmer.com Vol. 3, Issue. 4, Jul - Aug. 2013 pp-2111-2118 ISSN: 2249-6645

Transmission Congestion Management by Using Series Facts Devices and Changing Participation Factors Of Generators

G. Vinod Kumar[1], J. Srinivasa Rao[1], J. Amarnath[2]
[1]Department of Electrical and Electronics Engineering, QIS College of Engg & Technology, Ongole.
[2]Department of Electrical and Electronics Engineering, JNTUH College of Engg & Technology, Hyd.

Abstract: *The deregulated power system is quite popular in now a days. The increased power demand has forced the power system to operate very closer to its stability limits. So transmission congestion and voltage instability problems are arise in the power system. Due to the congestion in the network, not always possible to transmit the all contracted power. Congestion management is a tough task in deregulated power system. In this paper two different methodologies were used to manage the congestion in the network. The first methodology is congestion managed using series FACTS device. This method is tested on modified IEEE 5 bus system. The second method is congestion management by changing participation factors of generators. This method is tested on modified IEEE 9 bus system.*

Key Words: *Deregulated power system, congestion, Available Transfer Capability (ATC), Thyristor Controlled Series capacitor (TCSC), Transmission Load Relief (TLR) factors, Participation Factors.*

I. INTRODUCTION

In present days all our basic needs are relates with electricity. Like the growth of population, the demand for electricity is also tremendously increases day to day. So there may be a need to enhance either the existing power system or establish the new system to supply the power to meet the particular load demands. The establishment of new power system is very costliest choice. So we mostly concentrate on the first choice that is enhancing the existing power system. The main objective of the deregulation of a power industry is creating a competitive environment in between the power producers and prevents monopolies and also provides many choices to consumers to pick up a good utility. Due to the lack of coordination in between generation and transmission utilities, transmission congestion is occurs. So due to this transmission congestion, there may not be possible to dispatch all contracted power transactions. The series FACTS device TCSC is placed in series with the line for congestion management. In [1], sensitivity approach is used to find the optimal location for placement of TCSC. The reduction of total system reactive power losses method is one used to find optimal location of FACTS devices [4-7]. In this method, an over loaded sensitivity factor (power flow index) is used for optimal location of series FACTS device (i.e. TCSC) for static congestion management [8]. But for large systems, this enumerative approach is not practical given to the large number of combinations that have to be exam. In [2], here congestion is managed by Transmission line relief (TLR) method used in deregulated power industry [3]. In deregulated power systems, before permitting the power transactions, feasibility of transmission network components is required to be determined. It can be detected by evaluation of Available Transfer Capability (ATC) of the network for various applied power transactions [9-10]. ATC is an important term in restructured power system that affects the planning and controlling of transmission infrastructure. The FACTS devices are used to enhance ATC in deregulated power system [11]. Main constraints for ATC are thermal limits, voltage limits and steady state stability limits. The variable load is considered as data to calculate ATC of network, considering various sets of generator participation factors [12].

II. MODELLING [STATIC] OF TCSC

For static application like congestion management FACTS devices can be modelled as power injection model. The TCSC model shown as follows

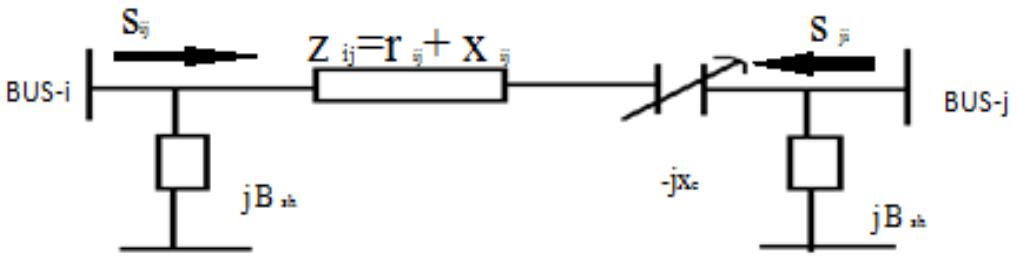

fig1. Modelling of TCSC

Let the complex voltage at bus i and bus j be denoted as $V_i \angle\delta_i$ and $V_j \angle\delta_j$ respectively. The expressions for real and reactive power flows from buses i to j and j to i can be written as follows

$$P^c_{ij} = V_i^2 G_{ij} - V_i V_j (G_{ij} \cos\delta_{ij} + B_{ij} \sin\delta_{ij}) \quad \& \quad P^c_{ji} = V_j^2 G_{ij} - V_i V_j (G_{ij} \cos\delta_{ij} - B_{ij} \sin\delta_{ij}) \qquad (1)$$

$$Q^c_{ij} = -V_i^2 (B_{ij} + B_c) - V_i V_j (G_{ij} \sin\delta_{ij} - B_{ij} \cos\delta_{ij}) \quad \& \quad Q^c_{ji} = -V_j^2 (B_{ij} + B_c) - V_i V_j (G_{ij} \sin\delta_{ij} + B_{ij} \cos\delta_{ij}) \qquad (2)$$

Hence, the change in the line flows due to series capacitance, the real power flow injection at bus i is

$P_{ic} = V_i^2 \Delta G_{ij} - V_i V_j (\Delta G_{ij} \text{Cos}\ \delta_{ij} + \Delta B_{ij} \text{Sin}\ \delta_{ij})$ (3)

$P_{jc} = V_j^2 \Delta G_{ij} - V_i V_j (\Delta G_{ij} \text{Cos}\ \delta_{ij} + \Delta B_{ij} \text{Sin}\ \delta_{ij})$ (4)

$Q_{ic} = -V_i^2 \Delta B_{ij} - V_i V_j (\Delta G_{ij} \text{Sin}\delta_{ij} - \Delta B_{ij} \text{Cos}\delta_{ij})$ (5)

$Q_{jc} = -V_j^2 \Delta B_{ij} + V_i V_j (\Delta G_{ij} \text{Sin}\delta_{ij} + \Delta B_{ij} \text{Cos}\delta_{ij})$ (6)

Where $\Delta G_{ij} = \frac{x_c r_{ij} (x_c - 2x_{ij})}{(r_{ij}^2 + x_{ij}^2)(r_{ij}^2 + (x_{ij} - x_c)^2}$ & $\Delta B_{ij} = \frac{-x_c (r_{ij}^2 - x_{ij}^2 + x_c x_{ij})}{(r_{ij}^2 + x_{ij}^2)(r_{ij}^2 + (x_{ij} - x_c)^2}$

The above equations were used to model (static) the TCSC for congestion management in deregulated power system.

III. SELECTION OF BEST LOCATION FOR TCSC PLACEMENT

The optimal location of FACTS devices is one of the important concepts. The main goal of the congestion management is to perform a best utilization of the existing transmission lines.

3.1 OPTIMAL PLACEMENT OF TCSC BASED ON SENSITIVITY APPROACH:

Based on sensitivity approach, we find the optimal location of TCSC for congestion management.

3.1.1 MITIGATION OF TOTAL SYSTEM VAR POWER LOSS:

A method based on the sensitivity of the total system reactive power loss with respect to the control variable of the TCSC. The reactive power loss sensitivity factors with respect to these control variables may be given as follows:

1. Loss sensitivity with respect to control parameter X_{ij} of TCSC placed between buses i and j,

$$a_{ij} = \frac{\partial Q_L}{\partial X_{ij}} \quad (7)$$

These factors can be computed for a base case power flow solution.

$$a_{ij} = \frac{\partial Q_L}{\partial X_{ij}} = [V_i^2 + V_j^2 - 2 V_i V_j \text{Cos}(\delta_i - \delta_j)] \frac{R_{ij}^2 - X_{ij}^2}{(R_{ij}^2 + X_{ij}^2)^2} \quad (8)$$

IV. LOAD CURTAILMENT METHOD BASED ON TLR SENSITIVITIES:

Transmission load relief sensitivities can be used for the purpose of congestion alleviation by load curtailment. In the method of congestion alleviation using load curtailment, TLR sensitivities at all load buses for the most overloaded line is considered**.** The TLR sensitivity at a bus k for a congested line i-j is S_{ij}^k and is calculated by

$$S_{ij}^k = \frac{\Delta P_{ij}}{\Delta P_k} \quad (9)$$

The excess power flow on transmission line i-j is given by

$$\Delta P_{ij} = P_{ij} - \Delta P_{ij}^* \quad (10)$$

Where P_{ij} = actual power flow through transmission line i-j

P_{ij}^* = flow limit of transmission line i-j

ΔP_k = change in load after curtailment at bus k

V. ATC CALCULATION

The Net work response method is the usual method for calculating ATC. In which bilateral transactions are only considered and then, whether the transaction is feasible for the network or not is concluded.

Mathematically, ATC is defined

$$\text{ATC} = \text{TTC-TRM-[ETC+CBM]} \quad (11)$$

Where, TTC= Total Transfer Capability

TRM = Transmission Reliability Margin

ETC=Existing Transmission Commitments

CBM= Capacity Benefit Margin

In above equation [11], the terms except TTC are decided by the load serving entities. If TRM and CBM are not considered, TTC represents ATC at the base load flow conditions. The term TTC is variable and changes according to the change in line flows, line limits and the transacted power between the buses.

5.1 PARTICIPATION FACTOR

This is an important factor in generator details. This participation factor is used to determine how the real power output of the generator changes in response to changes in load demand. It is given as,

$$X_i = \frac{\Delta T_{ik}}{\Delta P_k} \quad (12)$$

Where X_i = participation factor of generator

ΔT_{ik} = generator power changes at i^{th} bus due to change in load at k^{th} bus

ΔP_k = load change at k^{th} bus

The buyer and seller transactions are specified for the purpose of calculating ATC. This can be a single bus, slack, injection group, areas etc. when the multiple generators are exists in the transaction such as the case of areas or injection groups, participation factors needed to be assigned. So as to know the participation of generators or loads, the load flow solution must be known.

VI. SIMULATION RESULTS FOR MODIFIED IEEE 5 BUS SYSTEM:

In this study a modified IEEE 5 bus system has been analysed for congestion management. By optimal placement of FACTS device such as TCSC using power world simulator software based on sensitivity indices approach.

Fig 2 shows the modified IEEE 5 bus system drawn in power world simulator

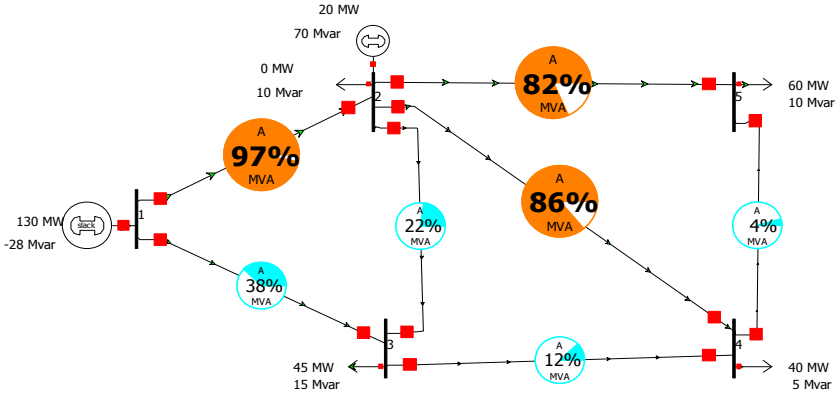

Fig 2: modified IEEE 5 bus system without TCSC

Fig 2 shows the transmission line flows without TCSC. It is observed that the lines 1-2, 2-4 and 2-5 are congested/overloaded compared to other lines.

The percentage loadability values for modified IEEE 5 bus system is tabulated below.

Table 1: OPF result without TCSC

LINES	FROM BUS	TO BUS	LODABILITY (%)	LINES	FROM BUS	TO BUS	LODABILITY (%)
1	1	2	**96.9**	5	2	5	**82.9**
2	1	3	37.6	6	3	4	11.8
3	2	3	22.4	7	4	5	4.1
4	2	4	**86**				

From the above table 1, the maximum loadable lines are 1-2, 2-4 and 2-5. Due to the increased loading, these lines are congested. So by using TCSC, congestion is going to be alleviated.

6.1 Mitigation of total system VAR power loss:

For placing TCSC at optimal location, we use sensitivity analysis. The sensitivity indices table of modified IEEE 5 bus system is shown below.

Table 2: Sensitivity indices

LINES	FROM BUS	TO BUS	SENSITIVITY INDEX (a_{ij})	LINES	FROM BUS	TO BUS	SENSITIVITY INDEX (a_{ij})
1	1	2	-7.759671	5	2	5	-1.69700
2	1	3	**-0.120364**	6	3	4	-32.19711
3	2	3	-0.303177	7	4	5	**-0.026715**
4	2	4	-1.145739				

From the above table 2, the lines 1-3 and 4-5 have the most positive sensitivity factors. So these are the best locations for placement of TCSC to relieve congestion in the network. By placing the TCSC in line 1-3, the congestion in the network is relieved.

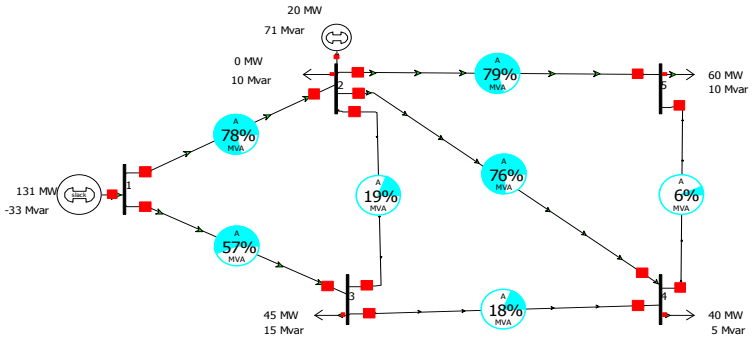

Fig 3: modified IEEE 5 bus system with TCSC in line 1-3

The fig 3 shows the transmission line flows with TCSC. It is observed that after placing TCSC the congestion in the network is relieved.

The list of power flows with and without TCSC is listed below as follows

Table 3: Power flow list of modified IEEE 5 bus system with and without TCSC

LINES	FROM BUS	TO BUS	WITH OUT TCSC	WITH TCSC		
				TCSC (20% COMP)	TCSC (40% COMP)	TCSC (65% COMP)
1	1	2	92.36	87.94	82.62	74.42
2	1	3	37.57	42	47.47	56.12
3	2	3	20.01	17.27	14.01	9.03
4	2	4	33.13	32.09	30.81	28.74
5	2	5	57.36	56.89	56.22	55.45
6	3	4	11.13	12.62	14.14	17.35
7	4	5	4.01	4.47	5.02	5.86

The Comparison of power flows with and without TCSC is shown as

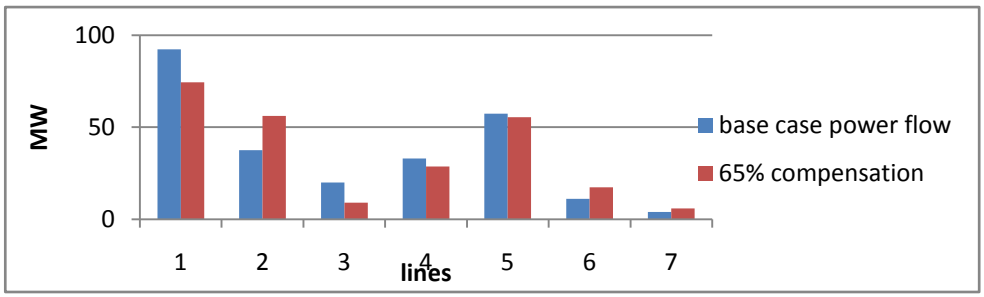

Chart 6.1: Comparison of power flows with and without TCSC

6.2 Transmission Load Relief (TLR) sensitivity method:

This transmission load relief method is based on the load curtailment. In this method of congestion management, TLR sensitivities at all the load buses for the most overloaded line are considered.

The TLR sensitivity values of modified IEEE 5 bus system is shown as follows

Table 4: TLR sensitivities

BUSES	CONGESTED LINES i-j		
	1-2	3-4	2-5
1	0	0	0
2	-0.857	0.032	0.016
3	**-0.571**	**-0.127**	**-0.063**
4	-0.762	-0.466	-0.233
5	-0.825	-0.134	-0.734

From the above table 4, the most positive TLR sensitive valued bus is bus3 from all congested lines. So by doing load curtailment on bus3 i.e. from 45 M.W to 5 M.W, then congestion is relieves from 97% to 72% at line 1-2, congestion is relieves from 86% to 72% at line 2-4 and congestion is relieves from 82% to 78% at line 2-5.

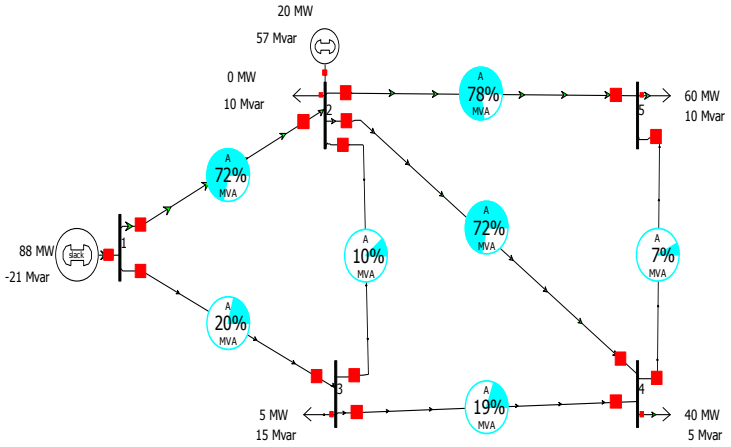

Fig 4: congestion relief by load curtailment at bus 3

So by doing load curtailment based on TLR sensitivity method at bus3 the congestion is relieved.

VII. SIMULATION RESULTS FOR MODIFIED IEEE 9 BUS SYSTEM:

The effect on ATC of the network by changing generator participation factors and by varying the load has been carried on below modified IEEE 9 bus system. In this modified IEEE 9 bus system, the bus1 is a slack bus, bus 2 and bus3 are generator buses. The bus5, bus7, bus9 are load buses. It is assumed that the load sharing by generator buses are x_i times the change in load.

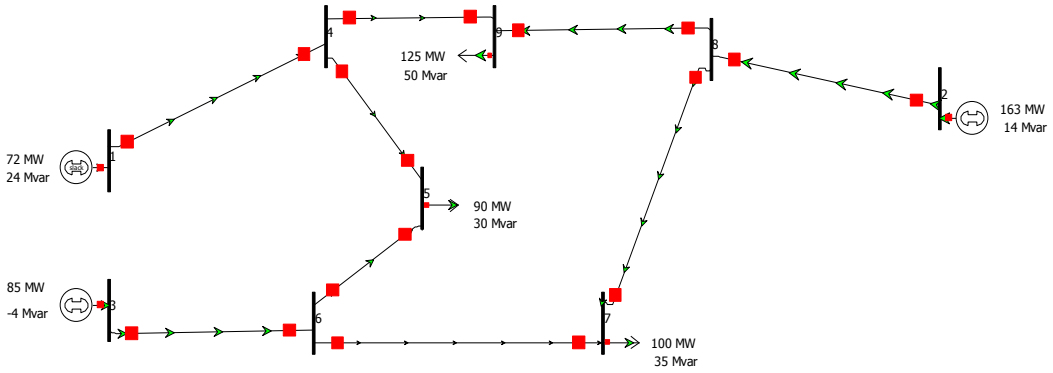

Fig 5: modified IEEE 9 bus system based on generator participation factor

For example, if 0.2, 0.2, 0.6 are the participation factors for the generators 1, 2, 3 respectively. For a change in load 10 M.W, then generator 1 additionally supplies 2 M.W, generator 2 additionally supplies 2 M.W and generator 3 additionally supplies 6 M.W.

The ATC contributions with changing generator participation factors and increment of load at particular bus is shown as follows

TABLE 5: Avilable Transfer Capability With Consideration Of Individual Bilateral Transactions And Changes In Load At Bus 5 (Initial Load At Bus 5=90mw And Participation FACTORS ARE x1=0.2, x2=0.2, x3=0.6)

S.NO	Applied change in load at bus 5 (MW)	Total load at bus 5 (MW)	Generator to load bus pair	Transacted power (MW)	Losses (MW)	N/W ATC for individual transactions (MW)	N/W ATC for simultaneous power transaction from all generator to bus 5 (MW)
1	10	100	1-----5	2	0	25.67	31.53
			2-----5	2		20.35	
			3-----5	6		41.04	
2	10	110	1-----5	5	1	23.25	21.54
			2-----5	4		13.90	
			3-----5	12		28.03	
3	10	120	1-----5	7	1	20.80	11.55
			2-----5	6		7.45	
			3-----5	18		15.03	
4	10	130	1----5	10	2	18.31	1.56
			2----5	8		1.01	
			3-----5	24		2.03	
5	10	140	1-----5	12	3	15.79	0
			2-----5	10		0	
			3-----5	31		0	

TABLE 6: AVILABLE TRANSFER CAPABILITY WITH CONSIDERATION OF INDIVIDUAL BILATERAL TRANSACTIONS AND CHANGES IN LOAD AT BUS5(INITIALLOAD AT BUS 5=90MW AND PARTICIPATION FACTORS ARE x1=0.4,x2=0.5,x3=0.1)

S.NO	Applied change in load at bus 5 (MW)	Total load at bus 5 (MW)	Generator to load bus pair	Transacted power (MW)	Losses (MW)	N/W ATC for individual transactions (MW)	N/W ATC for simultaneous power transaction from all generator to bus 5 (MW)
1	10	100	1----------5	4	0	22.14	37.65
			2----------5	5		24.30	
			3----------5	1		44.40	
2	10	110	1----------5	8	0	17.79	30.85
			2----------5	10		19.92	
			3----------5	2		40.16	
3	10	120	1----------5	13	1	13.42	24.06
			2----------5	15		15.53	
			3----------5	3		31.32	
4	10	130	1----------5	17	1	9	17.29
			2----------5	20		11.6	
			3----------5	4		22.50	
5	10	140	1----------5	21	1	4.56	10.52
			2----------5	25		6.79	
			3----------5	5		13.69	
6	10	150	1----------5	26	2	0.08	0.40
			2----------5	30		2.43	
			3----------5	6		4.89	
7	10	160	1----------5	30	2	0	0
			2----------5	35		0	
			3----------5	7		0	

Fig 6: congestion in network for participation factors x1=0. 2, x2=0.2, x3=0.6

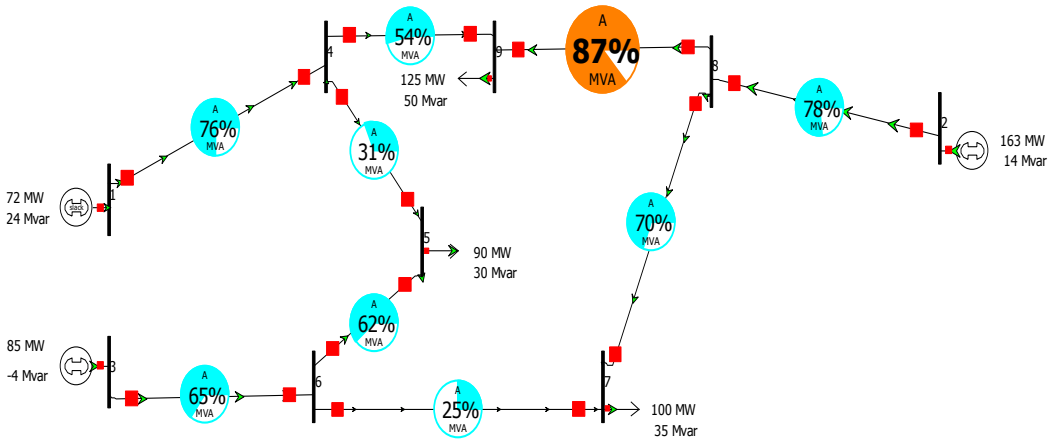

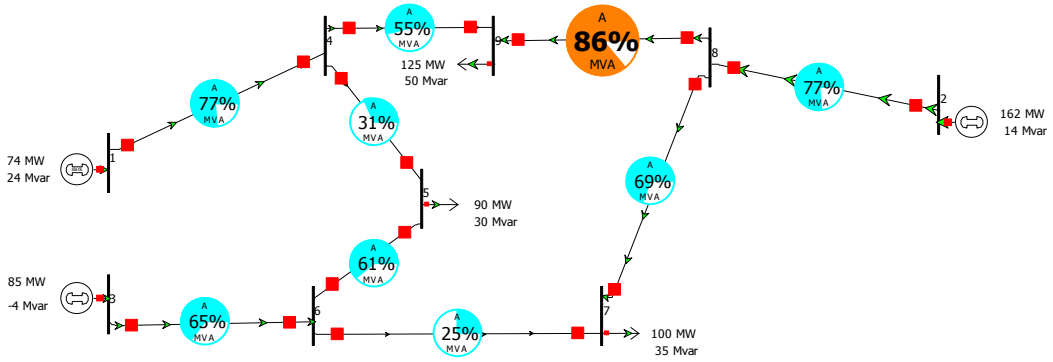

Fig 7: congestion in network for participation factors x1=0.4, x2=0.5, x3=0.1

The tables 5 and 6 represents the calculation of ATC values for increasing load is showed. For computation of Network ATC, the load at bus 5 is continuously increased in steps of 10 M.W till is leads to congestion in one or more transmission line of the power system. According to the initially placed generator participation factors, the generators responses for corresponding changes at the load bus 5. This change of load is shared by the generators as per the participation factors.

From the above tables it is observed that the ATC values of the network are decreases when the load at bus5 increases and also observed that ATC value of the network is changes when the generator participation factor is changed. The ATC values are also determined by power world simulator 16. The above table's shows that the total maximum load applied at load bus 5 for generator participation factors are

140 M.W for participation factors x1=0.2, x2=0.2, x3=0.6 and

160 M.W for participation factors x1=0.4, x2=0.5, x3=0.1.

The ATC values are determined by conventional Network response method. Generator with larger participation factor can have a more positive effect on improving the system power transfer capability. It can be observed from above two tables that as the load is continuously increased, ATC of network decreases leading to congestion in the transmission line. The below graphical representation shows the ATC and load variations for corresponding generator participation factors.

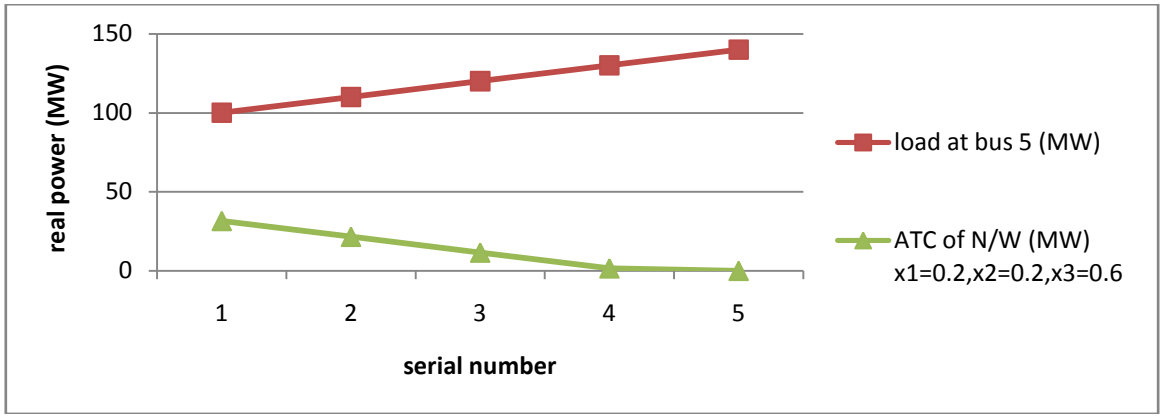

Graph 1: ATC and load variation for participation factors x1=0.2, x2=0.2, x3=0.6

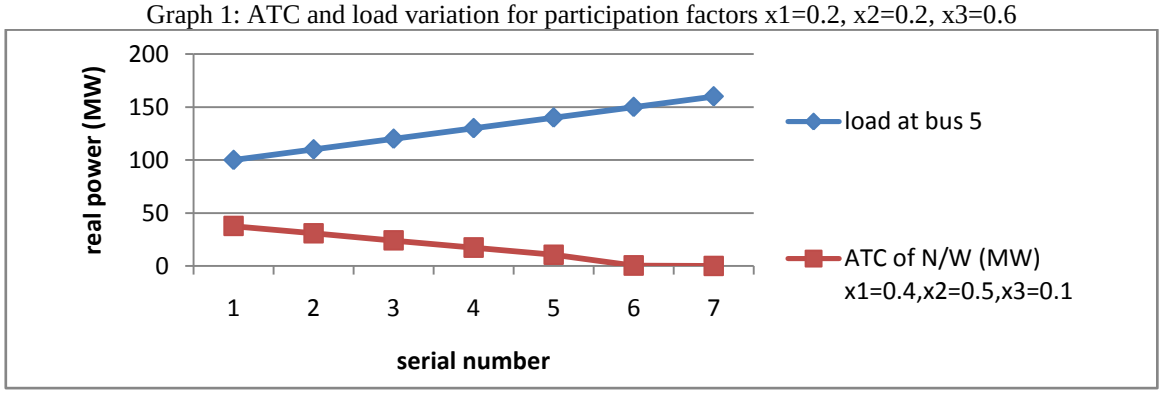

Graph 2: ATC and load variation for participation factors x1=0.4, x2=0.5, x3=0.1

VIII. CONCLUSION

Congestion management is one of the challenging and toughest tasks in deregulated power system environment. In this paper two different types of approaches were successfully used to relief the congestion in the network. One of approach is congestion management by use of FACT device i.e. TCSC and another approach is by changing generator participation

factors to alleviate congestion. The method of Mitigation of total system VAR power loss is used to allocate the TCSC in optimal location and transmission load relief (TLR) method is used to find load curtailed bus for congestion relief in the network. The loading on the network continuously increases, then ATC of the network will goes on decreases. From the results, it can be observed that the maximum load that can be applied to a particular bus also; there is no causing of network congestion because of changing generator participation factors. So generator participation factors are also used as one of tool for management of congestion in the network.

REFERENCES

[1] L.Rajalakshmi,M.V.Suganyadevi,S.Parameswari, "Congestion Management in Deregulated Power System by Locating Series FACTS Devices," International journal of Computer applications,Vol.13,pp 0975-8887,Jan2011.
[2] B.Likitha, J.Srinivasa Rao, J.Amarnath "Sensitivity Approach for Efficient Location of TCSC in a Deregulated Electricity Market," IOSR Journal of Engineering, ISSN:2250-3021,Vol.2, pp 09-15,June 2012.
[3] A.R Abhyankar,Prof.S.A.Khaparde "Introduction to Deregulation in Power Industry," IIT Bombay.
[4] Abouzar samimi, Peyman Naderi "A New Method for Optimal Placement of TCSC based on Sensitivity Analysis for Congestion management," Smart Grid and Renewable Energy, 2012, 3, 10-16.
[5] Madhura Gad, Prachi Shinde, Prof.S.U.Kulkarni,"Optimal Location of TCSC by Sensitivity Methods," International Journal of Computational Engineering Research, Vol.2, Oct.2012.
[6] Seyed Abbas Taher, Hadi Besharat "Transmission Congestion Management by Determining Optimal Location of FACTS Devices in Deregulated Power systems," American Journal of Applied Sciences 5(3):242-247, ISSN 1546-9239, 2008.
[7] K.Vijayakumar, "Optimal location of FACTS Devices for Congestion Management in Deregulated Power System," International Journal of Computer Applications,Vol.16, pp.0975-8887,feb2011.
[8] Mrinal Ranjan,B.Vedik, "Optimal Location of FACTS Devices in a Power System by Means of Sensitivity Analysis" Science Road Publishing Corporation- Trends in Electrical and Computer Engineering TECE 1(1) 1-9,2011.
[9] B.V.Manikandan, S.Charles Raja and P. Venkatesh, "AVAILABLE TRANSFER CAPABILITY ENHANCEMENT WITH FACTS DEVICES IN THE DEREGULATED ELECTRICITY MARKET" DOI:10.5370/JEET.2011.6.1.014
[10] D.Venu Madhava Chary, J.Amarnath, "COMPLEX NEURAL NETWORK APPROACH TO OPTIMAL LOCATION FACTS DEVICES FOR TRANSFER CAPABILITY ENHANCEMENT" APRN Journal of Engineering and Applied Sciences, Vol.5, ISSN 1819-6608,Jan 2010.
[11] K.Radha Rani and J.Amrnath, "APPLICATION OF FACTS DEVICES FOR ATC ENHANCEMENT IN COMPETITIVE POWER MARKET" international journal of electrical and electronics systems research, vol.3. june 2010.
[12] P.R.RANE,N.D.GHAWGHAWE, "CONGESTION MANAGEMENT BY CHANGING GENERATOR PARTICIPATION FACTOR," journal of information, knowledge and research in electrical engineering,ISSN:0975-6736,nov 10-10-11,vol.01,issue 2.

VINOD KUMAR .G is an M.Tech candidate in Power System Control & Automation at QIS College of Engineering & Technology, Ongole under J.N.T.U Kakinada. He received his B.Tech degree in Electrical & Electronics Engineering from St.Ann's College of Engineering & Technology, Chirala under J.N.T.U Kakinada. His current research interests are FACTS controller's applications to power systems, power quality issues and deregulated power system.

SRINIVASARAO.J is an associate professor in QIS College of Engineering &Technology at ongole. He is pursuing Ph.D under J.N.T.U Anantapur. He got his M-Tech degree from JNTU Hyderabad and his B-Tech degree from RVRJC Engineering College, Guntur. His Current research interests are power systems, power systems control and automation, Electrical Machines, power systems deregulation, FACTS applications.

AMARNATH.J obtained the B.E degree in electrical engineering from Osmania University, Hyderabad and the M.E. degree in power systems from Andhra University, Visakhapatnam. Presently he is professor in Electrical and Electronics engineering department, JNTU, Hyderabad. His research interests includes high voltage engineering, gas insulated substations, industrial drives, power electronics, power systems.

International Journal of Modern Engineering Research (IJMER)
www.ijmer.com Vol. 3, Issue. 4, Jul - Aug. 2013 pp-2119-2126 ISSN: 2249-6645

Develop and Apply Water Quality Index to Evaluate Water Quality of Tigris and Euphrates Rivers in Iraq

Dr. Sabah Obaid Hamad Al-Shujairi *
Ph D. in Environmental Engineering
** Environmental Department of Central Region -Ministry of Environment - Iraq*

Abstract: *This study is an attempt to develop Iraqi river water quality index (IRWQI) which can be applied to evaluate the general water quality of the main Iraqi' rivers (Tigris and Euphrates) in its entire stretch for public uses. The index proposed in this work is composed of seven measurable parameters: total dissolved solids (TDS), total hardness (TH), pH, dissolved oxygen (DO), biological oxygen demand (BOD), nitrate (NO_3) and phosphate (PO_4). IRWQI is a mean to summarize large amount of water quality data into simple terms (e.g., good or poor) for reporting to authorities management and the public in a consistent manner. IRWQI can be effectively used to evaluate the spatial and temporal variations of surface water quality in the two main rivers. Calculation of water quality rating (sub-indexes) were based on giving a rating scores of 100, 95, 90, 80, 70, 60, 50, 40, 30, 20, 10 and 5 corresponding to the 5^{th}, 10^{th}, 20^{th}, 30^{th}, 40^{th}, 50^{th}, 60^{th}, 70^{th}, 80^{th}, 90^{th}, 95^{th} and 99^{th} percentiles, respectively to long term parameter observations. The associated best-fit formulas to each parameter rating curve were used to calculate aggregated index. The unweighted harmonic square mean formula, as a method to aggregate sub index results, has been suggested. This formula allows the most impaired variable to impart the greatest influence on the water quality index and will pose differing significance to overall water quality at different times and locations. The IRWQI developed was applied to seven selected sampling stations (T1 to T7) along Tigris river, six selected sampling stations (E1 to E6) along Euphrates river and one common selected sampling station (ET) after meeting of Tigris with Euphrates at Al Qurna. The results showed that water quality varied from very good to very poor range. In general the water quality was degrades downstream. Tigris water quality better than Euphrates water quality. There was no large different in water quality between dry season and wet season where engineering controls on the rivers have greatly reduced their seasonality.*

Key words: *Euphrates Rivers, IRWQI, Rating curve, Tigris River, TDS, Water quality.*

I. INTRODUCTION

Most of the urban centers in Iraq and a large portion of its population are located along and near the Tigris and Euphrates rivers. Euphrates and the Tigris rivers are of vital importance to people in domestic water use. They are essential resources for economic activities.

The evaluation of water quality in developing countries has become a critical issue in recent years, especially due to the concern that fresh water will be scarce resource in the future. Whereas water monitoring for different purposes is well defined (e.g., aquatic life preservation, contact recreation, drinking water use), the overall water quality is sometimes difficult to evaluate from a large number of samples, each containing concentrations for many parameters [1].

Water quality index (WQI) is a mechanism for presenting a cumulatively derived numerical expression defining a certain level of water quality [2]. In other words, WQI summarizes large amounts of water quality data into simple terms (e.g., excellent, good, bad, etc.) for reporting to management and the public in a consistent manner. The index reflects the status of water quality in lakes, streams, rivers, and reservoirs.

A number of indices have been developed to summarize water quality data in an easily expressible and easily understood format [3]. These indices have been the product of efforts and research development from governmental agencies in different strata, as well as from masters' and doctorate research. There are various water quality indices (WQI) to compare various physico–chemical and biological parameters [4,5].

Despite the various water quality indices have been developed and published in the literature, but so far ministries of environment and water resource in Iraq has made insufficient progress in developing and utilizing specific water quality index. In this study an index has been developed which can be used with data on physical, chemical and biological variables routinely collected by **water resource monitoring program.** Although some information is lost when integrating multiple water quality variables, this loss is outweighed by the gained understand of water quality issues by the lay public and policy makers. Improving understanding is very import to water resource managers in terms of increasing support for water resource improvement efforts.

II. WATER QUALITY INDEX

Water quality index was first formulated by Horton (1965) and later on used by several workers for the quality assessment of different water resources. It is one of the aggregate indices that have been accepted as a rating that reflects the composite influence on the overall quality of numbers of precise water quality characteristics [6]. Water quality index provide information on a rating scale from zero to hundred. Higher value of WQI indicates better quality of water and lower value shows poor water quality. Therefore, a numerical index is used as a management tool in water quality assessment [7]. WQI basically acts as a mathematical tool to convert the bulk of water quality data into a single digit, cumulatively derived, numerical expression indicating the level of water quality. This, consecutively, is essential for evaluating the water quality of

different sources and in observing the changes in the water quality of a given source as a function of time and other influencing factors [8].

From literature review, it is clear that a great variety of water quality indices have been published. These indices differ from each other in term of fundamental structures and in term of the number and types of variables that have been selected for inclusion. The general procedure to calculate Water Quality Indexes depend on 3 common factors to develop it: 1) parameter selection, 2) determination of quality function for each parameter (sub-index) and 3) aggregation of sub-indices with mathematical expression.

2.1- Parameters included in WQI

Water quality assessment can be defined as the evaluation of the physical, chemical and biological nature of water in relation to natural quality, human effects and intended uses. In this study the WQI developed aids in the assessment of water quality for public uses (potable water supply, recreation, …) and to evaluate water quality management effectiveness. It can be used to improves comprehension of general water quality issues, communicate water quality status and illustrate the effectiveness of protective practice. In order to develop a water quality or river index for above purpose, there are seven parameters have been chosen. This parameters include: Total dissolved solids (TDS), total hardness (TH), dissolved oxygen (DO), pH, biological oxygen demand (BOD), nitrate (NO_3) and phosphate (PO_4) which monitored monthly among others by water resource monitoring program.

2.2- Quality rating formulas (sub-index)

The mean observed and predicted values of each water quality parameter were converted into sub-index scores for the parameter using the rating curves. These rating curves were developed in this study basically from statistical data analysis of raw data was acquired by long-term water resource monitoring program with assistance of water quality experts' opinions. Calculation of water quality rating (sub-indexes) were based on giving a rating scores of 100, 95, 90, 80, 70, 60, 50, 40, 30, 20, 10 and 5 corresponding to the 5^{th}, 10^{th}, 20^{th}, 30^{th}, 40^{th}, 50^{th}, 60^{th}, 70^{th}, 80^{th}, 90^{th}, 95^{th} and 99^{th} percentiles, respectively to each parameter observations. The associated best-fit formulas to each parameter rating curve were used to calculate aggregated index. Each of seven parameter sub-index (SI_i) used to calculate the overall water quality index have been listed below:

For TDS:
If TDS $\leq$ 450 $SI_{TDS} = 100$
If TDS > 5500 $SI_{TDS} = 10$
If 450 < TDS > 5500 $SI_{TDS} = -34.1 \ln (TDS) + 304.8$

For TH:
If TH $\leq$ 100 $SI_{TH} = 100$
If TH > 1200 $SI_{TH} = 10$
If 100 < TH $\leq$ 1200 $SI_{TH} = 6.57$ E-5*(TH)^2-0.1626 (TH)+111.1

For PH:
If 4.5 $\leq$ PH <7.0 $SI_{PH} = 1.9 EXP((PH-1)*0.66)$
If 7.0 $\leq$ PH $\leq$ 7.6 $SI_{PH} = 100$
If 7.6 <PH $\leq$ 10.5 $SI_{PH} = 100 EXP((PH-7.65)*-0.528)$
If 10.5 < PH < 4.5 $SI_{PH} = 10$

For DO:
If DO < 3.3 $SI_{DO} = 10$
If DO > 12.5 $SI_{DO} = 100$
If 3.3 $\leq$ DO $\leq$ 12.5 $SI_{DO} = -59.6 + 24.9*DO - 0.98*DO^2$

For BOD:
$SI_{BOD} = 100 * 0.86 ^ BOD$

For NO_3:
If $NO_3 \leq 1$ $SI_{NO3} = 100$
If $NO_3 > 1$ $SI_{NO3} = 102*0.8887^{(NO_3)}$

For PO_4:
If $PO_4 < 0.03$ $SI_{PO4} = 100$
If $PO_4 > 1.2$ $SI_{PO4} = 10$
If $0.03 \leq PO_4 \leq 1.2$ $SI_{PO4} = 99.5*0.17^{(PO_4)}$

2.3- Aggregation and calculation of water quality index

Aggregation is the process of combining and simplifying a group of sub- indices. The unweighted harmonic square mean formula, as a method to aggregate sub index results, has been suggested as an improvement over both the weighted arithmetic mean formula and the weighted geometric mean formula. The formula is given by Cude [9]:

$$WQI = \sqrt{\frac{n}{\sum_{i=1}^{n} \frac{1}{SI_i^2}}}$$

Where WQI is water quality index result, n is the number of sub-indices, and SI_i is sub-index. This formula allows the most impaired variable to impart the greatest influence on the water quality index and will pose differing significance to overall water quality at different times and locations.

2.4- Classification of WQI Scores

The index equation generates a number between 10 and 100, with 10 being the poorest and 100 indicating the excellent water quality. Within this range designations, present study have been set to classify water quality as illustrated in (Table 1) into six classes of water quality as very poor, poor, fair, good, very good and excellent.

Table .1 Classification scheme for water quality index scores.

WQI Range	Class	Statement
< 45	VI	Very poor
45 – 60	V	Poor
61 – 69	IV	Fair
70 – 79	III	Good
80 - 90	II	Very good
91 – 100	I	Excellent

III. MATERIAL AND METHODS

3.1- study sites

The Euphrates and Tigris Rivers flows within three of the Middle East countries: Turkey, Syria, and Iraq. The Tigris stretch section in Iraq about 1400 km while the length of the Euphrates in Iraq about 1060 km. Euphrates crosses Syria before flowing into Iraq and meeting Tigris, which also crosses Syria for short distance (about 40 km), and together they form Shat Al Arab in the south of Iraq. The Tigris–Euphrates Basin was shown in fig.1. Seven selected sampling stations located along the Tigris stretch and six selected sampling station along the Euphrates Rivers as well as one station after joint meeting between two rivers were chosen inside Iraq state to assess the water quality of two rivers. The selected sampling stations of Tigris river are T1 (Fishkhabor), T2 (Al Shirgat), T3 (Tarmiah), T4 (Baghdad), T5 (Aziziah), T6 (Kut) and T7 (Amarah). The selected sampling Stations of Euphrates river are E1 (Al Qaim), E2 (Fallujah), E3 (Al Kefil), E4 (Shnafia), E5 (Samawa) and E6 (Nasiria). The common sampling station ET (Al Qurnah), where Tigris river meet Euphrates river. It is worth mentioning that the first selected station for each river is located in the entry point of a river at Iraqi borders which often represents the baseline water quality to other downstream stations.

3.2- Methodology

This study did not involve any field data collection or laboratory water quality analysis. The available long-term water quality monitoring data of 39 sampling stations for Tigris river and 22 sampling stations for Euphrates river were analyzed to develop water quality index. The developed water quality index proposed in this study was applied to selected sampling stations along the Tigris and Euphrates rivers at 2012 to evaluate water quality of two rivers for public use. Seven related parameters (TDS, TH, pH, DO, BOD, NO_3 and PO_4) plays a significant role to assess general water quality based on common and important physical, chemical and biological parameters of surface water were chosen to calculate WQI at selected locations.

IV. RESULTS AND DISCUSSION

The water quality index was designed to permit comparison of water quality among different stretches along the same river or between different Iraqi rivers.

4.1- Parameters selection importance

Depending on the data availability and to ensure main Iraqi rivers water quality, seven water quality parameters were selected in WQI. With too many variables, small individual changes are not detectable in the aggregated water quality index value [9]. Understanding water quality parameters and their characteristics is important to identify the quality of the water, to know the reasons which led to changes in the quality, and to help in interpreting these changes**.** These parameters include: TDS, TH, pH, DO, BOD, NO_3 and PO_4.

An effort has been made by Bharti N and Katyal D. [10] to carry out a review of important indices formulated all over the world used in water quality assessment. From the analyses of 36 indices, it appears that they have 35 common parameters of which, the most common and frequent of the cases is the dissolved oxygen 15 indices, pH in 11 indices, BOD in 11 indices, total phosphorous and phosphates in 11 indices, nitrates in 10 indices, total dissolved solid in 8 indices and total hardness in 5 indices [11].

Total dissolved solids (TDS) are represents salts and minerals dissolved in the water (mg/L) that cannot be removed by conventional filtration [7]. Water salinity (expressed as TDS) is an increasing problem in Iraq. Salinity increases as the river water flows southward and evaporation, sewage effluent, dissolution of limestone and evaporate bedrock, and agricultural drainage all increase the salinity. River water can be classified by the amount of TDS as: fresh water < 1500 mg/L TDS, brackish water 1500 to 5000 mg/L TDS or saline water > 5000 mg/L TDS [12]. In this study TDS is considered to be a good indicator for water salinity, and it gives general information about the sum of ions in the water. TDS can be employed to establish potential water usage or to evaluate the quality of supplied water; it affects everything that consume, lives in, or uses water. If the TDS passes 1000 mg/l, water becomes less usable and it is no longer potable for human consumption [13]. Above 3000 mg/l, it is not suitable for most municipal or agricultural usages.

As shown in fig. (2), it is clearly demonstrated that the TDS increases steadily along the stretch of the Tigris river for both wet season (average of January, February and March months) and dry season (average of Jun, July and August months), while fig. (3) shows an exception for Euphrates river where TDS concentrations at upper stretch increased steadily especially at dry season then began decrease at downstream station E6 and later compared with previous stations. The main reason to decreasing TDS at lower stretch belong to partially dilution with better water quality discharged from Al Garraf branch river from Tigris. Primary sources for TDS in receiving waters are agricultural and residential runoff, leaching of soil contamination and point source water pollution discharge from industrial or sewage treatment plants [14].

Total hardness is mainly a reflection of major ions, e.g., Ca^{+2}, Mg^{+2}, CO_3^{-1} and HCO_3^{-1}, being present in the water. These ions enter the river water by leaching from minerals like Calcite, gypsum and Dolomite, which exist throughout the course of the river. Kannan [15] has classified water on the basis of hardness values in the following manner; 0- 60 mg/L, soft, 61-120 mg/L, moderately hard, 121-160 mg/L, hard and greater than as 180 mg/L very hard. Hardness below 300 mg/L is considered potable but beyond this limit produces gastrointestinal irritation [16]. Normally water hardness does not pose any direct health problem but may affect the consumer acceptability of water in terms of taste and cause economic problems [17]. The results was showed increase trend in hardness concentration along with downstream direction for Tigris and Euphrates rivers. There are strong correlation between TDS and hardness, however high TDS concentrations in water usually indicate high level of hardness in water [18]. Therefore, using both parameters in calculating WQI maximize the effect of TDS on water quality index which reflect the purpose of using index for public used.

pH is a measure of acidity or alkalinity. pH is an important parameter to monitor as it can significantly impact the physiological processes of aquatic biota when changes to the natural pH range occur [19]. Furthermore, it can influence the solubility of nutrients and pollutants. The measure of pH is very important as an indication of water quality due to the sensitivity of organisms to the pH of their environment. pH is also important in assessing the suitability of water for drinking [17]. The results as listed in table 1 and 2 showed variability along the course of rivers.

Dissolved oxygen (DO) is essential for water quality, ecological status, and health of a river. This is due to its importance as a respiratory gas, and its use in biological and chemical reactions [20]. DO is also important when assessing the suitability of water for drinking. Low DO in source water can increase the conversion of nitrate to nitrite and sulphate to sulphide as well as increase the concentration of ferrous iron in solution, leading to discoloration in drinking water [17]. The presence of pollutants can reduce the oxygen carrying capacity and the concentration value of dissolved oxygen in river water.

Biological oxygen demand (BOD) is the amount of dissolved oxygen needed by aerobic biological organisms in a body of water to break down organic material present in given water sample at certain temperature over a specific time period and considered as an important water quality indicator. BOD could be preferred over COD because BOD represents better the biodegradable pollutants in the water body and most of the water quality models can simulate this parameter [21].

Nutrients (nitrate and phosphate) are an important indicator of water quality and originate from a range of point and diffuse sources, particularly the discharge of sewage effluent and agricultural runoff (fertilisers, waste from livestock). Excessive nutrients can result in eutrophication and algal blooms, can significantly impact aquatic ecosystem health, and reduce ecological and recreational values of freshwater resources [22]. However, agricultural discharges may contribute with high nitrate levels resulting from excessive fertilizer use in agriculture, when microorganisms break down fertilizers, decaying plants, manures, animal feedlots or other organic residues.

4.2- Observed change in WQI

To calculate the WQI, the raw analytical results for each parameter, having different unit of measurement, are first transformed into non-dimensional sub-index values rating from 10 (worse case) to 100 (ideal) depending on the parameter's contribution to water quality impairment. These sub-indices are then combined to give a single water quality index rating value ranging from 10 to 100. The unweighted harmonic square mean formula used to combine sub-indices allows the most impacted parameter to impart the greatest influence on the water quality index [9]. Thus the result from all sampling stations in two seasons is showing that Water Quality Index is in very good range to very poor range because in method that assign fixed weights to variables will pose differing significance to overall water quality at different times and locations.

The quality of water in the Tigris river as shown in fig. 4 near the Turkey border (sampling station T1) is assumed to be ranged from good to very good quality, water quality degrades downstream, with major pollution inflows from urban

areas due to poor infrastructure of wastewater treatment. The diversion of excess water to prevent flooding problems from Tigris to the Al-Tharthar Depression caused considerable increase in the salinity (expressed as TDS) in return water to the river system, due to the very large evaporation rate, dissolution of salt and gypsum from soil of the depressions, and salt ground water effects. These three significant reasons have seriously diminished water quality [23]. The effect of Al-Tharthar Depression clear on the water quality at station T4 where the WQI status become fair at station T4 (Baghdad). Urbanization and an increasing population imply an increase in water consumption for domestic, industrial, and agricultural purposes. This increase in water demand consequently means an increase in the discharged waste water from all these sectors into river water [24,25]. After Tigris river joining Euphrates river (worse quality) at station ET (Al Qurna) the water quality more decreased, it become poor quality. At T6 the water quality slightly increased that may be belong to increasing the ability of river to self purification, where the concentration of nitrate decreased as well as the BOD. At lower stretch of Tigris river, the water quality can be severely affected by the irrigation return waters causing degrading in water quality, where at T7 and later quality of water was recording backing down.

The river water quality of the Euphrates as shown in fig. (5), is varying greatly from place to place along the river. This variation is due to a combination of natural factors and human activities. Euphrates starts with good or very good water quality index at sampling station E1 (the point of iterance Iraqi border from Syria), usually the TDS there is about 600 mg/l . Most other physiochemical parameter in good quality range. Gradually water quality decreases downstream, and the worse quality happen at stations (E4, E5 and E6) then the river water quality improved slightly from very poor quality to poor quality. At the mouth of the river into Shat al Arab where joining Tigris river (better quality), the quality of water convert to fair status.

The water quality of Euphrates River within Iraq especially south of Bagdad (at sampling stations E4 and later) is not satisfactory mostly [26]. Poor irrigation practices have led to major degradation of land and water. Inefficient irrigation techniques that are practiced have contributed to an increase in the salinity of the soil. Irrigation practices such as flood and furrow requires a lot of water to flood the farm land. As a result for this practice, a large quantity of excess water will be generated, which either seep into the groundwater or reaches to the river. There are more than 16 drains working and conveying drainage wastewater along Euphrates River especially at middle and lower stretch. These drains play a significant role in altering the quality of Euphrates river water. These drains discharging return irrigation water into the river which contains high concentration TDS, NO_3 and PO_4 [27]. This will led to an increase in the salinity and cause a massive increase in the growth of algae or plankton in Euphrates River. The final quality depends on how much water flows through the river and in which quality, as well as how much return water enters the river and the concentration of the water in the drains [18].

The Euphrates flows rapidly in the upper course due to large differences in elevations. In the middle and lower stretch in Iraq, the river velocity becomes very low and the river is consider to be a slow running stream [28]. The very gentle gradient of the Euphrates river [25] reduce the ability to self- purification and remove certain amount of pollutants by degrading or dispersing it.

The population growth in large suburban residential areas have developed along Tigris and Euphrates rivers stretch without adequate infrastructure, and sewage treatment plants are not enough for this expansion. Most of the solutions in this case are by constructing new bypasses to discharge the untreated wastewater into the river directly, which causes river water quality degradation [18].

In general, WQI in wet season as shown from fig. (4) and (5) for Tigris and Euphrates rivers respectively, is slightly less than in dry season. Although the amount of rain falling during wet season that may be reflected on the amount of river discharge and thus improve the quality of the water, but engineering controls on the rivers have greatly reduced their seasonality. In addition to the runoff and increasing the quantity of return flow from irrigation all that affect the water quality.

Water quality of the Euphrates entering Iraq is less than the Tigris, currently affected by return flow from irrigation projects in Turkey and Syria as well as sewage water system which are directed to the river (27). The quality of the water in both the Euphrates and the Tigris is further degraded by return flows from land irrigated in Iraq as well as urban pollution [29].

V. CONCLUSION

Developed Iraqi river water quality index (IRWQI) was applied to evaluate the water quality of Tigris and Euphrates rivers for public uses. The results showed that water quality varied from very good to very poor range. Tigris water quality was largely degraded after sampling station T3, where the effect of Al Tharthar depression was very clear on water quality. High impact of agriculture return flow on water quality was noticed at middle and lower stretch of Tigris and Euphrates rivers. Euphrates water quality was severely degraded at lower stretch (at sampling stations E4 and later). In general water quality of Tigris river better than in Euphrates. There was no large different in water quality between dry season and wet season where engineering controls on the rivers have greatly reduced their seasonality.

ACKNOWLEDGMENTS

I would like to thank very much **Mr. Sabah Al- Omran** Director General of the Department of Environment in central region/ Ministry of Environment and **Eng. Jabbar Abid Zayed**, the Head of water quality monitoring department in Environmental Ministry and **Dr. Hassan Hamid** from Ministry of water resource for their support and providing available data.

REFERENCE

[1] Bakan G., Ozkoc, H. B., Tulek S. and Cuce H., 2010, "Integrated environmental quality assessment of Kizilirmak river and its coastal environment", Turkish Journal of Fisheries and Aquatic Science",10:453-462.
[2] Bordalo, A. A., Teixeira, R., and Wiebe, W. J., (2006), A water quality index applied to an international shared river basin: The case of the Douro River, Environmental Management, 38, pp 910–920.
[3] Couillard, D. and Y. Lefebvre, 1985. Analysis of Water Quality Indices. Journal of Environmental Management 21:161-179.
[4] Pandey, M. and Sundaram, S. M., (2002), Trend of water quality of river Ganga at Varanasi using WQI approach, International Journal of Ecology and Environmental Science. New Delhi: International Scientific Publication, 28, pp 139–142.
[5] Ram, R. S. and Anandh, H., (1996), Water quality index of some Indian rivers, Indian Journal of Environmental Health, NEERI, Nagpur, 38(1), pp 21–34.
[6] Prati, L., Pavanello, R. and Pesarin, F., 1971, "Assessment of surface water quality by a single index of pollution", Water research 5, 741-751.
[7] Avvannavar, S. M., and Shrihari, S. (2007). Evaluation of water quality index for drinking purposes for river Netravathi, Mangalore, South India. Environmental Monitoring and Assessment
[8] Sarkar, C., and Abbasi, S. A. (2006). Qualidex – A new software for generating water quality indice. Environmental Monitoring and Assessment. 119, 201–231.
[9] Cude C. G. 2001. Oregon water quality index: a tool for evaluating water quality management effectiveness. Journal of the American Water Research Association 37:125–137
[10] Baharti, N. and Katyal, D., 2011, "Water quality indices used for surface water vulnerability assessment", International Journal of Environmental Science, 2: 154-173.
[11] Nelson F. , Alberto R. R. and Fredy S. (2004), *Physico - chemical water quality indices – a comparative review*, Revisal BISTUA, Colombia, 19 - 30.
[12] Ela, Wendell P., 2007, " *Introduction to Environmental Engineering and Science"*, Prentice Hall, 3rd ed. ISBN 0-13-148193-2
[13] WHO (World Health Organization) (1997) Guidelines for drinking water quality: surveillance and control of community supplies, 2nd ed. World Health Organization, Geneva.
[14] Al-Janabi, Z. Zahraw, Al-Kubasi, A. Abdul-Rahman and Al-Obaidy, Abdul-Hameed M., 2012, " Assessment of water quality of Tigris river by using water quality index (CCME WQI)", Journal of Al-Nahrain University 15 (1), pp.119-126.
[15] Kannan, K. 1991. Fundamentals of Environmental Pollution, S. Chand and Company Ltd., New Delhi.
[16] ICMR, 1975. Manual of standards of quality for drinking water supplies. ICMR, New Delhi.
[17] WHO. 2004. Guidelines for Drinking-water Quality. Third Edition Volume 1: Recommendations. World Health Organisation, Geneva.
[18] Al Bomola, Ahmed Hussein, 2011, "Temporal and spatial changes in water quality of Euphrates river-Iraq", PhD Thesis, Division of Water Resources Engineering Department of Building and Environmental Technology, Lund University
[19] ANZECC (Australian and New Zealand Environment and Conservation Council). 1992. Australian water quality guidelines for fresh and marine waters. Canberra, 202pp
[20] Mustapha. M. K. (2008). Assessment of the Water Quality of Oyun Reservoir, Offa, Nigeria, Using Selected Physico-Chemical Parameters. *Turkish Journal of Fisheries and Aquatic Sciences*, 8: 309-319.
[21] Abdullah-Al-Mamun and Azni Idris,2008 " Revised water quality indices for the protection of rivers in Malaysia", *Twelfth International Water Technology Conference, IWTC12 2008, Alexandria, Egypt*
[22] Davis, J.R. and Koop, K. (2001) Current understanding of the eutrophication process in Australia. In Schumann, A.H., Acreman, M.C., Davis, R., Marino, M.A., Rosbjerg, D. and Jun, X. (eds.) *Regional management of water resources*, International Association of Hydrological Sciences, Wellingford, Oxfordshire, ISBN 1-901502-51-1.
[23] Jehad, A.K., " Effect of Tharthar Canal Salty Water on the Quality of Euphrates Water", M.Sc. Thesis University of Tech., 1984.
[24] Kliot, Nurit, Water Resources and Conflict in the Middle East, London: Routledge, 1994, p. 100.
[25] Kolars, J., 1994. Problem of International River Management. In: The case of the Euphrates, International Waters of the Middle East from Euphrates-Tigris to Nile, Biswas, A.K. (Ed.). Oxford University Press, Oxford, pp:44-49
[26] FAO. 1994. Country information brief, Iraq. FAO-Representation in Iraq.
[27] Frenken, Karen (2009), Irrigation in the Middle East Region in Figures. AQUASTAT Survey 2008, Water Reports 34, Rome: FAO, ISBN 978-92-5-106316-3).
[28] Shahin, Mamdouh (2007), Water Resources and Hydrometeorology of the Arab Region, Dorecht: Springer, ISBN 9781 402054143. P251.
[29] Jawad, Laith A. (2003), "Impact of Environmental Change on the Freshwater Fish Fauna of Iraq", International Journal of Environmental Studies 60 (6): 581–593.
[30] Figure available at web reference, http://maps.unomaha.edu/Peterson/geog1000/MapLinks/SWAsia/40.gif

Figure (1). Tigris and Euphrates rivers [30]

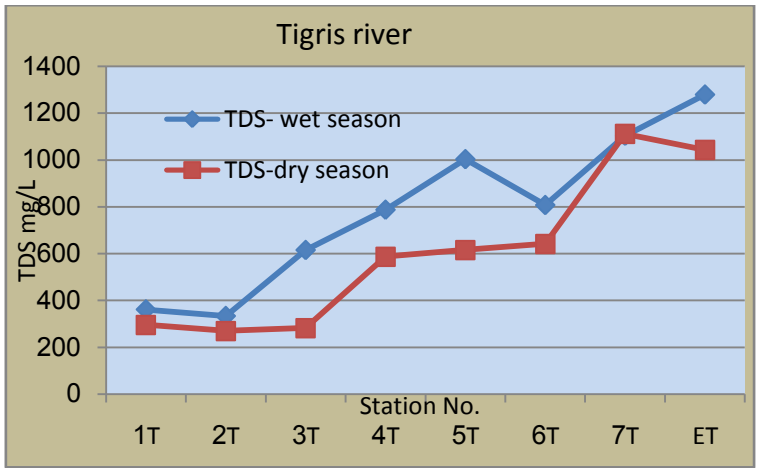

Figure (2). Changes in total dissolved solids along Tigris river.

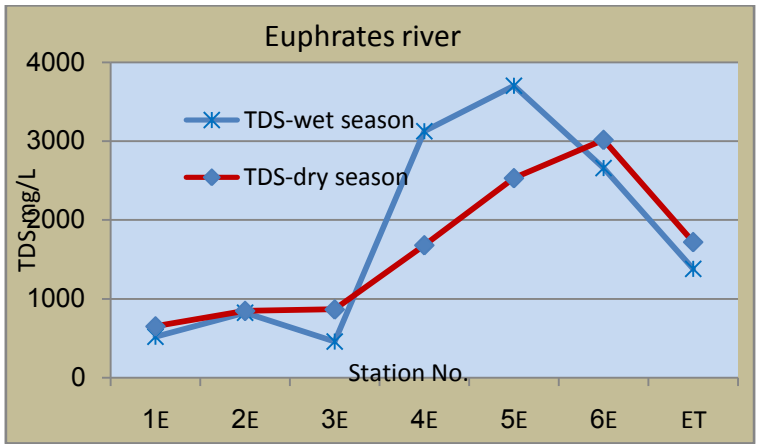

Figure (3). Changes in total dissolved solids along Euphrates river.

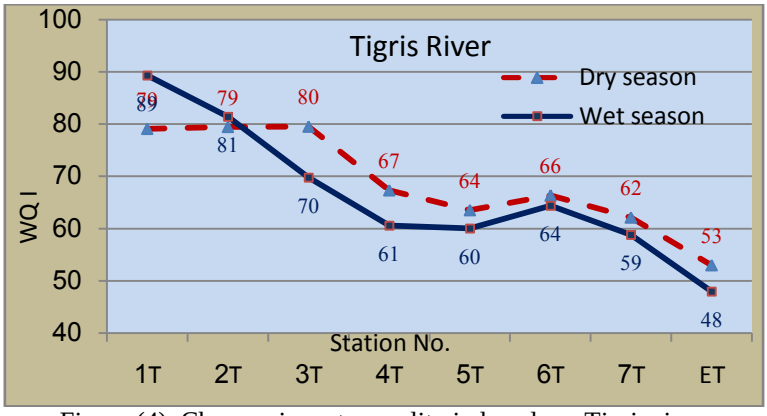

Figure (4). Changes in water quality index along Tigris river

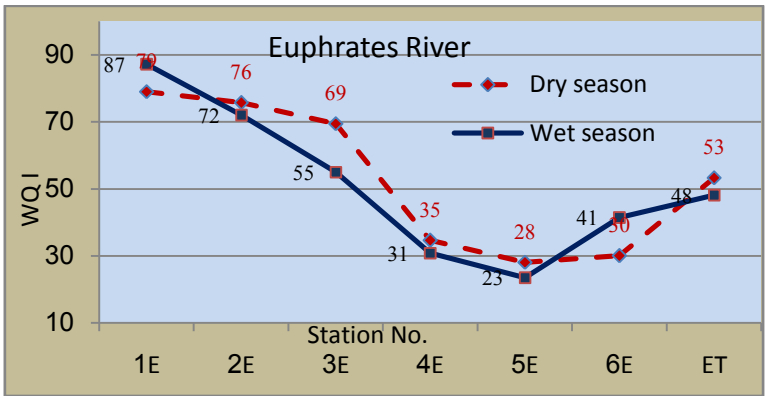

Figure (5). Changes in water quality index along Euphrates river.

International Journal of Modern Engineering Research (IJMER)
www.ijmer.com Vol. 3, Issue. 4, Jul - Aug. 2013 pp-2127-2132 ISSN: 2249-6645

Numerical Modelling of Wind Patterns around a Solar Parabolic Trough Collector

Mahesh Dundage[1], R. O. Bhagwat[2], Suhas Chavan[3]
[12]*Department of Mechanical Engineering, VJTI, Mumbai, India*
[3]*Solar-CoE, Thermax Limited, Pune, India*

ABSTRACT: *Solar based energy systems are now becoming very popular nowadays. Solar parabolic trough collectors are widely used for solar heating and solar thermal power plant. One aspect that is very important is the exact determination of drag force acting on the systems. To calculate drag force, drag coefficient, which is always associated with a particular area, is required. This drag coefficient can be determined by experimentally or by numerical simulation.*

This study reports on numerical predictions of drag coefficient, velocity and pressure fields in steady flow around a solar parabolic trough collector. Also the wind load acting on the collector is determined for each position of trough. In this paper drag coefficients are evaluated for different pitch angles (0^o to 180^o) of parabolic trough using the computational fluid dynamics (CFD) software for wind velocity of 12m/s. Also for 0^o pitch angle, drag coefficient is calculated varying wind velocity from 8m/s to 18m/s. It is found that maximum drag coefficient is 1.71 at 0^o pitch angle and drag coefficient remains constant for wind velocity range 8m/s to 18m/s. The present study has established that commercially available software like can provide a reasonable good solution of complicated flow structures.

Keywords: *CFD, Drag coefficient, Drag force, Numerical simulation, solar parabolic trough collector*

I. INTRODUCTION

It is an accepted fact that solar energy, which has attracted more attention during the recent years, is a form of sustainable energy. Sunlight can be used directly for heating and lighting residential and commercial buildings. The heat of sun can be harnessed for hot water heating, solar cooling, and other commercial and industrial uses. Today a great variety of solar technologies for electricity generation are available and among many, the application of parabolic collectors in large sizes is employed in many systems. Parabolic trough technology is currently the most proven solar thermal electric technology in the world. This is primarily due to nine large commercial scale solar power plants installed in USA. Large fields of parabolic trough collectors supply the thermal energy needed to produce steam for a Rankine steam turbine/generator cycle. Parabolic collectors have been also used or are under construction for commercial power plants in many countries such as Egypt, Greece, India, Mexico and Spain.

The major components of the parabolic collector are the receiver tube, the reflector, tracking system, collector structure, etc. The receiver is the element of the system, where solar radiation is absorbed and converted the radiated energy to thermal energy. It includes the absorber, its associated glass covers, and insulation. Solar parabolic trough collectors are arranged in modules so as to get required temperature rise and mass flow rate of the working fluid. For such solar collector, its ability to track the sun with respect to time very accurately is important. Any small off tracking as well as the collector structure stability will be affected by wind blowing from the regions, where the wind velocity is high.

Earlier wind flow studies around parabolic shape structure such as trough collectors were rare. But, today, with the increased interest in the solar energy, study of wind flow around parabolic trough is increasing. Wind load acting on an object can be determined using standard codes or by experimental graphs available. But these codes and graphs are for standard objects like sphere, rectangular plate, cylinder etc. Other shapes of objects need wind tunnel test or field test for wind load estimation. These tests are expensive and more importantly time consuming. Numerical modelling of flow can provide reasonably good values of drag coefficient and wind load estimates.

Farid C. Christo studied wind pattern around the full scale paraboloidal solar dish. In this paper velocity and pressure field around the dish were predicted using numerical modelling. The SST k-ω turbulence model, and a second-order upwind discretisation schemes are used for all equations. Study was done for different pitching angles (0^o to 180^o) and for different velocities. Aerodynamic coefficients for different positions were calculated. Analysis was done for both steady and unsteady flows around the dish and it was concluded that coefficients for steady and unsteady flows are same. It was found that aerodynamic coefficients were independent on wind velocity. The effects of installing windbreaks on aerodynamic forces were studied. Overall the results of numerical modelling were satisfactory. N. Naeeni et al. studied wind flow around a parabolic trough which is being used in solar thermal power plant. Computation is carried out for wind velocity ranging from 5 to 15 m/s and for different pitching angles (90^o, 60^o, 30^o, 0^o, -90^o,-60^o,-30^o). Simulation was done in two dimensions and using RNG k-ε turbulent model. Analysis included the effect of velocity boundary layer in the calculation. Girma T. Bitsuamlak et al. evaluated wind loads on solar panel modules using CFD method. In the analysis, position of the panel was fixed and angle of attack was varied. Calculations were done for stand-alone and arrayed panel type structure. Numerical results were validated with the experimental results. Yazan Taamneh carried out computational fluid dynamics (CFD) simulations for incompressible fluid flow around ellipsoid in laminar steady axisymmetric regime. Analysis was carried out for major to minor axis ratio ranged over 0.5 to 2. Flow around ellipsoid was visualized for different axis ratio. The simulation results are presented in terms of skin friction coefficient, separation angles and drag coefficient. Same simulation procedure was used for flow around sphere and simulation results were validated with experimental results. It was concluded

that commercially available software like FLUENT can provide a reasonable good solution of complicated flow structures including flow with separation. Shaharin A Sulaiman studied air flow over a two-dimensional cylindrical object using ANSYS CFD Flotran to obtain the surface pressure distribution, from which drag and lift were calculated using integral equations of pressure over finite surface areas. In addition the drag and lift coefficients were also determined. The simulation was repeated for various Reynolds numbers to check the robustness of the method. The CFD simulation results show close agreement with those of the experiment. Georgeta Văsieş et al. carried out the numerical simulations for analysis of wind action on solar panels, located on flat roofs with and without parapets. Analysis was done for wind incident angle of 45^{o} and the distribution of pressure on solar panels installed in a compact field on a flat roof was determined. Bo Gong et al. conducted an experiment on field to determine wind load on parabolic trough and characteristics of wind i.e. wind speed, wind direction and boundary layer formation. The objective of this study was to investigate wind loads and wind characteristics on parabolic trough solar collectors under wind action. The wind loads and wind characteristics on collector were measured using wind pressure transducers and propeller anemometers, respectively. Various test configurations were examined, consisted of 12 phases and every phase corresponds to a pitch angle of the solar collector.

The objectives of the study are; to determine the drag coefficient for a solar parabolic trough collector for different pitch angles; to determine the drag force acting on a solar parabolic trough collector for different pitch angles; to determine the effect of wind velocity on drag coefficient; to observe the velocity and pressure contours around the trough.

II. MODEL OF PARABOLIC TROUGH

In a solar thermal power plant there is an array of parabolic trough to reach the required high temperature. But for the study, geometry of a single repetitive unit has been considered. Several numerical and experimental studies have been performed to assess the heat transfer aspects of this parabolic trough. However, only a few studies of flow field have been published for parabolic trough.

The parabolic trough has a focal length of 500 mm and a total reflecting surface area (A) of approximately 7.931 m2. Its axis of rotation is assumed to be located approximately 1.233 m above ground level. The pitch angle of the parabolic trough is shown in Fig.1.

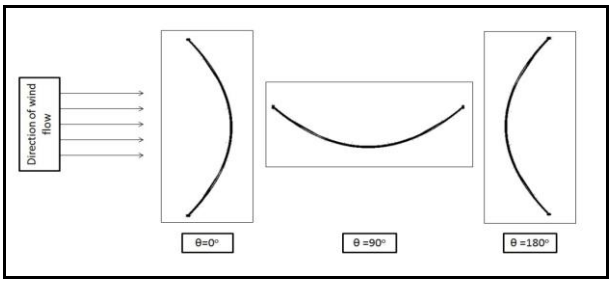

Figure 2: Parabolic trough collector in three positions with respect to wind

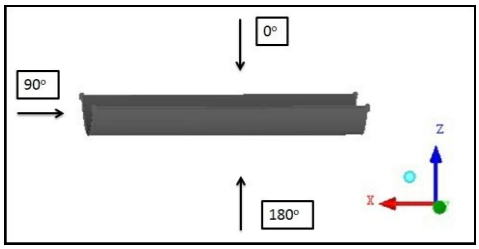

Figure 1: Wind incident angle from 0^{o} to 180^{o} for 0^{o} pitch angle

For pre-processing ICEM CFD was used. All calculations were performed using the ANSYS FLUENT package. A high-quality and fine mesh is constructed over the entire computational domain. The external domain around the parabolic trough extends 1000mm downstream and 500mm in lateral directions, resulting in the parabolic trough occupying less than 0.015% of the volume of the computation domain. This ratio is deemed adequate for modelling external flows with minimal effect of pressure boundaries proximity to the parabolic trough. Although the parabolic trough sits in an atmospheric boundary layer, the calculations assumed a uniform, rather than a boundary-layer, inlet velocity profile. This assumption represents a worst-case scenario for structural loading, hence effectively incorporates a design safety factor.

Steady-state calculations are performed for different pitch angle (θ) and wind speed (V) scenarios. The realizable k-ε turbulence model is used for all equations. Solution convergence is determined by ensuring all residuals of the transport equations drop below a pre-determined threshold and that drag coefficient does no longer vary with iterations.

III. MODEL VALIDATION

Validation of the numerical model is carried out using data from wind tunnel experiments conducted on a parabolic trough collector. In this experiment, parabolic trough is kept at 0^{o} pitch angle and wind incident angle (α) is changed from 0^{o} to 180^{o} i.e. over entire 180^{o} as shown in Fig.2. This reference is used because it provides sufficient information about the trough and the wind-tunnel geometry and flow conditions to generate an accurate numerical model. In the wind tunnel test results, drag coefficient at different wind incident angles for different wind speed were determined.

Numerical modelling was done for these test results. The predicted numerical drag coefficients (Fig.3) found to deviate by 15%, 16%, and 17%, 18%, 18% respectively, from the mean experimental values. Largest drag coefficient and drag force occurs at 0^{o} pitch angle. Overall the predicted drag coefficients are acceptable. This outcome therefore validates the accuracy of the calculations and provides confidence in the numerical model.Extensive experimental work is carried out on flow over the sphere. So the flow over the sphere was modelled numerically so as to check whether the numerical method gives results with minimum error or not. Maximum deviation for flow over sphere was about 18% (Fig.4).

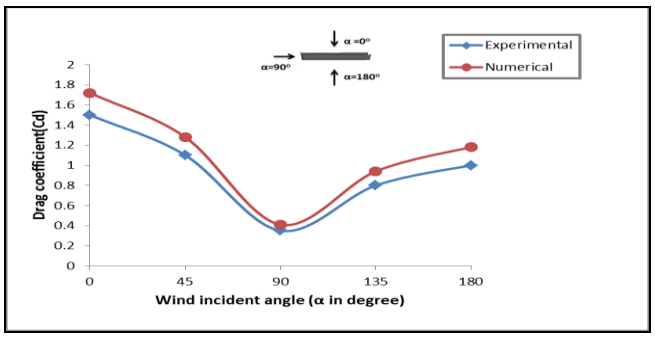

Figure 3: Experimental and numerical drag coefficient against wind incident angle for parabolic trough

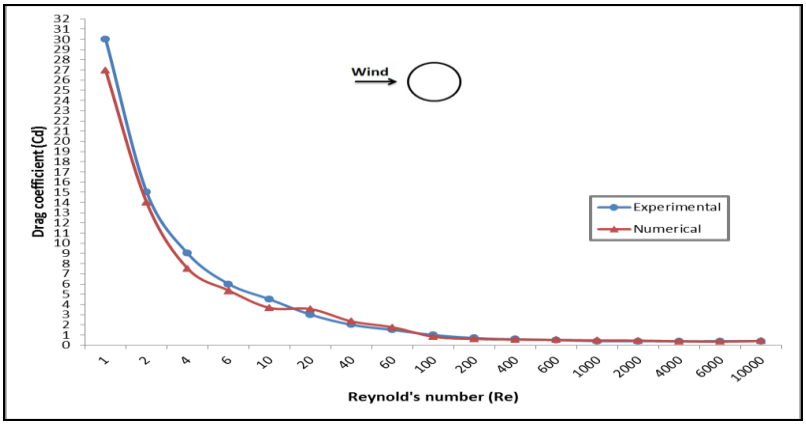

Figure 4: Experimental and numerical drag coefficient against Reynolds's number for sphere

In both the cases, maximum deviation from experimental value is about 18%. Nature of the curve in both the cases was nearly same. This outcome therefore validates the accuracy of the calculations and provides confidence in the numerical model.

IV. RESULTS AND DISCUSSIONS

Three-dimensional calculations are performed for the parabolic trough oriented at different pitch angles 0^o, 30^o, 60^o, 90^o, 120^o, 150^o, and 180^o. For pitch angle 0^o calculations are repeated for wind speed 8, 10,12,14,16 and 18m/s.

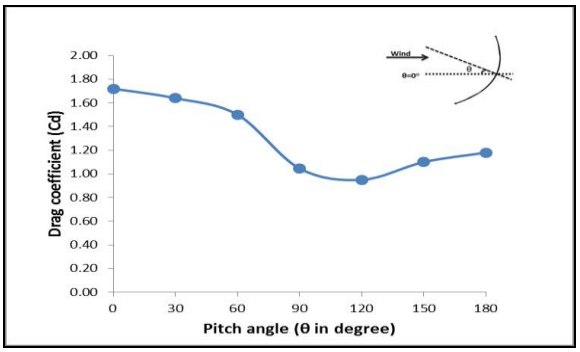

Figure 5: Predicted drag coefficient against pitch angle for parabolic trough

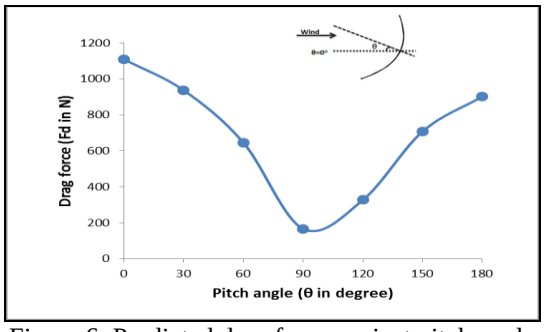

Figure 6: Predicted drag force against pitch angle for parabolic trough

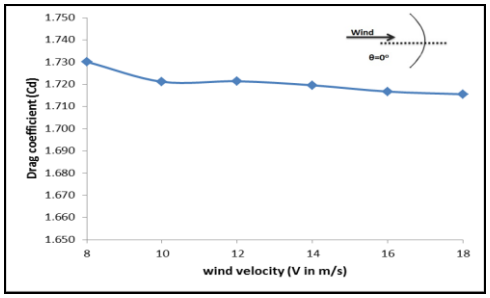

Figure 7: Drag coefficient against wind speed for trough at 0^o pitch angle

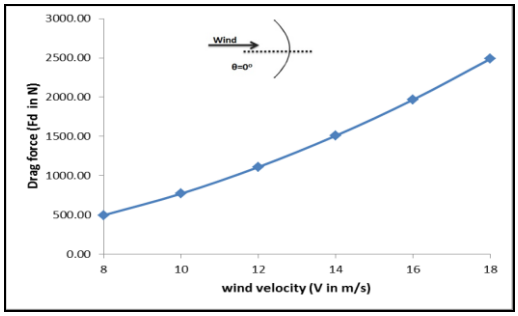

Figure 8: Drag force against wind speed for trough at 0^o pitch angle

For the steady-state flow conditions the predicted drag and coefficients (as expected) are independent of wind speeds, (Fig.8) but are strongly influenced by the pitch angle (Fig.6). Maximum drag coefficient occurs at 0^o pitch angle and minimum at 120^o pitch angle. Though the projected area is minimum at 90^o pitch angle, it is not a position of minimum drag coefficient. This is because drag coefficient depends on flow structure around trough and pressure difference caused around the trough. For the given range of velocity drag coefficient is constant. Drag force increases gradually with increase in the wind velocity (Fig.7). Maximum drag force occurs at 0^o position which is equal to 1100 N. Drag force decreases with increase in pitch angle up to 90^o pitch angle. Again it increases from 90^o to 180^o pitch angle.

The flow field around the trough is shown in the following figures. For different positions of trough, flow structure around the trough is different. Flow separation has occurred at upper edges of the trough (Fig.11). For 0^o and 180^o positions two vortexes are formed at leeward side of the trough. For other positions single vortex is formed. This is because 0^o and180^o positions are symmetrical positions. Single vortex is formed at lower region of the trough for 30^o pitch angle. 60^o position is slightly streamlined with the flow. No larger vortex appears for this position. But the vortex is visible at z=0 plane as shown in Fig.10. For 90^o position single vortex is formed inside the concave region of the trough. For 120^o and 150^o position single vortex is formed. For 120^o position vortex is formed at middle part of the trough and for 150^o position vortex is at upper part of trough. Last three positions i.e. 120^o, 150^o, 180^o positions are slightly streamlined. Hence the value of the drag coefficient for these positions is less than that of 0^o, 30^o, 60^o positions.

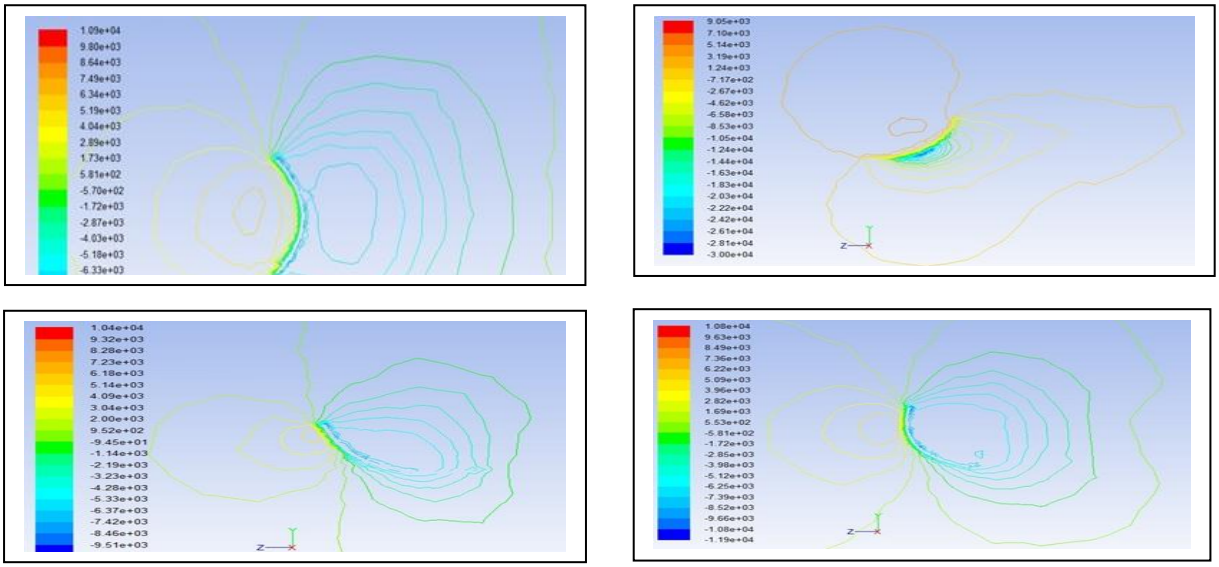

Figure 5: Contours of static pressure for 0^o, 60^o, 120^o, 150^o

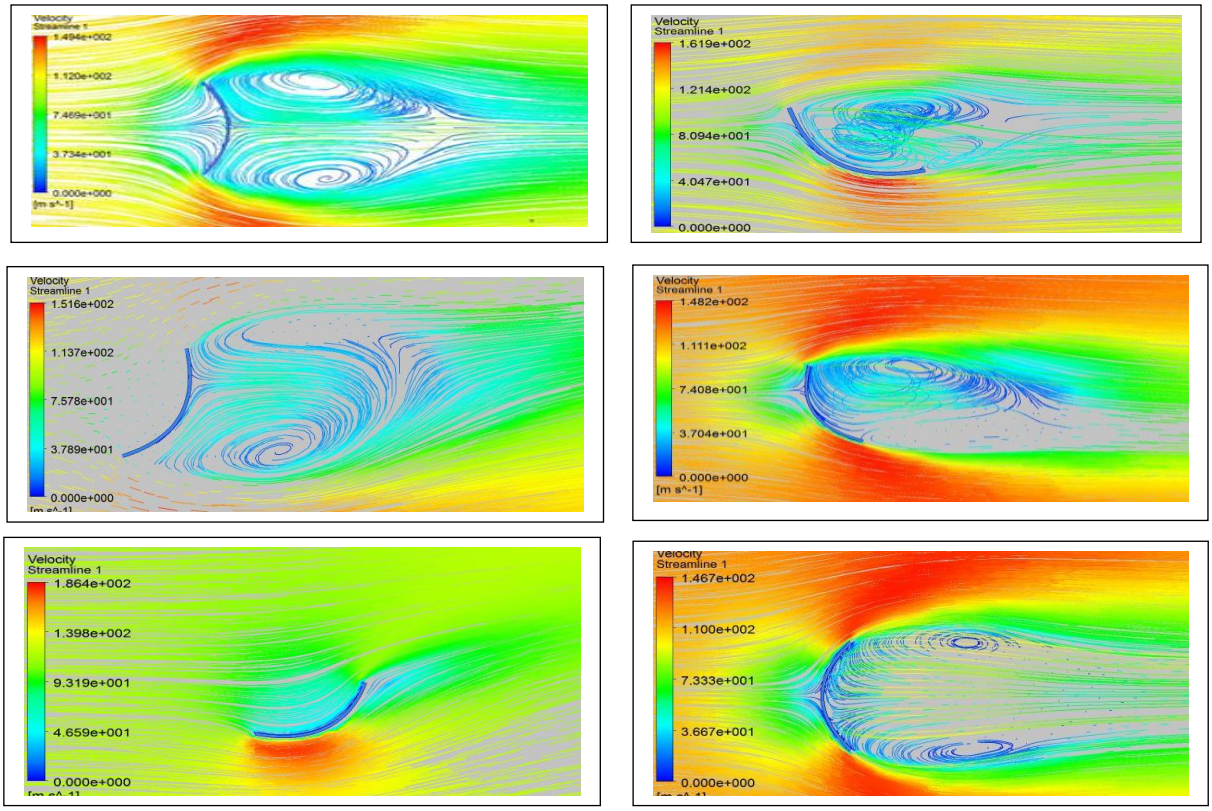

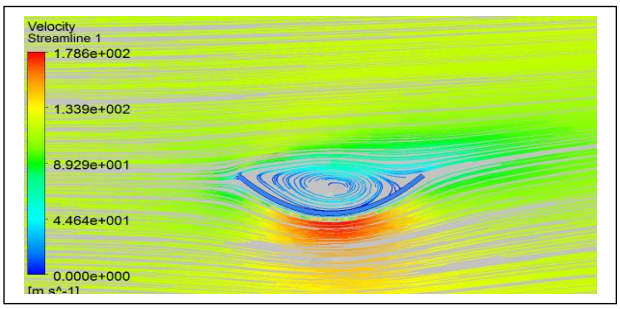

Figure 60: Contours of velocity streamlines for different trough positions

V. CONCLUSION

This validated numerical study provides a quantitative assessment of velocity and pressure fields around a parabolic trough collector.

- Maximum drag coefficient occurs at 0^o pitch angle and its value is 1.72. Minimum drag coefficient occurs at 120^o pitch angle and its value is 0.95.
- Maximum drag force is 1100N and minimum drag force is 167N occurs at 0^o and 90^o pitch angle respectively.
- Various recirculation regions can be found on the leeward and forward sides of the parabolic trough collector when the pitch angle changes with respect to wind direction.
- The resultant force on the collector structure is maximum when wind blows normal to the opening and minimum when the collector is oriented parallel with wind direction.
- The wind force on the collector structure and reflectors increases sharply when the wind speed increases, especially for large collector angles against wind direction.
- The resultant force on the mirrors to pull them from their support is maximum when the convex part of collector is against wind direction.
- Thus, this numerical method gives fairly good results of drag coefficient and flow structure around trough. This method is also useful for other solar concentrators like solar dish for determination of drag coefficient.

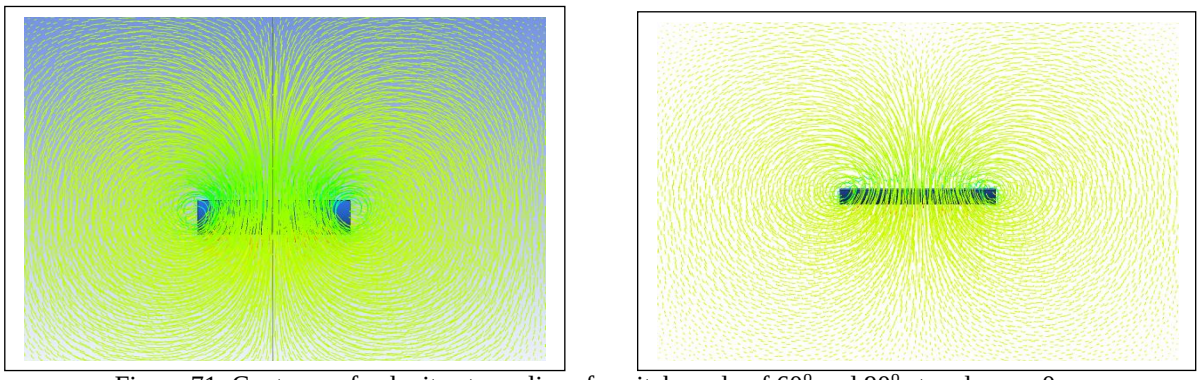

Figure 71: Contours of velocity streamlines for pitch angle of 60^o and 90^o at a plane z=0

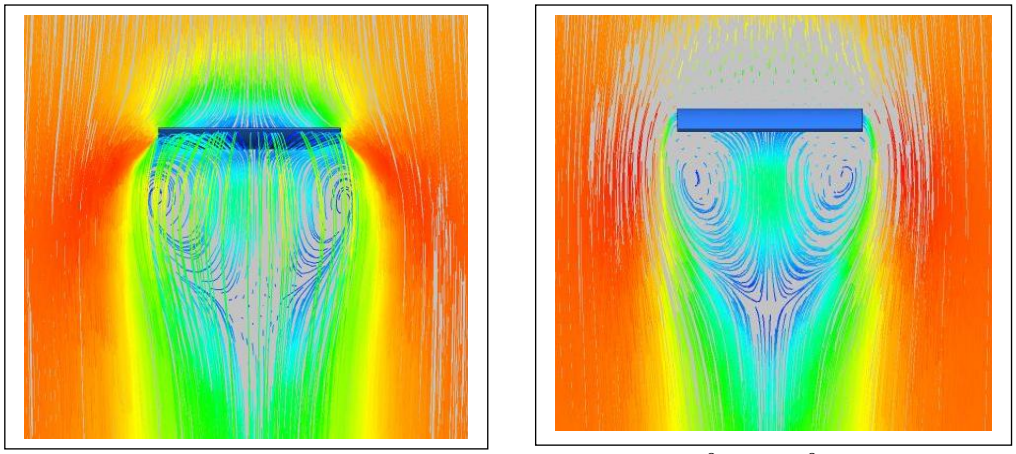

Figure 8: Contours of velocity streamlines for pitch angle of 0^o and 180^o at a plane y=0

VI. ACKNOWLEDGEMENTS

The work described in this paper was undertaken in Thermax Limited, Pune. Thanks to Thermax Limited, Pune for giving an opportunity to work on this project. Thanks to Mr. K. V. Deshpande, General Manager and Head- Solar CoE, Thermax Limited, Pune, for his encouragement and support while doing this work.

REFERENCES

[1]. Farid C. Christo, Numerical modelling of wind and dust patterns around a full-scale paraboloidal solar dish, *Renewable Energy, 39*, 2011, 356-366.
[2]. N. Naeeni, M. Yaghoubi, Analysis of wind flow around a parabolic collector (1) fluid flow, *Renewable Energy, 32*, 2006, 1898-1916.
[3]. Yazan Taamneh, CFD Simulations of Drag and Separation Flow Around Ellipsoids, *Jordan Journal of Mechanical and Industrial Engineering, 5*, 2011, 129-132.
[4]. Girma T. Bitsuamlaka, Agerneh K. Dagnewb, James Erwinc, Evaluation of wind loads on solar panel modules using CFD, *The Fifth International Symposium on Computational Wind Engineering (CWE2010), 2010.*
[5]. Shaharin A Sulaiman, Chen Jiun Horng, Determinations of Drag and Lift using ANSYS CFD Flotran Simulation, 2006
[6]. Georgeta Văsieș, Elena Axinte And Elena-Carmen Teleman, Numerical Simulation Of Wind Action On Solar Panel Placed On Flat Roofs With And Without Parapet, 2010.
[7]. Bo Gong, Zhifeng Wang, Zhengnong Li, Jianhan Zhang, Xiangdong Fu, Field measurements of boundary layer wind characteristics and wind loads of a parabolic trough solar collector, *Solar Energy, 86*, 2012, 1880-1898.
[8]. Jain A.K., *Fluid mechanics,* (Khanna Publishers, New Delhi, Tenth edition 2009).

International Journal of Modern Engineering Research (IJMER)
www.ijmer.com Vol. 3, Issue. 4, Jul.-Aug. 2013 pp-2133-2138 ISSN: 2249-6645

Low Cost Self-assistive Voice Controlled Technology for Disabled People

R. Puviarasi[1], Mritha Ramalingam[2], Elanchezhian Chinnavan[3]
[1](Asst.Prof,. Department of Electrical and Electronics Engineering, Saveetha University, India
[2](Lecturer, School of Engineering, AIMST University, Malaysia)
[3](Lecturer, School of Physiotherapy, AIMST University, Malaysia)

ABSTRACT: *This paper describes the design of an innovative and low cost self-assistive technology that is used to facilitate the control of a wheelchair and home appliances by using advanced voice commands of the disabled people. This proposed system will provide an alternative to the physically challenged people with quadriplegics who is permanently unable to move their limbs (but who is able to speak and hear) and elderly people in controlling the motion of the wheelchair and home appliances using their voices to lead an independent, confident and enjoyable life. The performance of this microcontroller based and voice integrated design is evaluated in terms of accuracy and velocity in various environments. The results show that it could be part of an assistive technology for the disabled persons without any third person's assistance.*

Keywords: *Disabled people, Home automation, Self-assistive, Voice control, Wheel chair,*

I. INTRODUCTION

Sometimes low-technology devices are the most appropriate and even preferred for their simplicity, ease of use, maintenance, and low cost. Naturally, a wheelchair voice control system should operate reliably for a large number of users, reduce the physical requirements; and if avoiding the need to move on one or more road extremities, should assist a user in maintaining well the chair position. However, the limited bandwidth of the voice makes it difficult to adjust frequently with the wheelchair's velocity, and also a voice input system may fail to identify a speaker. Thus, voice interface has yet become commercially viable for wheelchair control [1]. However, one implementation difficulty is that a voice input system may fail to recognize a user's voice. Indeed, speech activated interface between human and autonomous/semi-autonomous systems requires accurate detection and recognition. So the pitch and end-point detection plays an important role in speech recognition system [2]. The current power wheelchair control interfaces used may not be adequate to provide truly independent mobility for substantial number of person with disabilities [3]. The Respondents to the survey reported on average that approximately ten percent of the patients trained to operate a power wheelchair cannot use the chair upon completion of their training for activities of daily living or can do so only with extreme difficulty. The design and development of a speech recognition system can be used to interact with a home computer and to control domestic appliances at the command of a word (speech) [4]. The voice received is processed in the voice recognition system where the feature of the voice command is extracted and matched with the existing sample in the database. The module recognizes the voice and sends control messages to the microcontroller [5, 6]. Powered wheelchair users often struggle to drive safely and effectively and in more critical cases can only get around when accompanied by an assistant [7]. Without assistance, participants experienced multiple collisions whilst driving around the predefined route. These issues are proposed in a collaborative control mechanism that assists the user as and when they require help. The basic idea of the driving assistance module is to detour obstacles in a way that is most likely to be acceptable for the user. The automated wheel chair using head joystick [8] produces the driving assistance module by altering the translational and rotational velocities. A paper focuses specifically on the evaluation of shared control methodologies [9] surveys many components of wheelchair design: everything from mechanical aspects, interfaces and control algorithms to ISO standards that are being developed to assist users in driving safely.

The proposed system enables physically challenged persons like paralytic patients or physically disabled patients or patients having acute diseases like Parkinson's disease, to facilitate the control of a wheelchair. In particular, this is useful for the persons where they can move their wheelchair in their own directions, without any third party's help or support. The objective of this paper is divided into two targets. One is to control various home appliances by voice, and the other is to enable severely disabled person's movement independently using voice activated powered wheelchair, that provide reliability, safety and comfort. Moreover, home automation is an absolute benefit and can improve the quality of life for the user. Wheelchairs provide unique mobility for the disabled and elderly with motor impairments. The designed system is based on grouping a microcontroller with a new voice recognition processor.

The rest of the paper is organised as follows. After the introduction, Section 2 presents the design method. Section 3 discusses the experimental results and performance evaluation of the proposed design. Section 4 concludes the paper.

II. DESIGN METHOD

In the proposed design, the main idea of using voice activated technology for controlling the motion of the wheelchair and home automation is to prove that it can be an unique solution for severely disabled. The use of this new technology in conjunction with a mechanical system is, in order to simplify everyday life would spark interest in an ever growing modern society. Many people with disabilities do not have the dexterity necessary to control a joystick on an

electrical wheelchair. This can be a great drawback for the quadriplegics who is permanently unable to move any of the arms or legs. They can use their wheelchair easier only using voice commands and also they can control their home appliances. The aim of this study is to implement an interesting application using small and advanced vocabulary word recognition system. The methodology adopted is based on grouping a microprocessor with a speech recognition development kit for isolated word from a dependent speaker. The resulting design is used to control a wheelchair and home appliances for a disabled person based on the vocal command. It therefore involves the recognition of isolated words from a limited vocabulary. There are seven options for basic motions of a wheelchair & home appliances control to be applied by the user. The seven conditions of the wheelchair can be described as the following: moving forward to the front of the user, moving backward to the back of the user, turning to the right, turning to the left, static or stop condition, light on and light off

2.1 Mechanical and Electrical Design of the wheel chair

In this section, the manual wheelchair is modified into an electrical wheelchair which is controlled using voice command. The important part is to upgrade the manual wheelchair into an electrical wheelchair. Thus, the parts like motors, pulleys, belts and a battery are needed. With the combination of these mechanical and electrical parts, the manual wheelchair now is turned to be an electrical wheelchair. There are a number of possible driving wheel configurations (front wheel drive, rear wheel drive and mid wheel drive) which affect the characteristics of the chair in different situations, with turning while driving being the most complex. Further features can be added to assist the user such as lights, actuators and wireless links. The heart and brains of the powered wheelchair is in the controller as it provides both a conduit for the power to the motors and controls the overall system. The wheel which is connected with the motor is considered as the main wheel. The main wheel is 6" in diameter. Fig.1 (a) shows the main wheel that has a single bore at the centre. This bore is connected to the motor. A caster (or castor) wheel shown in Fig.1 (b) is an un driven, single, double, or compound wheel that is designed to be mounted to the bottom of a larger object (the "vehicle") so as to enable that object to be easily moved.

(a)  (b)  (c) 

Figure 1. (a**)** Main wheel (centre bore) (b) caster wheel (c) DC motor

This section mainly deals with the electrical components used in controlling the wheelchair and home automation. A DC motor shown in Fig.1 (c) is an electric motor that runs on direct current (DC) electricity. DC motors can operate directly from rechargeable batteries, providing the motive power for the vehicles. Today DC motors are still found in applications as small as toys and disk drives, or in large sizes to operate steel rolling mills and paper machines. Also step-down transformer, filter capacitors, rectifiers, transmitter-receivers are used in the system design. Fig.2 shows the basic components used in the design of the voice controlled wheel chair.

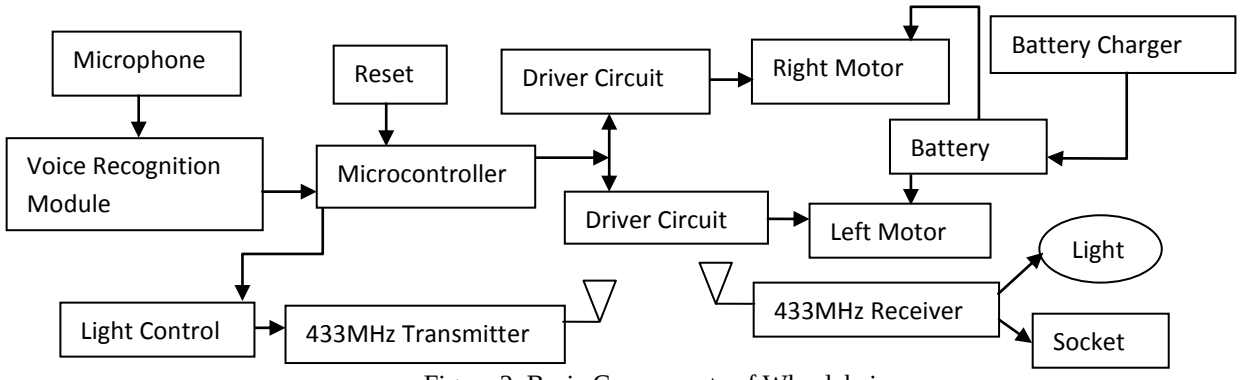

Figure 2. Basic Components of Wheelchair

2.2 Interfacing Circuits Design of wheel chair

The block diagram of the interfacing circuit of the wheel chair is shown in Fig 3. In this circuit, the HM 2007 processor is assembled with the input and output port, memory chip and the digital display. The instructions given by the supplier must be followed carefully so that the system can work properly. The voice recognition circuit operates as the main part of the system to store the commands in to the HM2007 processor. This speech recognition system uses a simple keypad and digital display to communicate with and program the HM2007 processor. When the circuit was turned on, the processor will check the static RAM. After this check out, the board displays "00" on the digital display and lights the red LED (READY). It is in the "Ready" state waiting for the command. In this system, the display board will be taking off from the output of voice recognition circuit and replace it by the interfacing circuit which will be connected to the motor driven

circuit. This is initialized by pressing the word number that wanted to be trained on the keypad. The circuit can be trained to recognize up to 40 words. The HM 2007 processor is assembled with the input and output port, memory chip and the digital display. The instructions given by the user must be followed carefully so that the system can work properly.

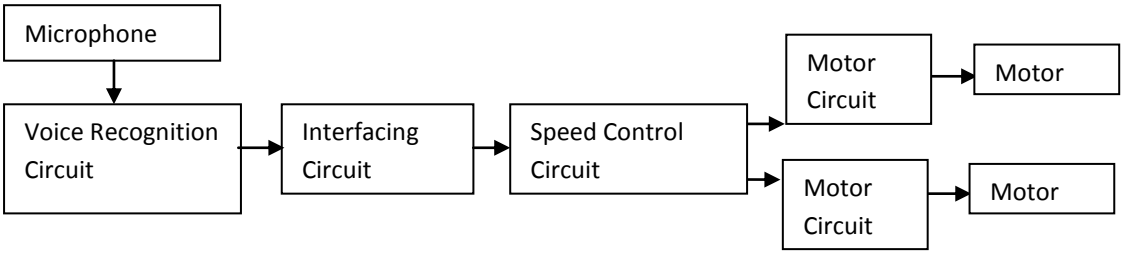

Figure 3: Interfacing Electronic circuit system

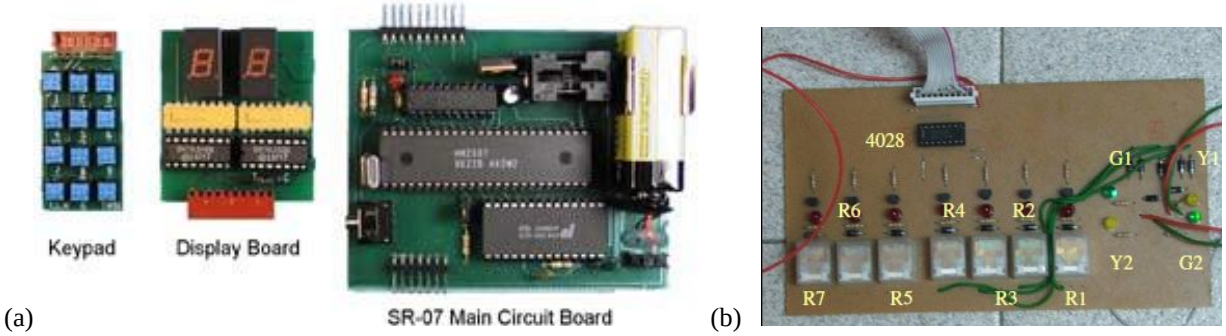

(a) (b)

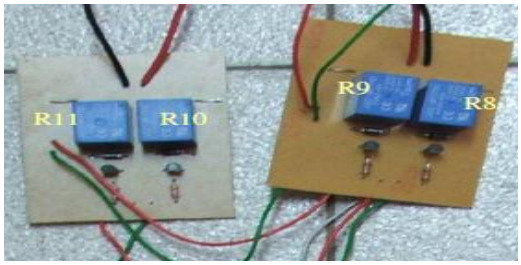

(c)

(d)

(e)

Figure 4 (a) Voice recognition circuit (b) Interfacing circuit (c) Speed control circuit to control motor
(d) Mechanical and Electrical design of the wheel chair (e) Hardware design of wheel chair with the interfacing circuits

The interfacing electronic circuit, Fig.4 (b) is used to connect the voice recognition circuit, Fig.4 (a) and speed control circuit Fig.4(c). The directions of motor are indicated by four LEDs on the interfacing circuit. In Fig 4 (d), with the combination of these mechanical and electrical parts, the wheelchair is designed manually. The manual wheel chair has been designed to be an electrical wheelchair with the interfacing circuits. The electrical powered wheelchair uses a wheelchair motor which was specially designed for the purpose to move the wheelchair with a load. The wheelchair motors normally have high torque and high revolution per minutes (rpm). These criteria will make sure that the electrical wheelchair can move smoothly when it is being used. The fig 4 (e) shows the hardware design of the wheel chair with the required interfacing circuits.

2.3 Voice controlled principle of the wheel chair

In this paper some advanced voice commands are designed so that the user can choose the speed. The user can select the speed in two levels, either slow or fast speed to move. For example if the user need only to move in a short distance or to approach object, he should use the slow speed. This speed selection is important for safety and extra manoeuvrability of the user. The main part of the design is to control the motion of the wheelchair. Fig. 5 shows the working principle of the wheel chair based on the voice recognition. There are four types of motions considered, moving forward, moving in reverse direction, moving to the left and moving to the right. For the speed, the user may use slow or fast speed. Slow speed is important as the user want to move in short distance or approaching an object. The system starts by

applying the supply voltage to the speech recognition circuit. The system will be in stand by condition in which the LED on circuit recognition board will be turned on.

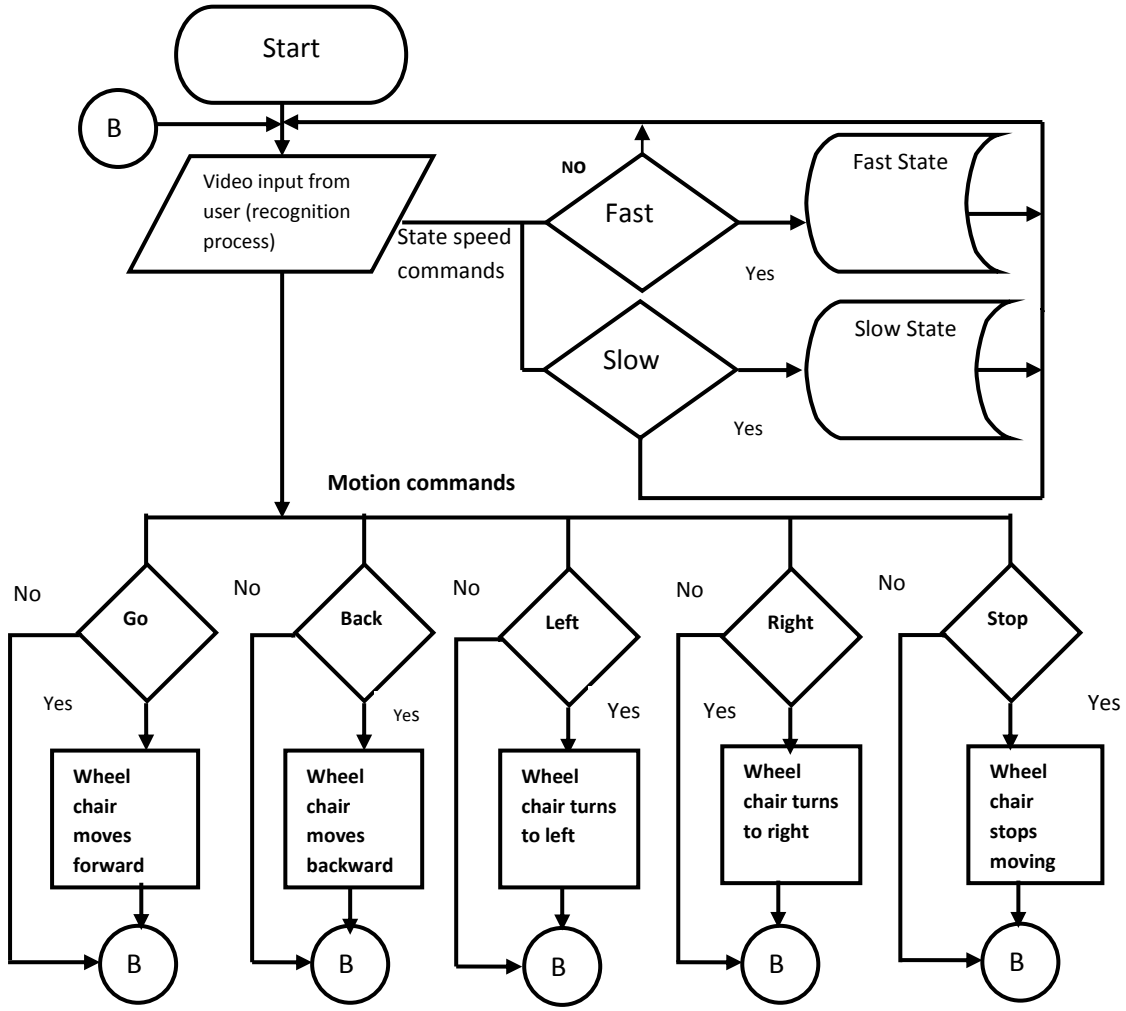

Figure 5 Voice controlled motion of the wheelchair

The system can be controlled in two speed conditions, fast and slow. For fast condition the system will supply higher current to the motors. If the user does not want the wheelchair to move in high speed, the slow speed can be set by applying low current supply to the motors. The direction and speed of the wheelchair depends on the user. For the forward command the wheelchair moves in forward direction. For the reverse direction the opposite movement of wheel rotation will occur. The left command will make right wheel moves forward and left wheel moves backward. The right command makes left wheel moves forward and right wheel rotate backward. In this system, by assigning the word command stop the rotation of both motors will stop. The wheelchair system will go back to the stand by condition or end the whole system by turning off the power supply of the speech recognition board. The voice commands used are as per Table 1. This processor is the best choice as it is easy to build programmable speech recognition circuit. The circuit is programmed in such a way that we train the words (or vocal utterances) that we want the circuit to recognize. This kit allows us to experiment with many facets of speech recognition technology. Unlike software based speech recognition systems like Dragon naturally speaking (tm) and Via Voice (tm), it is stand alone circuit and works without a personal computer. To train the voice control circuit, the keypad containing 12 switches is used. In this design the memory used is trained to recognize the voice as per the conditions in Table 1.

Table 1: Voice commands with binary values

Voice	Conditions	Digital display	Voice	Binary commands
FORWARD	Moves straight to the forward	01	FAST	0001
REVERSE	Moves straight to the backward	02	SLOW	0010
ON	Sets the wheelchair on	03	REVERSE	0011
OFF	Sets the wheelchair off	04	FORWARD	0100
LEFT	Turn to left	05	LEFT	0101
RIGHT	Turn to right	06	RIGHT	0110
STOP	Stop the system	07	STOP	0111

ON	Giving supply to wheelchair / home appliances	Switch		
OFF	Switching off the supply	Switch		

Fig. 6 shows the block diagram of the controlling mechanism for home appliances using voice recognition circuit. This system uses the 89c51 microcontroller and it has a flash programmable memory that is programmed using assembly programming to control the home appliances. The user of this wheel chair can operate the home appliances (like light, fan and TV) using their voice commands.

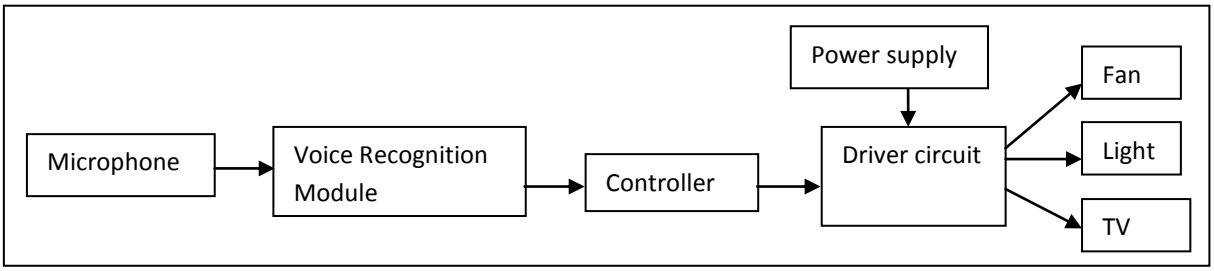

Figure 6 Block diagram of voice controlled home appliances

III. Results And Discussion

After the design and development of the wheel chair with respective interfacing circuits, the technology was tested for the motion of the wheel chair and home automation using trained voice. This design is experimented based on two important aspects, firstly, on the accuracy of the system and secondly, wheelchair velocity & home automation control by means of on & off control commands. The proposed design was implemented using normal people. This would be implemented for disabled people after having the smoothly furnished design of the wheel chair.

3.1 Accuracy of the Wheel Chair

This experiment was conducted in a room which is in silent condition to observe the result of the experiment. The purpose of the experiment is to find out the accuracy of the wheel chair in response to the speech (voice) in different conditions.

Condition 1: silent area

Five trials of experiments were done with the new design based on the commands listed at the Table 1. From Table 2, there are 4 over 5 commands were recognized by the speech recognition circuit to move the wheel chair. The percentage of the accuracy of the wheel chair in silent condition is 80% (Accuracy = 4/5 X100%= 80%).

	(a) Result in silent area						(b) Result in noisy condition					
Voice commands	Experiment trials					Total Response	Experiment trials					Total Response
	1	2	3	4	5		1	2	3	4	5	
On(HA)	1	1	0	1	1	4	0	1	1	1	0	3
OFF(HA)	1	1	1	1	0	4	0	0	1	1	0	2
Reverse	1	1	1	1	1	5	1	1	1	1	0	4
Forward	1	0	1	1	1	4	1	1	1	0	0	3
Right	1	1	0	1	1	4	1	1	0	0	0	2
Left	1	1	1	1	1	5	1	1	0	1	0	3
Stop	1	0	1	1	1	4	0	1	1	0	1	3

Table 2(a): Result in silent area; (b) Result in Noisy condition (HA-Home Appliances)

Condition 2: noisy area

The testing is done outside the silent room where it is considered as natural environment. From this experiment, the results are obtained as per the Table 2(b). From the table, there are 3 over 5 commands recognized by the trained speech recognition circuit. The percentage of the accuracy of speechRecognition circuit in noisy condition is 60%. This is calculated as, Accuracy = 3/5 X100 = 60%.

From Fig. 7, it is observed that the accuracy of the voice recognition circuit in silent condition is less compared to that in the noisy condition.

Figure 7 Graph of accuracy of the voice regonition circuit in two conditions

3.2 Velocity

The important aspect of the wheelchair system is to find its velocity. While the Voice controlled wheelchair moving in a straight line, the distance and time were noted for velocity. The velocity of the wheel chair needs to be experimented under two conditions. First the velocity is observed in unloaded condition. The wheelchair was made to move in a straight line and the result was observed. The distance measured was 6 meters and time is 6.34s. So, distance over time is 0.95m/s. Second, a person weighing around 20kg to 25kg was seated at the wheelchair. The voice controlled wheelchair was allowed to move in a straight line. Now the distance measured was 4 meters and time is 5.44s. So the velocity of the wheel chair with load is 0.74m/s. Based on the above result, the velocity of voice controlled wheelchair is affected by the load. It is observed that the velocity of the wheelchair system will decrease proportional to the load that is carried by the system.

IV. Conclusion

This proposed system contributes to the self dependency of physically challenged and older people. It reduces the manual effort for acquiring and distinguishing the command for controlling the motion of a wheelchair & home appliances. The speed and direction of the wheelchair now can be selected using the specified commands. Thus the only thing needed to ride the wheelchair is to have a trained voice. Besides that, the development of this project is done with less cost and affordable. However this system requires some improvements to make it more reliable. This design could be improved by implementing wireless communication in the wheel chair. By improving this system, we directly enhance the life style of the disabled people in the community. Lastly, we hope that this kind of system could contribute to the evolution of the wheelchair technology.

REFERENCES

[1] Linda Fehr, MS, W. Edwin, *et al.*, Adequacy of power wheelchair control interfaces for persons with severe disabilities: A clinical survey, *Journal of Rehabilitation Research and Development*, 37(3), 2000, 353-360.
[2] Simpson RC, Levine SP, Voice control of a powered wheelchair, *IEEE Trans Neural System Rehabilitation Eng.* 2000, 122-125.
[3] X. S. Li, *et al.*, Analysis and Simplification of Three-Dimensional Space Vector PWM for Three-Phase Four-Leg Inverters, *IEEE Trans. on Industrial Electronics, vol* 58, 2011, 450-464.
[4] R. Cooper, M. Boninger, *et al.*, Engineering better wheelchairs to enhance community participation, *IEEE Trans. Neural Systems Rehabilitation Eng*, 14(4), 2006, 438–455.
[5] C.Chandramouli and Vivek Agarwal, Speech Recognition based Computer Keyboard Replacement for the Quadriplegics, Paraplegics, Paralytics and Amputees, ACM publishers, *IEEE International Workshop on Medical Measurements and Applications*, 2009, 241-245.
[6] Kailash Pati Dutta, *et al.*, Microcontroller Based Voice Activated Wireless Automation System, *VSRD-IJEECE*, 2 (8), 2012, 642-649.
[7] Thomas Rofer, Christian Mandel and Tim Laue, Controlling an Automated Wheelchair via Joystick/Head-Joystick Supported by Smart Driving Assistance, *IEEE 11th International Conference on Rehabilitation Robotics*, 2009, 743-748.
[8] Ha, T.H. Tran and G. Dissanayake, A wavelet- and neural network-based voice interface system for wheelchair control, *Int. J. Intelligent Systems Technologies and Applications*, 1(2), 2005, 49-65.
[9] Tom Carlson and Yiannis Demiris, Collaborative Control for a Robotic Wheelchair: Evaluation of Performance, Attention and Workload, *IEEE Trans. on systems, man, and cybernetics:* part b, 2011, 1-12.

BIBLIOGRAPHY OF AUTHORS

R.Puviarasi	She is working as an Assistant Professor in Saveetha University, Chennai, India. She is graduated from Anna University, Coimbatore with M.E in Embedded & Control Systems and B.E in Electical & Electronics Engineering from Anna University, Chennai. Her research areas are Embedded systems, Renewable energy-solar and wind power systems, machines and control systems
Mritha Ramalingam	With ten years of teaching experience, she is currently working as a Lecturer in the Faculty of Engineering & Computer Technology, School of Engineering, AIMST University. She is graduated from ANNA University, Chennai with M.E Computer Science & Engineering(CSE) and B.E in CSE from University of Madras, Chennai. She worked as an Assistant Professor under Anna University, Chennai, India. Her research areas are embedded systems, network security, video steganography, computer networks and wireless networks
Elanchezhian Chinnavan	With fifteen years of teaching and clinical experience, he is currently working as a Lecturer in School of Physiotherapy, AIMST University. He worked as an Assistant Professor in Meenakshi University, Chennai, India. He worked as physiotherapist in many hospital organizations and in mentally retarded rehabilitation centers. He is specialized in Neurology.

International Journal of Modern Engineering Research (IJMER)
www.ijmer.com Vol. 3, Issue. 4, Jul - Aug. 2013 pp-2139-2146 ISSN: 2249-6645

Applying Classification Technique using DID3 Algorithm to improve Decision Support System under Uncertain Situations

Ahmed Bahgat El Seddawy[1], Prof. Dr. Turky Sultan[2], Dr. Ayman Khedr[3]
[1]*Department of Business Information System, Arab Academy for Science and Technology, Egypt*
[2, 3]*Department of Information System, Helwan University, Egypt*

Abstract: *Decision Support System (DSS) is equivalent synonym as management information systems (MIS). Most of imported data are being used in solutions like data mining (DM). Decision supporting systems include also decisions made upon individual data from external sources, management feeling, and various other data sources not included in business intelligence. Successfully supporting managerial decision-making is critically dependent upon the availability of integrated, high quality information organized and presented in a timely and easily understood manner. Data mining have emerged to meet this need. They serve as an integrated repository for internal and external data-intelligence critical to understanding and evaluating the business within its environmental context. With the addition of models, analytic tools, and user interfaces, they have the potential to provide actionable information that supports effective problem and opportunity identification, critical decision-making, and strategy formulation, implementation, and evaluation. The proposed system will support top level management to make a good decision in any time under any uncertain environment using classification technique by DID3algorithm.*

Key words: *DSS, DM, MIS, CLUSTERING, CLASSIFICATION, ASSOCIATION RULE, K-MEAN, OLAP, MATLAB*

I. INTRODUCTION

Decision Support System (DSS) is equivalent synonym as management information systems (MIS). Most of imported data are being used in solutions like data mining (DM). Decision supporting systems include also decisions made upon individual data from external sources, management feeling, and various other data sources not included in business intelligence. Successfully supporting managerial decision-making is critically dependent upon the availability of integrated, high quality information organized and presented in a timely and easily understood manner. Data mining have emerged to meet this need. They serve as an integrated repository for internal and external data-intelligence critical to understanding and evaluating the business within its environmental context. With the addition of models, analytic tools, and user interfaces, they have the potential to provide actionable information that supports effective problem and opportunity identification, critical decision-making, and strategy formulation, implementation, and evaluation. The proposed system will support top level management to make a good decision in any time under any uncertain environment [4]. This study aim to investigate the adoption process of decision making under uncertain situations or highly risk environments effecting in decision of investing stoke cash of bank. This applied for two types of usage investment - direct or indirect - or credit and any sector of investment will be highly or moderate or low risk. And select which one of this sectors risk 'rejected' or un-risk 'accepted' all that under uncertain environments such as; political, economical, marketing, operational, internal policies and natural crises, all that using the contribution of this study enhancing k-mean algorithm to improve the results and comparing results between original algorithm and enhanced algorithm. The paper is divided into four sections; section two is a background and related work it is divided into two parts, part one is about DSS, part two is about DM. Section three presents the proposed Investing Data Mining System 'IDMS. Section four presents conclusion and finally section five present future works2. Tables, Figures and Equations.

II. BACKGROUND AND RELATED WORK

1. Decision Support System (DSS)

DSS includes a body of knowledge that describes some aspects of the decision maker's world that specifies how to accomplish various tasks, that indicates what conclusions are valid in different circumstances [4].The expected benefits of DSS that discovered are higher decision quality, improved communication, cost reduction, increased productivity, time savings, improved customer satisfaction and improved employee satisfaction. DSS is a computer-based system consisting of three main interacting components:

- **A language system**: a mechanism to provide communication between the user and other components of the DSS.
- **A knowledge system**: A repository of problem domain knowledge embodied in DSS as either data or procedures.
- **A problem processing system**: a link between the other two components, containing one or more of the general problem manipulation capabilities required for decision-making.

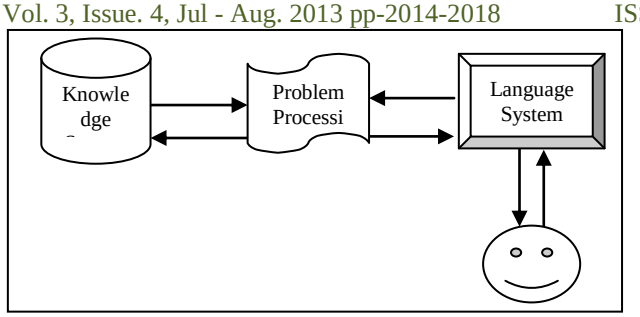

Fig 1: DSS Main Components

After surveying multiple decision support systems, it is concluded that decision support systems are categorized into the following [5]:

- **File drawer systems**: This category of DSS provides access to data items.
- **Data analysis systems**: Those support the manipulation of data by computerized tools tailored to a specific task or by more general tools and operators.
- **Analytical information systems**: Those provide access to a series of decision-oriented databases.
- **Accounting and financial models**: those calculate the consequences of possible actions.
- **Representational models**: those estimate the consequences of actions based on simulation models that include relationships that are causal as well as accounting definitions.
- **Optimization models**: those provide guidelines for actions by generating an optimal solution consistent with a series of constraints.
- **Suggestion models**: those perform the logical processing leading to a specific suggested decision or a fairly structured or well understood task.

This section describes the approaches and techniques mostly used when developing data warehousing systems that data warehousing approaches such as; Online Analytical Processing 'OLAP', Data Mining 'DM' and Artificial Intelligence 'AI'. And in this paper will using DM as approach and technique.

2. Data Mining Techniques (DM)

Data mining is the process of analyzing data from different perspectives and summarizing it into useful information [10]. DM techniques are the result of a long process of research and product development [10]. There are several processes for applying DM:

1. Definition of the business objective and expected operational environment.
2. Data selection is required to identify meaningful sample of data.
3. Data transformation that involves data representation in an appropriate format for mining algorithm.
4. Selection and implementation of data mining algorithm depends on the mining objective.
5. Analysis of the discovered outcomes is needed to formulate business outcomes.
6. Representing valuable business outcomes.

DM techniques usually fall into two categories, predictive or descriptive. Predictive DM uses historical data to infer something about future events. Predictive mining tasks use data to build a model to make predictions on unseen future events. Descriptive DM aims to find patterns in the data that provide some information about internal hidden relationships. Descriptive mining tasks characterize the general properties of the data and represent it in a meaningful way. Figure2 shows the classification of DM techniques.

Fig 2: DM Techniques [5]

2.1 Classification Technique

Classification is to use the model to predict the class of objects whose class label is unknown.

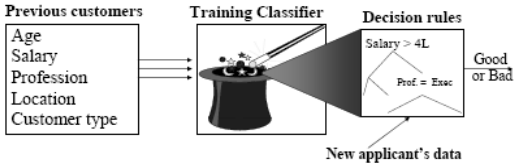

Fig 3: Example for classification procedures

Classification based on Bayes Theorem of classification is "composed of two steps supervised learning of a training set of data to create a model, and then classifying the data according to the model. Some well-known classification algorithms include Bayesian Classification, decision trees, neural networks and back propagation based on neural networks, k-nearest neighbor classifiers based on learning by analogy, and genetic algorithms" [10]. Classification can be used for predicting the class label of data objects. However, in many applications, one may like to predict some missing or unavailable data values rather than class labels. This is usually the case when the predicted values are numerical data, and is often specially referred to as prediction. Although prediction may refer to both data value prediction and class label prediction, it is usually connected to data value prediction and thus is distinct from classification. Also, prediction encompasses the identification of distribution trends based on the available data. Classification and prediction may need to be preceded by relevance analysis which attempts to identify attributes that do not contribute to the classification or prediction process.

2.1.1 Classification Tree

Trees used for regression and trees used for classification have some similarities - but also some differences, such as the procedure used to determine where to split. Some techniques use more than one decision tree for their analysis:

- A Random Forest classifier uses a number of decision trees, in order to improve the classification rate.
- Boosted Trees can be used for regression-type and classification-type problems.
- Rotation forest - in which every decision tree is trained by first applying principal component analysis (PCA) on a random subset of the input features.

There are many specific decision-tree algorithms such as, ID3 algorithm, C4.5 algorithm, CHi-squared Automatic Interaction Detector 'CHAID'. Performs multi-level splits when computing classification trees. And MARS extends decision trees to better handle numerical data.

2.1.1.1 ID3 Algorithm

ID3 is a simple decision tree learning algorithm developed by Ross Quinlan (1983) [74]. The basic idea of ID3 algorithm is to create a decision tree of given set, by using top-down greedy search to check each attribute at every tree node [75].

Table 2: Strengths and weakness of ID3 algorithm

Strengths	Weakness
• Understandable prediction rules are created from the training data. • Builds the fastest tree. • Builds a short tree. • Only need to test enough attributes until all data is classified. • Finding leaf nodes enables test data to be pruned, reducing number of tests. • Whole dataset is searched to create tree.	• Data may be over-fitted or over-classified, if a small sample is tested. • Only one attribute at a time is tested for making a decision. Classifying continuous data may be computationally expensive, as many trees must be generated to see where to break the continuum.

For building ID3 algorithm decision tree consists of nodes and arcs or sweeps which connect nodes. To make a decision, one starts at the root node, and asks questions to determine which arc to follow, until one reaches a leaf node and the decision is made. This basic structure is shown in figure 4.6

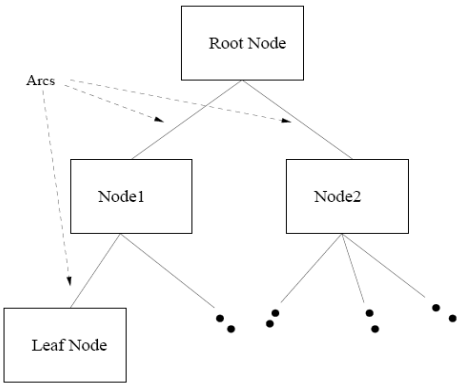

Fig 4: Basic decision tree structure

The main ideas behind the ID3 algorithm are:

Step 1: Each non-leaf node of a decision tree corresponds to an input attribute, and each arc to a possible value of that attribute. A leaf node corresponds to the expected value of the output attribute when the input attributes are described by the path from the root node to that leaf node.

Step 2: In a "good" decision tree, each non-leaf node should correspond to the input attribute which is the most informative about the output attribute amongst all the input attributes not yet considered in the path from the root node to that node. This is because we would like to predict the output attribute using the smallest possible number of questions on average.

Step 3: Entropy is used to determine how informative a particular input attribute is about the output attribute for a subset of the training data. Entropy is a measure of uncertainty in communication systems introduced by Shannon (1948). It is fundamental in modern information theory.

```
function ID3 (I, O, T) {
/*  I is the set of input attributes
*   O is the output attribute
*   T is a set of training data
*
*   function ID3 returns a decision tree
*/
    if (T is empty) {
        return a single node with the value "Failure";
    }
    if (all records in T have the same value for O) {
        return a single node with that value;
    }
    if (I is empty) {
        return a single node with the value of the most frequent value of
        O in T;
        /* Note: some elements in this node will be incorrectly classified */
    }

    /* now handle the case where we can't return a single node */
    compute the information gain for each attribute in I relative to T;
    let X be the attribute with largest Gain(X, T) of the attributes in I;
    let {x_j| j=1,2, .., m} be the values of X;
    let {T_j| j=1,2, .., m} be the subsets of T when T is partitioned
        according the value of X;
        return a tree with the root node labelled X and
        arcs labelled x_1, x_2, .., x_m, where the arcs go to the
        trees ID3(I-{X}, O, T_1), ID3(I-{X}, O, T_2), .., ID3(I-{X}, O, T_m);
}
```

Fig 5: Pseudo Cod of ID3 Algorithm

Enhanced ID3 to 'DID3'

After taking data from clustering technique by 'E_K-m' algorithm, and before inserting to next technique association rules need to classify data by ID3 algorithm, but before use it need to decompose data to several parts to can be managed, to be more accurate and faster that by enhancing ID3 using adding sample step called 'Decompose Data' to equal sized subsets. It shows also in next steps of algorithm.

1. Insert data from (E_K-m) to ID3,
2. Dividing data sets to 'K clusters',

Decompose data to K classification;

3. Run original DID3,
4. Create nods based on tree classification;

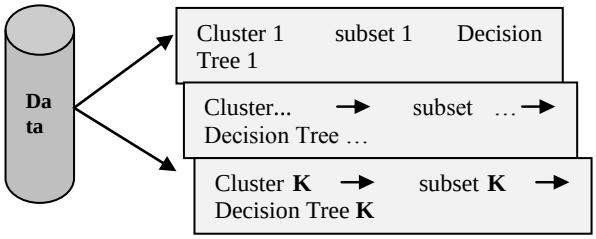

Fig 6: Example of decomposition data using ID3 Algorithm

3. Implementation

IDMS execution done via several techniques started with clustering technique using K-M and enhanced k-mean algorithm - it published in last paper [18], classification technique using ID3 algorithm that discussed in this paper. Next section will discuss the results of execution for second technique classification by DID3 algorithm.

4. Results

First step in classification results that get classification for all sectors related to every cluster which clustered in last step using enhanced K-M. Second step classification for uncertain situations may be appearing in IDMS for decision making.

4.1 Classification sectors and fields

Table 5.4 presents the set of data used in the implementation experiments for training data to set a best result and choosing an effective number of clusters and percentage of data set to apply the technique for the system the results of the simulation are shown in Table 5.4 for classify fields based on sectors.

Table 3: Simulation result of ID3 algorithm

Total Number of Instances	Correctly Classified Instances % (value)	Incorrectly Classified Instances % (value)	Time Taken (seconds)	Kappa Statistic
32	89.7143 % (157)	10.2857 % (18)	3.19	0.7858

In WEKA, all data is considered as instances and features in the data are known as attributes. The simulation results are partitioned into several sub items for easier analysis and evaluation. On the first part, correctly and incorrectly classified instances will be partitioned in numeric and percentage value and subsequently Kappa statistic, mean absolute error and root mean squared error will be in numeric value only. Also show the relative absolute error and root relative squared error in percentage for references and evaluation. The results of the simulation are shown in Table 5.5.

Table 4: Simulation errors

Mean Absolute Error	Root Mean Squared Error	Relative Absolute Error (%)	Root Relative Squared Error (%)
0.1062	0.3217	22.2878	65.1135

These graphs present classifications results of classified sectors that are used in investment department to find a good usage for cash in bank based on given data using ID3 algorithm through WEKA tools. The results have shows as next figures.

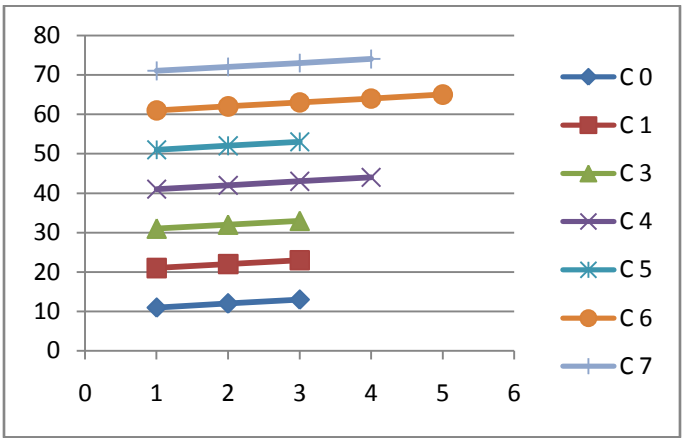

Fig 7: Distribution segments of sectors in testing set of data for a 7 classifications

Figure 7 describes the results of testing data. The results show that classification 1 of the data exist in cluster 0 refer to agriculture field and contain followed sectors, classification 2 of the data exist in cluster 1 refer to industry field and contain followed sectors, classification 3 of the data exist in cluster 2 refer to securities field and contain followed sectors, classification 4 of the data exist in cluster 3 refer to trading field and contain followed sectors, classification 5 of the data exist in cluster 4 refer to tourism field and contain followed sectors, classification 6 of the data exist in cluster 5 refer to petrochemicals field and contain followed sectors and classification 7 of the data exist in cluster 6 refer to technologies field and contain followed sectors.

Fig 8: Classification trees in testing set of data for a 7 classifications of fields

Figure 8 describes the results of testing data. These graph present clustering of sectors are used in investment sector to cluster sectors based on risk level.

4.2 Classification Uncertain Situations

Table 4 presents the set of data used in the implementation experiments for training data to set a best result and choosing an effective number of clusters and percentage of data set to apply the technique for the system the results of the simulation are.

Table 5: Simulation result of ID3 algorithm

Total Number of Instances	Correctly Classified Instances % (value)	Incorrectly Classified Instances % (value)	Time Taken (seconds)	Kappa Statistic
28	89.7121 % (157)	10.2871 % (18)	60.19	0.7858

Table 6: Simulation errors

Mean Absolute Error	Root Mean Squared Error	Relative Absolute Error	Root Relative Squared Error
0.1062	0.211	10.809 %	89.191 %

Figure 9 present classifications results of classified sectors that are used in investment department to find a good usage for cash in bank based on given data using DID3 algorithm through WEKA tools. The results have shows as next figures.

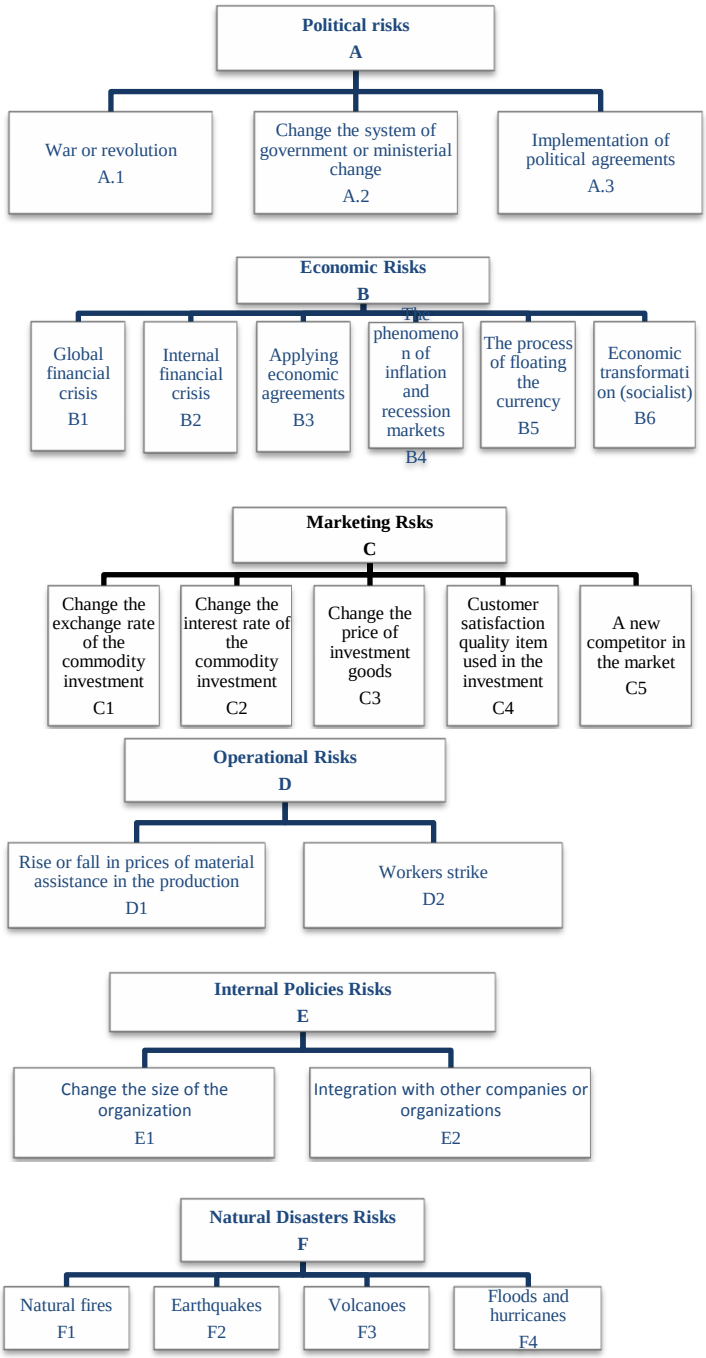

Fig 9: Classification trees in testing set of data for a 6 classifications of uncertain situations

Figure 9 describes the results of testing data. These graph present classification of fields based on sectors to use in IDMS.

III. CONCLUSIONS

This paper represents applying DM using classification technique using enhanced ID3 algorithm to "DID3" algorithm for DSS in banking sector especially in investment department which has been rarely addressed before. IDMS is a new proposed system which is simple, straightforward with low computation needs. The proposed preprocessing component is an aggregation of several known steps. The post processing component is an optional one that eases the interpretation of the investment results. The banking is planning a set of actions in accordance of IDMS outcomes for decision making in investment sector. The investment department in the banking is starting to analyze the approached investment sector, to introduce a good decision under uncertain situation.

IV. FUTURE WORK

In next step of this study implementing this proposed approach using association technique using apriori algorithm to give us a best result and support high level of management with a good decision and high accurate results.

ACKNOWLEDGMENT

I want to express my deepest gratitude for my professor's supervisors Prof. Dr. Turky Sultan and Dr. Ayman Khedr for their major help and support through all the phases of research and development.

REFERENCE

[1] A. Hunter and S. Parsons, "A review of uncertainty handling formalisms", Applications of Uncertainty Formalisms, LNAI 1455, pp.8-37. Springer -Verlag, 1998.
[2] E. Hernandez and J. Recasens, "A general framework for induction of decision trees under uncertainty", Modelling with Words, LNAI 2873, pp.26–43, Springer-Verlag, 2003.
[3] M. S. Chen, J. Han, and P. S. Yu. IEEE Trans Knowledge and Data Engineering Data mining. An overview from a database perspective, 8:866-883, 1996.
[4] U. Fayyad, G. Piatetsky-Shapiro and W. J. Frawley. AAAI/MIT, Press definition of KDD at KDD96. Knowledge Discovery in Databases, 1991.
[5] Gartner. Evolution of data mining, Gartner Group Advanced Technologies and Applications Research Note, 2/1/95.
[6] International Conferences on Knowledge Discovery in Databases and Data Mining (KDD'95-98), 1995-1998.
[7] R.J. Miller and Y. Yang. Association rules over interval data. SIGMOD'97, 452-461, Tucson, Arizona, 1997.
[8] Zaki, M.J., SPADE An Efficient Algorithm for Mining Frequent Sequences Machine Learning, 42(1) 31-60, 2001.
[9] Osmar R. Zaïane. "Principles of Knowledge Discovery in Databases - Chapter 8 Data Clustering". & Shantanu Godbole data mining Data mining Workshop 9th November 2003.
[10] T.Imielinski and H. Mannila. Communications of ACM. A database perspective on knowledge discovery, 39:58-64, 1996.
[11] BIRCH Zhang, T., Ramakrishnan, R., and Livny, M. SIGMOD '96. BIRCH an efficient data clustering method for very large databases. 1996.
[12] Pascal Poncelet, Florent Masseglia and Maguelonne Teisseire (Editors). Information Science Reference. Data Mining Patterns New Methods and Applications, ISBN 978 1599041629, October 2007.
[13] Thearling K, Exchange Applications White Paper, Inc. increasing customer value by integrating data mining and campaign management software, 1998.
[14] Noah Gans, Spring. Service Operations Management, Vol. 5, No. 2, 2003.
[15] Joun Mack. IEEE TRANSACTIONS ON PATTERN ANALYSIS AND MACHINE INTELLIGENCE. An Efficient k-Means Clustering Algorithm, Analysis and Implementation, VOL. 24, NO. 7, JULY 2002.
[16] Andrew Moore and Brian T. Luke. Tutorial Slides, K-means and Hierarchical Clustering and K-Means Clustering, Slide 15, 2003.
[17] E. Turban, J. E. Aronson, T. Liang, and R. Sharda, Decision Support and Business Intelligence Systems, eighth edition. Prentice Hall, 2007.
[18] Ahmed El Seddawy, Ayman Khedr, Turky Sultan, "Enhanced K-mean Algorithm to Improve Decision Support System under Uncertain Situation", International Journal of Modern Engineering Research (IJMER) Vol.2, No.3, Aug 2012.

Ahmed B. El Seddawy, M.S. degrees in Information System from Arab Academy for Science and Technology in 2009. He now with AASTMT Egypt Teacher Assisting BIS Department.

International Journal of Modern Engineering Research (IJMER)
www.ijmer.com Vol. 3, Issue. 4, Jul - Aug. 2013 pp-2147-2153 ISSN: 2249-6645

Power Quality Enhancement in an Isolated Power System Using Series Compensation

[1]Harinath Saggu, [2]Ch. Nagalaxmi, [3]V. K. R. Mohan Rao
[1]PG Scholar, [2]Assistant Professor, [3]Associate Professor, [1, 2, 3] Holy Mary Institute of Technology & Science

ABSTRACT: *In Isolated power systems the power quality problem is compounded as the drive converter loads are likely to fluctuate in conjunction with mining or exploration areas. The use of compensators in improving power quality of isolated power systems is considered. The roles of the compensators are to mitigate the effects of momentary voltage sags/swells, and to control the level of harmonic distortions in the networks. A control strategy for both series compensator and shunt compensator is developed to regulate power flow. However series compensator reduces harmonics to an acceptable level when compared to shunt compensator. This is achieved through phase adjustment of load terminal voltage. It leads through an increase in ride through capability of loads to the voltage sags/swells. Validity of the technique is illustrated through simulation. Hence series compensator with LC Filter is used in reducing the harmonic distortions in isolated power systems.*

KEYWORDS: *isolated power systems, series compensator, harmonics compensation, energy storage system.*

I. INTRODUCTION

The typical definition for a harmonic is a sinusoidal component of a periodic wave or quantity having a frequency that is an integral multiple of the fundamental frequency. Some references [1-2] refer to clean or pure power as those without any harmonics. Harmonics have been around for a long time and will continue to do so [3-5] with effects like:

- Overheated transformers, especially delta windings where triplen harmonics generated on the load side of a delta-wye transformer will circulate in the primary side.
- Nuisance operation of protective devices, including false tripping of relays and failure of a UPS to transfer properly, especially if controls incorporate zero-crossing sensing circuits.
- Bearing failure from shaft currents through uninsulated bearings of electric motors.
- Blown-fuses on PF correction caps, due to high voltage and currents from resonance with line impedance.
- Mis-operation or failure of electronic equipment
- If there are voltage subharmonics in the range of 1-30Hz, the effect on lighting is called flicker. This is especially true at 8.8Hz, where the human eye is most sensitive, and just 0.5% variation in the voltage is noticeable with some types of lighting.

The sensitive loads would be connected in parallel with the nonlinear drive. Often such sensitive loads also contain input rectifiers that are capacitive in nature. The combined sensitive loads may be represented by the parallel RC circuit shown in Fig. 1. While the total capacity of the sensitive loads could be much smaller than that of the main drives, the distorted supply voltage is harmful to the sensitive loads. Excessive voltage distortions could cause the sensitive loads to mal-operate. The loads are also sensitive to short-duration disturbances in the form of voltage sags or swells. The disturbances can be due to faults or most likely, the fluctuating load cycles of the main drives. In the latter case, voltage flickers can occur and they can be of major concern. Thus one important consideration in the design and operation of the power system would be to ensure that the quality of supply to the sensitive loads comply with that prescribed under industry standards, such as the ITI curve [3].A traditional method to achieve improved PQis to use passive filters connected at the sensitive load terminals [4]. However, this practice has some shortcomings: the effectiveness of the scheme could deteriorate as the source impedance or load condition changes; it can lead to resonance between the filter and the source impedance. For these reasons, active filters such as that described in [5] may be used. Essentially an active filter, connected at the sensitive load terminal, injects harmonic currents of the same magnitude but of opposite polarity to cancel the harmonics present there. However, as noted earlier, harmonic distortions are only part of the problem faced in such a network: the variations in the drive load would result in voltage sag/swell or flickers appearing in the upstream voltage. Thus, the challenge is to regulate the sensitive load terminal voltage so that its magnitude remains constant and any harmonic distortion is reduced to an acceptable level. In a recent study, [6] proposes a series compensation method to mitigate the harmonics problem for the power system shown in Fig. 1. However, compensation for voltage sag/swell or flicker has not been considered. Series voltage compensation methods have been discussed in [7], [8] for the mitigation of short-duration voltages/swells but the presence of harmonic voltages/current in the networks has been ignored. This paper intends to fill this gap. Specifically, the investigation is to develop a method to control the fundamental component of . The control is achieved by regulating power flow via phase angle adjustment. Unlike the previous methods of [6]–[8], the investigation also shows that the voltage-sag ride through capability of the sensitive load can be improved through importing harmonic power from the external system into the SC.

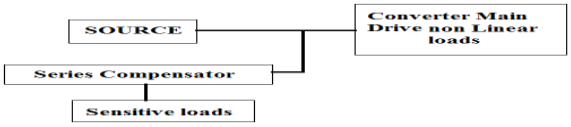

Fig.1 Typical isolated power system installed with a Series compensators.

II. HARMONIC MITIGATION AND POWER FLOW IN ISOLATED POWER SYSTEM

The simple isolated power system model shown in Fig. 2 is used to explain the principle of the proposed harmonics compensation method of the SC. The upstream generators are represented as an ideal voltage source and *ZS* represents the equivalent source impedance. The main drives or machinery loads are modeled as a lumped resistance-inductance load connected to the source through a power converter which is assumed to be an uncontrolled six-pulse rectifier in this study. The much smaller-capacity sensitive loads are assumed supplied through a separate feeder. Often, such critical or sensitive loads such as PC and control devices contain input rectifiers that are capacitive in nature. Although these loads could also be non-linear, however, their combined capacity is small compared to the main rectifier loads. Hence, the sensitive loads are assumed to be linear as their contributions towards the distortions in V_L is negligible. In the investigation, the load is modeled by a resistance *R* in parallel with a capacitor *C*. The value of *R* will be obtained based on the real power drawn by the sensitive load at the voltage $V_{L'}$. *C* can be obtained from the data supplied by the rectifier manufacture.

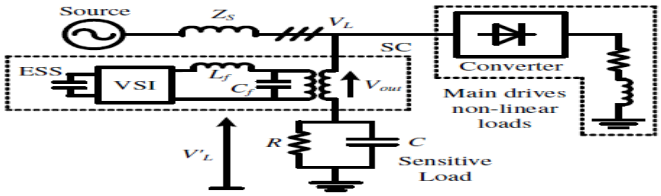

Fig.2 A typical isolated power system with SC

The series compensator (SC) is connected upstream of the sensitive load through an injection transformer. It is series connected with the sensitive load and its function is to ensure that the voltage across the load terminals is of high quality. The central part of the SC is the VSI and an energy storage system (ESS). PWM switching scheme is often used in the VSI. Due to the switching, harmonics are generated and filtering is required. L_f and C_f are the filter inductance and capacitance. While the detailed function of the SC under a voltage-sag can be found in [8], it is suffice to state that the VSI synthesizes the required voltage quantity (*Vout*) which would be injected in series with $V_{L'}$. The ESS would act as a buffer and provides the energy needed for load ride through during a voltage-sag. Conversely, during a voltage-swell, excess energy from the network would be stored in the SC so that $V_{L'}$ can be controlled.

Under steady-state conditions, harmonic currents generated by the main nonlinear converter-drive load will cause a voltage drop across *Zs*. Thus it results in distortions in the line voltage V_L: V_L consists of the fundamental and harmonic voltage components.

A. Principle of harmonics compensation

The underlying principle when the SC is used to compensate for upstream voltage sag/swell has been discussed in [8,9]. In Fig. 2, distorted voltage V_L will appear on the upstream source-side of the sensitive load and the phase voltages can be expressed as

$$V_{La}(t) = \sum_{n=1}^{\infty}[V_{0n} + V_{1n}\sin(n\omega t + \varphi_{1n}) + V_{2n}\sin(n\omega t + \varphi_{2n})] \quad (1)$$

$$V_{Lb}(t) = \sum_{n=1}^{\infty}[V_{0n} + V_{1n}\sin(n\omega t + \varphi_{1n} - 2n\pi/3) + V_{2n}\sin(n\omega t + \varphi_{2n} + 2n\pi/3)] \quad (2)$$

$$V_{Lc}(t) = \sum_{n=1}^{\infty}[V_{0n} + V_{1n}\sin(n\omega t + \varphi_{1n} + 2n\pi/3) + V_{2n}\sin(n\omega t + \varphi_{2n} - 2n\pi/3)] \quad (3)$$

where *n* is the harmonic order; V_{0n} is the zero phase sequence voltage component; V_{1n} and φ_{1n} are the magnitude and phase of the positive phase sequence voltage components; V_{2n} and φ_{2n} are the magnitude and phase of the negative phase sequence voltage components. Clearly, the distorted voltage is undesirable at the sensitive load terminals. The desirable terminal voltage for the sensitive load is the fundamental components of the voltages contained in (1)-(3), i.e.

$$V_{la}(t) = V_{11}\sin(\omega t + \varphi_{11}) \quad (4)$$

$$V_{lb}(t) = V_{11}\sin(\omega t - 2\pi/3 + \varphi_{11}) \quad (5)$$

$$V_{lc}(t) = V_{11}\sin(\omega t + 2\pi/3 + \varphi_{11}) \quad (6)$$

The proposed voltage injection method is to compensate for the difference between V_L and the desired voltage described by (4)-(6). This is achieved by injecting an ac voltage component in series with the incoming three-phase network. Hence from (1)-(6), the desired injection voltages are

$$V_{inja}(t) = V_{la}(t) - V_{La}(t) = \sum_{n=1}^{\infty} V_{0n} - \sum_{n=2}^{\infty} V_{1n}\sin(n\omega t + \varphi_{1n})$$

$$-\sum_{n=1}^{\infty} V_{2n}\sin(n\omega t + \varphi_{2n}) \qquad (7)$$

$$V_{injb}(t) = V_{lb}(t) - V_{Lb}(t) = \sum_{n=1}^{\infty} V_{0n} - \sum_{n=2}^{\infty} V_{1n}\sin(\omega t + \varphi_{1n} + 2\pi/3)$$

$$-\sum_{n=1}^{\infty} V_{2n}\sin(n\omega t + \varphi_{2n} + 2n\pi/3) \qquad (8)$$

$$V_{injc}(t) = V_{lc}(t) - V_{Lc}(t) = \sum_{n=1}^{\infty} V_{0n} - \sum_{n=2}^{\infty} V_{1n}\sin(\omega t + \varphi_{1n} - 2\pi/3)$$

$$-\sum_{n=1}^{\infty} V_{2n}\sin(n\omega t + \varphi_{2n} - 2n\pi/3) \qquad (9)$$

The above equations can be written in a compact form. From (4)-(6), define $\vec{V}_{Lf} = [\, V_{la}(t), V_{lb}(t), V_{lc}(t)]^T$ and from (1)-(3), denote $\vec{V}_L = [\, V_{La}(t), V_{Lb}(t), V_{Lc}(t)]^T$. Let V_{Lh} be the vector containing all the harmonic components in (1)-(3). Hence, from (7)-(9), the injection voltage of the SC would be

$$\vec{V}^* = \vec{V}_{Lf} - \vec{V}_L = -\vec{V}_{Lh} \qquad (10)$$

$\vec{V}_L$ can be measured online and its fundamental voltage $\vec{V}_{Lf}$ can be obtained using, for example, a Phase Locked Loop (PLL) scheme. Hence the injection voltage $\vec{V}^*$ can be generated online and used to mitigate the harmonic distortions in the manner described below.

B. Possible Mitigation Method

Fig. 3 shows a typical scheme whereby the SC, through the injection of the voltage V_{out}, compensates for the harmonic voltage. In this study, the resistance and leakage inductance of injection transformer is assumed negligible. The transformer turns-ratio is 1:n. Only the network branch pertaining to the sensitive load is included. The distorted source-side voltage V_L is represented as a harmonic voltage source. Z_{Load} denotes the parallel RC load shown in Fig. 2 and the load terminal voltage is V'_L. The corresponding line current is *ILoad*.

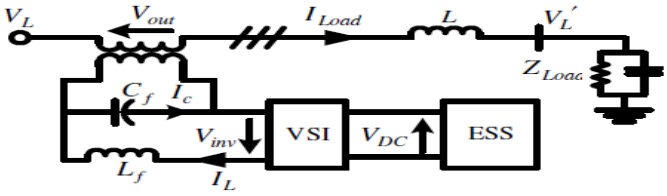

Fig. 3. Schematic diagram showing the interconnection of the SC with the sensitive load

The block diagram of the control scheme for a conventional SC designed for load ride-through enhancement function during a voltage-sag is given in Fig. 4. As an initial attempt, the same scheme may be considered for adoption herewith for the purpose of mitigating harmonic distortions. In this scheme, the injection voltage *Vout* is regulated to follow the reference voltage *V** which is described by (10). Thus it requires V_{out} to be compared with *V**. The error is multiplied by the voltage error feedback gain K_{2Cf} and fed to the second stage as the reference for the inductor current. This virtual inductor current reference is compared with the actual inductor current and the error is multiplied with the current error gain K_{1Lf} to form the inner feedback loop. The resulting quantity of this loop is subsequently fed to the PWM generator of the inverter.

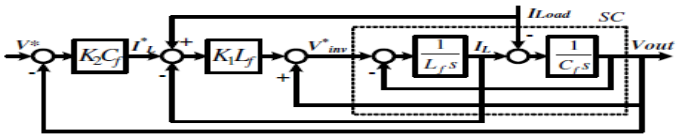

Fig. 4 Closed-loop control scheme for the SC

The load current I_{Load} is considered a disturbance caused by sensitive load changes. The effect of I_{Load} on the harmonic distortions is not the main concern in the design of this controller. Rather, the focus is on the control of V_{out} to track *V**, due to the distortions caused by the upstream main loads. For this purpose, the Closed-loop transfer function between V_{out} and *V** can be shown as:

$$G_{cl}(s) = \left.\frac{V_{out}}{V^*}\right]_{I_{Load}=0} = \frac{K_1K_2}{s^2 + K_1 s + K_1K_2} \qquad (11)$$

From Fig. 4, therefore V_{out} can be expressed as

$$V_{out}(s) = G_{cl}(s)V^*(s) + Z(s)I_{Load}(s) \qquad (12)$$

Where

$$Z(s) = -\frac{s}{s^2 + K_1 s + K_1 K_2} \cdot \frac{1}{C_f}$$

Z(s) is the equivalent impedance of the SC, while $G_{cl}(s)$ is as given by (11). $G_{cl}(s)$ is a second-order system; therefore, the damping ratio and the un-damped natural frequency of the SC control system are given as

$$\xi = 0.5\sqrt{K_1/K_2} \qquad (13)$$

$$\omega_n = \sqrt{K_1 K_2} \qquad (14)$$

In order to obtain a critically damped response, ξ=1 and this can be achieved when

$$K_2 = K_1/4 \qquad (15)$$

Substituting (15) into (11), G_{cl}(s) can be rewritten as

$$G_{cl}(s) = 1\Big/(1+\frac{s}{K_1/2})^2 \qquad (16)$$

For most systems, there is an upper limit on the proportional feedback gain in order to achieve a welldamped stable response. Thus, K_1 and K_2 should be selected with this consideration in mind.

III. CONTROL OF VOLTAGE IN THE ENERGY STORAGE SYSTEM

For the convenience of analysis and to avoid complicated mathematical expressions, a single-phase equivalent system is used to describe the three-phase system shown in Fig. 3. If the function of the SC is solely for the purpose of harmonics compensation, the instantaneous power at the SC output will be of the form

$$p(t)=V_{Lh}(t)I_{Load}(t)=\sum_{k=2}^{\infty}V_k\sin(k\omega t+\varphi_k)\sum_{k=1}^{\infty}I_k\sin(k\omega t+\theta_k) \qquad (17)$$

The average power is

$$P = \frac{1}{2}\sum_{k=2}^{\infty}V_k I_k\cos\phi_k \qquad (18)$$

Where $\phi_k = \varphi_k - \theta_k$.Note that only power components associated with the harmonics are contained in *P*. *P* is either imported into or exported from the SC to the external system. The losses in the VSI would be low and can be ignored. Hence the energy exchange between the SC and the external power system is

$$E = \frac{T}{2}\sum_{k=2}^{\infty}V_k I_k\cos\phi_k \qquad (19)$$

Over the time interval *T*. The SC supplies energy to the external system when $E \le 0$. As the only significant source of energy storage in the SC is the ESS, the export of the energy to the external system will result in a decrease in the voltage *VDC*. Conversely *VDC* will rise when $E \ge 0$.. Variation of V_{DC} will affect the compensation capability of the SC and excessive voltage rise will damage the ESS. Hence V_{DC} has to be controlled within certain range. In order to achieve this, there must be control on the energy flow. This can be achieved by adjusting the phase of the fundamental component of the reference voltage of the SC. If a phase shift is introduced to the reference voltage for, say phase "a" of (4), one obtains

$$v_L'(t)=V_1\sin(\omega t+\varphi_1+\alpha) \qquad (20)$$

Since only the fundamental voltage component is involved in the phase shift, the second subscript "1" in (4) has been omitted in (20). Furthermore, notice that the intention is not to change the magnitude of the fundamental component of the load-side voltage V'_L. Hence V'_L has the same magnitude as without the phase shift. With an assumed constant impedance load model, I_1 will also remain constant following the phase shift.
It then follows that the new injection voltage is

$$v_{inj}(t)=V_1\sin(\omega t+\varphi_1+\alpha)-V_1\sin(\omega t+\varphi_1)-V_{Lh} \qquad (21)$$

Refer to (18) and (19), the energy flow between the ESS and the external power system now becomes

$$E = \frac{T}{2}(V_1 I_1\cos(\phi_1+\alpha)-\sum_{k=2}^{\infty}V_k I_k\cos\phi_k) \qquad (22)$$

From (22), it can be seen that *E* could be forced to be zero if α is selected to be α_0 where

$$\alpha_0 = \arccos\Big(\frac{1}{V_1 I_1}\sum_{k=2}^{\infty}V_k I_k\cos\phi_k\Big)-\phi_1 \qquad (23)$$

So by the appropriate selection of the phase shift α in the fundamental component of V_{inj}, *E* and therefore V_{DC} can be controlled. In the proposed method, V_{DC} is monitored: if the voltage starts to decrease, it shows that there is a net energy flow from the SC to the external system. The SC should start to absorb energy from the external system to increase V_{DC}.

Conversely if V_{DC} rises, The SC should inject energy to the external system. The injection or absorption of energy is through the adjustments in α. Based on the above principle; the control strategy of α for different load conditions can be obtained. With the assumption of constant load power factor, the phasor diagram is shown in Fig. 5. $\vec{V}_{Lf}$ is the fundamental source-side voltage. $\vec{V}_{Lf}'$ is the load-side voltage after the phase shift. $\vec{V}^*$ is the injection voltage (also the reference voltage) and $\vec{I}_{Load}$ is the sensitive load current. θ is the load power factor angle. βis the phase difference between $\vec{V}^*$ and $\vec{I}_{Load}$. As only the phase shift is introduced, the loci of $\vec{V}_{Lf}$ and $\vec{V}_{Lf}'$ will lie on a circle with radius *V1*.

From Fig. 5, it can be seen that

$$\beta = 90^o + \theta - \alpha/2 \qquad (23)$$

Therefore, the active power flow between the SC and the external system is

$$P = \left|\vec{V}^*\right|\left|\vec{I}_{Load}\right|\cos\beta \qquad (24)$$

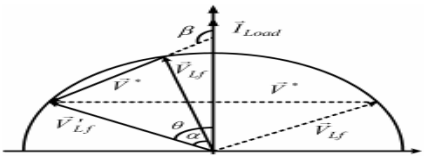

Fig.5 Phasor diagram showing voltage injection for a lagging power factor load.

Clearly when β > *90°*, *P < 0*, the SC absorbs energy from the external system. From (29), therefore, α should be adjusted such that $0° < \alpha < 2\theta$. Energy will be imported into the SC and V_{DC} will increase. When $\alpha = 2\theta$, V^* is then perpendicular to *ILoad*. It means that *P* is zero. This condition is shown by the dotted lines in Fig. 5. Conversely, for the SC to export energy to the external system, α should be within the range $2\theta - 360° < \alpha < 0°$. A decrease in V_{DC} will be observed.

The above analysis can be summarized in Table I, which shows how regulating V_{DC} for lagging and leading load power factor conditions can be achieved through the adjustments in phase shift α.

TABLE I

Load power factor	*0 < α < 2θ*	*2θ-360₀ < α <0*
Lagging: 0 ≤ θ ≤ π/2	V_{DC} increase	V_{DC} decrease
Leading:- π/2 ≤ θ ≤ 0	V_{DC} decrease	V_{DC} increase

From the above analysis, it is clear that in order to limit the variations in V_{DC}, a phase shift between the source-side fundamental voltage . $\vec{V}_{Lf}$ and the compensated load-side voltage $\vec{V}_{Lf}'$ is called for. The method of progressive phase shift similar to that described in [6] can be adopted. V_{DC} is continuously monitored and as soon as it is outside a set range, adjust α in the manner based on Table I until the voltage is within the set range.

IV. ILLUSTRATIVE EXAMPLE

The example of Fig. 2 is used to verify the effectiveness of the SC and its control strategy. The corresponding parametric values used are given in Table II and the simulations were accomplished using MATLAB. The capacity of the isolated system is assumed to be 1.5MVA, a typical level seen in practice. The source is assumed to have a reactance value of 1 p.u. The main load is assumed to be a six-pulse rectifier and is nominally at 1 MVA and that of the sensitive load is at 0.05MVA. The injection transformer is assumed to have a turns-ratio of 1:1. This is a reasonable assumption as the focus of the study is to demonstrate the principle of operation of the SC and not on the detailed design of the compensator. As the switching frequency of the VSI was chosen to be 20 kHz, the controller was based on the setting of ξ =1 and $\omega_n = 2\pi \cdot 500$ rad/sec. Thus *K1* $=2\pi \cdot 1000$ and *K2* $=2\pi \cdot 250$ were determined.

TABLE II SYSTEM PARAMETERS

Parameters	Values used in the simulation model
Source capacity	1.5MVA
Source reactance	1 p.u.
Sensitive load capacity	0.05 MVA
Injection transformer turn ratio	1:1

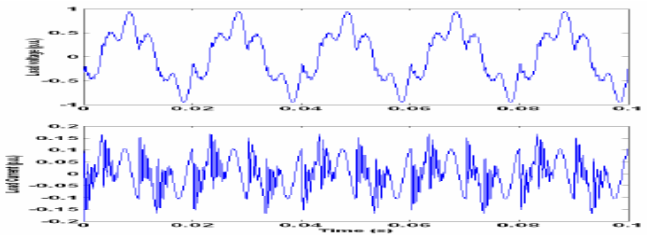

Fig. 6 Terminal voltage and current drawn by the sensitive load: without SC

Fig. 6 shows the waveforms of V_l and $_{ILoad}$ without the SC. It can be shown that V_l has a THD level of 37%. I_{Load} has a large harmonic content; its THD is 180%.

Fig. 7 shows the corresponding waveforms when the SC is in service. With harmonics compensation by the SC, the sensitive load is protected against the distortion introduced by the main drive load and the THD of the current has been significantly reduced to 6%.

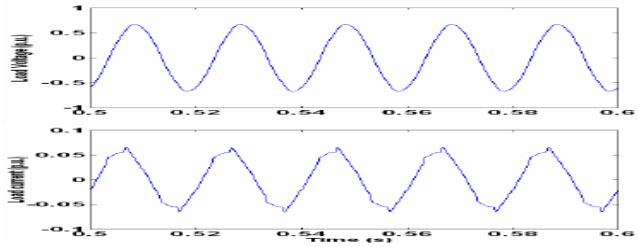

Fig. 7 Terminal voltage and current drawn by the sensitive load: with SC

Fig. 8 shows the voltage across the ESS but without phase shifting of the fundamental component of the reference voltage. It is shown that the voltage across the ESS decreases during injection, which means that the SC injects power to the external system. This is obviously un-sustainable for the continuous operations of the SC.

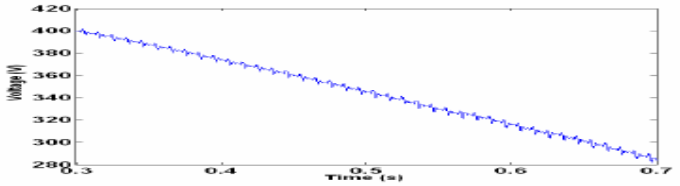

Fig. 8 Terminal voltage of ESS without phase shift in the reference voltage

Fig. 9shows the voltage of the ESS but with the proposed phase shifting of the fundamental component of the reference voltage. It shows that the voltage can be restored to its nominal level. Therefore the strategy can be applied for continuous operation of the power system. Indeed, in this study, a change in the main drive load from 1MVA to 1.1MVA has been introduced at t = 0.7 s. This is in order to assess how the SC would response to the load change. It seems that the technique is again effective in maintaining the voltage of the ESS. Fig. 15 shows the corresponding sensitive load terminal voltage and current, with the phase shift. THD are 1% and 9% for the voltage and current respectively.

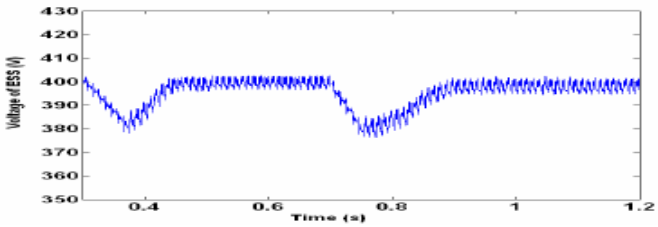

Fig.9 Terminal voltage of ESS with phase shift in the reference Voltage

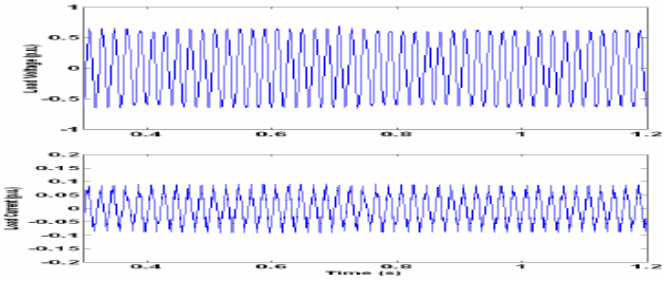

Fig. 10 Sensitive load terminal voltage and current

V. CONCLUSIONS

Power quality improvement in an isolated power system through series compensation has been investigated. A method to control the SC so that it can compensate for the harmonics under steady-state condition has been proposed. The proposed method is based on the control of the SC branch impedance. A feedback scheme is introduced through the control system of the SC. This is coupled with an inductive filter intended for mitigating high-order harmonic currents. In the process of harmonic voltage compensation, power exchange exists between the SC and the external network. It would result in the variation of the terminal voltage of the energy storage system of the SC. A method to maintain the voltage of the ESS through the phase shifting of the fundamental component of the reference voltage has been described. The effectiveness of the proposed method has been verified through simulation.

REFERENCE

[1]. Jonasson and L. Soder, ―Power quality on ships-a questionnaire evaluation concerning island power system,‖ in *Proc. IEEE Power Eng.Soc. Summer Meeting*, Jul. 2001, vol. 15–19, pp. 216–221.
[2]. J. J. Graham, C. L. Halsall, and I. S. McKay, ―Isolated power systems: Problems of waveform distortion due to thyristor converter loading,‖ in Proc. 4th Int. Conf. Power Electronics and Variable-Speed Drives, Jul.1990, vol. 17–19, pp. 327–330.
[3]. *ITI (CBEMA) Curve Application Note*, [Online]. Available: http://www.itic.org, Inf. Technol. Ind. Council (ITI).
[4]. J. C. Das, ―Passive filter—Potentialities and limitations,‖ *IEEE Trans. Ind. Appl.*, vol. 40, no. 1, pp. 232–241, Jan. 2004.
[5]. H. Akagi, ―New trends in active filter for power conditioning,‖ *IEEETrans. Ind. Appl.*, vol. 32, no. 6, pp. 1312–1322, Nov. 1996.
[6]. S. S. Choi, T. X. Wang, and E. K. Sng, ―Power quality enhancement in an isolated power system through series compensator,‖ presented at the 15th Power System Computation Conf., Liege, Belgium, Aug. 2005.
[7]. N. H. Woodley, L. Morgan, and A. undaram, ―Experience with an inverter-based dynamic voltage restorer,‖ *IEEE Trans. Power Del.*, vol. 14, no. 3, pp. 1181–1186, Jul. 1999.
[8]. S. S. Choi, B. H. Li, and D. M. ilathgamuwa, ―Dynamic voltage restoration with minimum energy injection,‖ *IEEE Trans. Power Syst.*, vol. 15, no. 1, pp. 51–57, Feb. 2000.
[9]. E. K. K. Sng, S. S. Choi, and D. M. Vilathgamuwa, "Analysis of series compensation and DC link voltage controls of a transformerless self-charging dynamic voltage restorer," *IEEE Trans. Power Delivery*, vol. 19, no. 3, pp. 1511 – 1518, July. 2004.

International Journal of Modern Engineering Research (IJMER)
www.ijmer.com Vol. 3, Issue. 4, Jul - Aug. 2013 pp-2154-2156 ISSN: 2249-6645

Parametric Analysis and Optimization of Turning Operation by Using Taguchi Approach

Mr. Manoj Kumar Sahoo
Department of Mechanical Engineering, Lakhmi Chand Institute of Technology, Bilaspur

ABSTRACT: *Every day scientists are developing new materials and for each new material, we need economical and efficient machining. Turning process is the one of the methods to remove material from cylindrical and non-cylindrical parts. Stainless steel is a widely used material in day to day applications. This paper deals with the optimization of turning process by the effects of machining parameters applying Taguchi methods so as to improve the quality of manufactured goods, and engineering development of designs for studying variation. There are three machining parameters i.e., Spindle speed, Feed rate and Depth of cut. Experiments are done by varying one parameter and keeping other two fixed so maximum value of each parameter was obtained. Taguchi orthogonal array is designed with three levels of turning parameters with the help of software Minitab 16. In the first run nine experiments are performed and material removal rate (MRR) is calculated. When experiments are repeated in second run again MRR is calculated. Taguchi method stresses the importance of studying the response variation using the signal–to–noise (S/N) ratio, resulting in minimization of quality characteristic variation due to uncontrollable parameter. The metal removal rate was considered as the quality characteristic with the concept of "the larger-the-better. S/N ratio values are calculated by taking the help of software Minitab 16. The MRR values measured from the experiments and their optimum value for maximum material removal rate. It is also predicted that Taguchi method is a good method for optimization of various machining parameters as it reduces the number of experiments.*

KEYWORDS: *Turning, Material Removal Rate, AISI 304 Steel, Taguchi, Minitab16*

I. INTRODUCTION

Experimental work includes the turning operation which is performed on the HMT NH26 lathe machine. The input parameters are taken as spindle speed, feed and depth of cut whereas the output parameter is taken as material removal rate. The values taken for spindle speed (in rpm) are 220, 350 and 540, the values for feed (in mm/rev) are 0.388, 0.418 and 0.462, and for depth of cut (in mm) the values are taken as 0.9, 1.0 and 1.1. The experiments are performed by HSS tool on AISI 304 steel bar work piece of 40 mm diameter and 60 mm length.

Table 1.1: Composition of AISI 304 Steel

Element	C	Mn	Si	Cr	Ni	P	S
Weight %	0.08	2	1	18-20	8-10	0.045	0.03

I.1.1 MATERIAL REMOVAL RATE: Material Removal Rate (MRR) Measurement From the initial and final weight of job, MRR is calculated and the relation is given below:

$$MRR = \frac{InitialWeight - FinalWeight}{TimeTaken}$$

II. LITERATURE REVIEW

Liu et al. (2006), has made use of the basic thermo mechanical properties and the molecular mechanical theory of friction. The main aim is to extend the knowledge of minimum chip thickness values to as many materials as possible when these materials are put to wide range of cutting conditions. [1]

H S Yoon et al., has proposed an orthogonal cutting force model based on slip-line field model for micro machining. Two material flow processes are being considered- chip formation process and ploughing. The paper takes into account the effects of parameters like effective rake angle, depth of deformation and minimum chip thickness. [2]

Z J Zhou et al. (1996), has taken up the case of ultra precision machining to study the effect of diamond tool sharpness on cutting surface integrity and minimum chip thickness. Good surface integrity is an essential requirement of machining processes. Good surface integrity implies smaller surface roughness and smaller residual stresses combined with high dimensional accuracy. However, the accuracy of the relative motion between the cutting edge and the work piece governs the achievable machining accuracy. So, the performance of machine tools needs to be studied. [3]

III. MATERIALS AND METHODS

III.1 TURNING OPERATION

Turning is the removal of metal from the outer diameter of a rotating cylindrical work piece. Turning is used to reduce the diameter of the work piece, usually to a specified dimension, and to produce a smooth finish on the metal. Often the work piece will be turned so that adjacent sections have different diameters. Turning is the machining operation performed on lathe that produces cylindrical parts.

The cutting tool material used in this experiment is high speed steel (HSS). The work piece taken for this experiment is AISI 304 steel bar of 40 mm diameter and 60 mm length. Experiment has been performed on HMT NH26 LATHE. Table 3.1 shows the experimental data:

Table 3.1: Observation of first run of experiment

Spindle Speed (rpm)	Feed (mm/rev)	Depth of Cut (mm)	Time (sec)	Initial wt. (gm)	Final wt. (gm)	Difference (gm)	MRR 1 (gm/sec)
220	0.388	1.1	16	737	714	23	1.44
220	0.418	1	15	757	738	19	1.27
220	0.462	0.9	11.7	762	744	18	1.53
350	0.388	1	9.9	762	740	22	2.20
350	0.418	0.9	9	758	740	18	2.00
350	0.462	1.1	8	784	766	18	2.25
540	0.388	0.9	7	753	746	7	0.99
540	0.418	1.1	7.1	758	742	16	2.25
540	0.462	1	6.5	727	716	11	1.72

Table 3.2: Observation of second run of experiment

Spindle Speed (rpm)	Feed (mm/rev)	Depth of Cut (mm)	Time (sec)	Initial wt. (gm)	Final wt. (gm)	Difference (gm)	MRR 2 (gm/sec)
220	0.388	1.1	15.66	714	692	22	1.40
220	0.418	1	15.41	738	718	20	1.30
220	0.462	0.9	11.71	744	726	18	1.54
350	0.388	1	10.00	740	718	22	2.20
350	0.418	0.9	8.75	740	722	18	2.06
350	0.462	1.1	8.13	766	748	18	2.21
540	0.388	0.9	6.10	746	740	6	0.98
540	0.418	1.1	6.54	742	728	14	2.14
540	0.462	1	6.39	716	704	12	1.88

III.1.1 TAGUCHI METHOD

Taguchi method is a powerful tool for the design of high quality systems. It provides simple, efficient and systematic approach to optimize design for performance, quality and cost. Taguchi method is efficient method for designing process that operates consistently and optimally over a variety of conditions. Taguchi approach to design of experiments easy to adopt and apply for users with limited knowledge of statics, hence gained wide popularity in the engineering and scientific community. The desired cutting parameters determined by handbook. Cutting parameters are reflected on surface roughness, surface texture and dimensional deviation on turned product. Taguchi method is especially suitable for industrial use but can also be used for scientific research.

III.1.1.1 DESIGN OF ORTHOGONAL ARRAY

Taguchi Orthogonal Array is designed in Minitab16 to calculate S/N ratio and Means.

III.1.1.1. ANALYSIS OF THE SIGNAL TO NOISE (S/N) RATIO

In the Taguchi approach, the term signal represents the desired value (mean) for the output characteristics and term noise represents the undesirable value (standard deviation) for the output
characteristics. Therefore, S/N ratio is the ratio of mean to the standard deviation. Taguchi uses the S/N ratio to measure the quality characteristics deriving from desired value. The S/N ratio is defined as given equation.

"the larger the better"

It is when the occurrences of some undesirable product characteristics is to be maximized. It is given by

$$S/N = -10\log_{10}\left[\frac{1}{n}\sum\frac{1}{y2}\right]$$

IV. RESULTS & DISCUSSION

After finding all the observation as given in Table 3.1 and 3.2, S/N ratio and Means are calculated and various graph for analysis is drawn by Minitab 16 software using Taguchi Method.

Table 4.1: Experiment Results and corresponding S/N ratios:

S.No.	Spindle Speed (rpm)	Feed (mm/rev)	Depth of Cut (mm)	MRR 1 (gm/sec)	MRR2 (gm/sec)	S/N Ratio
1	220	0.388	1.1	1.44	1.40	2.80549
2	220	0.418	1	1.27	1.30	3.69201
3	220	0.462	0.9	1.53	1.54	2.44400
4	350	0.388	1	2.20	2.20	5.57042
5	350	0.418	0.9	2.00	2.06	5.90939
6	350	0.462	1.1	2.25	2.21	8.48077
7	540	0.388	0.9	0.99	0.98	1.38411
8	540	0.418	1.1	2.25	2.14	5.54248
9	540	0.462	1	1.72	1.88	4.84202

Since, the greater S/N value corresponds to a better performance; therefore, the optimal level of the machining parameters is the level with the greatest value.

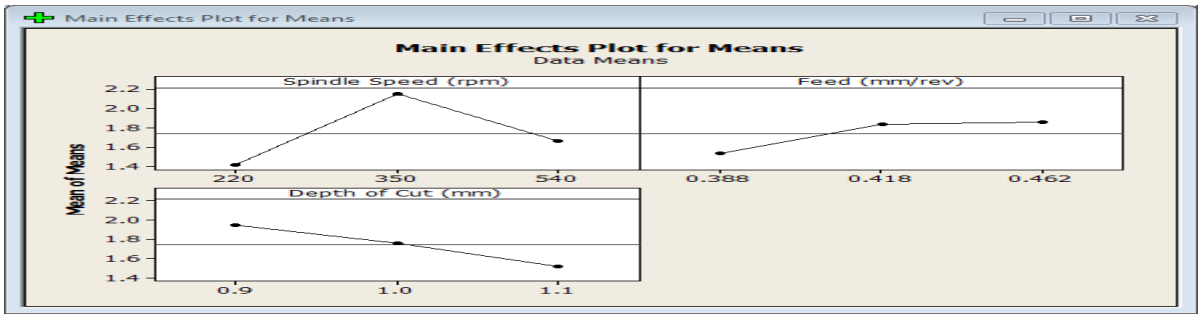

Fig 1. Effect of turning parameters on MRR for Means

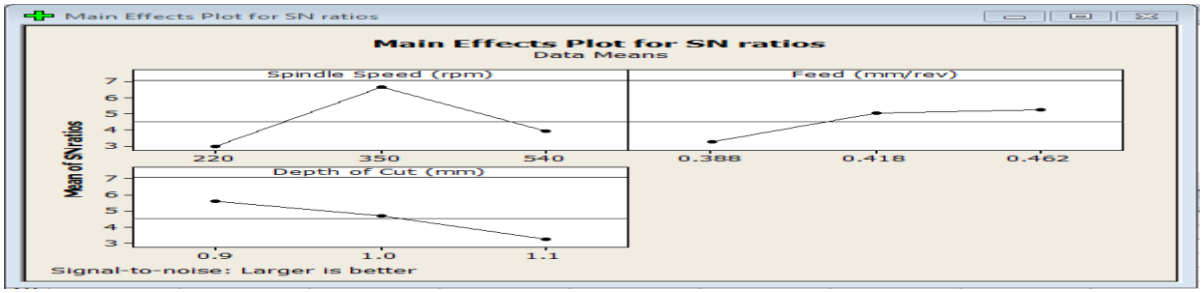

Fig 2. Effect of turning parameters on MRR for S/N ratio

V. CONCLUSIONS

The effect of parameters spindle speed on the metal removal rate values is shown above figure for S/N ratio. Its effect is increasing with increase in spindle speed upto 350 rpm beyond that it is decreasing. So the optimum spindle speed is level 2 i.e. 350 rpm.

The effect of parameters feed rate on the metal removal rate values is shown above figure S/N ratio. Its effect is increasing with increase in feed rate. So the optimum feed rate is level 3 i.e. 0.462 mm/rev.

The effect of parameters depth of cut on the metal removal rate values is shown above figure for S/N ratio. Its effect is decreasing with increase in depth of cut. So the optimum depth of cut is level 3 i.e. 1.1 mm.

REFERENCES

[1]. Liu X., DeVor R.E. and Kapoor S.G., "An Analytical Model for the Prediction of Minimum Chip Thickness in Micromachining", Journal of Manufacturing Science and Engineering, MAY 2006, Vol. 128, pp. 474-481.

[2]. H.S. Yoon, K.F. Ehmann, "A Slip-line field model for orthogonal micro-machining processes", Department of Mechanical Engineering, Northwestern University, IL, U.S.A.

[3]. Z.J. Yuan , M. Zhou, S. Dong, "Effect of diamond tool sharpness on minimum cutting thickness and cutting surface integrity in ultra precision machining", Journal of Materials Processing Technology 62 (1996), pp. 327-330.

[4]. Krishankant, Jatin Taneja, Mohit Bector, Rajesh Kumar, "Application of Taguchi Method for Optimizing Turning Process by the effects of Machining Parameters", International Journal of Engineering and Advanced Technology, ISSN: 2249 – 8958, Volume-2, Issue-1, October 2012, pp. 263-274.

[5]. Ashish Yadav, Ajay Bangar, Rajan Sharma, Deepak Pal, "Optimization of Turning Process Parameters for Their Effect on En 8 Material Work piece Hardness by Using Taguchi Parametric Optimization Method" International Journal of Mechanical and Industrial Engineering (IJMIE), ISSN No. 2231 –6477, Volume-1, Issue-3, 2012, pp. 36-40.

International Journal of Modern Engineering Research (IJMER)
www.ijmer.com Vol. 3, Issue. 4, Jul - Aug. 2013 pp-2157-2160 ISSN: 2249-6645

Parametric Study for Wind Design of Vertical Pressure Vessel as per Indian Standard

Chetan Chavan[1], Sachin Barve[2]
*(Research *Scholar, Mechanical Engineering Department, Veermata Jijabai Technological Institute, Mumbai, India)*
*** (Assistant Professor, Veermata Jijabai Technological Institute Matunga, Mumbai, India)*

ABSTRACT: *Like all other tall structures, determination of wind loads is important for industrial Pressure Vessel. All countries use different wind load standards. These different wind load standards are compared with each other in some studies. This paper describes a parametric study of wind load calculations on Vertical Pressure Vessel as per Indian Standard IS-875 (Part 4) (Ammendum 3rd 2006) with their latest addendums. The wind loads calculated, are applied to the design of structures to prevent failure due to wind. Calculated wind pressures as per different code on a Pressure Vessel produce actual loads on the structure. A good structural system for wind design is typically a strong, heavy system with robust connections to help resist loads as the wind blows across and over the structure.*

The Vertical Pressure Vessel is assumed to be made up of 3 components; First bottom dish which is supported on skirt, second intermediate Shell and Third top dish .The Vertical Pressure Vessel is 6.25 m tall and assumed which is located in urban terrain. The design wind speeds acting on vessel are to be calculated from corresponding codes.

The wind force are calculated on each component as per Code procedure and checked for variation occurred. The factors like Basic Wind Speed, Terrain Category, Exposure Category, Damping factor are changed during calculation, the variation on wind force is plotted on graph.

Keywords: *Gust Factor, IS-875, Parametric Study, Vertical Pressure Vessel, Wind Design.*

I. INTRODUCTION

Pressure vessels are containers for the containment of pressure either internal or external. This pressure comes from an external source or by the application of heat from a direct or indirect source or any combination of them. The pressure vessels are used to store fluid that may undergo a change of state inside as in case of boiler or it may combine with other reagent as in a chemical plant. Pressure vessels are commonly used in industry to carry both liquid and gases under pressure. The material comprising the vessel is subjected to pressure loading and hence stresses from all direction. The normal stresses resulting from this pressure are functions of radius of the element under consideration, the shape of the pressure vessel as well as the applied pressure.

Wind load is one of the important design loads for heighted structure greater than 10m. For Vertical Pressure vessel, tall buildings and high towers or mast structures, wind load may be taken as a critical loading, and complicated dynamic wind load effects control the structural design of the structure. In the on-going research project on tall buildings, the study of wind-induced demands is categorized as: along-wind and crosswind responses. Procedure for determining wind loads on buildings and other structures, in which pressures and/or forces and moments are determined for each wind direction considered, from a model of the building or other structure and its surroundings, in accordance with Different standards.

The IS code of practice (IS 875: Part 3 (1987)) and ASCE10 are widely used for estimating wind loads by the structural engineers all over the country.

II. PRESSURE VESSEL DESIGN

The Vertical Pressure Vessel is assumed to be made up of 3 components; First bottom dish which is supported on skirt, second intermediate Shell and Third top dish .The Vertical Pressure Vessel is 6.25 m tall and assumed which is located in urban terrain. The design wind speeds acting on vessel are to be calculated from corresponding codes.

2.1 Pressure Vessel Specification:

2.1.1 Design Parameters

Design Internal Pressure (for Hydro test)	6000.0 KPa.
Design Internal Temperature	280 C
Design External Pressure	103.419 KPa.
Design Internal Temperature	45 C
Minimum Design Metal Temperature	-29 C

2.1.2 Geometry Parameters

Part	I.D.	Height	Thickness	Corrosion Allowance
SKIRT	2500	2500	15	3
BOTTOM DISH	2500	50	15	3

SHELL	2500	3000	15	3
TOP DISH	2500	50	15	3
Note : All Dimensions are in mm.				

2.2 Design of Pressure vessel as per Wind Code (IS 875)

2.2.1: Determination of Velocity Pressure

There are some structural design standards that provide methods for developing wind loads and if we are to use them, we must make sure that we select the correct wind speeds for them to have the results be meaningful. Most established methods come with geographical wind distribution maps or tables that must be used with them. If we do that, we will find that the pressures generated by various methods are remarkably similar.

1] Basic wind speed, Vb (m/s) as per geographical location from IS 875 Part 3. Figure 1 gives basic wind speed map of India, as applicable to 10 m height above mean ground level for different zones of the country. Basic wind speed is based on peak gust velocity averaged over a short time interval of about 3 seconds and corresponds to mean heights above ground level in an open terrain (Category 2).

2] Selection of terrain categories shall be made with due regard to the effect of obstructions which constitute the ground surface roughness. The terrain category used in the design of a structure may vary depending on the direction of wind under consideration.

3] Design wind speed: The basic wind speed (Vb) for any site shall be obtained from Fig. 1 and shall be modified to include the following effects to get design wind velocity at any height (Vz) for the chosen structure.

a) Risk level;
b) Terrain roughness, height and size of structure; and
c) Local topography.

Vz = Vb x kl x k2 x k3,
Where kl = risk factor
k2 = terrain roughness factor
k3 = topography factor

4] Design wind pressure: The design wind pressure at any height above mean ground level shall be obtained by the following relationship between wind pressure and wind velocity:

$$Pz = 0.6 \times Vz2 / 9.81$$

2.2.2: Estimation of Aerodynamic Pressures or Forces

1] Force Coefficients (Cf)

The value of the force coefficient differs for the wind acting on different faces of a building or structure based on shape and height to breadth ratio are calculated from table 23.

2] Gust Factor (G)

Gust factor theory is designed which considers random nature of atmospheric wind speed. However, the wind speed at any height never remains constant and it has been found convenient to resolve its instantaneous magnitude into an average or mean value and a fluctuating component around this average value. The average value depends on the averaging time employed in analyzing the meteorological data and this averaging time varies from a few seconds to several minutes. The magnitude of fluctuating component of the wind speed which is called gust, which depends on the averaging time. In general, smaller the averaging interval, greater is the magnitude of the gust speed.

$$G = \frac{peak\ load}{mean\ load}$$

$$G = 1 + gfr\sqrt{[B(1+\emptyset)^2 + \frac{S*E}{\beta}]}$$

Value of Gust factor varies with variation in gfr factor, Background Factor, Size reduction factor.

3] Wind Force

The wind force on any object is given by

$$Fw = Cf \times Pz \times Ae \times Kp$$

Where Ae – Projected Area

III. PARAMETRIC STUDY

1] Design Wind Pressure

In general, wind speed in the atmospheric boundary layer increases with height from zero at ground level to a maximum at a height called the gradient height. The Pressure variation with height variation for different categories is shown below.

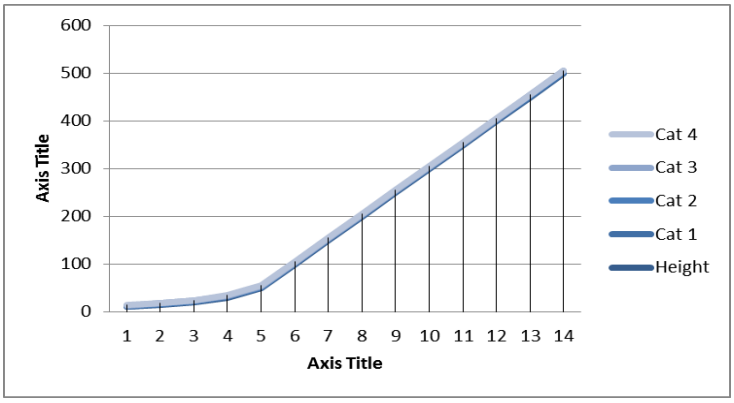

Figure 1 : pressure variation as variation in height and category

2] Gust Factor

Value of Gust factor varies with variation in gfr factor, Background Factor, Size reduction factor.

A] Gf*r Factor

Gf - peak factor defined as the ratio of the expected peak value to the root mean value of a fluctuating load.
R - Roughness factor which is dependent on the size of the structure in relation to the ground roughness.
The variation in product of peak factor and Roughness factor is shown with change in Vessel height and Category.

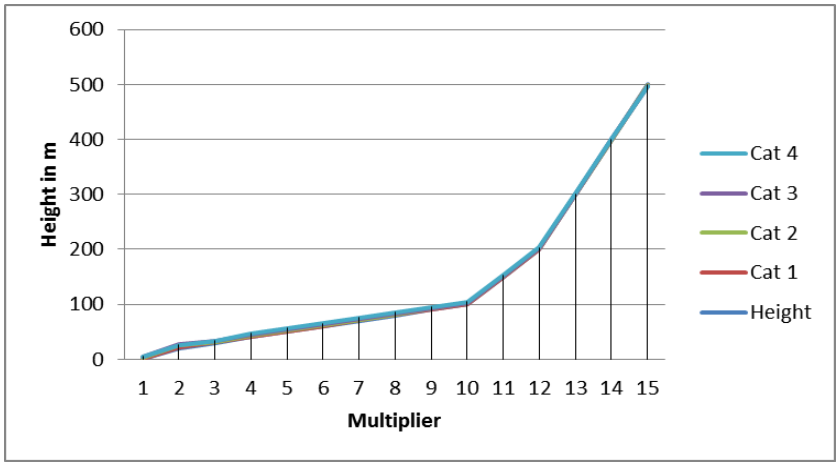

Figure 2: gust factor as variation in height and category

B] Background Factor,

Background factor indicates a measure of slowly varying component of fluctuating wind load. The Background Factor variation with Abscissa variation for different Lambda Values is shown below. Series in graph indicates different (Cy*b)/ (Cz*h) values.

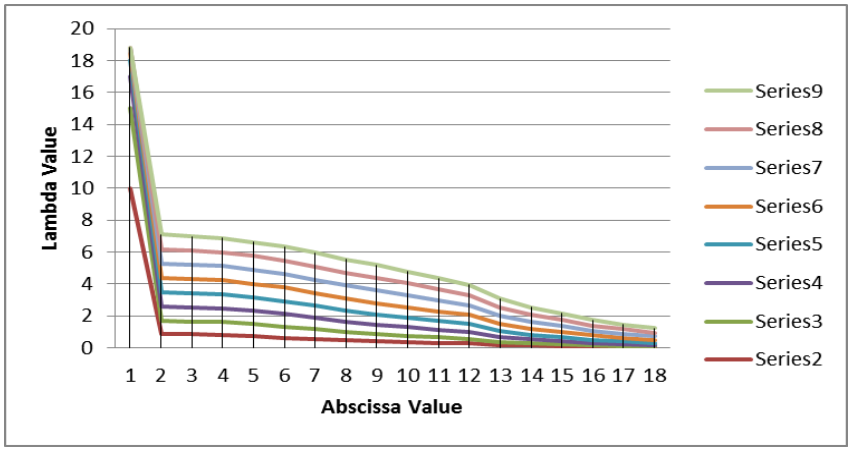

Figure 3: background factor variation as variation in lambda value

C] Size reduction factor

Size reduction Factor variation with Reduced Frequency variation for different Lambda Values is shown below. Series in graph indicates different (Cy*b)/ (Cz*h) values.

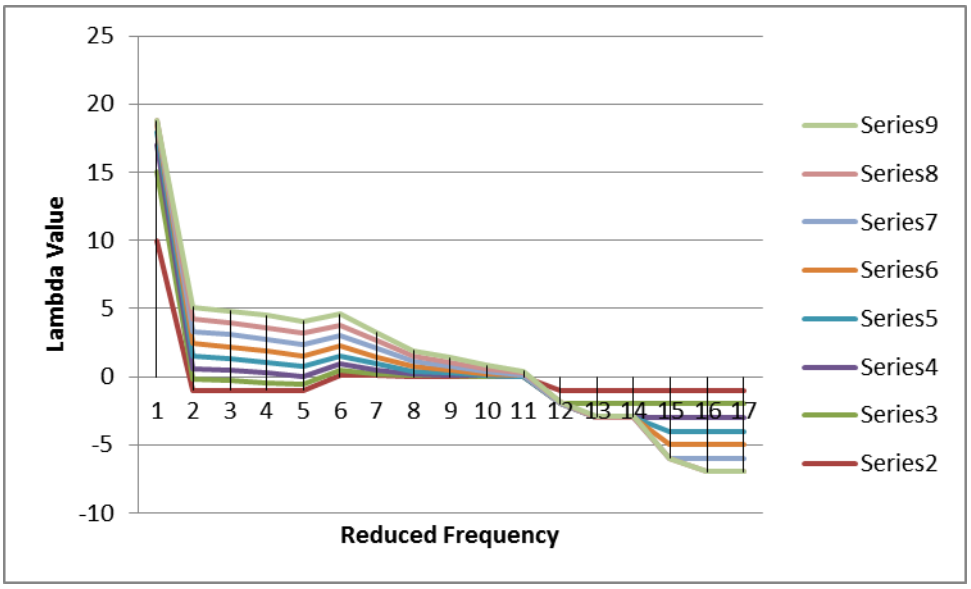

Figure 4: size reduction factor variation as variation in lambda value

IV. DISCUSSION AND CONCLUSION

In this study, structural wind load predictions for Simple Pressure Vessel using IS 875 have been calculated for different parameters keeping other parameters constant. Our results indicate that concerning the loads predicted by IS 875 code, the pressure values on edges stand much lower than that at higher values.

Among these 3 parameters that were evaluated in Gust factor, dynamic wind load, Background factor and Size reduction factor are two important parameters for safety criteria of pressure vessel that affect human perception to motion in the low range of Lambda value for different (Cy*b)/ (Cz*h) encountered in tall buildings.

Although many parameters were examined, the scope is limited to dynamically sensitive, Simple Pressure Vessel with 3 component supported on skirt. To accurately compare the parameters, the various equations in the codes/standards are written in a general format and corresponding graphs are plotted .

Research can be explored to take into account other parameters. Selection material referring to ASME standard can also been developed. The behaviors of pressure vessels in case of fluctuating load could be a challenging matter for future research.

REFERENCES

[1] Bureau of Indian Standards, *Indian Standard Code of Practice for design loads (other than earthquake) for buildings and structures*. Part 3 – Wind loads, IS: 875 (Part 3) -1987.

[2] John Holmes, Yukio Tamura, and Prem Krishna, Comparison of wind loads calculated by fifteen different codes and standards for low, medium and high-rise buildings, 11th Americas Conference on Wind Engineering- San Juan , Puerto Rico, *2009*.

[3] K. Suresh Kumar, Commentary on the Indian Standard for Wind Loads, International Conference on Wind Engineering, Amsterdam, Netherlands, *2011*.

[4] Ching-Wen Chien, and Jing-Jong Jang, Case Study Of Wind-Resistant Design And Analysis Of High Mast Structures Based On Different Wind Codes, Journal of Marine Science and Technology, *Vol. 16, No. 4, pp. 275-287, 2008*.

[5] Dennis Moss, *Pressure Vessel Design Manual* (Gulf Professional Publishing, Third Edition, 2005).

[6] Brownell and Young, *Process Equipment Design* (Wiley Eastern Limited, sixth reprint, 1991).

[7] Eugene F Megyesy, *Pressure Vessel Handbook* (Pressure Vessel Publications Inc., Tenth Edition).

International Journal of Modern Engineering Research (IJMER)
www.ijmer.com Vol. 3, Issue. 4, Jul - Aug. 2013 pp-2161-2165 ISSN: 2249-6645

Design and Analysis of Vapour Absorbing Machine

Prashant Tile[1], S. S.Barve[2]
[12]*Department of Mechanical Engineering, VJTI, Mumbai, India*

ABSTRACT: *A vapor absorption machine (VAM) is a machine that produces chilled water using a waste heat source rather than electrical input as in the more familiar vapor compression cycle. Vapor absorption machine works on the principle of absorption refrigeration cycle. Vapor absorption machine consists of two rectangular pressure vessel shells. Both shells operate under vacuum. As these pressure vessels are subjected to vacuum, there is a chance of external pressure failure. Therefore, design of components of vapor absorption machine is carried out using ASME and TEMA code. Design pressure is 1 Bar and design temperature is 150^{o}C. Modeling of vapor absorbing machine is carried out in PRO-E software. Finite element analysis of vapor absorption machine is done on ANSYS Workbench 11.0.*

Keywords: *Pressure vessel, ASME, TEMA, PRO-E, ANSYS vacuum, external pressure*

I. INTRODUCTION

Most of industrial process uses a lot of thermal energy by burning fossil fuel to produce steam or heat for the purpose. After the processes, heat is rejected to the surrounding as waste. This waste heat can be converted to useful refrigeration by using a heat operated refrigeration system, such as an absorption refrigeration cycle. Both vapor compression and absorption refrigeration cycles accomplish the removal of heat through the evaporation of a refrigerant at a low pressure and the rejection of heat through the condensation of the refrigerant at a higher pressure. The basic difference is that an electric chiller employs a mechanical compressor to create the pressure differences necessary to circulate the refrigerant whereas the absorption chillers use waste heat source and do not use a mechanical compressor.

Main components of vapour absorbing machine are evaporator, absorber, generator and condenser. VAM consists of two rectangular pressure vessel shells. Evaporator and absorber are contained inside lower shell and generator and condenser are contained inside higher shell. Pressure in the lower shell is of the order of 6 mm of Hg(abs). While, pressure in the higher shell is of the order of 80 mm of Hg(abs). Because of inside vacuum, there is a chance of failure of pressure vessel due to external atmospheric pressure of 1 Bar. Hence, pressure vessel is designed for external pressure of 1 Bar. Design temperature for vessel is 150^{o}C. Design of pressure vessel is carried out using ASME code. Procedure for deign of external pressure is given in UG-28 of ASME Sec viii Div 1.

Construction of rectangular pressure vessel of VAM consists of two L shape plates which are welded to form rectangular shell. This shell is closed on both sides by tube sheets. Tubes are inserted in these holes. In evaporator tubes carry water to be cooled. And in absorber tubes carry water required for absorber. Stay rods are used inside vessel to maintain shape of shell against external pressure. Stiffeners are welded externally to shell plate. Cross section of stiffener is 'C' shape. Water boxes are used for storing water flowing through evaporator and absorber. Water boxes are connected to tube sheet with the help of bolting.

ASME Sec viii Div 1 is used for the design of shell plate, tube sheet, stiffener and bolt required for connecting water box to tube sheet. Section 5 (Mechanical standards TEMA class RCB Heat exchangers) of TEMA code is used for the design of tube sheet. Model of VAM pressure vessel is created in PRO-E. It is followed by finite element analysis in ANSYS workbench 11.0. Equivalent stress and total deformation are determined in analysis.

II. EXTERNAL PRESSURE FAILURE

The mechanism of external pressure failure is different from internal pressure failure. Internal pressure failure can be understood as a vessel failing after stresses in part or a large portion exceeds the materials strength. In contrast, during external pressure failure the vessel can no longer support its shape and suddenly, irreversibly takes on a new lower volume shape. It loses its stability. The first picture shows an internal pressure failure. The second picture shows vessels of reduced volume after external pressure failure.

Stability: A stable system is one that is stronger than required. When the vessel is pushed on, it pushes back and returns to its original shape. As external pressure is added to the system, the vessel has less reserve strength left to push back. Eventually the vessel reaches a point where it has very little reserve strength. When push on the wall of the vessel is applied, it cannot push back. At this point the vessel can change shape to a smaller volume configuration.

Figure: 1) Failure due to internal pressure

Figure: 2) Failure due to external pressure

The factors which determine the ability of a pressure vessel to withstand external pressure are
1) Thickness (t)
2) Unsupported length of vessel (L)
3) Larger dimension of rectangular cross section of vessel shell (D)
4) Material of construction
Maximum allowable pressure for vessel can be increased by
1. Increasing thickness (t)
2. Decreasing unsupported length of vessel (L)
3. Decreasing larger dimension (D)
But D and L cannot be changed because vessel size is designed for required volume for reactions taking place inside. Hence only thickness can be changed.

III. DESIGN OF PRESSURE VESSEL

3.1. Shell plate design

Design procedure for calculating thickness of shell plate suitable to withstand external pressure is given in UG-28 of ASME Sec viii Div 1 code. First assume initial thickness and calculate maximum allowable external pressure (Pa). This calculated allowable pressure must be greater than external design pressure (P). If it is lower than external design pressure then thickness of vessel should be increased. Given input is D = 1734 mm, L = 3960 mm, t = 5mm, P = 1 Bar = 0.01033 Kg/mm2. Rectangular shell with above dimensions is shown in figure 3.

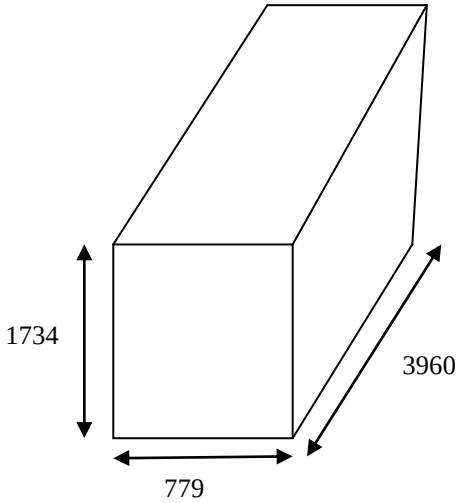

Figure 3: Rectangular pressure vessel

L/D_o=3960/1734= 2.283, D/t= 134/5 = 346.8.
For this ratios from figure G value of factor A = 0.00009.

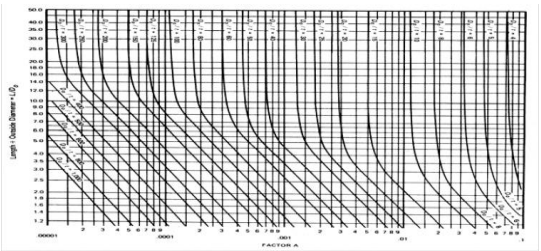
Figure 4: Graph G for determining factor A

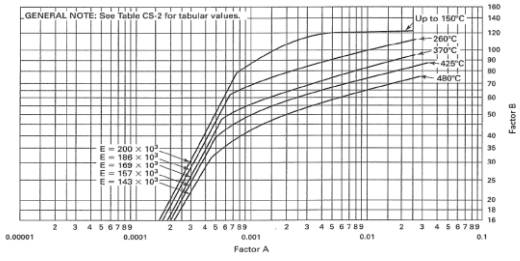

Figure 5: CS-2 chart for determining factor B

As A falls to left of curve use formula

$$P_a = \frac{2AE}{3(D_o/t)}$$

After substituting values we get max allowable pressure (pa) = 0.0037 Kg/mm2. It is lower than design pressure of 0.01033 Kg/mm2. Therefore 5 mm thickness is not safe. Hence, thickness is increased to 6mm. For 6 mm thickness again same calculations as above are performed. After calculation max allowable pressure is 0.00691 Kg/mm2. It is lower than design pressure. Hence, again thickness should be increased. But, continuous increase in thickness is not an economical option. Therefore to increase maximum allowable pressure unsupported length of vessel should be decreased. For this purpose stiffeners are used. Stiffener reduces the unsupported length of vessel. Four stiffeners are used at a distance of 792.4

mm thereby reducing unsupported length from 3960 mm to 792.4 mm. Calculations are performed with t = 6 mm and L = 792.4 mm.
L/D=792.4/1734 = 0.4569
D/t= 1734/6 = 289
D/t = 289 & L/D= 0.4569
From fig. G, Factor, A= 0.0073
From Chart CS-2, Factor, B = 6.2
Using formula

$$P_a = \frac{4B}{3(D_o/t)}$$

For this combination max allowable pressure was found to be 0.028 Kg/mm2. Now in this case it is greater than external design pressure (0.01033 Kg/mm2). Therefore design is safe.

3.2. Design of stiffener

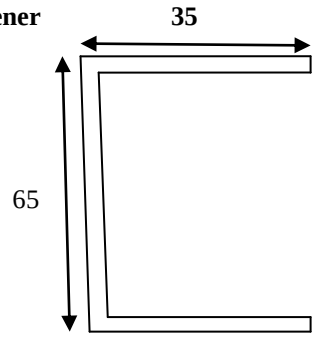

Figure 6: 'C' shape cross section of stiffener

Stiffeners have to satisfy certain requirements of moment of moment of inertia. Condition is that available moment Of inertia with neutral axis parallel to axis of shell should be greater than required moment of inertia. If above condition is not satisfied then stiffener with new cross section is taken. Required moment of inertia is calculated using procedure given in UG-29 of ASME Sec viii Div 1.

$$B = {}^{3}/_{4}\left(\frac{P * D}{t + {}^{A_s}/_{L}}\right)$$

From the formulaValue of factor B is 18.34
From value of B and from CS-2 chart value of factor A = 0.00017

Required moment of inertia is given by

$$I_s = \frac{\left[D^2 * L * \left(t + {}^{A_s}/_{L}\right) * A\right]}{14}$$

After substituting values we get Is = 199479.4 mm4.

Cross section of stiffener is 'C' shape. Available moment of inertia for 'C' shape cross section is 441203.5 mm4. Therefore, Available moment of inertia of stiffening ring is greater than required moment of inertia.

3.2.1 Strength of attachment weld

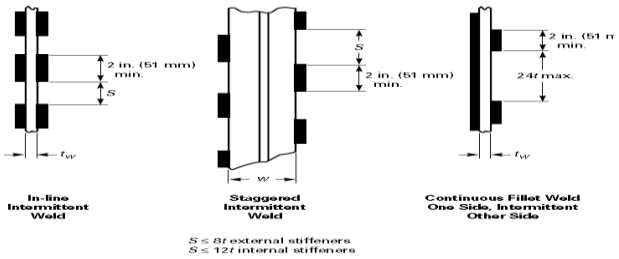

Figure 7: Arrangement of attachment weld

Stiffeners are welded to the shell with leg size of 6 mm. Procedure for checking of strength of attachment weld is given in UG-30 of ASME Sec viii Div 1. Criterion for checking weld strength is that actual load acting on the weld must be less than allowable weld for the load. The actual load on the weld is a combination of the radial pressure load between the stiffeners, the weld shear flow due to the radial load through the stiffener, and the external design load carried by the stiffener. After calculations of strength of attachment weld, it is found that actual load acting on weld is 108.04 N/mm. And allowable load for weld is 455.4 N/mm. Thus, allowable load for weld is greater than actual load on the weld. Therefore, fillet weld leg size of 6 mm is strong enough to withstand external pressure load.

3.3. Design of tube sheet

Tube sheet is a plate which is drilled with pattern of holes. Tubes are inserted in these holes. Rectangular shell is closed on both sides by tube sheets. Tube sheet is designed using both ASME and TEMA code.

a) Thickness of tube sheet after ASME calculations:

Design of non circular head with bolts is given in UG-34 of ASME sec viii Div 1. After calculations, thickness of tube sheet is 19 mm.

b) Thickness of tube sheet after TEMA calculations:

Section 5 of TEMA gives design of tube sheet. In TEMA tube sheet is designed for two conditions

1) For bending
   Tube sheet thickness for bending is 22 mm
2) For shear
   Tube sheet thickness for shear is 0.42 mm.
   Therefore according to TEMA, thickness of tube sheet is 22 mm

3.4. Design of bolts required to connect water box to tube sheet

Two water boxes are bolted to tube sheet. The bolts should be designed to contain the pressure and for the preload required to prevent leakage through the gasket. For sustaining such loads, provided area of bolts must be greater than required bolt area. Appendix 2 of ASME Sec viii Div 1 gives design procedure for bolts. After following the procedure we come to know that for evaporator side water box to maintain leak proof joint 36 bolts of M12 size are sufficient to withstand pressure of 1 Bar. And for absorber side water box 42 bolts of M12 size are sufficient to maintain leak proof joint.

IV. FINITE ELEMENT ANALYSIS OF VAPOUR ABSORBING MACHINE

Geometry of VAM is prepared in PRO-E. Then it is saved in IGES file format and imported to ANSYS workbench. Material used for vapor absorbing machine is low carbons steel SA 516 Gr 70. It is a linearly isotropic material.
Properties of material are given below:

Youngue's modulus	2.e+005 Mpa
Poisson's ratio	0.3
Density	7.856.e-006 kg/mm3
Tensile yield strength	250 Mpa
Tensile ultimate strength	460 Mpa

Element type used is Solid 186. It is a higher order 3-D 20-node solid element that exhibits quadratic displacement behavior. Meshing of geometry is carried out using hex dominant method. Meshing of geometry is shown below

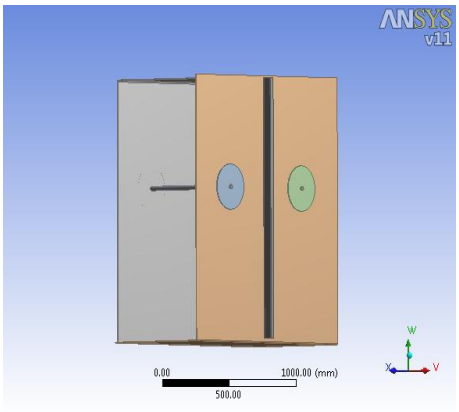

Figure 8: Geometry of VAM

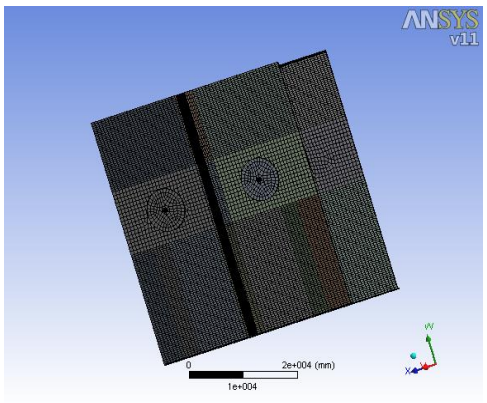

Figure 9: Meshing of VAM model

External pressure of 1 Bar is applied on geometry. Following boundary conditions are applied: Two fixed supports of 130 mm width at a distance of 150 mm from ends are given to the bottom plate of shell. Shell surface attached with tube sheet is fixed. Stay rods and stiffener are fixed to shell. After applying boundary conditions, model is solved for von-mises (equivalent) stress and total deformation occurring in the model. Results are shown below

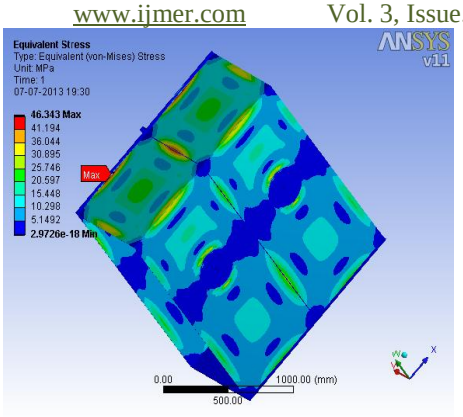

Figure 10: Equivalent stress in model

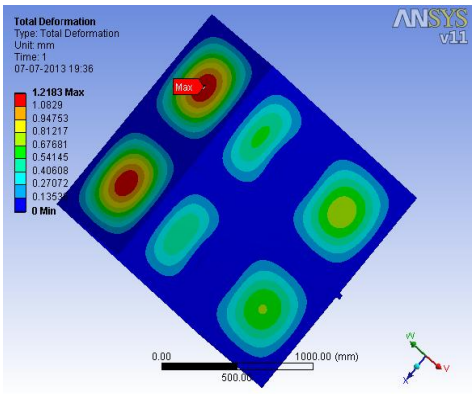

Figure 11: Total deformation

Maximum stress in the model is 46.34 Mpa and its location is at the connection of two L shape plate. And total deformation is 1.2183 mm. Max stress (46.34 Mpa) is lower than allowable stress (138 Mpa). Therefore there is no chance of failure due to external pressure.

V. CONCLUSION

Shell thickness of 6 mm with four stiffeners is safe for external design pressure of 1 Bar. Tube sheet thickness according to ASME code is 19 mm. And according to TEMA it is 22 mm. For external loading of 0.1 Mpa, 'C' shape cross section of stiffener with given dimension is suitable. Stiffener is welded to shell with one side continuous weld and other side intermittent weld. Weld leg size of 6 mm is enough to carry radial pressure load between stiffeners and weld shear flow doe to radial load between stiffeners. Forty two bolts with size of M 12 are sufficient to hold water box and absorber side tube sheet assembly for design pressure of 1 Bar. Thirty six bolts with size of M 12 are sufficient to hold water box and evaporator side tube sheet assembly for design pressure of 1 Bar. After finite element analysis on ANSYS we come to know that, maximum stress (46.34 Mpa) generating in the vessel is lower than allowable stress (138 Mpa) for vessel material.

REFERENCES

[1]. Rules for construction of pressure vessel ASME Sec vii Div 1 2001 Edition
[2]. ASME Sec ii Part D
[3]. Section 5 of tubular exchanger manufacturers association
[4]. "Pressure vessels design and practice", by Somnath Chattopadhyay. Publication: CRC Press. Ed: 2005
[5]. "Process equipment design", by Brownell and Young. Publication: Wiley Eastern Limited. Ed: 1959 sixth reprint Sept 1991.
[6]. "Pressure vessel design handbook", by Bednar, H.H. Second edition, CBS Publication
[7]. "Pressure vessel design manual'', by Dennis Moss 3rd Edition
[8]. Design and analysis of pressure vessel by Jimit Vyas and Mahavir Solanki
[9]. Mechanical design of process equipment by Coulson and Richardson
[10]. Vacuum Vessel Engineering Note for Cryomodule 2 (CM2) from FERMILAB Technical Division Authors: M. Wong
[11]. Structural analysis of the vacuum vessel for the LHCb vertex locator (VELO) by M. J. Kraan, J. Buskop, M. Doets, C. Snippe

International Journal of Modern Engineering Research (IJMER)
www.ijmer.com Vol. 3, Issue. 4, Jul - Aug. 2013 pp-2166-2169 ISSN: 2249-6645

Optimization of machining parameters of Electric Discharge Machining for 202 stainless steel

Singh Jaspreet[1], Singh Mukhtiar[2] and Singh Harpreet[3]
[1, 2, 3] *Lovely Professional University, Phagwara, Punjab.*

***ABSTRACT**: Electric discharge machining is used for machining of hard materials like steel. In this paper, the effect of electrical discharge machining (EDM) parameters such as pulse-on time (T_{ON}), pulse-off time (T_{OFF}), and current (I) on material removal rate (MRR) in 202 stainless steel was studied. The experiments are carried out as per design of experiments approach using L_{27} orthogonal array. The results were analyzed using analysis of variance and response graphs. From this study, it is found that different combinations of EDM process parameters are required to achieve higher MRR and greater surface finish. Signal to noise ratio (S/N) and analysis of variance (ANOVA) is used to analyze the effect of the parameters on MRR and also to identify the optimum cutting parameters. The contribution of each cutting parameter towards the MRR is also identified.*

***Keyword**: Material Removal Rate, Taguchi method, 202 stainless steel.*

I. INTRODUCTION

Electrical discharge machine (EDM) technology is increasingly being used in tool, die and mould making industries, for machining of heat treated tool steels and advanced materials (super alloys, ceramics, and metal matrix composites) requiring high precision, complex shapes and high surface finish. Traditional machining technique is often based on the material removal using tool material harder than the work material and is unable to machine them economically. An electrical discharge machining (EDM) is based on the eroding effect of an electric spark on both the electrodes used. Electrical discharge machining (EDM) actually is a process of utilizing the removal phenomenon of electrical-discharge in dielectric. Therefore, the electrode plays an important role, which affects the material removal rate and the tool wear rate. In non-traditional processing electrical discharge machining (EDM) has tremendous potential on account of the versatility of its application and it is except to be successfully and commercial utilized in modern industries (Habib,2009). In the EDM process to obtain the maximum material removal with minimum tool wear, the work material and tool must be set at positive and negative electrode (Che Haron et al.,2008). Electric discharge machining one of the most popular non-traditional material removals process and has become basic machining method for the manufacturing industries of aerospace, automotive, nuclear and medical . The source of energy used is amplified light, ionized material and high voltage. Examples are laser beam machining, ion beam machining, and plasma arc machining and electric discharge machining (Kiyak et al, 2007).

II. EXPERIMENTATION

Electric discharge machining of 202 stainless steel using different parameters:

The objective of the study is to evaluate the main effects of current, pulse on time, and pulse off time on the material removal rate (MRR) of the Following set of electrical of EDM process are expected to affect the resultant machining objective functions are given in the Table 2.1.

Table 2.1: Electrical and non-electrical parameters of EDM process

S No.	Electrical Parameters	Non-electrical Parameters
1	Peak current	Type of dielectric medium
2	Pulse-on time	Flushing Pressure
3	Pulse-off time	Volume fraction

After pilot experimentation the number of factors and the number of levels have been selected for the electrical parameters. The lists of factors studied with their levels are given in the Table 2.2 range of parameters available and used for experimentation.

Table 2.2: Range of parameters available and used for experimentation

SNo.	Machining parameter	Range	Used For Level 1	Used For Level 2	Used For Level 3
1	Current	0-30 A	3	9	15
2	Pulse-on time	0.5-2000µs	500	700	900
3	Pulse-off time	0.5-2000µs	500	700	900

The number of factors and their interactions and level for factors determine the total degree of freedom required for the entire experimentation.

Table 2.3: Orthogonal arrays experiments

S.No.	CURRENT	T-ON	T-OFF
1	3	500	500
2	3	500	700
3	3	500	900
4	3	700	500
5	3	700	700
6	3	700	900
7	3	900	500
8	3	900	700
9	3	900	900
10	9	500	500
11	9	500	700
12	9	500	900
13	9	700	500
14	9	700	700
15	9	700	900
16	9	900	500
17	9	900	700
18	9	900	900
19	15	500	500
20	15	500	700
21	15	500	900
22	15	700	500
23	15	700	700
24	15	700	900
25	15	900	500
26	15	900	700
27	15	900	900

ANOVA helps us to compare variability within experimental data. ANOVA table is made with help of MINITAB 15 software. When performance varies one determines the average loss by statistically averaging the quadratic loss.

III. RESULT AND DISCUSSION

The effect of parameters i.e. pulse on time, pulse off time and current some of their interactions were evaluated using ANOVA. A confidence interval of 95% has been used for the analysis. 27 experiments were completed so as to measure Signal to Noise ratio (S/N ratio) calculated by the formula $(S/N)_{HB} = -10\ log(MSD_{HB})$. The variation data for each factor and their interactions were F-tested to find significance of each calculated by the formula $F = \frac{MS\ for\ the\ term}{MS\ for\ the\ error\ term}$. The principle of the F-test is that the larger the F value for a particular parameter, the greater the effect on the performance characteristic due to the change in that process parameter. In this work, 202 stainless steel samples were machined with non-conventional method (EDM) by varying the EDM parameters, after that the experimental outcomes are optimized using ANOVA. The following conclusions were found from the optimized results after ANOVA. These significant values are shown in table. 3.1. In order to obtain the effect for machining parameters for each level, the S/N ratio value of each fixed parameter and level in each machining performance is summed up.

Table 3.1 Experimental result with S/N ratio for material removal rate

Exp.No.	CURRENT	T-ON	T-OFF	Material Removal Rate (gms/min)	S/N Ratio
1	3	500	500	16.000	24.0824
2	3	500	700	16.000	24.0824
3	3	500	900	12.000	21.5836
4	3	700	500	12.000	21.5836
5	3	700	700	8.000	18.0618
6	3	700	900	14.000	22.9226
7	3	900	500	6.000	15.5630
8	3	900	700	10.000	20.0000
9	3	900	900	10.000	20.0000
10	9	500	500	63.333	36.0326
11	9	500	700	73.333	37.3060
12	9	500	900	83.333	38.4164
13	9	700	500	66.667	36.4782
14	9	700	700	53.333	34.5400
15	9	700	900	80.000	38.0618
16	9	900	500	30.000	29.5424
17	9	900	700	13.333	22.4988
18	9	900	900	30.000	29.5424
19	15	500	500	75.000	37.5012
20	15	500	700	115.000	41.2140

21	15	500	900	80.000	38.0618
22	15	700	500	100.000	40.0000
23	15	700	700	75.000	37.5012
24	15	700	900	125.000	41.9382
25	15	900	500	95.000	39.5545
26	15	900	700	105.000	40.4238
27	15	900	900	110.000	40.8279

From the calculation of main effects for each level of the factors, the main effects values are presented in table 3.2. The main effect values and interactions are plotted in figures for current, pulse on time and pulse off time respectively. The main effect plot shows the influence of each level of factors on the machining performance for Higher is better.

Table 3.2: Response Table for Signal to Noise Ratios

Level	CURRENT	T-ON	T-OFF
1	20.88	33.14	31.15
2	33.60	32.34	30.63
3	39.67	28.66	32.37
Delta	18.79	4.48	1.75
Rank	1	2	3

Table 3.3: Analysis of Variance for SN ratios

Source	Sum of Squares	DF	Mean Square	% of contribution
Current	153.158	2	76.5789	0.501
Pulse-on time	11.284	2	5.6420	0.010
Pulse-off time	1.437	2	0.7186	0.489
Residual error	19.358	20	0.9679	
Total	185.237	26		

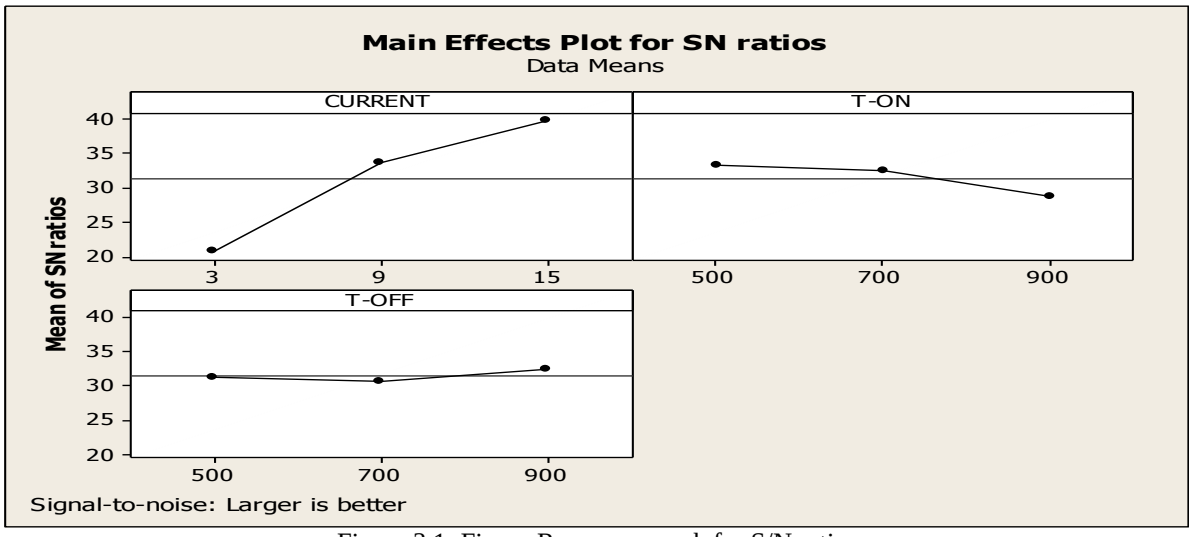

Figure 3.1: Figure Response graph for S/N ratio.

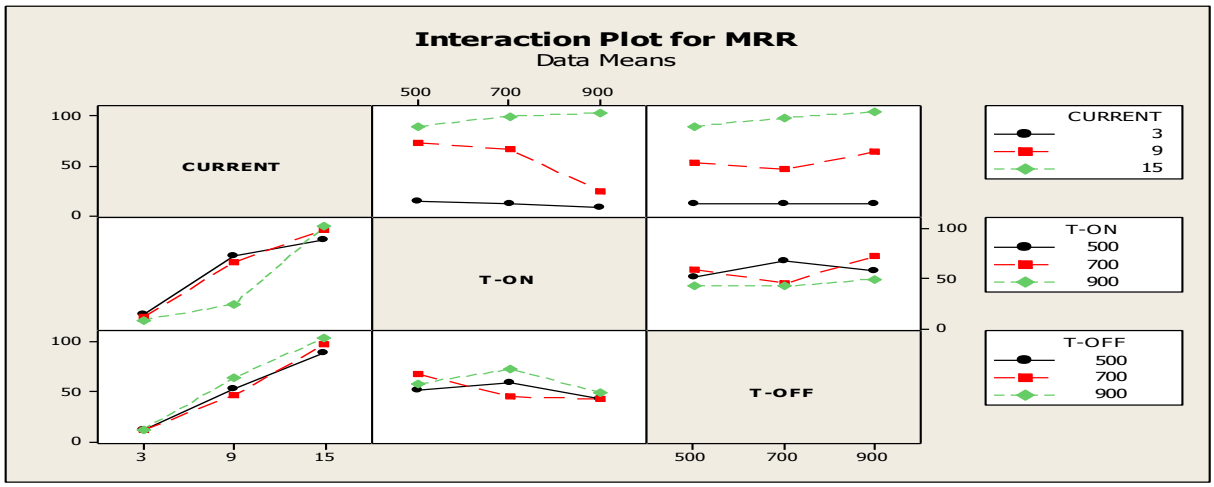

Figure 3.2: Interaction plot for S/N ratio

IV. CONCLUSION

The relative importance of the cutting parameters with respect to the pulse on time, pulse off time and current on MRR. From the analysis of the figures 3.1 & 2 and table 3.2 the optimal value for MRR is current 15A, pulse on time 500µs and pulse off time 900 µs. The according to percentage contribution data current and pulse off time are the affecting parameters.

REFERENCES

[1]. Habib, S. S., Study of the parameters in electrical discharge machining through response surface methodology approach. App. Math. Model. 33, 2009. 4397-4407.
[2]. Haron, C.H Che., Ghani, J.A., Burhanuddin, Y., Seong, Y.K., S wee, C.Y., Copper and graphite electrodes performance in electrical-discharge machining of XW42 tool steel. J. Mater. Process. Techno. 201, 2008. 570-573.
[3]. Kiyak, M., Cakir, O., 2007. Examination of machining parameters on surface roughness in EDM of tool steel. J. Mater. Process.
[4]. Santanu Dey, Dr. D.C.Roy Experimental Study Using Different Tools/Electrodes E.G.Copper, Graphite on M.R.R of E.D.M Process and Selecting The Best One for Maximum M.R.R in Optimum Condition International Journal of Modern Engineering Research (IJMER) Vol.3, Issue.3, May-June. 2013 pp-1263-1267

International Journal of Modern Engineering Research (IJMER)
www.ijmer.com Vol. 3, Issue. 4, July - Aug. 2013 pp-2170-2176 ISSN: 2249-6645

Analysis of Machining Characteristics of Cryogenically Treated Die Steels Using EDM

Singh Jaspreet[1], Singh Mukhtiar[2], Singh Harpreet[3]
[1, 2, 3] *Lovely Professional University, Phagwara, Punjab.*

***ABSTRACT*:** *The field of cryogenics was advanced during World War II when scientists found that metals frozen to low temperature showed more resistance to wear. Major advantages of these changes are to enhance the abrasion resistance hardness and fatigue resistance of the materials. To attain high accuracy in difficult to machine materials, the nonconventional machining has become the lifeline of any industry. One of the most important non-conventional machining methods is Electric discharge machining (EDM). In this research work, experimental investigations have been made to compare the machining characteristics of three die steel materials, before and after deep cryogenic treatment using EDM. The output parameters for study are material removal rate, tool wear and surface roughness. The results of study suggest that cryogenic treatment has a significant positive effect on the performance of work pieces, tool wear decreases and surface finish of the work piece after machining improves sharply for all three die steels. The best improvement in tool wear and surface roughness is reported by High Carbon High Chromium (HCHCr) followed by EN 8 and then by EN 31. It can be recommended that cryogenically treated die steels can be efficiently machined through EDM.*

KEYWORDS: *Austempered ductile iron (ADI), Electrical discharge machining (EDM), Surface modification, Surface finish*

I. INTRODUCTION

Electrical discharge machining (EDM) is a non-traditional machining method usually employed in production of die cavities via the erosive effect of electrical discharges between a tool electrode and a work-piece [3]. The advantage with EDM is its ability to machine complex cavities, small parts with sharp internal or external radii and fragile materials or work-pieces requiring the creation and modification of very thin walls. However, the occurrence of tool electrode wear is unavoidable and is a very critical issue since tool shape degeneration directly affects the final shape of die cavity. To improve the machining accuracy in the geometry of a work piece, methods to detect the tool electrode wear as well as to compensate the wear of the tool electrode are required [1]. The hard materials after Cryogenic processing makes changes to the crystal structure of materials. It is believed that cryogenically processing makes the crystal more perfect and therefore stronger. In Ferrous metals, it converts retained austenite to martensite and promotes the precipitation of very fine carbides.

Cryogenic processing will not itself harden metal like quenching and tempering. It is not a substitute for heat-treating. It is an addition to heat-treating. Most alloys will not show much of a change in hardness due to cryogenically processing. The abrasion resistance of the metal and the fatigue resistance will be increased substantially. Cryogenic Processing is not a coating. It affects the entire volume of the material. The change brought about by cryogenically processing is permanent. The EDM process on Cryogenic Processed material has actually altered the metallurgical structure and characteristics in this layer as it is formed by the unexpelled molten metal being rapidly cooled by the dielectric fluid during the flushing process and resolidifying in the cavity. This layer does include some expelled particles that have solidified and been re-deposited on the surface prior to being flushed out of the gap. This carbon enrichment occurs when the hydrocarbons of the electrode and dielectric fluid break down during the EDM process and impenetrate into the white layer while the material is essentially in its molten state. If this layer is too thick or is not removed by finer EDM finishes or polishing, the effects of this micro-cracking can cause premature failure of the part in some applications. Also, the existence of these micro-cracks lowers the corrosion and fatigue resistance of the material, so surface integrity should be the primary consideration when evaluating the performance of the EDM technique and the prime objective of EDM must be to establish the condition which suppresses this formation. The micro-cracks produced by EDM on Cryogenic Processed material are the result of thermal stresses created during the on-time phase of the EDM cycle. The depth of the micro-cracking is partially controlled by the EDM program and it goes without saying that as the spark intensity increases so does the depth. In the study, Taguchi quality design method was used to determine the significance of the machining parameters on the work piece removal rate [22]. The approach presented in this paper takes advantage the Taguchi method which forms a robust and practical methodology in tackling multiple response optimization problems. The paper also presents a case study to illustrate the potential of this powerful integrated approach for tackling multiple response optimization problems. The variance analysis is also an integral part of the study, which identifies the most critical and statistically significant parameters [4].

Different process parameters using Taguchi quality design. ANOVA and F-test to achieve a fine surface finish in EDM and found that the machining voltage, current type of pulse-generating circuit were identified as the significant parameters affecting the surface roughness in finishing process [23]. The test results were analyzed for the selection of an optimal combination of parameters for the proper machining.

II. PROBLEM FORMULATION

Most components made of hard alloys require high accuracy and complex machining. Therefore, the conventional method in machining of hard alloys is not suitable. Research on machining these using conventional machines mostly

highlights chipping, stresses, cutting tool wear and thermal problem during machining which are caused by mechanical energy. Instead of conventional machining, EDM process is a potential machining method to eliminate such problems.

However, not much work has been reported in the investigation of effect of Deep Cryogenic Treated work piece while machining through EDM. In this research work, efforts have been made to study the effect of cryogenically treatment on the performance of EDM machining characteristics using Taguchi design approach to analyze the material removal rate (MRR), tool wear (TW) and surface roughness (SR).

III. EXPERIMENTAL PROCEDURES

The main objectives of the research work are:

1. To study the effect of deep cryogenically treatment on the die steels while using EDM.
2. Comparison of the machining parameters of three different types of die steels, before and after cryogenically treatment.
3. Analysis of input machining parameters using Taguchi experimental design technique.

3.1 Parameter selection

There are several parameters in EDM e.g. Polarity, Gap voltage, pulse on- time, pulse off-time, Duty factor, Peak current, Dielectric pressure, Dielectric temperature, Dielectric conductivity, Pulse Width, Pulse duration, Electrode gap, Pulse wave form, Spark frequency etc. can be varied during the machining process.

S.no.	Parameters	Range	Material
1	Current: (A)	6 Amps	L1
		8 Amps	L2
		10 Amps	L3
2	On time: (B)	20 µSec	L1
		50 µSec	L2
		100 µSec	L3
3	Duty factor: (C)	8 pos	L1
		10 pos	L2
4	Voltage: (D)	30 V	L1
		35 V	L2
		40 V	L3
5	Polarity	Straight	Electrode Negative

Table: 3.1 *Parameter selected for EDM process*

But for this experimental work, it has been proposed to choose following four parameters as only these could be easily monitored:

1. Peak current (1 to 60A)
2. Pulse on-time (1 to 2000 µSec.)
3. Duty factor (1 to 12 steps, each step corresponding to 8%)
4. Gap Voltage (1 to 100V)

Various levels of the above four input machining parameters were taken and further L_{18} orthogonal array of Taguchi experimental design was chosen to conduct the experiments. Parameter assignments of this array are shown in table 3.2.

Experiment	Duty Factor (Pos) (A)	Current (Amps) (B)	Voltage (V) (C)	Pulse on-time (D)
1	10	6	30	20
2	10	6	35	50
3	10	6	40	100
4	10	8	30	20
5	10	8	35	50
6	10	8	40	100
7	10	10	30	20
8	10	10	35	50
9	10	10	40	100
10	12	6	30	20
11	12	6	35	50
12	12	6	40	100
13	12	8	30	20
14	12	8	35	50
15	12	8	40	100
16	12	10	30	20
17	12	10	35	50
18	12	10	40	100

Table: 3.2 Orthogonal Array L18 Matrix

Table contains an orthogonal matrix of treatments by assigning the various levels of each parameter in the corresponding columns and rows of the matrix. After setting up the machine as per the experiments were conducted according to the treatment combination. The observed values of response/ output parameters are tabulated.

3.2 Response parameters

Output parameters are material Removal Rate (MRR) higher the better, Tool Wear (TW) lowers the better and Surface Roughness (SR) lower the better. The work piece used in the experiments is 3 Die Steel (2 samples of each, out of which one is cryogenically treated & other is non-cryogenically treated) High Carbon High Chromium (HCHCr), EN8 and EN31. Tool steels for hot work applications, designated as group 'EN, D3' steels in the AISI classification system, have the capacity to resist softening during long or repeated exposures to high temperatures needed to hot work or for die-casting other materials. The outstanding characteristics of these tool steels are high toughness and shock resistance. They have air hardening capability from relatively low austenitizing temperatures and minimum scaling tendency during air cooling.

1	Workpiece	HCHCr EN8 EN31	Cryogenic Treated
2	Electrodes used	Copper electrode	14 mm in diameter
3	Dielectric used	EDM oil SEO 450	
4	Measuring Instruments	Surfcom	model 130A Resolution 0.001 µm

Table: 3.3 *E*xperimental details of materials used

IV. METHODOLOGY

Deep cryogenically treatment of die steels was done in a Cryogenic chamber. Liquid Nitrogen gas is used to perform the deep cryogenically treatment. Different set of parameters are used to perform the experiment on three different cryogenically treated die steels. Same set of parameters are used for non-cryogenically treated. Job material remains the same for all the cases. Performance of EDM is evaluated on the basis of Material Removal Rate (MRR), Tool Wear (TW) and Surface Roughness (SR).

The depth of cut is observed directly from the control panel, which is attached to the machine tool. Therefore, Material Removal Rate (MRR) for the EDM operation is calculated as *MRR (mm^3/min) = Depth of Cut (mm) × Area of Cut (mm)/ machining time (min).* Tool Wear (TW) for the EDM operation is calculated as *W (%) = (Initial weight- Final weight) × 100/ Initial weight*. The experiments were conducted at different combinations of input parameters. The results obtained in these experiments were optimized using Taguchi L18 orthogonal technique.

4.1 Deep cryogenically treatment of die steels

Deep cryogenically treatment of electrodes is done using 9-18-14 cycle. The temperature of cryogenically chamber is ramp down from atmospheric temperature to -184 °C in 9 hrs. The soaking period is 18 hrs. The temperature of cryogenically chamber is ramp up from -184 °C to atmospheric temperature in another 14 hrs. In this way 9-18-14 cycle is complete.

4.2 Taguchi experimental design and analysis

Taguchi method simplifies and standardizes the fractional design by introducing orthogonal array (OA) for constructing or laying out the design of experiments. It also suggests a standard method for the analysis of results. A factorial experiment with 4 parameters each at three levels would require (3^4=81) test runs whereas Taguchi L_{18} OA would require only 18 trial runs for providing same information. In the Taguchi method, the results of the experiments are analyzed to achieve one or more of the following objectives:

I. To establish the best or the optimum condition for a product and/or process.
II. To estimate the contribution of the individual variables and their interactions.
III. To estimate the response under the optimum conditions.

The optimum conditions are identified by studying the main effect of each of the parameters. The main effects indicate the general trend of influence of each parameter. The knowledge of the contribution of individual parameter plays an important role in deciding the nature of control to be established on a production process.

V. RESULTS AND DISCUSSION

5.1 Effect of cryogenic treatment on MRR

The standard procedure suggested by Taguchi is employed. The mean or the average values and S/N ratio of the response/quality characteristics for each parameter at different levels have been calculated from experimental data. For the graphical representation of the change in value of quality characteristic and that of S/N ratio with the variation in process parameters, the response curves have been plotted. These response curves have been used for examining the parametric effects on the response characteristics. ANOVA of the experimental data has been done to calculate the contribution of each factor in each response and to check the significance of the The third level of Pulse on-time (i.e.100µs) seems to be optimal as S/N ratio is higher. The main portion of material removal from work piece and electrode is due to occurrence of arcs. Since the MRR is contribution of discharges on total removed material is only due to the pulse train. model. Figure 5.1

indicates that increase in current results in improvement both in the average values and S/N ratio of MRR. Therefore, second level of current (i.e. 8 Amps) is optimal. The MRR will increase resulting into bigger crater on work surface and hence poor surface finish.

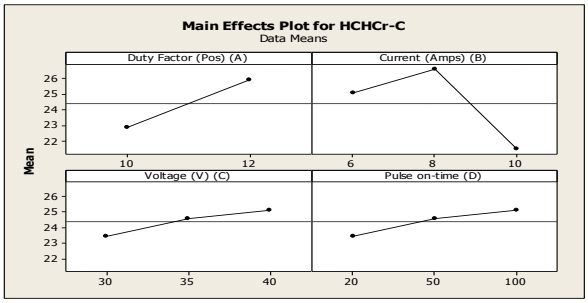

Fig 5.1: Work piece HCHCr (cryogenically treated)

Figure further suggest that second level of duty factor (i.e.12 pos) gives optimal results as regards to both average values and S/N ratio of MRR. As far as voltage is concerned, third level (i.e.40 V) is optimal as S/N ratio for this is highest.

Figure 5.2 indicates that increase in current results in improvement both in the average values and S/N ratio of MRR. Therefore, first level of current (i.e. 6 Amps) is optimal. The third level of Pulse on-time (i.e. 100 µs) seems to be optimal as S/N ratio is higher. First level of duty factor (i.e.10 pos) gives optimal results as regards to both average values and S/N ratio of MRR.

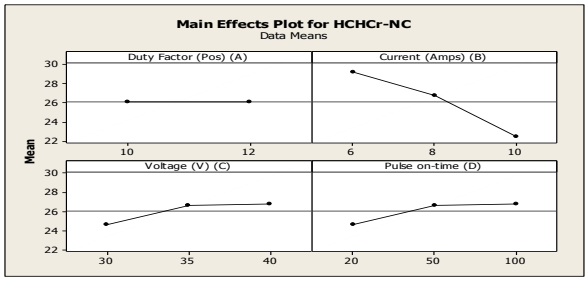

Fig 5.2: Work piece HCHCr (Non-cryogenically treated)

Voltage on third level (i.e.40 V) is optimal as S/N ratio for this is highest. Practically material removal rate is higher due to high spark energy. The first level of current (i.e. 6 Amps) is optimal. The third level of Pulse on-time (i.e. 50µs) seems to be optimal as S/N ratio is higher. Figure 5.3 further suggest that second level of duty factor (i.e.12 pos.) gives optimal results as regards to both average values and S/N ratio of MRR.

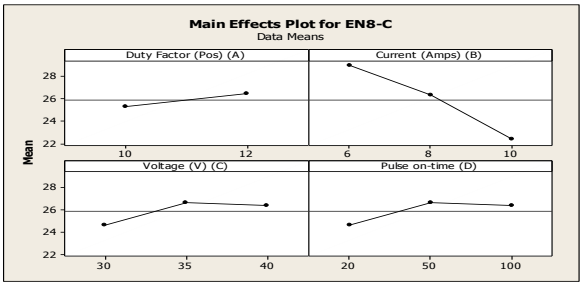

Fig 5.3: work piece EN 8 (cryogenically treated)

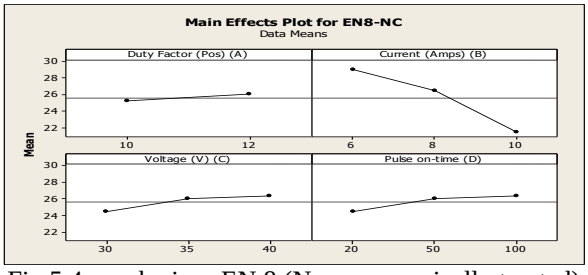

Fig 5.4: work piece EN 8 (Non-cryogenically treated)

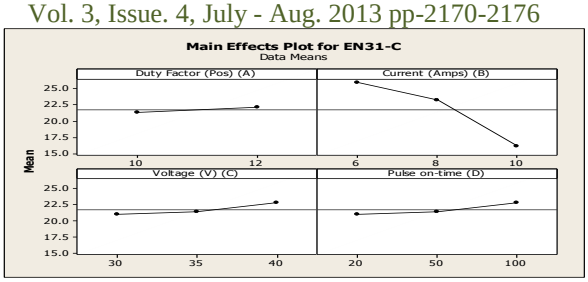

Fig 5.5: work piece EN 31 (cryogenically treated)

Similarly in figures 5.4-5.6 the maximum values are optimal values and representing the results for better MRR. The most favorable conditions (optimal settings) of process parameters in terms of mean response of characteristic have been established by analyzing response curves.

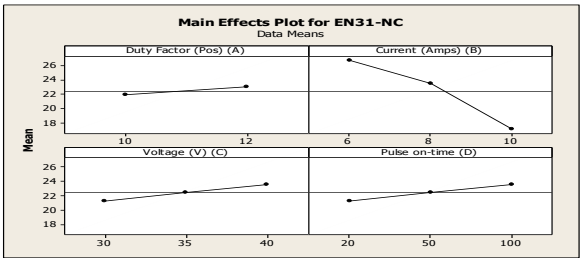

Fig 5.6: work piece EN 31 (Non-cryogenically treated)

5.2 Effect of cryogenic treatment on tool wear

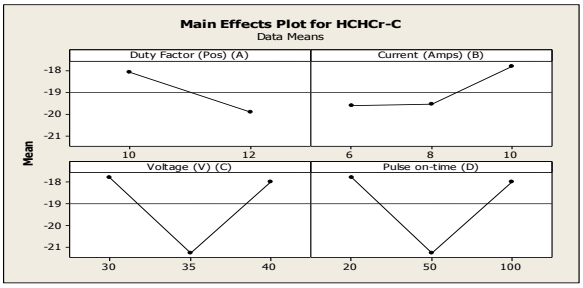

Fig 5.7: work piece HCHCr 8 (cryogenically treated)

It can be observed from figure 5.7 that high current increases the average value of TW. Third level of current (i.e.10 Amps) would be optimum as S/N ratio is maximum at this level.In case of Pulse on-time the second level (i.e.100 µs) would be optimal as it gives lowest average TW and highest S/N ratio. Figure further indicates that first level of duty factor (i.e.10 pos) is best as it gives maximum S/N ratio and lower average TW.

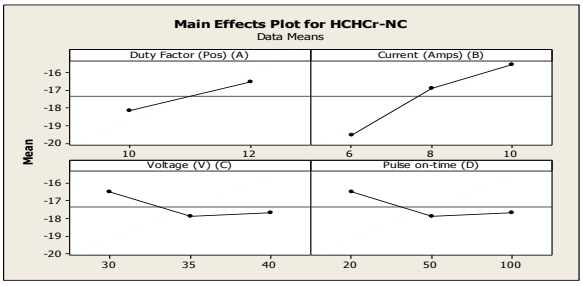

Fig 5.8: Work piece HCHCr (Non-cryogenically treated)

Figure 5.8 shows that first level of current (i.e.10 Amps) would be optimum as S/N ratio is maximum at this level. In case of Pulse on-time the third level (i.e. 20 µs) would be optimal as it gives lowest average TW and highest S/N ratio. The first level of duty factor (i.e. 12 pos.) is best as it gives maximum S/N ratio and lower average TW.

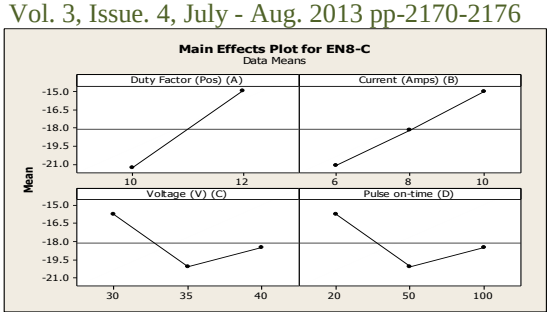

Fig 5.9: Work piece EN-8 (cryogenically treated)

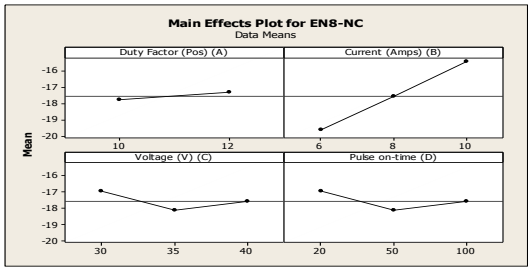

Fig 5.10: Workpiece EN-8(non-cryogenically treated)

It can be observed from figure 5.9 that first level of current (i.e.10 Amps) would be optimum as S/N ratio is maximum at this level. In case of Pulse on-time the second level (i.e.20µs) would be optimal as it gives lowest average TW and highest S/N ratio. Duty factor (i.e. 10 pos) is best as it gives maximum S/N ratio and lower average Tool wear.

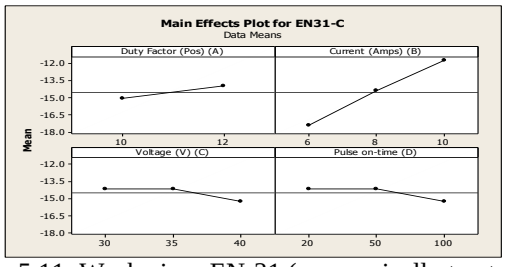

Fig 5.11: Work piece EN-31 (cryogenically treated)

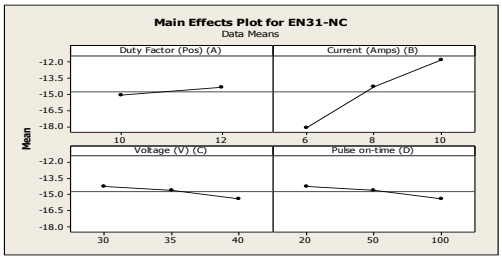

Fig 5.12: Work piece EN-31 (cryogenically treated)

Similarly in figures 5.10-5.12 the maximum values are optimal values and representing the results for less Tool Wear.

5.3 Effect of cryogenically treatment

From above main effect plots of MRR, TW and Ra, the optimum condition for them is concluded. After evaluating the optimal parameter settings, the next step of the Taguchi approach is to predict and verify the enhancement of quality characteristics using the optimal parametric combination. The estimated S/N ratio using the optimal level of the design parameters can be calculated: $\eta_{opt} = \eta_m + \sum_{i=1}^{o}(\bar{\eta}_i - \eta_m)$

Where $\eta_m$is the total mean S/N ratio $\bar{\eta}_i$is the mean S/N ratio at optimum level and **o** is the number of main design parameter that effect quality characteristic. Based on the above equation the estimated multi response signal to noise ratio can be obtained.

5.4 Comparison of results

Table5.1: Comparison of results

Electrode Material	Type of Electrode	Material Removal Rate	Tool Wear (%)	Surface Roughness (SR) (μm)
HCHCr	Cryogenically Treated	35.0917	0.05134	2.325
	Non Cryogenically Treated	31.0347	0.0784	7.7597
EN 8	Cryogenically Treated	37.1903	0.0385	1.6709
	Non Cryogenically Treated	30.907	0.0888	2.145
EN 31	Cryogenically Treated	15.0986	0.1758	1.1592
	Non Cryogenically Treated	13.8304	0.1499	2.3519

Table 5.2: Optimum combination of factors for the three response parameters

Electrode Material	Type of Electrode	Material Removal	Tool Wear	Surface Roughnes
HCHCr	Cryogenically Treated	A2 B2 C3 D3	A1 B3 C2 D2	A1 B3 C1 D1
	Non Cryogenically Treated	A2 B3 C3 D3	A1 B3 C2 D2	A1 B3 C1 D1
EN 8	Cryogenically Treated	A2 B3 C2 D2	A1 B3 C2 D2	A1 B3 C1 D1
	Non Cryogenically Treated	A2 B3 C3 D3	A1 B3 C2 D2	A1 B3 C1 D1
EN 31	Cryogenically Treated	A2 B3 C3 D3	A1 B3 C3 D3	A1 B3 C1 D1
	Non Cryogenically Treated	A2 B1 C3 D3	A1 B3 C3 D3	A1 B3 C1 D1

VI. CONCLUSIONS

1. Cryogenic treatment significantly affects the EDM machining parameters- tool wear decreases and surface finish of the work piece after machining improves sharply for all the three electrodes.
2. Some increment is also reported in Material Removal Rate (MRR) in all the three types of die steels after cryogenic treatment but in case of EN 31, it is comparatively less affected.
3. The best improvement in Tool Wear (56.64%) is reported by EN 8 followed by HCHCr (34.51%) and then EN 31 (14.39%).
4. The best improvement in surface finish (70.03%) is reported by HCHCr followed by EN 31 (50.71%) and then EN 8 (22.10%).
5. The optimum input parameters also get altered due to cryogenic treatment. It is observed that for the best value of surface roughness, pulse on-time undergoes a shift to the higher side for HCHCr; which may be an indication of strong crystal structure. Also, peak current undergoes a shift to higher side for the best values of tool wear for HCHCr which reflects the ability of tool electrode to withstand higher currents after cryogenic treatment.
6. Tool wear as well as surface finish of the work piece after machining are critical parameters in EDM. Since cryogenic treatment has a significant positive effect on both these parameters, it can be recommended that cryogenically treated die steels can be efficiently machined through EDM.

REFERENCES

[1]. Bannerjee, S., Prasad, B.V. S. S. S., Mishra, P. K. (1993), "A simple model to estimate the thermal loads on an EDM wire electrode". Journal of Materials processing Technology, Vol.39, pp.305-317.
[2]. Daniels, A. C. M. and Philps, George. (1978), "An energy distribution strategy in fast cutting EDM", Ann CIRP, Vol25 (2), pp. 521-525.
[3]. Dauw, D. F. and Albert, L. (1992), "About the evolution of tool wear performance in wire EDM ", Annals CIRP, Vol. 41(1), pp.221-225.
[4]. Dawei Luy and Jiju Antonyy, Optimization of multiple responses using a fuzzy-rule based inference system , int. j. prod. res., 2002, vol. 40, no. 7, 1613±1625, PP-33
[5]. Dhar A.R & Chhatopadhaya A.B, (2001), "The influence of cryogenic cooling on tool wear, dimensional accuracy and surface finish in turning AISI1040 and E4340 steels", Wear, Vol. 249, n10-11, pp 932-942.
[6]. Fores F.H, Yu.K & Nishimura,T,(2004) " Developing applications for Titanium", Journal of Cost-Affordable Titanium, Vol. 14, pp 19-26.
[7]. Guo, Z. N., Lee, T. C., Yue, T. M., Lau, W. S. (1997), "A study of Ultrasonic-aided Wire Electrical Discharge Machining", Journal of materials processing technology, Vol.63, pp.823-828.
[8]. Guo, Z. N., Lee, T. C., Yue, T. M., Lau, W. S. (1997), "Study on the machining mechanism of WEDM with Ultrasonic vibration of the wire", Journal of materials processing technology, Vol.69, pp.212-221.
[9]. Guo, Z. N., Wang, X., Huang, Z. G., Yue, T. M. (2002), "Experimental investigation into shaping particle-reinforced material by WEDM", Journal of Materials processing Technology, Vol.129, pp.56-59.
[10]. Han, Fujhu, Jiang, Jun., Dingwen, Yu. (2006), "Influence of machining parameters on surface roughness in finish cut of WEDM", International Journal of Advance manufacturing Technology, Vol. 67, pp. 134-140.
[11]. Hargrove, S. Keith. And Ding, Duowen.(2006), " Determining cutting parameters in wire EDM based on workpiece surface temperature distribution" International Journal of Advance manufacturing Technology, Vol. 154,pp. 24-27.
[12]. Huang, J. T. and Liao, Y. S., Hsue, W.J. (1999), "Determination of finish cutting operation number and machining parameters setting in wire electrical discharge machining", Journal of materials processing technology, Vol.87, pp.69-81.
[13]. Huang, J. T. and Liao, Y. S. (2003), "Optimization of machining parameters of wire EDM based on Grey relational and statistical analysis", International journal of production resources, Vol.41, No.8, pp.1707-1720.
[14]. Huang, Y. T., Zhu, Y. T., Liao, X. Z., Beyerlein, I. J.,Bouke, M. A., Mitchell, T. E. (2003), "Microstructure of cryogenic treated M2 tool steel" International Journal of Material Science Vol 339, pp. 241-244.
[15]. Juhr, H., Schulze, H. P., Wallenberg, G., Kunanz, K. (2004), "Improved cemented carbide properties after wire-EDM by pulse shaping", Journal of materials processing technology, Vol.149, pp.178-183.
[16]. Kinoshita, N., Fukui, M., Gamo,G. (1976) , "Study on EDM with wire electrode: a gap phenomenon", Annals CIRP, Vol.25 (1), pp.141-145.
[17]. Kinoshita, N., Fukui, M., Gamo, G. (1982) , "Control of wire EDM preventing from breaking", Annals CIRP, Vol.31, pp.111-114.
[18]. Kuriakose, Shajan. And Shunmugam, M. S. (2005), "Multi-objective optimization of wire electro-discharge machining process by non-dominated sorting Genetic Algorithm", Journal of materials processing technology, Vol.170, pp.133-141.

International Journal of Modern Engineering Research (IJMER)
www.ijmer.com Vol. 3, Issue. 4, Jul - Aug. 2013 pp-2177-2182 ISSN: 2249-6645

Energy Consumption and Distribution

Srinivasan Chinnammai
(Department of Economics, University of Madras, Chepauk, Chennai, TamilNadu, India)

ABSTRACT : *For as long as the global economy continues to operate on the basis of the limited energy and material supplies, its future prospects will be bleak. There are two incontrovertible reasons for this. Firstly, supply of fossil and mineral resources are limited; and secondly, the processes in which these resources are used inevitably also overstretch, damage and even destroy those limited planetary resources on which our lives depend: water, land and atmosphere. With respect to energy consumption, this second reason has become literally a burning issue.*

The fundamental economic reality of fossil fuels is that such fuels are found only in a relatively small number of locations across the globe, yet are consumed everywhere. The economic reality, by contrast, is that solar resources are available, in varying degrees, all over the world. Fossil fuel and solar resource use are thus poles apart – not just because of the environmental effects, but also because of the fundamentally different economical, logical and differing political, social and cultural consequences. These differences must be acknowledged if the full spectrum of opportunity for solar resources is to be exploited.

Therefore, this study concentrates on solar power as a renewable source of energy. It has many benefits compared to fossil fuels. It is clean and green, non-polluting and everlasting energy. For this reason it has attracted more attention than other alternative sources of energy in recent years. Many energy economists say that solar energy is going to play an increasingly important role in all our lives. To highlight the importance of such a source of energy becomes not only important but also inevitable.

Keywords: *Energy, power, Distribution, Consumption, Solar Power*

I. INTRODUCTION

Energy is a key infrastructure, which is the backbone and prime mover of the economic development of any country because it is required for all the sectors of economy which include agriculture, industries, service, information and technology, transport and others. Economic growth too is driven by energy in the form of finite resources such as coal, oil and gas or in renewable forms such as solar, hydro, wind and biomass, or its converted form, electricity.

Modern economists believe that an index of energy could be used as an index of capital because in "economic parlance, energy caters both to the direct consumption and the production of goods: as consumer goods, their consumption tends to vary with changes in income and consumer preferences; as an input in production, their availability and increasing quantities are a sine qua non of rising national income" [1].

Therefore, the availability of quality power in the required quantity is one of the most important determinants in the success of the country's development [2]. In addition providing adequate and affordable electric power is essential for economic development, human welfare and higher standard of living. India being a developing country with increasing population makes power the critical infrastructure. Hence, the study needs to know the real picture of power sector performance and its challenges therefore; power scenario of India has been examined.

II. REVIEW OF LITERATURE

There are divergent opinions regarding the application of energy as well as renewable source of energy. Accordingly different persons including scientists, technocrats, economists etc. view it from multiple angles. It is in this background, an attempt has been made to review the literature to understand the varied perspectives on conventional energy scenario, power development and its present position, renewable energy in general terms and solar energy in particular.

Anjaiah (2007) has highlighted in his intra-regional analysis, some economic issues pertaining to disparities in infrastructural facilities among the Indian states and union territories. But the infrastructure has wide spectrum such as roads and buildings, transport, tele-communication, power supply, banking and insurance services etc. Therefore, he has made an attempt to concentrate on power (electricity) issues such as production, supply and demand shortages and some other issues among the States. He has pointed out the reasons for the disparities among regions which is worth attention [3].

Vandana S. (2002) has stated that the conventional energy sources of the world like coal and petroleum are dwindling fast. Energy crisis have made us aware that and our total dependence on only one form of energy is not a wise step. The author has felt the need to tap additional sources of energy, to sustain satisfactory growth rate of our country. And she has mentioned that the ultimate solution of the energy crisis will be through the discovery of methods of harnessing the non –conventional energy sources. The extraction and utilization of non-conventional energy will not only help in meeting energy demands, but also help in their development [4].

Narasaiah M.L (2004) has focused on energy demand and supply of future in India. He has mentioned that the growing climate concerns would require massive reductions in fossil fuel use at the time when demand for energy is soaring. A shift to renewable energy sources such as solar energy and wind power holds great promise for meeting future energy demands without adverse ecological consequence, as per the author [5].

Chinnammai & Sasikala (2008) have, in their paper, highlighted the increasing energy pattern in India, characteristics of the energy in rural and urban areas, its impact on women, the various solar energy appliances available and

have empirically found out that solar energy can enhance the role of women. They have also forwarded various possible approaches to facilitate the sustenance of solar energy in India. By reaping the benefits of using solar energy appliances the increasing energy pattern, characteristics of household energy in rural and urban areas, its impact on women [6].

The Times of India (2008) has discussed Eco-friendly solar signals to direct traffic in Delhi which is now looking at installing solar-powered traffic signals at major intersections in the city. With this, traffic jams caused by signals rendered non-functional due to power failure or heavy rain may soon become a thing of the past. The traffic police are also installing inverters for back up at major points. The technology is expensive – and maintenance is high. With right research and development in this field experts feel that a futuristic technology, solarization, is an efficient means [7].

III. METHODOLOGY

The present study is empirical, based on secondary sources of data. The framework of the analysis has been constructed from the data collected through secondary sources. Secondary data, regarding net availability of power, distribution of power supply under state and all-India level have been collected from administrative reports, planning commission reports, books etc. These data have been used to highlight and substantiate the theoretical aspects of the solar power distribution. An attempt has been made to focus on the solar power sector growth and distribution in India.

IV. OBJECTIVES OF THE STUDY

To study the real picture of power sector performance and its challenges and
To analyse power scenario in India.

V. RESULT AND DISCUSSION

1.1 Indian Scenario

India is both a major energy producer and a consumer. India currently ranks as the world's seventh largest energy producer, accounting for about 2.49 percent of the world's total annual energy production. It is also the world's fifth largest energy consumer, accounting for about 3.45 percent of the world's total annual energy consumption in 2004. Since independence, the country has seen significant expansion in the total energy use with a shift from non-commercial to commercial sources. The share of commercial energy in total primary energy consumption rose from 59.7 percent in 1980-81 to 72.6 percent in 2006-07.

Table: 1 Demand and Supply of Primary Energy in India (In Mtoe #)

	1960-61	**1970-71**	**1980-81**	**1990-91**	**2000-01**	**2006-07**	**2011-12**
Domestic production of Commercial Energy	36.78	47.67	75.19	150.01	207.08	259.56	435
Demand of Commercial Energy	42.82	60.33	99.82	181.08	296.11	390.93	546
Non-Commercial Energy	74.38	86.72	108.48	122.07	136.64	147.56	169
Total Primary Energy Demand	117.20	147.05	208.30	303.15	432.75	538.49	715
Net Imports	**6.04**	**12.66**	**24.63**	**31.07**	**89.03**	**131.37**	**111**

Source: Planning commission Government of India'2008 Note: # Mtoe = million tonne of oil equivalen

i. Domestic production of commercial energy includes coal, lignite, oil, natural gas, hydro power, nuclear power and wind power.
ii. Net imports include coal, oil and LNG imports.

It must be noted, however, that India's per capita energy consumption is one of the lowest in the world. India consumed 455 kgoe per person of primary energy in 2003, which is around 26 percent of world average of 1750 Kgoe in that year. As compared to this, per capita energy consumption in China and Brazil was 1147 Kgoe and 1232 Kgoe, respectively [8].

Table: 1 shows the trend of primary energy demand and supply between 1960-61 and 2006-07 and projected requirement for 2011-12. While total primary energy demand registered 117.20 million tonne of oil equivalent (Mtoe) in 1960-61, it increased to 538.49 Mtoe during 2006-07. It has been projected to increase to 715 Mtoe in 2011-12. From the table it is observed that the net imports is on the rise; it can be inferred that India is not self sufficient in meeting our country's total energy demands.

The demand for energy, particularly for commercial energy, has been growing rapidly with the growth of the economy, changes in the demographic structure, rising urbanization, socio-economic development, and the desire for attaining and sustaining self-reliance in some sectors of the economy. The demand for commercial energy has increased to 390.93 mtoe during the period 1960-61 to 2006-07, it is projected to further the increase to 54.6 mtoe in 2011- 12. Non-

commercial energy resources include the traditional fuels such as wood; cow dung, crop residue, and biogas constitute a significant quantity of total primary energy demand. A large share of this fuel is used by the households, particularly in rural areas, for meeting their cooking and heating needs.

The consumption of 147.56 Mtoe of non-commercial energy in 2006-07 includes consumption of fuel wood, dung, and agricultural waste. It is projected to be at 169 Mtoe in 2011-12. From the table it is observed that there is a constant increase in demand for primary energy. Pattern of consumption also disturbs the power sector scenario; sudden increase in one sector's consumption level affects another sector. Nowadays domestic sector consumption of power is ever increasing due to increasing standard of living, increase in population and impact of globalization on social, economic and cultural stages of development. The next section has analyzed the distribution of consumption pattern of electricity in India. Table 2 indicates that consumption pattern of power by domestic, commercial, industry, railway traction, agriculture and others. The total utilization of power by industry has come down from 58.4 percent in 1980-81 to 45 percent in 1990-91. It further declined to 34 percent in 2000-01. There could be various reasons for this declining consumption of power. Many industries have switched to alternative sources of fuel while many others have established independent power producing plants.

Table: 2 Consumption Pattern of Electricity in India (In Percent)

Year	Domestic	Commer -cial	Industry	Railway Traction	Agricul -ture	Others	Total
1980-81	11.2	5.7	58.4	2.7	17.6	4.4	100
1981-82	11.6	5.8	58.8	2.8	16.8	4.2	100
1982-83	12.7	6.1	55.4	2.8	18.6	4.4	100
1983-84	12.9	6.4	55.8	2.6	17.8	4.5	100
1984-85	13.6	6.1	55.2	2.5	18.4	4.2	100
1985-86	14.0	5.9	54.5	2.5	19.1	4.0	100
1986-87	14.2	5.7	51.7	2.4	21.7	4.3	100
1987-88	15.2	6.1	47.5	2.5	24.2	4.5	100
1988-89	15.5	6.2	47.1	2.3	24.3	4.6	100
1989-90	16.9	5.4	46.0	2.3	25.1	4.3	100
1990-91	16.0	5.9	45.0	2.2	26.4	4.5	100
1991-92	17.3	5.8	42.0	2.2	28.2	4.5	100
1992-93	18.0	5.7	40.9	2.3	28.7	4.4	100
1993-94	18.2	5.9	39.6	2.3	29.7	4.3	100
1994-95	18.5	6.1	38.6	2.3	30.5	4.0	100
1995-96	18.7	6.1	37.8	2.3	30.9	4.2	100
1996-97	19.7	6.2	37.2	2.4	30.0	4.5	100
1997-98	20.3	6.5	35.4	2.3	30.8	4.7	100
1998-99	21.0	6.4	33.9	2.4	31.4	4.9	100
1999-2000	22.2	6.3	34.8	2.6	29.2	4.9	100
2000-01	23.9	7.1	34.0	2.6	26.8	5.6	100

Source: Buddhadeb Ghosh & Prabir De, India Infrastructure Database 2005, Vol.II, Book well, New Delhi, pp1087 to 1089.

Large industries are setting up their own captive power plants, instead of depending upon the inadequate and often undependable public utilities. However, consumption of power by agricultural sector in the total utilization of power has increased considerably over the years from 17.6 percent in 1980-81 to 26.8 percent in 2000-01. Increase in energized pump sets over the years and the promise made by most of the State Governments to provide free electricity for the farmers are considered to be the main reason for growth in the consumption of power by agricultural sector.

Table: 3 State Wise Consumption Pattern of Electricity in 2007– 2008 (In Mu)

Sl. No	State /UT	Domestic	Commer -cial	Industry	Agricul -ture	Railway Traction	Miscel- laneous	Total
1.	Andhra Pradesh	10679	2737	15383	15241	1209	3613	48861
2.	Arunachal Pradesh	48	10	77	0	0	35	170
3.	Assam	992	331	834	20	0	369	2544
4.	Bihar	1700	372	1103	659	385	175	4394
5.	Chattishgarh	1883	359	5150	1459	696	1066	10613
6.	Delhi(DVB)	7142	5008	2832	37	148	1161	16328
7.	Goa	602	160	1590	39	0	157	2548
8	Gujarat	7565	3534	20238	10946	588	1364	44236
9	Haryana	3477	1144	4990	7335	442	872	18260
10	Himachal Pradesh	1051	247	3100	27	0	595	5020

11	Jammu & Kashmir	1399	213	950	271	0	1197	4030
12	Jharkand	1346	225	8701	67	891	158	11387
13	Karnataka	6207	3614	11105	10844	22	2443	34235
14	Kerala	5624	1910	3198	241	109	708	11791
15	Madhya Pradesh	4943	1174	7516	7536	1541	882	23591
16	Maharashtra	15389	6476	29034	12676	2024	2332	67931
17	Manipur	118	13	9	1	0	58	197
18	Megalaya	212	39	508	1	0	134	893
19	Mizoram	116	9	2	0	0	52	179
20	Nagaland	127	10	13	0	0	33	183
21	Orissa	3313	705	6020	172	523	565	11299
22	Punjab	6349	1849	10558	10022	110	999	29887
23	Rajasthan	4464	1530	7407	8145	297	1816	23658
24	Sikkim	61	42	89	0	0	68	260
25	Tamil nadu	13006	6286	21114	10717	516	1314	52953
26	Tripura	220	41	65	24	0	48	398
27	Uttar Pradesh	13704	4089	8591	6200	653	4294	37532
28	Uttarakhand	1163	712	2288	300	9	263	4736
29	West Bengal	7001	3160	11335	1110	944	2698	26248
Total (States)		**119901**	**45999**	**183799**	**104090**	**11107**	**29469**	**494363**
Total (UTs)		**1017**	**686**	**5625**	**94**	**0**	**191**	**7614**
ALL INDIA		**120918**	**46685**	**189424**	**104184**	**11107**	**29660**	**501977**

Source: All India Electricity Statistics General Review 2009 by CEA

The same trend is seen in the domestic sector too. Consumption of power by domestic sector in the total utilization of power has increased from 11.2 percent in 1980-81 to 16.0 percent in 1990-91. It further increased to 23.9 percent in 2000-01. Growth and availability of various electronic goods for a quality living is considered to be the main reason for growth in consumption of power by domestic sector. But the growth seen in the consumption of power by commercial sector was very marginal. Consumption of power by commercial sector was 5.7 percent in the total utilization of power in 1980-81 and it increased to 5.9 percent in 1990-91 and 7.1 percent in 2000-01.

Table 3 clearly shows that out of 5, 01,977 million units (MU) total consumption, Industrial category accounted for 1, 89,424 MU, followed by Domestic sector for 1, 20, 918 MU. Of the total power consumption, other categories that is Agriculture consumed 1, 04184, Commercial accounted for 46,685, Railway consumed 11,107 and miscellaneous was about in terms of consumption 29,660. From the above table, there is a high rate of consumption in all sectors of some States. This gives a picture of the density of population, industrial, and infrastructural development of the Country.

The table further reveals that Maharastra is the leading state in the consumption of electricity by the following sectors, 15389 MU by domestic, 6476 MU by commercial, 29034 MU by industrial sector and 12676 MU by agricultural sector and followed by TamilNadu which consumed the high level of electricity at the rate of 13006 MU by domestic sector, 6286 MU by commercial sector, 21114 MU by industrial sector and 10717 MU by agricultural sector.

On the other hand, Arunachal Pradesh and Sikkim has shown the lowest consumption of electricity in India, because of their population and energy utility, at the rate of 48MU by Domestic sector, 10 MU by commercial sector, 77MU by industrial sector and 61 MU by Domestic sector, 42 MU by commercial sector, 89 MU by industrial sector respectively.

It is evident from the discussions above that India and TamilNadu are short of all energy resources and that coal will dominate India's energy basket. We need to expand our resources through research and development in the field of exploration of alternative sources of energy, energy saving techniques and usage of renewable sources of energy etc.

The environmental impact of various energy options is also a growing concern owing to widespread use of energy. It is necessary that the demand of energy in the country is met in an environment-friendly and sustainable manner. Therefore it is the need of the hour to pay much attention on renewable resources which are economical in long run and eco-friendly. Within renewable energy, solar power could be important for attaining energy independence as well as green house gas-free energy system in the long run.

The Sun is our nearest star and it is the source of energy for life on Earth. It is about 150 million km away a distance which sunlight cover in 8 minutes. The Sun is about 3, 00,000 times heavier than Earth. The energy output, solar constant is about 3.8 X 10^{33} ergs / sec. within forty minutes of the sun shining on the Earth, the Sun will have given off as much energy as the entire world population will use in a year. Only about one percent of this energy put out by the Sun is harnessed and utilized by earth's inhabitants.

Solar power can be harnessed in two ways, in the form of heat (or thermal energy), and in the form of light energy. The light rays of solar energy are harnessed for power generation through solar cells and are called Solar Photovoltaic (SPV) systems, where light is directly converted into electricity using silicon (solar) cells. The electricity thus generated can be used for lighting or other electrical applications [9].

1.2 Indian Scenario of Solar Energy

India was among the first countries in the world to have launched a major programme for renewable energy in the 1970s. During the Fifth Five-Year Plan (1975-80), a specific provision was made for Research and Development (R&D) on new and renewable sources of energy. During the Sixth Five-Year Plan (1980-85), a separate Department of Non-conventional Energy Sources (DNES) was set up in 1982. The programmatic emphasis of the DNES during the 1980s was on the development, dissemination, and demonstration of various Renewable Energy Technologies (RETs). The programme was led by government subsidies.

During the Seventh Five-Year Plan (1985-90), this programme was further intensified and major advances were made in areas such as solar thermal and solar photovoltaic among others. The renewable energy programme in India got a major boost when the DNES was upgraded to a full-fledged Ministry of Non-conventional Energy sources (MNES) in 1992. Around this time, it was realized that faster diffusion of renewable energy sources required great reliance on commercialization through fiscal rather than financial incentives involving the private sector. Thus, after the formation of the Ministry, the thrust of the programme has been on market development in order to facilitate and catalyze commercialization. India is probably the only country in the world with an independent ministry for the promotion of RETs in the energy economy of the country [10].

1.3 Progress of Solar Energy in India

In the area of solar energy, India has today achieved a leading position in the world in the development and use of technology. It is the second largest manufacturer in the world of crystalline silicon modules. Solar device based industrial production has touched a level of 7 MW/year.

The next section has assessed the usage of various levels of solar power in India.

Table: 4 Achievement of Solar Device in India (1996 To 2010)

Source/ systems	Units	Achievement up to 1996	Achievement up to 2005	Achievement up to 2007.	Achievement up to 2010.
I. Solar thermal Systems					
(i). Solar Water Heater	Sq.m	3,64,354	1 million collector area	2 .15 million collector area	3.25 million collector area
(ii.)Solar Cookers	Nos.	4,06,642	5,75,000	6,20,000	6,00,072
II.Solar Photovoltaic Systems					
(i) SPV Lantern	Nos	81,059	5,60,295	5,85,001	7,92,285.
(ii) SPV Street lights	Nos	32,870	54,795	69,549	88,297.
(iii) SPV Home lights	Nos	37,359	3,42,607	3,63,399	5,50,743.
(v)SPV Pumps	Nos	1,820	6818	7,068	7,247
III. SPV Power plants					
(a) Grid connected		-	-	2.12 MW	10.28 MW
(b) Stand alone		909.3 KWp	1566 KWp	2.18 MW	2.39 MW

Source: Annual reports of MNES, Government of India' 1996, 2005, 2007&2010.

Table 4 shows the cumulative achievements of solar device installed from 1996 to 2010. There were 3, 64,354 sq.m area covered by Solar water heaters and 4, 06,642 solar cookers were utilized in the country. This achievement rate has increased progressively by the policy of the government of India.

This apparently reveals with the current status of solar device installation. During 2010, 3.25 million sq.m areas have been covered by solar water heater devices installation. In the same year, 6, 00,072 lakh solar cookers have been distributed for usage. Under solar photovoltaic programme 792,285 numbers of solar lanterns, 88,297 numbers of solar street lighting systems and 5, 50,743 numbers of solar home lighting have installed. Besides these achievements 7247 numbers of solar water pumping installed for the benefit of agrarian society. More than 12.67 MW have so far been installed for voltage support for weak grids, for peak load saving and as diesel saving. This shows solar device technology not only entered into heating and lighting but also it extends its possibility in the area of water pumping and power producing through grid and off-grid.

VI. CONCLUSION

It can be seen that the solar energy technology is a natural endowment available freely and abundantly in the nature. At the time of increasing energy crisis, its full utilization will not only benefit the people but also helps to preserve the environment. Besides, it will be a contributing factor for improving the quality of life. Definitely, in future solar energy technology will become more popular and the development of this energy will drastically reduce the consumption of

commercial sources of energy like electricity, petrol, diesel, kerosene, natural gas etc. which in turn protects the environment and makes pollution free society.

REFERENCES

[1] S. Ramaswamy and T. Tamizh Chelvam, Energy and Economic Development, *Infrastructure Development for Economic Growth*, (Deep & Deep publications, New Delhi, 1997) pp.118
[2] Kula Saikia, *Energy Planning: Relevant Issues, Energy and Energy Resource Management,V.S. Mahajan, S.K. Agnihotri and R.P. Athparia (eds)* (Deep & Deep Publications, New Delhi,2000) pp23-24.
[3] Anjaiah J. ,Inter-Regional disparities in Electricity Generation in India *Southern Economist, Vol.46, No.14, November 15, 2007* pp5-8.
[4] Vandana S., Alternative energy, (APH publishing corporation, New Delhi, 2002).
[5] M.L.Narasaiah , Energy, Irrigation and Water supply, (Discovery Publishing house , New Delhi, 2004).
[6] S.Chinnammai, & M. R. Sasikala ,Women Environment and Energy, *Indian Journal of Human Rights and Social Justice , vol.3 No. 1-2 ,2008*, pp 327-353.
[7] Eco-friendly solar signals to direct traffic, (*The Times of India, 8th September, 2008).*
[8] Eleventh Five Year Plan 2007-12, Vol. III ,Planning Commission Government of India, (Oxford University press, New Delhi),pp342.
[9] Wolfgang Palz, Solar Electricity – An Economic Approach to Solar Energy, (Butterworths, UNESCO ,1978) pp 73.
[10] Sustainable Energy Development in India (Eu – India partnership for technology cooperation, organized and published by Teri, New Delhi, and 1999).pp22.

International Journal of Modern Engineering Research (IJMER)
www.ijmer.com Vol. 3, Issue. 4, Jul - Aug. 2013 pp-2183-2186 ISSN: 2249-6645

Worker Scheduling for Maintenance Modeling Software

Samuel C. Littlejohn[1]

*(Department of Industrial and Electrical Engineering Technology, South Carolina State University, United States of America)

ABSTRACT: *This article presents a brief discussion about the scheduling issues related to a maintenance modeling simulation software called, Improved Performance Research Integration Tool (IMPRINT). One of the areas of use for IMPRINT is for maintenance systems. A concise description of IMPRINT is presented. A description of possible application environments for use by IMPRINT is given. The discussions center on maintenance modeling and scheduling because these are primary applications for IMPRINT utilization.*

Keywords: *Maintenance, Scheduling, Maintenance Scheduling, Personnel Scheduling*

I. INTRODUCTION

In general, maintenance systems are created for the purpose of ensuring the serviceability and safety of equipment or systems so that maximum possible performance levels can be achieved. Scheduling and planning are two vital functions of the maintenance modeling paradigm. Scheduling is the arrangement of resources to be used. Planning is the act of ensuring that resources and tools are in order before the required tasks are to take place.

Within the construct of maintenance planning and scheduling, there are two categories. Category one consists of preventive maintenance, routine maintenance, and scheduled overhauls. Category two consists of unscheduled maintenance due to emergencies. Any maintenance schedule should consider both known and unknown circumstances. The primary objective of this research effort is to determine a possible scheduling approach for maintenance models of IMPRINT. IMPRINT is an acronym for Improved Performance Research Integration Tool.

II. IMPRINT OVERVIEW

IMPRINT is a simulation tool that can be used to perform maintenance modeling and analysis. IMPRINT maintenance models calculate the required manpower (number of maintenance workers needed to perform any desired task(s)). In this section, we present a brief overview of IMPRINT.

IMPRINT is a Microsoft Windows® based human performance modeling environment that has been developed by the Army Research Laboratory [1]. It is a stochastic network modeling tool that is designed to help assess the interaction of soldier and system performance throughout the system life cycle. The design originated from previous field testing and system upgrades.

IMPRINT is a simulation tool that is used for three primary reasons. Its first use is for the purpose of helping to set realistic system requirements. It is also used in order to identify soldier-driven constraints on system design. IMPRINT also has the ability to evaluate the potential of available manpower and personnel to effectively operate and maintain a system under given environmental stressors. In a strictly military context, IMPRINT can be used to target soldier performance concerns in system acquisition. IMPRINT is also used to estimate soldier-centered requirements early in the decision process. Another implementation of IMPRINT is as a simulation tool. It incorporates task analysis, workload modeling, performance shaping functions, degradation functions, stressors, and embedded personnel characteristics data. IMPRINT is used to facilitate a number of human factors analyses such as manpower projection, performance under environmental stress, and maintenance under manpower requirements[1].

Micro Saint® is the operating engine that is used by IMPRINT. Micro Saint is an embedded discrete event task network modeling language. The simulation employs task-level information to construct networks that represent the flow, performance time, and accuracy of a given system for operational and maintenance missions. The military uses IMPRINT to model both crew and individual soldier performance. In some instances, IMPRINT utilizes workload profiles that are generated so that crew-workload distribution and soldier-system task allocation can be examined. Other simulation applications may involve a maintainer (i.e., the actual maintenance worker) workload being assessed along with the resulting system availability. Furthermore, by using embedded algorithms, IMPRINT can model the effects of personnel characteristics, training frequency, and environmental stressors on overall system performance. Manpower requirement estimates can be generated for a single system, a unit, or Army-wide. IMPRINT outputs can be used as the basis for estimating manpower lifecycle costs[1].

III. IMPRINT MAINTENANCE MODELS

IMPRINT has maintenance modeling capabilities to predict manpower requirements: reliability, availability, and maintainability (system RAM). This is done by simulating the maintenance requirements of a unit as systems are at different stages. The first stage of a mission is the initiation stage, or the time at which the system operators are sent out. The next mission stage is where any required maintenance is performed. The final mission stage is after maintenance has occurred and the system is finally sent back into a pool of available systems.

When a particular system comes into maintenance, IMPRINT prioritizes and schedules repair based on the pools of maintainers with specialties available in the particular maintenance level that is required. There are other issues that affect the maintenance system such as spare availability, combat damage, maintenance shifting, and the criticality of individual system component failures.

There are certain limitations in the system RAM analysis capability that will affect the results of the program. First, the model assumes that all unit level (or first level) maintenance is performed "on equipment." This means the system will not be considered "available" to be sent out on any other mission until all unit level maintenance is completed. Second and third level maintenance (referred to as direct support (DS) and general support (GS)) are assumed to be performed "off equipment." In other words, the system is considered available before the repairs are complete because it is modeling maintenance as if the failed component has been removed from the system for repair. The model also assumes that maintenance is prioritized so that the system with the smallest amount of total repair time is repaired first. This is commonly referred to as shortest processing time (SPT) scheduling. All unit level maintenance must be completed before any DS level maintenance can begin. In the same way, all DS level maintenance must be completed before any GS level maintenance can begin.

IMPRINT's maintenance model is considered very high fidelity. A key aspect of the system RAM analysis capability is the concept of failure clocks. Each component of each system in the analysis has its own failure clock. The failure clock is used to provide a realistic estimation of component failures, and thus system maintenance requirements, throughout a particular scenario. The next sections discuss possible application environments for use by IMPRINT. The discussions center on maintenance modeling and scheduling because these are primary applications for IMPRINT utilization.

IV. MAINTENANCE MODELING

Under the umbrella of reliability and maintainability, [2] identifies maintenance planning and maintenance scheduling as areas that are directly related to this purpose. According to [2], these are the two most important elements of the maintenance function. They are a requirement for any effective maintenance control. Fig.1 shows a simple schematic breakdown of these two areas in maintenance modeling.

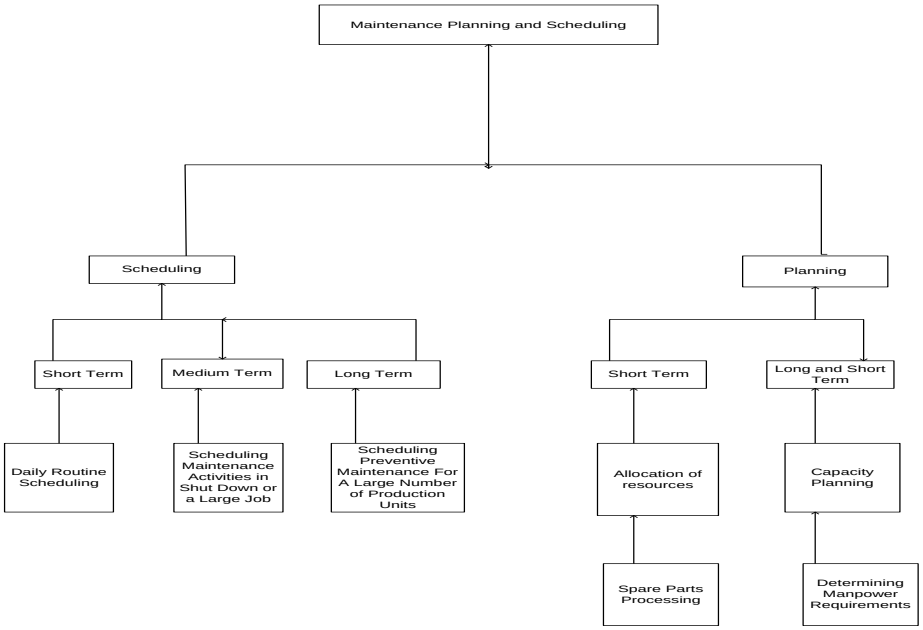

Figure 1: an overview of maintenance planning and scheduling areas [2]

There are three categories of maintenance requirements: manpower, material, and equipment. The most costly of these three categories is manpower. Human resources tend to have high variability when compared to material and equipment. By varying the usage of human resources, maintenance managers are able to have significant control over maintenance scheduling.

Reliability and maintenance are closely related. High quality maintenance corresponds directly to high reliability for any given piece of equipment. Complex maintenance equipment can account for a significant portion of costs associated with a particular piece of equipment. [3] Estimates that military maintenance costs encompass almost one-third of all incurred operating costs.

Three of the most common terms that are used are mean time between failures (MTBF), mean time to repair (MTTR), and availability. MTBF corresponds to the expected time between failures and MTTR represents the expected value of the time it takes to repair a piece of equipment. Availability is the average fraction of time the equipment operates.

Availability can be defined in terms of MTTR and MTBF:

(1) Availability $= \frac{MTBF}{MTBF + MTTR}$

For any operating equipment that exhibits an exponential failure behavior, it can be beneficial to replace the equipment even before it fails. This is especially important in situations in which the cost of replacing a piece of equipment before it fails is much less than the cost of having to replace a piece of equipment if it fails during operation. Because of associated costs, there are some military equipment that are replaced rather than repaired before they get to a point where they completely fail during operation. Therefore this equipment must be maintained on an ongoing basis so that it will not reach the point where repair is impossible. In these cases preventive maintenance is vital.

V. TOTAL COMPLETION TIME

It is important to note that a military maintenance scheduling system can possess characteristics of open shop scheduling with a minimizing total completion time objective. [4] Consider the problem of minimizing total completion time. They consider a unit-time open shop with release time and a constant number of machines ($Om \mid p_{ij} = 1, r_i \geq 0 \mid \sum C_i$). *Om* represents an open shop in which there are *m* number of nonparallel machines, *pij* is the processing time of job *i* on machine *j*, *ri* is the release time of job *i*, and the objective is to minimize the total completion time. Note that a unit time open shop is one in which all processing times are equal to one. They present an *O*(*n2*) dynamic programming algorithm to solve this problem. They then apply this to problems in which each operation requires one unit of an additional resource. This allows many problems to be solved in polynomial time. They believe that there is always an optimal schedule for in cases where each job is completed before time *Ci+m2*. The authors state two conclusions. The first is that this algorithm is not useful for a problem in which there is a large number of machines. The second conclusion is that if the number of machines is part of the input, the problem remains open.

A discussion of the scheduling of a two-machine open shop system with a hierarchical objective of minimizing the total completion time that is subject to minimum makespan is presented in [5]. They illustrate by use of counterexamples the distinct structure of the $O2 \| \sum C_i \mid C_{\max}$ problem in comparison to the related $O2 \| \sum C_i$ problem. They showed that it is possible to develop polynomial-time heuristics for special cases of the problem as long as there is the presence of a strongly dominant machine or a strongly dominant job. They also illustrate how this case can be extended to a similar three-machine problem represented as follows: ($O3 \| \sum C_i \mid C_{\max}$).

The problem of scheduling in a system containing two-machine preemptive open shops is discussed in [6]. The author develops a dynamic programming algorithm that can optimally solve the problem in both weighted and un-weighted forms. He proposes an efficient heuristic for solving large-sized problems. His computational results show that this proposed algorithm can handle problems with up to 30 jobs within a reasonable amount of time. He states that this heuristic has an average percentage deviation of less than 0.5% from the optimal solution for problems with 30 jobs or less.

VI. Maintenance Scheduling Introduction

The previous section discussed how a scheduling environment that can be utilized by IMPRINT may be classified as open shop. However it should be understood that that application of IMPRINT is not restricted to any particular maintenance scheduling system category. In fact many maintenance systems are not open shop. Maintenance scheduling problems can be modeled as job shop scheduling problems [7]. This is accomplished by first allowing a job in the job shop problem to be the maintenance work order. In this same way a machine in the job shop problem is considered to be a maintenance worker. This method transforms the job shop problem into a problem of scheduling workers to process work orders. In this context, a work order is created for preventive maintenance or for repair of machine breakdown. In order to gain insight into the relationship between scheduling theory and the notion of maintenance scheduling, the thesis first describes assumptions that define the traditional scheduling problem and then highlights the characteristics of the maintenance scheduling problem that distinguish it from the conventional scheduling framework.

6.1 Conventional Scheduling

Classical scheduling theory is well known to be inadequate in dealing with many real world problems. [8] lists the twelve assumptions that are common in the development of the classical scheduling theory. These twelve assumptions are discussed in brief.

1. The classical scheduling theory classifies an entity as being any job that is denoted by a work order. This means that a work order can actually be processed by one or more workers depending on the need for skills and the size of the job. The problem with this assumption is that it requires workers to process each operation of the work order in series. In other words, according to this assumption, workers are not allowed to work simultaneously on the same order.
2. Classical scheduling theory prohibits preemption. However, the ability to pre-empt a schedule is vital in any maintenance environment due to production breakdowns and other unpredictable events. Preemption allows the ability for workers to be reassigned to a different work order based on prioritization of jobs. In the same context, preemption also allows work orders to be fulfilled in stages, instead of having to be performed all at one time.

3. Each job has a specified number of operations, with no more than one operation per machine. This limits the ability of a worker to process more than one individual operation for each work order. This assumption disallows job cancellations, which limits the problem to being only deterministic in nature.
4. Classical scheduling theory assumes that processing times are independent of schedule. This assumption does not hold true in situations where the set-up time for a maintenance job is dependent on which job precedes it.
5. In process inventory allowance is permitted.
6. Maintenance workers with similar skills can be modeled as parallel machines with nonidentical processing speeds.
7. Machines (and consequently workers as well) are allowed to be idle.
8. A machine may not process more than a single operation at any given time. However, [7] states that this assumption does allow for a maintenance worker to work on two or more work orders as long as the work orders are close by (i.e., at the same location).
9. Machines (or workers) never break down, and are available throughout the scheduling period.
10. Technological constraints are always known in advance.
11. There is no randomness (everything is deterministic). Both the number of jobs and machines are fixed. The processing and ready times are known and fixed as well.
12. There are no cancellations. This means that once a job for corrective maintenance is scheduled, it cannot be unscheduled.

6.2 Maintenance Scheduling

Has also identified characteristics of maintenance scheduling which distinguish it from other scheduling archetypes. These characteristics are as follows:

1. Non-repetitive jobs are inherent to maintenance scheduling problems (i.e., all jobs do not have to be the same; each job can be different from one another).Maintenance jobs all have varying difficulties,performed tasks,and completion times.
2. Maintenance jobs include a dynamic diagnostic process. The scope of a required maintenance on a machine cannot be fully known until every problem is identified. This means that the complete nature of a maintenance task is not known until some form of diagnostic is performed. In reality, the amount of required maintenance can either be greater than or less than what is first projected.
3. Preventive maintenance due dates are specified as preferred time intervals. However, these dates (or schedules) can be changed (optimized) once objective criteria are selected. These objective criteria can include an accommodation of maintenance worker traveling time, to schedule concurrently with a breakdown task on the same machine, or a preventive maintenance task may be scheduled early to occur simultaneously with the downtime policy of an organization.
4. Maintenance scheduling also has the ability to be altered due to outside factors such as the rescheduling of other tasks.
5. Maintenance tasks do not have a fixed scope. Scheduling maintenance for machine breakdown requires the scheduler to consider various contingencies.
6. Maintenance scheduling must decide whether to schedule the maximum amount of maintenance allowed in order to perform all possible preventive maintenance requirements.
7. Maintenance schedulers commonly schedule only the minimum amount of maintenance that is necessary in order to get the machine back online.
8. Maintenance scheduling schedules for a level of maintenance that is somewhere in between the maximum and the minimum possibilities based on economic justifications.

VII. CONCLUSION

A brief summary of the research areas within maintenance, modeling, and scheduling was given. The foundational aspects of maintenance modeling were presented also. The differences between conventional scheduling and maintenance scheduling have been shown. This research has determined that it is beneficial to view certain maintenance scheduling environments that are modeled by IMPRINT as open shop environments. The objective of this maintenance scheduling environment is to increase the amount of time that the military systems are available. The article has briefly covered some of the pertinent issues related to understanding IMPRINT. Because IMPRINT is a tool that can be used for maintenance modeling and analysis, understanding these scheduling issues are important for proper utilization of this tool. This paper has not discussed possible applications of IMPRINT outside of maintenance scheduling. Other uses for this tool may be available. More work could be performed in order to determine optimum uses for IMPRINT.

REFERENCES

[1] ARL (2000). "IMPRINT Analysis Guide."
[2] Duffuaa, S. O.. *Maintenance modeling and optimization*. (Boston, Kluwer Academic Publisher, 2000).
[3] Nahmias, S. *Production and Operations Analysis*, (McGraw-Hill/Irwin, 2001).
[4] Woeginger, T. A.. Minimizing the total completion time in a unit-time open shop with release times. *Operations Research Letters* (20), 1997, 207 - 212.
[5] Koulamas, K. A.. Open shop scheduling with makespan and total completion time criteria. Computer and Operations Research (27): 2000, 15 - 27.
[6] Liaw, C.-F.. Scheduling two-machine preemptive open shops to minimize total completion time. Computers and Operations Research, 2003.
[7] Leigh, W., & Paz, N. (1993). Maintenance scheduling: issues, results and research needs. *International Journal of Operations and Production Management*. 1993, 47 - 69.
[8] French, S. (1982). *Sequencing and scheduling: An Introduction to the Mathematics of the Job Shop*. (Chichester, Ellis Horwood Limited, 1982).

International Journal of Modern Engineering Research (IJMER)
www.ijmer.com Vol. 3, Issue. 4, Jul - Aug. 2013 pp-2187-2189 ISSN: 2249-6645

Design and Stress Analysis of various cross section of Hook

Govind Narayan Sahu[1], Narendra yadav[2]
Department Mechanical Engineering
B.E. Scholar, Maha Maya College of Technology, Raipur Chhattisgarh India[1]
Asst. Prof., Rungta College of Engineering and Technology, Raipur Chhattisgarh India[2]

Abstract: *Hooks are employed in heavy industries to carry tonnes of loads safely. These hooks have a big role to play as far as the safety of the crane loaded is concerned. With more and more industrialization the rate at which these hooks are forged are increasing. This work has been carried out on one of the major crane hook carrying a larger load comparatively. The cad model of the crane hook is initially prepared with the help of existing drawings. It is then followed by implementation of modified cross section of hook in the static structural analysis workbench of catia v5. These results lead us to the determination of stress and deflections in the existing model. In order to reach the most optimum dimensions several models in the form of different dimensions of hook were tested and the most optimum dimension was selected. The selection was based on the satisfaction of several factors in the form of load carrying capacity, stress induced and deflection.*

Keywords: *Computer Aided Design (CAD), Computer Aided Engineering (CAE), Cross Section Area (CSA), Von Misses Stress (VMS).*

I. INTRODUCTION

Development of a hook is a long process which requires number of tests to validate the design and manufacturing variables. We have used CAE to shorten this development thereby reducing the tests. A systematic procedure is obtained where CAE and tests are used together. In fact, their use has enabled the automakers to reduce product development cost and time while improving the safety, comfort, and durability of the crane hook they produce. In this paper work is carried out on hook of any heavy crane. The objective of this work is to carry out computer aided design and analysis of hook. The material of the hook is Steel. The CAD modeling and finite element analysis is done in CATIA V5R20.

II. MATERIAL ASSIGNMENT

Many industries manufacture Hook by steel material. These materials are widely used for production of hook and beams of different cross sections. Other than the load carrying capacity of hook, it must also be able to absorb the vertical load and deflection (induced due to variable loads). Ability to store and absorb more amount of strain energy ensures the safety of crane. The mechanical properties of steel has been shown in Table2.1below

Table 2.1 Mechanical Properties of Steel Hook

PARAMETER	Material selected	Young's Modulus (E)	Poisson's Ratio	Tensile Strength Yield	Density	Thermal Expansion	Cross section area	Applied Load
VALUE	Steel	2x10^11 N/m^2	0.266	2.5e+008 N/m^2	7860 kg/m^3	$1.17x10^{-5}$ / ^oC	$0.008m^2$	4 Tonne (39240 N)

III. CAD MODELLING

CAD Modeling is the base of any project. Finite Element software will consider shapes, whatever is made in CAD model. The model of the four cross section of hook is prepared by using CATIA V5 R20 software. The 3D model of the Hooks shown in fig. 3.1 respectively

Fig. 3.1 Circular, Square, Curved and Modified Curved cross section Hook

IV. FINITE ELEMENT ANALYSIS

The Finite Element Method (FEM) has developed into a key, indispensable technology in the modeling and simulation of advanced engineering systems in various fields like housing, transportation, manufacturing, and communications and so on. In building such advanced engineering systems, engineers and designers go through a sophisticated process of modeling, simulation, visualization, analysis, designing, prototyping, testing, and lastly fabrication. Note, that much work is involved before the fabrication of the final product or system. The Crane hook taken into consideration is having a load carrying capacity of 4 Tonnes with factor of safety 4.

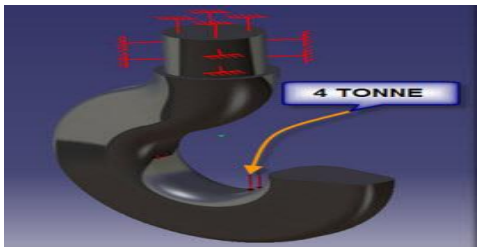

Fig. 4.1 Boundary conditions and application of load

FEA on circular CSA hook

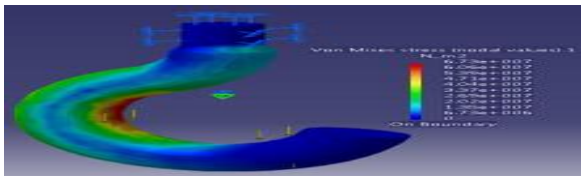

Fig.4.2 Stress Plot for circular CSA hook

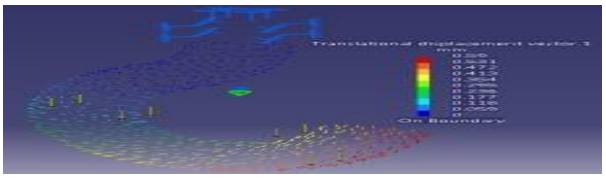

Fig. 4.3 Deflection Plot for circular CSA hook

FEA on rectangular CSA hook

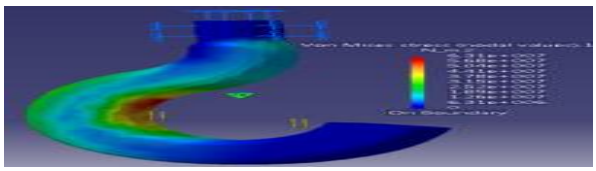

Fig. 4.4 Stress Plot for rectangular CSA hook

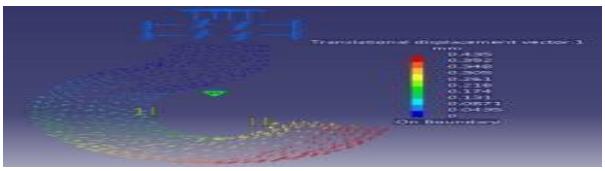

Fig. 4.5 Deflection Plot for rectangular CSA hook

FEA on curved CSA hook

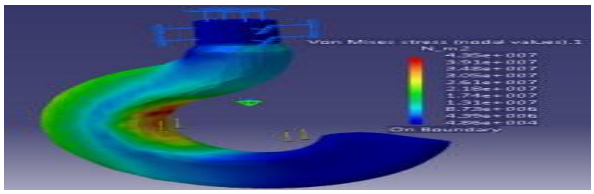

Fig. 4.6 Stress Plot for curved CSA hook

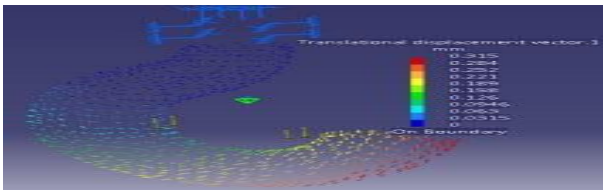

Fig. 4.7 Deflection Plot for curved CSA hook

FEA on modified curved CSA hook

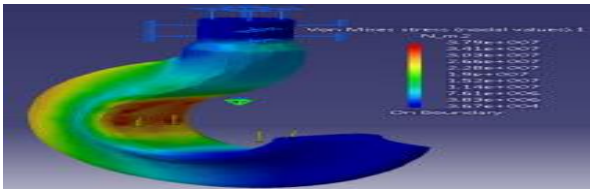

Fig.4.6 Stress Plot for modified curved CSA hook

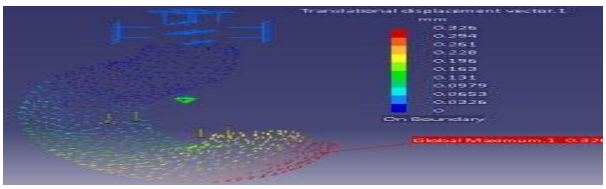

Fig.4.7 Deflection Plot for modified curved CSA hook

V. RESULTS & CONCLUSIONS

Stress induced and displacement in "Modified Curved Hook" is least because of curved shape and fillet edges as well as stress concentration are distributed uniformly. It have less mass due to this we are able to save the material and balance economy.

Table 5.1 Comparative Analysis for all hooks

Cross section	Mass (Kg)	V.M.S. (MPa)	Displacement (mm)
Square	45.108	63.1	0.435
Circular	50.203	67.3	0.590
Curved	51.798	43.5	0.316
Modified curved	45.725	37.9	0.326

REFERENCES

[1]. "**Rajendra Parmanik** "Design of Hoisting arrangement of E.O.T. crane hook" Posted on July 2008 by **http://rparmanik.wordpress.com/about-me-rajendra-parmanik/**

[2]. **R. Uddanwadiker**, "Stress Analysis of Crane Hook and Validation by Photo Elasticity," ***Engineering, Vol. 3 No. 9, 2011, pp. 935-941***

International Journal of Modern Engineering Research (IJMER)
www.ijmer.com Vol. 3, Issue. 4, Jul - Aug. 2013 pp-2190-2196 ISSN: 2249-6645

Experiment of Routing Protocol AODV (AdHoc On-demand Distance Vector)

Iyas Abdullah[1], Mohammad Odat[2]
[1, 2] *(Department of Information Technology /University of craiova, Romania)*

ABSTRACT: *In Mobile Ad hoc Network (MANET), routing protocols rely on asymmetric links so the received information for one connection is not useful at all for the other one. In this paper there are two approaches; the first approach is a simulation of MANET with many nodes in one network based FTP traffic. The second approach is a simulation of the combination between WiFi and WiMax wireless technologies in one network based on the IEEE 802.11 and IEEE 802.16 standards respectively. For these two approaches, the simulation considers the situation that the MANET receives traffic from another network via a common gateway. In addition, the mobile nodes are randomly placed in the network that will provide the possibility of multi-hop routes from a node to another. Several scenarios' simulations using WLAN technology were tested to investigate the behavior of the network performance for logical and office applications with fixed and mobile workstations. we considered to operate on a single-hop or multi-hop basis where nodes in the network are able to act as intermediaries (routers) for communications of other nodes. Nodes in networks are forced to operate with power limited batteries for power saving goal addition of the bandwidth constrained is considered.*

Keywords: *MANET, Routing, AODV, WLAN and OPNET Simulator.*

I. INTRODUCTION

In Mobile Ad hoc Network (MANET) is the establishment and maintenance of the ad hoc network through the use of routing protocols. The Ad hoc On Demand Distance Vector (AODV) routing algorithm is a routing protocol specifically designed for ad hoc mobile networks. AODV is capable of both unicast and multicast routing and it is an on demand algorithm, meaning that it builds routes between nodes only and only if it is desired by source nodes. It maintains these routes as long as they are needed by the sources [1][2].

In other words, the primary objectives of the algorithm are to broadcast discovery packets only when necessary in order to distinguish between local connectivity management and general topology maintenance and to disseminate information about changes in local connectivity to those neighboring mobile nodes that are likely to need information. [3][4]. Many researchers

Working with wireless routing protocols; Charles E. Perkins [5] studied a systematic performance analysis of Dynamic Source Routing (DSR) and AdHoc On-demand Distance Vector (AODV) routing protocols. Ferrari and Malvassori [6] proposed in a protocol called a MAODV (modified ad hoc on demand distance vector) which evaluated the benefits of using power control (PC) among selected routes in order to reduce the bite error rate at the destination node. Authors of [7] and [8] developed a reactive routing algorithm for multi-rate adhoc wireless networks which enhances the AODV protocol and shows in results the higher throughput over traditional adhoc routing protocols.

This paper submitted two study cases as follows; the first one related to using an AODV routing protocols in ad hoc network with Standard MAC 802.11. The second one is related to combining WiFi and WiMax networks then evaluating and analyzing the performance behavior of this network combination. we are build our implemented in OPNET 14.5 simulator. The rest of this paper is organized as follow. Section Two reviews some detailed description of AODV Routing. Section three describes the Path Discovery in AODV. Section four represents the MANET model architecture in OPNET simulation. Case studied scenarios (simulation experiments) are included in section five. The sixth section shows the researchers simulation results. Finally, the conclusions drawn are given in section seven.

II. (AODV) PROTOCOL

Ad hoc routing protocol is a network routing protocol developed with some mechanisms to cope with the dynamic nature of MANETs. The efficiency of a routing protocol is determined among other things by its power consumption of a participating node and routing of traffic into the network. How fast the routing protocol adapts to the connection tearing and mending is also considered paramount [9]. AODV is an on-demand routing protocol used in ad hoc networks, like any other on-demand routing protocols and facilitates a smooth adaptation to changes in the link conditions. In case a link fails, notifications are sent only to the affected nodes, this information enables the affected nodes invalidate all the routes through the failed link. It has low memory overhead and builds unicast routes from source to the destination.

There is minimal routing traffic in the network since routes are built on demand. It does not allow nodes to keep routes that are not in use. When two nodes in an ad hoc network are establishing a connection between each other, AODV will enable them to build multi-hop routes between the mobile nodes involved. AODV is a loop free protocol since it uses Destination Sequence Numbers (DSN) to avoid counting to infinity. This is the most important distinguishing feature of this protocol [10]. AODV is a reactive protocol, which plans the path for packets “as and when” it needs to. Updates to the routes are performed when needed and in the process of route discovery. The disadvantage of this general approach is the risk of full flooding which occurs when nodes receive a hit message, and flood the network with Route Request Packets [11].

A). Path Discovery in AODV

The Path Discovery process is initiated whenever a source node needs to communicate with another node for which it has no routing information in its table. The source node initiates path discovery by broadcasting a route request (RREQ) packet to its neighbors. The RREQ contains the following fields as shown in Fig.(1).

- Source address
- Source sequence number
- Broadcast ID
- Destination address
- Destination sequence number
- Hop count

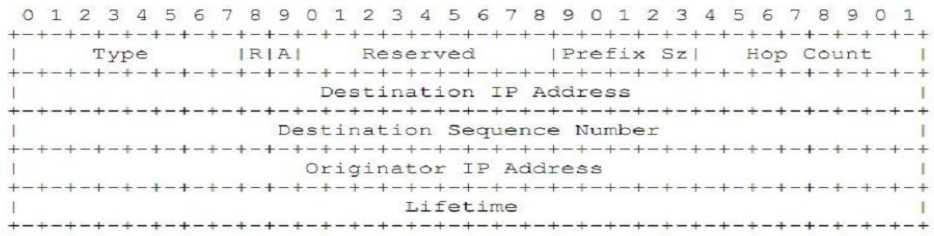

Figure 1. an example of RREQ message format [11].

The pair source address and broadcast ID uniquely identifies a RREQ. Broadcast ID is incremented whenever the source issues a new RREQ. Each neighbor either satisfies the RREQ by sending a route reply (RREP) back to the source or rebroadcasts the RREQ to its own neighbors after increasing the hop count. Notice that a node may receive multiple copies of the same route broadcast packet from various neighbors. When an intermediate node receives a RREQ, which it has already received with the same broadcast ID and source address, it drops the redundant RREQ and does not rebroadcast it.

B). Reverse Path Setup.

There are two sequence numbers included in a RREQ: the source sequence number, and the last destination sequence number known to the source. The source sequence number is used to maintain freshness information about the reverse route to the source, and the destination sequence number specifies how fresh a route to the destination before it can be accepted by the source [4][12].

Let's suppose the procedure shown in Fig. (2).When the source node S determines that it needs a route to the destination node D and it does not have the root available, then immediately node S starts broadcasting RREQ (Route Request) message to its neighboring nodes in quest of route to the destination. The nodes 1 and 4 being as neighbors to the node S receive the RREQ message. So nodes 1 and4 create a reverse link to the source from which they have received RREQ. Since the nodes 1 and 4 are not aware of the link to the node D, they simply rebroadcast this RREQ to their neighboring nodes 2 and 5. As the RREQ travels from a source to various destinations, it automatically sets up the reverse path from all nodes back to the source. This reverse route will be needed if the node receives a RREP back to the node that has originated the RREQ. Before broadcasting the RREQ, the originating node buffers the RREQ ID and the originator IP address. In this way, when the node receives the packet again from its neighbors, it will not reprocess and re-forward the packet [1].

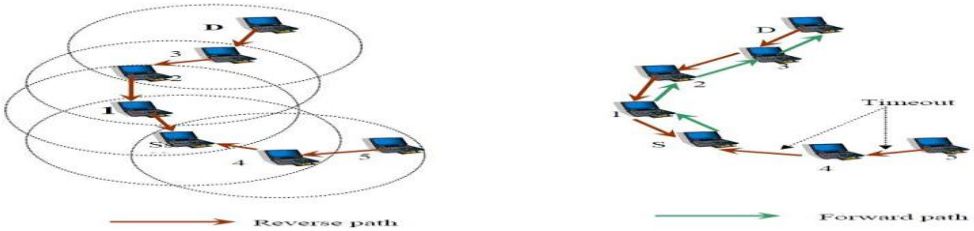

Figure (2): Forward Path Setting and Reverse Path.

C). Forward Path Setup.

Eventually, a RREQ will arrive at a node that possesses a current route to the destination or the destination itself. The receiving node first checks that the RREQ was received over a bi-directional link. If an intermediate node has a route entry for the desired destination, it determines whether the route is current by comparing the destination sequence number in its own route entry to the destination sequence number in the RREQ. If the RREQ's sequence number for the destination is greater than that recorded by the intermediate node, the intermediate node must not use its recorded route to respond to the RREQ. Instead, the intermediate node rebroadcasts the RREQ. The intermediate node can reply only when it has a route with a sequence number that is greater than or equal to that available in the RREQ. If it does have a current route to the destination and if the RREQ has not been processed previously, the node then unicasts a route reply packet (RREP) back to its neighbor from which it has received the RREQ.

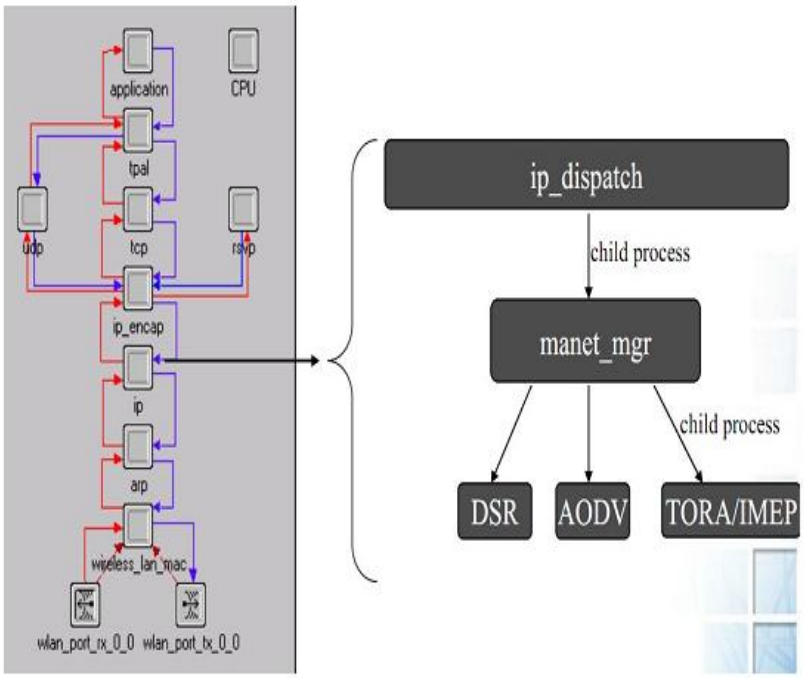

Figure (3): node model in OPNET simulator.

D). Manet Model Architecture in Opnet.

OPNET is widely being accepted as the frontrunner in simulation based tools in most universities and industry. This simulator helps to have a better understanding of how a wireless network is designed and implemented towards a real life scenario. It allows researchers to design and study communication networks, devices, protocols, and applications with great flexibility. OPNET provides a graphical editor interface to build models for various network entities from physical layer modulator to application processes. All the components are modeled in an object-oriented approach which gives intuitive easy mapping to real systems. Models of AODV and other ad hoc routing protocols are available in OPNET version 14.5. This section explains a model architecture, node models of MANET and all source, header and external files that are used by AODV process. Fig (3) Shows the node model in OPNET simulator [13].Traditionally, there are two profiles used to configure any network models [14];

- Profile Configuration -Profiles describe the activity patterns of a user or group of users in terms of the applications used over a period of time. Several different profiles run on a given LAN or workstation. These profiles can represent different user groups, for example, you can have an Engineering profile, a Sales profile and an Administration profile.
- Application Configuration- A profile is constructed using different application definitions. For each application definition, you can specify usage parameters such as start time, duration and repeatability. You may have two identical applications with different usage parameters; you can use different names to identify these as two distinct application definitions.

III. SOME OF CASIES

A) AODV Algorithm in Ad Hoc Network with Standard MAC 802.11

In this case the researchers used the following modeling standards given below for three proposed scenarios. A standard scenario contains (2-4) MANET Workstations and the Ad-Hoc Routing DSR or AODV depending on the scenarios . -The Workstation is connected wirelessly to the MANT Gateway at 2 –11MB.

-The Wireless Network BSS Identifier is 0. The scenario will take place in an office of size 100m x 100m.-Time of simulation is about 20 minutes.

Scenario 1: In this scenario, an office of 300m scale is chosen with Wireless LAN server and two nodes (source and destination) without any routing protocol. This scenario is shown in Fig.(4).

Scenario 2: For an ad-hoc network, AODV algorithm is used as shown in Fig.(5).By using node (0), the destination node can be connected to the network by AODV algorithm. The simulation duration is chosen as 20 minutes.

Scenario 3: As Fig.(6), two fixed node are added between source node and trajectory mobile node to see the effect of the trajectory and the number of nodes on distance vector and number of hopes. Figs.(7-9) show the simulation results of these three scenarios respectively. Figs (10-14) shows how the different number of nodes (different hopes) in the AODV simulation can have an effect on the network delay and throughput. The figures below show that increasing number of nodes (no. of hops) will decrease the network throughput.

Furthermore, it can be noted that the network delay with using AODV routing is less than any other network that uses any other routing algorithms.

Figure (4): scenario 1_network implementation

Figure (5): scenario 2_network implementation.

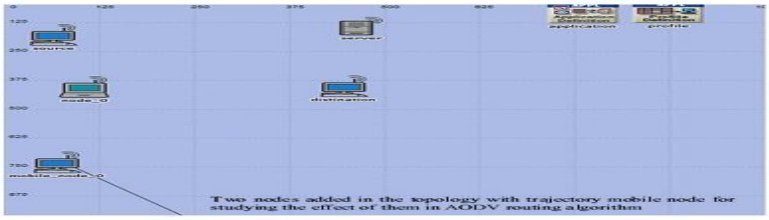

Figure (6): scenario 3_network implementation.

Figure (7): scenario 1_the results.

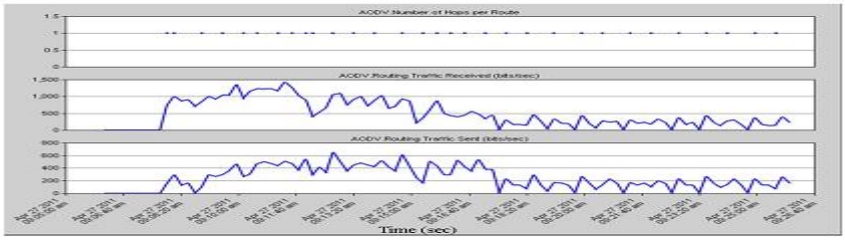

Figure (8-A): scenario 2_destination node results

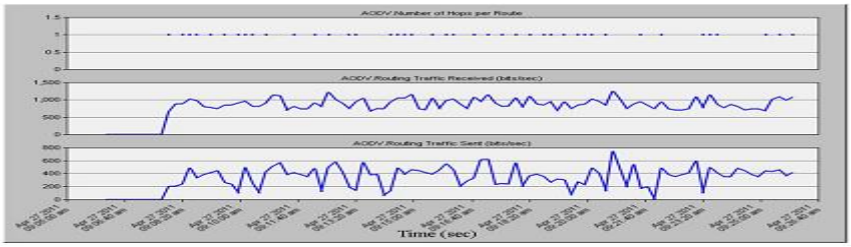

Figure (8-B): scenario 2_source node results.

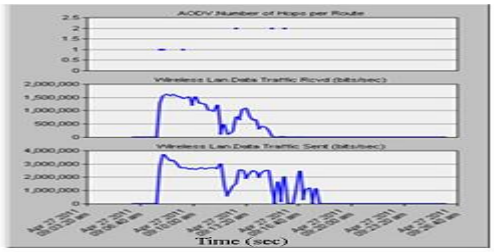

Figure (9): scenario 3_the results.

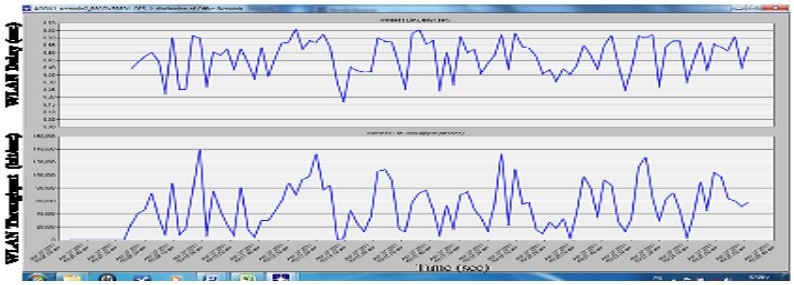

Figure (10): throughput and delay of AODV after adding two nodes.

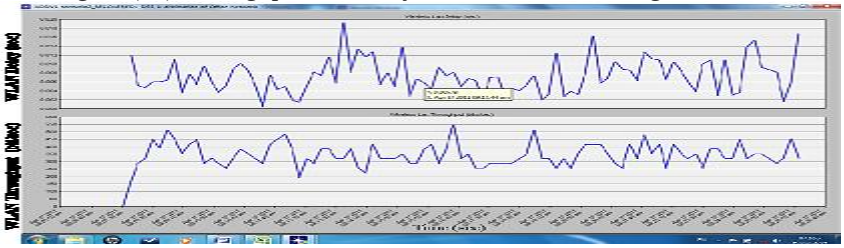

Figure (11): Throughput and Delay of AODV after adding three nodes.

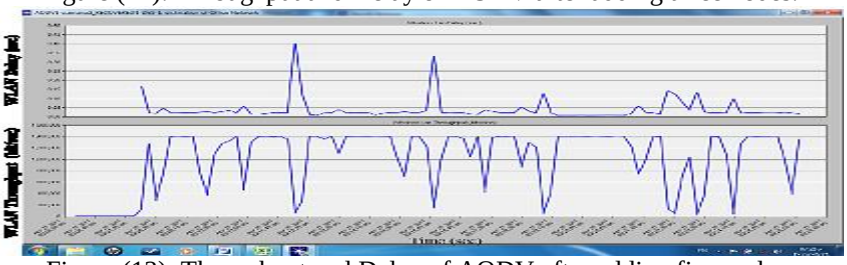

Figure (12): Throughput and Delay of AODV after adding five nodes.

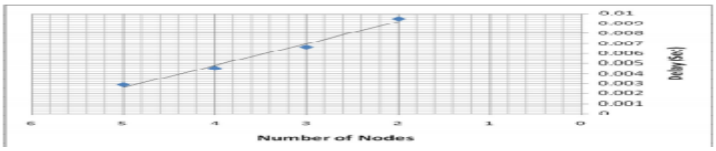

Figure (13): delay vs. no. of nodes.

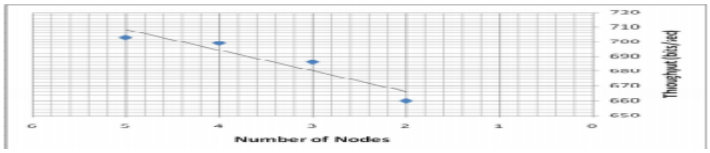

Figure (14): throughput vs. no. of nodes.

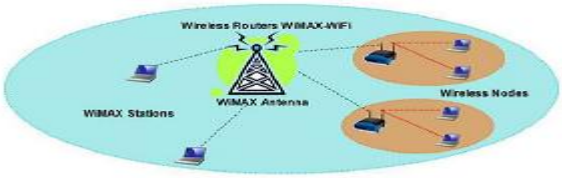

Figure (15): Wi-Fi and WiMax network convergence [15]

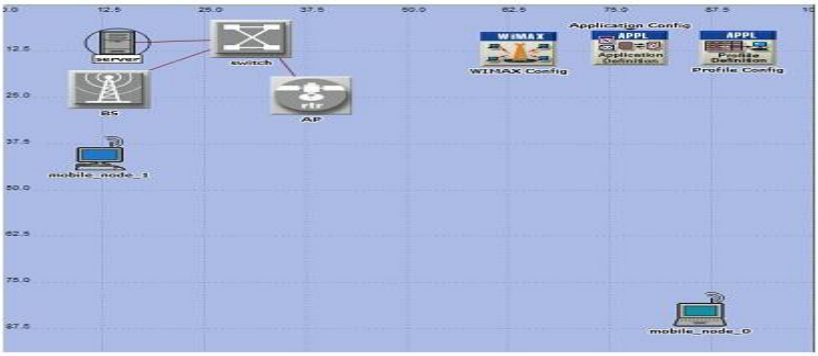

Figure (16): scenario 1_The WiMAX model implementation.

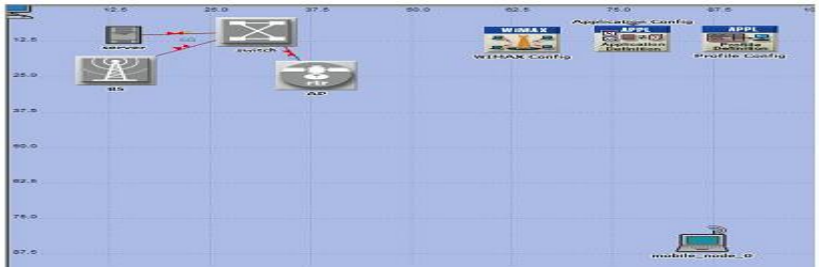

Figure (17): scenario 2_ WLAN-WiMAX packet flow and node movement.

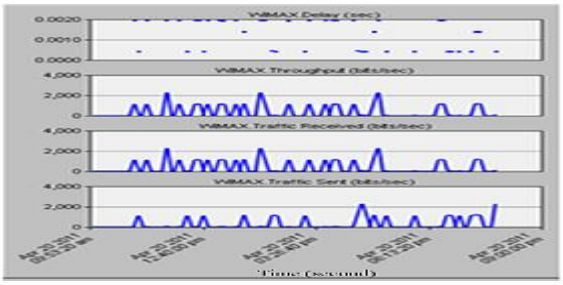

Figure (18): scenario 2_the simulation results.

B) WiFi and WiMax Evaluation and Network Performance.

WiMAX which is based on the IEEE802.16 standard provides a wireless broadband technology. Both the technical execution and the business cases show the differences between WiMAX and traditional Wi-Fi technology. As they are both wireless technology, most people consider WiMAX as the robust of WiFi. A simple comparison shows the advantage of WiMAX in larger network coverage area and faster transfer speed over Wi-Fi. Because of technologies reason and standardization issues, WiMAX does not present its better performance in market position In addition, the relatively high price also decreases the speed of WiMAX to occupy the market [15]. The main differences in protocol and services are shown in Table (1) below.

	3G	**WiFi 802.11**	**WiMax 802.16**	**Mobile-Fi 802.20**
Max Speed	2Mbps	54Mbps	100Mbps	16Mbps
Coverage	Several miles	300 feet	50 miles	Several miles
Airwave	Licensed	Unlicensed	Either	Licensed
Advantages	Range, mobility	Speed, Price	Speed, range	Speed, mobility
Disadvantages	Slow, Expensive	Short range	Interference issues	High Price

Table (1) comparison among different wireless technologies

The physical layer for WiMAX at the start stage is IEEE 802.16 which limits the physical layer to be operated in 10 GHz to 66 GHz. During going through the standard of IEEE 802.16a and IEEE 802.16e, WiMAX obtain benefits from the network coverage, self-installation, power consumption, frequency reuse and bandwidth efficiency. The standard IEEE802.16d is used on WMAN fixed and IEEE 802.16e is used on WMAN Portable. The throughput for Fixed WiMAX is up to 75 Mbps with the 20MHz bandwidth while the portable WiMAX is up to 30Mbps with 10MHz bandwidth. Also, the network coverage of fixed WiMAX and the portable WiMAX is 4-6 miles and 1-3 miles respectively. The conflict between WiMAX and Wi-Fi is the resistance for WiMAX to develop. In order to extend the reach of WiMAX technology, redundant efforts have been done to cooperate with the traditional Wi-Fi. This seems the only way to satisfy both the Wi-Fi supporters and those who focus on the higher speed and larger range. While the Wi-Fi is playing a smaller role in the wireless industry, the opportunity for wireless technologies to grow up and offer high speed appears. Fig.(15) gives an outline of how Wi-Fi and WiMAX is integrated to work together to approach a better performance in either distance or transfer speed [16][17].

IV. RESULTS AND DISCUSSION

A). WiMax Connection Model.

The basic components of WiMAX connection station is the wireless work station and WiMAX base station. The most common connections of WiMAX are PMP which means point to multi-point. The PMP topology, where a group of subscriber terminals are connected to a base station separately, is the best choice for most of the users who do not need entire bandwidth and extremely high speed. The basic WiMAX model is shown in Fig.(16) (scenario (1)). In this model, the components that have been used are; WiMAX config., WiMAX base station and WiMAX workstations. This model that has been built to test file transfer process contains the following:

- Application configuration.
- Profile configuration.

- Application server
- WiMAX_WLAN router

Model building steps are as follows; Creating the Topology, Configuring Node Mobility, Adding Traffic to the WiMAX Network Model and Configuring WiMAX Parameters). While load traffic are added to the WiMAX network model, the standard application models such as FTP, Email, and custom application is implemented in the WiMAX subscriber workstation and WiMAX application server.

B). WLAN-WiMAX Network Model.

Fig.(17) Shows the configuration for WLAN-WiMAX network model for scenario(2) and after the model was built, the file transfer performance of a WLAN-WiMAX was analyzed. The simulation result for this model can be seen in Fig. (18).

V. CONCLUSION

Our two approaches were discussed as two cases. For the first case study, AODV Algorithm in Ad-Hoc Network was used. It works by constructing routes between nodes on demand by source nodes, and they are kept until they are not needed so as to minimize the route discovery time. However the study shows that AODV is a faster protocol at finding the route due to using one route instead of multiple.

Following conclusions are made based on the analysis of simulation results:

-Using sequence numbers on route updated to find the latest route to destination that increase the speed and make the network fast and of high capacity.

With the increase of number of hops, throughput degrades due to higher delay.

The results show that AODV is the strongest candidate when experiencing an increase in nodes and bandwidth.

The performance of AODV is observed to improve with the increase in the number of sources. The hop-by-hop initiation in AODV helps to reduce the end-to-end delay. For the second case study (Wi-Fi and WiMAX), the network performance is evaluated and analyzed,. The following conclusions for this approach are: -By using these models together, the limitation of this network is the WLAN transfer performance. By improving the overall performance of the network, a WiMAX work station could be used instead the WLAN router with WLAN work stations.

The best way to enjoy the advantage of the WiMAX system is to combine the WiMAX and Wi-Fi systems together. The Simulation results show that throughput and lifetime become better by using WLAN-WiMAX model.

-Each access point has its own BSS. The connection change in this scenario considered a layer 2 handoff.

REFERENCES

[1]. Vijay k. Garg, “Wireless Communications and Networking”, article book, Elsevier Inc. Publishers, 2007.
[2]. G. Raj Kumar and K. Duraisamy, “a review of ad hoc on-demand distance vector routing protocol for mobile ad hoc networks”, Journal of Theoretical and Applied Information Technology,Vol. 36,No.1,2005.
[3]. N Qasim, F.Said and H. Aghvami, “Mobile Ad Hoc Networks Simulations Using Routing Protocols for Performance Comparisons”, Proceedings of the World Congress on Engineering, London, U.K, 2008.
[4]. P. Manickam, T. G.Baskar and M.Girija, “Performance Comparisons Of Routing Protocols in Mobile Ad Hoc Networks”, International Journal of Wireless & Mobile Networks (IJWMN), Vol. 3, No. 1, February 2011.
[5]. E. Charles, M. Elizabeth, and R.D. Samir, “Performance comparison of two on-demand Routing Protocols for ad-hoc networks”, IEEE personal communication, pp.16-28, February 2001.
[6]. G.Ferrari,S.A.Malvassori and O.K.Tonguz,“On Physical Layer Oriented outing With Power Control in Ad Hoc Wireless Networks”, IET Communications,Vol. 2 , No. 2,pp. 306-319,2008.
[7]. E. Charles and P. Bhagwat, “Highly Dynamic Destination-Sequenced Distance-Vector Routing (DSDV) for Mobile Computers”, In Proc. ACM SIGCOMM Conference (SIGCOMM '94), pp.234-244, 1994.
[8]. Z.Fan, “High Throughput Reactive Routing in Multi-rate Ad Hoc Networks”, Electronic Letters, Vol. 40, No.25,2004.
[9]. Sudip Misra, “Guide to Wireless Ad Hoc Networks”, Textbook, Springer-Verlag London Limited, 2009.
[10]. K.A.Shah, M.R.Gandhi, “Performance Evaluation of AODV Routing Protocol ith Link Failures”, IEEE International Conference on Computational Intelligence and Computing Research (ICCIC), 2010.
[11]. A.S.Tanenbaum, “Computer Networks”, Textbook, 3rdedition, Prentice Hall, 2003.
[12]. J.Lakkakorpi,“The Ad Hoc On-Demand Distance-Vector Protocol: Quality of Service Extensions”, Nokia Research Center, 2002.
[13]. Farzin, “OPNET Simulation of IEEE 802.11(Wi-Fi) and IEEE 802.16 (WiMAX) in a small area”, Final Project, spring publisher, 2010.
[14]. OPNET Modeler product documentation-release 14.5.
[15]. D. Xiao, Y.Fan and H.Xiaopeng, “ENSC 427 Communication Networks WLAN-WiMAX Analysis OPNET”, Final Report, Springer, 2009.
[16]. S. Ahmadi, “Mobile WiMAX A Systems Approach to Understanding IEEE 802.16 Radio Access Technology”, Textbook, Academic Press, UK, Nov. 2010.
[17]. V.Kulgachev and H.Jasani,“802.11 Networks Performance Evaluation Using OPNET”, Conference On Information Technology Education (CITC), Michigan, USA, 2010.

International Journal of Modern Engineering Research (IJMER)
www.ijmer.com Vol. 3, Issue. 4, Jul - Aug. 2013 pp-2197-2204 ISSN: 2249-6645

Further Results On The Basis Of Cauchy's Proper Bound for the Zeros of Entire Functions of Order Zero

Sanjib Kumar Datta[1], Manab Biswas[2]

[1](Department of Mathematics, University of Kalyani, Kalyani, Dist-Nadia, Pin- 741235, West Bengal, India)
[2](Barabilla High School, P.O. Haptiagach, Dist-Uttar Dinajpur, Pin- 733202, West Bengal, India)

ABSTRACT: *A single valued function of one complex variable which is analytic in the finite complex plane is called an entire function . The purpose of this paper is to establish the bounds for the moduli of zeros of entire functions of order zero. Some examples are provided to clear the notions.*

AMS Subject Classification 2010: *Primary 30C15, 30C10, Secondary 26C10.*

KEYWORDS AND PHRASES: *Zeros of entire functions of order zero, Cauchy's bound , Proper ring shaped region.*

I. INTRODUCTION, DEFINITIONS AND NOTATIONS

Let, $P(z) = a_0 + a_1 z + a_2 z^2 + a_3 z^3 + \ldots\ldots + a_{n-1} z^{n-1} + a_n z^n \; ; |a_n| \neq 0$

Be a polynomial of degree n . Datt and Govil [2] ; Govil and Rahaman [5] ; Marden [9] ; Mohammad [10] ; Chattopadhyay, Das, Jain and Konwar [1] ; Joyal, Labelle and Rahaman [6] ; Jain {[7] , [8]}; Sun and Hsieh [11] ; Zilovic, Roytman, Combettes and Swamy [13] ; Das and Datta [4] etc. worked in the theory of the distribution of the zeros of polynomials and obtained some newly developed results.

In this paper we intend to establish some of sharper results concerning the theory of distribution of zeros of entire functions of order zero.

The following definitions are well known :

Definition 1 The order ρ and lower order λ of a meromorphic function f are defined as

$\rho = \limsup_{r \to \infty} \frac{\log T(r,f)}{\log r}$ and $\lambda = \liminf_{r \to \infty} \frac{\log T(r,f)}{\log r}$.

If f is entire, one can easily verify that

$\rho = \limsup_{r \to \infty} \frac{\log^{[2]} M(r,f)}{\log r}$ and $\lambda = \liminf_{r \to \infty} \frac{\log^{[2]} M(r,f)}{\log r}$.

where $\log^{[k]} x = \log(\log^{[k-1]} x)$ for $k = 1, 2, 3, \ldots$ and $\log^{[0]} x = x$.

If $\rho < \infty$ then f is of finite order. Also $\rho = 0$ means that f is of order zero. In this connection Datta and Biswas [3] gave the following definition :

Definition 2 Let f be a meromorphic function of order zero. Then the quantities ρ^* and λ^* of f are defined by :

$\rho^* = \limsup_{r \to \infty} \frac{T(r,f)}{\log r}$ and $\lambda^* = \liminf_{r \to \infty} \frac{T(r,f)}{\log r}$.

If f is an entire function then clearly

$\rho^* = \limsup_{r \to \infty} \frac{\log M(r,f)}{\log r}$ and $\lambda^* = \liminf_{r \to \infty} \frac{\log M(r,f)}{\log r}$.

II. LEMMAS

In this section we present a lemma which will be needed in the sequel .

Lemma 1 If $f(z)$ is an entire function of order $\rho = 0$, then for every $\varepsilon > 0$ the inequality $N(r) \leq (\log r)^{\rho^* + \varepsilon}$ Holds for all sufficiently large r where $N(r)$ is the number of zeros of $f(z)$ in $|z| \leq \log r$.

Proof. Let us suppose that $f(z) = 1$. This supposition can be made without loss of generality because if $f(z)$ has a zero of order $'m'$ at the origin then we may consider $g(z) = c.\frac{f(z)}{z^m}$ where c is so chosen that $g(0) = 1$. Since the function $g(z)$ and $f(z)$ have the same order therefore it will be unimportant for our investigations that the number of zeros of $g(z)$ and $f(z)$ differ by m.

We further assume that $f(z)$ has no zeros on $|z| = \log 2r$ and the zeros z_i's of $f(z)$ in $|z| < \log r$ are in non decreasing order of their moduli so that $|z_i| \leq |z_{i+1}|$. Also let ρ^* suppose to be finite where $\rho = 0$ is the zero of order of $f(z)$.

Now we shall make use of Jenson's formula as state below

$$\log|f(0)| = -\sum_{i=1}^{n} \log\frac{R}{|z_i|} + \frac{1}{2\pi}\int_0^{2\pi} \log\left|f(R\,e^{i\phi})\right| d\phi \; . \qquad (1)$$

Let us replace R by $2r$ and n by $N(2r)$ in (1) .

$$\therefore \; \log|f(0)| = -\sum_{i=1}^{N(2r)} \log\frac{2r}{|z_i|} + \frac{1}{2\pi}\int_0^{2\pi} \log\left|f(2r\,e^{i\phi})\right| d\phi.$$

Since $f(0) = 1, \therefore \log|f(0)| = \log 1 = 0.$

$$\therefore \sum_{i=1}^{N(2r)} \log\frac{2r}{|z_i|} = \frac{1}{2\pi}\int_0^{2\pi} \log\left|f(2r\,e^{i\phi})\right| d\phi \qquad (2)$$

$$\text{L.H.S.} = \sum_{i=1}^{N(2r)} \log\frac{2r}{|z_i|} \geq \sum_{i=1}^{N(r)} \log\frac{2r}{|z_i|} \geq N(r)\log 2 \qquad (3)$$

because for large values of r,

$$\log\frac{2r}{|z_i|} \geq \log 2\,.$$

$$\text{R.H.S.} = \frac{1}{2\pi}\int_0^{2\pi} \log\left|f(2r\,e^{i\phi})\right| d\phi$$

$$\leq \frac{1}{2\pi}\int_0^{2\pi} \log M(2r)\, d\phi = \log M(2r). \qquad (4)$$

Again by definition of order ρ^* of $f(z)$ we have for every $\varepsilon > 0$,

$$\log M(2r) \leq \{\log(2r)\}^{\rho^*+\varepsilon/2}\,. \qquad (5)$$

Hence from (2) by the help of (3) , (4) and (5) we have

$$N(r)\log 2 \leq \{\log(2r)\}^{\rho^*+\varepsilon/2}$$

$$\text{i.e., } N(r) \leq \frac{(\log 2)^{\rho^*+\varepsilon/2}}{\log 2}\cdot\frac{(\log r)^{\rho^*+\varepsilon}}{(\log r)^{\varepsilon/2}} \leq (\log r)^{\rho^*+\varepsilon}\,.$$

This proves the lemma.

III. THEOREMS

In this section we present the main results of the paper.

Theorem 1 Let $P(z)$ be an entire function having order $\rho = 0$ in the disc $|z| \leq \log r$ for sufficiently large r. Also let the Taylor's series expansion of $P(z)$ be given by

$$P(z) = a_0 + a_{p_1}z^{p_1} + \ldots\ldots + a_{p_m}z^{p_m} + a_{N(r)}z^{N(r)},\ a_0 \neq 0,\ a_{N(r)} \neq 0$$

with $1 \leq p_1 < p_2 < \ldots\ldots < p_m \leq N(r) - 1$, p_i's are integers such that for some $\rho^* > 0$,

$$|a_0|(\rho^*)^{N(r)} \geq |a_{p_1}|(\rho^*)^{N(r)-p_1} \geq \ldots\ldots\ldots \geq |a_{p_m}|(\rho^*)^{N(r)-p_m} \geq |a_{N(r)}|\,.$$

Then all the zeros of $P(z)$ lie in the ring shaped region

$$\frac{1}{\rho^*\left(1+\frac{|a_{p_1}|}{|a_0|(\rho^*)^{p_1}}\right)} < |z| < \frac{1}{\rho^*}\left(1+\frac{|a_0|}{|a_{N(r)}|}(\rho^*)^{N(r)}\right).$$

Proof. Given that

$$P(z) = a_0 + a_{p_1}z^{p_1} + \ldots\ldots + a_{p_m}z^{p_m} + a_{N(r)}z^{N(r)}$$

where p_i's are integers and $1 \leq p_1 < p_2 < \ldots\ldots < p_m \leq N(r) - 1$. Then for some $\rho^* > 0$,

$$|a_0|(\rho^*)^{N(r)} \geq |a_{p_1}|(\rho^*)^{N(r)-p_1} \geq \ldots\ldots\ldots \geq |a_{p_m}|(\rho^*)^{N(r)-p_m} \geq |a_{N(r)}|\,.$$

Let us consider

$$\begin{aligned} Q(z) &= (\rho^*)^{N(r)}P\left(\frac{z}{\rho^*}\right) \\ &= (\rho^*)^{N(r)}\left\{a_0 + a_{p_1}\frac{z^{p_1}}{(\rho^*)^{p_1}} + \cdots\cdots + a_{p_m}\frac{z^{p_m}}{(\rho^*)^{p_m}} + a_{N(r)}\frac{z^{N(r)}}{(\rho^*)^{N(r)}}\right\} \\ &= a_0(\rho^*)^{N(r)} + a_{p_1}(\rho^*)^{N(r)-p_1}z^{p_1} + \ldots\ldots + a_{p_m}(\rho^*)^{N(r)-p_m}z^{p_m} + a_{N(r)}z^{N(r)}\,. \end{aligned}$$

Therefore

$$|\,Q(z)\,| \geq \left|a_{N(r)}z^{N(r)}\right| - \left|a_0(\rho^*)^{N(r)} + a_{p_1}(\rho^*)^{N(r)-p_1}z^{p_1} + \ldots\ldots + a_{p_m}(\rho^*)^{N(r)-p_m}z^{p_m}\right|. \qquad (6)$$

Now using the given condition of Theorem 1 we obtain that

$$\begin{aligned} &\left|a_0(\rho^*)^{N(r)} + a_{p_1}(\rho^*)^{N(r)-p_1}z^{p_1} + \ldots\ldots + a_{p_m}(\rho^*)^{N(r)-p_m}z^{p_m}\right| \\ &\leq |a_0|(\rho^*)^{N(r)} + |a_{p_1}|(\rho^*)^{N(r)-p_1}|z|^{p_1} + \ldots\ldots + |a_{p_m}|(\rho^*)^{N(r)-p_m}|z|^{p_m} \\ &\leq |a_0|(\rho^*)^{N(r)}|z|^{N(r)}\left(\frac{1}{|z|^{N(r)-p_m}} + \cdots\cdots + \frac{1}{|z|^{N(r)}}\right) \text{ for } |z| \neq 0\,. \end{aligned}$$

Using (6) we get for $|z| \neq 0$ that

$$\begin{aligned} |\,Q(z)| &\geq |a_{N(r)}||z|^{N(r)} - |a_0|(\rho^*)^{N(r)}|z|^{N(r)}\left(\frac{1}{|z|^{N(r)-p_m}} + \cdots\cdots + \frac{1}{|z|^{N(r)}}\right) \\ &> |a_{N(r)}||z|^{N(r)} - |a_0|(\rho^*)^{N(r)}|z|^{N(r)}\left(\frac{1}{|z|^{N(r)-p_m}} + \cdots\cdots + \frac{1}{|z|^{N(r)}} + \cdots\right) \\ &= |a_{N(r)}||z|^{N(r)} - |a_0|(\rho^*)^{N(r)}|z|^{N(r)}\left(\sum_{k=1}^{\infty}\frac{1}{|z|^k}\right). \end{aligned} \qquad (7)$$

The geometric series $\sum_{k=1}^{\infty}\frac{1}{|z|^k}$ is convergent for

$$\frac{1}{|z|} < 1$$

i.e., for $|z| > 1$

and converges to

$$\frac{1}{|z|}\frac{1}{1-\frac{1}{|z|}} = \frac{1}{|z|-1}.$$

Therefore

$$\sum_{k=1}^{\infty} \frac{1}{|z|^k} = \frac{1}{|z|-1} \text{ for } |z| > 1.$$

Using (7) we get from above that for $|z| > 1$

$$|Q(z)| \geq |a_{N(r)}||z|^{N(r)} - |a_0|(\rho^*)^{N(r)}|z|^{N(r)}\left(\frac{1}{|z|-1}\right)$$
$$= |z|^{N(r)}\left(|a_{N(r)}| - \frac{|a_0|(\rho^*)^{N(r)}}{|z|-1}\right).$$

Now for $|z| > 1$,

$$|Q(z)| \geq 0 \text{ if } |a_{N(r)}| - \frac{|a_0|(\rho^*)^{N(r)}}{|z|-1} \geq 0$$
$$\text{i.e., if } |a_{N(r)}| \geq \frac{|a_0|(\rho^*)^{N(r)}}{|z|-1}$$
$$\text{i.e., if } |z| - 1 \geq \frac{|a_0|(\rho^*)^{N(r)}}{|a_{N(r)}|}$$
$$\text{i.e., if } |z| \geq 1 + \frac{|a_0|(\rho^*)^{N(r)}}{|a_{N(r)}|} > 1.$$

Therefore $|Q(z)| \geq 0$ if

$$|z| \geq 1 + \frac{|a_0|(\rho^*)^{N(r)}}{|a_{N(r)}|}.$$

Therefore $Q(z)$ does not vanish for

$$|z| \geq 1 + \frac{|a_0|(\rho^*)^{N(r)}}{|a_{N(r)}|}.$$

So all the zeros of $Q(z)$ lie in

$$|z| < 1 + \frac{|a_0|(\rho^*)^{N(r)}}{|a_{N(r)}|}.$$

Let $z = z_0$ be any zero of $P(z)$. Therefore $P(z_0) = 0$. Clearly $z_0 \neq 0$ as $a_0 \neq 0$.
Putting $z = \rho^* z_0$ in $Q(z)$ we get that

$$Q(\rho^* z_0) = (\rho^*)^{N(r)}.P(z_0) = (\rho^*)^{N(r)}.0 = 0.$$

So $z = \rho^* z_0$ is a zero of $Q(z)$. Hence

$$|\rho^* z_0| < 1 + \frac{|a_0|(\rho^*)^{N(r)}}{|a_{N(r)}|}$$

$$\text{i.e., } |z_0| < \frac{1}{\rho^*}\left(1 + \frac{|a_0|(\rho^*)^{N(r)}}{|a_{N(r)}|}\right).$$

Since z_0 is an arbitrary zero of $P(z)$, therefore all the zeros of $Q(z)$ lie in

$$|z| < \frac{1}{\rho^*}\left(1 + \frac{|a_0|(\rho^*)^{N(r)}}{|a_{N(r)}|}\right). \quad (8)$$

Again let us consider

$$R(z) = (\rho^*)^{N(r)} z^{N(r)} P\left(\frac{1}{\rho^* z}\right).$$

Therefore

$$R(z) = (\rho^*)^{N(r)} z^{N(r)}.\left\{a_0 + a_{p_1}\frac{1}{(\rho^*)^{p_1} z^{p_1}} + \cdots\cdots + a_{p_m}\frac{1}{(\rho^*)^{p_m} z^{p_m}} + a_{N(r)}\frac{1}{(\rho^*)^{N(r)} z^{N(r)}}\right\}$$
$$= a_0(\rho^*)^{N(r)} z^{N(r)} + a_{p_1}(\rho^*)^{N(r)-p_1} z^{N(r)-p_1} + \ldots\ldots + a_{p_m}(\rho^*)^{N(r)-p_m} z^{N(r)-p_m} + a_{N(r)}.$$

Now

$$|R(z)| \geq \left|a_0(\rho^*)^{N(r)} z^{N(r)}\right| - \left|a_{p_1}(\rho^*)^{N(r)-p_1} z^{N(r)-p_1} + \ldots\ldots + a_{p_m}(\rho^*)^{N(r)-p_m} z^{N(r)-p_m} + a_{N(r)}\right|. \quad (9)$$

Also

$$\left|a_{p_1}(\rho^*)^{N(r)-p_1} z^{N(r)-p_1} + \ldots\ldots + a_{p_m}(\rho^*)^{N(r)-p_m} z^{N(r)-p_m} + a_{N(r)}\right|$$
$$\leq \left|a_{p_1}(\rho^*)^{N(r)-p_1} z^{N(r)-p_1}\right| + \ldots\ldots\ldots + \left|a_{p_m}(\rho^*)^{N(r)-p_m} z^{N(r)-p_m}\right| + \left|a_{N(r)}\right|$$
$$\leq \left|a_{p_1}\right|(\rho^*)^{N(r)-p_1}|z|^{N(r)-p_1} + \ldots\ldots\ldots + \left|a_{p_m}\right|(\rho^*)^{N(r)-p_m}|z|^{N(r)-p_m} + \left|a_{N(r)}\right|$$
$$\leq \left|a_{p_1}\right|(\rho^*)^{N(r)-p_1}\left(|z|^{N(r)-p_1} + \cdots\cdots + |z|^{N(r)-p_m} + 1\right). \quad (10)$$

Using (10) we get from (9) that for $|z| \neq 0$

$$|R(z)| \geq |a_0|(\rho^*)^{N(r)}|z|^{N(r)} - \left|a_{p_1}\right|(\rho^*)^{N(r)-p_1}\left(|z|^{N(r)-p_1} + \cdots\cdots + |z| + 1\right)$$
$$= |a_0|(\rho^*)^{N(r)}|z|^{N(r)} - \left|a_{p_1}\right|(\rho^*)^{N(r)-p_1}|z|^{N(r)}\left(\frac{1}{|z|^{p_1}} + \cdots\cdots + \frac{1}{|z|^{p_m}} + \frac{1}{|z|^{N(r)}}\right)$$

$$> |a_0|\,(\rho^*)^{N(r)}|z|^{N(r)} - |a_{p_1}|\,(\rho^*)^{N(r)-p_1}|z|^{N(r)}\left(\frac{1}{|z|^{p_1}} + \cdots\cdots + \frac{1}{|z|^{p_m}} + \frac{1}{|z|^{N(r)}} + \cdots\cdots\right).$$

Therefore for $|z| \neq 0$,

$$|R(z)| > |a_0|\,(\rho^*)^{N(r)}|z|^{N(r)} - |a_{p_1}|\,(\rho^*)^{N(r)-p_1}|z|^{N(r)}\left(\sum_{k=1}^{\infty}\frac{1}{|z|^k}\right). \tag{11}$$

Now the geometric series $\sum_{k=1}^{\infty}\frac{1}{|z|^k}$ is convergent for

$$\frac{1}{|z|} < 1$$

i.e., for $|z| > 1$

And converges to

$$\frac{1}{|z|}\frac{1}{1-\frac{1}{|z|}} = \frac{1}{|z|-1}.$$

So

$$\sum_{k=1}^{\infty}\frac{1}{|z|^k} = \frac{1}{|z|-1} \text{ for } |z| > 1.$$

Therefore for $|z| > 1$,

$$|R(z)| > |a_0|\,(\rho^*)^{N(r)}|z|^{N(r)} - |a_{p_1}|\,(\rho^*)^{N(r)-p_1}|z|^{N(r)}\left(\frac{1}{|z|-1}\right)$$
$$= |z|^{N(r)}\,(\rho^*)^{N(r)-p_1}\left(|a_0|\,(\rho^*)^{p_1} - \frac{|a_{p_1}|}{|z|-1}\right).$$

i.e., for $|z| > 1$

$$|R(z)| > |z|^{N(r)}\,(\rho^*)^{N(r)-p_1}\left(|a_0|\,(\rho^*)^{p_1} - \frac{|a_{p_1}|}{|z|-1}\right).$$

Now

$$R(z) > 0 \text{ if } \left(|a_0|\,(\rho^*)^{p_1} - \frac{|a_{p_1}|}{|z|-1}\right) \geq 0$$
$$\text{i.e., if } |a_0|\,(\rho^*)^{p_1} \geq \frac{|a_{p_1}|}{|z|-1}$$
$$\text{i.e., if } |z| - 1 \geq \frac{|a_{p_1}|}{|a_0|\,(\rho^*)^{p_1}}$$
$$\text{i.e., if } |z| \geq 1 + \frac{|a_{p_1}|}{|a_0|\,(\rho^*)^{p_1}} > 1.$$

Therefore

$$R(z) > 0 \text{ if } |z| \geq 1 + \frac{|a_{p_1}|}{|a_0|\,(\rho^*)^{p_1}}.$$

Since $R(z)$ does not vanish in

$$|z| \geq 1 + \frac{|a_{p_1}|}{|a_0|\,(\rho^*)^{p_1}},$$

all the zeros of $R(z)$ lie in

$$|z| < 1 + \frac{|a_{p_1}|}{|a_0|\,(\rho^*)^{p_1}}.$$

Let $z = z_0$ be any zero of $P(z)$. Therefore $P(z_0) = 0$. Clearly $z_0 \neq 0$ as $a_0 \neq 0$.
Putting $z = \rho^* z_0$ in $R(z)$ we obtain that

$$R\left(\frac{1}{\rho^* z_0}\right) = (\rho^*)^{N(r)}.\left(\frac{1}{\rho^* z_0}\right)^{N(r)} \cdot P(z_0)$$
$$= \left(\frac{1}{z_0}\right)^{N(r)} \cdot 0 = 0.$$

So

$$\left|\frac{1}{\rho^* z_0}\right| < 1 + \frac{|a_{p_1}|}{|a_0|\,(\rho^*)^{p_1}}$$
$$\text{i.e., } \left|\frac{1}{z_0}\right| < \rho^*\left(1 + \frac{|a_{p_1}|}{|a_0|\,(\rho^*)^{p_1}}\right)$$

$$\text{i.e., } |z_0| > \frac{1}{\rho^*\left(1+\frac{|a_{p_1}|}{|a_0|\,(\rho^*)^{p_1}}\right)}.$$

As z_0 is an arbitrary zero of $f(z)$, all the zeros of $P(z)$ lie in

$$|z| > \frac{1}{\rho^*\left(1+\frac{|a_{p_1}|}{|a_0|\,(\rho^*)^{p_1}}\right)}. \tag{12}$$

So from (8) and (12) we may conclude that all the zeros of $P(z)$ lie in the proper ring shaped region

$$\frac{1}{\rho^*\left(1+\frac{|a_{p_1}|}{|a_0|\,(\rho^*)^{p_1}}\right)} < |z| < \frac{1}{\rho^*}\left(1+\frac{|a_0|}{|a_{N(r)}|}(\rho^*)^{N(r)}\right).$$

This proves the theorem.

Corollary 1 In view of Theorem 1 we may conclude that all the zeros of

$$P(z) = a_0 + a_{p_1}z^{p_1} + \ldots\ldots + a_{p_m}z^{p_m} + a_n z^n$$

of degree n with $1 \le p_1 < p_2 \ldots\ldots < p_m \le n-1$, p_i's are integers such that for some $\rho^* > 0$,

$$|a_0| \ge |a_{p_1}| \ge \ldots\ldots \ge |a_{p_m}| \ge |a_n|$$

lie in the ring shaped region

$$\frac{1}{\left(1+\frac{|a_{p_1}|}{|a_0|}\right)} < |z| < \left(1+\frac{|a_0|}{|a_n|}\right)$$

on putting $\rho^* = 1$ in Theorem 1.

Theorem 2 Let $P(z)$ be an entire function having order $\rho = 0$. For sufficiently large r in the disc $|z| \le \log r$, the Taylor's series expansion of $P(z)$ be given by $P(z) = a_0 + a_1 z + \ldots\ldots + a_{N(r)}z^{N(r)}$, $a_0 \ne 0$. Further for some $\rho^* > 0$,

$$|a_0|(\rho^*)^{N(r)} \ge |a_1|(\rho^*)^{N(r)-1} \ge \ldots\ldots \ge |a_{N(r)}|.$$

Then all the zeros of $P(z)$ lie in the ring shaped region

$$\frac{1}{\rho^* t_0'} \le |z| \le \frac{1}{\rho^*}t_0$$

where t_0 and t_0' are the greatest roots of

$$g(t) \equiv |a_{N(r)}|t^{N(r)+1} - \left(|a_{N(r)}| + (\rho^*)^{N(r)}|a_0|\right)t^{N(r)} + (\rho^*)^{N(r)}|a_0| = 0$$

and

$$f(t) \equiv |a_0|\rho^* t^{N(r)+1} - (|a_0|\,\rho^* + |a_1|)t^{N(r)} + |a_1| = 0.$$

Proof. Let

$$P(z) = a_0 + a_1 z + \ldots\ldots + a_{N(r)}z^{N(r)}$$

by applying Lemma 1 and in view of Taylor's series expansion of $P(z)$. Also

$$|a_0|(\rho^*)^{N(r)} \ge |a_1|(\rho^*)^{N(r)-1} \ge \ldots\ldots \ge |a_{N(r)}|.$$

Let us consider

$$Q(z) = (\rho^*)^{N(r)}P\left(\frac{z}{\rho^*}\right)$$

$$= (\rho^*)^{N(r)}\left\{a_0 + a_1\frac{z}{\rho^*} + a_2\frac{z^2}{(\rho^*)^2} + \cdots\cdots + a_{N(r)}\frac{z^{N(r)}}{(\rho^*)^{N(r)}}\right\}$$
$$= a_0(\rho^*)^{N(r)} + a_1(\rho^*)^{N(r)-1}z + \ldots\ldots + a_{N(r)}z^{N(r)}.$$

Now

$$|Q(z)| \ge |a_{N(r)}||z|^{N(r)} - \left|a_0(\rho^*)^{N(r)} + a_1(\rho^*)^{N(r)-1}z + \ldots\ldots + a_{N(r)-1}z^{N(r)-1}\right|.$$

Also applying the condition $|a_0|(\rho^*)^{N(r)} \ge |a_1|(\rho^*)^{N(r)-1} \ge \ldots\ldots \ge |a_{N(r)}|$ we get from above that

$$\left|a_0(\rho^*)^{N(r)} + a_1(\rho^*)^{N(r)-1}z + \ldots\ldots + a_{N(r)-1}z^{N(r)-1}\right|$$
$$\le |a_0|(\rho^*)^{N(r)} + |a_1|(\rho^*)^{N(r)-1}|z| + \ldots\ldots + |a_{N(r)-1}||z|^{N(r)-1}$$
$$\le |a_0|(\rho^*)^{N(r)}\left(1 + |z| + \cdots\cdots + |z|^{N(r)-1}\right)$$
$$= |a_0|(\rho^*)^{N(r)} \cdot \frac{|z|^{N(r)}-1}{|z|-1} \text{ for } |z| \ne 1.$$

Therefore it follows from above that

$$|Q(z)| \ge |a_{N(r)}||z|^{N(r)} - |a_0|(\rho^*)^{N(r)} \cdot \frac{|z|^{N(r)}-1}{|z|-1}.$$

Now

$$|Q(z)| > 0 \text{ if } |a_{N(r)}||z|^{N(r)} - |a_0|(\rho^*)^{N(r)} \cdot \frac{|z|^{N(r)}-1}{|z|-1} > 0$$

i.e., if $|a_{N(r)}||z|^{N(r)} > |a_0|(\rho^*)^{N(r)} \cdot \frac{|z|^{N(r)}-1}{|z|-1}$

i.e., if $|a_{N(r)}||z|^{N(r)}(|z|-1) > |a_0|(\rho^*)^{N(r)}\left(|z|^{N(r)}-1\right)$

i.e., if $|a_{N(r)}||z|^{N(r)+1} - \left(|a_{N(r)}| + |a_0|(\rho^*)^{N(r)}\right)|z|^{N(r)} + |a_0|(\rho^*)^{N(r)} > 0.$

Let us consider

$$g(t) \equiv |a_{N(r)}|t^{N(r)+1} - \left(|a_{N(r)}| + |a_0|(\rho^*)^{N(r)}\right)t^{N(r)} + |a_0|(\rho^*)^{N(r)} = 0. \quad (13)$$

The maximum number of positive roots of (13) is two because maximum number of changes of sign in $g(t) = 0$ is two and if it is less, less by two. Clearly $t = 1$ is a positive root of $g(t) = 0$. Therefore $g(t) = 0$ must have exactly one positive root other than 1. Let the positive root of $g(t)$ be t_1. Let us take $t_0 = \max\{1, t_1\}$. Clearly for $t > t_0$, $g(t) > 0$. If not for some $t_2 > t_0$, $g(t_2) < 0$. Also $g(\infty) > 0$. Therefore $g(t) = 0$ has another positive root in (t_2, ∞) which gives a contradiction.

So for $t > t_0$, $g(t) > 0$. Also $t_0 \ge 1$. Therefore $|Q(z)| > 0$ if $|z| > t_0$. So $Q(z)$ does not vanish in $|z| > t_0$. Hence all the zeros of $Q(z)$ lie in $|z| \le t_0$.

Let $z = z_0$ be a zero of $P(z)$. So $P(z_0) = 0$. Clearly $z_0 \ne 0$ as $a_0 \ne 0$.

Putting $z = \rho^* z_0$ in $Q(z)$ we get that

$$Q(\rho^* z_0) = (\rho^*)^{N(r)} \cdot P(z_0) = (\rho^*)^{N(r)} \cdot 0 = 0.$$

Therefore $z = \rho^* z_0$ is a zero of $Q(z)$. So $|\rho^* z_0| \leq t_0$ or $|z_0| \leq \frac{1}{\rho^*} t_0$. As z_0 is an arbitrary zero of $P(z)$,

$$\text{all the zeros of } P(z) \text{ lie in the region } |z| \leq \frac{1}{\rho^*} t_0. \tag{14}$$

In the order to prove the lower bound of Theorem 2 let us consider

$$R(z) = (\rho^*)^{N(r)} z^{N(r)} P\left(\frac{1}{\rho^* z}\right).$$

Then

$$R(z) = (\rho^*)^{N(r)} z^{N(r)} \left(a_0 + \frac{a_1}{\rho^* z} + \cdots\cdots + a_{N(r)} \frac{1}{(\rho^*)^{N(r)} z^{N(r)}}\right)$$
$$= a_0 (\rho^*)^{N(r)} z^{N(r)} + a_1 (\rho^*)^{N(r)-1} z^{N(r)-1} + \ldots\ldots + a_{N(r)}.$$

Now

$$|R(z)| \geq |a_0| (\rho^*)^{N(r)} |z|^{N(r)} - \left|a_1 (\rho^*)^{N(r)-1} z^{N(r)-1} + \cdots\cdots + a_{N(r)}\right|.$$

Also

$$\left|a_1 (\rho^*)^{N(r)-1} z^{N(r)-1} + \cdots\cdots + a_{N(r)}\right| \leq |a_1| (\rho^*)^{N(r)-1} |z|^{N(r)-1} + \ldots\ldots + \left|a_{N(r)}\right|.$$

So applying the condition $|a_0| (\rho^*)^{N(r)} \geq |a_1| (\rho^*)^{N(r)-1} \geq \ldots\ldots \geq \left|a_{N(r)}\right|$ we get from above that

$$-\left|a_1 (\rho^*)^{N(r)-1} z^{N(r)-1} + \cdots\cdots + a_{N(r)}\right| \geq -|a_1| (\rho^*)^{N(r)-1} |z|^{N(r)-1} - \ldots\ldots - \left|a_{N(r)}\right|$$
$$\geq -|a_1| (\rho^*)^{N(r)-1} \left(|z|^{N(r)-1} + \cdots\cdots + 1\right)$$
$$= -|a_1| (\rho^*)^{N(r)-1} \cdot \frac{|z|^{N(r)-1} - 1}{|z| - 1} \text{ for } |z| \neq 1. \tag{15}$$

Using (15) we get for $|z| \neq 1$ that

$$|R(z)| \geq (\rho^*)^{N(r)-1} \left(|a_0| \rho^* |z|^{N(r)} - |a_1| \cdot \frac{|z|^{N(r)-1} - 1}{|z| - 1}\right). \tag{16}$$

Now

$$R(z) > 0 \text{ if } (\rho^*)^{N(r)-1} \left(|a_0| \rho^* |z|^{N(r)} - |a_1| \cdot \frac{|z|^{N(r)-1} - 1}{|z| - 1}\right) > 0$$
$$\text{i.e., if } |a_0| \rho^* |z|^{N(r)} - |a_1| \cdot \frac{|z|^{N(r)-1} - 1}{|z| - 1} > 0$$
$$\text{i.e., if } |a_0| \rho^* |z|^{N(r)} > |a_1| \cdot \frac{|z|^{N(r)-1} - 1}{|z| - 1}$$
$$\text{i.e., if } |a_0| \rho^* |z|^{N(r)} (|z| - 1) > |a_1| \left(|z|^{N(r)-1} - 1\right)$$
$$\text{i.e., if } |a_0| \rho^* |z|^{N(r)+1} - (|a_0| \rho^* + |a_1|) |z|^{N(r)} + |a_1| > 0.$$

Let us consider

$$f(t) \equiv |a_0| \rho^* t^{N(r)+1} - (|a_0| \rho^* + |a_1|) t^{N(r)} + |a_1| = 0.$$

Clearly $f(t) = 0$ has two positive roots, because the number of changes of sign of $f(t)$ is two. If it is less, less by two. Also $t = 1$ is the one of the positive roots of $f(t) = 0$. Let us suppose that $t = t_2$ be the other positive root. Also let $t_0' = \max\{1, t_2\}$ and so $t_0' \geq 1$. Now $t > t_0'$ implies $f(t) > 0$. If not then there exists some $t_3 > t_0'$ such that $f(t_3) < 0$. Also $f(\infty) > 0$. Therefore there exists another positive root in (t_3, ∞) which is a contradiction.
So $|R(z)| > 0$ if $|z| > t_0'$. Thus $R(z)$ does not vanish in $|z| > t_0'$. In otherwords all the zeros of $R(z)$ lie in $|z| \leq t_0'$.
Let $z = z_0$ be any zero of $P(z)$. So $P(z_0) = 0$. Clearly $z_0 \neq 0$ as $a_0 \neq 0$.
Putting $z = \frac{1}{\rho^* z_0}$ in $R(z)$ we get that

$$R\left(\frac{1}{\rho^* z_0}\right) = (\rho^*)^{N(r)} \cdot \left(\frac{1}{\rho^* z_0}\right)^{N(r)} \cdot P(z_0) = \left(\frac{1}{z_0}\right)^{N(r)} \cdot 0 = 0.$$

Therefore $\frac{1}{\rho^* z_0}$ is a root of $R(z)$. So $\left|\frac{1}{\rho^* z_0}\right| \leq t_0'$ implies $|z_0| \geq \frac{1}{\rho^* t_0'}$. As z_0 is an arbitrary zero of $P(z) = 0$,

$$\text{all the zeros of } P(z) \text{ lie in } |z| \geq \frac{1}{\rho^* t_0'}. \tag{17}$$

From (14) and (17) we have all the zeros of $P(z)$ lie in the ring shaped region given by

$$\frac{1}{\rho^* t_0'} \leq |z| \leq \frac{1}{\rho^*} t_0$$

where t_0 and t_0' are the greatest positive roots of $g(t) = 0$ and $f(t) = 0$ respectively.
This proves the theorem.

Corollary 2 From Theorem 2 we can easily conclude that all the zeros of

$$P(z) = a_0 + a_1 z + \ldots\ldots + a_n z^n$$

of degree n with property $|a_0| \geq |a_1| \geq \ldots\ldots \geq |a_n|$ lie in the ring shaped region

$$\frac{1}{t_0'} \leq |z| \leq t_0$$

where t_0 and t_0' are the greatest positive roots of

$$g(t) \equiv |a_n| t^{n+1} - (|a_n| + |a_0|) t^n + |a_0| = 0$$

and

$$f(t) \equiv |a_0|t^{n+1} - (|a_0| + |a_1|)t^n + |a_1| = 0$$

respectively by putting $\rho^* = 1$.

Remark 1 The limit of Theorem 2 is attained by $P(z) = a^2z^2 - az - 1$, $a > 0$. Here $P(z) = a^2z^2 - az - 1$, $a_0 = -1$, $a_1 = -a$, $a_2 = a^2$. Therefore $|a_0| = 1$, $|a_1| = a$, $|a_2| = a^2$. Let $\rho^* = a$. So $|a_0|(\rho^*)^2 \geq |a_1|\rho^* \geq |a_2|$ holds. Hence

$$g(t) \equiv |a_2|t^3 - (|a_2| + a^2|a_0|)t^2 + |a_0|a^2 = 0$$

i.e., $a^2(t^3 - 2t^2 + 1) = 0.$

Now $g(t) = 0$ has two positive roots which are $t_1 = 1$ and $t_2 = \frac{\sqrt{5}+1}{2}$. So $t_0 = \max(t_1, t_2) = \frac{\sqrt{5}+1}{2}$.

$$f(t) \equiv |a_0|\rho^*t^3 - (|a_0|\rho^* + |a_1|)t^2 + |a_1| = 0$$

i.e., $at^3 - (1.a + a)t^2 + a = 0$

i.e., $a(t^3 - 2t^2 + 1) = 0$

i.e., $t = 1$ and $t = \frac{\sqrt{5}+1}{2}$.

Again

$$t_0' = \max(\text{positive roots of } f(t) = 0)$$
$$= \frac{\sqrt{5}+1}{2}.$$

Hence by Theorem 2, all the zeros lie in

$$\frac{1}{\rho^* t_0'} \leq |z| \leq \frac{1}{\rho^*} t_0$$

i.e., $\frac{1}{a\frac{\sqrt{5}+1}{2}} \leq |z| \leq \frac{1}{a}\frac{\sqrt{5}+1}{2}$

i.e., $\frac{\sqrt{5}-1}{2a} \leq |z| \leq \frac{\sqrt{5}+1}{2a}$.

Now

$$P(z) = 0$$

i.e., $a^2z^2 - az - 1 = 0$

i.e., $z = \frac{1 \pm \sqrt{5}}{2a}$.

Let

$$z_1 = \frac{1+\sqrt{5}}{2a} \quad \text{and} \quad z_2 = \frac{1-\sqrt{5}}{2a}.$$

Clearly z_1 lie on the upper bound and z_2 lie on the lower bound of the boundary. Also here the order $\rho = 0$ because $M(r) = |a^2|r^2 = a^2r^2$ for large r in the circle $|z| = r$. Therefore

$$\rho = \limsup_{r \to \infty} \frac{\log\log M(r)}{\log r} = \limsup_{r \to \infty} \frac{\log\log a^2r^2}{\log r}$$
$$= \limsup_{r \to \infty} \frac{\frac{1}{\log a^2r^2} \cdot \frac{1}{a^2r^2} \cdot 2a^2r}{\frac{1}{r}} = \limsup_{r \to \infty} \frac{2}{\log a^2r^2} = 0.$$

Also $\rho^* = 2$ and $N(r) = 2 \leq (\log r)^{2+\varepsilon}$ for $\varepsilon > 0$ and sufficiently large r in $|z| \leq \log r$ and $a_n = 0$ for $n \neq N(r)$.

Corollary 3 Under the conditions of Theorem 2 and

$$P(z) = a_0 + a_{p_1}z^{p_1} + \ldots\ldots + a_{p_m}z^{p_m} + a_{N(r)}z^{N(r)}$$

with

$$1 \leq p_1 \leq p_2 \ldots\ldots \leq p_m \leq N(r) - 1,$$

where p_i's are integers a_0, a_{p_1}, ……., $a_{N(r)}$ are non vanishing coefficients with

$$|a_0|(\rho^*)^{N(r)} \geq |a_{p_1}|(\rho^*)^{N(r)-p_1} \geq \ldots\ldots \geq |a_{p_m}|(\rho^*)^{N(r)-p_m} \geq |a_{N(r)}|$$

then we can show that all the zeros of $P(z)$ lie in

$$\frac{1}{\rho^* t_0'} \leq |z| \leq \frac{1}{\rho^*} t_0$$

where t_0 and t_0' are the greatest positive roots of

$$g(t) \equiv |a_{N(r)}|t^{N(r)+1} - \left(|a_{N(r)}| + |a_0|(\rho^*)^{N(r)}\right)t^{N(r)} + |a_0|(\rho^*)^{N(r)} = 0$$

and

$$f(t) \equiv |a_0|(\rho^*)^{p_1}t^{N(r)+1} - \left(|a_0|(\rho^*)^{p_1} + |a_{p_1}|\right)t^{N(r)} - |a_{p_1}| = 0 \text{ respectively.}$$

Corollary 4 If we put $\rho^* = 1$ in Corollary 3 then all the zeros of

$$P(z) = a_0 + a_{p_1}z^{p_1} + \ldots\ldots + a_{p_m}z^{p_m} + a_nz^n$$

lie in the ring shaped region

$$\frac{1}{t_0'} \leq |z| \leq t_0$$

where t_0 and t_0' are the greatest positive roots of

$$g(t) \equiv |a_n|t^{n+1} - (|a_n| + |a_0|)t^n + |a_0| = 0$$

and

$$f(t) \equiv |a_0|t^{n+1} - \left(|a_0| + |a_{p_1}|\right)t^n - |a_{p_1}| = 0 \text{ respectively}$$

provided

$$|a_0| \geq |a_{p_1}| \geq \ldots\ldots \geq |a_{p_m}| \geq |a_n| \cdot$$

REFERENCES

[1]. Chattopadhyay, A.; Das, S.; Jain, V. K. and Knower, H.: Certain generalization of Eneström-Kakeya theorem, J. Indian Math. Soc., Vol. 72, No. 1 - 4(2005), pp.147 - 156.
[2]. Datta, B. and Govil, N. K.: On the location of the zeros of polynomial, J. Approximation Theory, Vol. 24(1978), pp. 78 - 82.
[3]. Datta, S.K. and Biswas, T.: On the definition of a meromorphic function of order zero, Int. Mat. Forum, Vol. 4, No. 37(2009), pp.1851 - 1861.
[4]. Das, S. and Datta, S. K.: On Cauchy's proper bound for zeros of a polynomial , International J. of Math. Sci. and Engg. Apples. (IJMSEA), Vol. 2, No. IV (2008), pp.241 - 252.
[5]. Govil, N. K. and Rahaman, Q. I.: On the Eneström-Kakeya theorem, Tohoku Math. J. Vol. 20(1968), pp.126 - 136.
[6]. Joyal, A., Labelle, G. and Rahaman, Q. I.: On the location of zeros of polynomials, Canad. Math. Bull., Vol. 10(1967), pp.53 - 63.
[7]. Jain, V. K. : On the location of zeros of polynomials, Ann. Univ. Mariae Curie-Sklodowska, Lublin-Polonia Sect. A, Vol. 30(1976), pp. 43 - 48.
[8]. Jain, V. K.: On Cauchy's bound for zeros of a polynomial, Truck. J. Math. Vol. 30(2006), pp.95 - 100.
[9]. Marden, M.: Geometry of polynomials, Amer. Math-Soc. Providence, R.I., 1966.
[10]. Mohammad, Q. G.: Location of zeros of polynomials , Amer. Math. Monthly, Vol. 74(1967) , pp. 290 - 292.
[11]. Sun, Y. J. and Hsieh, J. G.: A note on circular bound of polynomial zeros, IEEE Trans. Circuit Syst. Vol. 143(1996), pp. 476 - 478.
[12]. Valiron, G.: Lectures on the general theory of integral functions, Chelsea Publishing Company (1949).
[13]. Zilovic, M. S.; Roytman, L. M.; Combetts, P. L. and Swami, M. N. S. : A bound for the zeros of polynomials, *ibid* Vol. 39(1992) , pp. 476 - 478.

International Journal of Modern Engineering Research (IJMER)
www.ijmer.com Vol. 3, Issue. 4, Jul - Aug. 2013 pp-2205-2214 ISSN: 2249-6645

Optimal Control Problem and Power-Efficient Medical Image Processing Using Puma

Himadri Nath Moulick[1], Moumita Ghosh[2]

[1]*CSE, Aryabhatta Institute of Engg& Management, Durgapur, PIN-713148, India*
[2]*CSE, University Institute Of Technology, (The University Of Burdwan) Pin -712104, India*

ABSTRACT: *As a starting point of this paper we present a problem from mammographic image processing. We show how it can be formulated as an optimal control problem for PDEs and illustrate that it leads to penalty terms which are non-standard in the theory of optimal control of PDEs. To solve this control problem we use a generalization of the conditional gradient method which is especially suitable for non-convex problems. We apply this method to our control problem and illustrate that this method also covers the recently proposed method of surrogate functional from the theory of inverse problems. Graphics processing units (GPUs) are becoming an increasingly popularplatform to run applications that require a high computation throughput.They are limited, however, by memory bandwidth and power and, assuch, cannot always achieve their full potential. This paper presents thePUMA architecture - a domain-specific accelerator designed specificallyfor medical imaging applications, but with sufficient generality to makeit programmable. The goal is to closely match the performance achievedby GPUs in this domain but at a fraction of the power consumption. Theresults are quite promising - PUMA achieves upto 2X the performance of a modern GPU architecture and has up to a 54X improved efficiency on a floating-point and memory-intensive MRI reconstruction algorithm.*

KEYWORDS: *generalized conditional gradient method, surrogate functional, image processing, optimal control of PDEs*

I. INTRODUCTION

For many years medical imaging has aimed at developing fully automatic, software based diagnostic systems. However, the success of those automatic systems is rather limited and the human expert is as much responsible for the final diagnosis as in previous years. Hence, growing effort has been devoted to enhancing the techniques for presenting the medical images as well as additional information. In Germany a particular effort is made in mammography, i. e. X-ray scans of the female breast for early detection of breast cancer. The process of examination by the medical experts is divided into a very short recognition phase (< 1 sec.) and a second verification phase (≈ 1 min.). During the recognition phase, the expert first recognizes the coarse features, then more and more fine features. Tests have shown, that the experts usually form their decisions during this very short recognition phase. Nevertheless, the verification phase is the more critical one. The critical and difficult cases, where the recognition phase does not end with a preliminary diagnosis, most often applies to women in the early stages of cancer. During the verification phase the expert shifts forwards and backwards, thereby alternating in examining small details and in catching an overall impression of the location of critical patterns within the organ. The advent of programmable graphics processing units, or GPUs, for general-purpose computing is one of the major steps taken in computing over the last few years. These GPGPUs which, in the past, have been predominantly used for gaming and advanced image and video editing are now being used by many developers to accelerate inherently parallel programs in several other domains. Indeed, considerable amounts time and engineering effort are often spent in order to modify programs so that they may run effectively on GPUs.Several different application domains observe remarkable speedups when using GPUs, including the following [18]:• 4X to 100X speedup on medical applications, such as biomedical image analysis, 3D reconstruction of tissue structures for large sets of microscopic images and accelerating MRI reconstructions.• 8X to 260X speedup on electronic design automation, such as power grid analysis and statistical static timing analysis.• 4X to 327X speedup on physics applications, such as weather prediction and astrophysics.• 11X to 100X speed up financial applications such as instrument pricing using Monte-Carlo methods.

II. MOTIVATION FROM MEDICAL IMAGING

This process can be supported by presenting the expert different versions of the original image during close up and normal sub phases. More precisely, the expert sees a version with contrast enhanced small details in a close up phase (‘fine scale’), while he sees an image which preserves all major edges but smoothes within regions (‘coarse scale’) during the normal phase. For enhancing fine details in mammography images a variety of algorithm have been proposed. Many of them are based on the wavelet transform due to its property of dividing an image into different scale representations; see for example [7] and references therein. In this work we deal with the development of an optimized presentation for one cycle of the verification phase. To put the problem in mathematical terms, we start with a given image y0 assumed to be a function defined on $\Omega := [0,1]^2$. The fine scale and the coarse scale image are denoted yf and yc respectively. Under the natural assumption of finite energy images wemodel them as functions in $L^2(\Omega)$The goal is, to produce a movie (i. e. atime dependent function) y: $[0,1] \rightarrow L^2(\Omega)$, from the given images y0, yfand yc such that• the movie starts in y0, i. e. y(0) = y0,

the movie sweeps to the fine scale image and to the coarse scale image,e. g. y(t) ≈ yffor t∈[.2, .4] and y(t) ≈ ycfor t∈[.6, .8],• the movie sweeps in a "natural" way.An example for a mammography image, a fine scale, and coarse scale imageis shown in Fig 1. As a first guess one could try to make a linear interpolationbetween the fine scale and the coarse scale representation. Thismethod has one serious drawback: It does not take the scale sweep into account,i. e. all fine details are just faded in rather than developing one afteranother.

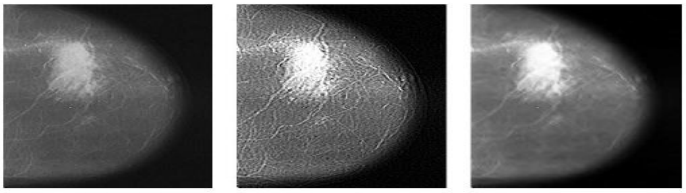

Fig 1: A mammography image. Left: original image y0, middle: fine scale image yf , right: coarse scale image yc
Modeling as an optimal control problem

III. PDES AND CONTROL PROBLEMS IN IMAGE PROCESSING

Parabolic partial differential equations are a widely used tool in image processing. Diffusion equations like the heat equation [14], the Perona-Malik equation [10] or anisotropic equations [13] are used for smoothing, denoising and edge enhancing. The smoothing of a given image $y_0 \in L^2(\Omega)$ with the heat equation isdone by the solution of the equation

$$\begin{aligned} y_t - \Delta y &= 0 \quad \text{in } [0,1] \times \Omega \\ y_\nu &= 0 \quad \text{on } [0,1] \times \partial\Omega \\ y(0) &= y_0 \end{aligned} \tag{1}$$

Where y_ stands for the normal derivative, i. e. we impose homogeneous Neumann boundary conditions.

The solution y: $[0,1] \to L^2(\Omega)$ gives a movie which starts at the image y0 and becomes smoother with time t. This evolution is also called scale space and is analyzed by the image processing community in detail since the 1980s. Especially the heat equation does not create new features with increasing time, see e. g. [5] and the references therein.
Thus, the heat equation is well suited to model a sweep from a fine scale image yf to a coarse scale image yc. Hence, we take the image yf as initial value. To make the movie y end at a certain coarse scale image yc instead of its given endpoint y(1) we propose the following optimal control problem:

$$\begin{aligned} \text{Minimize} \quad & J(y,u) = \frac{1}{2}\int_\Omega |y(1) - y_c|^2 dx + \frac{\alpha}{2}\int_0^1\int_\Omega |u|^2 \, dxdt \\ \text{subject to} \quad & y_t - \Delta y = u \quad \text{in } [0,1] \times \Omega \\ & y_\nu = 0 \quad \text{on } [0,1] \times \partial\Omega \\ & y(0) = y_f. \end{aligned} \tag{2}$$

In other words, the diffusion process is forced to end in yc with the help of a heat source u.

III.1: Adaption to image processing: The above described problem is classical in the theory of optimal control of PDEs, though not well adapted to image processing. The solution of this problem may have several drawbacks: The control u will be smooth due to the regularization and have a large support. This will result in very smooth changes in the image sequence y and, more worse, in global changes in the whole image. To overcome these difficulties, different norms can beused for regularization. A widely used choice in image processing is to use Besov norms because they are appropriate to model images. Besov norms can be defined in different ways, e. g. in terms of moduli of smoothness [12] or in terms of Littlewood-Paley decompositions [6]. Here we take another viewpoint and define the Besov spaces via norms of wavelet expansions [2, 9].For a sufficient smooth wavelet ψ the Besov semi norm of a function f on a set $M \subset \mathbf{R}^d$ is defined as

$$|f|^q_{B^s_{p,q}(M)} = \sum_j \left(2^{sjp} 2^{j(p-2)d/2} \sum_{i,k} |\langle f, \psi_{i,j,k}\rangle|^p \right)^{q/p} \tag{3}$$

Where j is the scale index, k indicates translation and i stand for the directions. The Besov space Bsp, q (M) is defined as the functions f∈Lp (M) that has a finite Besov semi norm. See [6, 9] for a more detailed introduction to wavelets and Besov spaces.

III.2: The solution of the PDE and the control-to-state mapping: The solution of the heat equation is a classical task. If we assume that the initial value yf is in L2(Ω) and the control u is in L2([0, 1] ×) the solution y is in L2(0, 1,H1(Ω)) ∩ C([0, 1],L2(Ω)). Especially y is continuous with respect to time and the point evaluation y(1) makes sense, see e. g. [8]. In our

case the solution operator $u \mapsto y$ is affine linear, due to the nonzeroinitial value. We make the following modifications to come back to a linear problem: We split the solution into two parts. The non-controlled part yn is the solution of

$$\begin{aligned} y_t^n - \Delta y^n &= 0 \\ y^n(0) &= y_f \end{aligned}$$

and the homogeneous part y^h is the solution of

$$\begin{aligned} y_t^h - \Delta y^h &= u \\ y^h(0) &= 0 \end{aligned} \tag{4}$$

(Both with homogeneous Neumann boundary conditions). Then the solution operator G : $u \mapsto y^h$ of equation (1) is linear and continuous from L2([0, 1],L2(Ω)) to L2(0, 1,H1(Ω)) ∩ C([0, 1],L2(Ω)). With the help of the point evaluation operator we have the control-to-state mapping K: $u \mapsto$ yh (1) linear and continuous from L2 ([0, 1],L2(Ω)) to L2(Ω). Then the solution is y = yn + yh and we can focus on the control problem for yh. Together with the thoughts of the previous subsection we end up with the following minimization problem:
Minimize

$$J(u) = \frac{1}{2}\|Ku - y_c + y^n(1)\|^2_{L^2(\Omega)} + \alpha |u|^p_{B^s_{p,p}([0,1]\times\Omega)}. \tag{5}$$

III.3. Solution of the optimal control problem: The minimization of the functional (2) is not straightforward. The no quadratic constraint leads to a nonlinear normal equation which can not be solved explicitly. Here we use a generalization of the conditional gradient method for the minimization.

IV. THE GENERALIZED CONDITIONAL GRADIENT METHOD

The classical conditional gradient method deals with minimization problems of the form

$$\min_{u \in C} F(u), \tag{6}$$

here C is a bounded convex set and F is a possible non-linear function. One notices that this constrained problem can actually be written as an "unconstrained" one with the help of the indicator functional

$$I_C(u) = \begin{cases} 0 & u \in C \\ \infty & u \notin C \end{cases}.$$

With Φ = IC, problem (3) thus can be reformulated as

$$\min_{u \in H} F(u) + \Phi(u). \tag{7}$$

To illustrate the proposed generalization, we summarize the key properties of F and Φ: F is smooth while Φ may contain non-differentiable parts. The minimization problem with Φ alone is considered be solved easily while the minimization of F is comparatively hard. The influence of Φ is rather small in comparison to F. With these assumptions in mind, the conditional gradient method can also be motivated as follows. Let u ∈H be given such that _(u) <∞. We like to find an update direction by a linearized problem. Since Φ is not differentiable, we only linearize F:

$$\min_{v \in H} \langle F'(u)|v\rangle + \Phi(v). \tag{8}$$

The minimizer of this problem serves as an update direction.So this "generalized conditional gradient method" in the (n+1)–st step reads as follows: Let un∈H be given such that Φ (un) <∞.

1. Determine the solution of (5) and denote it vn.
2. Set sn as a solution of

$$\min_{s\in[0,1]} F(u_n + s(v_n - u_n)) + \Phi(u_n + s(v_n - u_n)).$$

3. Let $u_{n+1} = u_n + s_n(v_n - u_n).$

To ensure existence of a solution in Step 1 we state the following condition:Assumption 1 Let the functional Φ : H →]−∞,∞] be proper, convex, lower semi-continuous and coercive with respect to the norm. Standard arguments from convex analysis yield the existence of a minimize in Step 1 of the algorithm [4]. So if F is G^ateaux-differentiable in H, the algorithm is well-defined. The convergence of the generalized conditional gradient method is analyzed in detail by the authors in [1]. The main result there is the following theorem.

Theorem 2 Let Φ satisfy Assumption 1 and let every set Et = {u ∈H | Φ (u) ≤ t} be compact. Let F be continuously Fr´echet differentiable, let F +_ be coercive and u0 be given such that Φ (u0) <∞. Denote (un) thesequence generated by the generalized conditional gradient method.Then every convergent subsequence of (un) converges to a stationarypoint of F + Φ At least one such subsequence exists.Two remarks are in order: First, we notice that the theorem is also validif the functional F is not convex. Second, the theorem only gives convergenceto a stationary point which may seem unsatisfactory, specially if one wantsto minimize non-convex functions. But this does not have to be a drawback,as we will see in the next section:

1. Application: Here we show the application of the above described methodology. Since the effects can be seen more clearly in artificial images, we will not use original images. The artificial images we used are shown in Fig 2.

Fig 2: Images used for illustration. Left: fine scale image, right: coarse scale image.

For illustration we use the values p = 1 and s = 3/2 + " > 3/2 in theminimization problem (2), since this is close to the BV -norm and we have $B_{1,1}^{3/2+\varepsilon}([0,1]\times\Omega) \subset L^2([0,1]\times\Omega)$ compactly.

The results are presented in Figure 3. The figure shows a comparison of the linear interpolation, the pure result of the application of the heat equation and the result of the optimal control problem. One sees that the linear interpolation is only fading out the details. In the uncontrolled result(middle column) the details are vanishing one after another but the process does not end in the desired endpoint. The result of the optimal control problem (right column) exhibits both a nice vanishing of the details and end in the given endpoint.

V. THE ADVANTAGES OF GPUs

GPUs have many appealing hardware features. Firstly, they lend themselves very well to both thread-level and data-level parallelism.Thread-level parallelism (TLP) is exploited by having a large numberof independent processing elements (PEs) on the GPU, each with itsown set of functional units (FUs) and local storage. Individual threadscan quite cleanly be assigned, either statically by the programmer ordynamically by the hardware, to each of these PEs and inter-threadcommunication is made possible by some form of interconnect fabricor through local storage such as caches. Programs with a large amountof data-level parallelism (DLP) can make use of vector-SIMD units inthese PEs which allow a single instruction to perform an operationon several data at the same time. DLP can also be extracted inprograms with compute-intensive loops that have little or no interiteration dependencies by executing operations from different iterationswithin a single SIMD instruction.Secondly, GDDR RAM and its increasingly fast successor's haveallowed for GPUs to have access to an immense amount of memorybandwidth. The AMD Radeon HD 4870 - the first GPU to supportGDDR5 memory - has a memory bandwidth of up to 115 GB/s.Above all, GPUs are commodity hardware products commonly availableas a part of many desktop and laptop computers. The tools toprogramthem are also easily available; NVIDIA's Compute UnifiedDevice Architecture (CUDA) package, for example, is free to downloadfrom their website [15]. CUDA is a general purpose parallel computingarchitecture which consists of the CUDA instruction set and the computeengine in the GPU. It provides a small set of extensions to the C programming language, which enables straightforward implementation of parallel algorithms on the GPU. CUDA also supports scheduling the computation between CPU and GPU, such that serial portions of applications run on the CPU and parallel portions are mapped to the GPU. Individual cores in Intel's up-and-coming Larrabee processor

implement the ubiquitous x86 ISA [23], allowing users to use a host of already-existing development tools to port their applications to it. Server products like Tesla [17] with even more compute power are also available.

VI. THE QUEST FOR PROGRAMMABLE AND SPECIALIZED HARDWARE

A wide range of architectures, in addition to GPUs, have beendesigned before to address the problem of providing high performancecomputation efficiently. These solutions maintain or sacrifice programmability to various degrees depending on the domain they target. Fig 3 shows the performance (on the y-axis) and programmability (on the x-axis) expectations from various architecture styles. The numbers next to each of the ovals shows the approximate performance-power ratio offered by each of these solutions.General purpose processors (GPPs) which fall on the lower rightcorner of the figure, are highly programmable solutions but are limitedin terms of the peak performance they can achieve. Further, structureslike instruction decoders and caches that are needed to support programmability consume energy. This results in a very low computational efficiency of about 1 MIPS-per-mW, for example, for the Intel Pentium- M processor. On the other end of the spectrum are Application-specific Integrated Circuits (ASICs). ASICs are custom-designed specifically for a particular problem, without extraneous hardware structures. Thus, ASICs havea high computational density with hardwired control, resulting in high computation efficiency up to 1,000 to 10,000 times more than that of GPPs. The space between these two extremes is populated by different solutions that have varying degrees of programmability. Application specific instruction-set processors (ASIPs) are processors with custom extensions for a particular application or applicationdomain. They can be quite efficient when running the applications for which they are designed, and they are also capable of running any other application, though with reduced efficiency. Examples include processors from Tensilica and ARC, transport triggered architectures [3] and custom-fit processors [9]. Domain loop accelerators are designed to execute computation intensive loops present in media and signal processing domains. Their design is close to that of VLIW processors, but with a much higher number of function units, and consequently, a higher peak performance. Very long instruction words in a control memory direct all FUs every cycle. However, domain loop accelerators (LAs) have less flexibility than GPPs because only highly computationally-intensive loops map well to them. Some examples of architectures in this design space are RSVP [1] and CGRAs [14]. Coarse-grain adaptable architectures have coarser-grain building blocks compared to FPGAs, but, like FPGAs, still maintain bit-level reconfigurability. The coarser reconfiguration granularity improves the computation efficiency of these solutions. However, non-standard tools are needed to map computations onto them and their success has been limited to the multimedia domain. PipeRench [10], RaPiD [6] are some examples of coarse-grain adaptable architectures.

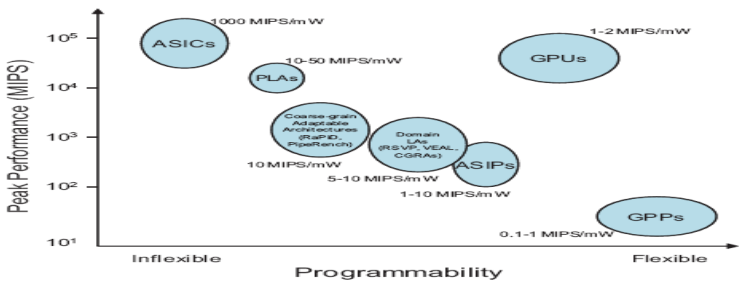

Fig. 3.Comparison of peak performance, power efficiency, and programmability of different architecture design styles.

1. **Programmable Loop Accelerators:** The programmable solutions shown in Figure 1 are all "universally"programmable, allowing any loop to be mapped on to them, although atvarying degrees of efficiency. There is a wide gap between the efficiency that can be achieved by ASICs and the efficiency that can be achieved by these programmable solutions. There are, for example, instances where there is a narrow requirement of flexibility. Using any of these above solutions is overkill for these instances as these solutions sacrifice too much efficiency for the needed flexibility. Further, most of the middlegroundsolutions listed above do not offer any support for fast floatingpoint computation, which limits the number of applications that they can be used for. This work advocates an open area in the design space where a non-trivial amount of programmability is provided in terms of intraprocessor communication, functionality and storage, but the application and domain-specific design, as a whole, resembles an ASIC more than a processor. The design point is labeled Programmable Loop Accelerator, or PLA (not to be confused with programmable logic array).

TABLE 1.Medical application characteristics

Benchmark	#instrs	%FP	Data Req'd $\frac{bytes}{instr}$
MRI.FH	38	42	0.95
MRI.Q	34	35	1.06
CT.segment	26	42	1.38
CT.laplace	20	30	1.20
CT.gauss	22	32	1.09

VII. TARGETING MEDICAL APPLICATIONS

Medical imaging devices are generally large, bulky and expensivemachines that have very limited portability and consume large amountsof power. There is an increasing focus on reducing the power ofthese medical imaging devices [20]. In order to address this issue,this work focuses on principle components of Computed Tomography

(CT) and Magnetic Resonance Imaging (MRI) image processing andreconstruction. A CT scan involves capturing a composite image from a series of X-Ray images taken from various angles around a subject. It produces a very large amount of data that can be manipulated using a variety of techniques to best arrive at a diagnosis. Oftentimes, this involves separating different layers of the captured image based on their radio densities. A common way of accomplishing this is by using a well known image-processing algorithm known as "image segmentation". In essence, image segmentation allows one to partition a given image into multiple regions based on any of a number of different criteria such as edges, colors, textures, etc. Being able to partition images in this manner allows for studying of isolated sections of the image rather than of all the information that was captured.The segmentation algorithm used in this work has three main floating-point- intensive components: Graph segmenting (CT.segment), Laplacian filtering (CT. Laplace) and Gaussian convolution (CT. gauss).

aplacian filtering highlights portions of the image that exhibit a rapid change of intensity and is used in the segmentation algorithm for edge detection. Gaussian convolution is used to smooth textures in an image to allow for better partitioning of the image into different regions. An MRI scan, instead of using X-Rays, uses a strong magnetic and radio frequency fields to align, and alter the alignment of, hydrogen atoms in the body. The hydrogen atoms then produce a rotating magnetic field that can be detected by the MRI scanner and converted to an image. The main computational component of reconstructing an MRI image is calculating the value of two different vectors, known here as MRI.FH and MRI.Q, respectively (explained in more detail in [13], [24]). Table I shows some characteristics of the benchmarks in consideration. All of these benchmarks are floating-point-intensive and require large amounts of data for the computation they perform, especially when compared to the 0.15 bytes/instruction supported by the GTX 280 GPU mentioned earlier.

The main loops in these benchmarks are "do-all" loops - there are no inter-iteration dependences. Prior work in this field has predominantly focused on using commercial products to accelerate medical imaging. For instance, in [11], the authors port "large-scale, biomedical image analysis" applications to multi-core CPUs and GPUs, and compare different implementation strategies with each other. In [21], the authors study image registration and segmentation and accelerate those applications by using CUDA on a GPU. In [24], the authors use both the hardware parallelism and the special function units available on an NVIDIA GPU to dramatically improve the performance of an advanced MRI reconstruction algorithm.

There are several other such examples of novel work in this field. In contrast with such research, this work focuses on designing a new, highly efficient, microarchitecture and architecture with the specific hardware requirements of medical imaging in consideration.

VIII. PUMA

PUMA, ***P***arallel ***micro***-architecture for ***M***edical ***A***pplications, is a tiled architecture as shown in Fig 4. It is specifically designed to maximize power-efficiency when executing medical imaging applications while still retaining full programmability. Each tile in PUMA is an instance of a specialized PLA - a generalized loop accelerator. The PLA tiles are connected to their neighboring tiles and to the external interface through a high-bandwidth mesh of on-chip routers.

1. **Background:** Fig. 5 shows the hardware schema for the single-function loop accelerator [7], [5]. The LA is designed to efficiently execute a modulo scheduled loop [19] in hardware. The lengths of the schedule, and the corresponding run-time of the loop, are determined by the *initiationinterval* (II) - the number of cycles between the beginnings of successive iterations of the loop. Thus, a lower II corresponds to a shorter schedule and increased performance. The modulo schedule contains a *kernel* that repeats every II cycles and may include operations from multiple loop iterations. The LA is designed to exploit the high degree of parallelism available in modulo scheduled loops with a large number of function units (FUs).Each FU performs a specific set of functions that is tailored for the particular loop. Each FU writes to a dedicated shift register file (SRF); in each cycle, the contents of the registers shift downwards to the next register. Point-to-point wires from the registers to FU inputs allow data transfer from producers directly to consumers. Multiple registers may be connected to each FU input; a multiplexer (MUX) is used to select the appropriate one. Since the operations executing in a modulo scheduled loop are periodic, the selector for this MUX is essentially a modulo counter. In addition, a central register file (CRF) holds static live-in register values that cannot be stored in the SRFs. The schema described is a template that is customized for the particular loop being accelerated. The number, types, and widths of the FUs, the widths and depths of the SRFs, and the connections from the SRFs to the FUs are all determined from the loop. During synthesis, the loop is first modulo scheduled to meet a given performance requirement, and then the details of the LA datapath are determined from the communication patterns in the scheduled loop.The control path for the single-function LA consists of a finite state machine with II states corresponding to each of time slots in the kernel of the modulo schedule. In each state, control signals direct the execution of FUs (for FUs capable of multiple operations) and control the MUXes at the FU inputs. Finally, a Verilog HDL realization of the accelerator is generated by emitting modules with pre-defined behavioral Verilog descriptions that correspond to the datapath elements. A simulation environment is used to verify that the Verilog properly implements the loop. Finally, gatelevel synthesis, placement, routing, power analysis and post-synthesis verification are performed on the design.

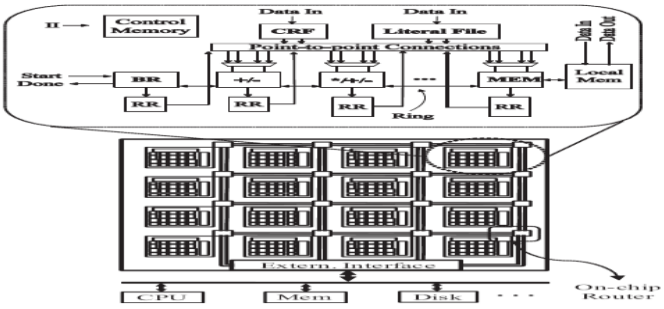

Fig. 4. PUMA. Each tile comprises of a programmable loop accelerator (template pictured) and the control and data memories required for its operation. On-chip routers transfer data between each tile and the external interface.

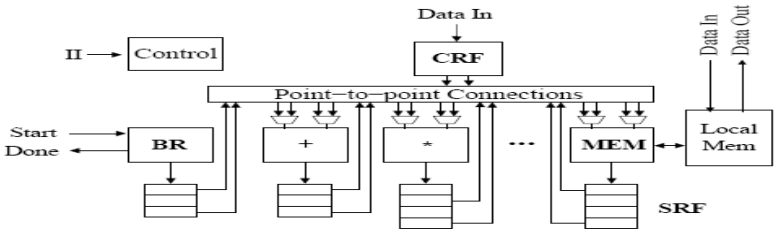

Fig. 5.Template for single-function loop accelerator.

2. PUMA Architecture

2.1. ***Base line PLA Design:*** A PLA is generalized loop accelerator,created by modifying the template datapath shown in Figure 5. A generic datapath template for the PLA is illustrated on the right side of Figure 4 The accelerator is designed for a specific loop at a specific throughput, but contains a more general datapath than the single-function LA to allow for different loops to be mapped onto the hardware [8]. These generalizations provide the LA with flexibility in functionality, storage, control and communication. To provide functionality, simple modifications were made to FUs inorder for them to support more operations; adders (both integer andfloating-point) are generalized to adder/subtracter units, left-shift unitsare generalized to left/right rotators, every FU can execute an identityoperation to act like a move instruction, etc. Even load-store units canbe generalized to integer adder/subtracter units if they already had thefunctionality to compute indirect addresses. Further, the input-muxes toFUs are redesigned to allow for operand-swapping as well.The SRFs used in the LA have limited addressability and fixed lifetimesfor variables. To overcome these constraints and provide moregenerality, these SRFs are replaced with rotating-register files (RRs).To improve controllability, the LA's finite state machine is replacedwith a control memory, the contents of which can be changed based onthe loop that needs to be executed. Further, numerical constants whichwere hard-coded in the LA are instead stored in a literal register file.To generalize communication, the PLA has a bus (in addition to thepoint-to-point connections) that connects all the RRs to all the FUs. Toreduce the hardware cost of having a potentially long bus, its width islimited to one operand, but has a predictable latency of one cycle.

$$\text{Maximize:}$$

$$\sum_{i \in T_\alpha} \sum_{j \in T_\beta} C_{ij} \qquad \forall \alpha \forall \beta : \alpha \neq \beta$$

$$\text{Subject to:}$$

$$\begin{array}{lll}
(1) & \sum_{j=0}^{\#FUs} X_{ij} = 5 & i \in [0, \#FUs) \\
(2) & X_{ii} = 1 & i \in [0, \#FUs) \\
(3) & C_{ii} = 1 & i \in [0, \#FUs) \\
(4) & X_{ij} = X_{ji} & i, j \in [0, \#FUs) \\
(5) & C_{ij} = C_{ji} & i, j \in [0, \#FUs) \\
(6) & C_{ij} \leq X_{ij} + I_{ij} & i, j \in [0, \#FUs)
\end{array}$$

Fig. 6.ILP formulation for FU arrangement on the PUMA ring

2.2. ***PUMA PLA:*** The PLA bus is not always a viable solution. Onemain disadvantage with the bus is that it is not a scalable solutionfor larger PLAs with many FUs. Further, the bus only carries a singleoperand per cycle, limiting the amount of programmability available inthe PLA and the sequences of opcodes that can be executed in parallel.To overcome these limitations, the intra-PLA communication fabricin PUMA is changed to a ring. A ring allows for as many operands to betransferred as there are connections to FUs. It does have its limitations,however. The assumed single-cycle latency to transfer data betweentwo arbitrary points in the PLA using the bus is no longer valid, asit takes one cycle to transfer an operand from one ring connection(or ring stop) to another. Also, the longer the distance an operandneeds to travel on the ring, the more FUs that have to execute moveinstructions to propagate the operand along at each ring stop. Theseadded instructions can potentially increase the loop's schedule lengthand reduce the accelerator's performance. In PUMA, the ring architecture actually consists of six rings (three sets of two rings going in opposite directions). The first set of rings has a

Bus/FU connector (or ring-stop) at every single FU. The second set of rings has a ring-stop at all the odd-numbered FUs, and the third set of rings has a ring-stop at all the even-numbered FUs. This effectivelyconnects an FU/RF pair to its two neighbors and also to its neighbors'neighbors; i.e. every FU can communicate with itself or with otherFUs one or two positions on either side of it on the ring. With thisconfiguration, the number of cycles required to transmit data betweenany two arbitrary FUs is no more than $\lceil \frac{\#FUs}{4} \rceil$, and regardless of theordering of FUs on the ring, every possible producer-consumer pairingcan be executed, provided sufficient time.In order to best maintain generality, we chose to arrange the FUs along the ring to allow maximum connectivity and to distribute the varioustypes of FUs as evenly as possible. This was done by formulatingthe problem as an integer linear program (ILP) as shown in Fig 6.In the objective function, T_ and T_ are two different sets of FUs, each set having all and only the FUs of a particular type. The subscriptsi and j are FU IDs and Cij is a binary variable that is 1 if a connectionexists between FU i and FU j. Essentially, this objective function aimsto maximize the number of connections between different types of FUs, subject to the following constraints: In constraint set (1), Xij is a binary variable that is 1 if FU i is"positioned" adjacent to FU j, implying that they are connected bythe ring. Every FU, therefore, is "positioned" next to 5 other FUs:itself, its two neighbors and the two additional FUs neighboringits neighbors. • Constraint sets (2) and (3) specify that every FU is "positioned"next to and connected to itself.• Constraint sets (4) and (5) specify that all added connections arebidirectional.• In constraint set (6), Iij is a binary number that is 1 if a connectionbetween FU i and FU j has already been inserted by the synthesistool. This constraint enforces the rule that a connection betweenFU i and FU j can only exist if they are either "positioned" nextto each other or are already connected. A 7th set of constraints was initially used which specified thatthere must always be a path between any two FUs with exactly $\lceil \frac{\#FUs}{4} \rceil$ connections between them This constraint was used toprevent insular sets of 5 FUs or sets of 5 FUs connected linearlyrather than in a ring (i.e. without a direct connection between thetwo ends). While this problem might occur in theory, the preexistingconnections put in place by the synthesis system preventit from happening in practice and these constraints were removedto reduce the size of the ILP. Once the optimal solution is obtained, the values of the Xij variables provide a unique ring arrangement.

IX. EXPERIMENTS AND RESULTS

1. Setup: All the PLAs in this work were synthesized for (and run at) afrequency of 450 MHz. The logic synthesis was done using SynopsysDesign Compiler 2006-06 and Synopsys Physical Compiler 2006-06,targeting a 65nm process technology with a nominal supply voltage of0.9 Volts. Energy numbers were obtained using Synopsys PrimeTime-PX 2006-12. For the purposes of this study, we assume that a peakmemory bandwidth of 142 GB/s is available to each PUMA system.This is the same amount of bandwidth afforded to the NVIDIA GTX280 processor.

2. PLA Characteristics: PUMA systems were built using PLAs for each of the five benchmarksin considerations (five systems, each composed entirely ofmultiple tiles of a single type of PLA). Table II shows variouscharacteristics of these accelerators. The "Peak Perf." columns show

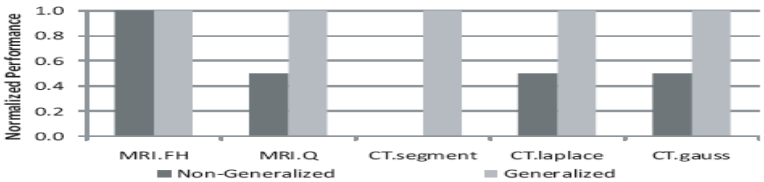

Fig. 7.Normalized performance of benchmarks on LA and PUMA PLA designed for MRI.FH

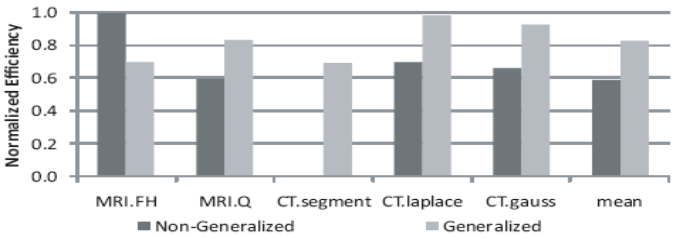

Fig. 8.Normalized $\frac{Performance}{Power}$ efficiency of benchmarks relative to MRI.FH

The throughput when executing floating-point operations and integer operations, respectively, in billions of operations per second. The nextcolumn shows the minimum bandwidth required by each applicationto prevent starvation. Finally, the last column shows the total numberof tiles of each PLA that would be present in a PUMA system. Thenumber of tiles was chosen to prevent data starvation, to make the mostefficient use of the resources available. For example, the number

of tilesin a system with MRI.FH tiles is $\left\lceil \frac{142}{16.2} \right\rceil$ or 9.Fig 8 shows the normalized performance difference betweenthe non-generalized and generalized loop accelerators across various

Benchmarks, to illustrate the effects of the modifications made to thebaseline accelerator to increase programmability. Each of the different benchmarks were compiled for the MRI.FH accelerator.The left column for each benchmark shows its normalized performance. The benchmarks MRI.Q, CT. Laplace and CT. gauss suffered a 50% reduction in performance; i.e. their II values had tobe doubled, from 1 to 2, in order for them to execute on the baselineloop-accelerator. The benchmark CT.segment could not be compiledfor the MRI.FH accelerator at all. For each benchmark, the column on the right shows the achieved performance on the generalized accelerator, with the hardware modificationsspecified in section III-B1. As shown, these modifications allowedall the benchmarks to run at full performance, at minimum II.Fig 8shows a graph similar to that in Fig 7, but showsthe normalized efficiency in terms of the accelerator's performance to-power ratio. Due to the increase in overall performance providedby the generalizations, the benchmarks MRI.Q, CT.laplace andCT.gauss had a significant increase in efficiency despite the poweroverhead of the additions. The MRI.FH benchmark, however, whichwould not experience any improved performance from the generalizations loses efficiency due to the increase in the accelerator's power consumption. On average, the generalizations increased the accelerator's efficiency increased by approximately 40%.

3. Commodity GPGPU Comparison: While other architectures may certainly be used for this domain,GPGPUs are the solutions that are currently in use in many medicalimaging applications and, therefore, the most suitable comparison point.For this reason, we assessed the performance and efficiency of fiveNVIDIA GPUs.

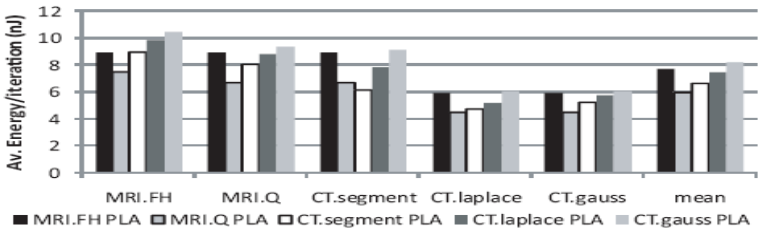

Fig. 9.Average energy consumed (per iteration) by each benchmark while running on PUMA systems designed around different PLAs

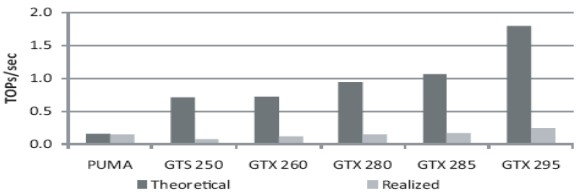

Fig. 10.Achieved performance of the MRI.FH benchmark (in trillions of operations) on the MRI.FH PUMA system and on various NVIDIA GPUs based on the GT200 architecture

Fig9 shows the result of direct performance comparisons betweenan MRI.FH PUMA system and the GPUs in consideration. Thecolumn on the left shows the total compute capability of each of theprocessors. The column on the right shows the realized performancewhile executing the MRI.FH benchmark, accounting for bandwidth restrictions. PUMA achieves a very small fraction of the peak performance offered by the GPUs, between 8.6% of the dual-GPU GTX 295 and 21.8% of the GTS 250. This gap changes dramatically, however, when accounting for the bandwidth-intensive nature of the application in question. PUMA delivers between 63% (on the dual-GPU GTX 295) and 2X the performance (on the GTS 250) of the GPUs.The case for PUMA is further underscored by examining the GPUs'power efficiency, as shown in Fig 10.

This graph shows how many*times* more efficient, in terms of number of operations per Watt, PUMAsystems are relative to the GPUs in consideration. These values rangefrom 20X, for the most complex benchmark running on the mostefficient GPU, to 54X, for the least complex benchmark running onthe least efficient GPU.

X. CONCLUSION

We have seen that the application of the theory of optimal control of PDEs to image processing problems is a fruitful field of research. Besides promising result, even for easy models like the linear heat equation, new interesting mathematical problems arise, like the treatment of non-quadratic penaltyterms. For future research, better adapted PDEs (like the anisotropic diffusion equations) could be investigated.The PUMA architecture is a power-efficient accelerator system designedspecifically for efficient medical image reconstruction. It consistsof tiles of programmable loop accelerators - ASICs with added hardwareto support general-purpose computing - designed around the computation requirements of the image reconstruction domain. As applications in this domain are normally executed on very high-performance GPGPUs, the latest NVIDIA GPU architecture was used to gauge the performance and efficiency of PUMA. The results are very encouraging – PUMA achieves up to 2 times the performance of a modern GPU architecture and has up to 54 times the power efficiency.

REFERENCES

[1]. K. Bredies, D. A. Lorenz, and P. Mass. Equivalence of a generalized conditional gradient method and the method of surrogate functionals.Preprint of the DFG Priority Program 1114? University of Bremen, 2005.
[2]. Cohen. Numerical Analysis of Wavelet Methods. Elsevier ScienceB.V., 2003.
[3]. Daubechies, M. Defrise, and C. De Mol. An iterative thres holding algorithm for linear inverse problems with a sparsity constraint. Com-munications in Pure and Applied Mathematics, 57(11):1413–1457, 2004.
[4]. Ekeland and R. Temam. Convex analysis and variational problems. North-Holland, Amsterdam, 1976.
[5]. L. Florack and A. Kuijper.The topological structure of Scale-Spaceimages. Journal of Mathematical Imaging and Vision, 12:65–79, 2000.
[6]. M. Frazier, B. Jawerth, and G. Weiss. Little wood-Paley theory and the study of function spaces. Number 79 in Regional Conference Series inMathematics.American Mathematical Society, 1991.
[7]. P. Heinlein, J. Drexl, and W. Schneider. Integrated wavelets for enhancement of micro calcifications in digital mammography. IEEE Trans-actions on Medical Imaging, 22(3):402–413, March 2003.
[8]. J.-L. Lions. Optimal Control of Systems Governed by Partial Differential Equations. Springer, 1971.
[9]. Y. Meyer. Wavelets and Operators, volume 37 of Cambridge Studies inAdvanced Mathematics.Cambridge University Press, 1992.
[10]. P. Perona and J. Malik.Scale-space and edge detection usinganisotropic diffusion. IEEE Transactions on Pattern Analysis and Ma-chine Intelligence, 12(7):629–639, 1990.
[11]. L. I. Rudin, S. J. Osher, and E. Fatemi. Nonlinear total variation basednoise removal algorithms. Physical D, 60:259–268, 1992.
[12]. H. Triebel. Theory of Function Spaces II. Monographs in Mathematics. Birkh¨ auser, 1992.
[13]. Weickert. Anisotropic diffusion in image processing. Teubner, Stuttgart, 1998.
[14]. P. Witkin. Scale-space filtering.In Proceedings of the International Joint Conference on Artificial Intelligence, pages 1019–1021, 1983.
[15]. S. Ciricescu et al. The reconfigurable streaming vector processor (RSVP).In *Proc. of the 36th Annual International Symposium on Microarchitecture*,pages 141–150, 2003.
[16]. CNET. The Gizmo Report: NVIDIA's GeForce GTX 280 GPU – introduction, 2008. http://news.cnet.com/8301-13512_3-9969234-23.html.
[17]. H. Corporal. TTAs: Missing the ILP complexity wall. *Journal of SystemArchitecture*, 45(1):949–973, 1999.
[18]. W. Dally et al. Merrimac: Supercomputing with streams. In *Proceedings ofthe 2003 ACM/IEEE conference on Supercomputing*, pages 35–42, 2003.
[19]. G. Dasika, S. Das, K. Fan, S. Mahlke, and D. Bull. DVFS in loopaccelerators using BLADES. In *Proc. of the 45th Design AutomationConference*, pages 894–897, June 2008.
[20]. C. Ebeling et al. mapping applications to the Rapid configurable architecture. In *Proc. of the 5th IEEE Symposium on Field Programmable CustomComputing Machines*, pages 106–115, Apr. 1997.
[21]. Fan et al. Cost sensitive modulo scheduling in a loop acceleratorsynthesis system. In *Proc. of the 38th Annual International Symposiumon Microarchitecture*, pages 219–230, Nov. 2005.
[22]. Fan et al. Modulo scheduling for highly customized data paths to increase hardware reusability. In *Proc. of the 2008 International Symposium on CodeGeneration and Optimization*, pages 124–133, Apr. 2008.
[23]. A. Fisher et al. Custom-fit processors: Letting applications definearchitectures. In *Proc. of the 29th Annual International Symposium onMicroarchitecture*, pages 324–335, Dec. 1996.
[24]. S. Goldstein et al. PipeRench: A coprocessor for streaming multimediaacceleration. In *Proc. of the 26th Annual International Symposium onComputer Architecture*, pages 28–39, June 1999.
[25]. T. D. Hartley, U. Catalyurek, A. Ruiz, F. Igual, R. Mayo, and M. Ujaldon. Biomedical image analysis on a cooperative cluster of GPUs and multicores.In *Proc. of the 2008 International Conference on Supercomputing*, pages15–25, 2008.
[26]. G. Lu et al. The MorphoSys parallel reconfigurable system. In *Proc.Ofthe 5th International Euro-Par Conference*, pages 727–734, 1999.
[27]. Mahesri et al. Tradeoffs in designing accelerator architectures forvisual computing. In *Proc. of the 41st Annual International Symposiumon Microarchitecture*, pages 164–175, Nov. 2008.
[28]. Mei et al. exploiting loop-level parallelism on coarse-grained reconfigurablearchitectures using modulo scheduling. In *Proc. of the 2003 Design, Automation and Test in Europe*, pages 296–301, Mar. 2003.
[29]. Nvidia. *CUDA Programming Guide*, June 2007.http://developer.download.nvidia.com/compute/cuda.
[30]. NVIDIA. GeForce GTX 280, 2008. http://www.nvidia.com/object/ product geforcegtx 280 us.html.
[31]. NVIDIA. NVIDIA Tesla S1070, 2008.http://www.nvidia.com/object/product tesla s1070 us.html.
[32]. Nvidia. Cuda Zone, 2009.http://www.nvidia.com/object/cuda home.html.
[33]. B. R. Rau. Iterative modulo scheduling: An algorithm for softwarepipelining loops. In *Proc. of the 27th Annual International Symposiumon Microarchitecture*, pages 63–74, Nov. 1994.
[34]. T. Review. Cheap, Portable MRI, 2006.http://www.technologyreview.com/computing/17499/?a=f.
[35]. Ruiz, M. Ujaldon, L. Cooper, and K. Huang.Non-rigid registration forlarge sets of microscopic images on graphics processors.*Springer Journalof Signal Processing*, May 2008.
[36]. Sankaralingam et al. Exploiting ILP, TLP, and DLP using polymorphismin the TRIPS architecture. In *Proc. of the 30th Annual InternationalSymposium on Computer Architecture*, pages 422–433, June 2003.
[37]. Seiler et al. Larrabee: a many-core x86 architecture for visual computing.*ACM Transactions on Graphics*, 27(3):1–15, 2008.
[38]. S. S. Stone et al. accelerating advanced MRI reconstructions on GPUs. In*2008 Symposium on Computing Frontiers*, pages 261–272, 2008.
[39]. Taylor et al. Evaluation of the Raw microprocessor: An exposed wire-delay architecture for ILP and streams. In *Proc. of the 31st AnnualInternational Symposium on Computer Architecture*, pages 2–13, June 2004.

International Journal of Modern Engineering Research (IJMER)
www.ijmer.com Vol. 3, Issue. 4, Jul - Aug. 2013 pp-2215-2218 ISSN: 2249-6645

Finite Element Analysis of Skirt to Dished junction in a Pressure Vessel

Sagar P. Tiwatane[1], Sachin S. Barve[2]
*(Department of Mechanical Engineering, V.J.T.I College, Mumbai University, India)
** (Department of Mechanical Engineering, V.J.T.I College, Mumbai University, India)

ABSTRACT: *Pressure vessels are probably one of the most widespread equipment within the different industrial sectors. In fact, there is no industrial plant without pressure vessels, steam boilers, tanks, autoclaves, collectors, heat exchangers, pipes, etc. The traditional method of proving a pressure vessel is to carry out mechanical design calculations in accordance with established codes .While so called design by rule approach is sufficient for majority of cases there are sometimes features of design which necessitates the use of design by analysis methods.*
Skirt to dished end junction in vertical pressure vessel is one of such critical junction which is often subjected to different loads. These loadings include internal pressure inside vessel, wind & seismic shear force and moments, operating weight of vessel& thermal stresses in the welds near the junction. This paper re-presents guidelines in structural analysis for skirt to dished end junction. Analysis is carried out in compliance with ASME Section VII Division 2. Finite elemental model of junction is prepared using UG-NX. It is then loaded in ansys 12.0 and results obtained are compared to code allowable.

KEYWORDS: *Finite element analysis, Skirt to dished end junction, Structural etc.*

I. INTRODUCTION

Most vertical vessels are supported by skirt. Skirt assembly generally consists of skirt shell, base-ring, top-ring & gussets. These supports transfer the loads by shear action. They also transfer loads to foundation through anchor bolts & bearing plates. Support skirts are welded directly to bottom of dished ends. Skirt carries entire weight of vessel as it supports whole assembly during operating condition. It includes weights of cylindrical shell, dished ends, internal trays, liners, nozzles & liquid column. All these loads are transferred to skirt shell through skirt to dished end junction only. Apart from these loads there are also wind and seismic loads junction have to withstand with.
Chemical reactions taking place inside vessels usually occur at high temperatures. So skirt to dished end junction experiences high temperature inside dished end and atmospheric temperature outside, which causes thermal stresses across the junction. All these loads make skirt to junction design critical.

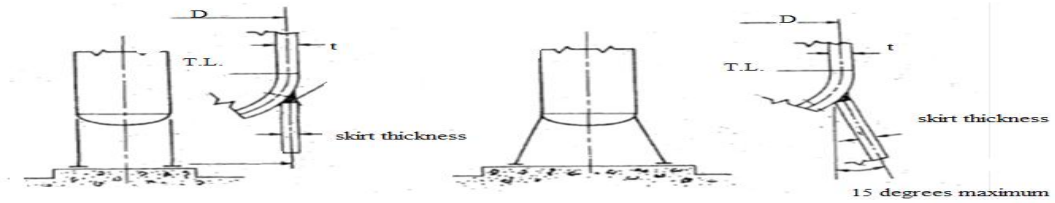

Fig.1-Pictures showing types of skirt constructions

UG-NX model of skirt to junction is depicted below.

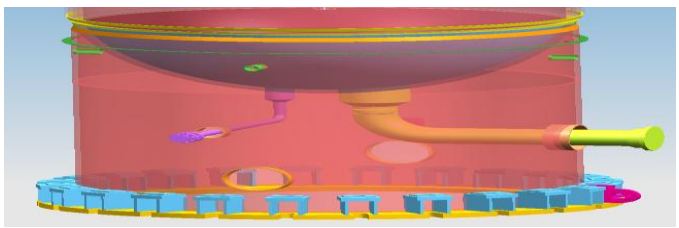

Fig.2- Assembly of skirt & dished end

II. DESIGN SPECIFICATIONS

II.1 Dished END

Design pressure	16.9
Design temperature	210 ° C
Dished end I.D	3472 mm
Dished end material	SA 537 CL2
Allowable stress s	209.47
Joint efficiency	1
Corrosion allowance	0 mm

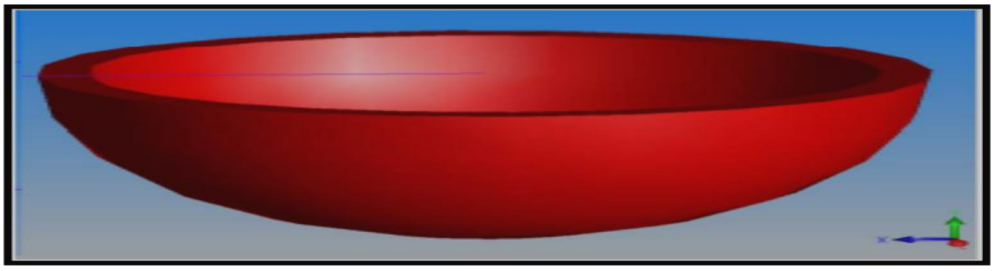

Fig 3- Bottom hemispherical dished end

Minimum Required Thickness as ASME SEC. VIII DIV 2 Part 4,

$$= \frac{D}{2}\left[e^{\frac{0.5P}{SE}} - 1\right]_+ C_i + C_o$$

$$= \frac{3472}{2}\left[e^{\frac{0.5\times16.988}{209.478\times1}} - 1\right]_+ 0 + 0$$

= 71.8173 + 0.000 + 0.000

= 71.8173 mm

Finished thickness = 78 mm

2.2 Skirt specifications:

Skirt material	SA 516 GR.70
Skirt thickness	45 mm
Corrosion allowance	0 mm

III. ANALYSIS DETAILS

The 180 ° sector 3D finite element model for head to skirt junction was prepared in Uni-graphics (UG). In order to reduce the overall size of FE model only half portion of the skirt to dished end assembly was considered. Meshing of model is carried out by using UG. This FEA analysis is carried out in order to know the stress distribution near head to skirt junction due to internal pressure, discontinuities, operating weight and seismic loads. ANSYS 11.0 was used for pre-processing, solution and post-processing of this finite element analysis. Stress classification lines were plotted to know distribution of stresses at critical junction. Finally, resulting von-misses stresses were compared to code allowable.

Component	Skirt to dished head junction
Software	ANSYS 12.0
Analysis type	Structural linear static
Element	Solid 45

III.1 Design data

Design code	ASME SEC VIII Div. 2
Design pressure	16.982 Mpa
Design temperature	210 ° C

III.2 Material data

Component	Material	Design temperature	Allowable stress S
skirt	SA516GR70	210 °C	138 MPa
Bottom dished end	SA 537CL2	210 °C	134 MPa

Allowable stresses for skirt & dished end material are obtained from table 5A,of ASME SEC. VIII Div.2,Ed 2010

III.3 Meshed model:

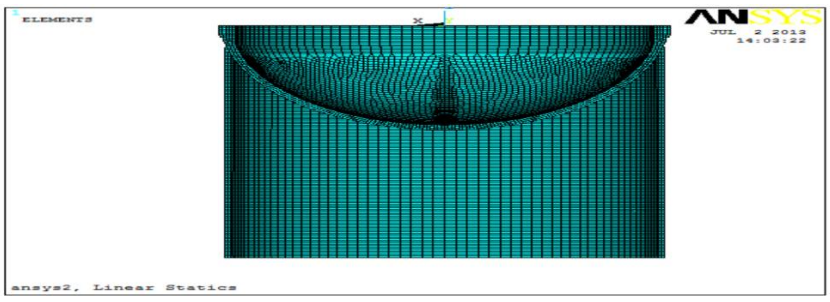

Fig 4- finite elemental model of skirt to dished junction

Stress classification lines (SCL) were plotted near junction and intensity of von misses stresses is observed across these junctions.

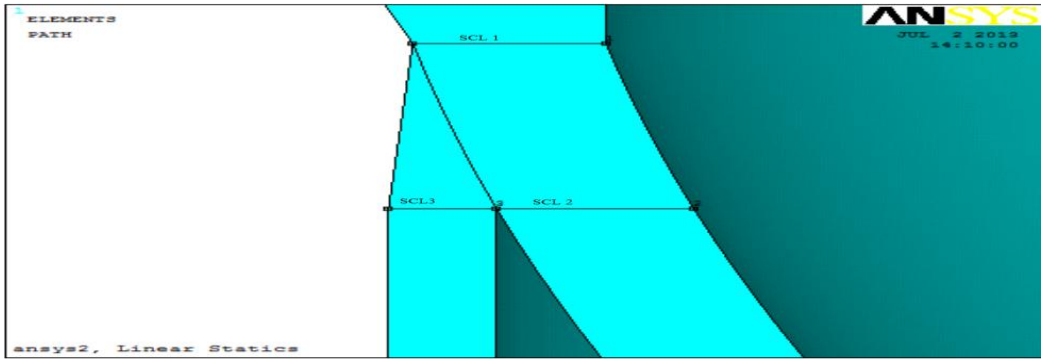

Fig 5- location of stress classification lines in the junction

IV. STRUCTURAL BOUNDARY CONDITIONS

1. Internal pressure has been applied on inside surface of dished end. P = 16.98 MPa
2. Operating weight of vessel including liquid and internals have been applied through center of gravity of vessel with the help of rigid elements.
3. W= 4208861 N
4. Horizontal Seismic shear force = 2212515 N
5. Seismic base moment = 28.827×10^9 N-mm
6. Seismic moment acting at C.G
7. = Seismic base moment – Seismic shear force distance from base model to top
8. = 28.827×10^9 – 2212515 × 11870
   = 2.564×10^9 N-mm
9. Axial thrust on dished end thickness
10. Longitudinal stress due to internal pressure = $\frac{PD}{4t}$
    = $\frac{16.982 \times 3414}{4 \times 135}$ = 107.36 MPa Stress due to operating weight = $\frac{4208861}{\frac{\pi}{4}(3684^2 - 3414^2)}$
    a. = 2.7962 MP
11. So, resulting axial thrust on dished end thickness = 107.36 – 2.7962 = 104.5638 MPa
12. Base of the skirt is constrained in all directions.

IV.1 Loads and boundary conditions:

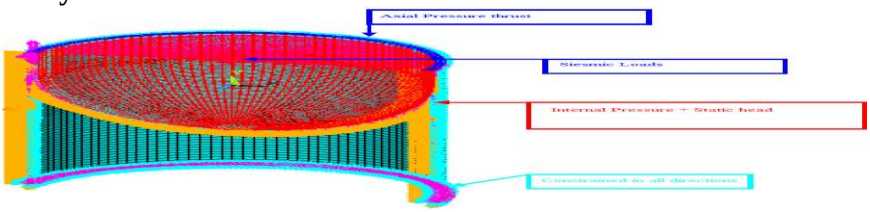

Fig 6- Boundary conditions

V. RESULTS & DISCUSSIONS

Model is solved for above mentioned loadings in ansys 12.0 deformation plot and von misses stress plot are obtained. Maximum primary stress, bending stress across stress classification lines in the junction are summarized in the table.

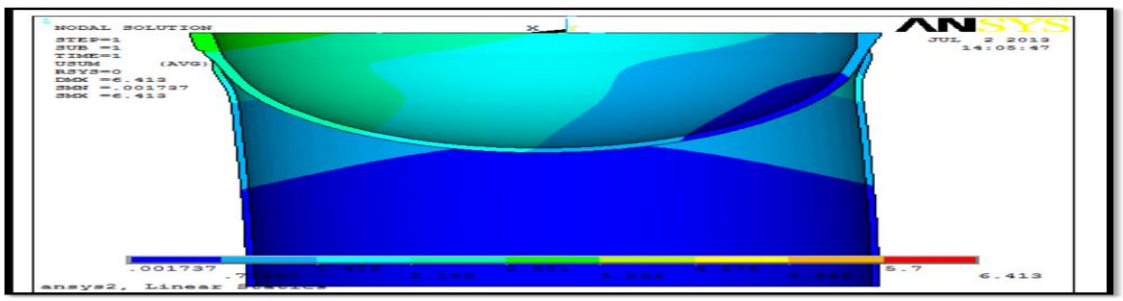

Fig 7- figure showing deformation in the junction

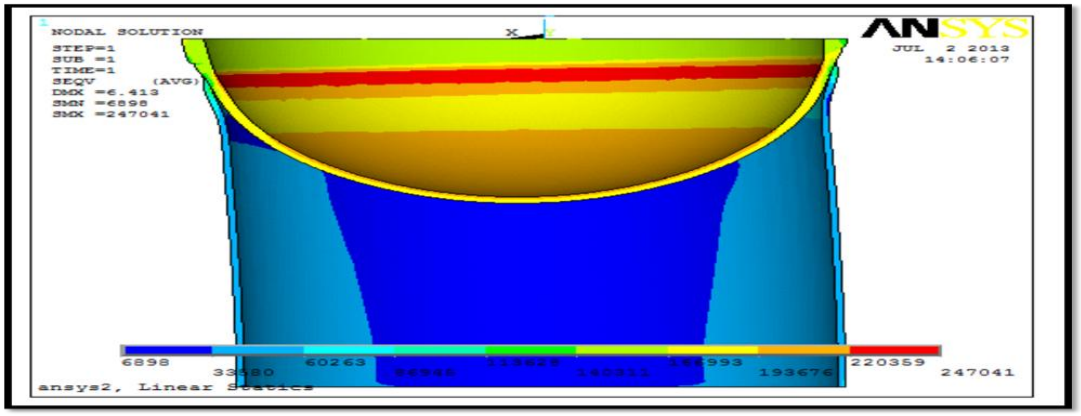

Fig 8 - Von misses stress plot

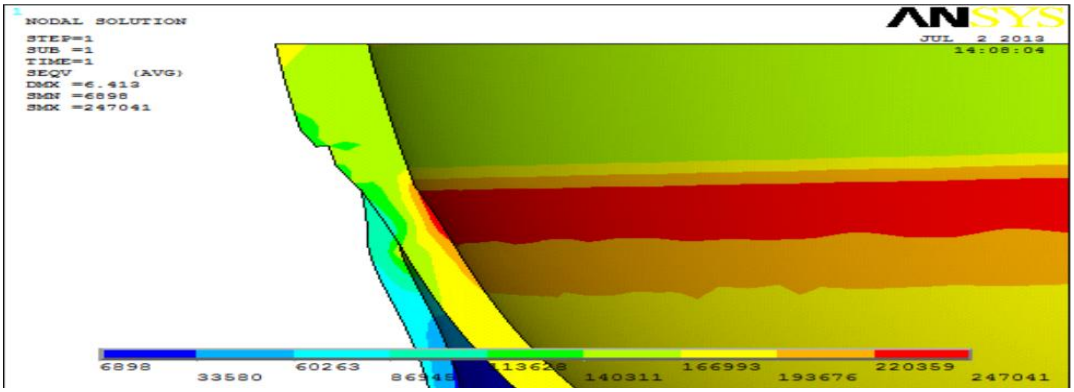

Fig 9-Von misses stress plot acros stress classificatio lines (SCL)

V.1 RESULTS TABLE

Stress Classification Line (SCL) [2]	Type of stress	Max Induced Von Misses stress (MPa)	Allowable Design stress (MPa) [1]
SCL 1: In Shell at Shell to Skirt Joint	Pl	154.4	1.5 S = 201
	Pl + Pb + Q	50.81	3 S = 402
SCL 2 : In Dish End at Shell to Skirt Joint	Pl	168.4	1.5 S = 201
	Pl + Pb + Q	74.04	3 S = 402
SCL 3: In Skirt at Shell to Skirt Joint	Pl	94.65	1.5 S = 207
	Pl + Pb + Q	36.06	3 S = 414

Primary & secondary stresses induced in the junction across stress classification lines are compared to code allowable & are found within allowable limit which justifies structural stability of the junction.

VI. CONCLUSION

a. This analysis throws light on various stresses encountered in the skirt to dished junction which makes its design critical.
b. After this analysis optimum parameters should be considered which can minimize stresses in junction. This can increase life of pressure vessel & reduce its cost.
c. It can be concluded that stress and other parameters are also decreased by changing weld size of skirt to dished end junction.

VII. ACKNOLEDGEMENT

Authors are grateful to M/S Larsen and Toubro Ltd, powai for allowing them to carry out the project work during the course of study. We are indebted to design department and the staff for their help.

REFERANCES

❖ **Books**

[1]. ASME code, Section VIII, Division 2, 2010 A-11
[2]. Moss D. R. Pressure Vessel Design Manual Third edition.

International Journal of Modern Engineering Research (IJMER)
www.ijmer.com Vol. 3, Issue. 4, Jul - Aug. 2013 pp-2219-2225 ISSN: 2249-6645

Nanotechnology: Shaping the world atom by atom

Sudipta Sen[1], Alapon Banerjee[2], Avishek Acharjee[3]
[1](Electrical Engineering, Techno India, India)
[2](Electrical Engineering, Techno India, India)
[3](Electronics & Telecommunication Engineering, Techno India, India)

ABSTRACT: *The ability to image, measure, model, and manipulate matter on the nanoscale is leading to new technologies that will impact virtually every sector of our economy and our daily lives. Nanoscale science and technology has the potential, for example, to increase the efficiency of lighting, enhance the performance of electronic devices, decrease waste and pollution during manufacturing, detect and treat disease at the earliest stages, and provide more cost-effective solar energy conversion. At the same time, care must be taken to develop new technologies for widespread use in a responsible manner. Achieving the benefits promised by nanotechnology will depend on advanced research in fields ranging from chemistry and engineering to biology and materials science; development and support of the necessary infrastructure, including user facilities and instrumentation; and education and training of a skilled workforce and an informed public.*

This report presents the strategic plan for shaping the world atom by atom. In developing this plan, I sought extensive advice and input from the academic, industrial, and government research communities and took into consideration the recommendations of the 2006 National Academies report.

Keywords: *1) Nanotechnology 2) Surfaces Galore 3) Nan tubes 4) Quantum 5) Atom*

I. INTRODUCTION

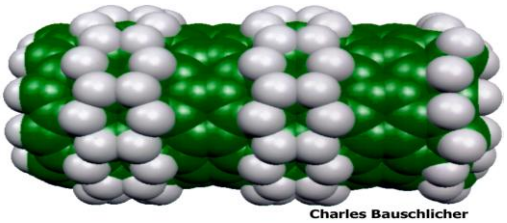

If you were to deconstruct a human body into its most basic ingredients, you'd get a little tank each of oxygen, hydrogen, and nitrogen. There would be piddling piles of carbon, calcium, and salt. You'd squint at pinches of sulfur, phosphorus, iron, and magnesium, and tiny dots of 20 or so other chemical elements. Total street value: not much. With its own version of what scientists call nanoengineering, nature transforms these inexpensive, abundant, and inanimate ingredients into self-generating, self-perpetuating, self-repairing, self-aware creatures that walk, wiggle, swim, sniff, see, think, and even dream. Total value: immeasurable. Now, a human brand of nanoengineering is emerging. The field's driving question is this: What could we humans do if we could assemble the basic ingredients of the material world with even a glint of nature's virtuosity? What if we could build things the way nature does—atom by atom and molecule by molecule? Scientists already are finding answers to these questions. The more they learn, the more they suspect nanoscience and nanoengineering will become as socially transforming as the development of running water, electricity, antibiotics, and microelectronics. The field is roughly where the basic science and technology behind transistors was in the late 1940s and 1950s.

II. WHAT IS NANOTECHNOLOGY?

In the language of science, the prefix nano means one-billionth of something like a second or a meter (see sidebar, p. 3). Nanoscience and nanotechnology generally refer to the world as it works on the nanometer scale, say, from one nanometer to several hundred nanometers. That's the natural spatial context for molecules and their interactions, just as a 100 yard gridiron is the relevant spatial context for football games. Naturally- occurring molecular players on the nanoscale field range from tiny three-atom water molecules to much larger protein molecules like oxygen- carrying hemoglobin with thousands of atoms to gigantic DNA molecules with millions of atoms. Whenever scientists and engineers push their understanding and control over matter to finer scales, as they now are doing on the nanoscale, they invariably discover qualitatively new phenomena and invent qualitatively new technologies For years now, scientists have been developing synthetic nanostructures that could become the basis for countless improved and completely new technologies. The way molecules of various shapes and surface features organize into patterns on nanoscales determines important material properties, including electrical conductivity, optical properties, and mechanical strength. So by controlling how that nanoscale patterning unfolds, researchers are learning to design new materials with new sets of properties. Some of these nanostructures may turn out to be useful as discrete nanostructures. New types of vaccines and medicines come to mind here.

The value of others may emerge only as they are assembled into larger structures like particles or fibers, which then would be processed into yet larger structures like textiles, films, coatings, bricks, and beams. Forward looking researchers believe they could end up with synthetic creations with life-like behaviors. Cover an airplane with paint containing nanoscale pigment particles that instantly reconfigure, chameleon-like, to mimic the aircraft's surroundings. You would end up with an airplane indistinguishable from the sky, that is, an invisible plane. How about bricks and other building materials that can sense weather conditions and then respond by altering their inner structures to be more or less permeable to air and humidity? That would go a long way toward improving the comfort and energy efficiency of buildings. And how about synthetic antibody- like nanoscale drugs or devices that might seek out and destroy malignant cells wherever they might be

in the body? For many years futurists steeped in the culture of science fiction and prone to thinking in time frames that reach decades ahead have been dreaming up a fantastic future built using nanotechnologies.

III. THE INCREDIBLE TININESS OF NANO

"Nano" derives from the Greek word for dwarf. Use it as a prefix for any unit like a second or a liter and it means a billionth of that unit. A nanosecond is one billionth of a second. A nanoliter is one billionth of a liter. And a nanometer is one billionth of a meter—about the length of a few atoms lined up shoulder to shoulder. The bottom of this letter, "l", spans about one million nanometers. A world of things is built up from the tiny scale of nanometers. Just consider the thousands of cellular proteins and enzymes that do everything from metabolizing hamburgers, to building up muscle fibers, to replicating DNA, whose twisty structure itself is a few nanometers thick. Enzymes typically are constructions of thousands of atoms in precise molecular structures that span some tens of nanometers. That kind of natural nanotechnology is about ten times smaller than some of the smallest synthetic nanotechnology humanity has made so far. The individual components of an Intel Pentium III microprocessor span about 200 nanometers. That's why these chips can harbor several million transistors and can translate a five-inch Digital Video Disc (DVD) into a seamless movie. Nanotechnology researchers say today's microelectronics are mere hints of what will come from engineering that begins on the even smaller scales of nanostructures.

In the summer of 1999, researchers reported making single molecules that behave like transistors. Talk of computers the size of sugar cubes suddenly became less speculative. Just as the prefix "micro" has infiltrated the general lexicon ever since early microscopists began observing the world on finer scales, the prefix "nano" has begun diffusing into popular culture. It's getting into screenplays and scripts for TV shows like the Xfiles and Star Trek: The Next Generation.

Companies are using it in their names. It's a favorite topic of science fiction writers. And it's on the agenda of corporate executives, deans, and government officials deciding how to allocate funds and resources among the many research and development projects vying for support.

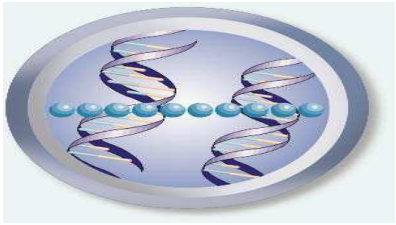

Nanometer: Ten shoulder to shoulder Hydrogen atoms (blue balls) span1 Nanometer, DNA molecules are about 2.5 nanometer wide.

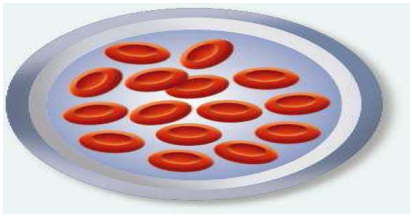

thousands of a nanometer Biological cell, like these red cells, have diameter in the range given above

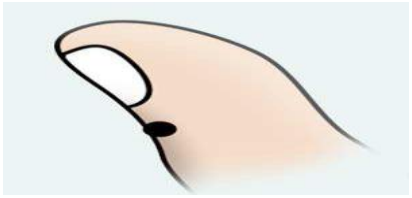

A MILLION NANOMETER: The pinhead sized patch of this thumb (circled in black) is a million nanometer across

IV. SOME DEEP ROOTS FOR A NANOTECHNOLOGICAL FUTURE

Nanotechnology is a new word, but it's not an entirely new field. Chemical catalysis, which underlies a significant portion of the country's gross national product, is an example of "old nanotechnology." Today, catalysts speed up thousands of chemical transformations like those that convert crude oil into gasoline, small organic chemicals into life-saving drugs and polymers, and cheap graphite into synthetic diamond for making industrial cutting tools. They're akin to biological catalysts—the enzymes in cells that orchestrate the chemistry of life. Most catalysts were discovered by trial and error—by "shaking and baking" metals and ceramics and then seeing how the result affects the reactions and their products. On closer examination with modern tools, many of these catalysts turn out to be highly organized metallic and/or ceramic nanostructures whose specific architectures trigger changes in molecules that temporarily dock to them. Researchers expect

NATURAL NANOTECHNOLOGY*: Much of the photosynthesis that powers forests unfolds inside tiny cellular power houses called chloroplasts (above). These contain nanoscale molecular machinery (including pigment molecules like*

chlorophyll) arranged inside stacked structures, called thylakoid disks that convert light and carbon dioxide into biochemical energy.

This nanoscale understanding of catalysis to lead to better, cleaner, and more capable industrial processes. Even an early instance of nanotechnology like catalysis really is young compared to nature's own nanotechnology, which emerged billions of years ago when molecules began organizing into the complex structures that could support life. Photosynthesis, biology's way of harvesting the solar energy that runs so much of the planet's living kingdom, is one of those ancient products of evolution. Scientists often perceive photosynthesis as the result of brilliantly engineered molecular ensembles—which include light harvesting molecules such as chlorophyll— arranged within cells on the nanometer and micrometer scales. These ensembles capture light energy and convert it into the chemical energy (which is stored in chemical bonds) that drives the biochemical machinery of plant cells. The abalone, a mollusk, serves up another perennial favorite in nature's gallery of enviable nanotechnologies. These squishy creatures construct super tough shells with beautiful, iridescent inner surfaces. They do this by organizing the same calcium carbonate of crumbly schoolroom chalk into tough nanostructured bricks. For mortar, abalones concoct stretchy goo of protein and carbohydrate. Cracks that may start on the outside rarely make it all the way through; the structure of the shell forces a crack to take a tortuous route around the tiny bricks, which dissipates the energy behind the damage. Adding to the damage control is that stretchy mortar. As a crack grows, the mortar forms resilient nanostrings that try to force any separating bricks back together. The result is a Lilliputian masonry that can withstand sharp beaks, teeth, even hammer blows. This clever engineering of the abalone shell reflects one of nanotechnology's most enticing faces: by creating nanometer- scale structures, it's possible to control the fundamental properties—like color, electrical conductivity, melting temperature, hardness, crack-resistance, and strength—of materials without changing the materials' chemical composition. The stuff of soft chalk becomes hard shell. Another feat of natural nanotechnology is in continuous operation every time you take a breath, move a muscle, live another second. Known antiseptically as F1-ATPase complexes, they're actually molecular motors inside cells. Each of these motors is a complex of proteins bound to the membranes of mitochondria, the cell's bacteria-sized batteries. About 10 nanometers across, the F1-AT Pase complexes are key players in the synthesis of ATP—the molecular fuel for cellular activity. Scientists have found that F1-ATPase complexes also generate rotary motion just like fan motors whirring in summertime windows. By attaching tiny protein filaments to the hub of F1-ATPase, researchers have visualized this rotary action. And it sets their own nanoengineering imaginations into motion with designs for human made nanometer-scale machines. Scientists using tools like electron microscopes to look at natural structures like abalone shells and protein complexes hope to emulate some of biology's nanoscale engineering. Their aim is to create structural materials for stronger, lighter, more damage-resistant and otherwise better man-made constructions ranging from buildings and cars to batteries and prosthetic limbs.

V. WHAT IS SO SPECIAL ABOUT NANO

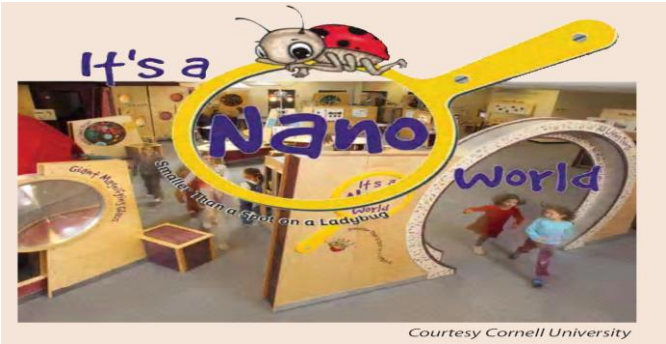

Nanotechnology stands out as a likely launch pad to a new technological era because it focuses on perhaps the final engineering scales people have yet to master. The pyramids in Egypt, the Brooklyn Bridge, and automobiles are conspicuous monuments to how well and how long people have controlled matter on large scales of meters and miles. The products of Swiss watchmakers even several centuries ago proved that human control over the material world had extended downward a thousand fold to the millimeter scale or so. Over the past few decades, researchers have pushed this control down another hundredfold. Using micro lithographic techniques, they've learned to inscribe silicon with ultra-dense patterns of circuitry whose individual components now are only visible with powerful electron microscopes. And all the while, chemists have been learning to mix, blend, heat, react, and otherwise process chemicals to produce millions of different specific molecular structures. This is about the finest level of material structure relevant for making things. In so doing, researchers have developed recipes and protocols for making the plastics, ceramics, semiconductors, metals, glass, fabrics, composites and other materials of the constructed landscape. But there's a big gap between the scale of individual molecular structures made by chemists and the sub-microscopic components on microprocessors made by electrical engineers. That gap, which spans from about one nanometer to several hundred nanometers, is where fundamental properties are defined. So with every advance researchers make in nanotechnology, they stitch together an unbroken engineering nexus from atoms on up to skyscrapers. Roald Hoffmann, a chemist and Nobel Prize laureate at Cornell University has put it this way: "Nanotechnology is the way of ingeniously controlling the building of small and large structures, with intricate properties; it is the way of the future, a way of precise, controlled building, with incidentally, environmental benignness built in by design."

VI. GOING QUANTUM

Many researchers expect that better control over the way atoms and molecules assemble into tiny structures could lead to a host of new technologies based on quantum phenomena that become prevalent only at nanometer scales. In the normal-sized realm of books, bricks, cars and houses, quantum mechanics—the conceptual framework scientists use to describe and predict the properties of matter on the levels of atoms and electrons—doesn't have much direct relevance. As long as bricks hold up the house, who cares about their quantum specifics? But now researchers.

actually are creating nano scale building blocks, such as metallic and ceramic particles, and all-carbon "nanotubes," that are hundreds of millions of times smaller than bricks used for houses and tubes used for plumbing. So scientists are finding themselves in the middle of quantum mechanics territory. In this nanoscale territory, electrons, for one, no longer flow through electrical conductors like rivers. On this scale, an electron's quantum mechanical nature expresses itself as a wave. This behavior makes it possible for electrons to do remarkable things, such as instantly tunnel through an insulating layer that normally would have stopped it dead. The payoff of this behavior is that electronic devices built on nanoscales not only can pack more densely on a chip but also can operate far faster—and with dramatically fewer electrons and less energy loss-than conventional transistors. These characteristics ultimately could yield more powerful computers that can help scientists mimic phenomena better and engineers design products better. In some specially designed materials with nanoscale layers made of different semiconductor materials, electrons exhibit behaviors not possible in less precisely organized settings. Researchers already

[Modern Pyramids. This nanoscale pyramid of germanium atoms— one kind of quantum dot—formed spontaneously atop a ground of Silicon. It could help researchers develop new generations of tinier electronic devices that are governed by quantum phenomena.]

Have exploited this quantum mechanical reality to design and build new solid state lasers that emit light in wavelengths good for tasks like monitoring pollution, tracking chemical reactions, and optical communications. What's more, researchers already have taken steps toward so-called quantum computers based on the energy states of atoms and electrons.

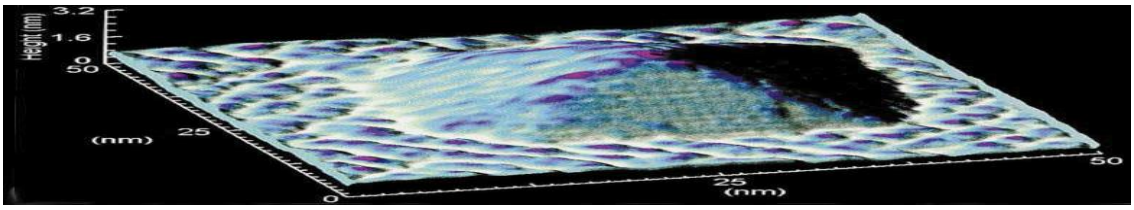

VII. SURFACE GALORE

Another major fountain of new technology is likely to spout from a simple fact of material reality: as objects become smaller, the proportion of their constituent atoms at or near the surface rises. Collections of very small particles, therefore, have high surface area compared to their volume. This characteristic is profound because so much of what happens in the world happens at surfaces. Photosynthesis Nano grains.

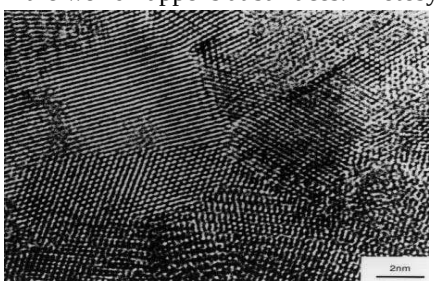

Each region of parallel lines reveals a nanoscale grain of palladium metal. Here, a dozen or so such particles are joined into a nanostructured metal. It has dramatically smaller grains with more internal boundaries than metals made from more conventional grains, and that leads to a stronger metal.

occurs on surfaces inside of cells. Catalysis happens on the surfaces of particles. Ice in the atmosphere forms on the surfaces of floating dust specks. Smaller industrial catalysts, or ones with labyrinthine interiors with nanoscale features, mean there's more surface area for thousands of chemical transformations. Make a ceramic brick or a metal part, such as a jet engine's turbine blade, out of nanoscale powder particles instead of conventional micro scale powder particles and the amount of internal surface goes up dramatically. There's no chemical difference between the two materials; only the size of their constituent particles differs. Yet, just for that the nanostructure brick or metal piece may be harder, less likely to crack, or stronger at higher temperatures, than the conventional brick. That's important for people who make things like armor or turbine blades for jet engines, which run more efficiently the hotter they become. The shift to nanoscale building blocks for making metal, ceramic, polymer and other material components is enabling researchers to "dial-in" many properties—like melting temperature, magnetic properties (e.g., the magnetic detection ability of materials in the read heads of hard disks), and color—that previously were impossible to obtain for a particular material.

VIII. FORTY YEARS OF GETTING AROUND TO IT

8.1 SEEING ATOMS: One of the biggest steps toward nanoscale control was in 1981 when researchers at IBM's Research Center in Switzerland—led by Gerd Binning and Heinrich Rohrer—told the world about their scanning tunneling microscope, or STM. It's essentially a superfine stylus that sweeps over a surface like a blind person's walking stick. But since the stylus is just a few atom widths away and it has a molecularly or perhaps atomically fine tip, something quantum mechanical happens. Electrons "tunnel" across the gap between the surface and the tip as the tip scans over the surface. This technique enables a computer to construct fantastically enlarged images of atomic or molecular landscapes normally impossible to see. The STM's inventors received a Nobel Prize because their invention quickly enabled thousands of researchers finally to "see" the atomic and molecular landscapes of things. So taken with the new view of the nanoworld STMs offered, scientists have developed a raft of related instruments now known collectively as scanning probe microscopes (SPMs). Now, besides STM images of surface structures, scientists use SPMs like scanning tunneling spectroscopes and near field scanning optical microscopes to analyze the identities of molecules and atoms on surfaces. They use scanning thermal microscopes to see how heat travels on and through nanostructures such as solid-state lasers, made like a cake with tensor hundreds of nanoscale layers of different semiconductor materials. They use scanning force microscopy to examine magnetic domains on storage media like hard disks.

Atom-by-atom chemistry

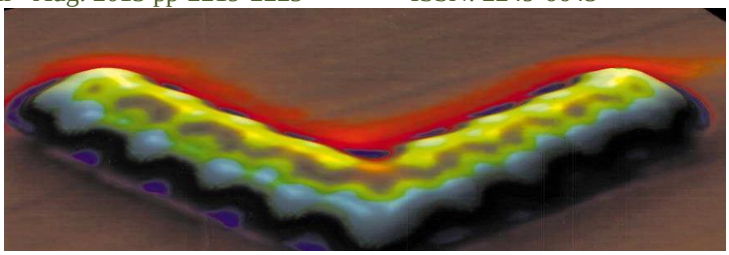

Drag 18 atoms of cesium and 18 atoms of iodine together with a scanning tunneling microscope and this is what you get. This is the beaker less, nanotechnology way of doing chemistry—you put the atoms where you want them and where physics will let you

8.2 MOVING ATOMS: SPMs can do more than just peek in on previously hidden nanoscale environments Donald Eigler of IBM's Almaden Research Center remembers the day in 1990 when he and Erhard K. Schweizer, who was visiting from the Fritz-Haber Institute in Berlin, moved individual atoms for the first time. In his laboratory notebook Eigler used big letters and an exclamation mark to write THIS IS FUN! Using one of the most precise measuring and manipulating tools the world had ever seen, the researchers slowly finessed 35 xenon atoms to spell out the three letter IBM logo atop a crystal of nickel. To be sure, it only worked in a vacuum chamber kept at temperatures that make the North Pole seem tropical. But it was the kind of submicroscopic manipulation that Feynman was talking about. The entire logo spanned under three nanometers. Since that feat, more researchers have used STMs to create letters, pictures, as well as exotic physical structures on surfaces one atom at a time. And some researchers now are developing atom- and molecule-moving tools that are easier to use. Consider a nanomanipulator that is being developed by a collaboration based at the University of North Carolina, Chapel Hill. With it, people can manipulate nanostructures in real time using what amounts to a sophisticated joy stick that controls a scanning tunneling microscope. The developers of the system built it with force-feedback so operators even "get a feel" for the atoms and molecules they are moving. What's more, the link between the joystick and the actual nanomanipulator is electronically mediated, which means it even can be controlled via the Internet. Students in a nearby North Carolina high school used this nanomanipulator across the Internet to see, feel and modify individual virus particles. These invaluable tools have opened many new doors of discovery. But using a single tip of a scanning probe microscopeeither for imaging or manipulating surfaces or tiny particles is painfully slow. In the past few years, SPM developers have been hooking up many SPM tips in arrangements that work in parallel. The difference is akin to building a house all by yourself versus getting a dozen friends to help.

SMALLEST WRITING: This famous set of images, now about 10 years old, helped prove to the world that people indeed can move atoms. The series shows how 35 atoms were moved to form a famous logo.

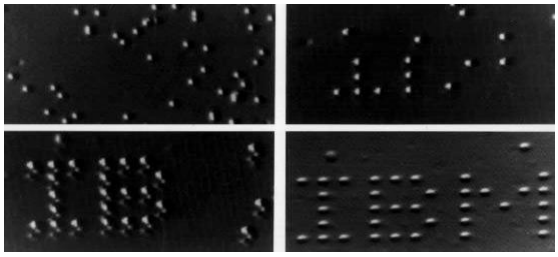

IX. NANOTUBES

All-carbon nanotubes (here with diameters of 1.2 nanometers) are promising for applications ranging from new structural materials that are stronger and lighter weight to electronic components for new supercomputers to drug delivery systems Carbon nanotube transistor by IBM and Delft University

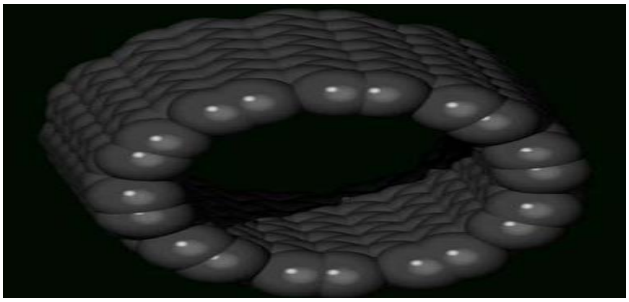

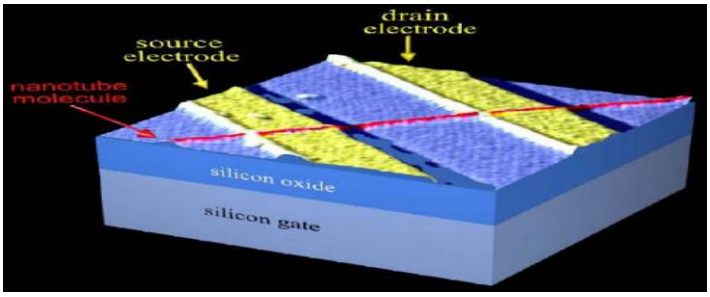

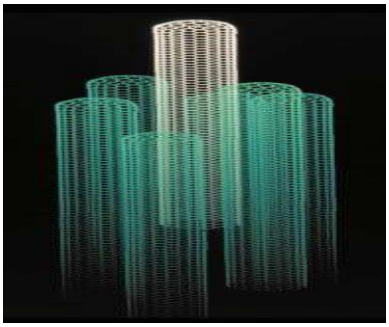

X. THE FUTURE OF NANOTECHNOLOGY

The list of nanotechnologies in various stages of conception, development and even commercialization already is vast and growing. If present trends in nanoscience and nanotechnology continue, most aspects of everyday life are subject to change. Consider these:

a. ***ELECTRONICS CENTRAL:*** By patterning recording media in nanoscale layers and dots, the information on a thousand CDs could be packed into the space of a wristwatch. Besides the thousand fold to million fold increases in storage capacity, computer processing speeds will make today's Pentium IIIs seem slow. Devices to transmit electromagnetic signals— including radio and laser signals—will shrink in size while becoming inexpensive and more powerful. Everyone and everything conceivably could be linked all the time and everywhere to a future World Wide Web that feels more like an all-encompassing information environment than just a computer network.

b. ***NANODOC:*** Nanotechnology will lead to new generations of prosthetic and medical implants whose surfaces are molecularly designed to interact with the body. Some of these even will help attract and assemble raw materials in bodily fluids to regenerate bone, skin or other missing or damaged tissues. New nanostructured vaccines could eliminate hazards of conventional vaccine development and use, which rely on viruses and bacteria. Nanotubules that act like tiny straws could conceivably take up drug molecules and release them slowly over time. A slew of chip-sized home diagnostic devices with nanoscale detection and processing components could fundamentally alter patient-doctor relationships, the management of illnesses, and medical culture in general.

c. ***SMOKELESS INDUSTRY:*** More and more materials and products will be made from the bottom-up, that is, by building them up from atoms, molecules, and the nanoscale powders, fibers and other small structural components made from them. This differs from all previous manufacturing, in which raw materials like sheet metal, polymer, fabric and concrete get pressed, cut, molded and otherwise coerced into parts and products. Bottom-up manufacturing should require less material and pollute less. What's more, engineers expect to be able to embed sophisticated, life-like functions into materials.Even concrete will get smart enough to internally detect signs of weakness and lifelike enough to respond by, say, releasing chemicals that combat corrosive conditions. In effect, the constructed world itself could become sensitive to damaging conditions and automatically take corrective or evasive action like a hand recoiling from a flame.

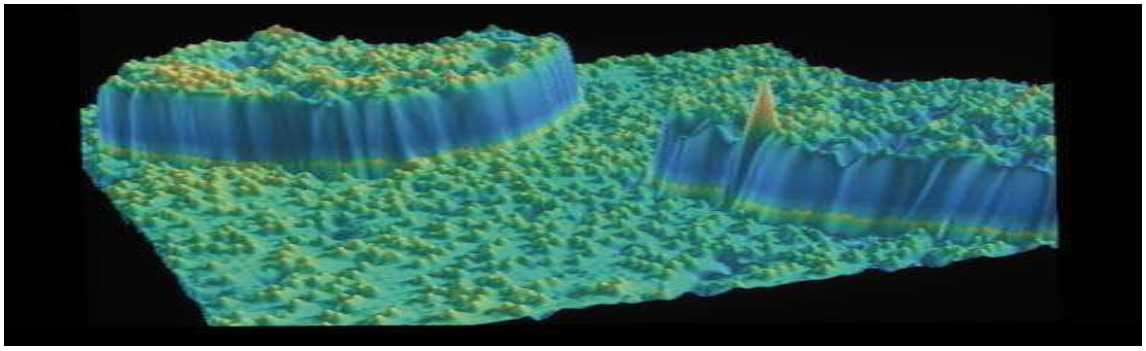

Memorable Clues: The raised mesas in this scanning tunneling microscope image are made of iron atoms. This atomic landscape forms when chromium deposits onto an iron surface. Nanoscale data like this could lead to new recording media.

d. ***PLANES, TRAINS AND AUTOMOBILES:*** Materials with an unprecedented combination of strength, toughness and lightness will make all kinds of land, sea, air and space vehicles lighter and more fuel efficient. Fighter aircraft designed with lighter and stronger nanostructured materials will be able to fly longer missions and carry more payloads. Plastics that wear less because their molecular chains are trapped by ceramic nanoparticles will lead to materials that last a lifetime. Some long-view researchers are taking steps toward self-repairing metallic alloys that automatically fill in and reinforcetiny cracks that can grow and merge into larger ones, including catastrophic ones that have caused plane crashes.

e. ***BUT, WAIT, THERE'S MORE!:*** Nanotechnology advocates say their field will leave no stone unturned. Their lengthy lists include artificial photosynthesis systems for clean energy; molecular layer-by-layer crystal growth to make new generations of more efficient solar cells; tiny robotic systems for space exploration; selective membranes that can fish out specific toxic or valuable particles from industrial waste or that can inexpensively desalinate sea water; chameleon-like camouflage that changes shape and color to blend anywhere, anytime; and blood substitutes.

XI. CONCLUSION

No one knows how much of nanotechnology's promise will prove out. Technology prediction has never been too reliable. In the March 1949 edition of Popular Mechanics, hardly a year after the invention of the transistor, experts predicted computers of the future would add as many as 5000 numbers per second, weigh only 3000 pounds, and consume only 10 kilowatts of power. Today's five-pound laptops add several million numbers per second using only a watt or so of power. And thumbnail-sized microprocessors run washing machines and kids' toys as well as hundreds of millions of computers.

What's more, computer technology spawned a new social epoch that some dub the Information Age or the Silicon

Age. And yet, many believe nanotechnology may do even more. Despite the advances researchers have made, it is hard to work on the nanoscale. And even assuming something like Feynman's vision of total nanoscale control comes about, the consequences are bound to be mixed. Like any extremely powerful new technology, nanotechnology will bring with it social and ethical issues. Just consider quantum computers. Theorists expect them to be so good at factoring huge numbers that the toughest encryption schemes in use today—which are enabling revolutionary things like e-commerce will become easy to crack. Or consider the claim that nanobiology will enable people to live longer, healthier lives. Longer average lifetimes will mean more people on Earth. But how many more people can the Earth sustain? For the moment, it's nanotechnology's promise that's on most peoples' minds. "Never has such a comprehensive technology promised to change so much so fast... Inevitably nanotech will give people more time, more value for less cost and provide for a higher quality of existence," predicts James Canton, president of the Institute for Global Futures. But maybe not for everyone. Says Canton: "Those nations, governments, organizations and citizens who are unaware of this impending power shift must be informed and enabled so that they may adequately adapt." It no longer seems a question of whether nanotechnology will become a reality. The big questions are how important and transformative nanotechnology will become, will it become affordable, who will be the leaders, and how can it be used to make the world a better place? — Questions that will, in time, are answered.

REFERENCES

[1]. Jack Uldrich & Deb Newberry, *the Next Big Thing Is Really Small* (March 2003)
[2]. Douglas Mulhall, *Our Molecular Future* (March 2002)
[3]. K. Eric Drexler , *Engines of creation: The coming era of Nanotechnology*
[4]. K. Eric Drexler, *Nanosystems: Molecular Machinery, Manufacturing, and Computation* (1992)
[5]. Ed Regis, Nano: *The Emerging Science of Nanotechnology.*
[6]. Robert A. Freitas Jr., *Nanomedicine: Basic Capabilities* (Vol. 1 by 1999 Reviews)
[7]. Glenn Fishbine, *the Investor's Guide to Nanotechnology and Micromachines* (January 2002)
[8]. Mark Ratner & Daniel Ratner, *Nanotechnology: A Gentle Introduction to the Next Big Idea*. (November 2002 Read reviews)

International Journal of Modern Engineering Research (IJMER)
www.ijmer.com Vol. 3, Issue. 4, Jul - Aug. 2013 pp-2226-2231 ISSN: 2249-6645

The Reliability in Decoding of Turbo Codes for Wireless Communications

T. Krishna Kanth[1], D. Rajendra Prasad[2]
[1]*M. Tech student, Dept of ECE, St.Ann's college of Engineering and Technology, Chirala, AP, India*
[2]*Assoc. Professor, Dept of ECE, St.Ann's college of Engineering and Technology, Chirala, AP, India*

ABSTRACT: *Turbo codes are one of the most powerful types of error control codes and high performance forward error correction codes currently available. They will be used later in the thesis as powerful building blocks in our search for better bandwidth efficient code schemes. Turbo codes emerged in 1993 and have since become a popular area of communications research. This paper provides a description of three turbo codes algorithms. Soft-output Viterbi algorithm, logarithmic-maximum a posteriori turbo algorithm and maximum- logarithmic-maximum a posteriori turbo decoding algorithms are the three candidates for decoding turbo codes. Soft-input soft-output (SISO) turbo decoder based on soft-output Viterbi algorithm (SOVA) and the logarithmic versions of the MAP algorithm, namely, Log-MAP decoding algorithm. The bit error rate (BER) performances of these algorithms are compared.*

KEYWORDS: *Turbo codes, Channel coding, Iterative decoding.*

I. INTRODUCTION

In information theory and coding theory with applications in computer science and telecommunication, error detection and correction or error control are techniques that enable reliable delivery of digital data over unreliable communication channels. Many communication channels are subject to channel noise, and thus errors may be introduced during transmission from the source to a receiver. Error detection techniques allow detecting such errors, while error correction enables reconstruction of the original data. The near Shannon limit error correction performance of Turbo codes and parallel concatenated convolutional codes have raised a lot of interest in the research community to find practical decoding algorithms for implementation of these codes. The demand of turbo codes for wireless communication systems has been increasing since they were first introduced by Berrou et. al. in the early 1990's.Various systems such as 3GPP, HSDPA and WiMAX have already adopted turbo codes in their standards due to their large coding gain. In it has also been shown that turbo codes can be applied to other wireless communication systems used for satellite and deep space applications.

The MAP decoding also known as BCJR algorithm is not a practical algorithm for implementation in real systems. The MAP algorithm is computationally complex and sensitive to SNR mismatch and inaccurate estimation of the noise variance . MAP algorithm is not practical to implement in a chip. The logarithmic version of the MAP algorithm and the Soft Output Viterbi Algorithm (SOVA) are the practical decoding algorithms for implementation in this system.

II. SHANNON–HARTLEY THEOREM

The field of Information Theory, of which Error Control Coding is a part, is founded upon a paper by Claude Shannon in 1948. Shannon calculated a theoretical maximum rate at which data could be transmitted over a channel perturbed by additive white Gaussian noise (AWGN) with an arbitrarily low bit error rate. This maximum data rate, the *capacity* of the channel, was shown to be a function of the average received signal power, W, the average noise power N, and the bandwidth of the system. This function, known as the *Shannon-Hartley Capacity Theorem*, can be stated as:

$C=W \log_2 (1+S/N)$ bits/sec

If W is in Hz, then the capacity, C is in bits/s. Shannon stated that it is theoretically possible to transmit data over such a channel at any rate $R \leq C$ with an arbitrarily small error probability

III. CODING IN WIRELESS COMMUNICATIONS

Coding theory is the study of the properties of codes and their fitness for a specific application and used for data compression, error correction and more recently also for network coding. Codes are studied by various scientific disciplines, such as information theory, electrical engineering, mathematics, and computer science for the purpose of designing efficient and reliable data transmission methods. This typically involves the removal of redundancy and the correction (or detection) of errors in the transmitted data. Most digital communication techniques rely on error correcting coding to achieve an acceptable performance under poor carrier to noise conditions. Basically coding in wireless communications are of two types:

III.1. Source coding: In computer science and information theory, 'data compression', 'source coding', or 'bit-rate reduction' involves encoding information using fewer bits than the original representation. Compression can be either lossy or lossless. The lossless compression reduces bits by identifying and eliminating statistical redundancy. No information is lost in lossless compression. Lossy compression reduces bits by identifying unnecessary information and removing it. The process of reducing the size of a data file is popularly referred to as data compression, although its formal name is source coding (coding done at the source of the data before it is stored or transmitted).

III.2. Channel coding: The channel coding also called as forward corrections codes (FEC).The purpose of channel coding is to find codes which transmit quickly, contain many valid code words and can correct or at least detect many errors. Channel coding is referred to the processes done in both transmitter and receiver of a digital communications system .While not mutually exclusive, performance in these areas is a trade off. So, different codes are optimal for different applications. The needed properties of this code mainly depend on the probability of errors happening during transmission. Channel coding is distinguished from source coding, i.e., digitizing of analog message signals and data compression.

Types of FEC Codes:

1. Linear block codes.
2. Convolutional codes.

1. Linear Block Codes: With Block Codes a block of data has error detecting and correcting bits added to it. One of the simplest error correcting block code is the Hamming Code, where parity bits are added to the data. By adding the error correcting bits to data, transmission errors can be corrected. However since more data has to be squeezed into the same channel bandwidth the more errors will occur. Linear block codes have the property of linearity, i.e. the sum of any two code words is also a code word, and they are applied to the source bits in blocks, hence the name, linear block codes. There are block codes that are not linear, but it is difficult to prove that a code is a good one without this property. Linear block codes are summarized by their symbol alphabets (e.g., binary or ternary) and parameters (n, m, d_{min}) where n is the length of the codeword, in symbols, m is the number of source symbols that will be used for encoding at once, d_{min} is the minimum hamming distance for the code. Block codes submit k bits in their inputs and forwards n bits in their output. These codes are frequently known as (n,k) codes. Apparently, whatever coding scheme is, it has added n-k bits to the coded block .Block codes are used primarily to correct or detect errors in data transmission. Commonly used block codes are Reed–Solomon codes, BCH codes, Golay codes and Hamming codes.

2. Convolutional Codes: Despite of block codes which are memory less, convolutional codes are coding algorithms with memory. Since, their coding rate (R) is higher than its counterpart in block codes they are more frequently used coding method in practice. Every convolutional code uses m units of memory, therefore a convolutional code represents with (n,k,m).In Convolutional coding the input bits are passed through a shift register of length K.N output bits are generated by modulo 2 adding selected bits held in different stages of the shift register. For each new data bit N output bits are produced. The output bits are influenced by K data bits, so that the information is spread in time. The channel code is used to protect data sent over it for storage or retrieval even in the presence of noise (errors).In practical communication systems, convolutional codes tend to be one of the more widely used channel codes. These codes are used primarily for real-time error correction and can convert an entire data stream into one single codeword. The Viterbi algorithm provided the basis for the main decoding strategy of convolutional codes. The encoded bits depend not only on the current informational k input bits but also on past input bits.

IV. TURBO CODES

Turbo codes are one of the most powerful types of error control codes (ECC) currently available and a class of high performance forward error correction (FEC) codes. They will be used later in the thesis as powerful building blocks in our search for better bandwidth efficient code schemes. Turbo codes emerged in 1993 and have since become a popular area of communications research. It is a combination of both block and convolutional codes. The encoder for a turbo code consists of two convolutional codes in parallel, with their inputs separated by a pseudo-random interleaver. The decoder consists of two Maximum A Posteriori (MAP) decoders connected in series via interleavers, with a feedback loop from the output of the second to the input of the first.

IV.1. Turbo Codes Encoding: The encoder for a turbo code is a parallel concatenated convolutional code. Figure 1 shows a block diagram of the encoder first presented by Berrou et al. The input sequence is passed into the input of a convolutional encoder, and a coded bit stream is generated. The data sequence is then interleaved. That is, the bits are loaded into a matrix and read out in a way so as to spread the positions of the input bits. The bits are often read out in a pseudo-random manner. The interleaved data sequence is passed to a second convolutional encoder, and a second coded bit stream is generated. The code sequence that is passed to the modulator for transmission is a multiplexed (and possibly punctured) stream consisting of systematic code bits and parity bits from both the first encoder and the second encoder.

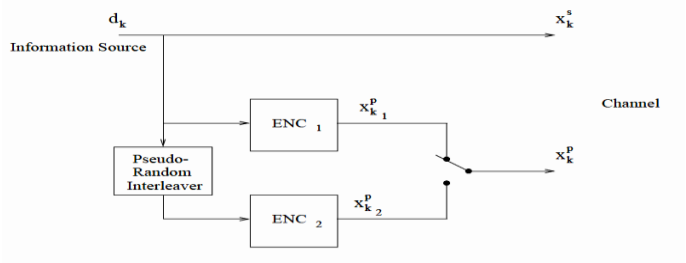

fig 1: Structure of Turbo Encoder

Interleaving: It is a device for reordering a sequence of bits or symbols. A familiar role of interleavers in communications is that of the symbol interleaver which is used after error control coding and signal mapping to ensure that fading bursts affecting blocks of symbols transmitted over the channel are broken up at the receiver by a de-interleaver, prior to decoding.

B. Turbo codes Decoding

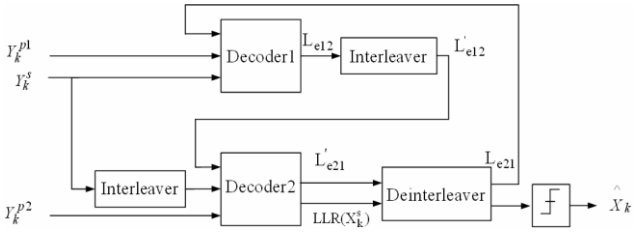

fig 2. Iterative Turbo Decoding

In a typical turbo decoding system (see Fig. 2), two decoders operate iteratively and pass their decisions to each other after each iteration. These decoders should produce soft-outputs to improve the decoding performance. Such a decoder is called a Soft-Input Soft- Output (SISO) decoder . Each decoder operates not only on its own input but also on the other decoder's incompletely decoded output which resembles the operation principle of turbo engines. This analogy between the operation of the turbo decoder and the turbo engine gives

This coding technique its name, "turbo codes" .Turbo decoding process can be explained as follows: Encoded information sequence X_k is transmitted over an Additive White Gaussian Noise (AWGN) channel, and a noisy received sequence Y_k is obtained. Each decoder calculates the Log-Likelihood Ratio (LLR) for the k-th data bit d_k, as

$$L(d_k) = \log [P(d_k=1|y / P(d_k=0|y)] \quad (1)$$

LLR can be decomposed into 3 independent terms, as

$$L(d_k) = L_{apri}(d_k) + L_c(d_k) + L_e(d_k) \quad (2)$$

Where $L_{apri}(d_k)$ is the a-priori information of (d_k), $L_c(d_k)$ is the channel measurement, and $L_e(d_k)$ is the extrinsic information exchanged between the constituent decoders. Extrinsic information from one decoder becomes the a-priori information for the other decoder at the next decoding stage. L_{e12} and L_{e21} in Figure 1 represent the extrinsic information from decoder1 to decoder2 and decoder2 to decoder1 respectively.

LLR computations can be performed by using one of the two main turbo decoding algorithms SOVA and MAP algorithms. The MAP algorithm seeks for the most likely data sequence whereas SOVA, which is a modified version of the Viterbi algorithm, seeks for the most likely connected

path through the encoder trellis. The MAP algorithm is a more complex algorithm compared to SOVA. At high SNR, the performance of SOVA and MAP are almost the same. However, at low Signal-to-Noise Ratios (SNRs) MAP algorithm is superior to SOVA by 0.5 dB or more. The following sections explain the MAP algorithm and its simplified versions Log-MAP and Max-Log-MAP algorithms.

V. DECODING ALGORITHMS TURBO CODES

We review now the decoding algorithms used within DEC_1 and DEC_2 to implement the soft input, soft-output processing needed for iterative decoding. We begin with the Maximum A Posteriori (MAP), algorithm. Decoding of convolutional codes is most frequently achieved using the Viterbi algorithm, which makes use of a decoding *trellis* to record the estimated states of the encoder at a set of time instants. The Viterbi algorithm works by rejecting the least likely path through the trellis at each node, and keeping the most likely one. The removal of unlikely paths leaves us, usually, with a single source path further back in the trellis. This path selection represents a 'hard' decision; on the transmitted sequence.

The Viterbi decoder estimates a maximum likelihood *sequence*. Making hard decisions in this way, at an early point in the decoding process, represents a loss of valuable information. It is frequently advantageous to retain finely-graded probabilities, 'soft decisions', until all possible information has been extracted from the received signal values. The turbo decoding relies on passing information about individual transmitted bits from one decoding stage to the next. The interleaving of the received information sequence between decoders limits the usefulness of estimating maximum likelihood *sequences*. So, an algorithm is required that can output soft-decision maximum likelihood estimates on a *bit-by-bit* basis. The decoder should also be able to accept soft decision inputs from the previous iteration of the decoding process. Such a decoder is termed a Soft Input-Soft Output (SISO). Berrou and Glavieux used two such decoders in each stage of their turbo decoder. They implemented the decoders using a modified version of an SISO algorithm proposed by Bahl, Cocke, Jelinek and Raviv [31]. Their *modified Bahl algorithm* is commonly referred to as the *Maximum A Posteriori* or MAP algorithm, and achieves soft decision decoding on a bit-by-bit basis by making two passes of a decoding trellis, as opposed to one in the case of the Viterbi algorithm. The MAP algorithm is an optimal but computationally complex SISO algorithm. The Log-MAP and Max-Log-MAP algorithms are simplified versions of the MAP algorithm. MAP algorithm calculates LLRs for each information bit as

$$L(d_k) = \ln\left[\frac{\sum_{S_k}\sum_{S_{k-1}} \gamma_1(S_{k-1}, S_k)\alpha(S_{k-1})\beta(S_k)}{\sum_{S_k}\sum_{S_{k-1}} \gamma_0(S_{k-1}, S_k)\alpha(S_{k-1})\beta(S_k)}\right]$$

Where α is the forward state metric, β is the backward state metric,γ is the branch metric, and k S is the trellis state at trellis time k . Forward state metrics are calculated by a forward recursion from trellis time k = 1 to, k = N where N is the number of information bits in one data frame. Recursive
calculation of forward state metrics is performed as

$$\alpha_k(S_k) = {}^1\textstyle\sum_{j=0}\ \alpha_{k-1}(S_{k-1})\gamma_j(S_{k-1}.S_k) \qquad (4)$$

Similarly, the backward state metrics are calculated by a backward recursion from trellis time k = N to, k = 1 as

$$\beta_k(S_k) = {}^1\textstyle\sum_{j=0}\ \beta_{k-1}(S_{k+1})\gamma_j(S_k.S_{k+1}) \qquad (5)$$

Branch metrics are calculated for each possible trellis transition as

$$\gamma_i(S_{k-1}, S_k) = A_k P(S_k \mid S_{k-1}) \exp\left[\frac{2}{N_o}\left(y_k^s x_k^s(i) + y_k^p x_k^p(i, S_{k-1}, S_k)\right)\right] \qquad (6)$$

Where i = (0,1) , k A is a constant, x^s_k and x^p_k are the encoded systematic data bit and parity bit, and, y^s_k and y^p_k are the received noisy systematic data bit and parity bit respectively.

LOG-MAP ALGORITHM: To avoid complex mathematical calculations of MAP decoding, computations can be performed in the logarithmic domain. Furthermore, logarithm and exponential computations can be eliminated by the following approximation.

$$\max^*(x,y) \triangleq \ln(e^x + e^y) = \max(x,y) + \log(1 + e^{-|y-x|})$$

So equations (3)-(6) become

$$L(d_k) = \max_{(S_k, S_{k-1})}{}^*\left(\bar{\gamma}_1(S_{k-1}, S_k) + \bar{\alpha}_{k-1}(S_{k-1}) + \bar{\beta}_k(S_k)\right) - \max_{(S_k, S_{k-1})}{}^*\left(\bar{\gamma}_0(S_{k-1}, S_k) + \bar{\alpha}_{k-1}(S_{k-1}) + \bar{\beta}_k(S_k)\right)$$

$$\bar{\alpha}_k(S_k) = \max_{(S_{k-1}, i)}{}^*\left(\bar{\alpha}_{k-1}(S_{k-1}) + \bar{\gamma}_i(S_{k-1}, S_k)\right)$$

$$\bar{\beta}_k(S_k) = \max_{(S_k, i)}{}^*\left(\bar{\beta}_{k+1}(S_{k+1}) + \bar{\gamma}_i(S_k, S_{k+1})\right)$$

$$\bar{\gamma}_i(S_{k-1}, S_k) = \frac{2}{N_o}\left(y_k^s x_k^s(i) + y_k^p x_k^p(i, S_{k-1}, S_k)\right) + \ln\left(P(S_k \mid S_{k-1})\right) + K$$

Where K is a constant.

The Log-MAP parameters are very close approximations of the MAP parameters and therefore, the Log-MAP BER performance is close to that of the MAP algorithm.

MAX-LOG-MAP ALGORITHM: The correction function $f_c = \log(1 + e^{|y-x|})$ in the * max (.) operation can be implemented in different ways. The Max-log-MAP algorithm simply neglects the correction term and approximates the * max (.) operator as at the expense of some performance degradation. This simplification eliminates the need for an LUT required to find the corresponding correction factor in the * max (.) operation.

VI. PRINCIPLES OF ITERATIVE DECODING

In a typical communications receiver, a demodulator is often designed to produce soft decisions, which are then transferred to a decoder. The improvement in error performance of systems utilizing such soft decisions is typically approximated as 2 dB, as compared to hard decisions in AWGN. Such a decoder could be called a soft input/ hard output decoder, because the final decoding process out of the decoder must terminate in bits (hard decisions). With turbo codes, where two or more component codes are used, and decoding involves feeding outputs from one decoder to the inputs of other decoders in an iterative fashion, a hard-output decoder would not be suitable. That is because a hard decision into a decoder degrades system performance (compared to soft decisions).

Hence, what is needed for the decoding of turbo codes is a soft input/ soft output decoder. For the first decoding iteration of such a soft input/soft output decoder, we generally assume the binary data to be equally likely, yielding an initial a priori LLR value of L(d)=0. The channel LLR value, Lc(x), is measured by forming the logarithm of the ratio of the values. The output L(d) of the decoder in Figure 3 is made up of the LLR from the detector, L'(d) , and the extrinsic LLR output, Le(d) ,representing knowledge gleaned from the decoding process. As illustrated in Figure 3, for iterative decoding, the extrinsic likelihood is fed back to the decoder input, to serve as a refinement of the a priori probability of the data for the next iteration.

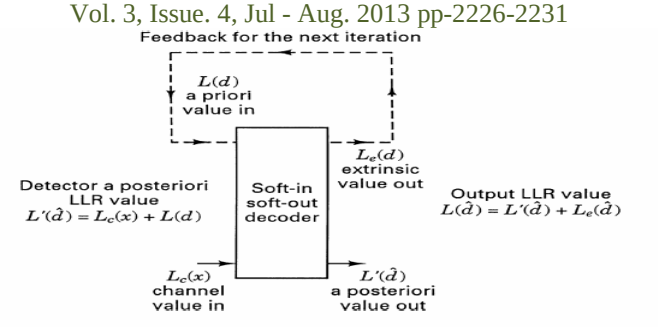

fig3:soft input soft output decoder

VII. SIMULATION RESULTS

The simulation curves presented shows the influence of iteration number, Block length, code rate and code generator. Rate ½ codes are obtained from their rate 1/3 counterparts by alternately puncturing the parity bits of the constituent encoders. In figures (4-5) BER for SOVA and LOG MAP as a function of Eb/No curves are shown for constituent codes of constraint length three and code rate ½. Eight decoding iterations were performed for Block length of 1024 . Also the improvement achieved when the block length is increased from 1024 to 4096 for both algorithms. For figure 6, LOG MAP shows better performance than SOVA for constraint length of three and for block length of 1024.And from the figure 7,we can observe the BER performances of LOG MAP and MAX-LOG MAP algorithms. The MAX-LOG MAP algorithm gives better BER performance.

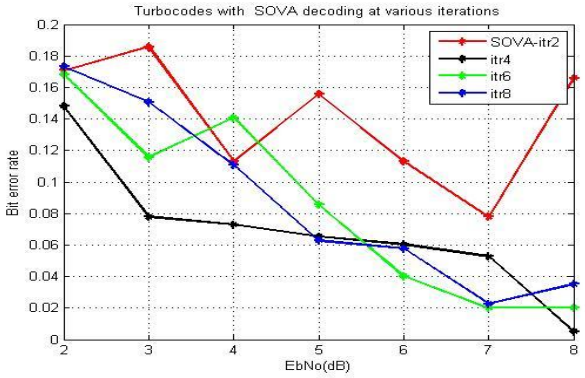

fig4: Iterations performed by sova decoding algorithm

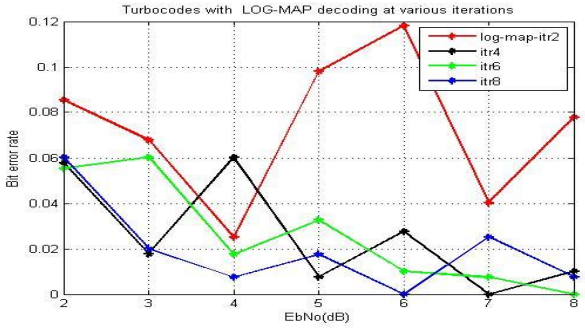

fig5: Iterations performed by log-map decoding algorithm

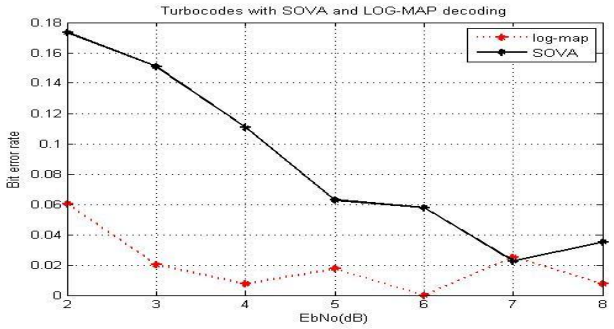

fig6:BER performances by SOVA and Log-Map decoding algorithms

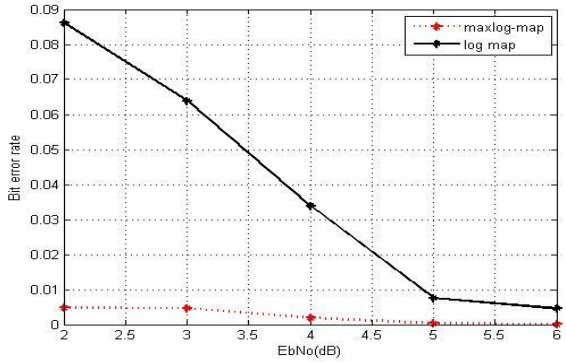

fig7:BER performances by Max Log-Map and Log-Map decoding algorithm

VIII. CONCLUSION

Our Simulation results shows that the decoding algorithms of Max-Log MAP performs better in terms of block length compared to SOVA and Log-MAP, and thus it is more suitable for wireless communication.

REFERENCES

[1]. Grace Oletu, Predrag Rapajic," The Performance of Turbo codes for Wireless Communication Systems,IEEE2011.
[2]. C. Berrou, A. Glavieux, and P. Thitimajshima, "Near Shannon Limit Error-Correcting Coding and Decoding: Turbo Codes, "Proceeding of IEEE ICC 93, pp. 1064-1070.
[3]. S. Benedetto, G. Montorsi, "Design of Parallel Concatenation Convolutional Codes: IEEE Trans. on communication, vol. 44,No.5, May 1996.
[4]. C. Berrou, "The Ten-Year-Old Turbo Codes are Entering into Service," IEEE Commun. Mag. vol. 41, no. 8, pp.110-116, Aug 2003.
[5]. L. Bahi, J. Cocke, F. Jelinek, and J. Raviv, "Optimum decoding of linear codes for minimizing symbol error rate," IEEE Trans.on Inf. Theory, vol. IT-20, pp. 284-287, Mar. 1974.
[6]. T.A. Summers and S.G. Wilson, "SNR Mismatch and Online Estimation in Turbo Decoding, "IEEE Trans. On Comm. vol.46, no.4, pp. 421-424, April 1998.
[7]. P. Robertson, P. Hoeher, and E. Villebrun, "Optimal and Sub-Optimal Maximum A Posteriori Algorithms Suitable for Turbo Decoding,"European Trans. on Telecomm. vol. 8, no. 2, pp. 119-126, March-April 1997.
[8]. P. Robertson, E. Villebrun, and P. Hoeher, "A Comparison of Optimal and Sub-optimal MAP Decoding Algorithms Operating in the Log Domain," International Conference on Communications, pp.1009-1013, June 1995.
[9]. S. Benedetto, G. Montorsi, D. Divsalr, and F. Pollara "Soft- Output Decoding Algorithm in Iterative Decoding of Turbo Codes," TDA Progress Report 42-124, pp. 63-87, February 15, 1996.
[10]. J. Hagenauer, and P. Hoeher, "A Viterbi Algorithm with Soft-Decision Outputs and Its applications, "Proc. Of GLOBECOM, pp.1680-1686, November 1989.
[11]. J. Hagenauer, Source-Controlled Channel Decoding, "IEEE Transaction on Communications, vol. 43, No. 9, pp.2449-2457, September 1995.
[12]. J.Hagenauer E.Offer, and L.Papke,"Iterative Decoding of Binary Block and Convolutional Codes," IEEE Trans.Inform. Theory, 42:429-45, March 1996.
[13]. W.J. Gross and P.G. Gulak, "Simplified MAP algorithm suitables for implementation of turbo decoders" Electronic Letters, vol. 34, no.16, August 6, 1998.
[14]. J. Hagenauer, L. Papke, "Decoding Turbo Codes With the Soft Output Viterbi Algorithm (SOVA)," in Proc. Int. Symp.On Information Theory, p164, Norway, June 1994.
[15]. J. Hagenauer, P. Robertson, L. Papke, "Iterative Decoding of Systematic Convolutional Codes With the MAP and SOVA Algorithms," ITG Conf., Frankfurt, Germany,pp 1-9, Oct. 1994
[16]. J. Hagenauer, E. Offer, L. Papke, "Iterative Decoding of Bloc and Convolutional Codes," IEEE Trans. Infor. Theory, Vol. IT. 42, No.2, pp 429-445, March 1996.

International Journal of Modern Engineering Research (IJMER)
www.ijmer.com Vol. 3, Issue. 4, July-august. 2013 pp-2232-2238 ISSN: 2249-6645

An Empirical Study on Identification of Strokes and their Significance in Script Identification

Sirisha Badhika
*Research Scholar, Computer Science Department, Shri Jagdish Prasad Jhabarmal Tibrewala University, India

***ABSTRACT**: India is a multilingual, multi-script country. There are totally 22 official languages and 12 scripts in India. People adopted to use two or more languages resulting in bilingual and trilingual documents. Many official documents are available with a combination of local language, English and sometimes Hindi. In this context script identification relies on the fact that each script has unique spatial distribution and visual attributes that make it possible to distinguish it from other scripts. Many script identification methods such as Distribution of an index of optical density method, identification of frequently occurring connected component templates, filtered pixel projection profiles vertical and horizontal projection profiles of document images were proposed earlier. In this work, a simple technique for script identification from a set of English, Telugu, and Devanagari document images in printed form is presented. The proposed system uses stroke features, pixel distribution along a sequence of words.*

***KEYWORDS:** strokes, vertical projection, Horizontal projection, script identification, peaks*

I. INTRODUCTION

Script identification is an important topic in pattern recognition and image processing based automatic document analysis and recognition. The objective of script identification is to translate human identifiable documents to machine identifiable codes. Script identification may seem to be an elementary and simple issue for humans in the real world but it is difficult for a machine, primarily because different scripts (a script could be a common medium for different languages) are made up of different shaped patterns to produce different character sets. OCR is of special significance for a multi-lingual country like India, where the text portion of the document usually contains information in more than one language. The official languages of India are Assamese, Bangla, (Bengali) English, Gujarati, Hindi, Kankanai, Kannada, Kashmiri, Malayalam, Marathi, Nepali, Oriya, Panjabi, Rajasthani, Sanskrit, Tamil, Telugu and Urdu. Of them, Devanagari script is used to write Hindi, Marathi, Rajasthani, Sanskrit and Nepali language while Bangla script is used to write Assamese and Bangla (Bengali) languages. The script of Hindi is Devanagari (which is also used to write Nepali, Marathi and Sindhi), while that of Bangla is called Bangla (also used to write Assamese and Manipuri). There is a strong structural similarity between Urdu and Arabic, the third most popular language in the world. Hindi and Bangla are the fourth and fifth most popular languages in the world respectively. Indian scripts differ from one another significantly. Most of the Indic scripts belong to the family of "syllabic alphabets" and include symbols to represent vowels (V), consonants (C), and vowel modifiers (M) for nasalization of vowels and consonants. A consonant that does not contain the implicit vowel sound is sometimes termed as a half-consonant (C'). Vowel symbols combine with consonants in the form of diacritical marks known as matras. A "character" in an Indic script refers to the orthographic syllabic unit [1]. Syllabic means that text is written using consonants and vowels that together form syllables. From the angle of language specificity, a word is derived from these syllables. In certain cases one syllable forms the complete word and in other cases the number of syllables in a word can be extended. Some scripts, like Hindi, Bengali and Assamese have horizontal and vertical linear features, while others like Telugu, Tamil and Malayalam have complicated curves. Many characters in Bangla and Devanagari script have a horizontal line at the upper part. Different Indian scripts also have different textural properties. Devanagari characters exhibit two-dimensional nature (Figure. 1) and thus the absolute positions of the strokes within the character or their relative positions with respect to the base consonant are generally regarded as important information for recognition.

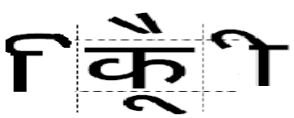

Figure 1: Two-dimensional structure: some possible matras for a Devanagari consonant

Generally human system identifies the script in a document using some visible characteristic features such as horizontal lines, vertical lines, strokes which are visually perceivable and appeal to visual sensation. Our present work is concerned with script separation and not the language separation. We are proposing to use vertical and horizontal projection profiles of document images for determining scripts in machine generated documents. Projection profiles of document images are sufficient to characterize different scripts at page level. The current paper uses horizontal and vertical projection profile features, stroke features for printed Devanagari, Telugu and English script.

II. LITERATURE REVIEW

Identification of stokes and their positions are considered as important information for online recognition of handwritten characters and words in oriental and Indic family of scripts especially because of their multi-stroke and two-dimensional nature. The significance of stroke size and position information for Devanagari word recognition by means of an empirical evaluation of three different word pre-processing schemes. These schemes involved retaining different degrees of stroke size and position information from the original input word. The experiments show that it is indeed possible to reliably recognize a handwritten Devanagari word written as discrete symbols, even in the absence of any size and position information [1]. Script recognition [2] by identifying stokes in document image segmentation were presented by identifying the valleys of the horizontal projection profiles and the position between two consecutive horizontal projections denotes the boundary of a text line. Using these boundary lines, document image is segmented into several text lines. Each text line is further segmented into several text words using the valleys of the vertical projection profile. To recognize online handwritten Gurumukhi words [3] a new step of rearrangement of recognized strokes in online handwriting recognition procedure were presented by classifying recognized strokes as dependent and major dependent strokes, and the rearrangement of strokes with respect to their positions. The combination of strokes to recognize character has achieved an overall recognition rate as 81.02% in online handwritten cursi handwriting for a set of 2576 Gurumukhi dictionary words. The script-line identification techniques in [4], [5] were modified in [6] for script-word separation in printed Indian multi-script documents by including some new features, in addition to the features considered earlier. The features used are headline feature, distribution of vertical strokes, water reservoir-based features, shift below headline, left and right profiles, deviation feature, loop, tick feature and left inclination feature. Tick feature refers to the distinct “tick” like structure, called “telakattu”, present at the top of many Telugu characters. This helps in separating Telugu script from other scripts. The vertical projection profile (or vertical histogram) of a print line consists of a simple running count of the black pixels in each column of that line. Baird et. al., [8] used the projection profile to horizontally segment characters and improved on this further by applying second order derivative on this profile. The resultant peak along with a threshold signifies in determination of the segmentation boundaries. Lu [9] designed a peak-to-valley function based on the ratio of sum of the differences between minimum value and the peaks on each side obtained from the second – order difference profile. This ratio exhibits low valleys with high peaks on both sides.

One early attempt to characterize script of a document without actually analyzing the structure of its constituent connected components was made by Wood et al. They proposed to use vertical and horizontal projection profiles of document images for determining scripts in machine generated documents. They argued that the projection profiles of document images are sufficient to characterize different scripts. For example, Roman script shows dominant peaks at the top and bottom of the horizontal projection profile, while Cyrillic script has a dominant midline and Arabic script has a strong baseline. On the other hand, Korean characters usually have a peak on the left of the vertical projection profile. However, the authors did not suggest how these projection profiles can be analysed automatically for script determination without any user intervention. Also, they did not present any recognition result to substantiate their argument [7]. Liang and others [10] improved the filtering to accommodate touching characters. They not only used the projection profile, an algorithm is proposed which used the differences between the upper and lower projection profiles of the script line are adapted for segmentation.

III. SCRIPT FEATURES

Every script defines a finite set of text patterns called alphabets. Alphabets of one script are grouped together giving meaningful text information in the form of a word, a text line or a paragraph. Thus, when the alphabets of the same script are combined together to yield meaningful text information, the text portion of the individual script exhibits a distinct visual appearance. The distinct visual appearance of every script is due to the presence of the segments like- horizontal lines, vertical lines, upward curves, download curves, descendants and so on. The presence of such segments in a particular script is used as visual clues for a human to identify the type of even the unfamiliar script. In most Indian languages, a text line may be partitioned into three zones. The upper-zone denotes the portion above the head-line, the middle zone covers the portion below head-line and the lower-zone is the portion below base-line. For the text having no head-line, the mean-line separates upper-zone and middle-zone. An imaginary line, where most of the uppermost (lowermost) points of characters of a text line lie, is called as mean- line (base-line). Examples of zoning are shown for English and Devanagari scripts are given below in fig 2(a &b).

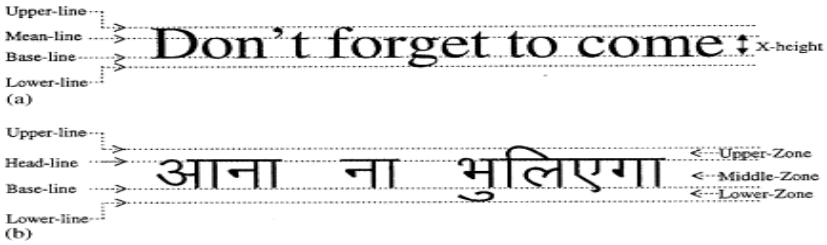

Figure 2: Text zone separation for English and Devanagari script

3.1 PRE-PROCESSING: After scanning the document, the document image is subjected to pre-processing for background noise elimination, skew correction and binarization to generate the bit map image of the text is necessary but in this project input images created saved as a bit map image. The pre-processed image is then subjected to feature extraction. Any language identification method requires conditioned image input of the document, which implies that the document should be noise free and skew free. Apart from these, some recognition techniques require that the document image should be segmented, thresholded and thinned. All these methods, help in obtaining appropriate features for text language identification processes. The pre-processing techniques such as noise removal and skew correction are not necessary for the data sets that are manually constructed by downloading the documents from the Internet.

3.2 FEATURE EXTRACTION: Projection profiles have been used extensively in the field of document analysis especially in skew removal and for block classification.

a. HORIZONTAL PROJECTION PROFILE: The horizontal projection profile of the document image and vertical white spaces are used to compute the separation between lines. First the number of columns and rows are computed for the document image in pixel count as i and j pixels. The horizontal projection is represented by equation (3.1) given below:

$$M \quad H[i] = \sum_{j=1}^{m} f[i, j] \quad - \quad (3.1)$$

Where m = number of pixels in the y direction i.e. vertically
i = Represent the row number.
j = Represent the column number.

In the binary image of each text line, count the number of black pixels in each row and take the count. This gives the horizontal projection profile of that image. Horizontal projection profile for English and Devanagari scripts are shown below. Horizontal projection for sample English script is presented in fig 3.

Once the range is selected can modify the formatting such as font size alignment including vertical alignment font color number formats borders background and so on. To access these settings choose format cells from the main menu bar or right click and choose Format Cells from the pop-up menu. This command opens the dialog box shown in Figure. If the text does not fit the width of the cell can increase the width by hovering the mouse over the line separating two columns until the cursor changes to a double arrow then click the left button.

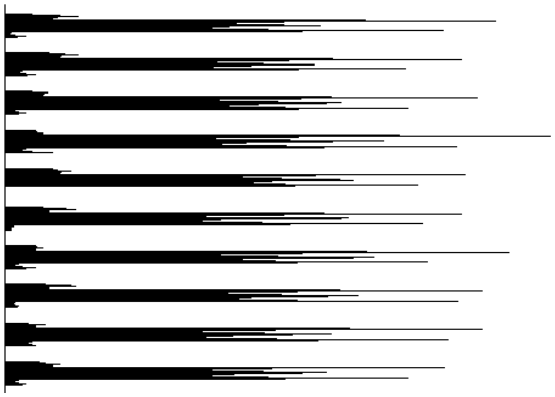

Figure 3: Horizontal projection profile of English script

Features calculated for this image are given below.
Number of peaks= 13
Number of valleys= 56
Number of Strokes= 22.6

Algorithm to calculate Peaks and Valleys:
1.Read the image
2.Convert the rgb image to binary image.
3.Count the number of black pixels in each row and obtain the vector of total image.
4.Normalize the vector
5.Then calculate the mean, maximum, minimum values for the normalized vector.
6.Calculate the peak vector and valleys vector as given below.

If there are continuous one's in a row greater than the horizontal maximum threshold value (horizontal threshold value is calculated for each text line. horizontal threshold value = 50% of the difference between maximum value and mean value), then such continuous one's are retained resulting in peaks. And, if there are continuous one's in a row less than the horizontal minimum threshold value (horizontal threshold value is calculated for each text line. Horizontal threshold value = 50% of the difference between mean value and minimum value), then such continuous one's are retained resulting in valleys.

Figure 4: Mean, Maximum, Minimum

b. VERTICAL PROJECTION PROFILE: Similarly the vertical projection profile of the document image and horizontal white spaces are used to compute the separation between words. First the number of columns and rows are computed for the document image in pixel count as i and j pixels. The vertical projection is represented by equation (3.2) given below:

$$H[i] = \sum_{j=1}^{m} f[i, j] \quad - \quad (3.2)$$

Where m = number of pixels in the x direction i.e. horizontally
i = Represent the column number.
j = Represent the row number.

The computation of the difference profile from the projection profile H For every entry in H starting from index 2 is presented by equation (3.3)

$$D[i] = H(i-1) - H(i) \quad - \quad 3.3$$

Where i = current element under evaluation between the range of
2: size of H

In the binary image of each text line, count the number of black pixels in each column of each row and take the count. This gives the vertical projection profile of that image. Vertical projection for sample English script is presented in fig 5.

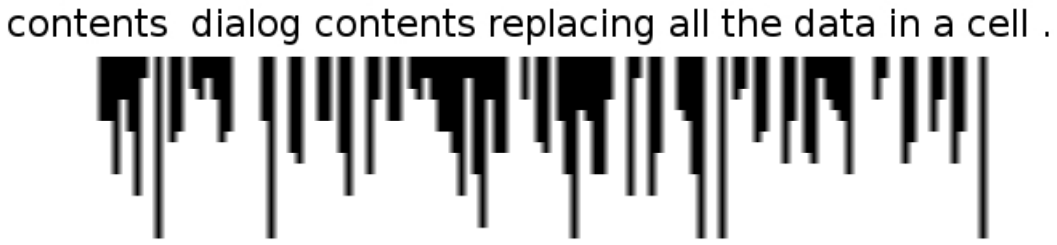

Figure 5: Vertical projection profile for English script

Features calculated for this image are given below.
Number of peaks= 13
Number of valleys= 60
Number of Strokes= 28
Stroke length= 478

Algorithm to calculate Strokes and stroke length:

1.Read an image
2.Convert rgb image to binary image
3.Get the top and bottom of the each text line in an image using vertical projection profile.
4.Measure the height of each text line.
5.For each and every row count the number of black pixels vertically. This gives the vertical projection profile vector.
6.Normalize the vector.
7.Then calculate the strokes and stroke lengths as given below.
If there are continuous one's in a column greater than the vertical threshold value (vertical thres hold value is calculated for each text line. Vertical threshold value = 75% of the X-height of that text line), then such continuous one's are retained resulting in a strokes.
8.Count the number of strokes, measure stroke lengths.

IV. RESULTS/FINDINGS

Three test sample images downloaded from internet (Google, Wikipedia for Hindi, Telugu and English) and the test sample values are given below.

Test Sample – 1:

इन व्यंजनों के हर प्रकार में पकवानों का एक अच्छा खासा विन्यास और पकाने के कई तरीकों का प्रयोग होता है यद्यपि पारंपरिक भारितीय भोजन महत्वपूर्ण हिस्सा शाकाहारी है लेकिन कई परम्परागत भारतीय पकवानों में मुर्गा बकरी भेड़ का बच्चा मछली और अन्य तरह के मांस भी शामिल हैं भोजन भारतीय संस्कृति का एक महत्वपूर्ण हिस्सा है जो रोज़मर्रा के साथ साथ त्योहारों में भी एक महत्वपूर्ण भूमिका अदा करता है कई परिवारों में हर रोज़ का मुख्य भोजन दो से तीन दौर में कई तरह की चटनी और अचार के सा रोटी और चावल के रूप में कार्बोहाइड्रेट के बड़े अंश के साथ मिष्ठान सहित लिया जाता है भोजन एक भारतीय परिवार के लिए सिर्फ खाने के तौर पर ही नहीं बल्कि कई परिवारों के एक साथ एकत्रित होने सामाजिक संसर्ग बढाने लिए भी महत्वपूर्ण है

Figure 6: Test Sample 1 of Devanagari Script

Four features (no. of strokes, stroke lengths, no. of peaks, no. of valleys) are calculated the values are tabulated in the below table (4.1):

Table 4.1: Features Values for the Test Sample - 1 (Devanagari script)

No. of strokes	Stroke length	No. of Peaks	No. of Valleys
1.2	21.6	9	56.7

Test Sample – 2:

Age 26, lean, hard, the consummate loner. On the surface he appears good-looking, even handsome; he has a quiet steady look and a disarming smile which flashes from nowhere, lighting up his whole face. But behind that smile, around his dark eyes, in his gaunt cheeks, one can see the ominous stains caused by a life of private fear, emptiness and loneliness. He seems to have wandered in from a land where it is always cold,

Figure 7: Test Sample 2 of English Script

Four features (no. of strokes, stroke lengths, no. of peaks, no. of valleys) are calculated the values are Tabulated in the below table (4.2).

Table 4.2: Features values for the test sample-2 (English script)

No. of strokes	Stroke length	No. of Peaks	No. of Valleys
24.9	428	13	57

TEST SAMPLE – 3:

కర్ణాటక సంగీత పితామహ. భగవంతుడు పురందర విఠలా వందనంతో అతని పాటలు ముగుస్తాయి కన్నడ భాషలో ఆయన సుమారు పాటలు కూర్చినట్లు భావిస్తున్నారు. అయితే ఈ రోజు వీటిలో వెయ్యి మాత్రమే తెలుసు. ప్రధాన వ్యాసం. భారతీయ నృత్యం కూడా జానపద మరియు శాస్త్రీయ రూపాలుగా విభజించబడింది. బాగా ప్రసిద్ధి చెందిన జానపద నృత్యాల్లో పంజాబ్‌కు చెందిన భాంగ్రా అస్సాంకు చెందిన బిహు జార్ఖండ్ ఒరిస్సాలకు చెందిన చావో రాజస్థాన్‌కు చెందిన ఘూమర్ గుజరాత్‌కు చెందిన దాండియా గార్బా కర్ణాటకకు చెందిన యక్షగాన మహారాష్ట్రకు చెందిన లావణి, గోవాకు చెందిన దెక్ని ఉన్నాయి. భారతదేశానికి చెందిన జాతీయ సంగీత నృత్య నాటక అకాడమీచే ఎనిమిది నృత్య రీతులు ఎక్కువగా కథనాత్మక రూపాలు హోదా పొందాయి.

Figure 8: Test Sample 3 of Telugu Script

Four features (no. of strokes, stroke lengths, no. of peaks, no. of valleys) are calculated the values are tabulated in the below table (4.3).

Table 4.3: Features values for the test sample-3(Telugu script)

No. of strokes	Stroke length	No. of Peaks	No. of Valleys
0	**0**	**12.8**	**54**

4.1 OBSERVATION:

Devanagari*:* It is observed that for Devanagari script the number of strokes vary between a minimum of 1 to 6. As the number of strokes vary so do the stroke length. It varies between 54 -59. The peak value is almost constant and is always in the vicinity of 9.

English: *The* average number of strokes for English is always greater than 20 which is unique to this script. The average stroke length is much greater than all other scripts under consideration and is greater than 400. This is due to the fact that English script is having more vertical line like structure characters. Peaks and Valleys for English are always constant and are 13 and 57 respectively.

Telugu**:** The no. of strokes and the stroke length are almost 0. Because vertical line like structure character are very less in Telugu script. The peak value is a constant with a value of 12 and the valley has an average value of 52.

Script identification: It is observed, if a test image after converted into black and white and calculate all the 4 features (no. of strokes, stroke lengths, no. of peaks, no. of valleys) and they are then compared with the training data base. And for each parameter, the script with minimum distance is identified and coded into a 1x4 vector.

- If more than two elements of the minimum distance vector-V has a same value X, then the test image script is identified as the script with code X. This condition is useful for identifying English, Telugu.
- If third element is either 2 or 4 and if remaining elements are not equal to 4 then the test image script is identified as the script with code 2. (This condition occurs only for Devanagari script.)

V. CONCLUSIONS

In this work a method to identify the document images of English, Hindi and Telugu scripts from a document image set is presented. The approach is based on the analysis of the horizontal projection profile and vertical projection profile of the document images and explores the features like strokes, peaks and valleys of pixel distribution.

In this work we observed that, vertical stroke features are efficient to classify south Indian languages from north Indian languages. To classify north Indian languages among themselves and also south Indian languages among themselves pixel distribution is used. To further improve the efficiency of classification and to cover even more scripts, additional features like entropy and energy distribution can be explored as a future task.

VI. ACKNOWLEDGMENT

I would like to record my sincere thanks to my research supervisor **Dr. L. PRATAP REDDY,** Director R&D Cell, Prof. in ECE Department, JNTUH College of Engineering and Mrs. Karunasri JNTUH College of Engineering. Their vision, breath of knowledge, perseverance and patience has been the motivating factors behind this work.

REFERENCES

[1]. Bharath A. and Sriganesh Madhvanath, "On the Significance of Stroke Size and Position for Online Handwritten Devanagari Word Recognition: An Empirical Study ", 2010 IEEE, International Conference on Pattern Recognition.

[2]. M.C. Padma and P. A. Vijaya, "Script Identification of Text Words from a Tri-Lingual Document Using Voting Technique",2010 International Journal of Image Processing, Volume (4): Issue (1)

[3]. Anuj Sharma, Rajesh Kumar and R.K. Sharma ,"Rearrangement of Recognized Strokes in Online Handwritten Gurumukhi Words Recognition",2009 10th International Conference on Document Analysis and Recognition

[4]. U. Pal and B.B. Chaudhuri, "Identification of Different Script Lines from Multi-script Documents," Image & Vision Computing, vol. 20, no. 13-14, pp. 945-954, Dec. 2002.
[5]. U. Pal, S. Sinha, and B.B. Chaudhuri, "Multi-script Line Identification from Indian Documents," Proc. Int'l Conf. Document Analysis & Recognition, Edinburgh, pp. 880-884, Aug. 2003.
[6]. S. Sinha, U. Pal, and B.B. Chaudhuri, "Word-wise Script Identification from Indian Documents," Lecture Notes in Computer Science: IAPR Int'l Workshop Document Analysis Systems, Florence, LNCS-3163, pp. 310-321, Sep. 2004
[7]. S.L. Wood, X. Yao, K. Krishnamurthy, and L. Dang, "Language Identification for Printed Text Independent of Segmentation," Proc. Int'l Conf. Image Processing, Washington D.C., vol. 3, pp. 428-431, Oct. 1995.
[8]. H.S. Baird, S. Kahan, and T. Pavlidis,"Components of an Omni- font Page Reader," Proc. Eighth Int'l Conf. Pattern Recognition, Paris, pp. 344- 348, 1986.
[9]. Y. Lu, "On the Segmentation of Touching Characters," lnt'l Conf. Document Analysis and Recognition, Tsukuba, Japan, pp. 440-443, Oct. 1993.
[10]. S. Liang, M. Ahmadi, and M. Shridhar, "Segmentation of Touching Characters in Printed Document Recognition," Proc. Int'l Conf. Document Analysis and Recognition, Tsukuba City, Japan, pp. 569-572, Oct. 1993.

International Journal of Modern Engineering Research (IJMER)
www.ijmer.com Vol. 3, Issue. 4, July-august. 2013 pp-2239-2243 ISSN: 2249-6645

Fabrication and Testing of Natural Fiber Reinforced Hybrid Composites Banana/Pineapple

Madhukiran.J[1], Dr. S. Srinivasa Rao[2], Madhusudan.S[3]

[1&2]Department of Mechanical Engineering M.V.G.R. College of Engineering,
Jawaharlal Nehru Technological University (Kakinada) Vizianagaram - 535005, A.P, India.
[3]Department of Mechanical Engineering Sir. C.R. Reddy College of Engineering,
Andhra University Eluru - 534 007, A.P, India.

ABSTRACT : *Work has been carried out to investigate the flexural properties of composites made by reinforcing banana and pineapple as the new natural fibers into epoxy resin matrix. The natural fibers were extracted by retting and manual process. The composites are fabricated using banana and pineapple fiber reinforcements. Hybrid composites were prepared using banana/pineapple fibers of 0/40, 15/25, 20/20, 25/15, and 40/0 Weight fraction ratios, while overall fiber weight fraction was fixed as 0.4Wf. It has been observed that the flexural properties increase with the increase in the weight fraction of fibers to certain extent. The hybridization of the reinforcement in the composite shows greater flexural strength when compared to individual type of natural fibers reinforced composites. All the composites shows increase in flexural strength in longitudinal direction. Similar trends have been observed for flexural modulus, inter laminar shear strength and break load values.*

KEYWORDS: *Natural fibers, Banana & Pineapple fibers, Hybrid composites, flexural properties, Inter laminar shear strength*

I. INTRODUCTION

Many researchers are searching for structural materials of high strength, less weight and low cost, in general strong materials are relatively dense and light materials have less strength. In order to achieve high strength and less weight, it requires combining two or more distinct materials to get composite materials. The combination results in superior properties not exhibited by the individual materials. Many composite materials are composed of just two phases one is termed as matrix phase, which is continuous and surrounds the other phase often called the dispersed phase or reinforcement phase [1-2]. The reinforcement is usually much stronger and stiffer than the matrix, and gives the composite good properties. The matrix holds the reinforcements in orderly pattern. The matrix materials can be metallic, polymeric or ceramic. A metal matrix composite consists of a matrix of metals or alloys reinforced with metal fibers such as boron carbon. When the matrix is a polymer the composite is called polymer matrix composite (PMC).Ceramic matrix composites consists of a matrix reinforced with ceramic fibers such as silicon carbide, alumina or nitride. The reinforcing phase can either be fibrous or non-fibrous (particulates) in nature and if the fibers are extracted from plants. The fiber reinforced polymers (FRPs) consist of fibers of high strength and modulus embedded in or bonded to a matrix with a distinct interface between them. In this form, both fibers and matrix retain their physical and chemical properties.

The matrix phase binds the fibers together and acts as medium by which an externally applied stress is transmitted and distributed to the fibers. Only a very small portion of an applied load is sustained by the matrix phase and major portion is sustained by the fibers. The fibers are basically two types. They are natural and synthetic Fibers. Cotton, jute and sisal are some examples for natural fibers and glass, nylon and carbon are some examples for synthetic fibers.

Natural fibers, as reinforcement, have recently attracted the attention of researchers because of their advantages over other established materials. They are environmentally friendly, fully biodegradable, abundantly available, and renewable. Plant fibers are light compared to glass, carbon and aramid fibers. The biodegradability of plant fibers can contribute to a healthy ecosystem while their low cost and high performance fulfils the economic interest of industry. When natural fiber-reinforced plastics are subjected, at the end of their life cycle, to combustion process or landfill, the released amount of CO_2 of the fibers is neutral with respect to the assimilated amount during their growth. Natural fibers such as banana, cotton, coir, sisal and jute have attracted the attention of scientists and technologists for application in consumer goods, low cost housing and other civil structures. It has been found that these natural fiber composites possess better electrical resistance, good thermal and acoustic insulating properties and higher resistance to fracture. They are also renewable and have relatively high strength and stiffness and cause no skin irritations. On the other hand, there are also some disadvantages, such as moisture absorption, quality variations and low thermal stability. Many investigations have been made on the potential of the natural fibers as reinforcements for composites and in several cases the results have shown that the natural fiber composites own good stiffness but the composites do not reach the same level of strength as the glass fiber composite [3]. Hybrid composite materials are made by combining two or more different types of fibers in a common matrix. Hybridization of two types of short fibers having different lengths and diameters offers some advantages over the use of either of the fibers alone in a single polymer matrix. Most of the studies are on the hybridization of natural fibers with glass fibers to improve the properties [4–10]. They possess a good calorific value and cause little concern in terms of health and safety during handling. In addition, they exhibit excellent mechanical properties, have low density and are inexpensive.

This good environmental friendly feature makes the materials very popular in engineering markets such as the automotive and construction industry.

S.M. Sapuan et al [12] investigated the tensile and flexural properties of banana fiber reinforced with epoxy. The statistical analysis carried out, showed an increase in mechanical properties. Maries Idicula et al [13] studies Dynamic studies on mechanical properties of randomly mixed sisal and banana fibers were carried out and it is observed that the flexural and tensile modulus shows improvement in results. The damping behavior also improved for sisal polyester composites. N.Venkateshwaran et al [14] studied the tensile, flexural and water absorption studies of banana-epoxy composite materials which showed a poor result and it can be improved in a better way by the addition of sisal fiber along with banana fiber in different weight percentages. V.Naga Prasad Naidu et al [15] in their paper the hybrid composites of unsaturated polyester based sisal/glass fiber hybrid composites were prepared. Glass/sisal fibers were combined in the same matrix (unsaturated polyester) to make hybrid composites and the tensile and flexural properties are studied. A significant improvement in tensile and flexural properties of sisal/glass fiber hybrid composites was found. With this background, an attempt has been made in this present investigation to fabricate and to evaluate the properties of natural fiber reinforced hybrid composites.

II. MATERIALS AND METHODS

II.1 Materials: Banana fiber (Musaceae family) a type of bast fiber, is extracted from the bark of banana tree. Pineapple is multi-cellular and lignocelluloses materials extracted from the leave of plant Ananas cosomus belonging to the (Bromeliaceous family). The fiber is extracted by hand scraping after beating the leaves to break up the pulpy tissue. Both fibers are purchased from Perfect Banana fiber & Articles Manufacturer, Coimbatore, Tamilnadu. Hardener and Resin was purchased from Shakti glass fibers and Traders, Chennai, India. The properties of banana and pineapple fibers are given in Table 1 [11].

II.2 Extraction of fibers: The obtained fibers are cleaned with water and dried. Then the segregations are gently dispersed with hand sitting patiently. Pineapple and banana fibers after retting the husks are beaten with a hammer. These fibers are ripped from the husks and separated from the comb. After drying at the room temperature, both the fibers were combed with a cotton carding frame for several times further separate the fibers in to individual state. After that, both the fibers are measured for proper weight and length.

II.3 Weight fraction of the fiber: The weight of the matrix was calculated by multiplying density of the matrix and the volume (volume in the mould). Corresponding to the weight of the matrix the specified weight percentage of fibers is taken. For hybrid combination the corresponding weight of fiber obtained is shared by two fibers.

Fig. 1 - Banana fibers and Pineapple fibers

II.4 Preparation of epoxy and hardener: Epoxy LY556 of density 1.15–1.20 g/cm^3, mixed with hardener HY951 of density 0.97–0.99 g/cm^3 is used to prepare the composite plate. The weight ratio of mixing epoxy and hardener is 10:1. This has a viscosity of 10-20 poise at 25^{0}C. Hardeners include anhydrides (acids), amines, polyamides, dicyandiamide etc.

II.5 Mould Preparation: Mould used in this work is made of well-seasoned teak wood of 200 mm X 200 mm X 3 mm dimension with five beadings. The fabrication of the composite material was carried out through the hand lay-up technique. The top, bottom surfaces of the mould and the walls are coated with remover and allowed to dry. The functions of top and bottom plates are to cover, compress the fiber after the epoxy is applied, and also to avoid the debris from entering into the composite parts during the curing time.

Fig. 2 - Resin and Hardener

II.6 Composite fabrication: The moulds are cleaned and dried before applying epoxy. The fibers were laid uniformly over the mould before applying any releasing agent or epoxy. After arranging the fibers uniformly, they were compressed for a few minutes in the mould. Then the compressed form of fibers (banana/pineapple) is removed from the mould. This was followed by applying the releasing agent on the mould, after which a coat of epoxy was applied. The compressed fiber was

laid over the coat of epoxy, ensuring uniform distribution of fibers. The epoxy mixture is then poured over the fiber uniformly and compressed for a curing time of 24 h, with load of 5kg. Composites are prepared by changing the weight fractions of both pineapple and banana fibers. Individual composites with banana and pineapple as reinforcement are also prepared under similar processing conditions for comparison purpose.

Table.1- Properties of Banana and Pineapple fiber.

Properties	Banana fiber	Pineapple fiber
Cellulose (%)	63–64	81-12
Micro febrile angle	11	14-8
Hemi cellulose (%)	6 - 19	16-19
Lignin (%)	5-10	4.6-12
Moisture content (%)	10-11	11-12
Density (kg/m^3)	1350	1440
Lumen size (mm)	5	2-3
Tensile strength (MPa)	529-914	413-1627
Young's modulus (GPa)	27-32	60-82

III. TESTING OF COMPOSITES

III.1 Flexural Test: Three point bend tests were performed in accordance with (ASTM) method D 790 [16] to measure flexural properties. The specimens were 100 mm long, 25 mm wide and 3 mm thick. In three point bending test, the outer rollers were 64 mm apart and samples were tested at a strain rate of 0.2 mm/min. Specimen were tested at a cross head speed of 2.5 mm/min, using associated universal testing machine (FIE) make. A three point bend test was chosen because it requires less material for each test and eliminates the need to accurately determine center point deflections with test equipment. In each case a set of five specimens were tested to obtain average value. The testing process is continued until the specimen fractures. A graph of load versus displacement curve was generated automatically by the computer. Flexural strength of the composite was calculated using the following relationship. $\sigma_f = 3PL/2bt^2$ Where σf = stress in the outer specimen at midpoint, P = load at a given point on the load deflection curve, L = support span, b = width of the sample d = depth of the sample.

Fig. 3 – Flexural Test Specimens

Flexural modulus is the ratio within the elastic limit of stress to corresponding strain. A tangent line will be drawn to the steepest initial straight line portion of the load deflection curve and the value can be calculated using equation $E_B=L^3M/4bd^3$ Where E_B = modulus of elasticity in bending, L = support span, M = slope of the tangent to the initial straight line portion of the load deflection curve, b = width of the sample, d = depth the sample.

III.2 Inter-Laminar Shear Test (ILST): It is three point bending test which generally promotes failure by inter-laminar shear. The short beam shear test (SBS) was carried out as per ASTM standard, using 5 Ton universal testing machine (FIE) make at a cross head speed of 2.5 mm/min. The inter-laminar shear strength (ILSS) is found out by using the equation ILSS= 3F/4bt .Where F is the maximum load, b the width of the specimen and t is the thickness of the specimen.

IV. RESULTS AND DISCUSSION

Table -2 Flexural Properties of different composite samples

% Weight fraction	Maximum Displacement	Flexural Strength (Mpa)	Flexural Modulus (Gpa)
0/40	2.63	212.15	0.506
15/25	2.26	203.40	0.319
20/20	3.45	192.47	0.474
25/15	3.77	277.77	0.706
40/0	4.33	137.17	0.252

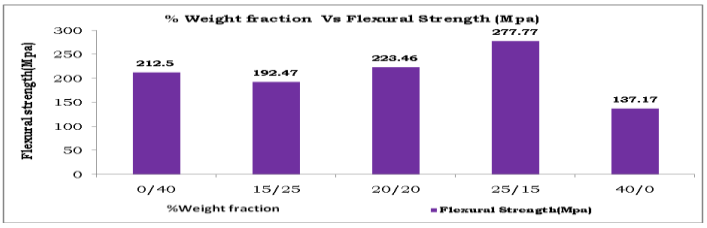

Fig. 4 – Flexural Strength Vs % Weight Fraction of Composites

The flexural strength of various composites with varying weight fractions are shown in figure 4. It can be observed that pure pineapple and pure banana composites shows a flexural strength of 212.5 Mpa and 137.17 Mpa respectively. The flexural strengths of the hybrid composites with weight fractions of 15/25 and 20/20 are found to be 192.47 Mpa and 223.46 Mpa respectively. The effect of hybridization is found to be negligible for the above two composites. However the flexural strength of the hybrid composite with 25/15 weight fraction is found to be 277.77 Mpa which is higher among the others. This behavior can be correlated to hybridization effect as both fibers contributed higher flexural strength to the composite.

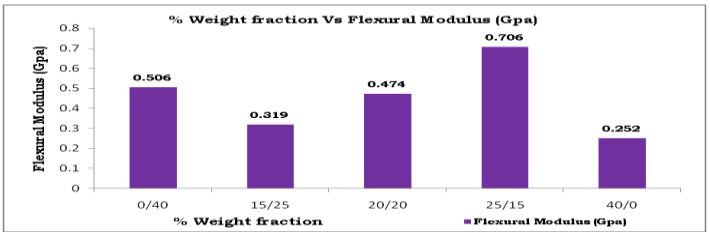

Fig. 5 – Flexural Modulus Vs % Weight Fraction of Composites

From the figure 5 it is evident that the flexural modulus of the pure banana composite (0/40) and pure pineapple composite (40/0) along longitudinal direction is 0.506 Gpa and 0.252Gpa respectively. The tensile modulus of hybrid composite (25/15) is 0.706 Gpa. This is higher among all the other composites. The tensile modulus of the other two hybrid composites with weight fractions 15/25, 20/20, is found to be 0.319 Gpa and 0.474 Gpa respectively, are very poor when compared to pure banana and 25/15 hybrid composite.

Table -3 Inter Laminar Shear Strength & Break load values of different composite samples

% Weight fraction	Inter Laminar Shear Strength (Mpa)	Break Load (Kn)
0/40	3.18	0.506
15/25	2.88	0.319
20/20	3.05	0.474
25/15	4.16	0.706
40/0	1.55	0.252

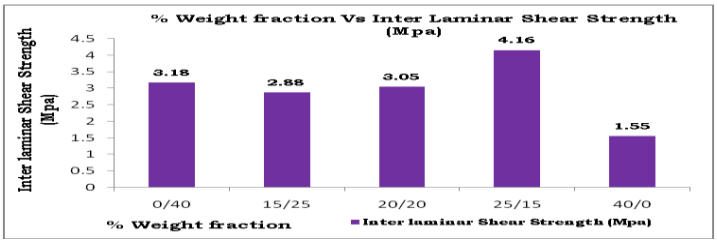

Fig. 6 – Inter Laminar Shear Strength Vs % Weight Fraction of Composites

The inter laminar shear strength of various composites with varying weight fractions are shown in figure 6. It can be observed that pure pineapple and pure banana composites shows inter laminar shear strength of 3.18 Mpa and 1.55Mpa respectively. Inter laminar shear strength of the hybrid composites with weight fractions of 15/25 and 20/20 are found to be 2.88 Mpa and 3.05 Mpa respectively. The effect of hybridization is found to be negligible for the above two composites. However the inter laminar shear strength of the hybrid composite with 25/15 weight fraction is found to be 4.16 Mpa which is higher among all the other composites. This behavior can be correlated to hybridization effect as both fibers contributed higher inter laminar shear strength to the composite.

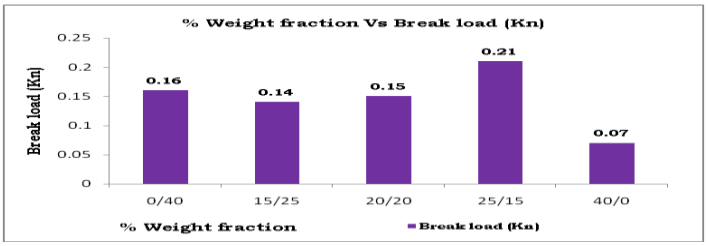

Fig. 7 – Break Load Vs % Weight Fraction of Composites

From figure 7, shows the trend of breaking strength with respect various weight fractions. Pure banana and pure pineapple composites have shown 0.16 Kn and 0.07 Kn at break point at 15/25 and 20/20 the values were observed to be low as compared to pure composite. This can be attributed to improper mixing, mismatch of individual fibers as a whole to the hybrid composite at 25/15, the hybrid composite has shown maximum breaking load (0.21 Kn) as compared to pure composite and other hybrid composites. This mixing ratio of both the fibers might have contributed proportionately thus resulted in superior breaking load capacity.

V. CONCLUSIONS

After determining the material properties of natural fiber reinforced epoxy hybrid composites with five different weight fractions of the materials, the following conclusions can be made.

1) The natural fiber reinforced epoxy hybrid composites are successfully fabricated using hand lay-up technique.
2) The banana/pineapple hybrid composite with weight fraction of 25/15 shows maximum flexural strength and maximum flexural modulus.
3) The banana/pineapple hybrid composite with weight fraction of 25/15 shows maximum inter laminar shear strength.
4) The hybridization of these natural fibers has provided considerable improvement of flexural strength when compared to individual reinforcement. This work also demonstrates the potential of the hybrid natural fiber composite materials for use in a number of consumable goods.
5) Due to the low density of proposed natural fibers compared to the synthetic fibers (Glass fibers, carbon fibers, etc...), the composites can be regarded as a useful materials in light weight applications.
6) The banana/pineapple hybrid composite with weight fraction of 25/15 shows maximum break load.

REFERENCES

[1]. K. John, S. Venkata Naidu, "Chemical resistance studies of sisal/glass., fiber hybrid composites*", Journal of Reinforced. Plastic Composites. 26(4) (2007) 373–376.*

[2]. H. P. S. Abdul Khalil, S. Hanida, C. W. Kang, N.A. Nikfuaad, Agro hybrid composite: "the effects on mechanical and physical properties of oil palm fiber (efb)/glass hybrid reinforced polyester composites", *Journal of Reinforced Plastic Composites. 26(2) (2007) 203–218.*

[3]. Oksman K, Skrivars M, Selin JF. "Natural fibers as reinforcement in polylactic acid (PLA) composites". *Composites Science and Technology 2003; 63(9):1317–24.*

[4]. Sreekalaa MS, George Jayamol, Kumaran MG, Thomas Sabu. "The mechanical performance of hybrid phenol–formaldehyde-based composites reinforced with glass and oil palm fibers". *Composites Science and Technology 2002; 62(3):339–53.*

[5]. Mishra S, Mohanty AK, Drzal LT, Misra M, Parijac S, Nayak SK, et al. "Studies on mechanical performance of bio fiber/glass reinforced polyester hybrid composites". *Composites Science and Technology 2003; 63(10):1377–85.*

[6]. Jacob Maya, Thomas Sabu, Varghese KT. "Mechanical properties of sisal/oil palm hybrid fiber reinforced natural rubber composites". *Composites Science and Technology 2004; 64(7– 8):955–65.*

[7]. Esfandiari Amirhossein. "Mechanical properties of PP/Jute Glass fiber composites – a statistical investigation". *Journal of Applied Sciences 2007; 7(24):3943–50.*

[8]. Velmurugan R, Manikandan V. "Mechanical properties of palmyra/glass fiber hybrid composites". *Composites Part a 2007; 38(10):2216–26.*

[9]. Thiruchitrambalam M, Alavudeen A, Athijayamani A, Venkateshwaran N, Elayaperumal A. "Improving mechanical properties of banana/kenaf polyester hybrid composites using sodium lauryl sulfate treatment" *Materials Physics and Mechanics 8 (2009) 165-173*

[10]. Jarukumjorn K, Supakarn Nitinnat. "Effect of glass fiber hybridization on properties of sisal fiber–polypropylene composites". *Composites Part B 2009; 40(7):623–7.*

[11]. Mukherjee KG, Satyanarayana KG. "Structure and properties of some vegetable fibers." *Journal of Material Science 1984; 19:3925–34.*

[12]. S. M. Sapuan, Leenie A, Harimi M, Beng YK. "Mechanical properties of woven banana fiber reinforced, epoxy composites". *Materials and Design 2006; 27(8):689–93.*

[13]. Maries Idicula, S.K. Malhotra, Kuruvilla Joseph, Sabu Thomas "Dynamic mechanical analysis of randomly oriented intimately mixed short banana/sisal hybrid fiber reinforced polyester composites". *Composites Science and Technology 65 (2005) 1077–1087.*

[14]. N. Venkateshwaran, A. ElayaPerumal, A. Alavudeen, M. Thiruchitrambalam "Mechanical and water absorption behaviour of banana/sisal reinforced hybrid composites" *Materials and Design 32 (2011) 4017–4021.*

[15]. V.Nagaprasad Naidu, M.Ashok kumar, G.Ramachndrareddy, M.Mohan reddy, "Tensile & flexural properties of sisal/glass fiber reinforced hybrid composites" *International Journal of Macromolecular Science 2011 1(1):19-22, ISSN-2249-8559.*

[16]. ASTM D790-07. Standard tests method for testing flexural properties of unreinforced and reinforced plastics and electrical insulating material.

International Journal of Modern Engineering Research (IJMER)
www.ijmer.com Vol. 3, Issue. 4, July-August. 2013 pp-2244-2249 ISSN: 2249-6645

Cross Spectral Density Analysis for Various Codes Suitable for Spread Spectrum under AWGN conditions with Error Detecting Code

CH.NISHANTHI[1], R.SUNDAR RAJAN[2]
Department of Electronics and Communication Engineering, JIET/ JNTUH, India
Professor, Department of Electronics and Communication Engineering, JIET/ JNTUH, India

***ABSTRACT*:** *CDMA is based around the use of direct sequence spread spectrum techniques. Essentially CDMA is a form of spread spectrum transmission which uses spreading codes to spread the signal out over a wider bandwidth then would normally be required. By using CDMA spread spectrum technology, many users are able to use the same channel and gain access to the system without causing undue interference to each other. Here this paper concentrates on the area where how to spread the signal with spread codes, So that more number of users can be accommodated in the spreaded bandwidth. Analyzing various correlation properties comparision between Pseudo Noise and Gold codes, to conclude which code best suits. Walsh Hadmard code has the capability of error detection and correction capability. The codes are simulated using MATLAB.*

KEYWORDS: *Correlation, gold codes, linear feedback shift register, Pseudo noise sequences, Spread Sequences, Walsh hadmard code.*

I. INTRODUCTION

Continuous growth in telecommunication industry in terms of users has led to utilize the available resources effectively and it provide maximum number of services. Spread spectrum (SS) is a technique where an already modulated signal or high frequency signal is modulated a second time in such a way as it produce interference in a barely noticeable way with some other signal operating in the same frequency band. So, in this interfering signals are transparent to spread spectrum signals and spread spectrum signals are transparent to interfering signals. Note that spread spectrum is not a modulation scheme. In this the main objective is preserved for generating PN sequence, like maintaining randomness, which is helpful to differentiate between users and also in generating noise like sequences, a very low correlation value, useful to avoid interference in the transmission channel and a high autocorrelation value to reject multipath fading. This paper illustrates the comparative capabilities of gold sequences and pseudo noise sequences for finding the better sequence by using their correlation properties and the simulation is done in Matlab environment for PN sequences, Gold Sequences, As well as Walsh hadmard codes.

The whole paper is sectionalized as follows. In section 2 spread spectrum techniques, pseudo noise sequences, gold sequences, Walsh hadmard codes are described. In section 3 generating PN and gold codes are described and generation of spread signal, how to generate despreaded signal along with cross correlation and auto correlation. In section 4 simulation comparisons of PN and Gold sequences in various scenarios how the Walsh hadmard code signal appears for a spread signal received without error in both cross correlation and autocorrelation cases. In section 5 results are described.

II. SPREAD SPECTRUM SEQUENCE

***II.1 Introduction*:** Spread spectrum is a means of transmission in which signal occupies a bandwidth in excess of the minimum necessary to send the information; the band spread is accomplished by a code which is independent of data and a synchronized reception with the code at the receiver is used for dispreading and subsequent data recovery. Spreading the bandwidth has several advantages like the resistance to narrowband interference and it covers the narrowband signal into a broadband signal.[3].
Spread codes are mainly:

- Pseudo Noise (PN) sequences
- Gold sequence
- Walsh Hadmard Codes
- Kasami Sequence

II.1 PN sequence: Pseudo noise (PN) sequence is a periodic binary sequence with noise like waveform but have deterministic value. The codes are usually generated by means of feedback shift registers, which are generated by using an algorithm which is deterministic and consists of some initial value called seed & therefore it produces sequence of numbers that are not stastically random. A pseudo noise (PN) sequence is a binary sequence of 1's and 0's.The PN code Properties are

Balance Property: In each period of maximum-length sequence, the number of 1s is always one more than the number of 0s. So there must be $2^m - 1$ones and $2^m - 1$zero in a full period of the sequence.

Run Length Property: *Here*, the 'run' represents a subsequence of identical symbols (1's or 0's) within one period of the sequence. The length of this subsequence is the length of the run. Among the runs of 1's and 0's in each period of a

maximum-length sequence, one-half the run of each kind are of length one, one-fourth are length two, one-eighth are of length three etc. For a maximum-length sequence generated by a linear feedback shift register of length m, the total number of runs is (N+1)/2 where N=$2^m - 1$

Correlation Property: The codes must have a low cross correlation value. Lower cross correlation allows more users in the system. This condition holds for both full-code correlation and partial-code correlation. Because in most situations there will not be a full period correlation of two codes, it is more likely that codes will only correlate partially due to random-access nature [2].

II.2 Linear Feedback shift Register: The PN sequences are generated by using linear feedback shift registers. LFSR is designed with Flip-flops and XOR gates with shifting operation. The number of states depends on number flip flops/registers involved in the LFSR. At each end of the clock edge the content in the registers are shifted to right by one position [1].to give feedback there is predefined taps in the registers. They will give feedback to the left most register through XNOR or XOR gate.

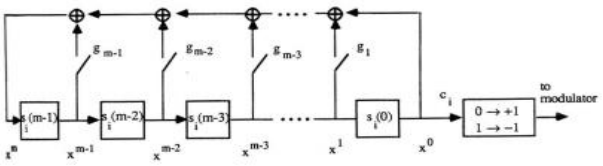

Figure 1:m-sequence Linear feedback shift Register

- Linear generator polynomial g(x) of degree m>0 g(x)=$g_m x^m + g_{m-1}x^{m-1} + \cdots + g_1 x + g_0$
- Recurrence Equation($g_m = g_0$=1) $x^m = g_{m-1}x^{m-1} + g_{m-2}x^{m-2} + \cdots . g_1 x + g_0$
- If g_i =1, the corresponding circuit switch is closed, otherwise $g_i \neq 1$, it is open. Output of the shift-register circuit is transformed to 1 if it is 0 and 1 if it is 1.

One of the two main parts of LFSR is the shift register and the other one is feedback function. The main function of the shift register is to shift its contents into adjacent positions within the register or if it is the position on the end, out of the register. the position on the other end id left empty unless some new content is shifted into the register[1].

II.3 Gold code: The particular class of PN sequences called Gold sequences. They can be chosen such that, the cross-correlation values between the codes over a set of codes are uniform and bounded. Gold codes can be generated by modulo-2 addition of two maximum-length sequences with the same length. The code sequences are added chip by chip by synchronous clocking. The generated codes are of the same length as the two m-sequences which are added together. In addition to their advantages Gold codes generates large number of codes. To define a set of Gold codes, preferred pairs of m sequences are used. If a is an m-sequence of length N, the second sequence a` can be obtained by sampling every q^{th} symbol of a. The second sequence is called decimation of the first sequence.

The figure2 illustrates about the gold sequence generator for the proffered pair gold sequences. Suppose we take an m sequence represented by a binary vector a of length N and generate a new sequence a' by sampling every q^{th} symbol a. We use multiple copies of a until we have enough samples to produce a sequence of a' of length N.The sequence a' is decimation of sequence a and is written as a=a[q].for gold sequences we need to start with preferred m-sequences that meet following conditions.

- n ≠ 0; that is, n is odd or n=2
- à =a[q] where q is odd and either
- q=$2^k + 1$ or q=$2^{2k} - 2^k + 1$
- GCD(n,k) = $\begin{cases} 1 \; for \; n \; odd \\ 2 \; for \; n \; even \end{cases}$

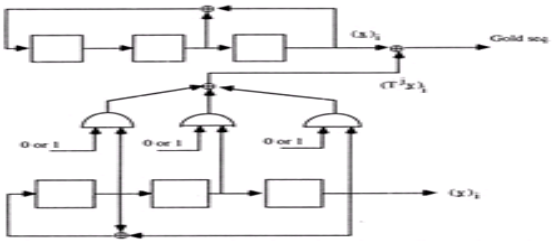

Figure2: Gold sequence generator for the preferred pair $g_1(x) = x^3 + x + 1$ and $g_2(x) = x^3 + x^2 + 1$

For shift register of length n,the cross correlation of the gold sequences produced by a preferred pair is bounded by $|R| \leq 2^{(n+1)/2}+1$ for n odd and $|R| \leq 2^{(n+2)/2}+1$ for n even. the two PN sequences are used as components in the program by XORing the two PN sequences we will get Gold-Code. Gold sequences help to generate more sequences out of a pair of m-sequences giving now many more different sequences to have multiple users. the m-sequences gave only one sequence of length (2^5-1).by combining two of these sequences, we can obtain up to 31 plus the two m-sequences themselves, generate 33 sequences that can be used to spread different input messages.

II.4 Walsh Hadmard code: Walsh codes are orthogonal codes. These codes are used in DSSS systems and also in FHSS systems to select the target frequency for next hop. The Hadamard-Walsh codes are generated in a set of $N=2^n$ codes with length $N=2^n$. The generating algorithm is as follows

$$H_{2N} = \begin{bmatrix} H_N & H_N \\ H_N & \overline{H_N} \end{bmatrix}$$

Figure3: Walsh Hadmard Matrix

Where N is a power of 2 and over score denotes the binary complement of the bits in the matrix. The smallest set of N=0 is $H_0 = [1]$ with the length 1. The rows or columns of matrix H_n are the Hadamard-Walsh codes since the matrix H_N is symmetric.

As shown above, in each set, the first row of the matrix consist all 1's and rest of the rows contains N/2 0's and N/2 1's. Also row N/2 starts with N/2 1's and ends with N/2 0's. Orthogonality is the most important property of Hadamard-Walsh codes. Because of this orthogonality property, the cross-correlation between any two Hadamard-Walsh codes of the same set (matrix) is zero, when system is perfectly synchronized. Walsh codes are not maximal length or PN type codes for spread spectrum. Although the members of the set are orthogonal, they do not give any spreading. They are used in forward channel of IS-95 CDMA type system for their orthogonality. Walsh code spreading can be used if all users of the same channel are synchronized in time, because the cross-correlation between different shifts of Walsh codes is not zero. Orthogonal functions are employed to improve the bandwidth efficiency of spread spectrum systems. The Walsh and Hadamard sequences make useful sets for CDMA.

The orthogonal functions have the following characteristic:

$$\sum_{k=0}^{M-1} \varphi_i(k\tau)\,\varphi_j(k\tau) = 0, i \neq j$$

$\varphi_i(k\tau)$, $\varphi_j(k\tau)$: Ith and jth orthogonal members of an orthogonal set.

III SPREAD CODES GENERATION

III.1Correlation: The correlation properties of PN codes play a major part in the code design for CDMA systems, since they determine not only the level of multiple access interference, i.e., the interference arising from other users of the channel and self interference due to multipath propagation, but also the code acquisition properties [6].correlation is the concept of determining how much similarity one set of data has with another. It is defined with range -1 to 1.Other value indicates partial degree of correlation.

TABLE 1. Correlation values

Correlation value	Interpretation
1	The second sequence m sequence matches the first sequence exactly
0	There is no relation between sequence
-1	The two sequences are mirror image of each other

III.1.1 Auto correlation: Autocorrelation is mainly of two types periodic autocorrelation and aperiodic autocorrelation In periodic autocorrelation The m-sequence have the best periodic autocorrelation in terms of minimizing the maximum value of the out-of-phase Autocorrelation. It is best utilized if the synchronization window is longer than on Period. In aperiodic autocorrelation If the synchronization window is only one period long or less, then the correlation is aperiodic.

The formal definition of aperiodic autocorrelation is

$x = x_0, x_1, \ldots\ldots\ldots\ldots x_{N-1}$ and $y = y_0, y_1, \ldots\ldots\ldots y_{N-1}$ is given by

$$C_{x,y}(i) = \begin{cases} \sum_{j=0}^{N-1-i} x_j\, y_{j+i}^* & 0 \le i \le N-1 \\ \sum_{j=0}^{N-1+i} x_{j-i}\, y_j^* & -(N-1) \le i < 0 \end{cases}$$

Auto correlation is the similarity of sequence with all phase shifts of itself[6].pure random data should have a correlation value close to 0 for all auto correlations with a phase shift other than 0.

$$R(\tau) = \frac{1}{N}\sum_{k=1}^{N} B_k B_{k-\tau} \quad where\ \tau = 0, N, 2N$$

III.1.2Cross correlation: In this case the comparision is made between two sequences from rather than a shifted copy of sequence with itself. In general cross correlation value produced by matching sequence with random sequence is low [6].the cross correlation between two sources A and B, is defined as

$$R_{A,B}(\tau) = \frac{1}{N}\sum_{k=1}^{N} A_k B_{k-\tau} \quad where\ \tau = 0, N, 2N$$

III.2 Transmitter block: It Gives output as spread signal means spreading of bandwidth. The spread signal is generated by modulating message signal with the gold code. Message signal is of 20 bit type and the bits are in the fashion of 0's and 1's.each and every code bit is mapped to string of six 1's and six 0's wherever 1's and 0' appears in the message signal. This is the key point in CDMA which increases the bandwidth of the message signal by keeping symbol per rate constant. Next step is to generate the gold code, it can be generated with the help of two PN sequences i.e. PN sequence 1 and PN sequence 2.

Generation of Gold Code

- At first there are two pseudo noise sequences produced named PN 1 and PN 2.
- The PN1 and PN2 are 20 bit long by XORing specific pattern and shifting each of them continuously.
- For PN1, the XORing pattern is obtained by taking bits 1, 4,6,7,13,19.
- For PN1,the XORing pattern is obtained by taking bits 1,2,3,5,7,9,10,13,14,16,17
- From the two sequences each output bit is XORed and stored in an array called Gold.

***Modulation of message signal with Gold code*:** The main idea for modulation is that replacing each 0 in the 20 bit message signal with the help of original gold codes. In the message signal each 1 is inverted to 20 bit gold codes. Therefore, 20 bit message signal is converted into (20 × 20) =400 bit spreaded signal**.**

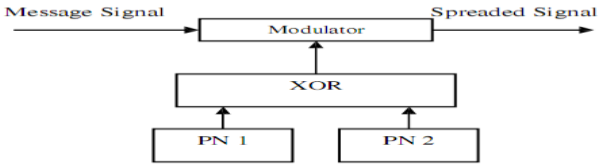

Figure4: Transmitter Block

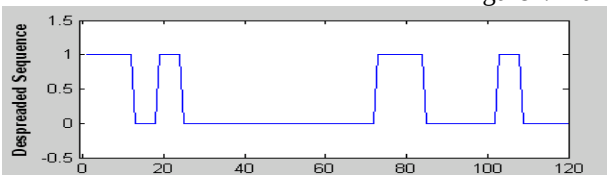

Figure5: Message signal

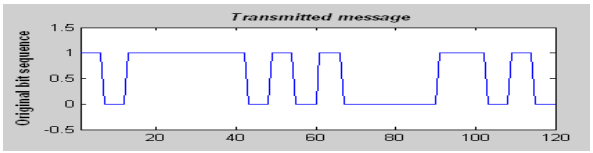

Figure6: Gold code

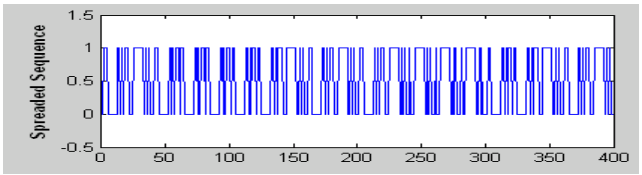

Figure7: Spread signal

III.3 Demodulation: In the demodulation process the transmitted signal is demodulated with the carrier signal like to get the original message signal at the end point.

In this section the received spreaded signal is demodulated with the gold codes for producing the original signal.

- As original message signal and gold code are 20 bit long, we have XORed each 20 bit of the received signal.
- The XORing results of the gold codes are either 0 or 1, as the message signal consists of either gold codes or inverted codes.
- The resulting 0 is stored in an array simply called despreaded signal and 1 is stored 1.
- This process is repeated up to 400 bits after each 20 bits.

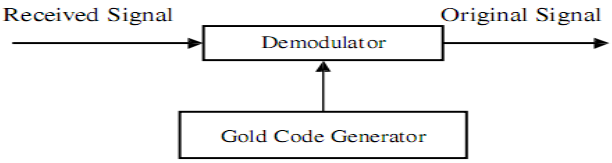

Figure8: Receiver block diagram

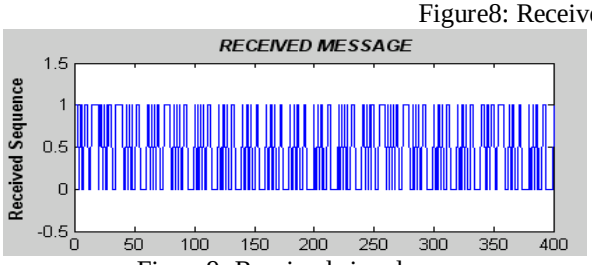

Figure9: Received signal

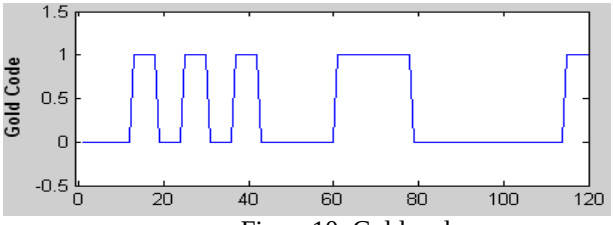

Figure10: Gold code

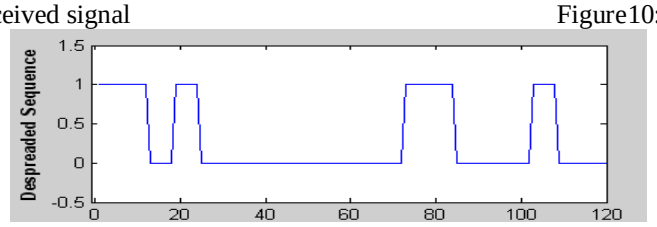

Figure11: Gold code

1.4 Walsh Hadmard code generation:

- We first generate 8 length Walsh codes using generateHadamardMatrix function in Matlab.
- To showcase auto correlation and cross correlation properties, we first perform Cross correlation of Walsh code 1 with the rest of the Walsh codes
- Auto Correlation is performed only using the first Walsh code.
- Results prove that Walsh codes have excellent cross-correlation property and poor autocorrelation property. Excellent cross-correlation property (zero cross-correlation) implies orthogonality, which makes it suitable for CDMA applications.

$$H_{2N} = \begin{bmatrix} H_N & H_N \\ H_N & \overline{H_N} \end{bmatrix}$$

Figure12: Walsh Hadmard Matrix

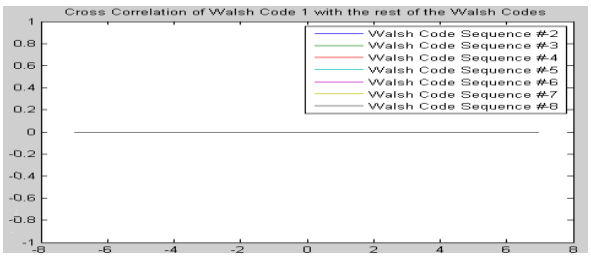

Figure13: Cross Correlated Walsh hadmard code

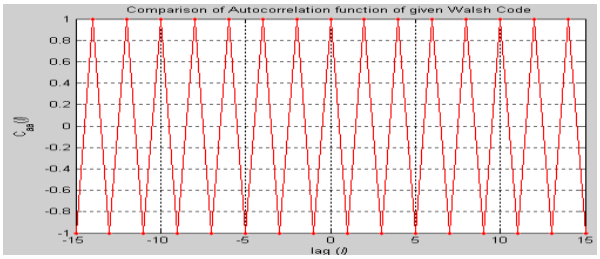

Figure14: Comparision of Auto correlated Walsh Hadmard Code

IV. SIMULATION RESULTS FOR CORRELATION

IV.1 Verification of Autocorrelation: Auto Correlation is the similarity of sequence with all phase shifts of itself . Pure random data should have a Correlation value close to 0 for all auto Correlations with a phase shift other then 0.

$$R(\tau) = \frac{1}{N}\sum_{k=1}^{N} B_k B_{k-\tau} \quad where\ \tau = 0, N, 2N$$

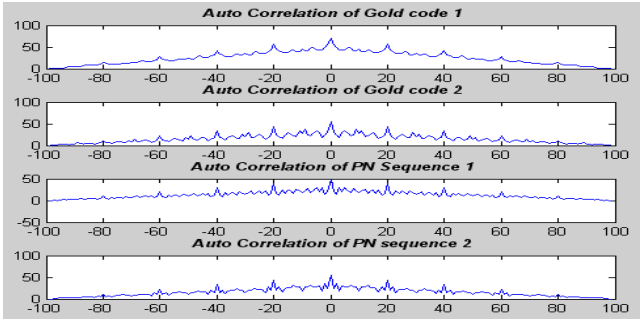

Figure15: Autocorrelation of spread codes

IV.2 Cross correlation: In this case the comparison is made between two sequences from rather than a shifted copy of sequence with itself. In general cross correlation value produced by matching sequence with random sequence is low . The cross correlation between two sources A and B, is defined as

$$R_{A,B}(\tau) = \frac{1}{N}\sum_{k=1}^{N} A_k B_{k-\tau} \quad where\ \tau = 0, N, 2N$$

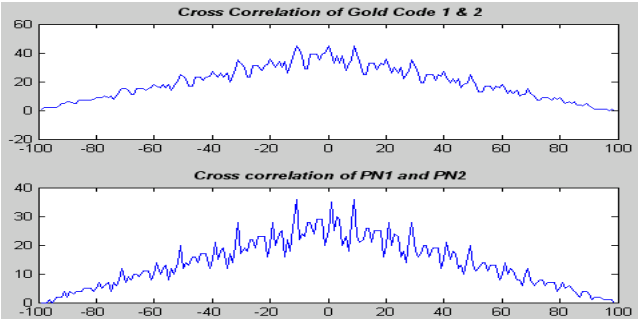

Figure16: Cross correlation of spread codes

V. RESULTS AND CONCLUSIONS

Correlations are tested which gives better result. From the graphs and results we can said that we have generated a 20 bit long gold code, modulated a message signal, produced 400 bits long spreaded signal and for producing the original message signal demodulated the spreaded signal by successfully. And from other graphs we can also said that the gold codes are better than PN sequences, therefore, gold codes are more appropriate for modulation process and to spread a message signal than PN sequences .Also these properties are verified for another type of code known as Walsh Hadamard code.

REFERENCES

[1]. Kamran Etemad, "CDMA 2000: Evolution-System Concepts & Design Principles", edition, John Wiley & sons, 2004, pp. 49, 121-123
[2]. Pal, M., Chattopadhyay," A novel orthogonal mini mum cross-correlation spreading code in CDMA system" Emerging Trends in Robotics and Communication Technologies (INTERACT), 2010 International Conference on Digital Object, 2010, pp. 80 – 84.
[3]. Theodore S.Rappaport "Wireless Communications Principle and Practice Prentice Hall, New Jersey, 1996." ISBN / ASIN: 0133755363 pp. 275-276
[4]. William Stallings, "Wireless Communications and Networks Second Edition" pp.160-170
[5]. [Online: November, 2011] Wikipedia, About gold codes http://en.wikipedia.org/wiki/Gold_code
[6]. William Stallings, "Wireless Communications and Networks Second Edition" pp.170-173

International Journal of Modern Engineering Research (IJMER)
www.ijmer.com Vol. 3, Issue. 4, July-august. 2013 pp-2250-2261 ISSN: 2249-6645

CNC PART PROGRAMMING AND COST ANALYSIS ON VERTICAL MACHINING CENTRE (VTC)

Dr. V.S.S. Murthy[1] P. Sreenivas[2]
[1](Professor and Principal of K.S.R.M *College of Engg, Dept of Mechanical Engineering, Kadapa, Andhra Pradesh, India)*
[2]*(Assistant Professor, Dept of Mechanical Engineering,*
K.S.R.M College of Engg, Kadapa, Andhra Pradesh, India)

ABSTRACT: *In the present study in view of the latest development and revolutionary changes taking place in CNC field through the world, Mechanical elements have to be designed and manufactured to precision, which is perfectly and easily possible through these modern CNC machines. This work is based on the capacity and capability of vertical machining Centre (VTC) with auto tool changer. The top slide which was part programmed can be machined using VTC. And Machining Time is compared in between carbide and hardened tools. The "Top slide" of lathe's called for powerful NC programming technique were used absolute position type data input system using G codes, M codes, polar coordinate programs, circular and linear interpolation, canned cycles etc. The above mentioned component – top slide being manufactured by using various Conventional machine tools like horizontal milling, vertical milling, surface grinding, boring machine and slotting machines. This involved a considerable lead time and usually delayed the assembly schedule. it has been modified and adopted for regular production on this machine, in two setups there by boosting their productivity and ensuring quality in each and every piece. Finally, we can establish for regular production.*

KEYWORDS: *CNC Programming, Machining Time, carbide & hardened Tools.*

I. INTRODUCTION

I.1.NUMERICAL CONTROL: Numerical control (NC) can be defined as a form of programmable automation in which the process is controlled by numbers, letters and symbols. In NC, the numbers form a program of instructions of designed for a particular work part or job.

The definition of NC given by electronic industries association (EIA) is "A system in which actions are controlled by direct insertion of numerical data at some point. The system must automatically interpret at least some portion of this data. "

A Numerical control (NC) system is used when

- The number of components per component is large
- Size of batches is medium
- Labour cost for the component is high
- The component requires special tooling
- Ratio of cutting time to non-cutting time is high
- Design changes are frequent

I.2. BASIC ELEMENTS OF A NC SYSTEM:

An operational numerical control system consists of three basic components

- Controller unit also known as machine control unit (MCU)
- Machine tool or other machining centre
- The program of instructions serves as the input to the controller unit, which in turn commands the machine tool or other process to be controlled.

I.2.1 PROGRAM OF INSTRUCTIONS: The program of instructions is the detailed step-by-step set of directions which instructs the machine tool what to do. It is coded in numerical or symbolic form on some type of input medium that can be interpreted by the controller unit. The input media used can be punched cards/ magnetic disk or tape/punched tape. There are two methods of inputs in the NC system.

- By manual entry of instructional data to the controller unit and this method is called manual data input (MDI) and is appropriate only for relatively simple jobs where the order will not be protected.
- By means of a direct link with a computer. This is called direct numerical control (DNC).

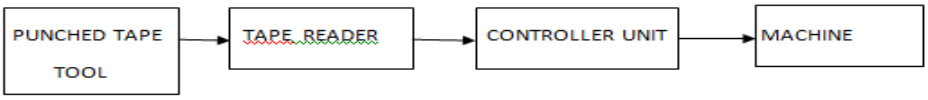

Fig.1 Basic Components of NC system

- Part programmer prepares the program of instructions. The programmer's job is to provide a set of detailed instructions by which the sequences of processing steps are to be performed.
- The processing steps for a machining operation are the relative movement between the cutting tool and the work piece

I.2.2 CONTROLLER UNIT: The controller unit consists of the electronics and hardware that reveals and interprets the program of instructions and converts it into mechanical actions of the machine tool. The controller unit elements are tape

reader, a data buffer, signal output to the machine tool Feedback, channel from the machine tool and data decoding control area.

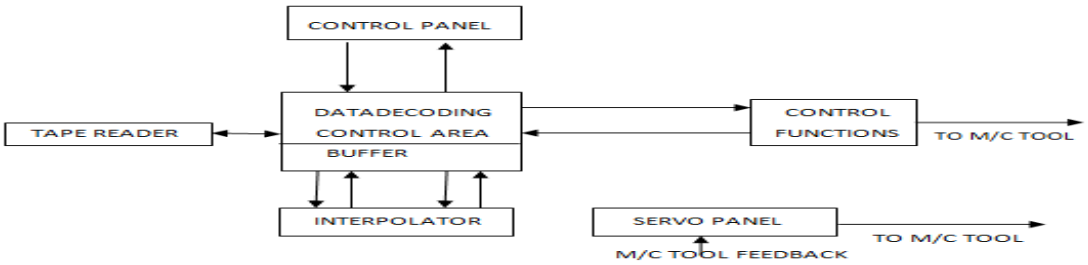

Fig 2. Machine controller unit

I.3. NUMERICAL CONTROL (NC) PROCEDURE:

The basic steps in NC procedure to utilize NC in manufacturing are

- Process planning
- Part programming
- Part program entry/ tape preparation
- Proving the part programs/ tape verification
- Production

I.3.1. PROCESS PLANNING: Process planning is the procedure of deciding what operations to be carried on the component, in what order and with what tooling and work holding facility. Both process planning and part programming for manufacturing occur after the detail drawing a component has been prepared.

1.3.2. PART PROGRAMMING: In part programming, sequence of steps to be performed by NC planned and documented. There are two methods by which a part program is accomplished manual part programming and computer assisted part programming.

In manual part programming the relative cutter/work piece positions which must be following to machine the part are listed in a format known as part program manuscript. For complex work piece geometries and jobs with many machining steps, computer-assisted part programming is used.

I.4 TOOLINGS FOR CNC (VERTICAL MACHINING CENTRE): The modern machine tools are designed to operate at higher speeds and feeds. They possess improved accuracy, higher rigidity and reduced noise levels. The cost of raw material input is very high-of the order of 40% for general purpose machine tools. This calls for optimizing the design of machine elements, selecting the right type of materials, judiciously imparting effective fabrication and treatment method.

I.5 GENERAL PRINCIPLES IN THE SELECTION OF MATERIALS FOR MACHINE TOOLS:

I.5.1 FUNCTIONAL REQUIREMENTS: The functional requirements must be met in terms of various properties. For example, in the selecting material for the main spindle of a machine tool, the modulus of elasticity and the surface hardness required for the spindle nose, bore and the locations of the bearings are important properties which need to be considered. Generally, low nickel-chromium alloy case carburized steel such as 15CrNi6 (as per DIN 17210) is selected, which meets the functional requirements.

1.5.2 EASE OF FABRICATION: The process of fabrication should be such that the part or component should be easy to make. If it is required in batch quantity, casting process is adopted. For example, machine tool elements or parts such as bed, headstock, etc. required in batch quantity are made out of casting process in the foundry. If the requirement is one or two numbers, a welding process is used to fabricate the part.

1.5.3 MACHINABILITY: This is another important parameter to be considered for selecting the raw material of machine tool components as extensive machining is involved. Construction steels such as medium carbon steel (C45 as per DIN 17200) and low alloy steel (15CrNi6 as per DIN 17210, 36CrNiMo4 as per DIN 17200 and 34CrAIMo5 as per DIN 17211) are chosen for many of the parts which have good machinability. In case of castings, grey cast iron is selected.

1.5.4. COST: Since the raw material cost plays a significant role in the overall cost of the machine tool, it becomes as important factor to be considered.

1.5.5. AVAILABILITY: The chosen material must be easily available so that the cost and delivery time are kept low. In fact, all the raw materials required for machine tools are easily available in India.

1.5.6. MATERIALS FOR CUTTING TOOLS: One of the main qualities that a cutting tool must possess is that it retains it's hardness at high temperatures generated during the cutting process. The most common cutting tool materials used in CNC application or HSS sintered carbides.

II. CANNED CYCLES

A canned cycle (fixed cycle) defines a series of machining sequences for drilling, boring, tapping.

The canned cycles G81 to G89 are stored as subroutines L81 to L89.

The user may deviate from a standard fixed cycle and redefine it to suit his specific machine or tooling requirements. The parameters R00 to R11 are used by subroutines to define the variable values necessary to correctly execute a fixed cycle prior to a subroutine call; all necessary parameters must be defined in the main program.

A fixed cycle call is initiated with G80 to G89. G81 to G89 are fixed cycles that are cancelled with G80. A boring cycle can be called with L81 to L89, however, L81 to L89 are not model. L81-L89 is performed only once in the block in

which it is (notable tungsten carbides), ceramic and polycrystalline diamond. High speed steel is tougher than cemented carbide but not so hard and therefore, cannot be used at such high rate of metal removal, not suitable from higher cutting speeds.

The hardness of the cemented carbide is almost equal to that of diamond. It deserves this hardness from its main constituent, tungsten carbide. In its pure form tungsten carbide is too brittle to be used as a cutting tool. So it is pulverized and mixed with cobalt. The mixture of tungsten carbide and cobalt powder is pressed into the required shape and then sintered. The cobalt metal binds the tungsten carbide gains in to a dense, non-porous structure.

In addition to tungsten carbide, the other metals as titanium and titanium carbides (TIC) are used and by providing tungsten carbide tool with a thin layer of titanium carbide tool, resistance of to wear and useful life are increased up to 5 times. Programmed. At the end of a fixed cycle the tool is re-positioned at the starting point.

II.1 USING CANNED CYCLES IN PROGRAMS

CALL-UP G81 (DRILLING, BORING, CENTERING, BORING AXIS Z)

N8101 G90 S48 F460 LF - Spindle ON
N8102 G00 D01 Z500 LF - Active tool offset
N8103 X100 Y150 LF - First drill position
N8104 G81 R02 360 R03 250 R11 3 LF - Call cycle
N8105 X250 Y300 LF - Second drill position and automatic G81 call
N8110 G80 Z500 LF - Cancelling G81 and returning to Starting plane

CALL-UP WITH L81:

N8101 G90 S48 F460 LF
N8102 G00 D01 Z500 LF
N8103 X100 Y150 LF
N8104 L81 R02 360 R03 250 R11 3 LF – Call up drilling cycle first hole
N8105 X250 Y300 LF
N8106 L81 R02. . . LF – Call- up drilling cycle, second hole
N8107 Z500 LF

As opposed to the call-up with G81, here the drilling cycle must be called up a new at every new drill position

CALL – UP G82 (DRILLING, COUNTER, SINKING)

N8201 … M03 F460 LF
N8202 G00 D01 Z500 L F
N8203 X100 Y150 LF
N8204 G82 R02 360 R03 250 R04 1 R11 3 LF
N8205 X250 Y300 LF
N8206 G80 Z500 LF

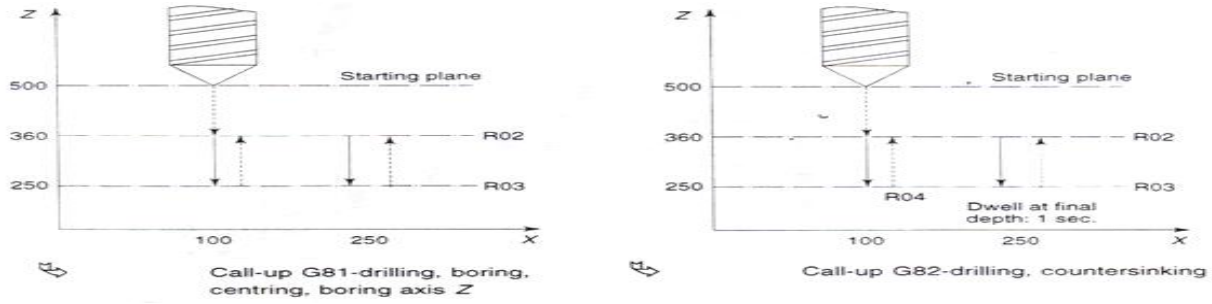

Fig 3

CALL – UP G83 (DEEP HOLE DRILLING)

First drilling depth 50 mm R01 50
Reference plane = retract plane 146 mm R02 146
Final drilling depth 5 mm R03 5
Dwell at starting point 5 s R00 5
Dwell at final depth 1 s R04 1
Degression value 20 mm R05 20
Drilling axis (z) 3 R11 3

N8301 … S48 M03 F460 LF
N8302 G00 D01 Z500 LF
N8303 X100 Y150 LF
N8304 G83 RO1 50 R02 146 R03 5 R00 5
RO4 1 R05 20 R11 3 LF
N8305 X250 Y300 LF
N8306 G80 Z500 LF

At the rapid traverse advance with respect to the new drilling depth, a safety distance of 1mm is kept (on account of the chips still remaining in the hole). With the inch system (G70) the safety distance must be changed accordingly.

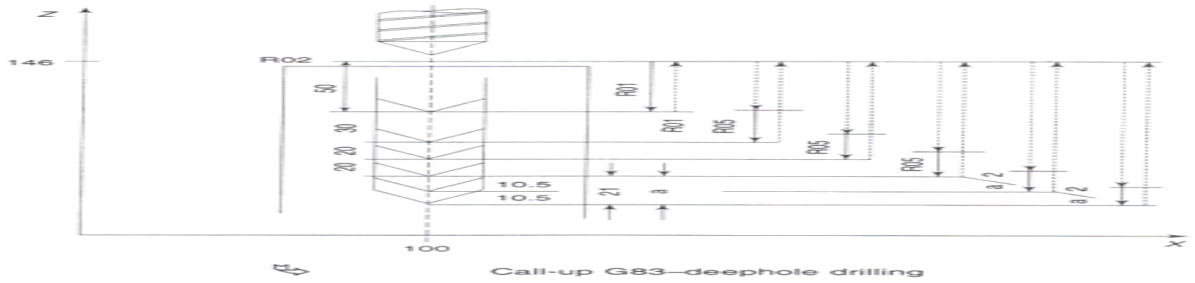

Fig 4

CALL – UP G84 (tapping cycle):-

N8401 . . . S48 M03 F460 LF
N8402 G00 D01 Z500 LF
N8403 X100 Y150 LF
N8404 G84 R02 360 R03 340 R06 04
R07 03 R11 3 LF
N8405 X250 Y300 LF
N8406 G80 Z500 LF

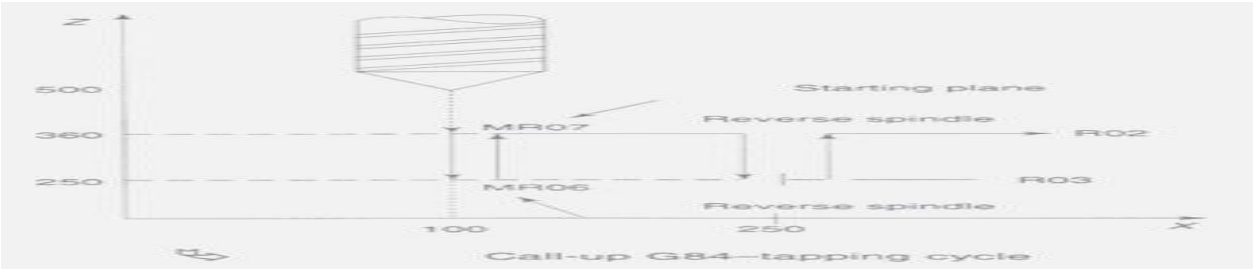

Fig 5

CALL – UP G85 (BORING 1) :

N8501 . . . S48 M03 F460 LF
N8502 D00 D01 Z500 LF
N8503 X100 Y150 LF
N8504 G85 R02 360 R03 250 R10 380 R11 3 LF
N8505 X250 Y300 LF
N8506 G80 Z500 LF

CALL – UP G86 (BORING 2):-

N8601 . . . S48 M03 F460 LF
N8602 G00 D01 Z500 LF
N8603 X100 Y150 LF
N8604 G86 R02 360 R03 250 R07 03
R10 380 R11 3 LF
N8605 X250 Y300 LF
N606 G80 Z500 LF

CALL – UP G87 (BORING 3):

N8701 . . . S48 M03 F460 LF
N8702 G00 D01 Z500 LF
N8703 X100 Y150 LF
N8704 G87 R02 360 R03 250 R07 03 R11 3 LF
N8705 X250 YY300 LF
N8706 G80 Z500 LF

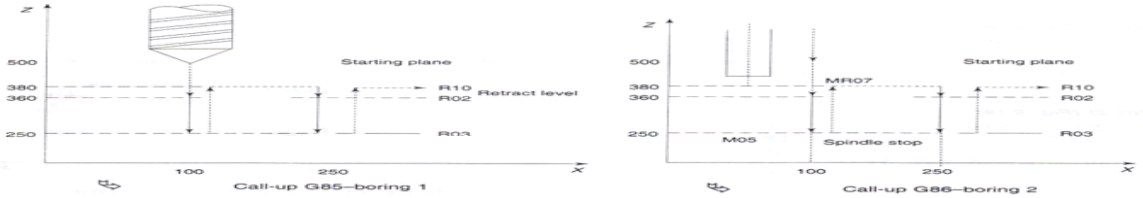

Fig 6

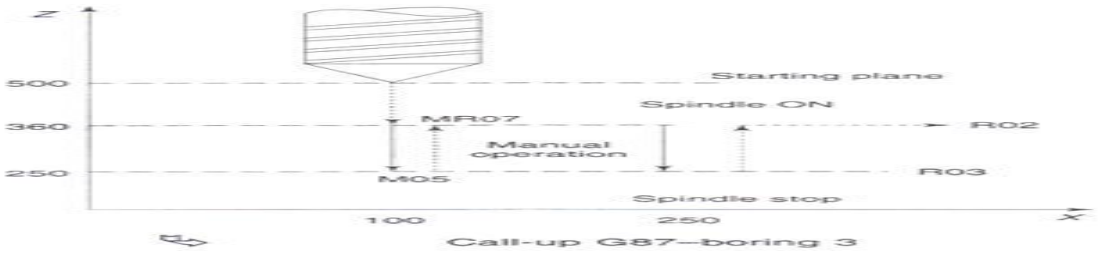

Fig 7

CALL – UP G88 (BORING 4):

```
N8801  . . . . .  S48   MO3    F460          LF
N8802  G00    D01   Z500                    LF
N8803  X100   Y150                          LF
N8804  G88    R02    360   R03 250 R04 1 LF
                R07   03   R11   3
N8805  X250   Y300                          LF
N8806  G80    Z500                          LF
```

CALL-UP G89 (BORING 5):-

```
N8901  . . . .  S48   M03    F460                LF
N8902           G00   D01    Z500                LF
N8903           X100  Y150                       LF
N8904           G89   R02    360  R03  250 R04   LF
                        1    R1103
N8905           X250  Y300                       LF
N8906           G80   Z500                       LF
```

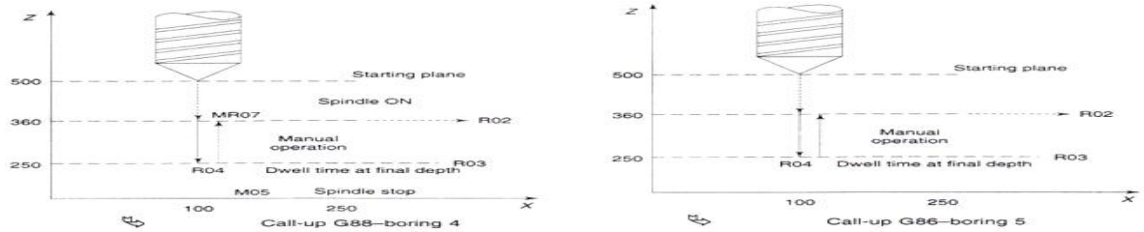

Fig 8

II.2 CALLING BORING CYCLES IN A SUBROUTINES:

If boring cycles are called in a subroutine, the following procedure is necessary:

```
%1R02 360 R03 250 R00 81 R11 3   LF- supply boring cycle parameters
L0101                            LF-boring positions
M30*                             LF
L0101   (Boring positions)
GR00 X1 Y1                       LF-First boring location
X2 Y2                            LF-Second boring location
X5 Y5                            LF-Third boring location
X10                              LF-Fourth boring location
G80 M17                          LF-Deselect boring cycle and end of subroutine
R02 360 R03 250 R00 81 R11 3   LF- supply boring cycle parameters
L0101                            LF-boring positions
M30*                             LF
L0101   (Boring positions)
GR00 X1 Y1                       LF-First boring location
X2 Y2                            LF-Second boring location
X5 Y5                            LF-Third boring location
X10                              LF-Fourth boring location
G80 M17                          LF-Deselect boring cycle and end of subroutine
```

II.3 POLAR COORDINATES G10/G11/G12/G13: Drawing dimensioned with an angle and radius can be entered directly in the program with the aid of the polar coordinates.

The following preparatory functions are available for Programming with coordinates:-

G10 Linear interpolation, rapid traverse

G11 Linear interpolation, federate (F)

G12 Circular interpolation, clockwise

G13 Circular interpolation, counter clockwise.

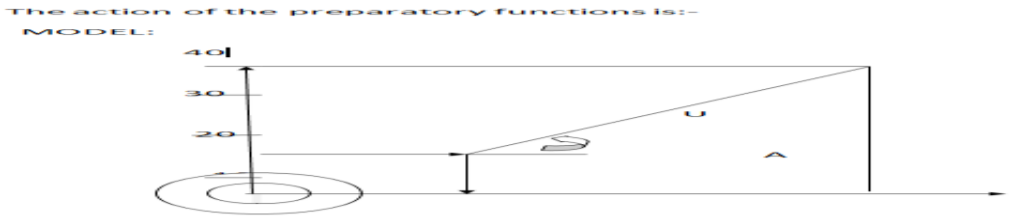

Fig 9

W - Work piece zero
M - Centre point of polar coordinate system
A - Angle
U - Radius

In order to determine the traverse path , the control requires the centre point, the radius and the angle .the centre point is entered with perpendicular coordinates (X,Y,Z) and on initial programming using absolute position data . A subsequent incremental position data input (with G91) always refers to the last centre point programmed.

2.3.1. Polar coordinates g110/g111: The functions G110 and G111 are used to adopt a new centre point or zero point when programming polar coordinates.
Using the new centre point, the angles are again taken from the horizontal and the radius is calculated from the new centre point. G110 and G111 have the following meanings.
G110 Adopt the set point reached as the new centre point
G111 Centre point programming with angle and radius without axis movement
(Example: setting the arc centre of a hole circle)
The following traversing movement must be programmed using G110
Ex: polar coordinates G110
Z385
(G110 polar coordinates) Lf
N05 G90 G 10 X0 Y0 U0 F1000 Lf
N10 G11 U30 A45 Lf
N15 G11 U20 A30 Lf
N20 M30 Lf

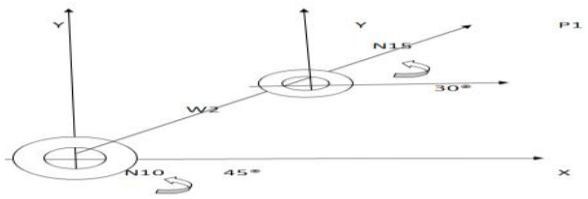

Fig 10

Feed rate F, G94/G95/G98
The federate F is programmed in mm/min or mm/rev
G94 F federate in mm/min
G95 F federate in mm/rev (is assigned to the leading spindle)
G98 F federate in rev/min (for rotary axes only)

II.3.2.Thread cutting G33/G34/G35: Threads can be cut both on drilling or boring and milling machines with a boring tool or a facing tool. These are various types of thread which can be cut as follows:

i. Threads with a constant lead
ii. Threads with a variable lead
iii. Single or multiple threads
iv. External or internal threads

The following preparatory functions are available for machining threads;

G33 threads cutting with constant lead
G34 thread cutting with linear lead increases
G35 thread cutting linear lead decreases

Fig 11.TOP SLIDE SECTIONAL VIEWS SET UP -1

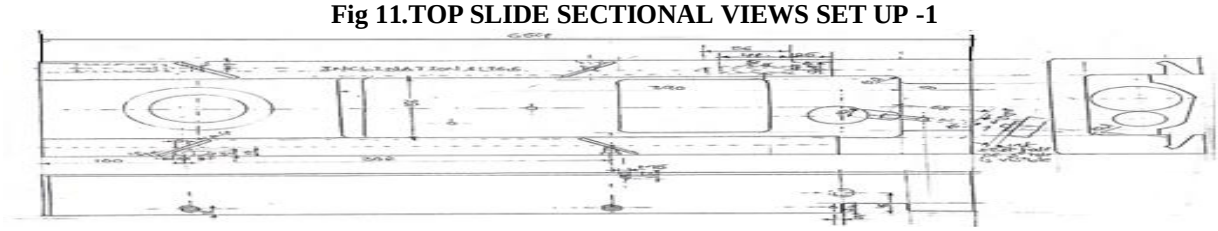

SCALE 1:3

FIG 12. Cross section of top slide for setup-1

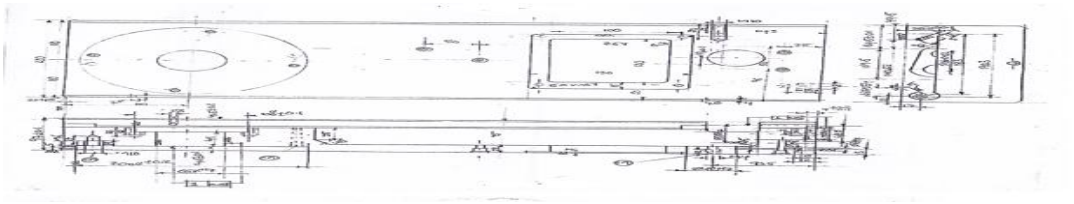

Fig 13. Cross section of top slide for setup-II

TOOL	DIAMETER
BW drill	60
Boring bar	64.5
BW drill	38
Boring bar	21.8
Inserted type end mill	25
Three lip end mill	12
Boring bar(Finishing)	65
Boring bar(finishing)	22
Shoulder milling cutter	63

III.1. MACHINE SPECIFICATIONS

VMC 1200
SOFTWARE SIEMENS
AXIS MOVEMENT 3
TOOLPOST CARRYING CAPACITY 24
X-AXIS 1200 MM
Y-AXIS 600 MM
Z-AXIS 600 MM
GUIDEWAYS T-SLOT BED
SPEED MAXIMUM 600 R.P.M
SPEED MINIMUM 50 R.P.M
FEED RATE 10 TO 250 MM/MIN

III.2. PART PROGRAM:

III.2.1 SETUP – I:

N5 L90; ……. [DIA60 CORE DRILL]
N10 T1
N15 M06
N20 G54 S200 M3 F30 D1
N25 G0 X0 Y0
N40 CYCLE 82 (150, 0, 2, -90, 1)
N50 MCALL
N55 M0
N60 L90: ….. [DIA64.5 SIF B. BAR]
N65 T2
N70 M06
N75 G54 S300 F30 D1
N80 G0 X0 Y0
N95 CYCLE 86 [DIA 38 BW DRL]
N105 MCALL
N110 M0
N115 N90; …. [DIA38 BW DRL]
N120 T3
N125 M06
N130 G54 S350 M03 F35 D1
N135 G0 X453.5 Y18.5
N150 CYCLE82 (150, 0, 2, -28, , 1)
N160 MCALL
N170 L90; …. [DIA 41.5 SIF B.BAR]
N175 T4
N180 M06
N185 G54 S400 M03 F30 D1
N190 G0 X453.5 Y1895
N205 CYCLE 86 (200, 0, 2, -28, , 2, 3, , ,)
N205 MCALL

```
N215  M0
N220  M0
N225  L90; …. [DIA 63  S/MILL]
N230  T5
N235  M06
N240  G54  S350  M03  F150  D1
N245  G0  X0  Y0
N250  R20 = 27  R21 = 3  R22 = 14.7
N255  MS1: G0  Z = -R20
N260  G01  X-50
N265  G02  X-50  Y0  I50  J0
N270  G01  X-67.5
N275  G02  X-67.5  Y0  I67.5  J0
N280  G01  X0  Y0
N285  IF  R20 == R22  GOTOF  MS2
N290  R20 = R20+R21
N295  G0T0B  MS1
N300  MS2  GO  Z200
N305  M0
N310  L90; ….[DIA25 END MILL]
N315  T6
N320  M06
N325  G54  S800  M03  F100  D1
N330  TRANS  X348  Y0
N335  GO  X-25  Y0
N340  Z-3.5
N345  G01  X-52.5
N350  Y67.5
N355  X52.5
N360  Y-67.5
N365  X-52.5
N370  Y0
N375  X-25
N380  TRANS  X0  Y0
N385  G0  Z200
N390  M0
N395  L90; ….[DIA12 END MILL]
N400  T7
N405  M06
N410  G54  S1000  M03  F100  D1
N415  GO  X-40  Y0
N425  Z-3.5
N430  G01  X-59
N435  Y74
N440  X59
N445  Y-74
N450  X-59
N455  Y0
N460  X-40
N465  TRANS  X0  Y0
N470  G0  Z200
N475  M0
N480  L90; ……[SPOT]
N485  T8
N490  M06
N495  G54  S1000  M03  F100  D1
N500  G0  X509  Y-19
N515  MCALL  CYCLE  82 (10, 0, 2, - 3.5, , 1)
N525  X509  Y-19
N530  Y31
N535  X242  Y0
N540  X192  Y31
N545  MCALL
N550  G0  Z200
N555  M0
N560  L90; …..[DIA200  SIF  BORE]
N565  T9
N570  M06
N575  G54  S100  M03  F10  D1
N580  G0  X0  Y0
N595  CCYCLE86 (200, 0, 2, -15, , 2, 3, , , , )
N605  MCALL
N610  M0
N615  L90; …… [DIA 42 H7]
N620  T10
N625  M06
N630  G54  S400  M03  F30  D1
N635  G0  X0  Y0
N650  CYCLE86 (150, -12, 2, -85, , 2, 3, , ,)
N660  MCALL
N665  M0
N670  L90; …… [DIA 42H7]
N675  T11
N680  M06
N685  G54  S600  M03  F30  D1
N690  G0  X453.5  Y18.95
N705  CYCLE86 (150, 0, 2, -28, , 2, 3, , , ,)
N715  MCALL
N720  M0
N725  L90; …. [DIA 100  SIM]
N730  T12
N735  M06
N740  G54  S300  M03  F200  D1
N745  G0  X-175  Y70
N750  Z0
N755  G01  X610
N760  G0  Y0
N765  G01  X-175
N770  G0  Y-70
N775  G01  X610
N780  G0  Z200
N785  M30
= = eof = =
```

III.2.2.SETUP - II

```
N5  L90; …..[DIA 63  S/M]
T5
M06
N10  G54  S400  M03  F200  D1
G0  X-55  Y202
Z-1
G01  X570
Y28
X-10
Y-40
N15  G0  X700  Y130
Z0
G01  X560
G0  Z250
M0
N16  L90; …..[SPOT]
T8
M06
N20  G54  S1000  M03  F50  D1
G0  X100  Y17
```

```
MCALL  CYCLE  82 (10, 0, 2, -3.5, , 0)
X100  Y17
X402
Y213
X100
MCALL
G0  Z200
M0
N30  L90; …..[OIL  GROVING]
T14
M06
N40  G54  S1000  M03  F100  D1
G111  X100  Y17
RP = 17.5  AP = 225  F = 100
G0  Z0
G01  Z-17
G111  X100  Y17
AP = 45  RP = 29
G0  Z2
G111  X402  Y17
RP = 17.55  AP = 315
G01  Z-1.7
G111  X402  Y17
RP = 29  AP = 13.5
G0  Z2
G111  X402  Y213
RP = 17.5  AP = 45
G01  Z-1.7
G111  X402  Y213
AP = 225  RP = 22.5
G0  Z2
G111  X100  Y213
RP = 17.5  AP = 135
G01  Z-1.7
G111  X100  Y213
AP = 315  RP = 29
G0  Z300
M0
N50  L90; ……..[DIA 63  S/MILL]
T5
M06
N60  S400  M03  F200  D1
G0  X-35  Y155.22
R20 = 4.4  R21 = 3  R22 = 25.4
MS1: G0  Z = -R20
G01  X0
X558  Y162.52
X563
G0  Y100
G01  Y74
X-35
G0  Y155.22
IF  R 20 == R22  GOTOF  MS2
R20 = R20 + R21
GOTOB  MS1
MS2: GO  Z100
N70  GO  X-40  Y115
Z-20
G01  X260
GO  Z-25.4
G01  X-45
G0  Z-25
N70  TRANS  X110  Y115
G0  X0  Y0
R20 = =29.4  R21 = 4  R22 = 41.4
PR1: G0  Z = -R20
G01  X17.5
G02  X17.5  Y0  I-17.5  J0
G01  X0  Y0
IF  R20 ==R22  G0T0F  PR2
R20 == R20 + R21
GOTOB  PR1
PR2: TRANS  X0  Y0
G0  Z200
M0
N70  L90; …..[50  DOVETAIL]
T15
M06
N80  G54  S80  M03  F50  D1
R20 = 74  R21 = 2  R22 = 66
XY:  X-45  Y = R20
Z-25.5
G01  X562
Y90
G0  X550
Z80
IF R20 == R22  G0TOF  XY2
R20 = R20-R21
GOTOB  XY1
XY2: M0
N90  X65.5
Z-25.5
G01  X562
Y90
G0  X550
Z80
N100  R20 = 5  R21 = 2  R22 = 63
X21: TRANS  Y = R20
G0  X-45  Y144.72
Z-25.5
G01  X0
X558  Y152.005
X562
TRANS  Y0
Y150
G0  X550
Z80
IF  R20 ==R22  GOTOF  XZ2
R20 = R20+R21
GOTOB  XZ1
MZ 2:  M0
N110  TRANS  X0  Y0
G0  X-55  Y115
Z-25.5
G01  X260
G0  Z300
M30
N90  L90; …[DIA 100  S/F]
T16
M06
N90  G54  S200  M03  F30  D1
G0  X110  Y115
CYCLE 86 (150, -24, 2, -41.5,  , 2, 3,  ,  ,  ,  ,  )
MCALL
M0
N100  L90
```

```
T17
M06
N110  S600  M03  F150  D1
G0  X574  Y-20
R20 = 8  R21 = 8  R22 = 32
JK 1: G0  Z= -R20
G01  Y70
N800  G01  Y701
N805  G0  Z10
N810  Y-20
N815  IF  R20 == R22  G0T0F  JK2
N820  R20 = R20 + R21
N825  G0T0B  JK1
N830  JK2:  G0  Z10
N835  G0  X574  Y12
N840  Z32
N845  G01  X674
N850  G0  Y40
N855  G01  X574
N860  G0  Z300
N865  Y400
N870  M0
N875  G0  X574  Y250
N880  R20 = 8  R21 = 8  R22 = 32
N885  JH1:  Z = -R20
N890  G01  Y175
N895  G0  Z10
N900  Y250
N905  IF  R20 == R22  G0T0F  JH2
N910  R20 = R20 + R21
N915  GOTOB  JH1
N920  JH2: G0  Z10
N925  G0  X574  Y250
N930  Z-32
N935  G01  Y218
N940  X674
N945  G0  Y188
N950  G01  X580
N955  G0  X200
N960  M30
= =eof = =
```

IV. MACHINIG TIME

IV.1 INTRODUCTION

Machining process converts raw material into useful finished product, surface finishing is needed to the foundry castings certain amount of material is added as a machining allowance for this purpose the size of the casting should be slightly over size than the dimensions shown on the finished drawings the machining operations generally performed on vertical machining center are:

- Drilling
- Boring
- Shaping
- Grinding
- Reaming
- Milling etc.

IV.2 PURPOSE OF ESTIMATING MACHINING TIME:

Estimation of machining time for different processes is required for the following processes:

To estimate the manufacturing time
To fix the delivery dates
To determine the cost of labour charges
To find out the cost of manufacturing different parts

IV.3 MACHINING TIME

Estimation of machining time means calculation of time required to finish the given component according to the drawings supplied after giving number of allowances in addition to the actual time taken for machining operations certain amount of extra time is given to the workers. They are:

- Setup time
- Handling inspection of jobs
- Team down time
- Fatigue allowance
- Tool changing allowance
- Measurement checking allowance
- Other allowances for cleaning
- Getting stock etc.

There for total machining time is the actual time for machining and all the time allowances as given above.
To calculate actual machining time the basic general formula used is

Machining time = length of cut / (feed × rpm)

IV.4 CUTTING SPEED:

The cutting speed of a cutting tool may be defined as the speed at which the cutting edge passes over the material. Cutting speed is generally expressed in m/min.

An estimator should consider the following while selecting a suitable cutting speed.

Low cutting speeds are required for hand materials.

- High speed steel cutting tools content high speeds and can bide tipped tools cut still higher speeds.
- If the depth of cut and feed is more/less cutting speed may be taken and vice-versa

- Cutting speeds can be increased by using good cutting fluids and coolants.
- The amount of stock removed in inversely proportional to the cutting speeds when stock is removed at high speeds.
- If the cutting speed increases the heat generated also increases and tool life decreases.

Cutting speed is given by the formula:

$S = (\pi DN) / 1000$ meters/min

IV.5. MACHINING TIME FOR CARBIDE TOOLS:

4.5.1. SETUP – I:

For DIA60mm core drill,

Cutting speed (s) $=\pi$ DN/1000= (1000 × 45)/(π ×60)= 200 rpm

Feed rate (F) = feed/tooth × no. of teeth × Rpm = 0.1 × 2 × 200 F = 30 mm/min

M/C time (or) operating time = length/feed= 92/30

Time = 4 min

For DIA 64.5 S/F B. BAR

Operating time = length/feed = 92/30 T = 4 min

For DIA 38 between DRL

C/s $=\pi dn/1000$

N = (45 × 1000) / (π ×38) N = 350 rpm (spindle speed)

Feed = 0.1× 1×350 = 35 mm/min

Operating time = 30/35 (length/feed) T = 1 min

For DIA 41.5 S/F B. BAR

C/s = $\pi dn/1000$

N = (1000 × 45) / (π × 41.5) = 300 rpm

F = 0.1 × 1 × 300= 30 mm/min

Operating time = length / feed= 30/30 = 1 min

For DIA 63 S/MILL S/s = 350 rpm [R = 67.5min]

Feed = 150 mm/min [no. of passes = 5]

Operating time = 2πR × no. of passes / feed= 2π×67.5×5/150= 15 min

For DIA 25 END MILL s/s = 800 rpm

Feed = 100 mm/min

Operating time = length/feed= 480/100 T = 5 min

For DIA 12 END MILL S/s = 1000 rpm

Feed = 100 mm/min

Operating time = length / feed= 532 /100 T = 6 min

For DIA 200 S/F BORE s/s = 100 rpm

Feed = 10 mm/min

Operating time = length /feed = 17 /10= 2 min

For DIA 42 H_7 S/S = 400 rpm

Feed = 30 mm/min

Operating time = length / feed= (87+30)/30 T = 4 min

For DIA 100 S/M S/s = 300 rpm

Feed = 200 mm/min

Operating time = length/feed= 1850/200 T = 10 min

TOTAL OPERATING TIME FOR SETUP – 1

= 4+4+1+1+15+15+6+2+4+10 T = 52 min

8.5.2.SETUP-II

For DIA 63 S/M S/s = 400 rpm

Feed = 200 mm/min

Operating time = length / feed= 1218 /200 T = 7 min

For spot

T = 5.5/50 = 1 min

For oil grooving

Feed = 100 mm/min

Time = length / feed= [(29 + 17.5)/100] × 4= 2 min

For 63 s/m

F = 200 mm/min

Operating time = length/feed= (length × no. of passes) / feed

= [(558×2 + 162×2)/200] × 8 T = 58 min

Total length = 2πR × no. of passes= 2π × 17.5 × 4

Time = (2π × 17.5 × 4)/200= 3 min

For 50 DOVETAIL S/s = 80 rpm

Feed = 50 mm/min

Operating time = (total length × no. of passes)/feed= [(607+90-74)×5]/50 T = 62 min

Operating time = [603+ (152.005-144.72)×4]/50 T = 49 min

Operating time = (260+55+155)/50 T = 8 min

For DIA 100 S/F S/s = 200 rpm

Feed = 30 mm/min

T = 43.5/30=2 min

No. of passes = 4

Total time = (574+70+20)*4/150= 17 min

IF $R_{20} == R_{22}$, S/s= 600 rpm

F= 150 mm/min

Total time = (total length × no. of passes)/feed= [((674+250)×2)/150]×4= 49 min

TOTAL OPERATING TIME FOR SETUP-II

= 7+1+2+58+3+3+62+49+8+2+17+9+49 T = 270 min

Total operating time for both setup-I & II = 270+52 = 322 min

IV.6. MACHINING TIME FOR HARDEND TOOLS

If the cutting tool is H.S.S/HARDEND cutting speed = 15 m/sec

4.6.1.SETUP-I

For DIA 60 core drill

C/s = πDN/1000

N = (1000×15) / (π×60)

N = 50 rpm

Feed = (feed/tooth)× no. of teeth's× rpm=0.1×2×50

F = 10 mm/min

Operating time = length / feed= 92/10 = 10 min

For DIA 64.5 S/F B. BAR s/s = 50 rpm

F = 10 mm/min

Operating time = length/feed = 92/10= 10 min

For DIA 38 BW DRL

C/s = πDN/1000 N = (1000×15)/ (π×38)= 120 rpm

Feed = 0.1×1×120= 12 mm/min

Operating time = 30/12= 3 min

For DIA 41.5 S/F BAR

C/S = πDN/1000N = (1000×15)/ (π×41.5)= 100 rpm

F = 0.1×1×100= 10 mm/min

Operating time = length/feed= 30/10 =3 min

For DIA 63 S/MILL

Spindle speed = 120 rpm

Feed = 50 mm/min

Operating time = (2πR× no. of passes)/feed= (2π×67.5×5)/50= 42 min

For DIA 25 END MILL

Spindle speed = 300 rpm

Feed = 30 mm/min

Operating time = length/feed= 480/30= 16 min

For DIA 12 END MILL

Spindle speed = 350 rpm

Feed = 35 mm/min

Operating time = 532/35 = 16 min
For DIA 200 S/F BORE
Spindle speed = 30 rpm
Feed = 5 mm/min
Operating time = length/feed= 17/5 = 4 min
For DIA 42 H_7.
Spindle speed = 150 rpm
Feed = 15 mm/min
Operating time = (87+30)/15 = 8 min
For DIA 100 S/M
Spindle speed = 100 rpm
Feed = 50 mm/min
Operating time = length/feed= 1850/50 = 37 min
Total operating time for setup –I
= 10+10+3+3+42+16+5+4+8+37= 154 min

IV.6.2 SET UP-II:

For DIA 63 s/m
Spindle speed = 150 rpm
Feed = 50 mm/min
Operating time = length/feed= 1218/50= 25 min
For spot
T= 5.5/20= 1 min
For oil grooving
Feed = 30 mm/min
Time = length/feed= [(29+17.5)/30]×4= 8 min
For 63 S/M F= 50 mm/min
Operating time = (length×no. of passes)/feed= (558×2+162×2)8/60= 230 min
Total length = 2πR ×no. of passes= 2π×17.5×4
Time = (2π×17.5×4)/80= 7 min
No. of passes = 4
Total time = (570+70+20)×4/40=67 min
Spindle speed = 200 rpm
Feed = 50 mm/min
Total time = [(674+250)×2 ×4]50= 147 min
Total time for setup-II= 25+1+8+230+7+160+145+22+5+67+147= 817 min
Total time for both setups I & II = 148+817= 965 min
Total machining time for carbide tools = 322 min
Total machining time for hardened tools = 965 min
By observing the carbide & hardened tools
The machining time for hardened tools is 3 times greater than the carbide tools

IV.7. COST ANALYSIS:

Given
M/c hour rate = Rs.800
For carbide tools total manufacturing cost for 4 pieces = (322×800×40)/60= Rs.17, 173
For Hardened tools total manufacturing cost for 4 pieces = (965×800×4)/60= Rs.51, 466
By using carbide tools, we saved Rs.34, 293 for 4 pieces.

IV. CONCLUSION

The 'TOP SLIDE' of horizontal lathe was machined successfully in two set ups on vertical set ups on vertical machining centre (VTC). It has been realised that CNC programming technique is so powerfull,that components of intricate profile and tight dimensional tolerance are machined with the sophisticated machine tool like VTC Machining of such components give way to a compact and revolutionary changes in industrial product. Concept of interchagibility is being felt verymuch .thus,maintance becomes very simple and economical.

It is also seen that numerically controlled machines because of their high initial cost and high machining hour rate are used mainly for highly intricate components requiring high degree of accuracy .It has been observed that the machining time for carbide tools is less as compared to hardened tools.

REFERENCES

[1]. NC MACHINES- By S.J. MARTIN,peace publishers Moscow 1965
[2]. NC MACHINES- By YOREM KOREM,industrial press new delhi,1993
[3]. MECHATRONICS- By TATA McGraw HILL pvt limited,new delhi
[4]. CAD/CAM- By ISHRAT M. MIRZANA radient publishers,2008

International Journal of Modern Engineering Research (IJMER)
www.ijmer.com Vol. 3, Issue. 4, July-august. 2013 pp-2262-2266 ISSN: 2249-6645

Fabrication and Characterization of PPS /40%GF/nano-$CaCo_3$ Hybrid Composites

Y.Haribabu[1], K. Ajay sir[2], B. ravikiran[3]
*(Mechanical department, M.V.G.R college of engineering, JNTU, INDIA)
** (Mechanical department, M.V.G.R college of engineering, JNTU, INDIA)
*** (Mechanical department, T.P.I.S.T college of engineering, JNTU, INDIA)

ABSTRACT: *In the present work fabrication of composite material(PPS+40%GF+NANO $CaCO_3$) was carried out and their tensile properties viz tensile strength, tensile strain(%),young's modulus, energy at maximum load and brinell hardness number were found and surface morphology of tensile fracture was analyzed by using SEM and EDS. Specimens of Polyphenylene sulfide (PPS)/Glass Fiber(GF) hybrid composites are prepared with four different compositions of nano-calcium carbonate($CaCO_3$), viz., 0,3,5 and 7%.Each specimen consisting of 40%GF.The specimens are fabricated by using micro-compounder with micro injection molding machine. Tests are conducted on these specimens to determine the tensile strength, tensile strain, young's modulus energy at maximum load and hardness number at room temperature using universal testing machine and Brinell hardness testing machine. The influence of the nano-$CaCO_3$ content on the mechanical properties tensile of hybrid composites was studied. Surface morphology of tensile fracture of the hybrid composites is analyzed by using Scanning electron Microscope (SEM).Point chemical analysis of the hybrid composites is analyzed by Energy Dispersive Spectrum (EDS).Thus it gives the various inorganic elements present at a particular location. It is found that the reinforcing and toughening effects of the PPS/GF hybrid composites are increased by adding nano-$CaCO_3$.The tensile strength, tensile strain, young's modulus and energy at max load of these composites increased nonlinearly with the addition of the nano-$CaCO_3$.*

Keywords: hybrid composites, PPS, GF Nano-$CaCo_3$, Tensile properties, hardness test, SEM, EDS

I. INTRDUCTION

Polyphenylene sulphide (PPS) composites are widely used especially in automotive main parts due to their easy process ability most automotive parts (especially the outer parts, like sun-roof, etc.) would either be exposed to natural weathering or to more extreme environments. It is an engineering thermoplastics, It possesses high temperature resistance, excellent electrical and mechanical properties.PPS has been widely used in corrosion resistant coating, mechanical parts, electric and electronic apparatus. PPS has a glass transition temperature of 80–90^{o}C and melting temperature of 280^{0}C. PPS has good dimensional stability, high strength, high modulus, chemical and fatigue resistance, and can be metal substitute engineering plastic. In electronics, PPS is typically found in connectors, plug boards, coil formers, relays, switches and chip carriers. Glass fiber is a material consisting of numerous extremely fine fibers of glass. Glassmakers throughout history have experimented with glass fibers, but mass manufacture of glass fiber was only made possible with the invention of finer machine tooling. Various researchers have investigated the effect of nano-inclusions on various polymers and also discussed the properties of Polyphenylene sulfide and other polymers. The influence of adding Nano-inclusions,to the polymers are studied. The comprehension of technical papers is given. Liang et al.[1] studied the how the mechanical properties such as tensile modulus, yield strength, and impact strength effect by add of the glass beads to polypropylene matrix. Impact strength of this composite has enhanced by 1.4 times of the unfilled polypropylene. Impact tests of notched specimens were also conduct at room temperature according to the ASTM D256.Morphology studies are also done by using SEM of unfilled polypropylene cross-section. Yang et al.[2] discussed application Poly (1,4-phenylene-sulfide) PPS is a special kind of engineering plastic with heat resistance, high mechanical strength, excellent chemical resistance, good electronic properties and good radiation resistance so widely used in many areas, especially in electronics, mechanical engineering ,chemical and petroleum industry and food industry. At present most PPS products are reinforced composites and polymer alloys like Ryton-PPS is a 40%Glass fiber reinforced composites Yanga et al.[3] studied The effect of surface treatment of glass beads with a silane coupling agent and the filler content on the notched IZOD Impact properties of the filled polypropylene (PP) composites has been investigated .It was found that the impact fracture energy of the composites increased with increasing the volume of the glass blends(wt%).The influence of surface treatment of the glass blends on was insignificant. Zhaobin et al.[4]The mechanical and tribological properties of carbon fiber (CF) reinforced polyamide 66 (PA66)/Polyphenylene sulfide (PPS) blend composite were studied in this. It was found that CF reinforcement greatly increases the mechanical properties of PA66/PPS blend. Impact strength(KJ/m^2) are observed as decreasing and increasing phenomenon.

II . EXPERIMENTAL ANALYSIS

Raw material: Polyphenylene sulphide with 40%GF was supplied by RK polymers, Mumbai, India. The melting temperature and density of PPS with 40%GF are 285^{0}C and 1600kg/m^3 respectively. The Nano-$CaCO_3$ was produced by Anyuan technical Industrial Co .Ltd, Jiangxi, and China. Mean diameter and density of the nano-particles are 80nm and 2500kg/m^3 respectively.

Preparation of test specimens: PPS with 40%GF are pre-dried for 3hours at 110-120^{0}C and nano-$CaCO_3$ particles pre-dried for 2hours at 80^{0}C in vacuum oven. The nano-$CaCO_3$ particles are mixed with the PPS and the glass fibre according to designated blending ratios .In this work ,the weight fraction of the glass fibre fixed as 40% and the weight fraction of the nano-$CaCO_3$ are 3%,5% and 7% and then the PPS/GF/nano-$CaCO_3$ blends are extruded in micro-compounder. These specimens are prepared as per the ASTMD638 STANDARD by Injection molding the specifications of specimens are 132x20x3.2mm^3

.

Fig: Tensile specimen As per ASTM D638

Instrument and Methodology: The tensile properties of PPS/GF/Nano-$CaCO_3$ hybrid composites are measured at room temperature by means of universal testing machine with extensometer (INSTRON, 3382) .Tests were conducted according to ASTM D638 standard with cross-head descending speed of 2mm/min. The various properties are found from the experiment are tensile strength, tensile elongation at break point, young's modulus energy at maximum load. The mean values of polymer nano composites have been noted. The hardness test of the PPS /GF/nano-$CaCO_3$ Ternary composites were measured at room temperature by means of a Brinell hardness testing machine. Hardness test is conducted according to ASTM E 10. All Brinell tests use a carbide ball indenter.

Fig: Tensile test specimen dies as per ASTM D638

Fig: Universal testing machine (UTM)

III. RESULTS AND DISCUSSION

This table shows the mean values of max load, tensile strength, tensile strain, young's modulus and energy at maximum load at different specimen labels.

S.NO	Specimen label s	Mean value Maximum Load (N)	Mean Tensile strength (MPa)	Mean Tensile strain at Break (%)	Mean value of Youngs Modulus (MPa)	Mean value of Energy at Maximum Load (J)
1	PPS+40%GF+0%NC	5904.058	134.287	3.8264	4091.106	10.90365
2	PPS+40%GF+3%NC	5629.149	146.087	4.0406	5666.22	12.43635
3	PPS+40%GF+5%NC	5789.238	145.1254	3.9386	4572.67	12.03635
4	PPS+40%GF+7%NC	5629.218	145.687	3.8664	4572.67	11.77555

1. Tensile strength: Fig 1.1 shows the dependence of the tensile strength of the PPS/ GF/ nano-$CaCO_3$ composites on the weight fraction of nano-$CaCO_3$ ($Ø_f$) particles. The value of tensile strength increased with the increase of addition of weight fraction of nano-$CaCO_3$ particles to the matrix PPS/40%GF.The graph varies non-linearly from base composite to the PPS/40%/7%nano-$CaCO_3$ Hybrid composite .The maximum increase of tensile strength observed when the addition of 3% of nano-$CaCO_3$ particles to matrix this increase observed as 8 compared to the base composite i.e. PPS/40%GF/nano-$CaCO_3$.

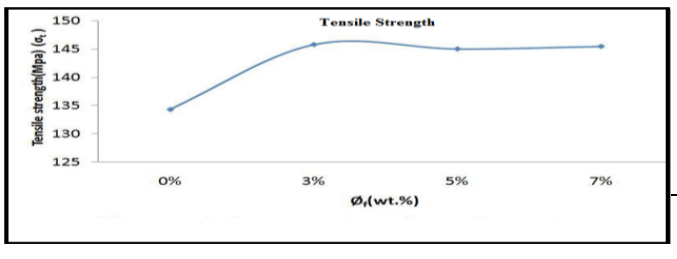

Fig 1.1: Effect of weight fraction of Nano-$CaCO_3$ ($Ø_f$) on tensile strength (σ_t)

2. Tensile strain: Fig 1.2 shows the dependence of the tensile strain of the PPS/GF/ Nano-$CaCO_3$ composites on the weight fraction of Nano-$CaCO_3$ particles.It can be seen that tensile strain increased non linearly with the addition of weight fraction of nano- $CaCO_3$.It means that the tensile strain of the PPS/GF binary composite materials filled with the increasing nano-$CaCO_3$ concentration will be enhanced effectively. The Max increase of the tensile strain ($€_t$) is observed at $Ø_f$ =3% is 5.59% as compared to the weight fraction of nano-$CaCO_3$ at $Ø_f$ = 0%.

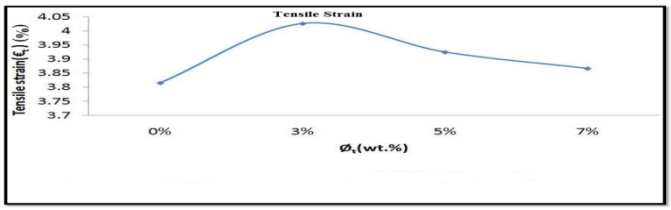

Fig 1.2: Effect of weight fraction of Nano-$CaCO_3$ ($Ø_f$) on Tensile Strain ($€_t$)

3. Young's modulus: Young's modulus is one major parameter for characterizing the tensile fracture toughness of materials.Fig 1.3 shows the effect of the weight fraction of the distribution of the particles in the matrix and the interfacial morphology between them are improved better. Consequently, the tensile fracture toughness of the PPS/GF/nano-$CaCO_3$ hybrid composite was enhanced correspondingly. The maximum increase of the young's modulus (E_t) at $Ø_f$ =3% is 11.77% as compared to the weight fraction of nano-$CaCO_3$ at 0%.Here the young's modulus (E_t) increased non linearly up to $Ø_f$ =3% , with the addition of wt. fraction of nano-$CaCO_3$ particles then decreases up to $Ø_f$ =5% then slightly decreases up to $Ø_f$ =7%.

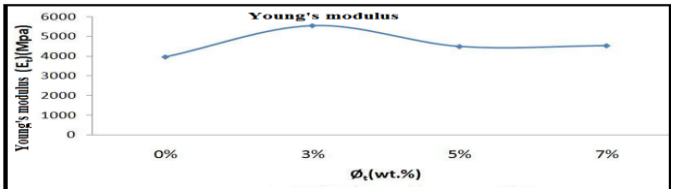

Fig 1.3: Effect of weight fraction of Nano-$CaCO_3$ ($Ø_f$) on young's modulus (E_t)

4. Energy at Maximum Load: Fig 1.4 shows the dependence of the energy at maximum load of the PPS/GF/ Nano-$CaCO_3$ composites on the weight fraction of Nano-$CaCO_3$ particles. It can be seen that the maximum increase of energy at maximum load(σ_E) is observed at $Ø_f$ =3% is3.24% compared to the weight fraction of nano-$CaCO_3$ at 0%. Here the energy at maximum load (σ_E) increased nonlinearly up to $Ø_f$ =3%, with the addition of wt. fraction of nano-$CaCO_3$ particles then gradually decreases up to $Ø_f$ =7%.

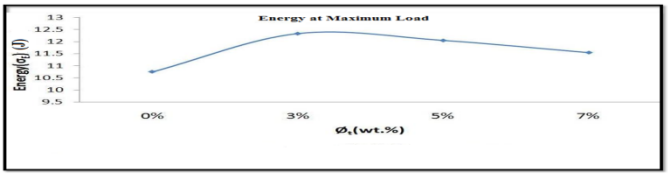

Fig:1.4 Effect of weight fraction of Nano-$CaCO_3$ ($Ø_f$) on Energy(σ_E)

5. Hardness test results: Hardness is extensively used to characterize materials and to determine if they are suitable for their intended use. The most common uses for hardness tests is to verify the heat treatment of a part and to determine if a material has the properties necessary for its intended use.It can be seen that the maximum increase of hardness number is observed at $Ø_f$ =5% is3.14% compared to the weight fraction of nano-$CaCO_3$ at 0%. Here the hardness number increased up to $Ø_f$ =5%. With the addition of wt. fraction of nano-$CaCO_3$ particles then gradually decreases at $Ø_f$ =7%.

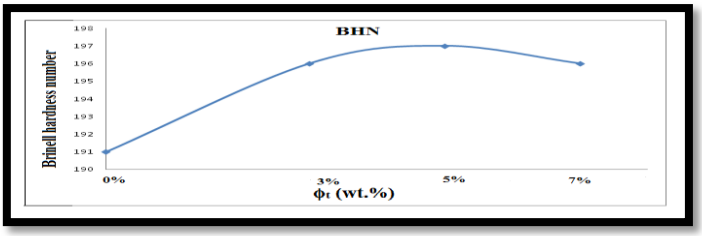

Fig.4.9 Effect of weight fraction of Nano-$CaCO_3$ ($Ø_f$) on Brinell hardness number (BHN)

IV. SURFACE MORPHOLOGY BY USING SCANNING ELECTRON MICROSCOPE (SEM)

1. SEM (scanning electron microscope): SEM photo graphs shows facture due to tensile load .These are shows surface morphology of the of polymer nano composites. I.e. how the nano particles distributed with increase of %wt. blending with PPS with 40%GF. And also seen, with an increasing loading of nano-$CaCO_3$, the nano particles could not be evenly distributed and form agglomerates. The SEM photo graphs can be shown as follows from figures 4.10 through 4.13.

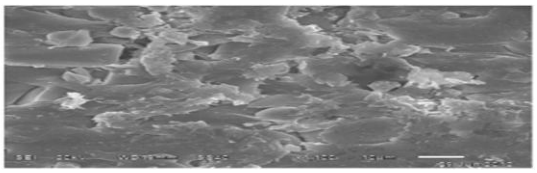

Fig 4.10 SEM: PPS/40%GF/0% nano-$CaCO_3$

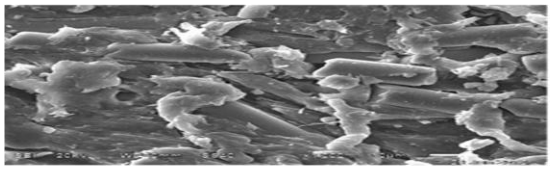

Fig 4.11 SEM: PPS/40%GF/3% nano-$CaCO_3$

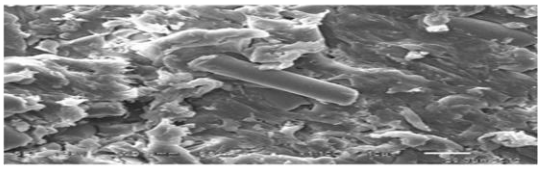

Fig 4.12 SEM: PPS/40%GF/5% nano-$CaCO_3$

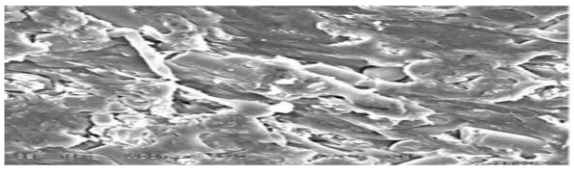

Fig 4.13 SEM: PPS/40%GF/7% nano-$CaCO_3$

2. Energy dispersive spectrum (EDS): This gives the chemical analysis of the composite materials and it also gives the various inorganic particles at a particular point in a composite material. The results of the EDS for Polymer nano composite material at various percentages of Nano-$CaCo_3$ Can be shown as follows from figures 4.14 through 4.17 and % of inorganic elements can also be in tables from 4.14 through 4.17 for each percentage of nano polymer composite .

Fig4.14 EDS: PPS/40%GF/0% nano-$CaCO_3$

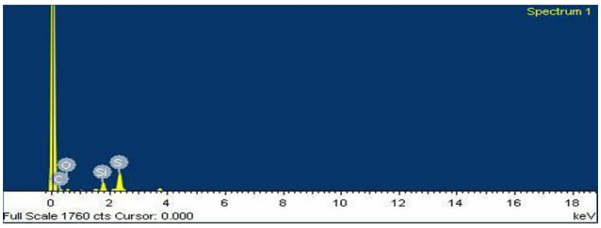

Fig4.15 EDS: PPS/40%GF/3% nano-$CaCO_3$

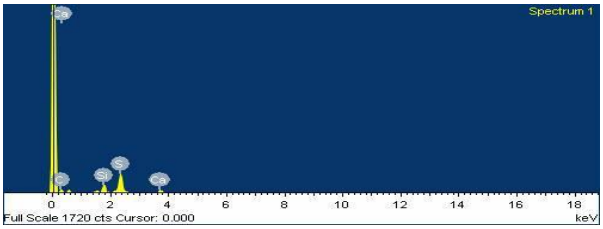

Fig4.16 EDS : PPS/40%GF/5% nano-$CaCO_3$

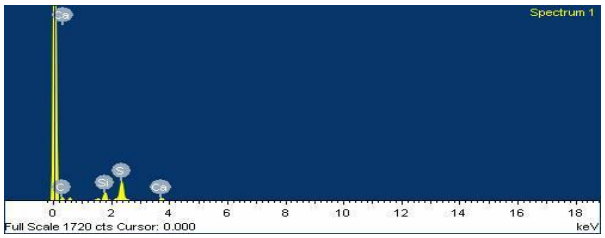

Fig4.17 EDS : PPS/40%GF/7% nano-$CaCO_3$

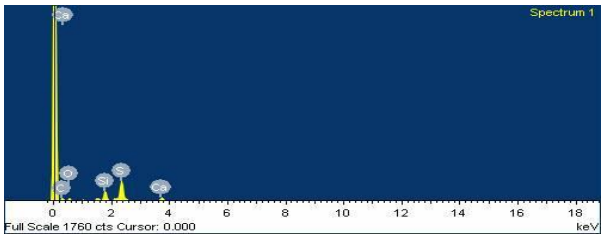

V. CONCLUSIONS

The following conclusions are dragged from the experimental investigations

[1] Reinforcing and toughening effects were found on PPS/GF/ nano-$CaCO_3$ composite materials.

[2] It was found that when the weight fraction of the nano particles was equal to 3%, the tensile strength and young's modulus and tensile strain were increased non linearly with the weight fraction of nano-$CaCO_3$ ($Ø_f$).

[3] The maximum increase of tensile strength observed when the addition of 3% of nano-$CaCO_3$ particles to matrix this increase observed as 8.78% compared to the base composite i.e., PPS/40%GF/nano-$CaCO_3$.

[4] The maximum increase of the tensile strain ($€_t$) is observed at $Ø_f$ =3% is 5.59% compared to the weight fraction of nano-$CaCo_3$ at $Ø_f$ = 0%.

[5] The maximum increase of the Young's Modulus (E_t) at $Ø_f$ =3% is 11.77% compared with the weight fraction of nano-$CaCO_3$ at 0%.Here the Young's Modulus (E_t) has been increased non linearly up to $Ø_f$ =3% with the addition of weight fraction of nano-$CaCO_3$ particles then decreases up to $Ø_f$ =5% then slightly decreases up to $Ø_f$ =7%.

[6] The energy at maximum load (σ_E) is increased non linearly up to $Ø_f$=3%, with the addition of weight fraction of nano-$CaCO_3$ particles then gradually decreases up to $Ø_f$ =7%

[7] It can be seen that the maximum increase of hardness number is observed at $Ø_f$ =5% is3.14% compared to the weight fraction of nano-$CaCO_3$ at 0%. Here the hardness number increased up to $Ø_f$ =5%, with the addition of wt. fraction of nano-$CaCO_3$ particles then gradually decreases at $Ø_f$ =7%.

[8] The mechanical properties of tensile strength, tensile strain and young's modulus at 3% and hardness at 5% showed that there was a good interfacial adhesion between the nano-$CaCO_3$ and the PPS matrix.

[9] SEM shows the surface morphology of the specimens with increase of load distribution of nano particles is un-even distributed and then agglomerated.

[10] From Energy Dispersive spectrum (EDS) it was found various inorganic elements present at a particular location in the specimen.

VI. ACHNOLOGEMENTS

I would like to tank for CIPET, Bhubaneswar, for providing fabrication and experimental facilities.

REFERENCES

[1]. Liang. and Li., "Mechanical Properties and Morphology of Glass Bead-Filled Polypropylene Composites, polymer composites*" polymer composites,Vol.19 No. 6 December 1998*.

[2]. Ji-Zhao Lianga, Lia., "Brittle-ductile transition in polypropylene filled with glass blends" *Elsevier polymer PP-3191-3195,1998.*

[3]. Kong Yang, Chaoyuan Wang, Jie Wei,"A study on biocomposite of nano apatite/poly(1,4-phenylene-sulfide)-poly (2,4-phenylene sulfide acid) *science direct Composites: Part B 38,PP-306-310, 1st November 2006.*

[4]. Zhaobin Chen, Xujun Liu, Renguo Lu , Tongsheng Li,"Friction and Wear Mechanisms of PA66/PPS blend reinforced with Carbon Fiber " *Wiley Inter Science, DOI 10.1002/app.25999, 28thMarch 2007.*

[5]. Shimpi, Verma and Mishra, "Dispersion of nano $CaCO_3$ on PVC and its Influence on Mechanical and Thermal propetie*" Journal of Composite Materials 2010 vol.44: 211 17th August 2009.*

[6]. Shimpi, Verma and Mishra, "Dispersion of nano $CaCO_3$ on PVC and its Influence on Mechanical and Thermal propetie" *Journal of Composite Materials 2010 vol.44: 211 17th August 2009.*

[7]. Dan Lu, Shiwei Pan, "Effects of Ball Milling Dispersion of Nano-SiOx Particles on Impact Strength and Crystallization Behavior of nano-SiOx–poly(phenylene sulfide) Nano composites" *Wiley InterScience,DOI 10.1002/pen.20547,2006.*

[8]. Knor,Walter,Haupert,"Mechanical and Thermal Properties of Nano-Titanium Dioxide-Reinforced Polyetheretherketone Produced by Optimized Twin Screw Extrusion" *Journal of Thermoplastic Composite Materials 2011 vol.24: 185 ,2010.*

[9]. Rajendra Kumar Goyal and Amol Kadam, "Polyphenylene sulphide/graphite composites for EMI shielding applications" *VBRI press Adv. Mat. Lett. 2010, 1(2), PP-143-147, 27 July 2010*.

[10]. Hanim, Ahmad Fuad, Zarina, Mohd Ishak and Azman Hassa, "Properties and Structure of Polypropylene/ Polyethylene-Octene elastomer/nano $CaCO_3$ Composites*" Journal of Thermoplastic Composite Materials vol.21: 123,2008.*

[11]. Qiyang, Limin, Guangxin and You "Preparation and Characterization of Acrylic/Nano-TiO2 Composite Latex High Performance Polymers *"High Performance Polymers vol.14: 383,2002.*

International Journal of Modern Engineering Research (IJMER)
www.ijmer.com Vol. 3, Issue. 4, July-august. 2013 pp-2266-2270 ISSN: 2249-6645

Designing and Characterization of koggestone, Sparse Kogge stone, Spanning tree and Brentkung Adders

V.Krishna Kumari [(1)], Y.Sri Chakrapani[(2)]
[(1)]M.Tech, Department of Electronics & Communication Engineering
[(2)]Associate Professor Department of Electronics & Communication Engineering
[(1)(2)]Gudlavalleru Engineering college, Gudlavalleru.

ABSTRACT: *Adders are known to be the frequently used ones in VLSI designs. In digital design we have half adder and full adder, by using these adders we can implement ripple carry adder(RCA). RCA is used to perform any number of additions. In this RCA is serial adder and it has propagation delay problem. With increase in ha & fa circuits, delay also increases simultaneously. That's the reason these parallel adders (parallel prefix adders) are preferred. The parallel prefix adders are KS adder(kogge-stone),SKS adder(sparse kogge-stone),Spanning tree and Brentkung adderS. These adders are designed and compared by using area and delay constraints. Simulation and synthesis by model sim6.4b, Xilinx ise10.1i.*

I. INTRODUCTION

In Processors (DSP) and microprocessor data path units, adder is an important element. As such, extensive research continues to be focused on improving the power-delay performance of the adder. In VLSI implementations, parallel-prefix adders are known to have the best performance. Reconfigurable logic such as Field Programmable Gate Arrays (FPGAs) has been gaining in popularity in recent years because it offers improved performance in terms of speed and power over DSP-based and microprocessor-based solutions for many practical designs involving mobile DSP and telecommunications applications and a significant reduction in development time and cost over Application Specific Integrated Circuit (ASIC) designs. The power advantage is especially important with the growing popularity of mobile and portable electronics, which make extensive use of DSP functions. However, because of the structure of the configurable logic and routing resources in FPGAs, parallel-prefix adders will have a different performance than VLSI implementations. In particular, most modern FPGAs employ a fast-carry chain which optimizes the carry path for the simple Ripple Carry Adder (RCA).

In this paper, the practical issues involved in designing and implementing tree-based adders on FPGAs. This work was supported in part by NSF LSAMP and UT-System STARS awards. The FPGA ISE synthesis software was supplied by the Xilinx University program described. An efficient testing strategy for evaluating the performance of these adders is discussed. Several tree- based adder structures are implemented and characterized on a FPGA and compared with the Ripple Carry Adder (RCA) and the Carry Skip Adder (CSA). Finally, some conclusions and suggestions for improving FPGA designs to enable better tree-based adder performance are given.

II. CARRY-TREE ADDER DESIGNS

Parallel-prefix adders, also known as carry-tree adders, pre-compute the propagate and generate signals. These signals are variously combined using the fundamental carry operator (fco) .

$(g_L, p_L) \circ (g_R, p_R) = (g_L + p_L \bullet g_R, p_L \bullet p_R)$ (1)

Due to associative property of the fco, these operators can be combined in different ways to form various adder structures. For, example the four-bit carry-look ahead generator is given by:

$c_4 = (g_4, p_4) \circ [(g_3, p_3) \circ [(g_2, p_2) \circ (g_1, p_1)]]$ (2)

A simple rearrangement of the order of operations allows parallel operation, resulting in a more efficient tree structure for this four bit example:

$c_4 = [(g_4, p_4) \circ (g_3, p_3)] \circ [(g_2, p_2) \circ (g_1, p_1)]$ (3)

It is readily apparent that a key advantage of the tree-structured adder is that the critical path due to the carry delay is on the order of $log_2 N$ for an N-bit wide adder. The arrangement of the prefix network gives rise to various families of adders. For a discussion of the various carry-tree structures. For this study, the focus is on the Kogge-Stone adder [4], known for having minimal logic depth and fanout (see Fig 1(a)). Here we designate BC as the black cell which generates the ordered pair in equation (1); the gray cell (GC) generates the left signal only, following. The interconnect area is known to be high, but for an FPGA with large routing overhead to begin with, this is not as important as in a VLSI implementation. The regularity of the Kogge Stone prefix network has built in redundancy which has implications for fault-tolerant designs. The sparse Kogge-Stone adder, shown in Fig 1(b), is also studied. This hybrid design completes the summation process with a 4 bit RCA allowing the carry prefix network to be simplified.

(a)

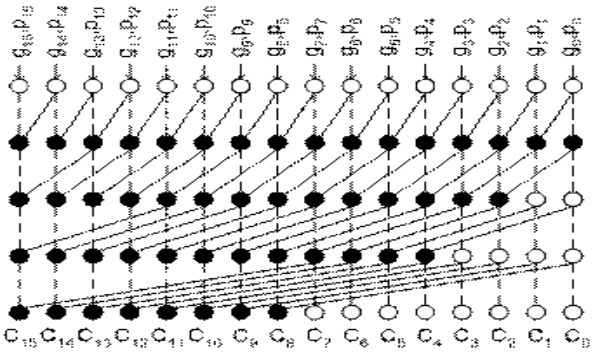

(b)

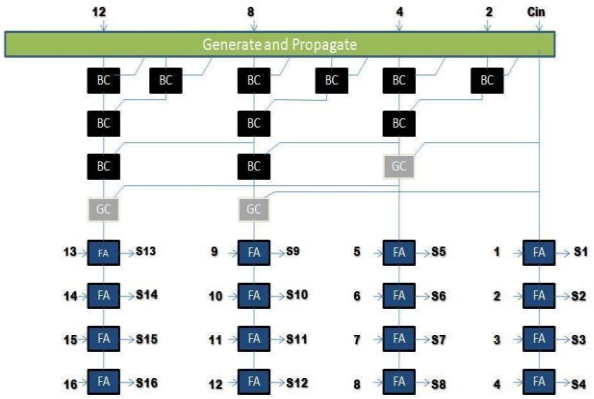

Fig. 1. (a) 16 bit Kogge-Stone adder and (b) sparse 16-bit Kogge-Stone adder

Another carry-tree adder known as the spanning tree and Brent kung carry-look ahead (CLA) adders are examined . Like the sparse Kogge-Stone adder, this design terminates with a 4-bit RCA. As the FPGA uses a fast carry-chain for the RCA, it is interesting to compare the performance of this adder with the sparse Kogge -Stone and regular Kogge-Stone adders. Also of interest for the spanning-tree CLA is its testability features .

(a)

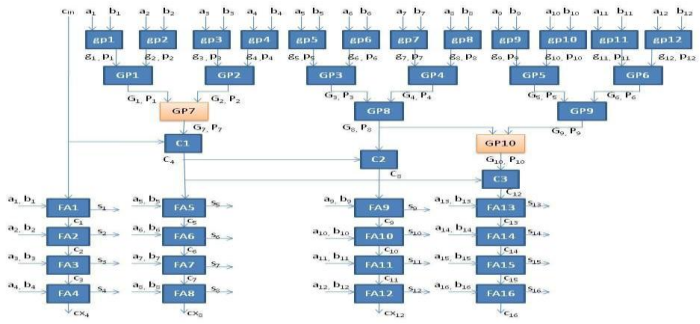

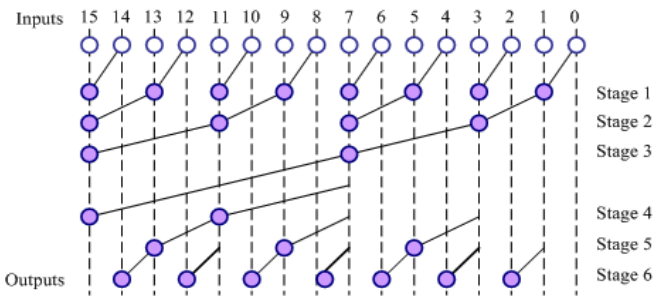

(b)

Fig. 2. (a)Spanning Tree Carry Look ahead Adder (16 bit) (b) 16 bit Brent kung adder.

III. RELATED WORK

The ripple carry adder with the carry-lookahead, carry-skip, and carry-select adders on the Xilinx 4000 series FPGAs. Only an optimized form of the carry-skip adder performed better than the ripple carry adder when the adder operands were above 56 bits. A study of adders implemented on the Xilinx Virtex II yielded similar results. In the authors considered several parallel prefix adders implemented on a Xilinx Virtex 5 FPGA. It is found that the simple RCA adder is superior to the parallel prefix designs because the RCA can take advantage of the fast carry chain on the FPGA.

This study focuses on carry-tree adders implemented on a Xilinx Spartan 3E FPGA. The distinctive contributions of this paper are two-fold. First, we consider tree-based adders and a hybrid form which combines a tree structure with a ripple-carry design. The Kogge-Stone adder is chosen as a representative of the former type and the sparse Kogge-Stone and spanning tree adder are representative of the latter category. Second, this paper considers the practical issues involved in testing the adders and provides actual measurement data to compare with simulation results. The previous works cited above all rely upon the synthesis reports from the FPGA place and route software for their results. In addition to being able to compare the simulation data with measured data using a high-speed logic analyzer, our results present a different perspective in terms of both results and types of adders .

The adders to be studied were designed with varied bit widths up to 128 bits and coded in VHDL. The functionality of the designs were verified via simulation with ModelSim 6.4b. The Xilinx ISE 10.1 software was used to synthesize the designs onto the Spartan 3E FPGA. In order to effectively test for the critical delay, two steps were taken. First, a memory block (labeled as ROM in the figure below) was instantiated on the FPGA using the Core Generator to allow arbitrary patterns of inputs to be applied to the adder design. A multiplexer at each adder output selects whether or not to include the adder in the measured results, as shown in Fig. 3. A switch on the FPGA board was wired to the select pin of the multiplexers. This allows measurements to be made to subtract out the delay due to the memory, the multiplexers, and interconnect (both external cabling and internal routing.

IV. IMPLEMENTATION

Xing and Yu noted that delay models and cost analysis for designs developed for VLSI technology do not map Second, the parallel prefix network was analyzed to directly to FPGA designs. They compared the design of determine if a specific pattern could be used to extract the worst case delay. Considering the structure of the Generate-Propagate (GP) blocks (i.e., the BC and GC cells), we were able to develop the following scheme, by considering the following subset of input values to the GP blocks.

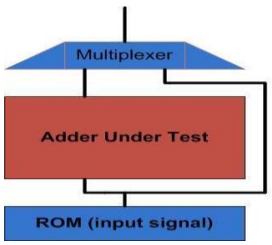

Fig. 3. Circuit used to test the adders adder

If we arbitrarily assign the (g, p) ordered pairs the values (1, 0) = True and (0, 1) = False, then the table is self-contained and forms an OR truth table. Furthermore, if both inputs to the GP block are False, then the output is False; conversely, if both inputs are True, then the output is True. Hence, an input pattern that alternates between generating the (g, p) pairs of (1, 0) and (0, 1) will force its GP pair block to alternate states.

Likewise, it is easily seen that the GP blocks being fed by its predecessors will also alternate states. Therefore, this scheme will ensure that a worse case delay will be generated in the parallel prefix network since every block will be active. In order to ensure this scheme works, the parallel prefix adders were synthesized with the “Keep Hierarchy” design setting turned on (otherwise, the FPGA compiler attempts to reorganize the logic assigned to each LUT). With this option turned on, it ensures that each GP block is mapped to one LUT, preserving the basic parallel prefix structure, and ensuring that this test strategy is effective for determining the critical delay. The designs were also synthesized for speed rather than area optimization.

The adders were tested with a Tektronix TLA7012 Logic Analyzer. The logic analyzer is equipped with the 7BB4 module that provides a timing resolution of 20 ps under the MagniVu setting. This allows direct measurement of the adder delays. The Spartan 3E development board is equipped with a soft touch-landing pad which allows low capacitance connection directly to the logic analyzer. The test setup is depicted in the figure below.

V. SIMULATION AND SYNTHESIS REPORT

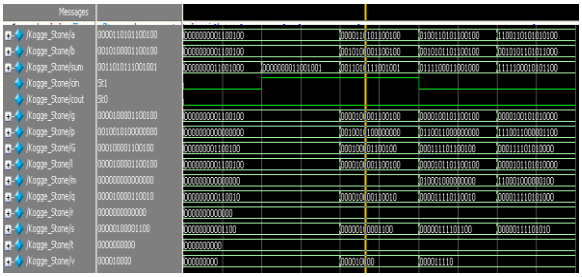

(a)

Device Utilization Summary			
Logic Utilization	**Used**	**Available**	**Utilization**
Number of 4 input LUTs	37	9,312	1%
Logic Distribution			
Number of occupied Slices	24	4,656	1%
Number of Slices containing only related logic	24	24	100%
Number of Slices containing unrelated logic	0	24	0%
Total Number of 4 input LUTs	37	9,312	1%
Number of bonded IOBs	50	232	21%

(b)

Fig.4:(a)Kogge stone simulated wave form (b) KS device utilization.

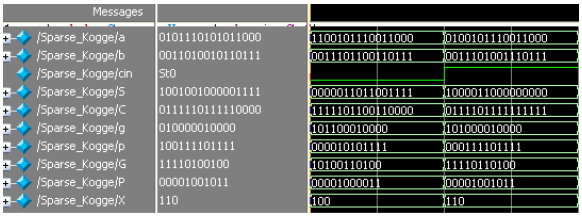

(a)

Device Utilization Summary			
Logic Utilization	**Used**	**Available**	**Utilization**
Number of 4 input LUTs	51	9,312	1%
Logic Distribution			
Number of occupied Slices	30	4,656	1%
Number of Slices containing only related logic	30	30	100%
Number of Slices containing unrelated logic	0	30	0%
Total Number of 4 input LUTs	51	9,312	1%
Number of bonded IOBs	65	232	28%

(b)

Fig.5:(a)Sparse kogge stone simulated wave form (b) SKS device utilization.

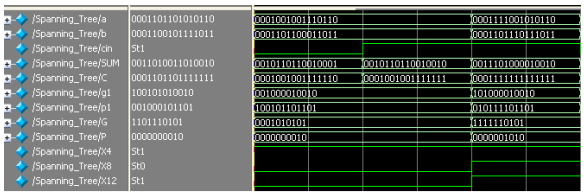

(a)

Device Utilization Summary			
Logic Utilization	**Used**	**Available**	**Utilization**
Number of 4 input LUTs	32	9,312	1%
Logic Distribution			
Number of occupied Slices	24	4,656	1%
Number of Slices containing only related logic	24	24	100%
Number of Slices containing unrelated logic	0	24	0%
Total Number of 4 input LUTs	32	9,312	1%
Number of bonded IOBs	65	232	28%

(b)

Fig.6:(a)Spanning tree simulated wave form (b) Spanning tree device utilization.

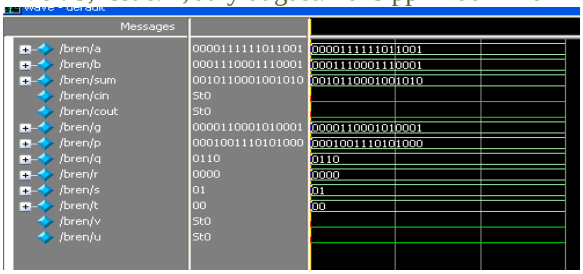

(a)

Device Utilization Summary (estimated values)			
Logic Utilization	Used	Available	Utilization
Number of Slices	24	4656	0%
Number of 4 input LUTs	43	9312	0%
Number of bonded IOBs	49	232	21%

(b)

Fig.7:(a) Brent kung simulated wave form (b) Brent kung device utilization

REFERENCE

[1]. K. Vitoroulis and A. J. Al-Khalili, "Performance of Parallel Prefix Adders Implemented with FPGA technology," *IEEE Northeast Workshop on Circuits and Systems*, pp. 498-501, Aug. 2007.
[2]. D. Gizopoulos, M. Psarakis, A. Paschalis, and Y. Zorian, "Easily Testable Cellular Carry Lookahead Adders," *Journal of Electronic Testing: Theory and Applications 19*, 285-298, 2003.
[3]. S. Xing and W. W. H. Yu, "FPGA Adders: Performance Evaluation and Optimal Design," *IEEE Design & Test of Computers*, vol. 15, no. 1, pp. 24-29, Jan. 1998.
[4]. M. Bečvář and P. Štukjunger, "Fixed-Point Arithmetic in FPGA," *Acta Polytechnica*, vol. 45, no. 2, pp. 67-72, 2005.
[5]. P. M. Kogge and H. S. Stone, "A Parallel Algorithm for the Efficient Solution of a General Class of Recurrence Equations," *IEEE Trans. on Computers*, Vol. C-22, No 8, August 1973.
[6]. P. Ndai, S. Lu, D. Somesekhar, and K. Roy, "Fine-Grained Redundancy in Adders," *Int. Symp. on Quality Electronic Design*, pp. 317-321, March 2007.
[7]. T. Lynch and E. E. Swartzlander, "A Spanning Tree Carry Lookahead Adder," *IEEE Trans. on Computers*, vol. 41, no. 8, pp. 931-939, Aug. 1992.
[8]. N. H. E. Weste and D. Harris, *CMOS VLSI Design*, 4th edition, Pearson–Addison-Wesley, 2011.
[9]. R. P. Brent and H. T. Kung, "A regular layout for parallel adders," *IEEE Trans. Comput.*, vol. C-31, pp. 260-264, 1982.
[10]. D. Harris, "A Taxonomy of Parallel Prefix Networks," in *Proc. 37th Asilomar Conf. Signals Systems and Computers*, pp. 2213–7, 2003.

International Journal of Modern Engineering Research (IJMER)
www.ijmer.com Vol. 3, Issue. 4, Jul - Aug. 2013 pp-2271-2274 ISSN: 2249-6645

Effect of artificial roughness on Thermal and Thermohydraulic efficiency in Rectangular Duct of a Double pass solar Air Heater by using transverse ribs on the absorber plate

Sudhanshu Dogra
Assistant Professor, Mechanical Engineering Dept., Lovely Professional University, Punjab, India

ABSTRACT: *This paper represents the effect of artificial roughness on the absorber plate in the form of transverse ribs of a double pass solar air heater. An experimental study has been carried out to see the effect of transverse ribs(α=90°) attached on both sides to the absorber plate of a Double pass solar air heater on the Thermal and Thermohydraulic efficiency in a rectangular Duct. The aspect ratio of the Duct (W/H) is 10. The range of Reynolds number varies from 4900 to 12000. The relative roughness pitch (p/e) is between 5-20 and fixed relative roughness height (e/Dh) 0.044 and fixed angle of attack (α) 90°. It has been observed that the maximum thermal and thermohydraulic efficiency of transverse ribs comes at relative roughness pitch (p/e) of 10.*

KEYWORDS: *Absorber Plate, Double pass solar air heater, Thermal efficiency, Thermohydraulic efficiency, Nusselt Number, Reynolds number.*

I. INTRODUCTION

Solar air heater is the simplest device which is used to convert the solar energy into heat energy. In solar air heater heat generated by solar energy is collected over a collector and that heat is then taken away by the fluid flowing i.e. air in the duct of solar air heater. The heat carried away by air is then used for various purposes and in many applications such as crop drying, space heating [1].

The efficiency of solar air heater is low due to low convective heat transfer between the absorber plate and the fluid flowing inside the duct. So to increase the thermal efficiency of solar air heater many investigators put forth their views.

Several methods have been used by various investigators to increase efficiency. Some of these are Use of artificial roughness on absorber plate, use of fins, electro hydrodynamic method, packed bed etc. Out of these the easiest and most acceptable method to enhance the thermal and thermo hydraulic efficiency is the creation of artificial roughness on the absorber plate of solar air heater.

Dhiman et al. [2] performed an analytical study to predict the thermal performance of a novel parallel flow packed bed solar air heater. They found that parallel flow solar air heater with packed bed material give a higher heat flux as compared to the conventional non-porous bed double flow system. Momin et al. [3] carried out an experimental investigation to show the effect of geometrical parameters of V-shaped ribs on heat transfer and fluid flow characteristics of rectangular duct of a solar air heater. They observed that using V- shaped ribs maximum heat transfer occurred at relative roughness height of 0.034 and at an angle of attack of 60°.

El-Sebaii et al. [4] carried out an experimental as well as analytical study for the thermal performance of a double pass flat and V-corrugated plate solar air heater. They found that double pass V-corrugated plate solar air heater is more efficient than double pass flat plate solar air heater by 11-14% and the maximum value of the thermo hydraulic efficiency of V as well as flat plate solar air heater occur at mass flow rate 0.02kg/s. Sudhanshu et al. [5] shows the effect of artificial roughness on heat transfer and friction factor characteristics on double pass solar air heater using transverse ribs. They found that by providing the artificial roughness on both sides of the absorber plate the heat transfer and friction factor gets improved with maximum heat transfer and friction factor occur at relative roughness pitch of 10. This study also shows that the Nusselt number increase by 1.06 times as that of the smooth one.

El-khawaja et al. [6] carried out an experimental study to show the thermal performance and the effect of using transverse fins on a double pass solar air heater using wire mesh as an absorber plate. He found that the thermal efficiency increases with the increase in mass flow rate and is highest in 0.042kg/s. Sahu and Bhagoria [7] experimentally studied the thermal performance of a solar air heater and show the variation in the thermal performance by using 90° broken ribs on the absorber plate and found that the thermal performance lie in the range of 51 to 83.5% with 90° broken ribs.

Aldabbagh [8] calculated the thermal performance of a single and double pass solar air heaters with steel wire mesh layer instead of a flat absorber plate and the results indicate that the efficiency increases with increasing the mass flow rate within the range of 0.012 to 0.038kg/s. Efficiency is more for double pass than single pass solar air heater by 34-45% for the same mass flow rate. Prasad and Saini[9] experimentally studied the effect of roughness and flow parameters on heat transfer and friction factor of a solar air heater. They observed that the maximum thermo hydraulic performance is achieved at relative roughness height of 0.033 and relative roughness pitch of 10. They also found that Nusselt number varies 2.38 times and friction factor varies 4.25 times as that of smooth one.

Nephon [10] performed a numerical study on the performance and entropy generation of a double pass solar air heater having longitudinal fins and mathematical model was developed for heat transfer characteristics for the mass flow rate of 0.02-0.1kg/s. He found that the thermal efficiency increases with increase in the number of fins and increase in their height

whereas entropy generation decreases with b the increase in the number of fins and their height. Suppramaniam and Satcunanathan [11] concluded that a simple two glass cover solar air heater can be operated as a two pass solar air heater by passing the air between glass panes before passing it through the blackened area which results in increase in the performance of collector with no further increase in cost.

The aim of this study is to show the effect of using transverse ribs on the absorber plate (upper side and lower side) on heat transfer and friction factor characteristics.

I.1 ARTIFICIAL ROUGHNESS

Thermal performance of solar air heater can be increased by using artificial roughness on the absorber plate to make it rough to increase the heat transfer rate and friction factor characteristics.

Due to this roughness, turbulent boundary layer with small laminar sub-layer is formed on the absorber plate. This laminar sub-layer offer very high resistance to the heat flow. So by breaking this layer to create turbulence the heat transfer rate and friction factor characteristics can be increased which further increases the thermal efficiency and thermo hydraulic performance of a solar air heater [12].

Hence, it is necessary that the turbulence must be created in the vicinity of heat transfer surface i.e. laminar sub layer only where the heat exchange takes place and the flow should not be unduly disturbed so as to avoid excessive friction losses. This can be done by keeping the height of the roughness element to be small in comparison with the duct dimensions. Although there are several parameters that characterize the arrangement and shape of the roughness, the roughness element height (e) and pitch (p) are the most important. These parameters are usually specified in terms of dimensionless parameters, namely, relative roughness height (e/D_h) and the relative roughness pitch (p/e). The roughness elements can be two dimensional ribs or three dimensional discrete elements, transverse or angled ribs or V-shaped continuous or broken ribs.

II. EXPERIMENTAL SET-UP

A Schematic view of double pass solar air heater is shown in fig 1. The rectangular duct of double pass solar air heater consists of two consecutive sections that is entry section and the test section. The size of the entire duct is 2070mm*250mm*25mm. Length of test section is 1600mm and entry length is 400mm. A space of 70mm is to be left out at the end for the movement of air towards upper duct. The entry length is considered on the basis of the American society heating refrigeration and air conditioning engineers (ASHRAE) std [13].

A heating source is provided so that we get required amount of intensity equivalent to that of 900W/m^2 which is equal to the intensity of sun. Halogen lights of 500W each is used as a heating source. These halogen lights are fixed on a flat board at a height of 1m above the duct. The intensity of radiations is measured with the help of pyranometer. A glass sheet of thickness 4mm is placed over the duct to make passage of air to make it double pass and also it makes the intensity comes from halogen lights to get directly falls over the absorber plate.

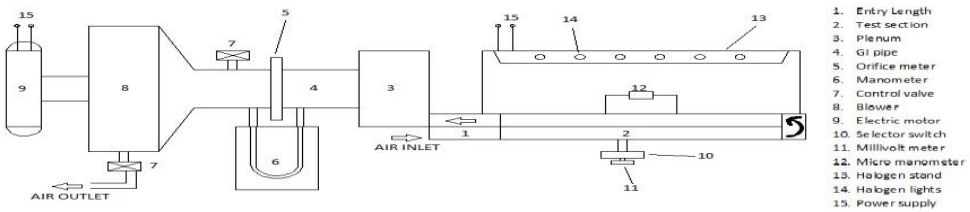

Fig 1. Schematic view of experimental set up

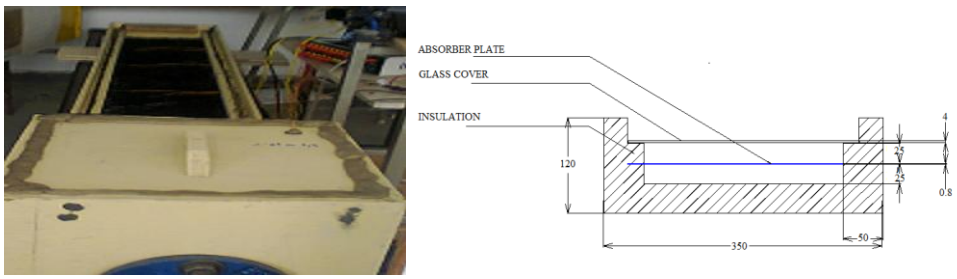

Fig 2. Pictorial and sectional view of Duct

The absorber plate is of galvanized iron (GI) having thickness of 0.8mm. Ribs are attached to the upper and lower side of the absorber plate with the help of glue. The material for ribs is aluminum wires of diameter 2mm. The schematic view of the absorber plate is given in fig 3.

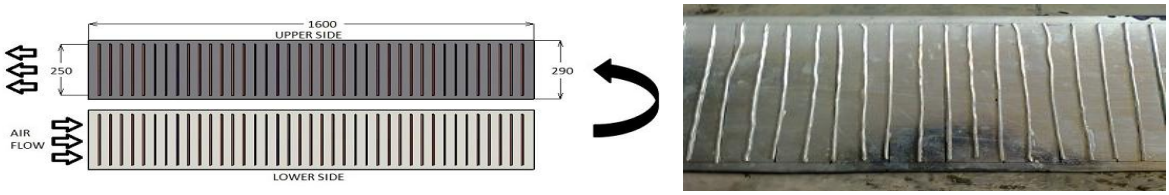

Fig 3. Schematic view of absorber plate

The mass flow rate of air through the duct is measured by means of a calibrated orifice meter which is inserted in the circular pipe and the flow is controlled by means of a control valve provided in blower which is attached to the circular pipe at the end. The copper-constantan thermocouple wire (T-type) was used to measure the air and absorber plate temperature at different locations. The pressure across the test section is measured with the help of micro manometer.

2.1 INSTRUMENTATION

A. Measurement of Air flow

The air flow rate through the duct was measured by using concentric orifice plate with 45° bevelled edges. It was designed, fabricated and fitted in the 80 mm pipe which carries the air from plenum to the blower. The orifice plate was calibrated against Pitot tube and the value of coefficient of discharge (C_d) was determined as 0.612. The pressure drop across the orifice meter was measured by means of a U-tube manometer.

B. Temperature Measurement

For measuring the temperatures of air and absorber plate Calibrated copper-constant (T type), thermocouples were used. Twelve Thermocouples were mounted on the upper side of the absorber plate to measure its mean temperature. For measuring the temperature of air two thermocouples were inserted at inlet and outlet section of the duct.

C. Pressure Drop Measurement

The pressure drop across the test section of the duct was measured with the help of a micro-manometer. It is having a least count of 0.01 mm. The movable reservoir is mounted using a lead screw having a pitch of 1.0 mm with a graduated dial having a 100 division. The meniscus is maintained at a fixed point by moving the reservoir up and down. Then the movement is noted, which gives the pressure difference across the two tapings.

2.2 DATA REDUCTION

The values of all the important parameters like temperature of absorber plate, air inlet and outlet temperature and pressure drop are required to calculate mass flow rate 'm', velocity of air, heat supplied to the air and heat transfer coefficient 'h' were calculated by using the following expressions.

Mass flow rate, $$m = C_d A_o \sqrt{\frac{2\rho(\Delta P_o)}{1-\beta^4}} \quad (1)$$

The heat transfer coefficient,

$$h = \frac{Q_u}{A_p(T_{pm} - T_{fm})} \quad (2)$$

Where heat transfer rate (Q_u) to the air is given by

$$Q_u = mC_p(T_o - T_i) \quad (3)$$

The heat transfer coefficient calculated is then used to determine the Nusselt number as given below;

$$Nu = \frac{hD_h}{k} \quad (4)$$

Where D_h is the hydraulic diameter of the duct.

The Darcy Wiesbach equation is then used to determine the friction factor by measured value of pressure drop $(\Delta P)_d$ across the test section length as below,

$$f = \frac{2(\Delta P)_d D_h}{4\rho L V^2} \quad (5)$$

III. RESULTS AND DISCUSSION

In this section of paper the effect of relative roughness pitch on thermal and thermohydraulic performance is given and discussed. Fig. 4(a) shows the variation of thermal efficiency as a function of Reynolds number for different values of Relative roughness pitch(p/e) 5-20 and fixed value of angle of attack 90° with a fixed value of relative roughness height (e/Dh) 0.044.

Fig. 4(a) shows that the maximum efficiency occurs at relative roughness pitch of (p/e) 10. This is due to the reason that at p/e = 10 maximum number of reattachment points are found and hence thermal efficiency get increased.Hence the maximum thermal efficiency occurs at relative roughness pitch (p/e) of 10.

Also at relative roughness pitch (p/e) of 5 thermal efficiency is more or less same as that of smooth plate, this is due to the reason that as the gap between the ribs is very less at this juncture hence the flow does not get separated and very less or no reattachment points has been formed.

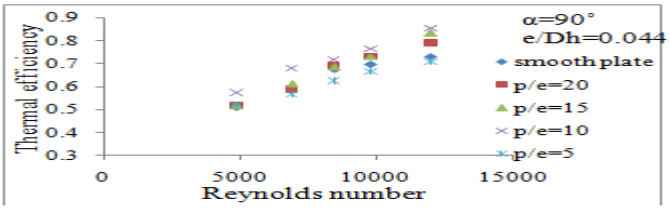

Fig 4(a). Variation of thermal efficiency with the Reynolds number for different values of relative roughness pitch and for fixed value of angle of attack 90° and relative roughness height

Fig 4(b) shows that the variation of thermo hydraulic efficiency as a function of Reynolds number for different values of relative roughness pitch (p/e) 5-20 and for a fixed value of angle of attack 90° with relative roughness height (e/Dh) 0.044. It can be seen from the figure that effective efficiency increases with the increase in Reynolds number and after a certain value it starts decreasing. This is due to the reason that the quality of collected heat decreases and pump work increases.

The maximum value of effective efficiency occurs at relative roughness height of 0.044 and relative roughness pitch of 10.

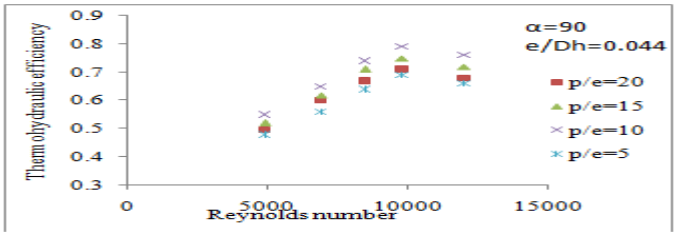

Figure 4(b). Variation of the thermohydraulic efficiency with the Reynolds number for different values of relative roughness pitch and for fixed value of angle of attack 90° and relative roughness height

REFERENCES

[1]. N.K.Bansal, "Solar air heater applications in India" 1998 published by Elsevier Science Ltd. PII: S0960-1481(98)00237-7.
[2]. Prashant Dhiman , N.S.Thakur, Anoopkumar, Satyendersingh, "An analytical model to predict the thermal performance of a novel parallel flow packed bed solar air heater," Applied energy 88(2011) 2157-2167.
[3]. Abdul- Malik Ebrahim Momin, J.S.Soni, S.C.Solanki, "Heat transfer and Friction factor in solar air heater duct with V-shaped rib roughness on absorber plate," Internantional journal of heat and mass transfer 45(2002) 3383-3396.
[4]. A.A.ElSebii, S.AboulEnein, M.R.I.Ramadan, S.M.Shalaby, B.M.Moharram, "Investigation of thermal performance of double pass flat and V-corrugated plate solar airheaters," Energy 36(2011) 1076-1086.
[5]. Sudhanshu Dogra, Nitin Chauhan, Gaurav Bhardwaj, "Effect of artificial roughness on heat transfer and friction factor characteristics in rectangular duct in double pass solar air heater" International Journal of Mechanical Engineering and Technology (IJMET), ISSN 0976 – 6340(Print), ISSN 0976 – 6359(Online) Volume 4, Issue 3, May - June (2013) © IAEME.
[6]. M.F.ElKhawajah, L.B.Y.Aldabbagh, F.Egelioglu, "The effect of using transverse fins on a double pass solar air heater using wire mesh as an absorber," Solar energy 86(2011) 1479-1487.
[7]. MM Sahu and JL Bhagoria, "Augumentation of heat transfer coefficient by using 90° broken transverse ribs on absorber plate," Renewal energy 2005; 30:2057-2063.
[8]. A.P.Omojaro, Aldabbagh, "Experimental performance of a single and double pass solar air heater with fins and steel wire mesh as an absorber," Applied energy 87(2010) 3759-3765.
[9]. B.N.Prasad and J.S.Saini, " Effect of artificial roughness on heat transfer and friction factor in a solar air heater," Solar energy vol.41, No. 6. Pp. 555-560, 1988.
[10]. PaisarnNaphon, " Perfrmance and entropy generation of the double pass solar air heater with longitudinal fins," Renewable energy 30(2005) 1345-1357.
[11]. Suppramaniam Satcunanathan and Stanley Deonarine, " A two pass solar air heater,"Solar energy 1973 , vol.15, pp.41-49.
[12]. Vikrant Katekar, AnkurVithalkar, Bhojraj Kale, "Enhancement of convective heat transfer coefficient in solar air heater of roughened absorber plate," ICETET' 09 Proceedings, IEEE comp. society, Washington DC, USA 2009, doi>10.11.09/ICETET-2009.
[13]. ASHARAE Standard 93–77. Method of testing to determine the thermal performance of Solar Air Heater, New York 1997; 1–34.

International Journal of Modern Engineering Research (IJMER)
www.ijmer.com Vol. 3, Issue. 4, Jul - Aug. 2013 pp-2275-2280 ISSN: 2249-6645

Effect on Efficiency of Two-phase Flow Distribution in a Parallel Flow Heat Exchanger with Reverse Upward Flow

Satish Choudhary[1], Dr. Bhupendra Gupta[2], Dr. Mukesh pandey[3]
Dr. Prashant Baredar[4]

[1]*Student, Master of Engineering, Heat Power, JEC, Jabalpur*
[2]*Assistant Professor, Jabalpur Engineering College, Jabalpur, India*
[3]*Professor, School of Energy and Environment, UIT, RGPV Bhopal, India*
[4]*Associate Professor, MANIT, Bhopal, India*

ABSTRACT: *The air and water flow distribution are experimentally studied for a round header – flat tube geometry simulating a parallel flow heat exchanger. The number of branch flat tube is 25. The effects of tube outlet direction, tube protrusion depth and quality are investigated. The flow at the header inlet is identified as annular. For the upward flow configuration, the water flow distribution is significantly affected by the tube protrusion depth. For flush-mounted configuration, most of the water flows through frontal part of the header. As the protrusion depth increases, minimum water is forced to the rear part of the header. Possible explanations are provided based on the flow visualization results.*

KEYWORDS*: Flow distribution; Parallel flow heat exchanger; Air and water flow measurement; Reverse upward flow; Two-phase; Experimental approach.*

I. INTRODUCTION

Two-phase flow distribution of Air and water was experimentally investigated in a parallel flow heat exchanger comprised of two horizontal headers and twenty five vertical channels. Most of the flow in the header inlet was identified as stratified flow. The effect of tube protrusion depth was also investigated. It was observed that, For upward flow, significant portion of liquid was forced to rear part of the header. The effect of quality and protrusion depth on the liquid distribution was also investigated.

Aluminum based heat exchangers consist of flat tubes of 5 mm hydraulic diameter. For the vertical header configuration, most of the liquid flowed through the frontal part of the header, and the effect of the inlet pipe direction was not significant. For a horizontal header, the flow distribution was highly dependent on the inlet pipe direction, and better distribution was obtained for the parallel configuration.

II. EXPERIMENTAL SETUP

The Experimental Setup used for this study is shown in Figure 2.1. The hydraulic diameter of the present flat tube is 5 mm, and the flow cross sectional area is 25 mm^2. The test section consists of the 16 mm internal Diameter round upper and lower headers, which are 90 cm apart, and 25 flat tubes inserted at 3 mm pitches. This configuration was chosen to simulate the actual parallel flow heat exchanger. Twenty five flat holes were machined at the bottom for insertion of flat tubes. An aluminum plate, which had matching flat holes, was installed underneath the header as illustrated in Fig. 2.1Flat tubes were secured, and the protrusion depth was adjusted using O-rings between the header and the aluminum plate. Transition blocks were installed in the test section to connect the flat tubes and the 5.0 mm ID round tubes. The round tubes served as flow measurement lines. At the inlet of the header, 1.0 m long aluminum tube having the same internal diameter as the header was attached. The tube served as a flow development section.

Figure 2.1: Experimental setup

Figure 2.2: Water flow meter

Figure 2.3: Flow distribution system

Figure 2.4: Electrical control panel

Table 2.1: Components used in Setup

Sr.No.	Name of component	Specification
1	Air blower	15 amp.220 v ac
2	Water heater	1000 w
3	Water pump	65w
4	Water flow meter	½ inch Diameter
5	Air flow meter	½ inch Diameter
6	Air and water Separator	4 inch Diameter
7	Flexible pipe	15 mm Diameter
8	Thirteen valve	½ inch Diameter
9	Vertical square aluminum pipe	Thickness 1.5mm
10	Vertical circular aluminum pipe	Thickness 1.5mm
11	Inlet tank	40Liters
12	Outlet tank	25 Liters
13	Electrical control panel	15 amp.

III. METHODOLOGY

III.1. UPWARD FLOW: An upward flow was observed at the header inlet. The liquid motion in the lower header was unstable and intermittent. Liquid was supplied into the channels by electrical water pump. The Air and water distribution is generally reverse to the liquid distribution. The flow visualization results that the liquid is forced to frontal part of the header as the quality increases. The liquid is forced to frontal part of the header as the quality decreases, yielding better liquid distribution. The explanation at lower quality, more liquid is supplied into the header, supplying more liquid to frontal part may be provided. The annular flow using air and water revealed that more water was forced to frontal part of the header at a higher quality. The reason was attributed to the increased water film thickness at the upper part of the header at increased quality. The part of the incoming water impinges at the first protrusion, separates at the top, reattaches at the bottom of the header due to the action of gravity. The separated water, along with the water from lower part of the header, is forced to the rear end of the header, and starts to fill in the tubes from backward.

IV. RESULT AND DISCUSSION

IV.1. Reverse upward flow: In reverse upward flow, the air and water are flow in the direction of upward and after that air and water are achieve in separator. Temperature at inlet is 50 °C., Temperature at outlet is 45.8 °C.
Time taken during reading = 10 sec.
Temperature at inlet =50 °C
Temperature at outlet =45.8 °C
H= witch insert in pipe
D= 16mm diameter of pipe

Table 4.1.1: Air flow in different h/d and Reverse upward flow

Sr. No.	Channel no.	Air flow (m^3 /sec) At h/d = 0/16 =0.0	Air flow (m^3 /sec) At h/d = 4/16 =0.25	Air flow (m^3 /sec) At h/d =8/16 =0.5
1	**1-5**	**0.5**	**1.5**	**1.5**
2	**6-10**	**1.2**	**1.4**	**1.2**
3	**11-15**	**1.3**	**1.2**	**1.0**
4	**16-20**	**0.5**	**0.5**	**1.0**
5	**21-25**	**0.2**	**0**	**0.0**

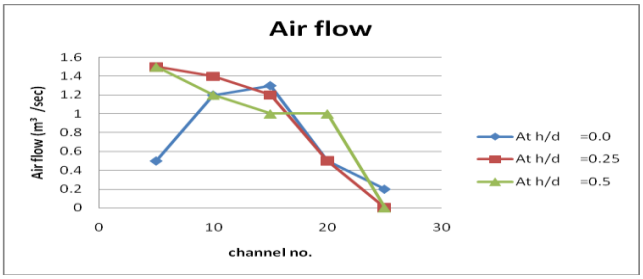

Fig. 4.1.1: Air flow in different h/d and Reverse upward flow

Table 4.1.2 Water flow in different h/d and Reverse upward flow

Sr. No.	Channel no.	Water flow (L/ sec) At h/d = 0/16 =0.0	Water flow (L/ sec) At h/d = 4/16 =0.25	Water flow (L/ sec) At h/d = 8/16 =0.5
1	1-5	2.0	0.5	0.4
2	6-10	0.5	0.4	0.5
3	11-15	0.4	0.4	0.5
4	16-20	1.0	0.5	1.4
5	21-25	2.2	1.5	2.3

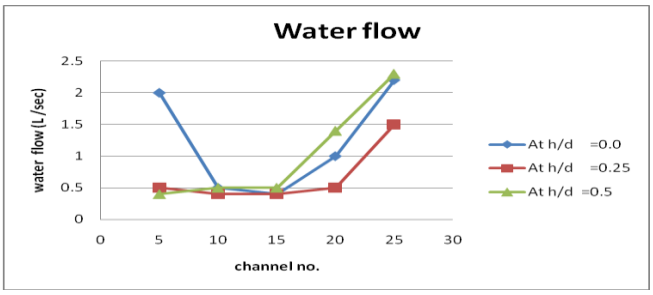

Figure 4.1.2: Water flow in different h/d and Reverse upward flow

Efficiency:
Temperature at inlet =50 °C
Temperature at outlet =45.8 °C
ή= (Temperature at inlet - Temperature at outlet) / Temperature at inlet
= (50-45.8)/50 =08.40%

IV.2. REVERSE UPWARD FLOW: In reverse upward flow, the air and water are flow in the direction of upward and after that air and water are achieve in separator. Temperature at inlet is 60 °C., Temperature at outlet is 53.6 °C.
Time taken during reading = 10 sec.
Temperature at inlet =60 °C.
Temperature at outlet =53.6 °C
H= witch insert in pipe
D= 16 mm diameter of pipe

Table 4.2.1: Air flow in different h/d and Reverse upward flow

Sr. No.	Channel no.	Air flow (m^3 /sec) At h/d = 0/16 =0.0	Air flow (m^3 /sec) At h/d = 4/16 =0.25	Air flow (m^3 /sec) At h/d =8/16 =0.5
1	1-5	0.6	1.6	1.5
2	6-10	1.3	1.5	1.3
3	11-15	1.4	1.3	1.2
4	16-20	0.7	0.4	1.1
5	21-25	0.2	0.3	0.1

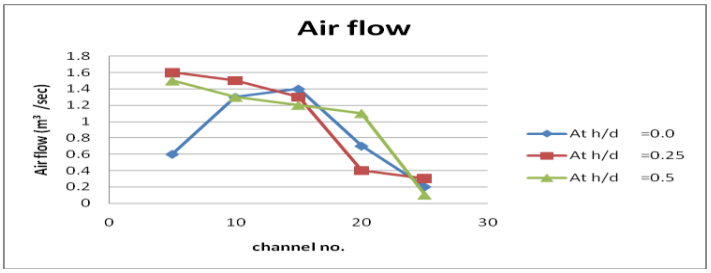

Figure 4.2.1: Air flow in different h/d and Reverse upward flow

Table 4.2.2: Water flow in different h/d and Reverse upward flow

Sr. No.	Channel no.	Water flow (L/ sec) At h/d = 0/16 =0.0	Water flow (L/ sec) At h/d = 4/16 =0.25	Water flow (L/ sec) At h/d = 8/16 =0.5
1	1-5	2.1	0.5	0.4
2	6-10	0.6	0.4	0.5
3	11-15	0.5	0.4	0.6
4	16-20	1.2	0.5	0.9
5	21-25	2.4	0.9	1.6

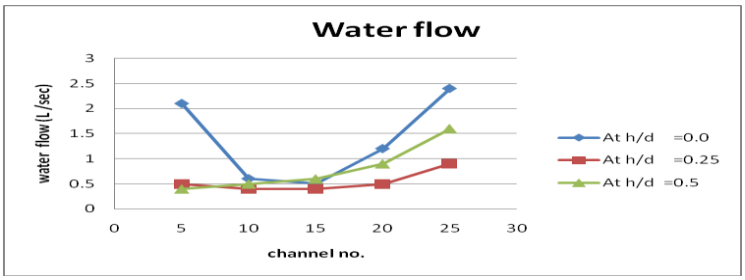

Figure 4.2.2: Water flow in different h/d and Reverse upward flow

Efficiency

Temperature at inlet =60 °C.
Temperature at outlet =53.6 °C
ή= (Temperature at inlet - Temperature at outlet) / Temperature at inlet
= (60-53.6)/60 =10.66%

IV.3. REVERSE UPWARD FLOW: In reverse upward flow, the air and water are flow in the direction of upward and after that air and water are achieve in separator. Temperature at inlet is 70 °C., Temperature at outlet is 63.8 °C.
Time taken during reading = 10 sec.
Temperature at inlet =70 °C
Temperature at outlet =63.8 °C
H= witch insert in pipe
D= 16mm diameter of pipe

Table 4.3.1: Air flow in different h/d and Reverse upward flow

Sr. No.	Channel no.	Air flow (m^3 /sec) At h/d = 0/16 =0.0	Air flow (m^3 /sec) At h/d = 4/16 =0.25	Air flow (m^3 /sec) At h/d =8/16 =0.5
1	1-5	0.7	1.7	1.6
2	6-10	1.4	1.6	1.3
3	11-15	1.6	1.4	1.2
4	16-20	0.8	0.5	1.2
5	21-25	0.1	0.9	0.2

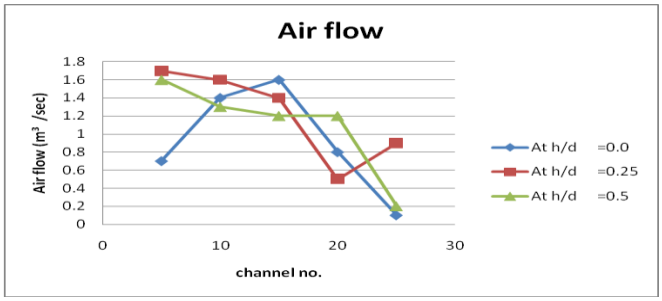

Figure 4.3.1: Air flow in different h/d and Reverse upward flow

Table 4.3.2: Water flow in different h/d and Reverse upward flow

Sr. No.	Channel no.	Water flow (L/ sec) At h/d = 0/16 =0.0	Water flow (L/ sec) At h/d = 4/16 =0.25	Water flow (L/ sec) At h/d = 8/16 =0.5
1	1-5	2.3	0.5	0.5
2	6-10	0.7	0.4	0.6
3	11-15	0.6	0.4	0.7
4	16-20	1.3	0.5	2.2
5	21-25	2.4	0.9	2.4

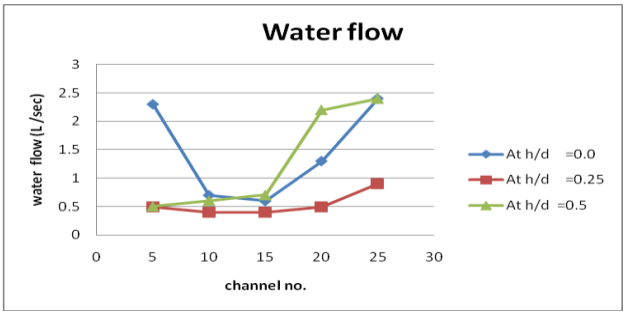

Figure 4.3.2: Water flow in different h/d and Reverse upward flow

Efficiency
Temperature at inlet =70 °C
Temperature at outlet =63.8 °C
ή= (Temperature at inlet - Temperature at outlet) / Temperature at inlet
= (70-63.8)/70 =8.85%

IV.4. REVERSE UPWARD FLOW: In reverse upward flow, the air and water are flow in the direction of upward and after that air and water are achieve in separator. Temperature at inlet is 80 °C and temperature at outlet is 73.2 °C.
Time taken during reading = 10 sec.
Temperature at inlet =80°C
Temperature at outlet =73.2 °C
H= witch insert in pipe
D= 16mm diameter of pipe

Table 4.4.1: Air flow in different h/d and Reverse upward flow

Sr. No.	Channel no.	Air flow (m^3 /sec) At h/d = 0/16 =0.0	Air flow (m^3 /sec) At h/d = 4/16 =0.25	Air flow (m^3 /sec) At h/d =8/16 =0.5
1	1-5	0.8	1.8	1.7
2	6-10	1.4	1.6	1.4
3	11-15	1.6	1.5	1.3
4	16-20	0.9	0.6	1.4
5	21-25	0.2	0.4	0.4

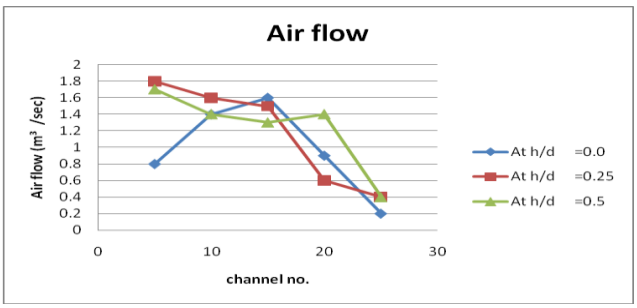

Figure 4.4.1: Air flow in different h/d and Reverse upward flow

Table 4.4.2: Water flow in different h/d and Reverse upward flow

Sr. No.	Channel no.	Water flow (L/ sec) At h/d = 0/16 =0.0	Water flow (L/ sec) At h/d = 4/16 =0.25	Water flow (L/ sec) At h/d = 8/16 =0.5
1	1-5	2.4	0.6	0.5
2	6-10	0.8	0.5	0.6
3	11-15	0.7	0.5	0.8
4	16-20	1.4	0.6	1.6
5	21-25	2.3	1.2	2.5

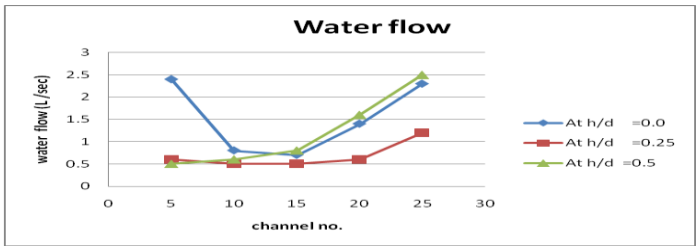

Figure 4.4.2: Water flow in different h/d and Reverse upward flow

Efficiency:

Temperature at inlet =80°C
Temperature at outlet =73.2 °C
ή= (Temperature at inlet - Temperature at outlet) / Temperature at inlet
= (80-73.2)/80 = 08.50%

V. CONCLUSION

[1] The effects of tube outlet direction, tube protrusion depth and quality are investigated. It is observed that the incoming water impinges at the protrusions, and the separated water reattaches at the rear part of the header. The reattachment length increases as the protrusion depth increases. The effect of quality is qualitatively the same as that of the protrusion depth. Increase of the mass flux or quality forces the water to rear part of the header.

[2] For the upward flow configuration, most of the water flows through the rear part of the header. The protrusion depth, quality does not significantly alter the flow distribution. Different from the downward flow configuration, the separated water from upper protrusions reattaches at the bottom of the header.

[3] Thus, the variation of reattachment length by the change of protrusion depth, quality is not like to significantly affect the flow distribution. Negligible difference on the water flow distribution was observed between the parallel flow and the reverse flow configuration. Using of Reverse upward flow the obtain maximum efficiency are 10.66% at Temperature at inlet =60 °C and Temperature at outlet =53.6 °C

REFERENCES

[1]. C. Schenone et.al. (2008) Experiments on two-phase flow distribution inside parallel channels of compact heat exchangers International Journal of Multiphase Flow 34 (2008) 128–144.
[2]. Galip Temir et. al. (2009) Heat transfer of horizontal parallel pipe ground heat exchanger and experimental verification Applied Thermal Engineering 29 (2009) 224–233.
[3]. Karen A. Thole et.al. (1999) Entry region of louvered ®n heat exchangers Experimental Thermal and Fluid Science 19 (1999) 223=232.
[4]. Lee, J.K., et.al.., (2004). Distribution of two-phase annular flow at header-channel junctions. Exp. Therm. Fluid Sci. 28, 217–222.
[5]. Rong, X., et.al. (1995). Two-phase header flow distribution in a stacked plate heat exchanger. Gas Liquid Flows Fed- Vol. 225, 115–215.
[6]. Tompkins, et.al. (2002). Flow distribution and pressure drop in micro channel manifolds. In: 9th Int. Refrigeration and Air Conditioning Conference at Purdue, R6-4.
[7]. Tae-Ryong Sin et. al. (2006) Two-phase flow distribution of air–water annular flow in a parallel flow heat exchanger International Journal of Multiphase Flow 32 (2006) 1340–1353.
[8]. Visit, S., et.al (2004). Two-phase flow distribution in compact heat exchanger manifolds. Exp. Thermal Fluid Sci. 28, 209–215.
[9]. Watanabe, et.al (1995). Two-phase flow distribution in multi-pass tube modeling serpentine type evaporator. ASME/JSME Thermal Eng. Conf. 2, 35–42.
[10]. Yansong Ma et. al. (2010) Experimental investigation of header configuration on two-phase flow distribution in plate-fin heat exchanger International Communications in Heat and Mass Transfer 37 (2010) 116–120.

International Journal of Modern Engineering Research (IJMER)
www.ijmer.com Vol. 3, Issue. 4, Jul. - Aug. 2013 pp-2281-2286 ISSN: 2249-6645

Optimization of WEDM Process Parameters on Titanium Alloy Using Taguchi Method

Lokeswara Rao T.[1], N. Selvaraj[2]
[1]Ph. D Research Scholar, National Institute of Technology, Warangal, India
[2]Professor, National Institute of Technology, Warangal, India

ABSTRACT : *This paper describes an optimum cutting parameters for Titanium Grade5 (Ti-6Al-4V) using Wire-cut Electrical Machining Process (WEDM). The response of Volume Material Removal Rate (MRR) and Surface Roughness (Ra) are considered for improving the machining efficiency. A brass wire of 0.25mm diameter was applied as tool electrode to cut the specimen. The Experimentation has been done by using Taguchi's L_{25} orthogonal array (OA) under different conditions like pulse on, pulse off, peak current, wire tension, servo voltage and servo feed settings. Regression equation is developed for the VMRR and Ra. The optimum parameters are obtained by using Taguchi method. This study shows that the stated problem is solved by minimum number of experiments when compared to full factorial design.*

KEYWORDS: *Optimization of Process parameters, Titanium alloy, Taguchi method, WEDM.*

I. INTRODUCTION

Wire cut EDM has been widely adopted as a machining tool for die materials which require high strength and hardness as well as good wear resistance, while the traditional manufacturing process needs a special tool or technique with a longer process time. In WEDM, a continuously moving conductive wire acts as an electrode and material is eroded from the work piece by series of discrete sparks between the work piece and wire electrode separated by a thin film of dielectric fluid. The dielectric is continuously fed to the spark zone to flush away the eroded material and it acts as a coolant. The schematic representation of the WEDM is as shown in Figure-1.

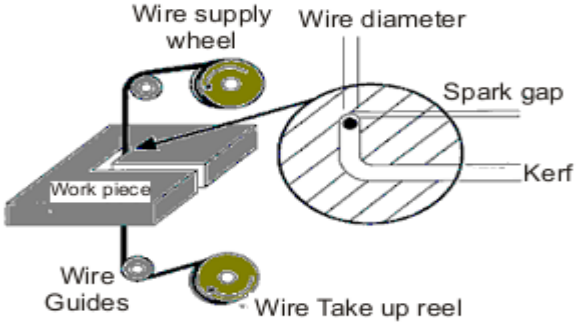

Fig.1: Schematic Representation of WEDM

Rajurkar K.P, et al, [1] used a factorial design method, to determine the optimal combination of control parameters in WEDM considering the measures of machining performance as metal removal rate and the surface finish. The study concluded that control factors are discharge current, the pulse duration and the pulse frequency. Y. S. Tarng, et al, [2] used a neural network model to estimate to the effects of parameters on the surface roughness as the response variable and machining speed. J. Prohaszka [3] in their paper they have discussed about effect of electrode material on machinability in wire electro-discharge machining that will lead to the improvement of WEDM performance. Experiments have been conducted regarding the choice of suitable wire electrode materials and the influence of the properties of these materials on the machinability in WEDM, the experimental results are presented and discussed. Y.S Liao et al.[4] derived an approach to determine machining parameter settings for WEDM process. Based on the taguchi quality design and the analysis of variance (ANOVA), the significant factors affecting the machining performance such as MRR, gap width ,surface roughness ,sparking frequency ,average gap voltage, normal ratio(ratio of normal sparks to total sparks) are determined. By means of regression analysis, mathematical models relating the machining performance and various machining parameters are established. Jose Maranon et.al [5] has investigated a new method of optimizing MRR using EDM with copper-tungsten electrodes. This paper describes an investigation into the optimization of the process which uses the effect of carbon which has migrated from the dielectric to tungsten copper electrodes.

Mustafa Ilhan et.al [6] have presented in their paper to select the most suitable cutting and offset parameter combination for the electrical discharge machining process in order to get the desired surface roughness value for the machined surface. A series of experiments have been conducted on 1040 steel material of thickness 30, 60 and 80 mm, and on 2379 and 2738 steel materials of thicknesses 30 and 60mm. S.H. Lee et al. [7] have studied the effect of machining parameters in EDM of tungsten carbide on the machining characteristics. The characteristics of EDM refer essentially to the output machining parameters such as material removal rate (MRR), relative wear ratio (RWR) and surface roughness (Ra). C. L. Lin, et al, [8] have described, the grey relational analysis based on an orthogonal array and fuzzy-based Taguchi method is applied for optimizing the multi-response process. They have used both the grey relational analysis method

without using the S/N (Signal/Noise) ratio and fuzzy logic analysis in orthogonal array Table in carrying out experiments for solving the multiple responses in the electrical discharge machining process. J. L. Lin et.al [9] has studied the optimization of multiple performance characteristics of WEDM using orthogonal array. In their paper, a new approach for optimization of the EDM with multiple performance characteristics based on the orthogonal array with grey relational analysis has been studied. The performance characteristics studied are MRR, surface roughness, and electrode wear ratio.

N. Tosun et.al [10] have investigated theoretically and experimentally about the effect of the cutting parameters on size on erosion craters of wire electrode in WEDM. The level of importance of the machining parameters on the wire crater size has been determined by using analysis of variance (ANOVA). K.H. Ho, et. al, [11] in their paper have discussed about wire EDM research involving the optimization of the process parameters surveying the influence of the various factors affecting the machining performance and productivity. The paper also highlights the adaptive monitoring and control of the process investigating the feasibility of the different control strategies of obtaining the optimal machining conditions. Scott F. Miller et al, [12] in their paper have discussed about wire electrical discharge machining (EDM) of cross-section with minimum thickness and compliant mechanisms is studied. This was supported by findings from SEM micrographs of EDM surface, subsurface, and debris. R.Ramakrishnan et.al [13] in their paper have applied the Taguchi's method, which is one of the methods of robust design of experiments to optimize multi responses of the wire cut electric discharge machining operations. Experimentation is carried out using Taguchi's L16 orthogonal array method. By applying the Taguchi's method, a good improvement was obtained. Swarup S. Mahapatra et.al [14] have described in their paper about Parametric Optimization of Wire Electrical Discharge Machining (WEDM) Process using Taguchi Method. The responses measured are Surface finish (Ra) and MRR. They have used Taguchi technique for the optimization of process parameters. Orthogonal array used is L27. They have proposed some optimized parameter values for machining the work piece.

The cutting of Tungsten Carbide ceramic using electro-discharge machining (EDM) with a graphite electrode by using Taguchi methodology has been reported by Mohd Amri Lajis et al [15]. The Taguchi method is used to formulate the experimental layout, to analyze the effect of each parameter on the machining characteristics, and to predict the optimal choice for each EDM parameter such as peak current, voltage, pulse duration and interval time. It is found that these parameters have a significant influence on machining characteristic such as metal removal rate (MRR), electrode wear rate (EWR) and surface roughness (SR). The analysis of the Taguchi method reveals that, in general the peak current significantly affects the EWR and SR, while, the pulse duration mainly affects the MRR. C. Bhaskar Reddy et.al, [16] have investigated for best parameter selection to obtain maximum Metal removal rate (MRR) and better surface roughness (Ra) by conducting the experimentation on CONCORD DK7720C four axes CNC Wire Electrical Discharge Machining of P20 die tool steel with molybdenum wire of 0.18mm diameter as electrode.

From the literature several researchers have been applied the Taguchi method is used to optimize the performance parameters in WEDM process. In the Present work Titanium alloy is considered for measuring the output parameters like material removal rate, surface rough using Taguchi method.

II. EXPERIMENTAL DESIGN

Proper experimental design significantly contributes towards the accurate characterization and optimization of the process. Here, the criterion for experimental design and analysis is to achieve higher VRR along with reduction in Surface Roughness. An orthogonal array for six controllable parameters is used to construct the matrix of five levels of controllable factors. The L25 orthogonal array contains 25 experimental runs at various combinations of six input variables. In the present study Table-1 represents various levels of process parameters and Table-2 represents experimental plan with assigned values.

Table 1: Levels of Various Process Parameters

S.NO	Process Parameters	Units	Level-I	LeveI-II	Level-III	Level-IV	Level-V
1.	Pulse On	µs	112	116	120	124	125
2.	Pulse Off	µs	60	56	52	48	44
3.	Peak Current	Amps	70	110	150	190	230
4.	Wire Tension	Kg-f	4	6	8	10	12
5.	Servo Voltage	Volts	10	30	50	70	90
6.	Servo Feed	mm/min	420	840	1260	1680	2100

Table 2: Experimental plan with assigned values

S.NO	Pulse on µs	Pulse Off µs	Peak Current Amps	Wire Tension Kg-f	Servo Voltage Volts	Servo feed mm/min
1.	112	60	70	4	10	420
2.	112	56	105	6	30	840
3.	112	52	145	8	50	1260
4.	112	48	185	10	70	1680
5.	112	44	215	12	90	2100
6.	116	60	105	8	70	2100
7.	116	56	145	10	90	420
8.	116	52	185	12	10	840
9.	116	48	215	4	30	1260
10.	116	44	70	6	50	1680
11.	120	60	145	12	30	1680
12.	120	56	185	4	50	2100

13.	120	52	215	6	70	420
14.	120	48	70	8	90	840
15.	120	44	105	10	10	1260
16.	124	60	185	6	90	1260
17.	124	56	215	8	10	1680
18.	124	52	70	10	30	2100
19.	124	48	105	12	50	420
20.	124	44	145	4	70	840
21.	128	60	215	10	50	840
22.	128	56	70	12	70	1260
23.	128	52	105	4	90	1680
24.	128	48	145	6	10	2100
25.	128	44	185	8	30	420

III. SELECTION OF MATERIAL

Titanium alloys are now the most attractive materials in aerospace and medical applications. The titanium its alloys are used extensively in aerospace, such as jet engine and airframe components, because of their excellent combination high specific strength (strength to weight ratio) and their exceptional resistance to corrosion at elevated temperature. In the present work Titanium grade 5 (Ti6Al4V) is used as work piece material and brass wire is used as electrode material. The chemical composition of the material is shown in Table -3. The variable process parameters and fixed parameters are given in Table-4 and Table-5 respectively.

Table 3**:** Chemical composition of Titanium Grade 5 Material

N	C	H	Fe	O	Al	V
0.05 %	0.08 %	0.015 %	0.40 %	0.20 %	6.75 %	4.5 %

IV. EXPERIMENTAL WORK

The experiments were planned according to Taguchi's L25 orthogonal array [17]. The experiments were carried out on ELEKTRA SPRINTCUT 734 four axis wire cut EDM machine is as shown in Figure.2. The basic parts of the WEDM machine consists of a wire Electrode, a work table, and a servo control system, a power supply and dielectric supply system. The following Fig shows the ELEKTRA SPRINTCUT 734 of wire EDM. . Therefore, the width of cut (W) remains constant. The VMRR for each WEDM operation was calculated using Eq. (1). Surface Roughness (Ra) is measured by handy surf (Mitutoyo surftest SJ-201P) equipment.

Fig. 2: CNC Wire cut EDM is used for experimentation

Table 4: process parameters of ELECTRONICA SPRINT CUT 734 CNC WEDM

Control parameters	Units	Symbol
Pulse On	µs	A
Pulse Off	µs	B
Peak Current	Amperes	C
Wire tension	Kg-f	D
Servo Voltage	Volts	E
Servo Feed	mm/min	F

Table 5: Variable and fixed parameters in WEDM

Machining Parameters	Working Range	Fixed Parameters	Value
Pulse On	115-131 machine unit	Composition of material	Ti6Al4V
Pulse off	63-45 machine unit	Work piece thickness	25mm
Peak current	70-230 Ampere	Wire electrode material	Brass wire Ø0.25mm
Wire tension	0-15 kg-f	Dielectric medium	Distilled water
Servo Voltage	0-99Volts	Wire feed	8m/min
Servo feed setting	0-2100 mm/min	Wire offset	0.00mm

Volume Material removal rate (VMRR) = Volume of the material removed / cutting time mm^3/min (1)

V. RESULTS AND DISCUSSIONS

The effect of machining parameters on material removal rate and surface roughness in machining Titanium (Ti-6Al-4V) are studied. From the results it is observed that, the pulse, pulse and peak current are the most significant factors for the performance measures. The wire tension, servo voltage and servo feed settings are less significant on performance measure. The results are obtained by analyzed using S/N Ratios, Response table and Response Graphs with the help of Minitab software. Table VI shows this experimental results then it is analyzed and obtained the optimum process parameters for MRR and Ra.

Table 6: Experimental results of output parameters

Run	A	B	C	D	E	F	Cutting Rate mm/min	Cutting time minutes	VMMR mm^3/min	Ra µm
1.	112	60	70	4	10	420	0.16	121.46	1.355	1.18
2.	112	56	105	6	30	840	0.55	33.24	4.952	1.24
3.	112	52	145	8	50	1260	0.65	30.54	5.389	1.28
4.	112	48	185	10	70	1680	0.72	29.21	5.635	1.31
5.	112	44	215	12	90	2100	0.35	59.56	2.777	1.16
6.	116	60	105	8	70	2100	0.36	60.21	2.733	1.20
7.	116	56	145	10	90	420	0.30	67.42	2.441	1.25
8.	116	52	185	12	10	840	1.35	15.02	10.959	1.52
9.	116	48	215	4	30	1260	2.21	9.12	18.049	2.11
10.	116	44	70	6	50	1680	1.88	11.40	14.439	2.03
11.	120	60	145	12	30	1680	1.72	11.56	14.239	2.01
12.	120	56	185	4	50	2100	1.64	12.15	13.548	1.93
13.	120	52	215	6	70	420	1.82	11.40	14.439	1.86
14.	120	48	70	8	90	840	2.35	7.41	22.214	2.89
15.	120	44	105	10	10	1260	2.19	8.52	19.320	2.76
16.	124	60	185	6	90	1260	1.47	13.56	12.139	1.29
17.	124	56	215	8	10	1680	1.82	10.58	15.558	1.37
18.	124	52	70	10	30	2100	2.74	7.11	23.151	2.45
19.	124	48	105	12	50	420	2.45	8.03	20.499	3.01
20.	124	44	145	4	70	840	1.73	11.25	14.632	1.54
21.	128	60	215	10	50	840	1.95	10.06	16.362	1.62
22.	128	56	70	12	70	1260	2.12	9.25	17.795	1.73
23.	128	52	105	4	90	1680	2.35	8.34	19.737	2.25
24.	128	48	145	6	10	2100	1.93	10.21	16.122	1.53
25.	128	44	185	8	30	420	2.42	8.12	20.272	2.08

VI. SELECTION OF OPTIMAL PARAMETER COMBINATION

The Experimental results shows the effect of six process parameters on material removal rate and surface roughness.Fig-4 shows the effect of Volume Material Removal Rate for the pulse on, pulse off, peak Current and Servo Voltage. From this Fig, it was observed that the VMRR increased when the pulse on time was increased due to number of discharges within a given period of time increase. In Fig.6, it shows that with an increase of pulse on time the surface quality of the machined surfaces were decreased because under longer pulse time on the electrical sparks generate bigger craters on the surface of work piece. Fig.3 and 5 shows the graphs for the S/N ratios.

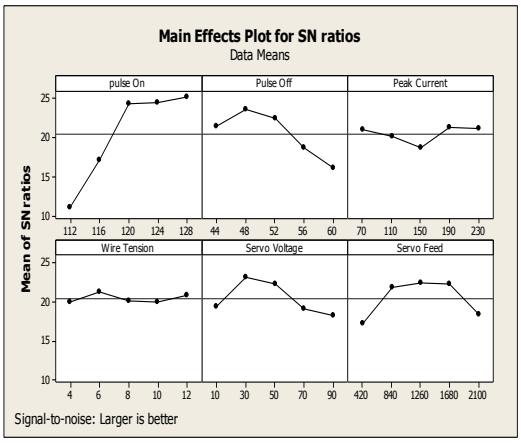

Fig. 3: Response Graphs for S/N ratios

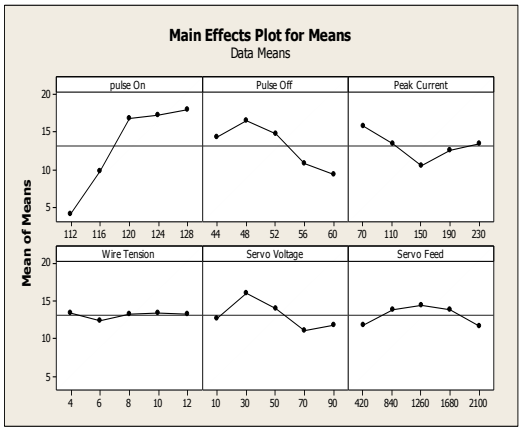

Fig. 4: Response Graphs for Means

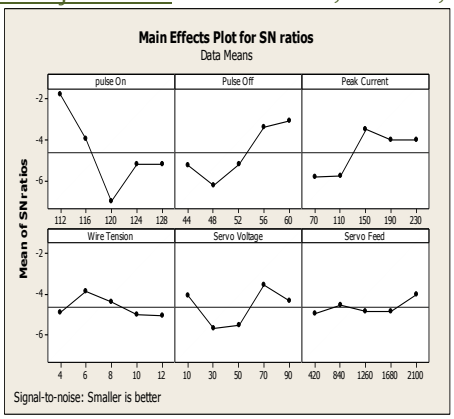

Fig. 5: Response Graphs for S/N ratios

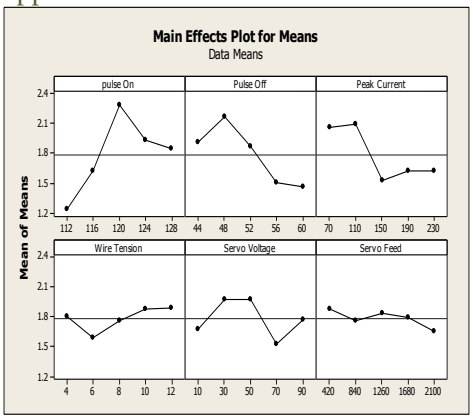

Fig. 6: Response Graphs for Means

In Taguchi Analysis the Volume Material Removal Rate versus Pulse on, Pulse off, Peak Current and Servo Voltage is carried out and average of each level is the parameter for raw data is given in Table 7 and average of each level in terms of S/N ratios are given in Table 8. Surface Rough versus Pulse on, Pulse off, Peak Current and Servo Voltage is carried out and average of each level is the parameter for raw data is given in Table 9 and average of each level in terms of S/N ratios and optimal parameter setting to obtain maximum Volume Material Removal Rate is given in Table 10. After observing all response graphs, Table 11 shows the Optimal Parameters Combination for VMRR and Ra.

Table 7: Response Table for Means Larger is better

Level	pulse On	Pulse Off	Peak Current	Wire tension	Servo voltage	Servo feed
1	11.01	21.45	21.01	19.92	19.43	17.19
2	17.12	23.49	20.10	21.22	23.10	21.84
3	24.31	22.36	18.58	20.05	22.19	22.43
4	24.47	18.58	21.25	2001	19.05	22.20
5	25.09	16.08	21.06	20.80	18.23	18.34
Delta	14.08	7.41	2.67	1.30	4.88	5.24
Rank	1	2	5	6	4	3

Table 8: Response Table for Signal to Noise Ratios

Level	pulse On	Pulse Off	Peak Current	Wire tension	Servo voltage	Servo feed
1	4.022	14.288	15.791	13.464	12.663	11.801
2	9.724	16.504	13.448	12.418	16.133	13.824
3	16.752	14.735	10.565	13.233	14.047	14.538
4	17.196	10.859	12.511	13.382	14.047	14.538
5	18.058	9.366	13.437	13.254	11.862	11.666
Delta	14.036	7.138	5.226	1.046	5.086	2.872
Rank	1	2	3	6	4	5

Table 9: Response Table for Means Smaller is better

Level	pulse On	Pulse Off	Peak Current	Wire tension	Servo voltage	Servo feed
1	-1.817	-5.274	-5.870	-4.886	-4.064	-4.940
2	-3.959	-6.263	-5.777	-3.863	-5.713	-4.533
3	-7.040	-5.200	-3.518	-4.408	-5.553	-4.884
4	-5.210	-3.403	-4.053	-5.015	-3.566	-4.867
5	-5.210	-3.097	-4.018	-5.064	-4.340	-4.012
Delta	5.223	3.165	2.352	1.202	2.146	0.928
Rank	1	2	3	5	4	6

Table 10: Response Table for Signal to Noise Ratios

Level	pulse On	Pulse Off	Peak Current	Wire tension	Servo voltage	Servo feed
1	1.234	1.914	2.056	1.082	1.672	1.876
2	1.622	2.170	2.056	1.802	1.672	1.762
3	2.290	1.872	1.522	1.764	.1.974	1.834
4	1.932	1.504	1.626	1.878	1.528	1.794
5	1.842	1.460	1.624	1.886	1.768	1.654
Delta	1.056	0.710	0.570	0.296	0.450	0.222
Rank	1	2	3	5	6	4

Table 11: Optimal Parameter Combination for MRR and Ra

Process Parameters	Optimum Level for VMRR	Optimum Level for Ra
Pulse On	128	112
Pulse Off	48	60
Peak Current	220	150
Wire Tension	6	6
Servo Voltage	30	70

DEVELOPMENT OF REGRESSION EQUATION

The objective of multiple regression analysis is to construct a model that explains as much as possible, the variability in a dependent variable, using several independent variables.

The Regression equations for VMRR and Ra

VMRR = - 69.7 + 0.889 pulse on - 0.387 Pulse Off - 0.0141 Peak Current + 0.027 Wire Tension - 0.0334 Servo Voltage - 0.00004 Servo Feed.

Ra = - 0.24 + 0.0381 pulse on - 0.0393 Pulse Off - 0.00333Peak Current + 0.0228 Wire Tension - 0.00129 Servo Voltage - 0.000098 Servo Feed.

VII. CONCLUSION

In this research, three different analyses are employed to obtain the following goals. Evaluating the effects on machining parameters on volume material removal rate, evaluating the effects on machining parameters on surface roughness and presenting the optimal machining conditions. Taguchi Analysis determines the factors which have significant impact on volume material removal rate. Equations which correlate machining parameters with material removal rate is found by regression analysis, and the optimal setting is found by S/N ratio analysis. Further research might attempt to consider the other performance criteria, such kerf, surface waviness, dimensional error as output parameters. This technique can also be applied for the various conventional machining operations and for machining of advanced materials like composites to improve the performance characteristics simultaneously. The present work was carried out by Taguchi analysis; further this work can be extended by considering any combination of fuzzy control, Grey relational analysis with Taguchi's orthogonal array technique, response surface methodology techniques.

REFERENCES

[1]. Rajurkar K.P., Scott D, Boyina S., "Analysis and Optimization of Parameter Combination in Wire Electrical Discharge Machining", International Journal of Production Research, Vol. 29, No. 11, 1991, PP 2189- 2207.

[2]. Y. S. Tarng., Ma S.C., Chung L.K., "Determination of Optimal Cutting Parameters in Wire Electrical Discharge Machining", International Journal of Machine Tools and Manufacture, Vol. 35, No. 12, 1995, PP. 1693-1701.

[3]. J.Prohaszka, A.G. Mamalis and N.M.Vaxevanidis, "The effect of electrode material on machinability in wire electro-discharge machining", Journal of Materials Processing technology, 69, 1997, PP 233-237.

[4]. (A) Y.S. Liao, Y.Y. Chu and M.T. Yan, Study of wire breaking process and monitoring of WEDM, International Journal of Machine Tools & Manufacture, 37 (1997) pp. 555-567. (B) Y.S Liao , J.T.Huang, A study on the machining parameter optimization of WEDM, Journal of Material Processing Technology,71(1997) pp. 487-493

[5]. Jose Marafona, Catherine Wykes., "A new method of optimizing MRR using EDM with Copper–tungsten electrodes". International journal of Machine tools and manufacturing. Vol. 40, 22 June 1999, PP 153-164.

[6]. Mustafa Ilhan Gokler, Alp Mithat Ozanozgu, "Experimental investigation of effects of Cutting parameters on surface roughness in the WEDM process". International journal of Machine tools and manufacture. Vol. 40, 2000, PP 1831-1848.

[7]. S.H.Lee, X.P Li, Study of the effect of machining parameters on the machining characteristics in electrical discharge machining of tungsten carbide, Journals of Material Processing Technology 115 (2001) pp.344-358.

[8]. C. L. Lin, J. L. Lin, T. C. Ko, "Optimization of EDM process based on the orthogonal array with fuzzy logic and grey relational analysis method". International journal of advanced manufacturing technology. Vol. 19, 2002, PP 271-227.

[9]. J. L. Lin., C. L. Lin., "The use of the orthogonal array with grey relational analysis to optimize the electrical discharge machining process with multiple performance characteristics". International journal of machine tools and manufacture, Vol. 42, 2002, PP 237-244.

[10]. N. Tosun, and H. Pihtili., "The Effect of Cutting Parameters on Wire Crater Sizes in Wire EDM", International journal of advanced manufacturing technology, Vol. 21, July 2003, PP 857-865.

[11]. K.H. Ho, S.T. Newman, S.Rahimifard, and R.D.Allen, "State of the art in wire electrical discharge machining (WEDM)", International journal of machine tools & manufacture,44, 2004, PP 1247-1259.

[12]. Scott F. Miller, Chen-C. Kao, Albert J. Shih, and Jun Qu "Investigation of wire electrical discharge machining of thin cross-sections and compliant mechanisms", International journal of machine tools & manufacture, 45, 2005, PP 1717-1725.

[13]. R.Ramakrishnan and L.Karunamoorthy. "Multi response optimization of WEDM operations using robust design", International journal of advanced manufacturing technology, Vol. 29, May 2006, PP 105-112.

[14]. Swarup S. Mahapatra, Amar Patnaik., "Parametric Optimization of Wire Electrical Discharge Machining (WEDM) Process using Taguchi Method", Journal of Brazil society of mech. Sci. & Eng, Vol. 28, No. 4, December 2006, PP 422-429.

[15]. Mohd Amri Lajis , H.C.D. Mohd Radzi, The Implementation of Taguchi Method on EDM Process of Tungsten Carbide, European Journal of Scientific Research ISSN 1450-216X Vol.26 No.4 (2009), pp.609-617.

[16]. C. Bhaskar Reddy et.al, Experimental Investigation of Surface Finish and Metal Removal Rate of P20 Die tool steel in wire-EDM using Multiple Regression Analysis, GSTF journal of Engineering Technology, V.1, number.1,june 2012,pp, 113-118.

[17]. A Hand Book on "Taguchi Techniques for Quality Engineering" by PHILLIP J. ROSS. 2005.

International Journal of Modern Engineering Research (IJMER)
www.ijmer.com Vol. 3, Issue. 4, Jul. - Aug. 2013 pp-2287-2295 ISSN: 2249-6645

Development of Methodology for Determining Earth Work Volume Using Combined Static and Kinematic GPS Observations

R. Ehigiator-Irughe[1], M. O. Ehigiator[2], T. U. Ilogho[3]

[1]*Siberian State Academy of Geodesy, Department of Engineering Geodesy and Geomatics, Novosibirsk, Russia.*
[2]*Faculty of Basic Science, Department of Physics, Benson- Idahosa University, Benin City, Nigeria.*
[3]*School of Environmental study, Department of Surveying and GeoInformatics , Auchi Polytechnic, Auchi.*

ABSTRACT: *Computing earthwork volumes is a necessary activity for nearly all construction projects and is often accomplished as a part of route surveying, especially for roads, Dredging and highways. If the area of the cross section at each station is known, then multiply that average end area by the known horizontal distance between the stations to determine the volume of cut. We present the results of precise static and kinematic point-positioning solutions obtained in post-processing, with a recursive Kalman filter estimator. The observations are dual frequency GPS carrier phase and pseudo-range, treated as two distinct data types, each with its own measurement equations. The receiver data is double differenced between satellites, to eliminate the receiver clock, and processed using precise satellite ephemerides and clock corrections. While estimating receiver coordinates, ionosphere-free carrier phase Lc biases, and tropospheric refraction model errors were treated accordingly. The motivation has been to show the possibility of the application of GPS in Topographical Survey and it associated accuracy. The method is fast, accurate and data was acquired using Trimble 4000SSI GPS Receiver and processed using Trimble Geomatics office.. The results indicate a precision at the level of a few centimeters, for static solutions, and below one decimeter, in kinematic mode.*

KEY WORDS: *Kalman filter, earthwork, GPS, Kinematic, integer ambiguities, Volume*

I. INTRODUCTION

Society recognises the need to move towards sustainable development. Construction has an important role to play within the sustainable development agenda not only because of the contribution to the national economy, but also because the built environment has a major impact on the quality of all of our lives, our comfort and security, our health and wellbeing and our productivity.

Road construction, maintaining and upgrading our existing Road has a potential environmental impact. The challenge today is to deliver road that can stand test of time and enhance the quality of life, while at the same time reducing the suffering encountered while embarking on a journey.

The purpose of the paper is to discuss the Geomatics modern approach used in the construction industries.

Earthwork computations are based on the design cross sections generated in the design process and cut and fill end areas computed and stored by that process.Earthwork computations are based on the design cross sections generated in the design process and cut and fill end areas computed and stored by that process. Additional required and optional data is needed for the earthwork computations. When subsurface data is provided, end areas for each material in cut are computed and is used as a basis for volumes. A compaction factor may be specified for each material, and volumes and mass ordinates will be computed accordingly.The earthwork parameters, such as compaction factors, added quantities, and forced balance stations, are used in computing the earthwork quantities for the designed roadways. These parameters are entered along with the other design data. These parameters are necessary in the compilation of earthwork volumes, mass ordinates and haul computations. Although these data are not strictly design data, they are entered and stored along with design data because the designer may then want to modify volume computation parameters and make new alternate volume computations.

A compaction factor is a characteristic assigned to a specific earth material which indicates how, and to what extent, its volume will change when that material, after having been cut from the original ground, is compacted as fill material. This characteristic is expressed as the ratio of a given volume of this material, in its original ground state, divided by the volume that same material would occupy when compacted as fill. Compaction factors produce an adjusted fill or cut volume to be used in computing earthwork volumes and mass ordinates. The compaction factors are applied when computing volumes. Volumes are computed separately for each roadway, and the appropriate compaction factor is selected and applied. Then these individual roadway volumes are summed to compute the design cross section volume.

II. GLOBAL POSITIONING SYSTEM (GPS)

Navigation and positioning is the art of determining position, speed and orientation of an object. The GPS program me was born in 1972 out of the quest for the US Navy and Air force to develop all weather Global Radio Navigation System. The GPS was designed to be a passive survivable continuous system which will provide any suitably equipped user with three dimensional position (x, y, z) velocity and precise time information.

The principle involves the measurement of distance (or range) to at least three Satellites whose *X*, *Y* and *Z* position is known, in order to define the user's X_p, Y_p and Z_p position. In its simplest form, the satellite transmits a signal on which the time of its departure (tD) from the satellite is modulated. The receiver in turn notes the time of arrival (tA) of this time mark. Then the time which it took the signal to go from satellite to receiver is (tA – tD) = Δt (called the delay time). The measured range *R* is obtained from (Andrew et.al 2004).

$$R1 = (t\mathrm{A} - t\mathrm{D})\ C = \Delta t\ C \qquad (1)$$

where c = the velocity of light.

Whilst the above describes the basic principle of range measurement, to achieve it one would require the receiver to have a clock as accurate as the satellite's and perfectly synchronized with it. As this would render the receiver impossibly expensive, a correlation procedure, using the pseudorandom binary codes (P or S), usually 'S', is adopted. The signal from the satellite arrives at the receiver and triggers the receiver to commence generating the S-code. The receiver-generated code is cross-correlated with the satellite code. The ground receiver is then able to determine the time delay (Δt) since it generated the same portion of the code received from the satellite (Abdel –Salem 2005).

However, whilst this eliminates the problem of an expensive receiver clock, it does not eliminate the problem of exact synchronization of the two clocks. Thus, the time difference between the two clocks, termed clock bias, results in an incorrect assessment of Δt. The distances computed are therefore called 'pseudo-ranges'. The effect of clock bias, however, can be eliminated by the use of four satellites rather than three. A line in space is defined by its difference in coordinates in an X, Y and Z system:

$$R = (\Delta X^2 + \Delta Y^2 + \Delta Z^2)^{1/2} \qquad (2)$$

If the error in R, due to clock bias, is (*_R) and* is constant throughout, then:

$$\begin{aligned}
R_1 + _R &= [(X_1 - X_p)^2 + (Y_1 - Y_p)^2 + (Z_1 - Z_p)^2]^{1/2} \\
R_2 + _R &= [(X_2 - X_p)^2 + (Y_2 - Y_p)^2 + (Z_2 - Z_p)^2]^{1/2} \\
R_3 + _R &= [(X_3 - X_p)^2 + (Y_3 - Y_p)^2 + (Z_3 - Z_p)^2]^{1/2} \qquad (3) \\
R_4 + _R &= [(X_4 - X_p)^2 + (Y_4 - Y_p)^2 + (Z_4 - Z_p)^2]^{1/2}
\end{aligned}$$

Where X_n, Y_n, Z_n = the coordinates of satellites 1, 2, 3 and 4 (n = 1 to 4)

X_p, Y_p, Z_p = the coordinates required for point P

R_n = the measured ranges to the satellites

Solving the four equations for the four unknowns X_p, Y_p, Z_p and $\_R$ eliminates the error due to clock bias. Whilst the use of pseudo-range is sufficient for navigational purposes and constitutes the fundamental approach for which the system was designed, a much more accurate measurement of range is required for positioning in Geodesy. This is done by measuring phase difference by means of the carrier wave in a manner analogous to EDM measurement (Schofield 1993).

III. KINEMATIC POSITIONING ALGORITHM

Kinematic positioning and alignment relies on the relationship of the carrier phase observations to the range observations described in the following equation (Raquet 1998).

$$\begin{aligned}
PR_1 &= R + bu_1 + bsv_{PR1} + T + I_1 + {}_{nPR1} \\
PR_2 &= R + bu_2 + bsv_{PR2} + T + I_1 \frac{\lambda_2^2}{\lambda_1^2} + {}_{nPR2} \\
-CPH_1 &= R + bu_{CPH1} + bsv_{CPH1} + T - I_1 + {}_{nCPH1} - N_1\lambda_1 \qquad (4) \\
-CPH_2 &= R + bu_{CPH2} + bsv_{CPH2} + T - I_1 \frac{\lambda_2^2}{\lambda_1^2} + {}_{nCPH2} - N_2\lambda_2
\end{aligned}$$

Where

PR = pseudo-range on L1 or L2 frequencies (meters), CPH = carrier phase on L1 or L2 frequencies, (meters), RT = true range (meters), bu = range equivalent receiver clock offset (meters), bsv = range equivalent satellite clock offset (meters)

T = tropospheric delay (meters), I = ionospheric delay (meters), n = measurement noise (meters), N = CPH integer (cycles), λ = carrier wavelength (meters)

The ionospheric delay is different on the L1 and L2 observations as it is inversely proportional to the frequency squared and so can be removed from the PR by differencing. The DGPS corrections will remove any errors in the navigation solution caused by satellite position and clock offsets. The accuracy of the PR derived DGPS corrected position solution is a function of the pseudo-range noise, which includes receiver noise and multipath errors. The GPS/inertial navigation solution will filter the short-term noise effects, but it cannot correct for correlated noise errors from multipath.

The major problem with static GPS is the time required for an appreciable change in the satellite/receiver geometry so that the initial integer ambiguities can be resolved. However, if the integer ambiguities could be resolved (and constrained in a least squares solution) prior to the survey, then a single epoch of data would be sufficient to obtain relative positioning to sub-centimeter accuracy. This concept is the basis of kinematic surveying. It can be seen from this that, if the integer ambiguities are resolved initially and quickly, it will be necessary to keep lock on these satellites while moving the antenna (Schofield 1993).

IV. RESOLVING THE INTEGER AMBIGUITIES

The process of resolving the integer ambiguities is called 'initialization' and may be done by setting-up both receivers at each end of a baseline whose coordinates are accurately known. In subsequent data processing, the coordinates are held fixed and the integers determined using only a single epoch of data. These values are now held fixed throughout the duration of the survey and coordinates estimated every epoch, provided there are no cycle slips. The initial baseline may comprise points of known coordinates fixed from previous surveys, by static GPS just prior to the survey, or by transformation of points in a local coordinate system to WGS 84 (Abdel – Salam 2005).

An alternative approach is called the 'antenna swap' method. An antenna is placed at each end of a short base (5–10 m) and observations taken over a short period of time. The antennae are interchanged, lock maintained, and observations continued. This results is a massive change in the relative receiver/satellite geometry and, consequently, rapid determination of the integers. The antennae are returned to their original position prior to the surveys. It should be realized that the whole survey will be invalidated if a cycle slip occurs. Thus, reconnaissance of the area is still of vital importance, otherwise re-initialization will be necessary. A further help in this matter is to observe to many more satellites than the minimum four required (Andrew et.al 2004).

IV.1. KALMAN FILTER

The Kalman filter is a digital algorithm that provides current estimates of a system variable such as position coordinates (Schoffield, 1993). The filter uses statistical models to properly weigh each new measurement relative to past information. It also determines up – to – date uncertainties of the estimates for real – time quality assessments (Kaplan 1996).

The Kalman filter is a multiple input multiple – output digital filter that can optimally estimate in real time the states of a system based on its outputs. These states are all the variables needed to completely describe the system behaviour as a function of time such as position and velocity. The Kalman filter filters noisy measurements to estimate the desired signals. The estimates are statistically optimal in the sense that they minimize the mean square estimation error. The Kalman filter contain a dynamic model of the GPS receiver platform motion and outputs a set of user receiver position, velocity and Time (PVT) state estimates as well as associated error variances [6]

The dynamic model can be derived by a Taylor's series expansion about the true position of the receiver. We let u (t) represent the true position of the receiver at a time t. Then at a time t_1 shortly after a time tu the receiver will be at a position (Kaplan 1996).

$$U(t) = U(t_o) + \frac{du(t)}{dt}\bigg|_{t=t_0}(t-t_0) + \frac{1}{2!}\frac{du^2(t)}{dt^2}\bigg|_{t=to}(t-t_0)^2 + \frac{1}{3!}\frac{du^3(t)}{dt^3}\bigg|_{t=to}(t-t_0)^3 \quad (5)$$

Where

$$\frac{du(t)}{dt}\bigg|_{t=tv} = Velocity \quad (5a)$$

$$\frac{1}{2!}\frac{du^2(t)}{dt^2}_{t=t_0} = acceleration \quad (5b)$$

$$\frac{1}{3!}\frac{du^3(t)}{dt^3}_{t=t_0} = jerk \quad (5c)$$

The third term in the expansion (Jerk) is regarded as negligible. The non negligible terms depend on the system being modeled and may be estimated for position measurement. Filters designed for PVT determination typically estimate either user states position (x_u, y_u, z_u), velocity $\left(\dot{x}_u, \dot{y}_u, \dot{z}_u\right)$ receiver clock offset (tu) and receiver clock drift $\left(\dot{t}_u\right)$.

IV.2. CODE MEASUREMENT

The GPS code measurement ρ is a linear measurement known as pseudo range in meters. Pseudo Range is a measure of the distance between the satellite and receiver at the time epoch of transmission and reception of the signals.

The transmit time of the signals is measured by comparing (correlating) identical Pseudo Random Noise (PRN) codes generated by the satellite and the receiver (Ehiorobo 2009).

$$\rho = R + C\,(dt - dT) + d_{ion} + d\,t_{rop} + d_{mpath.} \quad (6)$$

where

R = True range between the SV (at transmit time) and receiver (at r receiver time)

C = Speed of light (m/s)

dt = Receiver clock error (sec)

dT = Satellite clock error (sec)

d_{ion} = Ionospheric delay parameter

dt_{rop} = Measurement delay due to troposphere (m)

d_{mpath} = Measurement delay due to multipath

Most DGPS Processing involves generating a nominal "computed" range between the receiver and the satellite which is calculated from the known coordinate of the receiver locations and the satellite [6].

The true range vector **R** is

$$\mathbf{R} = P_{sv} - P_{rec} \quad (7)$$

Where; P_{sv} – is the computed position of the satellite at transmit time (From ephemeris)

P_{rec} is the nominal position of the receiver at receiver time.

IV.3. CARRIER MEASUREMENT

The constant motion of the GPS satellite constellation in orbit demands that the receiver be capable of taking care of the changing Doppler frequency shift on L_1.

In the case of Dual frequency receivers both L_1 and L_2 are tracked. L_1 wavelength is 19cm and L_2 wavelength is 24cm. The shift in frequency arises due to the relative motion between the satellite and the receivers. Integration of the Doppler frequency offset results in an extremely accurate measurement of the advance in signal carrier phase between time epochs (Gao et.al 2001).

Using Double Differencing Processing DD techniques on C/A or P(Y) – code carrier phase observables removes most of the error sources.

To achieve centimeter level accuracy, it is still necessary to carry out further refinement of the propagation path length measurement using carrier – cycle integer ambiguity resolution.

Once the receiver locks on to a particular satellite, it not only make C/A and or p(Y) code pseudo range measurements on L_1 and L_2 (if L_2 is present) but it also keeps a running count based upon the Doppler frequency shift present on L_1 and L_2 carrier frequencies.

Each epoch for running this cycle count is available for the receiver. It should be noted that the advance in carrier phase during an epoch is determined by integrating the carrier Doppler Frequency offset (fo) over the interval of the epoch. Frequency fo is the time rate of change of the carrier phase, hence integration over an epoch yields, the carrier phase advance during an epoch. At the conclusion of each epoch, a fractional phase measurement is made by the receiver. This measurement is derived from the carrier phase tracking loop of the receiver. Mathematically the relationship is as follows (Abdel – Salam):

$$\phi_{1.1n} = \phi_{1.1n-1} = \int_{I_{n-1}}^{In} f_{0_{1.1}}(r)dr + \phi_{1.10} \qquad (8)$$

$$Where \quad \phi_{1.10} = 0$$

$$\phi_{1.2n} = \phi_{1.2n-1} = \int_{I_{n-1}}^{In} f_{o_{1.2}}(r)dr + \phi_{1.20}$$

$$Where \quad \phi_{1.20} = 0$$

Where

ϕ is the accumulated phase at the epoch shown

n and n-1 are the current and immediate past epochs

f_D - is the Doppler frequency as a function of time

ϕ_1 is the fractional phase measured at the epoch shown

IV.4. IONOSPHERIC DELAY

The ionosphere is the part of the upper atmosphere where free electrons occur in sufficient density to have an appreciable influence on the propagation of radio frequency electromagnetic waves. It is a weak ionized plasma extending from approximately 50Km to 1000Km above the surface of the earth and can affect radio wave propagation in various ways (Kaplan 1996).

Ionosphere is a dispersive medium. The refractive index is a function of the operating frequency. The refractive index n of the ionosphere can be expressed as (Schofield 1993).

$$n^2 = 1 - \frac{X}{1 - iZ - \frac{Y_\tau^2}{2(1 - X - iZ)} \pm \left[\frac{Y_\tau^4}{4(1 - X - iZ)^2} + Y_L^2 \right]^{1/2}} \qquad (9)$$

Where

$$X = \frac{N_e e^2}{\varepsilon_n m \omega^2} \qquad ; Y_L = f_H \frac{Cos\theta}{f} \qquad ; Y_\tau = f_H \frac{\sin\theta}{f}$$

$$Z = \frac{\nu}{w} \qquad ; w = 2\Pi f$$

and

f	-	is frequency of incoming signal in Hz
N_e	-	is the electron density in electron / m^3
e	-	is the electron change = -1.602 X 10^{-19} Coulomb
ε_n	-	is the permeativity of free space = -8.854 X 10^{-12} Farad / m
m	-	is the rest mass of electron = 9.107 X 10^{-31} Kg
θ	-	is the angle of the ray with respect to the earth's magnetic field.
V	-	is the electron – neutron collision frequency and
f_H	-	is the electron gyro frequency typically 1.5MHz

IV.5. TROPOSPHERIC DELAY

Tropospheric delay occurs as a result of the GPS signals passage through the Earth's lower atmosphere. This region extends to an altitude approximately 10km above the earth's surface. The stratosphere is also considered part of the

lower atmosphere. It extends upward from the tropopause to an altitude of approximately 50 kilometers in these two sections of the atmosphere, electromagnetic refraction slows the GPS radio signals causing a delay in its arrival at the receiver [6].

IV.6. RECEIVER NOISE

Receiver noise can be considered as white noise as it is uncorrelated over time. In the case of GPS, it is the error in phase and code measurement due to imperfect tracking of the GPS signals by the phase and delay lock loops. The tracking error is random and is assumed to have a Gaussian distribution. The magnitude of the noise is a function of the measurement type and the signal strength.

The C/A – code measurement can be tracked with a typical accuracy of 1.5 meters but it may vary between 0.2 and 3 meter depending upon the strength of the receiver signal. Typical receiver noise for P(Y) code measurement is 10 – 30cm. Code and carrier phase measurement noise can be smoothed by an estimate of a "zero baseline" test (Kaplan 1996).

The GPS signal is split into two and fed to two separate but same types of receivers. In static application, the predominant error component in carrier phase noise is jitter of the phase lock loop caused by thermal noise. This can be expressed according to; (Schofield 1993).

$$\sigma_n = \sigma_{PLL} = \frac{\lambda}{2\pi}\sqrt{\frac{B_n}{C/\ n_o}\left(1+\frac{1}{\frac{2TC}{n_o}}\right)}\quad meters \qquad (10)$$

where

B_n - carrier loop noise band width in Hz

$\frac{C}{n_{io}}$ - is the carrier to noise power expressed as $10^{C/No/10}$ with C/No in dB - Hz

T - is the predetections integration time in seconds

λ - is carrier wavelength

IV.7. SATELLITE ORBIT ERRORS

Satellite orbit errors result from the uncertainty in orbital information. To compute the satellite position, we either use broadcast ephemeris or precise ephemeris. Although precise ephemeris information is much more accurate than those of broadcast information. The satellite positions are computed from a set of Keplerian orbit and perturbation parameters with clock parameters which are predicted states for the satellite orbit and are updated every two hours (Raquet 1998).

IV.8. MULTI PATH

Multi path refers to the existence of signals reflected from objects in the vicinity of a receiver's antenna that corrupt the direct line-of-sight signals from the GPS satellites, thus degrading the accuracy of both code-based and carrier phase-based measurements. The object may be tall buildings, television and Telephone masks, etc

IV.9. GEOMETRIC DILUTION OF PRECISION

In GPS observations, the position of the satellite affects the three dimensional angles of intersection between the satellite and the users position. When the satellites are close together or in a straight line, a low accuracy fix is obtained. When they are wide apart almost forming a square, a high accuracy is obtained (Abdel-Salam, 2005)

Thus, the dilution of precision is used to measure user position accuracy. The satellite configuration geometry with respect to the ground station is called the GDOP the geometric dilution of precision defined as (Ehioro 2008);

$$\text{GDOP} = \frac{1}{\sigma}\sqrt{\sigma_x^{\ 2}+\sigma_y^{\ 2}+\sigma_z^{\ 2}+\sigma_b^{\ 2}} \qquad (11)$$

Where; σ is the mean square error of the pseudo range, which has a zero mean

σ_x σ_y σ_z – measured r ms errors of the users position in the xyz direction and

σ_b is measured rms user clock error expressed in distance.

Other DOP parameters include

VDOP – vertical Dilution of Precision – One dimensional (1-D)

HDOP – Horizontal Dilution of Precision – Two dimensional (2-D)

PDOP – Position Dilution of Precision – Three dimensional (3-D)

The position dilution of precision is defined as

$$\text{PDOP} = \frac{1}{\sigma}\sqrt{\sigma_x^{\ 2}+\sigma_y^{\ 2}+\sigma_z^{\ 2}} \qquad (12)$$

The Horizontal Dilution of precision is defined as

$$\text{HDOP} = \frac{1}{\sigma}\sqrt{\sigma_x^{\ 2}+\sigma_y^{\ 2}} \qquad (13)$$

The Vertical Dilution of precision

$$VDOP = \frac{\sigma_z}{\sigma} \quad (14)$$

The time dilution of precision

$$TDOP = \frac{\sigma_b}{\sigma} \quad (15)$$

The smallest dilution of precision DOP value means the best satellite geometry for calculating user position. The observation is at the base of the tetrahedron. Under this condition, the DOP values are (Raquet 1998)

GDOP = $\sqrt{3} \approx 1.73$

PDOP = $2\sqrt{2/3} \approx 1.63$

HDOP = VDOP = $2/\sqrt{3} \approx 1.15$

And finally TDOP = $1/\sqrt{3} \approx 0.58$

V. CYCLE SLIPS

A cycle slip is a break in continuous satellite tracking. The wave fronts that the receiver counts during continuous tracking are also referred to as cycles. Therefore, when the receiver loses count because of an interruption in satellite tracking, the cycle or wave counting slips.

V.1 RESULTS OF ADJUSTMENTS OF OBSERVATIONS

The qualities to be obtained after field measurements and adjustment in a GPS network include baseline vector components and their covariance.

The final outcomes of baseline adjustment are the adjusted baseline vectors, estimated points coordinates and their covariance matrices. We present below results of adjustment using Trimble Geomatics office.

Table 1 - Baseline Processing Summary

Processing Summary

Baseline Summary B120 (3842 to AE000091)	
Processed:	Thursday, Jul 21, 2011 07:44:35PM
Solution type:	L1 fix
Solution acceptability:	Multiple
Ephemeris used:	Broadcast
Met Data:	Standard
Baseline slope distance:	2538.933m
Elevation mask:	13 degrees
Variance ratio:	0.0
Reference variance:	11.688
RMS:	0.008m
Horizontal Precision 1-sigma (scaled):	0.030m
Vertical Precision 1-sigma (scaled):	0.068m

Table 2 - Baseline Components (Mark to Mark)

From:	3842				
Grid		**Local**		**WGS 84**	
Northing	367124.091m	**Latitude**	7°19'01.50193"N	**Latitude**	7°19'02.82741"N
Easting	436929.511m	**Longitude**	6°22'02.87020"E	**Longitude**	6°22'00.44966"E
Elevation	365.672m	**Height**	365.672m	**Height**	366.558m

To:	AE000091				
Grid		**Local**		**WGS 84**	
Northing	368263.699m	**Latitude**	7°19'38.89654"N	**Latitude**	7°19'40.21925"N
Easting	434660.811m	**Longitude**	6°20'49.07818"E	**Longitude**	6°20'46.65650"E
Elevation	308.438m	**Height**	308.438m	**Height**	309.357m

Baseline:					
□ **Northing**	1139.607m	**NS Fwd Azimuth**	296°54'33"	□ **X**	48.700m
□ **Easting**	-2268.701m	**Ell. Distance**	2538.153m	□ **Y**	-2272.047m
□ **Elevation**	-57.235m	□ **Height**	-57.201m	□ **Z**	1132.082m

Table 3 - Standard Errors

Baseline Errors:					
□ □□ **Northing**	0.005m	□ **NS Fwd Azimuth**	0.517 seconds	□ □□ **X**	0.020m
□ □□ **Easting**	0.009m	□ **Ell.Distance**	0.008m	□ □□ **Y**	0.008m
□ □□ **Elevation**	0.020m	□ □□ **Height**	0.020m	□ □□ **Z**	0.005m

Table 4 - Occupations

		From	**To**
Point Name:		3842	AE000091
Data file:		38420790.DAT	30760790.DAT
Receiver Type:		4000SSi	4000SSi
Receiver Serial Number:		13842	13076
Antenna type:		Compact L1/L2	Compact L1/L2
Measured To:		Bottom of antenna	Bottom of antenna
Antenna height	**Measured**	1.270m	1.630m
	APC	1.332m	1.692m

Table 5 – Adjusted 3D Coordinate

Statistical Summary

Successful Adjustment in 1 iteration(s)
Network Reference Factor : 1.00
Chi Square Test (□ =95%) : PASS
Degrees of Freedom : 90.00
GPS Observation Statistics

Errors are reported using 1.96□ .

Point Name	Latitude	Longitude	Height	Northing	Easting
BM_5	7°19'02.77547"N	6°22'00.45644"E	345.315m	367122.496m	436929.726m
AE0001__	7°19'20.68657"N	6°21'11.59110"E	315.061m	367666.655m	435428.264m
AE000002	7°19'20.68709"N	6°21'11.59047"E	315.062m	367666.671m	435428.244m
AE000003	7°19'20.39312"N	6°21'11.91540"E	314.984m	367657.679m	435438.250m
AE000004	7°19'19.83339"N	6°21'11.34336"E	312.618m	367640.407m	435420.771m
AE000005	7°19'18.96313"N	6°21'10.67891"E	310.233m	367613.581m	435400.497m
AE000006	7°19'17.86287"N	6°21'09.61401"E	309.004m	367579.638m	435367.966m
AE000007	7°19'17.36933"N	6°21'07.72061"E	314.694m	367564.232m	435309.940m
AE000008	7°19'17.78599"N	6°21'06.86673"E	312.349m	367576.927m	435283.690m
AE000009	7°19'20.04550"N	6°21'04.33317"E	307.704m	367646.036m	435205.675m
AE000010	7°19'21.79386"N	6°21'05.17316"E	307.674m	367699.866m	435231.224m
AE000011	7°19'22.34130"N	6°21'04.59310"E	307.730m	367716.615m	435213.359m
AE000012	7°19'22.59900"N	6°21'03.57478"E	308.978m	367724.404m	435182.084m
AE000013	7°19'23.90880"N	6°21'00.67533"E	305.055m	367764.285m	435092.965m
AE000014	7°19'25.53640"N	6°20'58.39906"E	308.067m	367814.010m	435022.923m
AE000015	7°19'26.33917"N	6°20'58.24238"E	306.304m	367838.657m	435018.015m
AE000016	7°19'27.27521"N	6°20'57.19865"E	303.496m	367867.288m	434985.875m
AE000017	7°19'28.10378"N	6°20'55.42582"E	302.408m	367892.524m	434931.381m
AE000018	7°19'28.04179"N	6°20'52.51781"E	302.460m	367890.251m	434842.173m
AE000019	7°19'28.36471"N	6°20'50.60862"E	302.719m	367899.932m	434783.560m
AE000020	7°19'29.17996"N	6°20'49.09372"E	302.824m	367924.792m	434736.980m
AE000021	7°19'30.54718"N	6°20'48.80818"E	300.627m	367966.768m	434728.047m
AE000022	7°19'31.80050"N	6°20'47.82717"E	288.209m	368005.156m	434697.792m
AE000023	7°19'33.41452"N	6°20'48.26109"E	293.172m	368054.806m	434710.900m

AE000024	7°19'34.79316"N	6°20'48.74330"E	290.426m	368097.230m	434725.519m
AE000025	7°19'36.66374"N	6°20'46.95549"E	273.746m	368154.483m	434670.434m
AE000026	7°19'37.96679"N	6°20'47.67879"E	255.774m	368194.614m	434692.459m

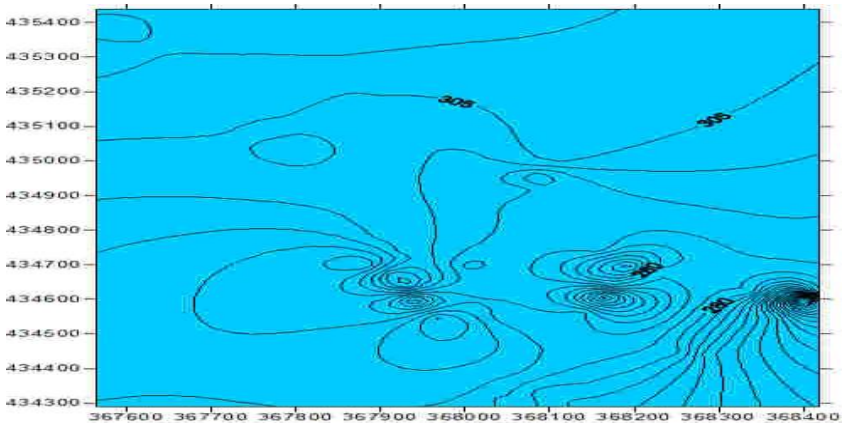

Figure 1 – Contour of the Site

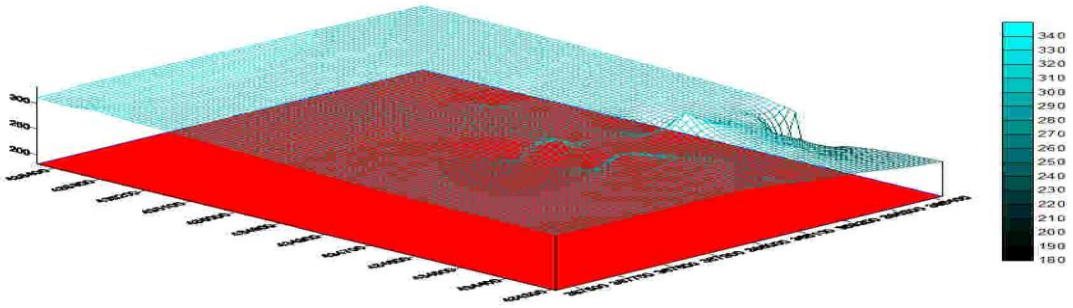

Figure 2 – 3D model of the Site

V.2 Grid Volume Computations

Volume calculations are made using the average end area method and distances along each roadway alignment. For a particular baseline, volume computations may be done for individual roadways, combinations of roadways, or the entire design, and may extend through any baseline station limits. Each volume calculation request generates volume calculations through the limits specified by the user by accessing the appropriate baseline cross section file to get the end area per station (established during the design process) and then determining the volume using the volume
parameters entered with the design data. A mass ordinate file is created as the volumes are calculated. Any design exceptions in the stationing are taken into account in the volume calculations. Corrections for horizontal curvature may be applied to the volume computation as desired.

The determination of earthwork quantities is based upon field crosssections taken in a specified manner before and after excavation. Crosssections are vertical profiles taken at right angles to the survey centerline. Every section is an area formed by the subgrade, the sideslopes, and the original ground surface.

Volumes are computed from cross-section measurements by the average end area method.

$$\text{Volume (metric) (} \quad \text{m3)} = \frac{\left[L \times (A1 + A2)\right]}{2} \qquad (16)$$

Where L is in meters A1 and A2 are in square meters

Specifications require this calculation. All the plans and bidding for the formula for average end areas is accurate only when the end areas are equal. For other cases, the formula generally gives volumes slightly larger than their true values. If applied to a pyramid, for example, the error would be the maximum and would be equal to 50 % of the correct volume.

From fig 2, the minimum upper surface in term of (XYZ) coordinate are (367564.24mN, 434290.11mE, 182.542m), while the maximum is (368418.331mN, 435438.297mE, 332.052m) at an interval of 12m spacing. The grid size is 100 rows by 75 columns. The lower surface is defined by Z value of 165m.

Using Trapezoidal Rule, the total volume of the surface was found to be 128594444.07633m^3. Using Simpson's Rule, the total volume was found to be 128591558.2169m^3. The positive volume (cut) was found to be 128594039.74377m^3, while the net Volume (cut – Fill) was found to be 128594039.74377m^3. The total planar area was found to be 980656.18301705m^2, while the positive Surface Area (cut) was found to be 996019.8002409m^2.

VI. DISCUSSION AND CONCLUSION

Our approach present baseline Static and kinematic GPS positioning by using standard Kalman filter process model. Table 1 is the baseline processed results. Table 2 is the result of the adjusted 3D coordinate of the site investigated. Figure 1 is the contour showing the nature of the terrain. Figure 2 is the presented Digital Terrain Model (DTM). The DTM reveal the area the will needed to be filled and cut. The quantity of material needed was also computed. The contour, 3D model, the area and Volume was derived using SUFFER 8.0 software.

Performance assessment of the measurement system carried during the data acquisition involved the use of three receivers, one control for static model and two rovers for Kinematic model both acquiring data at 5 seconds interval. From the results obtained it can be concluded that GPS observation by combining static and kinematic models gives very high accuracy for 3-D Survey.

REFERENCES

[1]. Andrew W. Sutter, Alan G. Evans (2004). Evaluation of Precise
[2]. Kinematic GPS Point Positioning. Proceedings of the Institute Of Navigation (ION) GNSS-2004 Meeting, Long Beach, California
[3]. Abdel-Salam, M. (2005) "Precise point positing using un-differenced code and carrier phase observation". Ph.D dissertation, Department of Geomatics Engineering, Schulich School of Engineering, University of Calgary, Alberta, Canada.
[4]. Raquet, F. J. (1998) " Development of a method of kinematics GPS carrier phase ambiguity resolution using multiple reference receivers" Ph.D Dissertation, Department of Geomatics Engineering, Schulich School of Engineering, University of Calgary, Alberta Canada.
[5]. Schofield, W. (2009): Engineering Surveying; Theory and Examination Problems for Students, Fifth Edition Kingston University.
[6]. Schofield, W. (1993) "Engineering Surveying". Butterworth –Heinemann Ltd, Oxford.
[7]. Kaplan, E.D. (1996) "Understanding GPS Principles and Application".
[8]. Artech House publishers, Norwood.
[9]. Ehiorobo O.J (2008) " Robustness analysis of a DGPS network for Earth Dam Deformation Monitoring". PhD thesis, department of Civil Engineering, University of Benin, Benin City Nigeria.
[10]. Ehiorobo O.J (2009) " Accuracy of static differential GPS techniques: Implications for structural deformation monitoring" Advanced materials Research, Trans Tech publications switzerland vol 62-64 pp 31-38.
[11]. Gao, Y and Chen, K. (2001) " Improving Ambuiguity Convergence in Carrier Phase Based Precise Point Positioning'', Proceedings 10N, GPS 2001, Salt Lake City, Utah.

International Journal of Modern Engineering Research (IJMER)
www.ijmer.com Vol. 3, Issue. 4, Jul. - Aug. 2013 pp-2296-2312 ISSN: 2249-6645

Optimal Placement of Distributed Generation on Radial Distribution System for Loss Minimisation & Improvement of Voltage Profile

Mohd Ilyas, Syed Mohmmad Tanweer, Asadur Rahman
Al-Falah School of Engineering & Technology, Dhauj, Faridabad, Haryana-121004, INDIA

ABSTRACT: *This project implements the IDENTIFICATION OF OPTIMAL DG LOCATIONS BY SINGLE DG PLACEMENT algorithm. This method first evaluates the voltage profile using the Newton-Raphson method and then it calculates the total I²R loss of the system. After that by placing the DG at each bus, it evaluates the corresponding total I²R losses and hence obtained the optimal placement of DG for loss reduction and best suited voltage profile evaluation.*

I. INTRODUCTION

Over the past few years, developments have been made in finding digital computer solutions for power-system load flows. This involves increasing the reliability and the speed of convergence of the numerical-solution techniques. The characteristics and performance of transmission lines can vary over wide limits mainly dependent on their system. Hence, the load flow method is used to maintain an acceptable voltage profile at various buses with varying power flow. The state of any power system can be determined using load flow analysis that calculates the power flowing through the lines of the system. There are different methods to determine the load flow for a particular system such as: Gauss-Seidel, Newton-Raphson, and the Fast-Decoupled method.

Distributed Generation (DG) is a promising solution to many power system problems such as voltage regulation, power loss, etc. Distributed generation is small-scale power generation that is usually connected to or embedded in the distribution system. Numerous studies used different approaches to evaluate the benefits from DGs to a network in the form of loss reduction.

This project implements the IDENTIFICATION OF OPTIMAL DG LOCATIONS BY SINGLE DG PLACEMENT algorithm. This method first evaluates the voltage profile using the Newton-Raphson method and then it calculates the total I²R loss of the system. After that by placing the DG at each bus, it evaluates the corresponding total I²R losses and hence obtained the optimal placement of DG for loss reduction and best suited voltage profile evaluation.

II. POWER SYSTEM

II.1Introduction: The state of a power system and the methods of calculating this state are very important in evaluating the operation and control of the power system and the determination of future expansion for this system. The state of any power system can be determined using load flow analysis that calculates the power flowing through the lines of the system. There are different methods to determine the load flow for a particular system such as: Gauss-Seidel, Newton- Raphson Load, and the Fast-Decoupled method.

Over the past few years, developments have been made in finding digital computer solutions for power-system load flows. This involves increasing the reliability and the speed of convergence of the numerical-solution techniques. In routine use, even few failures to give first-time convergence for physically feasible problems can be uneconomical.

The characteristics and performance of transmission lines can vary over wide limits mainly dependent on their system. Hence, the load flow method is used to maintain an acceptable voltage profile at various buses with varying power flow.

The transmission system is loop in nature having low R/X ratio. Therefore, the variables for the load−flow analysis of transmission systems are different from that of distribution systems which have high R/X ratio.

II.2 Power System History: The development of the modern day electrical energy system took a few centuries. Prior to 1800, scientists like William Gilbert, C. A. de Coulomb, Luigi Galvani, Benjamin Franklin, Alessandro Volta etc. worked on electric and magnetic field principles. However, none of them had any application in mind. They also probably did not realize that their work will lead to such an exciting engineering innovation. They were just motivated by the intellectual curiosity. In England, Michael Faraday worked on his induction principle between 1821 and 1831. The modern world owes a lot to this genius. Faraday subsequently used his induction principle to build a machine to generate voltage. Around the same time American engineer Joseph Henry also worked independently on the induction principle and applied his work on electromagnets and telegraphs.

For about three decades between 1840 and 1870 engineers like Charles Wheatstone, Alfred Varley, Siemens brothers Werner and Carl etc. built primitive generators using the induction principle. It was also observed around the same time that when current carrying carbon electrodes were drawn apart, brilliant electric arcs were formed. The commercialization of arc lighting took place in the decade of 1870s. The arc lamps were used in lighthouses and streets and rarely indoor due to high intensity of these lights. Gas was still used for domestic lighting. It was also used for street lighting in many cities.

However with the increase in load large voltage and unacceptable drops were experienced, especially at points that were located far away from the generating stations due to poor voltage regulation capabilities of the existing dc

networks. One approach was to transmit power at higher voltages while consuming it at lower voltages. This led to the development of the alternating current.

As a consequence of the electric utility industry deregulation and liberalization of electricity markets as well as increasing demand of electric power, the amount of power exchanges between producer and consumer are increases. In this process, the existing transmission lines are overloaded and lead to unreliable system. The countries like India with increasing demand of electric power day by day it is difficult to expand the existing transmission system due to difficulties in right of way and cost problem in transmission network expansion. So, we need power flow controllers to increasing transmission capacity and controlling power flows.

III. LOSSES IN POWER SYSTEM

III.1 Introduction: In India, average Transmission and Distribution losses, have been officially indicated as 23% of the electricity generated. However, as persample studies carried out by independent agencies, theselosses have been estimated to be as high as 50% in some states. In arecent study carried out by SBI Capital Markets for DVB, the Transmission and Distribution losses have been estimated as 58%. With the setting upof State Regulatory Commissions in the country, accurate estimation ofTransmission and DistributionLosses has gained importance as the level of losses directly affects the sales andpower purchase requirements and hence has a bearing on the determination ofelectricity tariff of a utility by the commission.

III.2. Transmission and Distribution Losses

III.2.1 Losses in Transmission lines: Losses in the transmission lines can be determined less complicated compared to transformers and distribution systems. The basic computation of it usually surrounds to the fundamentals of ohm's law. Due to the simplicity of the transmission lines configuration, solving for its line losses requires no advance knowledge in any electrical principles. However, there are also portion of these line losses that better understanding is necessary.

Total transmission lines losses can be broken down into three relevant parts namely; conductor losses, dielectric heating & radiation losses, and coupling & corona losses.It is because current flows through a transmission line and a line has a finite resistance there is an un-avoidable power loss. This is sometimes called conductor loss or conductor heating loss and is simply a power loss.

Conductor loss depends somewhat on frequency because of a phenomenon called the skin effect. In an AC system, the flow of current in the cross section of the wire is not uniformly distributed. Skin effect tends to make the current flow concentrated more in the outer layer of the conductor. Since a very small area of the wire carries that current, line resistance increases at the same time increases the dissipated power.

Corona is luminous discharge that occurs between the two conductors of a transmission line. When difference of potential between them exceeds the breakdown voltage of the dielectric insulator. Generally when corona occurs the transmission line is destroyed. If the separation between conductors in a metallic transmission line is appreciable fraction of wavelength. The electrostatic and electromagnetic fields that surround the conductor. Cause the line to act as if it were an antenna and transfer energy to any nearby conductive material. The energy radiated is called radiation loss and depends on dielectric material conductor spacing and length of transmission line. It reduces by properly shielding the cable e.g. STP and coaxial has less radiation loss It is also directly proportional to the frequency.

III.2.2. Losses in Distribution lines: The term "distribution line losses" refers to the difference between the amount of energy delivered to the distribution system from the transmission system and the amounts of energy customers' are billed. Distribution line losses are comprised of two types: technical and non-technical .

It is important to know the magnitude and causality factors for line losses because the cost of energy lost is recovered from customers. As a result of the composition and scale of the Hydro One distribution system it is not economic to provide metering and the supporting processes capable of measuring line losses directly. Since energy meters do not total data for the same periods, and load varies over time, a direct measurement of actual losses is not feasible. Instead, Hydro One relies on studies which are designed to calculate the magnitude, composition and allocation of system losses based on annual aggregate metering information for energy purchases, sales and system modeling methods. These studies are conducted with the energy assistance of industry experts in this field to ensure appropriate scientific methods and modeling techniques are utilized in establishing the magnitude, composition and allocation of losses.

III.3. Components of Transmission and Distribution losses

Energy losses occur in the process of supplying electricity to consumers due totechnical and commercial losses. The technical losses are due to energy dissipated in the conductors and equipment used for transmission, transformation,sub-transmission and distribution of power. These technical losses are inherentin a system and can be reduced to an optimum level. The losses can befurther sub grouped depending upon the stage of power transformation &transmission system as Transmission Losses (400kV/220kV/132kV/66kV), asSub transmission losses (33kV /11kV) and Distribution losses (11kV/0.4kv).The commercial losses are caused by pilferage, defective meters, and errors inmeter reading and in estimating unmetered supply of energy.

III.4. Reasons for Transmission and Distribution losses

Experience in many parts of the world demonstrates that it is possible to reduce the losses in a reasonably short period of time and that such investments have a high internal rate of return. A clear understanding on the magnitude of

technicaland commercial losses is the first step in the direction of reducing T&Dlosses. This can be achieved by putting in place a system for accurate energyaccounting. This system is essentially a tool for energy management and helps in breaking down the total energy consumption into all its components. It aims at accounting for energy generated and its consumption by various categories ofconsumers, as well as, for energy required for meeting technical requirement ofsystem elements. It also helps the utility in bringing accountability and efficiency in its working.

III.4.1 Reasons for high technical losses: The following are the major reasons for high technical losses in our country: -

1. Inadequate investment on transmission and distribution, particularly in sub-transmission and distribution. While the desired investment ratiobetween generation and T&D should be 1:1, during the period 1956 -97 itdecreased to 1:0.45. Low investment has resulted in overloading of thedistribution system without commensurate strengthening and augmentation.
2. Haphazard growths of sub-transmission and distribution system with the short-term objective of extension of power supply to new areas.
3. Large scale rural electrification through long 11kV and LT lines.
4. Too many stages of transformations.
5. Improper load management.
6. Inadequate reactive compensation
7. Poor quality of equipment used in agricultural pumping in rural areas, cooler air conditioners and industrial loads in urban areas.

III.4.2 Reasons for commercial losses: Theft and pilferage account for a substantial part of the high transmission and distribution losses in India. Theft / pilferage of energy is mainly committed bytwo categories of consumers i.e. non consumers and bonafide consumers. Antisocial elements avail unauthorized/unrecorded supply by hooking ortapping the bare conductors of L.T. feeder or tampered service wires. Some ofthe bonafide consumers willfully commit the pilferage by way of damaging and / or creating disturbances to measuring equipment installed at their premises. Some of the modes for illegal abstraction or consumption of electricity aregiven below:

1. Making unauthorized extensions of loads, especially those having "H.P." tariff.
2. Tampering the meter readings by mechanical jerks, placement of powerfulmagnets or disturbing the disc rotation with foreign matters.
3. Stopping the meters by remote control.
4. Willful burning of meters.
5. Changing the sequence of terminal wiring.
6. Bypassing the meter.
7. Changing C. T. ratio and reducing the recording.
8. Errors in meter reading and recording.
9. Improper testing and calibration of meters.

IV. LOAD FLOW STUDY

I.1 Introduction: In a three phase ac power system active and reactive power flows from the generating station to the load through different networks buses and branches. The flow of active and reactive power is called power flow or load flow. Power flow studies provide a systematic mathematical approach for determination of various bus voltages, there phase angle active and reactive power flows through different branches, generators and loads under steady state condition. Power flow analysis is used to determine the steady state operating condition of a power system. Power flow analysis is widely used by power distribution professional during the planning and operation of power distribution system.

3.2 Why we use it?

For planning the operation of a power system, its improvement and also its future expansion require following studies such as load flow studies, short circuit studies and stability studies. Load flow studies are used to ensure that electrical power transfer from generators to consumers through the grid system is stable, reliable and economic. Load flow studies are most important of all power system analysis, because these are used in planning studies of power system network to determine if and when specific elements will become overloaded. This is important, as the magnitudes of voltages at every bus are required to be held within a specified limit. The objectives of any load-flow study is to provide the following information-

•Voltage magnitude and phase angle at each bus.

•Real and Reactive power flowing in each element.

Once the bus voltage magnitudes and their angles are computed using the load flow, the real and reactive power flow through each line can be computed. Also based on the difference between power flow in the sending and receiving ends, the line losses in any particular line can also be calculated. It is helpful in determining the best location as well as optimal capacity of proposed generating station, substation and new lines. In the power flow problem, it is assumed that the real power P and reactive power Q at each Load Bus are known. For this reason, Load Buses are also known as PQ Buses. For Generator Buses, it is assumed that the real or active power generated P and the voltage magnitude V is known. For the Slack Bus, it is assumed that the voltage magnitude V and voltage phase angle of the buses are known. In this work Newton Raphson method for load flow is used, because of its reliability towards convergence and not sensitive nature to the starting

solution. In large-scale power flow studies, the Newton raphson has proved most successful because of its strong convergence characteristics.

3.3 Reactive Power: Power factor is defined as the ratio of real power to apparent power. This definition is often mathematically represented as Kw/Kva ,where the numerator is the active (real) power and the denominator is the (active+reactive) or the apparent power
Power Factor = Active power/Apparent power = kW/kVA = Active power/ (Active Power +Reactive Power)
= kW/(kW+kVAr)
The higher kVAr indicates low power factor and vice versa.

3.4 Objective of load flow study: Power flow analysis is very important in planning stages of new networks or addition to existing ones like adding new generator sites, meeting increase load demand and locating new transmission sites.

- The load flow solution gives the nodal voltages and phase angles and hence the power injection at all the buses and power flows through interconnecting power channels.
- It is helpful in determining the best location as well as optimal capacity of proposed generating station, substation and new lines.
- It determines the voltage of the buses. The voltage level at the certain buses must be kept within the closed tolerances.
- System transmission loss minimizes.
- Economic system operation with respect to fuel cost to generate all the power needed
- The line flows can be known. The line should not be overloaded, it means, we should not operate the close to their stability or thermal limits.

3.5 Importance of maintaining bus Voltage Profile in power system: One of the major aims of system operator is to maintain system parameters within feasible operational margin. During certain period of time in a day-load changes very rapidly, especially when it tends to increase, a generalized voltage decrement and stressed conditions for reactive power sources occurs. Maintaining Voltage profile under varying load conditions is need of today under unpredictable load scenario.

3.6 Classification of buses in load flow analysis: For load flow studies it is assumed that the loads are constant and they are defined by their real and reactive power consumption. It is further assumed that the generator terminal voltages are tightly regulated and therefore are constant. The main objective of the load flow is to find the voltage magnitude of each bus and its angle when the powers generated and loads are pre-specified. To facilitate this the different buses of the power system are classified as shown in below.

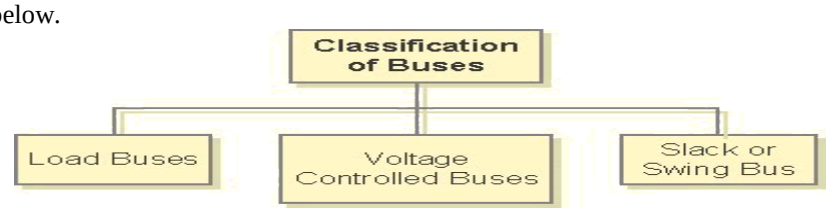

III.6.1 Load Buses (PQ): In these buses no generators are connected and hence the generated real power P_{Gi} and reactive power Q_{Gi} are taken as zero. The load drawn by these buses are defined by real power $-P_{Li}$ and reactive power $-Q_{Li}$ in which the negative sign accommodates for the power flowing out of the bus. This is why these buses are sometimes referred to as ***P-Q bus***. The objective of the load flow is to find the bus voltage magnitude $|V_i|$ and its angle δ_i.

III.6.2 Voltage Controlled Buses (PV): These are the buses where generators are connected. Therefore the power generation in such buses is controlled through a prime mover while the terminal voltage is controlled through the generator excitation. Keeping the input power constant through turbine-governor control and keeping the bus voltage constant using automatic voltage regulator, we can specify constant P_{Gi} and $|V_i|$ for these buses. This is why such buses are also referred to as P-V buses. It is to be noted that the reactive power supplied by the generator Q_{Gi} depends on the system configuration and cannot be specified in advance. Furthermore we have to find the unknown angle δ_i of the bus voltage.

III.6.3 Slack or Swing Bus: Usually this bus is numbered 1 for the load flow studies. This bus sets the angular reference for all the other buses. Since it is the angle difference between two voltage sources that dictates the real and reactive power flow between them, the particular angle of the slack bus is not important. However it sets the reference against which angles of all the other bus voltages are measured. For this reason the angle of this bus is usually chosen as 0°. Furthermore it is assumed that the magnitude of the voltage of this bus is known.

Now considering a typical load flow problem in which all the load demands are known. Even if the generation matches the sum total of these demands exactly, the mismatch between generation and load will persist because of the line I^2R losses. Since the I^2R loss of a line depends on the line current which, in turn, depends on the magnitudes and angles of voltages of the two buses connected to the line, it is rather difficult to estimate the loss without calculating the voltages

and angles. For this reason a generator bus is usually chosen as the slack bus without specifying its real power. It is assumed that the generator connected to this bus will supply the balance of the real power required and the line losses.

IV. Load Flow Solution

IV.1 Introduction: In Power System Engineering, the load flow study (also known as power flow study) is an important tool involving numerical analysis applied to a power system. Unlike traditional circuit analysis , a power flow study uses simplified notation such as a one line diagram and per unit system , and focuses on various forms of AC power (i.e. reactive ,real and apparent) rather than voltage and current. It analyses the power systems in normal steady state operation. There exist a number of software implementations of power flow studies.

IV.2 Formation of y-bus matrix by Direct Inspection method: The method of building network bus admittance and bus impedence matrix involves transformation and inversion of matrices .An alternative method for bus admittance matrix is based on the simple algorithm obtained by inspection of the network inter connections.

Bus admittance is often used in power system studies. In most of the power system studies it is required to form Y-bus matrix of the system by considering certain power system parameters depending upon the type of analysis.

Y-bus may be formed by inspection method, only if there is no mutual coupling between the lines. Every transmission line should be represented by Π -equivalent. Shunt impedances are added to diagonal element corresponding to the buses at which these are connected. The off diagonal elements are unaffected. The equivalent circuit of Tap changing transformer is included while formingY-busmatrix.

Conseder an *n* bus power system (excluding the ground).taking ground as referrance and considering the single phase equivalent of the balanced network.

$$\text{Generalized Y-bus} = \begin{bmatrix} Y_{11} & \cdots\cdots\cdots & Y_{1n} \\ \vdots & \vdots & \vdots \\ Y_{n1} & \cdots\cdots & Y_{nn} \end{bmatrix}$$

Where,
Y_{ii}=Self admittance
Y_{ij}=Transfer admittance

IV.2.1 Flow chart:

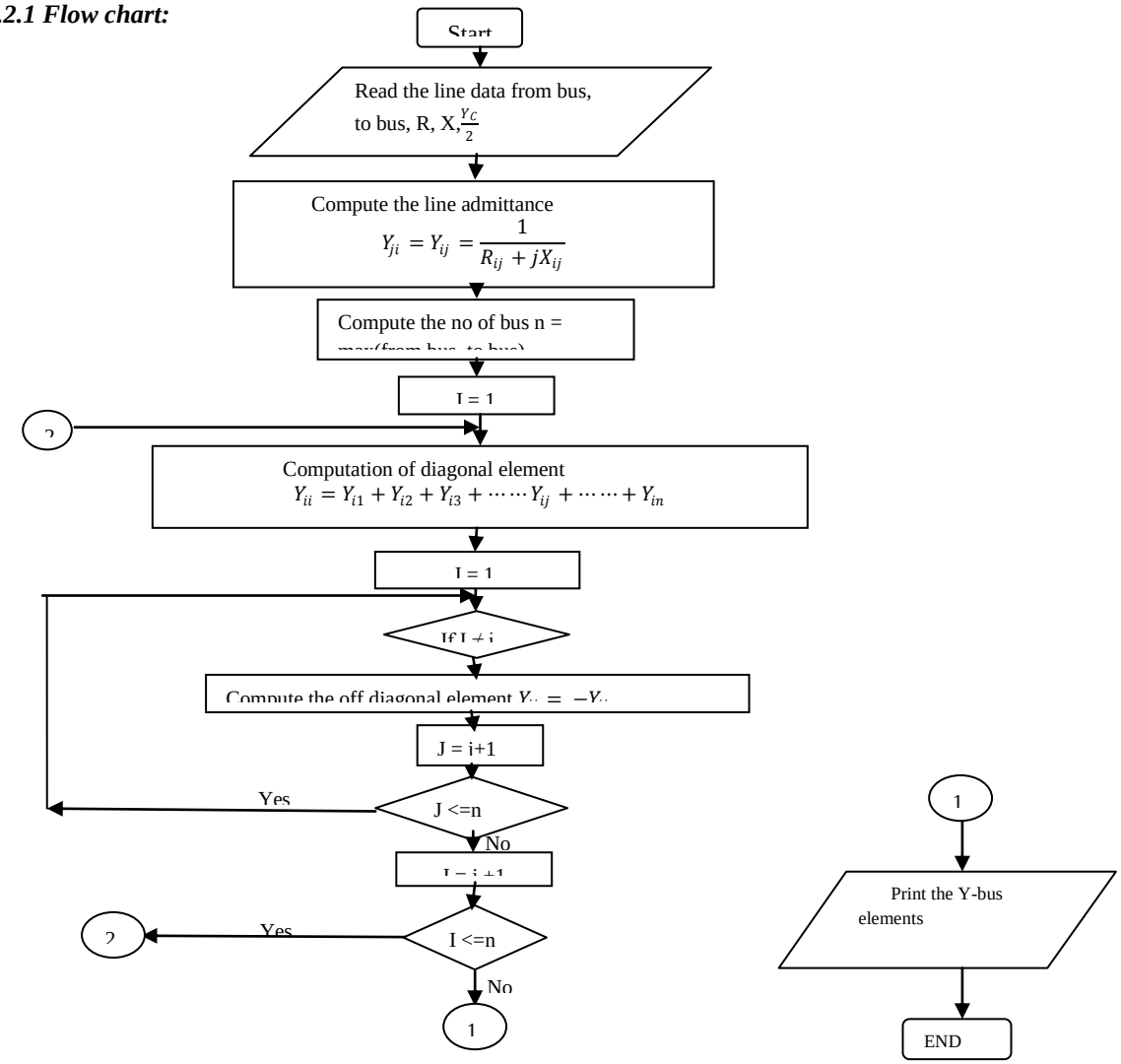

- The diagonal element Yii of the bus admittance matrix is the sum of the admittances of all the elements incident on bus *i* ,including the element between bus *i* and ground.
- The off diagonal element Yii is negative of the admittances of the element connected between buses *i* and *j*.
-

IV.3 Methods of load flow solution: There are mainly three methods for load flow studies:

- Gauss Siedel method
- Newton Raphson method
- Fast decoupled method

IV.3.1 Gauss Seidel Method: The Gauss seidel method is a iterative algorithm for solving non linear algebraic equations.An initial solution vector is assumed,choosen from the past experience,statistical data or from practical considerations.At every subsequent iteration ,the solution is updated till the convergence is reached.

IV.3.1.1 Steps for Gauss Seidal method: **Step 1**: Initially assume all the buses are PQ buses,except the slack bus.This means that the (n-1) complex bus voltages have to be determined.
Step 2:The Slack bus is generally numbered one.
Step 3:PV buses are numbered in sequence and PQ buses are ordered next in sequence.
From the equation of complex power we have,

$Si^*=Vi^*(\sum_{k=1}^{n} YikVk)$
Or, $Pi-jQi=Vi^*(\sum_{k=1}^{n} YikVk)$
Or, $\frac{Pi-jQi}{Vi*}=(\sum_{k=1}^{n} YikVk)$
Or, $\frac{Pi-jQi}{Vi*}=YiiVi+\sum_{\substack{k=1\\k\neq 1}}^{n} YikVk$
Or, $Vi=\frac{1}{Yii}*[\frac{Pi-jQi}{Vi*}-\sum_{\substack{k=1\\k\neq 1}}^{n} YikVk]$.....(a)

Above equation is an implicit equation,since the unknown variables appears on the both sides of the equation.Hence it needs to be solved by an iteration technique.

IV.3.1.2 Algorithm For Gauss Seidel Method: **Step1**: Prepare the required data.
Step2: Formulate the Ybus matrix by the method of direct inspection.
Step3: Assume initial voltages for all buses i= 2,3,4....n., (assume i=1 slack bus)
Step4: The complex bus voltagesand all n-1 buses(except the slack bus) are taken $1.0\angle 0\ p.u$.This is normally called a flat start.
Step5: Update the voltages in any (r+1)thiterations.The voltages are given by

$\mathbf{Vi(r+1)=\frac{1}{Yii}*[\frac{Pi-jQi}{Vi*}-\sum_{k=1}^{i-1} YikVk(r+1)-\sum_{k=i+1}^{n} YikVk(r)}$....(1)

Step6: Continue the iterations till

$|\Delta Vi(r+1)|=|Vi(r+1)-Vi(r)|<\in$

Where $\in$ is the tolerance value..Generally we use 0.0001 p.u.
Step7: Compute slack bus power after voltages have conversed using

$\mathbf{Si^*=Vi^*(\sum_{k=1}^{n} YikVk)}$

Step8: Compute all line flows of a line (or transformer) between the buses.

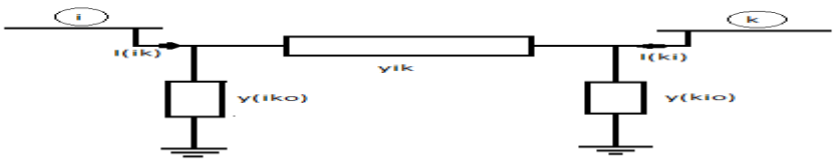

The figure represents the π model of a transmission line or a transformer. Here

I(ik)=(Vi-Vk)y(ik)+Vi*y(iko)
I(ki)=(Vk-Vi)y(ik)+Vk*y(iko)
S(ik)=ViI(ik)*
S(ki)= VkI(ki)*

The complex power loss in the line is given by S(ik)+S(ki). The total loss in the system is calculated by summing the loss over all the lines.

IV.3.1.3 Gauss Seidel method when p-v buses are present: Some of the buses in an n-bus power system are voltage controlled buses where real power(P) and bus voltage value(|V|) are specified,but reactive power Qi and voltage angle δ are unknown.Hence it is necessary to first make an estimate of Qi.We can find the value of Qi by using the following equation- $Qi= -Im\{Vi^*\sum_{k=1}^{n} YikVk\}$
Where ,Im stands for imaginary part.

At any (r+1)thiteration,at the ith PV bus

Qi(r+1)= -Im{(Vi(r))*$\sum_{k=1}^{i-1} YikVk(r+1) + (Vi(r)) * \sum_{k=i}^{n} YikVk(r)$} .....(2))

The steps for ith PV bus are as follows:

Step1: Compute Qi(r+1) , using equation (2)

Step2:Calculate Vi using equation (1) with Qi = Q i(r+1)

Step3:Since |Vi| is specified at the PV bus,the magnitude of Vi obtained in step 2 has to be modified and set to the specified value |Vi,sp|.Therefore,

Vi(r+1)=|Vi,sp|$\frac{Vi(r+1)}{|Vi(r+1)|}$

Stated another way,

Vi(r+1)=|Vi,sp|$\angle\delta i(r+1)$

The voltage computation for PQ buses doesnot change.

IV.3.1.4 Q-limit violations : If the limit of reactive power i.e. the Q limit is violated at voltage controlled bus or PV buses during any iteration(say,(r+1)th iteration at ith bus),the Q value is either less than the minimum Q value(Qi,min) or greater than the maximum Q value(Qi,max).It means that the voltage cannot be maintained at the specified value due to the lack of reactive power support.This bus is then treated as a PQ bus in the (r+1)th iteration and the voltage is calculated with the value of Qi set as follows:

If Qi<Qi,min then Qi=Qi,min

If Qi>Qi,max then Qi=Qi,max

If in the subsequent iteration, Qi falls within the limits, the bus can be switched back to PV status.

IV.3.1.5 Acceleration of convergence: The number of iterations increases with the increase in the size of the system, while we use Gauss Seidel method. The number of iterations required can be reduced if the correction in voltage at each bus is accelerated, by multiplying with a constant α.$\alpha$is called the acceleration factor.

In the (r+1)th iteration we can write,

Accelerated Vi(r+1)=Vi(r)+α(Vi(r+1)-Vi(r)),

Where, α is a real number.When α=1, the value of Vi(r+1) is the computed value. If 1< α <2, then the value computed is extrapolated.Generally, α is taken between 1.6 to 2.0.A wrong value may lead to divergence of the solution.

At PQ buses (pure load buses) if the voltage magnitude violates the limit.It simply means that the specified reactive power demand cannot be supllied, with the voltage maintained within acceptable limits.

IV.3.1.6 Flow Chart for Gauss-Seidal method:

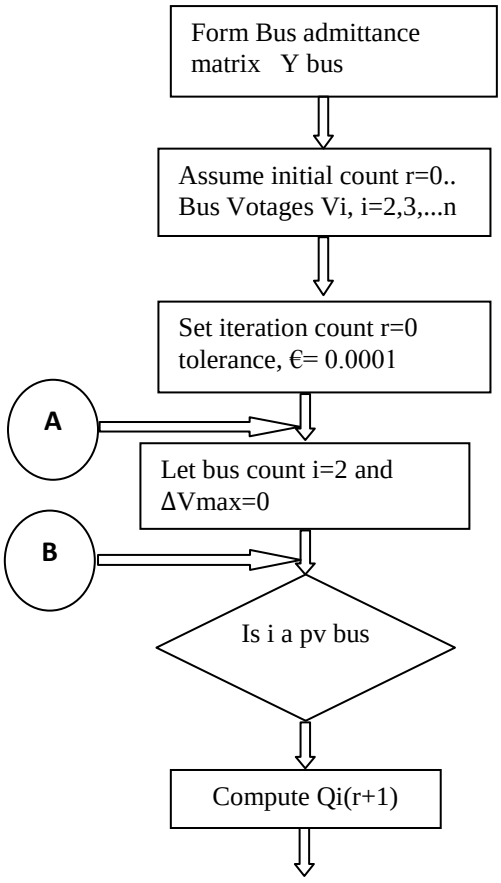

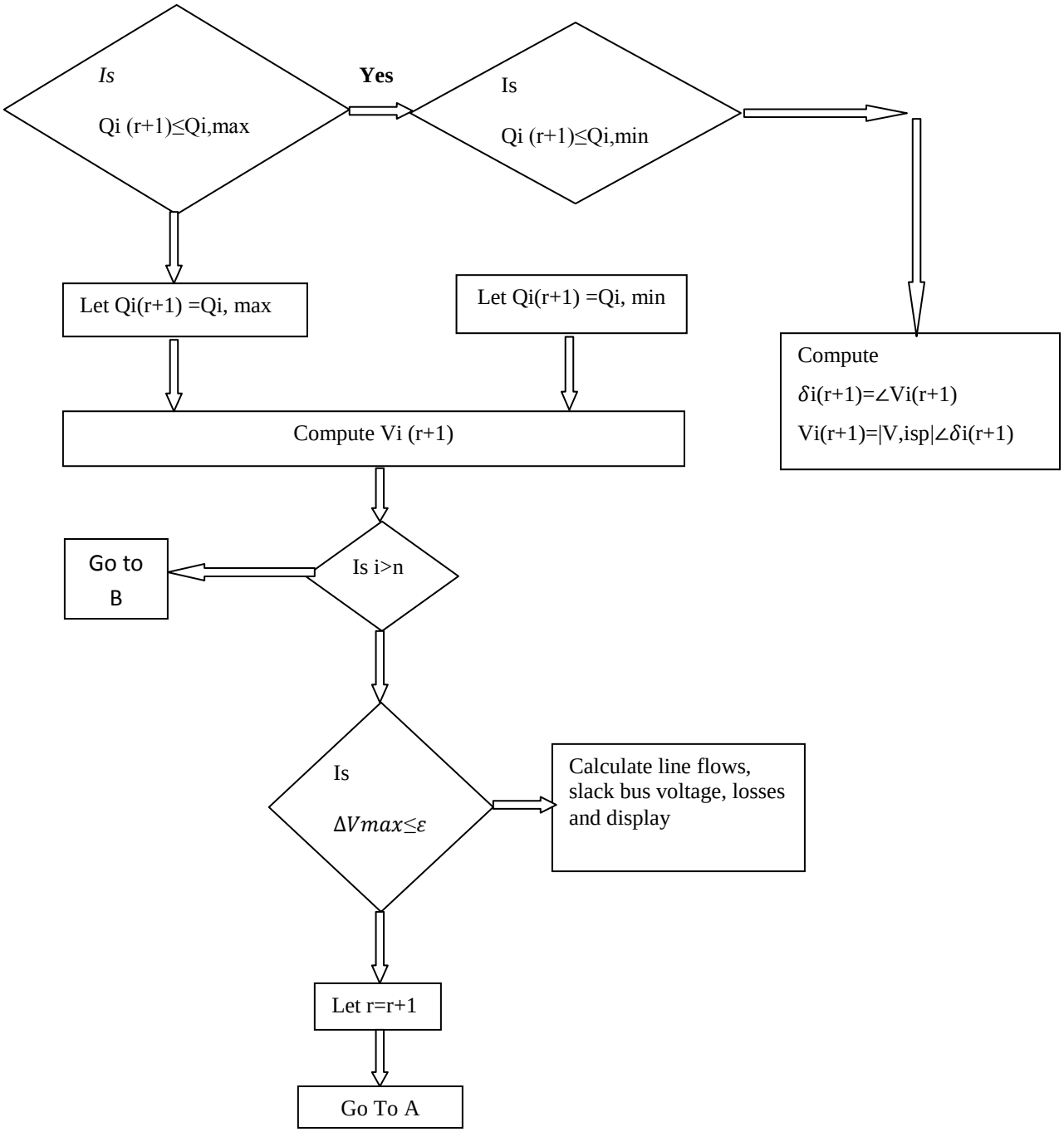

IV.3.2 Newton Raphson Method: In application of the NR method,we have to first bring the equations to be solved to the form f(x1,x2,...xn)=0,where x1,x2..xn are the unknown variables to be determined.Let us assume that the power system has n1 PV buses and n2 PQ buses.In polar co ordinates the unknown variable to be determined are.

IV.3.2.1 Steps for Newton-Raphson method: **Step1**: δi the angle of the complex bus voltage at bus i,at all the PV and PQ buses.This gives us n1+n2 unknown variables to be determined.

Step2: |Vi|, the voltage magnitude of bus i, at all PQ buses.This gives us n2 unknown variables to be determined.

Therefore the total number of unknown variables to be computed is n1+2n2 for which we n1+2n2 consistent equations to be solved. The equations to be solved are given by

$\Delta Pi = Pi,sp - Pi,cal = 0$

$\Delta Qi = Qi,sp - Qi,cal = 0$

Where,

ΔP =Active power residue

ΔQ= reactive power residue

Pi,sp =specified active power at bus i

Qi,sp =Specified reactive power at bus i

Pi, cal=calculated value of active power using voltage estimates
Qi, cal=calculated value of reactive power using voltage estimates

IV.3.2.2 Algorithm for N-R method: **Step1**: Formulate Bus Admittance Matrix Y bus.
Step2: Assume initial voltages as follows
Vi=|Vi, sp|∠0 (at all PV Buses) where Vi,sp=Specified voltage value
Vi=1∠0 (at all PQ buses)
Step3: At (r+1)th iteration calculate Pi(r+1),at all the PV and PQ Buses and calculate Qi(r+1) at all the PQ buses using Vi(r) values.
The formulae to be used are
Pi,cal=Gii$|Vi|^2 + \sum_{\substack{k=1 \\ k\neq i}}^{n} |Vi||Vk|(Gik * cos\,\delta ik + Bik * sin\delta ik)$
Qi,cal= Bii$|Vi|^2 + \sum_{\substack{k=1 \\ k\neq i}}^{n} |Vi||Vk|(Gik * sin\,\delta ik - Bik * cos\delta ik)$
Step4: Calculate the power mismatches i.e. Power residues
$\Delta Pi(r) = Pi, sp - Pi, cal(r+1)$ (at PV and PQ buses)
$\Delta Qi(r) = Qi, sp - Qi, cal(r+1)$ (at PQ buses)
Step5: Calculate the Jacobian [J(r)] using Vi(r)
Step6: Compute $\begin{matrix}\Delta\delta(r) \\ \frac{\Delta|V(r)|}{|V|}\end{matrix} = \frac{1}{[J(r)]} * \begin{matrix}\Delta P(r) \\ \Delta Q(r)\end{matrix}$
Step7:Update the variables as follows-
$\delta i(r+1) = \delta i(r) + \Delta\delta i(r)$ (at all buses)
|Vi(r+1)|=|Vi|(r)+Δ$|Vi|(r)$
Step8: Go to step 3 and iterate till the the power mismatches are within the acceptable limits.

3.3.2.3 Formation of Jacobian:

$$\begin{bmatrix} \vdots \\ \Delta P_n^o \\ \vdots \\ - - - \\ \vdots \\ \Delta Q_n^o \\ \vdots \end{bmatrix} = \begin{bmatrix} \vdots & \vdots & \vdots & \vdots & \vdots & \vdots & \vdots & \vdots & \vdots & \vdots & \vdots \\ \vdots & \frac{\partial P_n}{\partial \delta_{n-1}} & \frac{\partial P_n}{\partial \delta_n} & \frac{\partial P_n}{\partial \delta_{n+1}} & \vdots & \vdots & \vdots & \frac{\partial P_n}{\partial |V_{n-1}|} & \frac{\partial P_n}{\partial |V_n|} & \frac{\partial P_n}{\partial |V_{n+1}|} & \vdots \\ \vdots & \vdots & \vdots & \vdots & \vdots & \vdots & \vdots & \vdots & \vdots & \vdots & \vdots \\ - & - - - & - - - & - - - & - & - - & - - & - - - & - - - & - - - & - \\ \vdots & \vdots & \vdots & \vdots & \vdots & \vdots & \vdots & \vdots & \vdots & \vdots & \vdots \\ \vdots & \frac{\partial Q_n}{\partial \delta_{n-1}} & \frac{\partial Q_n}{\partial \delta_n} & \frac{\partial Q_n}{\partial \delta_{n+1}} & \vdots & \vdots & \vdots & \frac{\partial Q_n}{\partial |V_{n-1}|} & \frac{\partial Q_n}{\partial |V_n|} & \frac{\partial Q_n}{\partial |V_{n+1}|} & \vdots \\ \vdots & \vdots & \vdots & \vdots & \vdots & \vdots & \vdots & \vdots & \vdots & \vdots & \vdots \end{bmatrix} \begin{bmatrix} \Delta\delta_{n-1}^o \\ \Delta\delta_n^o \\ \Delta\delta_{n+1}^o \\ - - - \\ \Delta|V_{n-1}|^o \\ \Delta|V_n|^o \\ \Delta|V_{n+1}|^o \end{bmatrix}$$

There are some formulas given below for making the Jacobian in NR load flow method. theseare...
1) $\frac{\partial Pi}{\partial \delta i}$= -Qi-Bii$|Vi|^2$
2) $\frac{\partial Pi}{\partial \delta k}$= $|Vi||Vk|(Gik * \sin\delta ik - Bik * cos\delta ik)$
3) $\frac{\partial Pi}{\partial Vk}|Vk|$= $|Vi||Vk|(Gik * cos\delta ik + Bik * \sin\delta ik)$
4) $\frac{\partial Pi}{\partial |Vi|}|Vi|$ = Pi+Gii$|Vi|^2$
5) $\frac{\partial Qi}{\partial \delta i}$= Pi-Gii$|Vi|^2$
6) $\frac{\partial Qi}{\partial \delta k} = -|Vi||Vk|(Gik * cos\delta ik + Bik * \sin\delta ik)$
7) $\frac{\partial Qi}{\partial |Vi|}|Vi|$ = Qi-Bii$|Vi|^2$
8) $\frac{\partial Qi}{\partial |Vi|}|Vk| = |Vi||Vk|(Gik * \sin\delta ik - Bik * cos\delta ik)$

IV.3.2.4 Flow Chart for Newton Raphson method

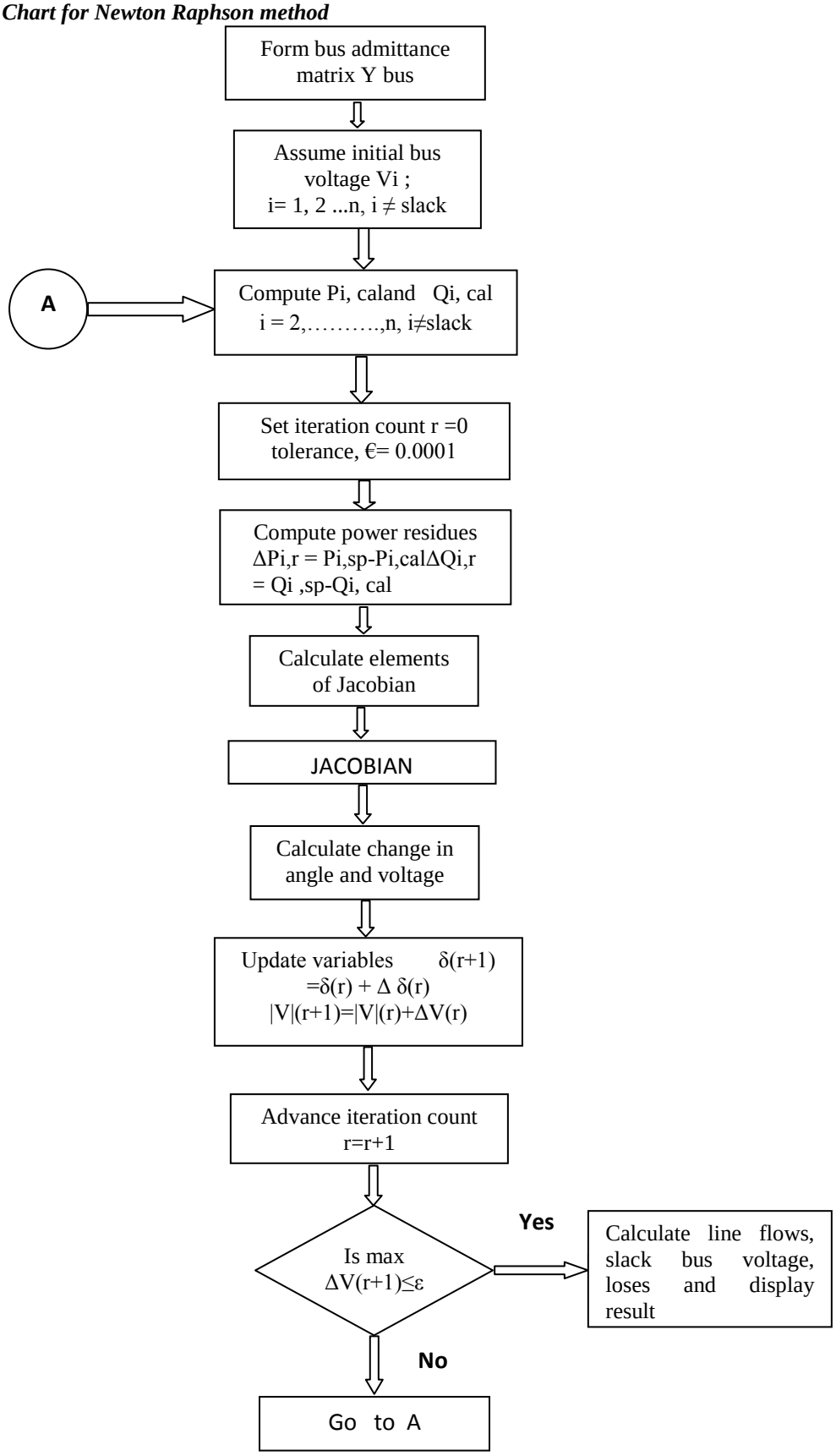

IV.3.3 Fast Decoupled method

If the co efficient matrices are constant,the need to update the jacobian at every iteration is eliminated.This has resulted in development of fast decoupled load flow.Assumptions used in this method are-

- $B_{ij} \gg G_{ij}$ (Since,the X/R ratio of transmission lines is high in well desighned system.
- Real power changes are less sensitive to voltage magnitude changes and are most sensitive to changes in phase angle $\Delta\delta$.

i.e $\cos(\delta_i - \delta_j) \approx 1$ and $\sin(\delta_i - \delta_j) \approx 0$

- Similarly, reactive power changes are less sensitive to changes in angle and are mainly dependent on changes in voltage magnitude.
- Therefore the element of theJacobian matrix become

$$H_{ik} = L_{ik} = -|Vi||Vk|Bik(i \neq k)$$
$$H_{ii} = L_{ii} = -Bii|Vi|^2$$

With this value we can perfom the load flow analysis by taking less time.

V. DISTRIBUTED GENERATION

V.1 Introduction to Distributed Generation

What is Distributed Generation?

Distributed generation is an approach that employs small-scale technologies to produce electricity close to the end users of power. DG technologies often consist of modular (and sometimes renewable-energy) generators, and they offer a number of potential benefits. In many cases, distributed generators can provide lower-cost electricity and higher power reliability and security with fewer environmental consequences than can traditional power generators. Distributed generation, also called on-site generation, dispersed generation, embedded generation, decentralized generation, decentralized energy or distributed energy, generates electricity from many small energy sources. Distributed generation reduces the amount of energy lost in transmitting electricity because the electricity is generated very near where it is used, perhaps even in the same building. This also reduces the size and number of power lines that must be constructed.

In contrast to the use of a few large-scale generating stations located far from load centers--the approach used in the traditional electric power paradigm--DG systems employ numerous, but small plants and can provide power onsite with little reliance on the distribution and transmission grid. DG technologies yield power in capacities that range from a fraction of a kilowatt [kW] to about 100 megawatts [MW]. Utility-scale generation units generate power in capacities that often reach beyond 1,000 MW.

Distributed generation takes place on two-levels: the local level and the end-point level. Local level power generation plants often include renewable energy technologies that are site specific, such as wind turbines, geothermal energy production, solar systems (photovoltaic and combustion), and some hydro-thermal plants. These plants tend to be smaller and less centralized than the traditional model plants. They also are frequently more energy and cost efficient and more reliable. Since these local level DG producers often take into account the local context, the usually produce less environmentally damaging or disrupting energy than the larger central model plants.

V.2 Benefits of Distributed Generation

What are the Potential Benefits of DG Systems?

Consumer advocates who favor DG point out that distributed resources can improve the efficiency of providing electric power. They often highlight that transmission of electricity from a power plant to a typical user wastes roughly 4.2 to 8.9 percent of the electricity as a consequence of aging transmission equipment, inconsistent enforcement of reliability guidelines, and growing congestion. At the same time, customers often suffer from poor power quality—variations in voltage or electrical flow—that results from a variety of factors, including poor switching operations in the network, voltage dips, interruptions, transients, and network disturbances from loads. Overall, DG proponents highlight the inefficiency of the existing large-scale electrical transmission and distribution network. Moreover, because customers' electricity bills include the cost of this vast transmission grid, the use of on-site power equipment can conceivably provide consumers with affordable power at a higher level of quality. In addition, residents and businesses that generate power locally have the potential to sell surplus power to the grid, which can yield significant income during times of peak demand.

Beyond efficiency, DG technologies may provide benefits in the form of more reliable power for industries that require uninterrupted service. The Electric Power Research Institute reported that power outages and quality disturbances cost American businesses $119 billion per year. In 2001, the International Energy Agency (2002) estimated that the average cost of a one-hour power outage was $6,480,000 for brokerage operations and $2,580,000 for credit card operations. The figures grow more impressively for the semiconductor industry, where a two hour power outage can cost close to $48,000,000. Given these numbers, it remains no mystery why several firms have already installed DG facilities to ensure consistent power supplies.

Perhaps incongruously, DG facilities offer potential advantages for improving the transmission of power. Because they produce power locally for users, they aid the entire grid by reducing demand during peak times and by minimizing congestion of power on the network, one of the causes of the 2003 blackout. And by building large numbers of localized power generation facilities rather than a few large-scale power plants located distantly from load centers, DG can contribute to deferring transmission upgrades and expansions—at a time when investment in such facilities remains constrained. Perhaps most important in the post-September 11 era, DG technologies may improve the security of the grid.

Environmentalists and academics suggest that DG technologies can provide ancillary benefits to society. Large, centralized power plants emit significant amounts of carbon monoxide, sulfur oxides, particulate matter, hydrocarbons, and nitrogen oxides.

Finally, DG can help the nation increase its diversity of energy sources. Some of the DG technologies, such as wind turbines, solar photovoltaic panels, and hydroelectric turbines, consume no fossil fuels, while others, such as fuel cells,

microturbines, and some internal combustion units burn natural gas, much of which is produced in the United States. The increasing diversity helps insulate the economy from price shocks, interruptions, and fuel shortages

V.3 Usage of Distributed Generation

How Much are Renewable and DG Systems Used in the American Electric Utility Sector?

Despite the immense environmental, technical, and financial promise of renewable energy systems, such generators still constitute a very small percentage of electricity generation capacity in the United States. Throughout the 1970s, some policy experts expected renewable energy systems to be used for much more generation capacity than they have. Dr. Arthur Rosenfeld, one of the five CEC commissioners serving from 2002 until the present, noted that President Carter had told him (during his presidency in the late 1970s) that he expected renewable energy systems to reach 10 percent of national electricity capacity by 1985. However, Carter's expectation went unfulfilled: excluding large hydroelectric generators, renewable energy technologies in 2003 comprised only about 2 percent of the U.S. electricity generation mix

The relatively minor use of renewable energy systems has created a general attitude among energy analysts, scholars, and laboratory directors that the technologies are not viable sources of electricity supply. For example, RodeySobin, former Innovative Technology Manager for the Virginia Department of Environmental Quality, argues that "in many ways, renewable energy systems were the technology of the future, and today they still are." Ralph D. Badinelli, a professor of Business Information Technology at Virginia Tech, explains that renewable energy technologies do not contribute significantly to U.S. generation capacity because "such sources have not yet proven themselves … Until they do, they will be considered scientific experiments as opposed to new technologies." Similarly, Mark Levine, the Environmental Energy Technologies Division Director at the Lawrence Berkeley National Laboratory, comments that despite all of the hype surrounding renewable energy, such systems are still only "excellent for niche applications, but the niches aren't large."

DG/CHP technologies have an only slightly better record. In 2004, the Energy Information Administration characterized only 3.1 percent of electricity generation capacity as commercial or industrial combined heat and power (33,217 MW out of 1.49 terrawatts [TW]). The EIA also estimated that in 2002 only 0.9 gigawatts (GW) of distributed generation capacity existed in the United States. Similarly, the EIA's 2005 Annual Energy Outlook projected that CHP systems are not widely used in the electric power sector, amounting to 0.053% of utility generation (197 billion kWh out of 3,700 billion kWh). Tom Casten, the Chair and Chief Executive Officer of Primary Energy, a manufacturer of fuel processing cogeneration steam plants, notes that even though CHP plants can reduce energy costs for industrial firms by over 40 percent, such plants remain "the exception instead of the rule."

V.4 Distriduted Generation in our system

5.4.1 Algorithm: The computational steps involved in finding the optimal Distribution Generator (DG) size and location to minimize the loss in a radial distribution system are summarized in following:

1. Perform the load flow analysis by using Newton Raphson method for determining the voltage profile and Total Loss for Radial Distribution system.
2. In load flow analysis obtain the branch current I_{ij} between two buses by using ,

$$I_{ij}=\frac{V_i-V_j}{R_{ij}}$$ Where, $V_i = Voltage\ of\ bus\ i$, $V_j = Voltage\ of\ bus\ j$, $R_{ij} = Resistance\ between\ bus\ i\ and\ j$

3. Obtain the active component, I_a and reactive component, I_r of the branch currents I_{ij}.
4. We calculate total I_a^2R loss by using,

$P_L = \sum_{i=1}^{n} I_i^2 R_i$

Where, $P_{La} = \sum_{i=1}^{n} I_{ai}^2 R_{ij}$ Due to active component of the current,

$P_{Lr} = \sum_{i=1}^{n} I_{ri}^2 R_{ij}$ Due to reactive component of the current,

5. We calculate the power loss P_{La}^{new} associated with the active component of branch current when DG is connected.It is given by

$P_{La}^{new} = \sum_{i=1}^{n} (I_{ai} + D_i I_{DG})^2 R_i$ where D_i=1; if branch i$\epsilon\alpha$

=0,otherwise

$'\alpha'$ is the set of branches connected between the source and the bus m where DG is placed.

6. Repeat **steps 1** to **steps 5** and calculate P_{La}(new) by placing DG at each bus.

7. Calculate the power saving by applying the formula given below

S=P_{La}-P_{La}^{new}

8. The DG current IDG that provides maximum saving can be obtained from

$\frac{\partial S}{\partial I_{DG}}$= -2$\sum_{i=1}^{n} (D_i I_{ai} + D_i I_{DG})\, R_i$=0

9.Calculate DG current for maximum power saving and is given by

$I_{DG} = -\frac{\sum_{i\epsilon\alpha} IaiRi}{\sum_{i\epsilon\alpha} Ri}$

10.Calculate the corresponding DG Size to be placed at each bus ,is given by

At Bus m,

P_{DG}=$V_m I_{DG}$, where V_m is the Voltage Magnitude of Bus 'm'

11.Update the active power component

$P_{new} = P_{GEN} + P_{DG} - P_{LOAD}$

12. Perform load flow analysis with updated active power component obtained in **step 11**.

13. Perform the **step 10** to **step 12 ,** and record the Voltage Profiles and Total line loss.

14. Obtain the Optomal location of Distributed Generation (DG) for Total line loss minimization and Voltage profile improvement.

V.4.2 Flow Chart

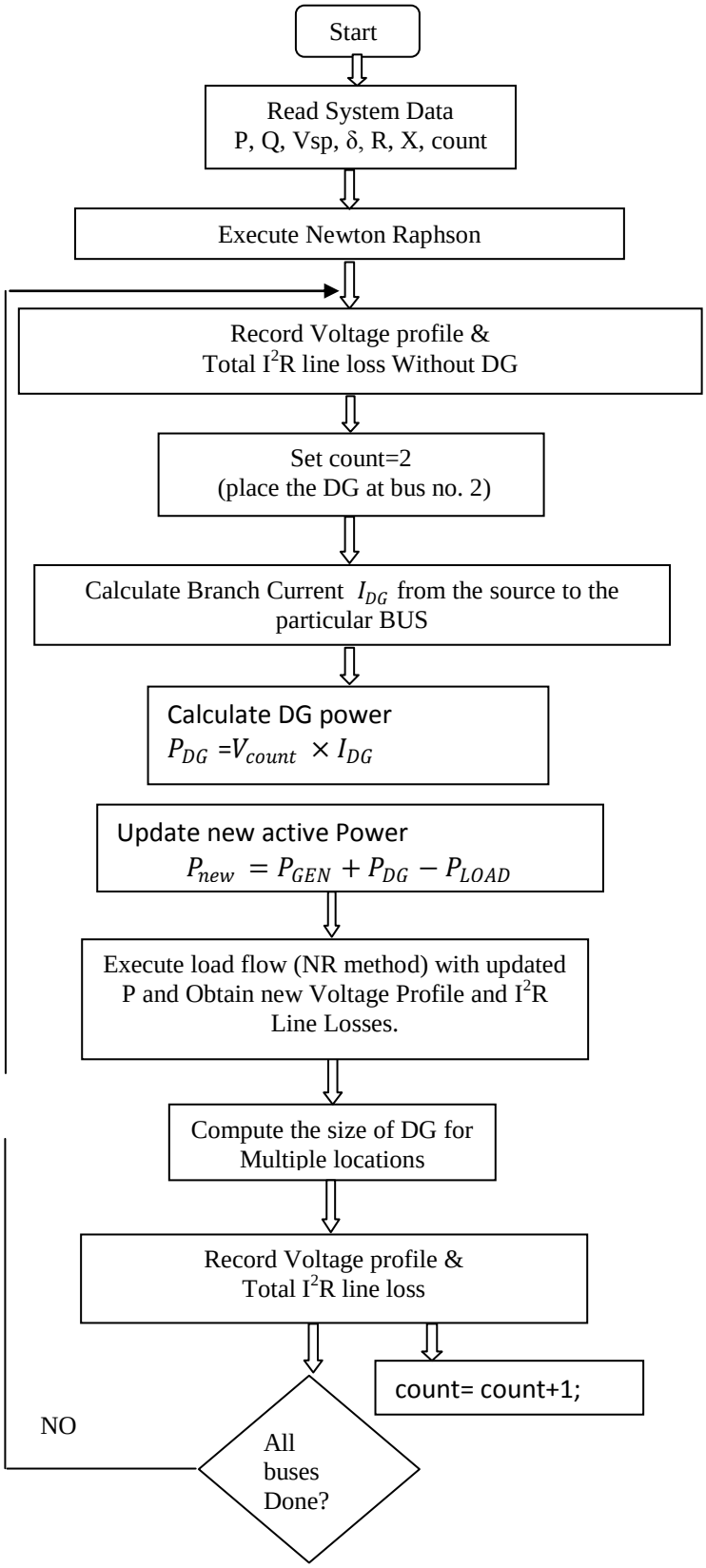

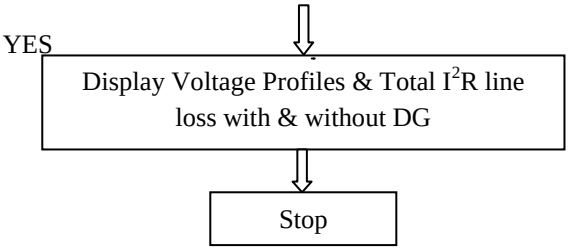

VI. TEST SYSTEM AND RESULTS

VI. 1 Test System (12-BUS Radial System)

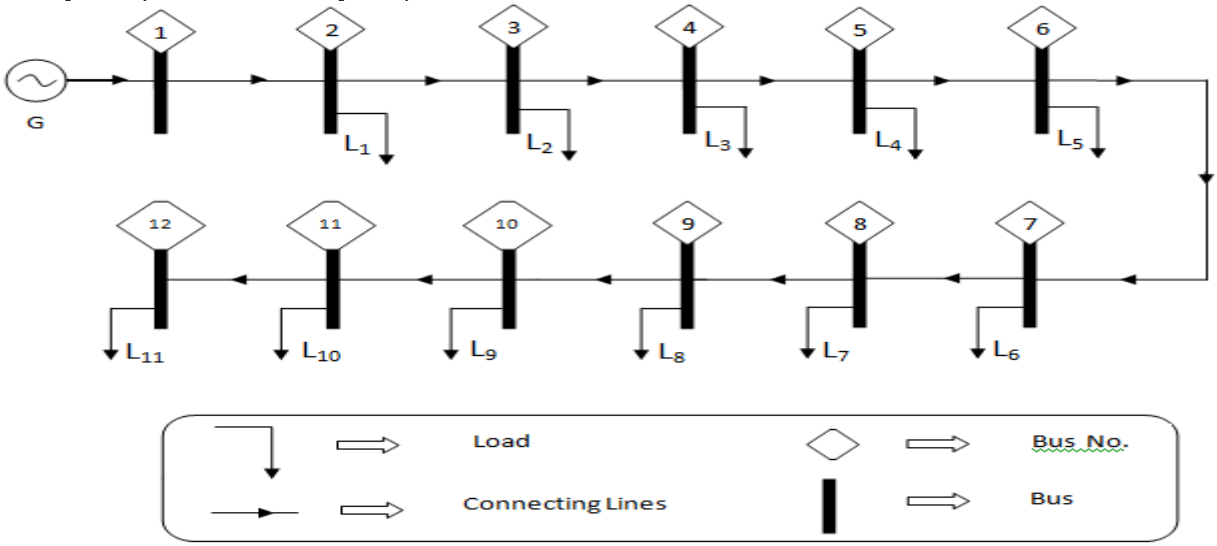

Figure: *A Radial Distribution Line with connecting Loads*

Number of buses in the system = 12
Number of slack bus = 1
Number of PV buses = 11
Number of PQ buses = 0
Number of lines in the system = 11
Maximum convergence value = 0.0001
Base value = 1000
Coding used for Buses:
Slack Bus – 1; PV Bus – 2; PQ Bus – 3

VI.1.1 SPECIFICATION OF TEST SYSTEM:

Bus	Type	Vsp (in pu)	Power angle	PGi (in kW)	QGi (in kVAR)	PLi (in kW)	QLi (in kVAR)
1	1	1.06	0	0	0	0	0
2	3	1	0	0	0	60	60
3	3	1	0	0	0	40	30
4	3	1	0	0	0	55	55
5	3	1	0	0	0	30	30
6	3	1	0	0	0	20	15
7	3	1	0	0	0	55	55
8	3	1	0	0	0	45	45
9	3	1	0	0	0	40	40
10	3	1	0	0	0	35	30
11	3	1	0	0	0	40	30
12	3	1	0	0	0	15	15

VI.1.2 LINE DATA:

From Bus	To Bus	Resistence, R (in Ω)	Reactance, X (in Ω)
1	2	1.093	0.455
2	3	1.184	0.494
3	4	2.095	0.873

4	5	3.188	1.329
5	6	1.093	0.455
6	7	1.002	0.417
7	8	4.403	1.215
8	9	5.642	1.597
9	10	2.890	0.818
10	11	1.514	0.428
11	12	1.238	0.351

VII. RESULTS & DISCUSSIONS

Performing the experiment in MATLAB Environment for Optimal Placement of DG with loss minimization technique and Voltage Profile improvement, we are having the results as described below:

1. Optimal Placement of DG for Loss Minimization:

For finding the optimal location of DG for Total Loss Minimization we placed single DG at each Bus and Total loss obtained in each step is compared as such.

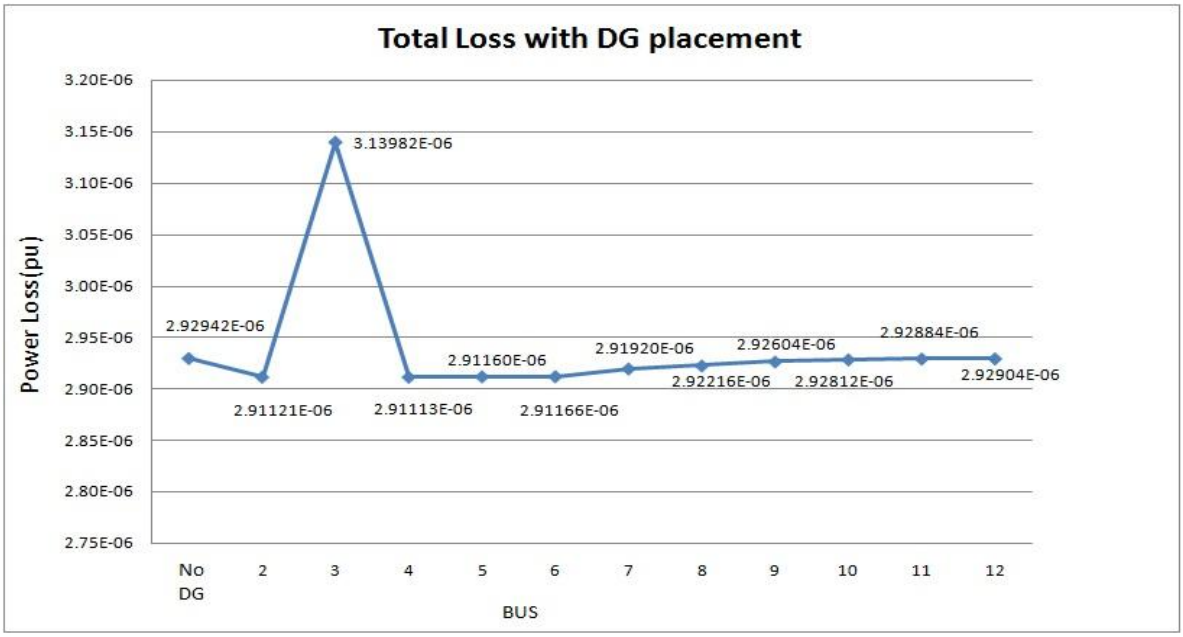

Fig: Optimal DG location for Total Line Loss minimization

- From the graph we observe that when we place DG at BUS No. 4 the Total Line Loss compared to DG placement at other buses is minimum. The Elapsed time for execution of the MATLAB program is 0.385176 seconds with total line loss = $2.91113X10^{-6}$ p.u.
- So, we can suggest that for Total Line Loss reduction in our test system, the optimal location for the single DG placement is at BUS No. 4

2. Optimal Placement of Voltage Profile Improvement:

For finding the optimal location of DG for Voltage Profile improvement we placed single DG at each Bus and compared the obtained voltage profile with the reference value (1 p. u)

		DG at										
	No DG	bus 2	bus 3	bus 4	bus 5	bus 6	bus 7	bus 8	bus 9	bus 10	bus 11	bus 12
BUS 1	1.06000	1.06000	1.06000	1.06000	1.06000	1.06000	1.06000	1.06000	1.06000	1.06000	1.06000	1.06000
BUS 2	1.00412	1.00430	1.00212	1.00430	1.00429	1.00429	1.00422	1.00419	1.00415	1.00413	1.00413	1.00412
BUS 3	1.00498	1.00516	1.00285	1.00516	1.00515	1.00515	1.00508	1.00505	1.00501	1.00499	1.00498	1.00498
BUS 4	1.00685	1.00704	1.00457	1.00704	1.00703	1.00703	1.00695	1.00692	1.00688	1.00686	1.00685	1.00685
BUS 5	1.01059	1.01078	1.00813	1.01078	1.01078	1.01078	1.01069	1.01065	1.01061	1.01059	1.01059	1.01058
BUS 6	1.01187	1.01207	1.00938	1.01207	1.01206	1.01206	1.01197	1.01193	1.01189	1.01187	1.01187	1.01186
BUS 7	1.01266	1.01286	1.01016	1.01286	1.01285	1.01285	1.01276	1.01272	1.01268	1.01266	1.01266	1.01265
BUS 8	1.02096	1.02116	1.01900	1.02115	1.02114	1.02114	1.02107	1.02102	1.02097	1.02095	1.02095	1.02095
BUS 9	1.03394	1.03409	1.03220	1.03408	1.03408	1.03408	1.03401	1.03398	1.03394	1.03393	1.03392	1.03392
BUS 10	1.04034	1.04047	1.03863	1.04046	1.04046	1.04046	1.04040	1.04037	1.04034	1.04032	1.04032	1.04032
BUS 11	1.04272	1.04285	1.04102	1.04284	1.04284	1.04284	1.04278	1.04275	1.04272	1.04271	1.04271	1.04270
BUS 12	1.04341	1.04353	1.04171	1.04353	1.04352	1.04352	1.04347	1.04343	1.04341	1.04340	1.04339	1.04339

Table: Voltage Profile before and after placing DG

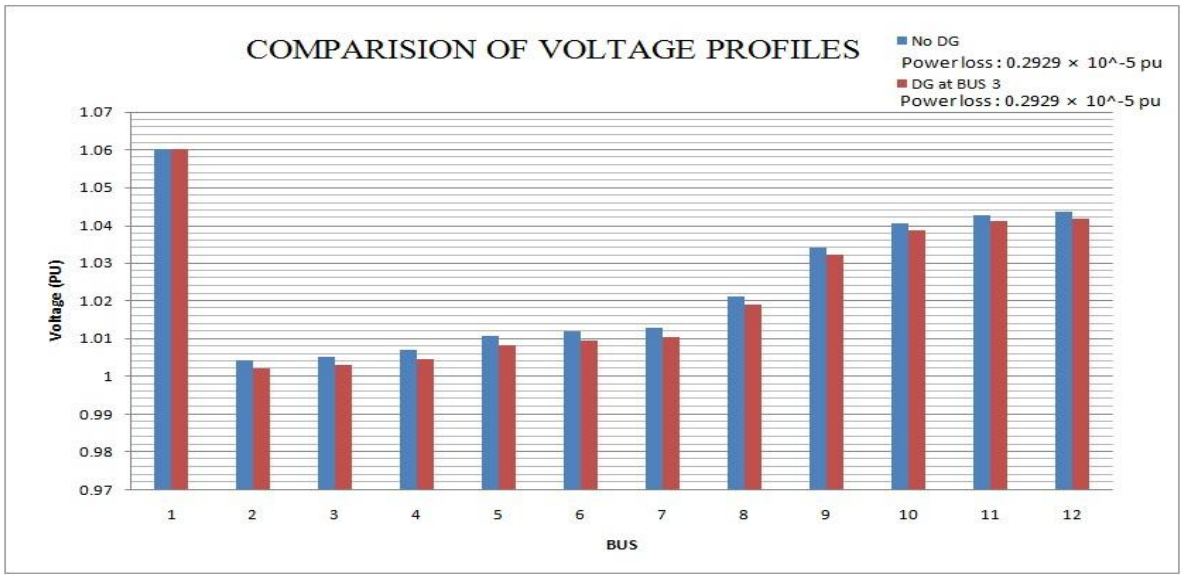

Figure: Optimal DG location for Voltage Profile improvement

[1]. In the graph Blue bar represents the voltage profile of the 12 Bus radial distribution system without DG placement and Red bar represents the voltage profile after placing the DG at bus no. 3

[2]. Comparing the two Voltage Profiles with reference value (1 pu), we observed that , when the DG is placed at Bus No. 3 the obtained voltage is much nearer to the reference value.

REFERENCES

[1]. Halpin, S. M. Power Quality. In: Grigsby, L. L. *The Electric Power Engineering Handbook*. United State of America: CRC Press LLC. Chap. 15: 1-26. 2001.

[2]. Santoso, Surya and Grady, W. M. Understanding Power System Harmonics. *IEEE Power Engineering Review*. 2001. 21 (11): 8-11.

[3]. Galli, W., Skvarenina, T. L., Chowdhury, B. H. and Akagi, H. Power Quality and Utility Interface Issues. In: Skvarenina, T. L. *The Power Electronics Handbook*. United State of America: CRC Press LLC. Chap. 17: 1-48. 2002.

[4]. Akagi, Hirofumi. Trends in Active Power Line Conditioners. *IEEE Transactions on Power Electronics.* 1994. 9 (3): 263-268.

[5]. Clemmensen, J. M. Estimating the Cost of Power Quality. *IEEE Spectrum*.1993. 40-41.

[6]. Bhavaraju, V. B. *Analysis and Design of Some New Active Power Filters for Power Quality Enhancement*. Ph.D. Thesis. Texas A&M University;1994.

[7]. Akagi, Hirofumi. Active Filters for Power Conditioning. In Timothy L.Skvarenina. *The Power Electronics Handbook: Industrial Electronics Series*. United State of America: CRC Press. Chap. 17:30-63. 2002.

[8]. Peng, F. Z., Akagi, H. and Nabae, A. A Novel Harmonics Power Filter.*IEEE Transactions on Power Electronics Specialists Conference*. April 11-14. PESC '88 Record: IEEE. 1988. 1151-1159.

[9]. Akagi, Hirofumi. New Trends in Active Filters for Power Conditioning. *IEEE Transactions on Industry Application.* 1996. 32 (6): 1312-1322.

[10]. Casaravilla, G, Salvia, A., Briozzo, C. and Watanabe, E. Control Strategies of Selective Harmonics Current Shunt Active Filter. *IEE Proc.- Generation, Transmission and Distribution*.2002. 149 (6): 689-694.

[11]. Grady, W. M., Samotyi, M. J. and Noyola, A. H. Survey of Active Line Conditioning Methodologies. *IEEE Transactions on Power Delivery*.1990. 5 (3): 1536-1542.

[12]. Bhattacharya S. and Divan D., "Synchronous frame based controller implementation for a hybrid series active filter system," IEEE Conf. On Industry applications, vol.4,(1995):pp. 2531–2540

[13]. Lin C. E., Su W. F., Lu S. L, Chen C. L., and Huang C. L., "Operation strategy of hybrid harmonic filter in demand-side system," IEEE-IAS Annul. Meeting, Industry applications, (1995):pp. 1862–1866.

[14]. Dahono P.A, "New hysteresis current controller for single-phase bridge inverters" IET journal on Power electronics, vol.2 (2009):pp. 585-594.

[15]. Hongyu Li., Fang Zhuo, Zhaoan Wang, Lei W. and Wu L., "A novel time domain current detection algorithm for shunt active power filters" IEEE Trans. power systems, vol.20, (2005):pp. 644–651.

[16]. Buso S., Malesani L., Mattavelli P. and Veronese R., "Design and fully digital control of parallel active filters for thyristor rectifier to comply with ICE 1000-3-2 standard" IEEE Trans. Ind. Applicat., vol. 34, (1998):pp. 508–517.

[17]. B.O. Slim, Braha A. and Ben saoud s. "Hardware design and Implementation of digital controller for Parallel Active Filters" IEEE Conf. Design and test of integrated systems in nanoscale technology, (2006): pp. 331-334.

[18]. Haque, M. T. and Ise, T. Implementation of Single Phase pq Theory. *Proceedings of the Power Conversion Conference 2002.* April 2-5. Japan. PCC Osaka: IEEE. 2002. 761-765.

[19]. Bhattacharya S., Divan, and B. Benejee, "Synchronous Reference Frame Harmonic Isolator Using Series Active Filter", 4th European Power Electronic Conf., Florence, Vol. 3, (1991):pp.30-35.

[20]. Ching-Tsai Pan and Ting-Yu Chang, **"**An Improved hysteresis current controller for reducing switching frequency" IEEE Trans. Power Electronics, vol. 9, (1994): pp.97-104.

[21]. B. K. Bose, "An adaptive hysteresis band current control technique of a voltage feed PWM inverter for machine drive system", IEEE Trans. Ind. Electron. vol.37, (1990):pp. 402–406.

[22]. Kale M. and Ozdemir E. "An adaptive hysteresis band current controller for shunt active power filter" Electrical power sys.

Research.Vol.73, (2005): pp.113-119.
[23]. Zeliang Shu, Yuhun Guo, Jisan Lian "Steady state and dynamic study of active power filter with efficient FPGA based control algorithm" IEEE Trans. Industrial Electronics, vol. 55, (2008),pp. 1527-1536.
[24]. Angelo Baggini. 'Hand book of power quality', John Wiley and Sons, Ltd
[25]. Narain G. Hingoranl, Laszlo Gyugyi. 'Understanding FACTS', A John Wiley & Sons, Inc., Publication.
[26]. Hirofumi Akagi, Edson Hirokazu Watanabe, Mauricio Aredes. 'Instantaneous power theory and applications to power conditioning', A John Wiley & Sons, Inc., Publication.
[27]. Kim Y.S., Kim, J.S., Ko S.H., "Three-phase Three-wire series active power filter, which compensates for harmonics and reactive power" IET Journals, Electric Power Applications, Vol.151, (2004):pp.276-282.
[28]. Hafner J., Aredes M., Heumann K., "A shunt active power filter applied to high voltage distribution lines" IEEE Trans. Power delivery, Vol.12, (1997):pp.266-272.
[29]. Sangsun Kim, Enjeti P.N, "A new hybrid active power filters (APF) topology" IEEE Trans. Power Electronics, vol.17, (2002):pp.48-58.
[30]. Grino, R., Cardoner R., Costa-Castello R., Fossas E, "Digital repetitive control of a Three- phase four-wire shunt active filter" IEEE Trans. Industrial Electronics, Vol. 54, (2007):pp.1495-1503.
[31]. Karuppanan P., Mahapatra K.K., "PLL with fuzzy logic controller based shunt active power filter for harmonic and reactive power compensation" IEEE Conference, IICPT, Power Electronics, (2011):pp.1-6.
[32]. V. S. C. Raviraj and P. C. Sen "Comparative Study of Proportional–Integral, Sliding Mode, and Fuzzy Logic Controllers for Power Converters" IEEE Trans. Industry Applications, Vol. 33, (1997):pp. 518-524.
[33]. C. N. Bhende, S. Mishra, and S. K. Jain "TS-Fuzzy-Controlled Active Power Filter for Load Compensation" IEEE Trans. Power Delivery, Vol. 21, (2006):pp. 1459-1465.
[34]. Computer techniques and Models in Power Systems by K. Uma Rao **(Book)**
[35]. Electrical Power Systems by C. L. Wadhwa **(Book)**
[36]. http://ethesis.nitrkl.ac.in/2464/1/load_flow_in_power_system.pdf **(Internet)**
[37]. Optimal DG Placement for Maximum Loss Reduction in Radial distribution System Using ABC Algorithm **(IEEE Journal)**

Bibliography

Mr. Mohammad Ilyas is working in Department EEE of Al-falah school of Engg & Tech as a assistant prof since twelve Years & serving to the community . He did his graduation Electrical Engg in 1999 and M-Tech in Electrical power system Management From Jamia Milia Islamia University New Delhi in 2010 and now perusing Ph D From Maharishi Dayanand University. He attended many national & international seminars & work shop.

Mr. Syed Mohmmad Tanweer is student of M-Tech Power system in Department of EEE, Al-falah school of Engg & Tech (MDU) . He did his graduation in Electrical & Electronics in 2009 from Bju Patnaik University of Technology. He is author of SENSORS & TRANSDUCERS & attended many national seminars & workshops at IIT ROORKEE & IIT MUMBAI.

Mr. Asadur Rahman
B. TECH (EEE), M. TECH (PESE) NIT-SILCHAR,
Worked as Asst. Prof. at G.I.M.T, Guwahati (Assam), EE Dept. (Aug'2011 to July'2013)
Presently pursuing Ph.D in the dept. of Electrical Engineering, NIT-SILCHAR.

International Journal of Modern Engineering Research (IJMER)
www.ijmer.com Vol. 3, Issue. 4, Jul. - Aug. 2013 pp-2313-2316 ISSN: 2249-6645

Live Streaming With Receiver-Based P2P Multiplexing for Future IPTV Network

Md. Amanatulla[1], G. Sri Devi[2], Syed Sadat Ali[3]
[1]*M. Tech (CSE), Nimra College of Engineering & Technology, Vijayawada, A.P., India*
[2]*Assoc.Professor, Dept.of CSE, Nimra College of Engineering & Technology, Vijayawada, A.P., India*
[3]*Professor, Dept.of CSE, Nimra College of Engineering & Technology, Vijayawada, A. P., India*

ABSTRACT: *Future broadcast network concentrates on IPTV (Internet Protocol TeleVision). The main hurdle in IPTV is streaming of audio and video signals. A number of commercial systems are built to study and analyze the behaviour of live streaming of audio and video signals. Peer to Peer multiplexing (P2P) provides a good solution for this problem. In this paper a variation of P2P multiplexing is proposed which is called as receiver based P2P multiplexing. To analyze the performance of the proposed multiplexing techniques the very famous European network "Zatto" is considered. This paper also describes the network architecture of Zatto and uses the data collected from the provider to evaluate the performance of the proposed variation in P2P multiplexing.*

KEYWORDS: *IPTV, Live Streaming, Peer to Peer Multiplexing.*

I. INTRODUCTION

Current generation broadcast network for TV is DTH which will be slowly replaced by the next generation Internet Protocol Television (IPTV) network. There is an emerging market for IPTV. Numerous commercial systems now offer services over the Internet that is similar to traditional over-the-air, cable, or satellite TV. Live television, time-shifted programming, and content-on-demand are all presently available over the Internet. Increased broadband speed, growth of broadband subscription base, and improved video compression technologies have contributed to the emergence of these IPTV services [1][6]. IPTV systems deliver video and audio channels to viewing devices by switching a single channel to multiple sources. IP Television networks are primarily constructed of computer servers, gateways, access connections and end user display devices. Servers control the overall system access and processing of channel connection requests and gateways convert the IP television network data to signals that can be used by television media viewers.

Content aggregation is the process of combining multiple content sources for distribution through other communication channels. A head end is part of a television system that selects and processes video signals for distribution into a television distribution network. The core network is the central network portion of a communication system. The core network primarily provides interconnection and transfer between edge networks. An access network is a portion of a communication network (such as the public switched telephone network) that allows individual subscribers or devices to connect to the core network. A premises distribution network (PDN) consists of the equipment and software that are used to transfer data and other media in a customer's facility or home. A viewing device is a combination of hardware and software that can convert media such as video, audio or images into a form that can be experienced by humans. The network archicture of IPTV is shown in Fig1.

Peer to peer multiplexing is mainly used for Live streaming of video and audio. User draw a distinction between three uses of peer-to-peer (P2P) [1] networks: delay-tolerant file download of archival material, delay-sensitive progressive download (or streaming) of archival material, and real-time live streaming. In the first case, the completion of download is elastic, depending on available bandwidth in the P2P network. The application buffer receives data as it trickles in and informs the user upon the completion of download. The user can start playing back the file for viewing in the case of a video file. Bit torrent and variants are examples of delay-tolerant file download systems. In the second case, video playback starts as soon as the application assesses it has sufficient data buffered that, given the estimated download rate and the playback rate, it will not deplete the buffer before the end of file. If this assessment is wrong, the application would have to either pause playback or rebuffed or slow down playback. While users would like playback to start as soon as possible, the application has some degree of freedom in trading off playback start time against estimated network capacity. Most video-on-demand systems are examples of delay-sensitive progressive-download application. The third case, real-time live streaming has the most stringent delay requirement. While progressive download may tolerate initial buffering of tens of seconds or even minutes, live streaming generally cannot tolerate more than a few seconds of buffering. Taking into account the delay introduced by signal ingest and encoding, and network transmission and propagation, the live streaming system can introduce only a few seconds of buffering time end-to-end and still be considered ―live‖ . The Zattoo peer-to-peer live streaming system was a free-to-use network serving over 3 million registered users in eight European countries at the time of study, with a maximum of over 60 000 concurrent users on a single channel. The system delivers live streams using a receiver-based, peer-division multiplexing scheme.

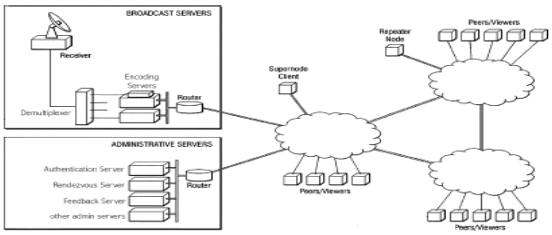

Fig. 1 Architecture of IPTV

To ensure real-time performance when peer uplink capacity is below requirement, Zattoo subsidizes the network's bandwidth requirement, as described in. After delving into Zattoo's architecture in detail, large-scale measurements collected during the live broadcast of the UEFA European Football Championship, one of the most popular one-time events in Europe, in June 2008 [5]. During the course of that month, Zattoo served more than 35 million sessions to more than 1 million distinct users.

II. SYSTEM ARCHITECTURE

The Zattoo system rebroadcasts live TV, captured from satellites, onto the Internet. The system carries each TV channel on a separate peer-to-peer delivery network and is not limited in the number of TV channels it can carry. Although a peer can freely switch from one TV channel to another, thereby departing and joining different peer-to-peer networks, it can only join one peer-to-peer network at any one time. Users are required to register themselves at the Zattoo Web site to download a free copy of the Zattoo player application. To receive the signal of a channel, the user first authenticates itself to the Zattoo *Authentication Server*. Upon authentication, the user is granted a ticket with limited lifetime. The user then presents this ticket, along with the identity of the TV channel of interest, to the Zattoo *Rendezvous Server*. If the ticket specifies that the user is authorized to receive signal of the said TV channel, the Rendezvous Server returns to the user a list of peers currently joined to the P2P network carrying the channel, together with a signed channel ticket. If the user is the first peer to join a channel, the list of peers it receives contain only the Encoding Server. The user joins the channel by contacting the peers returned by the Rendezvous Server, presenting its channel ticket, and obtaining the live stream of the channel from them. Zattoo uses the Reed–Solomon (RS) error correcting code (ECC) for forward error correction [2]. The RS code is a systematic code: of the n packets sent per segment, k<n packets carry the live stream data, while the remainder carries the redundant data [3]. Due to the variable-bit rate nature of the data stream, the time period covered by a segment is variable, and a packet may be of size less than the maximum packet size.

III. RECEIVER BASED P2P MULTIPLEXING

A. P2P Multiplexing

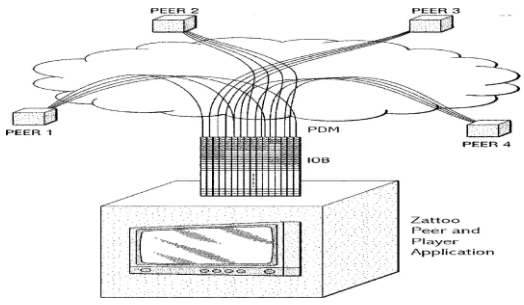

Fig 2. Peer system with an IOB

FWhen a new peer requests to join an existing peer, it specifies the substream(s) it would like to receive from the existing peer [4]. These substreams do not have to be consecutive. Contingent upon availability of bandwidth at existing peers, the receiving peer decides how to multiplex a stream onto its set of neighboring peers, giving rise to our description of the Zattoo live streaming protocol as a receiver-based, peer-division multiplexing protocol. To minimize per-packet processing time of a stream, the Zattoo protocol sets up a virtual circuit with multiple fan outs at each peer. When a peer joins a TV channel, it establishes a peer-division multiplexing (PDM) scheme among a set of neighboring peers by building a virtual circuit to each of the neighboring peers. Baring departure or performance degradation of a neighbor peer, the virtual circuits are maintained until the joining peer switches to another TV channel. With the virtual circuits set up, each packet is forwarded without further per-packet handshaking between peers. The PDM establishment process consists of two phases: the *search* phase and the *join* phase. *Search Phase:* To obtain a list of potential neighbors, a joining peer sends out a SEARCH message to a random subset of the existing peers returned by the Rendezvous Server. The SEARCH message contains the substream indices for which this joining peer is looking for peering relationships. The joining peer continues to wait for SEARCH replies until the set of potential neighbors contains at least a minimum number of peers, or until all SEARCH replies have been received. *Join Phase:* Once the set of potential neighbors is established, the joining peer sends JOIN requests to each potential neighbor. The JOIN request lists the substreams for which the joining peer would like to construct virtual circuit with the potential neighbor.

B. Stream Management: The IOB is referenced by an *input pointer*, a *repair pointer*, and one or more *output pointers*. The input pointer points to the slot in the IOB where the next incoming packet with sequence number higher than the highest

sequence number received so far will be stored. The repair pointer always points one slot beyond the last packet received in order and is used to regulate packet retransmission and adaptive PDM [3] as described later. Different peers may request for different numbers of, possibly nonconsecutive, substreams. To accommodate the different forwarding rates and regimes required by the destinations, we associate a packet map and forwarding discipline with each output pointer. Fig. 3 shows the packet map associated with an output peer pointer where the peer has requested substreams 1, 4, 9, and 14. Every time a peer pointer is repositioned to the beginning of a sub-buffer of the IOB, all the packet slots of the requested substreams are marked NEEDed and all the slots of the substreams not requested by the peer are marked SKIP. When a NEEDed packet arrives and is stored in the IOB, its state in the packet map is changed to READY. As the peer pointer moves along its associated packet map, READY packets are forwarded to the peer and their states changed to SENT. A slot marked NEEDed but not READY, such as slot n+4

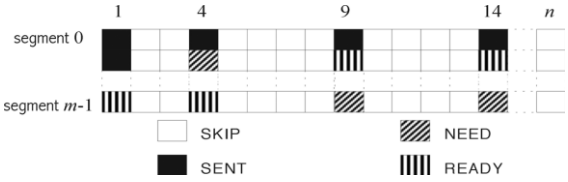

Fig. 3 Packet Map Associated with peer map

In addition to achieving lossless recording, we use retransmission to let a peer recover from transient network congestion. A peer sends out a retransmission request when the distance between the repair pointer and the input pointer has reached a threshold of R packet slots, usually spanning multiple segments. A retransmission request consists of an R bit packet mask, with each bit representing a packet, and the sequence number of the packet corresponding to the first bit. Marked bits in the packet mask indicate that the corresponding packets need to be retransmitted. When a packet loss is detected, it could be caused by congestion on the virtual circuits forming the current PDM or congestion on the path beyond the neighboring peers. In either case, current neighbor peers will not be good sources of retransmitted packets.

C. Adaptive PDM: Peers on the Zattoo network can redistribute a highly variable number of substreams, reflecting the high variability in uplink bandwidth of different access network technologies [7]. For a full-stream consisting of 16 *constant*-bit rate substreams, our prior study showed that based on realistic peer characteristics measured from the Zattoo network, half of the peers can support less than half of a stream, 82% of peers can support less than a full-stream, and the remainder can support up to 10 full streams (peers that can redistribute more than a full stream is conventionally known as supernodes in the literature) [5]. With variable- bit rate streams, the bandwidth carried by each substream is also variable. To increase peer bandwidth usage, without undue degradation of service, we instituted measurement-based admission control at each peer. In addition to controlling resource commitment, another goal of the measurement-based admission control module is to continually estimate the amount of available uplink bandwidth at a peer.

The amount of available uplink bandwidth at a peer is initially estimated by the peer sending a pair of probe packets to Zattoo's Bandwidth Estimation Server. Once a peer starts forwarding substreams to other peers, it will receive from those peers quality-of-service feedbacks that inform its update of available uplink bandwidth estimate. A peer sends quality-of-service feedback only if the quality of a substream drops below a certain threshold [9]. Upon receiving quality feedback from multiple peers, a peer first determines if the identified substreams are arriving in low quality. If so, the low quality of service may not be caused by limit on its own available uplink bandwidth—in which case, it ignores the low quality feedbacks. Otherwise, the peer decrements its estimate of available uplink bandwidth. If the new estimate is below the bandwidth needed to support existing number of virtual circuits, the peer closes a virtual circuit. To reduce the instability introduced into the network, a peer closes first the virtual circuit carrying the smallest number of sub streams. Each peer on the Zattoo network is assumed to serve a user through a media player, which means that each peer must receive, and can potentially forward, all sub streams of the TV channel the user is watching. The limited redistribution capacity of peers on the Zattoo network means that a typical client can contribute only a fraction of the sub streams that make up a channel. This shortage of bandwidth leads to a global bandwidth deficit in the peer-to-peer network. In the Zattoo system, two separate centralized collector servers collect usage statistics and error reports, which we call the ―stats‖ server and the ―user-feedback‖ server respectively.The ―stats‖ server periodically collects aggregated player statistics from individual peers, from which full session logs are constructed and entered into a session database. The session database gives a complete picture of all past and present sessions served by the Zattoo system. A given database entry contains statistics about a particular session, which includes join time, leave time, uplink bytes, download bytes, and channel name associated with the session. Receiver based multiplexing ensures error free and feedback based server in Zatoo collects the feedback and tries to reduce the delay in data delivery.

IV. CONCLUSION

A receiver-based, peer-division multiplexing engine to deliver live streaming content on a peer-to-peer network. The same engine can be used to transparently build a hybrid P2P/CDN delivery network by adding Repeater nodes to the network. By analyzing a large amount of usage data collected on the network during one of the largest viewing events in Europe, we have shown that the resulting network can scale to a large number of users and can take good advantage of available uplink bandwidth at peers. We have also shown that error-correcting code and packet retransmission can help improve network stability by isolating packet losses and preventing transient congestion from resulting in PDM reconfigurations.

REFERENCES

[1]. R. auf der Maur, ―Die Weiterverbreitung von TV- und Radioprogrammenüber IP-basierte Netze,‖ in Entertainment Law, F. d. Schweiz, Ed., 1st ed. Bern, Switzerland: Stämpfli Verlag, 2006.
[2]. Euro2008,‖ UEFA [Online]. Available: http://www1.uefa.com/ [3] S. Lin and D. J. Costello Jr., Error Control Coding, 2nd ed. Englewood Cliffs, NJ: Pearson Prentice-Hall, 2004.
[3]. S. Xie, B. Li, G. Y. Keung, and X. Zhang, ―CoolStreaming: Design, theory, and practice,‖ IEEE Trans. Multimedia, vol. 9, no. 8, pp. 1661–1671, Dec. 2007.
[4]. K. Shami et al., ―Impacts of peer characteristics on P2PTV networks scalability,‖ in Proc. IEEE INFOCOM, Apr. 2009, pp. 2736–2740.
[5]. Bandwidth test statistics across different countries,‖ Bandwidth- Test.net [Online]. Available: http://www.bandwidth-test. net/stats/country/
[6]. X. Hei, C. Liang, J. Liang, Y. Liu, and K. W. Ross, ―Insights into PPLive: A measurement study of a large-scale P2P IPTV system,‖ in Proc. IPTV Workshop, Int. World Wide Web Conf., May 2006.
[7]. B. Li et al., ―An empirical study of flash crowd dynamics in a P2Pbased live video streaming system,‖ in Proc. IEEE GLOBECOM, 2008, pp. 1–5.
[8]. J. Rosenberg et al., ―STUN—Simple traversal of User Datagram Protocol (UDP) through network address translators (NATs),‖ RFC 3489, 1993.
[9]. Ali, A. Mathur, and H. Zhang, ―Measurement of commercial peer-to-peer live video streaming,‖ in Proc. Workshop Recent Adv. Peer-to-Peer Streaming, Aug. 2006.
[10]. Hyunseok Chang, Sugih Jamin, and Wenjie Wang – Live Streaming with Receiver Based PDM || in IEEE/ACM TRANSACTIONS ON NETWORKING, vol. 19, no. 1, Feb 2011.

International Journal of Modern Engineering Research (IJMER)
www.ijmer.com Vol. 3, Issue. 4, Jul. - Aug. 2013 pp-2317-2319 ISSN: 2249-6645

An Efficient PDP Scheme for Distributed Cloud Storage

Jimnisha Shaik[1], Syed Gulam Gouse[2]
[1]*M. Tech, Nimra College of Engineering & Technology, Vijayawada, A.P., India*
[2]*Professor, Dept.of CSE, Nimra College of Engineering & Technology, Vijayawada, A.P., India*

***ABSTRACT*:** *Cloud computing is the use of Internet for the tasks performed on the local computer, with the hardware and software demands maintained elsewhere. It represents a different way to architect and remotely manage various computing resources. Cloud is widely used everywhere owing to its convenience, be it in simple data analytic program or composite web or mobile applications. Cloud computing is being driven by many which includes Amazon, Google and Yahoo as well as traditional vendors including IBM, Microsoft and Intel. The data should be available in the cloud for it to be accessed by many users. There are four main types of cloud storage- Multi Cloud Storage or distributed cloud storage, Public Cloud Storage, Private Cloud Storage, Mobile Cloud Storage. Distributed cloud is a combination of public and private cloud storage where some critical data resides in the enterprise's private cloud while other data is stored and accessible from a public cloud storage provider. Provable data possession (PDP) is a technique for ensuring the integrity of data stored in storage outsourcing. In this paper, we propose a method called cooperative PDP (CPDP) scheme based on homomorphic verifiable response and hash index hierarchy.*

INDEX TERMS: *Cloud, Hash index, Integrity, PDP.*

I. INTRODUCTION

In recent years, the concept of parallel computing has emerged to solve the problems with a greater computational speed. It's operation is based upon the principle that larger problems can be reduced to a number of smaller ones, then which are solved parallely.Parallel computing can be implemented in several ways of computing like bit level, instruction level, task and data parallelism. Based on the level at which the hardware supports parallelism, it can be classified as- multi-core and multi-processor. Generally in a computer system a problem can be solved using a stream of instructions. Only one instruction is executed at a time, and then the others are executed. On the other hand in parallel computing, uses the multi-processing elements to solve a problem. This is accomplished by breaking the problem into various independent parts so that each processing element can execute its part of the algorithm simultaneously with others. There is another important concept which is responsible for the effective and efficient computation of our problem is, distributed system. Using high performance computers connected by using high speed communication links, it is possible to build a single system consisting of multiple computers and using it as a single consolidated system.

In a distributed system, the computers are not independent but are interconnected by a high-speed network. Here are a few requirements for a distributed system- Like reliability and security, consistency of replicated data, concurrent transactions, and fault tolerance. The major aim of constructing the distributed system is that its behavior should be transparent to the user. In a distributed memory architecture if we take into account each processor has its own local storage and all the processing is done locally. All systems are interconnected using a LAN.

In any kind of computer system which involves data storage and retrieval, availability is one of the major security issues to be concerned. Provable Data Possession (PDP) is such a technique which ensures data availability or proof of retrievability (POR).It's the proof which is provided for the storage provider, in order to prove the ownership and integrity of client's data without being downloading it. The proof-checking of the data without being downloading is very important, especially when it comes to very large sized data blocks. It is necessary because it is to be ensured that the data is not deleted or altered. PDP schemes are very useful when it comes to these kinds of issues. However, this scheme will be effective only for single cloud storage, but not for the distributed-cloud storage environment.

II. RELATED WORK

To check the availability and integrity of the outsourced data in cloud storages, researchers have proposed two basic approaches called Provable Data Possession (PDP) [1] and Proofs of Retrievability (POR) [2]. In [1], the authors first proposed the PDP model for ensuring possession of files on un trusted storages and provided an RSA-based scheme for a static case that achieves the O(1) communication cost. In order to support dynamic data operations, the authors developed a dynamic PDP solution called Scalable PDP [3]. They proposed a lightweight PDP scheme based on cryptographic hash function and the symmetric key encryption, but the servers can deceive the owners by using previous metadata or responses due to the lack of the randomness in the challenges.

In [4], the authors introduced two Dynamic PDP schemes with a hash function tree to realize O(log n) communication and computational costs for a n-block file. The basic scheme, called DPDP-I, retains the drawback of Scalable PDP method, and in the 'blockless' scheme, called DPDPII. In [2], the authors presented a POR scheme, which relies largely on preprocessing steps that the client conducts before sending a file to a CSP. Several POR schemes and models have been recently proposed including in [5][6]. In [5], the authors introduced a distributed cryptographic system that allows a set of servers to solve the PDP problem. This system is based on the integrity protected error correcting code (IP-ECC), which improves the security and efficiency of the existing tools, like POR.

III. PROPOSED METHOD

In this section, we introduce the principles of our cooperative provable data possession for distributed clouds, including the main technique, model, fragment structure, index hierarchy, and the architecture to support our scheme.

A. ***Homomorphic Verifiable Response:*** A homomorphism is the map f : P → Q between two groups such that f(g1+g2) = f(g1)×f(g2) for all g1, g2 ∈ P, where + denotes the operation in P and × denotes the operation in Q. This notation is used to define the Homomorphic Verifiable Tags (HVTs): Given two values σi and σj for two message mi and mj , anyone can combine them into a value σ′ corresponding to the sum of the message mi + mj.

B. ***Cooperative PDP:*** A cooperative provable data possession(CPDP) scheme S′ is a collection of two algorithms and an interactive proof system, S′ = (K, T, P).

KeyGen(1^k): It takes a security parameter k as the input, and returns a secret key sk or a public-secret key pair (pk, sk);
TagGen(sk, F,P): It takes as inputs a secret key "sk", a file
F, and a set of cloud storage providers P = {Pk}, and returns the triples (ζ ,ψ, σ), where ζ is the secret of tags, ψ = (u,H) is a set of verification parameters u and an index hierarchy
H for F, σ = {σ(k)}Pk∈ P denotes a set of all tags, σ(k)is the tags of the fraction F (k) of F in Pk.

Proof(P, V): It is a protocol of proof of the data possession between the CSPs (P = {Pk }) and a verifier (V), that is,(∑Pk∈ P Pk(F(k), σ(k)), V) (pk, ψ), where each Pk takes as input a file F(k) and a set of tags σ(k), and a public key pk and a set of public parameters ψ is the common input between P and V . At the end of the protocol run, " V" returns a bit {0|1} denoting false and true where, $\sum_{P_K \in p}$ denotes the collaborative computing in Pk ∈ P.

C. ***Fragment Structure of Cooperative PDP:*** We propose a fragment structure of CPDP scheme as shown in the Figure 1, which has following characters:

- A file is split into n × s sectors and each block (or s sectors) corresponds to a tag, so that the storage of signature tags can be reduced with the order of s.
- The verifier can check the integrity of the file by random sampling approach, which is a matter of the utmost importance for large or huge files.
- This structure relies on the homomorphic properties to aggregate the data and tags into a constant size response, which minimizes network communication overheads.

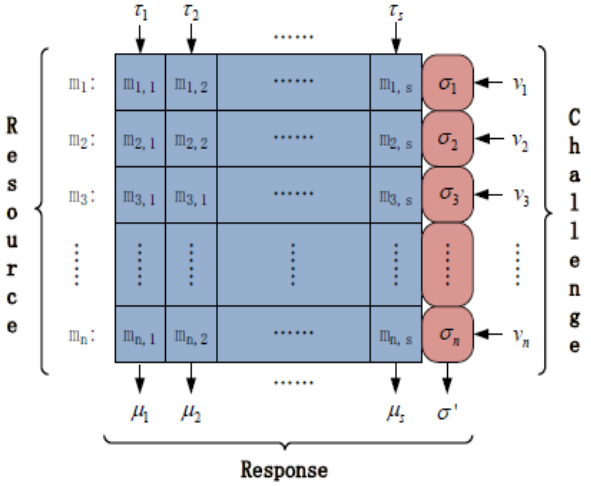

Figure 1: The fragment structure of Cooperative PDP model

The above structure, considered as a common representation for some existing schemes in [1][7], can be converted to MAC-based, ECC or RSA schemes. By using BLS signatures and the random oracle model, it is easy to design a practical CPDP scheme with the shortest homomorphic verifiable responses for public verifiability. This structure also creates favorable conditions for the architecture of the CSPs.

D. ***Hash Index Hierarchy:*** The Architecture for data storage in distributed clouds is shown in Figure 2. This architecture is based on a hierarchical structure with three layers to represent the relationship among all blocks for stored resources. Three layers can be described as follows:

- First Layer (Express Layer): It offers an abstract representation of the stored resources
- Second Layer (Service Layer): It promptly offers and manages cloud storage services
- Third Layer (Storage Layer): It directly realizes data storage on many physical devices.

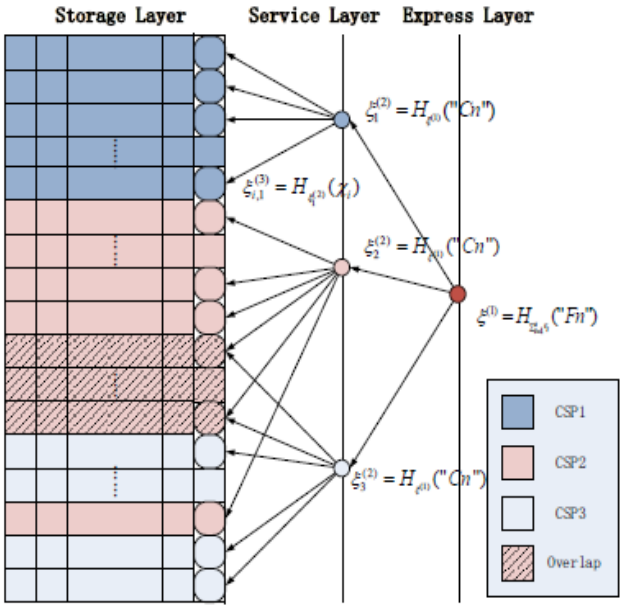

Figure 2: The architecture of Cooperative PDP model

This architecture naturally accommodates the hierarchical representation of the file systems. We make use of a simple hierarchy to organize the multiple CSP services, which involve private clouds or public clouds, by shading the differences between these clouds. As shown in Figure 2, the resources in the Express Layer are split and stored into three CSPs in the Service Layer. In turn, each CSP fragments and stores the assigned data into the storage servers at the Storage Layer. We distinguish different CSPs by different colors, and the denotation of the Storage Layer is the same as in Figure 1. Moreover, we follow the logical order of data blocks to organize Storage Layer. This architecture could provide some special functions for the data storage and management, e.g., there may exist an overlap among data blocks (as shown in dashed line) and discontinuous blocks (as shown on a non continuous color).

IV. CONCLUSION

With the techniques such as homomorphism verifiable response and hash index hierarchy, cooperative provable data possession (CPDP) concept has been achieved and hence integrity and availability is verified .The zero- knowledge proof system is used and hence increases the security so it can be used widely in public cloud services thereby increasing their performance. By this approach the computation time and as well as cost is reduced. Our system can be used as a new method for data integrity verification in out sourcing data storage on distributed cloud environment.

REFERENCES

[1]. G. Ateniese, R. C. Burns, R. Curtmola, J. Herring, L. Kissner, Z. N. J. Peterson, and D. X. Song, "Provable data possession at untrusted stores," in ACM Conference on Computer and Communications Security, P. Ning, S. D. C. di Vimercati, and P. F. Syverson, Eds. ACM, 2007, pp. 598–609.

[2]. Juels and B. S. K. Jr., "Pors: proofs of retrievability for large files," in ACMConference on Computer and Communications Security, P. Ning, S. D. C. di Vimercati, and P. F. Syverson, Eds. ACM, 2007, pp. 584–597.

[3]. G. Ateniese, R. D. Pietro, L. V. Mancini, and G. Tsudik, "Scalable and efficient provable data possession," in Proceedings of the 4th international conference on Security and privacy in communication netowrks, SecureComm, 2008, pp. 1–10.

[4]. C. Erway, A. K¨upc¸ ¨u, C. Papamanthou, and R. Tamassia, "Dynamic provable data possession," in ACM Conference onComputer and Communications Security, E. Al-Shaer, S. Jha, and A. D. Keromytis, Eds. ACM, 2009, pp. 213–222.

[5]. K. D. Bowers, A. Juels, and A. Oprea, "Hail: a high-availability and integrity layer for cloud storage," in ACM Conference on Computer and Communications Security, E. Al-Shaer, S. Jha, and A. D. Keromytis, Eds. ACM, 2009, pp. 187–198.

[6]. Y. Dodis, S. P. Vadhan, and D. Wichs, "Proofs of retrievability via hardness amplification," in TCC, ser. Lecture Notes in Computer Science, O. Reingold, Ed., vol. 5444. Springer, 2009, pp. 109–127.

[7]. H. Shacham and B. Waters. Compact proofs of retrievability. In ASIACRYPT, pages 90–107, 2008.

International Journal of Modern Engineering Research (IJMER)
www.ijmer.com Vol. 3, Issue. 4, Jul. - Aug. 2013 pp-2320-2323 ISSN: 2249-6645

A Novel Method for Blocking Misbehaving Users over Anonymizing Networks

A. N. Venkata Krishna Gopichand[1], Syed Gulam Gouse[2]
[1]*M. Tech, Nimra College of Engineering & Technology, Vijayawada, A.P., India.*
[2]*Professor, Dept.of CSE, Nimra College of Engineering & Technology, Vijayawada, A.P., India*

ABSTRACT: *Nymble is a system that allows websites to selectively blacklist the users of anonymizing networks such as Tor without knowing the user's IP-address. Users not on the blacklist enjoy anonymity while the blacklisted users are not allowed future connections for a duration of time while their previous connections remain unlinkable. Nymble is based on two administratively separate "manager" servers, called the Pseudonym Manager (PM) and the Nymble Manager (NM). The PM is responsible for pairing a user's IP address with the pseudonym deterministically generated based on the user's IP address. The NM pairs a the user's pseudonym with the target server. The major problem is that the security of this system greatly depends on the assumption that the involved participants are honest and they are not going to collude to identify a user and link his connections. Another problem is that this system is neither scalable nor robust since there is only one Nymble Manager (NM) that has to be involved in the nymble ticket generation and complaining mechanisms. This paper presents a novel method for constructing a dynamic nymble system for solving the problems in original nymble system.*

KEYWORDS: *Anonymizing network, Nymble, Pseudonym.*

I. INTRODUCTION

Anonymizing networks such as Tor[1][2] route traffic through independent nodes in separate administrative domains to hide the client's IP address. Unfortunately, some users have misused such networks—under the cover of the anonymity, users have repeatedly defaced popular Web sites such as Wikipedia. Since Web site administrators cannot blacklist individual malicious users' IP addresses, they blacklist the whole anonymizing network. Such measures eliminate the malicious activity through anonymizing networks at the cost of denying anonymous access to behaving users. Anonymizing networks such as Tor are widely deployed to preserve the privacy of the users while they access a service provided by a web server. These networks constitute an important class of a Privacy Enhancing Technology. However, some servers simply deny requests of users who connect through the anonymizing network since they don't have any protocol to punish misbehaving users.

Nymble[3] is basically a system that intends to bind the identity of an anonymous user to a pseudonym[4][5], generated from user's IP address using a one-way function, and simulates a service request with a ticket acquisition. This idea enables a server to complain about the misbehaviour of a user and blacklist his future tickets. Using this system honest users remain anonymous, a server can blacklist the future connections of particular users. Moreover, all the connections of a blacklisted user before the complaint remain anonymous and finally a user can check whether he is blacklisted or not at the beginning of a connection.

Nymble offers the following properties:

- **Anonymous blacklisting:** A server can block the Internet protocol (IP) address of a misbehaving user without knowing the identity of the user or his/her IP address.
- **Privacy:** Honest and misbehaving users both remain anonymous, which provides privacy.
- **Backward anonymity:** The blacklisted user's previous activity remains anonymous or unlinkable, and is refused future connections.
- **Blacklist-status awareness:** A user can check whether he/she has been blocked before accessing the services at the server.
- **Subjective judging:** Since misbehaving users are blocked without compromising their privacy, the servers can provide their own definition of "misbehavior".

II. EXISTING SYSTEM

Nymble is based on two administratively separate "manager" servers, called the Pseudonym Manager (PM) and the Nymble Manager (NM). The PM is responsible for pairing a user's IP address with the pseudonym deterministically generated based on the user's IP address. The NM pairs a the user's pseudonym with the target server. As long as the two managers are not colluding with each other, the user's connections remain anonymous to the PM, pseudonymous to the NM (note that the user does not communicate directly with the NM, and connects to the NM through Tor), and anonymous to servers that the user connects to. The user (in this case, Alice) must first demonstrate the control over a resource, that is the Alice's IP-address. To do this Alice must first connect directly with the PM before receiving the pseudonym. The PM has knowledge of existing the Tor routers, and thus can ensure that Alice is communicating with it directly. Note that the PM has no knowledge of the user's destination, similar to the entry node in Tor network. The PM's sole responsibility it to map IP addresses to the pseudonyms. Alice then connects to the NM through Tor network presenting her pseudonym and her target server. The NM does not know that the IP address of the user, but the pseudonym provided by the PM guarantees that some unique IP address maps to the pseudonym. She receives a set of "nymble" tickets as her credential for the target server.

These nymble tickets are unlinkable, and therefore Alice can present them nymble tickets (once each) to gain anonymous access at the target server. Figure 1 shows how a user connects to a server.

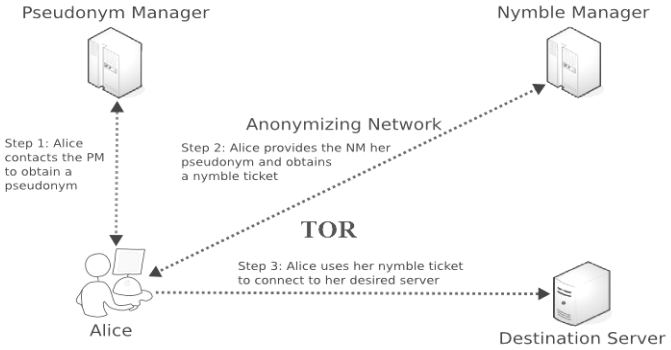

Figure 1: Connecting to a server

Servers can present the user's nymble ticket to the NM as part of a complaint. The NM extracts the linking token from the nymble ticket, that will allow the server to link future connections by the blacklisted user. The NM also issues the servers with blacklists, which the users can examine before performing any actions at the server. By checking servers' blacklists, the blacklisted users are assured that their privacy is not compromised. We now explain the process of blacklisting in a little more detail- nymble tickets are bound to certain "time periods" and "linkability windows.". Figure 2 shows the process of blacklisting a user.

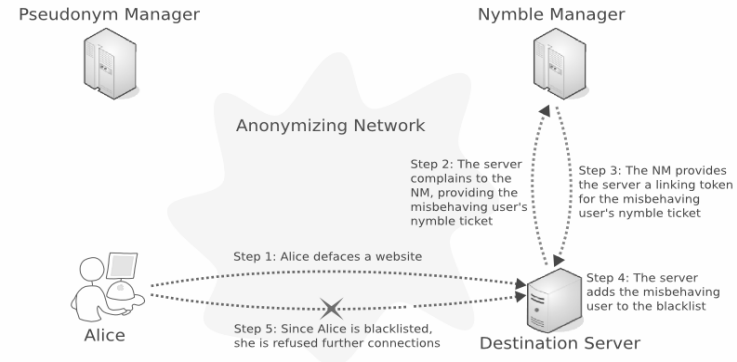

Figure 2: Blacklisting a user

The major problem is that the security of this system greatly depends on the assumption that the involved participants are honest and they are not going to collude to identify a user and link his connections. Another problem is that this system is neither scalable nor robust since there is only one Nymble Manager (NM) that has to be involved in the nymble ticket generation and complaining mechanisms.

III. PROPOSED SYSTEM

In the existing system, Pseudonym Manager (PM) is mapping IP addresses to pseudonyms. The pair (IP, pnym) is of more of real security concern. Here, one more layer of security is needed to add to that pair. In our proposed work (Figure 3), to do that, it requires some changes in the design of PM. The new pseudonym protocol needs two rounds of communication between the user and the set of Pseudonym Managers: In the first round, the user must choose a random PM and connect to it directly to request the codename, which is a pseudonym of his IP address. A request is valid if the user IP address does not come from a known anonymzing network and it has not been used before obtaining a codename in this likability window. The user chooses another random PM in the second round of the pseudonym registration. The user connects to that PM using an anonymizing network and sends her (codename,σ) pair to him. After obtaining the pair and verifying the ring signature [6], the PM issues a pseudonym, that the user can use it to connect to the Nymble Managers.

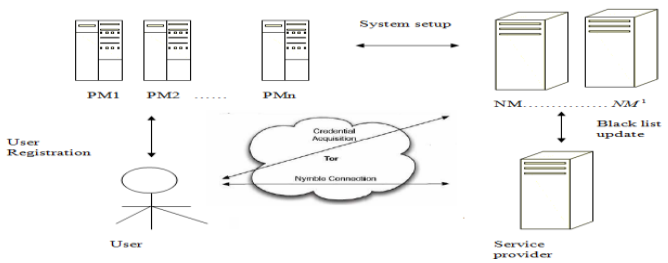

Figure 3: Pseudonym Construction

In the design of Nymble system, the Nymble Manager is an entity that is involved in ticket generation, linking token extraction and blacklist refreshment. Therefore, it might be heavily loaded if the system has many anonymous users and service providers. On the other hand, if Nymble Manager goes out of service for any reason like a a DoS attack or system failure, new users cannot subscribe into the system and service providers cannot extract linking token of misbehaving users. So we need more than one nymble manager. In this design every Nymble Manager should be able to do the following:

- Generate a chain of nymble tickets for the user
- Verify integrity of the nymble ticket without knowing the identity of its issuer
- Extract a linking token from the nymble ticket possibly issued by another Nymble Manager
- Guarantee freshness of the server's blacklist

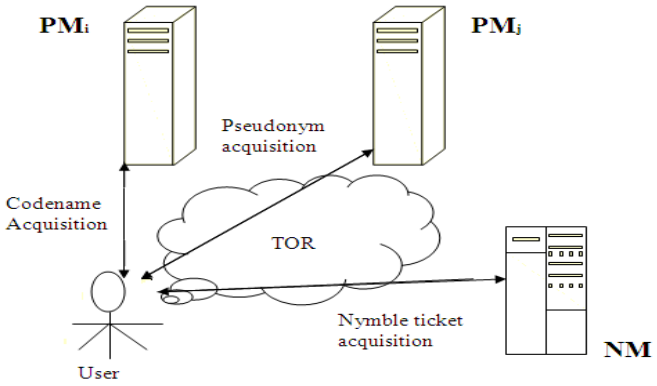

Figure 4: Integrity verification of Pseudonym by NM

The tasks of NM are: Nymble manager should first verify integrity of pseudonym and then generate nymble tickets for that connection (Figure 4). The NM should first verify the integrity of the nymble ticket and then decrypt it to obtain the linking token (Figure 5).

The Nymble Manager first runs NMVerifyPseudonym to check whether the pseudonym is valid or invalid. Then it runs NMCreateCredential to create the list of nymble tickets(called *creds*) for the user and sign every ticket using a ring signature scheme that allows other NMs and all servers to verify it. Algorithm 1 is used to verify the pseudonym by NM.

Algorithm 1: NMVerifyPseudonym
Input: {pnym,w}
Output: {true or false}
1 Extract verifyKeyPM1…n from keys in nmState
2 (nym,σnym) := pnym
3 return σnym == RingSig:Verify(nym|| || w, verifyKeyPM1…n)

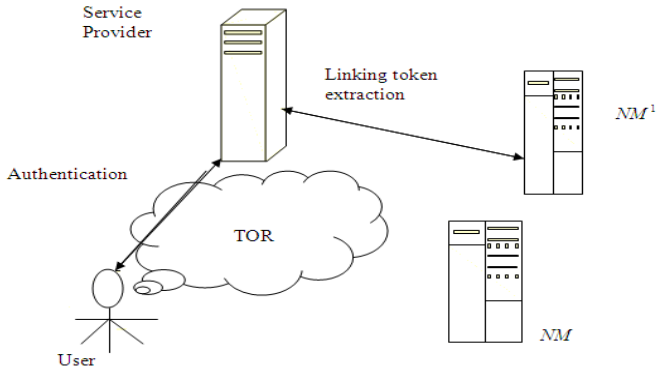

Figure 5: Integrity verification of Nymble ticket by NM

The Nymble manager verifies the nymble ticket by using algorithm 2.

Algorithm 2: NMVerifyTicket
Input: {sid,t,w,ticket}
Output: {true or false}
1 Extract verifyKeyNM1, NM2, NM3…NMm from keys in nmState
2 (nymblet,ctxt, σ_{ticket}) := ticket
3 return RingSig:Verify(sid||t||w|| $nymble_t$ ||ctxt, σ_{ticket} , verifyKeyNM1, NM2, NM3…NMm)

The Nymble Manager should also verifies the integrity of blacklist by running algorithm 3.

Algorithm 3: NMVerifyBL
Input: {sid, t, w, blist, cert}
Output: {true or false}
1 Extract verifyKeyNM1…m from keys in nmState
2 (td,daisy,ts, σ_{BL}) := cert
3 if td $\neq$t v td < ts then
4 return false
5 target := h(td−ts)(daisy)
6 return RingSig.Verify(sid||ts||w||target||blist, σ_{BL} ;
verifyKeyNM1…m)

IV. CONCLUSION

Nymble is a system which provides a blocking mechanism to a server to protect it from various misbehaving users without de- anonymization while allowing anonymous access to behaving users. But, the earlier design for Nymble had a disadvantage. The original design was based on an unrealistic assumption that the trusted third parties(TTP), Pseudonym Manager and Nymble Manage are not going to collude to identify the user. To eliminate this one, we propose a distributed nymble system. Our distributed architecture is not only scalable and robust, but it is more efficient than TTP free anonymous blacklisting systems like BLAC and PEREA.

REFERENCES

[1]. R. Dingledine, N. Mathewson, and P. Syverson, "Tor: The Second- Generation Onion Router," Proc. Usenix Security Symp., pp. 303- 320, Aug. 2004.
[2]. http://www.torproject.org.in/
[3]. Patrick P.Tsang, Apu Kapadia, Cory Cornelius, and Sean W. Smith. Nymble: Blocking misbehaving users in anonymizing networks. IEEE Transactions on Dependable and Secure Computing, 99(1),2011.
[4]. Lysyanskaya, R.L. Rivest, A. Sahai, and S. Wolf, "Pseudonym Systems," Proc. Conf. Selected Areas in Cryptography, Springer, pp. 184-199, 1999.
[5]. D. Chaum, "Showing Credentials without Identification Transfeering Signatures between Unconditionally Unlinkable Pseudonyms," Proc. Int'l Conf. Cryptology (AUSCRYPT), Springer, pp. 246-264, 1990.
[6]. Nishanth Chandran, Jens Groth, and Amit Sahai. Ring signatures of sub-linear size without random oracles. In ICALP, pages 423–434, 2007.

International Journal of Modern Engineering Research (IJMER)
www.ijmer.com Vol. 3, Issue. 4, Jul. - Aug. 2013 pp-2324-2326 ISSN: 2249-6645

Dynamic Organization of User Historical Queries

M. A. Arif[1], Syed Gulam Gouse[2]
[1]*M. Tech, Nimra College of Engineering & Technology, Vijayawada, A.P., India.*
[2]*Professor, Dept. of CSE, Nimra College of Engineering & Technology, Vijayawada, A.P., India*

ABSTRACT: *With the increasing number of published electronic materials, the World Wide Web (WWW) has become a vast resource for the individuals to acquire knowledge, solve problems, and complete tasks that use the Web information. To better support the users in their long term information quests on the Web, search engines keep track of their queries and clicks while searching online. In this paper, our goal is to automatically organize a user's search history into query groups, each containing one or more related queries and their corresponding clicks. Each query group corresponds to the atomic information. First and foremost, query grouping allows the search engine to better understand the user's session and potentially tailor that user's search experience according to her needs. Once query groups have been identified, the search engines can have a good representation of the search context behind the current query using queries and clicks in the corresponding query group. This will help to improve the quality of the key components of search engines such as result ranking, query suggestions, query alterations, sessionization, and collaborative search.*

KEYWORDS: *Log, Search engine, Query, WWW.*

I. INTRODUCTION

As the web is growing very rapidly, the user interacts very often and carries out many complex-task oriented operations over the net. The burst in the size and the richness of web is directly proportional to a variety and the complexity of task performed by user. Hence, the behavior of the user is unpredictable and untraceable as in a user may perform many different search terms over small period of time or may perform many similar searches at different times. Query log is generated by any user are hence no longer related to issuing simple navigational queries. Various studies on query logs[1][2] reveal that only about twenty percent of queries are navigational, while remaining are just transactional or navigational.

The main reason is now the user follows much elaborate task-oriented goals and operations such as planning a tour, planning a purchase and related decisions, managing their finances. The main way of accessing the information over the internet is through the keywords and queries using a search engine. A search engine has become a very important component of internet and they are broadly used for accessing the information over the net. However, a user decomposes the complex task oriented operation into number of smaller and simplified the queries, such as purchasing decision can be broken down into number of co-dependent steps over a period of time. Each step requires one or more queries, and each query results in one or more clicks on the relevant pages. During their complex search online, one of the important step towards providing the services and features that can help users is the capability to identify and group related queries together. This can be traced by using a new feature provided by any search engine which gives the user about their post navigational and task-oriented clicks and queries generally termed as "search histories".

In fact, identifying groups of related queries has applications beyond helping the users to make sense and keep track of queries and the clicks in their search history. Hence query grouping allows the search engine to better understand the user search behavior according to his/her need and his session. Once the query grouping is identified, the search engine can represent the result of the current queries and clicks by the user in the context. Query suggestions, result ranking, query alterations, sessionization, and collaborative search are the key components of the search engines, which may be improved via proper query grouping. Query grouping can also help different users by promoting the task level collaborative search. For example, a group of queries provided by some expert users, we can select the one which is highly relevant to the current user's activity and can suggest it to him. In this paper, we study the main concept of organizing users historical queries.

II. RELATED WORK

In [3][4], the authors investigate the search-task identification problem. More specifically, in [3], the authors considered a search session to consist of a number of tasks (missions), and each task further consists of a number of sub-tasks (goals). In [4], the authors employed similar features to construct a query flow graph, where two queries linked by an edge were likely to be part of the same search mission. In [5][6], the authors used the overlap of terms of two queries to detect changes in the topics of the searches. In [7], the authors studied the different refinement classes based on the keywords in queries, and attempted to predict these classes using a Bayesian classifier. In [8], the authors identified query sequences, called chains, by employing a classifier that combines a timeout threshold with textual similarity features of the queries, as well as the results returned by those queries. The problem of online query grouping is also related to query clustering in [9], [10]. In [9], the authors found query clusters to be used as possible questions for a FAQ feature in an Encarta reference Web site by relying on both text and click features. Graphs based on query and click logs [11] have also been used in previous work for different applications such as query expansion [12], query suggestions [4], ranking [13]. In several cases, variations of random walks have been applied on the graph in order to identify the most important nodes. In [13], a Markov random walk was applied on the click graph to improve ranking. In [14], a random walk was applied on the click-through graph to determine useful keywords.

III. QUERY RELEVANCE USING SEARCH LOGS

In this paper, we develop the machinery to define the query relevance based on Web search logs. Our measure of relevance is aimed at capturing two important properties of relevant queries, namely- (1) queries that frequently appear together as reformulations and (2) queries that have induced the users to click on similar sets of pages. We start our discussion by introducing three search behavior graphs that capture aforementioned properties. Following that, we show how we can use these graphs to compute the query relevance and how we can incorporate the clicks following a user's query in order to enhance our relevance metric. One way to identify the relevant queries is to consider query reformulations that are typically found within the query logs of a search engine. If two queries that are issued consecutively by many users occur frequently enough, they are likely to be used for reformulations of each other. To measure the relevance between any two queries issued by a user, the time-based metric, sometime, makes use of the interval between the timestamps of the queries within the user's search history. In contrast, our approach is defined by the statistical frequency with which any two queries appear next to each other in the entire query log, over all of the users of the system.

A different way to capture relevant queries from the search logs is to consider the queries that are likely to induce users to click frequently on the same set of URLs. For example, although the queries "ipod" and "apple store" do not share any text or appear temporally close in a user's search history, they are relevant because they are likely to have the resulted in clicks about the ipod product. In order to capture such property of relevant queries, we construct a graph called the query click graph (QCG). The query reformulation graph (QRG) and the query click graph (QCG) capture two important properties of relevant queries respectively. In order to make more effective use of the both properties, we combine the query reformulation information within QRG and the query click information within QCG into a single graph, QFG = (VQ, EQF), that we refer to as the query fusion graph. At a high level, EQF contains a set of edges that exist in either EQR or EQC. The weight of the edge (qi, qj) in QFG, wf (qi, qj), is taken to be a linear sum of the edge's weights, wr (qi, qj) in EQR and wc(qi, qj) in EQC,as follows:

wf (qi, qj) = _ × wr(qi, qj) + (1 − α) × wc (qi, qj)

The following Algorithm is used for calculating the query relevance by simulating random walks over the query fusion graph.

Relevance (q)

Input:

1) the query fusion graph, QFG
2) the jump vector, g
3) the damping factor, d
4) the total number of random walks, numRWs
5) the size of neighborhood, maxHops
6) the given query, q

Output:

the fusion relevance vector for q, relF q
(1) Initialize relF q = 0
(2) numWalks = 0; numVisits = 0
(3) while numWalks < numRWs
(4) numHops = 0; v = q
(5) while v 6= NULL ^ numHops < maxHops
(6) numHops++
(7) relF q (v)++; numVisits++
(8) v = SelectNextNodeToVisit (v)
(9) numWalks++
(10) For each v, normalize relF q (v) = relF , q (v)/numVisits

We use the jump vector "gq" to pick the random walk starting point. At each node v, for a given damping factor d, the random walk either continues by following one of the outgoing edges of v with a probability of d, or stops and then re-starts at one of the starting points in gq with a probability of (1−d). Then, each outgoing edge, (v, qi), is selected with the probability wf (v, qi), and the random walk always re-starts if v has no outgoing edge. The selection of the next node to visit based on the outgoing edges of the current node v in QFG and the damping factor d is performed by the SelectNextNodeToVisit process in the Step (7) of the algorithm. In addition to the query reformulations, user activities also include clicks on the URLs following each query submission.

IV. QUERY GROUPING USING THE QFG

In this section, we outline our proposed similarity function "simrel" to be used in the online query grouping process. For each query, we maintain a query image, which represents the relevance of the other queries to this query. For each query group, we maintain the context vector, which aggregates the images of its member queries to form an overall representation. We then propose a similarity function simrel for any two query groups based on these concepts of context vectors and query

images. Note that our proposed of query reformulation graph, query images, and the context vectors are crucial ingredients, which lend significant novelty to the Markov chain process for determining relevance between queries and query groups.

For each query group, we maintain the context vector which is used to compute the similarity between the query group and the user's latest singleton query group. The context vector for a query group s, denoted "cxts", contains the relevance scores of each query in VQ to the query group s, and is obtained by aggregating the fusion relevance vectors of the queries and clicks in s. If s is a singleton query group containing only {qs1 , clks1}, it is defined as the fusion relevance vector rel(qs1,clks1). For a query groups = h{qs1 , clks1}, . . . , {qsk , clksk}i with k > 1, there are a number of different ways to define cxts. For instance, we can define it as the fusion relevance vector of the most recently added query and the clicks, rel(qsk ,clksk). Other possibilities include the average or the weighted sum of all the fusion relevance vectors of the queries and the clicks in the query group.

V. CONCLUSION

This paper shows how to organize user's historical queries in the search engine, means if the user search in the search engine, then that user query and URL will be stored in the history log. To reduce the burden on the users, in this paper we have created a feature called "Query Group". In this group we store the user queries. This Query Group having only related queries and the query groups will be created with different related queries. For example several users have been searching for the banks, then that time a new Query Group will be created about bank and another user have been searching for Hospitals information then the new Query Group will be created automatic and Dynamic fashion. This feature will be useful to the users for selecting or searching the related queries.

REFERENCES

[1]. J. Teevan, E. Adar, R. Jones, and M. A. S. Potts, "Information reretrieval: repeat queries in yahoo's logs," in SIGIR. New York, NY, USA: ACM, 2007, pp. 151–158.
[2]. Broder, "A taxonomy of web search," SIGIR Forum, vol. 36, no. 2, pp. 3–10, 2002.
[3]. R. Jones and K. L. Klinkner, "Beyond the session timeout: Automatic hierarchical segmentation of search topics in query logs," in CIKM, 2008.
[4]. P. Boldi, F. Bonchi, C. Castillo, D. Donato, A. Gionis, and S. Vigna, "The query-flow graph: Model and applications," in CIKM, 2008.
[5]. D. He, A. Goker, and D. J. Harper, "Combining evidence for automatic Web session identification," Information Processing and Management, vol. 38, no. 5, pp. 727–742, 2002.
[6]. H. C. Ozmutlu and F. C¸ avdur, "Application of automatic topic identification on Excite Web search engine data logs," Information Processing and Management, vol. 41, no. 5, pp. 1243–1262, 2005.
[7]. T. Lau and E. Horvitz, "Patterns of search: Analyzing and modelling Web query refinement," in UM, 1999.
[8]. F. Radlinski and T. Joachims, "Query chains: Learning to rank from implicit feedback," in KDD, 2005.
[9]. J.-R. Wen, J.-Y. Nie, and H.-J. Zhang, "Query clustering using user logs," ACM Transactions in Information Systems, vol. 20, no. 1, pp. 59–81, 2002.
[10]. J. Yi and F. Maghoul, "Query clustering using click-through graph," in WWW, 2009.
[11]. R. Baeza-Yates, "Graphs from search engine queries," Theory and Practice of Computer Science (SOFSEM), vol. 4362, pp. 1–8, 2007.
[12]. K. Collins-Thompson and J. Callan, "Query expansion using random walk models," in CIKM, 2005.
[13]. N. Craswell and M. Szummer, "Random walks on the click graph," in SIGIR, 2007.
[14]. Fuxman, P. Tsaparas, K. Achan, and R. Agrawal, "Using the wisdom of the crowds for keyword generation," in WWW, 2008.

International Journal of Modern Engineering Research (IJMER)
www.ijmer.com Vol. 3, Issue. 4, Jul. - Aug. 2013 pp-2327-2329 ISSN: 2249-6645

Three Party Authenticated Key Distribution using Quantum Cryptography

V. Padmaja[1], Sayeed Yasin[2]
[1]*M. Tech, Nimra College of Engineering & Technology, Vijayawada, A.P., India.*
[2]*Asst. Professor, Dept.of CSE, Nimra College of Engineering & Technology, Vijayawada, A.P., India*

***ABSTRACT*:** *Cryptography is the science of writing in secret message and is an ancient art. In data and telecommunications, cryptography is necessary when communicating over any untrusted medium, which includes just about any network, particularly over the Internet. Over the last two decades an interesting field of the cryptography has raised from non classical atomic theory, Quantum Physics. This field is known as Quantum cryptography. Unlike the classical cryptography of public and private key ciphers which analyse the strength of a cipher by means of mathematical attacks and formulas, the security of the quantum cryptography is ensured by laws of Quantum Physics. In this paper, we present a method for three party authentication using quantum cryptography. Our method depends on partial trusted third party, so that the key is not revealed to the trusted third party.*

KEYWORDS*:** *Authentication,* ***Cryptography, Photon, Secret key.

I. INTRODUCTION

Cryptography[1] plays an important role in modern life as it allows for secure communication over insecure channels, even in the face of powerful adversaries. Cryptography has been used for the military and government communications for more than 2000 years, but only in the past 20 years has cryptography come to be used in day-to-day life. The expansion of the Internet from a small scale academic network to a global network enabling hundreds of billions of dollars of the electronic commerce was due in no small part to the availability of cryptography. The successful design of the multitudes of secure cryptographic algorithms — public key agreement, digital signatures, block and stream ciphers, hash functions, message authentication codes — and secure protocols that employ these primitives is a remarkable achievement. Of those that have been widely adopted, the majority have remained fundamentally secure despite years of intensive cryptanalysis and the advancing computer technology.

Various security problems abound on the Internet. The servers of governments and the major corporations are subjected to denial of service attacks. Spyware, viruses, and malware are installed on the users' computers. Individuals fall victim to phishing attacks and the identity theft. Devices are subject to attacks that exploit the subtle variations in their power usage. These security problems do not arise as a result of a break of the cryptographic algorithms or protocols. Rather, they arise by working around the cryptography- why exert billions of hours of computer effort to break an advanced encryption protocol to crack a user's password when you can simply trick the user into telling you their password directly?

In symmetric key cryptography, both parties must possess a secret key(shared key) which they must exchange prior to using any encryption. Distribution of the secret keys has been problematic until recently, because it involved face-to-face meeting, use of a trusted courier, or sending the key through an existing encryption channel. The first two are often impractical and always unsafe, while the third depends on the security of the previous key exchange. One solution is based on the mathematics, public key cryptography**.** In public key cryptography, the key distribution of the public keys is done through public key servers. When a person creates a key-pair, he/she keeps one key private and the other, public-key, is uploaded to a server where it can be accessed by anyone to send the user a private, encrypted, message. Another approach is based on physics- quantum cryptography. While public-key cryptography relies on the computational difficulty of certain hard mathematical problems, quantum cryptography relies on the laws of the quantum mechanics**.**

II. QUANTUM CRYPTOGRAPHY

Quantum cryptography[2] uses quantum mechanics to guarantee a secure communication. It enables two parties to produce a shared random bit string known only to them, which can be used as a shared key to encrypt and decrypt messages. An important and unique property of the quantum cryptography is the ability of the two communicating users to detect the presence of any third party trying to gain knowledge of the key. This results from a fundamental part of quantum mechanics- the process of measuring a quantum system in general disturbs the system. A third party trying to eavesdrop on the key must in some way measure it, thus introducing a detectable anomalies. By using quantum superpositions or quantum entanglement and transmitting information in the quantum states, a communication system can be implemented which detects eavesdropping. If the level of eavesdropping is below a certain threshold a key can be produced which is guaranteed as secure, otherwise no secure key is possible and the communication is aborted.

The security of the quantum cryptography relies on the foundations of quantum mechanics, in contrast to traditional public key cryptography which relies on the computational difficulty of certain mathematical functions, and cannot provide any indication of eavesdropping or guarantee of key security. Quantum cryptography is only used to produce and distribute the key, not to transmit any message data. This key can then be used with any chosen encryption algorithm to encrypt and decrypt the message, which can then be transmitted over a standard communication channel. The algorithm most commonly associated with QKD is the one-time pad, as it is provably secure when used with the secret, random key.

III. RELATED WORK

There are two three party quantum key distribution protocols(QKDps), one with implicit user authentication and the other with explicit mutual authentication[3], are combined to demonstrate the merits of combining both classical and quantum cryptography. Also when compared with the classical three-party key distribution protocols, the proposed QKDPs easily resist replay attacks. This work presents a new direction in designing QKDPs by combining the advantages of classical with the quantum cryptography. There are few quantum key distribution protocols described in [4] such as B92 quantum cryptographic protocol, BB84 quantum cryptographic protocol, Entanglement-based quantum key distribution and Quantum Bit Commitment (QBC) protocols. Also this paper includes protocol evaluating and comparison, using such criteria as the error possibility, quantum and classical memory bounds, noise sensitivity.

Some of the advantages of the Quantum Cryptography over classical cryptography described in[5] i.e., it gives us perfectly secure data transmission. Also it discusses about Quantum Key Distribution and how important the quantum cryptographic protocols are to it. It also tells about how eavesdropping will be in quantum cryptography and its effects. The security of some of the quantum cryptographic protocols such as Six-state protocol, BB84 protocol, SARG04 protocol, Symmetric and Asymmetric three-state protocol is described in [6]. The authors also compare their performances in both the ideal case and in the realistic case and found that Efficient BB84 and Six-state protocols tolerate the highest QBER.

IV. EXISTING SYSTEM

In [3], the authors proposeda three-party quantum authenticated key distribution protocol (QAKD). This three-party QAKD is immune to the man-in-the-middle attack, while it performs both authentication and the key distribution with one step by utilizing a trusted third party. The weakness of this scheme is that it relies 100% on the trusted third party(TTP). The TTP has the ability to read all communication packets. In cryptography or network security, an authentication between parties unknown to each other is not possible without the third party that guarantees the identities of the participating parties. Thus, a TTP, which is a disinterested party trusted to complete a protocol [7], needs to be introduced. However, in a real world, such an idealized assumption cannot be always possible. For example, it may be too optimistic to make an assumption in key distribution schemes for medical applications. Patient information should be shared only between the patient and the doctors, so the third party for the key distribution system should not be able to read the encrypted confidential data. There must be a safeguard to protect the confidentiality even from the trusted third party in such applications.

V. PROPOSED SYSTEM

Let Alice and Bob intended to share an authenticated shared key 'K', which is an n- bit random number. Here we assume that every participant shares a secret shared key with the trusted centre in advance. Let $K_{A,T}$ is the key shared between the Alice and Trusted Centre(TC), and $K_{B,T}$ is the key shared between Bob and TC. Let h(K,M) is a hash value of a message M with key "k", generated using a hash function(e.g., SHA-1 or MD5). Assume that the TC has been notified to start the authentication session as follows:

The TC generates two random numbers r_A and r_B and then computes:

$$X = h(K_{A,T}, r_A) \oplus (U_A \| U_B)$$

$$Y = h(K_{B,T}, r_B) \oplus (U_B \| U_A)$$

Now $r_A \| r_B \| X$ is polarized and encrypted using the pre- shared key $K_{A,T}$ and the result is transmitted to Alice over a Quantum channel. Also $r_B \| r_A \| Y$ is polarized and encrypted Using the pre- shared key $K_{B,T}$ and the result is transmitted to Bob over another Quantum channel.

Alice decrypts and measures the received qubits. She computes a hash value using $K_{A,T}$ and r_A and obtain the values of $U_A \| U_B$. Then she verifies the values of U_A and U_B.

Bob decrypts and measures the received qubits. She computes a hash value using $K_{B,T}$ and r_B and obtain the values of $U_B \| U_A$. Then she verifies the values of U_A and U_B. Thus after the successful completion of the session, both Alice and Bob are implicitly authenticated using the TC.

A secret key 'K' is going to be established between Alice and Bob. The secret key will not revealed to others, even to Trusted centre. Key establishment is based on Shamir's three- pass protocol and Quantum superposition states. Here classical Shamir's three- pass protocol is combined with superposition states, because classical shamir's protocol is vulnerable to attacks[8].

In the following discussion, without losing generality, we can assume that message M is single photon encoded as M= |0> (i.e.., n=1 and i_1=0) and Alice initiates a key distribution.

(i) First, Alice and Bob generate their session keys $K_A = \theta_A$ and $K_B = \theta_B$.

(ii) Alice encrypts M with her encryption key K_A. The resulting state can be described as

E_{K_A} [M] : R(θ_A)|0>= $\begin{pmatrix} \cos\theta_A & \sin\theta_A \\ -\sin\theta_A & \cos\theta_A \end{pmatrix}\begin{pmatrix} 1 \\ 0 \end{pmatrix}$

= cos θ_A . |0> - sin θ_A . |1>= $|\psi_1\rangle$,

Where E_{K_A} indicates an encryption with K_A. Such a resulting state is called as a superposition state . Alice sends the resulting state $|\psi_1\rangle$ to Bob.

(iii) Bob receives the photon in $|\psi_1\rangle$ and encrypts it with his key K_B .

E_{K_B} [E_{K_A} [M]]: R(θ_B).$|\psi_1\rangle$

= cos($\theta_B + \theta_A$) |0> - sin ($\theta_B + \theta_A$) |1>

= $|\psi_2\rangle$

The resulting state $|\psi_2\rangle$ is still a superposition state. Bob send it back to Alice.

(iv) Alice receives and decrypts it by rotating it back with the angle θ_A (i.e., rotation of - θ_A)and sends the resulting superposition state $|\psi 3\rangle$ to Bob.

D_{K_A} [E_{K_B} [E_{K_A} [M]]]= E_{K_B} [M]: R(- θ_A).$|\psi_2\rangle$

= cos θ_B . |0> - sin θ_B . |1> = $|\psi 3\rangle$

Where D_{K_A} indicates a decryption with K_A.

(v) Bob receives and decrypts it by rotating it back with the angle θ_B (i.e., rotation of - θ_B).

D_{K_B} [E_{K_B} [M]]: R(- θ_B). $|\psi 3\rangle$

= $\begin{pmatrix} \cos(-\theta_B) & \sin(-\theta_B) \\ -\sin(-\theta_B) & \cos(-\theta_B) \end{pmatrix}.\begin{pmatrix} \cos\theta_B \\ -\sin\theta_B \end{pmatrix}$

= $\begin{pmatrix} 1 \\ 0 \end{pmatrix}$ = $|0\rangle$.

Now, Bob has the original message M= $|0\rangle$.

After the key distribution phase, both the participants ave the key 'K'.

VI. CONCLUSION

This paper presents a Quantum authenticated key distribution protocol that can perform key distribution and also ensure that the participants of the communication are authentic, both implicitly and explicitly. This protocol provides new directions in Classical cryptography and Quantum cryptography. The Participants of the protocol trust the third party regarding the authentication part only. Thus the proposed protocol will be preferable for network systems which deal with highly sensitive information, such as military, hospitals, research facilities. Our protocol utilizes polarized photons in superposition states for authentication and key distribution which provides high security against many attacks.

REFERENCES

[1]. W. Stallings, Cryptography and Network Security: Principles and Practice 3/e. Prentice Hall, 2003.
[2]. C.H. Bennett, G. Brassard, "Quantum cryptography: public key distribution and coin tossing, in: Proc. IEEE Int. Conf. on computers, Systems and Signal Processing, Bangalore, India, pp. 175-179, 1984.
[3]. Tzonelih Hwang, Kuo-Chang Lee, chuan-Ming Li, "Provably Secure Three-Party Authenticated Quantum Key Distribution Protocols," IEEE Transactions on Dependable and Secure Computing, vol. 4, No. 1, January-March 2007.
[4]. Lelde Lace, Oksana Scegulnaja-Dubrovska, Ramuns Usovs, Agnese Zalcmane, "Quantum Cryptographic Key Distribution Protocols", The European Social Fund(ESF), 2008.
[5]. Rajni Geol, Moses Garuba and Anteneh Girma, " Research Directions in Quantum Cryptography", International Conference on Information technology, 2007.
[6]. Chi-Hang Fred Fung, Hoi-Kwong Lo, "A survey on quantum cryptographic protocols and their security", IEEE, 2007.
[7]. B. Schneier, Applied Cryptography, John Wiley, New York, 1996.
[8]. Rolf Oppliger "Contemporary Cryptography", Artech House, Computer security series, 2005, pp. 408- 410.

International Journal of Modern Engineering Research (IJMER)
www.ijmer.com Vol. 3, Issue. 4, Jul. - Aug. 2013 pp-2330-2334 ISSN: 2249-6645

Optimal Location of Statcom for Power Flow Control

S. S. Chandrakanth, A. Ramulu
M. Tech (PS&A) GITAM University, Visakhapatnam, India

ABSTRACT: *Power flow control in a long transmission line plays a vital role in electrical power system. This paper uses the shunt connected STATCOM for the control of voltage and power flow. The proposed device is used in different locations such as sending end, middle and receiving end of the transmission line. The PWM control is used to generate the firing pulses of the controller circuit. Simulation modeling of the system is carried out using MATLAB/SIMULINK. Based on a voltage-source converter, the STATCOM regulates system voltage by absorbing or generating reactive power. This paper deals with a cascaded multilevel converter model, which is a 48-pulse (three levels) GTO converter. The simulation studies are carried for sending end, middle and receiving end of the transmission line. The objective is to define the reactive power generated and voltage control at different locations (at sending end, middle, receiving end) of transmission line using STATCOM.*

KEYWORDS: FACTS device, STATCOM, SVC, PWM, MATLAB /Simulink.

I. INTRODUCTION

The power system is an interconnection of generating units to load centres through high voltage electric transmission lines and in general is mechanically controlled. It can be divided into three subsystems: generation, transmission and distribution subsystems. In order to provide cheaper electricity the deregulation of power system, which will produce separate generation, transmission and distribution companies, is already being performed. At the same time electric power demand continues to grow and also building of the new generating units and transmission circuits is becoming more difficult because of economic and environmental reasons. Therefore, power utilities are forced to rely on utilization of existing generating units and to load existing transmission lines close to their thermal limits. However, stability has to be maintained at all times. Hence, in order to operate power system effectively, without reduction in the system security and quality of supply, even in the case of contingency conditions such as loss of transmission lines and/or generating units, which occur frequently, and will most probably occur at a higher frequency under deregulation, a new control strategies need to be implemented.

The future growth of power systems will rely more on increasing capability of already existing transmission systems, rather than on building new transmission lines and power stations, for economical and environmental reasons. Ideally, these new controllers should be able to control voltage levels and flow of active and reactive power on transmission lines to allow for their secure loading, to full thermal capability in some cases, with no reduction of system stability and security.

The location of STATCOM for power flow control in transmission system has been presented [1]. The FACTS devices are introduced in the power system transmission for the reduction of the transmission line losses and also to increase the transfer capability. STATCOM is VSC based controller to regulate the voltage by varying the reactive power in a long transmission line. The effectiveness of SVC and STATCOM of same rating for the enhancement of power flow has been demonstrated [2]. The modeling of converter-based controllers when two or more VSCs are coupled to a dc link has been presented [3].The optimal location of shunt FACTS devices in transmission line for highest possible benefit under normal condition and has been investigated [4].A shunt connected controllable source of reactive power, and two series connected voltage-sourced converters - one on each side of the shunt device was presented [5]. An overview of how series connected and combined series/shunt connected FACTS controllers are studied in an AC system has been highlighted [6]. The optimum required rating of series and shunt flexible ac transmission systems controllers for EHVAC long transmission lines by computing `optimum compensation requirement' (OCR) for different loading conditions has been demonstrated [7]. A series passive compensation and shunt active compensation provided by a static synchronous compensator (STATCOM) connected at the electrical centre of the transmission line to minimize the effects of SSR has been presented [8].A novel approach for damping inter-area oscillations in a large power network using multiple STATCOMs was given [9]. The effective utilization of FACTS device called unified power flow controller (UPFC) for power flow control was presented [10].

II. OPERATING PRINCIPLE

A STATCOM consists of a coupling transformer, an inverter and a DC capacitor as shown in fig 1.

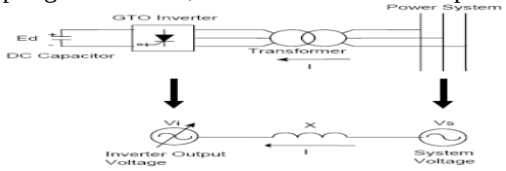

Fig 1 Equivalent circuit of STATCOM

Using the classical equations that describe the active and reactive power flow in a line in terms of Vi and Vs, the transformer impedance (which can be assumed as ideal) and the angle difference between both bars, we can define P and Q.

The angle between the Vs and Vi in the system is δ. When the STATCOM operates with δ =0 we can see how the active power send to the system device becomes zero while the reactive power will mainly depend on the voltage module. This operation condition means that the current that goes through the transformer must have a +/-90º phase difference to Vs. In other words, if Vi is bigger than Vs, the reactive will be send to the STATCOM of the system (capacitive operation), originating a current flow in this direction. In the contrary case, the reactive will be absorbed from the system through the STATCOM (inductive operation) and the current will flow in the opposite direction. Finally if the modules of Vs and Vi are equal, there won´t be neither current nor reactive flow in the system as shown in fig 2.

Thus, we can say that in a stationary state Q only depends on the module difference between Vs and Vi voltages. The amount of the reactive power is proportional to the voltage difference between Vs and Vi.

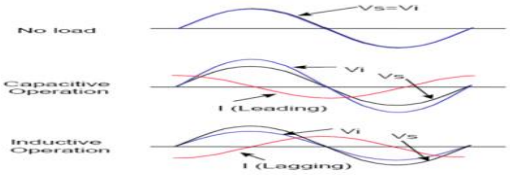

Fig 2 Operation Characteristics of STATCOM

III. CHARACTERISTICS OF STATCOM AND SVC

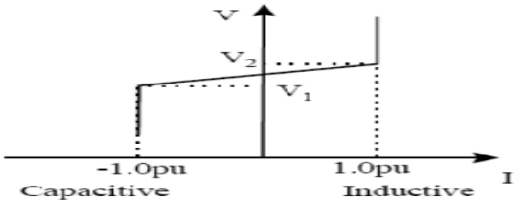

Fig 3 V-I Characteristics of STATCOM

The STATCOM smoothly and continuously controls voltage from V1 to V2 as shown in fig 3. However, if the system voltage exceeds a low-voltage (V1) or high-voltage limit (V2), the STATCOM acts as a constant current source by controlling the converter voltage (Vi) appropriately.

With the active power constraint imposed, the control of the STATCOM is reduced to one degree of freedom, which is used to control the amount of reactive power exchanged with the line. Accordingly, a STATCOM is operated as a functional equivalent of a static var compensator; it provides faster control than an SVC and improved control range. Each GTO converter generates a voltage that is stepped up by a line-side-series-connected multi-stage converter transformer. The converter transformer enables the build-up of a sine-wave voltage in both magnitude and phase. Because STATCOMs with multi-stage converter transformers do not generate significant internal harmonics, they generally require minimal or no harmonic filtering. If the number of firing pulses for the GTOs is increased (i.e., pulse-width modulation (PWM) order), the harmonics are further decreased.

Static Var Compensator is "a shunt-connected static Var generator or absorber whose output is adjusted to exchange capacitive or inductive current so as to maintain or control specific parameters of the electrical power system (typically bus voltage)". SVC is based on thyristors without gate turn-off capability. The operating principal and characteristics of thyristors realize SVC variable reactive impedance. SVC includes two main components and their combination: (1) Thyristor-controlled and Thyristor-switched Reactor (TCR and TSR); and (2) Thyristor-switched capacitor (TSC).

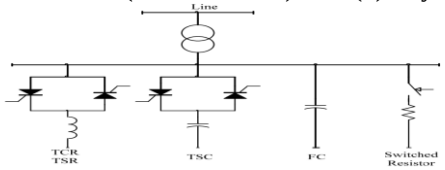

Fig 4 Static VAR Compensators (SVC)

IV. SIMULATION AND RESULTS

STATCOM has a rating of +/- 100MVA. This STATCOM is a phasor model of a typical three-level PWM STATCOM. STATCOM is having a DC link nominal voltage of 40 KV with an equivalent capacitance of 375 µF.The circuit diagram without compensation is shown in Figure5. In this circuit the power is directly measured in the 600km long transmission line at the three stages like sending end, middle and receiving end and also tabulated the result of voltage and reactive power in table1.The circuit diagram when STATCOM is connected at the middle of the long transmission line is shown in fig 6.

Similarly the connections are made when the STATCOM is connected at the sending end and receiving end of the long transmission line. In this circuit the voltage and reactive power are directly measured and tabulated the result in table3. For comparison purpose, the result is tabulated in table2 with SVC (replacing STATCOM) at different positions.

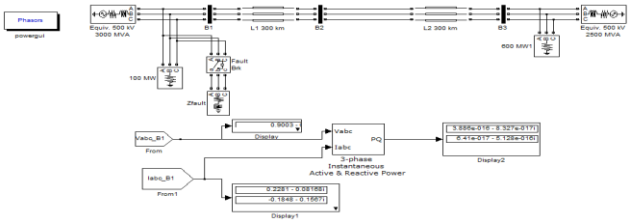

Fig 5 Simulink model of uncompensated transmission line

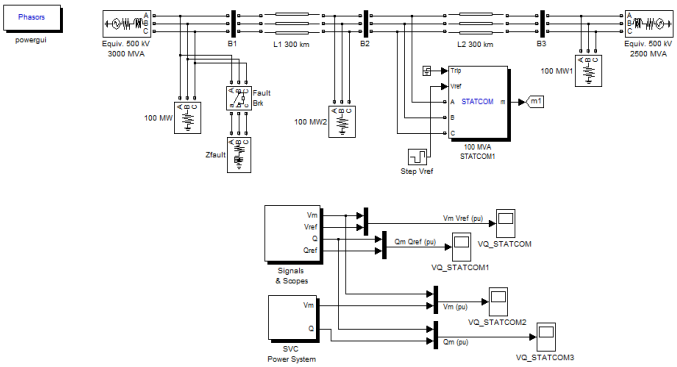

Fig 6 Simulink model of compensated transmission line

Table 1

Simulink data of uncompensated transmission line

UNCOMPENSATED	VOLTAGE (PU)	REACTIVE POWER (PU)
SENDING END	0.903	6.41E-17
MIDDLE	0.691	2.884E-16
RECEIVING END	0.385	5.76E-16

Table 2

Simulink data of SVC in transmission line

SVC	VOLTAGE (PU)	REACTIVE POWER (PU)
SENDING END	0.96	-0.9357
MIDDLE	0.98	-0.5944
RECEIVING END	0.98	-0.9798

STATCOM	VOLTAGE (PU)	REACTIVE POWER (PU)
SENDING END	0.98	4.72E-12
MIDDLE	1.002	0.06
RECEIVING END	0.99	-0.02

Table 3

Simulink data of STATCOM in transmission line

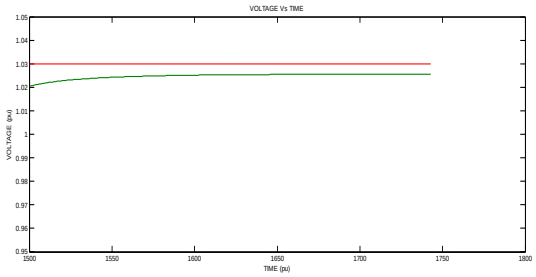

Fig7. Voltage of STATCOM at middle of transmission line

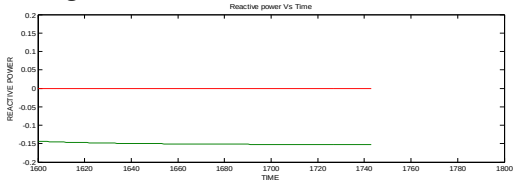

Fig8. Reactive power of STATCOM at middle of transmission line

When STATCOM is placed at the middle of the transmission line the voltage and the reactive power obtained are 1.002 pu and 0.060 pu respectively and they are improved when compared with all the locations of SVC.

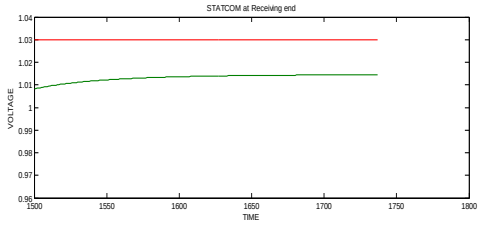

Fig9.Voltage of STATCOM at receiving end of transmission line

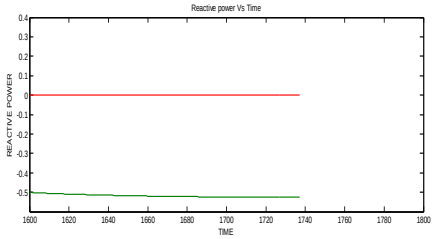

Fig10.Reactive power of STATCOM at receiving end of transmission line

When STATCOM is placed at the receiving end of the transmission line the voltage and the reactive power values are 0.99 pu and -0.02 pu respectively. The reactive power value is not compensated when compared with the other ends of the long transmission line. But by comparing, it is clear that the reactive power is compensated (-0.02 pu) with STATCOM when compared to SVC (-0.9798 pu).

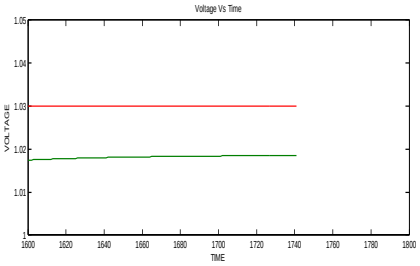

Fig11. Voltage of STATCOM at sending end of transmission line

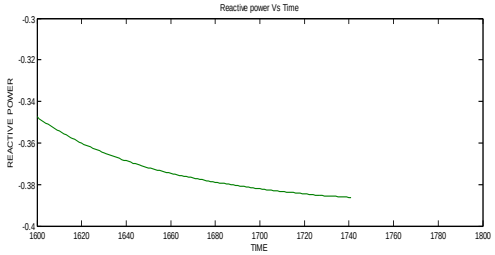

Fig12. Reactive power of STATCOM at sending end of transmission line

When STATCOM is placed at the sending end of the transmission line the voltage profile and reactive power values are 0.98 pu and 4.72e-12 pu respectively and reactive power is improved when compared with SVC at all locations of the transmission line.

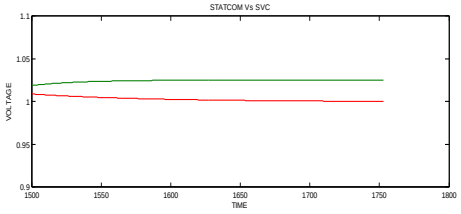

Fig13.Voltage of STATCOM and SVC at middle of transmission line

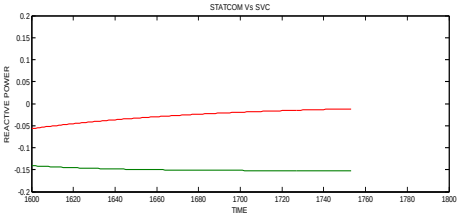

Fig14.Reactive power of STATCOM and SVC at middle of transmission line

By observing the values in table 2 and 3, voltage profile is increased with the placement of STATCOM rather than with SVC. The reactive power is compensated much better with the STATCOM when compared with SVC. The voltage profile and the reactive power compensation values are 1.002 pu and 0.06 pu respectively are much improved at middle of the transmission line with the placement of STATCOM, when compared with other places like sending end, receiving end of the long transmission line. The uncompensated voltage and reactive power values of a long transmission line are also shown in table 1.

V. CONCLUSION

STATCOM and SVC are connected at the various locations such as sending end, middle and receiving end of the transmission line. Based on a voltage source converter, the statcom regulates system voltage by absorbing or generating reactive power. The results are obtained with and without compensation using matlab/simulink environment. The simulation results reveal that the reactive power obtained for STATCOM is better when compared with SVC at the middle of the transmission line. So, the location of STATCOM is optimum when connected at the middle of the long transmission line. The numerical results of the system analysis are elaborated in the tables 1, 2 & 3.

REFERENCES

[1]. M.Karthikeyan, Dr.P.Ajay-D-Vimalraj "Optimal Location of Shunt Facts Devices for Power Flow Control". IEEE, 2011.
[2]. Tan, Y.L., "Analysis of line compensation by shunt-connected FACTS controllers: a comparison between SVC and STATCOM", IEEE Transactions on Power Engineering Review, Vol.19, pp 57-58, Aug 1999.
[3]. Xia Jiang Xinghao Fang Chow, J.H. Edris, A.-A. Uzunovic, E. Parisi, M. Hopkins, L. "A Novel Approach for Modeling Voltage-Sourced Converter-Based FACTS Controllers", IEEE Transactions on Power Delivery, Vol.23(4), pp 2591-2598, Oct 2008.
[4]. Chandrakar, V.K. Kothari, A.G. "Optimal location for line compensation by shunt connected FACTS controller", The Fifth International IEEE Conference on Power Electronics and Drive
[5]. Systems", Vol 1, pp 151-156, Nov 2003.
[6]. Bebic, J.Z. Lehn, P.W. Iravani, M.R. "The hybrid power flow controller - a new concept for flexible AC transmission", IEEE Power Engineering Society General Meeting, DOI-10.1109/PES.2006.1708944, Oct 2006.
[7]. Johnson, B.K. "How series and combined multiterminal controllers FACTS controllers function in an AC transmission system", IEEE Power Engineering Society General Meeting, Vol.2, pp 1265-1267, June 2004.
[8]. Shankaralingappa, C.B. Jangamashetti, S.H. "FACTS Controllers to Improve Voltage Profile and Enhancement of Line Loadability in EHV Long Transmission Lines", International IEEE Conference on POWERCON, pp 1-5, Oct 2008.
[9]. K.R. Padiyar N. Prabhu "Design and performance evaluation of subsynchronous damping controller with STATCOM", IEEE Transactions on Power Delivery, Vol.21(3), pp 1398-1405, July 2006.
[10]. Zarghami, M. Crow, M.L. "Damping inter-area oscillations in power systems by STATCOMs", 40thNorth American Symposium 2008, pp 1-6, 978-1-4244-4283-6, Sept 2008.
[11]. Yap, E.M. Al-Dabbagh, M. Thum, P.C. "Applications of FACTS Controller for Improving Power Transmission Capability", IEEE Conference on TENCON 2005, pp 1-6, Nov 2005.

International Journal of Modern Engineering Research (IJMER)
www.ijmer.com Vol. 3, Issue. 4, Jul. - Aug. 2013 pp-2335-2337 ISSN: 2249-6645

A Study of Secure Efficient Ad hoc Distance Vector Routing Protocols for MANETs

P. Saraswathi Devi[1], A. Veerabhadra Rao[2]
[1]*M. Tech, Sri Sai Madhavi Institute of Science & Technology, A.P., India*
[2]*Asst. Professor, Dept. of CSE, Sri Sai Madhavi Institute of Science & Technology, A.P., India*

***ABSTRACT*:** *A mobile ad hoc wireless network (MANET) consists of a number of wireless mobile nodes that are capable of communicating with each other without the use of a network infrastructure or any centralized administration. In such a network, each mobile node operates not only as a host but also as a router, forwarding packets for other nodes that may not be within the direct wireless transmission range. Thus, nodes must discover and maintain routes to all other nodes. Due to the mobility of the nodes, routers for MANETs need to be dynamically renovated to reflect the changes in topology. Therefore, the design of the routing protocols for such networks is more challenging than that for wired networks. The MANETs are more prone to suffer from the malicious behaviors than the traditional wired networks. Therefore, we need to pay more attention to the security issues regarding routing protocols in the MANETs. This paper presents the study of three secure efficient ad hoc routing protocols for MANETs- SEAD, I- SEAD and SEAD- FHC.*

KEYWORDS: *HASH value, MANET, SEAD, TESLA.*

I. INTRODUCTION

In recent years, the explosive growth of mobile computing devices, which mainly include personal digital assistants (PDAs), laptops and handheld digital devices, has impelled a revolutionary change in the computing world- computing will not merely rely on the capability provided by the personal computers, and the concept of ubiquitous computing emerges and becomes one of the research hotspots in the computer science society [1]. In the ubiquitous computing environment, the individual users utilize, at the same time, several electronic platforms through which they can access all the required information whenever and wherever they may be [2]. The nature of the ubiquitous computing has made it necessary to adopt the wireless network as the interconnection method- it is not possible for the ubiquitous devices to get wired network link whenever and wherever they need to connect with other ubiquitous devices. The Mobile Ad Hoc Network(MANET) is one of the wireless networks that have attracted most concentrations from many researchers.

A MANET is a system of wireless mobile nodes that dynamically self-organize in arbitrary and temporary network topologies. People and vehicles can thus be internetworked in the areas without a preexisting communication infrastructure or when the use of such infrastructure requires wireless extension [3]. In the MANET, nodes can directly communicate with all the other nodes within their radio ranges; whereas nodes that not in the direct communication range use intermediate nodes to communicate with each other. In these two situations, all the nodes that have participated in the communication automatically form a wireless network; therefore this kind of formed wireless network can be viewed as mobile ad hoc network. The MANET has the following typical features [4]:

- Unreliability of wireless links between the nodes. Because of the limited energy supply for the wireless nodes and the mobility of the nodes, the wireless links between the mobile nodes in the ad hoc network are not consistent for the communication participants.
- Constantly changing topology: Due to the continuous motion of the nodes, the topology of the mobile ad hoc network changes constantly- the nodes can continuously move into and out of the radio range of the other nodes in the ad hoc network, and the routing information will be changing all the time because of the movement of the nodes.
- Lack of incorporation of security features in statically configured wireless routing protocols not meant for the ad hoc environments. Because the topology of the ad hoc networks is changing constantly, then it is necessary for each pair of adjacent nodes to incorporate in the routing issue so as to prevent some kind of potential attacks that try to make use of vulnerabilities in the statically configured routing protocol.

Because of the features listed above, the MANET are more prone to suffer from the malicious behaviors than the traditional wired networks. Therefore, we need to paymore attention to the security issues regarding routing protocols in the mobile ad hoc networks.

II. ATTACKS AND SECURITY MECHANISMS IN MANETS

A. Attacks in MANETs: MANETs are more easily attacked than a wired network. The attacks prevalent on MANET routing protocols can be broadly classified into passive and active attacks[5]. There are two classifications of attacks in the MANETs.

- Active attack: In order to perform some harmful operations, the misbehaving node has to bear some energy costs are known as active attacks.
- Passive Attacks: Passive attack is mainly about lack of the cooperation with the purpose of energy saving. Nodes that perform the active attacks with the aim of damaging other nodes by causing network outage are considered to be malicious while nodes that perform passive attacks with the aim of saving battery life for their own communications are considered to be selfish.

B. Security mechanisms for MANETs: Message encryption and digital signatures are two important mechanisms for data integrity and the user authentication. There are two types of data encryption mechanisms, called symmetric and asymmetric (or public key) mechanisms. Symmetric cryptosystems use the same secret key for encryption and decryption of a message, and asymmetric cryptosystems use one key, called the public key, to encrypt a message and another key, called the private key to decrypt it. Public and private keys are related in such a way that only the public key can be used to encrypt messages and only the corresponding private key can be used for decryption process. Even if the attacker comprises a public key, it is virtually impossible to deduce the private key. Any code attached to the electronically transmitted message that uniquely identifies the sender is known as digital code. Digital signatures are the key component of most authentication schemes. To be effective, the digital signatures must be non-forgeable.

Hash functions are used in creation and verification of the digital signature. It is an algorithm which creates a digital representation or a fingerprint in the form of a hash value (or hash result) of a standard length which is usually much smaller than the message and unique to it. Any change to the original message will produce a different hash result even when the same hash function is used. In the case of a secure hash function, also known as the one-way hash function, it is computationally infeasible to derive the original message from knowledge of its hash value. In MANETs, the secrecy of the key does not ensure the integrity of the message. For this purpose, message Authentication Codes (MAC) [6] are used. It is a hashed representation of the message and even if MAC is known, it is impractical to compute the message that generated it. A MAC, which is a cryptographic checksum, is computed by the message initiator as the function of the secret key and the message being transmitted and it is appended to the message. The recipient recomputes the MAC in the similar fashion upon receiving the message. If the MAC computed by the receiver matches with the MAC received then the recipient is assured that the message was not modified.

III. SECURE EFFICIENT ROUTING PROTOCOLS

A. SEAD Protocol: The Secure and Efficient Ad hoc Distance vector routing protocol (SEAD) [7] is based upon the DSDV [8] routing protocol. It uses efficient one-way hash functions to authenticate the lower bound of the distance metric and the sequence number in the routing table. More specifically, for authenticating a particular sequence number and the metric, the node generates a random initial value x $\in (0,1)^{\rho}$ where ρ is the length in bits of the output of the hash function, and computes the list of values h0,h1,h2,h3,…,hn, where h0=x , and hi = H(hi-1) for 0< i ≤ n , for some value n. As an example, given an authenticated hi value, the node can authenticate hi-3 by computing H (H (H(hi-3))) and verifying that the resulting value equals hi. Each node uses one authentic element of the hash chain in each of the routing update it sends about itself with metric 0. This enables the authentication process for the lower bound of the metric in other routing updates for that node. The use of the hash value corresponding to sequence number and metric in a routing update entry prevents any node from advertising a route greater than the destination's own current sequence number.

The receiving node authenticates the route update by applying the hash function according to the prior authentic hash value obtained and then compares it with the hash value in the routing update message. The update message is authentic if both the values match. The source must be authenticated using some kind of the broadcast authentication mechanism such as TESLA [9]. Apart from the hash functions used, SEAD protocol doesn't use average settling time for sending triggered updates as in DSDV in order to prevent eavesdropping from neighboring nodes.

The advantage of using SEAD protocol is that it is robust against multiple uncoordinated attackers, active attackers or compromised nodes. It uses efficient, inexpensive cryptographic primitives and this plays an important role in the computation and bandwidth-constrained nodes. The disadvantages of SEAD is that it doesn't provide a way to prevent an attacker from tampering with "next hop" or "destination" columns. Instead, it relies on doing neighbor authentication, which is a bad thing. Hash chains are consumed very fast, either new h_n needs to be released very often and the hash chain has to be rather long.

B. I- SEAD Protocol: In SEAD protocol, the nodes exchange their routing tables periodically and broadcast their hash value to their neighbors, so that the neighbors can verify the correctness of the value by using one way hash function. Because of the periodic and triggered updating, SEAD protocol increases the routing overhead significantly. In I-SEAD protocol [10], it can let the neighbors check the correctness of the hash value and reduce the routing overhead. We describe the procedure as follows: When the start node sends the route request(RREQ), it randomly chooses a number as a seed. The start node computes a list of values with the seed. Before sending the route request message, the start node computes its MAC value by its TESLA key to protect its hash value. Each node can verify the received value after a certain period of time. For example, given an authenticated h_i value, a node can authenticate h_{i-3} by computing H(H (H (h_{i-3}))) and verifying that the resulting value equals h_i as in the SEAD protocol.

C. SEAD Fixed Hash Chain Protocol: The SEAD protocol uses one-way hash chains to prevent an attacker from forging better metrics or sequence numbers. But SEAD protocol does not prevent an attacker from tampering other fields or from using the learned metric and sequence number to send new routing updates. The Secure Efficient Ad hoc Distance Vector with fixed hash chain length(SEAD-FHC) protocol[11] is used to minimize and stabilize the computational complexity that leads minimization in delay time and maximization in throughput.

The SEAD- FHC protocol is explained as follows: SEAD- FHC authenticates packets that are transmitted serially in the given network. A current password is selected for the current packet to be transmitted. p_C Includes current data d_C. A secure hash function $f_{(h)}$ is applied to the pw_C current password to form a current tag t_C . A password pw_n is selected for a packet p_n that is in sequence and allows p_C, which includes data d_n , and $f_{(h)}$ is applied to pw_n to form a tag t_n. $f_{(h)}$ is then applied to the d_n, t_n and pw_C to obtain a hashed value H_C. p_C is then transmitted that includes the H_C, d_C, t_C and password pw_p of packet p_p that sent before p_C in sequence to authenticate d_C.

IV. COMPARATIVE STUDY

We summarize the various secure routing protocols that have been explained in section III. We consider various attributes and comment on these attributes with respect the each of the protocol discussed above. The following Table 1 presents the comparative study on various security parameters and security attacks.

Table 1: Comparative study of protocols

Performance parameters	SEAD	I- SEAD	SEAD- FHC
Base Protocol	DSDV	DSDV	DSR
Encryption Algorithm	Symmetric	Symmetric	Symmetric
Synchronization	Yes	Yes	Yes
Integrity	No	Yes	Yes
Nonrepudiation	No	No	No
Authentication	Yes	Yes	Yes
Confidentiality	No	No	Yes
DoS Attacks prevention	Yes	Yes	Yes

V. CONCLUSION

SEAD is a proactive routing protocol based on DSDV protocol. It does not rely on the asymmetric encryption primitive but instead it relies on one-way hash chain for security. The basic idea of SEAD protocol is, to authenticate the sequence number and metric of a routing table update message using hash chains elements. In SEAD protocol, the nodes exchange their routing tables periodically and broadcast their hash value to their neighbors, so that the neighbors can verify the correctness of the value by using one way hash function. Because of the periodic and triggered updating, SEAD protocol increases the routing overhead significantly. In I-SEAD protocol [10], it can let the neighbors check the correctness of the hash value and reduce the routing overhead. The Secure Efficient Ad hoc Distance Vector with fixed hash chain length(SEAD-FHC) protocol is used to minimize and stabilize the computational complexity that leads minimization in delay time and maximization in throughput.

REFERENCES

[1]. Marco Conti, Body, Personal and Local Ad Hoc Wireless Networks, in Book The Handbook of Ad Hoc Wireless Networks (Chapter 1), CRC Press LLC, 2003.
[2]. M. Weiser, The Computer for the Twenty-First Century, Scientific American, September 1991.
[3]. M.S. Corson, J.P. Maker, and J.H. Cernicione, Internet-based Mobile Ad Hoc Networking, IEEE Internet Computing, pages 63–70, July-August 1999.
[4]. Amitabh Mishra and Ketan M. Nadkarni, Security in Wireless Ad Hoc Networks, in Book The Handbook of Ad Hoc Wireless Networks (Chapter 30), CRC Press LLC, 2003.
[5]. C.Siva Ram Murthy and B. S. Manoj. "Ad hoc wireless networks: Architecture and Protocols". Prentice Hall Publishers, May 2004, ISBN 013147023X.
[6]. Zapata, M., "Secure Ad hoc On-Demand Distance Vector Routing.," ACM Mobile Computing and Communications Review (MCZR), Vol. 6. No. 3, July 2002, pp. 106-107. pp. 1516-1521
[7]. Y. C. Hu, D. B. Johnson, and A. Perrig, "SEAD: Secure Efficient Distance Vector Routing for Mobile Wireless Ad Hoc Networks," Ad Hoc Networks Journal, 1, 2003
[8]. C Perkins and P. Bhagwat, "Highly dynamic destination sequenced distance vector routing (DSDV) for mobile computers", ACM SIGCOMM, (October 1994).
[9]. William Stallings. "Network Security essentials: Application and Standards", Pearson Education , Inc 2003, ISBN 0130351288.
[10]. Wei-Shen Lai, Chu-Hsing Lin, Jung-Chun Liu, Yen-Lin Huang, Mei-Chun Chou, "I-SEAD: A Secure Routing Protocol for Mobile Ad Hoc Networks", pages 45- 54, International Journal of Multimedia Ubiquitous Engineering Vol. 3, No. 4, October, 2008.
[11]. Prasuna V G, Dr. S. Madhusudhana Verma, "SEAD-FHC: Secure Efficient Distance Vector Routing with Fixed Hash Chain length", Global Journal of Computer Science and Technology Volume 11 Issue 20 Version 1.0 December 2011.

International Journal of Modern Engineering Research (IJMER)
www.ijmer.com Vol. 3, Issue. 4, Jul. - Aug. 2013 pp-2338-2340 ISSN: 2249-6645

A Novel Sybil Attack Detection Mechanism in Urban Vehicular Networks

J. Geetha Renuka[1], Syed Gulam Gouse[2]
[1]*M. Tech, Nimra College of Engineering & Technology, Vijayawada, A.P., India.*
[2]*Professor, Dept. of CSE, Nimra College of Engineering & Technology, Vijayawada, A.P., India*

***ABSTRACT*:** *In vehicular networks, moving vehicles are enabled to communicate with each other using inter vehicle communications as well as with road side units (RSUs) in vicinity via roadside-to-vehicle communications. In urban vehicular networks where the privacy, especially the location privacy of the vehicles should be guaranteed vehicles need to be verified in an anonymous manner. A wide spectrum of applications in such a network relies on collaboration and information aggregation among the participating vehicles. Without the identities of participants, such applications are vulnerable to the Sybil attack where a malicious vehicle masquerades as multiple identities, overwhelmingly influencing the result. The consequence of Sybil attack happening in urban vehicular networks can be vital. For example, in safety-related applications such as hazard warning, passing assistance and collision avoidance biased results caused by a Sybil attack can lead to severe car accidents. This paper presents a novel method for detecting sybil attacks in urban vehicular networks.*

KEYWORDS: *Malicious vehicle, RSU, Sybil attack, Trajectory.*

I. INTRODUCTION

Recent advances in various Dedicated Short Range Communication (DSRC) techniques provide easy and effective communication between the vehicles with high mobility. A Vehicular Ad Hoc Network (VANET)[1] is a type of Mobile Ad Hoc Network (MANET) where intermediate nodes are moving vehicles connected using DSRC to form a multi-hop network. Drivers are provided critical information from VANET, which helps their safe and comfortable driving, such as intersection collision avoidance, emergency warning of approaching vehicles, news group broadcast, opportunistic access into internet, etc. One specific application we envision is the information exchange over the VANET in the urban area. Urban vehicular networks are quite different from those with inter-city environment in many aspects, such as the the complexity of road network structure, traffic density and the like. Drivers on different vehicles exchange information, such as emergency warnings, witness of accidents, traffic conditions, among the citywide network to assist driving. Each vehicle acts as an information provider that observes the surrounding environment and contributes useful information to the VANET. Meanwhile each urban vehicle is also an information consumer that queries the items of particular interest and retrieves them from the VANET.

The recent gain of interest for wireless communication in Vehicular Ad hoc Network (VANET) implies an always increasing the number of potential applications in this kind of network. These applications have different goals going from driving assistance (road traffic alert or emergency brake) to the comfort of the passenger (distributed games). All these applications need to exchange data using other vehicles. The communication security problem must be taken into account due to the critical goal of safety related to functions such as emergency brake. As data is broadcasted over a shared communication media, it is simple for a malicious vehicle to intercept, inject or modify data in VANET. Moreover, due to the limited communication range of the vehicle, the cooperation between nodes is essential. Exchanging data with other nodes allows to discover its neighborhood and to share data. This necessity of co- operation shows the vulnerability of these networks if no security mechanism is available. How to trust data received from the other node? Is this node even a physical entity? The multiplication of fake nodes in a wireless network in order to launch different kind of attack called as the Sybil attack [2].

The Sybil attack was first described and formalized by in [2]. It consists in sending multiple messages from one node , called the attacker node, with multiple identities. Hence, the attacker simulates several nodes in the overall network. Different types of attacks that can be launched using Sybil nodes in sensor networks are described in [3]. Applications of the Sybil attack to VANETs have been discussed in [4][5]. Goal of these attacks may be simply to give illusion of a traffic jam to force the other vehicles to leave the road to the benefit of the attacker. Nevertheless, the attack may be more dangerous, trying to provoke collision in the vehicle platoon [4]. This shows the importance of Sybil attack detection in urban vehicular networks.

II. EXISTING WORK

There are so many methods used previously to detect sybil attacks. They are explained as follows: To eliminate the threat of the Sybil attacks, it is straightforward to explicitly bind a distinct authorized identity (e.g., PKI-based signatures) [6][7] to each vehicle so that each participating vehicle can represent itself only once during all communications. Using explicit identities of vehicles has the potential to completely avoid Sybil attacks but violates the anonymity concern in the urban vehicular networks. As an alternative scheme, resource testing [8][9] can be conducted to differentiate between malicious and the normal vehicles, where the judgment is made whether a number of identities possess fewer resources (e.g., computational and storage ability) than would be expected if they were distinct. This scheme fails in heterogeneous environments where the malicious vehicles can easily have more resources than normal ones.

Considering the fact that a vehicle can present itself at only one location at a time, then localization techniques or other schemes like the Global Positioning System (GPS) aiming to provide location information of vehicles can be exploited to detect hostile identities. However, these schemes often fail in
complicated urban settings- for example bad GPS signals due to urban canyons, inaccurate localizations due to highly dynamic wireless signal quality. Later, two group signature-based schemes [10][11] have been proposed, where a message received from multiple distinct vehicles is considered to be trustworthy. Using group signatures can provide anonymity of vehicles and suppress the Sybil attacks by restraining duplicated signatures signed by the same vehicles. One practical issue of these schemes is that different messages with similar semantics may be ignored from making the decision, which leads to either a biased or no final decision.

Recently, location hidden authorized message generation scheme have been proposed, where the RSU signatures on the messages are signer ambiguous so that the RSU location information is concealed from the resulted authorized message and two authorized messages signed by the same RSU within the same given period of time are recognizable so that they can be used for identification purpose. The issue of this scheme is that the RSU is considered to be trust worthy, which can also be compromised.

III. PROPOSED WORK

A. Attack Model: In order to launch the Sybil attack, a malicious vehicle must try to present multiple distinct identities. This can be achieved by either generating a legal identity or by impersonating other normal vehicles. With the following capabilities, an attacker may succeed to launch a Sybil attack in urban vehicular networks: Heterogeneous configuration— malicious vehicles can have more communication and computation resources than the honest vehicles.

B. Design Goals: The design of a Sybil attack detection scheme in urban vehicular networks should achieve the following three goals:

1. Location privacy preservation: A particular vehicle would not like to expose its location information to other vehicles and the RSUs as well since such information can be confidential. The detection scheme should prevent the location information of the vehicles from being leaked.
2. Online detection: When a Sybil attack is launched, then the detection scheme should react before the attack has terminated. Otherwise, the attacker vehicle could already achieve its purpose.
3. Independent detection: The essence of Sybil attack happening is that the decision is made based on the group negotiations. To eliminate the possibility that the Sybil attack is launched against the detection itself, the detection should be conducted independently by the verifier without collaboration with others.

C. RSU Deployment: In Footprint, vehicles require authorized messages issued from the RSUs to form trajectories, which should be statically installed as the infrastructure. When considering the deployment of the RSUs, two practical questions are essential. A simple solution is to deploy RSUs at all intersections. This can result fine trajectories with a sufficient number of authorized messages which will facilitate the recognition of the vehicle. However, deploying such a huge number of RSUs in one time is prohibitive due to high cost.

D. Location hidden authorized Message Generation: In order to be location hidden, authorized messages issued for the vehicles from an RSU should possess two properties. The temporarily linkable property requires that two authorized messages are recognizable if and only if they are generated by the same RSU within the same given period of time.

E. Sybil attack Detection: During a conversation, upon request from the conversation holder, all the participating vehicles provide their trajectory-embedded authorized messages issued within specified event for identification. With submitted messages, the conversation holder verifies that each trajectory and refuses those vehicles that fail the message verification. After that, the conversation holder conducts an online Sybil attack detection before further proceeding with the conversation.

In Footprint, vehicles have wide freedom to create their own trajectories. For example, a vehicle is allowed to request multiple authorized messages from the RSU using different temporary key pairs. Thus, the vehicle can use different authorized messages for different conversations. This capability, however, can be leveraged by a malicious vehicle that tries to launch the Sybil attack by using multiple different messages in a single conversation. The Sybil attack problem is hard due to three following factors:

1. Authorized messages generated for different vehicles are to be asynchronous.
2. Authorized messages are temporarily linkable, which means that there is no invariable mapping between an RSU signature and the real RSU who signed this signature.
3. A malicious vehicle can abuse the freedom of the trajectory generation and the neighbor relationship among RSUs to generate elaborately designed trajectories.

For example, in Figure 1, an attacker can legally generate multiple trajectories which appear different from each other even under a very simple RSU topology. Assume that the real path of the attacker is {R1, R2, R3, R4} (indicated by solid arrows). It can start a new trajectory at any RSU by using a temporary key pair. Therefore, besides the trajectory {R1, R2, R3, R4}, trajectories such as {R1, R2, R3}, {R2, R3, R4}, {R1, R2}, {R2, R3},{R3, R4}, {R1}, {R2}, {R3} and {R4} are all

legitimate. In addition, knowing the neighboring relationship of both R2 andR4, the attacker can generate forged trajectories like {R1, R2, R4}, {R1, R4}, and {R2, R4} (indicated by the dash arrow).

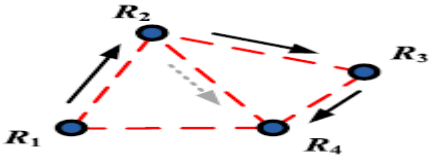

Figure 1: Sybil Trajectory Generation

F. Social Relationship among Trajectories: Despite the asynchrony and temporarily linkable properties of the authorized messages, there are two basic facts that can be exploited to judge whether two trajectories are from two actual vehicles. First, it is very hard, if not impossible, for a single vehicle to traverse between a pair of RSUs shorter than a given time limit. Second, within a limited time period, the total number of RSUs traversed by using a single vehicle is less than a limit. Based on these features an exclusion test is used to examine whether two trajectories are distinct. There are two cases where a pair of trajectories can pass this test. In first case, there are two distinct RSUs appearing within a sliding time window (called check window) when checking two trajectories. We can set the size of the check window equals to traverse time limit. For example, in Figure 2, trajectories T 1 and T 2 are distinct since there exists a pair of different RSUs within the check window, denoted by the box of dash line, i.e., R2 and R3. In the second case, the number of RSUs contained in the merged RSU sequence of the two trajectories is larger than the trajectory length limit.

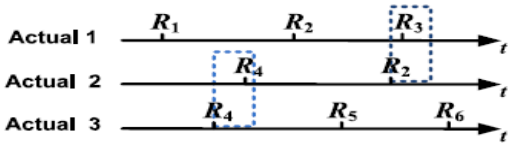

Figure 2: Checking for distinct trajectories a check window

IV. CONCLUSION

Malicious vehicle can easily obtain messages between two other communicating entities by using eavesdropping on the wireless channel. Footprint, all messages delivered through wireless communication. If a malicious vehicle can succeed in using authorized message issued for other vehicle it can masquerade as multiple identities launching a Sybil attack. In existing systems, location Hidden Authorized Message Generation Scheme was implemented In this scheme the Road Side Unit (RSU) is compromised by the forged vehicle and also it is not trustworthy. If an RSU is compromised, it can help a malicious vehicle generate fake legal trajectories, for example by inserting link tags of other RSUs into a forged trajectory. In that case, Footprint mechanism cannot detect such trajectories. However, the corrupted RSU cannot deny a link tag generated by itself nor forge the link tags generated by other RSUs, which can be utilized to detect a compromised RSU in the system. In our proposed work, first, consider the scenario where a small fraction of the RSUs are compromised. We will develop cost-efficient techniques to fast detect the corruption of the RSU. Second, we will delve into designing process better linkable Signer-Ambiguous Signature Schemes such that the computation overhead for signature verification and the communication overhead can be reduced. Third, a threshold ElGamal system based key management scheme for safeguarding urban vehicular networks from the compromised RSUs and their collusion with the malicious vehicle.

REFERENCES

[1]. C. Harsch, A. Festag, and P. Papadimitratos, "Secure Position-Based Routing for VANETs," In Proc. of IEEE VTC, 2007.
[2]. J. Douceur. The Sybil Attack. In First International Workshop on Peer-to-Peer Systems, pages 251–260, March 2002.
[3]. J. Newsome, E. Shi, D. Song, and A. Perrig. The Sybil Attack in Sensor Networks: Analysis & Defenses. In Proceedings of the third international symposium on Information processing in sensor networks, pages 259–268, 2004.
[4]. J. Blum and A. Eskandarian. The Threat of Intelligent Collisions. IT Professional, 6(1):24–29, January-February 2004.
[5]. M. Raya and JP. Hubaux. Securing Vehicular Ad Hoc Networks. Journal of Computer Security, Special Issue on Security of Ad Hoc and Sensor Networks, 15(1):39– 68, 2007.
[6]. M. Castro, P. Druschel, A. Ganesh, A. Rowstron, and D.S.Wallach, "Secure Routing for Structured Peer-to-Peer Overlay Networks," Proc.
[7]. Symp. Operating Systems Design and Implementation (OSDI '02), pp. 299-314, Dec. 2002.
[8]. S.Chang, Y.Qi, H.Zhu, J.Zhao, and X.Shen, "Footprint: Detecting Sybil Attacks in Urban Vehicular Networks", IEEE Trans. Parallel and Distributed Systems, vol.23, June. 2012.
[9]. C. Piro, C. Shields, and B.N. Levine, "Detecting the Sybil Attack in Mobile Ad Hoc Networks," Proc. Securecomm and Workshop, pp. 1-11, Aug. 2006.
[10]. N. Borisov, "Computational Puzzles as Sybil Defenses," Proc. Sixth IEEE Int'l Conf. Peer-to- Peer Computing (P2P '06), pp. 171-176, Oct. 2006.
[11]. Q. Wu, J. Domingo-Ferrer, and U. Gonzalez Nicola´ s, "Balanced Trustworthiness, Safety and Privacy in Vehicle-to-vehicle Communications,"
[12]. IEEE Trans. Vehicular Technology, vol. 59, no. 2, pp. 559-573, Feb. 2010.
[13]. L. Chen, S.-L. Ng, and G. Wang, "Threshold Anonymous Announcement in VANETs," IEEE J. Selected Areas in Comm., vol. 29, no. 3, pp. 1-11, Mar. 2011.

International Journal of Modern Engineering Research (IJMER)
www.ijmer.com Vol. 3, Issue. 4, Jul. - Aug. 2013 pp-2341-2343 ISSN: 2249-6645

An Ontology Model for Knowledge Representation over User Profiles

Shaik Haseena Sultana[1], Ch. N. Santhosh Kumar[2], V. Sitha Ramulu[3]
[1]*M. Tech, Swarna Bharathi Institute of Science & Technology, Khammam, A.P., India*
[2]*Assoc. Professor, Dept. of CSE, Swarna Bharathi Institute of Science & Technology, Khammam, A.P., India*
[3]*Assoc. Professor, Dept. of IT, Swarna Bharathi Institute of Science & Technology, Khammam, A.P., India*

ABSTRACT: *The amount of information on the world wide web increases rapidly. But gathering the required information from the web has become the most challenging job in today's scenario. People are only interested in the relevant information from the web. The web information gathering systems before this satisfy the user's requirements by capturing their information needs. For this reason user profiles are created for user background knowledge representation and description. The user profiles represent the concepts models possessed by user while gathering the useful web information. The concept of Ontologies is utilized in personalized web information gathering which are called ontological user profiles or personalized ontologies. In this paper, an ontology model is proposed for representing the user background knowledge for personalized web information gathering. Personalized ontology attempts to improve the web information gathering performance by using ontological user profiles. The model constructs user personalized ontologies by extracting world knowledge from the Library of Congress Subject Headings system and discovering user background knowledge from user local instance repositories.*

KEYWORDS: *Ontologies, Specificity, User profiles, WWW.*

I. INTRODUCTION

Over the last decade, we have witnessed an explosive growth in the information available on the World Wide Web (WWW). Gathering useful information from the WWW has become a challenging issue for users. The Web users expect more intelligent systems or agents to gather the useful information from the huge size of Web related data sources to meet their information needs. The user profiles are created for the user background knowledge description [1][2][3]. User profiles represent the concept models possessed by users when gathering the web information. A concept model is implicitly global analysis method, which is an effective method for gathering the global knowledge. Local analysis is used for analyzing the user behavior in the user profiles. In some works, users provided with a set of documents from that background knowledge can be discovered. The user background knowledge can be better discovered if we integrate both global and the local information. It can be better improved by using the ontological user profiles. A multidimensional ontology mining method, Specificity and exhaustivity, for analyzing the concept of specified machine-readable documents.

The goal of ontology learning is to semi automatically possessed by the users and is generated from their background knowledge. This knowledge is used to gather relevant information about a user's choices and preference. World knowledge is a common sense knowledge acquired by the people from experience and education[4]. For representing the user profiles, the user background knowledge must be gathered by using local or global analysis. Global analysis uses worldwide knowledge base for representing background knowledge. The commonly used knowledge bases include generic ontologies e.g. Thesauruses, digital libraries, word net. Compared with the other benchmark models, ontology model is successful.

II. RELATED WORK

A. Ontology Learning: Ontologies are the means of knowledge sharing and reuse. They are called semantic containers. The term "Ontology" has various definitions in various domains, texts and applications. Many existing knowledge bases are used by many models for learning ontologies. In [1] and [5], the authors learned personalized ontologies from the Open Directory Project to specify users‟ preferences and interests in web search. King developed "IntelliOnto" method based on the basis of the Dewey decimal classification. The Dewey Decimal Classification (DDC) system is a general knowledge organization system that is used continuously revised to keep pace with knowledge. The DDC is used around the world in 139 countries, over sixty of these countries also use Dewey to organize their national bibliographies. Over the lifetime of the system, the DDC has been translated into more than 30 languages [6]. In [7], the authors used Wikipedia which helps in understanding user interests in queries. The above work discovered user background knowledge but the performance is limited by the quality of the global knowledge base. Much work has been done for discovering user background knowledge from the user local information. Pattern reorganization and association rule mining technique to discover the knowledge from user local information is used by [3].

A domain ontology learning approach was proposed in [3] that uses various data mining and natural language understanding techniques to discover knowledge from user local documents for ontology construction. Semantic relations and concepts are discovered in [9] for which he developed a system called Ontolearn. OntoLearn system is an infrastructure for automated ontology learning from the domain text. It is the only system, as far as we know, that uses the natural language processing and machine learning techniques. In [8], the authors use content mining techniques to find semantic knowledge from domain-specific text documents for ontology learning. Much of the user background knowledge is discovered using

these data mining technique. In many work, ontologies are used for getting better performance in knowledge discovery process.

B. User Profiles: In the web information gathering, user profiles were used to understand the semantic meanings of the queries and capture user Information needs. User profiles are used for user personalization and modeling. It is used to reflect the interests of users. Li and Zhong defined user profiles as the interesting topics of a users information need. The user profiles are categorized into two diagrams- the data diagram and which are acquired by analyzing a database or a set of transaction whereas the information diagram user profiles acquired by using manually such as interviews and questionnaires or automatic techniques such as information retrieval and machine learning. User profiles are categorized into three groups: they are- interviewing, semi-interviewing, and non-interviewing [1][3].

III. PROPOSED WORK

In proposed work, by using ontology mining we can discover interesting and on-topic knowledge from the concepts, semantic relations and instances in ontology. Here we discuss 2D ontology mining method callded specificity and exhaustivity. Our focus on a given topic is described by Specificity and subject's semantic space dealing with the topic is restricted by exhaustivity. Using this method we can investigate the subject and the strength of their association in ontology. The subject's specificity has two focuses which are known as semantic specificity and topic specificity.

A. Semantic Specificity: Semantic specificity is also called absolute specificity, denoted by spe_a (s). Let $\partial(\Gamma)$ is a world knowledge base. The semantic specificity is measured based on the hierarchical semantic relations(is-a and part-of) held by the subject and its neighbors in tax^s. The A(s') and part of(s') are two functions in the algorithm satisfying: A(s')∩part of(s')=Ø.As the tax^s of $\partial(\Gamma)$ is a graphic taxonomy, the leaf subjects have no descendants. If a subject has direct child subjects mixed with relations is-a and part-of relationships, a spe_a and spe_a are addressed separately with respect to the relations is-a and part-of child subjects. The following algorithm illustrates semantic relations for specificity:

Algorithm:

Input: a personalized ontology $\partial(\Gamma)$:= < tax^s ,rel> ;
A coefficient Θ between (0,1).

Output: spe_a (s) applied to specificity.

Step 1: set k=1, get the set of leaves s_o from tax^s,
for(s_o ϵ S_o) assign spe_a (s_o) = k;

Step 2: get S' which is the set of leaves in case we remove the nodes S_o and the related edges from tax^s;

Step 3: if (S' == Ø) **then** return;// the terminal condition;

Step 4: for each s' ϵ S' do

Step 5: if (is A(s') == Ø) then spe_a^1 (s')=k;

Step 6: else spe_a^1 (s') = Θ * min{ spe_a (s)|sϵ isA(s')};

Step 7: if (part of(s') == Ø) then spe_a^2 (s')=k;

Step 8: else spe_a^2 (s')=Σsϵ partOf(s') spe_a (s)/|partOf(s')|;

Step 9: spe_a (s')=min(spe_a^1(s'), spe_a^2 (s'));

Step 10: End

Step 11: k=k*Θ, $S_o = S_o$ U S', go to step 2.

B. Topic Specificity: The topic specificity of a subject is investigated, based on the user background knowledge discovered from the user's local information. User background knowledge can be discovered from the user's local information collections. Populate the ontology with the instances generated from the user's local information collections. Such a collection called as user local instance repository (LIR). Generating the user's local LIRs is a challenging issue. The documents in LIRs may be semi- structured or an unstructured .In semi- structured web documents, content-related descriptors are specified in the meta-data sections. These descriptors have direct reference to the concepts specified in the global knowledge base. These documents are ideal to generate the instances for the ontology population. The documents in the user local repository have content-related descriptors referring to the subjects in O(T). The reference strength between an instance and the subject needs to be evaluated. Hence, denoting an instance by "i", the strength of i to a subject s is determined by:

$$str(i, s)= \frac{1}{priority(s,i)Xn(i)}$$

The subject str (i, s) aims to select the right instances to populate O(T). With the str(i, s) determined, the relationship between the LIR and O(T) can be defined. Let Ω= {i1, i2 ,i3,……. ik } be a finite and non- empty set of instances in an LIR, and min_str be the minimal str values for filtering out the noisy pairs with weak strengths.

C. Architecture of the Ontology Model: The proposed ontology model aims to discover the user's back-ground knowledge and learns personalized ontologies to rep-resent user profiles. Figure 1 illustrates the architecture of the ontology model. A personalized ontology is constructed using a given topic. Two knowledge resources, the global world knowledge base and the user's local instance repository, are utilized by using the model. The world knowledge base provides the taxonomic structure for the personalized ontology representation. The user background knowledge is discovered from the user's local instance repository. Against the given topic, the specificity and exhaustivity of the subjects are investigated for user background knowledge discovery.

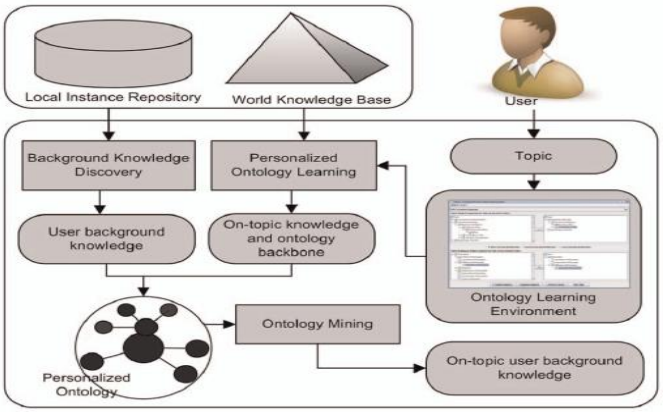

Figure 1: Architecture of the ontology model

From the figure, we can hypothesize that user background knowledge can be better discovered and represented if we can integrate global and the local analysis within a hybrid model. The knowledge formalized in the global knowledge base will con-strain the background knowledge discovery from the user local information. Such a personalized ontology model should produce a superior representation of the user profiles for web information gathering.

IV. CONCLUSION

Every user has a distinct background and a specific goal when searching for information on the World Wide Web. The goal of Web search personalization is to tailor the search results to a particular user based on that user's interests and preferences. Effective personalization of information access involves two important challenges- accurately identifying the user's context and organizing the information in such a way that matches the particular contexts. We present an approach to personalized search that involves building models of the user's context as ontological profiles by assigning implicitly derived interest scores to existing concepts in domain ontology. A spreading activation algorithm is used to maintain the interests scores based on user ongoing behaviour.

REFERENCES

[1]. S. Gauch, J. Chaffee, and A. Pretschner,"Ontology-Based Personalized Search and Browsing," Web Intelligence and Agent Systems, vol. 1, nos. 3/4, pp. 219-234, 2003.
[2]. Y. Li and N. Zhong, "Web Mining Model and Its Applications for Information Gathering," Knowledge-Based Systems, vol. 17, pp. 207-217, 2004.
[3]. Y. Li and N. Zhong, "Mining Ontology for Automatically Acquiring Web User Information Needs,"IEEE Trans. Knowledge and Data Eng., vol. 18, no. 4, pp. 554-568,Apr. 2006.
[4]. S.E. Robertson and I. Soboroff, "The TREC 2002 Filtering Track Report," Proc. Text Retrieval Conf., 2002.
[5]. Sieg, B. Mobasher, and R. Burke, "Web Search Personalization with Ontological User Profiles," Proc. 16th ACM Conf. Information and knowledge Management(CIKM" 07),pp.525-534,2007
[6]. J.D. King, Y. Li, X. Tao, and R. Nayak, "Mining World Knowledge for Analysis of Search Engine Content," Web Intelligence and Agent Systems, vol. 5, no. 3, pp. 233-253, 2007
[7]. D. Downey, S. Dumais, D. Liebling, and E. Horvitz, "Understanding the Relationship between Searchers" Queries and Information Goals," Proc. 17th ACM Conf. Information and Knowledge Management (CIKM " 08), pp. 449-458, 2008
[8]. X. Jiang and A.-H. Tan, "Mining Ontological Knowledge from Domain-Specific Text Documents," Proc. Fifth IEEE Int" l Conf. DataMining (ICDM " 05), pp. 665-668, 2005.
[9]. R. Navigli, P. Velardi, and A. Gangemi, "Ontology Learning and Intelligent Systems, vol. 18, no. 1, pp. 22-31, Jan./Feb. 2003.Its Application to Automated Terminology Translation," IEEE Intelligent Systems, vol. 18, no. 1, pp. 22-31, Jan./Feb. 2003.

International Journal of Modern Engineering Research (IJMER)
www.ijmer.com Vol. 3, Issue. 4, Jul. - Aug. 2013 pp-2344-2346 ISSN: 2249-6645

A Novel Data Extraction and Alignment Method for Web Databases

Sravan Kumar Teegala[1], Ch.N.Santhosh Kumar[2], V. Sitha Ramulu[3]
[1]*M. Tech, Swarna Bharathi Institute of Science & Technology, Khammam, A. P., India*
[2]*Assoc. Professor, Dept. of CSE, Swarna Bharathi Institute of Science & Technology, Khammam, A.P., India.*
[3]*Assoc.Professor, Dept. of IT, Swarna Bharathi Institute of Science & Technology, Khammam, A.P., India.*

ABSTRACT**:** *Online databases, also called web databases, comprise the deep web tag and value. Compared with WebPages in the surface web, which can be accessed by using a unique URL, pages in the deep web are dynamically generated in response to a user query submitted through the query interface of a web database. Upon receiving a user's query, a web database returns the relevant data, either structured or semi structured, encoded in the HTML pages. Many web applications, such as data integration, met querying and comparison shopping, need the data from multiple web databases. For these applications to further utilize the data embedded in HTML pages, the automatic data extraction is necessary. Only when the data are extracted and organized in a structured manner, such as tables, can they be aggregated and compared. Hence, accurate data extraction is vital for these applications to perform process correctly. This paper focuses on the problem of automatically extracting data records that are encoded in the query result pages generated from web databases.*

KEYWORDS: *Data extraction, HTML, Query, Tag tree.*

I. INTRODUCTION

World Wide Web(WWW) is a powerful source of information. Search engines are very important tools for users to get the desired information on the web. Not only web users but many web applications also need to interact with the search engines. For decision making many business applications have to depend on the web in order to aggregate information from different web sites. By analyzing and summarizing web data we can find the latest market trends, price details, product specification etc. Manual data extraction is time consuming and leads to errors. In this context automatic web information extraction plays an important role. Example of web information extraction are: Extract competitor's price list from the web page regularly to stay ahead of competition, extract data from the web pages and transfer it to another application, extract people's data from the web pages and put it in a database.

Automatic data extraction plays an important role in processing results provided by the search engines after submitting the query by user. Wrapper is an automated tool which extracts Query Result Records (QRRs) from HTML pages returned by the search engines. Automated extraction is easier with the web sites having web service interfaces like Google and Amazon. But it's difficult for those that support B2C i.e. business to customer applications which does not have the web service interfaces. Normally Search engine result consists of query independent contents (static contents), query dependent contents (dynamic contents), while some contents are affected by many queries but independent of the content of specific query (semi-dynamic). As the web evolved web page creation process changed from manual to a more dynamic procedure using the complex templates. Many web pages are not created in advance, but are generated dynamically by querying the database server and sending the results to a predefined page structure. Automatic data extraction is very important for many applications, such as data integration , meta-querying and comparison shopping, that need to co-operate with multiple web databases to collect data from multiple sites and provide services.

II. RELATED WORK

In [1], the authors presented a novel data extraction method, ODE (Ontology-assisted Data Extraction), which automatically extracts the query result records from the HTML pages. To label attributes it is necessary that the labels appear in the query interfaces or query result pages within the domain. If the query result records are arranged into two or more different formats in the query result pages, then only one format will be identified as "query result section". Finally, the performance of ODE on certain types of query result pages is far from satisfactory only. In [2], the authors presented an overview of the issues involved in measuring data linkage and de duplication quality and complexity. It is shown that measures in the space of the record pair comparisons can produce deceptive accuracy results. It is recommended that the quality be measured using the precision-recall or F-measure graphs rather than using single numerical values, and that quality measures that include the number of true negative matches should not be used due to their large number in the space of record pair comparisons.

In [3], the authors made a thorough analysis of the literature on duplicate record detection. The similarity metrics that are commonly used to detect the similar field entries and an extensive set of duplicate detection algorithms that can detect approximately duplicate records in a database are covered. The lack of standardized, large scale benchmarking data sets can be a big obstacle as it is almost impossible to convincingly compare new techniques with the existing ones. In [4], the authors studied the problem of structured data extraction from arbitrary Web pages. In this paper, a novel and effective technique, called DEPTA, to perform the task of Web data extraction automatically is proposed. This method has the following drawbacks- When an object is very dissimilar to its neighboring objects, DEPTA misses it. This also causes a few identified data records to contain an extra information or to miss part of their original data items.

In [5], the authors presented a technique for automatically producing wrappers that can be used to extract search result records from dynamically generated result pages returned by search engines. The main problem with this method is its reliance on the tag structure in the query result pages, due to which it suffers from very poor results. In [6], the authors addressed the problem of unsupervised Web data extraction using a fully-automatic information extraction tool called ViPER. The tool is able to extract and separate data exhibiting recurring structures out of a single Web page with high accuracy by identifying the tandem repeats and using visual context information. However, this technique lacks overall performance in few datasets.

III. PROPOSED WORK

In this section, we describe the methods that are use in the process of Data extraction and Alignment. There is method for automatically extracting data records that are encoded in the query result pages generated by the web databases.

Figure 1 shows the framework for QRR extraction.

A. Tag Tree Construction: The first step is constructing a tag tree for the page rooted in the <HTML> tag. Each node represents a tag in the HTML page and its children are tags enclosed in it. Each internal node n of the tag tree has a tag string "tsn", which includes the tags of n and all tags of n's descendants, and a tag path tpn, which includes the tags from the root to n.

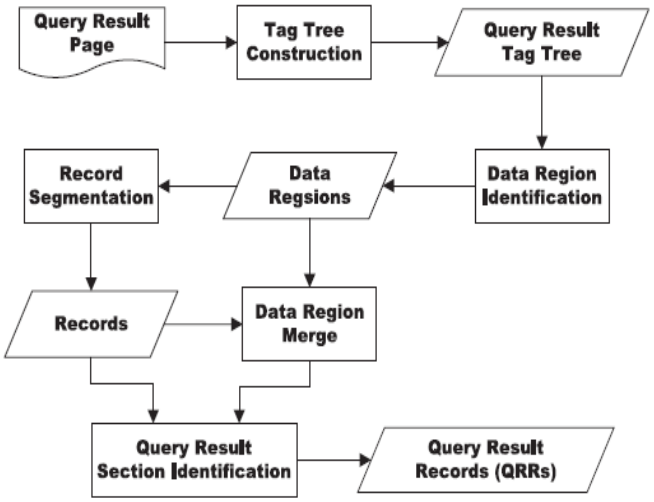

Figure 1: QRR Extraction framework

B. Data Region Identification: Similar data records of the same parent node are grouped as a "data region". It deals with the non- contiguous data records as well. Here we propose a new method that considers the auxiliary information leading to accurate data extraction. For this we need a temporary file which buffers the attributes as well as their values. These are further filtered which used to identify the exact data regions.

C. Record Segmentation: In a tag tree[4], the tandem repeats within a data region is initially found out. If only one repeat is found out then it corresponds to a record. In case of multiple repeats then any one has to be selected. Heuristics for record segmentation are as follows:

- Within a data region, if any auxiliary information is encountered, the tandem repeat that stops is the correct one since the auxiliary information cannot be inserted in the middle of the record.
- If the above two heuristics are failed to be used, then the tandem repeat that starts the data region is selected.

D. Data Region Merge: The data region identification step may identify various data regions in a query result page. Moreover, the actual data records may span several data regions identified. In the websites we examined, 12% had QRRs with different parents in the HTML tag tree. Thus, before we can identify all the QRRs in a query result page, we need to determine whether any of the data regions identified should be merged. Given any two data regions, we treat them as similar if the segmented records they contain are very similar. The similarity between any two records from two data regions is measured by using the similarity of their tag strings. The similarity between the two data regions is calculated as the average record similarity.

E. Query Result Section Identification: Even after performing the data region merge step, there may still be multiple data regions in the query result page. However, we assume that at most one of the data regions contains the actual QRRs. Three heuristics are used to identify this data region, called as the query result section:

- The query result section usually occupies a large space in the query result page
- The query result section is usually located at the center of the query result page

- Each QRR usually contains more raw data strings than the raw data strings in other sections.

F. ***QRR Alignment:*** The data values that belong to the same attribute generally show similarity in the data values and may include similar strings. Data value similarity [7] is calculated between every pair of values .The pairwise alignment determines whether the paired data values belong to the same attribute on the basis of calculated the data value similarity. Similarity of the record path is a constraint .The alignment of the data values between two QRRs must be unique. There should not be any cross alignment as well. After the pairwise alignment all data values of the same attribute are put in to the same table column globally by using of holistic alignment. This is similar to finding the connected components in an undirected graph . The vertices from the same record are not included in the same component. If any vertices breach this constraint, then the breach path is to be established. However the connected components are not allowed to intersect with each other. Finally a nested processing is needed to handle the attributes that having multiple values.

IV. CONCLUSION

In this project a novel data extraction method is proposed to automatically extract QRRs from a query result page. This method employs two steps for this task: The first step identifies and segments the QRRs to improve the existing techniques by allowing the QRRs in a data region to be non- contiguous. The second step is used to align the data values among the QRRs. An alignment method is used in which the alignment is performed in three consecutive steps: pair wise alignment, holistic alignment, and nested structure processing.

REFERENCES

[1]. W. Su, J. Wang, and F.H. Lochovsky, "ODE: Ontology-Assisted Data Extraction," ACM Trans. Database Systems, vol. 34, no. 2, article 12, p. 35, 2009.
[2]. P. Christen and K. Goiser, "Quality and Complexity Measures for Data Linkage and Deduplication," Quality Measures in Data Mining, F. Guillet and H. Hamilton, eds., vol. 43, pp. 127-151, Springer, 2007.
[3]. A. K. Elmagarmid, P.G.Ipeirotis, and V.S.Verykios, "Duplicate Record Detection: A Survey", IEEE Trans. Knowledge and Data Eng., vol. 19, no. 1, pp. 1-16, Jan.2007.
[4]. Y. Zhai and B. Liu, "Structured Data Extraction from the Web Based on Partial Tree Alignment," IEEE Trans. Knowledge and Data Eng., vol. 18, no. 12, pp. 1614-1628, Dec. 2006.
[5]. H. Zhao, W. Meng, Z. Wu, V. Raghavan, and C. Yu, "Fully Automatic Wrapper Generation for Search Engines," Proc. 14th World Wide Web Conf., pp. 66-75, 2005.
[6]. K. Simon and G. Lausen, "ViPER: Augmenting Automatic Information Extraction with Visual Perceptions," Proc. 14th ACM Int'l Conf. Information and Knowledge Management, pp. 381-388, 2005.
[7]. Weifeng Su, Jiying Wang, Frederick H.Lochovsky and Yi Liu, "Combining Tag and Value Similarity for Data Extraction and Alignment,"IEEE Transactions on Knowledge and Data Engineering,vol. 24, no. 7, pp. 1186-1199, 2012.

International Journal of Modern Engineering Research (IJMER)
www.ijmer.com Vol. 3, Issue. 4, Jul. - Aug. 2013 pp-2347-2349 ISSN: 2249-6645

Combating Bit Losses in Computer Networks using Modified Luby Transform Code

Anand P.[1], George M. Joseph[2], Arun A. S.[3], Dhanish Vijayan[4], Jerryl James Abraham[5], Gopalakrishnan P. N. Nair[6], Bob P. George[7]

[1](*M.Tech Student, Department of ECE, SCT College of Engineering,* India)
[2](*Assistant Professor, Department of ECE, SCT College of Engineering, India)*
[3](*M.Tech Student, Department of ECE, SCT College of Engineering, India)*
[4](*M.Tech Student, Department of ECE, College of Engineering, Trivandrum, India)*
[5, 6, 7](*Project Engineer, Elementz Engineers Guild Pvt. Ltd., India)*

ABSTRACT : *Erasure channels like computer networks are of great importance. Due to the large amount of packet retransmission that takes place in the currently existing methods to combat bit losses in erasure channels, they are either inefficient or time consuming. Through this paper, we propose a Modified Luby Transform (MLT) coding scheme to efficiently combat bit losses on transmitted data over computer networks, while eliminating the need for retransmission. The simulation and implementation results of the proposed MLT code confirm the efficiency of the encoding scheme. The MLT code is tested on a live computer network and applicability of the code in real world situations is verified and confirmed.*

Keywords: *Erasure channel, Fountain Codes, Luby Transform Codes, Wired Networks, Wireless Networks*

I. INTRODUCTION

Bit losses in erasure channels are of great concern. Files sent over the internet or a wired / wireless LAN network are converted to bits / packets, and each bit / packet is either received without error or not received, that is they behave like erasure channels. Also if you take the case of a mail server, when you send a mail, the recipient either receives the mail or does not receive it. There is no chance for the content to be received incorrectly. Erasure codes are codes that work on such erasure channels and combat bit losses / erasures. The erasure channel is described by the probability of erasure of that channel. Say if the probability of erasure is 0.1, it means that 10% of the data transmitted would be lost and the rest 90% would be received without any error.

Common methods for communicating over such channels employ a feedback channel from receiver to sender that is used to control the retransmission of erased bits / packets. The receiver might send back messages which enable identification of the missing packets, which are then retransmitted. Alternatively, the receiver might send back acknowledgements for each received packet; the sender keeps track of which packets have been acknowledged and retransmits the others until all packets have been acknowledged.

These retransmission protocols have the advantage that they will work regardless of the erasure probability but if the erasure probability is large, the number of feedback messages sent by the first protocol will be large. If the system uses the second protocol, it is very likely that the receiver will end up receiving multiple redundant copies of many packets, and heavy use is made of the feedback channel [1]. Fountain codes are provided as a solution for reliable communication in lossy networks [2] [3] [4]. They eliminate the need of retransmission request which increases the bandwidth consumption and increases the delay. Luby transform (LT) codes are special case of fountain codes [2]. LT encoder chooses randomly from a set of K packets, and according to a distribution, a subset of d packets, and XOR them [2]. In practice, decoding may be possible from a set S of such encoded packets, for S slightly larger than K.

In [5], a new method was designed to integrate the notion of network coding with the technique of connected dominating set which represents the source independent backbone in order to improve the broadcast process in ad hoc wireless network. When using the source independent backbone, the intermediate nodes are either responsible for retransmitting all or none of packets. This increases network coding efficiency since forwarder nodes use all available packets in encoding [5]. In [6], some of the nodes are chosen to retransmit messages, independent on coding process. Decoding process is improved in [7]. Fountain codes were used in [8] to broadcast n packets from the source. The source generates m encoded packets using LT codes, and floods each of them into the network. Each recipient retransmits each received packet with certain fixed probability. When a recipient has received enough data, it can decode original packets [8]. In all the above cases, LT codes are used along with retransmission protocols or relaying-based protocols to improve the efficiency. But they do not consider the delay caused by these methods. In practical cases, all the above methods cause delays which are inappropriate for live networks. Through this paper, we propose a Modified Luby Transform (MLT) code which can efficiently combat bit losses and can be efficiently used in a live network without any need for concatenating it with any retransmission or relay-based protocols. Using the MLT codes, we can eliminate the use of the feedback channel and also improve the performance of the receiver.

II. MODIFIED LUBY TRANSFORM (MLT) CODE

We propose a modified decoding algorithm for a particular LT encoding pattern. In the proposed MLT codes, the input bits are divided into sets of four bits and each four bit input is encoded to form an eight bit encoded packet. During encoding, the first and last bit of the encoded packet is set to be the first bit of the input. The other bits of the encoded packet

would be the XORed version of the previous bit of the encoded packet with the next input bit. Let [a b c d] be the input bits and [E1 E2 E3 E4 E5 E6 E7 E8] be the bits of the encoded packet, then

E1 = a
E2 = E1 xor b = a xor b
E3 = E2 xor c = a xor b xor c
E4 = E3 xor d = a xor b xor c xor d
E5 = E4 xor a = b xor c xor d
E6 = E5 xor b = c xor d
E7 = E6 xor c = d
E8 = a

The MLT encoding process is depicted in Fig. 1 below

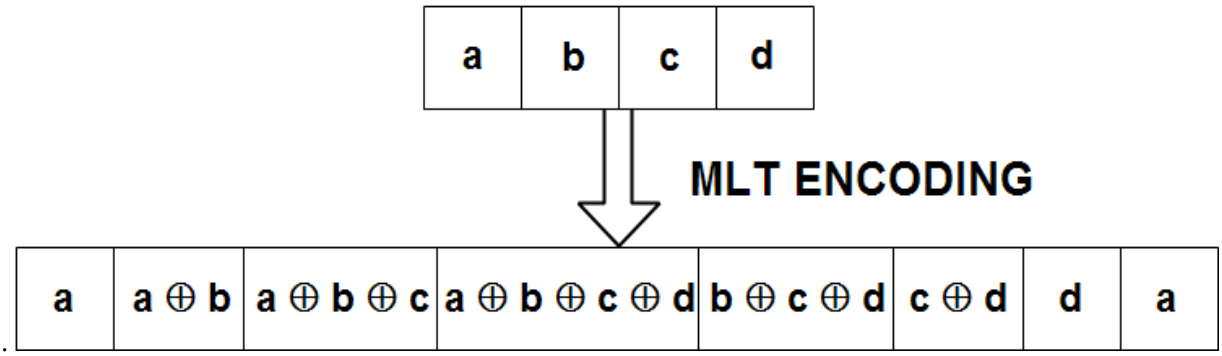

Fig. 1 Modified Luby Transform (MLT) Encoding

While transmitting through the channel, the bits of the encoded packets may get lost. So what we get would be a punctured form of the transmitted bit. At the receiver end, we need to get back the original information from the punctured form of received packet. Here we use a modified decoding algorithm. It is an iterative process. During the first iteration, we make use of the normal LT decoding process in which successive XORing of the bits of the encoded packets will result in the input bits. Since some of the bits of the packet are lost, all the input bits cannot be correctly retrieved. Now, using the retrieved bits and the correctly received bits, we can make further XORed combinations of the input bits. This is used in the next iteration and we look for decoding the input bits by successive XORing of the generated bits in the previous iteration along with the correctly received bits, say we had received 'E4' (b xor c xor d) and correctly retrieved bits, 'b' and 'd' but we could not retrieve 'c'; we can generate a combination 'b xor d' from the correctly retrieved bits and then XOR the generated bit with the 'E4' to correctly retrieve 'c'. The iteration is continued till all input bits are retrieved or if all bits could not be retrieved even after eight iterations levels.

The MLT decoding process is depicted in Fig. 2 below. The blank portions indicate the bits lost during data transmission and recovery of original data is possible even though all the bits of the received packet are not received properly at the receiver end.

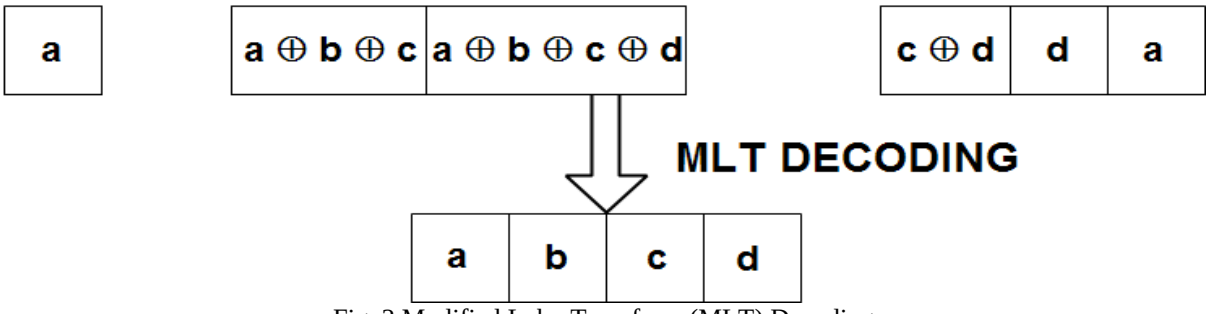

Fig. 2 Modified Luby Transform (MLT) Decoding

III. SIMULATION AND HARDWARE IMPLEMENTATION

The MLT codes were simulated using MATLAB R2012a on a computer with Intel i5 2.4GHz (with turbo boost upto 3.2GHz) processor and 4GB RAM. The simulation results of MLT codes are compared with the results obtained for LT codes and for systems with no encoding.

The MLT codes were implemented on a live peer to peer computer network. All data to be transmitted from one computer to another computer were encoded using MLT codes and the data received at the receiving end is decoded to get back the original data. Results from hardware implementation are compared with the simulation results and are discussed in Section IV.

IV. RESULTS AND ANALYSIS

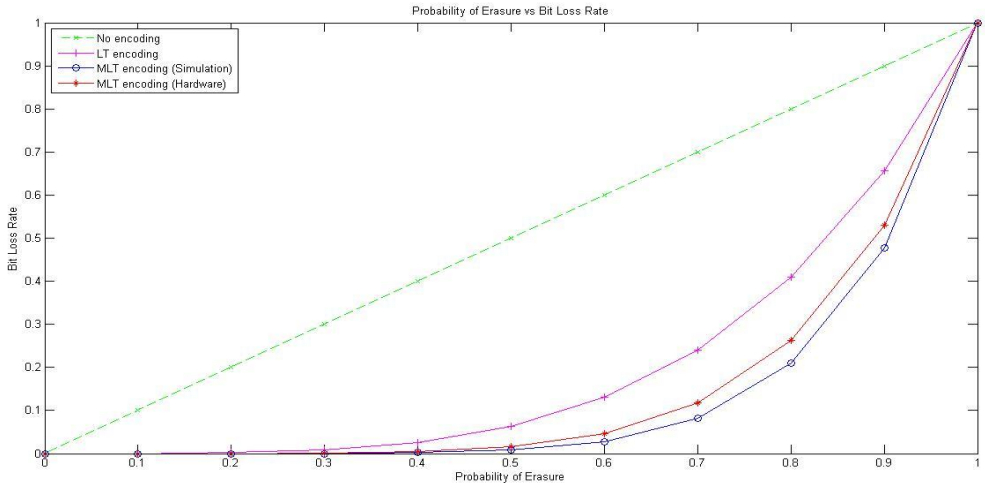

Fig. 3. Performance Analysis using Probability of Erasure vs Bit Loss Rate graph – (a) No encoding (b) LT encoding (c) MLT encoding (Simulation Results) (d) MLT encoding (Hardware Implementation Results)

From Fig. 3, we can see that bit loss rate is considerably reduced using MLT encoding. For channels with probability of erasure less than 0.45, we can see that the bit loss rate is almost zero. This means that we can correctly decode all the data even if almost half of the transmitted data is lost, we can efficiently decode the original data without any need for retransmission. Using LT codes, we can achieve lossless transmission only for channels with probability of erasure less than 0.3. In real situations, probability of erasure would be in range of 0.2 to 0.5 only, if it is more than 0.5, it would mean more or less break in channel or loss of channel as such. Say we have a live network, erasure of over 0.5 occurs when the channel is non-existent or if the router resets itself and is recreating the communication link as such. Even if retransmission is done in any of the above cases, it is more probable that the retransmitted packet is also lost and the retransmission process becomes wasteful and time-consuming. This can be avoided. MLT codes provide an efficient way to transfer data within computer networks by combating bit losses and eliminating retransmission delays.

V. CONCLUSION

A Modified Luby Transform (MLT) code is designed for computer networks and the analysis is done for channels with different probabilities of erasure. The results were compared with the results obtained by using LT codes and those without any encoding. The comparison results show that the bit loss rate can be efficiently reduced using MLT codes. The hardware implementation is done to ensure usability and reliability in live computer networks without using any retransmission process. Thus, we can conclude that by using MLT codes without any retransmission protocol, we can efficiently transmit data over wired / wireless computer networks and avoiding time delays to a large extent.

ACKNOWLEDGEMENTS

We would like to acknowledge Elementz Engineers Guild Private Limited for providing us with the facilities needed for simulation of the MLT codes and for allowing us to test it on live networks at their office premises.

REFERENCES

[1]. D.J.C. MacKay, Fountain codes, Capacity Approaching Codes Design and Implementation Special Section, IEEE Proceedings - Communication Vol.152, No. 6, December 2005
[2]. Luby, “LT codes,” in FOCS: IEEE Symposium on Foundations of Computer Science (FOCS), 2002.
[3]. Anand P., et al., “Design, Analysis and Implementation of Modified Luby Transform Code,” IOSR Journal of Electronics and Communication Engineering, volume 7, issue 1, pp. 42-51, 2013.
[4]. Shokrollahi, “Raptor codes,” IEEE Transactions on Information Theory, vol. 52, no. 6, pp. 2551–2567, 2006.
[5]. Khaldoun Al Agha, Nour KADI, Ivan Stojmenovic, Fountain Codes with XOR of Encoded Packets for Broadcasting and source independent backbone in Multi-hop Networks using Network Coding, Vehicular Technology Conference, 2009. VTC Spring 2009. IEEE 69th
[6]. E. L. Li, R. Ramjee, M. M. Buddhikot, and S. C. Miller, “Network coding-based broadcast in mobile ad-hoc networks,” in INFOCOM. IEEE, 2007, pp. 1739–1747. [Online]. Available: http://dx.doi.org/10.1109/INFCOM.2007.203
[7]. N. Kadi and K. A. Agha, “Optimized MPR-Based Flooding in Wireless Ad Hoc Network using Network Coding,” in IFIP/IEEE Wireless days’08. Dubai, UAE: IEEE Explorer, November 2008.
[8]. R. Kumar and A. Paul and U. Ramachandran, “Fountain broadcast for wireless networks,” in IEEE Int. Workshop on Network Sensing Systems, San Diego, USA, 2005.

International Journal of Modern Engineering Research (IJMER)
www.ijmer.com Vol. 3, Issue. 4, Jul. - Aug. 2013 pp-2350-2355 ISSN: 2249-6645

Design and Implmentation of Circular Cross Sectional Pressure Vessel Using Pro-E and Ansys

[1]M. Pradeep Kumar, [2]K. Vanisree, [3]Sindhuja Raj
Assistant professor in Aeronautical Engineering
[1]Aurora Scientific &Technological Institue Ghatkesar , Andhra Pradsh
Assistant professor in Aeronautical Enginnering

ABSTRACT: *In this paper we design and analyse of high pressure frame assembly for submarine mounted EW system(Electronic Warfare System). High pressure frame assembly is a leak proof container design to hold precious electronics at a pressure substantially different from the abient pressure.Design is carired according to American Society of Mechanical Engineers (ASME) code,deals with the study of various parts like flanges,support etc.various methods of facbrication and testing are also included.Using PRO-E software different 3D models are generated and analysised by using ANSYS software, a versatile Finite Element pakage.The final AHU "(Antenna Head Unit)" frame assembly has to be designed in a tradeoff between strength, weight maintenance and thermal aspects. To overcome the problems in existing rectangle cross sectional vessel design, in our proposed design the stresses developed in the circular cross section with hemispherical end caps are very less as compared to rectangle cross sectional vessel. Also in the circular cross section, the stresses and deflections are minimum. and from the results Factor of safety in the case with hemispherical end caps is 1.8.*

KEYWORDS: *high-pressure vessel, Elastic analysis, Torispherical Head, Bott Circular shape om Head, hemispherical end caps*

I. INTRODUCTION

The process of conversion from one material into another by chemical or physical means requires handling or storing of large quantities of materials in containers of varied constructions, depending upon the existing state of the material, a container or vessel is usually referred as pressure vessel which are in accordance with ASME code. The ASME gives thickness and stress of basic components, it is up to the designer to select appropriate analytical as procedure for determining stress due to other loadings. The pressure vessels are leak proof containers for fluids subjected to pressure and they may be of any shape ranging from types of processing equipment. Most process equipment units may be considered as vessels with various modifications necessary to enable the units to perform certain required functions, e.g. an autoclave may be considered as high-pressure vessel equipped with agitation and heating sources.

The designer must familiarize with the various types of stresses and loadings in order to accurately apply the results of analysis and also consider some adequate stress or failure theory in order to confine stress and set allowable stress limits. The methods of design are primarily based on elastic analysis and also other criteria such as stresses in plastic region, fatigue, creep, etc. which need consideration in certain cases. Elastic analysis is developed on the assumption that the material is isotropic and homogeneous and that it is loaded in the elastic region. This analysis is not applicable in the plastic range. Under cyclic variation of load causing plastic deformation, while due to residual stresses or strain hardening the steady state is perfectly elastic. This phenomenon is called shakedown of plastic deformation under cyclic loading. therefore Elastic analysis is the most important method of designing pressure vessel shells and components beyond the elastic limit, the material yields and the plastic region spreads with increased value of load. The load for which this occurs is called collapse load and also called as limit load.

In Limit analysis when calculating the load or pressure due to yielding failure of structural material occurs hence this method is not suitable for design the pressure vessels. When vessels are subjected to cyclic loading, it is necessary to consider requirements for elastic cycling of the material and the effects of this on component behavior. In the case of a discontinuity of shape, load may give rise to plastic cycling under these conditions, shakedown will occur and the maximum shakedown load is twice the first yield load. Therefore under cyclic loading conditions an elastic analysis is valid up to the range of load A factor of safety on the stress or a factor of safety of twenty is applied on the numbers cycles. Design stress is accepted as the lower value.

1.2 Presser Vessel

It is a closed container designed to hold gases or liquids at a pressure substantially different from the ambient pressure. The pressure vessels may be thin or thick. When the ratio of the plate thickness to mean radius of the pressure is less than 1/15 then the pressure vessel is termed as a thin pressure vessel, otherwise, a thick pressure vessel. Pressure vessels are used in a variety of applications in both industry and the private sector. They appear in these sectors as industrial compressed air receivers and domestic hot water storage tanks.

1.3 Classification of Pressure Vessels: There are two different factors in the classification of pressure vessel
According to thickness

i. Thin cylinder
ii. Thick cylinder

According to end construction

i. Closed ended
ii. Open ended

If "t" is smaller than of "d" then it is said to be as thin cylinder.

Where $\frac{t}{d}$ must be less than 0.1 "or" $\frac{t}{d}$<0.1

i.e., 10% of the internal diameter, if the ratio exceeds then the cylinder is said to be a thick cylinder.

1.4 Selection Of Pressure Vessels

The first step in the design of any vessel is the selection of the type best suited for the particular service in question. The primary factors influencing this choice are,

- The operating temperature and pressure.
- Function and location of the vessel.
- Nature of fluid.
- Necessary volume for storage or capacity for processing

It is possible to indicate some generalities in the existing uses of the common types of vessels. For storage of fluids at atmospheric pressure, cylindrical tanks with flat bottoms and conical roofs commonly used. Spheres or spheroids are employed for pressure storage where the volume required is large. For smaller volume under pressure, cylindrical tanks with formed heads are more economical.

1.5 Scope Of The Paper

The sophisticated pressure vessels encountered in engineering construction are high pressure; extremes of temperature and severity of functional performance requirements pose exciting design problems. The word "DESIGN" does not mean only the calculation of the detailed dimensions of a member, but rather is an all-inclusive term, incorporating the reasoning that established the most likely mode of damage or failure, the method of stress analysis employed and significance of results and the selection of materials type and its environmental behavior.

The ever-increasing use of vessel has given special emphasis to analytical and experimental methods for determining their emphasis to analytical and experimental methods for determining their operating stresses. Of equal importance is the appraising the significance of these stresses. This appraisal entails the means of determining the values and extent of the stresses and strains, establishing the behavior of the material involved, and evaluating the compatibility of these two factors in the media or environment to which they are subjected. Knowledge of material behavior is required not only to avoid failures, but also equally to permit maximum economy of material choice and amount used

1.6 Organization Of The Paper

The paper is organized as follow chapter 2 deals with brief discussion about pressure vessel. The chapter 3breify discussed about design implementation of pressure vessels .chapter 4 deals with Analysis of pressure vessels. Chapter 5 discussed about performance analysis .chapter 6 deals with conclusion and future work.

II. DESIGN PROCEDURE & CALCULATION

2.1 Design Of Shell & Its Components: Most of the components are fabricated from plates or sheets. Seamless or welded pipes can also be used. Parts of vessels formed are connected by welded or riveted joints. In designing these parts and connections between them, it is essential to taken the efficiency of joints into account. For welded joints, the efficiency may be taken as 100%, if the joint is fully checked by a radiograph and taken as 85%, even if it is checked at only a few points. If the radiographic test is not carried out 50 to 80% efficiency is taken. Efficiencies vary between 70 to 85% in the case of riveted joints. All these are made for pressure vessels operating at pressures less than 200kg/km^2.

2.2 Design Calculations: ***2.2.1 Design Of Thickness Of The Pressure Vessel Shell:***

According to the Lame's Equation, the thickness (t) of the shell

$$t = r_i \left[\sqrt{\frac{\sigma_t}{\sigma_t - 2P}} - 1\right] \qquad (2.1)$$

P = operating pressure in pa
t = thickness of shell in mm
r_i = inner radius of shell mm
σ_t = Max allowable stress in N/mm^2

Table2.1: Thickness calculation for different cases

S.No	Type	Material	Max allowable stress σT	Thickness t
1	CASE - I	:SA-240 316L	115.142 N/mm^2	$t = 50.04 \sim 50$
2	CASE - II	SA-516 70	137.895 N/mm^2	$t = 40.7499 \sim 41$

2.2.2Design of Cylinder Shells under Pressure: The equations for determining the thickness of cylindrical shells of vessels under internal pressure are based upon a modified membrane-theory equation. The modification empirically shifts the thin wall equation to approximate the "Lame" equation for thick-walled vessels shown above.

Table:2.2: Thickness calculation of cyclinderal shells with internal radius 500nm

S.No	pressure	Maximum Allowable Stress	Joint efficiency	Thickness
1	45 bar	137.895145864 N/mm^2	80%	20mm
2	100bar	137.895145864 N/mm^2	80%	47.33mm

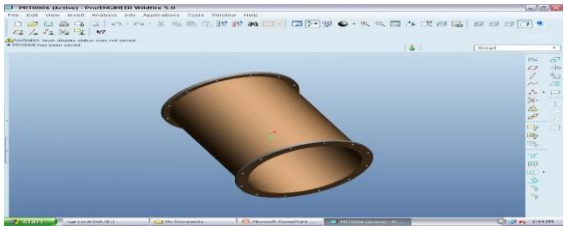

Fig 2.2: design of cylindrical shells

2.2.3Cylinder flange: Pitch should be between 20√d1 and 30√d1

Where d1 = hole diameter

Pitch circle formula Outer diameter formula

Dp = D + 2t + 3d1 Do = Dp + 3d1 "or" Do = D + 2t + 6d1

Where,

Dp = Pitch circle

D = Cylinder diameter

t = Wall thickness

Do = Outer diameter of the flange

Table2.3: outer diameter of SA 51670 material

s.no	thickness t	d1	Dp	Do
1	40mm	20mm	1140mm	1200mm
2	47mm	20mm	1154mm	1214mm

2.3 Design of Head's:A 2:1 Torispherical Head is selected

According to UG 31 of ASME Sec VIII Div 1,

Minimum thickness required 'tr' = $\frac{P * D + C}{2\,S * E - 0.2 * P}$

Where,

D = Internal diameter

E = Joint efficiency = 1.0

C = Corrosion allowance = 3mm

2.4 calculation of top and bottom head diameter for material SA 51670

Equipment Head	Design Pressure	Diameter	tr
Top	100 bar = 10 N/mm^2	1000mm	36.5mm
Bottom	100 bar = 10 N/mm^2	1000mm	36.5 mm

Height of the torispherical head,

h = D/4 = 1000/4 = **250 mm**

2.4 Design of Nozzle:

Table 2.5:Nozzle specification

1	Nozzle Mark	V-shape
2	Equipment	Vent with valve
3	Size	100mm
4	Code	ASME Sec VIII Div 1
5	Material	SA 106 Gr B
6	Max allowable stress	118mm^2
7	Design pressure	100 bar = 10 N/mm^2

From ANSI 3.36.10

Outside diameter D_0 = 110mm, Outside Radius Ro = 90mm

Thickness of the nozzle,

$$A' = \frac{P*Ro+C}{S*E+0.4\,P} = \frac{10*90+3}{118*1.0+0.4*10}$$

$$= 7.40 \sim 10 \text{ mm}$$

B' = head thickness + C = 40 + 3 = 43 mm

2.5 Pro-E Design:

Antenna specifications

1. Dimensions are 600 diameter & 1000mm height.
2. Test pressure 45 bar.

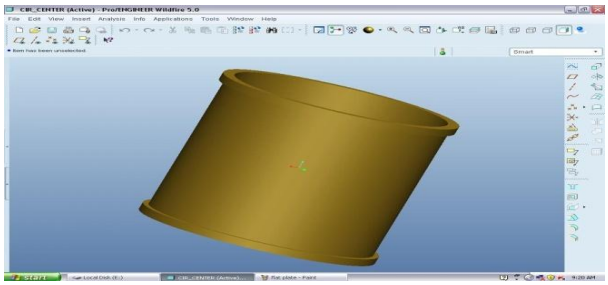

Fig2.2: Design of the Shell

Cylinder when orbited with an angle. The design is done on the basis of the given dimensions which are calculated in designing procedure. Length of 1500mm and having a diameter of 1000mm, the pressure vessel can sustain its max pressure of 100 bar i.e. 10 N/mm^2. With a supporting flanges welded on both sides have a good rigid fitting to the shell as well as with the end caps attached/welded to it.

III. DESIGN OF PRESSURE VESSEL

3.1 Design of Top and Bottom Head: The design of the top head is most important part of the project workbeacuse according to the lames equation that has been shown above relates that the pressure in the thick cylinders exerts its max intensity of force longitudinally and thus longitudinal stress is more in thick cylinders. Therefore the top/bottom head plays the main role in design work.

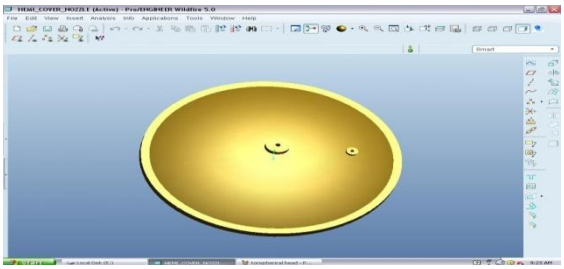

Fig3.1: Top Head with a Nozzle

The figure 3.1 shows that the design work of the top head with dimensions of 607mm outer radius and 47mm thickness. The height of the top head will also be shown with D/4 ratio. That is 250mm as its height. The nozzle welded on the top of the head will be at the center so as to supply equivalent pressure into the pressure vessel. Its main purpose is to vent the pressure into the pressure vessel.

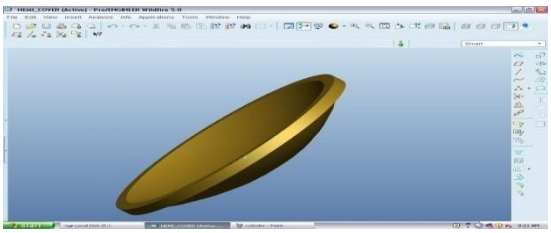

Fig3.2: Bottom Head with designed supports

The figure 3.2 shows that the designed supports on the head are welded to the bottom head to withstand the pressure acting downwards i.e. along –y axis. As the pressure vessel gets pitted into the pit, legs or supports are not required.

3.2 Design of External Lugs: External lugs are welded to the top head with designed dimensions. They act like an agent which are used to life the top head and place the antenna inside the pressure vessel for testing purpose.

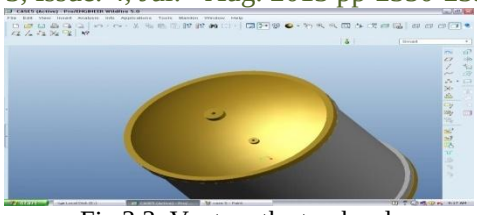

Fig 3.3: Vent on the top head

The fig 3.3 shows that that the designed structure of the lugs which are welded on the top head.

IV. PERFORMANCE ANALYSIS

4.1 CASE – I: The vessel first was designed in square shaped with flat end caps with dimensions of height 1500mm and diameter 1000mm. This vessel was then tested in ANSYS. The below diagram shows the failure of the square designed vessel which fails at the center of the end caps. This is due to the non-distributive stresses acting inside the vessel. The longitudinal stress will act on the center of the end caps. Centrifugal stresses are not distributed equally and on the whole will lead to a failure structure.

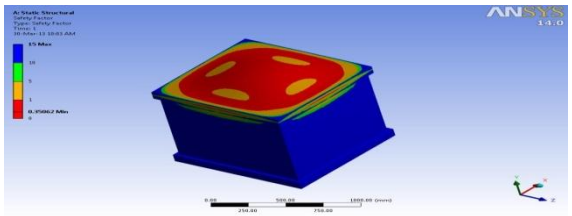

4.1 Non-distributive stresses acting inside the square designed vessel

4.2 CASE – II: Second vessel was designed in Circular shape tank with flat end caps with flat end caps with dimensions of height 1500mm and diameter 1000mm. This vessel was then tested in ANSYS. The below diagram shows the failure of the Circular shape tank with flat end caps with flat end caps. This is due to the non-distributive stresses acting inside the vessel. The longitudinal stress will act on the center of the end caps. Centrifugal stresses are distributed equally but may not withstand stress, due to flat end caps. Thus leads to a failure structure.

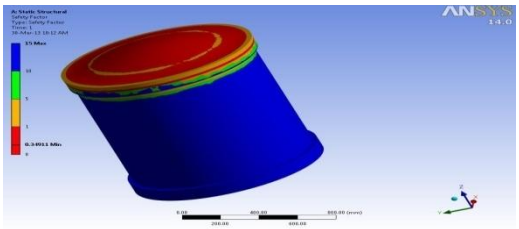

4.2 Failure of the Circular shape tank with flat end caps with flat end caps

4.3 CASE – III: The third vessel was designed Circular shape tank with one side hemispherical end cap & other side flat end caps with dimensions of height 1500mm and diameter 1000mm. This vessel was then tested in ANSYS. The below diagram shows the failure of the Circular shape tank with one side hemispherical end cap & other side flat end caps. This is due to the non-distributive stresses acting inside the vessel. The longitudinal stress will act on the center of the end caps. Centrifugal stresses are not distributed equally and on the whole will lead to a failure structure.

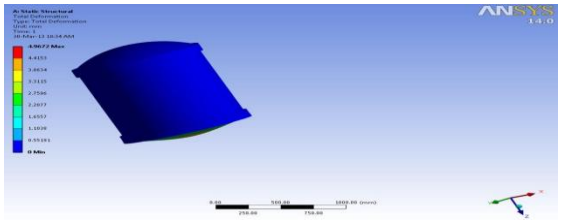

4.3 failure of the Circular shape tank with one side hemispherical end cap & other side flat end caps

4.4 CASE – IV:

The third vessel was designed Circular shape tank with both sides hemispherical end cap with dimensions of height 1500mm and diameter 1000mm. This vessel was then tested in ANSYS. The below diagram shows the failure of the Circular shape tank with both sides hemispherical end cap. This is due to the non-distributive stresses acting inside the vessel. The longitudinal stress will act on the center of the end caps. Centrifugal stresses are distributed equally and on the whole will lead to a good structure.

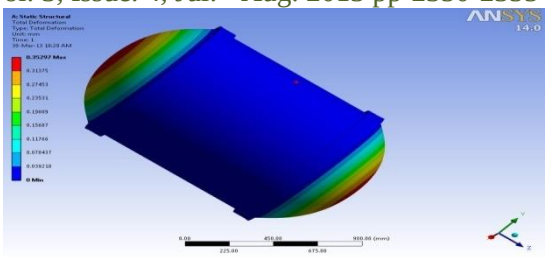

4.4 Failure of the Circular shape tank with both sides hemispherical end cap.

4.5 CASE – V: The third vessel was designed Case 4 with nozzle & test gauge mounting arrangement with dimensions of height 1500mm and diameter 1000mm. This vessel was then tested in ANSYS. The below diagram shows In this case the pressure vessel is design with the nozzle and a vent hole for the pressure to go inside the pressure vessel. The design is based on the torispherical head – top/bottom the pressure gets distributed equally. This design and results known after testing ANSYS. The below figure shows the longitudinal stresses/centrifugal stresses are acting equally in the pressure vessel design.

Hence the present design satisfies the requirements.

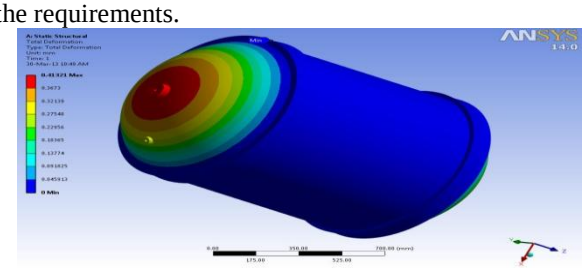

4.5 Longitudinal stresses/centrifugal stresses acting equally in the pressure vessel design with nozzle and a vent hole

V. CONCLUSION

Pressure vessel was modeled and analyzed in different types of configuration. According to Case I analysis the rectangle cross sectional vessel and flat end caps are not suitable for electronic warfare antenna because of the high stresses developed in it. If the thickness is increased, then the weight of the base frame also increases, which is not feasible. If the thickness is decreased to resist the loads acting on it. Hence we proved our proposed circular cross section with hemispherical analysis the stresses developed in the end caps are very less as compared to existing rectangle cross sectional vessel. Also in the circular cross section deflections are minimum.

From the results, excluding pointed stress concentration node results, Factor of safety in case5 is 1.8. We have concluded that circular cross section vessel with CASE5 configuration is adequate for given environment. In future using finite element analysis create a FE model depends on the user, the discretization needs an intuition of how the model could fail, considering the loads acting. Also we need to fine tune manufacturing version based on intricate requirements.

REFERENCES

[1]. Myer Kutz and Wiley," Mechanical Engineers' Handbook", Interscience
[2]. Publication, 1986.
[3]. Frank Kreith," The CRC Handbook of Mechanical Engineering",- CRC Press, Inc1998.
[4]. Tirupathi ,R Chandrupatla and Belegundu," Introduction to Finite Elements in Engineering", Second Edition, Prentice Hall India.
[5]. Chandrakanth S Desai and John F Abel," Introduction to the Finite Element Method",1987, CBS Publishers & Distributors.
[6]. Harold A. Rothbart," McGraw Hill Encyclopedia of science and technology", McGraw Hill Inc,2nd Edition.
[7]. O.C.Zeinkiewicz," The Finite Element Method", Tata McGraw Hill publishing Company Ltd.

International Journal of Modern Engineering Research (IJMER)
www.ijmer.com Vol. 3, Issue. 4, Jul. - Aug. 2013 pp-2356-2359 ISSN: 2249-6645

A Subgraph Pattern Search over Graph Databases

Zareen Nikhat[1], Ch. N.Santhosh Kumar[2], V. Sitha Ramulu[3]
[1]*M. Tech, Swarna Bharathi Institute of Science & Technology, Khammam, A.P., India.*
[2]*Assoc. Professor, Dept.of CSE, Swarna Bharathi Institute of Science & Technology, Khammam, A.P., India.*
[3]*Assoc. Professor, Dept.of IT, Swarna Bharathi Institute of Science & Technology, Khammam, A.P., India.*

***ABSTRACT*:** *Graphs has been used in various real applications such as social network modeling and chemical compound analysis. Due to their wide usages, many interesting graph problems are extensively studied, for example, sub graph search, graph reachability, and keyword search in graphs. Given an example, during a chemical reaction, the structures of the chemical compounds often change along the reaction process. We can model these evolving graphs as graph streams, that is, a sequence of graphs which grow indefinitely over time . However, most of the previous works assume that graph data are rather static, which raises challenges when applying to the graph streams. Compared to the static graphs, graph streams not only inherit the complexity of graphs but also possess their own characteristics. In this paper, we study the problem of continuous sub graph pattern search over graph databases, which can be used in many real applications.*

KEYWORDS: *Graph, NNT, Stream, Trees.*

I. INTRODUCTION

Graph pattern matching is a routine process in a variety of applications, e.g., knowledge discovery, computer vision, biology, chem- informatics, dynamic network traffic, intelligence analysis and social networks. It is often defined in terms of sub- graph isomorphism [1], graph simulation [2] or bounded simulation [3]. Given a pattern graph GP and a data graph G, the graph pattern matching is to find the set M(GP, G) of matches in G for GP . For sub graph isomorphism, M(GP,G) is the set of all the sub graphs of G that are isomorphic to the pattern GP . For bounded simulation, M(GP, G) consists of a unique maximum match, a relation defining edge-to-edge (edge-to-path) mappings. Graph pattern matching is very costly: NP-complete for subgraph isomorphism [4], cubic-time for bounded simulation [3], and quadratic-time for simulation [5]. In practice, a data graph G is typically very large, and moreover, is frequently updated. This is particularly evident in, e.g., social networks [6], Web graphs [7] and also traffic networks [8]. It is often prohibitively expensive to re compute the matches starting from the scratch when G is updated. These highlight the need for incremental algorithms to compute the matches.

Given a pattern graph GP , a data graph G, that matches M(GP, G) in G for GP and changes ΔG to G, the incremental matching problem is to compute changes ΔM to the matches such that $M(GP,G \oplus \Delta G) = M(GP,G) \oplus \Delta M$, where (a) ΔG consists of a set of edges to be inserted into or deleted from G, and (b) operator $\oplus$ applies changes ΔS to S, where S is a data graph G or matching results M. As opposed to batch algorithms that re compute the new output from the scratch, an incremental matching algorithm aims to minimize unnecessary recomputation and improve response time. Indeed, when the changes ΔG to G are very small, the increment ΔM to the matches is often small as well, and is much less costly to find than recompute the entire $M(GP, G \oplus \Delta G)$. While real life graphs are constantly updated, the changes are typically minor; for example, only 5% to 10% of the nodes are updated weekly in a Web graph [7]. We can cope with the dynamic nature of the social networks and Web graphs by computing matches once on the entire graph via a batch algorithm, and then incrementally identifying their changes in response to updates. That is, we find new matches by making maximal use of the previous computation, without paying the price of the high complexity of graph pattern matching.

II. RELATED WORK

A lot of interesting works have been done to address the sub graph search problem. In [9], the authors proposed a closure-tree (C-tree) to organize graphs into a tree-based multi-dimensional index and used the graph closures as bounding boxes. The C-tree can support both exact sub graph queries and the similarity-based sub graph queries. In [10], the authors decomposed a graph into a full set of sub graphs and indexed the hash value of canonical forms of the sub graphs.

In [11], the authors proposed GCoding for graph search, which assigns a signature to each vertex based on its local structures. Then, they produced a spectral graph code by combining all vertex signatures in the graph. Based on the spectral graph codes, a necessary condition for sub graph isomorphism was derived. In [12], the authors proposed gIndex which uses frequent sub graphs as filtering features. Because of anti- monotonicity, once a sub graph pattern is not frequent, any super graph that contains it will not be frequent as well. In [13], the authors used frequent sub graphs as indexing features and constructed a nested inverted-index, thus, a frequent graph query could be answered directly. Only an infrequent graph query needs to be verified for the sub graph isomorphism. In [14], the authors proposed an improved subgraph isomorphism checking method using tree features. They also integrated indexing with the sub graph searching. Thus, not only the sub graph isomorphism verification time was reduced as well.

III. PROPOSED WORK

In this paper, we focus on answering continuous sub graph patterns over graph databases. More specifically, we assume a user has a set of sub graph patterns and starts monitoring graph streams from timestamp zero. Then, as time

evolves, the user wants the system to continuously report the appearances of certain sub graph patterns on the graph streams at each and every timestamp.

A. Node- neighbour tree: Node-neighbor tree or NNT, which captures the local structure around each vertex. An example graph *G* together with the NNTs of all its vertices and edges under *l* = 2 is shown in Figure 1(a). In the example, *G* has 4 vertices with ids from 1 to 4, which have labels *A,A,B,C* respectively. The NNTs of vertices 1 and 2 have the same structure, thus, we use only one tree to represent *T*1 and *T*2 in this example. *T*3 rooted at vertex 3 has only two branches consisting of the same labels *A*, which indicates that node 3 has two distinct neighbors with label *A*. *T*4 has two different branches rooted at the node with label *B*. In node-neighbor trees, each node is identified by the lower case character in the figure. The numbers in the brackets are referring to the node IDs in the original graph "*G"*.

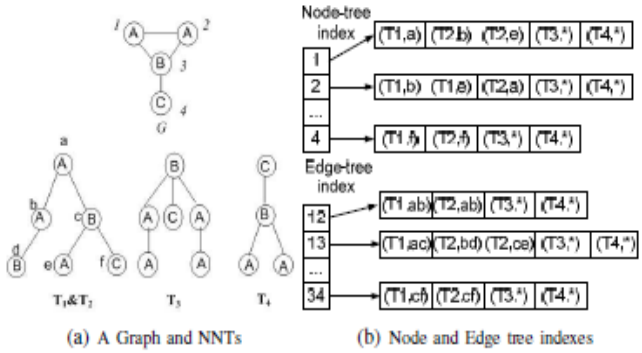

Figure 1: Graph, Node- neighbour trees and index

For example, in *T*1, the node *a* is referring to node 1 in *G* and then nodes *b*,*e* are all referring to 2 in *G*. Figure 1(b) shows an example of node-tree index for the NNTs in Figure 1(a). In the example index, node 2 appears in positions *b* and *e* of tree *T*1 rooted at node 1, thus in the entry 2 of the node tree index, (*T*1, *b*) and (*T*1, *e*) are stored.

B. Projecting to Numerical Vectors: In this section, we propose a novel encoding method to transform a NNT to a set of vectors and approximate sub- tree isomorphism checking by dominant relationship verification between two vector sets. Figure 2 shows an example of dimension derived from the query graph Q (upper left). We show that the NNTs of vertices l = 2. Thus, there are fourteen possible dimensions from the NNTs, < 1,A,A >, < 2,A,A >, . . ., < 2, C,B >. Based on these dimensions, we can apply Procedure 1 to project a NNT into a node projected vector (NPV).

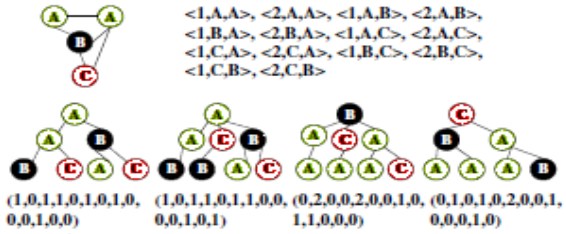

Figure 2: Projecting NNTs to Numerical Vectors

Procedure 1: Tree Projection
{**Input:** A NNT tree up to depth of l
Output: Node projected set
(1) NPV ← 0
(2) for each level li in Input
(3) for each edge (u, u^1) at level li
(4) NPV [(li, label(u), label(u^1))] ← NPV [(li, label(u), label(u^1))] + 1
(5) return NPV}

C. Search in the Vector Space: After projecting NNTs to their NPVs, we can check every possible joinable pair of streams and the query graphs based on the dominant relationship of NPVs using a nested loop algorithm. We set this nested loop algorithm as the baseline and propose two improved search strategies: the first improved method utilizes the idea of checking the dominated vector set as a whole instead of checking the whole dominant relationship pair by pair. When the stream graph of the next timestamp comes, for each dimension, we only need to update the number of dominated vectors of *Q*, when the position of the projected node vector in *G* changes. The detailed steps are listed in Procedure 2. Second, for each

vector of the stream graph, we maintain two counter vectors for it, namely, the position counter vector and the dominant counter vector.

Procedure 2: Dominated Set Cover Join
{**Input:** stream graphs {G1, ...Gk1}, query graphs {Q1, ...Qk2}
Output: Reported positive pairs
(1) for i ← 1 to k1
(2) for u ∈ Gi
(3) for each non-zero dimension of NPV (u) {
(4) update u's position counter NPV (u)pos
(5) update u's dominant counter NPV (u)dom
(6) mark query vectors dominated by Gi based on
NPV(u)dom }
(7) for j ← 1 to k2
(8) if Gi dominates all vectors in Qj
(9) answer ← answer U (i, j)
(10) return answer

D. Search in Uncertain Graph Streams: For sub- graph pattern search over uncertain graph streams, besides using the structural features, we want to utilize the probabilities to reduce the search space. Specifically, other than removing the stream graph G^1 that does not contain the query graph Q, that is, the probability of G^1 containing Q is zero, we also want to filter out a stream graph that contains Q but with a probability less than $\in$. Thus, for sub- graph search over uncertain graph streams, we would like to conduct the pruning in two steps: For structural pruning, we can utilize procedure 2. Compared to certain graph streams, for uncertain graph streams, we have to make some modifications for projecting the node- neighbour trees (NNTs) to numerical vectors, since each of the NNT of an uncertain graph has a probability associated with each of its edges. We call the converted vectors from NNTS of an uncertain graph called as Probability Node Projected Vectors (PNPV). The basic idea of the probability pruning is to derive an upper bound for the probability of a stream uncertain graph G^1 containing the query graph Q, called matching probability upper bound, denoted as MPbound. Based on the global mapping probability upper bounds, we have:
MPbound=max{min{Plocal-mapping(NPV (u), PNPV (v))}

From the above equation, we can observe that we need to compute local mapping probability upper bound before we derive MPbound. Therefore, we listed detailed steps on computing this local mapping bound in Procedure 3.

Procedure 3: Local Mapping Bound
{**Input:** Query vector NPV (u), PNPV (v) of the uncertain graph node
Output: Probability bound
(1) check if PNPV (v) dominates NPV (u)
(2) if no, return 0
(3) bound = 1
(4) for each dimension i in NPV (u)
(5) k ← value of i dimension in NPV (u)
(6) l ← kth largest probability of the probability array pointed by p of i dimension in PNPV (v)
(7) if l < bound bound = l
(8) return bound}

Now we propose one exact solution and one approximate solution. The exact solution will derive the exact MPbound(procedure 4). The approximate solution will get an approximate solution(procedure 5), whose value is less than MPbound, but much faster than the exact solution.

Procedure 4: Exact MP Bound
{**Input:** weighted bipartite graph G
Output: MPbound
(1) low = 0, high = 1
(2) while low + δ < high
(3) mid = (low + high)/2
(4) remove from G all edges having weights less than mid
(5) use Hopcroft-Karp algorithm to check if there is a maximum matching
with regard to the number of nodes in query graph
(6) if yes, low = mid, otherwise high = mid
(7) return low}

Procedure 5: Approximate MP Bound
{**Input:** weighted bipartite graph G
Output: Approximate MPbound
(1) bound = 1
(2) for each node u in query graph
(3) find the edge incident to u with maximum probability p
(4) if p < bound bound = p
(5) return bound}
Finally, the overall query procedure for the sub graph search over uncertain graph stream is presented in Procedure 6.

Procedure 6: Uncertain Join
{**Input:** uncertain stream graphs {G1, ...Gk1}, query graphs {Q1, ...Qk2}, and a probability threshold ε
Output: Joinable query-stream pairs
(1) answer ← ϕ , answer2 ← ϕ
(2) conduct Skyline with Early Stop or
Dominated Set Cover algorithm to obtain structural
filtering results to answer
(5) for each query-stream pair (Qj,Gi) $\in$ answer
(6) bipartite graph G ← ϕ
(7) for each node u in Qj
(8) for each node v in Gi
(9) call Procedure Local Mapping Bound and store return value in p
(10) if p is non-zero, add (u, v) with weight p to G
(11) call Procedure Exact MP Bound or Procedure Approximate MP Bound
with parameter G to derive MPbound
(12) if MPbound $\geq$ ε , then answer2 ← answer2 U (i, j)
(13) return answer2}

IV. CONCLUSION

In this paper, we propose a continuous sub graph patterns over graph databases. We introduce a light-weight yet effective feature structure called Node-Neighbor Tree to filter out false candidate query-stream pairs. Later we propose a novel encoding method to transform a NNT to a set of vectors and approximate sub- tree isomorphism checking by dominant relationship verification between two vector sets. After projecting NNTs to their NPVs, we can check every possible joinable pair of streams and the query graphs based on the dominant relationship of NPVs using a nested loop algorithm. After projecting NNTs to their NPVs, we can check every possible joinable pair of streams and the query graphs based on the dominant relationship of NPVs using a nested loop algorithm. for sub- graph search over uncertain graph streams, we would like to conduct the pruning in two steps: structural and probability pruning. This reduces search space for capturing patterns over uncertain graph streams.

REFERENCES

[1]. Stotz, R. Nagi, and M. Sudit. Incremental graph matching for situation awareness. FUSION, 2009.
[2]. S. Abiteboul, P. Buneman, and D. Suciu. Data on the Web. From Relations to Semistructured Data and XML. Morgan Kaufman, 2000.
[3]. W. Fan, J. Li, S. Ma, N. Tang, Y. Wu, and Y. Wu. Graph pattern matching: From intractability to polynomial time. In PVLDB, 2010.
[4]. M. Garey and D. Johnson. Computers and Intractability: A Guide to the Theory of NP-Completeness. W. H. Freeman and Company, 1979.
[5]. M. R. Henzinger, T. Henzinger, and P. Kopke. Computing simulations on finite and infinite graphs. In FOCS, 1995.
[6]. S. Garg, T. Gupta, N. Carlsson, and A. Mahanti. Evolution of an online social aggregation network: An empirical study. In IMC, 2009.
[7]. Ntoulas, J. Cho, and C. Olston. What's new on the Web? The evolution of the Web from a search engine perspective. In WWW, 2004.
[8]. Z. Chen, H. T. Shen, X. Zhou, and J. X. Yu. Monitoring path nearest neighbor in road networks. In SIGMOD, 2009.
[9]. H. He and A. K. Singh, "Closure-tree: An index structure for graph queries," Proc. 22nd Int'l Conf. Data Eng. (ICDE), 2006.
[10]. D. W. Williams, J. Huan, and W. Wang, "Graph database indexing using structured graph decomposition," Proc. 23rd Int'l Conf. Data Eng. (ICDE), 2007.
[11]. L. Zou, L. Chen, J. X. Yu, and Y. Lu, "A novel spectral coding in a large graph database," Int. Conf. on Extending Database Technology (EDBT), 2008.
[12]. X. Yan, P. S. Yu, and J. Han, "Graph indexing: a frequent structurebased
[13]. approach," Proc. ACM SIGMOD, 2004.
[14]. J. Cheng, Y. Ke, W. Ng, and A. Lu, "FG-index: towards verification-free query processing on graph databases," Proc. ACM SIGMOD, 2007.
[15]. H. Shang, Y. Zhang, X. Lin, and J. X. Yu, "Taming verification hardness: an efficient algorithm for testing subgraph isomorphism," Proc. 34th Int'l Conf. Very Large Data Bases (VLDB), 2008.

International Journal of Modern Engineering Research (IJMER)
www.ijmer.com Vol. 3, Issue. 4, Jul. - Aug. 2013 pp-2360-2363 ISSN: 2249-6645

Experimental study with different cathode and anode humidification temperatures in PEM fuel cell

Babua Ram Sahu[1], Mahesh Kumar Yadav[2], Dr. Bhupendra Gupta[3], Prof. Amit Dutta[4]
[1&2] *Students, Master of Engineering, (Heat power), Jabalpur Engineering College, Jabalpur, India*
[3] *Assistant Professor, Jabalpur Engineering College, Jabalpur*
[4] *Assistant Professor, GRKIST, Jabalpur*

ABSTRACT: *The paper gives experimental study and analysis of PEM Fuel cell with different humidification temperature. The paper focuses on the effect on the voltage and power obtained from fuel cell under variable humidification temperatures. An experimental setup of PEM fuel cell has been developed for this study.*

The effects of different operating parameters on the performance of proton exchange membrane (PEM) fuel cell have been studied experimentally using pure hydrogen on the anode side and air on the cathode side. Experimental analysis has been done with different cathode and anode humidification temperatures. The experimental results are presented in the form of polarization curves, which show the effects of the various operating parameters on the performance of the PEM fuel cell. The possible mechanisms of the parameter effects and their interrelationships are discussed.

KEYWORDS*: PEM fuel cell, Anode material, Cathode Material, Pressure Range, humidification Temperature Range.*

I. INTRODUCTION

Proton exchange membrane (PEM) fuel cells have been widely recognized as the most promising candidates for future power generating devices in the automotive, distributed power generation and portable electronic applications. The proton exchange membrane fuel cell (PEMFC) is of great interest in energy research field because of its potential application for conversion of chemical energy into electrical energy with high efficiency, high power density, low pollution and low operating temperature.

II. Principle of PEM Fuel Cell

The working of PEM Fuel cell is shown in the Figure 2.1. Hydrogen is fed to the anode side, while oxygen is fed to the cathode side. The fuel, in this case hydrogen, is oxidized at the anode to produce positively charged protons and negatively charged electrons. The protons can pass through the hydrated PEM to the cathode as hydronium ions, while the electrons travel along an external circuit, also to the cathode. In this way, electro-neutrality (charge balance) is maintained. The protons and oxygen molecules are combined with the electrons at the cathode. Oxygen is reduced by the electrons and combined with the protons to produce pure water and heat. Again, the process can be simplified into separation (anode) and recombination (cathode) of charges, and the associated increase (energy source) or decrease (energy sink) in the system's electrical energy.

Fuel cell electrochemical reactions (Thermodynamics): A hydrogen PEM fuel cell operates on two coupled half reactions, that of the hydrogen oxidation reaction (HOR) at the anode, and the oxygen reduction reaction at the cathode (ORR). Other fuels can be oxidized at a PEM fuel cell anode, such as methanol, ethanol, and formic acid. The anode and cathode electrochemical reactions are shown below.

$H_2 = 2H^+ + 2e^-$ ……(1)

Where the corresponding anode thermodynamic potential is $E^o_a = 0.00$ V versus SHE (under standard conditions).

$½O_2 + 2H^+ + 2e^- = H_2O$ ……..……(2)

Figure 2.1: Schematic Diagram of PEM Fuel Cell

Again, the corresponding cathode potential is $E^o_c = 1.229$ V versus SHE (under standard conditions).

The overall hydrogen PEM fuel cell reaction is therefore:

$H_2 + ½O_2 = H_2O$ + heat ……(3)

With the standard equilibrium electromotive force calculated to be 1.229 V.

III (A). Experimental Setup

Experimental setup are the combination of two major plates such as , anode plates and cathode plates, which has been well design and construction with as per specification. A single unit cell with active surface aria of 7.2 x 7.2 c.m. was used for experiment in this study. The membrane electrode assembly (MEA) consists of a Nafion in combination with platinum loadings of 0.4 mg/cm^2 per electrode. The gas diffusion layers are made of carbon fiber cloth. The MEA positioned between two graphite plates is pressed between two gold-plated copper plates. The graphite plates are grooved with serpentine gas channels. In the test station, reactant gases are humidified by passing through external water tanks. Regulating the water temperature controls the humidification of the reactant gases.

III (B). Experimental procedure

The procedure for each experiment is as follows:

1. Power on the Fuel Cell Test Station and open the valves of the gas cylinders of hydrogen, oxygen.
2. Before starting experiments, purge the anode side with hydrogen to ensure no oxygen is present.
3. Set the experimental parameters of mass flow rate of the gas cylinders of hydrogen, oxygen.
4. Set the maximum voltage, minimum voltage and voltage increment step of the fuel cell polarization data by Ammeter and Voltmeter.
5. Set the delay between every two voltage and current data points.

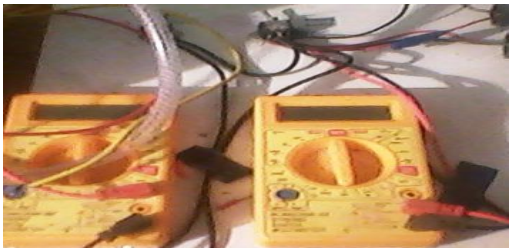

Figure 3.1: Ammeter and Voltmeter

Figure 3.2: Hose Pipe Zone

Figure 3.3: Pressure Gauge

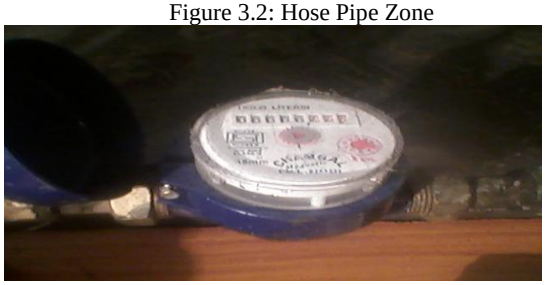

Figure 3.4: Flow Meter Arrangement

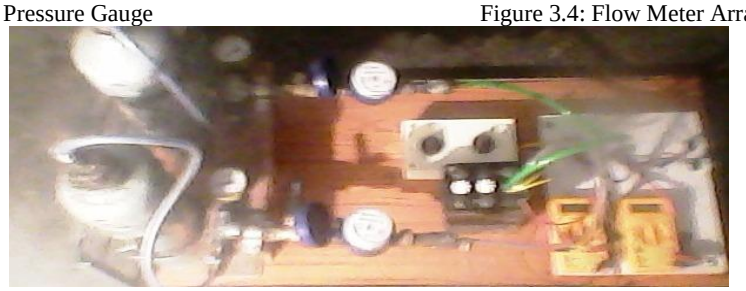

Figure 3.5: Experimental setup of PEM Fuel cell

IV. Result and discussion

4.1 Effect of the humidification in plates

When the anode humidification temperature is at 40◦C, the current density of the fuel cell is the lowest at a given voltage. graph shows that the linear portion of the polarization curve for different anode humidification temperatures are almost parallel to each other, which indicates that the electrical resistance of the fuel cell causing the ohmic losses does not vary significantly.

At low current densities, lower the anode humidification temperature, the lower the cell voltage. This phenomenon could be explained by the decrease of the active catalyst surface area caused by lack of water in the catalyst layers. When the anode is dry, the water transfer through the membrane from the cathode side to the anode side due to back-diffusion is dominant.

This is even more pronounced at low current densities, when water transfer due to electro-osmosis is low. The result of the combined effect is water de1ciency in the cathode catalyst layer. At higher current densities, the cell voltages at different anode humidification temperatures come closer. This, again, could be explained by hydration of the catalyst layer. At high current densities, water generation rate is high and water transfer due to electro-osmosis is high. Thus the cathode catalyst layer is better hydrated even though the anode humidification is low.

Table 1: Data for different humidification temperatures, backpressures are 4 atm on both the anode and cathode sides and hydrogen flow rates are 1.0 ml/s and Oxygen flow rates 2.0 ml/s.

Sr. No.	Current density (A/cm^2)	Voltage at humidification temperature 40^0C	Voltage at humidification temperature 60^0C	Voltage at humidification temperature 80^0C
1	0.2	0.91	0.92	0.93
2	0.4	0.78	0.80	0.83
3	0.6	0.74	0.75	0.77
4	0.8	0.71	0.72	0.73
5	1.0	0.69	0.70	0.71
6	1.2	0.61	0.64	0.68

Table 2: Data for different humidification temperatures, backpressures are 4 atm on both the anode and cathode sides and hydrogen flow rates are 2.0 ml/s and Oxygen flow rates 4.0 ml/s.

Sr. No.	Current density (A/cm^2)	Voltage at humidification temperature 40^{0}C	Voltage at humidification temperature 60^{0}C	Voltage at humidification temperature 80^{0}C
1	0.2	1.02	1.04	1.05
2	0.4	0.96	0.97	0.98
3	0.6	0.94	0.95	0.96
4	0.8	0.92	0.93	0.94
5	1.0	0.90	0.91	0.92
6	1.2	0.78	0.801	0.821

Table 3: Data for different humidification temperatures, backpressures are 4 atm on both the anode and cathode sides and hydrogen flow rates are 3.0 ml/s and Oxygen flow rates 6.0 ml/s

Sr. No.	Current density (A/cm^2)	Voltage at humidification temperature 40^{0}C	Voltage at humidification temperature 60^{0}C	Voltage at humidification temperature 80^{0}C
1	0.2	1.09	1.11	1.12
2	0.4	0.99	1.08	1.09
3	0.6	1.02	1.04	1.05
4	0.8	0.96	0.97	0.98
5	1.0	0.94	0.95	0.96
6	1.2	0.92	0.93	0.94

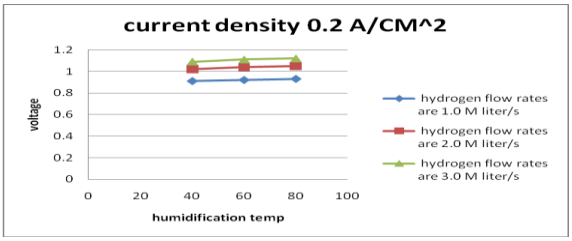

Fig. 4.1. Different mass flow rates curves for cell humidification temperature vs. cell voltage at 0.2 current density

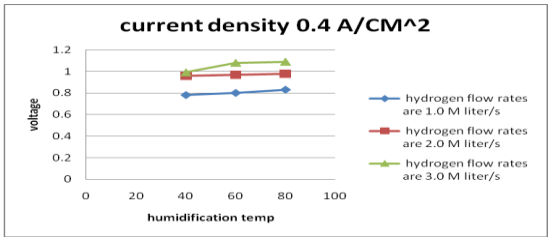

Fig. 4.2. Different mass flow rates curves for cell humidification temperature vs. cell voltage at 0.4 A/cm^2 current density

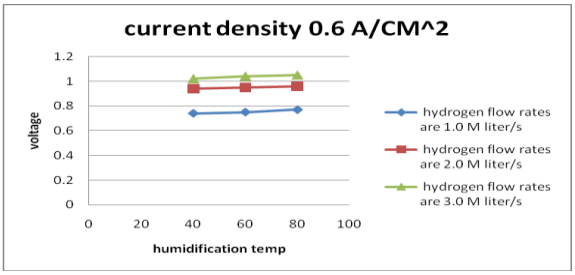

Fig. 4.1. Different mass flow rates curves for cell humidification temperature vs. cell voltage at 0.6 A/cm^2 current density

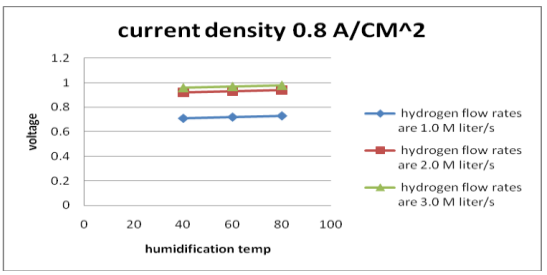

Fig. 4.2. Different mass flow rates curves for cell humidification temperature vs. cell voltage at 0.8 A/cm^2 current density

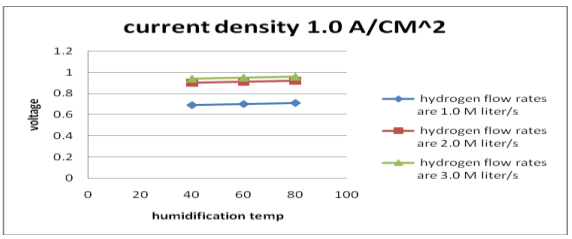

Fig. 4.1. Different mass flow rates curves for cell humidification temperature vs. cell voltage at 1.0A/cm^2 current density

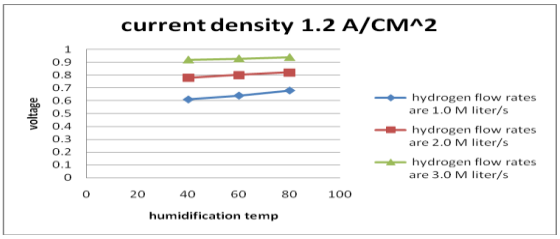

Fig. 4.2. Different mass flow rates curves for cell humidification temperature vs. cell voltage at 1.2 A/cm^2 current density

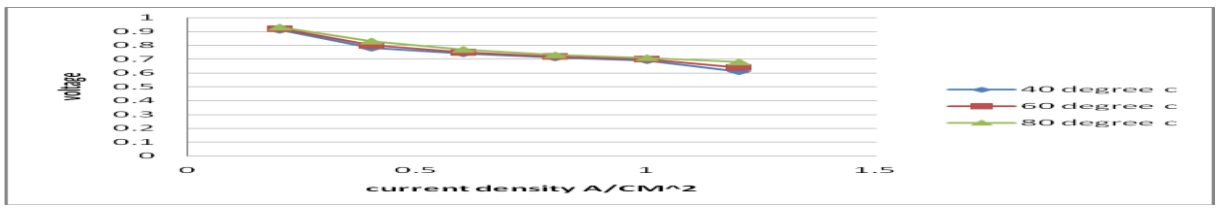

Figure 4.6: Humidification temperatures with hydrogen flow rates are 1.0 ml/s and Oxygen flow rates 2.0 ml/s.

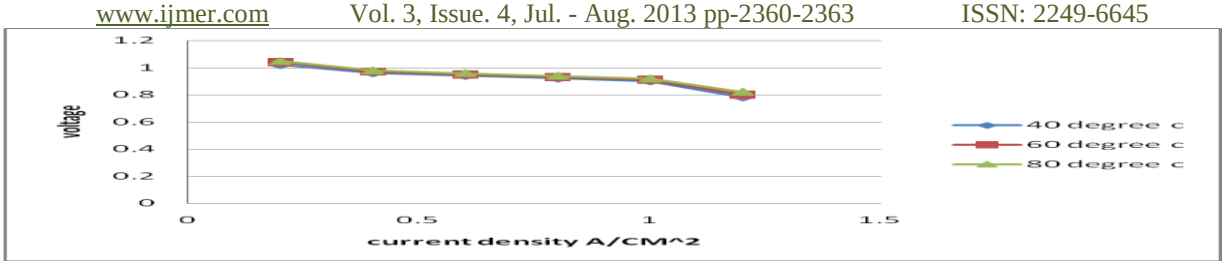

Figure 4.7: Humidification temperatures with hydrogen flow rates are 2.0 ml/s and Oxygen flow rates 4.0 ml/s.

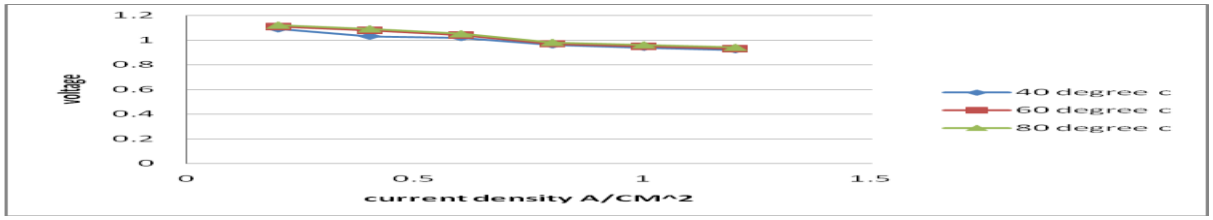

Figure 4.8: Humidification temperatures with hydrogen flow rates are 3.0 ml/s and Oxygen flow rates 6.0 ml/s.

V. CALCULATIONS

Table 5.1 presents the Improvement in Voltage of variable Mass Flow Rate and Current Density of Fuel Cell

Table 5.1: Improvement in Voltage of variable Mass Flow Rate and Current Density of Fuel Cell

Current density (A/cm^2)	Humidification Temperature (^0C)	hydrogen flow rates (case I) (ml/s)	Oxygen flow rates (case I) (ml/s)	Voltage (caseI) (V)	hydrogen flow rates (case II) (ml/s)	Oxygen flow rates (case II) (ml/s)	Voltage (case II) (V)	Increase in voltage (%)
0.2	80	1.0	2.0	0.93	3.0	6.0	1.12	20.43%
0.4	80	1.0	2.0	0.83	3.0	6.0	1.09	31.32%
0.6	80	1.0	2.0	0.77	3.0	6.0	1.05	36.36%
0.8	80	1.0	2.0	0.73	3.0	6.0	0.98	34.24%
1.0	80	1.0	2.0	0.71	3.0	6.0	0.96	35.21%
1.2	80	1.0	2.0	0.68	3.0	6.0	0.94	38.23%

VI. CONCLUSION

In this work, humidification temperatures and pressures have been performed. Voltage is increase 38.23% by increasing the different humidification temperatures and mass flow rates**.** When enough humidification is provided, the performance of the PEM fuel cell improves with the increase of operation temperature.

1. During the process we found that Voltage is increased 38.23%, when the fuel cell is 80^0C and at fixed Current density of 1.2 A/cm^2.
2. During the process we found that Voltage is increased 35.21%, when the fuel cell is 80^0C and at fixed Current density of 1.0 A/cm^2.
3. During the process we found that Voltage is increased 34.24%, when the fuel cell is 80^0C and at fixed Current density of 0.8 A/cm^2.
4. During the process we found that Voltage is increased 32.36%, when the fuel cell is 80^0C and at fixed Current density of 0.6 A/cm^2.
5. During the process we found that Voltage is increased 31.32%, when the fuel cell is 80^0C and at fixed Current density of 0.4 A/cm^2.

REFERENCES

[1]. A.B. La Conti, M. Hamdan, R.C. McDonald, W. Vielstich, H.A. Gasteiger, A. Lamm. Handbook of Fuel Cells: Fundamentals Technology and Applications, vol. 3, John Wiley & Sons Ltd., 2003, pp. 647–662.

[2]. A Fischer, J. Jindra, H. Wendt, Porosity and catalyst utilization of thin layer cathodes in air operated PEM-fuel cells, J. Appl. Electrochem. 28 (1998) 277–282.

[3]. E.A. Ticianelli, C.R. Derouin, A. Redondo, S. Srinivasan, Methodsto advance technology of proton exchange membrane fuel cells, J.Electrochem. Soc. 135 (1988) 2209–2214

[4]. Jinfeng Wua, Xiao Zi Yuan, Jonathan J. Martin "A review of PEM fuel cell durability: Degradation mechanisms and mitigation strategies". Journal of Power Sources 184 (2008) 104–119

[5]. Lin Wang, Attila Husar, Tianhong Zhou, Hongtan Liu "A parametric study of PEM fuel cell performances". International Journal of Hydrogen Energy 28 (2003) 1263 – 1272

[6]. Pan Zhao, Jiangfeng Wang, Lin Gao, Yiping Dai "Parametric analysis of a hybrid power system using organic Rankine cycle to recover waste heat from proton exchange membrane fuel cell". International Journal of hydrogen energy 37 (2012) 3382-3391.

[7]. S. Litster, G. McLean "PEM fuel cell electrodes" Journal of Power Sources 130 (2004) 61–76

[8]. V.A. Paganin, E.A. Ticianelli, E.R. Gonzalez, Development and electrochemical studies of gas diffusion electrodes for polymer electrolyte fuel cells, J. Appl. Electrochem. 26 (1996) 297–304.

[9]. Xiao-guang Lia, Liu-lin Caoa, Zhi-xiang Liub, Cheng Wangb "Development of a fast empirical design model for PEM stacks" International Journal of hydrogen energy 35 (2010) 2698 – 2702.

[10]. X. Cheng, B. Yi, M. Han, J. Zhang, Y. Qiao, J. Yu, Investigation of platinum utilization and morphology in catalyst layer of polymer electrolyte fuel cells, J. Power Sources 79 (1999) 75–81.

International Journal of Modern Engineering Research (IJMER)
www.ijmer.com Vol. 3, Issue. 4, Jul. - Aug. 2013 pp-2364-2366 ISSN: 2249-6645

Token Based Packet Loss Control Mechanism for Networks

Pathan Uddandu[1], Sayeed Yasin[2]
[1]M. Tech, Nimra College of Engineering & Technology, Vijayawada, A.P., India.
[2]Asst. Professor, Dept. of CSE, Nimra College of Engineering & Technology, Vijayawada, A.P., India.

ABSTRACT: *Modern IP network services provide for the simultaneous digital transmission of data, voice, and video. These services require congestion control algorithms and protocols which can solve the packet loss parameter can be kept under control. Congestion control is therefore, the cornerstone of the packet switching networks. It should prevent congestion collapse, provide fairness to competing flows and optimize transport performance indexes such as throughput, loss and delay. In this paper we propose a congestion control mechanism with application to Packet Loss in networks with P2P traffic is proposed. In this new method the edge and the core routers will write a measure of the quality of service guaranteed by the router by writing a digital number in the Option Field of the datagram of the network packet. This is called as "token". The token is read by the path routers and then interpreted as its value will give a measure of the congestion especially at the edge routers. Based on the token number, the edge router at the source's edge point will shape the traffic generated by the source, thus reducing the congestion on the path.*

KEYWORDS: *Congestion, CSFQ, STLCC, Token.*

I. INTRODUCTION

There are a number of very good reasons to avoid loss in today's computer networks. Many of these stem from the fact that the loss is often a symptom of overflowing router buffers in the network, which can also lead to high latency, jitter, and poor fairness. In the last few years considerable effort has been expended on the design and implementation of the packet switching networks [1] [2]. A principle reason for developing such packet networks has been to facilitate the sharing of computer resources. In this paper, we study whether the benefits of a network architecture that embraces rather than avoids widespread packet loss outweigh the potential loss in efficiency of the network. We propose an alternative approach to Internet congestion control called as decongestion control.

In a departure from conventional approaches, end hosts strive to transmit packets faster than the network can deliver them, leveraging end-to-end erasure coding and in-network fairness enforcement. In this paper we present a protocol design and philosophy that supports the sharing of resources that exist in various packet switching networks. After a brief introduction to inter network protocol issues, we describe the function of a gateway as an interface between the network and discuss its role in the protocol [3][4]. We then consider the various details of the proposed work, including addressing, formatting, buffering, sequencing, flow control, error control, and so forth.

A typical packet switching network is composed of a set of computer resources called as hosts, a set of one or more packet switches, and a collection of communication media that interconnect the packet switches. The ensemble of packet switches and communication media is called as packet switching subnet as shown in Figure 1. In a typical packet switching subnet, data of a fixed maximum size are accepted from a source node, together with a formatted destination address which is used to route the data in a store and forward fashion.

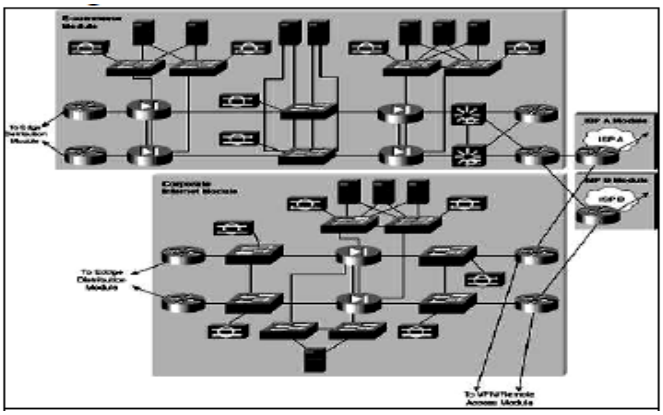

Figure 1: packet switching communications at network Edge

II. RELATED WORK

The basic idea of peer- to- peer network is to have peers participate in an application level overlay network and operate as both A number of approaches for queue management at Internet gateways have been studied previously. Droptail gateways are used almost universally in the current Internet because of their simplicity. A droptail gateway drops an incoming packet only when the buffer becomes full, thus providing congestion notification to protocols like TCP. While simple to implement, it distributes losses among the flows arbitrarily[5]. This often results in the bursty losses from a single TCP connection, thereby reducing its window sharply. Thus, the flow rate and consequently the throughput for that flow

drops. Tail dropping also results in multiple connections simultaneously suffering from losses leading to global synchronization [6]. Random early detection(RED) addresses some of the drawbacks of droptail gateways. The RED gateway drops incoming packets with a dynamically computed probability when the exponential weighted moving average queue size avg q exceeds a threshold.

In [6], the author does per-flow accounting maintaining only a single queue. It suggests changes to the RED algorithm to ensure fairness and to penalize the misbehaving flows. It puts a maximum limit on the number of packets a flow can have in the queue. Besides it also maintains the per flow queue occupancy. Drop or accept decision for an incoming packet is then based on the average queue length and the state of that flow. It also keeps track of the flows which consistently violate the limit requirement by maintaining a per-flow variable called as strike and penalizes those flows which have a high value for strike. It is intended that this variable will become high for non- adaptive flows and so they will be penalized aggressively. It has been shown through simulations [7] that FRED fails to ensure the fairness in many cases. CHOKe [8] is an extension to RED protocol. It does not maintain any per flow state and works on the good heuristic that a flow sending at a high rate is likely to have more packets in the queue during the time of the congestion. It decides to drop a packet during congestion if in a random toss, it finds another packet of the same flow. In [9], the authors establish how rate guarantees can be provided by simply using buffer management. They show that the buffer management approach is indeed capable of providing reasonably accurate rate guarantees and the fair distribution of excess resources.

III. PROPOSED WORK

In the proposed work, a model called the Terminal Dependent Congestion Control case which is a best-effort service in the Internet that was originally designed for a cooperative environment which is the congestion control but still it is mainly dependent on the TCP congestion control algorithm at terminals, supplemented with load shedding at congestion links is shown in Figure 2. In high speed networks Core Stateless Fair Queuing (CSFQ) is enhanced to fairness

set up an open- loop control system at the network layer, which inserts the label of the flow arrival rate onto the packet header at edge routers and drops the packet at core routers based on the rate label if congestion happens. At the core routers CSFQ is the first to achieve approximate fair bandwidth allocation among flows with O (1) complexity.

CSFQ can provide fairness to competing flows in the networks with P2P traffic, but unfortunately it is not what end-users really want. By an end user Token Based Congestion Control (TBCC) restricts the total token resource consumed. It cannot obtain extra bandwidth resources when TBCC is used so no matter how many connections the end user has set up. The Self Verifying CSFQ tries to expand the CSFQ across the domain border. It randomly selects a flow, and then re-estimates the flow's rate, and checks whether the re-estimated rate is consistent with the label on the flow's packet. Consequently Self-Verifying CSFQ will put a heavy load on the border router and makes the weighted CSFQ null as well as void.

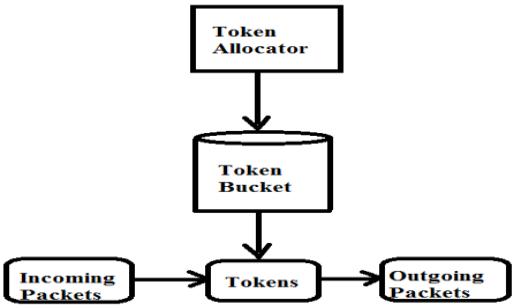

Figure 2: Packet Loss Control

The congestion control architecture re- feedback, which aims to provide the fixed cost to end-users and bulk inter-domain congestion charging to network operators. Re- feedback not only demands very high level complexity to identify the malignant end user, but also is difficult to provide the fixed congestion charging to the inter domain interconnection with low complexity. There are three types of inter domain interconnection polices: the Internet Exchange Points, the private peering and the transit. In the private peering polices, the Sender Keep All (SKA) peering arrangements are those in which the traffic is exchanged between two domains without mutual charge. As Re-feedback is based on the congestion charges to the peer domain, it is difficult for re- feedback to support the requirements of SKA.

The modules of the proposed work are:

- NETWORK CONGESTION
- STABLE TOKEN LIMIT CONGESTION CONTROL (STLCC)
- TOKEN
- CORE ROUTER
- EDGE ROUTER

Network Congestion: Congestion occurs when the number of packets being transmitted through the network crosses the packet handling capacity of the network. Congestion control aims to keep number of packets below the level at which performance falls off dramatically.

Stable Token Limit Congestion Control (STLCC): STLCC is able to shape output and input traffic at the inter domain link with O(1) complexity. STLCC produces a congestion index, pushes the packet loss to the network edge and improves the overall network performance. To solve the oscillation problem, the Stable Token-Limited Congestion Control (STLCC) is also introduced. It integrates the algorithms of XCP and TLCC [10] altogether. In STLCC, the output rate of the sender is controlled using the algorithm of XCP, so there is almost no packet lost at the congested link. At the same time, the edge router allocates all the access token resources to the incoming flows equally. When congestion happens, the incoming token rate increases at the core router, and then the congestion level of the congested link will also increased as well. Thus STLCC can measure the congestion level analytically, and then allocate network resources according to the access link, and further keep the congestion control system stable.

Token: A new and better mechanism for the congestion control with application to Packet Loss in networks with P2P traffic is proposed. In this new method the edge and the core routers will write a measure of the quality of service guaranteed by the router by writing the digital number in the Option Field of the datagram of the packet. This is called as token. The token is read by the path routers and then interpreted as its value will give a measure of the congestion especially at the edge routers. Based on the token number, the edge router at the source, thus reducing the congestion on the path.

Core Router: A core router is a router designed to operate in the Internet Backbone (or core). To fulfill this role, a router must be able to support multiple telecommunications interfaces of the highest speed in use in the core Internet and must be able to forward the IP packets at full speed on all of them. It must also support the routing protocols being used in the backbone. A core router is distinct from the edge routers.

Edge Router: Edge routers sit at the edge of a backbone network and connect to the core routers. The token is read by the path routers and then interpret as its value will give a measure of the congestion especially at the edge routers. Based on the token number of the edge router at the source, thus reducing the congestion on the path.

IV. CONCLUSION

In this paper the architecture of Token based Congestion Control (TBCC) provides fair bandwidth allocation to end users in the same domain is introduced. The two congestion control algorithms CSFQ and TBCC are elevated in this proposed work. STLCC is accessible and the simulation is designed to demonstrate its validity. The Unified Congestion Control Model which is the abstract model of the CSFQ, Re-feedback and STLCC. The simple version of the STLCC is introduced and can be deployed on the current Internet. The inter domain router is added to the TBCC system as the two TBCC domains are inter-connected.

REFERENCES

[1]. G. Appenzeller, N. McKeown, J. Sommers, and P. Barford, “Recent Results on Sizing Router Buffers,” in Proceedings of the Network Systems Design Conference, Oct. 2004.
[2]. M. Enachescu, Y. Ganjali, A. Goel, N. McKeown, and T. Roughgarden, “Part III: Routers with very small buffers,” ACM/SIGCOMM Computer Communication Review, vol. 35, pp. 83- 90, July 2005.
[3]. L. Zhang, S. Shenker, and D. Clark, “Observations on the dynamics of a congestion control algorithm: The effects of two-way traffic,” in Proceeedings of ACM SIGCOMM, pp. 133–147, Sept. 1991. [3] F. R. E. Dell, “Features of a proposed synchronous data network,” in Proc. 2nd Symp. Problems in the Optimization of Data Communications Systems, 1971, pp. 50—57.
[4]. R. A. Scantlebury and P. T. Wilkinson, “The design of a switching system to allow remote access to computer services by other computers and terminal
[5]. devices,” in Proc. 2nd Symp. Problems in the Optimization of Data Communications Systems, 1971, pp. 160-167.
[6]. F. Dabek, M. F. Kaashoek, D. Karger, R. Morris, and I. Stoica. Widearea
[7]. cooperative storage with CFS. In Proceedings of the 18th ACM Symposium on Operating Systems Principles (SOSP ’01), Chateau Lake Louise, Banff, Canada, October 2001.
[8]. Das and R. Srikant. Diffusion approximations for a single node accessed by congestion-controlled sources. IEEE Transactions on Automatic Control, 45(10):1783–1799, October 1998. [11] G. de Veciana and X. Yang. Fairness, incentives and
[9]. Sally Floyd, Van Jacobson, Link-sharing and Resource Management Models for Packet Networks, IEEE\ACM Transactions on Networking, Vol.3, No.4, 1995.
[10]. John Nagle, RFC896 congestion collapse, January 1984.
[11]. S. H. Low and D. E. Lapsey, “Optimization flow control—I: Basic algorithms and convergence,” IEEE/ACM Trans. Networking, vol. 7, pp. 861–874, Dec. 1999.
[12]. Dina Katabi, Mark Handley, and Charles Rohrs, "Internet Congestion Control for Future High Bandwidth-Delay Product Environments." ACM Sigcomm 2002, August 2002.

International Journal of Modern Engineering Research (IJMER)
www.ijmer.com Vol. 3, Issue. 4, Jul. - Aug. 2013 pp-2367-2373 ISSN: 2249-6645

Mitigation of Fault in the Distribution System by using Flexible Distributed Static Compensator (FD-STATCOM)

B. Giri Prasad Reddy[1], V. Obul Reddy[2]
M. Tech (power electronics), Aurora Engineering College, JNTU Hyderabad, AP, India[1]
Assistant professor, Aurora's Engineering College, JNTU Hyderabad, Andhra Pradesh, India[2]

ABSTRACT: *This paper proposes a flexible D-STATCOM (Distribution Static Compensator) and its new controller system, that be able to mitigate all types of faults (LG, DLG, LL, LLL and LLLG), and improve the distribution system performance. This paper validates the performance of D-STATCOM system to mitigate the power quality problems such as voltage flickers, voltage sags/swells harmonics and improve the distribution system performance under all types of system related disturbances and system unbalanced faults (LG, LL, DLG), balanced faults (LLL and LLLG). A 12-Pulse converter based STATCOM was used to mitigate the voltage flicker with respect to the harmonic problem. A multilevel converter has several advantages over a conventional 12-pulse converter such a Staircase waveform quality, Common-mode (CM) voltage, Input current and harmonic control. Multi level based D-STATCOM configuration with IGBT is designed and the graphic models of the D-STATCOM is developed using the MATLAB/SIMULINK*

KEYWORDS: *Distribution System, D-STATCOM, Voltage Sags, Faults.*

I. INTRODUCTION

The modern power distribution network is constantly being faced with an ever-growing load demand. Distribution networks experience distinct change from a low to high load level every day. Electric load growth and higher regional power transfers in a largely interconnected network becoming more complex and less secure power system operation. Power generation and transmission facilities are unable to meet these new demands. Many loads at various distribution ends like domestic utilities, computers, process industries, adjustable speed drives, printers, and microprocessor based equipment etc. have become intolerant to voltage fluctuations, harmonic content and interruptions[1]. Electrical power losses in distribution systems correspond to about 70% of total losses in electric power systems. One of the most severe problems faced by distribution networks operators is voltage drop along distribution feeders, which is caused by real and reactive power flow. Voltage control is a difficult task because voltages are strongly influenced by random load fluctuations. Voltage profile can be improved and power losses can be considerably reduced by installing Custom Power Devices or Controllers at suitable location.

These controllers which are also named Distribution formally defined as the employment of power electronic or static controllers in distribution systems rated up to 38 kV for the purpose of supplying a level of reliability or PQ Flexible AC Transmission System (D- FACTS) are a New generation of power electronics-based equipment flows in low-voltage distribution networks. Custom power that is needed by electric power customers who are sensitive to power variations. Custom power devices or controllers include static switches, inverters, converters, injection transformers, master-control modules and energy-storage modules that have the ability to perform current-interruption and voltage-regulation functions within a distribution system [2].

The STATCOM is applied in distribution system is called D-STACOM (Distribution STACOM) and its configuration is the same, or with small modifications, oriented to a possible future amplification of its possibilities in the distribution network at low and medium voltage implementing the function so that we can describe as flicker damping, harmonic, filtering and short interruption compensation. D-STATCOM exhibits high speed control of reactive power to provide voltage stabilization, flicker suppression, and other types of system control. The D-STATCOM utilizes a design consisting of a GTO- or IGBT-based voltage sourced converter connected to the power system via a multi-stage converter transformer. This paper proposes a flexible D-STATCOM system designed to mitigate the voltage sags caused by LG, LL, DLG, 3-Phase and 3-Phase to ground faults. And improve the power quality of the distribution system. Reactive power compensation is an important issue in the control of distribution systems. The main reason for reactive power compensation in a system is the voltage regulation increased system stability, better utilization of machines connected to the system, reducing losses associated with the system and to prevent voltage collapse as well as voltage sag. Reactive current increases the distribution system losses, reduces the system power factor, shrink the active power capability and can cause large-amplitude variations in the load-side voltage [3]. Various methods have been applied to mitigate voltage sags. The conventional methods use capacitor banks, new parallel feeders, and uninterruptible power supplies (UPS).The D-STATCOM has emerged as a promising device to provide not only for voltage sag mitigation but also for a host of other power quality solutions such as voltage stabilization, flicker suppression, power factor correction. By a similar argument, the D-STATCOM is also suitable for reducing the impact of voltage transients The DSTATCOM configuration consists of a typical Three-level voltage source converter arrangement, a dc energy storage device; a coupling transformer connected in shunt with ac system, and associated control circuits. The configurations that are more sophisticated use multi pulse and/or multilevel configurations [4]. The VSC converts the dc voltage across the storage device into a set of three-phase ac output voltages. These voltages are in phase and coupled with the ac system of network through the reactance of the coupling transformer.

A control method based on RMS voltage measurement has been presented. Where they have been presented a PWM-based control scheme that requires RMS voltage measurements and no reactive power measurements are required. In addition, in this given method, Clark and Park transformations are not required. However, they have been investigated voltage sag/swell mitigation due to just load variation while no balanced and unbalanced faults have been investigated. In this paper, a new control method for mitigating the load voltage sags caused by all types of fault is proposed. A Lookup Table is used to detect the proportional gain of PI controller, which is based only on Trial and Error [5].

While in this paper, the proportional gain of the PI controller is fixed at a same value, for all types of faults, by tuning the transformer reactance in a suitable amount. Then the robustness and reliability of the proposed method is more than the mentioned methods. In this method, the dc side topology of the D-STATCOM is modified for mitigating voltage distortions and the effects of system faults on the sensitive loads are investigated and the control of voltage sags are analyzed and simulated.

II. THE PROPOSED D-STATCOM STRUCTURE

The basic electronic block of the DSTATCOM is the voltage source inverter that converts an input dc voltage into a three-phase output voltage at fundamental frequency.

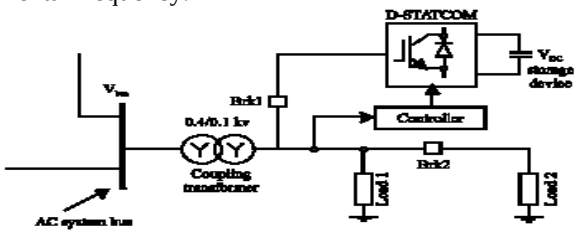

Fig.1 Block diagram of D-STATCOM

These voltages are in phase and coupled with the ac system through the reactance of the coupling transformer. Suitable adjustment of the phase and magnitude of the D-STATCOM output voltages allow effective control of active and reactive power exchanges between the D-STATCOM and the ac system

III. CONTROL STRATEGY

The block diagram of the control scheme designed for the FD-STATCOM is shown in Fig. 3 [6]. It is based only on measurements of the voltage VRMS at the load point.

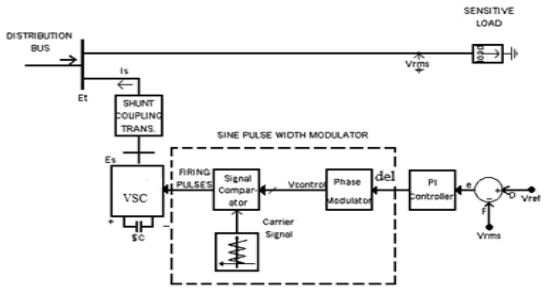

Fig.3. Control scheme designed.

D-STATCOM: The voltage error signal is obtained by comparing the measured VRMS voltage with a reference voltage, VRMSRef. A PI controller processes the difference between these two signals in order to obtain the phase angle δ that is required to drive the error to zero. The angle δ is used in the PWM generator as the phase angle of the sinusoidal control signal. The switching frequency used in the sinusoidal PWM generator is 1450 Hz and the modulation index is 1. The modulating angle δ is applied to the PWM generators in phase A. The angles of phases B and C are shifted 120 and 240 degrees, respectively [7].

IV. PROPOSED CONTROL METHOD

In this paper, in order to mitigate voltage sags caused by LG, LL, DLG, 3-Phase and 3-Phase to ground faults and improve the power quality improvement of the distribution system. Considering this fact that all types of fault may occur in distribution system, controller system must be able to mitigate any types of voltage sags. The control of a D-STATCOM is developed to mitigate such problems and enhance power quality and improve distribution system reliability [8]. D-STATCOM is connected to the Y-Y and Y- Δ transformers for creating the 30 degrees phase shift. Harmonics mitigation will takes place by creating the 30 degrees phase shift.

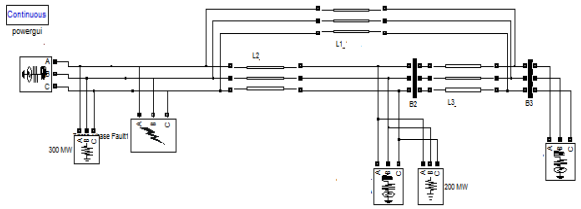

Fig 4: SIMULINK diagram WITHOUT D-STATCOM

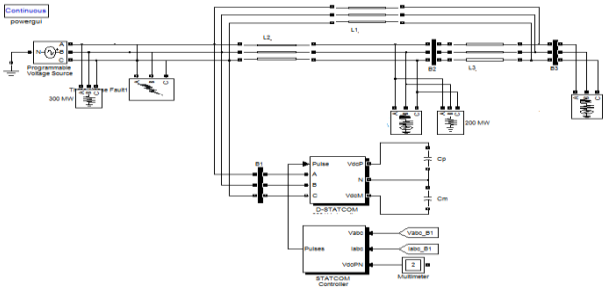

Fig 5: SIMULINK diagram WITH D-STATCOM

Table 1: Specifications of test system

Parameters	Values
Source 1	11KV
Source 2	11KV
Source 3	11KV
Load 1	300KW
Load 2	200KW
Length BW B1 to B2	25Km
Length BW B2 to B3	20Km

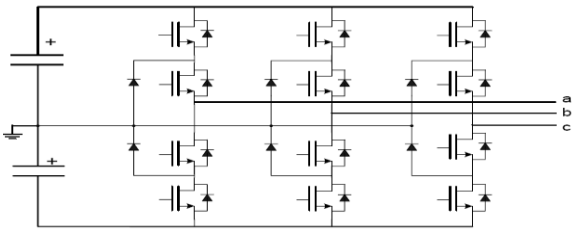

Fig 6: Simulink model for D-STATCOM

V. SIMULATION RESULTS

Fig. 3 shows the test system implemented in MATLAB/SIMULINK to carry out simulations for the FDSTATCOM. The test system comprises a 11 kV transmission system. A balanced load is connected to the 11 kV, secondary side of the transformer. Brk. 1 is used to control the operation period of the FD-STATCOM. A Three-level FD-STATCOM is connected to the tertiary winding by closing Brk. 1 at 0.2 s, for maintaining load RMS voltage at 1pu. The dc side provides the FD-STATCOM energy storage capabilities. The simulations are carried out for both cases where the FD-STATCOM is connected to or disconnected from the system.

The simulations of the FD-STATCOM in fault condition are done using LL and DLG faults and under islanded operating condition. In LL and DLG faults the faulted phases are phases A and B while in islanded operating condition, three conductors open by Brk. 2 in 0.4 – 0.5 s. The duration of the islanding condition are considered for about 0.1 s and the LL and DLG faults are considered for about 0.3 s. The faults are exerted at 0.4 s. The total simulation time is 1.6 s. In this paper, the FD-STATCOM uses the proposed control method to mitigate the load voltage sags due to all types of faults. The simulations are done for all types of faults introduced in the 11 kV distribution systems as follows:

A. Simulation results for Line-to-Line fault.

Fig. 7 and 8 show the RMS voltage and Vab (line Voltage) at the load point, respectively, for the case when the system operates without FD-STATCOM and under LL fault. In this case, the voltage drops by almost 20% with respect to the reference value. At t = 0.2 s, the FD-STATCOM is connected to the distribution system. The voltage drop of the sensitive load point is mitigated using the proposed control method.

Fig. 9 shows the mitigated RMS voltage using this new method where a very effective voltage regulation is provided.

Fig. 10 shows the compensated Vab at the load point in interval 0.4 - 0.7 s, (when the voltage drops by almost 20% because of the unbalanced LL fault by operating Timed Fault Logic). Fig. 11 shows the Vab frequency spectrums during mitigation of voltage sag that is presented in percent. The THD in percent for Vab in during mitigation of LL fault occurrence is 0.034%. Because of a 12-pulse FD-STATCOM is used in this paper, then the THD for Vab is very small.

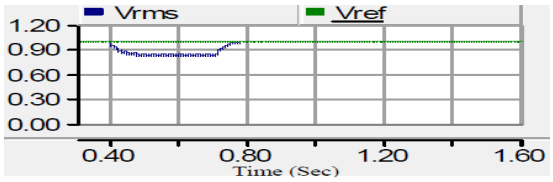

Fig 7: The RMS voltage (VRMS) at PCC without FD-STATCOM

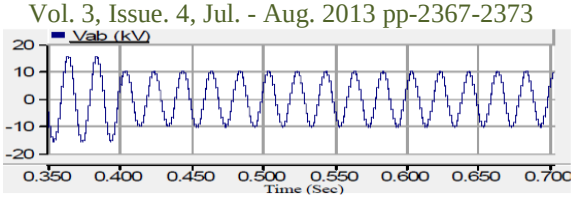

Fig 8: Vab at PCC without FD-STATCOM

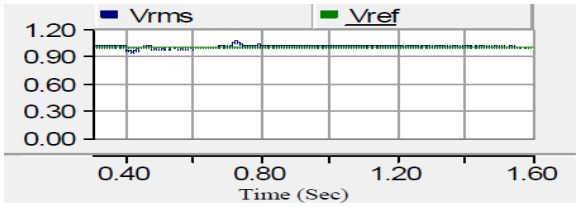

Fig 9: Compensated RMS voltage under LL fault

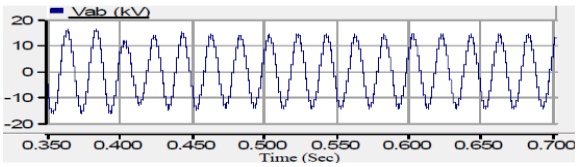

Fig 10: Compensated line voltage (Vab) at the load point

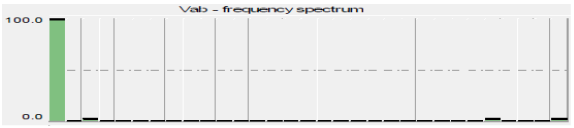

Fig 11: Frequency spectrum for Vab during mitigation of LL fault

B. Simulation results for Double Line to Ground fault

Figs. 12 and 13 show the RMS voltage and line voltage Vab at the load point, respectively, for the case when the system operates without FD-STATCOM and unbalanced DLG fault is occurred. The RMS voltage faces with 20% decrease with respect to the reference voltage.

Figs. 14 and 15 show the compensated RMS voltage and mitigated voltage of Vab at the load point, respectively, under DLG fault using proposed method. It is observed that the proposed method has correctly mitigated voltage sag.

Fig. 16 shows the Vab frequency spectrums during mitigation of voltage sag. The THD of Vab in during mitigation of DLG fault occurrence is very suitable and 0.036%.

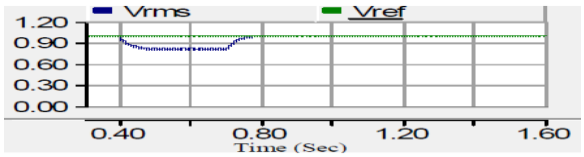

Fig 12: The RMS voltage (VRMS) at PCC without FD-STATCOM

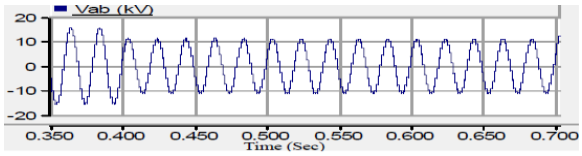

Fig 13: Vab Line voltage at PCC without FD-STATCOM

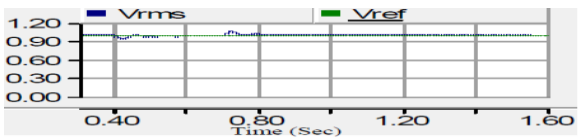

Fig 14: Compensated RMS voltage

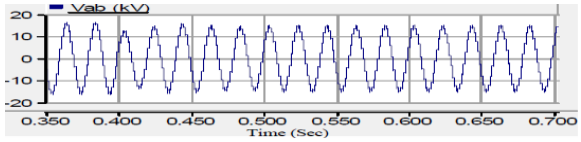

Fig 15: Mitigated line voltage Vab at the load point

The THD of Vab under islanded operating condition is very close to zero and 0.03%. The proposed method merits with respect to the classic methods are simplicity and control convenience and being flexible, i.e. it can mitigate voltage distortions caused by both LL/DLG faults and islanded operating condition only with the same control system setting.

The presented results show that the proposed FDSTATCOM and its controller system not only could mitigate voltage distortions caused by the faults but also have a suitable performance under the islanded operating condition as a FDG.

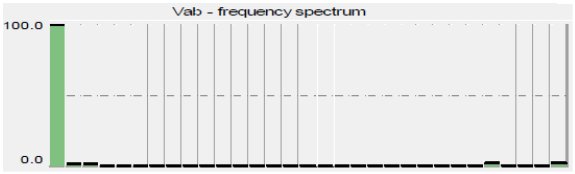

Fig 16: Frequency spectrum for Vab during mitigation of DLG fault

C. Simulation results under islanded operating condition

Figs. 17, 18 and 19 show the RMS voltage, line voltages and load currents (versus kA) at the PCC, respectively, for the case when the system operates without FD-STATCOM and under islanded operating condition.

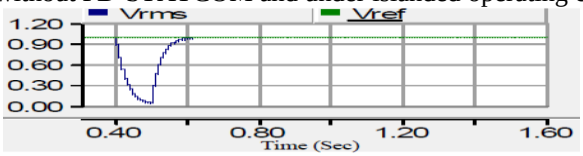

Fig 17: VRMS at PCC without FD-STATCOM under islanding condition

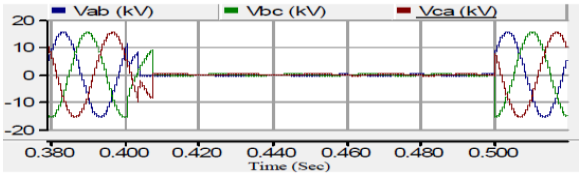

Fig 18: Line voltages at PCC without FD-STATCOM

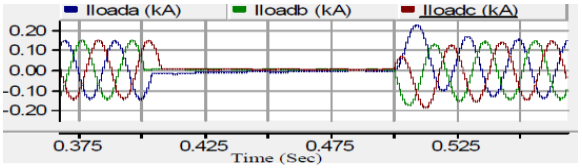

Fig 19: Load currents without FD-STATCOM in islanding condition

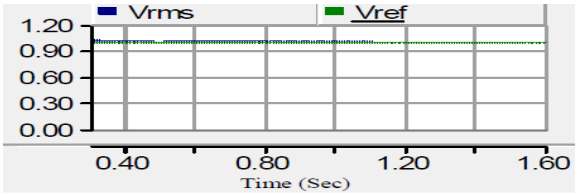

Fig 20: Compensated RMS voltage

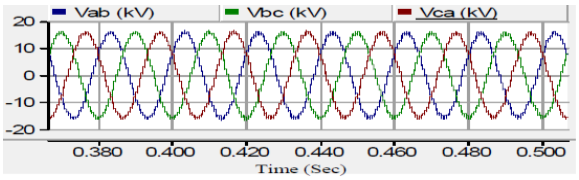

Fig 21: Compensated line voltages at the load point

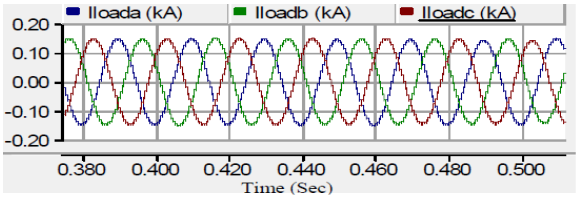

Fig 22: The mitigated load currents (in kA)

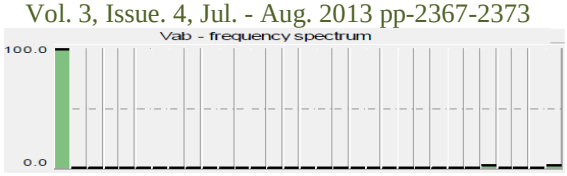

Fig 23: Frequency spectrum for Vab under islanded operating condition

Figs. 20, 21 and 22 shows the mitigated RMS voltage, line voltages at the load point and compensated load currents, respectively, using the proposed method.

It is observed that the RMS load voltage is very close to the reference value, i.e., 1pu and FD-STATCOM is able to supply power to sensitive loads, correctly. Fig. 23 shows the Vab frequency spectrums during mitigation of voltage sag caused by islanding condition. The THD of Vab under islanded operating condition is very close to zero and 0.03%.

The proposed method merits with respect to the classic methods are simplicity and control convenience and being flexible, i.e. it can mitigate voltage distortions caused by both LL/DLG faults and islanded operating condition only with the same control system setting. The presented results show that the proposed FDSTATCOM and its controller system not only could mitigate voltage distortions caused by the faults but also have a suitable performance under the islanded operating condition as a FDG.

Compression of different types of faults without D-STATCOM and with D-STATCON on distributed system

Type of Fault	Without D-STATCOM	With D-STATCOM	IMPROVEMENT IN VOLTAGE
L L Fault	✓ One phase voltage is reduced. ✓ Voltage drops by 20% w.r.t reference voltage. ✓ THD fault occurrence 0.034%	Voltage drop is reduced 10.571KV (voltage reference is 11kV)	96.1%
L L G Fault	✓ Two phase voltage are get affected. ✓ Voltage drops by 22.727% w.r.t reference voltage. ✓ THD fault occurrence 0.036%	Voltage drop is reduced 10.01KV (voltage reference is 11KV)	91%
Islanded Fault	✓ Supply disconnects. ✓ Voltage drops by 36.36% w.r.t reference voltage. ✓ THD fault occurrence 0.03%	Voltage drop is reduced 9.656KV (voltage reference is 11KV)	87.75%

VI. CONCLUSIONS

In this paper, the D-STATCOM and its control system proposed that could mitigate the voltage sags (such as LG, LL, DLG, 3-Phase and 3-Phase to Ground faults) and improved the power quality of the distribution system such as voltage flickers and power factor correction. The D-STATCOM is connected to the Y-Y and Y-Δ, the harmonics generated by a power electronic component is mitigated by providing the 30 degrees phase shift. The operation of the D-STATCOM and its control system are developed in MATLAB/SIMULINK for mitigating the voltage sags and improving the power quality of the distribution system.

REFERENCES

[1]. N. Hingorani, ―FACTS—Flexible ac transmission systems, in Proc. IEE 5th Int.Conf. AC DC Transmission, London, U.K., 1991, Conf. Pub.345, pp. 1–7.
[2]. S. Nilsson, ―Special application considerations for Custom Power systems, in Proc.IEEE Power Eng. Soc., Winter Meeting 1999, vol. 2, 1999, pp. 1127–1130.
[3]. C. J. Gajanayake, D. M. Vilathgamuwa, P. C. Loh, F. Blaabjerg, and R. Teodorescu, ―A z- source inverter based flexible DG system with Presonance and repetitive controllers for power quality improvement of a weak grid,‖ in Proc. IEEE Power Electronics Specialists Conference, 2007, pp. 2457-2463.
[4]. M. I. Marei, E. F. El-Saadany, and M. M. A. Salama, Flexible distributed generation: (FDG), in Proc. IEEE Power Engineering Soc. Summer Meeting, 2002, vol. 1, pp. 49- 53.
[5]. G. F. Reed, M. Takeda, and I. Iyoda, ―Improved power quality solutions using advanced solid-state switching and static compensation technologies, in Proc. IEEE Power Engineering Society Winter Meeting, 1999, vol.2, pp. 1132-1137.
[6]. L. S. Patil and Ms. A. G. Thosar, ―Application of D-STATCOM to mitigate voltage sag due to DOL starting of three phase induction motor, in Proc. IEEE International Conference on Control, Automation, Communication and Energy Conservation, 2009, pp. 1-4.
[7]. O. Anaya-Lara and E. Acha, ―Modelling and analysis of custom power systems by PSCAD/EMTDC,‖ IEEE Trans. Power Del., vol. 17, no. 1, pp. 266- 272, Jan. 2002.
[8]. H. Hatami, F. Shahnia, A. Pashaei, and S.H. Hosseini, ―Investigation on D-STATCOM and DVR operation for voltage control in distribution networks with a new control strategy,‖ in Proc. IEEE Power Tech., 2007, pp. 2207-2212.
[9]. E. Babaei, A. Nazarloo, and S. H. Hosseini, ―Application of flexible control methods for D-STATCOM in mitigating voltage sags and swells,‖ in Proc. IEEE International Power and Energy Conference (IPEC), Singapore, 2010, pp. 590-595.
[10]. S. H. Hosseini, A. Nazarloo, and E. Babaei, ―Application of DSTATCOM to improve distribution system performance with balanced and unbalanced fault conditions,‖ in Proc. IEEE Electrical Power and Energy Conference (EPEC), Canada, 2010.
[11]. N. Mariun, H. Masdi, S. M. Bashi, A. Mohamed, and S. Yusuf, ―Design of a prototype D STATCOM using DSP controller for voltage sag mitigation,‖ in Proc. IEEE International Power and Energy Conference, 2004.

BIOGRAPHIES

V. OBUL REDDY was born in Andhra Pradesh, India, 1986. He received the B.Tech degree in Electrical and Electronics Engineering from JNTU Hyderabad, India, 2009, and the M.Tech. Degree in Power electronics from JNTU Hyderabad, India, 2011. He is presently working as a Asst. Professor in Aurora's Engineering College, AP, India. His main research areas are Switched Mode Converters, Renewable Energy Sources and Electric Drives.

B. Giri Prasad Reddy was born in Nemallagunta Palli,Chittoor at Andhra Pradesd received his B.tech degree from Sindhura College of Engineering and Technology, Ramagundam, Affiliated to JNTU Hyderabad. He is M.Tech degree from Aurora's Engineering College, Bhongir, Hyderabad Affiliated to JNTU Hyderabad. His area of interest is Application of FACTS devices in Power systems.

International Journal of Modern Engineering Research (IJMER)
www.ijmer.com Vol. 3, Issue. 4, Jul. - Aug. 2013 pp-2374-2381 ISSN: 2249-6645

Alternatives for Cellulase Production in Submerged Fermentation with Agroindustrial Wastes

Fernanda Miranda Zoppas[1], Álvaro Meneguzzi[2], Francine Tramontina[3]
*(Laboratório de Corrosão, Proteção e Reciclagem de Materiais, Universidade Federal do Rio Grande do Sul, Porto Alegre, Brasil.)

ABSTRACT: *This article presents a review of the alternatives for cellulase production in submerged fermentation using agroindustrial residues as carbon sources. Among the wastes that are cited, the residue of grapes shows promise for producing these enzymes. The advantages associated with this process refer to the removal of industrial waste from the environment that is associated with the same added value through the production of enzymes.*

KEYWORDS: *Aspergillus niger. Cellulase. Grape marc. Submerged fermentation*

I. INTRODUCTION

The southern region of Brazil stands out in the wine industry by volume and quality of wines. As a consequence of this economic activity, grape residues are produced in large quantity per year. These residues are rich in cellulose and can be reused as a carbon source for several processes, including the production of enzymes.

Cellulases are enzymes that form a complex capable of acting on the cellulose and promote its hydrolysis. These enzymes are commonly used in various areas of industry, including food, beer and wine, agriculture, paper, textiles, detergent and animal feed, is also an alternative for generating energy. This paper presents a review of alternatives for production of cellulases in submerged fermentation using agroindustrial residues as carbon source, emphasizing the grape waste.

1.1. Lignocellulosic Materials, Agroindustrial Wastes: Lignocellulosic materials are the most abundant organic compounds in the biosphere, representing 50% of terrestrial biomass [1], which corresponds mainly by agribusiness materials, the urban waste, and the wood of angiosperms and gymnosperms [2].

According to Castro and Pereira Jr. (2010) [2], the lignocellulosic biomass is composed of three main polymer fractions: lignin, hemicellulose, and cellulose, which are joined to each other by covalent bonds, forming a complex network resistant to microbial attacks.

The cellulose from natural materials is the world's most abundant biopolymer that is formed by residues of β-D-glucose bound together by β-1,4, bonds, and it maintains a linear and flat structure; cellobiose (Fig. 1, adapted of BON, et al., 2008), the disaccharide 4-O-β-D-glucopyranosyl-D-glucopyranose, is the repeating unit of the polymer [3] that can be hydrolyzed to glucose with the help of acids. The microbial degradation of cellulose is total and specific and has encouraged the use of cellulolytic fermentation processes by man. In nature, these processes represent the largest source of carbon to the soil [4].

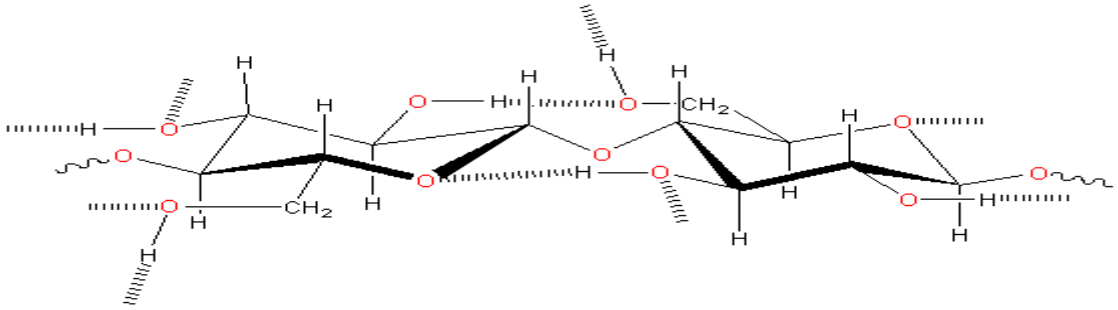

Figure1. Chemical structure of cellulose.

1.1.1. ***Agroindustrial wastes:*** Agroindustrial waste materials are rich in lignocellulosic materials that are inevitably produced by agricultural and industrial activities. The following can be cited as being among the lignocellulosic residues produced in bulk by the Brazilian agroindustrial activity: sugarcane bark, bagasse and straw, rice straw and rice bran, corn cobs and straw, chaff and bran from wheat, banana straw, cotton waste, wood scraps, and waste based on paper. Most of these materials are either partly or entirely not taken, being transformed into pollutants from the environment. Agricultural wastes contain 20–60% cellulose, 20–30% hemicellulose, and 15–30% lignin. The available quantity of these materials in the world is very large [5, 6].

Considering renewable resources, residues has a low cost as raw material for other processes and they can be purchased in regions that are located close to the local processing of the material. Due to the difficulty experienced by cellulose degradation in environmental conditions, cellulosic wastes accumulate, which makes them a nuisance to the environment. The use of lignocellulosic biomass derived from agriculture waste, forestry waste, and sewage can bring savings to the production of fuels and other products as well as reduce waste [2, 7].

1.1.1.1. Wastes from Winery: *According to Mendes and Araújo (2006) [8], more than 20% of the fermentation process of grapes for wine production involves waste that can generate environmental problems; therefore, it is necessary to search for an appropriate destination to them. Among the various solutions to this problem are composting, anaerobic digestion, animal feed processing, the use of seeds to produce oil as biofuel, soil deposition for fertilization, and pyrolysis.*

The same authors claim that in the process of making wine, every 1000 grams of grapes harvested, after crushing, generates about 350 grams of waste (bark, stems, and seeds), which are usually utilized in the soil of vineyards of the wine industry, serving as organic material for fertilization.

According to Mello (2003) [9], the Brazilian wine industry has advanced a great extent in manufactured products such as wines and juices as in the production of grapes for fresh consumption.

In 2009, grape production in Rio Grande do Sul (viniferous and regular) was 534,123,176 pounds. Being the main state producer of grapes and wines in the country, Rio Grande do Sul continues with being the largest area cultivated in Brazil, with 50 400 ha. [10, 11].

Another factor to be considered is the pruning of vines, which releases lignocellulosic material, and burning in the same field is responsible for the formation of toxic compounds emanating from the burning of lignin [6]. In this way, the use of grape marc for the production of enzymes appears as an alternative of biomass emanating from the pruning of the vines.

The grape marc waste differs from the others due to its composition, the presence of protein, starch, and lipids; while the rice husk, sugarcane bagasse, and bark of black acacia have the vast majority of lignocellulosic material composition [12].

In Table 1, we can observe some work that uses agroindustrial residues as a carbon source in the production of enzymes and other products of microbial origin.

Table 1. Agroindustrial wastes as a carbon source in the production of enzymes and other products of microbial origin.

Agroindustrial residue	**Microrganisms used**	**Authors**
Coconut shell	*Aspergillus niger*	COELHO *et al.*, (2001)
grape marc	*Aspergillus phoenicis*	SILVA, (2008)
grape marc	*Aspergillus awamori*	BOTELLA *et al.*, (2005)
grape marc	*Monascus purpureus*	DAROIT *et al.*, (2007)
grape marc	*Monascus purpureus*	SILVEIRA *et al.*, (2008)
grape marc and Orange peel	*Aspergillus awamori*	DÍAZ *et al.*, (2012)
Bagasse from sugarcane	*Aspergillus niger*	AGUIAR *et al.*, (2008)
Sawdust of *Pinus sp* and grape marc	*Pleurotus sajorcaju* PS-2001	DEON *et al.*, (2009)
Coconut shell	*Aspergillus phoenicis*	OLIVEIRA *et al.*, (2009)
Passion fruit peel	*Aspergillus niger*	SOUZA *et al.*, (2010)

As shown in Table 1, the use of waste grape has been described as an alternative substrate for the production of other products of microbial origin, which can be highlighted in the production of β-glucosidases, and pigments by the fungus Monascus purpureus and the production of hydrolytic enzymes such as exo-polygalacturonases, CMC-ase, and xylanase [12-16].

Based on the studies just cited, we can observe the high potential of grape waste as a substrate for cellulase production, with current efforts focusing on the use of agroindustrial by-products as a substrate and looking for products with high commercial value and low cost production from naturally abundant substrates in each region.

1.1.2. Enzymes and Cellulases: Enzymes: *Enzymes are proteins that exhibit catalytic activity. The enzyme complex molecular structure consists of one part of protein, but it can be connected to other molecules such as carbohydrates and lipids [17]. Enzymes are present in all living cells, which exercise the function of catalysts of the reactions that compose the anabolic and catabolic pathways of cellular metabolism [6].*

As Filho (2006) [18] explains, the great interest in the use of enzymes can be explained by several factors, including the large variety of reagents in which the same act, the complex reactions which the enzymes are capable of catalyzing on routes where the generation of waste and by-products is reduced, and that they have the capacity to operate as catalysts at high speeds in conditions of reduced energy needs (mild conditions of pressure and temperature).

The catalytic action of enzymes involves the delivery of a specific environment of the enzyme where the enzyme reaction is energetically more favorable, and this region where the reaction is called active site. The molecule that binds to the active site and acts on the enzyme is called the substrate. In general, the substrate binding site is a slot or groove on the surface of an enzyme, complementary to the shape of the substrates (geometric complementarily). In addition, the amino-acid residues that form the binding site are arranged to form specific interactions of attraction with the substrate (electronic complementarily). The reaction becomes more favorable, because the interaction between the amino-acid residues and the reactant molecules decreases the activation energy that is required for the rearrangement of covalent bonds and the performance of non-covalent interactions between the enzyme and the substrate [18, 19].

1.1.3. Cellulases: *To meet the challenge associated with degrading cellulose, cellulolytic microorganisms produce a complex mixture of enzymes called cellulases. These enzymes, which collectively have links to specific β-1, 4 cellulose, are necessary for the complete solubilization of cellulose, existing synergism between that [6].*

The complex cellulolytic enzymes are hydrolases that cleave O-glycosidic bonds and are classified by the Enzyme Commission (EC) with the coding 3.2.1.x, where the value of x varies with the cellulase evaluated. The classification of cellulases, according to their site of action in the cellulosic substrate, allows them to be categorized into three groups: endoglucanases (EnG), which cleave internal cellulosic fiber bonds; exoglucanases (ExG) or celobiohidrolases (BNG), which work in the external region of the cellulose; and β-glucosidases (BG), which hydrolyze soluble glucose oligosaccharides [2, 6].

Figure 2, adapted of LYND et al., (2002), illustrates the synergistic action between exoglucanases, endoglucanases, and β-glucosidases in the hydrolysis of cellulose fiber.

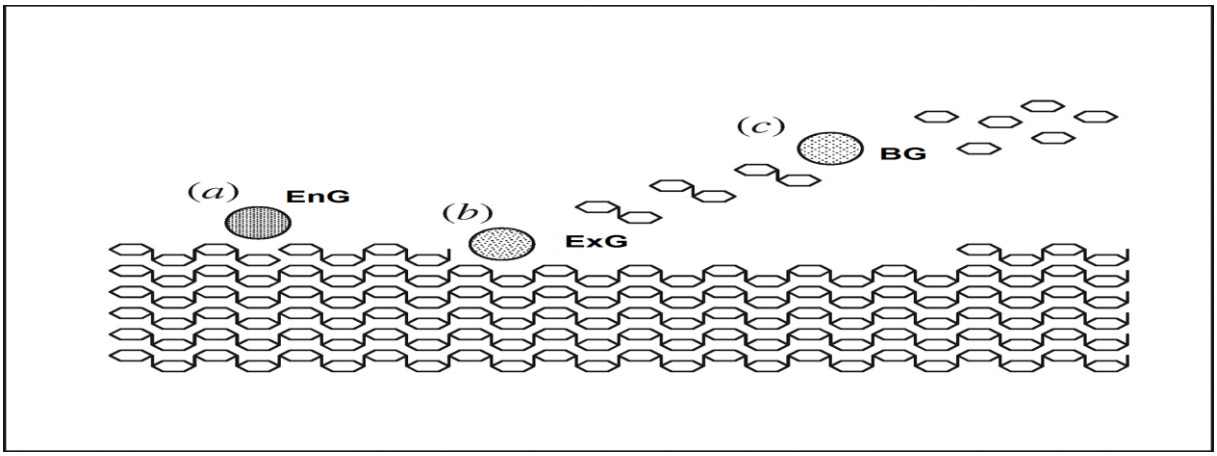

Figure 2. Mode of action of enzymes of the cellulolytic complex

1.1.3.1. Endoglucanases: *Endoglucanases are also known as endo-β-1, 4 glucanase and carboxymethyl cellulase. They catalyze the hydrolysis of internal bonds β-1, 4-D-glucosides of cellulose, randomly generating oligosaccharides of various sizes and, consequently, new chain terminals. Cellulose and xiloglicana serve as their natural substrate. They act only in the amorphous portion of cellulose, and their activity decreases along with shortening the length of the cellulose chain [20].*

1.1.3.2. Exoglucanases: *They act in a progressive way in reducers and nonreducer portions of the cellulose chains, liberating either glucose (glucanohidrolases) or cellobiose (celobiohidrolases) as the main products. They act on microcrystalline cellulose, thereby shortening the polysaccharide chains and have a limited effect on substrates such as carboxymethylcellulose (CMC) and hydroxyethylcellulose (HEC) [21].*

1.1.3.3. β-glucosidase: *This is necessary to hydrolyze short-chain oligosaccharides and soluble cellobiose into glucose, and can also be called β-D-glucoside glucohidrolase (EC 3.2.1.21). It loses activity with increasing the length of the cellulose chain and also performs the hydrolysis of terminal β-D-glucose oligosaccharides [20, 21, 22].*

When working together, the complex cellulolytic enzymes have a better yield than the sum of the individual income, that is, when acting in isolation from each other [2].

1.2. Characterization and properties of cellulases: *With the aim of using cellulases in industrial processes under the conditions of their best performance, it is essential that their properties are determined, especially with regard to kinetic factors and physical chemists [2].*

Another property of cellulolytic enzymes commonly reported in the literature is their ability to be influenced by other molecules, especially metals, and this characteristic is suffering from inhibitory or inductive effects at the moment. Among the ions studied, the ones that more often inhibit cellulases are those of mercury, copper, silver, and zinc (Hg^{+2}, Cu^{+2}, Ag+, and Zn2+), which even lead to the total loss of catalytic activity, and are present at concentrations as low as 2.0 mM [2]. For the characterization of crude cellulase preparations with regard to their activity, different substrates of endoglucanases are used, stressing, however, that the synergy between the two types of enzyme prevents a precise quantification [6]. A substituted cellulose derivative such as carboxymethyl cellulose (CMC), which is soluble, is used as a substrate for endoglucanase activity. The enzyme attacks the polymer in a random mode, producing a rapid change in the degree of polymerization. After the enzymatic reaction, the formation of reducer sugars is determined, which is known as CMCase activity. The microcrystalline cellulose is one of the substrates used in the tests for measuring the activity of exoglucanases. The measurement of enzyme activity is commonly used as a reference for determining the activity in both cellulosic global academic work and for commercial enzyme preparations [6,23].

1.3. ***Applications of cellulases:*** Cellulases have been investigated mainly with regard to their potential as an additive in the detergent industry, textile industry, and also in the bioconversion of agricultural biomass into products with commercial value [6]

In the food industry, cellulases are used in maceration processes, usually along with hemicellulases and pectinases, such as the extraction of fruit juice and oil seeds. They also have an important role in the filtration and clarification of fruit juices, which increases the effectiveness of the extraction of color and juices in the liquefaction of plant tissue, thereby allowing for a better extraction of pigments from fruits [22, 24-27].

Cellulases have great potential use in the production of glucose syrups from cellulosic materials that compete with starch and sucrose in the production of alternative sweeteners which are used in food and beverage industries. Hydrolyzed cellulose can also be used as a nutrient in fermentation for the production of various chemicals, including enzymes for food processing and food ingredients such as citric acid and acetic acid, and amino acids [6].

The animal feed industry moves a market of more than 50 billion dollars worldwide. In ruminants, the use of cellulases, along with pectinases and hemicellulases, increases the digestion of forage plants, the basis of animal nutrition, and, thus, increases the quality and digestibility of feed [22, 24, 26].

In the textile industry, cellulases are used for the removal of excess dyes in denim fabrics, a process called Bio-Stonewashing [27]. Other benefits associated with the addition of these cellulases are a reduction in the time of use of the machines involved in the process, increased productivity, improved security conditions in the work environment, and conditions of process automation [22, 24, 28, 29]. Cellulases are also present in the Biopolis tissue process, that is, the removal of surface fibrils caused by pilosity, which increases with use and washing processes. These enzymes then promote the reduction of the tendency of pellets, which is actually the formation of small balls in the tissue [6]. A major challenge associated with the application of cellulases in the textile and laundry industries is the correct use of formulations for the use of enzymes [24].

In the manufacturing of pulp, woody materials that harm the quality of pulp are removed. The use of Trichoderma cellulases in the process allows an energy savings of 20% but can reach up to 40%, depending on the time and type of the enzyme applied. The use of cellulases is present in the modification of the properties of the fibers, increasing the speed of manufacture of paper [24].

There is a worldwide trend of enzymatic hydrolysis of lignocellulosic materials, seeking to ferment sugars for the production of bioethanol on a large scale [30]. An obstacle to the use of cellulases is the cost of production, which can be overcome using genetically modified organisms (bacteria, yeasts, and plants) for the production of enzymes, and the need to produce more efficient enzymes [31]. Another option is the use of agroindustrial residues that serve as a carbon source, promoting the reduction of production costs of cellulases through the economy in the purchase of raw materials, and also collaborating with the environmental problem of waste generation from these industries.

1.4. Enzyme Production by Microorganisms: *Microorganisms are the main sources of industrial enzymes that are unique because of their wide variety of catalytic activities, the possibility of the production of enzymes by fermentation processes, and the large-scale regularity and simplicity of the nutritional requirements [6].*

1.4.1. Characteristics and nutrition: *According to Bon et al. (2008) [6], the first step in the microbial production of an enzyme of interest is the identification and acquisition of the producer organism, which can either be a wild strain or one that is modified by molecular biology techniques. The lineage of interest can be either acquired from culture collections or scientific service, or selected from samples of soil, water, air, and plant tissues such as stems or decaying fruit and other sources. Additionally, according to the same authors, ideally, the microorganism that is used in the case just mentioned should have the following characteristics: It should be safe from the biological point of view; have a high capacity for the synthesis and excretion of the enzyme; withstand environmental conditions related to osmotic pressure, temperature, and ionic strength; and be tolerant to the presence of toxic substances that can be generated during the treatment process of raw materials or by cellular metabolism.*

The maintenance and preservation of organisms are extremely important steps that ensure their viability and prevent genetic changes which lead to a reduction or loss of phenotypic properties [6].

1.4.1.1. Culture media in the production of enzymes: *The physicochemical characteristics of the culture media are of fundamental importance, not only for cell growth but also for the yield of a product. This is because the cells are able to respond to physical and chemical stimuli from the external environment through biochemical mechanisms that regulate gene expression and physiology of the organism and, by extension, its performance in the formation of the desired product [6].*

The physical and chemical constituents of the medium, such as nutrient composition, pH, temperature, dissolved oxygen, and mechanical forces, exert changes in the formation of mycelium [32]. The study of variables such as the formation of pellets is essential; it is a positive factor for citric acid production by A. niger; whereas it is harmful for the production of amylase [33].

The use of different nitrogen sources allows greater productivity in the secretion of cellulase enzymes, as seen in the work of Hanif et al., (2004) [34]. During hydrolysis, some factors can interfere by way of access to the surface area due to the porosity of the material, the presence of crystalline cellulose fibers, and the presence of lignin and hemicellulose, which hinder access to the cellulose enzyme, thus resulting in a reduced-efficiency hydrolysis process [31].

Different proportions of grape residue and culture media were analyzed by Silva (2008) [12], with the objective of determining the best ratio between the substrate and culture medium for cellulase production by Aspergillus phoenicis. For

total cellulase activity, higher activity was observed after treatment with 15 g/L of grape residue and 7.5 g/L of peptone (0.094 FPU). However, when the concentration of peptone decreased to 1.5 g/L or increased to 8.5 g/L, a low enzyme activity of 0.029 FPU occurred. The change in the concentration of grape residue of 3 g to 17 g caused a reduction in enzyme activity, averaging 0.034 FPU, which is significant for a confidence level of 95%.

In this sense, it is important to consider to what extent the increase in substrate concentration will increase the production of cellulase, without any form of inhibition, which would cause waste of raw material and growing medium, affecting the yield of the process. This is a definite factor, as the culture medium contains all the nutrients necessary for the organism to develop and generate product interest.

1.4.2. Fungal decomposers of lignocelluloses: *Fungi are one of the most important groups of microorganisms in the activity of decomposition of organic matter due to their expertise in degradation. This activity occurs mainly through their mycelium or vegetative stage. During vegetative and reproductive phases, the formation of biomass depends on the production of extracellular enzymes, which are fundamental components of the degradation of substrates, mainly lignocellulose [35].*

Cellulases as well as other extracellular enzymes that are required for hydrolysis are induced and secreted by microorganisms to grow on cellulose. Among them are cellulases produced by fungi of the genus Trichoderma, Penicillium, and Aspergillus [36].

The most common genus of filamentous fungi is Aspergillus, and it is also one of the most well studied. The species composing this genus are widely distributed worldwide and are present in the earth's surface, air, and water, in both the bodies of plants and animals, besides being associated with the deterioration of plant materials and food, especially in tropical and sub-tropical regions. Many Aspergillus species are used to obtain enzymes in the chemical biosynthesis and processing of compounds [37].

Despite the existence of pathogenic species, the genus is present in the food and industrial microbiology like positive, so that micro-organisms of the species Aspergillus oryzae and Aspergillus niger are considered safe, according to the Food and Drug Administration (FDA), an agency responsible for the control of food and medicine in the United States of America, being generally named and recognized as Safe (GRAS). Industrially, the genus is present in the production of enzymes, drugs, and antibiotics that are used in food fermentation [32, 33, 38-40]. The genus Aspergillus is widely reported in the literature as being a producer of cellulases [13, 20, 22, 41-44].

The fermentation kinetics of Aspergillus niger was studied by Aguiar et al. (2008) [45], using sugar cane bagasse as a substrate. The fungus Aspergillus niger used proved to be a producer of cellulases under the conditions studied, with activity equal to 0.408 UI. There was also a decrease in pH, due to the production of organic acids by the fungus (for example, citric acid, gluconic, oxalic, etc.).

In the study of Coelho et al. (2001) [7], Aspergillus niger was used for the production of enzymes (cellulases, xylanases, and pectinases) with green coconut shell as a substrate, because this material contains large amounts of compounds such as cellulose, hemicellulose, pectin, and others, with no need for large nutrient additions that would enhance appropriate microbial development.

However, Silva (2008) [12] observed differences in the results of enzymatic activities among isolates of the same genus, which shows that not all members of the same genus have the same potential for the production of enzymes.

As observed in the work just mentioned, Aspergillus niger is a great producer of enzymes such as cellulases, presenting a great potential for the production thereof with various cellulosic substrates, and is also very promising; therefore, the use of grape waste for the production of enzymes, given the need for regional use of this residue.

1.5. Bioprocesses for Enzymes Production: *The industrial enzymes are usually produced by microorganisms, although some of them are extracted from animal and plant tissues [6]. According to Lima et al. (2001) [46], the production of enzymes on an industrial scale is done mostly by submerged fermentation; whereas in eastern countries, there is an established tradition of using solid-state fermentation.*

In any bioprocess, biomass is a crucial parameter for the characterization of cell growth [6]. The bioprocess can be divided into two kinds: The first kind indicates the production of biomass, whereas the second kind involves the production of metabolites (primary or secondary). In the first case, the measure of biomass is very important, because it is the main objective of the process of submerged or solid-state fermentation. The production of these metabolites can be proportional to the amount of biomass. Thus, in order to improve the production of metabolites, especially a secondary metabolite, it is necessary to improve cell growth [6, 17, 42].

Environmental factors such as temperature, pH, water activity, oxygen levels, and concentrations of nutrients and products significantly affect microbial growth and product formation. In submerged cultures, environmental control is relatively simple due to the homogeneity of the suspension of microbial cells, the nutrient solution, and the products in the liquid phase [17].

1.5.1. Solid-state Fermentation: *The term solid-state fermentation (SSF) is described as the fermentation in which the growth of microorganisms in solid substrates occurs in the absence of liquid in the free form. The free water is essential to the growth of microorganisms and is either adsorbed on a solid support or complexed within a solid matrix. The SSF is considered more natural than other types of fermentation, because their processes are similar to the conditions under which most microorganisms grow in nature [17].*

1.5.2. Submerged Fermentation: *The submerged fermentation is also known as submerged culture, and its main characteristic is the use of a liquid fermentation media with soluble nutrients. This fermentation process can be performed in shaken flasks (Erlenmeyer flasks, for example), on a fermenter's bench, or on an industrial-scale fermenter [47]. In this type of fermentation, the substrate is dissolved or suspended in a water source where water is not a limiting factor [1], and it can generate different metabolites [32, 33]. Among them, it is worth mentioning enzymes, antibiotics, organic acids [32], carotenoids, biotin [33] recombinant proteins [33, 35, 48], and amino acids [49].*

Most commercial enzymes are obtained by submerged fermentation, as modern methods of control are more easily adapted to fermentation, the yields are higher, and the costs and risks of contamination are lower [12].

For the successful cultivation of filamentous fungi under water, it is necessary to study several variables. Operating parameters such as pH, temperature, oxygen consumption, and carbon dioxide formation are measured and tightly controlled [6, 50]

According to Volpato (2009) [51], submerged cultures may occur in two ways: in a rotating incubator, where the control of pH and oxygen transfer is more difficult, or in bioreactors, which enable the control of various parameters such as temperature, pH, agitation speed, and pressure, among others.

With regard to the semi-solid culture, submerged cultivation has the advantage of being able to have better rationalization and standardization of the process, which is crucial for the industry and allows a homogeneous culture system. Thus, according to Silva (2008) [12], the main advantages of the submerged processes are ease in controlling the physicochemical process, greater efficiency of nutrient absorption, and excretion of metabolites through the cells, leading to lower process times and, consequently, productivity gains.

Among the disadvantages, the following can be cited: the high cost of aeration and agitation, especially when used a reaction media with high viscosity and complex rheology; Foaming.

The submerged fermentation is used to produce several enzymes of industrial interest, as described in several studies. These can be cited in the submerged fermentation in bottle production by recombinant yeast endoxilanases P. pastoris using culture media containing "Yeast Nitrogen Base" (YNB), peptone, and yeast extract as sources of nitrogen and methanol as carbon source [52]. The lipase production in submerged cultivation allows the obtention of 3.15 U / mL in 96 hours of fermentation in synthetic medium and of 2.22 U / mL at 72 hours of fermentation in the industrial environment, with the fungus Penicilllium verrucosum [47] showing that the crop is promising for various purposes.

Among the challenges associated with submerged growth are the mechanisms of growth of the fungus, the dynamic aggregation of the mycelium, fragmentation, quantification of the morphology, and mathematical models for the growth and formation of products of cultivation [32]. A better system of homogenization with submerged growth is achieved by agitation, so that in this way, the pellets are not formed, the whole system hifal may be exposed to the environment. Therefore, the limitations imposed by lack of oxygen and reducing the rate of diffusion of nutrients can be overcome [53]; however, one should consider that the processes carried out in shaken flasks have difficulty in controlling certain parameters, such as, for example, aeration [47].

Among the studies using submerged cultivation, we can highlight Sridevi (2009) [54], who evaluated the capacity of cellulase production by Aspergillus niger in pretreated lignocellulosic residues such as sawdust, wheat straw, bagasse, and rice bran in submerged fermentation, obtaining satisfactory results, as seen in Alberton (2004) [17], who studied the use of different natural substrates in the production of xylanase, and Aguiar and Menezes (2000) [55], who studied the production of cellulase by Aspergillus niger IZ-9, grown on sugarcane bagasse chemically treated, as a substrate.

Many research groups distributed around the world have been studying strains of microorganisms with high cellulolytic activities, different lignocellulosic materials as a carbon source, and the stabilization and immobilization of these enzymes with a view to their application in large-scale processes. In this aspect, the use of grape waste as a carbon source for cellulase production proves to be very promising, possibly because of it being a residue that can be used on an industrial scale in the future. It is important to stress the need to use controls, both the ability of cellulase production by the strain chosen as the capacity of the grape marc serve as a carbon source, using data obtained from literature, to give credibility to the results obtained.

1.6. Market and Perspectives for Use of Enzymes in Brazil: *According to data from the Ministry of Development and Foreign Trade of the federal government on the enzymes market in Brazil, in 2005, the total Brazilian imports of enzymes were $ 95.7 million, while the exports were $ 5.4 million, showing that the Brazilian market is essentially an importer and also indicating strategic and technological disadvantages in terms of production and the use of enzymes in the country. Thus, the use of bagasse is an alternative to production the oxidative and hydrolytic enzymes of biotech industries to obtain a cheaper cost compared with enzymes that are available in the market [6].*

The use of enzyme catalysts in many different industries has been a growing trend worldwide, and the total market value is estimated at 2.3 billion dollars annually [27]. The market is divided into three segments: the enzyme techniques (formed by detergent, starch, textile, ethanol, pulp and paper pulp, and leather industries), enzymes in the food industry, and animal feed enzymes [27, 28].

Advances in enzyme technology in Brazil are favored by the enormous quantity and variety of renewable raw materials that can be enzymatically transformed into useful products for the strategic sectors of the economy. There are also the country's knowledge of the technologies used for the production of enzymes on a large scale, and extractive fermentation processes, as well as the greatest biodiversity as a source of biocatalysts [6].

II. CONCLUSIONS

It is possible to produce cellulases from agroindustrial residues as the residue of grapes, but larger studies are needed in order to quantify these enzymes, their separation, and the optimization of the production process, so that they could be later used in a pilot-scale production of the same or at even an industrial scale.

With regard to the environmental question, one should always stress the importance of removing the residual of the environment and adding value to it, so that industries in various sectors such as food, textiles, and beverages could later take advantage of this proposal through the use of cellulases that are obtained from grape residue. For this to happen, further studies are needed for the purification of enzymes and their marketing, so that regional demands are met by these enzymes.

ACKNOWLEDGMENTS

The authors acknowledge the support rendered by the Universidade Estadual do Rio Grande do Sul, Universidade Federal do Rio Grande do Sul, and CNPq.

REFERENCES

[1]. Sarko, *How much do we know about its estructure?, in Wood and Cellulosics: Industrial Utilization*. John Wiley & Sons, New York, 1997.
[2]. A.M. De CASTRO, and N. PEREIRA JR., Produção, propriedades e aplicação de celulases na hidrólise de resíduos agroindustriais. *Química Nova. 33* (2010), pp. 181-188.
[3]. E.A. Bayer, and R. Lamed, The cellulose paradox: pollutant par excellence and/or a reclaimable natural resource. *Biodegradation. 3* (1992) pp. 171-188.
[4]. J.M. Lynch, J.H. Slater, J.A. Bennett, and S.H.T. Harper, Cellulase activities of some aerobic microorganisms isolated from soil. *Journal of General Microbiology* 127 (1981) pp. 231-236.
[5]. G. Pauli, *Upzing,* (Porto Alegre, L&PM, 1998).
[6]. E.P.S. Bon, M.A. Ferrara, M.L. Corvo, A.B. Vermelho, C.L.A.M. Paiva, R.B. De Alencastro, and R.R.R. Coelho, *Enzimas em biotecnologia: Produção, aplicações e Mercado.* Rio de Janeiro. Interciência, Portugal, 2008.
[7]. M.A.Z Coelho, S.G.F. Leite, M.F. Rosa, and A.A.L. Furtado, *Aproveitamento de resíduos agroindustriais: produção de enzimas a partir da casca de coco verde.* Boletim CEPPA. 19 (2001) pp. 33-42.
[8]. M.A. Mendes, and J.H.B. Araújo, *Transformação de resíduos da indústria vinícola em produtos de interesse comercial.* Mostra de Iniciação Científica e Tecnológica Interdisciplinar, Colégio Agrícola de Camboriú, UFSC, Balneário Camboriú, 2006.
[9]. L.M.R. Mello, *Produção e comercialização de uvas e vinhos – Panorama 2003***,** (Bento Gonçalves, Embrapa Uva e Vinho, Brasil, 2003).
[10]. EMBRAPA, *Uva e Vinho,* Bento Gonçalves, 2010. Available at: www.cnpuv.embrapa.br.
[11]. UVIBRA, União Brasileira de Vitivinicultura. *Dados estatísticos, 2010*. Available at: http://www.uvibra.com.br/dados_estatisticos.htm.
[12]. Silva, L.A.D; *Produção e caracterização de enzimas celulásicas por Aspergillus phoenicis***.** Master's Thesis, Universidade Federal do Rio Grande do Sul, 2008.
[13]. Botella, I. De Ory, C. Webb, D. Cantero and A. Blandino, Hydrolytic enzyme production by Aspergillus awamori on grape pomace. *Biochemical Engineering Journal* 26 (2005), pp. 100 -106.
[14]. D.J. Daroit, S.T. Silveira, P.F. Hertz, and A. Brandelli, Production of extracellular b-glucosidase by Monascus purpureus on different growth substrates. *Process Biochemistry* 42 (2007) pp. 904-908.
[15]. S.T. Silveira, D.J. Daroit, A. Brandelli, Pigment production by Monascus purpureus in grape waste using factorial desing. *Food Science and Technology* 41 (2008), pp. 170-174.
[16]. A.B. Díaz, I. De Ory, I. Caro, A. Blandino, Enhance hydrolytic enzymes production by Aspergillus awamori on supplemented grape pomace. *Food and Bioproducts Processing* 90 (2012), pp. 72-78.
[17]. L.R. Alberton, *Produção de xilanase em resíduos agroindustriais por Streptomyces viridosporus t7a e aplicação do extrato bruto em veterinária.* Doctoral thesis, Universidade Federal do Parana, 2004.
[18]. U.C. Filho, Apostila: *Cinética enzimática e uso e produção de enzimas*; Universidade Federal de Uberlândia, 2006.
[19]. A.L. Lehninger, D.L. Nelson, M.M. Cox, *Princípios de bioquímica*. (São Paulo, Sarvier, 2006).
[20]. L.R. Lynd, P.J. Weimer, W.H.V. Zyl, I. S. Pretorius. Microbial Cellulose Utilization: Fundamentals and Biotechnology. *Microbiology and Molecular Biology Reviews* 66 (2002), pp. 506-577.
[21]. Singh and K. Hayashi, Microbial cellulases: Protein architeture, molecular properties, and biosynthesis. *Advances in Applied Microbiology*, 40 (1995), pp. 1-44.
[22]. M.K. Bhat and S. Bhat, Cellulose degrading enzymes and their potential industrial applications. *Biotechnology Advances* 15 (1997) pp. 583-620.
[23]. T.K. Ghose, Measurement of cellulase activities. *Pure & Applied Chemistry* 59 (1987), pp. 257-268.
[24]. M.K. Bhat, Cellulase and related enzymes in biotechnology. *Biotechnology Advances* 18 (2000) pp. 355-383.
[25]. F. Vaillant, P. Milan, G. O' Brien, M. Dornier, M. Decloux and M. ReyneS, Crossflow microfiltration of passion fruit juice after partial enzymatic liquefaction. *Journal of Food Engineering*, 42 (1999), pp. 215 -254.
[26]. F. Niehaus, C. Bertoldo, M. Kahler and G. Antranikian, Extremophiles as a source of novel enzymes for industrial application. *Applied Microbiology and Biotechnology* 51 (1999), pp. 711-729.
[27]. S.I. Mussatto, M. Fernandes and A.M.M. Milagres, Enzimas: Poderosa ferramenta na indústria. *Ciência Hoje*, 41 (2007), pp. 28-33.
[28]. O. Kirk, T.V. Borchert and C.C. Fuglsang, *Industrial enzyme applications. Current Opinion in Biotechnology* 13 (2002), pp. 345–351.
[29]. J. Chen, Q. Wang, Z. Hua and G. Du, Research and application of biotechnology in textile industries in China. *Enzyme and Microbial Technology* 40 (2007), pp. 1651-1655.
[30]. Y.H.P. Zhang, M.E. Himmel and J.R. Mielenz, Outlook for cellulose improvement: Screening and selection strategies**.** *Biotechnology Advances*, 24 (2006), pp. 452–481.

[31]. Y. Sun and J. Cheng, Hydrolysis of lignocellulosic materials forethanol production: a Review. *Bioresource Technology*, 83 (2002), pp. 1–11.
[32]. M. Papagianni, Fungal morphology and metabolite production in submerged mycelia processes. *Biotechnology Advances* 22 (2004), pp. 189–259.
[33]. P.A. Gibbs, R.J. Seivour and F. Schimid, Growth of filamentous fungi in submerged culture: Problems and possible solutions. *Critical Reviews in Biotechnology* 20 (2000), pp. 17–48.
[34]. Hanif, A.; Yasmeen, A. Rajoka, M.I. Induction, production, repression, and de-repressionof exoglucanase synthesis in Aspergillus Niger. Bioresource Technology, Oxford, v. 94, p. 311–319, 2004
[35]. M.A. Velazquez-Cedeño, G. Mata, J.M. Savoie, Waste reducing cultivation of Pleurotus ostreatus and Pleurotus pulmonarius on coffe pulpe changes in the production of some lignocellulolytics enzymes. *World Journal of Microbiology and Biotechnology* 18 (2002), pp. 201-207.
[36]. L.A. Serafini, N.M. Barros and J.L. Azevedo, *Biotecnologia na agricultura e na agroindústria***.** *(*Guaíba, Agropecuária, 2001).
[37]. C.A.R. Rosa, S.G. Campos and F.A. Baroni, *Práticas de micologia veterinária*. (Rio de Janeiro, Seropédica, 2002).
[38]. J.W. Bennett, Mycotechnology: the role of fungi in biotechnology. *Journal of Biotechnology* 66, (1998) pp. 101-107.
[39]. O.P. Ward, W.M. Qin, J. Dhanjoon, J. Ye and A. Singh, Physiology and biotechnology of Aspergillus. *Advances in Applied Microbiology*, 58 (2006), pp. 1-75.
[40]. L.H. Grimm, S.Kelly, R. Krull and D.C. Hempel, Morphology and productivity of filamentous fungi. *Applied Microbiology and Biotechnology*, 69 (2005), pp. 375-384.
[41]. J.C. Stewart and J.C. Parry, Factors influencing the productions of cellulase by Aspergillus fumigatus (Fresenius). *Journal of General Microbiology* 125 (1981), pp. 33-39.
[42]. S.W. Kang, Y.S. Park, J.S. Lee, S.I. Hong and S.W. Kim, Production of cellulases and hemicellulases by Aspergillus niger KK2 from lignocellulosic biomass. *Bioresource Technology* 91 (2004), pp. 153-156.
[43]. Mamma, E. Kourtoglou, P. Christakopoulos, Fungal multienzyme production on industrial by-products of the citrus-processing industry. *Bioresouce Technolology***,** 99 (2008) pp. 2373-2383.
[44]. T.B. Ng, Peptides and proteins from fungi. *Peptides*, 25 (2004), pp. 1055-1073.
[45]. C.M. de Aguiar, M.H.L. Margonar and S.L. Lucena, *Produção de Celulases por Aspergillus niger: Cinética da Fermentação.* XVI Encontro de Química da Região Sul, Blumenau, 2008.
[46]. U.A. Lima, W. Schimdell, E. Aquarone and W. Borzani, *Biotecnologia industrial: Processos Fermentativos e Enzimáticos.* (São Paulo, Edgar Blüncher, 2001).
[47]. T.L.F. Pinheiro, *Produção de lipases por fermentação em estado sólido e fermentação submersa utilizando Penicillium verrucosum como microrganismo***.** Master's Thesis. Universidade Regional Integrada, 2006.
[48]. L. Wang, D. Ridgway, T. Gu and M. Moo-Young, Bioprocessing strategies to improve heterologous protein production in filamentous fungal fermentations. *Biotechnology Advances*, 23 (2005), pp. 115 -129.
[49]. J. Gomes and D. Kumar, *Production of L-methionine by submerged fermentation: A Review. Enzyme and Microbial Technology*, 37 (2005), pp. 3-18.
[50]. European Commission. *Final Report: Collection of information on Enzymes.* Austria, 2002.
[51]. G. Volpato, *Produção, purificação e imobilização de lipases de staphylococcus warneri EX17 produzidas em glicerol;* Doctoral thesis. Universidade Federal do Rio Grande Do Sul, 2009.
[52]. W.R. Carvalho, *Caracterização bioquímica da endoxilanase recombinante (HXYN2r) do fungo termofílico Humicola grisea var. thermoidea e sua aplicação na sacarificação de resíduos agrícolas.* Doctoral thesis, Universidade Federal de Goiás, 2008.
[53]. D.H. Griffin, *Fungal physiology*, (New York, Wiley-Liss, 1994).
[54]. Sridevi, G. Narashimha and B.R. Reddy, Production of Cellulase by Aspergillus niger on natural and pretreated lignocellulosic wastes. *The Internet Journal of Microbiology***.** 7 (2009).
[55]. C.L. Aguiar, T.J.B Menezes, *Produção de celulases e xilanase por Aspergillus Níger IZ9 usando fermentação submersa sobre bagaço de cana-de-açúcar*. Boletim Centro de Pesq Process Alimentos, 18, 2000.
[56]. M. Deon, L.O. Da Rosa, R.A. Saggin, J.M. Finimundi and A.J.P. Dillon, *Produção de Cogumelos de Pleurotus sajor-caju PS-2001 em Resíduos Lignocelulosicos constituídos de Serragem de Pinus sp e Bagaco de Vitis labrusca*. XVII encontro de jovens pesquisadores da UCS, Caxias do Sul, 2009.
[57]. S.L.R. Oliveira, T.C. Maciel, A.L.F. Pereira and S. Rodrigues, *Produção de Celulase por Aspergillus phoenicis URM 4924 utilizando a casca do coco verde (Cocos nicifera L.) como substrato.* IX ENPPG, IX ENICIT, III SIMPIT, Ceará, 2009.
[58]. R.L.A. De Souza, L.S.C. Oliveira, F.L.H. Silva and B.C. Amorim, Caracterização da poligalacturonase produzida por fermentação semi-sólida utilizando-se resíduo do maracujá como substrato. *Revista Brasileira de Engenharia Agrícola e Ambiental* 14 (2010), pp.987–992.

International Journal of Modern Engineering Research (IJMER)
www.ijmer.com Vol. 3, Issue. 4, Jul. - Aug. 2013 pp-2382-2388 ISSN: 2249-6645

Heavy Metals in Irrigated Crops along Tatsawarki River in Kano, Nigeria

[1]Bichi, M. H., [2]Bello, U. F.
[1,2]*Department of Civil Engineering, Bayero University, Kano-Nigeria*

***ABSTRACT*:** *Surface and ground irrigation water samples were collected from the three different farmlands along the Tatsawarki River. Control surface and ground water samples were collected from farmlands located away from away from the river. Samples of three crops (tomatoes, onions, and pepper) were collected from the three irrigated farmlands along the river banks. Each of the three crops was collected from each of the farmlands irrigated with surface water as well as from each of the farmlands irrigated with ground water. Sample crops were also collected from control farmland irrigated with fresh water. The analyses of heavy metals (Cr, Cu, Cd, Zn, Co, Fe, Pb, and Mn) concentrations were carried out with an Atomic Absorption Spectrophotometer (AAS). The concentrations of the heavy metals in irrigation water was found to be higher than the FAO guideline values with the exception of Fe and Pb which were found to be below the FAO guideline values. All irrigation water samples were also found to have higher metals level in comparison with the levels found in control sample with the exception of Pb. The crops irrigated with the polluted irrigation water were found to be unfit for human consumption. The high concentration of these heavy metals in the irrigated crops was directly attributed to the metals in the irrigation water as the control crops sample shows low or no heavy metals concentration. It is recommended that the source of food and vegetables consumed in the area should be checked so as to avoid food and vegetables irrigated with polluted water. The consumers should also eat foods that are rich in antioxidants like selenium, vitamin C, E, and beta carotene, since they depend against heavy metals in the food chain. The farmers should also be made aware of the dangers involved and encourage them to grow crops that are less susceptible to heavy metals uptake.*

KEYWORDS: *Heavy Metals, Industrial Pollution, Irrigated Crops, Kano*.

I. INTRODUCTION

The increasing industrial manufacturing at large scale is now being parallel with a corresponding challenge of waste management and disposal even in developing countries. Thus the hitherto clean, fresh and safe ecological setting is today exposed to the hazard of environmental pollution which has a potential of deleterious effect to both plants and animals. An irrigation activity that is gradually gaining recognition is the one being practiced under the urban and peri-urban agriculture (UPA). The system involves the use of stream water to irrigate lands at the banks with the objective of producing fruits and vegetables for the consumption of city dwellers [1]. The heavy metals pollution of Rivers affects on the irrigation water quality along the river, as well as crops irrigated with it. The irrigated crops may take-up these heavy metals and consequently, introduce them into food chain, resulting to gradual accumulation in the humans, and thereafter, present health hazard.

Studies ([2], [3]) have shown that intake of trace metals from dietary sources may represent a significant exposure pathway for human populations. However, dietary exposure to trace metals is highly variable. For example, [4] has observed that for Cd, the principal exposure route for the general population is through uptake by food plants. Where metal concentrations in crops exceed the limits, it may be possible to use this produce in animal feeds in order to minimize the effect upon the human diet. However, animals fed on a metal-enriched diet may have elevated concentrations of these metals in their tissues and milk. Reference [3] has noted that regular consumption of metal-enriched animal products may lead to adverse health effects in humans. Furthermore, [5] have observed that the greatest degree of metal accumulation occurs in offal, such as livers and kidneys.

In vegetables, contaminants as well as micronutrients generally accumulate in the outer skin layer (peel). Reference [6], for example, found that total As and Cu in carrot peel was approximately 2 times and 2.5 times respectively greater than in the core of the carrot. Higher Cd concentrations were also found in potato peel than in the potato tuber [7]. Other findings in India [8] have shown that Cd, Pb and Zn levels in important vegetables like spinach, beet, cauliflower and radish regularly exceed acceptable limits set by the Government of India posing food safety threat to urban consumers using products for home consumption.

Reference [9] presented an overview of knowledge on heavy metal phytotoxicity to plants in Australian environment. From the overview, it became evident that metal concentrations at which plants showed phytotoxicity were dependent on a number of factors that included soil type, plant type, soil properties and the bioavailable metal concentrations. Different soils may have the same total metal concentrations but remarkably different effect on plant metal uptake and potential for metal phytotoxicity. This suggested that total metal concentration may not be appropriate and sensitive indicator for phytotoxicity.

Reference [10] investigated alfalfa plants grown in soil at different growth stages using separate batches of Cr (VI) at 100 mg/L, and Cd(II), Cu(II), Ni(II), or Zn(II) at 500mg/L. Four days after germination, all metals, except Zn (II), had lethal effects on the seedlings. When applied 16 days after germination, Cr(VI) and Ni(II) still had lethal effects on the seedlings and Cd(II) and Cu(II) destroyed more than 50% of the plant population. While approximately 90% of the plants exposed to Cd(II), Cu(II) and Zn(II) were able to grow without apparent negative effects 20 days after germination, Cr (VI)

and Ni(II) still showed lethal effects. These results demonstrated that the tolerance of alfalfa plants to Cd, Cu and Zn was positively correlated with the age of the plants. Thus, alfalfa seedlings tolerated Zn(II) at 500 mg/l at the growth stage of 4 days after germination. Alfalfa plant could be considered potentially feasible to be transplanted in uncontaminated soils where the concentrations of Cd, Cu or Zn are high enough to interfere with alfalfa seed germination.

Reference [11] concluded that heavy metals are largely transported apoplastically in plant tissue. To be able to reach the xylem vessels of the roots, the metals have to cross the endodermis and the suberinized casparian strips. Consequently, most of the metal uptake is performed by the younger parts of the roots where the casparian strips are not yet fully developed. Studies ([12], [13]) have also shown that the translocation of metals to the shoot is performed in the xylem and is promoted by transpiration of water via leaves. A young plant, however, has a small ratio of shoot-to-root mass and in such plants the root pressure determines the translocation of xylem sap to the shoot. Translocation is also promoted for some metal ions by cation exchange at the negative charges of the xylem vessel walls.

Reference [8] have studied the soil to plant transfer of some heavy metals (arsenic, copper, lead, thallium and zinc) by vegetables bean (phaseolus vulgaris L. and dwarf bean), kohlrabi (Brassica oleracea var. gongylodes L.), mangold (Beta vulgaris var. macrorhiza), lettuce (Lactuca sativa L. 'American gathering brown'), carrot (Daucus carota L.'Rotin', Sperlings's), and celery [Apium graveiolus var. dulce (Mill.) Pers.] from a control soil (Ap horizon of an Entisol) and from a contaminated soil (1:1 soil-slag mixtures). The transfer coefficients for plant uptake of As, Cu, Pb, and Zn from soils contaminated by two slags were considerably smaller compared with an uncontaminated soil. The results revealed that for a given type of slag and a given metal, not only the concentration ratios, but also the relative availability of a metal in the slag for plant uptake with respect to its uptake from a control soil depended strongly on the plant species. Thallium from both types of slags was more available for plant uptake by kohlrabi, carrots, and celery than soil-borne TI. For several vegetables, however, the availability for root uptake from slag with respect to the control soil was reduced by the same factor. The results thus demonstrated that the factor by which the metal uptake of a plant from slag is decreased (or increased) with respect to an uncontaminated soil could be plant specific, suggesting that some plants are able to mobilize the metals in the slag to a higher extent. Thus, plant-specific effects for metal mobilization might therefore be a cause for a moderate success of estimation in the laboratory for the availability of a metal for plant uptake from solid contaminant by leaching tests with extractants.

In this study, the transfer of heavy metals in to crops that are irrigated with the effluent polluted waters along River Tatsawarki in Kano, Nigeria was examined. The level of heavy metals in crops irrigated along the river bank was determined and compared with the level of heavy metals obtained in the control crops irrigated away from the river bank. The results were also compared with the standards acceptable limits set by the Food and Agricultural Organization (FAO). The research was conducted in the dry season, as it represents the worst condition, when the river bears low flow with high concentration of pollutants.

II. MATERIALS AND METHODS

II.1 Project Area and Sampling Locations

The project area lies in the Southern part of Kano within the Kano River basin. The river basin drains the southern part of Kano metropolis, including two of the largest industrial estates of Challawa and Sharada which also discharges mostly untreated effluents within the basin. Rivers Tatsawarki collects the entire domestic and industrial wastes from the southern part of the metropolis and discharges into the Challawa River, just before its confluence point with the Kano River [14]. The basin, besides being the main source of water for metropolitan Kano, is also extensively being used for irrigation of vegetable crops.

Three irrigation areas were selected at Magami village (M-Upstream); Gidan Kwanso village (G- Midstream) just before the confluence with the effluent channel from the nearby Tamburawa Water Works; and Tsafe (T-Downstream) just before the discharge point in to River Challawa (Figure 1). The control farmland was located at Kwarin Matage village, away from the river bank and uses fresh surface and ground waters.

II.2 Surface and Ground Water Sampling

Surface water samples were collected from the three different points along the River. Sample S1: at the beginning of the project area; Sample S2: before its confluence with the waste water channel from Tamburawa water works, and Sample S3: before its confluence with River Challawa (Fig. 1). Ground water samples were also collected from farmlands located in the three areas (G1, G2, and G3). Control surface and ground water samples were collected from farmlands located away from away from the river.

Sample collection was done as described by the Department of waters affairs and forestry Pretoria (SA) [15]. The sample label, zone and time and date of collection, place of collection and pH were recorded at the site of collection. Two litres (2L) polyethylene bottles, after being thoroughly washed with detergent, rinsed with water and then distilled water and then soaked in 5% HNO_3 for 24 hours were used for collection of the water samples. The samples are preserved using 1-2 ml of concentrated HNO_3 in order to get a required pH of 2.2 to 2.8. The samples were refrigerated in order to stabilize the metal before analyzing.

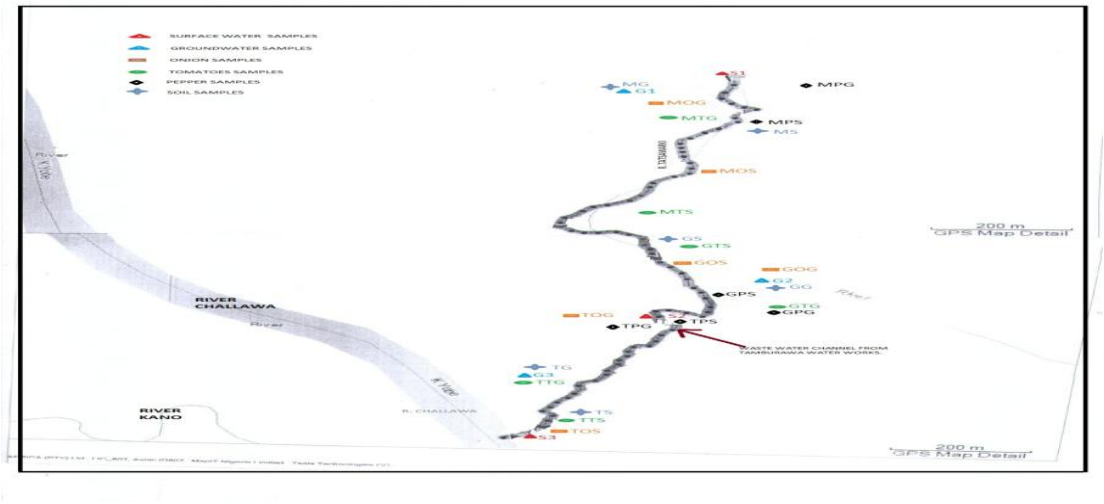

Figure 1: Location of Sampling Points

II.3 Sampling of Vegetable Crops

Three crops (tomatoes, onions, and pepper) that are normally irrigated along the river bank were selected. The sample crops were collected from the three irrigated farmlands along the river banks (Figure 1). Each of the three crops was collected from each of the farmlands irrigated with surface water (TMS, TGS, and TTS for Tomatoes; OMS, OGS, and OTS for Onions; PMS, PGS, and PTS for Pepper); as well as from each of the farmlands irrigated with ground water (TMG, TGG, and TTG for Tomatoes; OMG, OGG, and OTG for Onions; PMG, PGG, and PTG for Pepper). Sample crops were also collected from control farmland irrigated with fresh water. The sampling was done using the procedure described by the Department of waters affairs and forestry Pretoria (SA) [15].

II.4 Analysis of Heavy Metals

2.4.1 Pre-treatment of Samples for Analysis of Metals in Water Samples: The open-beaker digestion (OBD) method was employed using HNO_3 as described in [16] for the chemical analysis of water samples. 50ml of the water samples was measured into a beaker and 10ml HNO_3 was added. The beaker and the content were placed on a hot plate and digested until the brown fumes of HNO_3 escaped. The heating continued until the content reduced to 10ml; the content was then washed into a 50ml volumetric flask and made up to the mark. The digest obtained was subjected to determination of the metals.

2.4.2 Pre-treatment of Samples for Analysis of Metals in Vegetable Samples: The plant samples were thoroughly washed, rinsed with tap water and then with double-distilled water to remove any attached soil particles. It was then cut into small portions and placed in a large crucible where they were oven dried at 60˚C overnight. The dried plant was then grounded into fine particles using a clean mortar and pestle.

The triacid method of digestion was employed. The acids that were used are Nitric acid (HNO_3), Perchloric acid ($HClO_4$) and concentrated sulphuric acid (H_2SO_4) in the ratio of 65:8:2 respectively. 0.2g of the powdered crop sample was weighed into a 100ml glass beaker. 30ml of the acid mix was added and the content swirled and placed on a hot plate. The beaker was heated until the brown fumes of the nitric acid went off; and the heating continued till the content of the beaker reduced to about 5ml. The content was then allowed to cool and a little amount of distilled water added and the beaker swirled again. The content was then poured into 50ml volumetric flask and made up to the required mark. The digest obtained was used for the determination of the metals.

2.4.3 Determination of Heavy Metals: The measurement of heavy metal concentrations were carried out with an Atomic Absorption Spectrophotometer (AAS). All concentrations were determined using the absorbance made with air-acetylene flame. Eight working solutions were prepared from the stock solutions for each of the metals (Cr, Cu, Cd, Zn, Co, Fe, Pb, and Mn) by successive serial dilution and each of the standard solutions was then aspirated into the flame of AAS and the absorbance recorded in each case. A plot of the concentration against the corresponding absorbance gives the calibration curve of each metals. The samples were aspirated into the flame and the absorbance obtained. The values were then extrapolated from the calibration plot to obtain the corresponding concentration.

III. RESULTS AND DISCUSSIONS

The results of the analysis of heavy metal concentration in irrigation waters are presented in Table 1, together with the limiting FAO values [17]. The concentrations of heavy metals in the irrigated crops are presented in Tables 2, 3, and 4 for tomatoes, onions, and pepper respectively. The results are discussed according to each of the heavy metals analyzed.

Table 1: Concentrations of Heavy Metals in Surface and Ground Waters used for Irrigation

S/No	Parameters	FAO [17] Guideline for irrigation water	Surface Water					Ground Water				
			Control Sample	S1	S2	S3	Aver-age	Control Sample	G1	G2	G3	Aver-age
1	Chromium (mg/l)	0.1	0.8	8.8	8.5	9.1	8.8	0.8	4.0	4.0	2.0	3.3
2	Copper (mg/l)	0.2	1.2	4.7	4.7	5.3	4.9	1.2	1.3	1.3	2.7	1.8
3	Cadmium (mg/l)	0.01	4.1	17.0	12.2	12.0	13.7	4.1	9.0	8.0	15.0	10.7
4	Zinc (mg/l)	2.0	2.0	11.4	10.3	9.6	10.4	2.0	5.0	5.5	6.8	5.8
5	Cobalt (mg/l)	0.05	0.5	1.9	1.8	1.9	1.9	0.5	1.0	1.0	0.8	0.9
6	Iron (mg/l)	5.0	1.0	0.7	0.9	1.5	1.0	1.0	2.0	1.0	1.5	1.5
7	Lead (mg/l)	5.0	1.9	1.4	1.1	1.4	1.3	1.9	1.4	1.0	1.9	1.4
8	Manganese (mg/l)	0.2	0.9	2.5	3.2	3.5	3.1	0.9	5.0	2.5	3.0	3.5

S1 – Samples collected at point A (upstream)
S2 – Samples collected at point B (midstream)
S3 – Samples collected at point C (downstream)
G1 – Samples collected at Magami Irrigated farmlands
G2 – Samples collected at Gidan-kwanso irrigated farmlands
G3 – Samples collected at Tsafe irrigated farmlands

Table2: Concentrations of Heavy Metals in Tomatoes

SN		PARAMETERS (ppm)							
		Pb	Cr	Cd	Fe	Mn	Co	Zn	Cu
	Control Tomato	**1.3**	**0.4**	**0.4**	**1.2**	**0.9**	**0.0**	**2.3**	**1.6**
1	Sample TMS	1.0	3.6	2.0	1.3	1.5	0.8	7.6	3.0
2	Sample TGS	0.9	1.8	1.4	1.2	2.5	0.8	5.0	3.3
3	Sample TTS	1.1	3.6	1.6	1.3	2.0	0.8	9.0	4.8
	Average	**1.0**	**3.0**	**1.7**	**1.3**	**2.0**	**0.8**	**7.2**	**3.7**
1	Sample TMG	1.4	2.0	1.0	1.5	2.0	0.7	5.6	2.0
2	Sample TGG	0.5	2.2	1.2	1.7	2.8	0.8	6.8	2.1
3	Sample TTG	1.0	2.0	0.5	1.6	3.0	0.4	7.6	2.3
	Average	**1.0**	**2.1**	**0.9**	**1.6**	**2.6**	**0.6**	**6.7**	**2.1**

TMS – Tomato crop – Magami – Surface water irrigated
TGS – Tomato crop – G/kwanso – Surface water irrigated
TTS – Tomato crop – Tsafe – Surface water irrigated
TMG – Tomato crop – Magami – Groundwater irrigated
TGG – Tomato crop – G/kwanso – Groundwater irrigated
TTG – Tomato crop – Tsafe – Groundwater irrigated

Table 3: Concentrations of Heavy Metals in Onions

SN		PARAMETERS (ppm)							
		Pb	Cr	Cd	Fe	Mn	Co	Zn	Cu
	Control Onion	**1.6**	**0.3**	**0.2**	**1.0**	**1.2**	**0.2**	**3.3**	**1.2**
1	Sample OMS	1.0	2.0	2.0	1.0	2.5	1.0	9.1	3.1
2	Sample OGS	1.2	2.0	0.9	1.0	1.2	0.6	7.0	2.7
3	Sample OTS	1.4	1.8	0.0	0.9	3.5	0.7	7.0	2.9
	Average	**1.2**	**1.9**	**1.0**	**1.0**	**2.4**	**0.8**	**7.7**	**2.9**
1	Sample OMG	1.0	1.8	2.0	1.5	5.0	0.4	5.5	2.0
2	Sample OGG	2.4	2.0	1.0	1.5	3.2	0.4	7.0	1.9
3	Sample OTG	0.5	1.4	0.0	1.5	3.1	0.4	9.2	2.2
	Average	**1.3**	**1.7**	**1.0**	**1.5**	**3.8**	**0.4**	**7.2**	**2.0**

OMS – Onion crop – Magami – Surface water irrigated
OGS – Onion crop – G/kwanso – Surface water irrigated
OTS – Onion crop – Tsafe – Surface water irrigated
OMG – Onion crop – Magami – Groundwater irrigated
OGG – Onion crop – G/kwanso – Groundwater irrigated
OTG – Onion crop – Tsafe – Groundwater irrigated

Table 4: Concentrations of Heavy Metals in Pepper

SN		PARAMETERS (ppm)

		Pb	Cr	Cd	Fe	Mn	Co	Zn	Cu
	Control Pepper	**1.1**	**0.1**	**0.0**	**0.7**	**0.9**	**0.0**	**2.3**	**1.2**
1	Sample PMS	1.0	4.5	0.3	1.5	2.1	1.0	6.0	4.3
2	Sample PGS	0.8	2.3	0.1	1.5	1.2	0.8	6.2	1.8
3	Sample PTS	1.1	2.2	0.2	1.0	1.8	0.9	5.2	2.0
	Average	**1.0**	**3.0**	**0.2**	**1.2**	**1.7**	**0.9**	**5.8**	**2.7**
1	Sample PMG	1.0	2.0	0.0	2.0	2.5	0.8	6.0	1.6
2	Sample PGG	1.0	2.0	0.0	1.4	5.0	0.9	5.8	1.3
3	Sample PTG	1.2	3.6	0.0	1.4	5.5	0.8	7.1	1.9
	Average	**1.0**	**2.5**	**0.0**	**1.6**	**3.3**	**0.8**	**6.3**	**1.8**

PMS – Pepper crop – Magami – Surface water irrigated
PGS – Pepper crop – G/kwanso – Surface water irrigated
PTS – Pepper crop – Tsafe – Surface water irrigated
PMG – Pepper crop – Magami – Groundwater irrigated
PGG – Pepper crop – G/kwanso – Groundwater irrigated
PTG – Pepper crop – Tsafe – Groundwater irrigated

III.1 Chromium, Cr

The concentration of chromium in the crops irrigated along river Tatsawarki was in the range of 1.8ppm – 4.5ppm, with pepper exhibiting a highest average concentration of 3.0ppm for surface water irrigated pepper and an average concentration value of 2.5ppm by that irrigated with groundwater, while the control pepper crop exhibit chromium concentration of 0.1ppm (Table 4). The concentration of chromium in tomatoes was 3.0ppm on average by surface water irrigated tomatoes and 2.1ppm on average by that irrigated with ground water, while the control tomato crop shows a concentration value of 0.4ppm (Table 2). The chromium concentration in onions irrigated with surface water shows 1.9ppm on average and an average concentration of 1.7ppm for groundwater irrigated onions, while the control onion crop exhibits a concentration of 0.3ppm (Table 3). All the crops show higher chromium contents than the FAO limiting values.

III.2 Copper, Cu

The concentration of the metal copper in the crops samples was in the range of 1.2ppm – 4.8ppm, with tomatoes exhibiting a higher average concentration of 3.7ppm for surface water irrigated tomato and 2.1ppm average for groundwater irrigated tomatoes, while the control tomatoes exhibits a copper concentration of 1.6ppm (Table 2). The concentration of copper in onions irrigated along river Tatsawarki exhibits an average concentration of 2.9ppm for onions irrigated with surface water and 2.0ppm for that irrigated with groundwater, while the control onion was found to have a concentration of 1.2ppm (Table 3). The concentration of copper in pepper samples were found to be 2.7ppm on average for pepper irrigated with surface water and 1.8ppm for pepper irrigated with groundwater, while the control pepper crop shows a concentration value of 1.2ppm (Table 4). The copper concentration in all the crops exceeded the FAO limiting concentrations.

III.3 Iron, Fe

The concentration of iron obtained in the crops irrigated in the research area was in the range of 0.9ppm – 2.0ppm. The concentration of iron was higher in tomatoes which exhibit an average concentration of 1.6ppm by tomatoes irrigated with groundwater and 1.3ppm by that irrigated with surface water, while the control tomato crop exhibits a concentration of 1.2ppm (Table 2). The concentration of iron in pepper was higher than the concentration obtained in onions, as the concentration was found to be 1.6ppm on average for pepper irrigated with groundwater and an average concentration of 1.2ppm for that irrigated with surface water, while the control pepper exhibit a concentration value of 1.0ppm (Table 4). The concentration of iron in the onion crops shows slightly lower value than the value obtained in pepper crops as the concentration was found to be 1.5ppm on average for ground water irrigated onions and an average concentration of 1.0ppm for onions irrigated with surface water, while the concentration of iron in the control sample was 1.0ppm (Table 3). The higher concentration of iron in the crops irrigated with groundwater can be attributed to the higher concentration of iron exhibited by the groundwater more than the surface water (Table 1). All the crops contain lower iron concentrations than the minimum limiting concentrations set by the FAO.

III.4 Manganese, Mn

The concentration of manganese in the crops irrigated in the three irrigated farmlands was found to be in the range of 1.2ppm – 5.5ppm. Onions exhibits the highest concentration of manganese with an average value of 3.8ppm on onions irrigated with groundwater and 2.4ppm on that irrigated with surface water, while the control onion exhibits a concentration of 1.2ppm (Table 3). The manganese concentration in pepper shows a higher value than that observed in tomatoes with an average concentration of 3.3ppm on pepper irrigated with groundwater and 1.7ppm average on that irrigated with surface water, while the concentration of 0.9ppm was observed in the control pepper (Table 4). The average concentration of manganese in tomatoes was found to be 2.6ppm on crops irrigated with groundwater and 2.0ppm on crops irrigated with surface water, while the control tomatoes exhibits a concentration of 0.9ppm. The higher concentration of manganese in the crops irrigated with groundwater can also be attributed to the higher concentration of manganese exhibited by the

groundwater more than the surface water (Table 1). The manganese concentrations in all the crops exceeded the FAO limiting values.

III.5 Led, Pb

The concentration of lead in the crops samples in the research area was within the range of 0.5ppm – 2.4ppm. The concentration of the metal in onions was found to be higher than the other vegetables and was found to be 1.3ppm average in crops irrigated with groundwater and 1.2ppm average in that irrigated with surface water, while the control onions exhibit a concentration value of 1.6ppm, higher than the average value obtained in the test samples (Table 3). The concentration of lead obtained in tomatoes was lower than the value obtained in onions and slightly higher than the value obtained in pepper with an average lead concentration of 1.0ppm for both surface and groundwater irrigated crop samples, while the control exhibit a higher lead concentration of 1.3ppm (tables 2 and 3). The concentration of the metal in pepper was of the value 1.0ppm on average for pepper irrigated with surface water and an average value of 0.8ppm in pepper irrigated with groundwater, while the control sample shows a concentration value of 1.1ppm (Table 4). The high lead concentration observed in all control samples can be directly related to the high lead content observed in the control irrigation water as well as high lead concentration in the soil on which the control samples were grown. The lead concentrations in all the samples indicated lower values than the FAO limiting values.

III.6 Zinc, Zn

The concentration of the metal zinc in the crops samples were found to be in the range of 5.0ppm – 9.1ppm, with onions exhibiting a higher average concentration of 7.7ppm for surface water irrigated onions and 7.2ppm average for groundwater irrigated onions, while the control onions exhibits a zinc concentration of 3.3ppm (Table 3). The concentration of Zinc in tomatoes irrigated along river Tatsawarki exhibits an average concentration of 7.2ppm for tomatoes irrigated with surface water and 6.7ppm for that irrigated with groundwater, while the control tomatoes was found to have a zinc concentration of 2.3ppm (Table 2). The concentration of copper in pepper samples was 5.8ppm on average for pepper irrigated with surface water and 6.3ppm for pepper irrigated with groundwater (Table 4), while the control pepper crop was having a concentration value of 2.3ppm. All the crop samples indicated higher Zinc concentrations than the FAO limiting values.

III.7 Cobalt, Co

The concentration of cobalt in the crops irrigated along river Tatsawarki was in the range of 0.4ppm – 1.0ppm, with pepper exhibiting a slightly higher average concentration of 0.9ppm for surface water irrigated pepper than the average concentration value of 0.8ppm shown by that irrigated with groundwater, while in the control pepper crops no cobalt was found (Table 4). The concentration of cobalt in tomatoes was found to be 0.8ppm on average by surface water irrigated tomatoes and 0.6ppm on average by that irrigated with groundwater, while the control tomato crop was found to have no cobalt in it (Table 2). The cobalt concentration in onions irrigated with surface water was 0.8ppm on average and an average concentration of 0.4ppm for groundwater irrigated onions, while the control onion crop exhibits a concentration of 0.2ppm (Table 3). All the experimental samples indicated higher Cobalt concentrations than the limiting values set by FAO.

III.8 Cadmium, Cd

The concentration of cadmium in the crops irrigated along river Tatsawarki was in the range of 0.0ppm – 2.0ppm, with tomatoes exhibiting a higher average concentration of 1.7ppm for surface water irrigated tomatoes and an average concentration value of 0.9ppm by that irrigated with groundwater, while the control tomatoes crop exhibit cadmium concentration of 0.4ppm (Table 2). The concentration of cadmium in onions was found to be 1.0ppm on average by both surface and groundwater irrigated onions, while the control onion crop was found to have a cadmium concentration value of 0.2ppm (Table 3). The cadmium concentration in pepper irrigated with surface water shows 0.2ppm on average while the groundwater irrigated pepper and the control pepper were found to have no cadmium in them (Table 4). The ground and surface water samples indicated higher Cadmium contents than the FAO limiting values. Higher values were also observed in all the onion and tomato samples as well as pepper samples irrigated with surface water. Only the pepper samples irrigated with the ground water and the control pepper samples show no cadmium contents.

IV. CONCLUSION

The concentrations of the heavy metals in irrigation water was found to be higher than the FAO guideline values with the exception of Fe and Pb which were found to be below the FAO guideline values. This is thus unfit for irrigation. All irrigation water samples were also found to have higher metals level in comparison with the levels obtained in control sample with the exception of Pb. The crops irrigated with the polluted irrigation water were found to be unfit for human consumption as they contain some of these metals in high concentrations. The high concentration of these heavy metals obtained in the irrigated crops is directly attributed to the metals in the irrigation water as the control crops sample shows low or no heavy metals concentration.

As an interim measure, the source of food and vegetables in the affected communities should be regularly checked so as to avoid food and vegetables irrigated with polluted water since the linkage between crops heavy metals content and heavy metals in irrigation water has been established. The communities should also eat foods that are rich in antioxidants like selenium, vitamin C, E, and beta carotene, since they depend against heavy metals as these food crops may end up in the

food chain. Awareness should be created among the farmers about the dangers involved and they should be encouraged to grow crops that are less susceptible to heavy metals uptake. The authorities and other stakeholders should device means of and methods to clean the irrigation soils and water off the heavy metals, and the discharges of untreated effluents in to the river system controlled.

REFERENCES

[1]. Binns, J.A. Maconachie, R.A. Tanko, A.I., Water, land and health in urban and peri-urban food production: The case of Kano, Nigeria, 2003. www.cityfarmer.org/WaterLandHealthKano
[2]. Baes III CF Sharp RD Sjoreen AL & Shor RW., Review and analysis of parameters for assessing transport of environmentally released radionuclides through agriculture, US Department of Commerce, National Technical Information Service, Virginia, 1984.
[3]. Reilly, C., Metal contamination of food. (Second edition. Elsevier Applied Science London and New York, 1991).
[4]. Lopez-Artiguez, M. Soria, M. L. Camean, A. & Repetto, M., 'Cadmium in the diet of the local population of Seville (Spain)', Bulletin of Environmental Contamination and Toxicology 50, p417-424, 1993.
[5]. Beresford, N. A. Mayes, R. W. Crout, N. M. J. Maceachern, P. J. Dodd, B. A. Bernett, C. L. & Lamb, C. S., 'Transfer of cadmium and mercury to sheep tissues', Environmental Science and Technology 33, 2395-2402, 1999.
[6]. Helgesen, H. & Larsen, E. H., 'Bioavailability and speciation of arsenic in carrots grown in contaminated soil', Analyst, 123(5): 791–6, 1998.
[7]. McLaughlin, M J. Williams, C M J. McKay, A. Kirkham, R. Gunton, J. Jackson, K J., 'Effect of cultivar on uptake of cadmium by potato tubers', Aust J Ag Res; 45:1483–95, 1994.
[8]. Bunzl, K. Trautmannsheimer, M. Schramel, P. and Reifenhauser, W., 'Availability of Arsenic, Copper, Lead, Thallium, and Zinc to Various Vegetables Grown in Slag-Contaminated Soils', Journal of Environmental Quality. 30: 934-939, 2001.
[9]. Naidu, R. Smith, E. Owens, G. Bhattacharya, P. Nadebaum, P., Managing arsenic in the environment: from soil to human health. Melbourne: CSIRO Publishing. pp565, 2003.
[10]. Peralta-Videa, J.R., De la Rosa, G., Gonzalez, J. H and Gardea-Torresdey, T. (2004): Effects of the growth stage on the heavy metal tolerance of alfalfa plants. Advances in Environmental Research, (8): 679-685.
[11]. Marschner, H (1995): Mineral nutrition of higher plants. (2nd edition. London, Academic Press. 889p., 1995)
[12]. Van de Geijn, S.C and Petit, C.M (1979): Transport of divalent cations: cation exchange capacity of intact xylem vessels. *Plant Physiology*, 64: 954-958., 1979.
[13]. Wolterbeek, H.T, 'Cation exchange in isolated xylem cell walls of tomato. I, Cd and Rb exchange in adsorption experiments', Plant, Cell Environ. 10: 30–44, 1987.
[14]. Bichi, M. H. , "Surface Water Quality in the Kano Industrial Environment" in Falola, J. A.; Ahmed, K; Liman, M. A.; and Malwada, A (eds), "*Issues in Land Administration and Development in Northern Nigeria*", Department of Geography, Bayero University, Kano. pp 305-313, 2000.
[15]. DWAF, Standard procedures for sample collection and preservation by the Department of waters affairs and forestry Pretoria South Africa, 1992.
[16]. Dike, N I; Ezealor, A U; Oniye, S J., 'Concentration of Pb, Cu, Fe, and Cd during the dry season in river Jakara, Kano Nigeria', Chem Class Journal, 1:78-81, 2004.
[17]. FAO, Food and Agriculture Organisation of the United Nations, Wastewater treatment and use in agriculture – FAO irrigation and drainage paper 47, 1992. http://www.fao.org/docrep/T0551E/t0551e0c.htm

International Journal of Modern Engineering Research (IJMER)
www.ijmer.com Vol. 3, Issue. 4, Jul. - Aug. 2013 pp-2389-2395 ISSN: 2249-6645

Utilization of DVR with FLC to Inject Voltage in a Transmission Line

R. Udaya Sree[1], T. Vijay Kumar[2]
[1](M.Tech Student, S.K.T.R.M College of Engineering, Kondair-509125, Mahabubnagar, Andhra Pradesh)
[2] (EEE Department, S.K.T.R.M College of Engineering, Kondair-509125, Mahabubnagar, Andhra Pradesh)

ABSTRACT: *In this paper a Dynamic Voltage Restorer (DVR) is used for power quality improvement on transmission side for the voltage regulation, grid stabilization and efficient utilization. The DVR normally installed between the source voltage and critical or sensitive load. The vital role of DVR depends on the efficiency of the control technique involved in switching circuit of the inverter. The DVR is controlled by using PI with fuzzy logic controller. The Fuzzy logic controller based on fuzzy logic provides a means of converting a linguistic control strategy based on expert knowledge into automatic control strategy. This paper presents a Digital validation conducted for different cases of fault conditions using the Mat lab/Simulink/Sim-Power software environment with the Dynamic Voltage Restorer scheme with fuzzy controller for effective voltage compensation, in rush current conditions and transmission line loss reduction.*

KEYWORDS**:** *Dynamic Voltage stabilization, PI with fuzzy controller, Phase detection, voltage source converter, voltage sag.*

I. INTRODUCTION

The various power quality problems are due to the increasing use of non linear and power electronic loads. Harmonics and voltage distortion occur due to these loads. The power quality problems can cause malfunctioning of Sensitive equipments, protection and relay system [1]. These problems include a variety of electrical disturbances, which may originate in several ways and have different effects on various kinds of sensitive loads. As a result of this vulnerability, increasing numbers of industrial and commercial facilities are trying to protect themselves by investing in more sophisticate equipment to improve power quality [2]. Voltage magnitude is one of the major factors that determine the quality of power supply. Loads at distribution level are usually subject to frequent voltage sags due to various reasons. Voltage sags are highly undesirable for some sensitive loads, especially in high-tech industries. It is a challenging task to correct the voltage sag so that the desired load voltage magnitude can be maintained during the voltage disturbances. The effect of voltage sag can be very expensive for the customer because it may lead to production downtime and damage. Voltage sag can be mitigated by voltage and power injections into the distribution system using power electronics based devices, which are also known as custom power device. Different approaches have been proposed to limit the cost causes by voltage sag. One approach to address the voltage sag problem is dynamic voltage restorer (DVR). It can be used to correct the voltage sag at distribution level [3].

Distribution system is mainly affected by voltage sag and Swell power quality issue. Short circuits, lightning strokes, faults and inrush currents are the causes of voltage sags. Start/stop of heavy loads, badly dimensioned power sources, badly regulated transformers, single line to ground fault on the system lead to voltage swells. Voltage sag is a decrease of the normal voltage level between 10 and 90% of the nominal rms voltage at the power frequency, for durations of 0.5 cycle to 1 minute. Voltage swells are momentary increase of the voltage, at the power frequency, outside the normal tolerances, with duration of more than one cycle and typically less than a few seconds [4]. The Dynamic Voltage Restorer (DVR) are now becoming more established in industry to mitigate the impact of voltage disturbances on sensitive loads [5].The Dynamic Voltage Restorer (DVR) is a device that detects the sag or swell and connects a voltage source in series with the supply voltage in such a way that the load voltage is kept inside the established tolerance limits [6].Other than voltage sags and swells compensation, DVR also has added other features like: line voltage harmonics compensation, reduction of transients in voltage and fault current limitations.

This paper explores design and analysis of a novel Dynamic Voltage Restorer along with fuzzy controller (mamdani rule base) for efficient stabilization and utilization. Fuzzy inference systems have been successfully applied in fields such as automatic control, data classification, decision analysis, expert systems, and computer vision [7], [8]. Because of its multidisciplinary nature, fuzzy inference systems are associated with a number of names, such as fuzzy-rule-based systems, fuzzy expert systems, and fuzzy logic controllers [9]. The Mamdani rule base is a crisp model of a system, i.e. it takes crisp inputs and produces crisp outputs. It does this with the use of user-defined fuzzy rules on user-defined fuzzy variables. The idea behind using a Mamdani rule base to model crisp system behavior is that the rules for many Systems can be easily described by humans in terms of fuzzy variables. Thus we can effectively model a complex non-linear system, with common-sense rules on fuzzy variables [10], [11]. The proposed scheme proved success in improving the power quality, enhancing power factor, reduce transmission losses and limit transient over voltage and inrush current conditions. The paper is organized in seven sections. Section II deals with the Dynamic Voltage Restorer. Section III Proposed DVR with fuzzy controller with mat lab models. Section IV presents the Digital simulation results when different faults occur, Section VI concludes the work.

II. DYNAMIC VOLTAGE RESTORER

A DVR is a solid state based power electronics switching device consisting of either MOSFET or IGBT, a capacitor bank as an energy storage device and injection transformers. It is linked in series between a distribution system and a load that shown in Figure.1. The basic idea of the DVR is to inject a controlled voltage generated by a forced commuted converter in a series to the bus voltage by means of an injecting transformer.

A DC to AC inverter regulates this voltage by sinusoidal PWM technique. All through normal operating condition, the DVR injects only a small voltage to compensate for the voltage drop of the injection transformer and device losses. However, when voltage sag occurs in the distribution system, the DVR control system calculates and synthesizes the voltage required to preserve output voltage to the load by injecting a controlled voltage with a certain magnitude and phase angle into the distribution system to the critical load [12].

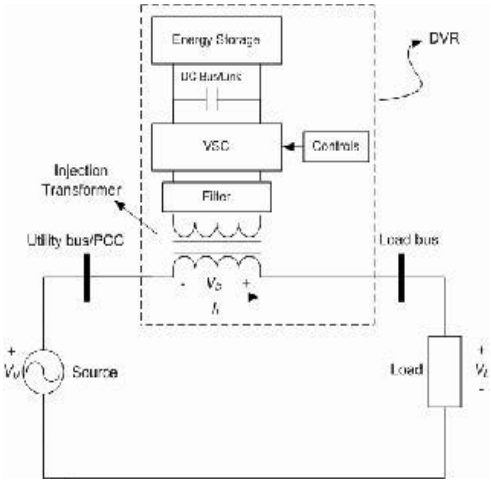

Fig. 1: DYNAMIC VOLTAGE RESTORER

III. PROPOSED DVR WITH FUZZY CONTROLLER WITH MAT LAB MODELS

Discrete PI Controller shown in Fig.2 is a feedback controller which drives the plant to be controlled with a weighted sum of the error and the integral of that value. The proportional response can be adjusted by multiplying the error by constant K_P, called proportional gain. The contribution from integral term is proportional to both the magnitude of error and duration of error. The error is first multiplied by the integral gain, K_i and then was integrated to give an accumulated offset that have been corrected previously.[13]

A. Proportional-Integral (PI) Controller

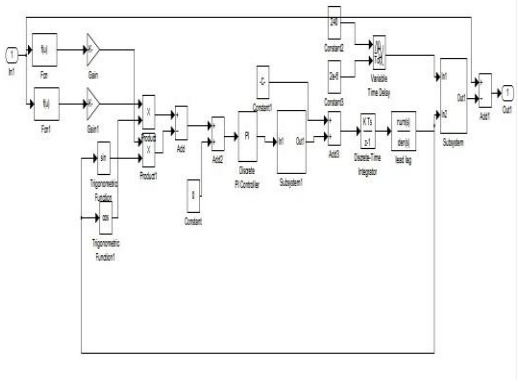

Fig. 2 Discrete PI controller

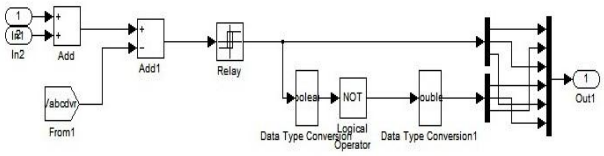

Fig. 3: Control circuit using PI with fuzzy logic controller

Fig.3 shows the control circuit designed in Matlab/Simulink software. The input of the controller come from the output voltage, V3 measured by three-phase V-I measurement at Load in pu. V3 is then transformed in dq term (expressed as instantaneous space vector). The voltage sag is detected by

measuring the error between the dq- voltage and the reference values. The d-reference is set to rated voltage whilst q reference is set to zero. The dq components of load voltage are compared with the reference values and the error signal is then entering to PI controller. Two PI controller block are used for error signal-d and error signal-q separately. For error signal-d, K_P is set to 40 and K_i is set to 100 whilst for error signal-q, K_P is set to 30 and K_i is set to 150 respectively. All the gains selected use to tune up the error signal d and q so that the signal is stable and well responses to system disturbances. The outputs of the PI controller then are transformed back into V_{abc} before forwarded to PWM generator. B. Fuzzy Logic Controller (FLC)

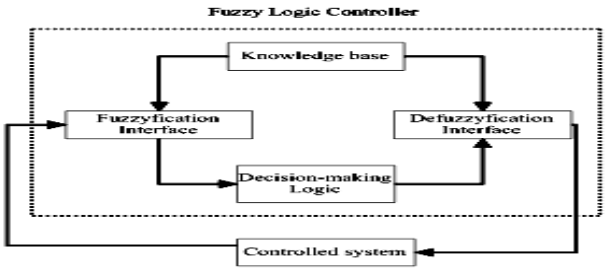

Fig. 4: Basic configuration of FL controller

Unlike Boolean logic, fuzzy logic allows states (membership values) between 0 or 1. Its major features are the use of linguistic variables rather than numerical variables. Linguistic variables, defined as variables whose values are sentences in a natural language (such as small and big), may be represented by fuzzy sets [14]. The general structure of an FLC is represented in Fig.4 and comprises four principal components:
• a fuzzyfication interface which converts input data
into suitable linguistic values;
• a knowledge base which consists of a data base with the necessary linguistic definitions and control rule set;
• a decision making logic which, simulating a human decision process, infers the fuzzy control action from the knowledge of the control rules and the linguistic variable definitions; and
• a defuzzyfication interface which yields a nonfuzzy control action from an inferred fuzzy control action.

In this paper, two FL controller block are used for error signal-d and error signal-q as shown in Fig.3. The process also same as before except the controller now is Fuzzy Logic. For both blocks (error signal-d and q) the FL controller consists of three linguistic variables from input which is; Negative (N), Zero (Z) and Positive (P). Each parameter from linguistic variables for error signal is shown in Fig.5.

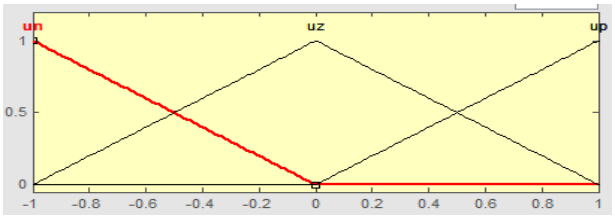

Fig. 5: Linguistic variables from error

For delta error, there are three linguistic variables, Negative (N), Zero (Z) and Positive (P). Both variables can be depicted as in Fig.6.

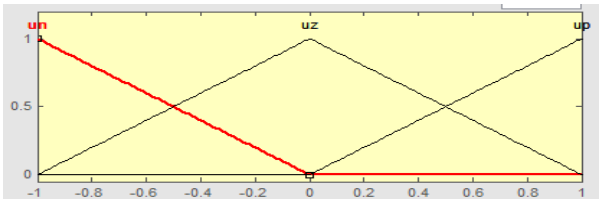

Fig. 6: Linguistic variables from delta error

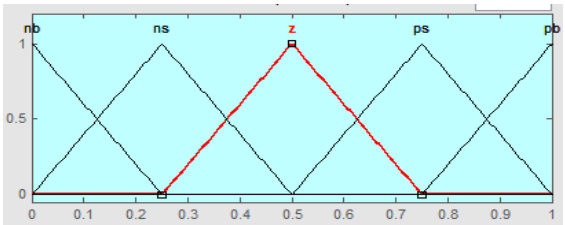

Negative Big (NB), Negative Small(NS), Positive Big(PB), Positive Small (PS), Fig.7. Shows each parameter for output signal.

Table 1: Rule Base

E /DE	N	Z	P
N	NB	NS	Z
Z	NS	Z	PS
P	Z	PS	PB

In the decision-making process, there is rule base that linking between input (error signal) and output signal. Table 1 show the rule base used in this FL controller.

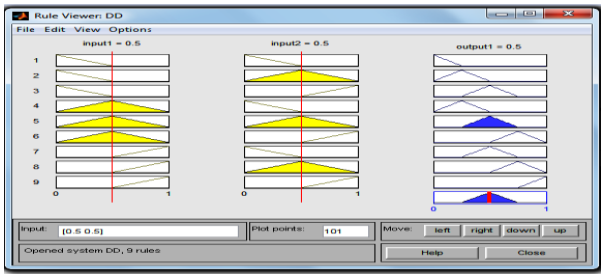

Fig. 8: Rule viewer of d reference

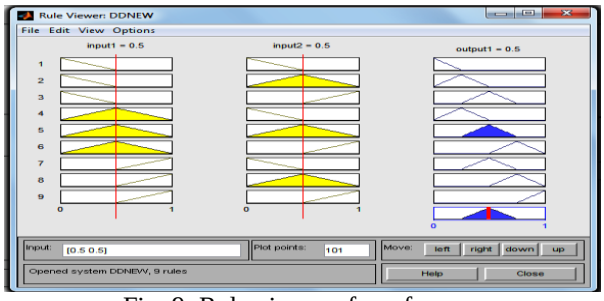

Fig. 9: Rule viewer of q reference

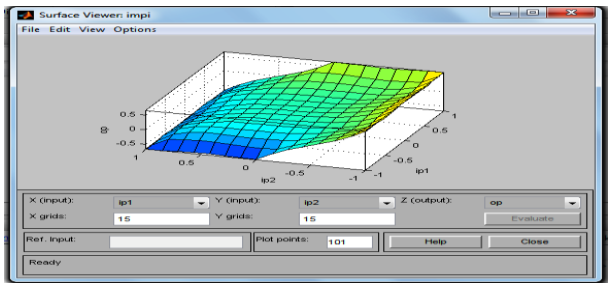

Fig. 10: Surface viewer

IV. SIMULATION RESULTS

In order to understand the performance of the DVR along with control, a simple distribution network as shown in Fig.11 is implemented. There are different fault conditions like normal system, single line to ground fault, double line to ground fault, three phase fault and voltage sag simulated using MATLAB/SIMULINK software. PI with fuzzy logic controller is used for the control purpose. The DVR system connected to the distribution system using a booster transformer.

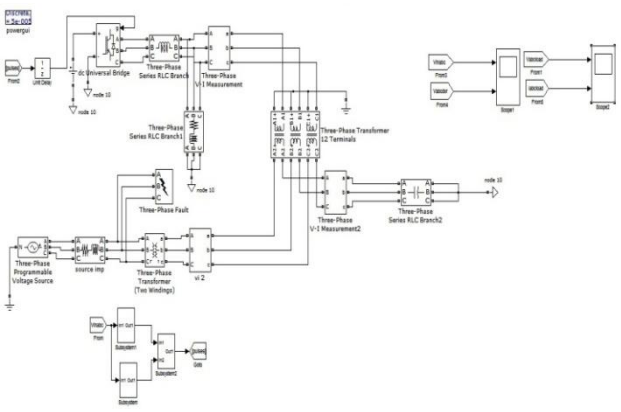

Fig. 11: Simulink Model of DVR Test System

In this system different fault conditions like normal system, single line to ground fault, double line to ground fault, three phase fault and voltage sag with feeder for the duration of 0.2s to 0.3s with fault resistance is 20 ohms and the ground resistance is 0.001 ohms. The output results for the above system are shown below.

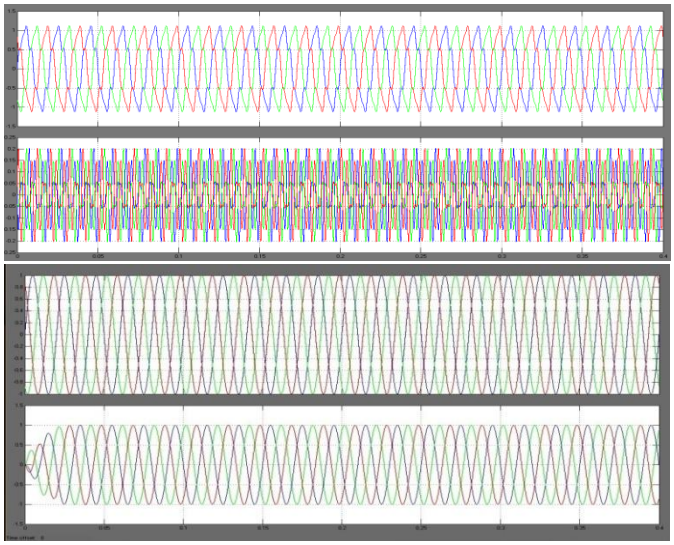

Time (s)

Fig. 12: Normal system (a) Supply voltage, (b) Injection voltage, (c) Load voltage and (d) Load current

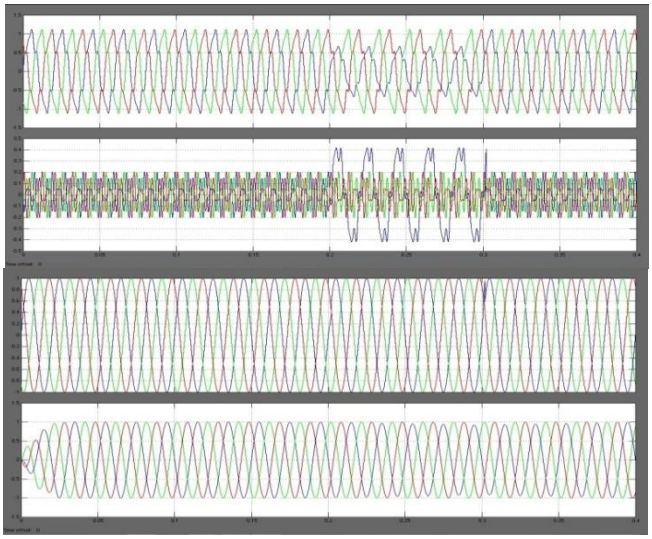

Time (s)

Fig. 13: Single line to ground fault; (a) Supply voltage, (b) Injection voltage, (c) Load voltage and (d) Load current

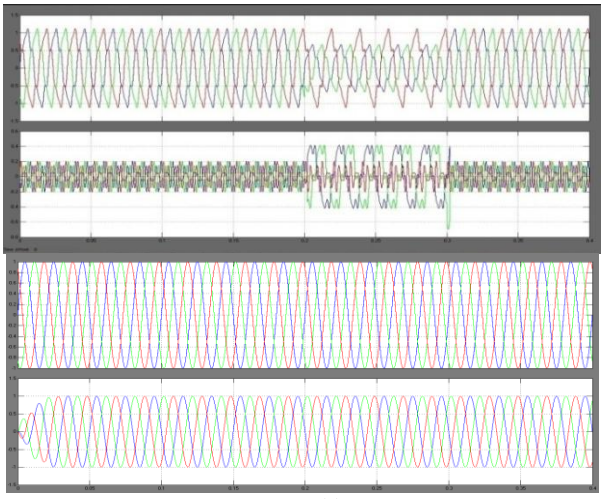

Time (s)

Fig. 14: Double line to ground fault; (a) Supply voltage, (b) Injection voltage, (c) Load voltage and(d) Load current

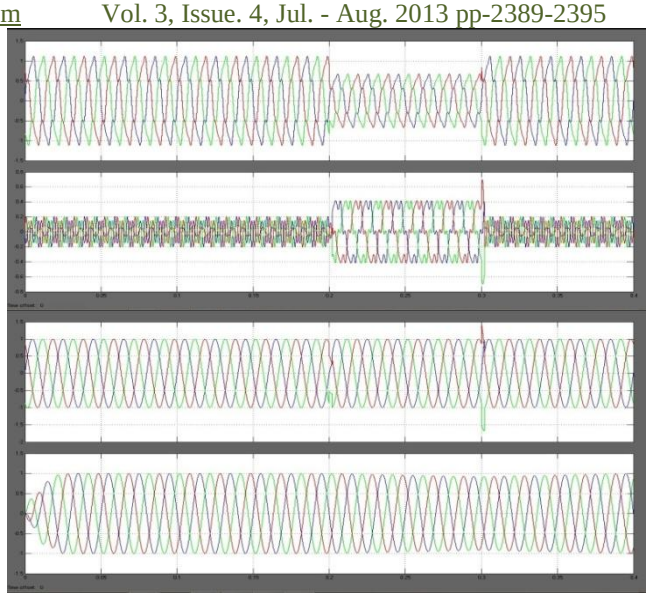

Time (s)

Fig. 15: Three phase fault; (a) Supply voltage, (b) Injection voltage, (c) Load voltage and (d) Load current

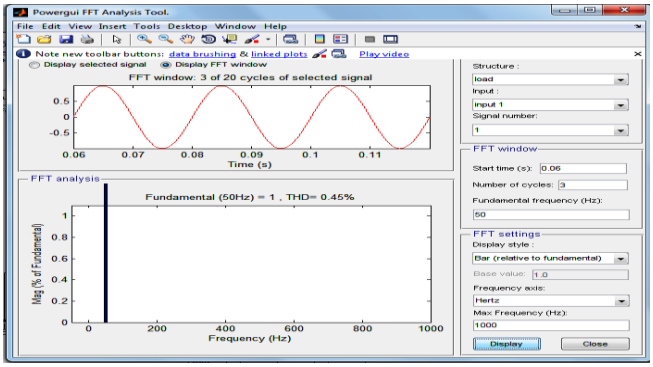

Fig. 17: THD for load voltage using PI with Fuzzy Logic controller

Table 2: THD for V_{dc}

Sl.No.	V_{dc} (V)	
1.	250	0.45
2.	200	0.39
3.	150	0.30
4	100	0.19
5.	50	0.08

V. CONCLUSION

This project thesis examined the problems of power quality in the distribution systems and the need for the mitigation of these problems using the effective and efficient power quality equipment. The Voltage sag was created in a sampler power system by a three phase symmetrical fault in Simulink and a prototype of Dynamic Voltage Restorer was constructed in Simulink. The corresponding Injected voltage was generated for the appropriate Sag voltage occurred in the line.

Finally DVR model can able to mitigate the voltage sag dynamically without any change in the parameters of the internal system and the corresponding compensating voltage is also generated in the distribution system. The simulations carried out showed that the DVR provides relatively better voltage regulation capabilities. There are some limitations; those are the voltage limit, power limit, and energy limit.

REFERENCES

[1]. Anita Pakharia, Manoj Gupta "DYNAMIC VOLTAGE RESTORER FOR COMPENSATION OF VOLTAGE SAG AND SWELL: A LITERATURE REVIEW" International Journal of Advances in Engineering & Technology, Vol. 4, Issue 1, pp. 347-355,July 2012

[2]. M. Rahmani, A. Arora, R. Pfister, P. Huencho, "State of the Art Power Quality Devices and Innovative Concepts", *in VII Seminario de Electrónica de Potencia*, Valparaíso, Chile, Abril 1999.

A. de Almeida, L. Moreira. J. Delgado, "Power Quality Problems and New Solutions

[3]. Chellali BENACHAIBA, Brahim FERDI, "Voltage Quality Improvement Using DVR" Electrical Power Quality and Utilisation, Journal Vol. XIV, No. 1, 2008.

[4]. Rosli Omar,N.A. Rahim and 3Marizan Sulaiman, "Dynamic Voltage Restorer Application for Power Quality Improvement in Electrical Distribution System: An Overview" Australian Journal of Basic and Applied Sciences, 5(12): 379-396, 2011.
[5]. M. E. C. Brito, M. C. Cavalcanti, L. R. Limongi and F. A. S. Neves, "Low Cost Dynamic Voltage Restorer" International Conference on Renewable Energies and Power Quality, 28th to 30th March, 2012.
[6]. L.A.Zadeh,"fuzzysets,"Informat.control.vol.8.pp.338-353
[7]. Jang, J.-S. R. and C.-T. Sun, *Neuro-Fuzzy and Soft Computing: A Computational Approach to Learning and Machine Intelligence*, Prentice Hall, 1997.
[8]. Mamdani, E.H. and S. Assilian, "An experiment in linguistic synthesis with a fuzzy logic controller," *International Journal of Man-Machine Studies*, Vol. 7, No. 1, pp. 1-13, 1975.
[9]. Sugeno, M., *Industrial applications of fuzzy control*, Elsevier Science Pub. Co., 1985.
[10]. Zadeh, L.A., "Outline of a new approach to the analysis of complex systems and decision processes," *IEEE Transactions on Systems, Man, and Cybernetics*, Vol. 3, No. 1, pp. 28-44, Jan. 1973.
[11]. H.P. Tiwari and Sunil Kumar Gupta *"Dynamic Voltage Restorer against Voltage Sag"*,International Journal of Innovation, Management and Technology vol.1,no.3, pp.232-237, 2010.
[12]. Nise, N. S. "Control Systems Engineering" 5th
[13]. Edition, John Wiley & Son, Inc. 2008.
[14]. Mattavelli, P. Rossetto, L. Spiazzi, G. Tenti, P. *"General-Purpose Fuzzy Controller for DC- DC Converter" IEEE Transactions* on Power Electronics, Vol. 12, No. 1, January 1997.
[15]. R. H. Salimin and M. S. A. Rahim *"Simulation*
[16]. *Analysis of DVR Performance for Voltage Sag Mitigation"* The 5th International Power Engineering and Optimization Conference (PEOCO2011),Shah Alam,Selangor, Malaysia: 6-7 June 2011, pp. 261-266.
[17]. Paisan Boonchiam[1] Promsak Apiratikul[1] and Nadarajah Mithulananthan[2] *"Detailed Analysis of Load Voltage Compensation for Dynamic Voltage Restorers" IEEE Transactions*, 2006.
[18]. Omar R and Rahim, N.A. *"New Control*
[19]. *Technique Applied in Dynamic Voltage Restorerfor Voltage Sag Mitigation"* Industrial Electronics and Applications, 2009. ICIEA 2009. 4th IEEE Conference, pp.848 --852.
[20]. Teke K. Bayindir and M.Tu¨may*"Fast sag/swell detection method for fuzzy logic controlled dynamic voltage restorer"* IET Gener. Transm. Distrib., 2010, Vol. 4, Iss. 1, pp. 1–12.
[21]. B.Panda, A.K. Mahapatra and D.P. Bagarty***** And S. Behera****** *"Fuzzy Logic Controller – Based Dynamic Voltage Restorer For Mitigation of Voltage Sag"* International Journal of Engineering Science and Technology (IJEST), Vol. 3 No. 2 Feb 2011, pp. 996-1007.
[22]. S. S. Choi, B. H. Li and D. D.Vilathgamuwa, *"Dynamic Voltage Restoration with Minimum Energy Injection," IEEE Trans.* Power Syst, vol. 15, pp. 51–57, Feb. 2000.

BIOGRAPHIES

R. Udaya Sree is born in 1987 in India. She is graduated from JNTU Hyderabad in 2009. Presently she is doing Post graduation in Electrical Power Systems Specialization at J.N.T.U.H, Hyderabad. Her main areas of interest include Electrical machines, Power systems, Power Electronics & FACTS.

T. VijayKumar. M.Tech, working as Associate Professor in S.K.T.R.M College of Engineering, Affiliated to JNTUH, Approved by AICTE. New Delhi. He completed his M.Tech in 2009 from JNTU. He has nine years teaching experience in Electrical Engineering. He has done two Conferences in Electrical Engineering.

International Journal of Modern Engineering Research (IJMER)
www.ijmer.com Vol. 3, Issue. 4, Jul - Aug. 2013 pp-2396-2402 ISSN: 2249-6645

High speed customized serial protocol for IP integration on FPGA based SOC applications

[1]R. Renukanath, [2]D. R. Srinivas, M.S. (Ph.D)
[1](ECE Department, GPR College of Engineering, Kurnool, Indian)
[2](ECE Department, Associate Professor of GPR College of Engineering, Kurnool, Indian)

ABSTRACT: *The serial communication is very commonly used communication protocol between various peripherals and processor. The current trend is all high speed buses are built with serial communication interface. As the key processing equipment of comprehensive task processing system, Mission management computer needs to crosslink with various equipments and the types of communication interface are different, a serial communication interface based on FPGA (Field Programmable Gate Array) has been designed in this project used for data communication with other equipment . It guarantees the realization of the serial communication function under the condition of without any increasing in hardware resources.*

*The Xilinx **Micro Blaze** soft processor and PowerPC hard processor are widely used in FPGA based CSOC (configurable system on chip) applications. These processers do not have programmable serial links for interfacing with embedded peripherals which are mostly off chip. In this project it is proposed to implement dynamically configurable serial communication block in VHDL. The developed module shall be interfaced with **Micro Blaze** processor as a general purpose IO port. The serial interface blocks shall be implemented to handle high data rate serial links and provide parallel interface to the processor. The serial interface transceiver shall consist of PISO, SIPO shift registers, clock switching modules, counters and control logic.The Xilinx Embedded development kit (EDK) shall be used for developing the test application in C programming language. The serial interface blocks which are coded in VHDL shall be synthesized using Xilinx ISE. The Modelsim simulation software shall be used for simulation. The Spartan 3 family FPGA board shall be used for verifying the results on board.*

Key words: *Serial Communication, Parallel to Serial Conversion, FPGA.*

I. INTRODUCTION

As the key processing equipment of comprehensive task processing system, mission management computer implements comprehensive control and management of the system, data processing, information processing, data decoding and so on, it needs to crosslink with many equipments and the types of communication interface are various. Generally standard interface as RS232, RS422, RS485, ARINC429, simulation and on off, can satisfy the requirements, but there are some equipment which has special requirements.

In order to guarantee normal correspond, private communication interface design is needed. The implement of standard module guarantees the stability and the reliability of the system in largely, and reduces the design personnel repeat work and effectively improves the work efficiency. But the design requirements of mission management computer are diverse, how possible on the base of without any increasing in existing module kinds to satisfy increasingly rich design requirements is currently hardware design personnel need to consider problems. The FPGA (Field Programmable Gate Array) has the characteristics of the reconstruction, the rapidity, design flexibility and the high –density of logical resources [1]; we make full use of the programmable resources of FPGA on a great extent to module function expansion and to meet increasingly complex requirements[2]. The implement mode of private communication interface based on FPGA is presented in this paper; under the condition of without anyincreasing in original module Har dware resources, it has realized module function expansion, shortened the development cycle, and satisfied the module standardization requirements.

II. REALIZATION OF THE MODULES BLOCKS DIAGRAM

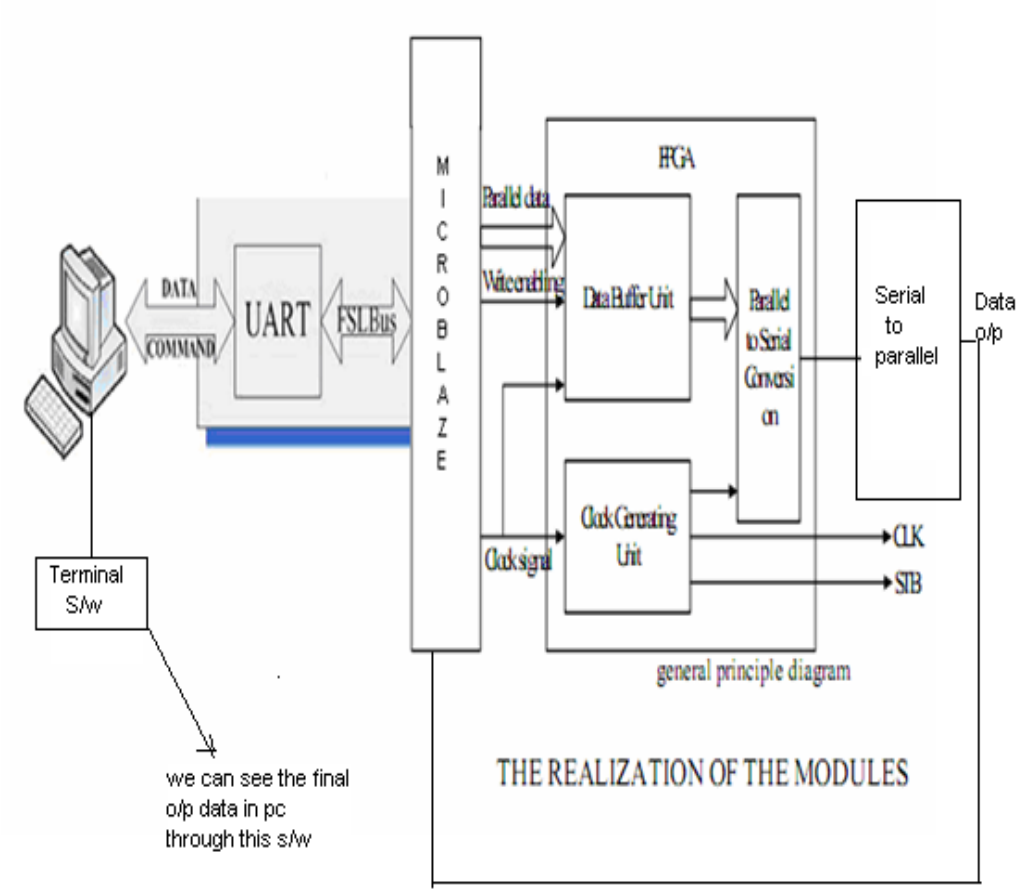

Fig.1. REALIZATION OF THE MODULES BLOCK DIAGRAM

2.1 IMPLEMENTATION OF THE TOTAL BLOCKS DIAGRAM:

The main theme of the project is to prove the serial communication is speed compared to the parallel communication. This is possible in our project by the new configuration board of fpga which is named as Spartan 3E and also the clock signal which is a 50 MHz clock. In this project whatever we used the modules and also the functions of the each and every block will be discussed in below paragraphs. First we are taking the information which is 32 bit from the pc through rs232 cable and also micro blaze is use to send the commands those are various 32 bits of inputs when we want to change the input data immediately it will automatically changed by the micro blaze commands and after receiving the 32 bits of data from the micro blaze this will passed to buffer unit for the storage purpose and after that depends on the parallel and serial clock signals this data will be send to the parallel to serial unit and here we get the output as serial and again this serial data is converted back into the paralle data by the serial to parallel conversion block and now this final parallel data will be sent back to the micro blaze port this data will appears in PC through terminal software and RS232 cable**.**

2.2 COMMUNICATIONS PROTOCOL:

Mission management computer sends control information and high-speed information to aviation administer transponder by CLK, STB and DI signal, CLK denotes data sending clock, DI denotes data(including control and state data), STB denotes data sending finish symbol . Figur2 and Figure 3 respectively shows the signal formats of CLK, STB and DI. Figure 2 shows the interval in figur1. The cycle of CLK is 13us, duty-cycle is 3/10, the 32 bits of data is sent in bytes every time, it has 32us interval between bytes, 4bytes have been sent 8us later, STB is effective; And after keeping 28us, STB is ineffective. A data sending is finished.

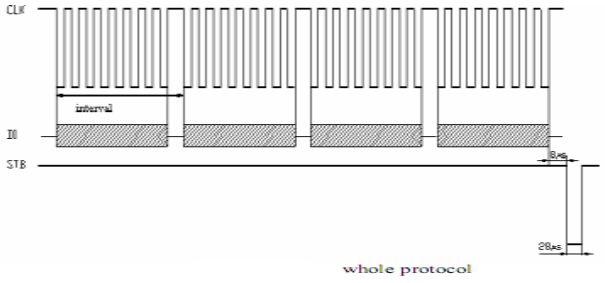

Fig.2

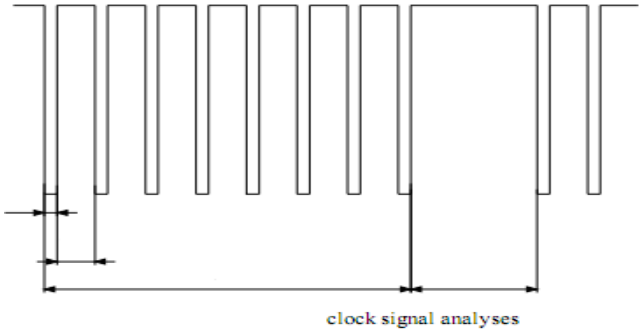

Fig.3

This interface control logic is located on data processing module, FPGA communicates with MicroBlaze processor by internal bus . Figure 1 shows the integral design diagram of this interface logic. FPGA adopts the Xilinx Company's Spartan3e series, the input signal includes 50MHz clock, data/address multiplexing bus and write enabling signals. The output signal is CLK, STB, DI which are the signal the protocol requires**(in our case clk and serial enable and final parallel data ports in our vhdl logic**). The above communication protocol will be changed in our project for the effectiveness of the output that is we are receiving the 8 bit data from the uart and at a time we will receive the 32 bits of by receiving the 4 bytes of data from the uart .then the microblaze will form the 32 bits of data and sends it to the data buffer unit for the storing purpose.

2.2.1 THE INTERFACE LOGIC MAINLY INCLUDES THREE FUNCTION MODULES:

The data buffer unit: The data buffer unit is the functional unit that is mainly responsible for the storage control of parallel data; at the same time it receives upper software order; if there are sending requirements, it sends the parallel data in buffer to parallel to serial conversion unit to process. The clock generating unit: The clock generating unit is the functional unit that is mainly responsible for generating various required clock signal according to protocol requirements; input is the interval bus clock signal which Microblaze output; frequency is 50MHz; at the same time it provides sampling basic clock for parallel to serial conversion unit and generates sending finish signal STB(serial_en signal).The parallel to serial conversion unit: The parallel to serial conversionunit is the functional unit that is mainly responsible for theconversion of parallel data is to serial data; the data is output on the CLK clock edge according to protocol requirements. After the module are electrified, firstly the data which will be sent is wrote in data buffer unit; then the module receives upper software order to send data; the data buffer unit sends the data to parallel to serial conversion unit to data transform and produces serial DI data; After waiting serial data ready, clock generating unit produces CLK signal according to protocol requirements and produces STB signal after data sending has been finished for some time , this data sending has been finishedAnd also we have added another unit in this paper that is serial to parallel unit which is used to convert the serial output of the block parallel to serial into the form of parallel. why we need this block is to just to see the output of out project in separate software called terminal and this final parallel data will be again sent back to the microblaze to see the output in terminal in pc through rs232 cable.

2.2.2 THE DATA BUFFER UNIT:

The data buffer unit is the functional unit that is responsible for the storage of the parallel data in internal bus through FPGA built-in "distributed double-port RAM" resource to achieve ; the principle diagram is shown in Figure 4. This module's input signal includes write enabling (WR_EN), read enabling(RD_EN), write clock(WR_CLK), read clock(RD_CLK), write address(WR_ADDR), read address(RD_ADDR) and write data(WR_DATA), Output port uses synchronized output RD_sDATA. After the power is reset, if WR_EN is effective, then data is wrote to WR_ADDR corresponding data unit under the action of the WR_CLK clock edge; if WR_EN is ineffective, then write port is closed. When RD_EN is effective, the data in RD_ADDR address space is read under the action of the RD_CLK clock edge as the initial data in the parallel to serial conversion unit.

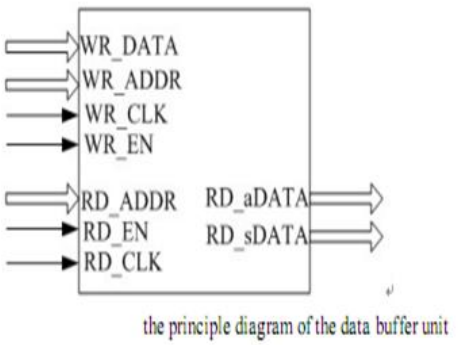

Fig.4

2.3UART BLOCK DIAGRAM:

The UART block diagram for the fpga implementation is shown in Fig. It consists of 4 blocks namely transmitter, receiver, enable generator and baud generator. The uart transmitter and receiver are deigned in the same block which is shown in below. The UART is a serial interface with a frame format of start bit of active low '0'at the beginning and 8 bit of information with a stop bit of active high'1' signal at the end. The operation of UART is controlled by Clock signal which is fed from external crystal.

Baud Generator:-Baud generation section is a clock divider ckt, FPGA board clock runs at 50MHz, but UART transfer data at predefined standards that hade to be maintained, in present system is designed for a rate of 9600/sec(i.e $50x10^6$ is scaled down for 9600). Generates a 9600 pluses for a sec, this implies the speed of UART is 9600 bits per sec. another clock with a 16 times faster is required to the receiver section so that the data will not be corrupted, baud out is given to the enable generator section.

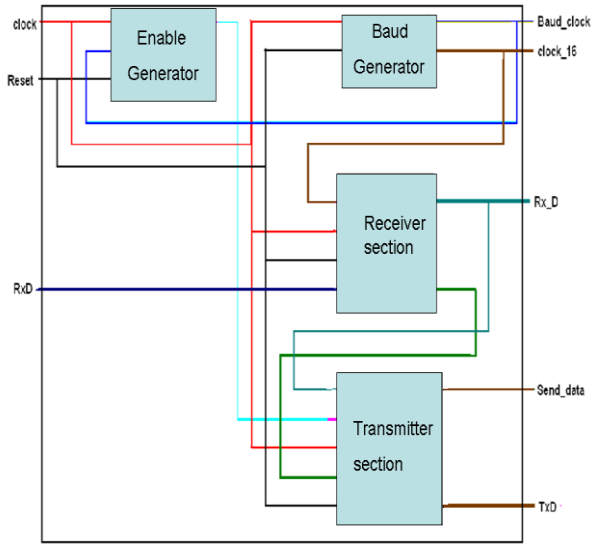

Fig.5

Enable Generator:- this section receives baud_clock signal as a enable signal and gives enable out signal to the transmitter section as a enable input signal. This signal is used to synchronize the transmitter section when ever the data is to transferred.

Transmitter: - The transmitter block is responsible for the transmission of serial data from UART. It takes 8-bit data from the receiver section (in this architecher it takes data after processing image operation block) in parallel and send data in serial form. Data inserted between start and stop bits. An optional parity bit also may be used for error detection. state machine for transmitter is shown in Fig. Transmitter stays in IDLE state unless transmit enable (tx_enable) is made as '1'.The data transmission starts with tx_enable = 1. As mandated by the protocol, a '0' is transmitted to indicate start of transmission or start bit. This is done in START state. Then data bits 0 to 7 are transmitted in states DATA0 to DATA7. If parity is enabled in configuration register, the data is attached with parity in PARITY state. Then transmitter enters STOP state and sends a '1'. This indicates the completion of transmission. Then the transmitter enters the IDLE state and waits for next data transmission.

Receiver: - UART receiver handles reception of data from RS232 port. main functions of receiver block are to convert the serial data to parallel data, check the correctness of data from parity and store the received data.

UART receiver state machine is shown in Fig. The receiver is in IDLE state by default. When the serial data pin goes low, indicating the start bit, the state machine enters DATA0 state. The data is received, one bit at a time from LSB to MSB in states DATA0 to DATA7.

If parity is enabled, the state machine checks the parity bit received against the parity obtained from received data. If the data received is fine, the data_rx (data_rx_done) bit is set to '1' and the receiver goes back to IDLE state again.

Top Module: - top module is a combination of uart and a selected image processing applications. Type of operation is selected by slider switches on the FPGA board each and every block is explained in detail below.

2.4 IMPLEMENTATION OF MICROBLAZE:

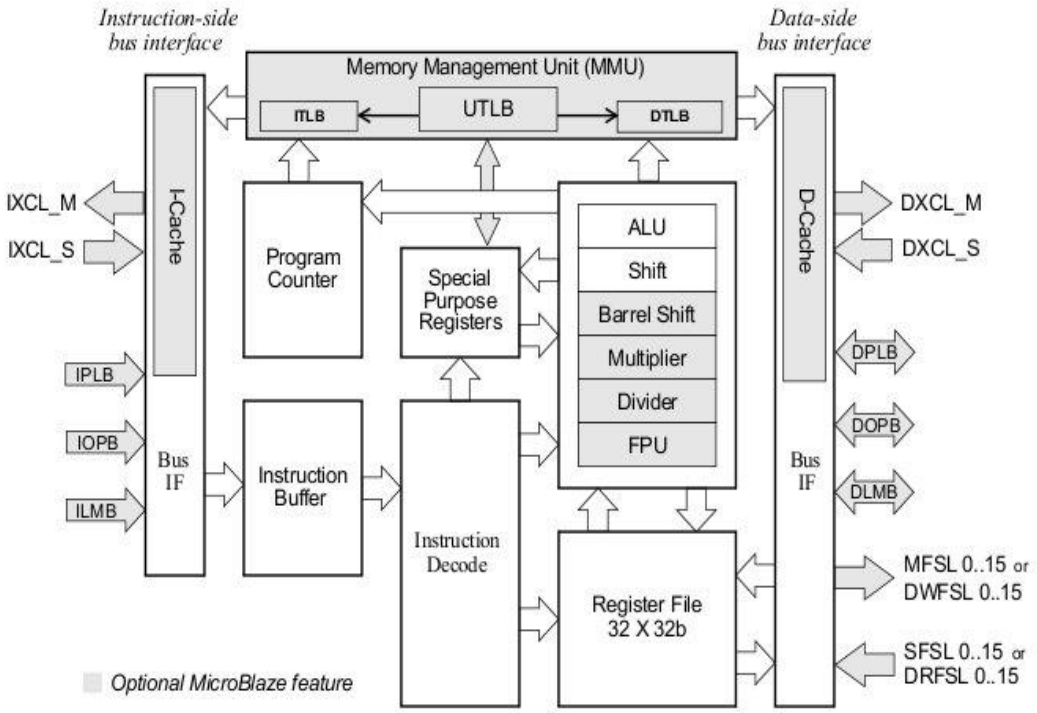

Fig.6

2.4.1.MICROBLAZE: Which is a soft core processor, the part of the FPGAwill acts as a micro blaze processor by implementing the hardware description language means by the vhdl code we are making a act the part of fpga as micro blaze. So it is called as soft core processor. No need of any external hardware circuitry. if we compared with the power pc hard core processor we won't require any separate memory block in FPGA for the micro blaze so the FPGA memory will acts as a micro blaze memory for to build a processor. we will get this soft core processor micro blaze by the ip core generation of Xilinx tool. And sdk tool of Xilinx tool.

2.4.2.POWER PC: It is hard core processor, means it is different than microblaze. In this we should require the some space in fpga hardware to build a power pc that means in if we want to use the power pc for the processor based application then that particular fpga will consist the power pc hardware in the memory block means in the memory space some memory will be accessed for power pc.So in this project we are implementing Microblaze soft core processor only. And this processor will take the information from the Pc by using UART. So from the we receive the commands in hexa,ascii format. By using these commands only we can change our parameters of modulation techniques like setting frequency ,setting azimuth angle, changing work mode, self testing and output RF signal. This function we will implementing by coding. Acoording to these commands the modulation techniques are select in the synthesized unit.

III. THE PARALLEL TO SERIAL CONVERSION UNIT

The parallel to serial conversion Unit mainly implements the conversion of parallel data to serial data. Spartan 3E provides plenty of parallel to serial conversion resources, so it can implement 2 frequency doubling to 8 frequency doubling parallel to serial conversion, and this is suitable for high-speed continuous conversion situation. This module conversion rate is quite low, and the quantity of data is small. Adopting the combination of data buffer and shift register realize the conversion of parallel data to serial data. This method is simple and suitable for low-speed and little data situation, and it can transplant to implement the control of serial interface AD/DA. The example realization code is following:

```
process (sampling clock, output control)
begin
if (output control is ineffective) then
serial output<='0';
count<="0000";
pdata_tmp<=parallel data input;
elseif( the falling edge of the sampling clock) then
if (count="1001") then
count<="0000";
else
count<=count+1;
end if;
pdata_tmp<=pdata_tmp(6 downto 0) &
pdata_tmp(7);--shift register
```

```
sdata_tmp<=pdata_tmp(7);--high bit as
serial data output
if (count="0000") then
pdata_tmp<=pdata_tmp1;-- after
8 bits are been converted, then load the new parallel data
end if;
end if;
end process;
```

IV. THE PARALLEL TO SERIAL CONVERSION UNIT

Already we had mention in above session about the purpose of the serial to parallel unit. In the main IEEE paper they won't tell about this unit but we had added as a extra feature for the effectiveness of the final output And we know the main working function of the serial to parallel conversion unit it takes the serial information from the parallel to serial unit and it again converts into the parallel data which is sends back to the micro blaze to observe in pc through the terminal software.

V. FINAL SIMULATION RESULTS

After the design has been completed, we carry on the emulation to the function. The parallel input data is in turn"11111111", "00001111", "01010101", and "10101010".Figure 8 shows the waveform diagram. From this waveform diagram, we can see that this program has realized the extraction of effective data bits to input data, and carried on serial output according to certain baud rate. Data transmission is steady; data output satisfy the protocol requirements; the specific function and capability have been validated in system-test.

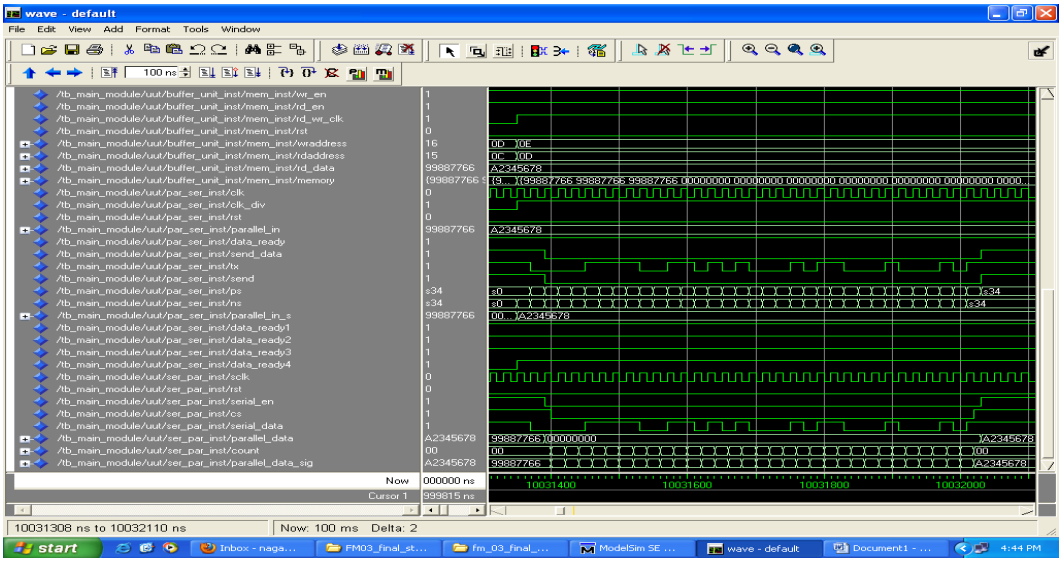

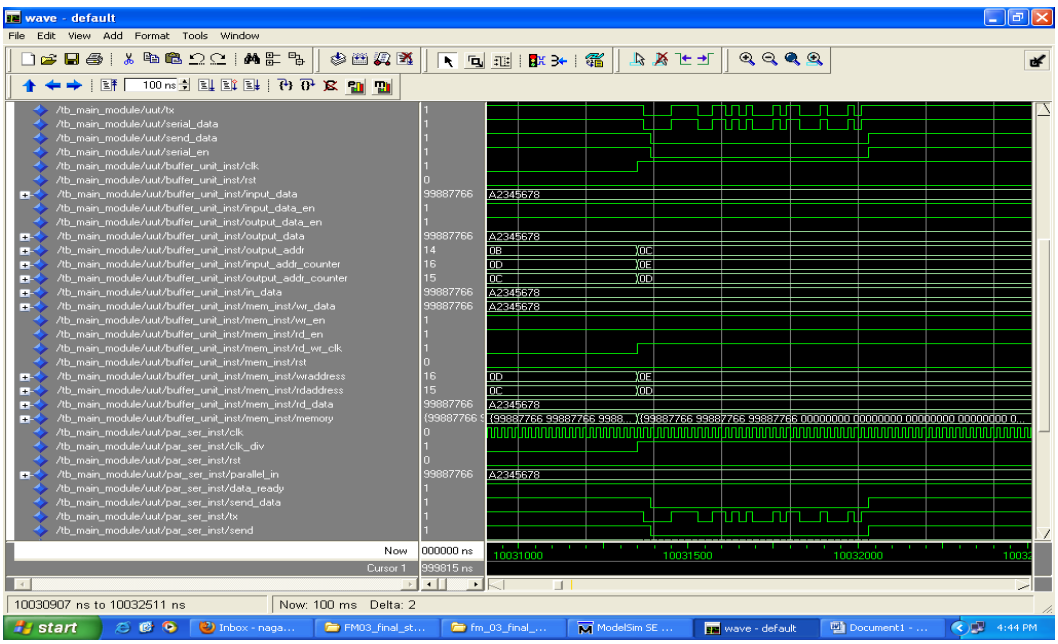

VI. APPLICATIONS

The Xilinx Microblaze soft processor and PowerPC hard processor are widely used in FPGA based CSOC (configurable system on chip) applications.

VII. ADVANTAGES

- High speed devices such as serial ADC/DACs can be interfaced to Microblaze
- Serial processing on high speed sensors is enabled with our application

VIII. CONCLUSIONS

With the enhancement of the comprehensive mission management system integration rate, the equipments with which mission management computer needs to cross-link are more and more. In this paper the design method of the private serial interface based on FPGA is shown, it has realized the new function, shortenned the development cycle, reduced manpower investment and adhered to the principle of the module standardization in the case of without increasing original module kind. This design method is worth promoting in future design.

REFERENCES

[1] Design of Serial Communication Interface Based on FPGA Peng Hui-ling; Nie Ya-lin; Dept. of Comput. & Inf. Eng., Luoyang Inst. of Sci. & Technol., Luoyang, China.
[2] Computer Science and Automation Engineering (CSAE), 2011 IEEE International Conference.
[3] LIU Wan, HE Dao-jun, TAN Ming. The Design and Application of FPGA. Beijing: Tsinghua University Press, China, June 2006.
[4] Guo Shu-tao, JING Yong-zhi. Serial Communication Based on FPGA. The transaction of Beijing Electronic Science and Technology Institute China, Vol .14, No.4, December 2006.
[5] LIU-An-jie, HOU lv, DUAN Zhi-jiao. VGA Display and Serial Communication Based on FPGA. Indurstry Control computer, China, Vol. 19, No.6, 2006.

International Journal of Modern Engineering Research (IJMER)
www.ijmer.com Vol. 3, Issue. 4, Jul - Aug. 2013 pp-2403-2406 ISSN: 2249-6645

Prospective Evaluation of Intra operative Nucleus 22-channel cochlear implant Radiographs

Goutam Goyal[1], K. K. Dhawan[2], Dr. S. S. Tiwari[3]
[1]*M. E., Biomedical Engineering Research Group , Singhania University Rajasthan , India, Email Dr. Ph.D. Director,*
[2]*Shekhawati Group Of College Shekhawati, Rajasthan, India*
[3]*Ph. D., Managing Director , Sensors Technology Pvt. Ltd. , Gwalior , India*

Abstract: *To investigate the clinical utility of intra operative plain radiographs in cochlear implant surgery. Eighty consecutive adult and pediatric cochlear implant operations at a facility capable of intra operative radiographs were evaluated over 06 months. A carefully designed study to evaluate the performance of individuals who received the Nucleus 22-channel cochlear implant. All patients were profound-totally deaf, adults with a post lingual onset of impairment. The preoperative evaluation, prosthesis fitting, training, and postoperative testing were consistent across clinics . Single- subject studies, where each patient acted as his/her own control, revealed that of the 80 subjects, 16–24 obtained significant improvement (P~0 .001) on unpracticed, unfamiliar recorded speech tests from the Minimal Auditory Capabilities (MAC) Battery, when using hearing alone (no lip-reading). In addition, virtually all patients showed improvement in recognition of speech material with lip-reading. The data support the efficacy of a feature extraction coding system where specific formant and amplitude information are transmitted via direct electrical stimulation to the cochlea.*

I. Introduction

The two most common approaches have been to stimulate the cochlea with one electrode (single channel) or more than one electrode (multichannel). Both systems can be divided into those that deliver the speech signal without speech specific processing or those that extract the speech features in some way (2) . The primary rationales for multichannel stimulation are to provide more information and to take advantage of the tonotopic organization of the cochlea.

The purpose of this paper is to provide a description of a technologically advanced 22-electrode speech feature extraction type cochlear prosthesis and to present some preliminary results of the clinical study to date.

Preoperative Patient Selection

The primary criteria for selection of cochlear implant candidates are

1) Postlingually deafened;
2) Profound deafness, bilaterally ;
3) 18 years of age or older;
4) No benefit from any sensory device (tactile or hearing aid) as defined by less than 1 percent open-set discrimination when aided; and
5) Positive CAT scan or tomogram demonstrating patency of the basal turn of the scala tympani.

There are three stages of evaluation. If the patient is considered suitable after completing the first stage, he or she progresses to the next. The initial steps Stage I are those taken to evaluate patients before they are considered as implant candidates. During this stage the degree of hearing loss is established and trials with new hearing aids are conducted if inappropriate amplification has been provided in the past. It is in stage I that promontory stimulation is performed. It is administered by placement of an electrocochleography needle electrode on the promontory. Those patients who do not obtain any sensation of sound in response to electrical stimulation are not considered candidates, at this time.

Stage II considers results obtained from speech discrimination testing using the Minimal Auditory Capabilities Battery and selected subtests from the Iowa Cochlear Implant Battery (4, 7) . These tests are prerecorded by an Unfamiliar speaker and are presented to potential candidates in a controlled fashion (i .e., using standard audiometric Equipment in a sound field presentation) . All tests are performed with a sensory device. For baseline purposes a measure of speech reading is also obtained.

Stage III is the final step in patient selection and occurs only if the candidate meets stages I and II criteria. It involves counseling for appropriate expectations, both with the patient and the family. Further, a tinnitus questionnaire is administered, the surgical procedure is fully explained, and the patient is scheduled for implantation.

Prelingually deafened adults consist of a very heterogeneous group of patients. A substantial number of individual factors, such as etiology of deafness, communication mode, residual hearing, and educational experience, could all affect the post implantation outcomes. Consequently, a valid assessment of the effectiveness of CIs would require a study with a large number of patients or a very well-controlled group of subjects. The speech recognition scores of these patients were examined longitudinally over the 06-month clinical trial period to evaluate the effectiveness of cochlear implantation in providing auditory perceptual benefits. Undertaken to prospectively

II. PATIENTS AND METHODS

In a prospective manner, 73 consecutive adult and pediatric cochlear implant patients (undergoing 80 consecutive cochlear implant operations) were studied at a tertiary care referral center. Patients underwent implantation in standard fashion via a facial-recess approach. All patients were examined with an intra operative plain radiograph obtained in a Tran orbital view. The use and timing of the intra operative radiograph was at the discretion of the surgeon. The surgeon evaluated

the radiograph before final skin closure. In addition, the implanting surgeon completed a questionnaire regarding the device implanted, patient anatomy, surgical procedure, timing of the intra operative radiograph, manner in which the intra operative radiograph was used, and whether the radiograph changed the course of the surgery.

III. RESULTS

The patients included in this study are summarized in Table 1.

TABLE 1. *Patients and cochlear implant operations*

Condition	No. of patients
Patient age	
Adult patients (mean, 58 ± 3 yr)	40
Pediatric patients (mean, 4 ± 3 yr)	33
Total No. of patients	73
Operation	
Primary cochlear implant operation	75
Bilateral cochlear implant operation	7
Revision cochlear implant operation	5
Total No. of cochlear implants	80
Morphology of inner ear	
Normal	71
Abnormal	5
Postmeningitic ossification	4
Total No. of operated ears	80

Forty adult patients and 33 pediatric patients were studied. Seventy-five operations were performed for initial cochlear implantation and five operations were performed for revision cochlear implantation. Of the initial cochlear implantation surgeries, seven operations were performed as bilateral cochlear implantations. For the purposes of this study, the bilateral operations were considered as two initial cochlear implants. The morphology of the implanted inner ears was normal in 71 ears, abnormal in 5 ears, and ossified in 4 ears. On the basis of surgeon questionnaires, the number of insertions of the electrode array and the use of the intra-operative radiograph were compared (Table 2).

TABLE 2. *Electrode insertions and radiographs* Electrode insertion attempts

TABLE 2. *Electrode insertions and radiographs*

Electrode insertion attempts	No. of imaging studies	No. of implants
Single	Single	53
Single	Multiple	11
Multiple	Single	10
Multiple	Multiple	6

In 53 patients, the electrode array was inserted completely into the cochleostomy in a single attempt and a single radiograph was obtained. In 11 patients, the electrode array was inserted into the cochleostomy in a single attemptand multiple radiographs were obtained. Ten patients required multiple insertions of the electrode array to achieve complete insertion and a single radiograph was obtained. In six patients, multiple insertions of the electrode array were required and multiple imaging studies were obtained. The utility of the intraoperative radiograph was assessed through the surgeon questionnaire. In 79 operations, the radiograph was used to confirm the normal operative findings of electrode insertion into the cochlea, and patient management was not changed on the basis of radiographic findings

TABLE 3. Management decisions and radiographs

Condition	No. of implants
Radiograph confirmed normal operative findings	79
Radiograph changed intraoperative management	1
Postoperative CT scans obtained	4

CT, computed tomographic.

In one operation, the intra operative radiograph was used to alter the management of the patient. This case was a second revision cochlear implant performed on a patient who had been ossified from meningitis. The revision was performed for intractable headaches at the site of the ground electrode. On inspecting the round window area, it was observed that there had been two previously performed "cochleostomies."

In this case, the first intra operative radiograph was obtained of an insertion test device in an attempt to confirm the site of the true cochleostomy before reimplantation. Four patients required postoperative computed tomography (CT) scans to aid in their management despite adequate intra operative plain radiographic evaluation. One adult patient received significant facial stimulation at initial device settings and a CT scan was obtained to further clarify device placement. One pediatric patient with significant inner ear malformations and a lack of normal surgical landmarks was evaluated with CT scanning after implantation to verify insertion of the electrode array into the severely abnormal cochlea. Two other pediatric patients underwent CT scanning several months after implantation as part of the evaluation for apparent no stimulation with the implant device. In each of these cases, the CT scan showed correct intra cochlear placement of the electrode arrays. In one revision surgery, the intra operative plain radiograph was useful for confirming the cochleostomy site. In the remaining 79 operations, no changes in the electrode arrays were made on the basis of the information provided by intraoperative plain radiographs.

IV. Conclusions

In this cohort, intra operative plain radiographs were not useful for uncomplicated implant operations; however, they may be useful for complicated operations. These results may have implications for surgical cost and patient radiation exposure. Cochlear implants are a common and well-accepted method for habilitation of hearing in the profoundly hearing-impaired population. The traditional facial recess approach to cochlear implantation provides an adequate view of the middle ear space and round window niche to accomplish electrode insertion. The insertion of the electrode array into the cochlea is often verified with a plain radiograph obtained in the intra operative or early postoperative period (1–9). Accumulated experience with cochlear implants at the study institution has suggested plain radiography may not be useful in assessing implant placement. This study was undertaken to prospectively assess the utility of intra operative plain radiographs in cochlear implantation. In this prospective analysis of intra operative plain radiographs, there appear to be several interesting findings. First, in primary cochlear implant operations, the utility of plain radiographs in patient management is negligible. In no primary implant cases were management decisions changed on the basis of the appearance of the intra operative plain radiograph. A second finding concerns revision cochlear implant surgery. This study included five revision implant cases. In four of the five revision cases, the intra operative radiograph was of negligible utility, confirming what was already known from the procedure. In the remaining revision case, an intra operative radiograph was used to determine which of two previously drilled cochleostomies was the proper one to use for reimplantation. In this case, the electrode array had been removed without visualization from the proper cochleostomy site earlier in the operation. Had the electrode array been left in the true cochleostomy with removal under direct visualization of the promontory, the need for the intra operative radiograph may have been eliminated. A third finding concerns more complicated implant cases. In severely malformed inner ears, the utility of the plain radiograph is questionable. Numerous malformed inner ears were implanted during this study. Specifically, two patients with complete aphasia of the vestibular system, one patient with enlarged vestibular aqueduct, one patient with bilateral facial nerve cysts of the descending segment (10), and one patient with severe cochlear hyperplasia resulting from branchio-oto-renal syndrome underwent implantation during this study. In addition, four patients with post meningitis cochlear ossification underwent implantation during the study period. Of these complicated implant cases, one patient with a malformed inner ear and intra operative questions regarding electrode placement progressed to CT scanning despite the appearance of an adequate intra operative plain radio-Postoperative CT scans obtained 4 CT, computed tomographic. graph. A second patient with inner ear malformations and an adequate intra operative plain radiograph progressed to CT scan evaluation in the postoperative period for apparent lack of stimulation from the implant. Both of these CT scans revealed intra cochlear placement of the electrode array. On the basis of these findings, an argument can be made that CT scan is the study of choice for evaluating cochlear implants in the malformed inner ear when questions arise as to electrode placement because the plain radiograph, again, did not alter management decisions. In 13 of the 17 operations with

multiple imaging performed, the further images were required because of suboptimal radiologic technique. (The four remaining cases with multiple imaging underwent subsequent CT scan evaluation in the postoperative period as detailed above.) Although each plain radiograph delivers 280 mrad of radiation to the lens, the cumulative exposure is concerning in the cochlear implant population. In addition to a preoperative CT scan (approximately 4,200 mrad), many patients (13 patients, 16% of the study population) required more than one intra operative plain radiograph to properly visualize the implant. The utility of the plain radiograph in choosing speech-processing strategies (12). Furthermore, the intra operative radiographs are often obtained at less-than optimal angles, given the constraints of patient positioning and the sterile nature of the procedure. This leads to difficulty in interpreting electrode movement on subsequent comparison films obtained at a later time. With no clear use for the intra operative plain radiograph in operative decision-making, initial postoperative programming, or as a basis for comparison with subsequent radiographs, the risks and costs of the plain radiograph deserve consideration.

REFERENCES

[1] Rosenberg RA, Cohen NL. Intraoperative verification of multi channel scale tympani electrode position. Laryngoscope 1986; 96: 1293–4.
[2] Rosenberg RA, Cohen NL, Reede DL. Radiographic imaging for the cochlear implant. Ann Otol Rhinol Laryngol 1987; 96:300–4.
[3] Gray RF, Evans RA, Freer CEL, et al. Radiology for cochlear implants. J Laryngol Otol 1991;105:85–8.
[4] Marsh MA, Xu J, Blamey PJ, et al. Radiologic evaluation of multichannel intra cochlear implant insertion depth. Am J Otol 1993; 14:386–91.
[5] Ito J. Considerations of cochlear implant surgery. Clin Otolaryngol 1993;18:108–11.
[6] Shpizner BA, Holliday RA, Roland JT, et al. Postoperative imaging of the multichannel cochlear implant. AJNR Am J Neuroradiol 1995; 16:1517–24.
[7] Czerny C, Steiner E, Gstoettner W, et al. Postoperative radiographic assessment of the Combi 40 cochlear implant. Am J Radiol 997; 169:1689–94.
[8] Lawson JT, Cranley K, Toner JG. Digital imaging: a valuable technique for the postoperative assessment of cochlear implantation.Eur Radiol 1998; 8:951–4.
[9] Wang CY, Lai CH, Huang TS. Image study on cochlear-implanted patients. In Kim CS, Chang SO, Lim D, eds. Updates in Cochlear Implantation. Basel: Karger, 2000:67–74.
[10] Pertzborn SL, Reith JD, Maucuso AA, Antonelli PJ. Epineural pseudocysts of the infratemporal facial nerve. Otol Neurotol 2003; 24:490–3.
[11] Wilde G, Sjostrand J. A clinical study of radiation cataract formation in adult life after gamma irradiation of the lens in early childhood.Br J Ophthalmol 1997; 81:261–6.
[12] Cohen LT, Xu J, Xu SA, et al. Improved and simplified methods for specifying positions of the electrode bands of a cochlear implant array. Am J Otol 1996; 17:859–65.
[13] CLARK GM, BLACK R, FORSTER IC, PATRICK JF, TONG YC: Design criteria of a multiple-electrode cochlear implant hearing prosthesis. J Acoust Soc Am 63: 631-633, 1978.
[14] MECKLENBURG DJ, BRIMACOMBE JA : An overview of the Nucleus cochlear implant program . Sem Hearing 41-51, 1985.
[15] OWENS E, TELLEEN C: Speech perception with hearing aids and cochlear implants . Arch Otolaryn 107 : 160-163, 1981 .
[16] TONG YC, BLACK RC, CLARK GM, FORSTER IC, MILLAR JB, O'LOUGLIN BJ, PATRICK JF : A preliminary report on a multiple channel cochlear implant operation . J Laryn Otol 93 : 679-695,1979.
[17] THORNTON AR, RAFFIN MJM : Speech discrimination scores modeled as a binomial variable . J Speech Hear Res 21: 507-518, 1978.
[18] TYLER RS, PREECE JP, LOWDER MW: The Iowa Cochlear Implant Test Battery. Department of Otolaryngology, Head and Neck Surgery, University of Iowa, 1983.

International Journal of Modern Engineering Research (IJMER)
www.ijmer.com Vol. 3, Issue. 4, Jul - Aug. 2013 pp-2407-2411 ISSN: 2249-6645

The Efficiency of Meteorological Drought Indices for Drought Monitoring and Evaluating in Kohgilouye and Boyerahmad Province, Iran

Arash Asadi, Seyed Farnood Vahdat
[1]*Islamic Azad University Dehdasht branch, Iran*
[2]*Ph.D. Candidate, Water Science Dept., Science and Research Branch, Islamic Azad University, Tehran, Iran*

Abstract: *Drought is one of the most common natural events that have a great negative impact on agriculture and water resources. Recently, a new index for drought assessment and monitoring is presented called Reconnaissance Drought Index (RDI). RDI is calculated based on precipitation and potential evapotranspiration. In this study, indices of SPI (Standardized Precipitation Index) and RDI were calculated using 30 years meteorological data (1982 to 2012) for Kohgilouye and Boyerahmad Province located in iran. The negative values show the dry years of the historical record. It can be seen that the most sever drought occurred during the year 2007- 2010. Correlation analysis is performed to identify differences of the SPI and RDI in different time scales. Results show the presented correlation coefficients increase in the longer time scales such as (9 and 12 months). The Map of Spatial distribution of drought severity for 2010 obtained based on the SPI and RDI by means of geostatistics methods in the study area. It can be observed that East part of the watershed lie in the moderately class and the rest of area is generally characterized by severe drought. In this paper however it was shown that RDI can be used for monitoring purposes and to a certain extent for short period drought forecasting.*

Keywords: *Drought, Standardized precipitation index (SPI), Reconnaissance drought index (RDI), Kohgilouye and Boyerahmad*

I. Introduction

Drought as an environmental disaster is associated with a deficit of water resources over a large geographical area, which extends for a significant period of time (Rossi, 2000). It occurs in areas with high and low rainfall and all climate conditions. The different drought indices are presented for drought monitoring. They are useful tools for decision makers to identify weather abnormal conditions for a region (Wilhite et al., 2000).

There are many literatures on the drought evaluation by using different indices, models and water balance simulations (Jain et al., 2010). There are different indices for drought monitoring, such as: Palmer Drought Severity Index (PDSI), Crop Moisture Index (CMI), Surface Water Supply Index (SWSI), Percent of Normal Index (PN), Standardized Precipitation Index (SPI) (Mishra and Singh, 2010).

Along the various indices for meteorological drought monitoring, SPI were widely accepted and used (Shamsnia and Pirmoradian, 2009).The SPI was presented by McKee and his colleagues at Colorado State University . SPI is completely related to probability. This Index use precipitation as the most effective parameter in the calculation of the drought severity. The SPI is normally distributed so it can be applied to monitor wet as well as dry periods. During the last decade the SPI has become very popular due to its low data requirements. This index can be useful for drought monitoring and forecasting (Shamsnia et al., 2009). Recently, a new index for drought assessment and monitoring is presented called Reconnaissance Drought Index (Tsakiris et al., 2007). RDI is calculated based on precipitation and potential evapotranspiration. Precipitation alone cannot show the impact of drought on agricultural production and vegetation. Applying both of the P and PET in drought severity calculation and monitoring, increases the validity of the results (Tsakiris et al., 2007). Also, this index has a strong correlation with SPI (Asadi Zarch et al., 2011). The RDI was used in Greece (Tigkas, 2008), Cyprus (Pashiardis and Michaelides, 2008), Malta (Borg, 2009) and Iran (Khalili et al., 2011) for monitoring or analysis of historical droughts. To achieve this objective, we used Geostatistical tools to mapping. Geostatistical Analyst creates a continuous surface by using sample points taken at different locations. Using interpolation techniques are frequently used in recent years to mapping drought risk.

The Study Area

Drought is a common natural disaster in many countries as well as Iran. Previous studies show that Iran is exposing drought with different severities. To evaluate drought, Kohgilouye and Boyerahmad Province in the southwest of Iran were selected. This province is located in the southwest part of Iran, at 49° 57' to 51° 42 E longitude and 30° 9' to 31° 32' N latitude, with an area of 26416 Km2. Elevation in the study area ranges from 500 m to 4400 m. The climate is characterized by dry and warm summers, and cool wet winters. The annual mean of precipitation for the province ranges from 400 to 1300mm. Most of the annual average precipitation falls as rain during winter. The Location of study areas and monitoring station are shown in Figs 1.

Data used

Rainfall data were collected from 17 meteorological stations complied by the Meteorology Organization of Iran and Kohgilouye and Boyerahmad Regional Water Authority. After, annual rainfalls data during 30 years from 1982-2012 were

chosen to later analysis. Missing data was computed by use of relationship between elevation and rainfall. To this order, linear regression was calculated in Spss software.

II. Method

Calculation of meteorological indices

The Standardized Precipitation Index

The standardized Precipitation Index (SPI) is one of the indices that were presented for drought monitoring. It is calculated in short-term (3, 6 and 9 months) and long-term (12, 24 and 48 months) periods. In any time scale, the SPI mean may reach zero in a location and its variance become equal to 1.Using the SPI, quantitative definition of drought can be established for each time scale. A drought event for time scale i is defined here as a period in which the SPI is continuously negative and the SPI reaches a value of -1.0 or less. The drought begins when the SPI first falls below zero and ends with the positive value (Mckee et al., 1993). The SPI is calculated by using the following equation:

$$\boldsymbol{SPI = \frac{P_i - \overline{P}}{S}} \quad (1)$$

Where P_i and $\boldsymbol{\overline{P}}$ are the precipitation and average precipitation of selected period, S is standard deviation of precipitation.

The Reconnaissance Drought Index (RDI)

The Reconnaissance Drought Index (RDI) is calculated in three stages: Initial value of RDI (a_0), normalized RDI (RDIn) and standardized RDI (RDIst). Initial value may be calculated for each month, seasons (3-month, 4-month, etc.) or hydrological year. The a_0 is calculated by using the following equation (Tsakiris et al., 2007; Asadi Zarch et al., 2011)

$$\boldsymbol{a_0^{(i)} = \frac{\sum_{i=1}^{12} P_{ij}}{\sum_{j=1}^{12} PET_{ij}} ; i = 1(1)N \text{ and } j = 1\ (1)12} \quad (2)$$

Where $P_{ij}$and PET_{ij} are the precipitation and potential evapotranspiration of the jth month of the i_{th} hydrological year. Hydrological year is starting from October in Iran. N is the total number of years of the available data.

A second step, the Normalized RDI(RDI_n)is computed using the following equation for each year, in which it is evident that the parameter a_0 is the arithmetic mean of a_0 values (Tsakiris et al., 2007; Asadi Zarch et al., 2011).

$$\boldsymbol{RDI_n^{(i)} = \frac{a_0^{(i)}}{\overline{a}} - 1} \quad (3)$$

The third step, the Standardized RDI(RDI_s), is computed following a similar procedure to the one that is used for the calculation of the SPI: The equation for the Standardized RDI is:

$$\boldsymbol{RDI_{st(k)}^{(i)} = \frac{y_k^i - \overline{y}_k}{\hat{\sigma}_{yk}}} \quad (4)$$

Where y_k is the $ln(a_0; \overline{y}_k)$ is its arithmetic mean of y_k , and $\hat{\sigma}_{yk}$ is its standard deviation.

The RDI is based on the ratio of two aggregated quantities which are precipitation and potential evapotranspiration. It can be estimated for all time scales. However 3, 6, 9 and 12 month are suggested since they are more useful for comparing different locations (Tsakiris and Vangelis, 2005).

Estimation of potential evapotranspiration for drought monitoring using RDI

Several methods have been suggested for PET estimation. The Penman–Monteith (PM) equation is one of the standard methods of calculating PET by using meteorological data. It is remarkable that the international scientific community has accepted this equation as the exact method (Jabloun and Sahli, 2008). Although PM equation in different climates has shown positive results, but because of the full meteorological data requirement such as minimum and maximum air temperature, minimum and maximum relative humidity, solar radiation and wind speed, its widespread use is limited. In some studies for drought monitoring using RDI, alternative methods such as Thornthwaite method and Blaney-Criddle equation has been used for PET estimation (Kanellou et al., 2010). Therefore in this research was used the Calibrated Thornthwaite method (Ahmadi and Fooladmand, 2008) for Kohgilouye and Boyerahmad Province. The Calibrated Thornthwaite equation is :

$$\boldsymbol{PET = 16(10\frac{T_{eff}}{I})^a} \quad (5)$$

Where PET is mm month^{-1},T_{eff} is the effective monthly temperature (°C). I is a thermal index imposed by the local normal climatic temperature regime, and the exponent a is a function of I.

Effective temperature is calculated as (Camargo et al., 1999):

$$\boldsymbol{T_{eff} = K(T_{ave} + A)} \quad (6)$$

$$\boldsymbol{A = T_{max} - T_{min}} \quad (7)$$

Where T_{min}, $T_{max}$and $T_{eff}$are the minimum, maximum and effective monthly temperature (°C) respectively. $K$is the calibrated coefficient.

Time Scales

In this study, Monthly SPI and RDI were calculated using the monthly precipitation and evapotranspiration data of 17 stations in Kohgilouye and Boyerahmad Province. SPI and RDI values were calculated in the period of hydrological years from 1982 to 2012 for the time scales of 1, 3, 6, 9 and 12 months. Because of data limitations, SPI with time scales longer than 24 months may be unreliable. The RDI_{st} behaves similar to the SPI. Drought classification of these indices is shown in Table 1. The values from -0.5 to -0.99 and +0.5 to +0.99 considered as nominal class of mild drought and slightly wet (Shamsnia and Pirmoradian, 2009).

III. Results and discussions

Correlation analysis between RDI and SPI

The correlation coefficients (r) between SPI and RDI for each area and each time scales are described in Table 2. Results show the presented correlation coefficients increase in the longer time scales such as (9 and 12 months). The maximum value of r between SPI and RDI was obtained for 12-month time scale and the minimum value for 1-month time scale in all areas (Table 2). In time Scale 9 and 12 months in all stations, correlation coefficient (r) is more than 0.9. Because SPI index is related to precipitation parameters for drought assessment, the results show that precipitation parameters are more effective in drought with a longer time scale. By contrast, the effect of potential evapotraspiration parameters that were used in the RDI index will be reduced by increasing the time scale. The wet, drought and normal periods have more fluctuation on the short time scales such as 1, 3 and 6 months, because of the low number of effective months and effects of other meteorological parameters on the severity of drought. In other words, changes of dry and wet periods on short time scales, in addition to precipitation, depend on the evapotraspiration and the other weather parameters.

Identification of Drought Events

Fig 2 shows the annual SPI and RDI in the yasuj station for the period 1982 to 2012. The negative values show the dry years of the historical record. It can be seen that the most sever drought occurred during the year 2007- 2010.

Drought Maps

Drought maps were produced using the estimated annual values of SPI and RDI. Also, By means of kriging method spatial severity of drought was mapping. Fig 3 and 4 shows Spatial distribution map of SPI and RDI in 2010 in the study area. It can be observed that north and west parts of the area lie in the extremely class and the rest of area is generally characterized by severely and moderately drought. Such spatial drought map can be useful to forecast drought in the further studies. In most cases, the results from both indices are similar. However, in some cases, depending on the local conditions, the results from RDI are more sensitive.

IV. Conclusions

SPI and RDI were calculated in a period of 30 years data (1982 to 2012) for Kohgilouye and Boyerahmad Province. Correlation analysis is performed to identify the differences of the standardized precipitation index (SPI) and the reconnaissance drought index (RDI). From the presentation of some popular indices for drought assessment it seems that SPI is becoming the most widely used index. This is probably due to its simplicity, universality and to its least data demanding nature. In this paper however it was shown that water deficit cannot be estimated only on the input (e.g. precipitation) but also on the output variable (water consumption). Based on the logic a new index, RDI was purposed using data of two determinants, precipitation and potential evapotranspiration. It can be more effectively associated with hydrological and agricultural drought. Also it is an ideal index to study the effects of climate instability conditions. Due to its easy calculation RDI can be used for monitoring purposes and to a certain extent for short period drought forecasting.

References

[1] Ahmadi, S.H. and Fooladmand, H.R. (2008). Spatially distributed monthly reference evapotranspiration derived from the calibration of Thornthwaite equation: a case study, South of Iran. Irrig Sci. 26:303–312.
[2] Asadi Zarch, M.A., Malekinezhad, H., Mobin, M.H., Taghi Dastorani, M. and Kousari, M.R. (2011). Drought Monitoring by Reconnaissance Drought Index (RDI) in Iran. Water Resour Manag. 25(13):3485-3504.
[3] Borg, D.S. (2009). An application of drought indices in Malta, case study. European Water. 25/26:25-38/
[4] Kanellou, E., Domenikiotis, C., Tsiros, E. and Dalezios, N.R. (2008). Satellite-based drought estimation in Thessaly. European Water, 23/24:111-122.
[5] Kanellou, E., Domenikiotis, C., Tsiros, E. and Dalezios, N.R. (2008). Satellite-based drought estimation in Thessaly. European Water, 23/24:111-122.
[6] Khalili, D.,Farnoud, T., Jamshidi, H., Kamgar-Haghighi, A.A. and Zand-Parsa, Sh. (2011). Comparability analyses of the SPI and RDI meteorological drought indices in different climatic zones. Water Resour Manag. 25(6): 1737-1757.
[7] Jabloun, M. and Sahli, A. (2008). Evaluation of FAO-56 methodology for estimating reference evapotranspiration using limited climatic data. Application to Tunisia. Agric Water Manage. 95:707–715.
[8] Jain, S.K., Keshri, R., Goswami, A. and Sarkar, A. (2010). Application of meteorological and vegetation indices for evaluation of drought impact: a case study for Rajasthan, India. Natural Hazards. 54: 643-656.

[9] McKee, T.B., Doesken, N.J. and Kleist, J. (1993). The relationship of drought frequency and duration to time scales, Preprints, 8th conference on applied climatology, January 17 22, Anaheim, California, pp 179–148
[10] Mishra, A.K. and Singh, V.P. (2010). A review of drought concepts. Journal of Hydrology. 391: 202-216.
[11] Pashiardis, S. and Michaelides, S. (2008). Implementation of the standardized precipitation index (SPI) and the reconnaissance drought index (RDI) for regional drought assessment: A case study for Cyprus. European Water. 23/24: 57-65.
[12] Rossi, G (2000). Drought mitigation measures: a comprehensive frame work. In Drought and Drought Mitigation in Europe. J. Voght and F. Somma (eds), Kluwer Academic Publishers, Dordrecht.
[13] Shamsnia, S.A. and Pirmoradian, N. (2009). Rectification of the Standardized Precipitation Index (SPI) Classification for Drought Evaluation in Fars Province (IRAN). 2nd India Disaster Management Congress. National Institute of Disaster Management. 4-6 November.
[14] Tigkas, D. (2008). Drought Characterisation and monitoring in regions of Greece. European Water. 23/24:29-39.
[15] Tsakiris, G., Pangalou, D. and Vangelis, H. (2007). Regional drought assessment based on the reconnaissance drought index (RDI). Water Resource Management. 21:821-833.
[16] Wilhite, D., Sivakumar, M. and Wood, D. (2000). Early Warning Systems for Drought Preparedness and Drought Management. Proceedings of an Expert Group Meeting, 5-7 Sep, Lisbon, Portugal.WMO TD No. 1037.

Table 1. Drought classification according to the SPI and RDI_{st} values

SPI and RDI_{st} value	Category
2 or more	Extremely wet
+1.5 to +1.99	Severely wet
+1 to +1.49	Moderately wet
+0.5 to +0.99	Slightly wet
-0.49 to +0.49	Normal
-0.5 to -0.99	Mild drought
-1 to -1.49	Moderately drought
-1.5 to -1.99	severely drought
-2 and less	Extremely drought

Table 2. Correlation coefficient (r) of the SPI and RDI in different time scales

Row	Station	Time Scales (Month)				
		1	3	6	9	12
1	Yasuj	0.838	0.965	0.979	0.990	0.992
2	Dashtroom	0.521	0.746	0.899	0.948	0.985
3	Dehnoo	0.640	0.831	0.954	0.977	0.991
4	Patave	0.532	0.764	0.842	0.971	0.989
5	Abchirak	0.615	0.856	0.941	0.983	0.997
6	Nazmakan	0.654	0.832	0.932	0.955	0.984
7	Tolchega	0.543	0.683	0.742	0.886	0.979
8	Ghaleraesi	0.725	0.846	0.921	0.964	0.993
9	Bibihakime	0.626	0.754	0.878	0.943	0.996
10	Likak	0.537	0.622	0.774	0.865	0.947

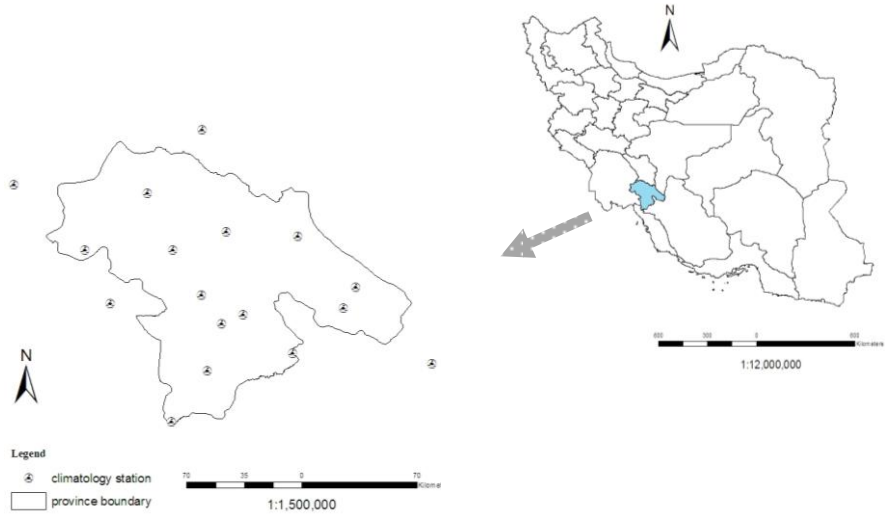

Fig 1. Regional map of Iran , location of study area and monitoring stations

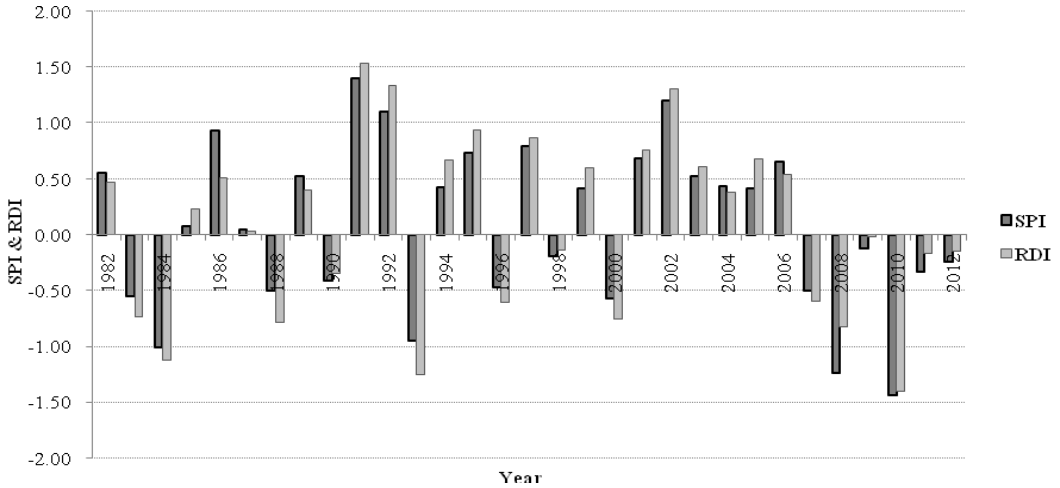

Fig 2. Annual SPI & RDIst for each hydrological year (Oct-Sep) for yasuj station

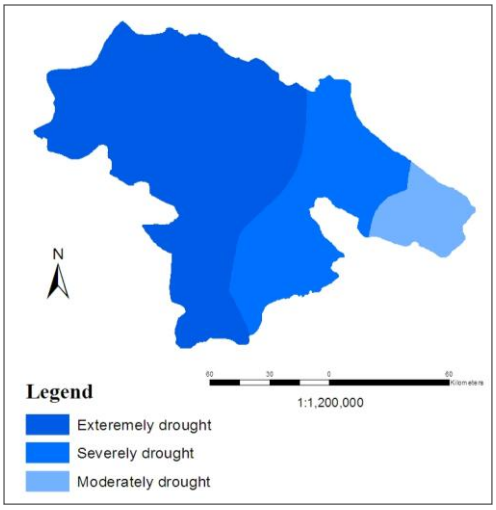

Fig 3. Spatial distribution map of SPI in 2010 in the study area

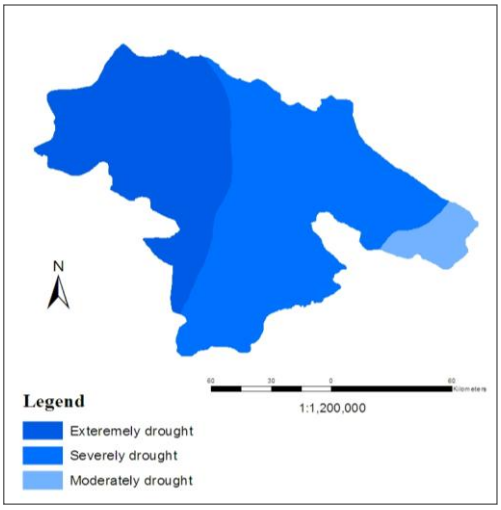

Fig 4. Spatial distribution map of RDI in 2010 in the study area

International Journal of Modern Engineering Research (IJMER)
www.ijmer.com Vol. 3, Issue. 4, Jul - Aug. 2013 pp-2412-2418 ISSN: 2249-6645

Review on Digital Elevation Model

Dr. Pratibha P. Shingare[1], Mr. Sumit S. Kale[2]
[1](Department of Electronics & Telecomm., College of Engineering Pune, India)
[2](Department of Electronics & Telecomm., College of Engineering Pune, India)

ABSTRACT: *Digital Elevation Models commonly known as DEM's are widely used in Terrain Analysis & image processing applications. A Digital Elevation Model is commonly used for Analysis of various features & objects which are remotely sensed by various devices & Techniques of Modern Era. Detail Literature Review of DEM by referring various Journals & Research papers is proposed in this paper. Various Remote sensing techniques to capture Terrain Surface are studied along with their practical use in the field of Geoanalysis. We enlisted various Interpolation algorithms, Global DEM's, Quality Parameters & practical use of DEM's.*

Keywords: *DEM, Geomorphology, Interpolation, Raster, Vector*

I. INTRODUCTION

The concept of Digital Elevation Model is relatively recent & came from the concept of Digital Terrain Analysis (DTM). The Term Digital Terrain Analysis (DTM) is attributed to two American Engineers namely Miller & Laflamme at the Massachusetts Institute of Technology during the late 1950s (Nasel El Shelmy).Since the 1960's the main research area was on surface modelling & contouring from DEM. The Model is an object or concept which is used to represent something else. It is reality scaled down & converted to a form which we can comprehend (Mayer 1985). Model permit abstraction based on logical formation using a convenient language expressed in a shorthand notation, thus enabling one to better visualize the main element of a problem while the same time satisfying communication, decreasing ambiguity & improving the chance of agreement on the result (Saaty & alexander 1981). According to Burrough (1986) **"**Digital Elevation Model is regular gridded matrix representation of the continuous variation of relief over space". Elevation can be defined as "the height above the horizon". The term horizon refers to the sea level. DEM involves creation of regular array of elevations in the form of squares or hexagon pattern over the terrain. DTM represents the altitude of ground itself while DEM refers to the maximum altitude everywhere. DEM Have become widely used tool & product in last 25 years for providing snap shot of landscape & landscape features along with elevation values (G.Toz, M. Erdogan).They describe as a spatially referenced Geo-dataset. DEM have ability to represent complex terrain structures with adequate resolution. They can be directly compatible with remotely sensed data sources. The need of Study highlights the importance of Terrain analysis & DEM in numerous applications for modeling & analyzing spatial topographic information. DEMs are widely used in numerous applications including military, environmental, engineering, commercial GIS applications etc. Digital Elevation Model includes four important steps namely (i) Data Acquisition (ii) data Modeling (iii) Data Management (iv) Application development. The data acquisition refers to capturing of Terrain Images with the help of various techniques including Photogrammetry, Surveying, Remote Sensing and Cartography. In Computation & modeling numerous disciplines used such as photogrammetry, surveying, cartography, geography, computational geometry, computer graphics, image processing etc. In data management & manipulation various techniques can be used such as spatial database technique, data coding & compression technique, data structuring, computer graphics. In application discipline all geosciences are involved including surveying, photogrammetry, cartography, remote sensing, geography, geomorphology, civil engineering, mining engineering, geological engineering, landscape design, Urban planning, Environmental management, resource management, facility management, flight simulation, battle simulation, tank route planning, missile & airplane navigation, computer games etc. A fundamental architecture of DEM derives from the data model which is used to represent it. Basically DEMs can be represented by Image Method or Mathematical method. Various data structures have been tried for storing & displaying topographic surfaces (i) Rectangular Grid which can also be called as Elevation Matrix structure (ii) Triangulated Irregular Network (TIN) (iii) Contours. These above models are derived on the basis of sampling method. As earth have infinite number of points that can be measured it is very difficult to record every point. So to simplify this drawback sampling method must be used which extract the representative points of the Earth Surface. According to ESRI- 1992 guidelines, the data structure should: (i) accurately represent the surface (ii) Suitable for efficient data collection (iii) Minimize data storage requirements (iv) Maximize data handling capacity (v) Suitable for given surface analysis.

II. DEM DATA STRUCTURES

DEM data structures are usually classified as: (i) Rectangular Grids are also known as Computed DEM (Minnesota Department of Natural Resources). Grids are matrix structure that implicitly records topological relation between data points. The data structure of Grid is similar to the array storage structure of digital computers. Raster type DEM is included in it. Raster is a grid of digital, uniform, square cells covering an area on the earth's surface where each cell is given a value of

whatever you want to map. In the case of DEMs, each cell is given the elevation value of the land (or water) surface that it overlies. The cells of a given DEM may be almost any size but most frequently are in the range from 5 to 30 meters square. Raster's are relatively fast to process by a computer because the location of each cell can be determined solely from its order value in the grid. Because every vertex in a vector map requires two pieces of data to be located - the x and y - it is slower to process than a raster cell. A raster also represents the values of a continuous surface such as elevation more precisely than vector. A vector contour map shows elevation only at specific intervals represented by the contour lines (e.g. 100 ft, 110 ft, 120 ft). Raster cells, however, show elevation values not only at the specific intervals but in-between them as well (e.g. 100 ft, 101 ft, 102 ft, and 120 ft). (ii) The TIN model was developed as a simple way to build a surface from a set of irregularly spaced points (Peucker et al. 1978). TIN are also known as Measured DEM. They are vector type data. It utilizes digital points, lines and polygons to represent features on the earth's surface (e.g. point: stream gage, line: roadway, polygon: forested area). Every feature in vector format is composed of a set of vertices, each having explicit x and y (or longitude and latitude) location coordinates. TIN include nodes, Edges, Triangles, Topology. The vector advantage is that it is locationally more precise than raster. A point feature in vector format is represented by a single coordinate pair (x, y) which, on the computer screen, is only a pinpoint that has no measurable width. The same point feature represented in raster, however, would be at least one cell in width (e.g. 30 m). Also, to give a vector map greater resolution is less costly in terms of data storage space than increasing the resolution of a raster map. (Resolution can be measured by the amount of data (i.e. vertices or cells) in a given area.) On a vector map, the number of *vertices* for a set of features may be doubled and this only increases the data storage requirement by two. For a raster map, however, doubling the resolution ups the data storage requirement by four or, in other words, the square of the resolution increase. (iii) Contour is also known as isolines. They are most familiar representation of terrain surface. The accuracy of contour becomes high when they have been captured as primary data from aerial photograph. However in today's scenario Grid & TIN are most widely used data structures to create DEMs. To enhance & extract the exact DEM according to end users need, topographic attributes plays very important role.

III. TOPOGRAPHIC ATTRIBUTES FOR DEM

Topographic attributes are commonly of two types (i) Primary (ii) Secondary. Primary topographic attributes are derived directly from DEM. They include: (i) Surface Derivatives- It measures the rate at which elevation Changes as per location (X & Y coordinates) (ii) Slope- It measures the rate of change of elevation in the direction of steepest descent. It affects the velocity of the surface & subsurface flow including soil water content, erosion potential, Soil formation etc. (iii) Aspect & Primary Flow Direction- Aspect is the orientation of line of steepest descent. It is useful for visualizing landscapes. (iv) Curvature- They based on rate of change of second derivative like slope, aspect etc. Basically in DEM we use Plane Curvature (Rate of change of Aspect along a contour) & Profile Curvature (Rate of Change of slope down a flow line). (v) Upslope contributing Area- It is the area above a certain length of contour the contribute flow across the contour. It is also referred to as drainage area or catchment area. (vi)Flow Width (vii) Maximum Flow Path Length- It is the maximum length of all paths from catchment boundary to a given point in the DEM. Secondary topographic attributes are computed from two or more Primary Topographic attributes. They include: (i) Topographic Wetness Index- It gives relationship between Specific catchment area & product of Slope gradient & soil transmitivity. (ii) Stream power Indices (iii) Radiation Indices (iv) Temperature Indices.

IV. DEM DATA STRUCTURES

DEM data structures are usually classified as: (i) Rectangular Grids are also known as Computed DEM (Minnesota Department of Natural Resources). Grids are matrix structure that implicitly records topological relation between data points. The data structure of Grid is similar to the array storage structure of digital computers. Raster type DEM is included in it. Raster is a grid of digital, uniform, square cells covering an area on the earth's surface where each cell is given a value of whatever you want to map. In the case of DEMs, each cell is given the elevation value of the land (or water) surface that it overlies. The cells of a given DEM may be almost any size but most frequently are in the range from 5 to 30 meters square. Raster's are relatively fast to process by a computer because the location of each cell can be determined solely from its order value in the grid. Because every vertex in a vector map requires two pieces of data to be located - the x and y - it is slower to process than a raster cell. A raster also represents the values of a continuous surface such as elevation more precisely than vector. A vector contour map shows elevation only at specific intervals represented by the contour lines (e.g. 100 ft, 110 ft, 120 ft). Raster cells, however, show elevation values not only at the specific intervals but in-between them as well (e.g. 100 ft, 101 ft, 102 ft, and 120 ft). (ii) The TIN model was developed as a simple way to build a surface from a set of irregularly spaced points (Peucker et al. 1978). TIN are also known as Measured DEM. They are vector type data. It utilizes digital points, lines and polygons to represent features on the earth's surface (e.g. point: stream gage, line: roadway, polygon: forested area). Every feature in vector format is composed of a set of vertices, each having explicit x and y (or longitude and latitude) location coordinates. TIN include nodes, Edges, Triangles, Topology. The vector advantage is that it is locationally more precise than raster. A point feature in vector format is represented by a single coordinate pair (x, y) which, on the computer screen, is only a pinpoint that has no measurable width. The same point feature represented in raster, however,

would be at least one cell in width (e.g. 30 m). Also, to give a vector map greater resolution is less costly in terms of data storage space than increasing the resolution of a raster map. (Resolution can be measured by the amount of data (i.e. vertices or cells) in a given area.) On a vector map, the number of *vertices* for a set of features may be doubled and this only increases the data storage requirement by two. For a raster map, however, doubling the resolution ups the data storage requirement by four or, in other words, the square of the resolution increase. (iii) Contour is also known as isolines. They are most familiar representation of terrain surface. The accuracy of contour becomes high when they have been captured as primary data from aerial photograph. However in today's scenario Grid & TIN are most widely used data structures to create DEMs. To enhance & extract the exact DEM according to end users need, topographic attributes plays very important role.

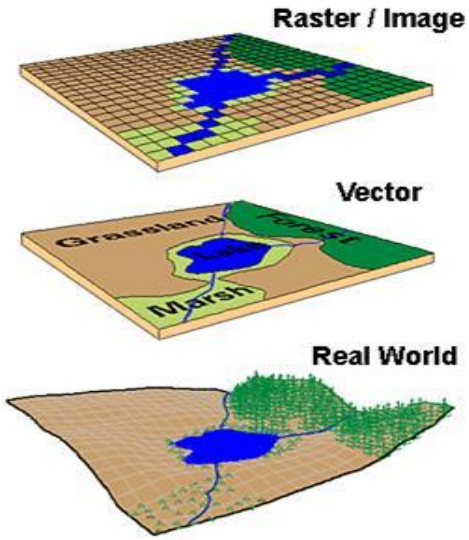

Fig.1.dem data structures

V. DEM DATA SOURCES

Various techniques & methods are used to capture the Terrain data remotely from the surface of the Earth. (i) Aerial & Space Images- Most valuable data source for large scale production of high quality DEM. High precision photographs are taken from metric cameras mounted on aerial planes. By referring fiducial marks of Photograph the center of the photograph can be determined. Mathematically it can be expressed as;

$$1/u + 1/v = 1/f \quad (1)$$

Where, u represents distance between object & lens, v represents distance between the image plane & the lens & f represents the focal length of the lens. To determine the scale of the aerial photograph we can use;

$$1/s = f/H \quad (2)$$

Where H is flying height, f is focal length. (ii) Field Surveying- It involves capturing of terrain directly from surface data by using total station theodolite & GPS. (iii) Existing topographic maps (iv) Photogrammetry- It signifies "measuring graphically by means of light" (Whitemore & Thompson 1966). Fundamental principle behind it is making use of stereo pair of image to construct 3D object & measure the coordinates of object from generated 3D view. Stereo pair can be defined as two images of the same scene captured at two slightly different places to make certain degree of overlap. Each photograph represents six orientation elements, three angular elements (X, Y, Z) along with three translations (geocodic coordinate system). Photogrammetry basically classified as Analog & Digital type. However currently DPW technique also used widely. DPW means Digital Photogrammetric Workstation. In this method when given an image point on the left image, the system will automatically search corresponding point of right image under Image matching process. (v) Radar Interferometry- Synthetic Aperture Radar (SAR) is most widely used technique under this category. SAR is a microwave imaging radar & is based on principle of Doppler frequency shift. The radar source mounted on the flying platform transmits a cone shaped microwave beam to ground continuously & measures reflected energy. In case of Environmental monitoring & reconnaissance of remotely sensed data, SAR Interferometry is best suitable method. It is a signal processing technique which can derive height information by using the interferogram. Interferogram records the phase difference between two complex radars images of the same area taken by two SARs. (vi) Airborne LASER Scanning (LIDAR) - Various experiments demonstrated the Power of using Lasers in remote sensing including lunar laser sensing, satellite laser ranging, atmospheric monitoring, and oceanographic study (Flood 2001). It is an active remote sensing technique. The principle behind LIDAR illustrates that the transmitted electromagnetic energy can be reflected back from the surface of the earth. Depending upon the various objects of the earth the intensity of the scattered light varies which can be used to determine the height of that object. Airborne Laser scanning include: (i) Filtering- It refers to the removal of unwanted measurements such

as erroneous object or obstacles. (ii) Classification- it means to find a specific geometric or statistic structure such as building, vegetation etc. (iii) Modeling- It refers to the Generalization of classified object. (vii) Cartographic Digitization- It is mainly of two type's viz. Vector based & Raster based. There are two modulating schemes used in LIDAR which are useful for obtaining range measurement (i) Pulse Modulation (ii) Sinusoidal continuous wave (CW) Modulation (Baltsavias 1999). Pulse modulation generates rectangular pulse of width from 10 to 15 ns (Wehr & Lohr 1999). The position of point can be calculated by considering distance (d), Laser angle (a) from sensor vertical axis, sensor altitude & sensor position. The distance can be calculated as;

$$t = 2(d / c) \quad (3)$$

Where, t is total elapsed time, d is the path distance or range of the pulse; c is speed of the light. There are four scanning techniques employed in LIDAR; (i) Constant Velocity –rotating mirror- Produce measurement that appear as parallel lines on the ground which removes acceleration type errors in angle observation (ii) Oscillating Mirror- All commercial users like Optech, TopEye uses this system in which the mirror rotates back & forth. As mirror always pointing towards ground the data collection is continuous. (iii) Fiber Optical array- It have fewer & smaller moving parts which increases scanning rate up to great extent. (iv) Palmer / Elliptical Scanner- This method was used in ASLRIS (Hu et al. 1999). Currently there are various commercial LIDAR systems used viz. ALTM 3100, TopoSys Falcon which have operating- 80-3500m, distance resolution-1-2 m, scan width- 0 to 25^0, Scan rate- 20-70 Hz, Effective measurement rate- 5000 to 10,000 per sec etc.

VI. GLOBAL DEMS

It is also known as Global Elevation Data Sources. According to International Steering Committee for Global Mapping (ISCGM), global data is defined as that which meets certain criteria: covers the entire earth, is at a scale of 1:1,000,000 or as resolution of 1 KM & is includes specific core data layers (ISCGM 1996). On the basis of above criteria some of the global elevation data which are used in current applications are enlisted: (i) GLOBE- It is Global Land One Km Base Elevation. It have nominal 1 Km grid, Absolute vertical accuracy of 10 to 500 m. There are plenty of sources like satellite imagery, aerial photography, satellite altimetry, cadastral survey data & hardcopy topographic maps. The Source data can be converted to 16 bit binary raster grids. (ii) DTED- It is Digital terrain elevation database. It is provided by National Imagery & Mapping agency (NIMA). It has resolution of 30 arc seconds (nearly 1 Km). (iii) GTOP30- It is widely used by U.S. It has resolution of 30 arc seconds (1 Km). (iv) SRTM- It is Shuttle Radar Topographic Mission. It is joint project between National Geospatial Agency (NGA) & National Aeronautics & space administration (NASA). It has capability to analyze terrain surface through clouds. It has resolution of 3 arc second (1 arc second= 30 meter).

VII. SPATIAL SCALES FOR DEM

Fine Toposcale- It has resolution about 5-50m.It can be obtained from Airborne & space borne radar & laser, Aerial photography. It is Used in spatial analysis of soil properties, hydrological modeling, Topographic aspect correction of remotely sensed images, study of effects like solar radiation, evaporation etc. (ii) Coarse Toposcale- It has resolution about 50-200m. It can be obtained from contour & stream line data analysis, digitization of data from existing topographic maps etc. It is used in analysis of broader scale distributed parameter hydrological modeling, sub catchment of lumped parameter hydrological modeling etc. (iii) Mesoscale- It has resolution about 200m – 5Km. It can be obtained from surface specific points & streamline data digitized from existing topographic maps. It is used in analysis of surface roughness, continental drainage divisions. (iv) Macro scale- It has resolution about 5-500 KM. It can be obtained from ground surveys, Extraction of data from digitized maps etc. It is used in generation of circulation models.

VIII. SURFACE CLASSIFICATION FOR DEM

Based on representation, continuity, smoothness the DEM surfaces can be classified as: (i) Functional Surface:- It is capable of storing a single Z value for a given (X,Y) locations. Functional Surfaces are used to represent statistical surface describing climate, demographic data, concentration of resources, biological data etc. They can also be used to represent mathematical functions & arithmetic expressions which denotes surface. Ex. Terrain surface of earth (ii) Solid Surface:- They are true 3D models capable of storing multiple Z values for a given (X,Y) location. Ex. Buildings, Bridges, Dams etc. (iii) Continuous Surface:- When approaching a given (X,Y) location on a functional surface from any direction, will get same Z value. It is the type of Functional Surface. (iv) Discontinuous Surface:- Different Z values can be obtained based on direction of approach. Ex. Vertical fault across the surface of the earth. (v) Smooth Surface:- The direction of normal vector remains same irrespective of direction of approach towards specified location. The smoothness property mainly deals with changing surface normal from one location to another. (vi) Rough Surface: - The surface normal varies continuously across the surface. However Surface normal is normal vector to the surface's first derivative usually slope Ex. Ridges, Valleys, Mountains.

IX. FACTORS AFFECTING DEM QUALITY

The quality of a DEM is a measure of how accurate elevation is at each pixel (absolute accuracy) and how accurately is the morphology presented (relative accuracy). These factors are mentioned as below: (i) Accuracy of data source (ii) sampling density (iii) Terrain roughness (iv) Grid resolution which also noted as Pixel size (v) Interpolation Source. The accuracy of source data varies with technique depends upon various techniques used to capture it like active airborne sensors, field surveying etc. Terrain roughness is the representation of characteristics of the surface such as flat, hilly, mountainous etc. Standard deviation of slope, standard deviation of elevation, slope convexity, variability of plan convexity (contour curvature), or some other measure of topographic texture is known as terrain roughness. The sampling density is the number of recorded samples per unit distance. For more accurate & detail terrain data sampling density should be high. Interpolation algorithms also affect quality of DEM. On the basis of some factors like aim of study, required output, type of area like hilly, smooth etc. we can choose best suitable algorithm. Interpolation is a method of constructing new data points within the range of a discrete set of known data points (Thomas K Poikar). Interpolation is required to generate DEMs from surface specific points & from contours & stream line data. Basically DEM interpolation methods classified in two approaches as Global Interpolation Methods like thin plate splines & Local Interpolation methods like IDW, Local Kriging, TIN etc.

X. DEM FILE FORMATS

The DEM format originates from 1992. Starting in 1995, the 7.5-minute USGS DEM data was converted to the newer SDTS format. In 2011, DEM datasets in SDTS format are available for download from GeoCommunity at the GIS Data Depot. Starting in 2006, USGS no longer distributes elevation data in the DEM format. However, USGS elevation data in the DEM format is available from other sources, e.g., WebGIS Terrain Data. Other entities still issue elevation data in the USGS "native". Currently we have four DEM file formats viz. (i) USGS DEM (ii) SDTS DEM (iii) DTED (iv) DIMAP. The USGS DEM standard is a geospatial file format developed by the United States Geological Survey for storing a raster-based digital elevation model. It is an open standard, and is used throughout the world. It has been superseded by the USGS's own SDTS format but the format remains popular due to large numbers of legacy files, self-containment, relatively simple field structure and broad, mature software support. The USGS DEM format is a self-contained (single file) set of ASCII-encoded (text) 1024-byte blocks that fall into three record categories called A, B, and C. There is no cross-platform ambiguity since line ending control codes are not used, and all data including numbers is represented in readable text form. There is no known binary analogue of the format, although it is common practice to compress the files with gzip. Floating-point numbers are encoded using Fortran scientific notation, so C/C++ programs need to swap the "D" exponent-indicating character with "E" when parsing (and vice versa when writing). The A record appears once as the file's header, the C record also appears once as the trailer, and multiple B records (called Profiles) comprise the elevation data. A and C records each fit within one block but a single B record typically requires multiple blocks. When such block-spanning occurs, data is shifted to start cleanly on each block boundary. A records also come in "old" and "new" flavors, because the USGS added several fields to the A record. The fields in the A record hold the origin, type, summary statistics and the measurement systems used by the profiles. One of the key items is the quadrangle, which is a set of four terrestrial coordinates describing the four-sided polygon enclosing the area of interest. B records (profiles) are a variable-length longitudinal column of raster elevations that start at a specified location. They are some multiple of 1024 bytes long and contain a small header summarizing the profile. The elevations are contiguous; breaks or other discontinuities are expressed using "void" elevations of value -32767. Each elevation is described as a six-character readable integer occupying a fixed location in a block. The profile header only appears in the first block, so subsequent blocks hold more elevation values. When reading the DEM file from first byte to last, one reads the profiles as columns from west to east. The elevations within a profile run from south to north. The variable-location and variable-length nature of profiles stems mainly from the use of the UTM (Universal Transverse Mercator) ground reference system. Since measurements within UTM employ fixed distances (e.g., 30 meters between elevation samples), the quadrangle must slightly distort to map such locations onto the spherical Earth. This distortion usually manifests as a rotated square, hence the elevation columns near the east and west edges start more northward and contain fewer samples. The C record contains root-mean squared error (RMSE) quality control data, using ten six-character integer fields. A USGS DEM can be classified into one of four levels of quality. This is due to the multiple methods of data collection, and certainty in the data. The levels are (i) Level 1 which gives DEM series of 7.5 minute & 30 minute (ii) Level 2 which gives all DEM series (iii) Level 3 which gives DEM series of 7.5 minutes (iv) Level 4 which gives all DEM series. SDTS is a standard used to describe earth-referenced spatial data. It was designed to easily transfer and use spatial data on different computer platforms. DTED (or Digital Terrain Elevation Data) is a standard of digital datasets which consists of a matrix of terrain elevation values. This standard was originally developed in the 1970s to support aircraft radar simulation and prediction. Terrain elevations are described as the height above the Earth Gravitational Model 1996 (EGM96) geoid, not the WGS84 reference ellipsoid. DTED supports many applications, including line-of-sight analyses, terrain profiling, 3-D

terrain visualization, mission planning/rehearsal, and modeling and simulation. DTED is a standard National Geospatial-Intelligence Agency (NGA) product that provides medium resolution, quantitative data in a digital format for military system applications that require terrain elevation. The DTED format for level 0, 1 and 2 is described in U.S. Military Specification Digital Terrain Elevation Data (DTED) MIL-PRF-89020B, and amongst other parameters describes the resolution for each level: Level 0 has a post spacing of ca. 900 meters, Level 1 has a post spacing of ca. 90 meters, Level 2 has a post spacing of ca. 30 meters. The precise spacing is defined by dividing the world into zones based on latitude North South as 0^0-50^0, 50^0-70^0, 70^0-75^0, 75^0-80^0, 80^0-90^0. The DIMAP format is the format for SPOT products, introduced for the SPOT 5 launch in May 2002 and developed with CNES. The DIMAP format is a public format for describing geographic data. Although it was specially designed for image data, it can also handle vector data. SPOT products in DIMAP format now consist of two parts, one for the image and the other for a description of the image. (i)Image- By default it is described in GeoTIFF format, consisting of a TIFF part, as TIFF is the most widely used image format in the world, recognised by all software on the market and easily integrated and a Geo part, recognised by all geographic information processing software. It adds georeferencing information for the image file (coordinates in the upper left-hand corner of the image and pixel size) to the basic TIFF file and may also describe the map projection used and its corresponding geographic system (ii) Metadata -This is written in XML. XML, similar to HTML, is more highly structured and allows users to create their own keywords with their corresponding values. It can be read directly by standard Internet browsers and can be linked to an XSL style sheet which sorts and does the HTML layout of the information contained in the XML file.

XI. INTERPOLATION

Interpolation can be defined as “the process of estimating the value of attributes at some sites from measurements made at surrounding point locations which can be denoted as sample points & can be used for reference purpose”. The basic need of Interpolation technique for DEM creation is: (i) Remove the errors due to sampled surface having different level of resolution & Orientation (ii) the sampled elevations need to be transformed from one format to another. (iii) The point data must be converted to surface representation for analysis & modeling purpose. The Interpolation methods can be classified on the basis of criteria’s like: (i) Compatibility between the interpolated elevations at the sampled points & original elevations (ii) The spatial extent of the utilized samples for the estimation of the elevation at a given interpolation point. (iii) The utilized terrain & data characteristics within the Interpolation mechanism. On this basis they are classified as: (i) Exact Interpolation- Estimates an elevation at a reference point location that is the same as the given elevation at that point. It generates a surface that passes through the reference points (ii) Inexact Interpolation- It yields a different elevation value at the reference points when compared to given elevations at that point. The quality of Inexact Interpolation can be determined by statistical difference between the given & interpolated elevations at the sample points. (iii) Global Interpolation- It uses all the available samples to estimate the elevation at the interpolation point. Ex. Kriging, Trend Surface analysis, Fourier analysis (iv) Local Interpolation- It estimates the unknown elevation using nearest sample points. Ex. Triangular Irregular Networking (TIN), Inverse Distance Weighting (IDW) (v) Stochastic Interpolation- It consider statistical properties of the surface like slope, elevation & sampled elevations at the reference points throughout the Interpolation procedure (vi) Deterministic Interpolation- It does not consider the statistical properties of the surface & sampled elevations within the Interpolation mechanism. Few of the most popular Interpolation methods are enlisted below: (A) Triangulation: - Rather than using a grid, the triangulation method defines a surface from irregularly spaced points. This characteristic often results in more accurately defined features. Since triangulation does not average information during interpolation, it is better equipped to deal with data sets with abrupt peaks or changes. The triangulation method can be computed quickly because it uses fewer points than Kriging, but it will not create as smooth of a surface. The formation of TIN based mainly on following 3 aspects (i) Method of Picking sample points which include Flower & Little Algorithmic Method, Very Important point Algorithmic Method & Drop heuristic method. (ii) Method of connection of points to form triangle which include Distance ordering & Delauney Triangulation (iii) Method of modeling surface within each triangle. (Thomas K Poikar). On the basis of above aspects most popular implementations are: (I) Very Important Point Algorithm (VIP)- VIP works by examining the surface locally using a window. This is a simplification of the technique used in ESRI's ARC/INFO. Because of its local nature, this method is best when the proportion of points deleted is low. It is less satisfactory on curved surfaces diagram. Procedure:- (i)Each point has 8 neighbours, forming 4 diametrically opposite pairs, i.e. up and down, right and left, upper left and lower right, and upper right and lower left (ii) For each point, examine each of these pairs of neighbours in turn, connect the two neighbors by a straight line, and compute the perpendicular distance of the central point from this line diagram & average the four distances to obtain a measure of "significance" for the point (iii) Delete points from the DEM in order of increasing significance, deleting the least significant first (iv) This continues until one of two conditions is met: (1) the number of points reaches a predetermined limit (2) the significance reaches a predetermined limit. (II) Delauney Triangulation - 3 points form a Delaunay triangle if and only if the circle which passes through them contains no other point diagram. Procedure:- (i)Partition the map by assigning all locations to the nearest vertex. (ii) The boundaries created in this process form a set of polygons called Thiessen polygons or Voronoi or Dirichlet regions overhead - Delaunay triangles from Thiessen polygons (iii) Two vertices are connected in the Delaunay triangulation if their Thiessen polygons share an edge. This method is preferred for Fat triangles. Convex hull is again an important parameter in TIN. It is formed due to boundary edges of Delaunay network. (B) Spline is a polynomial between each pair of tabulated Points, but one whose coefficients are determined “slightly” non-locally. The non-locality is designed to guarantee global smoothness in the interpolated function up to some order of derivative. Splines are basically of 3 types (i) Linear Spline (ii) Cubic Spline (iii) Simple Spline. Out of

all 3 types' Cubic spline method is more popular. Spline interpolation avoids the problem of Runge's phenomenon, which occurs when interpolating between equidistant points with high degree polynomials. (i) Cubic Spline - The goal of cubic spline interpolation is to get an interpolation formula that is continuous in both the first and second derivatives, both within the intervals and at the interpolating nodes. It will give us a smoother interpolating function. In general, if the function you want to approximate is smooth, then cubic splines will do better than piecewise linear interpolation;

$$f = Afk + Bfk + 1 \quad (4)$$

The problem with a linear function is that, the first derivative is not continues at the boundary between two adjacent intervals, while we want the second derivative to be continuous, even at the boundary. Cubic spline technique is used to generate a function to fit the data. Moreover, it can be shown that data generated by a particular function is interpolated by a spline which behaves more or less like the original function. This is testimony to the consistency of splines (Sky McKinley and Megan Levine). (C) Kriging- The weights are determined according to the distance between the interpolation & reference points as well as the stochastic properties of the surface. The elevation at the interpolation point is determined as a weighted average of the observed elevations at the reference points. Optimal interpolation based on regression against observed *z* values of surrounding data points, weighted according to spatial covariance values. Kriging assigns weights according to a (moderately) data-driven weighting function, rather than an arbitrary function. Simple Kriging, Ordinary Kriging, Cokriging & Arbitrary kriging are some types of Kriging. Kriging Help's to compensate for the effects of data clustering, assigning individual points within a cluster less weight than isolated data points (*or*, treating clusters more like single points). It Gives estimate of estimation error (kriging variance), along with estimate of the variable, *Z*, itself (but error map is basically a scaled version of a map of distance to nearest data point, so not that unique). Availability of estimation error provides basis for stochastic simulation of possible realizations of *Z*(u) (Geoff Bohling 1999).

XII. CONCLUSION

In this paper we proposed all basic information regarding DEM & its applications. Raster DEM is easy to process & extract the DEM due to its Matrix structure which is compatible with current computer systems as compared to TIN. Satellite Photogrammetry can be useful for extraction of high quality of DEM with the help of Remote sensing software's like ENVI, Geomatica etc. while extracting DEM from any source one should consider Scope of work & purpose of extraction & then apply respected Interpolation techniques. There is no "best" interpolation algorithm that is clearly superior to all others & appropriate for all applications. To get best general result for more advanced analysis & visualization use Kriging method while to get fastest result use IDW. In future we are going to implement all basic algorithms like Kriging, IDW, TIN with the help of MATLAB & IDW (Interactive Data Language). Also we are going to extract DEM of same area from two different sources & fuse them to analyze the difference.

ACKNOWLEDGEMENT

This work is part of Digital Elevation Model (DEM) Fusion Project funded by Indian Space Research Organization (ISRO), India.

REFERENCES

Journal Papers:

[1] H. papasaika, D.Poli, E. Balsavias- *A Framework for the Fusion of Digital Elevation Models commission II, WG II/7*

[2] T.Ch. Malleshwara Rao, K.V Rao, A.Ravi Kumar, D.P Rao, B.L Deekshatula- *DTM from IRS satellite data from the overlap area of two adjacent paths using Digital Photogrammetric technique NRSC, PE & RS June 1996*.

[3] Saffet Ergoden *A comparison of Interpolation methods for producing Digital Elevation Models at Fine scale Earth Surf. Process. Landforms 34, 366–376 (2009)*

[4] R.Sunita, K.Kallo *A comparison of geostatistics and fuzzy application for digital elevation model the international archives of the photogrammetry, remote sensing and spatial information sciences, vol. 34*

[5] Tomaz Podobnikar *Methods for visual quality assessment of a digital terrain model S.A.P.I.E.N.S 2.2 | 2009 : Vol.2*

Books:

[6] Naser El-Sheimy Caterina Valeo Ayman Habib, *Digital Terrain Modelling Acquisation, Manpulation & Applications (*Artech House, Incorporated, 2005*)*

[7] Zhilin Li, Qing Zhu, Christopher Gold- *Digital Terrain Modelling Priciples & Methodology* (CRC press 2005)

International Journal of Modern Engineering Research (IJMER)
www.ijmer.com Vol. 3, Issue. 4, Jul - Aug. 2013 pp-2419-2423 ISSN: 2249-6645

Influence choice of the injection nodes of energy source on on-line losses of a distribution network

Houndedako S.[1], Daï Tometin D.[1], Vianou A.[1] Espanet Ch.[2]
[1]*Laboratoire d'Electrotechnique, de Télécommunication et d'Informatique Appliquée (LETIA) Ecole Polytechnique d'Abomey-Calavi, Université d'Abomey-Calavi 01 BP 2009 Cotonou, Bénin.*
[2]*FEMTO-ST Département Energie, Université de Franche-Comté, France. 2, Avenue Jean moulin 90000 Belfort, France*

ABSTRACT: *One of the problems which contribute today to the energy dependence of Benin to more (90%) in 2012 of its own production constitutes the losses, of which on-line losses. Certain more remarkable consequences of this situation constitute the energy low level of cover, the large financial losses for the Distribution firm of Benin (SBEE). The object continued by the authors is to determine with precision, the points of injection of the photovoltaic power stations to connect to the distribution network of the SBEE in order to minimize on-line losses. With this intention, the authors have with the premium on board modeled with software NEPLAN, the network "COTONOU-EST" of the SBEE. They have according to the results obtained with NEPLAN, dimensioned with the software PVsyst the photovoltaic power stations. The behavior of the power stations was studied using Matlab/Simulink. Lastly, the authors determined by simulation with software NEPLAN the points of injection minimizing on-line losses.*

Keywords: *Electrical network, Electrical energy, On-line losses, photovoltaic Energy, Node of injection.*

I. Introduction

The liberalization of the energy sector, but especially the energy problem of deficit very accentuated in certain countries in the process of development like Benin, makes that the managers of the electrical networks connect energy sources dispersed on their distribution network. The form of the sources of production decentralized more in vogue nowadays is that of renewable energies. Indeed, one attends the connection of the photovoltaic and wind power stations more and more on the distribution networks electric, especially in the developed countries. This operation contributes in what relates to them, not only to solve the environmental problems by limiting the gas emissions to greenhouse effect in the respect of conventions of the protocol of Kyoto, but still to reduce the technical losses. Research is made indeed more and more to help the managers of network to reduce on-line losses. There were many studies on the reconfiguration of the distribution networks for the reduction of the losses. An exchange algorithm of switch was proposed in [1]. In [2], an approximate technique of flow of power was developed to analyze the reduction of the losses by the reconfiguration of the network. In [3], Fan and Zhang formulated the problem of reconfiguration like linear problem of programming and applied a method of optimization to only one loop to solve the reconfiguration of network. Other techniques such as the genetic algorithm, and the algorithm of research by colony of ants (ACS) were used for purposes of the reconfiguration of the network to reduce the losses. For the optimal site of condenser "a well-known gold rule," or "rule 2/3" for the reduction of the losses is presented in [4]. This method would bring back good solutions in the system where the loads are uniformly distributed. In distribution systems, the Autonomous Source (AS) can provide part of power active and/or reactive so that the current in the wire is reduced and the profile of tension can be improved with the reduction of the losses. However, the studies indicate that the bad choice of the place and the size would lead to losses higher than the losses without sources of decentralized production [4] and [5]. A technique for the site of AS using the rule "2/3" was presented in [4]. Although the rule of 2/3 is simple and easy to apply, this technique cannot be effective in distribution with the loads not uniformly distributed. It is strong of that it was published useful for the authors of this article to study the influence of the connection of AS in the case of a real distribution network where the loads are not distributed uniformly. Does the geographical location of the point of coupling to a real distribution network of these power stations, have an influence on the losses of the network? To give an exact answer to this question, the authors of this article analyzed the evolution of the losses by connecting a source of autonomous production of 3 MW on the portion of network "Cotonou Est" of SBEE. Software NEPLAN was used as basic tool to evaluate before and after the operations of injection of energy.

II. Material and methodology

2.1. Mathematical formulation of the objective to be optimized

The problem of optimization is related to one or more objectives which one tries to minimize (or to maximize). The main objective here is the minimization of the Joules losses. The authors expressed this objective by mathematical expressions which are integrated in the algorithms of optimization.

2.2. The losses Joules

The reduction of the Joules losses becomes a priority for the operators of distribution networks, especially in a deregulated and competing context. A minimization of the losses allows a reduction of the costs of energy distribution and involves an increase in the margins of transit on the electric lines as well as an improvement of the profile of voltage. To express this objective in an algorithm of optimization, the authors used the following expression:

$$f_{objectif} = \sum_k R_k . I_k^2 \quad (1)$$

where: R_k : the resistance of the branch K;

I_k: the module of the complex current in the branch K;

To minimize the expression (1) led to a reduction of one of the costs of exploitation.

2.3. Formulation of the constraints of safety

The constraints of safety are the constraints related to the voltage on the level of each node of the network and with the currents on each branch of the network.

2.3.1. Amplitude of the voltage

Concerning the amplitude of the voltage, each company of electricity is held to respect an interval in which the voltage can vary during the exploitation by taking account of the regulations of the international standards. It is necessary thus, when one seeks a network configuration, that the voltage in each node is included/understood between $V_{nominal} = \pm 5\ \%$ for HV distribution network and $U_{nominal} = +6$ and $-10\ \%$ for LV network (according to the European standards and French in particular). This constraint is expressed in the following way:

$$\frac{V_{in} - V_i}{V_{in}} < \varepsilon_{i\ max} \quad (2)$$

where : V_{in} : nominal voltage to node i

V_i : module of voltage to node i

$\varepsilon_{i\ max}$: variation of maximum voltage acceptable

In general, in the distribution networks, the loads are inductive. We thus observe voltage drops rather than of rises. However, the connection of the independent producers leads to local rises in voltage which could exceed the acceptable limits.

2.3.2. Acceptable currents

Another constraint of safety is related to the currents on the branches which should not exceed the acceptable maximum currents in permanent mode, guaranteed by the manufacturers. We express this constraint in the form:

$$\frac{|I_j|}{I_{j\ \max\ adm}} < 1 \quad (3)$$

where I_j: the current on the branch j

$I_{j\ \max\ adm}$: the acceptable maximum current in the branch j

2.4. Representation of the network "Cotonou Est"

The network "Cotonou Est" of SBEE is the electrical network of the city "Cotonou", which feed the feeders of the source station of Akpakpa. It now comprises 230 transformers HV/LV) and 620 nodes.

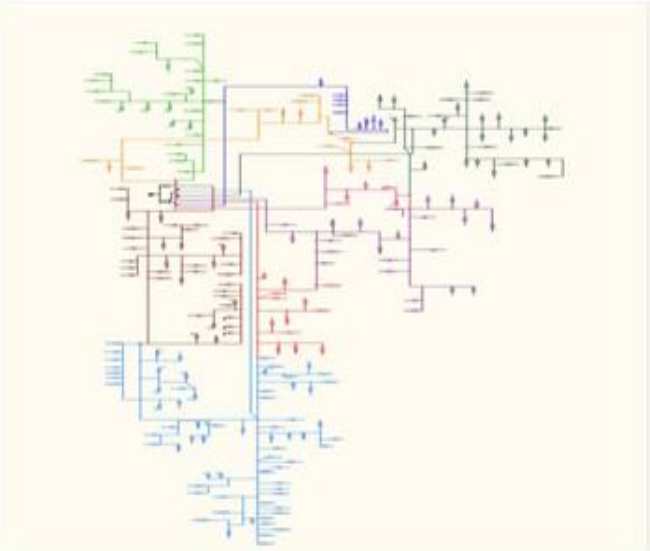

Figure 1: Network "Cotonou Est" SBEE

2.5. Modeling of the source station of Akpakpa with software NEPLAN

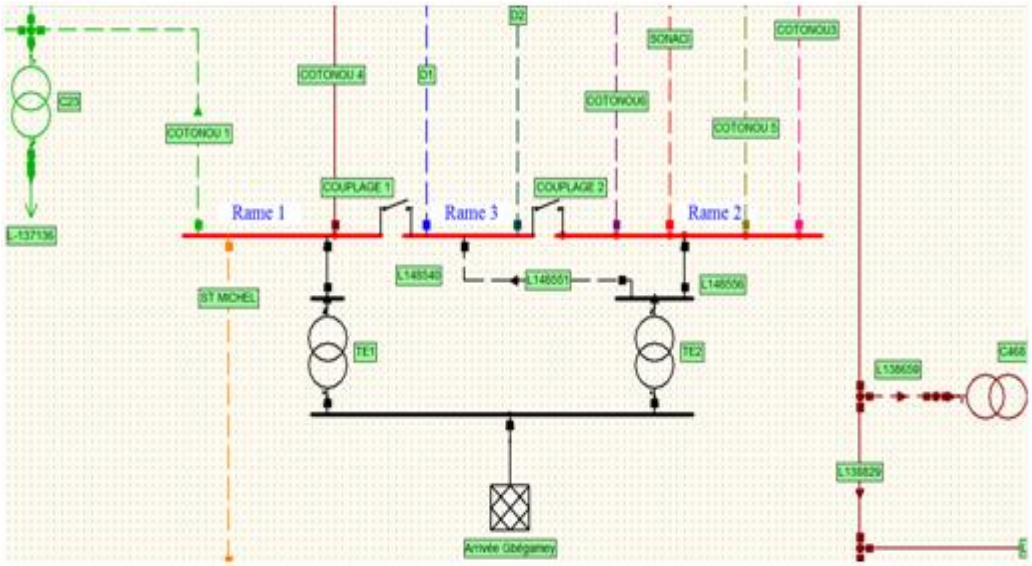

Figure 2: Source station of Akpakpa

The source station of Akpakpa have three (03) main nodes (Rame1, Rame2, Rame3), supplied with two named transformers HV/LV TE1 of power 20 MVA and TE2 of power 31,5 MVA. In normal circumstances of exploitation, when no coupling is closed, TE1 feeds Rame1, while TE2 feeds Rame2 and Rame3. There is a possibility of coupling Rame1 and Rame3 by closing the switch of coupling 1, Rame2 and Rame3 by closing the switch of coupling 2.

The source station of Akpakpa has 9 feeders which are: Cotonou1, Cotonou3, Cotonou4, Cotonou5, Cotonou6, St Michel, D1, D2 and Sonaci

Simulation and validation of the model with software NEPLAN

To validate the model, the authors have:

- compared the total load simulated by feeder, with the series of measurement of the loads by transformers on each feeder;
- compared the simulated value of the total power factor by feeder with the power factor measured during the series of measurement

Table 1, presents the comparison between the simulated values and the actual values:

Table 1: Comparison between real consumption and that simulated by feeder

	Real consumption			Simulated consumption			|Ecart| en %		
	P (MW)	Q (MVAR)	Cos Φ	P (MW)	Q (MVAR)	Cos Φ	P	Q	Cos Φ
Total	24.18	13	0.887	24.6	13.728	0.88	1.7	5.3	0.8
St Michel	2.0	1.3	0.85	1.81	1.074	0.86	9.5	17.4	1.2
Cotonou 1	3.1	1.6	0.90	3.632	1.861	0.89	14.6	14	1.1
Cotonou 4	2.1	1.4	0.84	4.011	2.38	0.86	47.6	41.2	2.3
Cotonou 5	2.5	0.8	0.95	2.169	0.857	0.93	13.2	6.7	2.1
Cotonou 6	1.6	0.9	0.84	2.335	1.508	0.84	31.5	40.3	0
SONACI	0.9	0.1	0.96	2.296	0.575	0.97	60.8	82	1
D1	5.3	2.5	0.90	3.227	1.375	0.92	39.1	45	2.2
D2 Cotonou 3	6.6	3.6	0.86	5.4 0.685	3.06 0.271	0.87 0.93	18.2	15	1.1
TE 1	7.5	4.6	0.85	9.425	6.334	0.83	20	22.6	2.3
TE 2	17.1	8.2	0.90	16.036	4.973	0.89	6.2	39.3	1.1

It is thus noted that the difference between the simulated model and the real model is very weak overall when one carries out an analysis of the 'Total' line `' of table 1. The few strong variations noted on certain feeders are prone state of the switches on the network. We can validate our model from these results. Then, the authors carried out the calculation of load flow in the network studied before the connection of the autonomous source of production.

2.6. Power sum

The Power sum before the connection of the autonomous power station of production of 3 MW is presented in the table the 2 as well as losses per level of voltage.

The total active losses of the network rise to 1062 kW, for a load of 24.51 MW, while the total power in the network is evaluated to 25.573 MW.

Table 2: Load flow in the network "Cotonou Est" in its actual position (before injection energy of autonomous source)

TOTAL POWER SUM						
	P losse MW	Q losse MVar	P imp MW	Q imp MVar	P load MW	Q load MVar
Network« Cotonou Est »	**1.062**	**5.273**	**25.573**	**15.721**	**24.511**	**10.448**
POWER SUM BY LEVEL OF VOLTAGE						
Un (kV)	P_online_losses (MW)	Q_ online_losses (MVar)	P_transfo_losses (MW)	Q_transfo_losses (MVar)		
15	0.54	0.214	0.42	2.025		
63	0	0	0.102	3.034		

The Power sum by feeder is in table 3. The active losses of the feeder D1 on which we connected the autonomous source raise to 346 kW.

Table 3: Power sum by feeder

POWER SUM BY FEEDER						
Node	Feeder	P losse	Q losse	P imp	Q imp	P load	Q load
Rame 1	COTONOU1	0.086	0.296	3.603	1.795	3.517	1.498
Rame 1	COTONOU4	0.057	0.284	2.615	1.666	2.558	1.382
Rame 1	ST MICHEL	0.04	0.126	1.656	0.999	1.616	0.872
Rame 2	COTONOU3	0.008	0.049	0.458	0.14	0.45	0.091
Rame 2	COTONOU5	0.046	0.139	2.144	0.665	2.098	0.526
Rame 2	COTONOU6	0.06	0.198	2.463	1.362	2.403	1.164
Rame 2	SONACI	0.022	0.078	1.193	0.244	1.171	0.167
Rame 3	**D1**	**0.346**	**0.637**	**5.621**	**2.722**	**5.275**	**2.085**
Rame 3	D2	0.293	0.43	5.716	3.094	5.423	2.664

III. Results

3.1. Evolution of the losses by simulation of the injection point on the feeder D1

By varying the node of connection of a Dispersed Energy Source (DES) of 3 MW, we obtain the evolution of losses on the nodes of the longest line of the feeder D1. According to the power sum recapitulated in table 2, the power imported on the feeder D1 is of 5.621 kW.

Figure 3 gives the profile of losses according to the distances compared to the source station of Akpakpa.

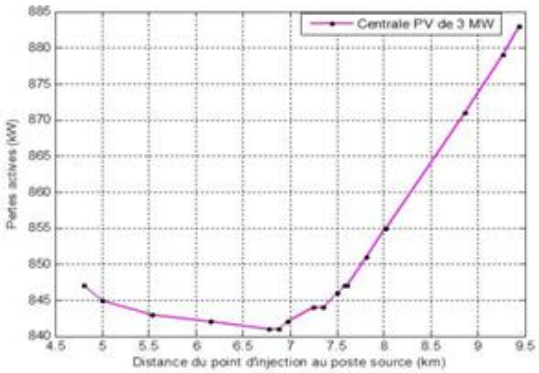

Figure 3: Evolution of the losses with the change of the point of injection on D1

For better appreciating the influence of the choice of the point of injection on on-line losses, the authors, not only chose various nodes of connection, but also varying the power of the DES. The results of simulation are related to figure 4:

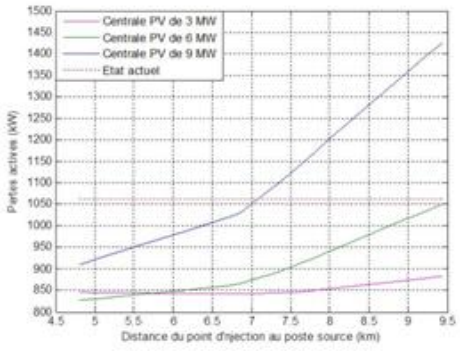

Figure 4: Evolution of the losses with the change of the point of injection on D1 for various powers of DES

IV. Discussion

The losses thus evolve from 841 to 883 kW on figure 3 for a total loss of 1.062 MW on the whole of the network, that is to say a maximum profit in power of 42 kW in HTA. Thus, we can reduce the power forwarded up to 42 kW by judiciously choosing the point of connection for an injection of 3 MW on the feeder D1, value which is lower than the power imported on this departure (5.621 kW) in the actual position of the network. The losses were minimized when we made connection with a node located at approximately 6.8 km of the source station of Akpakpa (figure 3).

An interpretation of this figure leads us to affirm with certainty that an electrical network admits a "center of load" which is function of the load-distribution in the network. When an injection of power is made with the node center, the losses are then minimized.

The analysis of the compared evolution of on-line losses (figure 4) according to the node of connection shows that on-line losses evolve proportionally with the power of the additional source, when this one is higher than the power imported on the feeder concerned. In this case, the center of the loads moves at the head of feeder. Thus, when the power of the autonomous source is higher than the imported power of the feeder on which it will be connected, connection must be made with the nodes at the head of feeder to minimize on-line losses. But when the connected power is lower than the imported power, it is important to seek the center of the loads which is not any more at the head of feeder. Figure 4 also shows us that the losses can become much more important than they are it in the actual position of the network, when the power injected is higher than the power imported on the feeder in the initial state of the network. It comes out the importance from it to decentralize the autonomous sources of production, by distributing the total power to inject in several small powers not to increase the rate of losses on the feeders.

V. Conclusion

We analyzed in this article, the influence of the choice of the injection nodes of the autonomous sources on the losses of the network "Cotonou Est" while using the simulation software NEPLAN with various values of powers from 3 to 9 MW exits of our photovoltaic power stations. The feeder D1 was retained on the network for our simulation, thus, it was determined the suitable node of connection for which the losses are minimized on the network "Cotonou Est", i.e. to 6.8 km of the source station.

Apart from the minimization of on-line losses, the injection of the DES will make it possible to make up the energy deficit of Benin which currently knows a dependence of more than 90% of its energy need.

For a number of seven inhabitants per hearth on average, requiring according to a publication of UNDP of 0.99 kW energy per hearth, this recovery of loss of electrical energy of 42 kW can be used for supplying approximately 42 additional hearths and thus contributing the policy of reduction of poverty to the Benin.

REFERENCE

[1] Civanlar S., Grainger J. J., Yin H., and Lee S. S. H., Distribution feeder reconfiguration for loss reduction, IEEE Transactions on Power Delivery, vol. 3(3), 1988, 1217 1223.
[2] Baran M. E. and Wu F. F., Network reconfiguration in distribution systems for loss reduction and load balancing, IEEE Transactions Power Delivery, vol. 4(2), 1989, 1401–1407.
[3] Fan J. Y., Zhang L., and McDonald J. D., Distribution network reconfiguration: single loop optimization, IEEE Transactions Power Systems, vol. 11(3), 1996, 1643–1647.
[4] Schmill, J. V., Optimum size and location of shunt capacitors on distribution feeders, IEEE Transactions Power Apparatus Systems, vol. PAS-84(9), 1965, 825–832.
[5] Acharya N., Mahat P.and Mithulananthan N., An analytical approach for DG allocation in primary distribution network, Electrical Power and Energy Systems, vol. 28, 2006, 669–678.
[6] T. Ackermann, G. Andersson, and L. Soder, Distributed generation: A definition, Elect. Power Syst. Res., vol. 57, 2001, 195–204.
[7] N. Hadjsaid, J. Canard, and F. Dumas, Dispersed generation impact on distribution networks, IEEE Comput. Appl. Power, vol. 12(2), Apr. 1999, 22–28.
[8] Peter. Daly, Understanding the potential Benefits of DG on Power Delivery System, a paper presented at Rural Electric Power conference 2001, Little Rock, Arkansas, 2001.
[9] P. Chiradeja, Benefit of distributed generation: A line loss reduction analysis, in Proc. IEEE-Power Eng. Soc. Transmission and Distribution Conf. Exhib.: Asia and Pacific, Dalian, China, Aug. 15–17, 2005.
[10] Chiradeja, Ramkumar , An Approach to quantify the Benefits of Distrributed Generation Systems, IEEE trans. On Energy Conversion, Vol. 19, Dec 2004, 764 – 773.

International Journal of Modern Engineering Research (IJMER)
www.ijmer.com Vol. 3, Issue. 4, Jul - Aug. 2013 pp-2424-2428 ISSN: 2249-6645

A Review Paper on Fingerprint Image Enhancement with Different Methods

Purneet Kaur[1], Jaspreet Kaur[2],
[1]*Student of Baba Banda Singh Bahadur Engineering College, Fatehgarh*
[2]*Assist.prof.of Baba Banda Singh Bahadur Engineering College, Fatehgarh*

Abstract: *Image enhancement plays an important role in Fingerprint Recognition System. In this paper, we study the different techniques of enhancement of a fingerprint image in which have been used in previous work. There are so many techniques for enhancement which uses so many different image processing approaches. During study some approaches are found in spatial domain, frequency domain, some are neural network based and some are fuzzy based. Most of the fingerprint techniques use contextual filters or multi-resolution filters whose parameters depends on the local ridge frequency and orientation .The main drawback of these methods lie in the fact that false estimate of local ridge direction will lead to poor enhancement. But the estimate of local ridge directions is unreliable in the areas corrupted by noise where enhancement is most needed.*

I. INTRODUCTION

Fingerprints are today the most widely used biometric features for personal identification. Most automatic systems for fingerprint comparison are based on minutiae matching [11]. Minutiae characteristics are local discontinuities in the fingerprint pattern which represent terminations and bifurcations. A ridge termination is defined as the point where a ridge ends abruptly. A ridge bifurcation is defined as the point where a ridge forks or diverges into branch ridges (Fig. I). Reliable automatic extracting of minutiae is a critical step in fingerprint classification. The ridge structures in fingerprint images are not always well defined, and therefore, an enhancement algorithm, which can improve the clarity of the ridge structures, is necessary. Skin on human fingertips contains ridges and valleys which together forms distinctive patterns. These patterns are fully developed under pregnancy and are permanent throughout whole lifetime. Prints of those patterns are called fingerprints. Injuries like cuts, burns and bruises can temporarily damage quality of fingerprints but when fully healed, patterns will be restored. Through various studies it has been observed that no two persons have the same fingerprints, hence they are unique for every individual.

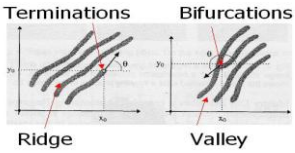

Fig(1.1)Ridge and valley structure


Fig(1.2)Fingerprint

II. Why we need enhancement of fingerprint before minutiae extraction?

The performance of minutiae extraction algorithm is heavily depends upon the quality of input image. In fingerprint image minutiae can be precisely located from the thinned ridges.

However, in practice due to the factor of sensor environment and state of human finger, a significant percentage of acquired fingerprint image is of poor quality. The ridge structure in poor quality image is always not well defined so that they cannot be detected correctly. Otherwise this will lead to the following problems, which can be:

a) A significant number of unreliable minutiae pattern can be created.
b) A large percentage of genuine minutiae can be ignored.
c) We will get false matching results.

So, In order to avoid these problems this is necessary to use enhancement algorithm which can improve the quality of the image.

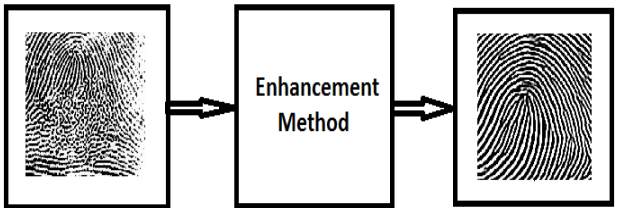

Fig.(2.1) Enhancement method

The reason for performing enhancement (2.1) is to eradicate the noise in the fingerprint images, Illuminate the parallel ridges and valleys. The efficiency of fingerprint image enhancement algorithm is greatly depends on the quality of the fingerprint images. In order to obtain robust performance of a finger print image enhancement algorithm, that can improve the transparency of the ridge structures, is very essential.

The main objective of fingerprint image enhancement is to improve the ridge characteristics of the image, as these ridges carry the information of characteristics features required for minutiae extraction. Ideally, in a well-defined fingerprint image, the ridges and valleys should alternate and flow in a locally constant direction. This regularities facilitates the detection of ridges and consequently allow minutiae to be precisely extracted from the thinned ridges. Thus, the corruption or noise has to be reduced through image enhancement techniques to get enhanced definition of ridges against valleys in the fingerprint images.

2.1Fingerprint enhancement can be conducted on either

1) Binary ridge image
2) Gray level image

Binary ridge image is an image where all the pixel values assigned to one and non pixel values are assigned to zero. The binary image is obtained by applying minutiae extraction algorithm on a gray level fingerprint image. In binary ridge image, a number of simple heuristics can be used to differentiate the spurious ridge configuration from the true ridge configuration since ridge and valley in the image run parallel to each other in a local neighborhood.

Gray level image is a image in which ridge and valleys form a sinusoidal-shaped plane wave which has a well defined frequency and orientation. A number of techniques that can take the advantage of this information that is used for the enhancement of the gray level image.

As we said most of the techniques use contextual filter and multi-resolution filter. But these methods also have some limitations in terms of that false estimate of local ridge direction will lead to poor enhancement. One another method which is pixel wise method, it is the simpler method Common operations include normalization, intensity transformations, histogram processing, image subtraction, image averaging. Good enhancement results can be achieved exploiting pixel-wise methods as pre-processing in advanced fingerprint recognition algorithms. Image enhancement techniques can be divided into two broad categories and Normally, enhancement techniques use various combinations of methods from these two categories. 1. Spatial domain methods. 2. Frequency domain methods.

Spatial domain refers to the image plane itself, and image processing methods in this category are based on direct manipulation of pixels in an image. Spatial domain above can be denoted by the expression:

$$g(x,y) = T[f(x,y)] \quad \ldots\ldots\ldots\ldots\ldots\ldots (1)$$

Where f (x,y) is the input image, g (x,y) is the output image and T is an operator on defined over a neighborhood of point (x,y).

Frequency domain This method consists of modifying the Fourier transform of an image and then computing the inverse transform [Discrete Fourier Transform (DFT)] to get back to input image .Thus given a digital image f (x,y), of size M x N, the basic filtering equation in which we are interested has the form:

$$g(x,y) = \Im^{-1}[H(u,v)F(u,v)] \quad \ldots\ldots (2)$$

Where $\Im^{-1}$ is the IDFT, F (u,v) is the DFT of the input image f (x,y), H (u,v) is the filter function and g (x,y) is the filtered output image. Specification of H (u,v) is simplified considerably by using functions that are symmetric about the center. This is accomplished by multiplying the input image by (-1) x+y prior to computing its transform.

III. Fingerprint Enhancement Methods

There is not any particular method of image enhancement. There are numerous techniques are available for fingerprint enhancement we need to choose between the choices of algorithms. When an image is processed the viewer is the judge who can decide how well a particular methods works. There have existed a variety of research activities along the ability of reducing noises and increasing the contrast between ridges and valleys in the gray-scale fingerprint images

3.1 Algorithm for Enhancing Fingerprint Images (B. G. Sherlock, D. M. Munro, and K. Millard) [1994]

In his proposed method Sherlock et al. [1] has described finger print image enhancement, based on non-stationary directional Fourier domain filtering. Fingerprints smoothed using directional filter and orientation is matched to local ridge orientation. The enhancement consists of filtering followed by thresholding stage. Filtering produces directionally smoothed version of the image from which most of the unwanted information has been removed. Thresholding yields the binary enhanced image. Experiment result leads to significant improvement in speed and accuracy of AFIS.

3.2 Fingerprint Image Enhancement: Algorithm and Performance Evaluation (L.Hong, Y.Wan & A.Jain)[1998]

L. Hong et al. [9] have developed a fingerprint enhancement algorithm in the minutiae extraction module. They incorporated a fast fingerprint enhancement algorithm, which can adaptively improve the clarity of ridge and valley structures of input fingerprint images based on the estimated local ridge orientation and frequency, was applied. Based on the local orientation and ridge frequency around each pixel, the Gabor filter is applied to each pixel location in the image. The performance of the image enhancement algorithm was evaluated using the goodness index of the extracted minutiae and the accuracy of an online fingerprint verification system. Experimental results show that incorporating the enhancement algorithm improves both the goodness index and the verification accuracy.

3.3 Hybrid Fuzzy Logic and Neural Network Model For Fingerprint Minutiae Extraction (Vijay Kumar Sagar and Koh Jit Beng Alex) [1999]

The presented research based on fuzzv- neuro technology in automated fingerprint recognition for the extraction of fingerprint features, known as minutiae. The work presented here is carried out earlier. In this research three minutiae extraction techniques presented are: classical approach, fuzzy approach and fuzzy neural approach. The hybrid fuzzy and neural network model performs the minutiae extraction in two stages, a fuzzy front-end and a neural back-end. Experiment results shows that using the fuzzy neural hybrid model, fingerprint minutiae extraction is more accurate since fewer false minutiae and more true minutiae are identified.

3.4 Fingerprint Image Enhancement using Filtering Techniques (S Greenberg, M. Aladjem, D. Kogan and I. Dimitrov) [2000]

S.Greenberg et al. [11] has proposed two methods for fingerprint image enhancement. The first one is based on using local histogram equalization, Wiener filtering, and image binarization. The second method is carried out by a unique anisotropic filter for direct grayscale enhancement. The results achieved are compared with those obtained through some other methods. Both methods show some improvement in the minutiae detection process in terms of either efficiency or time required.

3.5 New Enhancement Algoithm for Fingerprint Images (Byung-Gyu Kim, Han-Ju Kim and Dong-Jo Park) [2002]

Kim et al. [2] presented an improved algorithm for enhancement of fingerprint image on the basis of the image normalization and Gabor Filter. Firstly, the adaptive normalization based on block processing is suggested for improvement of fingerprint images. An input image is partitioned into sub-blocks with the size of K x L at first and the region of interest (ROI) of the fingerprint image is acquired. Secondly, a new technique for selection of two important parameters of Gabor filter is devised. The proposed algorithms were tested with NIST fingerprint images and show significant improvement in the experiments

3.6 A modified Gabor filter design method for fingerprint image enhancement (Jianwei Yang, Lifeng Liu, Tianzi Jiang,Yong Fan) [2003]

In this research work has proposed a novel filter design method for fingerprint image enhancement[5]. Yang developed an improved version of the TGF, called the modified Gabor filter (MGF). The modification of the TGF made the MGF more accurate in preserving the fingerprint image topography. The remarkable advantages of the MGF over the TGF consist in preserving fingerprint image structure and achieving image enhancement consistency. Experimental results indicate that the proposed MGF enhancement algorithm can reduce the FRR of a fingerprint matcher by approximately 2% at a FAR of 0.01%.

3.7 Fingerprint image Enhancement method using directional median Filter (Chaohong Wu, Zhixin Shi and Venu Govindaraju) [2004]

Chaohong Wu et al. [3] proposed a new approach to fingerprint image enhancement, which is based on integration of Anisotropic Filter and directional median filter (DMF). DMF join broken fingerprint ridges, fill out the holes of fingerprint images, smooth irregular ridges and remove some annoying small artifacts between ridges. Experiment results show that Gaussian-distribute noises are reduced by Anisotropic Filter and impulse noises efficiently by DMF.

3.8Fingerprint Enhancement and Matching by Genetic Algorithms (Xuejun Tan, Bir Bhanu)[2005]

In this paper, Xuejun Tan et al. propose a fingerprint-matching approach based on genetic algorithms (GA), which tries to find the optimal transformation between two different fingerprints. Enhancement has done by the the following steps: Block direction, computation, smoothing, segmentation and binarization. In order to deal with low-quality fingerprint images, which introduce significant occlusion and clutter of minutiae features, they design a fitness function based on the local properties of each triplet of minutiae. The experimental results on National Institute of Standards and Technology fingerprint database, NIST-4, not only show that the proposed approach can achieve good performance even when a large portion of fingerprints in the database are of poor quality, but also show that the proposed approach is better than another approach, which is based on mean-squared error estimation.

3.9 Adaptive Fingerprint Binarization by Frequency Domain Analysis (J. Strom Bartunek, M. Nilsson, J. Nordberg and I. Claesson) [2006]

J.S. Bartunek et al. [6] proposed a new method for fingerprint enhancement by using directional filters and binarization. They derived a technique where the proper size of the local area is automatically determined for each individual fingerprint. Frequency analysis is also carried out in local area to design directional filters. The proposed algorithm was tested on numerous fingerprint images taken from the different databases. The proposed adaptive fingerprint binarization algorithm shows a good ability to tune itself to each fingerprint image.

3.10 Fingerprint Image Enhancement Using STFT Analysis (Sharat S. Chikkerur, Alexander N. Cartwright and Venu Govindaraju) [2007]

S. Chikkerur et al. [12] introduced a new approach for fingerprint enhancement based on Short Time Fourier Transform (STFT) Analysis. STFT is a well known technique to analyze non-stationary signals. The algorithm estimates all

the intrinsic properties of the fingerprints such as the foreground region mask, local ridge orientation and local frequency orientation. Chikkerur compared the presented approach to other filtering method and showed that their technique performs efficiently. They also objectively measured the improvement in recognition rate due to enhancement and obtained a 17% improvement in the recognition rate on a set of 800 images from the FVC2002 database.

3.11Image Enhancement for Fingerprint Minutiae- Based Algorithms Using CLAHE, Standard Deviation Analysis and Sliding Neighborhood [2008]

Sepasian et al. [10] presented a method to investigate the performance of a three-step procedure for the fingerprint enhancement, using CLAHE (contrast limited adaptive histogram equalization) together with Clip Limit, standard deviation and sliding neighborhood as stages during processing of the fingerprint image. In first step CLAHE with clip limit is applied to enhance the contrast of the small tiles to eliminate the artificially induced boundaries existing in the fingerprint image. In a second step, the image is decomposed into an array of distinct blocks and the discrimination of the blocks is obtained by computing the standard deviation of the matrix elements to remove the image background and obtain the boundaries for the region of interest. In final step by using a slide neighborhood processing, an enhancement of the image is obtained by clarifying the Minutiae in each specific pixel, process known as thinning. The analysis of its possible advantages is carried out through a simulated investigation.

3.12 An enhancement algorithm for low quality fingerprint image based on edge filter and Gabor filter (Xue Jun-tao, Liu Jie & Liu Zheng-guang) [2009]

Jun-tao et al. [16] proposed an enhancement algorithm based on edge filter and Gabor filter. In first step, a gray based algorithm is used to enhance the edge and segment the image. Then a multilevel block size method is used to extract the orientation field from segmented fingerprint image. In final step, Gabor filter is used to fulfill the enhancement of the fingerprint image. The experiment results show that the proposed enhancement algorithm is effective than the normal Gabor filter algorithm. The fingerprint image enhance by the algorithm has better enhancement effect.

3.13 On Latent Fingerprint Enhancement (SoweonYoon, Jianjiang Feng and Anil K. Jain) [2010]

Yoon et al. [13**]** proposed a latent fingerprint enhancement algorithm which requires manually marked region of interest (ROI) and singular points. The core of the proposed enhancement algorithm is a novel orientation field estimation algorithm, which fits orientation field model to coarse orientation field estimated from skeleton outputted by a commercial fingerprint SDK. Experimental results on NIST SD27 latent fingerprint database indicate that by incorporating the proposed enhancement algorithm, the matching accuracy of the commercial matcher was significantly improved.

3.14 A New Framework for improving low Quality Fingerprint Images (J. Choudhary, Dr.S. Sharma, J.S. Verma) [2011]

This method present a fingerprint image enhancement method which can adaptively improve the clarity of ridge and furrow structures of input fingerprint image based on the frequency and spatial domain filtering, local orientation estimation, local frequency estimation and morphological operation. The proposed Enhancement algorithm is tested on 100 fingerprint images which are selected randomly and without repetition from database DB-finger to evaluate the efficiency. There set of operation applied on the database DB-Finger that Improve the quality of fingerprint Image.

3.15 An Efficient Fuzzy Based Filtering Technique for Fingerprint Image Enhancement (K. Srinivasan and C. Chandrasekar) [2012]

K. Srinivasan et al. [8] developed an efficient fingerprint enhancement technique via fuzzy based filtering. In his work they employed a fuzzy modeling approach for removing the noise as well as for improving the luminosity of the ridges. Moreover, the fuzzy filter values are evaluated and superior results are produced in the image domain. The probabilities of gray values are measured from the position of the input image pixel. The proposed technique is implemented in MATLAB. The quality of the reconstructed images is determined by measuring the PSNR of FVC2002 fingerprint database. The proposed fingerprint enhancement system using fuzzy based filtering techniques gives high PSNR and low MSE when compared to the Gabor filtering based fingerprint enhancement method.

3.16 Fingerprint Image Enhancement: Segmentation to Thinning (I. G. Babatunde, A. O.Charles, A. B. Kayode and O. Olatubosun) [2012]

I.G. Babatunde et al. [9] modified some of the submodels of an existing mathematical algorithm for the fingerprint image enhancement to obtain new and improved versions. The new versions consist of different mathematical models for fingerprint image segmentation, normalization, ridge orientation estimation, ridge frequency estimation, Gabor filtering, binarization and thinning. The implementation was carried out in an environment characterized by Window Vista Home Basic operating system as platform and Matrix Laboratory (Matlab) as frontend engine. The results show that the modified sub-models perform well with significant improvement over the original versions. The results also show the necessity of each level of the enhancement.

IV. CONCLUSION

During this different techniques of fingerprint enhancement of fingerprint are studied. Most of the existing enhancement techniques are based on Gabor filter. Gabor filters are both frequency and orientation selective tuned by ridge

direction and ridge frequency. It works on both spatial and frequency domains. The main drawback of these methods lies in the fact that false estimate of local ridge direction will lead to poor enhancement. Gabor filter is time consuming and parameter selection such as ridge centre frequency, radial bandwidth and central orientation, requires am empirical setup. There are also some more techniques for this purpose such as normalization, ridge orientation estimation, ridge frequency estimation, region of interest extraction, block direction, computation, segmentation, filtering, binarization, morphological thinning then the final step minutiae extraction and matching. Techniques using histogram equalization which is followed by binarization with further preprocessing gives very good results and consumes less time as compared to Gabor filters.

REFERENCE

[1] B. G. Sherlock, D. M. Munro, and K. Millard, "Algorithm for Enhancing Fingerprint Images," Electronics Letters,Vol. 28, no. 18, pp. 1720-1721, 1994.
[2] Byung-Gyu Kim, Han-Ju Kim and Dong-Jo Park, "New Enhancement Algorithm for Fingerprint Images", IEEE proceedings,Vol.4651,no.2,pp. 1051- 1055, 2002
[3] Chaohong Wu, Zhixin Shi and Venu Govindaraju, "Finger print image Enhancement method using directional median Filter", Elsevier Science, pp. 250- 256, 2004
[4] I. G. Babatunde, A. O.Charles, A. B.Kayode and O. Olatubosun,"Fingerprint Image Enhancement: Segmentation to Thinning",IJACSA,Vol.3,no.1,pp.15-24,2012.
[5] J. Yang, L. Liu, T. Jiang, Yong Fan, "An improved method for extraction of fingerprint features" In: Proc. 2nd ICIG, SPIE, Vol. 4875, no.1, pp. 552–558, 2003.
[6] J. Strom Bartunek, M. Nilsson, J. Nordberg and I.Claesson, "Adaptive Fingerprint Binarization by Frequency Domain Analysis", IEEE transaction,pp.598-602,2006
[7] J. Choudhary, Dr.S. Sharma, J.S. Verma, "A New Framework for improving low Quality Fingerprint Images", IJCTA, Vol.2, no.6, pp. 1859 -1866,2011.
[8] K. Srinivasan, C. Chandrasekar,"An Efficient Fuzzy Based Filtering Technique for Fingerprint Image Enhancement", AJSR,ISSN 1450-223X, no.43, pp. 125-140, 2012
[9] L. Hong, Y. Wan, A. Jain, "Fingerprint Image Enhancement: Algorithm and Performance Evaluation", IEEE Trans. Pattern Analysis & Machine Intelligence, Vol. 20, no.8, pp.777-789, 1998.
[10] M. Sepasian, W. Balachandran and C. Mares, "Image Enhancement for Fingerprint Minutiae- Based Algorithms Using CLAHE, Standard Deviation Analysis and Sliding Neighborhood", WCECS, pp.1199-1203, 2008.
[11] S. Greenberg, M Aladjem, D Kogan, and I Dimitrov, "Fingerprint image enhancement using filtering techniques", ICPR, Vol. 3, pp. 326–329, 2000.
[12] Sharat S. Chikkerur, Alexander N. Cartwright and Venu Govindaraju, "Fingerprint Image Enhancement using STFT Analsis",Pattern Recognition,Vol.40,pp. 198-211,2007.
[13] Soweon Yoon, Jianjiang Feng and Anil K. Jain, "On Latent Fingerprint Enhancement",Michigan State University, MI 48824, USA,2010
[14] Vijay Kumar Sagar and Koh Jit Beng Alex, "Hybrid Fuzzy Logic and Neural Network Model for Fingerprint Minutiae Extraction", IEEE Transaction, 7803, pp.3255-3259, 1999.
[15] Xueju Tan, Bir Bhanu "Fingerprint Matching by Genetic Algorithms" The journal of Pattern Recognition 39 (2005) 465 – 477
[16] Xue Jun-tao, Liu Jie & Liu Zheng-guang, "An enhancement algorithm for low quality fingerprint image based on edge filter and Gabor filter", Proc. Of SPIE, Vol. 7383, 2009.

International Journal of Modern Engineering Research (IJMER)
www.ijmer.com Vol. 3, Issue. 4, Jul - Aug. 2013 pp-2429-2433 ISSN: 2249-6645

AC-DC-AC-DC Converter Using Silicon Carbide Schottky Diode

Y. S. Ravikumar
Faculty of TE, SIT, Tumkur

Abstract: *Silicon carbide (SiC) is the perfect cross between silicon and diamond. The crystal lattice of SiC is identical to silicon and diamond, but, exactly half the lattice sites are occupied by silicon atoms and half by carbon atoms. Like-diamond siC has electronic properties superior to silicon, but, unlike diamond it is also manufacturable. The thermal leakage current (dark current) in SiC is sixteen orders-of magnitude lower as well. As temperature increases, the leakage current increases, but, the temperature where the leakage current would disrupt circuit operation is over 1000 °C in SiC, compared to about 250 °C in silicon. The SiC electronic revolution began in the early 1990's when single-crystal wafers became commercially available for the first time. During the intervening years, many different electronic devices have been demonstrated in SiC, with performance often exceeding the theoretical limits of silicon. These include pin diodes, MOS field-effect transistors (MOSFETs), metal-semiconductor field-effect transistors (MESFETs), and bipolar transistors (BJTs), as well as specialized devices such as CCD imagers, Schottky diodes, static induction transistors (SITS) and impact-ionization- avalanche-transit-time (MATT) microwave oscillators. These early digital logic gates and linear elements are based on n-channel MOS technology, but, quickly followed by more sophisticated CMOS integrated circuits.*

Key words: *DC-DC Converter, Energy band, Silicon Schottky diode, Silicon Carbide Schottky diode, MOSFET, Recovery time, switching losses*

I. INTRODUCTION

Semiconductor power devices, especially diodes play important role in switching response. Low power dissipation on the switching devices will give rise to highly efficient power electronic system. For example, if a semiconductor device operates in a linear mode such as in power amplifiers of in linear regulators, it is expected that some amount of energy will be lost in the power circuit before its energy reaches the output. High efficiency of power converter requires a minimal loss of this energy from source to load. One of the energy can be easily dissipated in the diodes in terms of heat leading to a lower efficiency of the converter [1]. The unipolar Silicon Schottky (Si) and Silicon carbide Schottky (SiC) diodes are commonly used in power converters circuits. In spite of both diodes come from the same unipolar family, the issues of higher switching losses with regards to reverse recovery losses have yet been solved. Nevertheless, the new SiC diode has emerged in the market in recent years where they are expected to improve the efficiency of the converter by allowing a further reduction in reverse recovery energy losses and hence increasing the performance. The additional substance of carbide element in the power Schottky diode may eventually lower the reverse charge current thus, improve the overall transient response in the converter. An ideal semiconductor device would inhibit large breakdown voltage, low voltage drop in the on-state, high switching speed and low power loss. However in order to increase the performance of a semiconductor device, several additional doping enhancements will be added during the fabrication stage, where the characteristics of the device will altered by adding some impurity atoms to the pure semiconductor material. Today's technology requires extensive research to develop more powerful devices, not only to have lower switching losses, higher efficiency but also improve reliability. For this reason, power losses in the device must be put into consideration. The main contribution in this work is to verify that SiC high power diode having larger energy bandgap can indeed produce better results in DC-DC converter. The analyses are mainly done using circuit simulator.

II. SILICON SCHOTTKY DIODE FAMILY

The Silicon Schottky diode of Schottky barrier diode is widely used as a mixer or detector diode. In addition to its low forward voltage drop, it may lead to lower levels of power losses in the circuit [2]. Since Si diode is a unipolar device, the current transport is mainly due to majority carriers and therefore the speed is faster. In addition, it has low turn-on voltage, high frequency capability and low capacitive effect [3]. SiC diode is a wide-bandgap (WBG) semiconductor family from III-V group. It has the advantages in faster recovery rimes as well as no dependence on temperature [4] and has the potential to operate more efficiently. In Si diode however, the temperature may rise due to the increasing in electron's thermal energy leading to higher peak reverse recovery current [5]. This eventually gives higher power loss in the device.

In addition to smaller package and higher weight, SiC diodes also have higher critical field and barrier heights compared to Si diode. This results in reduced on-state resistance and lower leakage current or SiC diode [6]. It also has been demonstrated that the SiC diode has the potential to improve power FET performance [7]. Its energy bandgap is three times higher than Si and ten times higher in electrical breakdown strength. Therefore, SiC can operate at operating voltage of 20 times with current densities up to 400 times higher than Si diode [8]. SiC Schottky diode has a small forward voltage and the reverse breakdown voltage cannot be made too high (currently about 200 V). It is used for rectification of power supplies for low voltage and high current applications or in high frequency systems due to its small reverse recovery time.

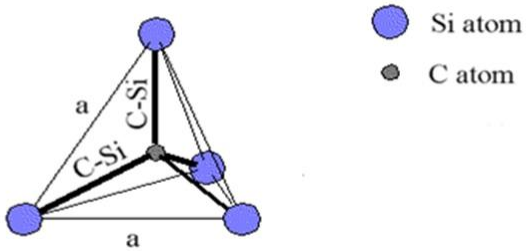

Fig.1 The tetragonal bonding of a carbon atom with the four nearest silicon neighbors. The distance **a** and C-SiC are approximately 3.08Å and 1.89 Å respectively.

Fig. 1 shows four Si atoms made a covalent bonding with a single Carbon © atom to form a SiC. The C atom is located in the middle of the structure and the distances between all atoms which marked C-Si are equal. The SiC possess increase tolerance to radiation damage, marking it a material suitable for defense and aerospace applications. Due to high tolerance of temperature in SiC, it is chosen in various industries, such as aircraft, automotive communications, power and power spacecraft.

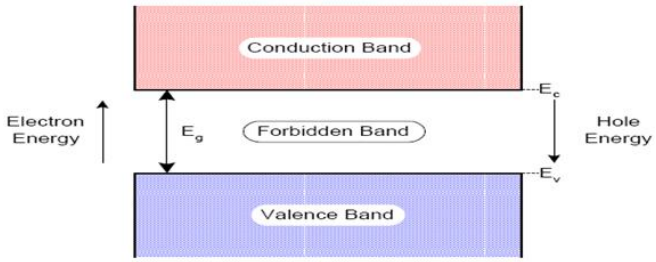

Fig. 2 Energy Band Diagram of a Semiconductor.

The characteristics of SiC diode as a wide bandgap semiconductor device results in a more energy to excite the electron from its covalent bond during turn-off compared to Si. Referring to Fig. 2, the wide bandgap is measured from the distance between the conduction band and valance band. An insulator would have a larger bandgap that would take lots of energy for the electrons to travel from the valence to conduction band while a conductor would have no forbidden band. The energy is calculated from the difference between both bands. The wider the bandgap, more thermal energy is required to excite the electrons enabling the device to operate at higher temperature without affecting its electrical properties.

III. REVERSE RECOVERY

Reverse recovery is one of the properties in a diode. It can be a factor in determining the efficiency of the applications. When a diode has been conducting in a forward bias long enough for it to establish steady, there will be charges due to the presence of minority charge carriers. This charge must be removed to block in reverse direction.

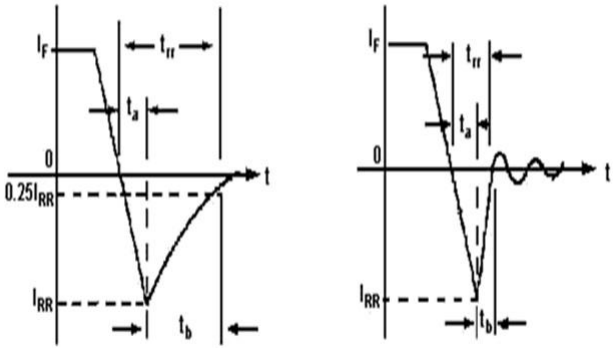

a. Soft recovery b. abrupt recovery

Fig. 3 Reverse Recovery Current Characteristic

The characteristics of reverse recovery current experienced by a diode is represented Fig. 3 above, t_{rr} represents the reverse recovery time, I_{rr} is the peak reverse current whilst t_a is the transition time due to charge stored in depletion region of the p-n junction and t_b is the time for the current to relax to zero. The peak reverse recovery current depends on the falling rate of change in current during turn-off. In SiC diode, there will be less or none reverse recovery current due to its ability to immediately remove stored charge. However, there are differences observed during the recovery from the peak values. This is merely reflected from different device's fabrication techniques.

Normally, in SiC, the rising current rate takes a longer time (t_{rr}) as shown in part (a) in Fig 3. This eventually reduces the turn-off speed. In other SiC type, The speed can also be slightly faster due to smaller t_b but with the cost of higher dissipation. This can be seen in part (b) as oscillation exists during the end stage of turn-off time. In addition, if the falling current rate during the beginning of turn-off time is high as in the case of non-schottky diode, the reverse current would also be high, leading to both high power dissipation and lower in turn-off speed.

IV. DIODE CHARACTERISTICS

4.1 Static Characteristics

The I-V and reverse current are among the static characteristics of the device. Due to higher level of majority carrier injection in Si diode, this causes a lower voltage drop and hence smaller capacitance to bias the junction for turn-on process. This is the only advantages of Si diode compared to SiC. Here, SiC diode requires a higher voltage to forward bias the device. Apart from that, SiC diode can handle larger reverse voltage as compared to Si.

4.2 Dynamic Characteristics

The characteristic that changes with time is inherited in both devices. Si and SiC diodes are compared in terms of the reverse recovery time, reverse recovery current and corresponding switching losses. The comparisons in dynamic characteristics between two devices are tabulated in Table I. The SiC and Si diodes used are of part number UPSC600 and B530C respectively.

Table I. Comparison of Dynamic Characteristics

Characteristics	SiC Schottky (UPSC600)	Si Schottky (B530C)
Reverse Recovery Time	Time Unchanged with temperature variation	Increases as temperature increases
Reverse Recovery Current	Negligible	Increases as temperature increases
Switching Losses	Low	Slightly higher

Table I shows that SiC diode has advantages in all dynamic characteristics. Si diode suffers from higher reverse recovery current and switching losses. This clearly indicates that additional carbide substance in the device may improve switching speed and reduce power dissipation.

V. AC-DC-AC-DC Converter Using SiC

Figure 1 shows the circuit diagram of AC-DC-DC converter (switched mode), the LT spice simulation package is used for simulating this circuit. Table II give the parameters of the active devices used in this ciruit simulation. The input 230 V, 50 Hz 1ϕ sine wave is used. Using MUR460 power diodes (D1-D4), bridge rectifier is constructed and capacitor C2 is connected across bridge rectifier output to reduce the ac component. The switching device M1 (STP8NM60) MOSFET used as switch. The gate pulse of amplitude 7 V with 25 µsec. on period of 50 µsec. total period is applied. Gate pulse Vg1is shown in Figure 2 The primary and secondary (diode) currents are shown in Figure 3 and Figure 4 respectively. The load for this circuit is used as resistive load 10Ω. The laod current for this circuit design is 700 mA with 50 µsec duration and it is shown in Figure 5 and Figure 6 gives the current through load capacitor. The peak power of the diode is 6.3 W as shown in the Figure7.

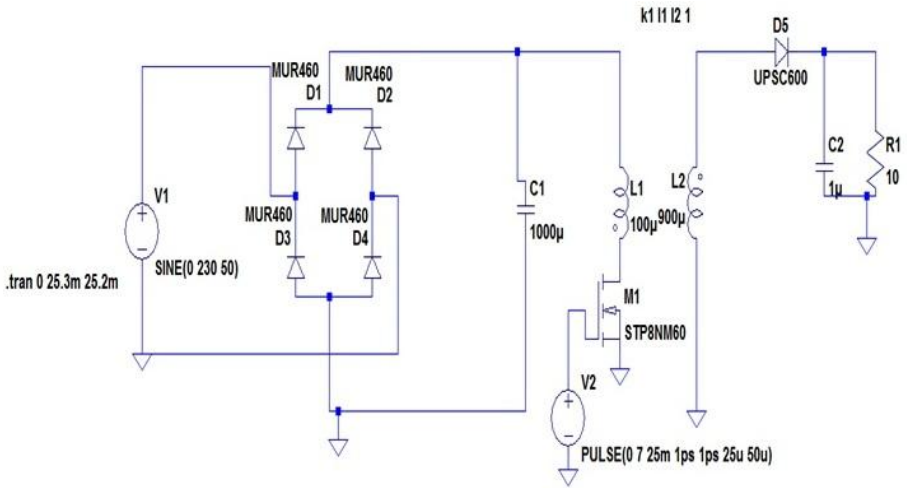

Figure 1 Circuit diagram of AC-DC-AC-DC converter using SiC (Switched mode

Table II Device parmeters in the test circuit

MOSFET Properties		Diode properties	
MOSFET	STP8NM60		
Manufacturer	STMicroelectronics	Manufacturer	Microsemiconductor
Polarity	N-chan	Type	SiC Schottky
Vds[V[	650	Average forward current[A]	1
Rds[on]Ω	0.9	Breakdown voltage[v]	600
Qgate[C] 1	$1.3e_{.008}$		

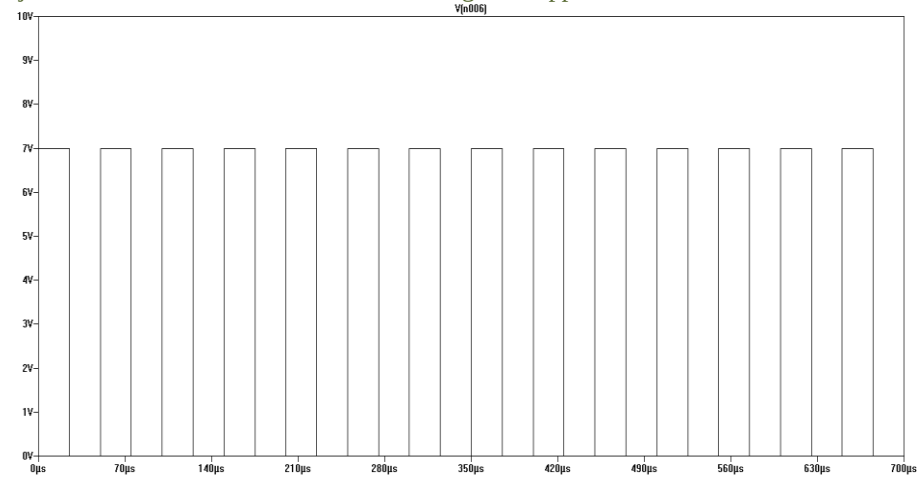

Figure 2 Gate to source voltage (Vgs)

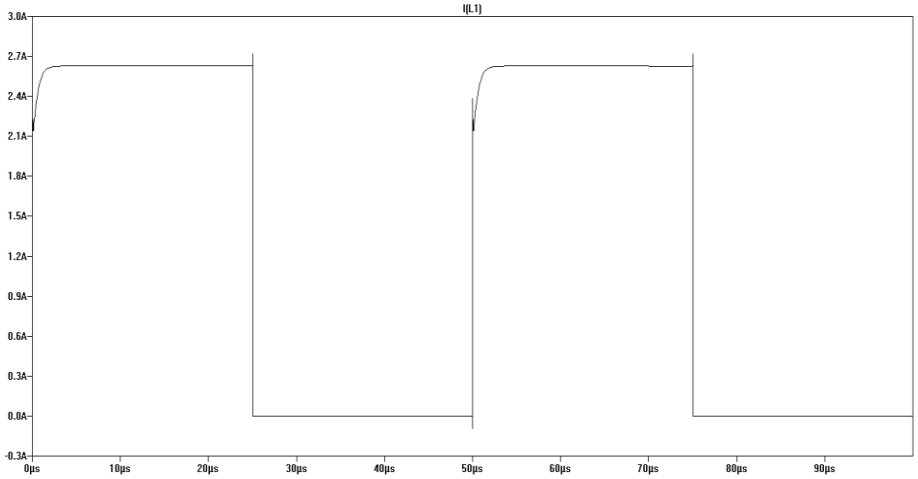

Figure 3 Primary current

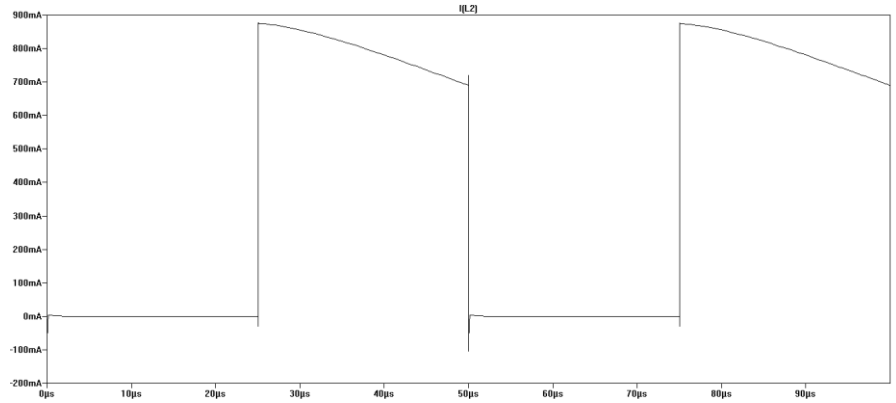

Figure 4 Secondary current (current through diode)

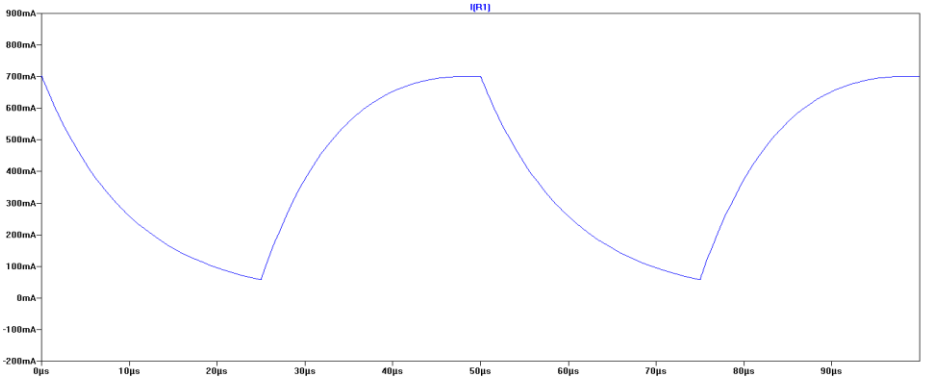

Figure 5 Current through Load Resistor

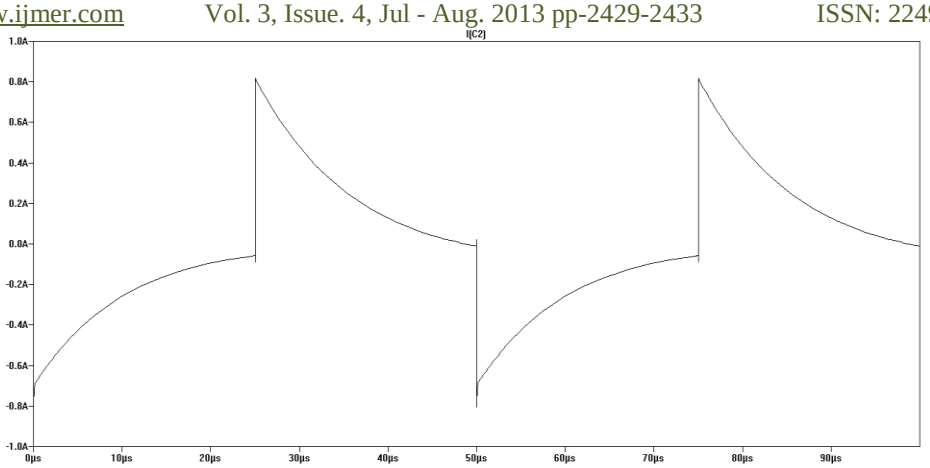

Figure 6 Current through Load Capacitor

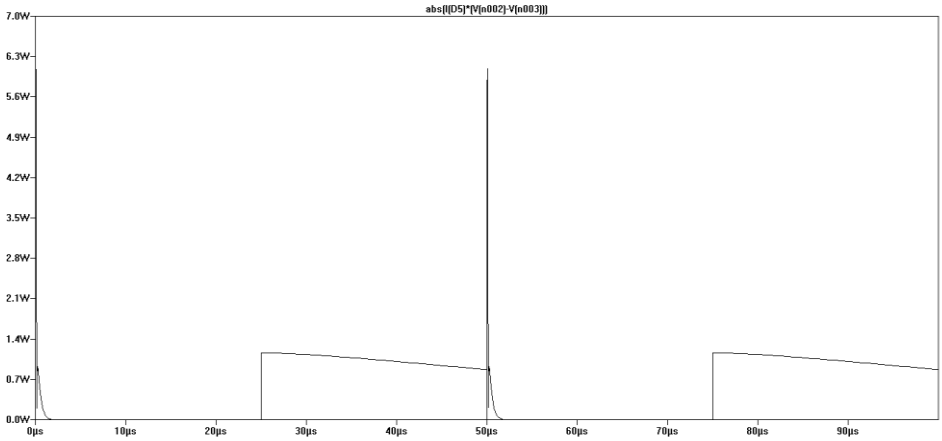

Figure 7 Power in diode

VI. Results and Discussion

The maximum primary current in the circuit is 2.6 and maximum secondary current (through the diode) is 900 mA by simulation using LT spice simulation tool. The maximum current through the load and capacitor is 0.8 A at 25µsec. The switching power loss in the SiC Schottky diode is 6 W. The results are shown in Figures 5.26 to 5.31 and these are simulated characteristics using LT spice simulation tool.

REFFERENCES

[1] I. Batarseh "Power Electronic Circuits", University of Central Florida, John Wiley &Sons, Inc., 2004.
[2] A.P. Malvino, "Transistor Circuit Approximation", McGraw-Hill, Inc., 3rd Ed., 2007
[3] F. Mohammed, M.F. Bain, F.H. Ruddell, D. Linton, H.S. Gamble and V.F. Fusco, "A Novel Silicon Schottky Diode for NLTL Applications", *IEEE Transactions on Electron Devices*, vol. 52, iss. 7, pp. 1384-1391, July. 2005.
[4] B. Ozpineci and L.M. Tolbert, "Characterization of SiC Schottky Diodes at Different Temperatures", *IEEE Power Electronics Letters*, vol. 1, no. 2, pp. 54-57, Jun. 2003.
[5] M.S. Chinthavali, B. Ozpineci and L.M. Tolbert, "Temperature-Dependent Characterization of SiC Power Electronic Devices", *IEEE Power Electronic in Transportations*, pp. 43-47, Oct. 2004.
[6] M.J. Kearney, M.J. Kelly, A. Condie and L. Dale, "Temperature Dependent Barrier Heights in Bulk Unipolar Diodes Leading to Improved Temperature Stable Performance", *IEEE Electronic Letters*, vol. 26, iss. 10, pp. 671-672, May 1990.
[7] B.J. Baliga, "Power Semiconductor Device Figure of Merit for High-Frequency[8] Purdue University Nanoscale Center, Wide Bandgap Semiconductor Devices. Applications", *IEEE Electron Device Letters*, vol. 10, iss. 10, pp. 455-457, Oct. 1989.
[8] Purdue University Nanoscale Center, Wide Bandgap Semiconductor Devices.

ACKNOWLEDGMENT

The authors are grateful for the support and encouragement of Dr. M. N. Channabasappa, Director, and Dr. Shivkumaraiah, Principal of Siddaganga Institute of Technology, Tumkur.

BIOGRAPHIES

Y. S. Ravikumar received B. E degree from Bangalore University in1981 and M.S. Degree from BITS, Pilani in 1985 Since 1983 he had been with Electronics and Communication Engineering Department, SIT, Tumkur. At present he is an Associate Professor in the Department of Telecommunication Engineering, SIT, Tumkur. His research interests are in SiC device and electronics technology, and power electronics devices. He has two international conference papers and four publications to his credit.

International Journal of Modern Engineering Research (IJMER)
www.ijmer.com Vol. 3, Issue. 4, Jul - Aug. 2013 pp-2434-2441 ISSN: 2249-6645

Comparative study on Garments dyeing process and Fabric dyeing process on various parameters (PH, M: L, softener etc)

Amit Saha[1], Anup Saha[2], Pallab Sutradhar[3], Tanvir Ahmed[3], MD.Fazle Rabbi[3]
[1]*Department of Textile Engineering, City University, Bangladesh*
[2,3] *Department of Industrial and Production Engineering, Shahjalal University of Science and Technology, Bangladesh*

Abstract: *Today is the world of most scientific and advanced level of dyeing. There are huge numbers of process to do coloration. Natural and man-made colors are also used. In this research, the difference of garments dyeing and fabric dyeing are analyzed. At first we compare garments dyeing and fabric dyeing process with using respectively direct dye and reactive dye. Compare two processes we find out when we change pH in polyester fabric & get different types of shade. When we take less pH (3) then the shade become lighter, poor fastness to wash. When we take pH (6) the shade become more saturated, excellent fastness to wash. But in the process of garments dyeing shade variation less occur. We get some different types of result such as M: L, time, shade, variation, pH, cost etc.*

Keywords: *Garments dyeing, Fabric dyeing, ph, M: L, Softener*

I. INTRODUCTION

Textile coloration is combination of same series processes such as scouring, bleaching, dyeing & after treatment which can be carried out at different stages of fiber processing in different forms like staple, yarn, fabric (rope or open-width, piece & garments) Dyeing of staple forms(loose fiber) is better for achieving better colorfastness, maximum penetration and uniform migration of dues over dyeing. Piece (batch) dyeing is carried out open width or rope form in depending on machine type & end-dyes. Usually these materials are dyed in exhaust dyeing method in a single dyeing machine. But lightweight woven fabrics & garments are also possible to dye with same principle in different form of dyeing machine such as jet dyeing machine. During garment dye process, some dyeing parameter should be adjusted according to form of products-righty weaved and heavy garments need the dyes with better migration properties, higher dyeing temperature, lower liquor ration & careful circulation of goods.

Usually, textile coloration is carried out impart attracting of textiles & pretreatment is first stage of textile coloration process, plats very role on coloring on textiles. Generally loose fiber, yarn, knit fabric, garment & very lightweight synthetic woven fabric are dyed batch wise in single machine. So the batch preparation is the early step of pretreatment in coloration process.

II. GARMENTS DYEING

This method is the best process of the dyeing of goods. However, the penetration of the dye solution may not be completely passed to the fibers such as between the seams, buttons, zippers etc. Normally, it is used for lingerie, socks, sweater dyeing etc.

In woven fabric processing generally various types of dyeing process is used. Those are:

i. Pad Dry Steam (PDS)
ii. Pad Dry Cure (PDC)
iii. Cold Pad Steam (CPS)

Machine required for those process:

i. Cold pad batch
ii. Thermosol
iii. Pad steam

Cold pad batch: It is the simple & easiest way of woven fabric dyeing. In this process only dark shade can be produced successfully & economically. But limitation is medium or light shade is difficult to match. It takes a long time because after dyeing it required a rotation of 8 to 12 hours.

Thermosol: It is a dyeing machine but it cannot produce the color as finally required or permanent. But in PDS process it can be provide finished product. By this machine only color is migrated from liquor to fabric. The it is dried on pre dryer & followed by hot air flow drying in thermosol unit. After this process color is developed in pad steam by chemical padding.

Pad stream: Thermosol run fabric must pass through pad steam for the development of color when CPS process is carried out. Here chemical padding is done through which color is fixed on the fabric. CPB run fabric does not require pad steam process. Here based on requirement additional dye can also added.

2.1 Garments Dyeing Machine Specification:

No. of machine: 01: Belly Machine
Brand Name: Nagai Shina
Origin: China
Capacity: 250 kg
Model No: NS-2260
RPM: 28
Total Quantity: 18 pcs
Maximum Temperature- 100° c

No. of machine: 02: Front Loading Machine/Computer Machine.
Brand Name: DANIS
Origin: Turkey
Capacity: 450 kg
Model No: MKM-525
RPM: 30(Fixed)
Total Quantity: 08 pcs

No. of machine: 03: Hydro Machine
Brand Name: DANIS
Origin: Turkey
Capacity: 250 kg
Model No: D-2233
RPM: 800N-1000N
Total Quantity: 08 pcs

No. of machine: 04: Dryer Machine (Steam Dryer)
Brand Name: DANIS
Origin: Turkey
Capacity: 180 kg
Model No: D-2218
RPM: 30
Total Quantity: 06 pcs

No. of machine: 05: Dryer Machine (Gas Dryer)
Brand Name: DANIS
Origin: Turkey
Capacity: 180 kg
Model No: D-2218
RPM: 30
Total Quantity: 08 pcs

2.2 Flow chart for garments dyeing (medium / dark shade):

M : L – 1 : 8

Garments Load - 2 kg
↓
Level in water 16 liter
↓
Wetting agent 0.5g/l NOF (70° c × 5’)
↓
Normal Wash
↓
Leveling agent LDR (60° c× 5’)
↓
Color dosing (60° c× 10’)
RG Yellow RGB - (0.44%)
RG Red RGB - (0.254%)
RG Blue RR - (0.898%)
Run 10’
↓
Salt dosing {(50g/l) 60° c × (10’ + 10’}
↓

Soda dosing {(16g/l) (60° c × 10')}
↓
Run Time 35' (sample check)
↓
A – Acid (1 g/l × 5')
↓
Fixing agent (E.C) (1g/l) – (40° c × 5 min)
↓
Raise temp. 50° c
↓
Run time 5
↓
Drain
↓
Level in
↓
Cold wash (27° c × 2min)

2.3 Flow chart for garments dyeing (light shade):

Level in Raise temp. (70° c × 5min)
□
Wetting + Detergent (NOF)
↓
Leveling agent (LDR) 60° c × 5min)
↓
Color dosing {60° c × (10 +10)}
{CIBA Yellow FNR - 0.048%
CIBA Red FNR – 0.048%
CIBA Blue FNR – 0.048%}
↓
Salt dosing (24g/l){60° c × (10+10)}
↓
Soda dosing {(8g/l) (60° c × 10')}
↓
Run time 35 min (sample check)
↓
Normal Wash
↓
Acetic Acid (1 g/l)
↓
Cold wash
↓
Fixing agent (E.C) (1 g/l) – (40° c × 5 min)
↓
Raise temp. 50° c
↓
Run time 5 min
↓
Drain
↓
Level in
↓
Cold wash (27° c × 2 min)

2.4 Work procedure

2.4.1 Desizing:

This process to remove the size material and increase the absorbency power of the fabric to make the fabric suitable for the next process is called Desizing.

Chemical Types:

1. Detergent – 200gm
2. Caustic soda – 400gm
3. Water – 400 L

4. Hydrogen Peroxide – 600gm
5. Temperature - 70°c

At first mixed the chemical then run the machine 10 minutes at 70°c. After this process to proper clean the machine with 800 L water.

2.4.2 Neutral: Neutral is done to control the pH of this process pH must be checked. Some chemical are use for the process. At first Acetic Acid (100gm) with water 400 L to run the machine 5 minutes at 45°c. Then after this process to proper clean the machine with 800 L water for the next process.

2.4.3 Dyeing: This process by which is a textile material is to be changed physically or chemically, so that it looks mono uniform colored is called Dyeing.

Dyeing Curve:

Figure 1: Dyeing curve

Alfatex + Anticrease = 45°c – 5min
Dye Chemical = 55°c – 5min + Salt after 20min
Fixing Agent
Softening Agent
Rinsing Wash
Dain

2.4.4 Objects of dyeing:

1. The textile goods are dyed uniformly with single color.
2. To increase the attractiveness of the textile goods.
3. To make the fabric suitable for various usage.
4. To make textile goods suitable for decorative purposes.

Some necessary chemicals are needed for this process. Such as

1. Alfatex – 500gm
2. Anticrease – 500gm

Anticrease removes crease mark. The Belly Machine run 5 minute with chemical and water at 80°c temperature then add dyestuff.

- Indosol Scarlet BL – 350GM
- Rose RR – 66.25gm
- Red BA – 153.5gm
- Salt – 15kg

Those chemical are mixed in a bath. Those chemical are taken in a Belly Mache with 800 L water to run the machine 5 minute at 80°c temperature then check garments to match the shade.

2.4.5 Fixing: This is a very important process because it helps to carry dye in garments. It increases durability dye in the garments. For this process fixing agent such as hydrocol sun (300gm) and water is needed to run machine 5 minute at 40°c. Then after this process to proper clean the machine with 800 L water for the next process.

2.4.6 Enzyme:

This process is done when the garments carry excess dye than the buyer requirement. But when garments carry light that time enzyme process is not necessary. For enzyme process Jak powder (150gm) and pocket clear (100gm) are needed with water to run the machine 5 minute at 40°c temperature. After this process to proper clean the machine with 800 L water.

2.4.7 Softener: Softener is used to soft the garments. For this process IMA and Acetic Acid are needed with water to run the machine 5 minute at 40°c temperature then garments out. After Finishing those process garments are taken out for finish dry process. Time, Temperature, Liquor Ratio must be controlled.

2.4.8 Garments dyeing process with vat dyes:

The following process is suitable specially for garment dyeing.
Typical recipe:
Wetting agent = 0.5 – 1.0 g/l
Sequestering agent = 1.0 - 2.0 g/l
Leveling agent = 1.0 - 2.0 g/l
Retarding agent – 5 - 7 g/l (If necessary use in hot dyes)
Dyes = 7% (owf)
Caustic soda = 5 %(according to vender recommendation)
Hydros (sodium hydrosulfite) = 5%(according to vender recommendation)
Temperature = 70°c - 80°c
Time = 30 – 50 min
M: L = 1:10

Table 1: Different dye percentage of vat dye

Dye%(owf)	Reagents	Warm dyeing	Hot dyeing
1.0	Caustic flakes Hydroz Common salt	=3.0 - 4.0 g/l =3.0 - 4.0 g/l =5.0 - 8.0 g/l	=6.0 - 7.0 g/l =6.0 - 7.0 g/l =00
4.0	Caustic flakes Hydroz Common salt	=4.0 - 4.5 g/l =3.0 - 4.5 g/l =10.0 - 12.0 g/l	=7.0 - 8.0 g/l =7.0 - 8.0 g/l =00
8.0	Caustic flakes Hydroz Common salt	=4.5 - 5.0 g/l =4.5 - 5.0 g/l =12.0 - 15.0 g/l	=8.0 - 9.0 g/l =8.0 - 9.0 g/l =00

Note: considering M: L = 1:10

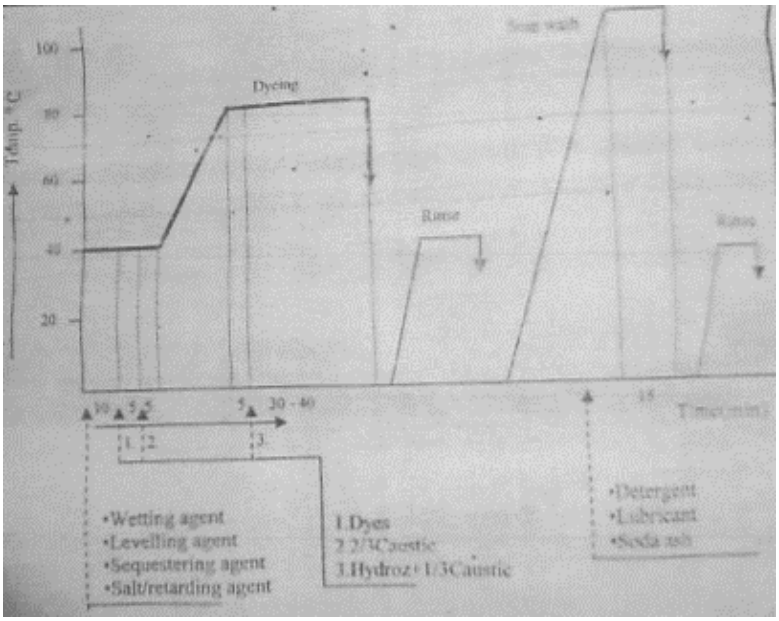

Figure 2: Process curve (dyeing of cotton goods with vat dyes)

Procedure:

1. First, settle dye bath with substrate at 40°c and wetting, sequestering agent, leveling, retarding agent (if necessary) and then run for 5 – 10 min.
2. Add dyes according to substrate weight and run the bath for 5 min.
3. Add 2/3 of caustic soda requirements and run for 5 min.
4. Raise the temperature to 70 – 80 at 2-3c/min and run for 5 min.
5. Add Sodium hydrosulfite (hydroz) to the bath with rest 1/3 amount of caustic requirements.
6. Run the bath for 30 min and maintain reduction by checking with vat reduction paper.
7. Overflow rinse until with cold water.

2.4.9 Oxidation: After dyeing cycle penetrated and distributed dye molecules are oxidized to convert insoluble form into the fiber. The oxidation process can be done in contact of air or other oxidizing agent. For example, the oxidation process can be carried out treating the dyed goods with 0.5 – 1.0 g/l hydrogen 35% at 30 – 35 for 10 min.

2.4.9.1 Soaping:

Detergent = 1.0 – 2.0 g/l
Soda ash = 1- 2 g/l
Glucose = 95 – 100c
Time = 15 – 30 min
M: L = 1: 10 – 1: 20
The rinse the goods with cold-hot-cold water successively.

2.4.9.2 Softening:

1. That the good with 1.0 – 2.0% softening agent at 10 min.
2. Drop
3. Finally dry the goods uses.

III. FABRIC DYEING

Fabric dyeing is the method after weaving, knitting or non-woven to make fabrics. This is very popular method of dyeing as the dyed fabrics will be processed further to garment industries very easily. Dyeing forms of the fabric dyeing can be used in 2 ways.

1. Open width form using the fabrics to spread without any creases and dye them.
2. Rope form using the fabrics with the form like a rope.

3.1 Dyeing work flow chart:

Scouring & bleaching
↓
Per oxide hot with a/acid
↓
Enzymes wash with a/acid
↓
Leveling with sequestering
↓
Dyeing dosing
↓
Salt dosing
↓
Soda dosing
↓
Sample
↓
Drain
↓
Washing off
↓
A/acid
↓
Softener
↓
Unload

3.2 Dyeing machine:

Name of the m/c: Dyeing machine
Brand Name: Dilmenlar
Manufacturing Company: Turkey
Year of Manufacturing: 2004
Machine capacity: 150 kg
No. of nozzle: 02
Maximum Temperature: 135°c
Motor: 01
Winch Motor: 01
Pump Motor: 01

3.3 The controlled Parameters for dyeing procedure:

a. pH:
- During H_2O_2 bleaching Ph: 10.50 – 12

- During neutralization : 6.50 – 7.0
- During Enzyme : 4.50 – 7.0
- During reactive dyeing pH: 9.5 – 11.50
- During Soda dosing : 10.0 – 11.0
- Soaping : 4.50 – 6.0
- During disperse dyeing pH : 4.50 – 5.0

b. Temperature:
- For cotton scouring : 98°c
- For cotton enzyme : 55°c - 60°c
- For cotton dyeing : 98°c (For hot brand)
- For salt, Soda : 60°c
- Polyester dyeing : 135°c
- For cotton cold wash : 30°c - 40°c
- For cotton hot wash : 80°c - 90°c
- For cotton acid wash : 50°c - 60°c
- OBA application : 98°c

c. Time:
- For scouring & bleaching : 60 minute (when temp. 98°c) If 110°c, time 30min.
- For cotton enzyme : 60 minute
- For reactive dyeing : 30 minute
- For disperse dyeing : 30 minute
- For salt dosing : 30 minute
- For soda dosing : 45 – 60 min

d. M: L ratio:
- For reactive dyeing M: L ratio maintained between 1: 8
- For disperse dyeing M: L ratio maintained between 1: 10

3.4 The calculated formula followed in production:

01. Color (%) – Required dye (gm)= Total fabric × Recipe / 100
02. Chemical + Auxilaries (gm/l) - Required chemical (gm)= Total liquor × chemical(gm/l) / 1000

3.5 Working Procedure:

Firstly the detergent, Anti-creasing agent, Anti-foaming agent and Stabilizer are mixed in mixing tank, then load to machine at 50°c

↓

The temperature is risen to 60°c. Now the Caustic Soda is given to bath

↓

The Hydrogen Peroxide is given at 70°c

↓

Raise the temperature at 98°c and run for 60 minutes. Here the Ph = 11-12

↓

Rinse the fabric

↓

Hot wash is done at 80°c × 10 → Drain → Normal wash → Drain

↓

Peroxide is applied at 60°c and run for 15 minutes → Hot wash

↓

Add Acetic Acid at same temperature and run 10 minutes

↓

pH checked (pH=6.5) → Normal wash

↓

Now Acetic Acid applied at 55°c for pH control (pH= 4.50) and then Enzyme is given to bath at same temperature with 60 minute

↓

Raise the temperature (Grade rate → 2 C/min) at 80°c and run 6 minute

↓

Cold wash is done 2 times and the drained out.

IV. DIFFERENCE BETWEEN THE GARMENTS DYEING AND FABRIC DYEING

Table 2: Difference between the garments dyeing and fabric dyeing

Garments Dyeing	Fabric Dyeing
1. When garments are made from grey fabric and then the garments are dyed in required color and shade called garments dyeing.	1. Fabric dyeing is the method after weaving, knitting or non woven to make fabric. This is a very popular method of dyeing of the dyed fabrics will be processed further to garments industries very easily.
2. Less time is required.	2. More time is required.
3. Comparatively low cost of production.	3. Comparatively higher cost of production then garments dyeing process.
4. For direct dyeing M: L ratio maintained between 1: 10	4. For reactive dyeing M: L ratio maintained between 1: 8
5. Wales per centimeter is not increases after dyeing process.	5. Wales per centimeter increases after dyeing process. Because during dyeing fabric is continuously revolved. Therefore fabric gets lengthwise tension & it causes increases of WPCM.
6. GSM is increase after dyeing.	6. GSM is also increase after dyeing.
7. Generally Belly machine is used for garments dyeing.	7. Generally Jet/Jigger/Pad/ Winch dyeing machine are used
8. Less production than Fabric Dyeing.	8. Higher production than Garments Dyeing.
9. Comparatively lower space is needed.	9. Comparatively higher space is needed.
10. No possibility of shade variation.	10. It has possibility of shade variation.
11. For direct dye pH is needed 4-7.	For reactive dye pH is needed 9-11.
12. Sewing thread used for making the garments should be of same fiber like the garments fabric, otherwise color difference may occur between garments fabric and sewing thread.	12. No need of sewing thread.
13. After dyed garments no need processed further to garments industries.	13. After dyed fabrics must be processed further to garments industries.

V. CONCLUSION

We find out that different type of using pH shade variation occur in fabric dyeing. But the garment dyeing has less shade variation. From the recipe of garments dyeing and fabric dyeing we realize that garments dyed needed M: L 1: 10. But for the fabric dyeing needed M: L 1:8 for the reason of production. After dyed garment no need processed to garments industries but for fabric dyeing fabric must be processed further to garments industries. Because garment dyeing is done after finished garments and fabric dyeing is done after weaving process. Time variation occur between two dyeing method. Because fabric dyeing is a long process and garments dyeing is a short process. Production occurs in garments dyeing is low and fabric dyeing is a high production. The capacity of fabric dyeing machine is low than the fabric dyeing machine.

References

[1] Yahya. Faruk. "Textile Dyeing and Printing Technology", Madina Printer & packager. 1997
[2] https://en.wikipedia.org/wiki/Dyeing (Last modified on 18 July 2013 at 07:48, Retrieved: 24 July 2013)
[3] http://wiki.answers.com/Q/What_is_garment_dyeing (Retrieved: 27 July 2013)
[4] Rahman. Moshiur. "Wet Processing Technology Part-2", Books Fair Publications. 2008
[5] Rahman. Moshiur. " Wet Processing Technology Part-1", Books Fair Publications. 2006
[6] https://textiledictionary.com (Retrieved: 07 Jan 2013)
[7] Dr. V.A. Shennai. Currently, Technical consultant, Former Professor of Textile Chemistry, Department of Chemical Technology, University of Bombay

International Journal of Modern Engineering Research (IJMER)
www.ijmer.com Vol. 3, Issue. 4, Jul - Aug. 2013 pp-2442-2445 ISSN: 2249-6645

Implementation of Cryptography Architecture with High Secure Core

R. Vijaya Durga[1], K. V. Ramana Rao[2], K. Prasanna Kumar[3]
[M.tech] Department of Electronics and Communication Engineering, Pydah College of engineering and Technology, Affliated to JNTUK, Ghambheeram, Visakhapatnam-531163

ABSTRACT: *The continuous increase in demand for security in electronic systems and communication systems which lacks a secure architecture has resulted in the need to provide cryptography architecture with high secure core. The hardware implementation of the cryptography core which incorporates multiple algorithm for security purpose was already developed but if the architecture is capable of switching between the algorithms used for encryption /decryption as controlled by the host computer dynamically, then the security over the data path will be increased by making the attempt for hacking too difficult. The switching between heterogeneous algorithms will also increase the confusion level. This proposed architecture implements three symmetric algorithms namely the standard AES, standard DES and proposed modified DES (MDES) algorithms. Representing these algorithms in the functional block level and also using the new concept of common S-Box , results in operations that are common to all the three algorithms, allows us to merge them in a single architecture and thus there is an area reduction of 14.5% in cryptography core with 2 S-Boxes rather than using 11 S-Box. The operation of this cryptography core is controlled by the control signals, selecting which algorithm to work at time, making it difficult to hack the information transferred through the data line.*

I. INTRODUCTION

The cryptography technique users always have demanded high security for the data they transfer, and this demand increases day-by-day as the information transferred is hacked unlawfully. To meet this needs, though some works with different architectures are designed, this project introduces a simple new technique having three algorithms onto a single core, making the architecture to function as any one of the algorithm at different time instance helps in increasing the security level. In the proposed cryptography architecture we have implemented the private key algorithm and the algorithms used here are standard AES which is a 128-b block cipher algorithm, standard DES and MDES both of which are 64-b block cipher algorithms.

A cryptography system can be implemented either in software or hardware. Software implementation allows multiple algorithms to be supported on the same platform but they are usually slow and are considered to be more vulnerable to side channel attack, which uses physical measurements on the devices, for example the power consumption of the processor to detect the encryption / decryption key while on the other hand the hardware implementation is comparatively faster and more secure as compared to that of software. The main concept used in order to increase the security is that, the inputs to core module is a 128-b data and 128-b key and the output is also 128-b which generally confuses the hacker since AES generates an output which is 128-b data but the other two algorithm generates output of 64-b data which is hidden in the 128-b data that is coming out of the module and also the control signal which selects the algorithms operation increases the security level because before the hacker hacks the information the encrypted/decrypted data will be transmitted since he doesn't know which algorithm is used at what time as it is been controlled by the host medium with the control signal being sent via the secure data channel with the help of private key algorithm.

II. STRATEGY

Some of the strategy used in designing algorithm is as follows. In designing the Key Schedule module for AES encryption, we had used on the fly key method i.e. the keys are generated in accordance with the working of each round in AES flow. Instead of pre-generating the keys required for the encryption process which consumes lot of time and reduces the frequency and speed of operation, but by using this strategy keys are generated whenever the round operation works helping in increasing the throughput.

The technique used to design common S-Box is show in the Fig.1 we know that the number of S-Boxes used for DES algorithm is 8 and each box contain 64 elements of 4-b each. So the number of elements as a whole is 64 X 8 = 512 elements. And the common S-Box that we are going to use is (16 x 16 = 256) capable of holding 256 elements of 8-b each this is nothing but the S-Box that we use for AES and DES algorithms. Now, what we do is we club two elements starting from starting element till end and represent them in the hexadecimal value and dump it into the common S-Box. As already told the total elements in DES is 512 and each is of 4-b. Now, we just club two elements from DES S-Box i.e. of 4-b each and represent it as 8-b elements that fits into the Common S-Box. As show in the example the element 14 and 4 of 4-b each is clubbed and represented as E4 and the value is dumped into the first location of the Common S-Box and as such this is done for the rest of the elements and thus all the elements of DES S-Box is dumped into Common S-Box and hence the required functionality is achieved. But there is a small change because of this common box in the cipher function of the DES algorithm i.e. instead of using 6 i/p □ 4o/p LUT , we require an LUT of 8 i/p □ 8 o/p. And by using this technique we now require 2 S-Box as a whole instead of 11 S-Box, one for AES- inv-S-Box which is mandatory and other S-Box that is common to all the three algorithms and because of this strategy there is area reduction in the whole of the architecture.

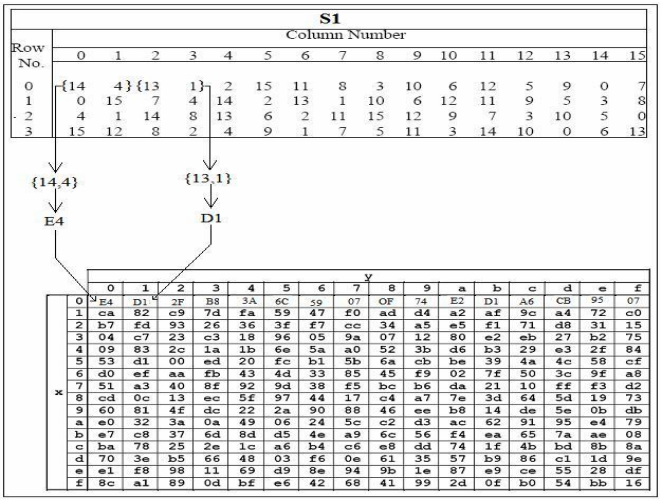

Fig.1. Common S-Box Technique

III. CRYPTOGRAPHY CORE ARCHITECHTURE

The complete cryptography architecture is designed using Verilog HDL language and is synthesized using Xilinx and cadence RTL compiler. The cryptography core functions as standard AES or standard DES or MDES according to the selection of the control signals. The block diagram of the complete cryptography architecture is shown in the Fig.2.

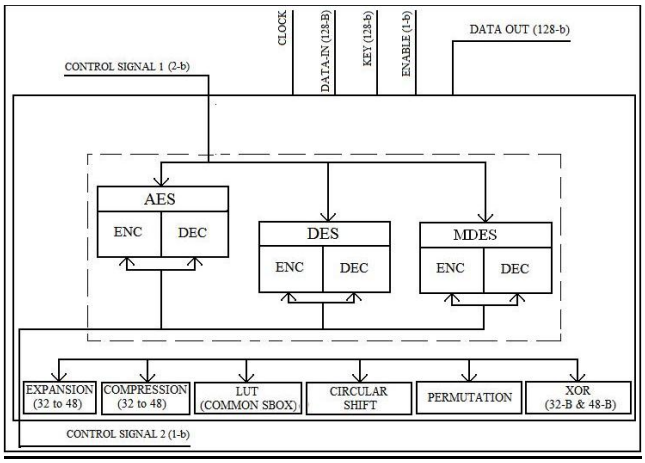

Fig.2. Cryptography architecture

IV. CRYPTOGRPHY CORE OPERATION

The working of the core is started with the help of enable signal. As soon as the architecture is given enable signal, the structure start working as any of these algorithms on the basis of the control signal provided the algorithms works in flow with the clock signal.

ENABLE	CONTROL1	CONTOL2	OUTPUT
0	??	?	HIGH IMPEDANCE
1	00	1	AES ENCRYPTION
1	00	0	AES DECRYPTION
1	01	1	DES ENCRYPTION
1	01	0	DES DECRYPTION
1	10	1	MDES ENCRYPTION
1	10	0	MDES DECRYPTION

Table.1. Working Operation of Cryptography Core

The Table.1 reveals the combinations of the control signal and is corresponding algorithm selection for functioning of the architecture.

The necessary operations required for direct implementation of the cryptography algorithm is shown in Below Table.2.

ALGORITHM	Expand / Permutation	LUT Logical	XOR	Circular/Logical Right/Left shift	LUT (S-box)
AES	-	8in=> 8out		32 (32 by 8b)	2
DES	32,48,56,64	6in=> 4out	32, 48	28(by 1b or 2b)	8
MDES	32,48,56,64	8in=> 8out	32,48 ,64	28(by 1b or 2b)	1

Table.2.Basic Operation Required For Implementation of the algorithm

This gives us an idea on what are the operations that governs the working condition of the algorithm.

ALGORITHM	Expand / Permutation	LUT Logical	XOR	Circular/Logical Right/Left shift	LUT (S-box)
AES	-	8in=> 8out		32 (32 by 8b)	2
DES	32,48,56,64	6in=> 4out	32, 48	28(by 1b or 2b)	8
MDES	32,48,56,64	8in=> 8out	32,48 ,64	28(by 1b or 2b)	1

Table.3. Basic Operation Required For Implementation after Reordering

The procedure for designing this cryptography core is to express the high level operations of each algorithm in terms of basic arithmetic and logical operations to maximize the Number of common operations among the algorithms and also using the common S-Box technique results in minimize the overall required architecture area. Hence some of the operations that are common to the algorithms are expansion (32 to 48), compression (48 to 32), LUT, permutation, xor operation, which gets plugged into architecture of the algorithm whenever it is called for functioning. Table.3 shows the operations required for each algorithm after reorganization of the architecture.

V. SECURITY ENHANCEMENT IN CRYPTOGRAPHY CORE

In the working operation of the cryptography core a simple technique is used in order to increase the security level to the data being transferred. Fig.3 shows technique show the technique used.

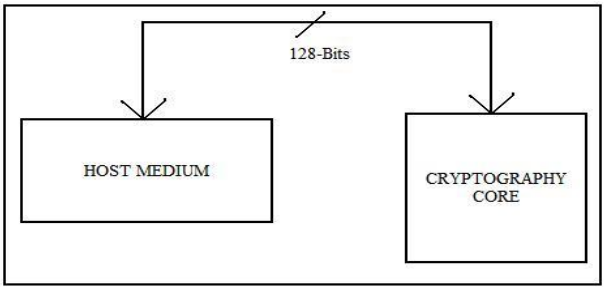

Fig.3. Security Enhancement Technique

Here the data input and the key to core is of 128-b and the data out is also128-b. In general when the data's are encrypted using AES algorithm, the output transferred is 128-b, but when the other two algorithms are used for encryption process the data out should be 64-b as these two algorithms are 64-b block cipher algorithms as explained before, but the data coming out of this core is of 128-b, i.e. the 64-b encrypted/decrypted data is embedded into the 128-b data coming out.

This helps in increasing the security level because in general if it is going to be 64-b data, the hacker has to try all 2^{64} combinations to data out to crack and find the information which takes a longer time, but here as the important data is embedded into 128-b data coming out, it's a tough job to hack the information and apart from this, the selection of which algorithm to work at what time by the host medium too increase security level.

VI. EXPERIMENTAL RESULTS

The Table.4 shows the result of the cell usage and other details when the design is targeted to ASIC and synthesized using the Xilinx's RTL compiler. Here the cell usage of cryptography core using 2 S-Box is less when compared to that of using 11 S-Box.

ALGORITHM	No of Cells Used	Power(w)	Time Period(ns)	Frequency of Operation (MHz)
CRYPCORE(11 S-BOX)	288153	0.156	24.597	40.683
CRYPCORE(2 S-BOX)	245838	0.082	24.733	40.431

Table.4. Area and Timing Report for Design Using Xilinx's RTL Compiler Targeting 180 nm

VII. CONCLUSION

A simple technique to address the important issue of performance improvement of the cryptography core is discussed in this work and also explains the design of cryptography core for electronic devices and other desired applications used for secure data transmission using private Key algorithm. Through the simulation and synthesize results, we have inferred that performance level of the cryptography core is increased and we have achieved this by expressing the operations of the three algorithms namely the standard AES, standard DES and MDES in terms Of basic arithmetic and logical operations that maximizes the number of common blocks among them and also using common S-Box technique, resulting in merging of these three algorithms in a single core. And, this design also increasing the security level by controlling the core to Operate in different algorithms at a particular time with the help of control signal which is transferred via secure data line using private key algorithm, making it too difficult for hacking and other external attacks. A few extra works that can be added to this design in future to enhance its capabilities are implementing the private key cryptography algorithm onto this core, which helps in secure transfer of keys and the control signals used for the operation of the core.

REFERENCES

[1] Data Encryption Standards (DES), Oct.1999.FIPS standards publications.
[2] Advanced Encryption Standard (AED), Nov.2001.FIPS standards publication 197.
[3] AES and DES Algorithm, "Wikipedia-Free Encyclopaedia".
[4] Atul Kahate, "Cryptography and Network Security", 2003.
[5] William stalling, ''Cryptography and Network Security Principles and Practice''.
[6] John Daemen and Vincent Rijmen, "AES proposal: Rijndael".
[7] J.Bhaskar, "Verilog HDL primer and Verilog HDL synthesize".

International Journal of Modern Engineering Research (IJMER)
www.ijmer.com Vol. 3, Issue. 4, Jul - Aug. 2013 pp-2446-2450 ISSN: 2249-6645

Simulation of three-phase bridge rectifier using MATLAB/ SIMULINK for harmonic mitigation

Himanshu Chaturvedi[1], Anil K. Chaudhary[2], C. Veeresh[3]
[1, 2, 3](Department of Electrical and Electronics Engineering, MIT Mandsaur (M.P.), India)

ABSTRACT: *Power quality standards (IEEE-519) compel to limit the total harmonic distortion (THD) within acceptable range caused by rapid usage of power electronic equipment. This paper envisages on the simulation of instantaneous active and reactive theory based shunt active filter with MATLAB/Simulink, as a better solution for reduction of the harmonics.*

Key words: *Active Filters, THD, Instantaneous Power Theory*

I. INTRODUCTION

In a modern power system, due to the broader applications of nonlinear loads such as power electronic equipment or arc furnaces, the degree of waveform distorted is increasingly serious now [1]. These loads may cause poor power factors, lead to voltage notch, or result in a high degree of harmonics. Such cases have brought the power quality as an increasing concern. Moreover, from economical viewpoints, a utility's revenue may get affected at a higher cost. Therefore, efficient solutions for solving these pollution problems have become highly critical for both utilities and customers [3].

The amount of distortion in the voltage or current waveform is quantified by means of an index called the total harmonic distortion (THD) [1]. The THD in current is defined as

$$\%THD = 100 * \sqrt{\sum_{n\neq 1}\left(\frac{I_{sn}}{I_{sl}}\right)^2}$$

Conventionally methods are of harmonics/current reference and classified either as time or frequency-domain and are limited steady-state analysis. This paper envisages on the instantaneous power theory validating both the steady and transient-state analysis. The compensation command signals are obtained from the instantaneous active power and the instantaneous reactive power. This method does not require the phase synchronization.

The harmonic causes problems in power systems and in consumer products such as equipment overheating, motor vibration, excessive neutral currents and low power factor. Conventionally, passive LC filters and capacitors have been used to eliminate line current harmonics and to compensate reactive power by increasing the power factor. But these filters have the disadvantages of large size, resonance, and fixed compensation behavior so these conventional solutions becomes ineffective [4]. Therefore concept of active power filters was proposed to mitigate harmonic problems and to compensate reactive power. Since then the theories and applications of active power filters have become more popular and have attracted great attention .It is to be noted that non sinusoidal current results in many problems for the utility power supply company, such as low power factor, low energy efficiency, electromagnetic Interference (EMI), distortion of line voltage etc [6].

II. INSTANTANEOUS POWER THEORY

Moinuddin k SYED [1] proposed a theory based on instantaneous values in three-phase power systems with or without neutral wire, and is valid for steady-state or transitory operations, as well as for generic voltage and current waveforms called as Instantaneous Power Theory or Active-Reactive (p-q) theory which consists of an algebraic transformation (Clarke transformation) of the three-phase voltages in the a-b-c coordinates to the α-β-0 coordinates, followed by the calculation of the p-q theory instantaneous power components:

$$\begin{bmatrix} V_0 \\ V_\alpha \\ V_\beta \end{bmatrix} = \sqrt{\frac{2}{3}} \begin{bmatrix} 1/\sqrt{2} & 1/\sqrt{2} & 1/\sqrt{2} \\ 1 & -1/2 & -1/2 \\ 0 & \sqrt{3}/2 & \sqrt{3}/2 \end{bmatrix} \begin{bmatrix} V_a \\ V_b \\ V_c \end{bmatrix} \quad (1)$$

$$\begin{bmatrix} V_a \\ V_b \\ V_c \end{bmatrix} = \sqrt{\frac{2}{3}} \begin{bmatrix} 1/\sqrt{2} & 1 & 0 \\ 1/\sqrt{2} & -1/2 & \sqrt{3}/2 \\ 1/\sqrt{2} & -1/2 & -\sqrt{3}/2 \end{bmatrix} \begin{bmatrix} V_0 \\ V_\alpha \\ V_\beta \end{bmatrix} \quad (2)$$

Where V_a, V_b , V_c are phase voltages. Identical relations hold for line currents i_a, i_b, i_c.

The instantaneous three - phase power is given by:

$$P_{3\phi}(t) = v_a i_a + v_b i_b + v_c i_c = v_\alpha i_\alpha + v_\beta i_\beta + v_0 i_0$$
$$= p_a(t) + p_b(t) + p_c(t) = p_\alpha(t) + p_\beta(t) + p_0(t)$$
$$= p(t) + p_0(t) \quad (3)$$

Where $p = p_\alpha + p_\beta$ is instantaneous real power, and $p_0(t) = v_0 i_0$ is the instantaneous zero-sequence power.

One advantage of using the transformation of α-β-0 is to separate the zero-sequence component of the system.

The reactive power measurement can be give by $q(t) \approx v_\alpha i_\beta - v_\beta i_\alpha$ (4)

Rewritten in terms of a-b-c components as

$$q = -[(v_a - v_b)i_c + (v_b - v_c)i_a + (v_c - v_a)i_b]/\sqrt{3} \quad (5)$$

The power p and q can be rewritten as

$$\begin{bmatrix} p \\ q \end{bmatrix} = \begin{bmatrix} v_\alpha & v_\beta \\ -v_\beta & v_\alpha \end{bmatrix} \begin{bmatrix} i_\alpha \\ i_\beta \end{bmatrix} \quad (6)$$

From this matrix equation, for $\Delta = {v_\alpha}^2 + v_\beta^2$

$$\begin{bmatrix} i_\alpha \\ i_\beta \end{bmatrix} = \frac{1}{\Delta} \begin{bmatrix} v_\alpha & -v_\beta \\ v_\beta & v_\alpha \end{bmatrix} \begin{bmatrix} p \\ q \end{bmatrix} \quad (7)$$

Separating the Active and Reactive parts

$$\begin{bmatrix} i_\alpha \\ i_\beta \end{bmatrix} = \frac{1}{\Delta} \left\{ \begin{bmatrix} v_\alpha & -v_\beta \\ v_\beta & v_\alpha \end{bmatrix} \begin{bmatrix} p \\ 0 \end{bmatrix} + \begin{bmatrix} v_\alpha & -v_\beta \\ v_\beta & v_\alpha \end{bmatrix} \begin{bmatrix} 0 \\ q \end{bmatrix} \right\}$$

$$\cong \begin{bmatrix} i_{\alpha p} \\ i_{\beta p} \end{bmatrix} + \begin{bmatrix} i_{\alpha q} \\ i_{\beta q} \end{bmatrix} \quad (8)$$

Where, the current components are

$$i_{\alpha p} = v_\alpha p/\Delta \ , \quad i_{\alpha q} = -v_\beta q/\Delta \quad (9)$$

$$i_{\beta p} = v_\beta p/\Delta \ , \quad i_{\beta q} = -v_\alpha q/\Delta \quad (10)$$

Power in phases α and β can be separated as

$$\begin{bmatrix} p_\alpha \\ p_\beta \end{bmatrix} = \begin{bmatrix} v_\alpha & i_\alpha \\ v_\beta & i_\beta \end{bmatrix} = \begin{bmatrix} v_\alpha & i_{\alpha p} \\ v_\beta & i_{\beta p} \end{bmatrix} + \begin{bmatrix} v_\alpha & i_{\alpha q} \\ v_\beta & i_{\beta q} \end{bmatrix}$$

$$\cong \begin{bmatrix} p_{\alpha p} \\ p_{\beta p} \end{bmatrix} + \begin{bmatrix} p_{\alpha q} \\ p_{\beta q} \end{bmatrix} \quad (11)$$

Where, the power components are

$$p_{\alpha p} = v_\alpha i_{\alpha p} = v_\alpha^2 p/\Delta \quad (12)$$

$$p_{\alpha q} = v_\alpha i_{\alpha q} = -v_\alpha v_\beta q/\Delta \quad (13)$$

$$p_{\beta p} = v_\beta i_{\beta p} = v_\beta^2 p/\Delta \quad (14)$$

$$p_{\beta q} = v_\beta i_{\beta q} = v_\alpha v_\beta q/\Delta \quad (15)$$

Therefore the three phase active power can be rewritten

$$p_{3\phi} = p_\alpha + p_\beta + p_0$$

$$= p_{\alpha p} + p_{\alpha q} + p_{\beta p} + p_{\beta q} + p_0$$

$$= p_{\alpha p} + p_{\beta p} + p_0 \quad (16)$$

Thus from equations (13) and (15)

$$p_{\alpha q} + p_{\beta q} = 0 \quad (17)$$

Thus

$p_{\alpha p} - \alpha$ axis instantaneous active power.

$p_{\beta p} - \beta$ axis instantaneous active power.

$p_{\alpha q} - \alpha$ axis instantaneous reactive power.

$p_{\beta q} - \beta$ axis instantaneous reactive power.

It is observed that the reactive power corresponds to the parts of instantaneous power, which is dependent on the instantaneous imaginary power q, in each independent phase and vanishes when added $(p_{\alpha q} + p_{\beta q} = 0)$, in a two-phase $(\alpha - \beta)$ system.

Instantaneous real power p, gives the net energy per second being transported from source to load and vice-versa at any time, which is dependent only on the voltage and currents in phases α and β and has no zero-sequence present.

Non-linear Load

The three phase sinusoidal voltages supplying a non-linear load are represented as

$$v_a = \sqrt{2} v sin\omega t$$

$$v_b = \sqrt{2} v sin(\omega t + 120°)$$

$$v_c = \sqrt{2} v sin(\omega t - 120°) \quad (18)$$

And the currents being

$$i_a = \sum_{n=1}^{\infty} \sqrt{2}\, I_n \sin(n\omega t - \emptyset_n)$$

$$i_b = \sum_{n=1}^{\infty} \sqrt{2}\, I_n \sin[n(\omega t + 120°) - \emptyset_n]$$

$$i_c = \sum_{n=1}^{\infty} \sqrt{2}\, I_n \sin[n(\omega t - 120°) - \emptyset_n] \quad (19)$$

Then,

$i_\alpha = \sum_{n=1}^{\infty} \frac{2}{\sqrt{3}} I_n \sin(n\omega t - \emptyset_n)\,[1 - \cos(n120°)]$ (20)

$i_\beta = \sum_{n=1}^{\infty} 2I_n \cos(n\omega t - \emptyset_n) \sin(n120°)$ (21)

$i_0 = \frac{1}{\sqrt{3}}(i_a + i_b + i_c)$

$\sum_{n=1}^{\infty} \sqrt{6}\, I_{3n} \sin(3n\omega t - \emptyset_{3n})$ (22)

The power components p, q, p_0 and $p_{3\emptyset}$ are

$P = v_\alpha i_\alpha + v_\beta i_\beta = p_{\alpha p} + p_{\beta p}$

= $3VI_1\cos\phi_1$ - $3VI_2\cos(3\omega t-\phi_2)$ + $3VI_4\cos(3\omega t+\phi_4)$ – $3VI_5\cos(6\omega t-\phi_5)$ + $3VI_7\cos(6\omega t+\phi_7)$ - …. (23)

$q = v_\alpha i_\beta - v_\beta i_\alpha$

= $3VI_1\sin\phi_1$ - $3VI_2\sin(3\omega t-\phi_2)$ + $3VI_4\sin(3\omega t+\phi_4)$ – $3VI_5\sin(6\omega t-\phi_5)$ + $3VI_7\sin(6\omega t+\phi_7)$ - …. (24)

$P_0 = v_0 i_0 = 0$ and $P_{3\emptyset}$= p (25)

Thus, these expressions are

$P = \bar{P} + \tilde{P}$ and $q = \bar{q} + \tilde{q}$ (26)

Each of these expressions represents the mean-value and alternating components with mean-value equal to zero.
From (23) and (24) it can be concluded that

$\bar{P} = P_{3\emptyset}$ and $\bar{q} = Q_{3\emptyset}$ (27)

Thus the harmonic power is given by

$H = \sqrt{\tilde{P}^2 + \tilde{Q}^2}$ (28)

Where $\tilde{P}$ and $\tilde{Q}$ are the RMS values of $\tilde{p}$ and $\tilde{q}$, respectively.

III. COMPENSATION STRATEGY

The reactive and harmonic compensation is carried by injecting appropriate currents into the circuit through a compensator i.e., shunt active filter as shown in Fig.1.

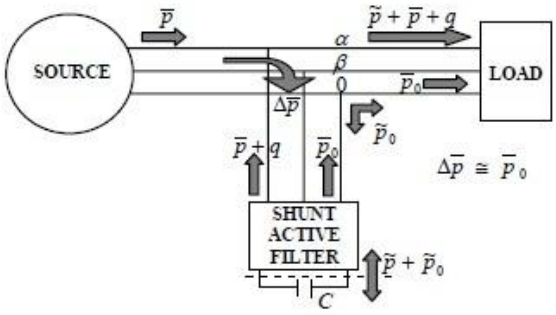

Fig.1. Strategy of Instantaneous Power Theory

In order to compensate $P_{\alpha q}$ and $P_{\beta q}$, currents $i_{\alpha c}$ and $i_{\beta c}$ are injected equivalent to reactive currents as

$i_{\alpha c} = i_{\alpha q}$, and (29)

$i_{\beta c} = i_{\beta q}$ (30)

Where, $i_{\alpha q}$ and $i_{\beta q}$ are given by (9) and (10). The current $i_{\alpha c}$ is in shunt with the voltage source v_α, thus supplies the power $P_{\alpha q} = v_\alpha i_{\alpha q}$. Similarly, the current source $i_{\beta c}$ supplies $P_{\beta q} = v_\beta\, i_{\beta q}$. Thus, the voltage source v_α and v_β need to supply only $P_{\alpha p}$ and $P_{\beta p}$. From (17), the power necessary to compensate for $i_{\alpha q}$ is equal to the negative of the power necessary to compensate for $i_{\beta q}$.

The current source $i_{\alpha c}$ and $i_{\beta c}$ represent active power filters that are generated from the VSI inverter controlled to generate $i_{\alpha q}$ and $i_{\beta q}$. As such, no DC source is necessary and also no large energy storage element is necessary to compensate the reactive power. Instantaneously, the reactive power required by one phase can be supplied by the other one. This means that, the size of the capacitor does not depend on the amount of reactive power to be compensated. In fact, in actual systems only a small capacitor is used because the switching of the inverters.

As stated in (26), p can be decomposed in two parts as $\bar{p}$ and $\tilde{p}$. As $\bar{p}$ is the actual working power, only $\tilde{p}$ has been compensated.

Thus (12) and (14) are modified to:

$P_{\widetilde{\alpha p}} = v_\alpha i_{\widetilde{\alpha p}} = v_\alpha^2 \tilde{p}/\Delta$ (31)

$P_{\widetilde{\beta p}} = v_\beta i_{\widetilde{\beta p}} = v_\beta^2 \tilde{p}/\Delta$ (32)

The above power terms have mean-value equal to zero but their summation is not zero at every instant, that is, $P_{\widetilde{\alpha p}} + P_{\widetilde{\beta p}} \neq 0$. The capacitor receives energy when $\tilde{p}$ is negative and supplies when $\tilde{p}$ is positive.

IV. SIMULATION RESULTS

The simulation of the proposed instantaneous power theory is carried on MATLAB/Simulink as represented in the Fig.2.

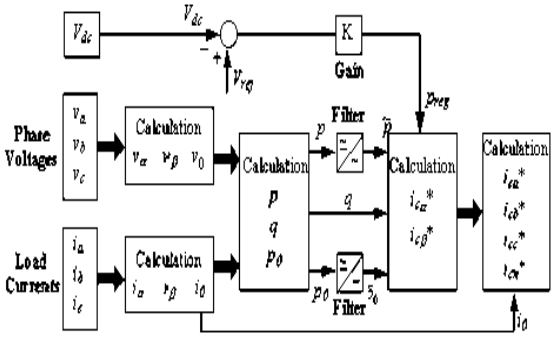

Fig.2. Proposed power control strategy

The source supply is designed with amplitude of 360 volt and frequency of 315 rad/sec with a phase difference of 2.0944 rad between phases.

The load is simulated to include harmonic distortion by injecting the diode current generated from a three phase uncontrolled diode rectifier of 36KW and a three phase fully controlled thyristor rectifier of 12KW with 60˚ firing delay angle.

A VSI inverter is instantaneous and infinitely fast to track current reference and is implemented as a current amplifier with unity gain block with unity value.

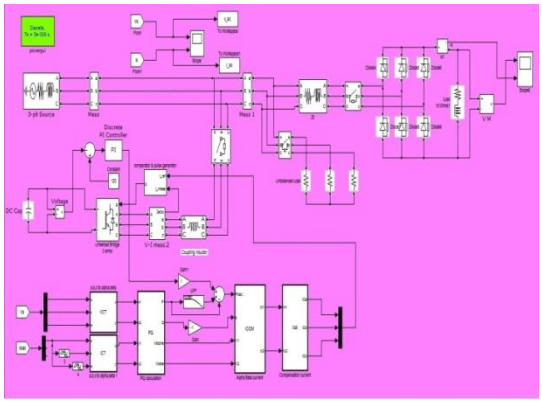

Fig.3. Circuit diagram of PWM Control Technique of Shunt Active Power Filter

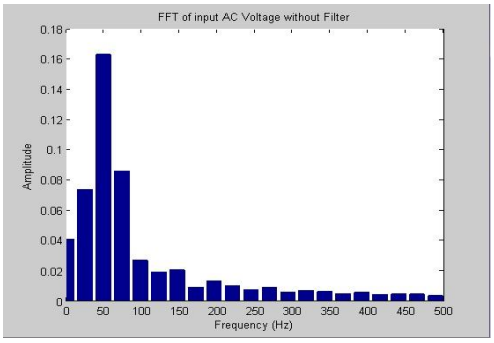

Fig.4. FFT of input AC Voltage without Filter

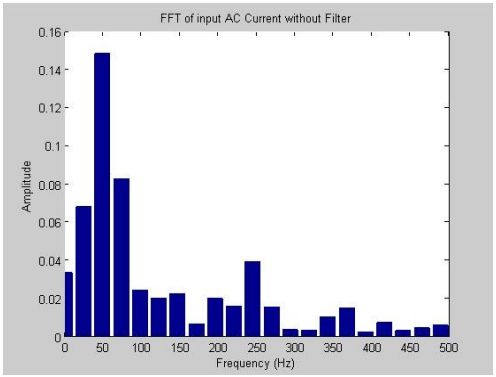

Fig.5. FFT of input AC Current without Filter

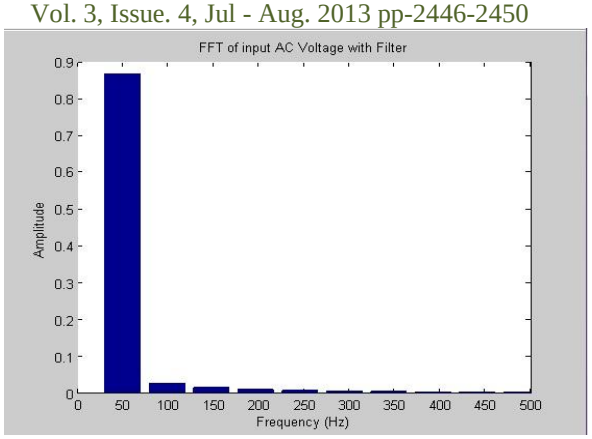

Fig.6. FFT of input AC Voltage with Filter

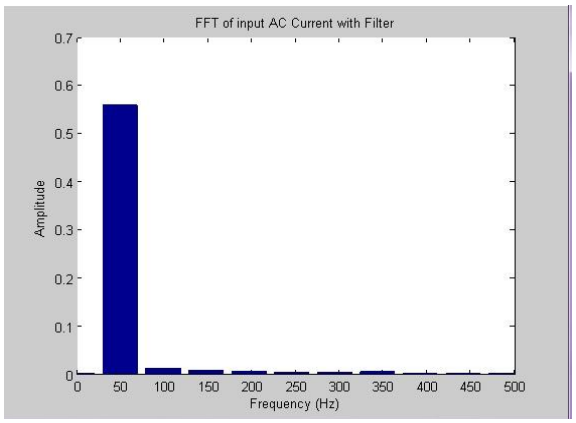

Fig.7. FFT of input AC Current with Filter

V. CONCLUSIONS

Instantaneous power theory gives a piecemeal approach in analysis and control of the active and reactive components of the harmonic load and introduces the active power filter for appropriate corrective measure for the total harmonic distortion for improvement of the power quality as per the scheduled standards.

Energy efficient power supplies incorporating active power supplies shall govern the future in the electrical power quality standardizations.

REFERENCES

[1] Moinuddin k SYED, "Instantaneous Power Theory Based Active Power Filter: A Matlab/ Simulink Approach" Journal of Theoretical and Applied Information Technology.
[2] Bhim Singh, "A Review of Active Filters for Power Quality Improvement" Vol.46, No.5, 1999.
[3] M. Chakravarthy,"Control of shunt active power filters in power system using MATLAB/SIMULINK" Vol. 1, pp 226, 2012
[4] R. M. Potdar," Comparison of topologies of shunt active power filter implemented on three phase four wire system", Vol-1, Issue-5, 2011
[5] Suresh Mikkili, "Simulation and RTDS Hardware implementation of SHAF for mitigation of current harmonics with p-q and I_d-I_q control strategies using PI controller", Vol.1, No.3, 2011
[6] Sachine Hirve, "PLL-Less Active Power Filter based on one-cycle control for compensating unbalanced loads in three-phase four wire system" Vol.22, No.4, 2007
[7] Javid Akhtar, "Modeling and Simulation of STATCOM for a power system network using MATLAB/SIMULINK", Vol2, Issue8, pp 12-17
[8] Sindhu.S, "Implementation of Three phase Shunt Hybrid Filter using ICOSØ Algorithm, Vol.5, No.1, Aug2011, pp7
[9] Ibrahim A., "Shunt Active Power Filter Based on Diode Clamped Inverter and Hysteresis band current controller", pp84
[10] Vaibhav Purwar, "Simulation of shunt active Power Line conditioner (APLC) for three phases AC/DC converter", IJEECE, Vol.1 (9), 2011, 504-513
[11] George Adam, "A MATLAB-SIMULINK APPROACH TO SHUNT ACTIVE POWER FILTERS
[12] I. Zamora, "Simulation by MATLAB/Simulink of active filters for reducing THD created by industrial systems,
[12] Mr. D.R. Dobariya, Matlab Simulation Of Hybrid Active Power Filter Using Instantaneous Reactive Power Theory
[13] Consalva J. Msigwa, "Control Algorithm for Shunt Active Power Filter using synchronous reference frame theory,WASET,2009
[14] N. Senthilnathan, "A novel control strategy for Line harmonics reduction using three phase shunt active filter with balanced and unbalanced supply, EJSR, Vol.67,Nov.3,pp456-466
[15] Y. Satish kumar, Instantaneous Power theory active power filter, IJASTR, Vol.4, Issue 2, 2012, pp342.
[16] J. Chelladurai, "Investigation of various PWM techniques for shunt active filter, WASET, 2008, PP192.

International Journal of Modern Engineering Research (IJMER)
www.ijmer.com Vol. 3, Issue. 4, Jul - Aug. 2013 pp-2451-2455 ISSN: 2249-6645

Investigating Waste Water Treatment in a Closed Environment

T. S. Nurudeen[1], R. A. Kareem[2], S. O. Salawu[3]
[1, 2]*Department of Mathematics, Lagos State Polytechnic, Ikorodu, Nigeria*
[3]*Department of Mathematics, University of Ilorin, Ilorin, Nigeria*

Abstract: *This paper focuses on the investigation of the claim of 'The Sound and Environmental Water and Effluent Re-cycling company' that water can be completely purified if a population of at least 10 organisms per cubic centimeter can be maintained in its cleaning tank for a period of at least 8 days. We investigated the growth patterns of each of these organisms and make recommendations about which one will provide the most efficient water treatment and how many organisms should be introduced initially.*

Keyword: *Environment, Waste, Micro-organisms and Water Treatment,*

I. INTRODUCTION

The importance of these kinds of investigations as well as the complimentary experimental works, say in large-scale water treatment and redistribution networks, thus makes them of great relevance [1-6]. It should however be remarked that to date, the literature on the waste water treatment is still quite sparse. This then forms the crux of the current investigation [8]. Untreated water supply causes a serious socio-ecological hazard. If the problem is not carefully controlled and monitored, large communities can be exposed to extensive health risks. It then requires taking immediate corrective measure to redress and mitigate against its impact in the society [9].

The use of micro organisms to clean waste water and make it safe for re-use is good idea for water treatment. The micro-organisms feed on harmful bacteria, thus removing them from the water. The efficiency of this method depends upon choosing the correct species of micro-organism and ensuring that it is able to thrive in the tank of waste water successfully for long enough to consume all the bacteria [7]. However, it is important that the population declines after completing its function, since the ecological balance could be upset by discharge number of micro-organism into the environment.

II. MODEL EQUATION

The growth of micro-organism in a closed environment (such as the cleaning tank) is determined by three principle factors.

- The reproduction rate
- The effect of increased crowding
- The build-up of toxins produced as waste products by the organisms.

This can be modeled by the equation [9]

$$\frac{du}{dt} = au - bu^2 - cu\int_0^t u(\tau)d\tau \qquad (1)$$

Where $u(t)$ the number of organisms per cubic centimeter of water is, a is the reproduction ratio, b is the crowding coefficient, and c is a measure of the sensitivity of the organisms to toxins. The integral term is necessary since the toxins in the environment are built up gradually over a period of time at a rate proportional to the number of organisms present.

The model equation in (1) which is in Integra-differential equation is reduced to differential equations of the form

Let $x(t) = \int_0^t u(\tau)d\tau$

$$\frac{dx}{dt} = \int_0^t \frac{d}{dt}u(\tau)d\tau + u(t)$$

$$\frac{dx}{dt} = u(t)$$

$$x' = u \qquad (2)$$

Then (1) becomes

$$\frac{du}{dt} = au - bu^2 - cux$$

$$u' = au - bu^2 - cux \qquad (3)$$

III. NUMERICAL SOLUTION

The claim of SEWER scientists that water can be completely purified if a population of at least 10 organisms per cubic centimeter can be maintained in its cleaning tank for a period of at least 8 days. We investigated by a MATLAB code for equations (2) and (3) that give the plots below on which the investigation is made.

The maximum permissible population within water discharged into the environment is 0.05 per cubic centimeter. We considered the micro-organism (multiplicanda numerosa, solo anti-socials and reproductio sensitova) whose growth is determined by the three principle factors a, b and c defined above. Alternatively, they could use the combination of these three. These can be categorized into 7 cases for the organism coefficients.

Case 1
Multiplicanda numerosa

$$a = 20, b = 0.01, c = 0.003$$

Case 2
Solo anti-socialis

$$a = 5, b = 0.5, c = 0.01$$

Case 3
Reproductio sensitova

$$a = 0.5, b = 0.001, c = 0.08$$

Case 4
Multiplicanda numerosa and Solo anti-socialis

$$a = 25, b = 0.51, c = 0.013$$

Case 5
Multiplicanda numerosa and Reproductio sensitova

$$a = 20.5, b = 0.011, c = 0.083$$

Case 6
Solo anti-socialis and Reproductio sensitova

$$a = 5.5, b = 0.501, c = 0.09$$

Case 7
Multiplicanda numerosa, Solo anti-socialis and Reproductio sensitova

$$a = 25.5, b = 0.511, c = 0.093$$

In summary the following table shows the different cases.

Case	Organism	Reproduction rate	Crowding effect	Toxin Build-up
1	mn	20	0.01	0.03
2	sa	5.0	0.5	0.01
3	rs	0.5	0.001	0.08
4	$mn + sa$	25	0.51	0.013
5	$mn + rs$	20.5	0.011	0.083
6	$sa + rs$	5.5	0.501	0.09
7	$mn + sa + rs$	25.5	0.511	0.093

Where
mn = Multiplicanda numerosa
sa = Solo anti-socialis
rs = Reproductio sensitova

Plot for cases 1 -7 are given in figures 1 – 7 below for 50 days in which the analysis of the results are based. The number of organisms per cubic centimetre chosen by experiments as initial values is 10, 20 and 30. The plots are given together for comparison from which the following inferences are drawn.

Case 1

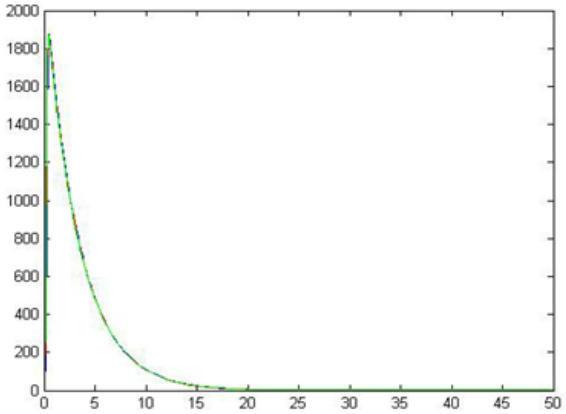

Figure 1: a = 20; b = 0:01; c = 0:03

Case 2

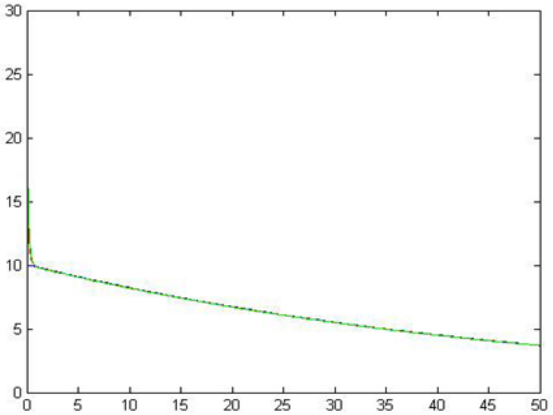

Figure 2: a = 5; b = 0:5; c = 0:01

Case 3

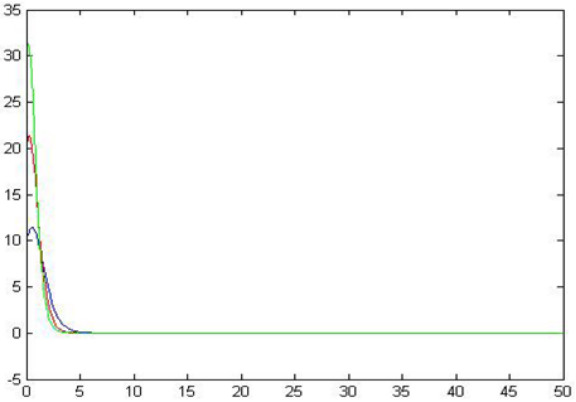

Figure 3: a = 0:5; b = 0:001; c = 0:08

Case 4

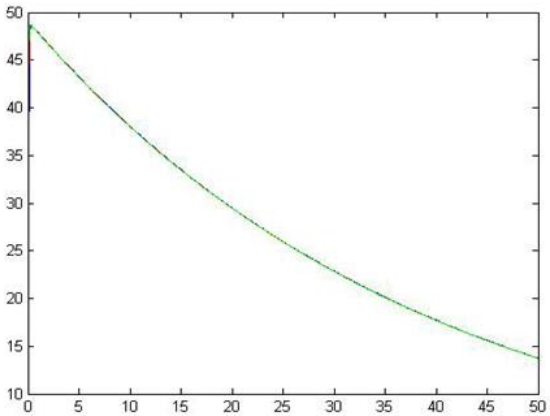

Figure 4: a = 25; b = 0:51; c = 0:013

Case 5

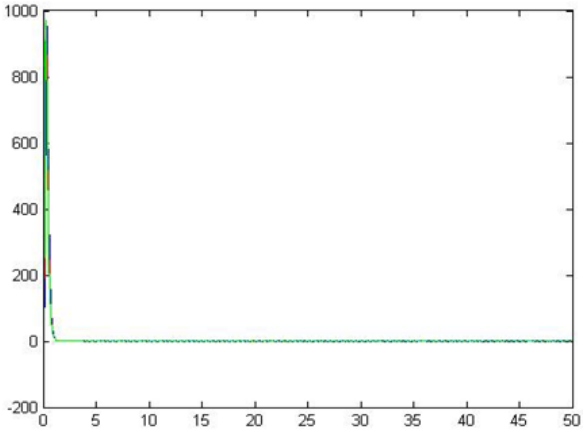

Figure 5: a = 20:5; b = 0:011; c = 0:083

Case 6

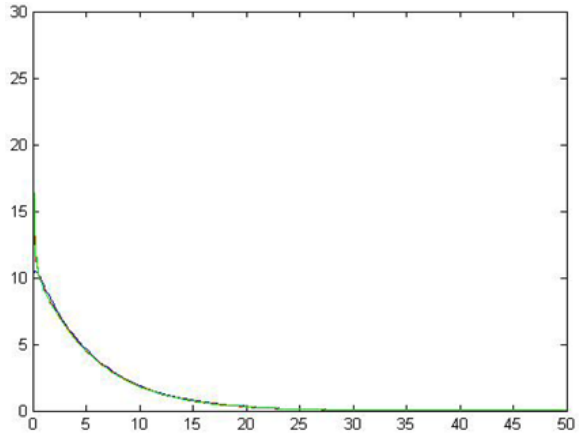

Figure 6: a = 5:5; b = 0:501; c = 0:09

Case 7

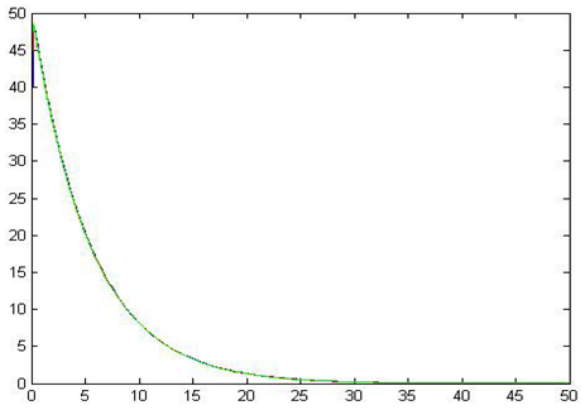

Figure 7: a = 25:5; b = 0:511; c = 0:093

IV. DISCUSSION OF RESULTS

It is observed from figures 1, 4, and 7 that number of organisms is more than 10 so growth of organisms is limited due to crowding effects. Toxin build-up only dominating in the long run, hence the population is insensitive to toxins. They are all good methods of treatment.

Also for figures 2, 3, 5 and 6, it is observed that the number of organisms is less than 10. Growth is immediate due to lack of crowding effects and checked by accumulation of toxins. The populations are sensitive to toxins. They are not good methods of waste water treatment.

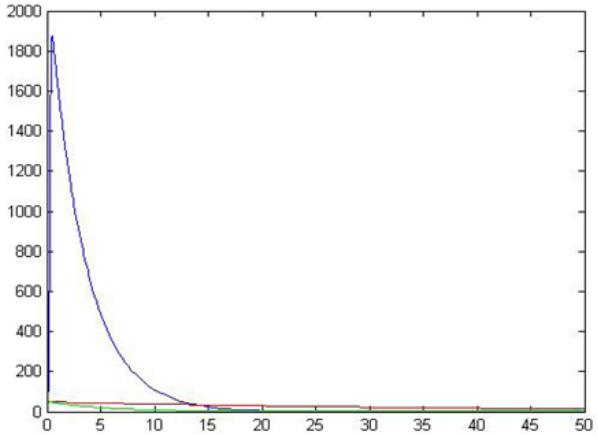

Figure 8a

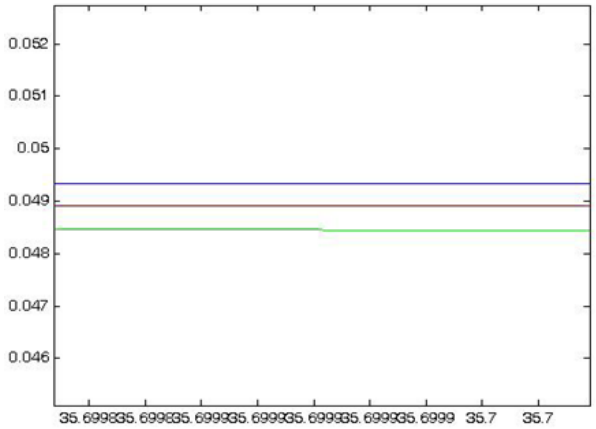

Figure 8b

V. CONCLUSION

Cases 1, 4 and 7 provide more efficient water treatment as evident in the observation compared to cases 2, 3, 5 and 6. From the figures, it is obvious that case 1 (i.e. Multiplicanda numerosa) with the largest amplitude curves brings the logistic curve with slow decay will provide the most efficient water treatment because it can successfully thrive in the tank of waste water to consume all the bacteria in fewer days and has the maximum permissible population below 0.05 per cubic centimeter (see figure 8b) within water discharge into the environment. This is evident in figure 8a which shows the comparison between 1, 4 and 7. So from figure 8b, 10 organisms should be introduced initially and this confirms the claim of the SEWER scientists.

REFERENCE

[1] C. Zheng and G. D. Bennett Applied Contaminant Transport Modeling: Theory and Practices, Van Nostrand Rienhold, 1995.
[2] P. Dulal and S. Khan, "A time dependence mathematical model for dispersion of air pollutant from point sources," International Journal of Environmental Studies, vol. 35, pp. 197–208, 1990.
[3] M. Summerfield and W. Krebs, "Particle dispersion in a swirling confined jet flow source," Particle Characterization, vol. 7, pp. 16–24, 1990.
[4] J. F. Sini, S. Anquetin, and P. G. Mestayer, "Pollutant dispersion and thermal effects in urban street canyon," Atmospheric Environment, Urban Atmospheric, vol. 30, pp. 2659–2677, 1996.
[5] O. D. Makinde, R. J.Moitsheki, and B. A. Tau, "Similarity reductions of equations for river pollution," Applied Mathematics and Computation, vol. 188, no. 2, pp. 1267–1273, 2007.
[6] R. J. Moitsheki and O. D. Makinde, "Symmetry reductions and solutions for pollutant diffusion in a cylindrical system," Nonlinear Analysis: Real World Applications, vol. 10, no. 6, pp. 3420–3427, 2009.
[7] SEWER, '' The uses of Micro-organisms to clean waste water and make it safe for re-use'' 2009
[8] T. chinyoka and O.D. Makinde, '' Analysis of Nonlinear Dispersion of a poolutant ejected by an External Source into a Channel Flow: Hindaawi Publication Corporation Mathematical Problems in Engineering. p17. 2010
[9] M. S. Kalamkin, '' Mathematical Modelling'': Classroom notes in Applied Mathematics. 2010.
[10] T. I eldho, ''Management of Waste Water'': Department of Civil Enginering, IIT Bombay, 2011.

International Journal of Modern Engineering Research (IJMER)
www.ijmer.com Vol. 3, Issue. 4, Jul - Aug. 2013 pp-2456-2459 ISSN: 2249-6645

OXYSTELMA ESCULENTUM Stem Extracts as Corrosion Inhibitor for Mild Steel in Acid Medium

S. Ananth Kumar[1], A. Sankar[1], M. Vijayan[2], S. Ramesh Kumar[3]
[1]*Kandaswami Kandar's College, P. Velur, Namakkal-638 182, India*
[2]*Scientist, centre for conducting polymers, Electrochemical materials science division, Central Electrochemical research Institute, Karikudi-630006, India*
[3]*PSG College of Technology Peelamedu, Coimbatore 641 004, India*

Abstract: *The corrosion inhibitive action of oxystelma esculentum stem on mild steel corrosion in 0.5 M H_2SO_4 solution was studied using weight loss method, potentiodynamic polarization and EIS measurements. The results obtained indicate that the extracts functioned as good inhibitors in 0.5 M H_2SO_4 solution. Inhibition efficiency was found to increase with extract concentration. The adsorption of constituents in the plant extract on the surface of the metal is proposed for the inhibition behavior.*

Key words: *Inhibitor, Mass loss, Impedance, Polarization, oxystelma esculentum*

I. Introduction

Corrosion inhibitors are widely used in industry to reduce the corrosion rate of metals and alloys in contact with aggressive environments. Most of the corrosion inhibitors are synthetic chemicals, expensive, and very hazardous to environments. Therefore, it is desirable to source for environmentally safe inhibitors [1-3]. There are some reports on the inhibition effects of non-toxic compounds on the Corrosion of metals. We have recently reported the inhibition effect of amino acids on the steel [1] and aluminum [4] corrosion in acidic media. The rare earth metals have been proposed as corrosion inhibitors [5-8]. The inhibition effects of some non-toxic organic compounds have been also reported for steel corrosion [9, 10] but they are expensive. The aim of this study was to investigate the inhibition effect of *Oxystelma esculentum extract* as a cheap, raw and non-toxic corrosion inhibitor on mild steel corrosion in 0.5M H_2SO_4. The electrochemical measurements were used to evaluate the inhibition efficiencies.

II. MATERIAL AND METHODS

2.1 Preparation of oxystelma esculentum extract:

An aqueous extract of oxystelma esculentum stem extract was prepared by grinding 5g of plant stem, with distilled water, filtering the suspending impurities, and making up to 100 ml. The extract was used as corrosion inhibitor in the present study.

2.2 Preparation of specimens

Carbon steel specimens (0.022% S, 0.038% Mn, 0.027%P, 0.086 C) of dimension 1.0 cm *4.0cm*0.2cm were polished to a mirror finished with the emery sheets of various grades and degreased with trichloroethylene.

2.3 Weight loss method.

Carbon steel specimens in triplicate were immersed in 100 mL of the inhibited and uninhibited 0.5M H_2SO_4 solutions in the presence and absence of KI for two hours. The weight of each specimen before and after immersion was determined using shimadzu balance, model Ay 62.The inhibition efficiency (IE) was then calculated using the expression;

$$IE\% = \left(\frac{W_1 - W_2}{W_1}\right) \times 100$$

Where $W_1$and W_2 are the corrosion rates in the absence and presence of the inhibitor, respectively.

2.4 Electrochemical impedance measurements

The impedance measurements were performed using a computer –controlled potentiostat (model Solartron SI-1260) and the data were analyzed using gain phase analyser electrochemical interface (Solartron SI-1287). A three electrode set up was employed with Pt foil as the auxiliary electrode and a saturated calomel electrode as the reference electrode. The Teflon coated mild steel rod, with the surface prepared as described in the weight loss experimental method, served as the working electrode. The measurements were carried out in the frequency range 10^6–10^{-2} Hz at the open circuit potential by superimposing sinusoidal AC signal of small amplitude, 10 mV, after an immersion period of 30 min in the corrosive media. The double layer capacitance (C_{dl}) and charge transfer resistance (R_{ct}) were obtained from the impedance plots as described elsewhere**11**. Because R_{ct} is inversely proportional to corrosion current density, it was used to determine the inhibition efficiency (IE%) using the relationship;

$$IE\% = \frac{Rct - R^{0}ct}{Rct} \times 100$$

Where R_{ct} and R^{0}_{ct} are the charge transfer resistance values in the inhibited and uninhibited solutions respectively.

2.5. Polarization measurements

The potentiodynamic polarization curves were recorded using the same cell setup employed for the impedance measurements. The potentials were swept at the rate of 1.66mV/s, primarily from a more negative potential than E_{ocp} to a more positive potential than E_{ocp} through E_{corr}. The inhibition efficiencies were calculated using the relationship **12**;

$$IE\% = \frac{I^{0}corr - Icorr}{I^{0}corr} \times 100$$

Where I^{0}_{corr} and I_{corr} are the corrosion current densities in the absence and in the presence of inhibitor, respectively

III. RESULTS AND DISCUSSION

3.1 Analysis of results of mass loss method

The corrosion rates and inhibition efficiency values, calculated using weight loss data, for various concentrations of oxystelma esculentum extract in the presence and absence of KI the corrosion of carbon steel in 0.5M H_2SO_4 solution are presented in Table.1. It is apparent that the inhibition efficiency increased with the increase in inhibitor concentration in the presence and absence of KI . This behavior can be explained based on the strong interaction of the inhibitor molecule with the metal surface resulting in adsorption. The extent of adsorption increases with the increase in concentration of the inhibitor leading to increased inhibition efficiency. The maximum inhibition efficiency was observed at an inhibitor concentration of 100 ppm. Generally, inhibitor molecules suppress the metal dissolution by forming a protective film adsorbed to the metal surface and separating it from the corrosion medium. The corrosion suppressing ability of the inhibitor molecule originates from the tendency to form either strong or weak chemical bonds with Fe atoms using the lone pair of electrons present on the O and π electrons in benzene ring. It is also seen from table.1 that the leaf extract of oxystelma esculentum at 25 ppm and 100 ppm concentrations shows 55.55 % and 66.00 % inhibition efficiencies respectively, Then the values increased to 80.14 % after adding 25 ppm of KI solution in 0.5M H_2SO_4 solutions containing 100 ppm of plant extract respectively. This showed a good synergistic effect between oxystelma esculentum extract and KI.

Table1. Corrosion rate (CR) of mild steels in 0.5M H_2SO_4 solutions the absence and presence of inhibitor and the inhibition efficiency (IE) obtained by weight loss method.

. Inhibitor concentration (ppm)	KI (0) ppm	
	CR (mg cm^{-2} h^{-1})	IE %
0	136.00	-
10	65.42	51.90
25	58.26	57.16
50	46.06	66.13
75	41.26	69.66
100	37.75	72.24

3.2 INFLUENCE OF KI ON THE INHIBITION EFFICIENCY OF STEM EXTRACTS

Inhibitor concentration (100ppm)	KI (25) ppm	
	CR (mg cm^{-2} h^{-1})	IE %
100	24.26	82.16

3.3 Electrochemical impedance spectroscopic measurements (EIS)

Impedance spectra obtained for corrosion of mild steel in 0.5 M H_2SO_4 contains a semicircle, representing the interaction of metal surface with the corrosive environment.. The -R(CR) model best describes this situation. The semicircle in the impedance plots contain depressed semicircles with the centre below the real axis. The size of the semicircle increases with the inhibitor concentration, indicating the charge transfer process as the main controlling factor of the corrosion of mild steel. It is apparent from the plots that the impedance of the inhibited solution has increased with the increase in the in which

the second one represents the interaction of metal surface with the corrosive environment. The first semicircle represents the nature of the corrosive media .Since the conductivity of the corrosive medium is very low, this also behaves like a leaky capacitor. The CR-CR model best describes this situation. The second semicircle in the impedance plots contain depressed semicircles with the centre below the real axis. The size of the semicircle increases with the inhibitor concentration, indicating the charge transfer process as the main controlling factor of the corrosion of mild steel. It is apparent from the plots that the impedance of the inhibited solution has increased with the increase in the concentration of the inhibitor. The experimental results of EIS measurements for the corrosion of mild steel in 0.5 M H_2SO_4 in the absence and presence of inhibitor are given in Table 3. Said that sum of charge transfer resistance (R_{ct}) and adsorption resistance (Rad) is equivalent to polarization resistance (Rp).

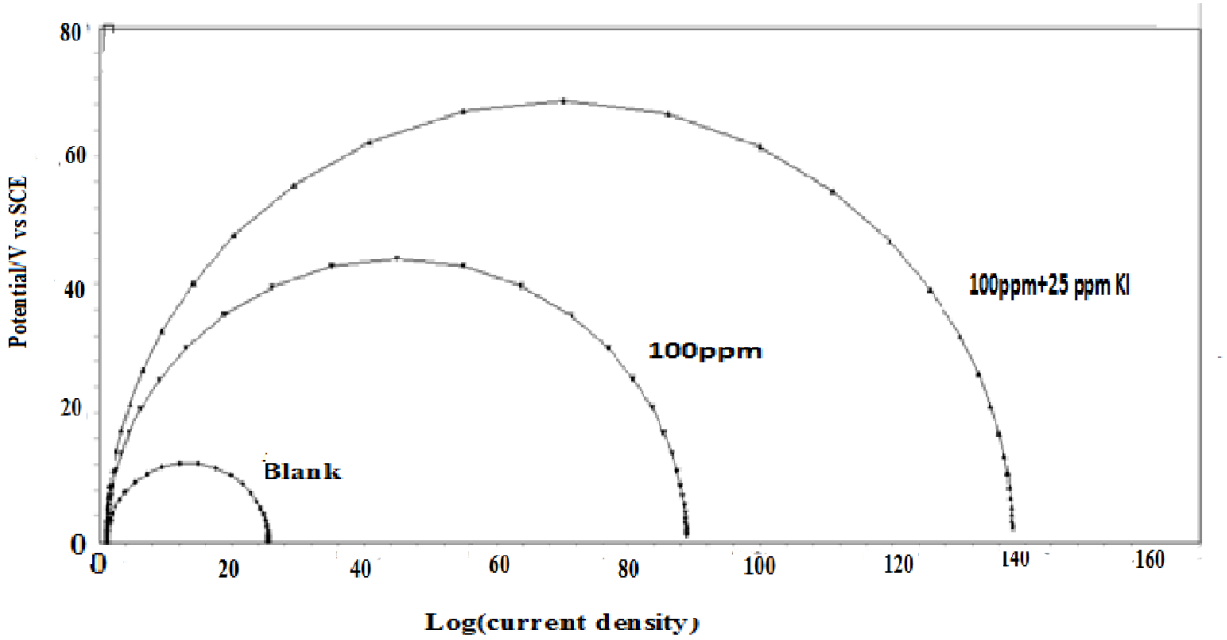

Table 3. Impedance parameters obtained from electrochemical impedance studies.

Inhibitor concentration ppm	Rct Ohm cm^2	C_{dl} µF	IE%
0	17.2	9.2578×10^{-6}	-
100	63.00	2.5275×10^{-6}	73.00
100+ 25ppmKI	104	1.5311×10^{-6}	83.50

3.4 Potentiodynamic Polarization studies :

Fig 2. Potentiodynamic polarization curves of mild steel immersed in 0.5M H_2SO_4 solution in the absence and presence of inhibitors

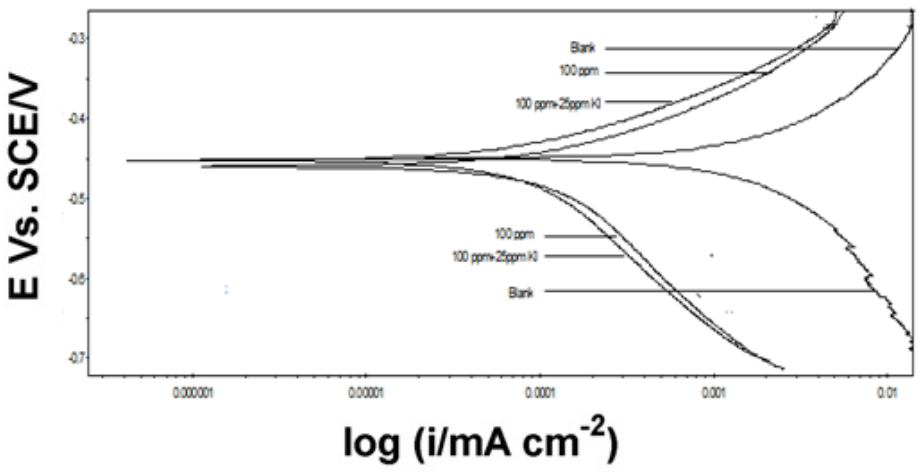

Table 4. Corrosion parameters in the presence and absence of inhibitor obtained from polarization measurements.

Inhibitor concentration ppm	$-E_{corr}$ (mV)	β_c (mV/)	β_a (mV)	$I_{corr}\times10*6$ µA	IE%
0	447	127	68	1.35	
100	450	173	72	0.378	72.0
100+25ppmKI	453	195	94	0.278	82.4

The polarization curves obtained for the corrosion of mild steel in the inhibited (100 ppm) and uninhibited 0.5 M H_2SO_4 solutions in the absence and presence of KI are shown in Fig.2. Electrochemical parameters such as corrosion potential (E_{corr}), corrosion current density (I_{corr}), cathodic and anodic tafel slopes (β_c and β_a) and percentage inhibition efficiency according to polarization studies are listed in table 4. Here I_{corr} decreased with increasing inhibitor concentration. From the figures, it can be interpreted that the addition of this inhibitor to corrosive media changes the anodic and cathodic tafel slopes. The changes in slopes showed the influence of the inhibitor both in the cathodic and anodic reactions. However, the influence is more pronounced in the cathodic polarization plots compared to that in the anodic polarization plots. Even though β_c and β_a values (table.3) change with an increase in inhibitor concentrations, a high β_c value indicates that the cathodic reaction is retarded to a higher extent than the anodic reaction[13].

From Fig.2 it is also clear that the addition of the inhibitor shifts the cathodic curves to a greater extent toward the lower current density when compared to the anodic curves. The E_{corr} value is also shifted to the more negative side with an increase in the inhibitor concentration. These shifts can be attributed to the decrease in the rate of the hydrogen evolution reaction on the mild steel surface caused by the adsorption of the inhibitor molecule to the metal surface[14]. It has been reported that a compound can be classified as an anodic and cathodic type inhibitor on the basis of shift of E_{corr} value. If displacement of E_{corr} value is greater than 85 mv, towards anode or cathode with reference to the blank, then an inhibitor is categorized as either anodic or cathodic type inhibitor otherwise inhibitor is treated as mixed type[15,16]. In our study, maximum displacement in E_{corr} value was around 6 mV, indicating the inhibitor is a mixed type and more anodic nature and does not alter the reaction mechanism. The inhibition effect has occurred due to simple blocking of the active sites, thereby reducing available surface area of the corroding metal[17,18]. The increase in inhibitor efficiency of inhibited (10mL) 0.5M H_2SO_4 solution for the corrosion of mild steel after adding 25 ppm KI shows synergism between inhibitor molecules and KI.

IV. CONCLUSIONS

Results obtained from both electrochemical methods showed that the oxystelma esculentum stem acts as an inhibitor for corrosion of steel in 0.5 M H_2SO_4 media. Corrosion inhibition action of oxystelma esculentum stem increased as its concentration increases. Inhibition of steel in 0.5 M H_2SO_4 solution by oxystelma esculentum stem is attributed to adsorption of the phytochemical compounds in this extract.

ACKNOWLEDGEMENTS

The authors generously acknowledge the support by Dr.R.Somasundaram M.D Dr. R. Arul M.Sc., Ph.D., Dr.S.Vedanayaki M.Sc.,Ph.D.,President ,Principal and head of the department chemistry respectively of kandaswami Kandar's college,P.Velur for providing necessary chemical and lab facilities to carry out chemical studies

References

[1] H. Ashassi-Sorkhabi, M. R. Majidi and K. Seyyedi, *Applied Surface Science*,225(2004)176
[2] A.Y. El-Etre, *Corrosion Science*,45(2003)2485
[3] A.Y. El-Etre, *Corrosion Science*,40 (1998)1845
[4] H. Ashassi-Sorkhabi, Z. Ghasemi and D. Seifzadeh, *Applied Surface Science*,249 (2005)408
[5] M. Bethencourt, F.J. Botana, J.J. Calvino and M. Marcos,*Corrosion Science*,40(1998)1803
[6] S. Virtanen, M.B. Ives, G.I. Sproule, P. Schmuki and M.J. Graham, *Corrosion Science*,39(1997)1897.
[7] B. Davó and J.J. de Damborenea, *Electrochimica Acta*,49(2004)*4957*
[8] A. Aballe, M. Bethencourt, F. J. Botana and M. Marcos, *Journal of Alloys and Compounds*, 323-324(2001)*855*
[9] K. C. Emregül and M. Hayvalı, *Materials Chemistry and Physics*,83(2004)209
[10] S. A. Abd El-Maksoud, *Electrochimica Acta*,49(2004) 4205
[11] Ashassi-Sorkhabi.H,.Shaabani.B,Seifzadeh.D, Electrochim. Acta,**2005** ,50 ,3446.
[12] Shahin.M, Bilgie.S, Yilmaz.H, *Appl. Surf. Sci*.**2003**,195, 1
[13] Silverman D. C., "*Practical Corrosion Prediction Using Electrochemical Techniques*", ch. 68 *in Uhlig's Corrosion Handbook, 2nd edition* (Revie,.R.W, ed.), *The Electrochemical Society*, 2000.
[14] Prabhu., T.V. Venkatesha, A.V. Shanbhag. Praveen. B.M, Kulkarni. G.M,.Kalkhambkar R.G, *Mater. Chem. Phys*. **2008**,108 , 283
[15] Sanghvi. R.A, M.J., et al., *Bull. Electrochem*.**1999**, 13, 358.
[16] Felicia Rajammal Selvarani, S.Santhanalakshmi, J. Wilson sahayaraja, A. John Amalraj,and Susai Rajendran , *Bull. Electrochemistry*.**2004**, 20 , 561-565.
[17] Susai RajendranS. Mary Reenkala, Noreen Anthony and Ramaraj,R. *Corros Sci*,**2002**, 44, 2243-2252.
[18] Scully. J. R., "*Polarization Resistance Method for Determination of Instantaneous Corrosion Rates*", *Corrosion, Vol.**2000***,56, p. 199.

International Journal of Modern Engineering Research (IJMER)
www.ijmer.com Vol. 3, Issue. 4, Jul - Aug. 2013 pp-2460-2463 ISSN: 2249-6645

Secure and Efficient Hierarchical Data Aggregation in Wireless Sensor Networks

Shaik Nagul Shareef[1], Syed Sadat Ali[2]
[1]*M. Tech, Nimra College of Engineering & Technology, Vijayawada, A.P., India.*
[2]*Assoc. Professor & Head, Dept.of CSE, Nimra College of Engineering & Technology, Vijayawada, A.P., India.*

***Abstract*:** *A wireless sensor network (WSN) is a wireless network consisting of spatially distributed autonomous devices that use sensor nodes to monitor physical or environmental conditions. These distributed autonomous devices, or nodes, combine with routers and a gateway to create a typical WSN system. The distributed sensor nodes communicate wirelessly to a central gateway, which provides a connection to the wired world where you can collect, process, analyze, and present your measurement data. Due to the broadcast nature of the transmission media they use, sensor networks are vulnerable to various security attacks, such as eavesdropping, jamming and node capture attacks. In this paper, we provide a solution for node capture attack. Node capture attacks result from the combination of active, passive and physical attacks by an intelligent adversary. In order to initialize or set up a node capture attack, the adversary will collect information about the WSN by eavesdropping on message exchanges, either local to a single adversarial device or throughout the network with the aid of a number of adversarial devices deployed throughout the network. Hence in order to securely aggregate data in a wireless sensor network, we must not only provide protection against eavesdroppers, but we should also prevent intermediate sensors from having access to the data.*

Keywords*: *Aggregation, Sensor node, Slicing, WSN.

I. INTRODUCTION

Wireless sensor networks (WSN) (Figure 1) are self organizing networks of small, battery powered sensors used to monitor the environment for events such as enemy troop movements in military, forest fires, pollutant levels. A large number of small, battery powered computing devices with built-in radio equipment are spread over the area to be monitored. Upon activation, these sensor nodes self-organize into a multi-hop network, which connects to the users via a powerful base station in order to achieve a common goal [1]. As each sensor surveys the area within its sensing range, the information is sent towards the base station along a multi- hop path. A sensor network is able to remotely cover a large sensing area since these low cost sensors organize into a multi-hop network without human assistance. Since sensor nodes are typically battery powered and a WSN contains thousands of sensors, replacing the batteries is not a possibility. In terms of energy usage, communication is much more expensive than any internal computations [2]. In data aggregation, intermediate results are calculated along the multi-hop path whenever two or more messages are routed along the same path. Depending on the routing structure, power savings may be by as much as eight times [3].

Security in sensor networks includes confidentiality, integrity and availability. Confidentiality in WSNs is accomplished by preventing outsiders from eavesdropping on transmissions. This is generally achieved by enciphering the relevant parts of a packet. Integrity in general means that the receiver is assured that the network packet was not tampered with or the message altered in some way. By ensuring the availability we mean that the data is available in a timely fashion so that it is useful to the user. Availability in WSNs is of great concern to the user of the network. Unfortunately, many existing security primitives can not be used in WSNs, either because the computing power of the sensors is too limited or the additional work created by the protocols causes excessive network traffic [4].

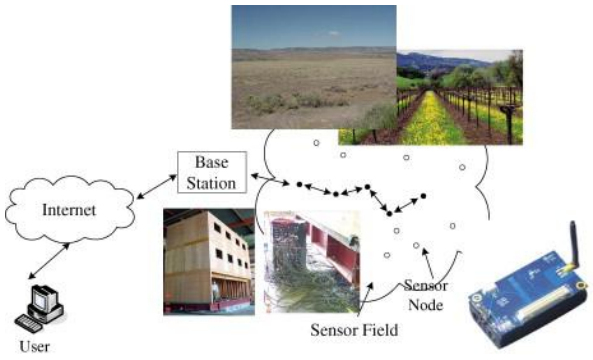

Figure 1 : Wireless sensor network example

Sensors in WSNs can become corrupted due to the environment such as water, wind or sand acting on the sensor. In hostile environments, a sensor may deliberately be corrupted by an attacker. A corrupted sensor may appear to participate in the mission of the network but falsify make sensor readings, improperly apply an aggregation function, exclude legitimate messages from the aggregate result or create a fictitious result. A sensor corrupted by an hacker may behave in this way in order to get the base station to accept an incorrect result that is favorable to the attacker. Hence in order to securely aggregate data in a sensor network, we must not only provide protection against eavesdroppers, but we should also prevent the intermediate sensors from having access to the data.

II. DATA AGGREGATION IN WSNS

In a typical WSN, a large number of sensor nodes collect application specific information from the environment and this information is transferred to a central base station where it is processed, analyzed, and used by the application. In these resource constrained networks, the general approach is to jointly process the data generated by different sensors while being forwarded toward the base station [5]. Such distributed in-network processing of data is generally called as data aggregation and involves combining the data that belong the same phenomenon. The main objective of hierarchical data aggregation is to increase the network lifetime by reducing the resource consumption of sensor nodes (such as battery energy and bandwidth). While increasing network lifetime, data aggregation protocols may degrade the important quality of service metrics in wireless sensor networks, such as data accuracy, latency, fault-tolerance, and security. Therefore, the design of an efficient data aggregation protocol is an inherently challenging task because the protocol designer must trade off between energy efficiency, data accuracy, fault-tolerance, latency, and security.

In order to achieve this trade off, data aggregation techniques are tightly coupled with how packets are routed through the sensor network. Hence, the architecture of the WSN plays a vital role in the performance of different data aggregation protocols. There are several protocols that allow routing and aggregation of network packets simultaneously. These protocols can be categorized into two parts: cluster-based data aggregation protocols and tree based data aggregation protocols. To reduce the latency due to tree based data aggregation, recent work on data aggregation process tends to group sensor nodes into clusters so that data are aggregated in each group for improved efficiency.

III. NODE CAPTURE ATTACK

WSNs are vulnerable to node capture attacks[6] because sensor nodes are usually deployed in unattended manner. Once attacker captures the sensor nodes, he can compromise them and launch various types of attacks with those compromised nodes. A straightforward strategy for sensor node compromise is to launch a node capture attack in which adversary physically captures all sensor nodes, removes them from the network, compromises and redeploys them in the network. After redeploying compromised nodes, he can mount a variety of attacks with the compromised nodes. For example, he can simply monitor a significant fraction of the network traffic that would pass through these vulnerable nodes. Alternatively, he could jam legitimate signals from benign nodes or inject falsified data to corrupt monitoring operation of the sensor nodes. A more aggressive attacker could undermine common sensor network protocols, including routing, cluster formation and data aggregation, thereby causing continual disruption to the network operations. Hence, node capture attacks are very dangerous and thus should be detected as quickly as possible to minimize the damage incurred by them.

IV. EXISTING SYSTEM

In Existing System, the aggregate data to be transmitted through sensor nodes, a security threat is originate by any node. So, that time attacker achieves full control over a sensor node through direct physical path in wireless sensor network. It makes to data loss and risk of data privacy. A typical sensor network consists of a large number of sensor nodes randomly deployed over a wide area. Sensor nodes are typically low cost hardware components with severe limitations on energy, memory and communication resources. The disadvantages of the existing system are:

1. Sensor nodes are exposed to maximum failures.
2. Sensor nodes which make use of the broadcast communication pattern and have severe bandwidth restraint.
3. Sensor nodes have inadequate amount of resources.

V. PROPOSED SYSTEM

In Proposed System, to avoid data loss initially sensor network is separated into different clusters each cluster is headed by an aggregator and directed connected to sink. So, this idea basically dispersed data processing measures to save the power and minimize the medium access layer contention in wireless sensor networks. It proposed the distinct Structure and Density Independent Group Based Key Management Protocol (DGKE) [7]. The protocol offers:

- A better secure communication,
- Secure data aggregation,
- Confidentiality and
- Resilience against node capture and
- Replication attacks using reduced resources.

A. Wireless Sensor Network

WSNs consist of numerous low cost, little devices and are in nature self organizing ad hoc systems. The job of the WSN is to monitor the physical environment, gather and transmit the information to other sink nodes. Generally, radio transmission ranges for the WSNs are in the orders of the magnitude that is lesser that of the geographical scope of the unbroken network. Hence, the transmission of the data is done from hop-by-hop to the sink in a multi-hop manner. Reducing the amount of the data to be relayed thereby reduces the consumption of energy in the network.

B. Hierarchical Secure Data Aggregation

Combine the data from various sources, redirect it with the removal of the redundancy and thereby reducing the number of transmissions and also saves energy. The inbuilt redundancy in the raw data gathered from various sensor nodes can be banned by the in-network data aggregation. Two securities in the data aggregation of sensor network is data Confidentiality: In particular, the fundamental security issue is the data privacy that protects the transmitted data which is

sensitive from the passive attacks like eavesdropping. The significance of the data confidentiality is in the hostile environment, where the wireless channel is more prone to eavesdropping attack. Though cryptography provides plenty of methods, such as the process related to complicated enciphering and deciphering, like modular multiplication of large numbers in public key based on cryptosystems, utilizes the sensor's power speedily. Data Integrity: It avoids the modification of the last aggregation value by the negotiating source nodes (aggregator nodes). Sensors can be without difficulty compromised because of the lack of the expensive tampering-resistant hardware. The otherwise hardware that has been used may not be reliable at all times. A compromised message is able to modify, forge and discard all messages.

C. Countering Node Capture Attacks

The process of getting hold of the sensors through a physical attack is termed as node capture attack. For example: uncovering the sensor node and adding wires in any place. This attack essentially differs from getting hold of a sensor via certain software bug. Since sensor nodes are typically supposed to operate the same software, specifically, the operating software which discovers the suitable bug permits the adversary to manage the entire sensor network. Distinctly, the node capture attacks can be set over the small segment of adequately large network. There are two types of node captures possible: Random node capture and Selective node capture. The following algorithm is used to detect node capture attacks.

Algorithm Node_Capture_Attack (node, aggregator, key, cluster, AGGadv)
{
// ui is a member node in cluster Cj where j = 1to n.
// Aj is the aggregator of the cluster Cj.
// AGGadv represents Aggregator Advertisement Message
// R1 is the first round of aggregation.
// TS1 is R1's respective time stamp.
// Aj possess a secret key (kjsec) which is shared with the sink.

$$A_j \xrightarrow{AGGadv} u_i$$

// In R1, the aggregator broadcasts the AGGadv to all the nodes.

$$u_i \xrightarrow{ACK} A_j$$

// ui sends acknowledgment (ACK) message to Aj.
// ACK = {wi, g} Where wi = node's ID, g = node's category. // based on ACK messages, the Aj selects c nodes (c<n) randomly.
Set Q = {u1, u2, …..uc}. // selected c nodes are represented by the set Q

$$A_j \xrightarrow{V} Q$$

V = [(w1, Kw1), (w2, Kw2), ……, (wc, Kwc)]
// the Aj broadcasts a set of unique values V to all nodes in Q. //V consists of the node ids of Q and their authentication key.
// Kwi denotes the authentication keys of the corresponding node wi.

$$u2 \xrightarrow{encr(1to(c-1))} u_3$$

X=1+2+…+C.
//X represents data which sliced into c pieces.
//assume u2 wants to send the data to any node .First u2 send encrypted data to nearest node u3.
//In c slices, one of them is kept inside that node itself.

$$X(1 \text{ to } (c\text{-}1)) \xrightarrow{decr(1 \text{ to } (c\text{-}1))} u3$$

//u3 waits for a time t, which assures that all slices of this round of aggregation are received. 1+2+…. +(c-1) =Sc
// sums up the received slices

$$u_3 \xrightarrow{encr(Sc)} Ai$$

//Sc is again encrypted with the authentication key of the respective node and sent to the Aj

$$Aj \xrightarrow{MAC(ED,TS)} Sink$$

// Aj aggregates and encrypts the data with the shared key kjsec and forwards it to towards sink.
//The message in the form MAC (ED, TS1) where TS1 = time stamp, ED = encrypted data.

If (TS1 → expires)
{
R1 → ends R2 → starts TS2→ begins
}
//The same procedure is repeated for R2 except that the set of nodes in Q is reselected with new
//set of authentication keys.
}

D. Slicing Technique

The Slicing technique is described using the slicing architecture shown in Figure 2. Consider the node 2 in below figure. When it wants to send data to its neighboring nodes, it slices the data "X" into 8 pieces (since network size u=8). It holds the one of the slices with it. The remaining slices are encrypted with their respective authentication keys and sent to rest of the sensor nodes.

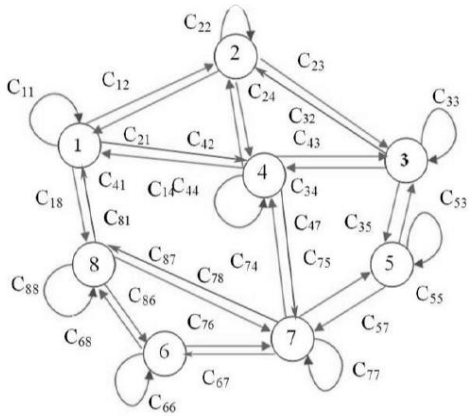

Figure 2: Slicing Technique

When the node 1 receives the encrypted data slice from node 2, then it decrypts the slice using its authentication key K1. Then Node 1 waits for reception of the rest of the slices until time "t". When "t" expires, the node 1 stops receiving the data slice. After complete decryption of the received slices, the node 1 sums them up along with the slice within it and this sum is represented as "S1".

$$S1 = C11 + C21 + C41 + C81$$

The node 1 encrypts "S1" with k1 and sent to the aggregator A1. The aggregator encrypts the data with a secret shared key (kjsec) and forwards it to the sink.

VI. CONCLUSION

WSNs are increasingly becoming the networks of choice in various industrial, medical and military applications, including remote plant control, health monitoring and target surveillance. Wireless sensor network consists of a huge number of tiny electromechanical sensor nodes that are capable of sensing, computing and communicating. Serious security threat is originated by node capture attacks in hierarchical data aggregation where a attacker achieves full control over a sensor node through direct physical access in wireless sensor networks. It makes a high risk of data privacy. In this propose, we propose a method for countering node capture attacks for hierarchical data aggregation in wireless sensor networks.

REFERENCES

[1] L. Clare, G. Pottie, and J. R. Agre, "Self-organizing distributed sensor networks," SPIE-The International Society for Optical Engineering, pp. 229–237, 1999.
[2] R. W. Heinzelman, J. Kulik, and H. Balakrishnan, "Adaptive protocols for information dissemination in wireless sensor networks," in MobiCom '99: Proceedings of the 5th annual ACM/IEEE international conference on Mobile computing and networking. ACM Press, 1999, pp. 174–185.
[3] W. Heinzelman, A. Chandrakasan, and H. Balakrishnan, "Energyefficient communication protocol for wireless microsensor networks," in HICSS '00: Proceedings of the 33rd Hawaii International Conference on System Sciences-Volume 8. Washington, DC, USA: IEEE Computer Society, 2000, p. 8020.
[4] J. Albath and S. Madria, "Practical algorithm for data security (pads) in wireless sensor networks," in MobiDE '07: Proceedings of the 6th ACM international workshop on Data engineering for wireless and mobile access. New York, NY, USA: ACM Press, 2007, pp. 9–16.
[5] R. Rajagopalan, P.K. Varshney, Data aggregation techniques in sensor networks: a survey, IEEE Commun. Surveys Tutorials 8 (4) (2006).
[6] Conti, M., Pietro, R., Mancini, L., & Mei, A. (2008). Emergent Properties: Detection of the Node-capture Attack in Mobile Wireless Sensor Networks. In ACM WiSec, April 2008.
[7] K. Kifayat, M. Merabti, Q. Shi, D. Llewellyn-Jones, ―Group Based Secure Communication for Large-Scale Wireless Sensor Networks‖ , journal of information assurance and security, Vol 2, Issue 2, June 2007 .

International Journal of Modern Engineering Research (IJMER)
www.ijmer.com Vol. 3, Issue. 4, Jul – Aug. 2013 pp-2464-2468 ISSN: 2249-6645

Deformation Analysis of a Triangular Mild Steel Plate Using CST as Finite Element

Mr. Amit Karkamkar
*(Mechanical Engineering Final year Student / National Institute Of Technology Warangal, India)

ABSTRACT: *This research work aims to analyse isotropic triangular mild steel plate constrained by boundary condition using Finite Element Analysis with CST as master element. Static deformation analysis of a mild steel triangular plate fixed at one end under point loads at the free end has been performed using Constant Strain Triangle (CST) as finite element. FEA analysis techniques are used to find the deformation of the plate. Problem Modelling and simulation of the plate is done in ANSYS and the results obtained by the finite element analysis using Constant Strain Triangle (CST) are compared. Good agreement has been found out in the deformation results by both the methods. Simulation results are critically studied and salient conclusions have been drawn.*

Keywords: *ANSYS, Constant Strain Triangle (CST), Deformation, FEA, Mild steel plate*

I. INTRODUCTION

Finite element analysis (FEA) is a powerful computational technique used for solving engineering problems having complex geometries that are subjected to general boundary conditions. In the FE analysis technique, the system is divided into discrete finite number of parts or elements by expressing the unknown field variable in terms of the interpolation functions within each element. The ease of computation depends on the linearity and the nature of the interpolation functions. This paper focuses on the use of the three node triangular element as the finite element. Geometry and displacement variables follow isoparametric representation . It is also known as Constant strain triangle(CST) because the localized strain in the element remains constant as it depends only on the nodal displacements. The shape functions for this elements allow ease of calculations. The paper first relates the shape functions to the displacement variables and element stiffness matrix for the CST element has been found out. Later the deformation in the plate is studied by finding out the nodal displacements in given loading and boundary condition. Accuracy of the results have been found out by comparing the results with ANSYS analysis.

II. DESCRIPTION

A triangular mild steel plate is considered in this paper for analysis. Mild steel is the most common form of steel used in industries because of its low cost and good mechanical properties. Mild steel is a general term for a range of low carbon steel (about 0.3%). They have good strength and can be bent, worked or can be welded into an variety of shapes for uses from vehicles to building materials. A typical CAD model for such a plate is shown in FIG .1 The model is generated in the designing software package PRO-E.

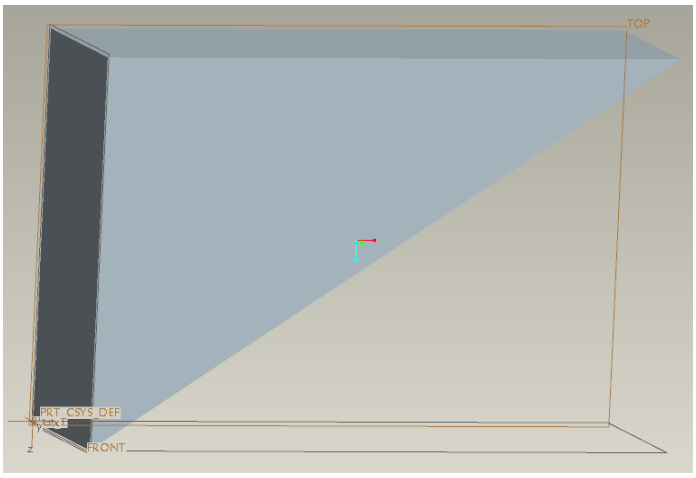

FIG. 1

For the deformation analysis a typical boundary condition is considered. One edge of the plate is fixed and point loads applied at the free end of the plate. The objective is to study the deformation in the plate under the influence of the loads that is the amount of deflection of the free end both in horizontal and vertical direction. For the analysis Finite element analysis method is utilized and Constant strain triangle is taken as the basic element type. For the purpose of analysis typical values of the point loads are assumed and the condition of plane stress condition is considered.

2.1) Constant Strain Triangle (CST) :

In the finite element method, the displacements at points inside the element need to be represented in terms of the nodal displacements of the elements. For the constant strain triangle, the shape functions or the interpolation functions are linear over the element. The independent shape functions are represented by ξ and η. CST will have three nodes at each of the vertices of the triangle and each having two degrees of freedom. Let us define the DOF in X positive X axis as q_{2i-1} and DOF in Y axis as q_{2i}. where, I is the node number. FIG. 2 shows the three nodes 1, 2 and 3. Thus q_1, q_2, q_3, q_4, q_5, q_6 represent the displacements at the three nodes.

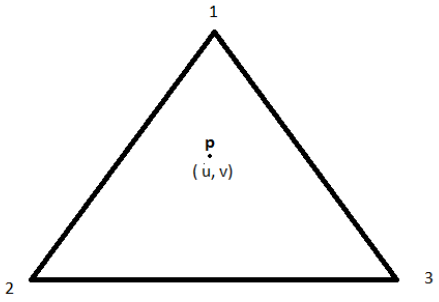

FIG. 2

The displacements inside the element are now written using the shape functions and the nodal values of the unknown displacement field.

$$u = (q_1 - q_5)\xi + (q_3 - q_5)\eta + q_5$$
$$v = (q_2 - q_6)\xi + (q_4 - q_6)\eta + q_6$$

For the triangular element, the coordinates x, y can also be represented in terms of nodal coordinates using the same shape functions. This is isoparametric representation. From reference [1], for the triangular element,

$$\zeta = Bq \quad \text{..... (1)}$$

Where, ζ is the strain matrix and q is the displacement matrix. B is a (3 x 6) element strain - displacement matrix relating the three strains to the six nodal displacements and is given by

$$B = \frac{1}{\det J}\begin{bmatrix} y_{23} & 0 & y_{31} & 0 & y_{12} & 0 \\ 0 & x_{32} & 0 & x_{13} & 0 & x_{21} \\ x_{32} & y_{23} & x_{13} & y_{31} & x_{21} & y_{12} \end{bmatrix} \quad \text{..... (3)}$$

Where, $x_{ij} = x_i - x_j$ and $y_{ij} = y_i - y_j$

i and j represent the node numbers.

det J is the Jacobian of the transformation. Analysis shows that Value of det J is equal to twice the area of the triangular element [2].

$$\det J = 2 \times A_e \quad \text{..... (4)}$$

Where A_e is the area of the triangular element.

Thus it can be seen from equation (1) that the strain in this triangular element remains constant throughout and that is why a lot of computational time is saved by using Constant strain triangle as model element when using Finite element method. This paper aims at verifying the computational accuracy of this method when compared to the ANSYS analysis method.

The element stiffness matrix k^e is given by

$$k^e = t_e A_e B^T D B$$

Where,

t_e = Thickness of the element

A_e = Area of the triangular element

D = Material property matrix

Value of D matrix can be taken depending on the plane stress or the plane strain condition. In this analysis plane stress condition is considered for the deformation of the mild steel plate under loading.

Now , by the finite element analysis method,

$$KQ = F \quad \text{.....(5)}$$

where, K is the global stiffness matrix, Q is the displacement matrix, and F is the force vector.
Equation (3) is solved for the vector matrix Q which will give the values of displacement under the influence of the force vector F.

III. PROBLEM STATEMENT

FIG. 3 clearly elaborates the direction and the magnitude of the point loads acting on the plate . The plate is 20 mm in height and 30 mm in width and 10 mm in thickness. A point load of 100 N is acting in the negative Y direction at the free end of the plate and point load of 50 N in the positive X direction. The plate is fixed along the edge AB.

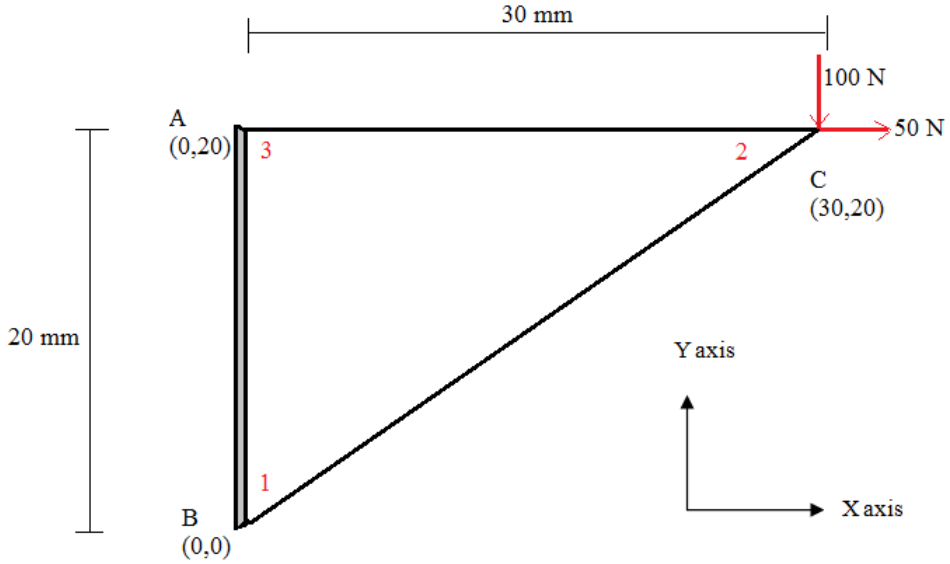

FIG. 3

Now this triangular plate is mapped to a isoparametric constant strain triangle. The problem is solved using FEA and one element. Thus the points 1, 2 and 3 represent the nodes of the constant strain triangular element. Coordinate system used indicating the positive directions is shown in the figure. Point B is considered as origin for the simplicity of analysis.

3.1) Material Properties of mild steel:

The material properties of mild steel are shown in the following TABLE 1.

TABLE 1

Material Used	Young's modulus (E)	Poisson's Ratio (ν)	Density (ρ)
Mild Steel	210 GPa	0.3	7850 kg/m^3

IV. CALCULATIONS

To study the deformation in the plate, under given force vectors and the dimensions of the plate , plane stress condition is assumed. Thus the value of matrix D is given as

$$D = \frac{E}{1-\nu^2}\begin{pmatrix} 1 & \nu & 0 \\ \nu & 1 & 0 \\ 0 & 0 & \frac{1-\nu}{2} \end{pmatrix} = \frac{210x10^3}{0.91}\begin{pmatrix} 1 & 0.3 & 0 \\ 0.3 & 1 & 0 \\ 0 & 0 & \frac{1-0.3}{2} \end{pmatrix} = 230769.23\begin{pmatrix} 1 & 0.3 & 0 \\ 0.3 & 1 & 0 \\ 0 & 0 & 0.35 \end{pmatrix}$$

Using eq. 4;

det J = 2 x A_e = 2 x $(\frac{1}{2}x20x30)$ = 600

Using eq. 3 , value of matrix B is found out.

$$B = \frac{1}{600}\begin{bmatrix} 0 & 0 & 20 & 0 & -20 & 0 \\ 0 & -30 & 0 & 0 & 0 & 30 \\ -30 & 0 & 0 & 20 & 30 & -20 \end{bmatrix}$$

$k^e = t_e A_e B^T DB$ = 10 x 300 x $B^T DB$

Using the program MATLAB above complex multiplication has been carried out and the value for the element stiffness matrix is

$$k^e = 1923.07 \begin{bmatrix} 315 & 0 & 0 & -210 & -315 & 210 \\ 0 & 900 & -180 & 0 & 180 & -900 \\ 0 & -180 & 400 & 0 & -400 & 180 \\ -210 & 0 & 0 & 140 & 210 & -140 \\ -315 & 180 & -400 & 210 & 715 & -390 \\ 210 & -900 & 180 & -140 & -390 & 1040 \end{bmatrix}$$

In this case as shown in FIG 3; only one CST element is considered for analysis. Thus,

$k^e = k_g$, where k_g is the global stiffness matrix.

Global force vector will be given by, $F = \begin{Bmatrix} 0 \\ 0 \\ 50 \\ -100 \\ 0 \\ 0 \end{Bmatrix}$

Using equation (5);

$$1923.07 \begin{bmatrix} 315 & 0 & 0 & -210 & -315 & 210 \\ 0 & 900 & -180 & 0 & 180 & -900 \\ 0 & -180 & 400 & 0 & -400 & 180 \\ -210 & 0 & 0 & 140 & 210 & -140 \\ -315 & 180 & -400 & 210 & 715 & -390 \\ 210 & -900 & 180 & -140 & -390 & 1040 \end{bmatrix} \begin{Bmatrix} q_1 \\ q_2 \\ q_3 \\ q_4 \\ q_5 \\ q_6 \end{Bmatrix} = \begin{Bmatrix} 0 \\ 0 \\ 50 \\ -100 \\ 0 \\ 0 \end{Bmatrix} \quad \text{.....(6)}$$

The edge AB of the mild steel plate is fixed as shown in FIG .3 Thus the DOFs q_1, q_2, q_5 and q_6 will be constrained to be zero. So now using the elimination method to solve the equation no. (6) striking off the rows and columns corresponding to the constrained Degrees of freedoms, we get,

$$1923.07 \begin{bmatrix} 400 & 0 \\ 0 & 140 \end{bmatrix} \begin{Bmatrix} q_3 \\ q_4 \end{Bmatrix} = \begin{Bmatrix} 50 \\ -100 \end{Bmatrix}$$

Solving the above equation , we get,

q_3 = 6.5 x 10^{-5} mm ; q_4 = - 3.71 x 10^{-4} mm ..... . (7)

Let σ be the stress generated in the element.

σ = DBq , where q is the element nodal displacement vector.

$$\therefore \quad \sigma = \frac{230769.23}{600} \begin{pmatrix} 1 & 0.3 & 0 \\ 0.3 & 1 & 0 \\ 0 & 0 & 0.35 \end{pmatrix} \begin{bmatrix} 0 & 0 & 20 & 0 & -20 & 0 \\ 0 & -30 & 0 & 0 & 0 & 30 \\ -30 & 0 & 0 & 20 & 30 & -20 \end{bmatrix} \begin{Bmatrix} 0 \\ 0 \\ 6.5x10^{-5} \\ -3.71x10^{-4} \\ 0 \\ 0 \end{Bmatrix}$$

$\sigma = \{0.49, 0.15, -0.99\}^T$ *MPa* ..... (8)

V. ANSYS Modeling

Commercially available software ANSYS 13.0 is used to model the problem and solve for deformation. ANSYS parametric design language (APDL) is utilized for this purpose. A model is generated in the work plane for the given dimension and thickness of the mild steel plate. After specifying the material properties and real constants as shown in TABLE 1, boundary condition is applied. That is both the nodes 1 and 3 are fixed thus constraining their displacement to zero. At the node 2, constant point load of 50 N in the positive X axis and 100 N in the negative Y axis direction is applied. The generated model is shown in FIG. 4. Deformation analysis finding the nodal displacements using the numeric method is done by the ANSYS postprocessor. The stress generated in the element is also found out. The displacement in the positive X direction of the node 2 is 0.65E-04 mm and in the negative Y direction 0.37E-03 mm. Using the command plot results- a deformed shape of the plate is generated by the ANSYS software. This is shown in the FIG 5

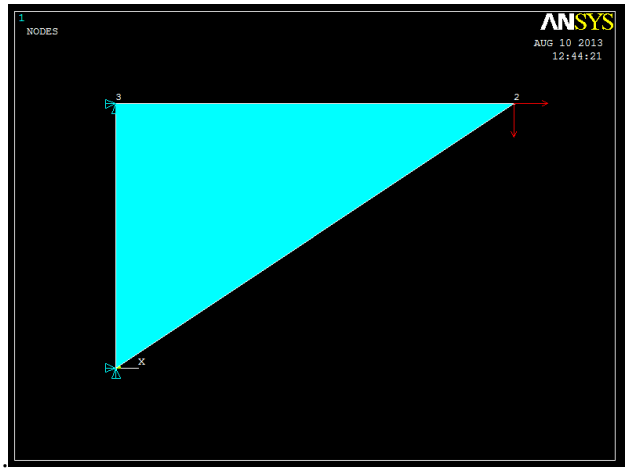

FIG. 4

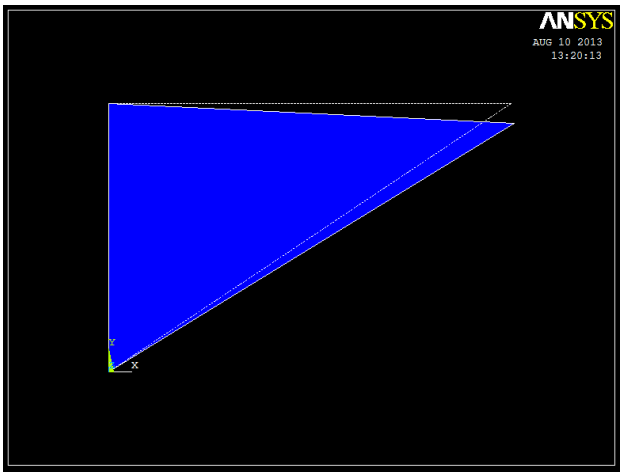

FIG 5

VI. Results & Discussions

From eq. (7) and (8) and the results obtained from ANSYS modeling, it can be conclusively averred that the results of the finite element analysis using Constant Strain Triangle and that of ANSYS show good agreement. The deformation of the plate subjected to given boundary condition and loading and the corresponding Von-Mises Stress generated were equal in both the methods.

VII. Conclusions

This paper mainly focused on finding the deformation of the triangular mild steel plate subjected to a boundary condition under the influence of point loads. The deformation analysis is first carried out by finite element method using the three node Constant Strain Triangle (CST) as a basic geometric shape. Later, for the same structure and load, boundary conditions, analysis has been performed using analysis software ANSYS (APDL). Finally, the results obtained from FEA and ANSYS are compared and they are closely converging. Thus use of Constant Strain Triangle as a master element for

FEA in complex stress and deformation analysis is proposed because of the following reasons:

1) The stress value in the basic modeling element is constant and depends on nodal displacements. This saves a lot of computational effort and time required for analysis. The shape functions are linear over the element. Isoparametric representation allows use of same shape functions for representing geometry and displacements inside the element. This approach lends simplicity of development and retains uniformity with other complex elements.

2) The results obtained by FEA using CST as modeling element are in good agreement with the solution.

REFERENCES

Books:

[1] A. D Belegundu , T.R Chandrupatla ,*Finite elements in Engineering* second edition (Prentice hall India).
[2] S. S Rao , *The Finite Element Method in engineering* fourth edition (Elsevier Science & Technology).
[3] E. Madenci , I. Guven , *The finite element method and applications in engineering using ANSYS* (Springer NY USA).
[4] Y. Kwon, *The Finite element method using MATLAB* (CRC press Washington DC).

International Journal of Modern Engineering Research (IJMER)
www.ijmer.com Vol. 3, Issue. 4, Jul - Aug. 2013 pp-2469-2471 ISSN: 2249-6645

A Review on Brain Disorder Segmentation in MR Images

Savitha C. K.[1], Prajna M. R.[2], Ujwal U. J.[3]
Department of Computer Science, K. V. G. College of Engineering, V T U, India

ABSTRACT: *Brain tumor is one of the major causes of death among people. It is evident that the chances of survival can be increased if the tumor is detected and classified correctly at its early stage. Magnetic resonance (MR) imaging is currently an indispensable diagnostic imaging technique in the study of the human brain. Computer aided diagnosis systems for detecting Brain tumor for medical purpose have been investigated using several techniques. In this Review paper, it is intended to summarize and compare the methods of automatic detection of brain tumor through Magnetic Resonance Image (MRI) used in different stages of Computer Aided Detection System (CAD). Various segmentation approaches are reviewed with an emphasis placed on revealing the advantages and disadvantages of these methods for medical imaging applications. The use of image segmentation in different imaging modalities is also described along with the difficulties encountered in each modality.*

Keywords: *Brain tumor, MR images, Computer Aided Detection System, Classification, Segmentation.*

I. Introduction

Brain cancer is a very serious type of malignancy that occurs when there is an uncontrolled growth of cancer cells in the brain. Brain cancer is caused by a malignant brain tumor. Not all brain tumors are malignant (cancerous). Some types of brain tumors are benign (non-cancerous).Malignant brain tumors (or) cancerous brain tumors can be counted among the most deadly diseases. In Figure 1 one normal and abnormal Brain image has been showed.

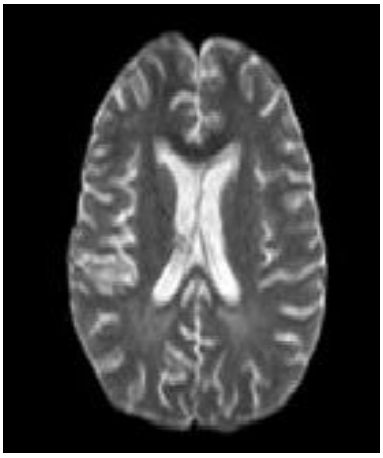

Fig.1 (a). Normal,

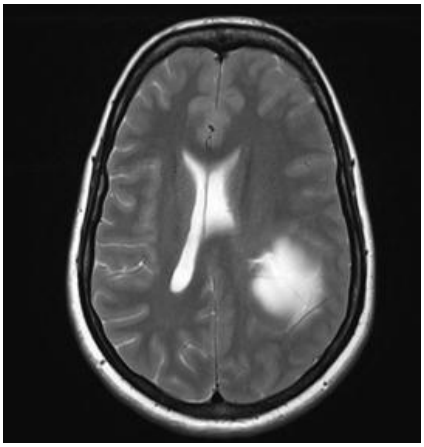

1(b) abnormal

According to the World Health Organization, brain tumor can be classified into the following groups:
Grade I: Pilocytic or benign, slow growing, with well defined borders.
Grade II: Astrocytoma, slow growing, rarely spreads with a well defined border.
Grade III: Anaplastic Astrocytoma, grows faster.
Grade IV: Glioblastoma Multiforme, malignant most invasive, spreads to nearby tissues and grows rapidly.

Many diagnostic imaging techniques can be performed for the early detection of brain tumors such as Computed Tomography (CT), Positron Emission Tomography (PET) and Magnetic Resonance Imaging (MRI). Compared to all other imaging techniques, MRI is efficient in the application of brain tumor detection and identification, due to the high contrast of soft tissues, high spatial resolution and since it does not produce any harmful radiation, and is a non invasive technique.

Although MRI seems to be efficient in providing information regarding the location and size of tumors, it is unable to classify tumor types, hence the application of invasive techniques such as biopsy and spinal tap method, which are painful and time consuming methods. Biopsy technique is performed where, the surgeon makes a small incision in the scalp and drills a small hole, called a burr hole, into the skull and passes a needle through the burr hole and removes a sample of tissue from the brain tumor, to check for cancerous cells (Or) the spinal tap method, where the doctor may remove a sample of cerebrospinal fluid and check for the presence of cancerous cells. This inability related to invasive technique requires development of new analysis techniques that aim at improving diagnostic ability of MR images.

Computer Aided Diagnosis is gaining significant importance in the day-to-day life. Specifically, the usage of the computer aided systems for computational biomedical applications has been explored to a higher extent. Medical image analysis is an important biomedical application which is highly computational in nature and requires the aid of the automated systems. These image analysis techniques are often used to detect the abnormalities in the human bodies through scan images. Automated brain disorder diagnosis with MR images is one of the specific medical image analysis methodologies.

The automated diagnosis involves image segmentation step which is used to extract the abnormal tumor portion which is essential for volumetric analysis. This volumetric analysis determines the effect of the treatment on the patient which can be judged from the extracted size and shape of the abnormal portion. Over the last decade various approaches have been proposed for the same. Some regarded the segmentation task a tissue recognition problem, which meant using a well-trained model that can determine whether a pixel/voxel belongs to a normal or abnormal tissue based on classification methods such as neural network approach.

II. Literature Review

Image segmentation and classification techniques are increasingly being used on MR images to properly identify abnormal lesions from normal regions of the brain. Broadly speaking segmentation is a technique which reveals the region-of-interest [ROI] in the images by suppressing background and the rest. In this paper, we will discuss an illustrate a number of approaches and show improvements in segmentation performance that can be achieved by combining methods from distinct categories such as techniques in which edge detection methods combined with thresholding. The segmentation approaches were studied under 5 categories. These are as follows- 1) Thresholding approaches, 2) Region growing approaches, 3) Genetic Algorithm approaches,4) Clustering approaches ,5) Neural network approaches. Several authors suggested various algorithms for segmentation.

The **threshold technique** is by making decision based on the local raw pixel information and Edge based method is centered on contour. Jaskirat Kaur, Sunil Agrawal & Renu Vig.'s paper presented thresholding and edge detection being one of the important aspects of image segmentation comes prior to feature extraction and image recognition system for analyzing images. It helps in extracting the basic shape of an image, overlooking the minute unnecessary details. In this paper using image segmentation (thresholding and edge detection) techniques different geo satellite images, medical images and architectural images are analyzed. [1]. Manoj K Kowar, Sourabh Yadav**,** proposed a method based on histogram thresholding [2]. They follow a concept that after dividing the image into two equal halves, histograms are compared to detect the tumor and cropping method is used to find an appropriate physical dimension of brain tumor.

In the **Region based technique** the images are partitioned by organizing the nearest pixel of similar kind. N. Senthilkumaran and R. Rajesh proposed region-based techniques with an assumption that adjacent pixels in the same region have similar visual features such as grey level, color value, or texture. Split and merge approaches were used & its performance largely depends on the selected homogeneity criterion [3]. Instead of tuning homogeneity parameters, the seeded region growing (SRG) technique is controlled by a number of initial seeds. If the number of regions were approximately known & used it to estimate the corresponding parameters of an edge detection process., it is possible to combine region growing and edge detection for image segmentation.

The important process in the automated system is brain image classification. The main objective of this step is to differentiate the different abnormal brain images based on the optimal feature set. An interactive tool to classify the healthy and the tumorous MR brain images is proposed by Michael R, Simon K, Nabavi A, Peter M, Ferenc A, Kikinis R [4]. Though this approach claimed a faster convergence rate, it may not be much useful because of its low accuracy than Artificial Intelligent (AI) techniques. Ahmed Kharrat & Karim Gasmi proposed a hybrid approach for classification of brain tissues in MRI based on **genetic algorithm [5]**. The optimal texture features are extracted from normal and tumor regions by using spatial gray level dependence method. It is concluded that, Gabor filters are poor due to their lack of orthogonality that results in redundant features at different scales or channels. While Wavelet Transform is capable of representing textures at the most suitable scale, by varying the spatial resolution and there is also a wide range of choices for the wavelet function.

A survey on different **clustering techniques** to achieve image segmentation is performed in[6]. In order to increase the efficiency of the searching process, only a part of the database need to be searched. For this searching process clustering techniques can be recommended. Clustering can be termed here as a grouping of similar images in the database. Clustering is done based on different attributes of an image such as size, color, texture etc. The purpose of clustering is to get meaningful result, effective storage and fast retrieval in various areas. Amir Ehsan Lashkar [7] used neural network-based method using Zernike and Geometric moments using 200 MRI images. Yu Sun et al [8] employed the technique of symmetry integration in several steps associated with segmentation, clustering and classification. However, use of small and unstructured dataset restricts the generality and clinical applicability.

The application of Kohonen neural networks for image classification is explored by [9]. Some modifications of the conventional Kohonen neural network are also implemented in this work which proved to be much superior to the conventional neural networks. J. Zhou et al [10] carried out image segmentation using one-class support vector machine (SVM). A hybrid approach such as combination of wavelets and Support Vector Machine (SVM) for classifying the abnormal and the normal images is used by [11]. This report revealed that the hybrid SVM is better than the Kohonen neural networks in terms of performance measures. But the major drawback of this system is the small size of the dataset used for implementation.

Mohd Fauzi Bin Othman, Noramalina Bt Abdullah [12] in 2011, performed classification of brain tumor using wavelet based feature extraction method and Support Vector Machine (SVM). Feature extraction was carried out using Daubechies (db4) wavelet and the approximation coefficients of MR brain images were used as feature vector for classification. Accuracy of only 65% was obtained, where, only 39 images were successfully classified from 60 images. It was concluded that classification using Support Vector Machine resulted in a limited precision, since it cannot work accurately for a large data due to training complexity.

Application of various **artificial neural networks** for image classification is analyzed by [13]. The lack of faster convergence rate of the conventional neural networks is also explained in the report. This lay an emphasis on the

requirement of modified neural networks with superior convergence rate for image classification applications. The modified Probabilistic Neural Network for tumor image classification is used by [14]. Abnormal images such as metastase, glioma and meningioma are differentiated using the least square feature transformation based PNN. A comparative analysis is also performed with SVM. This work inferred that the transform based PNN is superior to the SVM in terms of classification accuracy. Various research works have been performed in classifying MR brain images into normal and abnormal Whereas, classifying MR brain images into normal, cancerous and non cancerous brain tumors in particular, is a crucial task, a wavelet and co occurrence matrix method based texture feature extraction and Probabilistic Neural Network for classification has been used as new method of brain tumor classification[15].

III. Future Scope

After evaluation of well-known segmentation techniques it is clearly shown the various methods which can detect the tumor efficiently and provide accurate results. These can be further improved by incorporating discrete and continuous-based segmentation methods. Computational time will also be considered to compare this technique efficiently. Segmentation methods have proved their utility in research areas and are now emphasizing increased use for automated diagnosis and radiotherapy. These will be particularly important in applications such as computer integrated surgery, where envision of the anatomy is a significant component.

IV. Conclusion

Computer-aided segmentation is a key step for finding application in computer aided diagnosis, clinical studies and treatment planning. A survey of brain tumor detection has done based on several segmentation approaches. The use of computer technology in medical decision support is now widespread and pervasive across a wide range of medical area.MRI plays an important role in progressive researches. First we have seen Region- or edge-based methods, and then we have done a detailed analysis of segmentation algorithms proposed so far are based on classification or clustering approaches. Finally, it is concluded that the results of the present study are of great importance in the brain tumor detection which is one of the challenging tasks in medical image processing. This work will be extended for new algorithm for brain tumor detection which will provide more efficient results than existing methods in near future.

References

[1] Jaskirat Kaur,Sunil Agrawal and Renu Vig, A Comparative Analysis of Thresholding and Edge Detection Segmentation Techniques, International Journal of Computer Applications 39(15):29-34, February 2012. Published by Foundation of Computer Science, New York, USA (2012).
[2] Manoj K Kowar, Sourabh Yadav, Brain Tumor Detection and Segmentation Using Histogram Thresholding, International Journal of Engineering and Advanced Technology, ISSN: 2249 – 8958, Volume-1, Issue-4, April 2012.
[3] N. Senthilkumaran and R. Rajesh, A Study on Split and Merge for Region based Image Segmentation,Proceedings of UGC Sponsored National Conference Network Security (NCNS-08) , 2008, pp.57-61.
[4] Michael R, Simon K, Nabavi A, Peter M, Ferenc A, Kikinis R.,Automated segmentation of MR images of brain tumors, Radiology 2000; 218:586-91.
[5] Ahmed kharrat, Karim Gasmi, et.al, A Hybrid Approach for Automatic Classification of Brain MRI Using Genetic Algorithm and Support Vector Machine, Leonardo Journal of Sciences, pp.71-82, 2010.
[6] S.Thilagamani and N. Shanthi;||A Survey on Image Segmentation Through Clustering|| International Journal Of Research and Reviews in Information Sciences Vol. 1,No. 1, March 2011.
[7] Lashkari Amir Ehsan "A Neural Network-Based Method for Brain Abnormality Detection in MR Images Using Zernike Moments and Geometric Moments", IJCA-10.
[8] Yu Sun, Bir Bhanu, Shiv Bhanu, "Automatic Symmetry-integrated Brain Injury Detection in MRI Sequences", 2009 IEEE
[9] Messen W, Wehrens R, Buydens L. "Supervised Kohonen networks for classification problems". Chemometrics and Intelligent Laboratory Systems 2006; 83:99-113.
[10] Zhou J, Chan KL, Chongand VFH, Krishnan SM "Extraction of brain tumor from MR images using one-class support vector machine" IEEE (2005).
[11] Chaplot S, Patnaik M, Jagannathan N.,Classification of magnetic resonance brain images using wavelets as input to support vector machine and neural network,Biomedical Signal Processing and Control, 2006;1:86-92.
[12] Mohd Fauzi Bin Othman, Noramalina Bt Abdullah, et.al,MRI Brain Classification using Support Vector Machine," IEEE, 2011.
[13] Egmont P, De D, Handels H.,Image processing with neural networks-a review, Pattern Recognition ,2002;35:2279-301.
[14] Mohd Fauzi Bin Othman, Noramalina Bt Abdullah, et.al., MRI Brain Classification using Support Vector Machine, IEEE, 2011.
[15] Pauline John, Brain Tumor Classification Using Wavelet and Texture Based Neural Network, International Journal of Scientific & Engineering Research 3(10), October-2012 1 ISSN 2229-5518.

International Journal of Modern Engineering Research (IJMER)
www.ijmer.com Vol. 3, Issue. 4, Jul - Aug. 2013 pp-2472-2475 ISSN: 2249-6645

The Impacts of Social Networking and Its Analysis

Prajna M. R.[1], Savitha C. K.[2], Ujwal U. J.[3]
Department of computer science and engineering, KVGCE Sullia

ABSTRACT: *Social networking sites are playing very significant role in today time; it has a direct impact on all age group people. Though it has many cons but still these are like an effective tool in communicating millions of people and spreading our expressions and view worldwide. We all need a change in the pattern of use, in order to prevent miss-happenings on these sites. If we will be active and aware these sites will serve us their batter and will bring some more revolution in the world of cyber technology. Social network analysis (SNA) is the methodical analysis of social networks. Social network analysis views social relationships in terms of network theory, consisting of nodes (representing individual actors within the network) and ties (which represent relationships between the individuals, such as friendship, kinship, organizational position etc.). These networks are often depicted in a social network diagram, where nodes are represented as points and ties are represented as lines.*

Keywords: *Nodes, Social network analysis, Ties.*

I. INTRODUCTION

A social network can be defined as a social structure of interactions between individuals, which are directly or indirectly based on a common thread of interest. It represents networks with vertices as a people or group of people. The advent of online social networks can be considered as a milestone in the web industry.

Whatever may be the country the urge for being social is increasing day-by-day. Social networking is the outcome of this. It can be defined as internet based system designed to facilitate communication, collaboration and information sharing across users. Communication may takes place between computers or mobile devices without the knowledge of the users. Social networking gives control to the users. It is the user to decide what information is shared and how it is shared. Users can form public groups and private groups. In public group access is to everybody. In private group access is restricted. There are many popular social networking services.

- Video sharing- you tube
- Photo management and sharing- flickr
- Microblogs –Twitter
- Social networking of professionals
- Social utility- facebook
- Power point presentations and sharing- slideshare

The popularities of social networking are posting messages, downloading music, downloading videos, posting photos, blogging, polls and surveys.

Benefits of social networking

- These sites give users a platform across the globe to express their feelings and views.
- It helps users to get interact with other users, no matter from where s/he operates these sites in world.
- These sites help users to organize and participate in any events..
- It is a great source of communication between two users, irrespective of the distance between them.
- SNS boosts many organizations and business, through their promotions on these sites.
- It helps in building credibility amongst the customers.
- It helps to make people and community aware of any issue.
- It helps to bring social change in society.
- It helps to be in touch with our interested, loved ones, relevant group or people or community.
- These sites are not only a source of creating social activities but also a great way to participate and enhance our skill through participating in many contests and activities etc.

Disadvantages of social networking

One of the major demerits of these sites are increment in criminal activities, as there is no hard restrictions on creating account on these sites.

- Another important issue is security of our personal data and information, as its free to everyone, most of the users create face accounts and misuse the personal information of other users/celebrities.
- Sometime some non genuine and face account users attacks to some religious communities and political groups.
- These sites unnecessarily waste our valuable time, when user spend time on these sites and get addicted.
- Addictions of these sites can even affect our mental conditions, sometime is became a big reason of depression and tension.
- User's reliability is not sure; it's very hard to trust on any stranger on these sites.
- Many of time it has been seen that it became the reason of one's death, as it becomes the medium to get in touch with the victim.
- It encourages many scamse etc.

II. IMPACTS OF SOCIAL NETWORKING

News- Social media has become an important source of news. While the credibility of some sources can clearly be contested, news channels tweet or give updates on significant happenings all over the world. Their availability on social networks makes news more accessible. Additionally, news quickly gets passed around the networks in ways never experienced before.

Interaction- Social media has furthered interaction by such a massive scale that is hard not to notice it. It allows people to keep in touch in a more regularly, and sometimes, more intimately, than was ever before because of time and space constraints. People cities or continents apart can keep in touch so effortlessly, creating an opportunity to experience different cultures.

Political Landscapes- Social media has enabled greater political awareness and organization, which has in some cases rewritten entire political landscapes. It has particularly played a large part in the Iran elections, and Obama's reelection for a second term as US President, and inspired the political unrests in Egypt.

Learning- Social media has also played a large part in fostering literacy. Children who start using the platforms develop early communication skills, and generally become more literate. This is an encouraging trend, and thanks to the huge availability of information, both simplistic and complex on the internet, anyone can become as smart or intelligent as they desire.

Marketing- The whole dynamics of marketing has been changed, and rather than investing in mass channels ads, companies are becoming more consumer-centered through interactions made over social media. They are able to understand the needs of the market from the market itself, greatly altering the way marketing has been done in the past.

III. SOCIAL NETWORK ANALYSIS

Social network research has come a long way since the notable six degree separation experiment. Social network analysis is the social networking to understand their structure and behavior. Social network analysis dates back to the early 20th century, with initial studies focusing on small group behavior from a sociological perspective. The emergence of the internet and subsequent increase in the use of online social networking application has caused a shift in the approach to this field. Faced with complex, large datasets, researchers need new methods and tools for collecting, processing, and mining social network data. The increasing computing power allows more memory expensive algorithms and statistical methods to analyze large social networks.

Online social networks (OSN) have revolutionized the way we interact and share information over the internet, and social networking applications such as you tube, facebook etc, have millions of active users. While already being enormously popular, these applications only scratch the surface of online social networking possibilities. Networks such as facebook, Twitter and Linkdln have quickly become communication juggernauts, providing a vast and unprecedented record of social interactions. But they have left mathematicians struggling to keep up. It is challenge for researchers to visually convey the intricate system that make up OSNs. Novel mathematical models of how online social networks are formed, and are trying to find creative ways to use the resulting network topologies to efficiently share/distribute information. The models and results provide surprising insights into how and why the social network that we form and use in our everyday life are so important and efficient.

Social network is easy to formulate but difficult to assess. Network analysts like to know what groups of individuals are unusually closely interconnected with each other, relative to the average for the population as a whole and most importantly which are the influential points. Apart from relational concepts, nodes of actors and their actions are as interdependent. Network model focus on individuals and network structure is treated as individual interaction. The attributes of actors are not considered. It focuses on uncovering the pattern of people's interaction. Analysis is based on the intuitive notion that these patterns are features of individuals.

Social networks are self-organizing, emergent, and complex, such that a globally coherent pattern appears from the local interaction of the elements that make up the system. These patterns become more apparent as network size increases. However, a global network analysis of, for example, all interpersonal relationships in the world is not feasible and is likely to contain so much information as to be uninformative. Practical limitations of computing power, ethics and participant recruitment and payment also limit the scope of a social network analysis. The nuances of a local system may be lost in a large network analysis, hence the quality of information may be more important than its scale for understanding network properties. Thus, social networks are analyzed at the scale relevant to the researcher's theoretical question. Although levels of analysis are not necessarily mutually exclusive, there are three general levels into which networks may fall: micro-level, meso-level, and macro-level.

3.1. Micro level

At the micro-level, social network research typically begins with an individual, snowballing as social relationships are traced, or may begin with a small group of individuals in a particular social context.

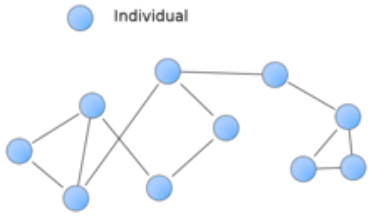

Figure: Social network diagram, micro-level.

Dyadic level: A dyad is a social relationship between two individuals. Network research on dyads may concentrate on structure of the relationship (e.g. multiplexity, strength), social equality, and tendencies toward reciprocity/mutuality.

Triadic level: Add one individual to a dyad, and you have a triad. Research at this level may concentrate on factors such as balance and transitivity, as well as social equality and tendencies toward reciprocity/mutuality.[36]

Actor level: The smallest unit of analysis in a social network is an individual in their social setting, i.e., an "actor" or "ego". Egonetwork analysis focuses on network characteristics such as size, relationship strength, density, centrality, prestige and roles such as isolates, liaisons, andbridges.[38] Such analyses, are most commonly used in the fields of psychology or social psychology, ethnographic kinship analysis or othergenealogical studies of relationships between individuals.

Subset level: Subset levels of network research problems begin at the micro-level, but may cross over into the meso-level of analysis. Subset level research may focus on distance and reachability, cliques, cohesive subgroups, or other group actions or behavior

3.2. Meso level

In general, meso-level theories begin with a population size that falls between the micro- and macro-levels. However, meso-level may also refer to analyses that are specifically designed to reveal connections between micro- and macro-levels. Meso-level networks are low density and may exhibit causal processes distinct from interpersonal micro-level networks.

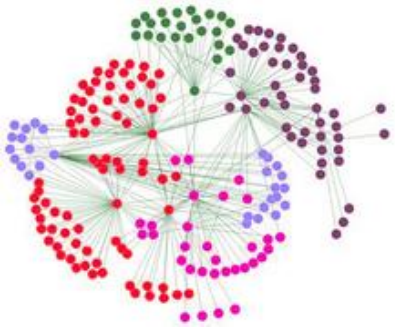

Figure: Social network diagram, meso-level

Organizations: Formal organizations are social groups that distribute tasks for a collective goal. Network research on organizations may focus on either intra-organizational or inter-organizational ties in terms of formal or informal relationships. Intra-organizational networks themselves often contain multiple levels of analysis, especially in larger organizations with multiple branches, franchises or semi-autonomous departments. In these cases, research is often conducted at a workgroup level and organization level, focusing on the interplay between the two structures.

Randomly-distributed networks: Exponential random graph models of social networks became state-of-the-art methods of social network analysis in the 1980s. This framework has the capacity to represent social-structural effects commonly observed in many human social networks, including general degree-based structural effects commonly observed in many human social networks as well as reciprocity and transitivity, and at the node-level, homophily and attribute-based activity and popularity effects, as derived from explicit hypotheses about dependencies among network ties.Parameters are given in terms of the prevalence of small subgraph configurations in the network and can be interpreted as describing the combinations of local social processes from which a given network emerges.

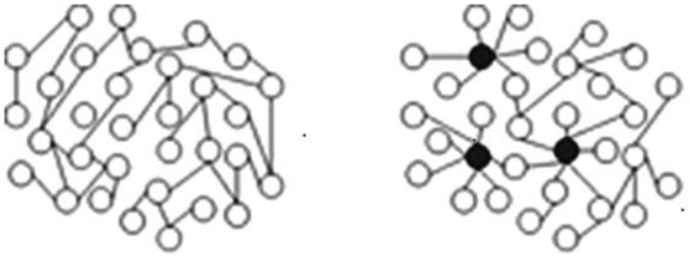

Figure : Examples of a random network and a scale-free network. Each graph has 32 nodes and 32 links. Note the "hubs" in the scale-free diagram (on the right).

Scale-free networks: A scale-free network is a network whose degree distribution follows a power law, at least asymptotically. In network theory a scale-free ideal network is a random network with a degree distribution that unravels the size distribution of social groups. Specific characteristics of scale-free networks vary with the theories and analytical tools used to create them, however, in general, scale-free networks have some common characteristics. One notable characteristic in a scale-free network is the relative commonness of vertices with a degree that greatly exceeds the average. The highest-degree nodes are often called "hubs", and may serve specific purposes in their networks, although this depends greatly on the social context. Another general characteristic of scale-free networks is the clustering

coefficient distribution, which decreases as the node degree increases. This distribution also follows a power law. The Barabási model of network evolution shown above is an example of a scale-free network.

3.3. Macro level

Rather than tracing interpersonal interactions, macro-level analyses generally trace the outcomes of interactions, such as economic or other resource transfer interactions over a large population.

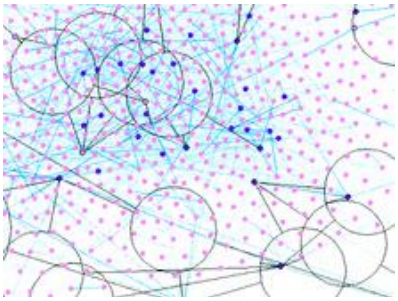

Figure: section of a large-scale social network

Large-scale networks: Large-scale network is a term somewhat synonymous with "macro-level" as used, primarily, in social and behavioral sciences, in economics. Originally, the term was used extensively in the computer sciences (see large-scale network mapping).

Complex networks: Most larger social networks display features of social complexity, which involves substantial non-trivial features of network topology, with patterns of complex connections between elements that are neither purely regular nor purely random (see, complexity science,dynamical system and chaos theory), as do biological, and technological networks. Such complex network features include a heavy tail in the degree distribution, a high clustering coefficient,assortativity or disassortativity among vertices, community structure, and hierarchical structure. In the case of agency-directed networks these features also include reciprocity, triad significance profile (TSP, see network motif), and other features. In contrast, many of the mathematical models of networks that have been studied in the past, such as lattices and random graphs, do not show these features.

IV. CONCLUSION

Social network analysis has gained significant prominence, largely due to the popularity of the networking and media sharing sites. There has been an increased interest in network analysis in organization studies and information research. There has been many groups working in different areas, still a gap exist between techniques developed by research community and their deployment. This is coming in a big way as a new approach to the problem solving, assuming people are interconnected which has consequences in performance.

REFERENCES

[1]. NETWORKS AN INTRODUCTION: MARK NEWMAN, OXFORD UNIVERSITY PRESS.
[2]. Social network data analystics: Charu C Aggarwal(ed.)
[3]. Pinheiro, Carlos A.R. (2011). Social Network Analysis in Telecommunications. John Wiley & Sons.p.4. ISBN 978-1-118-01094-5.
[4]. D'Andrea, Alessia et al. (2009). "An Overview of Methods for Virtual Social Network Analysis". In Abraham, Ajith et al. Computational Social Network Analysis: Trends, Tools and Research Advances. Springer. p. 8. ISBN 978-1-84882-228-3.
[5]. Senekal, B. A. 2012. Die Afrikaanse literêre sisteem: 'n Eksperimentele benadering met behulp van Sosiale-netwerk-analise (SNA), LitNet Akademies 9(3)
[6]. "Social Network Analysis". Field Manual 3-24: Counterinsurgency. Headquarters,Department of the Army. pp. B–11 – B–12.
[7]. en.wikipedia.org/wiki/Social_network_analysis
[8]. Journal on Introduction to stochastic actor-based models for network dynamics Snijders, T.A.B., van de Bunt, G.G., Steglich, C.E.G.
[9]. www.sciencedirect.com/science/journal/03788733
[10]. lrs.ed.uiuc.edu/tse-portal/analysis/social-network-analysis/
[11]. Using Social Network Analysis to Analyze Relationships Among IS Journals Greta L. Polites, Richard Watson
[12]. Utilization and value of Social Networking relationships in family and nonfamily firms in an African transition economy Original Research Article European Management Journal, Volume 29, Issue 5, October 2011, Pages 347-361 Moses Acquaah
[13]. Social Networking sites and the legal profession: Balancing benefits with navigating minefields Original Research Article Computer Law & Security Review, Volume 29, Issue 2, April 2013, Pages 164-174
[14]. Online Social Networking for Quality of Life Original Research Article Procedia Social and Behavioral Sciences, Volume 35, 2012, Pages 713-718 Noorriati Din, Saadiah Yahya, Raja Suzan, Raja Kassim
[15]. The effect of Social Networking websites on positive self-views: An experimental investigationOriginal Research Article Computers in Human Behavior, Volume 28, Issue 5, September 2012, Pages 1929-1933 Brittany Gentile, Jean M. Twenge, Elise C. Freeman, W. Keith Campbell
[17] . Article on Understanding social network analysis by Mini Ulanat and K Poulose
[18]. Social network analysis: a powerful strategy, also for the information sciences**:** Evelien Ott**e,** Ronald Rousseau
[19]. Social network analysis: An approach and technique for the study of information exchange :Library & Information Science Research, Volume 18, Issue 4, Autumn 1996, Pages 323-342
[20]. Article on Social networking –Impact and Ramification by Dr. P Chenna Reddey

International Journal of Modern Engineering Research (IJMER)
www.ijmer.com Vol. 3, Issue. 4, Jul - Aug. 2013 pp-2476-2480 ISSN: 2249-6645

"Comparison of Histogram Equalization Techniques for Image Enhancement of Grayscale images of Dawn and Dusk"

Dinesh Sonker[1], M. P. Parsai[2]
[1, 2] (*Department of Electronics and Comm. Engineering, Jabalpur Engineering College, Jabalpur, M.P., 482011, India*)

ABSTRACT: *Various enhancement schemes are used for enhancing an image which includes gray scale manipulation, filtering and Histogram Equalization (HE). Histogram equalization is one of the well known image enhancement became a popular technique for contrast enhancement because this method is simple and effective. In the latter case, preserving the input brightness of the image is required to avoid the generation of non-existing artifacts in the output image. Although these methods preserve the input brightness on the output image with a significant contrast enhancement, they may produce images which do not look as natural as the input ones. The basic idea of HE method is to re-map the gray levels of an image. HE tends to introduce some annoying artifacts and unnatural enhancement. To overcome these drawbacks different brightness preserving techniques are used which are covered in the literature survey. There are different images used in different time period and comparison on the basis of subjective and objective parameters. Subjective parameters are visual quality and computation time and objective parameters are Peak signal noise ratio (PSNR), Mean squared error (MSE), Normalized Absolute Error (NAE), Normalized Correlation, Error Color and Composite Peak Signal to Noise Ratio (CPSNR).*

KEYWORD: *Contrast enhancement, Histogram equalization, PSNR, MSE, NAE, CPSNR, Visual Contrast quality.*

I. INTRODUCTION

Contrast enhancement techniques are used widely in image processing. One of the most popular automatic procedures is histogram equalization (HE). Out of the five senses sight, hearing, touch, smell and taste which humans use to perceive their environment, sight is the most powerful. Receiving and analyzing images forms a large part of the routine cerebral activity of human beings throughout their waking lives. In fact, more than 99% of the activity of the human brain is involved in processing images from the visual cortex. This is less effective when the contrast characteristics vary across the image. Adaptive Histogram Equalization (AHE) overcomes this drawback by generating the mapping for each pixel from the histogram in a surrounding window. In future we will take different type of images in different time period and use Adaptive Histogram Equalization (AHE) and compare histogram equalization of images.

A. Image Enhancement: Image enhancement is among the simplest and most appealing areas of digital image processing. Basically, the idea behind enhancement techniques is to bring out detail that is obscured or simply to highlight certain features of interest in an image. A familiar example of enhancement is shown in Fig.1 in which when we increase the contrast of an image and filter it to remove the noise "it looks better." It is important to keep in mind that enhancement is a very subjective area of image processing. Improvement in quality of these degraded images can be achieved by using application of enhancement technique.

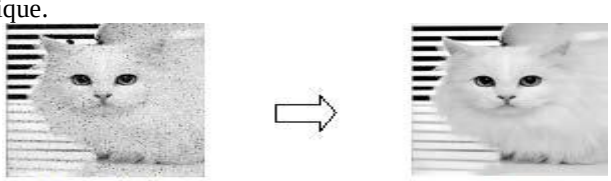

Distorted Image Enhanced Image

B. Adaptive Histogram Equalization method: This is an extension to traditional Histogram Equalization technique. It enhances the contrast of images by transforming the values in the intensity image. The AHE process can be understood in different ways. In one perspective the histogram of grey levels (GL's) in the output is maximally black; if it has the median value in its window the output is 50% gray's window around each pixel is generated first. The cumulative distribution of GL's, that is the cumulative sum over the histogram, is used to map the input pixel GL's to output GL's. If a pixel has a GL lower than all others in the surrounding window

C. Dualistic sub-image histogram equalization method: This is a novel histogram equalization technique in which the original image is decomposed into two equal area sub-images based on its gray level probability density function. Then the two sub-images are equalized respectively. At last, we get the result after the processed sub-images are composed into one image. In fact, the algorithm can not only enhance the image visual information effectively, but also constrain the original image's average luminance from great shift. This makes it possible to be utilized in video system directly.

D.Dynamic histogram equalization for image contrast Enhancement: It employs a partitioning operation over the input histogram to chop it into some sub histograms so that they have no dominating component in them. Then each sub-histogram goes through HE and is allowed to occupy a specified gray level range in the enhanced output image. Thus, a better overall contrast enhancement is gained by DHE with controlled dynamic range of gray levels and eliminating the

possibility of the low histogram components being compressed that may cause some part of the image to have washed out appearance.

E.Contrast Limited Adaptive Histogram Equalization Method (1)**Algorithm Steps**:Obtain all the inputs: Image, Number of regions in row and column directions, Number of bins for the histograms used in building image transform function (dynamic range), Clip limit for contrast limiting (normalized from 0 to 1).

Pre-process the inputs: Determine real clip limit from the normalized value if necessary, pad the image before splitting it into regions.

Process each contextual region (tile) thus producing gray level mappings: Extract a single image region, make a histogram for this region using the specified number of bins, clip the histogram using clip limit, and create a mapping (transformation function) for this region

Interpolate gray level mappings in order to assemble final CLAHE image: Extract cluster of four neighboring mapping functions, process image region partly overlapping each of the mapping tiles, extract a single pixel, apply four mappings to that pixel, and interpolate between the results to obtain the output pixel; repeat over the entire image.

II. METRICS FOR GRAY SCALE IMAGES

1. Peak-signal-to-noise-ratio (PSNR): PSNR is the evaluation standard of the reconstructed image quality, and is important measurement feature. PSNR is measured in decibels (dB) and is given by:

PSNR*= 10log (255^2/*MSE)

Where the value 255 is maximum possible value that can be attained by the image signal. Mean square error (MSE) is defined as Where M*N is the size of the original image. Higher the PSNR value is, better the reconstructed image.

2. Contrast: Contrast defines the difference between lowest and highest intensity level. Higher the value of contrast means more difference between lowest and highest intensity level.

Histogram Technique for Equalization: Enhance contrast using histogram equalization

Syntax:

J = histeq(I, hgram)
J = histeq(I, n)
[J, T] = histeq(I,...)
newmap = histeq(X, map, hgram)
newmap = histeq(X, map)
[newmap, T] = histeq(X,...)

Description: Histeq enhances the contrast of images by transforming the values in an intensity image, or the values in the color map of an indexed image, so that the histogram of the output image approximately matches a specified histogram.

J = Histeq (I, hgram) transforms the intensity image I so that the histogram of the output intensity image J with length (hgram) bins approximately matches hgram. The vector hgram should contain integer counts for equally spaced bins with intensity values in the appropriate range: [0, 1] for images of class double, [0, 255] for images of class uint8, and [0, 65535] for images of class uint16. Histeq automatically scales hgram so that sum (hgram) = prod (size (I)). The histogram of J will better match hgram when length (hgram) is much smaller than the number of discrete levels in me.

J = Histeq (I, n) transforms the intensity image I, returning in J an intensity image with n discrete gray levels. A roughly equal number of pixels is mapped to each of the n levels in J, so that the histogram of J is approximately flat. (The histogram of J is flatter when n is much smaller than the number of discrete levels in I.) The default value for n is 64.

[J, T] = Histeq (I...) returns the grayscale transformation that maps gray levels in the image I to gray levels in J.

New map = Histeq(X, map, hgram) transforms the color map associated with the indexed image X so that the histogram of the gray component of the indexed image (X,newmap) approximately matches hgram. The histeq function returns the transformed color map in new map. Length (hgram) must be the same as size (map,1).

New map = Histeq(X, map) transforms the values in the color map so that the histogram of the gray component of the indexed image X is approximately flat. It returns the transformed color map in new map.

[new map, T] = Histeq(X,...) returns the grayscale transformation T that maps the gray component of map to the gray component of new map.

Class Support: For syntax that includes an intensity image I as input, I can be of class uint8, uint16, int16, single, or double. The output image J has the same class as I.

For syntax that includes an indexed image X as input, X can be of class uint8, single, or double; the output color map is always of class double. The optional output T (the gray-level transform) is always of class double.

Examples

Enhance the contrast of an intensity image using histogram equalization.

```
I = imread ('tire.tif');
J = Histeq (I);
imshow (I)
```

Figure, imshow (J)

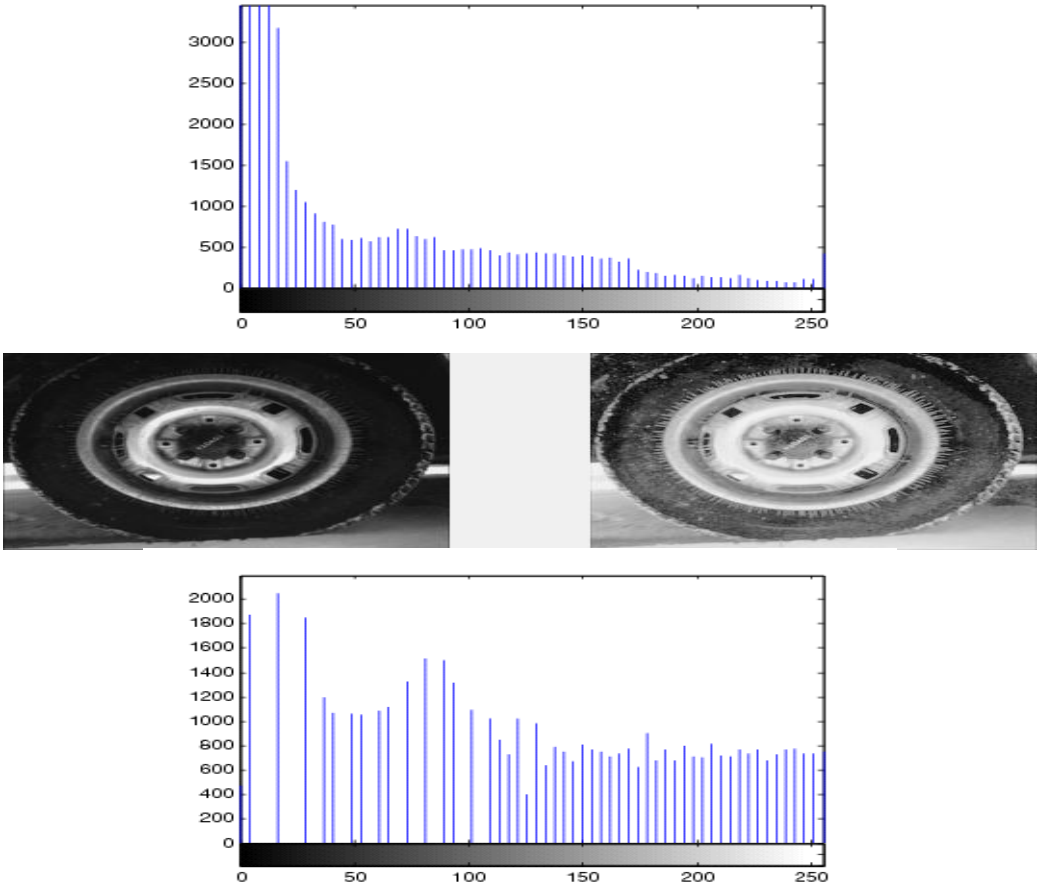

(a).Original image of tire (b) HE image of tire

Results of test image "Rice"

(a) Original image

(a) Histogram of Image

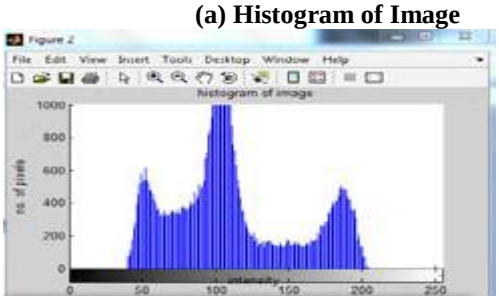

(b) DHE Image

(b) DHE Histogram

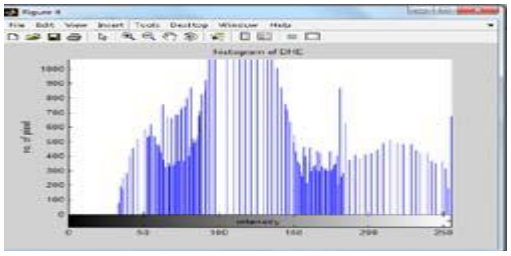

(c)DSIHE Image

(c) DSIHE Histogram

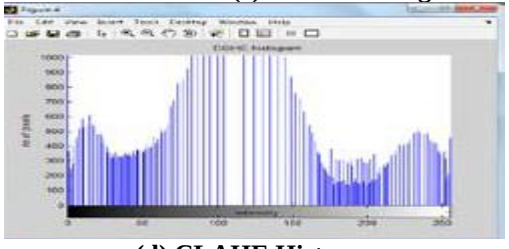

(d) CLAHE Image

(d) CLAHE Histogram

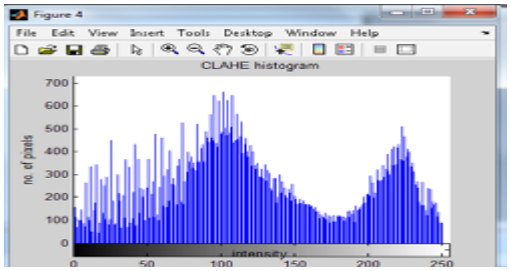

Equalized Histograms for Image "Rice" as shown in Image a, b, c, d as original, CLAHE, DHE, DSIHE Respectively.

Table 1: Comparison of Various Parameters for "Rice" Image:

Parameter Technique	AMBE	Contrast	PSNR
CLAHE	10.576	21.681	0.0266
DSIHE	3.908	31.876	0.0244
DHE	10.476	9.154	0.1021

III. CONCLUSION AND FUTURE ASPECT

IN future we will use different images in different time either are in morning or evening, Natural or Unnatural light and that's images are compare different time duration and take out its equalization. We will be compared images by Histogram Equalization. In this Paper; a frame work for image enhancement based on prior knowledge on the Histogram Equalization has been presented. Many image enhancement schemes like Contrast limited Adaptive Histogram Equalization (CLAHE), Equal area dualistic sub-image histogram equalization (DSIHE), Dynamic Histogram equalization (DHE) Algorithm has been implemented and compared. The Performance of all these Methods has been analyzed and a number of Practical experiments of real time images have been presented. From the experimental results, it is found that all the three techniques yields Different aspects for different parameters. In future, for the enhancement purpose more images can be taken from the different application fields so that it becomes clearer that for which application which particular technique is better both for Gray Scale Images and color Images.

Histogram Equalization images in different Time Period

M1

M2

M3

M4

Morning Period Images (at 06:00 to 10:00 am)

E1

E2

E3

E4

Evening Period Images (at 6:00 to 6:45pm)

REFERENCE

[1]. M. Abdullah-Al-Wadud, Md. Hasanul Kabir, M. Ali Akber Dewan, Oksam Chae, "A dynamic histogram equalization for image contrast enhancement", IEEE Transactions. Consumer Electron. vol. 53, no. 2, pp. 593- 600, May2007.
[2]. Histogram Equalization Techniques For Image Enhancement "Rajesh Garg, Bhawna Mittal, Sheetal Garg, H.I.T., Sonepat, Haryana, India3S.M.Hindu Sr.Sec.School, Sonepat, Haryana, India IJECT Vol. 2, Issue 1, March 2011.
[3]. T. Tom and G. J. Wolfe, "Adaptive histogram equalization and its applications," SPIE Applicat. Dig. Image Process. IV, vol. 359, pp.
[4]. Rafael C. Gonzalez, Richard E. Woods, "Digital Image Processing", 2nd edition, Prentice Hall, 2002.
[5]. K. Jain, "Fundamentals of Digital Image Processing". Englewood Cliffs, NJ: Prentice-Hall, 1991.
[6]. J. M. Gauch, "Investigations of image contrast space defined by variations on histogram equalization," CVGIP: Graph. Models Image Process, vol. 54, pp. 269–280, July 1992.
[7]. Stephen M. Pizer, R. Eugene Johnston, James P. Ericksen, Bonnie C. Yankaskas, Keith E. Muller, "Contrast-Limited Adaptive Histogram Equalization Speed and Effectiveness, IEEE Int. Conf. Neural Networks & Signal Processing, Nanjing, China, December 14-17, 2003.

International Journal of Modern Engineering Research (IJMER)
www.ijmer.com Vol. 3, Issue. 4, Jul - Aug. 2013 pp-2481-2488 ISSN: 2249-6645

Design of Neural Network Controller for Active Vibration control of Cantilever plate with piezo-patch as sensor /actuator

Amit Kumar[1], Deepak Chhabra[2]

[1](M.Tech Scholar, Department of Mechanical Engineering, University Institute of Engineering and Technology, Maharishi Dayanand University Rohtak , India)

[2](Asst. Professor, Department of Mechanical Engineering, University Institute of Engineering and Technology, Maharishi Dayanand University Rohtak , INDIA)

ABSTRACT: *The purpose of this work is to control the vibration of the plate with the help of neural network controller. Using augmented equations, a finite element model of a two-dimensional cantilever plate instrumented with a piezoelectric patch sensor-actuator pair is derived. The contribution of piezoelectric sensor and actuator layers on the mass and stiffness of the plate is considered. As mesh size (8x8) is found best for the future modeling and analysis of the plate has been taken.LQR controller tuning has been designed with the help of Neural Network training. It is observed that neural network controller has found suitable and gave effective control to suppress the first three modes of vibration of cantilever plate. With the help of MATLAB simulation results are presented.*

Nomenclature

$\{D\}$	electric displacement vector	ω_m	m[th] modal frequency
$\{E\}$	electric field vector	$[e]$	piezoelectric stress coefficient matrix
$\{\varepsilon\}$	strain vector	$[\in]$	permittivity constant matrix
$\{\sigma\}$	stress vector	$\in_0$	absolute permittivity
$[d]$	piezoelectric strain coefficient matrix	q	charge applied on piezoelectric material
$[c]$	elasticity matrix	v	voltage generated in piezo electric patch
Y	Young's modulus of elasticity	ζ_m	m[th] Modal damping ratio
μ	Poisson's ratio	f_m	m[th] Modal force vector
ρ	Density	$\{s\}$	state variable
$\{p\}$	pyroelectric constant vector	$[A]$	system state matrix
$\{\alpha\}$	coefficient of thermal expansion vector	$[B]$	control matrix
u,v,w	displacements along, respectively x, y and z-axis	$[C]$	output matrix
$\alpha_2^* \alpha_1^*$	coefficient associated with Kinetic energy and Strain energy	$[M]$	mass matrix
$\{F^e\}$	external force vector on an element	$[K]$	stiffness matrix
{x}	displacement vector	$[C]$	damping matrix
		A	area
η_m	m[th] modal state vector	d	thickness of piezoelectric patch
$[N]$	Hermite's interpolation function	T_e	kinetic energy of element
V_e	potential energy of element	W_{elect}	Electric energy of element
$[m_s^e]$	substrate element mass matrix	*Superscripts*	
$[m_p^e]$	piezoelectric element mass matrix	T	transpose
G	noise influence matrix	*Subscripts*	
K_e	Kalman filter gain	s	substrate
		p	piezoelectric
		i	in the i[th] direction

Key words: *Smart structure, Finite element model, Active vibration control, Neural Network Controller*

I. INTRODUCTION

Vibration control is the strategy in which an external source of energy is used to control structural vibrations is called active vibration control (AVC). It essentially consists of sensors to capture the structural dynamics, a processor to manipulate the sensor signals, actuators to obey the order of processor and a source of energy to actuate the actuators. Such a structure is known as a 'smart structure'. Piezoelectric materials possess excellent electromechanical properties viz. fast response, easy fabrication, design flexibility, low weight, low cost, large operating bandwidth, low power consumption, generation of no magnetic field while converting electrical energy into mechanical energy, etc. So, they are extensively used as sensors and actuators in AVC [12].

Damble, Lashlee, Rao and Kern [1] studied an integrated approach to design and implement robust controllers for smart structures. Jha and Jacob Rower [2] purposed neural networks for identification and control of smart structures is investigated experimentally. Piezoelectric actuators are employed to suppress the vibrations of a cantilevered plate subject to

impulse, sine wave and band-limited white noise disturbances. The neural networks used are multilayer perceptron trained with error back propagation. Jha and Chengli He [3] purposed a neural-network-based adaptive predictive controller is developed and validated experimentally. On-line nonlinear plant identification is performed using a multilayer perceptron neural network with tapped delay inputs. Q. Song, J. C. Spall and Y.C. Soh [4] studied robust neural network tracking controller using simultaneous perturbation stochastic approximation. They consider the problem of robust tracking controller design for a nonlinear plant in which the neural network is used in the closed-loop system to estimate the nonlinear system function. Liu, Lin and Lee [5] proposed a novel neural network approach for the identification and control of a thin simply supported plate. The motion behaviour of a two dimensional model of piezoelectric materials bounded to the surface of the plate is analytically investigated.

Yu and Jinde Cao [6] studied robust control of uncertain stochastic recurrent neural networks with time varying delay. They consider a novel control method which is given by using the Lyapunov Functional method and linear matrix inequality (LMI) approach. Chun-Fei Hsu [7] proposed an adaptive recurrent neural network control (ARNNC) system with structure adaptation algorithm for the uncertain nonlinear systems. The developed ARNNC system is composed of a neural controller and a robust controller. Roy and chakraborty [8] purposed genetic algorithm (GA) based linear quadratic regulator (LQR) control scheme has been proposed for active vibration control of smart Fiber Reinforced Polymer (FRP) composite shell structures under combined mechanical and thermal loading.

Mei, Wu and Jiang [9] purposed a neural network robust adaptive control for a class of time delay uncertain nonlinear systems. They describe a robust adaptive control scheme based on neural network is proposed for a class of time delay uncertain nonlinear system. M. Adhyaru, I. N. Kar, M. Gopal [10] studied bounded robust control of nonlinear systems using neural network–based HJB solution. They use Hamilton–Jacobi–Bellman (HJB) equation–based optimal control algorithm for robust controller design is proposed for nonlinear systems. J. F .de Canete, Perez Saz-Orozco and I. Garcia-Moral [11] studied robust stability in multivariable neural network control using harmonic analysis. In the research they describe robust stability and performance are the two most basic features of feedback control systems. Gupta, Sharma, Thakur and S P singh [12] A new scheme for active structural vibration control using piezoelectric patches at elevated temperatures is analytically derived and experimentally verified. A control law is derived using augmented piezoelectric constitutive equations which include the temperature dependence of piezoelectric stress coefficient and permittivity.

In this paper, the design of a Neural Network controller is to be done. Here two inputs and six outputs are taken with the help of LQR controller to design the Neural Network controller. The two inputs of LQR controller are the coefficient associated with Kinetic energy and Strain energy and six outputs are taken as Control Gain to control first three modes of vibration.

II. METHODOLOGY

2.1 Plate

An isotropic elastic rectangular plate of homogenous material is considered with its dimensions length L, breadth B, and thickness H. The plate is simply supported at two opposite sides and is subjected to vibrations. The vibration of the boundaries will be uniform and synchronous, i.e., the amplitude will be constant along the sides and all points along the boundaries will be vibrating in-phase. The remaining degrees of freedom along the sides of the structure will be locked. The plate is discretised into some finite number of smaller elements of identical shapes and sizes. The structure will be modeled by means of the FEM. It is supposed that the pair of piezoelectric patches can be added to the structure as sensor and actuator in piece coinciding with the surface area of each element.

Considering M is the number of elements along the length of the plate and N are the number of elements along the breadth. Each element is considered to be rectangular in shape with nodes i, j, l and m; and with dimensions length 2a and breadth 2b and thickness h.

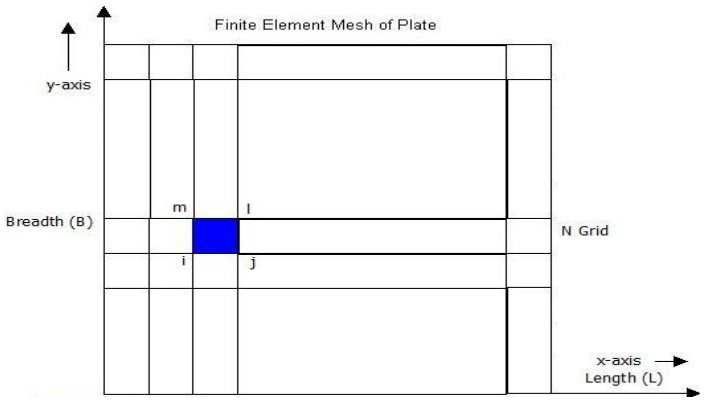

Fig. 1: Finite Element Mesh of Plate

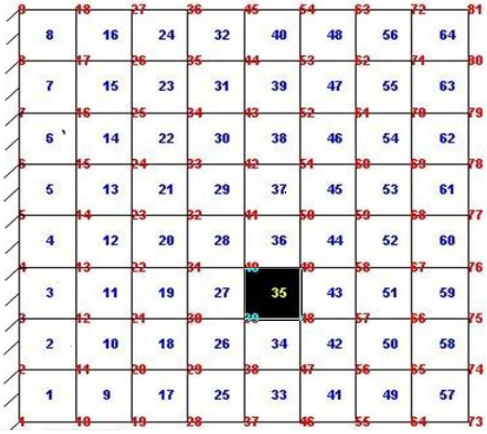

Fig. 2: Smart piezoplate structure divided into 64 finite elements with 81 nodes.

2.2 Finite Element Formulation

Consider a flexible elastic plate structure (fig.1). The plate is instrumented with piezo-patches collocated sensor–actuator pair polarized in the thickness direction. The top and bottom surface of each piezo-patch is covered by electrodes. At the piezo location, the structure is composite in the thickness direction with two piezo-patches and one elastic layer. The plate is modeled using the finite element method. It is divided into discrete finite elements where 'ζ' and 'η' are the natural coordinates of the finite element and they are related to global coordinates *(x, y)* as:

$$\zeta = \frac{x}{a} \tag{1}$$

$$\eta = \frac{y}{b} \tag{2}$$

Each finite element has four nodes and each node has three degrees of freedom: one translational w and two rotational θ_x and θ_y . If $\{u_e\}$ is the displacement vector of an element then displacement in the *z*-direction can be interpolated as:

$$w = [N]_{1\times12}\{u_e\}_{12\times1} \tag{3}$$

Where $[N]_{1\times12}$ is Hermite's interpolation function.

Ignoring shear deformations in the plate and using Kirchhoff's classical plate theory, strains developing in the plate can be written as:

$$\{\varepsilon\} = \{\frac{\partial u}{\partial x} \quad \frac{\partial v'}{\partial y} \quad \frac{\partial v'}{\partial x} + \frac{\partial u}{\partial x}\}^T \tag{4}$$

Where $u = -z\frac{\partial \omega}{\partial x}$ and $v' = -z\frac{\partial \omega}{\partial y}$

After substituting values of 'u' and 'v'' in the above equation, we get:

$$\{\varepsilon\}_{3\times1} = z[B_u]_{3\times12}\{u_e\}_{12\times1} \tag{5}$$

Where $[B_u]_{3\times12} = [-\frac{z\partial^2}{\partial x^2} - \frac{z\partial^2}{\partial y^2} - \frac{2z\partial^2}{\partial x\partial y}]^T_{3\times1}[N]_{1\times12}$

Kinetic energy of one finite element: $T_e = \frac{1}{2}\int_s \rho_s \omega^2 d\tau + \frac{1}{2}\int_p \rho_p \omega^2 d\tau$ (6)

Potential energy of one finite element:

$$V_e = \frac{1}{2}\int_s \{\varepsilon\}^T\{\sigma\}d\tau + \frac{1}{2}\int_v \{\varepsilon\}^T\{\sigma\}d\tau \tag{7}$$

Electric energy stored in one finite element:

$$W_{elect} = \frac{1}{2}\int_P \{E\}^T\{D\}d\tau \tag{8}$$

External surface traction or a point force can act on a smart structure. These forces would do work on the smart structure and as a result, energy stored per element is:

$$W_{ext\,(1)} = \int_{A_s} \{w\}^T\{f_s^e\}dA_s \tag{9}$$

Work required to apply external charge on the surface of a piezoelectric is:

$$W_{ext\,(11)} = -\int_{A_P} qvdA_P \tag{10}$$

Now, the Lagrangian for one finite element of the smart structure can be obtained as:

$$L = T_e - V_e + \left(W_{elect} + W_{ext\,(1)} + W_{ext\,(11)}\right) \tag{11}$$

The Lagrangian can be calculated using finite element relations and augmented constitutive equations. The equation of motion of one finite element is derived using Hamilton's principle:

$$\delta\int_{t1}^{t2} Ldt = 0 \tag{12}$$

The resulting variational contains two variables namely '$\{u_e\}$' and 'v'. Taking variation with respect to $\{u_e\}$, we get:

$$([m_s^e] + [m_P^e])\{\ddot{u_e}\} + ([k_s^e] + [k_P^e])\{u_e\} + [k_{uv}^e]v = \{F_S^E\} \tag{13}$$

And taking variation with respect to 'v', we get:

$$[k_{vu}^e]\{u_e\} - [k_{vv}^e]v = 0 \tag{14}$$

$$v = [k_{vv}^e]^{-1}[k_{vu}^e]\{u_e\} \tag{15}$$

Where $[m_s^e] = \int_s \rho_s [N]^T[N]d\boldsymbol{\tau}$

$[m_P^e] = \int_P \rho_P [N]^T [N] d\boldsymbol{\tau}$

$[k_s^e] = \int_s z^2 [B_u]^T [c_s][B_u] d\boldsymbol{\tau}$

is the substrate element stiffness matrix,

$[k_P^e] = \int_P z^2 [B_u]^T [c_s][B_u] d\boldsymbol{\tau}$

is the piezoelectric element stiffness matrix,

$[k_{uv}^e] = [k_{uv}^e]^T = \int_P z\{B_u\}^T [e^t][B_v] d\tau$ is the electromechanical interaction matrix.

Put the value of v from eqation (14), in the equation, we get the equation of motion of one finite element of the smart plate structure as:

$$[M_e]\{\ddot{u}_e\} + [K_e]\{u_e\} = \{F_e\} \quad (16)$$

Where $[M_e]$, $[K_e]$and $\{F_e\}$ are elemental mass matrix, elemental stiffness matrix and total force on the finite element respectively.

Applying assembly procedure and boundary conditions, the global equation of motion of the smart cantilevered plate structure is obtained as:

$$[M]\{\ddot{x}\} + [C]\{\dot{x}\} + [K]\{\dot{x}\} = \{F\} \quad (17)$$

Where the damping term $[C] = \alpha[M] + \beta[K]$. '$\alpha$' and '$\beta$' are Rayleigh mass and stiffness damping coefficients respectively. This is the equation of motion of a two dimensional smart cantilevered plate instrumented with one collocated piezoelectric sensor–actuator pair.

2.3 LQR Controller

LQR optimal control theory is used to determine the active control gain. The following quadratic cost function is minimized $$\mathrm{j} = \frac{1}{2}\int_0^\infty (\mathrm{x^T\,Q\,x + u^T Ru})\mathrm{dt} \quad (18)$$

Q and R represent weights on the different states and control channels and their elements are selected to provide suitable performance. They are the main design parameters. J represents the weighted sum of energy of the state and control. Assuming full state feedback, the control law is given by

$$\mathrm{u=-kx} \quad (19)$$

With constant control gain, $$\mathrm{k = R^{-1}B^T S} \quad (20)$$

Matrix S can be obtained by the solution of the Riccati equation, given by

$$\mathrm{A^T S + SA + Q - SBR^{-1}B^T S = 0} \quad (21)$$

The closed loop system dynamics with state feedback control is given by

$$\mathrm{\dot{x} = (A - Bk)x + Er(t)} \quad (22)$$

2.3 Determination of weighting matrices

Weighting matrices $[Q]$ and $[R]$ are important components of the LQR optimization process. The compositions of $[Q]$ and $[R]$ elements influence the system's performance. Ang. *et al* [13] proposed that weighting matrices could be determined, considering the weighted energy of the system, as follows

$$[Q] = \begin{bmatrix} \alpha_2^*[\psi]^T[K][\psi] & [0] \\ [0] & \alpha_1^*[\psi]^T[M][\psi] \end{bmatrix} \quad (23)$$

$$[\mathrm{R}] = 1 \quad (24)$$

A vast research have been done so far for neural network controller but in this research the neural network controller training used for tuning LQR controller which gave the minimum settling time and gave effective control to suppress the first three modes of vibration of cantilever plate.

Table 1: Input and Output of LQR controller

S No.	α_2^*	α_1^*	k1	k2	k3	k4	k5	k6
1	10	20	0.068194	13.01451	5.832724	-2.2212	-49.4622	2033.436
2	20.14	30.14	0.137404	26.16566	11.727	-3.34731	-74.4928	2714.578
3	32.25	42.25	0.24224	46.02262	20.62714	-4.69217	-104.345	3408.725
4	44.45	54.45	0.368897	69.93655	31.34608	-6.047	-134.375	4022.424
5	55.5	65.5	0.499835	94.58898	42.39643	-7.27409	-161.535	4525.661
6	75.6	85.6	0.773395	145.9095	65.40166	-9.50611	-210.845	5348.572
7	95.1	105.1	1.078137	202.8389	90.9225	-11.6714	-258.568	6063.211
8	106.14	116.14	1.266419	237.9043	106.6426	-12.8973	-285.537	6439.785
9	117.15	127.15	1.464863	274.7825	123.1758	-14.1198	-312.397	6798.588
10	128.2	138.2	1.674296	313.6208	140.5882	-15.3467	-339.318	7143.947
11	139.4	149.4	1.896662	354.772	159.038	-16.5903	-366.569	7480.639
12	150	160	2.116142	395.3081	177.2125	-17.7672	-392.325	7788.21
13	161.24	171.24	2.358146	439.9166	197.2134	-19.0151	-419.602	8103.736
14	172.7	182.7	2.614407	487.0587	218.3508	-20.2875	-447.375	8415.236
15	180	190	2.782525	517.9356	232.1956	-21.0979	-465.046	8608.718
16	190	200	3.01884	561.2733	251.6279	-22.2081	-489.229	8867.974

2.4 Design of Neural Network Controller

The design of Neural Network controller is based on simple human reasoning. The design of the neural network controller (NNC) is based on the inversion of the plant model (Neural Network Identifier). The NNC (figure) has five hidden neurons and a single output neuron, which gives the controller voltages. The inputs consist of excitation signals, control signals and time-delayed target values. There are many practical applications, where the disturbance is known or measurable. A neural network (also known as 'artificial neural network') is a massively parallel interconnection of simple processors or neurons that has the ability to learn from its environment and store the acquired knowledge for future use. Properly formulated and trained NNs are capable of approximating any linear or nonlinear function to the desired degree of accuracy. The neural networks used in the current research are known as multilayer perceptron (MLP). The MLPs comprise a layer of input signals, one or more hidden layers of neurons, and an output layer of neurons. A layer consists of a single or multiple neurons. Differences between the desired outputs (targets) and the network outputs give the errors. The connection strengths ('weights') and 'biases' are updated during training (or learning) such that the network produces the desired output for the given input.

Mathematically, neuron *j* having *m* inputs is described as follows:

$$y_j = \varphi_j(v_j) \tag{24}$$

Where $v_j = \left(\sum_{i=1}^{m} w_{ji}\, x_i + b_j\right)$

$x_i - input\ signals, w_{ji} - weights\ and\ b_j\ is\ bias$

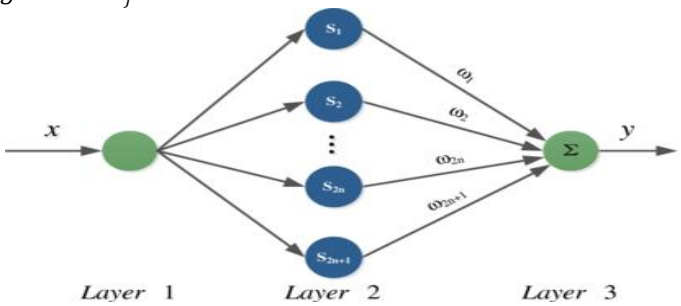

Fig. 3 Neural Network Controller

For a given set of inputs to the network, outputs are computed for each neuron in the first layer and forwarded to the next layer. The signals propagate on a layer-by-layer basis until the output layer is reached. The weights and biases remain unchanged during the 'forward pass'. The output of the network is compared with the desired value (t_j) and difference gives the error.

$$e_j = t_j - y_j \tag{25}$$

The total error is defined by equation (28), where *c* is the number of neurons in the output layer.

$$E = \frac{1}{2}\sum_{j=1}^{c} e_j^2 \tag{26}$$

The error *E* represents the cost function, and the weights and biases are updated to minimize it.

The computed partial derivatives (sensitivity) $\partial E/\partial w_{ji}$ determine the search direction for updating the weights w_{ji} as

$$w_{ji}(k+1) = w_{ji}(k) - \eta\frac{\partial E(k)}{\partial w_{ji}(k)} \tag{27}$$

k is the current time and (*k* + 1) is the next time step. The above update formula is refined using a 'momentum term' that has a stabilizing effect on the back-propagation algorithm. The training of the NN is complete when the error (or change in the error) reduces to a predetermined small value.

Using neural network fitting tool the inputs (coefficient associated with Kinetic energy and strain energy) and output (control gain) are given in the form of matrix i.e. of 16X2 and 16X6 in the range of 0 to 200 with training 70%, validation 15% and testing 15%. The hidden neurons are taken as 10. Network has been trained with the help of Levenberg-Marquardt back propagation algorithm which gave the regression plot for the neural network controller (Fig 4)

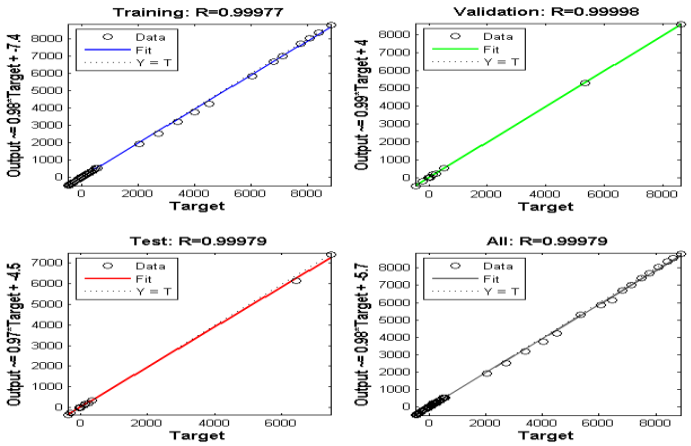

Fig 4 Regression Plot of Neural Network Controller

III. RESULT

Settling time for each patch placed in the 8X8 mesh under various control laws are as shown in the table2:

Table 2: Input parameters (Piezolocation, α_2^*, α_1^*) and settling time obtained using neural network controller

Sr. No.	Piezolocation	coefficient associated with Kinetic energy (α_2^*)	coefficient associated with Strain energy (α_1^*)	Settling Time
1	60	10	20	3.84
2	55	20.14	30.14	8.14
3	35	55.5	65.5	1.34
4	64	44.45	54.45	8.38
5	20	117.15	127.15	4.99
6	15	139.4	149.4	7.56
7	18	172.7	182.7	7.52
8	9	20.14	30.14	4.99
9	25	95.1	105.1	7.65
10	30	32.25	42.25	1.91
11	30	10	20	2.45
12	45	180	190	7.98
13	11	190	200	7.55
14	50	75.6	85.6	8.17
15	39	20.14	30.14	2
16	28	32.25	42.25	1.91

The Neural Network Controller is designed based on simple human reasoning. Using Neural Network Fitting tool input and output has been given in the form of matrix with 10 hidden neurons. Network has been train with the help of Levenberg-Marquardt back propagation algorithm. Input to the controller consists of coefficient associated with Kinetic energy and Strain energy of the structure and output of the controller are the gains applied to the actuator. Neural Network is used in such a way that voltage given to the actuator within breakdown voltage limits and provides stability to the system. The proposed neural network controller is tested for active vibration control of a cantilever plate to suppress first three modes of vibrations. A finite element model of 2D cantilever plate instrumented with a piezoelectric patch as sensor/actuator has been taken. While controlling first three modes simultaneously with a single sensor/actuator pair, effective control is observed with present approach. The position of sensor/actuator has been varied 1 to 64 positions which are available on finite element plate. The value of the coefficient associated with Kinetic energy and Strain energy has also been varied from 0 to 200. Thus by varying the sensor/actuator location and value of coefficient associated with Kinetic energy and strain energy, we found out the minimum settling time using Neural Network Controller. Table2. shows the settling time of using Neural Network Controller at various locations and values of coefficient associated with Kinetic energy and strain energy. The settling time are calculated by changing various position of piezo-patches and both coefficient associated with Kinetic energy and strain energy on MATLAB software. Some settling time figures are shown below. The best time settling is obtained at 35th piezo-patches and co-efficient associated with Kinetic energy and strain energy positions are 55.5 and 65.5 respectively. Figure 5 shows controlled and uncontrolled coefficient of kinetic energy (32.25) and strain energy (42.25) when piezoactuator is placed at 28th position. Figure 6 shows controlled and uncontrolled coefficient of kinetic energy (32.25) and strain energy (42.25) when piezoactuator is placed at 30th position. Figure 7 shows controlled and uncontrolled coefficient of kinetic energy (55.5) and strain energy (65.5) when piezoactuator is placed at 35th position. Figure 8 shows controlled and uncontrolled coefficient of kinetic energy (10) and strain energy (20) when piezoactuator is placed at 60th position.

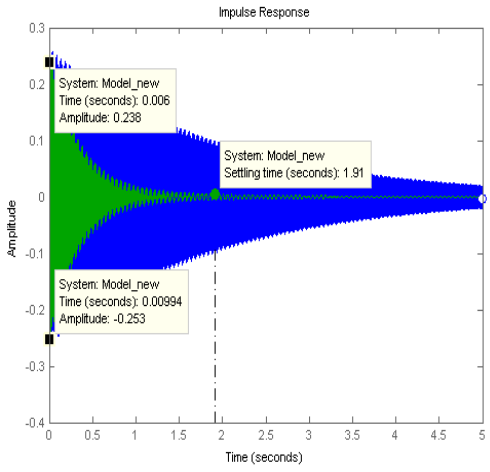

Fig 5 Controlled and Uncontrolled coefficient of Kinetic energy and strain energy When piezoactuator placed at 28th position (al=32.25 and bet=42.25)

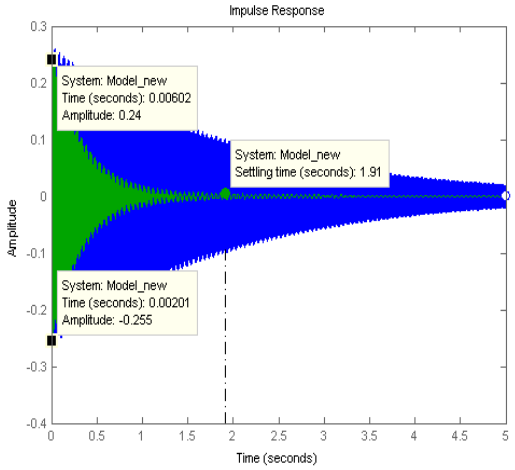

Fig 6 Controlled and Uncontrolled coefficient of Kinetic energy and strain energy When piezoactuator placed at 30th position (al=32.25 and bet=42.25)

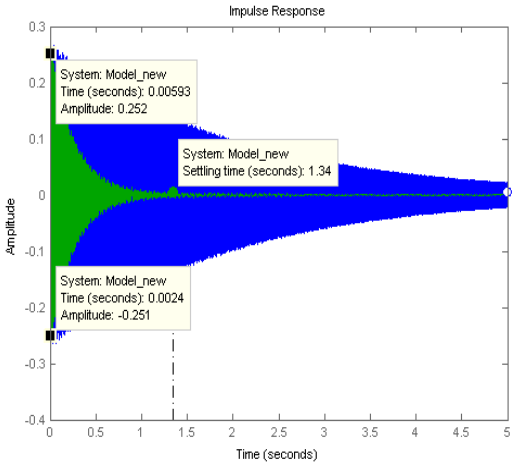

Fig 7 Controlled Uncontrolled coefficient of Kinetic energy and strain energy When piezoactuator placed at 35th position (al=55.5 and bet=65.5)

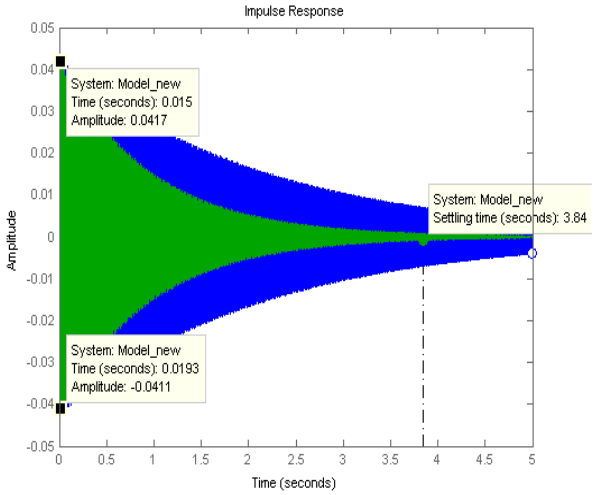

Fig 8 Controlled and Uncontrolled coefficient of Kinetic energy and strain energy When piezoactuator placed at 60th position (al=10 and bet=20)

IV. CONCLUSION

This work shows the basic techniques for analysis of active vibration control using piezoelectric sensor and actuator. A general scheme of analyzing and designing piezoelectric smart cantilever plate with Neural Network control tuned with LQR controller is successfully developed in the study. The two inputs of LQR controller are taken as coefficient associated with Kinetic energy and Strain energy to determine the weighing matrices Q & R and six outputs are taken as

Control Gain to control first three modes of vibration. The present scheme has flexibility of designing the collocated and non-collocated system. The best location of sensor/actuator pair is 35^{th} which gives the minimum settling time i.e.1.34 sec and the concern coefficient of Kinetic energy and strain energy are 55.5 and 65.5 respectively.

REFERENCES

[1] Damble, Lashlee, Rao and Kern, 1993"Identification and robust control of smart structures using artificial neural network" *Smart Mater. Struck*-3
[2] Jha and Jacob Rower, 2001"Experimental investigation of active vibration control using neural networks and piezoelectric" *Smart Mater. Struct.* 11 (2002) 115–121
[3] Jha and Chengli He,2002" Neural Network based adaptive predictive control for vibration suppression of smart structures" *Smart Mater. Struct*. 11 (2002) 909–916
[4] Q. Song, J. C. Spall and Y.C. Soh, 2003, "Robust neural network tracking controller using simultaneous perturbation stochastic approximation" *IEEE* 0-7803-7924-1
[5] Liu, Lin and Lee,2004" Neural-network-based identification and control of a thin plate using piezoelectric actuators and sensors" *IJSS* 0020–7721
[6] Wenwu Yu and Jinde Cao, 2007, " Robust Control of Uncertain Stochastic Recurrent Networks with Time-varying Delay" *Springer Science Business Media*, 26:101–119
[7] Chun-Fei Hsu , 2007, " Adaptive recurrent neural network control using a structure adaptation algorithm*" Springer-verlag* 18:115–125
[8] Roy and chakraborty, 2009"Genetic algorithm based optimal control of smart composite shell structures under mechanical loading and thermal gradient" *Smart Mater. Struct*. 18 (2009)
[9] J. Fernandez de Canete, S. Gonzalez-Perez, P. del Saz-Orozco, and I. Garcia-Moral, 2009,"Robust stability in multivariable neural network control using harmonic analysis" *IJIE* 3:1
[10] Rong Mei, Qing-Xian Wu and Chng-Sheng Jiang, 2010, "Neural network robust adaptive control for a class of time delay uncertain nonlinear systems" *ICIC* 1349-4198
[11] Deepak M. Adhyaru, I. N. Kar, M. Gopal ,2010,"Bounded robust control of nonlinear systems using neural network–based HJB solution" *Springer-Verlag* 20:91–103
[12] Gupta, Sharma, Thakur and S P singh, 2011"Active vibration control of a smart plate using a piezoelectric sensor–actuator pair at elevated temperatures" *Smart Mater. Struct*. 20
[13] Ang K K, Wang S Y and Quek S T, 2002"Weighted energy linear quadratic regulator vibration control of piezoelectric composite plates" *Smart Mater. Struct*. 11 98–106

International Journal of Modern Engineering Research (IJMER)
www.ijmer.com Vol. 3, Issue. 4, Jul - Aug. 2013 pp-2489-2491 ISSN: 2249-6645

Colour Rendering For True Colour Led Display System

N. Venkata Narendra[1], Dr. T. C. Sarma[2]
(Department of Electronics, Sreenidhi Institute of Science and Technology, India)

ABSTRACT: *This paper deals finding primary colours (Red, Green, Blue) depth values for each pixel in selected image or text to display the true colour of an image on the RGB LED display panel and transmitting those values to the controller via Ethernet. True colour having the colour depth of 2^8 (=256) for each primary colour in RGB colour space. So, we are able to display 256X256X256=1.6 billion colours on the RGB LED display panel.*

Keywords: *Ethernet, MATLAB, MBI5030 LED Driver, RGB LED panel.*

I. Introduction

Light Emitting Diodes (LEDs) are commonly used as indicator lights in electronic devices such as televisions and computers. LEDs, as with all semiconductors devices, have material and process variation which yields products with corresponding variation in performance. LEDs are binned and packed to balance the nature of manufacturing process with needs of the lighting industry. Color rendering is essentially an experiment where secondary color is generated by adding the appropriate proportion of primary colors.This paper describes how we are displaying the image or the video on RGB LED panel. Firstly we are generating the RGB values of image or video for each pixel, then we perform the gamma correction for RGB pixels separately, then after the operation we transfer each RGB values of each pixel via the frames using Ethernet to the STM controller. In the controller it processes and gives each pixel to LED driver. From the driver each pixel values are passed to the RGB LED panel and the image is displayed.

II. Accompanying Hardware and Software

The firmware describes in this paper is included with the STM32F207V Evaluation board. This board is specifically developed for hardware circuitry that is exhibited on the board. This board also includes a PC software that displays color output produced by the board by using Kiel software.

III. High Level Firmware

This firmware performs four tasks (refer to figure 1).The chart in this figure represents the procedural execution of the associated project.

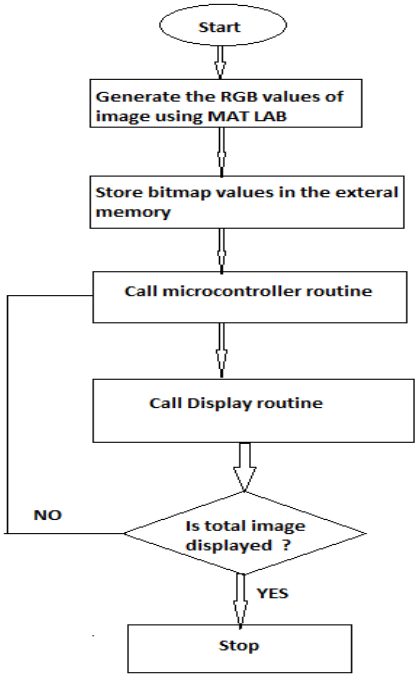

Fig 1.High Level Flow Chart of Firmware Execution

The important tasks are generating the RGB values for each pixel of an image and displaying it on the LED panel. And the other primary tasks are storing the bit map values and performing the gamma correction. Give three bit inputs (8 different combinations) to the decoder on display board to select each row in top & bottom 8 rows of one brick (display board consist of two active bricks).Activate first row LEDs of two bricks at a time and load internal buffers with respective gray values in LED drivers using D latch of LED driver .Set Global clock pin to glow all LEDs at a time with respective

gray values. Activate second, 3rd up to 8th row of two bricks and repeat process of glowing LEDs with the row refresh time of 312 micro seconds.

Before exploring the displaying of image, we must know more about the inputs and outputs of the system.

IV. Colour Rendering Inputs

This firmware uses RGB values of each pixel as the input to be serviced. First we should select an image, for that image we are going to generate the RGB values for the each pixel depends on the image resolution. This is done by using the Mat lab software. By using the image read function we are going to read the data of the particular image and by image pixel format we are going to generate R value separately, G value separately and B value separately. Then for this values gamma correction is performed. The gamma correction is a name of a nonlinear operation used to code and decode luminance or tristimulus values in video or image systems i.e it is used to display the text, image in accurate manner. The gamma correction is done to each pixel value of R,G,B by using the expression:

$\Gamma = R * G\_LUT[R] / 0xFFFF$ (For Red Pixels) .....(1)

And similarly in case of the green and blue colors. After the gamma correction these values are stored in external memory .By using the Ethernet we are going to the bitmap values from memory to STM controller via frames.The Ethernet peripheral enables the STM32F207V to transmit and receive data over Ethernet in compliance with the IEEE 802.3-2002 standard. Ethernet frames read from the system memory are pushed into the FIFO by the DMA. The frames are then popped out and transferred to the MAC core. When the end-of-frame is transferred, the status of the transmission is taken from the MAC core and transferred back to the DMA. The Transmit FIFO has a depth of 2 Kbyte. FIFO-fill level is indicated to the DMA so that it can initiate a data fetch in required bursts from the system memory, using the AHB interface. The data from the AHB Master interface is pushed into the FIFO. When the SOF is detected, the MAC accepts the data and begins transmitting to the MII. The time required to transmit the frame data to the MII after the application initiates transmission is variable, depending on delay factors like IFG delay, time to transmit preamble. Then it gives the bitmap data to controller via the com port.

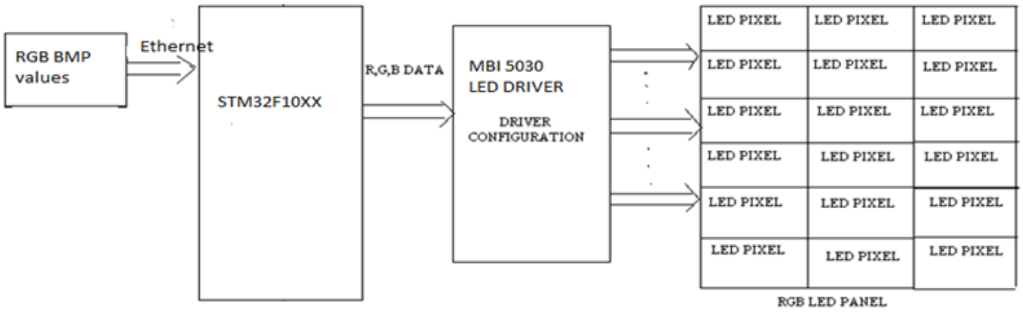

Fig 2.Firmware Input and Output

V. Colour Rendering Outputs

The challenge in developing this system lies in controlling LEDs .Here the controller used is STM32F207V.The features available in this controller are JTAG,LCD , Ethernet ,Decoder. The bitmap data from the controller is MBI5030 LED driver bit by bit.MBI 5030 is designed for LED video applications using internal pulse width modulation control with selectable 12-bit color depth. This features a 16-bit shift register which converts serial input data into each pixel gray scale of output. Suppose in order to display a 8*8 resolution image, their is need of 64 LEDs to drive 64 RGB LEDs .If we are using total 64 LED drivers in system it will become too complex as well as cost will be more, so in order to this drawback we are going use a decoder so that number of LED driver should use will be less. Give three bit inputs (8 different combinations) to the decoder on display board to select each row in top & bottom 8 rows of one brick (display board consist of two active bricks).Activate first row LEDs of two bricks at a time and load internal buffers with respective gray values in LED drivers using D latch of LED driver .Set Global clock pin to glow all LEDs at a time with respective gray values. Activate second, 3rd up to 8th row of two bricks and repeat process of glowing LEDs on RGB LED panel with the row refresh time of 312 micro seconds. so that image or video can seen by us clearly as refresh rate is very low.

VI. Mathematical Model

Fig.2 shows the inputs of the firmware and translated outputs .The mathematical functions in this section describe how the dimming value are obtained from CIE color space in order to a specific color. For some multi-LED applications, mixing white LEDs from a variety of bins is a cost effective way to achieve good color quality while minimizing LED costs. In this Illustration we show four LEDs can achieve the same perceived result as if four LEDs from one of the central sub-bins were used instead. Mathematically the results come because color and flux are additive. LEDs are typically characterized by chromaticity (x,y in the 1931 CIE color space) and flux (Φ =Y). Luminous flux is an additive metric just as perceived color is additive.

Tristimulus values, used in color mixing math, can be calculated as follows:

$X=x*(Y/y)$ ----------(2)

$Y=Y$ ----------(3)

$Z=(Y/y)*(1-x-y)$------(4)

The combined color is the result of the added tristimulus values:

Xmix=X1+X2+X3+X4
Ymix=Y1+Y2+Y3+Y4
Zmix=Z1+Z2+Z3+Z4

After finding Xmix, Ymix, Zmix, calculate xmix, ymix, zmix

xmix = Xmix/(Xmix+ Ymix+Zmix)
ymix = Ymix/(Xmix+Ymix+Zmix)
Φmix = Y1+Y2+Y3+Y4

VII. Conclusion

The final two primary tasks in fig 1 are generating the RGB values of the image with the dimming values for the each pixel and passing it to the STM controller on evaluation board via the Ethernet and gamma correction is performed and the bit by bit data is send to RGB LED panel via the LED driver and the image , video can be displayed on the LED panel which has true colour. This application mainly useful in Large LED Screens for Stadiums, Railway Stations, Bus stands etc.

VIII. Output

9.1 This is the one color rendered output, that is displayed on the RGB LED panel.

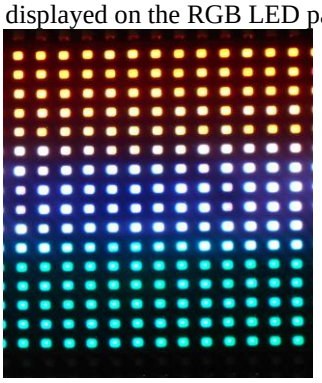

9.2 This is the procedure of connecting STM evaluation kit to LED panel and the output is display panel.

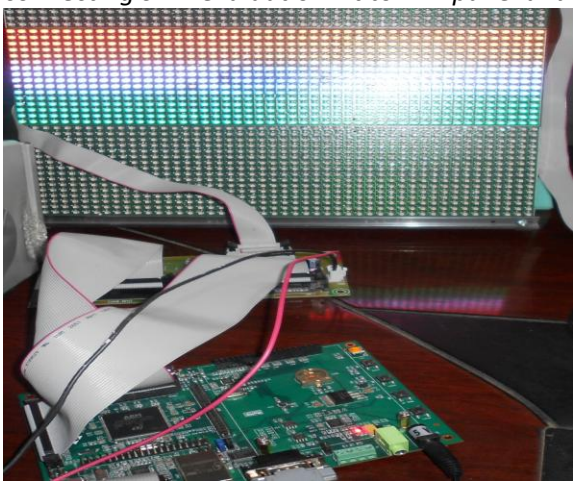

References

[1] Golbert A. and Israel I."Trends in microprocessor cache architectures" IEEE on March,1991
[2] Jaber Hasan and Simon S. Ang, "A High-Efficiency Digitally Controlled RGB Driver for LED Pixels" IEEE paper.
[3] Qin Song, Yan Sun "ARM9-based Control System for LED Large Screen Display" 2010 IEEE paper
[4] A guided tour of color space, Charles poynton,Newyork,1997
[5] Firmware for RGB color mixing .-EZ-color,AN16035,2010
[6] Cree's LED color mixing-Basics and Background,2010
[7] STM32F2XX datasheet "Doc ID 15818 Rev 8" www.stm.com.
[8] Yao Yingbiao, Zhang Jianwu, and Zhao Danying "Survey on microprocessor architecture and development trends" IEEE on November, 2008
[9] Microblock MBI5030 16-channel constant current LED driver
[10] http://www.colourbasics.com.

International Journal of Modern Engineering Research (IJMER)
www.ijmer.com Vol. 3, Issue. 4, Jul - Aug. 2013 pp-2492-2497 ISSN: 2249-6645

Modeling & Simulation of PMSM Drives with Fuzzy Logic Controller

Praveen Kumar[1], Anurag Singh Tomer[2]
[1](ME Scholar, Department of Electrical Engineering, RCET, Bhilai, India)
[2](Assoc. Prof., Department of Electrical Engineering, RCET, Bhilai, India)

ABSTRACT: *The Permanent-magnet-synchronous-machine (PMSM) drives have been increasingly applied in a variety of industrial applications which require fast dynamic response and accurate control over wide speed ranges. In this thesis the control of a Permanent Magnet Synchronous Motor (PMSM) is studied. Usually, a proportional-integral (PI) controller is used as a speed controller for a Permanent Magnet Synchronous Motor (PMSM). However, a PI controller is sensitive to speed changes, load disturbances and parameters variation without continuous tuning of its gains. The conventional approach is to tune the proportional and integral gains manually by observing the response of the system. The tuning of the PI parameters must be made on-line and automatic in order to avoid tedious tasks in manual control. For this reason the design of using fuzzy logic controller (FLC) which replace the proportional-integral (PI) controller.*

KEYWORDS: *AC drives, Fuzzy logic controller (FLC), Permanent Magnet Synchronous Machine (PMSM), Pulse Width Modulation (PWM),* P*roportional-Integral (PI) controller.*

I. INTRODUCTION

Recent availability of high energy-density permanent magnet (PM) materials at competitive prices, continuing breakthroughs and reduction in cost of powerful fast digital signal processors (DSPs) and micro-controllers combined with the remarkable advances in semiconductor switches and modern control technologies have opened up new possibilities for permanent magnet brushless motor drives in order to meet competitive worldwide market demands [1].

The popularity of PMSMs comes from their desirable features :

- High efficiency
- High torque to inertia ratio
- High torque to volume ratio
- High air gap flux density
- High power factor
- High acceleration and deceleration rates

Permanent magnet synchronous motor requires a "drive" to supply commutated current. This is obtained by pulse width modulation of the DC bus using a DC-to-AC inverter attached to the motor windings. The windings must be synchronized with the rotor position by using position sensors or through sensor less position estimation techniques. By energizing specific windings in the stator, based on the position of the rotor, a rotating magnetic field is generated. , only two of the three stator windings are energized in each commutation sequence [1].

The fuzzy logic is a class of artificial intelligence with a recent history and application. The concept of fuzzy logic was first introduced by 1965 by a computer scientist Lotfy Zadeh, a professor at the University of California at Berkley. Fuzzy-logic provides a simple way to arrive at a definite conclusion based upon vague, ambiguous, imprecise, noisy, or missing input information. Its approach to control problems mimics how a person would make decisions, much faster [2], [3], [4].

II. MATHEMATICAL MODEL OF PMSM

Equation is often written in expanded form as

$$V_{ds} = R_s I_{ds} + L_d \frac{d\, Ids}{dt} - \omega_r L_q I_q$$
$$V_{qs} = R_s Iq_s + L_q \frac{d\, Iqs}{dt} + \omega_r (L_d I_{ds} + \lambda_m)$$
$$V_{0s} = R_s I_{0s} + L_0 \frac{d\, I_0s}{dt}$$

Under balanced steady-state conditions, the electrical angular velocity of rotor ωr is considered constant and equal to that of the synchronously rotating reference frame. In this mode of operation, with the time rate of change of all flux linkages neglected, the steady state versions of above equations become

$$V_{ds} = R_s I_{ds} - \omega_r L_q I_{qs}$$
$$V_{qs} = R_s I_{qs} + \omega_r (L_d I_{ds} + \lambda_m)$$
$$V_{0s} = R_s I_{0s} = 0$$

Electromagnetic torque can be expressed with the stator variables in the rotor reference frame as

$$T_e = \left(\frac{3}{2}\right)\left(\frac{P}{2}\right)(\lambda_{ds} I_{qs} - \lambda_{qs} I_{ds})$$

Appropriate substitution of into the above torque equation yields

$$T_e = \left(\frac{3}{2}\right)\left(\frac{P}{2}\right)[\ \lambda_m I_{qs} + (L_d - L_q) I_{qs} I_{ds}\ ]$$

The torque equation can also be expressed in the following way,

$$T_e = T_m + J\frac{d}{dt}\omega_r + B\,\omega_r$$

III. Pmsm Drives With Fuzzy Controller

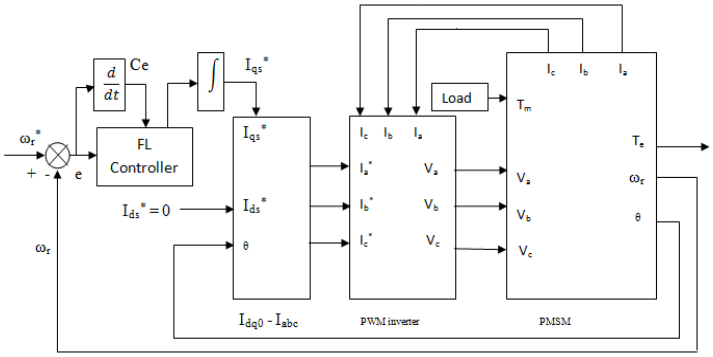

Figure 1: PMSM Drive with Fuzzy Logic (FL) controller

3.1 Pulse width modulation (PWM) technique

Pulse width modulation (PWM) technique is used to generate the required voltage or current to feed the motor or phase signals. This method is increasingly used for AC drives with the condition that the harmonic current is as small as possible. Generally, the PWM schemes generate the switching position patterns by comparing the three-phase sinusoidal wave forms with a triangular carrier.

The most widely used method of pulse width modulation are carrier based. This method is also known as the sinusoidal (SPWM), triangulation, subharmonic, or suboscillation method [5], [6].

3.2 Fuzzy Logic Controller

The FLC has two inputs speed error e(k) and change in speed error ce(k) and one output u(k) which represents the change in quadrature reference current $I_q^*(k)$.

e(k) and ce(k) are calculated as in equations for every sampling time:

$$e(k) = \omega_r^*(k) - \omega_r(k)$$

$$ce(k) = e(k) - e(k\text{-}1)$$

Where $\omega_r^*(k)$ is reference speed and $\omega_r(k)$ is actual speed value.

To obtain normalized inputs and output for fuzzy logic controller, the constant gain blocks are used as scaling factors G_E, G_{CE} and G_U as shown in Fig (2)

$$E(k) = G_E\, e(k)$$

$$CE(k) = G_{CE}\, ce(k)$$

$$U(k) = G_U\, u(k)$$

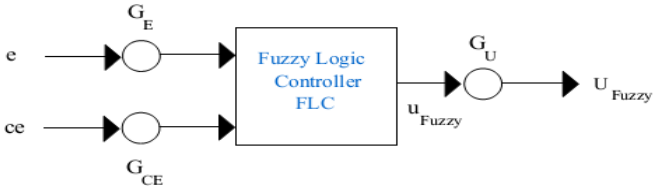

Figure 2: Scaling Factors for FLC

The FLC consists of three stages: the fuzzification, rule execution, and defuzzification. In the first stage, the crisp variables e(k) and ce(k) are converted into fuzzy variables E(k) and CE(k) using the triangular membership functions.

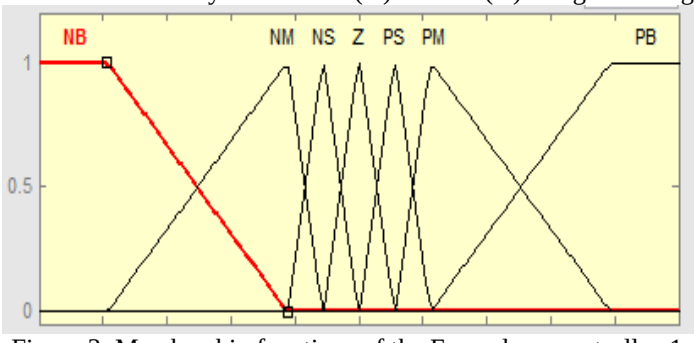

Figure 3: Membership functions of the Fuzzy logy controller-1

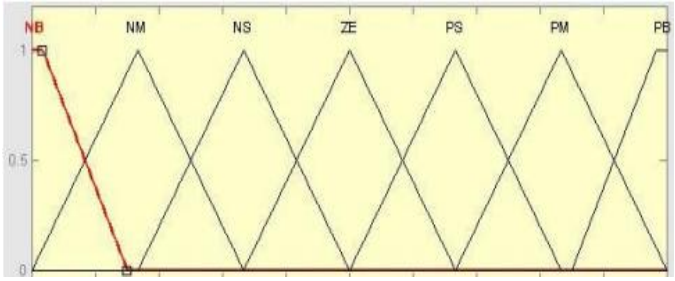

Figure 4**:** Membership functions of the Fuzzy logy controller-2

Each universe of discourse is divided into five fuzzy sets: NB (negative big), NM (negative medium), NS (negative small), ZE (zero), PS (positive small), PM (positive medium) and PB (positive big).

In the second stage of the FLC, the fuzzy variables E and CE are processed by an inference engine that executes a set of control rules contained in (7 X 7) rule bases. The control rules are formulated using the knowledge of the PMSM behavior. Each rule shown in Table

Table I: Rule Base for Fuzzy Logic Controller

CE→ E↓	NB	NM	NS	ZE	PS	PM	PB
NB	NB	NB	NB	NB	NM	NS	ZE
NM	NB	NB	NB	NM	NS	ZE	PS
NS	NB	NB	NM	NS	ZE	PS	PM
ZE	NB	NM	NS	ZE	PS	PM	PB
PS	NM	NS	ZE	PS	PM	PB	PB
PM	NS	ZE	PS	PM	PB	PB	PB
PB	ZE	PS	PM	PB	PB	PB	PB

Different inference algorithms can be used to produce the fuzzy set values for the output fuzzy variable u Fuzzy. In this paper, the max-min inference algorithm is used, in which the membership degree is equal to the maximum of the product of E and CE membership degree.

The inference engine output variable is converted into a crisp value U FUZZY in the defuzzification stage. Various defuzzification algorithms have been proposed in the literature. In this paper, the centroid defuzzification algorithm is used, in which the crisp value is calculated as the centre of gravity of the membership function.

The definition of the spread of each partition, or conversely the width and symmetry of the membership functions, is generally a compromise between dynamic and steady state accuracy. Equally spaced partitions and consequently symmetrical triangles are a very reasonable choice. So, we need to multiply the controller input and output variables by adjusting gains in order to accommodate these variables into the normalized intervals.

The reference current $I_q^*(k)$ for the vector control system is obtained by integrating u(k) as in equation

$I_q^*(k) = I_q^*(k-1) + u(k)$

IV. Simulink Models And Parameter:

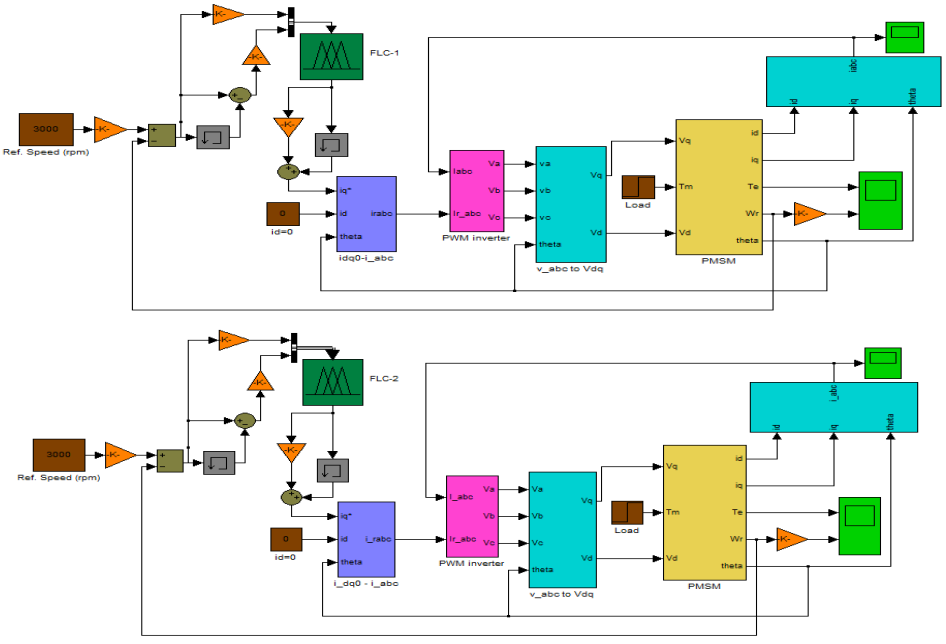

Figure 5: PMSM drive with FLC-1 and FLC-2 controller

PMSM drive model are simulated in MATLAB simulink are shown above Fig 5. In PMSM Model following PMSM parameters are used.

Table II: PMSM Parameter

S. NO.	Parameter	Value
1.	Direct axis Resistance, R_d	1.4 Ω
2.	Quadracture axis Resistance, R_q	1.4 Ω
3.	d axis inductance, L_d	0.0066 H
4.	q axis inductance, L_q	0.0058 H
5.	Rotor permanent-magnet flux, λ_m	0.1546 (wb)
6.	Moment of Inertia, J	0.00176 ($kgm^{2)}$
7.	combined viscous friction, B	0.00038818 (Nm / (rad / s))
8.	no. of poles, P	6

V. Results And Discussion:

The simulation of PMSM drive system with Fuzzy controller has been carried out using MATLAB. The speed, torque and current responses of PMSM are observed with Fuzzy controller. The performances are observed under various speed and the results are presented.

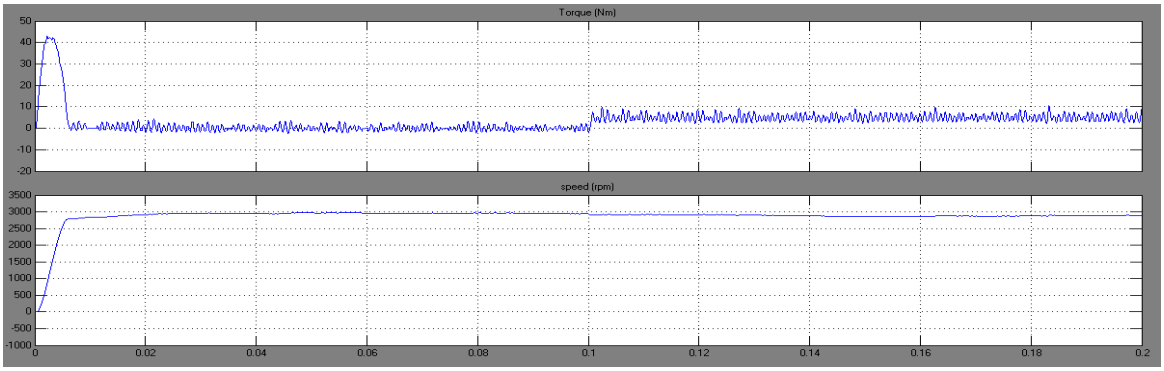

(a) Torque and Speed

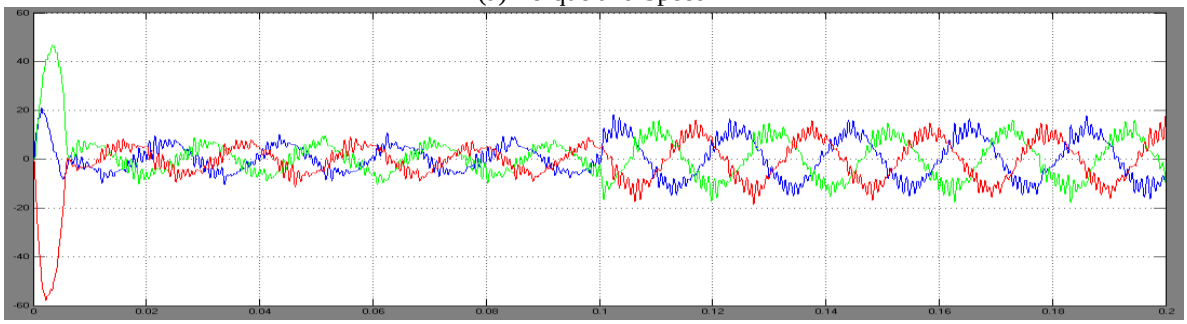

(b) Currents

Figure 6 Speed (rpm), Torque (Nm) & Current (Amp) for reference speed 3000 using FLC-1

The Fuzzy Logic controller FLC-1 performance for speed ω_r = 3000 RPM, Peak Overshoot at starting is M_p=0%, Rise Time t_r = 0.006 sec, Steady State error e_{ss} = 9, Speed drop at load is 3.6667%, Settling time after load is 0.008 sec.

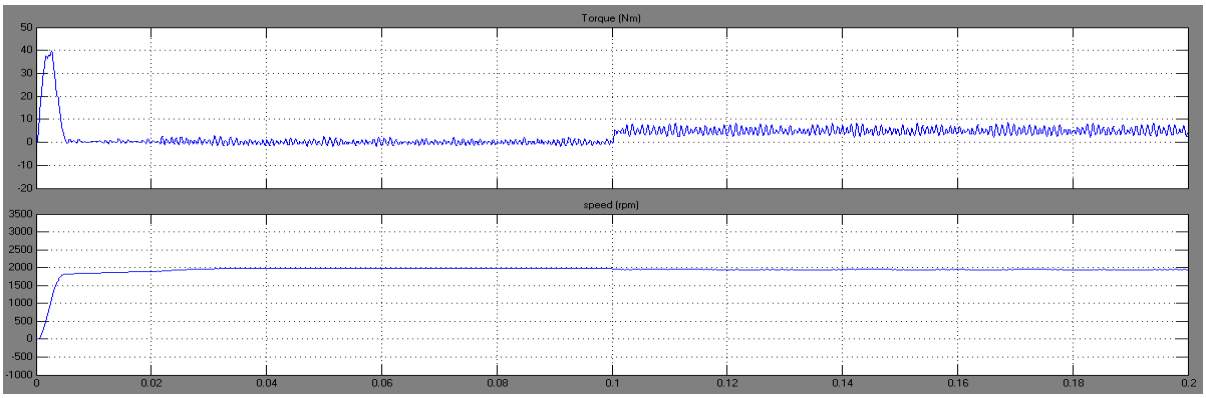

(a) Torque and Speed

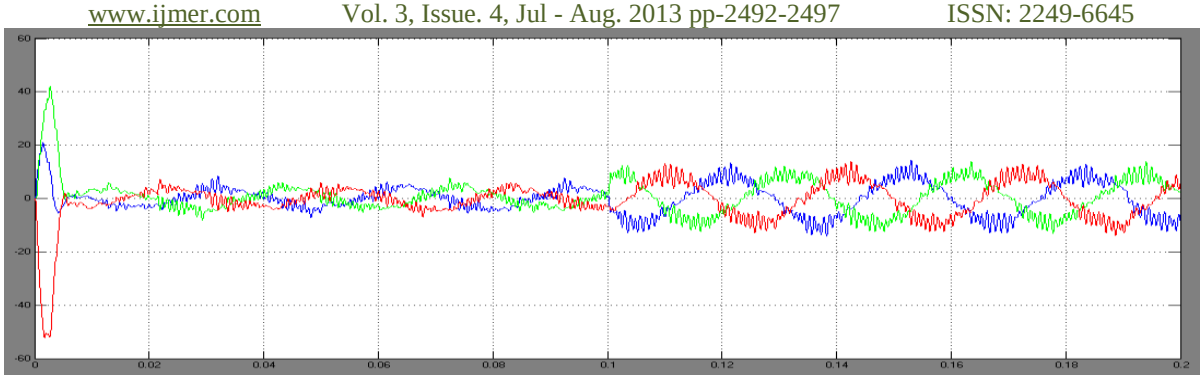

(b) currents

Figure 7 Speed (rpm), Torque (Nm) & Current (Amp) for reference speed 2000 using FLC-1

The Fuzzy Logic controller FLC-1 performance for speed ω_r = 2000 RPM, Peak Overshoot at starting is M_p=0%, Rise Time t_r = 0.0045 sec, Steady State error e_{ss} = 6, Speed drop at load is 2%, Settling time after load is 0.003 sec.

Performance of Fuzzy logic controller FLC-2 is shown below

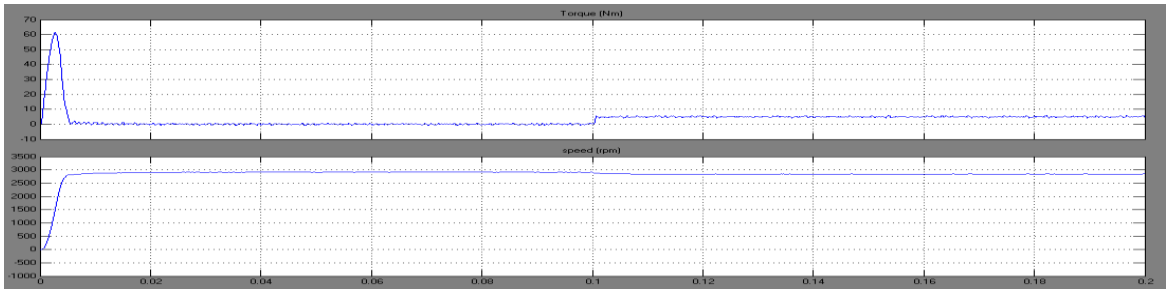

(a) Torque and Speed

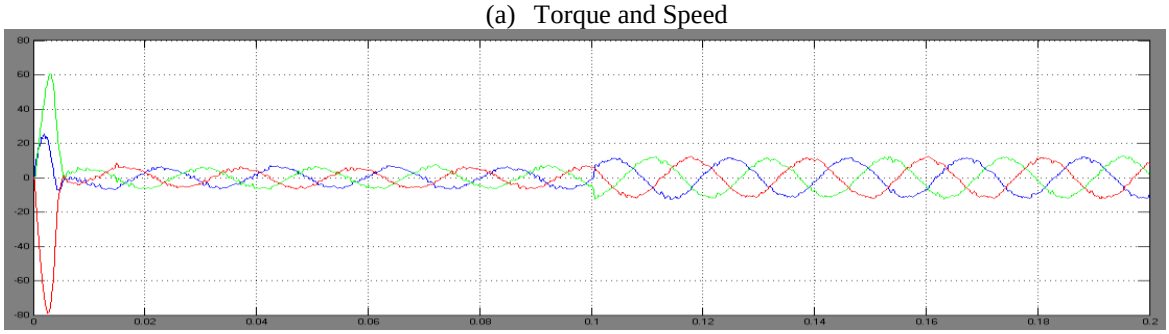

(b) Currents

Figure 8 Speed (rpm), Torque (Nm) & Current (Amp) for reference speed 3000 using FLC-2

The Fuzzy Logic controller FLC-2 performance for speed ω_r = 3000 RPM, Peak Overshoot at starting is M_p=0%, Rise Time t_r = 0.005 sec, Steady State error e_{ss} = 16, Speed drop at load is 1.6667%, Settling time after load is 0.0028 sec.

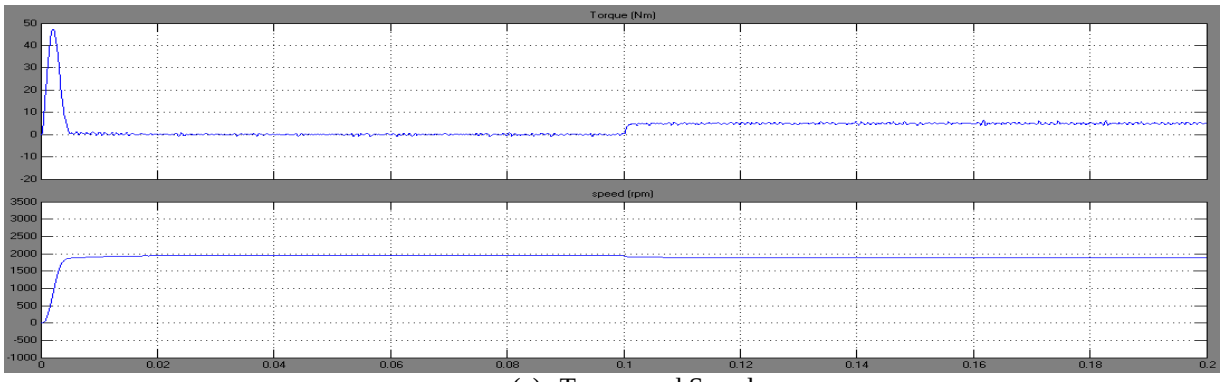

(a) Torque and Speed

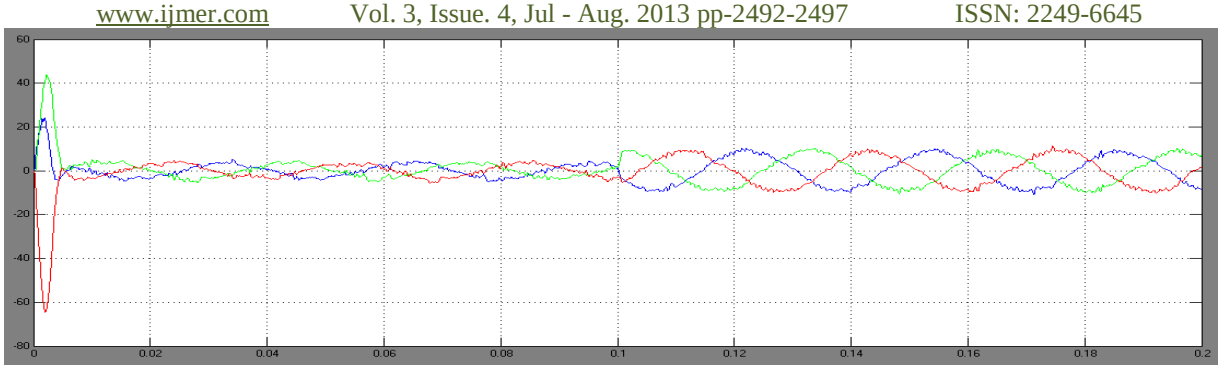

(b) Currents

Figure 9 Speed (rpm), Torque (Nm) & Current (Amp) for reference speed 2000 using FLC-2

The Fuzzy Logic controller FLC-2 performance for speed ω_r = 2000 RPM, Peak Overshoot at starting is M_p=0%, Rise Time t_r = 0.0044 sec, Steady State error e_{ss} =12.3 , Speed drop at load is 3%, Settling time after load is 0.0021 sec.

VI. Conclusion

These Fuzzy Logic controllers are used successfully in speed Control system for PMSM. The design of Fuzzy logic controller and its performance shows that the error is minimized. The no overshoot in the speed curve and the ripples in the torque curve are maintained minimum.

References

[1] A. Khurram, *Position and speed sensorless control of permanent magnet synchronous motor*, Ph. D. dissertation, Michigan State University, East Lansing, MI, 2001.
[2] R. Krishnan, *Permanent Magnet Synchronous and Brushless DC Motor Drives*, Electrical and Computer Engineering Department, Virginia Tech Blacksburg, Virginia,U.S.A., CRC Press Taylor & Francis Group, 2010.
[3] LEONID REZNIK, *Fuzzy Controllers*, Victoria University of Technology, Melbourne, Australia, Reed Elsevier plc group, 1997
[4] Chunhua Zang, *Vector controlled PMSM Drive based on Fuzzy Speed Controller*, 2nd International Conference on Industrial Mechatronics and Automation, 2010, pp 199-202
[5] B. K. Bose, *Modern Power Electronics and AC drives*, (Prentice-Hall, 2002).
[6] J. Holtz, *Pulse width modulation for electronic power conversion*", Proceedings of the IEEE, Vol. 82, Issue: 8, Aug. 1994, pp.1194-1214.

International Journal of Modern Engineering Research (IJMER)
www.ijmer.com Vol. 3, Issue. 4, Jul – Aug. 2013 pp-2498-2501 ISSN: 2249-6645

A Novel Computing Paradigm for Data Protection in Cloud Computing

Bhagya Lakshmi Nandipati[1], G. Sridevi[2]
[1]*M. Tech, Nimra College of Engineering & Technology, Vijayawada, A.P., India*
[2]*Assoc. Professor, Dept.of CSE, Nimra College of Engineering & Technology, Vijayawada, A.P., India*

***Abstract*:** *Cloud computing is the term given to the use of several server computers via a digital network as if they were one computer. The 'Cloud' itself is a virtualization of various resources such as networks, servers, applications, data storage and services – which the end user has on-demand access to. Cloud computing services are divided into three types, according to the abstraction level of the capability provided and the service model of providers, namely: Infrastructure as a service(IaaS), Platform as a service(PaaS) and Software as a service(SaaS). This paper proposes a novel cloud computing paradigm, data protection as a service (DPaaS). DPaaS is a suite of security primitives offered by a cloud computing platform, which enforces data security and privacy and offers evidence of privacy to data owners, even in the presence of potentially compromised or malicious applications.*

***Keywords*:** *Auditing, Cloud, Data protection, Service.*

I. INTRODUCTION

Now minute and average business organizations are realizing that simply exchange to the cloud can get access to excellent business claims and increase up their infrastructure assets in a very low cost, Internet on an as-needed basis [1]. This new and exciting paradigm has generated significant interest in both the marketplace and the academic world [2], resulting in a number of notable commercial and individual cloud computing services, e.g., form Amazon, Google, Microsoft, Yahoo, and Sales force [3]. Also, top database vendors, like Oracle, are adding cloud environment support to their databases. The providers are enjoying the superficial opportunity in the marketplace but they should ensure that they possess the right security features. The cloud computing provide facilities like fast development, lower cost on pay-for-use, quick flexibility, quick provisioning, everywhere network contact, hypervisor defense against network vulnerability, economical failure recovery and data storage solution, on-request security checks, synchronized detection of system altering and rapid re-construction of services. The cloud environment provides this compensation, until some of the risks are better understood.

The basic concept of the cloud computing, based on the services they offer, from application service provisioning, grid and service computing, to Software as a Service [4][5]. Despite of the specific architecture, the dominant concept of this cloud computing model is that customers' data, which can be of individuals, organizations or enterprises, is processed remotely in unknown machines about which the user not aware. The ease and efficiency of this approach, however, comes with both privacy and security risks [6]. Secrecy of data is the main hurdle in implementation of cloud services. A huge data centers are established in cloud computing environment, but the deployment of data and services are not trustworthy. These create different new security challenges. These challenges are vulnerabilities in accessibility, web and virtualization, such as SQL injection, cross site scripting, physical access issues, privacy and control issues happening from third parties having physical control of data, issues related to identity and credential , data loss and theft, issues related to data confirmation, changing and privacy, issues related to integrity and IP spoofing.

II. CLOUD COMPUTING SERVICE MODELS

There are three primary classes of cloud computing service models (Figure 1):

A. *Infrastructure as a Service (IaaS)*

A cloud based virtual server providing networking and mass storage services and other infrastructure services. The user does not manage or control the data centre but may have control over the data or operating systems placed into the infrastructure. For example, Amazon web service (AWS).

B. *Platform as a Service (PaaS)*

It is the service level where a computable platform upon which the user can host and develop applications and services by using programming language and API's37 is provided. The user can control the deployed applications and sometimes the application-hosting environment as well. However, the infrastructure (servers, OS, storage) is still in the control of the cloud provider. Examples include Windows Azure and Google App engine.

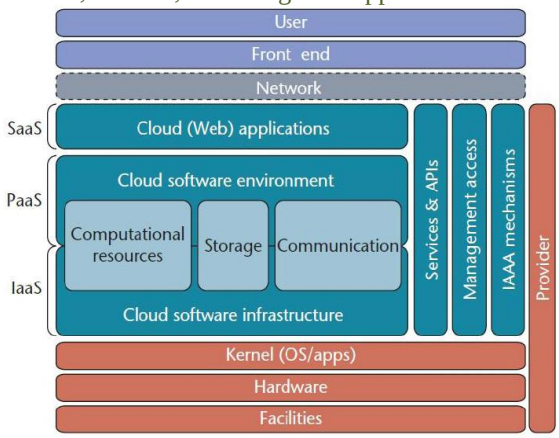

Figure 1: Cloud Computing Architecture

C. *Software as a Service (SaaS)*

In SaaS, applications are running on a cloud infrastructure or platform which is accessible via a thin client interface (browser) or program interface. The user only has the possibility to manage some user specific settings, because the provider does not accommodate cloud features; they only provide applications running 'in the cloud'. SaaS is an alternative to having the software running on local machines and good examples are online office applications (Google Docs), online CRM systems (SalesForce CRM), webmail (Google Mail) and Social Network Sites (Twitter, Facebook).

III. DATA PROTECTION AS A SERVICE

For organizations embarking on cloud computing environment, storage management is extremely important. To avoid loss, the cloud computing system must provide data protection and resiliency. If loss does occur, the computing environment must be able to recover the data quickly in order to restore access to the cloud services. This need is equally true whether the cloud computing environment is private, public or hybrid. It is possible to obtain data storage and protection services from the companies that specialize in storage, and many organizations that handle their own computing and applications choose this option for outsourcing storage. When outsourcing applications, however, an organization should never assume that the service provider includes storage management, data protection or disaster recovery among its services—not all of them do. It is therefore important to ensure from the beginning that the service provider delivers the necessary data storage and protection services, and to be familiar with the technologies and products used for storage management in the cloud environment. To ensure a practical solution, we considered the following goals relating to data protection in cloud.

- **Integrity:** The customer's stored data won't be corrupted.
- **Privacy:** Secret data won't be leaked to any unauthorized entity.
- **Access transparency:** Logs will clearly indicate who or what accessed any type of data.
- **Ease of verification:** Customers will be able to easily verify what platform or application code is running, as well as whether the cloud has strictly enforced their data's privacy policies.
- **Rich computation:** The cloud platform will allow efficient, rich computations on sensitive user data.
- **Development and maintenance support**: Because they face a long list of challenges—bugs to find and fix, frequent software upgrades, continuous usage pattern changes, and customer demand for high performance— developers will receive both development and maintenance support.

IV. DAAS ARCHITECTURE

Figure 2 shows architecture to explore the design space of Data Protection as a Service [7].

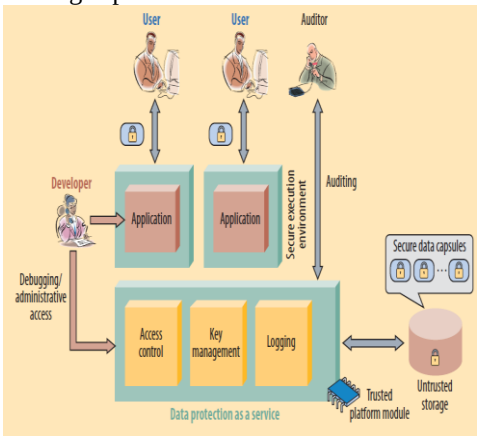

Figure 2: DPaaS Architecture

A. Lightweight Confinement

A Secure Data Capsule (SDC) is an enciphered data unit packaged with its security policy, e.g., Access Control List (ACL). To avoid unauthorized leakage of customer's data in the presence of potentially buggy or compromised applications, we confine the execution of various applications to mutually isolated environments, henceforth referred to as Secure Execution Environments (SEEs). There are different levels of inter-SEE isolation we could impose; stronger isolation in general exacts the greater performance cost due to context switching and data marshalling. At one end, a SEE could be a virtual machine with an output channel back to the requesting customer. In other words, the thread pool of the traditional server would be replaced with a pool of VMs or containers, whose data state is reset before being loaded with a new data unit.

B. Sharing and authorization

It is a basic requirement of our target applications that units of data that should be sharable; that is why SDCs are bound to a full ACL versus a particular customer. The key to enforcing those ACLs is that we can control the Input/Output channels available to SEEs. To confine data, we mandate that the data in an SDC is deciphered by the platform only for an SEE, and even then, only at an authorized user's request. The output may be funneled either directly to the customer or to another SEE which provides a service; in either case, the channel is mediated by the platform.

C. Auditor and Data Access Auditing

The auditor is one who audits the overall performance of the computing system. The auditor can track the transactions and logins of users with correct time and date. Here auditor is software component that is capable of tracking the transactions. Cloud storage offers movement of data into the cloud. It has great convenience to the customer because users can store their data in the cloud safely without the knowledge about the storage space. Since the platform mediates all access to the data, authenticates customers, and runs binaries, it knows what data is being accessed, by what user, and using which application. It can generate meaningful audit log files containing all these parameters and optionally incorporate additional information from the application layer. There are four basic types of actions we can log:

- Ordinary online data accesses occur in response to external requests from customers, and take place when a user is online and using an application.
- Access control modification by authorized customers. Knowing the provenance of these changes can be helpful for diagnosing or forensics sharing problems.
- Batch/offline access to handle requests while users are offline (e.g., e-mail delivery), to compute aggregates, or to reorganize data such as during schema changes.
- Administrative access for maintenance operations like debugging.

D. Key Management

The concept of key come from the branch of science called "cryptography". There are basically two kinds of keys.

- Public key
- Private key

A public key known to everyone and a private or shared secret key known only to the recipient of the message. When Alice wants to send a secure message to Bob, he uses Jane's public key to encrypt the message. Bob then uses her private key to decrypt it. In our system we encrypt the file using a key and stored in the cloud. The user should enter the key in order to decrypt the file. So multiple protection schemes are used here for protecting the files in the cloud.

E. Authorization for Debugging, Maintenance, and Batch Access

While ordinary customer access is governed by the ACL on the data, administrative access needs its own separate policy. That in turn can be audited to hold developers as well as administrators accountable. Each specific invocation of the administrative policy, because it may entail user access to data for, e.g., debugging or account recovery, should be logged and made available for auditing. The same kind of mechanism would be used for batch access, with perhaps different logging granularity; and to prevent misuse, the code for the batch process can be restricted only to an approved set. That might mean requiring controlled or quantifiable information release, such as differential privacy [8] or quantitative information flow [9].

F. Verifiability of the Platform

The DPaaS paradigm provides logging and auditing at the platform level, sharing the benefits with all applications running on top. Offline, the auditor can verify that the paradigm implements each data protection feature as promised. At runtime, the platform provider can use trusted computing (TC) technologies to attest to the particular software that is running. Trusted computing uses the tamperproof TPM as well as the virtualization and isolation features of modern processors, such as Intel VT or AMDV.

V. CONCLUSION

Cloud computing environment enables highly scalable services to be easily consumed over the Internet on an as-needed basis. A major feature of the cloud computing services is that customers' data are usually processed remotely in unknown machines that users do not own or operate. Offering strong data protection to cloud customers while enabling rich

applications is a challenging task. We explore a novel cloud platform architecture called Data Protection as a Service, which dramatically reduces the per-application development effort required to offer data protection, while still allowing rapid development and maintenance.

REFERENCES

[1] T. Mather, S. Kumaraswamy, and S. Litif, Cloud Security and Privacy: An enterprise perspectives on Risks and Compliance (Theory in Practice). O' Reilly, 2009.
[2] IEEE International Conference on Cloud Computing. 2009.
[3] P.T.Jaeger, J.Lin, and M. grimes, Cloud computing and information policy: Computing in a policy cloud? Journal of Information Technology and politics, 2009.
[4] Cloud Computing: Clash of the clouds. the economist., 2009.
[5] B.P.Rimal, E.Choi, and I.Lumb. A taxonomy and survey of Cloud Computing Systems. in Networked Computing and Advanced Information Management, International Conference. 2009.
[6] B.R. Kandukuri, R.P.V., and A. Rakshit. Cloud security issues. in IEEE International Conference on Services Computing (SCC). 2009.
[7] P. Maniatis, D. Akhawe, K. Fall, E. Shi, S. McCamant, and D. Song. Do You Know Where Your Data Are? Secure Data Capsules for Deployable Data Protection. In HotOS, 2011.
[8] C. Dwork, "The Differential Privacy Frontier Extended Abstract," Proc. 6th Theory of Cryptography Conf. (TCC 09), LNCS 5444, Springer, 2009, pp. 496-502.
[9] S. McCamant and M. D. Ernst. Quantitative information flow as network flow capacity. In PLDI, pages 193–205, 2008.

International Journal of Modern Engineering Research (IJMER)
www.ijmer.com Vol. 3, Issue. 4, Jul - Aug. 2013 pp-2502-2506 ISSN: 2249-6645

Modelling Nozzle throat as Rocket exhaust

Keshava Rao P.[1], Komma Rahul[2], Souda Dinesh[3]
[1](Mechanical Engineering, CBIT College, India)
[2](Mechanical Engineering, RGUKT (IIIT Basar), India)
[3](Concurrent Analysis Pvt Ltd, Hyderabad, India)

ABSTRACT: *The ejector mode of rocket-based combined cycles is a concept that has the ability to gain thrust from atmospheric air and reduce fuel consumption and thus reduce the cost of rocket launches. This thesis develops a three-dimensional rocket nozzle design that includes the potential for incorporating the ejector effect. The nozzle is designed such that the diverging portion of the nozzle geometry must pass through a gate that is placed on the outer perimeter whose shape does not have to remain axisymmetric, thus creating a void for air intake into the centre of an annular rocket exhaust stream. Viscous effects are included via Edenfield's displacement thickness δ correlation for turbulent boundary layers. Comparison of computational fluid dynamics to a predefined Mach number distribution is within 1.6% of an inviscid solution and 6.8% for a viscous simulation using the k-ε turbulence model.*

I. COMBINED CYCLES

Air-augmented rockets also known as Combined Cycles (CC), that present the notion of increasing thrust in addition of mass flow, 70% reducing propellant mass fraction, 10–20% increasing the specific impulse at atmospheric conditions. It leads to reducing launch costs of atmospheric flight. These Cycles are classified as hybrid rocket, operates better than the rocket or ramjet separately.

Combined Cycles is attained through the addition of a diffuser downstream of the exhaust. It includes three parts that is ejector, air intake, thrust chamber. In the thrust chamber propellant energy of fuel converts into kinetic energy accelerating exhaust gases. Through air intake valves air enters into chamber. Ejector effect is achieved by mixing of air and propellant flow. Momentum from the high rocket exhaust velocity is transferred to entrained air. Due to air flow through valves in chamber specific impulse and thrust increases. Ejectors create a vacuum at outlet, reducing the risk of plume overexpansion.

Combined cycle operates at low-altitude environments below 100km identified as von Karman line known to be optimistic upper limit for air augmented systems.

The main aim of this thesis is to show that using **CCPS** (combined cycle propulsion system) in rockets and other systems in aerospace technology reduces the amount of oxidizer for Trans-atmospheric flight by using oxygen in the atmosphere.

Propulsion systems are classified as CCPS only if all the propulsion subsystems are in use all the times during flight. By this statement turbo ramjet is not classified into CCPS systems.

II. SUBSYSTEMS OF COMBINED-CYCLE PROPULSION SYSTEMS

The incitement for manufacturing a CCPS is that none of the propulsion systems is effectual throughout the entire range of Mach numbers that an aircraft undergoes. CCPS utilizes two or more subsystems, air-breathing and other systems.
The Thrust equation for CCPS is

$$T = mv_2 + ((p_2 - p_3)\,A_2)$$

Where,
m = mass flow rate,
v2 = nozzle exit velocity (equal to c)
p2 = pressure at the nozzle exit
p3 = pressure of the atmosphere
A2 = area of the nozzle exit

Effective exhaust velocity (assuming isentropic Flow through the nozzle). This is a reasonable assumption for a converging-diverging nozzle where the maximum fraction of the thermal energy of the gases is converted into kinetic energy in a reversible process

$$v_2 = \sqrt{\frac{2K}{K-1}\frac{R'T_1}{\mathfrak{M}}\left[1-\frac{p_2}{p_1}\right]^{\frac{(K-1)}{K}}}$$

k = the ratio of specific heats
R' = universal gas constant
T1 = stagnation temperature of the chamber or nozzle inlet
$\mathfrak{M}$ = average molecular mass of the fuel
p1 = chamber pressure
p2 = pressure at the nozzle exit

III. MODELLING AND MESHING

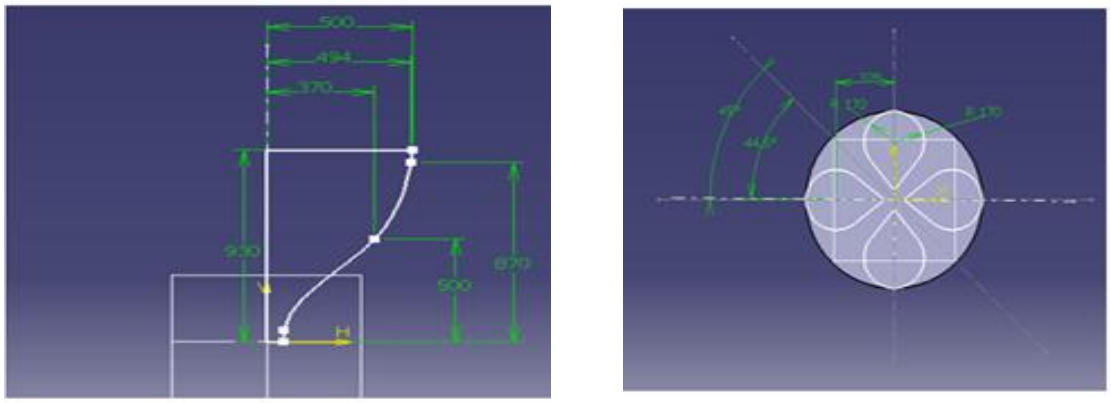

3D Model

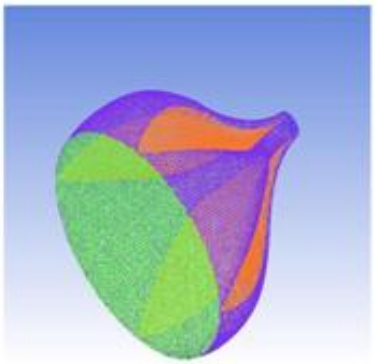

3.1 MESH (ICEM CFD)

Mesh Type = Tetra/ Mixed
Total elements: 6, 55,092

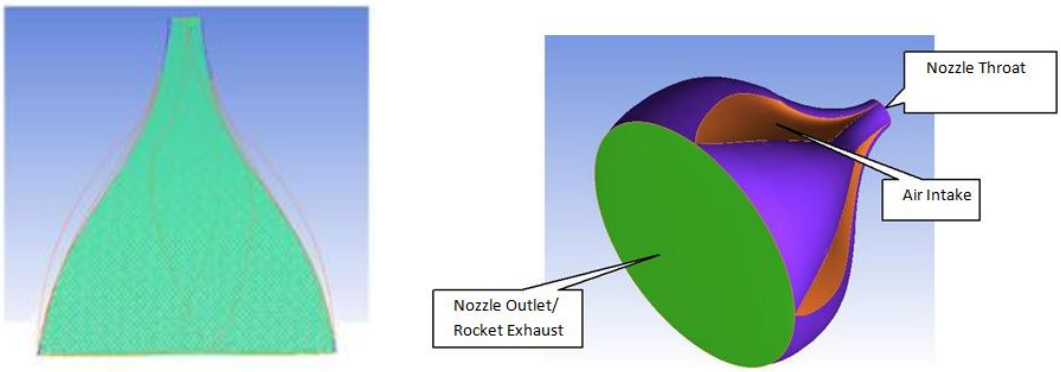

Mesh views

IV. SIMMULATION

4.1 CALCULATIONS

Speed of Sound depends on temperature and can be calculated using the following formula:

$$\text{Speed of sound } c = 331.5 \cdot \sqrt{\frac{\vartheta + 273.15}{273.15}} = 331.5 \cdot \sqrt{1 + \frac{\vartheta}{273.15}} \text{ in m/s; temperature } \vartheta \text{ in } °C$$

By using above formula
Speed of Sound has been calculated as 1060.95 m/sec
For Mach Number 1.05, Velocity at nozzle throat has been calculated as 1114 m/sec

4.2 MATERIAL USED&BOUNDARY CONDITIONS

Fluid – Kerosene – Vapour
Chemical Formula – C12H23

Density – 7.1 Kg/m3
Thermal Conductivity -0.0178 w/m-k
Viscosity – 7 e-08 Kg/m-s
For Nozzle Throat
Velocity = 1114 m/sec
Supersonic Gauge Pressure = 2475.6 K Pa (2577 Kpa – Operating Pressure (101325 Pa)) Temperature = 3668 K
For Air Intake = Pressure Inlet
For Nozzle Outlet = Pressure Outlet
Operating Pressure = 101325 Pa
Wall Temperature = 500 K
K-ξ Turbulence has been used with 5% as turbulence intensity at boundaries.

4.3 COMPARISON OF NOZZLE JET PROPULSION SYSTEM

4.3.1 SINGLE AIR INTAKE OPENING

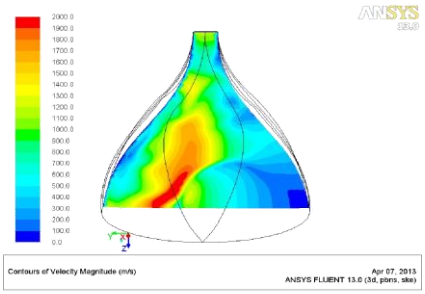

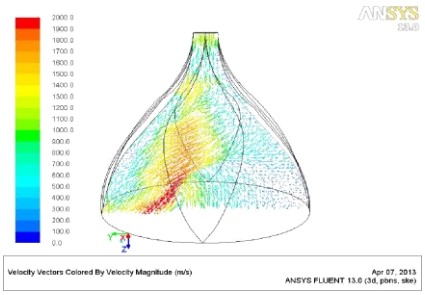

4.3.2 DOUBLE AIR INTAKE OPENING

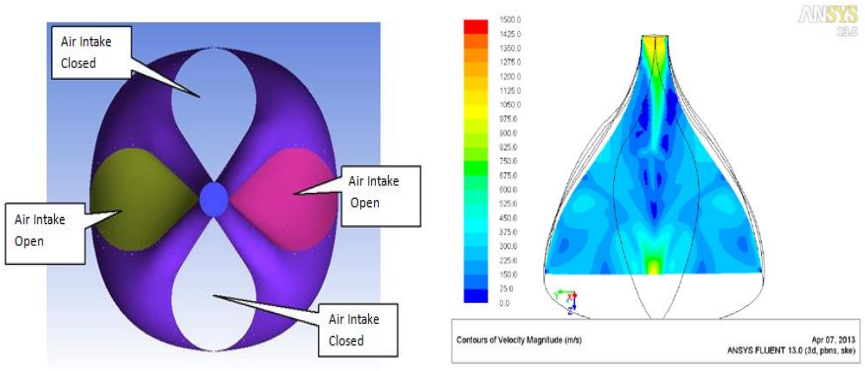

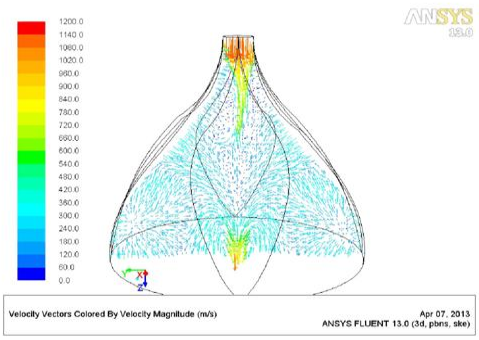

4.3.3 TRIPLE AIR INTAKE OPENINGS

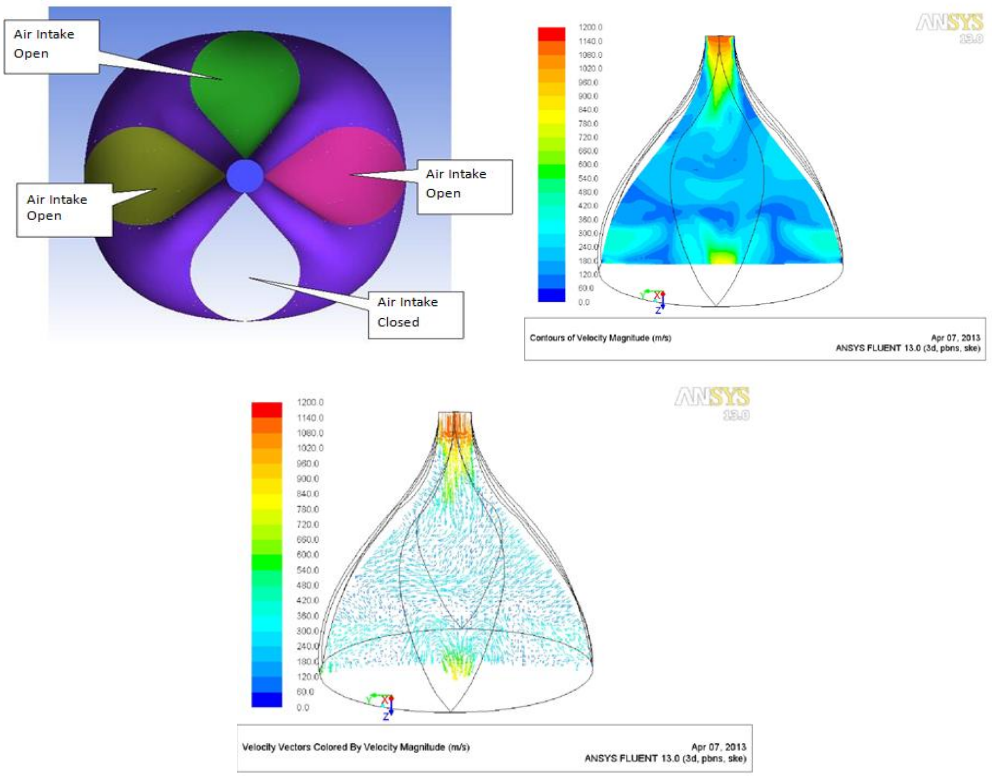

4.3.4 QUADRAPLE AIR INTAKE OPENINGS

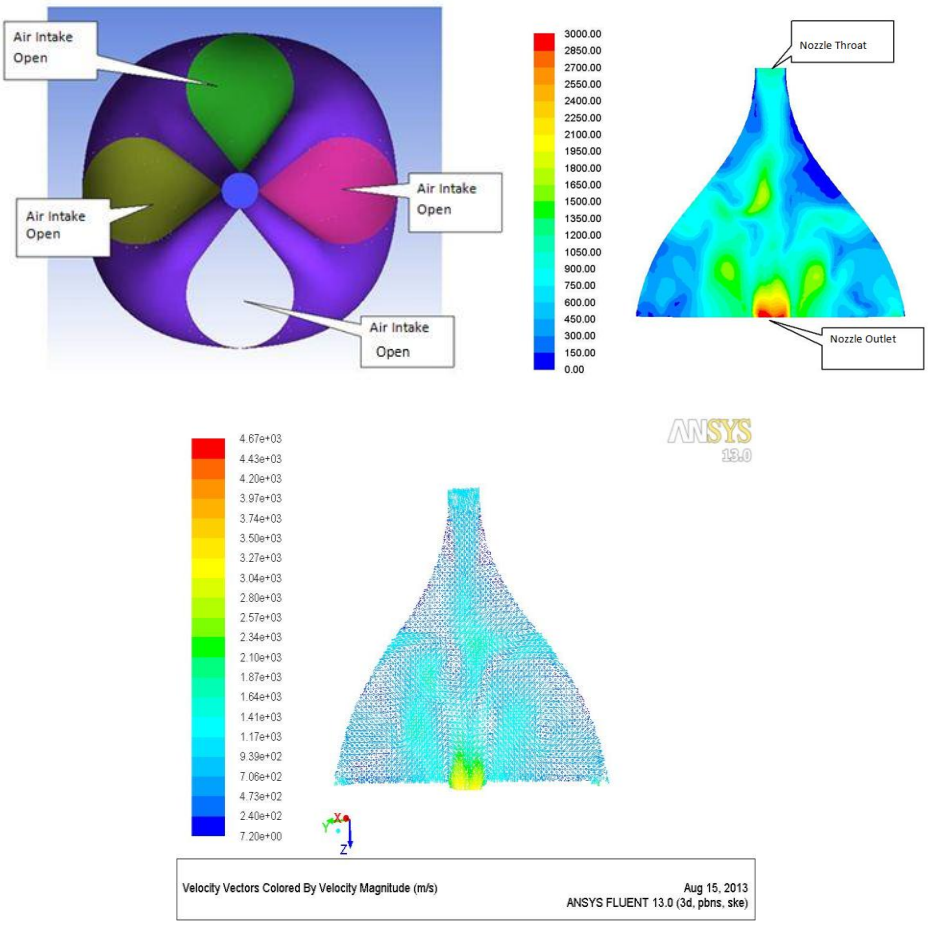

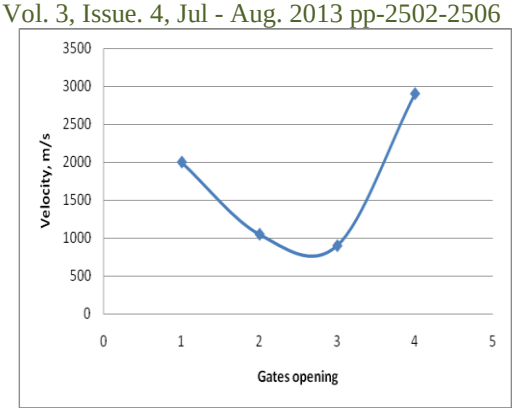

Graph between gates opening to the velocity

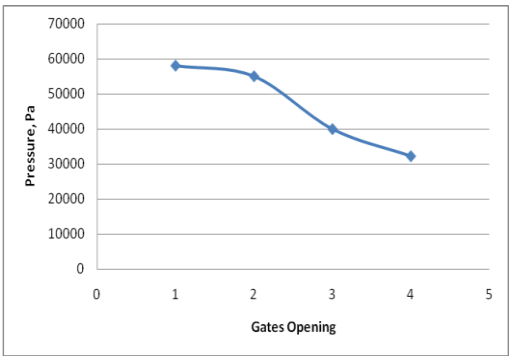

Graph between gates opening to the Pressure

In the first case even though the velocity of exhaust gases is high (2000 m/s) it is not concentrated exactly at the centre of exhaust opening as shown in velocity contours. Due to this divergence of velocity vector forces act on the walls of nozzle causing manoeuvring and maintenance problems. In the second and Third case the velocity magnitude is low (900-1125 m/s) which is not desirable.

In the fourth case both the velocity of exhaust is high about 2.75 Mach number and the velocity magnitude is concentrated at the correct position at the exhaust.

V. Conclusion

As a result of void formation air entrainment into the centre of annular rocket exhaust stream occurs.

Isentropic expansion takes place as the wall curvature is convex. Velocity contours diverge into the cross sectional thickness hence velocity first increases along these surfaces.

The direction of the velocity vectors is related to the curvature as the streamlines parallel the nozzle walls

Reduction of the outlet arc angle ψ should reduce the magnitude of the circumferential velocity components and avoid the likely presence of strong oblique shocks at the nozzle outlet Increasing the air intake size is beneficial for increased mass flow, the air entrainment capability must consider shock waves or expansion fans induced by the geometry design.

In this thesis comparison among the air inlet with single, double, triple & all open conditions have been performed. Result plots of velocity contours have been published in this report The highest Mach number of 2.75 (2900 m/sec) occurs in Quadruple air intake case.

Investigation of the specific impulse and thrust performance characteristics are necessary to confirm that the design concept leads to improvement over existing thrust chambers.

References

[1] Turner, M. J. L., *Rocket and Spacecraft Propulsion: Second Edition*, Praxis Publishing Ltd., 2005.
[2] Tajmar, M., *Advanced Space Propulsion Systems*, Springer-Verlag/ Wien, 2003.
[3] Sutton, G. P., *History of Liquid Propellant Rocket Engines*, American Institute of Aeronautics and Astronautics, 2006.
[4] Kraemer, R. S., *Rocketdyne: Powering Humans into Space*, American Institute of Aeronautics and Astronautics, 2006.
[5] Daines, R. and Segal, C., "Combined Rocket and Airbreathing Propulsion Systems for Space-Launch Applications," *Journal of Propulsion and Power*, Vol. 14, No. 5, 1998, pp. 605–12.
[6] Jones, T. D., "Final countdowns: The shuttle's last years," *Aerospace America*, Vol. 45, No. 1, January 2007, pp. 16–8.
[7] C´aceres, M., "A sputtering market for nanosats and picosats," *Aerospace America*, Vol. 44, No. 11, November 2006, pp. 16–8.
[8] Braeunig, R. A., "Rocket & Space Technology," [electronic resource], 2005, URL: http://www.braeunig.us/space/, [cited 11 June 2007].
[9] Shebalin, J.-P. and Tiwari, S. N., "NOZ-OP-2D: A CFD-Based Optimization System for Axially Symmetric Rocket Nozzles," AIAA Paper 2001–1062, 2001, presented at the 31st Joint Propulsion Conference.
[10] Hagemann, G., Immich, H., Nguyen, T. V., and Dumnov, G. E., "Advanced Rocket Nozzles," *Journal of Propulsion and Power*, Vol. 14, No. 5, September-October 1998, pp. 620–34.
[11] White, F. M., *Fluid Mechanics*, Boston: McGraw-Hill, 5th ed., 2003.
[12] Hopkins, D. F. and Hill, D. E., "Transonic Flow in Unconventional Nozzles," AIAA *Journal*, Vol. 6, No. 5, 1968, pp. 838–42.

International Journal of Modern Engineering Research (IJMER)
www.ijmer.com Vol. 3, Issue. 4, Jul - Aug. 2013 pp-2507-2509 ISSN: 2249-6645

A Bayesian Probit Online Model Framework for Auction Fraud Detection

Sirisha Vegunta[1], G. Minni[2]
[1]M. Tech, Nimra College of Engineering & Technology, Vijayawada, A.P., India
[2]Asst. Professor, Dept. of CSE, Nimra College of Engineering & Technology, Vijayawada, A.P., India

Abstract: *Individual users are able to buy and sell a broad variety of goods and services worldwide on online auction and shopping websites, e.g. eBay.com and Taobao.com. However, attackers have also attempted to conduct fraudulent activities against honest parties for the purpose of illegitimate profit. On Internet auction sites, auction fraud mainly involves fraud attributable to the non-delivery of products purchased through an Internet auction site or the misrepresentation of a product advertised for sale. Malicious sellers may post a non existing item for bidding with false description to deceive the buyer concerning its true value, and request payments to be wired directly to them. Similarly, malicious buyers may make a purchase through a fraudulent credit card where the address of the card holder does not match the shipping address. Both consumers as well as merchants can be victims of online auction fraud, as well as the commercial auction websites. In this paper we study the problem of building models for the online auction fraud detection system, which essentially evolves dynamically over time. We propose a Bayesian probit online model framework for auction fraud detection.*

Keywords: *Fraud detection, Probit, Regression, SSVS.*

I. INTRODUCTION

Online auction networks, such as eBay.com and taobao.com, have become popular trading platforms, with a large variety of products available with competitive prices. Today, these networks have hundreds of billions dollars in trading volume, and hundreds of billions dollars in revenue. While online auction networks have many advantages over traditional retail stores, many usres are still reluctant to sell/buy products on these networks with the concern that sellers/buyers on these networks may not be reliable. To help users assess each other's honesty and integrity, online auction networks often use some reputation-based systems. For example, eBay allows the seller and the buyer to leave feedback to each other for each transaction and the feedback may be viewed by other users. A seller or buyer with more positive comments can be regarded as a more reliable user.

Fraudsters, however, can collude with accomplices to accumulate bogus positive feedback to manipulate the reputation systems, which makes it very hard to evaluate a user's reliability according to the reputation (feedback). It has been observed in [1] that the fraudsters and accomplices are likely to form a dense bipartite core as the fraudsters receive most of the feedback from the accomplices, and are interested in receiving a large number of feedback comments as quick as he/she can. In this paper we study the problem of building models for the online auction fraud detection moderation system, which essentially evolves dynamically over time. We propose a Bayesian probit online model framework for the fraud detection. We apply the stochastic search variable selection (SSVS) [2], a well known technique in the statistical literature, to handle the dynamic evolution of the feature importance in a principled way.

II. RELATED WORK

In the past, attempts have been made to help usres identify potential fraudsters. However, most of them are "common sense" approaches, recommended by a variety of authorities such as newspapers articles [3], law enforcement organizations [4], or even from auction sites themselves [5]. These approaches usually suggest that user be cautious at their end and perform background checks of sellers that they wish to transact with. Such suggestions however, require peoples to maintain constant vigilance and spend a considerable amount of time and effort in investigating potential dealers before carrying out a transaction. Reputation systems are used extensively by many auction sites to prevent fraud. But they are usually very simple but can be easily foiled. In [6], the authors summarized that modern reputation systems face many challenges which include the difficulty to elicit honest feedback and to show faithful representations of users' reputation. In [7] and [8], the authors conducted empirical studies which showed that selling prices of goods are positively affected by the seller's reputation, implying people feel more confident to buy from trustworthy sources. In summary, reputation systems might not be an effective mechanism to prevent online fraud because fraudsters can easily trick these systems to manipulating their own reputation.

In [9], the authors have categorized auction fraud into different types, but they did not formulate methods to combat them. They suggest that an effective approach to fight online auction fraud is to allow law enforcement and auction sites to join forces, which unfortunately can be costly from both monetary and managerial perspectives. Authority propagation, an area closely related to online fraud detection, has been studied extensively in the context of Web search. PageRank [10] and HITS [11] treat a Web page as an "important" if other "important" pages point to it. In effect, they propagate the importance of web pages over hyperlinks connecting them. Trust propagation was used by TrustRank [12] to detect Web spam. Here, the goal was to distinguish between the "good" and "bad" sites (e.g, phishers, sites with adult con- tent, etc).

III. PROPOSED WORK

A. Online Probit Regression

Consider splitting the continuous time into many equal- sized intervals. For each time interval we may observe multiple expert labeled cases indicating whether they are considered as fraud or non-fraud. At time interval "t" suppose there are nt observations. Let us denote the i-th binary observation as 'yit". If yit = 1, the case is consider as fraud; otherwise it is consider as non-fraud. Let the feature set of case i at time interval t be xit. The probit model can be written as follows:

$$P[y_{it} = 1|x_{it}, \beta_t] = \Phi(x'_{it}\beta_t)$$

where "$\Phi(\cdot)$" is the cumulative distribution function of the standard normal distribution N(0, 1), and "β t" is the unknown regression coefficient vector at time t.

Through data augmentation, the probit model can be expressed in the hierarchical form as follows: For each observation i at time interval t assume a latent random variable zit. The binary response yit can be viewed as the indicator of whether zit > 0, i.e. yit = 1 if and only if zit > 0. If zit <= 0, then yit = 0. zit can then be modeled by using a linear regression

$$z_{it} \sim N(x'_{it}\beta_t, 1)$$

In a Bayesian modeling framework it is common practice to put a Gaussian prior on β t as follows:

$$\boldsymbol{\beta_t \sim N(\mu_t, \Sigma_t)}$$

B. Coefficient Bounds for Fraud Detection

It is always important to incorporate domain knowledge into the modeling framework, which can sometimes boost the model performance. In our online fraud detection system, the feature set x was proposed by experts with years of experience. Currently all the features are in fact binary "rules", i.e. any violation of any one of the rule should somehow increase the probability of fraud. However, simply fitting the model might generate a negative coefficient on some of the features, because given limited training data, the sample size might be very small for those coefficients to converge to the right values, or when some features are highly correlated. Hence we bound the coefficients of those binary "rules" to force them to be equal or greater than zero. Specifically, we consider the following optimization problem:

$$\min_{\beta} \quad \sum_i w_i[y_i \log(1+\exp(-x'_i\beta)) +$$

$$(1-y_i)\log(1+\exp(x'_i\beta)) + \rho\|\beta\|_k]$$

C. Online Feature Selection through SSVS

For regression problems with many features, proper shrinkage on the regression coefficients is usually required to avoid the case of over fitting. For instance, two common shrinkage methods are L1 penalty (Lasso) and L2 penalty (ridge regression). Also, experts often want to monitor the importance of the selection rules so that they can make appropriate adjustments (e.g. change rules or add new rules). However, the illegal sellers change their behavioral pattern quickly: Some rule-based feature that does not help today might helps a lot tomorrow. Therefore it is necessary to build an online feature selection framework that evolves dynamically to provide both intuition and optimal performance. In this paper we embed the stochastic search variable selection (SSVS) into our online probit regression framework.

At time interval t, let β jt be the j-th element of the coefficient vector β t. Instead of putting the Gaussian prior on β jt, the prior of β jt now is

$$\beta_{jt} \sim p_{0jt}1(\beta_{jt} = 0) + (1 - p_{0jt})N(\mu_{jt}, \sigma^2_{jt})$$

where p0jt is the prior probability of β jt being exactly zero.

D. Multiple Instance Learning

When we looked into the actual expert reviewing and the labeling process, we noted that the experts actually assign labels in a "bagged" fashion, i.e. for each seller identification number, one expert looks through all of his/her posted items, and if the expert finds any item as fraud, all of this seller id's posted items are labeled as fraud. In literature the models for this scenario is known as "Multiple Instance Learning" . Suppose for each labeled seller i, there are Ki number of cases. For these cases, the labels should be same, thus can be denoted as yi. The multiple instance learning model with the logistic function becomes

$$P[y_i = 1] = 1 - \prod_{j=1}^{K_i} \frac{1}{1+\exp(x'_j\beta)}$$

which is essentially a noisy-or likelihood function. The noisy-or likelihood function only requires a subset of the events in the bag are fraud rather than all are fraud events. The optimization problem can thus be written as:

$$\min_{\beta} \quad \sum_i w_i[-y_i \log(1 - \prod_{j=1}^{K_i} \frac{1}{1+\exp(x_j'\beta)})$$

$$+(1-y_i)\sum_{j=1}^{K_i} \log(1+\exp(x_i'\beta)) + \rho K_i \|\beta\|_k]$$

$$+\sum_i \tilde{w}_j[\log(1+\exp(z_j'\beta)) + \rho\|\beta\|_k]$$

IV. CONCLUSION

Online auction and online shopping have achieved more and more recognition due to the emergence of the world wide open and the problem of building online machine-learned models for identifying the auction deception in e-commerce web sites is considered. As users are enjoying the advantages from online trading, fraudsters are also taking advantages to accomplish deceptive activities against candid parties to obtain dishonest profit. Therefore to detect and prevent such illegal and deceptive activities, proactive fraud detection moderation systems are commonly applied in practice. We show that our proposed online probit model framework is based on the real word online auction fraud detection data, which combines bounding coefficients from proficient knowledge, online feature selection and several instance learning and can extensively develop over baselines and the human-tuned model. This online modeling frame can be simply extended to various other applications. The adjustment of the selection bias in the online model training process is included to one direction and has proven to be very efficient for offline models too.

REFERENCES

[1] D. H. Chau, S. Pandit, and C. Faloutsos, "Detecting fraudulent personalities in networks of online auctioneers," in Proceedings of the 10th European conference on Principle and Practice of Knowledge Discovery in Databases, 2006, pp. 103–114.
[2] E. George and R. McCulloch. Stochastic search variable selection. Markov chain Monte Carlo in practice, 68:203–214, 1995.
[3] Usa today: How to avoid online auction fraud. http://www. usatoday.com/tech/columnist/2002/05/07/yaukey.htm, 2002.
[4] Federal trade commission: Internet auctions: A guide for buyers and sellers. http: //www.ftc.gov/bcp/conline/pubs/online/auctions.htm, 2004.
[5] ebay: Avoiding fraud. http: //pages.ebay.com/securitycenter/avoiding fraud.html, 2006.
[6] P. Resnick, R. Zeckhauser, E. Friedman, and K. Kuwabara. Reputation systems. Communications of the ACM, 43, 2000.
[7] M. Melnik and J. Alm. Does a seller's ecommerce reputation matter? evidence from ebay auctions. Journal of Industrial Economics, 50:337–49, 2002.
[8] P. Resnick, R. Zeckhauser, J. Swanson, and K. Lockwood. The value of reputation on ebay: A controlled experiment, 2003.
[9] C. Chua and J. Wareham. Fighting internet auction fraud: An assessment and proposal. In Computer, volume 37 no. 10, pages 31–37, 2004.
[10] S. Brin and L. Page. The anatomy of a large-scale hypertextual web search engine. In WWW, 1998.
[11] J. Kleinberg. Authoritative sources in a hyperlinked environment. In Proc. 9th ACM-SIAM Symposium on Discrete Algorithms, 1998.
[12] Z. Gyongyi, H. G. Molina, and J. Pedersen. Combating web spam with trustrank. In VLDB, 2004.

International Journal of Modern Engineering Research (IJMER)
www.ijmer.com Vol. 3, Issue. 4, Jul - Aug. 2013 pp-2510-2513 ISSN: 2249-6645

A Distributed Cut Detection Method for Wireless Sensor Networks

Meer Khursheeda Sulthana[1], Syed Sadat Ali[2]
[1]*M. Tech, Nimra College of Engineering & Technology, Vijayawada, A.P., India.*
[2]*Assoc. Professor & Head, Dept.of CSE, Nimra College of Engineering & Technology, Vijayawada, A.P., India.*

Abstract: *Wireless sensor networks (WSNs) consisting of large numbers of low- power and low- cost wireless nodes, have recently been employed in many applications: military surveillance, disaster response and medical care among others. The inherent nature of sensor networks such as unattended operation, battery-powered nodes, and harsh environments pose major challenges. One of the challenges is to ensure that the network is always connected. The connectivity of the sensor network can easily be disrupted due to unpredictable wireless channels, early depletion of node's energy, and physical tampering by hostile users. Network disconnection, typically referred as a network "cut", may cause a number of problems. For example, ill-informed decisions to route the data to a node located in a disconnected segment of the network might lead to data loss, wasted power consumption, and congestion around the network cut. This paper presents a distributed cut detection method for WSNs.*

Keywords: CCOS, Cut, DOS, WSN.

I. INTRODUCTION

Wireless sensor network (WSNs) (Figure 1) is composed of a powerful base station and a set of low-end sensor nodes. Base station and the sensor nodes have wireless capabilities and communicate through a wireless, multi-hop, ad-hoc network[1]. WSNs have emerged as an important new technology for purpose of instrumenting and observing the physical world. Sensor networks are a capable scenario for sensing large areas at high spatial and positive resolution. However, the small size and low cost of the processing machines that makes them attractive for large deployment also causes the loss of low operational reliability[2]. The basic building block of these networks is a small microprocessor integrated with one or more MEMS (micro-electromechanical system) sensors, actuators, and a wireless transceiver.[3]

A WSN is usually collection of hundreds or thousands of different sensor nodes. These sensor nodes are often densely deployed in the sensor field and have the ability to gather data and route data back to a base station (BS). A sensor has 4 basic parts: a processing unit, a sensing unit, a transceiver unit, and a power unit [4]. Most of the WSNs routing techniques and sensing tasks require knowledge of location, which is provided by a location finding system. WSNs contains large number of nodes and each node may be very close to each neighbor. Since WSN should use multi- hop techniques because it consume less power than single hop techniques.

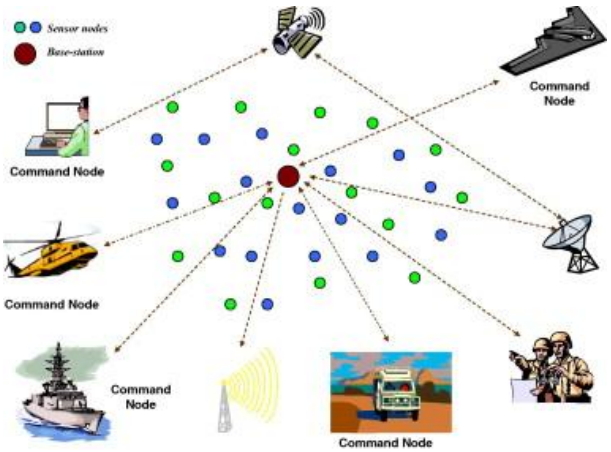

Figure 1 : Wireless sensor network example

II. CUTS IN WSNS

One of the unique challenges in wireless networking environments is the phenomenon of network partitioning, which is the breakdown of a connected network topology into two or more separate, disconnected topologies[1]. Similarly sensor nodes become fail for several reasons and the network may breaks into two or more divided partitions so can say that when a number of sensor fails so the topology changes. A node may fail due to a variety of conditions such as electrical or mechanical problems, environmental degradation, and battery reduction. In fact, node failure is expected to be quite common anomaly due to the typically limited energy storage of the nodes that are powered by small batteries. Failure of a set of sensor nodes will reduce the number of multi-hop paths in the network. Such failures can cause a subset of sensor nodes –

that have not failed – to become disconnected from the rest of the network, resulting in a partition of the network also called a "cut".

Two sensor nodes said to be disconnected if there is no path between them [2].And as we know that sensor nodes has disconnectivity from the network is normally referred as a partition of the network of cut in the wireless sensor network, which arise many problems like data loss, unreliability , performance degradation. Because of cuts in WSNs many problems may arise like a wired network means data loss problem arises, means data reach in a disconnected route. Due to cuts, if any sensor node breaks down then the network is separated into different parts so the topology of the network changes but still network works. But because partition affects reliability, QOS of the network, data loss, efficiency, data processing speed. Because if any data passes unfortunately in the wrong route so data loss occurs this also shows unreliability of the network.

III. RELATED WORK

In [5], the authors developed a partitionable group communication service which allows so called "partition-aware applications" to operate in separated network topologies and, after two or more partitions merge, reconfigure themselves. The partitioning problem is handled by a simple PING or ACK mechanism. A sensor node sends a PING message to another node. If it does not receive an ACK in a certain period of time, that node is added to a list of suspects. A dynamic timeout mechanism is helpful which leads to a reasonably accurate suspect list. This scheme lacks the ability to distinguish between the node failure and partitioning which for most applications is desirable. In [3], the authors challenges posed by the possibility of network partitioning in WSNs has been recognized in several papers but the problem of detecting when such partitioning occurs seems to have received a little attention. To the best of our knowledge, the work in [3] is the only one that addresses the problem of detecting cuts in WSNs. They developed an algorithm for detecting the linear cuts, which is a linear separation of sensor nodes from the base station. The reason for the restriction to the linear cuts is that their algorithm relies critically on a certain duality between straight line segments and points in 2D, which also restricts the algorithm in [3] to sensor networks deployed in the 2D plane.

In contrast to the algorithm designed in [3], the DSSD algorithm proposed in [6] is not limited to linear cuts; it can detect cuts that separate the network into multiple components of arbitrary shapes. Furthermore, the DSSD algorithm is not restricted to sensor networks deployed in 2D, it does not require deploying sentinel nodes, and it allows every node to detect if a cut occurs. The DSSD algorithm involves only the nearest neighbor communication, which eliminates the need of routing messages to the source node. This feature makes the algorithm applicable to the mobile nodes as well. Since the computation that a node has to carry out involves only averaging, it is particularly well suited to wireless sensor networks with nodes that have limited computational capability. In this paper, the proposed algorithm is an extension of the previous work [6], which partially examined the DOS detection problem.

IV. PROPOSED WORK

A. Problem Statement

Consider a WSN as a time-varying graph G(k) = (V(k), E(k)), whose node set V(k) represents the sensors active at time k and the edge set E(k) consists of pairs of nodes (u, v) such that nodes u and v can directly exchange messages between each other at time k. By an "active" node we mean a node that has not failed permanently. All graphs considered here are called undirected, i.e., (i, j) = (j, i). The neighbors of a node i is the set Ni of nodes connected to i, i.e. Ni = {j|(i, j) € E}.

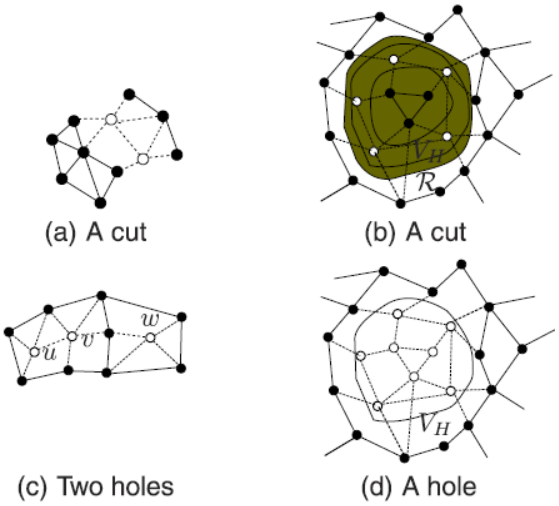

Figure 2: Examples of Cut and Holes

The number of neighbors of i, |Ni(k)|, is known its degree, which is denoted by di(k). A path from nodes i to j is a sequence of edges connecting i and j. A graph is called connected if there is a path between every pair of the nodes. A component Gc of a graph G is a maximal connected sub- graph of G (i.e., no other connected subgraph of G contains Gc as its subgraph). In terms of these definitions, a "cut" event is formally defined as the increase of the number of components of a graph due to the failure of a subset of nodes (Figure 2). The number of cuts associated with a cut event is the increase in

the number of the components after the event. The problem we seek to address is a twofold. First, we have to enable every sensor node to detect if it is disconnected from the source.

B. Disconnected from source(DOS) Detection

We say that a Disconnected from Source (DOS) event has occurred for node u. The algorithm allows each node to detect the DOS events. The sensor nodes use the computed potentials to detect if DOS events have occurred (i.e., if they are disconnected from the source node). The approach here is to exploit the fact that if the state is close to zero then the node is disconnected from the source, otherwise not. In order to reduce the sensitivity of the algorithm to variations in network size and structure, we use a normalized state. DOS detection part consists of normalized state computation, steady-state detection and connection or separation detection. A sensor node keeps track of the positive steady states seen in the past using the following method. Each sensor node i computes the normalized state difference δ xi(k) as follows:

$$\delta x_i(k) = \begin{cases} \dfrac{x_i(k) - x_i(k\text{-}1)}{X_i(k\text{-}1)}, & \text{if } x_i(k-1) > \epsilon_{zero} \\ \infty, & \text{otherwise} \end{cases}$$

Where $\in$ zero is a small positive number.

Each sensor node keeps an estimate of the most recent "steady state" observed, which is denoted by $x_i^{ss}(k)$. This estimate is updated at every time "k" according to the following rule: if PSSR(k)=1, then $x_i^{ss}(k) \leftarrow x_i$ k; otherwise $x_i^{ss}(k) \leftarrow x_i$ k− 1 . It is initialized as $x_i^{ss}(0) = \infty$. Every sensor node i also keeps a list of steady states seen in the past, one value for each unpunctuated interval of time during which the state was detected to be steady. This information is kept in a vector $x_i^{ss}(k)$, which is initialized to be empty and is updated as follows: If PSSR(k) = 1 but PSSR(k −1) = 0, then $x^{ss}(k)$ is appended to $x_i^{ss}(k)$ as a new entry. If steady state reached was detected in both k and k - 1 (i.e., PSSR(k) = PSSR(k − 1) = 1, then the last entry of $x^{ss}(k)$ is updated to $x_i^{ss}(k)$.

C. Connected Cut Occurred Somewhere (CCOS) Detection

The algorithm for detecting CCOS events relies on finding a shortest path around a hole, if it exists, and is partially inspired by the jamming detection algorithm [7]. The method utilizes sensor node states to assign the task of hole-detection to the most appropriate nodes. When a sensor node detects a large change in its local state as well as failure of one or more of its neighbors, and both of these events occur within a (predetermined) small time interval, the node initiates a PROBE message. The probe messages that are initiated by certain nodes that encounter failed neighbors, and are forwarded from one node to another in a way that if a short path exists around a "hole" created by node failures, the message will reach the initiating node. The pseudo code for the algorithm that decides when to initiate a probe message is included. Each probe message "p" contains the following information:

- A unique probe ID,
- Source Node id S
- Destination node,
- Path traversed (in chronological order), and
- The angle traversed by the probe message.

The list of probes is the union of the probe messages it received from its neighbors and the probe it decided to initiate, if any probe is forwarded in a manner such that if the probe is triggered by the creation of a cut or small hole(with circumference less than lmax) the probe traverses a path around the hole in a counter clockwise (CCW) direction and reaches the node that initiated the probe. Since it is only used to compute destinations of the probe messages.

V. CONCLUSION

Wireless sensor networks (WSNs) are a promising technology for monitoring large regions at high spatial as well as temporal resolution. The failure of some of its sensor nodes, which is called "cut" can separate the network into multiple connected components. The ability of detecting the cuts by the disconnected nodes and source node of a wireless sensor network will lead to the increase in the operational lifetime of the network. The Distributed Cut Detection (DCD) algorithm proposed here enables every sensor node of a sensor network to detect Disconnected from Source events if they occur. Second, it enables a subset of sensor nodes that experience CCOS events to detect them and estimate the approximate location of the cut in the form of a list of active sensor nodes that lie at the boundary of the cut. The algorithm is based on ideas from both electrical network theory and parallel iterative solution of linear equations. A key strength of the DCD method is that the convergence rate of the iterative scheme is quite fast and independent of the size and structure of the network.

REFERENCES

[1] A Partition Detection System for Mobile Ad-Hoc Networks: Hartmut Ritter, Rolf Winter, Jochen Schiller
[2] Akyildiz, I.F., Su, W., ankarasubramaniam, Y., Cayirci, E.: Wireless Sensor Networks: A Survey. Computer Networks Journal (Elsevier), Vol. 38, No.4 (2002)pp. 393-422.
[3] N. Shrivastava, S. Suri, and C. D. T´oth, "Detecting cuts in sensor networks,"in IPSN '05: Proceedings of the 4th international symposiumon Information processing in sensor networks, 2005, pp. 210–217.
[4] A Survey on Sensor Setworks,‖ : I. F. Akyildiz et al IEEE Commun. Mag., vol. 40, no. 8, Aug. 2002, pp. 102–112.
[5] Ö. Babaoglu, R. Davoli, A. Montresor, Group Communication in Partitionable Systems: Specification and Algorithms, IEEE Transactions on Software Engineering, 2001, vol. 27, no.4.
[6] P. Barooah, "Distributed Cut Detection in Sensor Networks," Proc. 47th IEEE Conf. Decision and Control, pp. 1097-1102, Dec.2008.
[7] A.D. Wood, J.A. Stankovic, and S.H. Son, "Jam: A Jammed-Area Mapping Service for Sensor Networks," Proc. IEEE Real Time Systems Symp. 2003.

International Journal of Modern Engineering Research (IJMER)
www.ijmer.com Vol. 3, Issue. 4, Jul - Aug. 2013 pp-2514-2521 ISSN: 2249-6645

An Efficient Distributed Control Law for Load Balancing in Content Delivery Networks

S. K. Mehertaj[1], K. V. Subbaiah[2], P. Santhi[3], T. Bharath Manohar[4]

[1,3]*M. Tech 2ndyr, Dept of CSE, PBRVITS (Affiliated to JNTU Anantapur), Kavali, Nellore. Andhra Pradesh. India.*
[2] *Assoc. Prof., Dept of CSE, PBRVITS (Affiliated to JNTU Anantapur), Kavali, Nellore. Andhra Pradesh.India.*
[4] *Asst. Professor, Dept of CSE, CMR College of Engineering &Technology,*
(Affiliated to JNTU Hyderabad)Hyderabad.Andhra Pradesh.India.

Abstract: *Content Delivery Networks (CDN) aim at overcoming the inherent limitations of the Internet. The main concept at the basis of this technology is the delivery at edge points of the network, in proximity to the request areas, to improve the user's perceived performance while limiting the costs. This paper focuses on the main research areas in the field of CDN, pointing out the motivations, and analyzing the existing strategies for replica placement and management, server measurement, best fit replica selection and request redirection. In this paper, we face the challenging issue of defining and implementing an effective law for load balancing in Content Delivery Networks .A formal study of a CDN system, carried out through the exploitation of a fluid flow model characterization of the network of servers.This result is then leveraged in order to devise a novel distributed and time-continuous algorithm for load balancing, which is also reformulated in a time-discrete version.*

Keywords: *CDN's Fluid flow model, Load balancing Algorithm.*

I. INTRODUCTION

Content Delivery Network (CDN) represents a popular and useful solution to effectively support emerging Web applications by adopting a distributed overlay of servers. By replicating content on several servers, a CDN is capable to partially solve congestion issues due to high client request rates, thus reducing latency while at the same time increasing content availability

- In this paper, we face the challenging issue of defining and implementing an effective law for load balancing in Content Delivery Networks.
- A formal study of a CDN system, carried out through the exploitation of a fluid flow model characterization of the network of servers.
- This result is then leveraged in order to devise a novel distributed and time-continuous algorithm for load balancing, which is also reformulated in a time-discrete version.

II. MOTIVATION

- In this paper, we face the challenging issue of defining and implementing an effective law for load balancing in Content Delivery Networks.
- A formal study of a CDN system, carried out through the exploitation of a fluid flow model characterization of the network of servers.
- This result is then leveraged in order to devise a novel distributed and time-continuous algorithm for load balancing, which is also reformulated in a time-discrete version.

SCOPE:

The most important performance improvements derived from the adoption of such a network concern two aspects:

1) Overall system throughput, that is, the average number of requests served in a time unit (optimized also on the basis of the processing capabilities of the available servers);
2) Response time experienced by clients after issuing a request. The decision process about these two aspects could be in contraposition. As an example, a "better response time" server is usually chosen based on geographical distance from the client, i.e., network proximity; on the other hand, the overall system throughput is typically optimized through load balancing across a set of servers. Although the exact combination of factors employed by commercial systems is not clearly defined in the literature, evidence suggests that the scale is tipped in favor of reducing response time.

Drawbacks of Existing System

- Goal of CDN can be achieved in many different ways, not all of which provide local stability guarantees, as well as balancing of the servers' queues.
- Indeed, it might happen that the overall condition is met, but one or more local server's queues overflow, thus bringing to packet losses and unavailability of the overloaded servers.

PROBLEM STATEMENT

- We focus exclusively on critical conditions where the global resources of the network are close to saturation.
- This is a realistic assumption since an unusual traffic condition characterized by a high volume of requests, i.e., a flash crowd, can always overfills the available system capacity.
- In such a situation, the servers are not all overloading which we have local instability conditions where the input rate is greater than the service rate.

NEW SYSTEM PROPOSAL

- We first design a suitable load-balancing law that assures equilibrium of the queues in a balanced CDN by using a fluid flow model for the network of servers.
- We present a new mechanism for redirecting incoming client requests to the most appropriate server, thus balancing the overall system requests load.
- Our mechanism leverages local balancing in order to achieve global balancing. This is carried out through a periodic interaction among the system nodes.

III. LITERATURE SURVEY

The commercial success of the Internet and e-services, together with the exploding use of complex media content online has paved the way for the birth and growing interest in Content Delivery Networks (CDN). Internet traffic often encounters performance difficulties characteristic of a non dedicated, best effort environment. The user's urgent request for guarantees on quality of service have brought about the need to study and develop new network architectures and technologies to improve the user's perceived performance while limiting the costs paid by providers. Many solutions have been proposed to alleviate the bottleneck problems and the most promising are based on the awareness of the content that has to be delivered. The traditional *"content-blind"* network infrastructures are not sufficient to ensure quality of service to all users in a dynamic and ever increasing traffic situation. New protocols and integrated solutions must be in place both on the network and on the server side to distribute, locate and download contents through the Internet. The enhancement of computer networks by means of a content aware overlay creates the new architectural paradigm of the CDN. Today's CDN act upon the traditional network protocol stack at various levels, relying on dynamic and proactive content caching and on automatic application deployment and migration at the edge of the network, in proximity to the final users. Content replicas in a CDN are geographically distributed, to enable fast and reliable delivery to any end-user location: through CDN services, up-to-date content, can be retrieved by end-users locally rather than remotely.

CDNs were born to distribute heavily requested contents from popular web servers, most of all image files. Nowadays, a CDN supports the delivery of any type of dynamic content, including various forms of interactive media streaming. CDN providers are companies devoted to hosting in their servers the content of third-party content providers, to mirroring or replicating such contents on several servers spread over the world, and to transparently redirecting the customers requests to the 'best replica' (e.g. the closest replica, or the one from which the customer would access content at the lowest latency). Designing a complete solution for CDN therefore requires addressing a number of technical issues: which kind of content should be hosted (if any) at a given CDN server (replica placement), how the content must be kept updated, which is the 'best replica' for a given customer, which mechanisms must be in place to transparently redirect the user to such replica. A proper placement of replica servers shortens the path from servers to clients thus lowering the risk of encountering bottlenecks in the non-dedicated environment of the Internet. A request redirection mechanism is provided at the access routers level to ensure that the best suited replica is selected to answer any given request of possibly different types of services with different quality of service agreements. The CDN architecture also relies on a measurement activity that is performed by cooperative access routers to evaluate the traffic conditions and the computational capacity and availability of each replica capable of serving the given request. Successfully implemented, a CDN can accelerate end user access to content, reduce network traffic, and reduce content provider hardware requirements.

IV. SYSTEM ANALYSIS

DISTRIBUTED LOAD-BALANCING ALGORITHM

We want to derive a new distributed algorithm for request balancing that exploits the results are presented. First of all, we observe that it is a hard task to define a strategy in a real CDN environment that is completely compliant with the model proposed. As a first consideration, such a model deals with continuous-time systems, which is not exactly the case in a real packet network where the processing of arriving requests is not continuous over time. For this reason, in the following of this section, we focus on the control law are described. The objective is to derive an algorithm that presents the main features of the proposed load-balancing law and arrives at the same results in terms of system equilibrium through proper balancing of servers' loads, as assessed by Lemma.

Algorithm Description

The implemented algorithm consists of two independent parts: a procedure that is in charge of updating the status of the neighbors' load, and a mechanism representing the core of the algorithm, which is in charge of distributing requests to a node's neighbours. The pseudocode of the algorithm is reported. Even though the communication protocol used for status information exchange is fundamental for the balancing process, in this paper we will not focus on it. Indeed, for our simulation tests, we implemented a specific mechanism: We extended the HTTP protocol with a new message, called *CDN*, which is periodically exchanged among neighboring peers to carry information about the current load status of the sending node. Naturally, a common update interval should be adopted to guarantee synchronization among all interacting peers. For this purpose, a number of alternative solutions can be put into places, which are nonetheless out of the scope of the present work.

```
// peer status update
prob_space[0]=0; load_diff = 0; load_diff_sum = 0;
for(j=1; j<=n; j++){
     if(load_i – peer[j].load){
          load_diff = load_i – peer[j].load;
          //insert the new difference
          build_prob_space(load_diff, prob_space);
          load_diff_sum = load_diff_sum + load_diff;
     }
     //normalize the vector elements
     update_prob_space(load_diff_sum, prob_space);
}

// balancing process
if(prob_space[] == NULL) //no neighbors with lower load
     //serve locally the request
     serve_request();
else{
     float x = rand(); //random number generator
     int req_sent = 0; int i = 0;
     while(prob_space[i] == 1 or req_sent == 1){
          if(prob_space[i-1] <= x < prob_space[i]){
               //send request to the chosen peer
               send_to(peer[i-1].addr);
               req_sent = 1;
          }
          i++;
     }
}
```

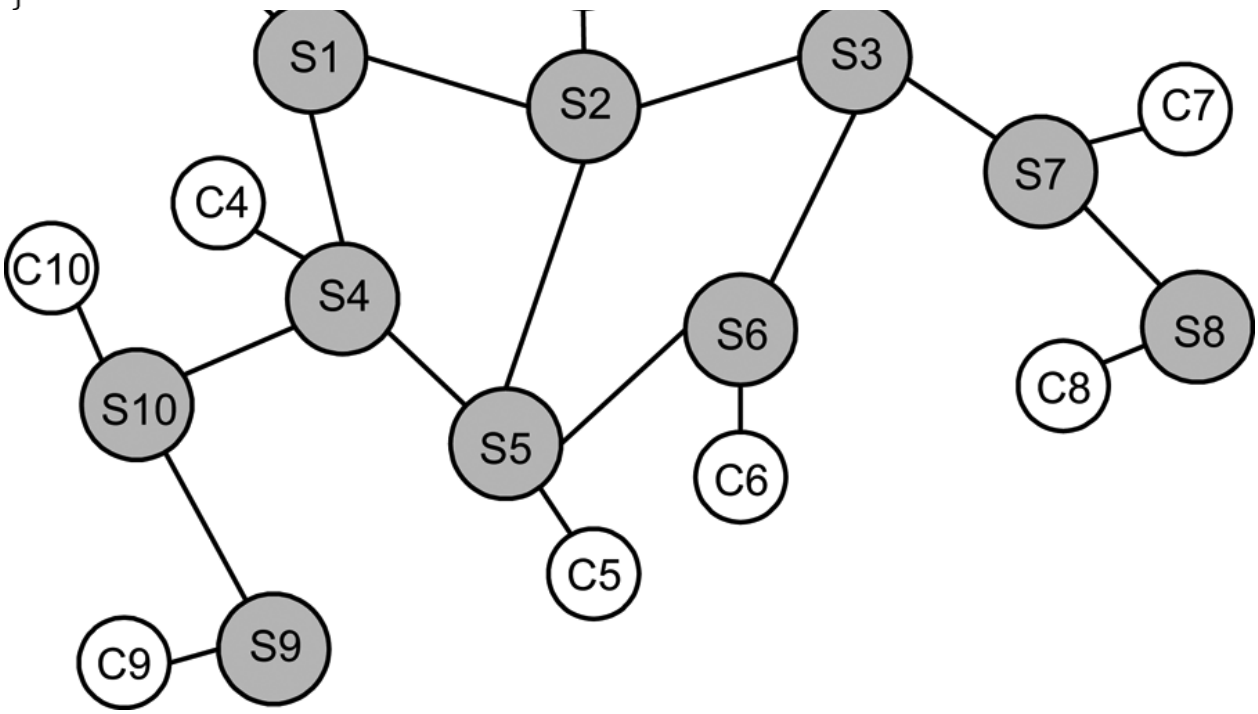

Fig: Pseudocode description of the proposed algorithm

Functional Requirements Specification

This section outlines the use cases for each of the active readers separately. The reader, the author and the reviewer have only one use case apiece while the editor is main actor in this system

Different use cases in the system

1. Admin

He/she enters into the mobile sink they are end mobile agents who participate in the communication .mobile agents passes /submits query to anonymizer and it sends to location-based service.

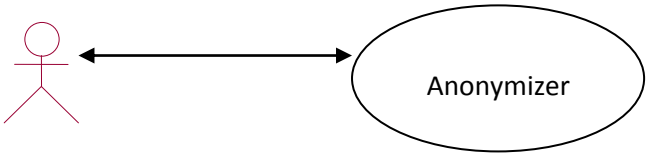

2. Anonymizer

It is an interface between user i.e. mobile agent and main server .It receives messages from user and signals to LBS/BS and then passes information to mobile nodes.It also selects local database and checks the databases for localization of mobile agents.

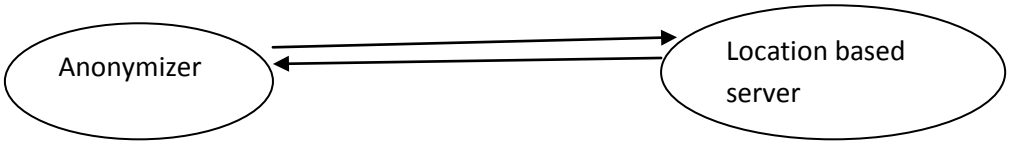

Mobile user (MU), issues the query and public key to the nearby anonymizer, Anonymizer passes the query and key to the base station (BS). As the LBS server is deployed at the BS, LBS processes the query and returns the result back to the BS , the BS knows that the user is in its region and gives a active signal to all the anonymizers in that particular region.

3. LBS (LOCATION BASED SERVER)

It is the main server acts as a base station and processes the requests from clients and sends message to mobile agents. It signals the anonymizer about mobile locations.

Overall Description

In this paper, we presented a novel load-balancing law for cooperative CDN networks. We first defined a model of such networks based on a fluid flow characterization. We hence moved to the definition of an algorithm that aims at achieving load balancing in the network by removing local queue instability conditions through redistribution of potential excess traffic to the set of neighbors of the congested server. The algorithm is first introduced in its time-continuous formulation and then put in a discrete version specifically conceived for its actual implementation and deployment in an operational scenario. Through the help of simulations, we demonstrated both the scalability and the effectiveness of our proposal, which outperforms most of the potential alternatives that have been proposed in the past.

External Interface Requirements

The only link to an external system is the link to the Historical Society (HS) Database to verify the membership of a Reviewer. The Editor believes that a society member is much more likely to be an effective reviewer and has imposed a membership requirement for a Reviewer. The HS Database fields of interest to the Web Publishing Systems are member's name, membership (ID) number, and email address (an optional field for the HS Database).

- The *Assign Reviewer* use case sends the Reviewer ID to the HS Database and a Boolean is returned denoting membership status. The *Update Reviewer* use case requests a list of member names, membership numbers and (optional) email addresses when adding a new Reviewer. It returns a Boolean for membership status when updating a Reviewer.
- Product Functions

Logical database requirement

DATA BASE ARCHITECTURE

There are three types of architecture: ONE TIER ARCHITECTURE TWO-TIERED THREE-TIERED ONE TIER ARCHITECTURE

The application and the data reside together logically. These are not usually database programs. The logic and its data reside together. Figure below shows a model of a single-tier application.

TWO-TIERED

The application resides in a different logical location than the data. These are usually database applications. Most client/Server applications fit into this category. figure shows a model of a two-tier application.

THREE-TIERED

In a three-tiered system, the application resides in a different logical location than the logic of the application and the data.

To put it another way, the client software makes a call to a remote service. that remote service is responsible for interacting with the data and responding to the client. the client has no knowledge of how and where the data is stored. All it knows about is the remote service has no knowledge of the clients that will be calling it. It only knows about the data.

E-R DIAGRAMS AND DATA FLOW DIAGRAMS

Data flow diagram

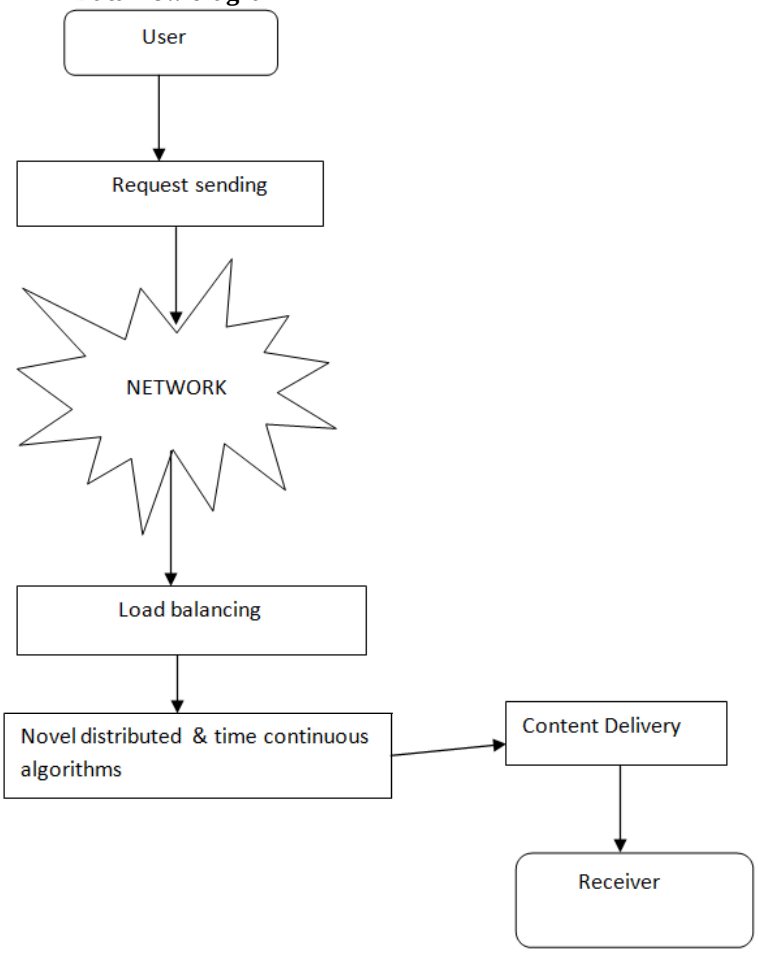

ENTITY RELATIONSHIP MODELS

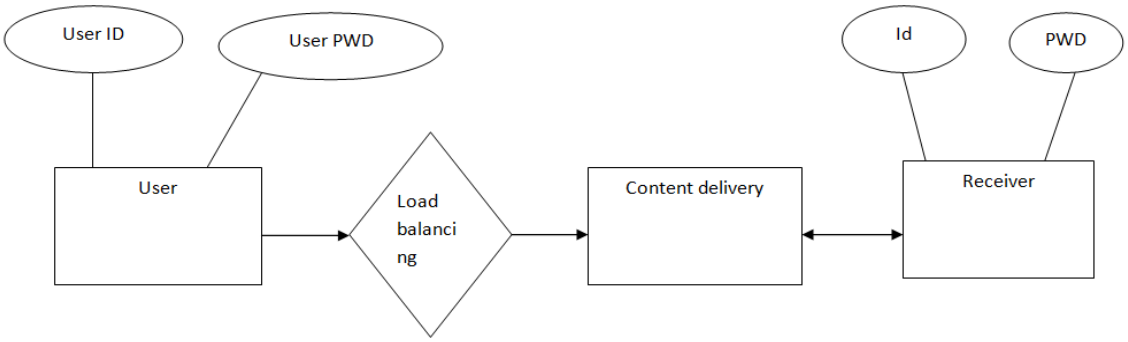

CLASS DIAGRAM

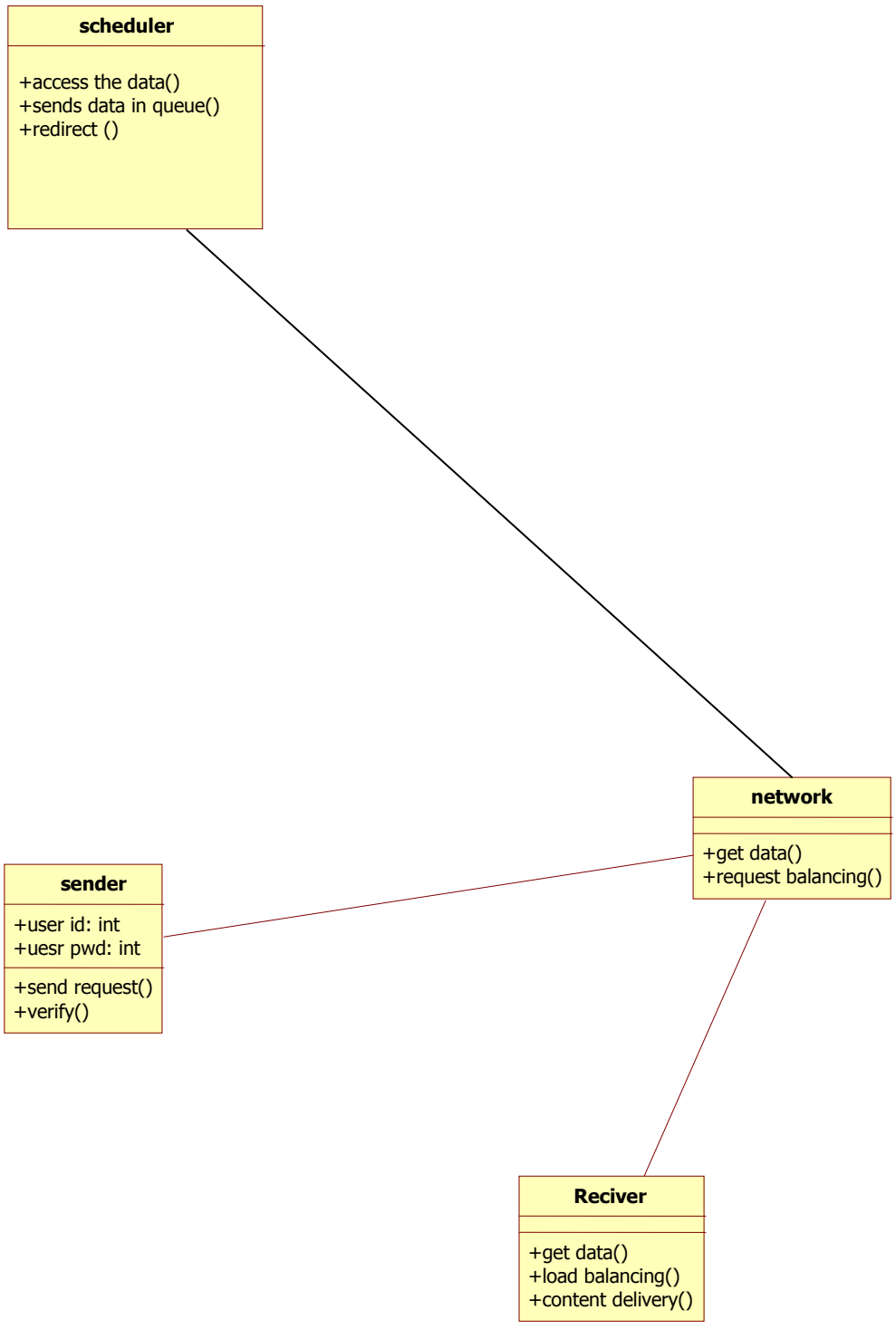

USE CASE DIAGRAM

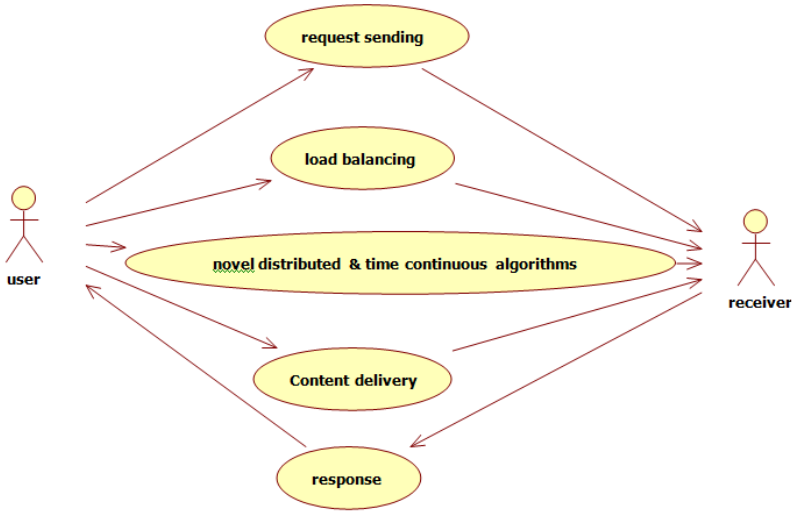

SEQUENCE DIAGRAMS

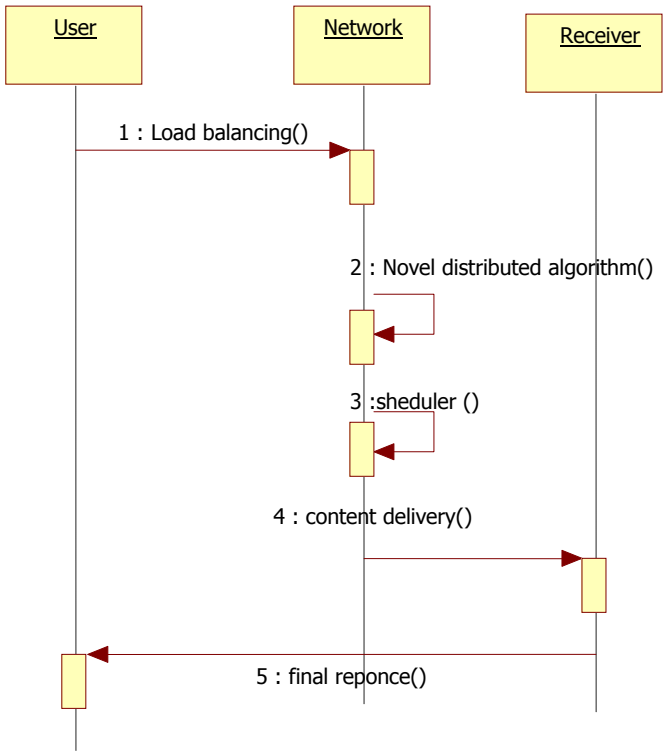

STATE CHART DIAGRAMS

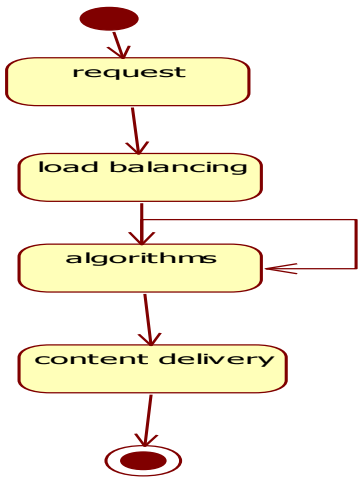

V. CONCLUSION

In this paper, we presented a novel load-balancing law for cooperative CDN networks. We first defined a model of such networks based on a fluid flow characterization. We hence moved to the definition of an algorithm that aims at achieving load balancing in the network by removing local queue instability conditions through redistribution of potential excess traffic to the set of neighbors of the congested server. The algorithm is first introduced in its time-continuous formulation and then put in a discrete version specifically conceived for its actual implementation and deployment in an operational scenario. Through the help of simulations, we demonstrated both the scalability and the effectiveness of our proposal, which outperforms most of the potential alternatives that have been proposed in the past. The present work represents for us a first step toward the realization of a complete solution for load balancing in a cooperative, distributed environment. Our future work will be devoted to the actual implementation of our solution in a real system, so to arrive at a first prototype of a load-balanced, cooperative CDN network to be used both as a proof-of-concept implementation of the results obtained through simulations and as a playground for further research in the more generic field of content-centric network management.

ACKNOWLEDGMENT

I would like to express my sincere thanks to my Guide and my Co-Authors for their consistence support and valuable suggestions.

REFERENCES

[1] M. Arlitt and T. Jin, *A Workload Characterization Study of 1998 World Cup Web Site*, IEEE Network, pp. 30-37, May/June 2000.
[2] J. Dilley, B. Maggs, J. Parikh, H. Prokop, R. Sitaraman and B. Weihl, *Globally Distributed Content Delivery*, IEEE Internet Computing, pp. 50-58, September/October 2002.
[3] M. Zukerman, T. D. Neame and R. G. Addie, *Internet Traffic Modeling and Future Technology Implications*, IEEE INFOCOM, 2003.
[4] Akamai Technologies, Inc. www.akamai.com, 2006
[5] F. Douglis, M. F. Kaashoek, *Scalable Internet Services*, IEEE Internet Computing, vol. 5, no. 4, 2001, pp.36-37.
[6] G. Pallis and A. Vakali, *Insight and Perspectives for Content Delivery Networks*, Communications of the ACM, vol. 49, no. 1, ACM Press, NY, USA, January 2006. pp. 101-106.
[7] S. Jamin, C. Jin, Y. Jin, D. Raz, Y. Shavitt and L. Zhang, *On the placement of Internet Instrumentation*, In Proceedings of IEEE INFOCOM conference, pp. 295-304, Tel-Aviv, Israel, March 2000.
[8] P. Krishnan, D. Raz, Y. Shavitt, *The Cache Location Problem*, IEEE/ACM Transaction on Networking, 8(5), 2000.
[9] L. Qiu, V. N. Padmanabhan, G. M. Voelker, *On the Placement of Web Server Replicas*, In Proceedings of IEEE INFOCOM conference, pp. 1587-1596, Anchorage, Alaska, USA, April 2001.
[10] S. Jamin, C. Jin, A. R. Kure, D. Raz and Y. Shavitt, *Constrained Mirror Placement on the Internet*, In Proceedings of IEEE INFOCOM Conference, Anchorage, Alaska, USA, April 2001.
[11] Y. Chen, R. H. Katz and J. D. Kubiatowicz, *Dynamic Replica Placement for Scalable Content Delivery*, In Proceedings of International Workshop on Peer-to-Peer Systems (IPTPS 02), LNCS 2429, Springer-Verlag, pp. 306-318, 2002.
[12] A. Vakali and G. Pallis, *Content Delivery Networks: Status and Trends*, IEEE Internet Computing, IEEE Computer Society, pp. 68-74, November-December 2003.
[13] N. Fujita, Y. Ishikawa, A. Iwata and R. Izmailov, *Coarse-grain Replica Management Strategies for Dynamic Replication of Web Contents*, Computer Networks: The International Journal of Computer and Telecommunications Networking, vol. 45, issue 1, pp. 19-34, May 2004.
[14] G. Peng, *CDN: Content Distribution Network*, Technical Report TR-125, Experimental Computer Systems Lab, Department of Computer Science, State University of New York, Stony Brook, NY 2003. [20] J. Kangasharju, J Roberts and K. W. Ross, *Object Replication Strategies in Content Distribution Networks*, Computer Communications 25(4), pp. 367-383, March 2002.
[15] M. Day, B. Cain, G. Tomlinson and P. Rzewski, *A Model for Content Internetworking (CDI)*, Internet Engineering Task Force RFC 3466, February 2003.
[16] W. Y. Ma, B. Shen and J. T. Brassil, *Content Services Network: Architecture and Protocols*, In Proceedings of 6th International Workshop on Web Caching and Content Distribution(IWCW6), 2001.
[17] M. Hofmann and L. R. Beaumont, *Content Networking: Architecture, Protocols, and Practice*, Morgan Kaufmann Publishers, San Francisco, CA, USA, pp. 129-134, 2005.

International Journal of Modern Engineering Research (IJMER)
www.ijmer.com Vol. 3, Issue. 4, Jul - Aug. 2013 pp-2522-2525 ISSN: 2249-6645

Performance Based Evaluation of Shear Walled RCC Building by Pushover Analysis

P. B. Oni[1], Dr. S. B.Vanakudre[2]
[1, 2] *(Department of Civil Engg, SDM College of Engg and Tech, India)*

***ABSTRACT**: As the world move towards the implementation of Performance Based Engineering philosophies in seismic design of Civil Engineering structures, new seismic design provisions require Structural Engineers to perform both linear and nonlinear analysis for the design of structures. In the present work three storey and six storey building models with plus shape Shear wall have been considered. Equivalent static and response spectrum methods are carried out as per IS:1893 (Part 1) -2002 using finite element analysis software ETABS v9.1.1. Seismic performance is assessed by pushover analysis as per ATC-40 guidelines for earthquake zone V in India. The paper also deals with the effect of the variation of the building height on the structural response of the shear wall. This paper highlights the accuracy of Push over analysis in comparison with the most commonly adopted Response Spectrum Analysis and Equivalent Static Analysis.*

***Keywords**: Equivalent Static method, Pushover Analysis, Response Spectrum Analysis, Shear Wall, Storey height.*

I. INTRODUCTION

Recently there has been a considerable increase in the tall buildings both residential and commercial and the modern trend is towards more tall and slender structures. Thus the effects of lateral loads like wind loads, earthquake loads and blast forces are attaining increasing importance and almost every designer is faced with the problems of providing adequate strength and stability against lateral loads. This is the new development as the earlier building designers designed the buildings for vertical loads and as an afterthought checked the final design for lateral loads as well. Now the situation is quiet different and a clear understanding of effect of the lateral loads on the building and the behavior of various components under these loads is essential.

Structural design of buildings for seismic loading is primarily concerned with structural safety during major earthquakes, but serviceability and the potential for economic loss are also of concern. Seismic loading requires an understanding of the structural behavior under large inelastic deformations. Behavior under this loading is fundamentally different from wind or gravity loading, requiring much more detailed analysis to assure acceptable seismic performance beyond the elastic range. Some structural damage can be expected when the building experiences design ground motions because almost all building codes allow inelastic energy dissipation in structural systems.

II. OBJECTIVES

The main objectives of present study include:

1. The effect of Plus shaped shear wall on structural response under seismic loading.
2. Analysis of framed structures using Static Non linear Pushover analysis, Response Spectrum Method and Equivalent Static Method.

III. STRUCTURAL MODELLING

The finite element analysis software ETABS v 9.1.1 is utilized to create 3D model and run all analyses. The software is able to predict the geometric nonlinear behavior of space frames under static or dynamic loadings, taking into account both geometric nonlinearity and material inelasticity. The software accepts static loads (either forces or displacements) as well as dynamic (accelerations) actions and has the ability to perform eigen values, nonlinear static pushover and nonlinear dynamic analyses.

Table 1. Structural Details

Young's modulus of M20 concrete, E	2.48×10^7 kN/m^2
Grade of concrete	M20
Grade of steel	Fe 415
Density of Reinforced Concrete	25 kN/m^3
Modulus of elasticity of brick masonry	2100×10^3 kN/m^2
Density of brick masonry	20 kN/m^3
No of storey	G+2, G+5
Beam size	0.25m x 0.45 m
Column size	0.5 m x 0.5m
Shear wall thickness	0.4 m
Slab thickness	0.125 m
Height of all storeys	3 m

3.1 Nonlinear Hinge Assignment for Pushover Analysis

Shear walls: Typically, PMM hinges with axial force-moment interaction were assigned at the wall ends near floor levels and shear hinges were assigned at the mid-height level of walls.

Columns:

PMM hinges were assigned at the columns ends and at a few equally-spaced intermediate points.

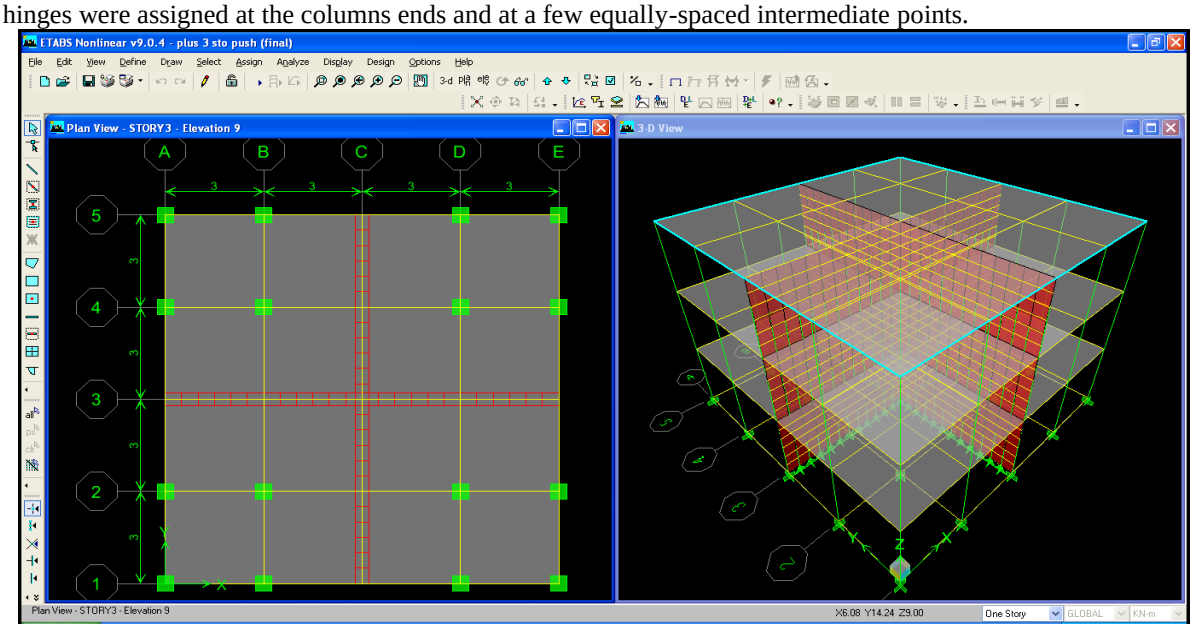

Figure 1. Plan and elevation of the three storey building

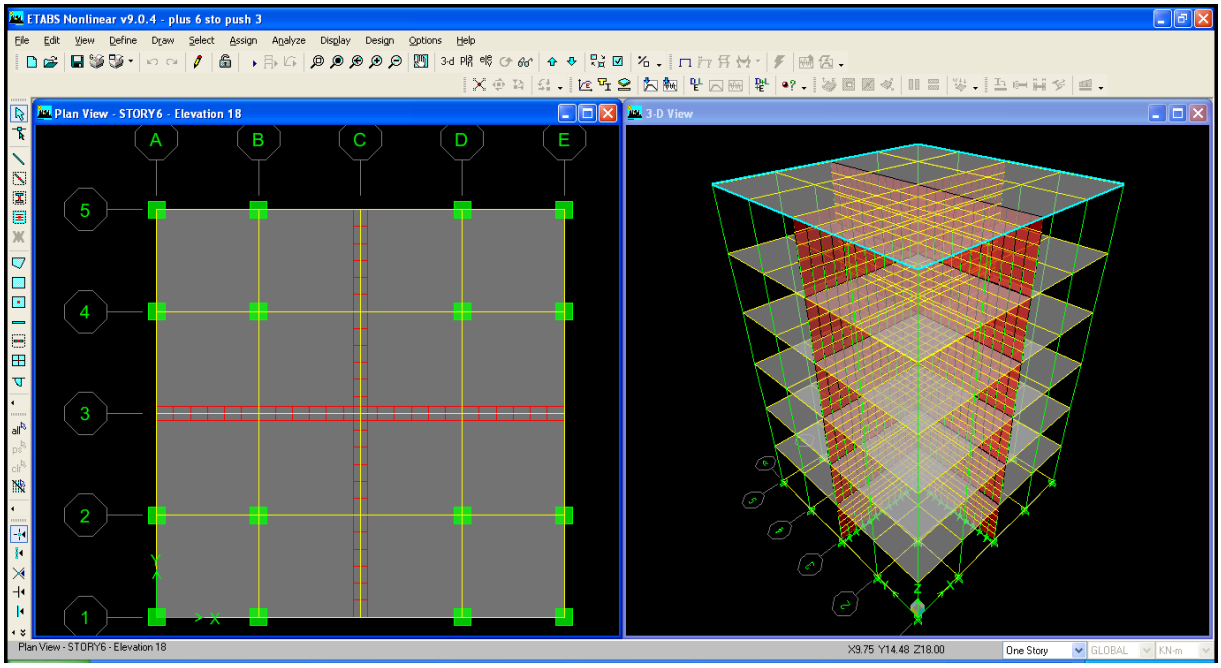

Figure 2. Plan and elevation of the six storey building

IV. RESULTS AND DISCUSSIONS

Table 2. Base Shear calculations

No of Storeys	Longitudinal Direction		Transverse Direction	
	$\overline{V_B}$ (kN)	V_B (kN)	$\overline{V_B}$ (kN)	V_B(kN)
6	1201.09	1462.3	1201.09	1462.3
3	692.8	635.34	692.8	637.34

4.1 Comparison between Equivalent Static Method and Response Spectrum Method

Equivalent static method is a linear static method for the seismic analysis whereas response spectrum method is a linear dynamic method. Figure.3 illustrates the comparison of storey drift using equivalent static method and response spectrum method for three storey building with plus shaped shear wall. The percentage variation between the two methods of analysis for the above case is 3.4%.

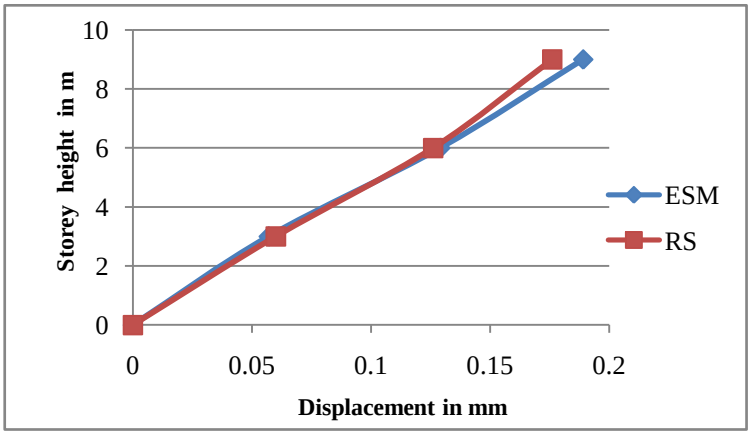

Figure 3. The comparison of storey drift using equivalent static method and response spectrum method for three storey building with plus shaped shear frame.

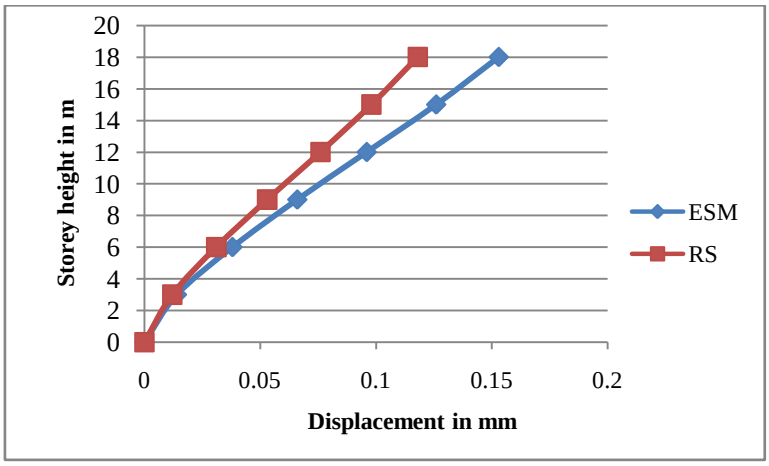

Figure 4 . The comparison of storey drift using equivalent static method and response spectrum method for six storey building with plus shaped shear frame.

Figure 4 illustrates the comparison of storey drift using equivalent static method and response spectrum method for six storey building with plus shaped shear frame. The percentage variation between the two methods of analysis for the above case is 7.1%.

4.2 Comparison between Response Spectrum Method and Pushover analysis method

A comparison between response spectrum method and push over analysis is carried out for storey drift for three storey and six storey building with infill walls for Plus shape shear wall. Figure. 5 illustrates the comparison of storey drift using response spectrum method and push over analysis method for three storey building with plus shaped shear frame .The percentage variation between the two methods of analysis for the above case is 10.39%.

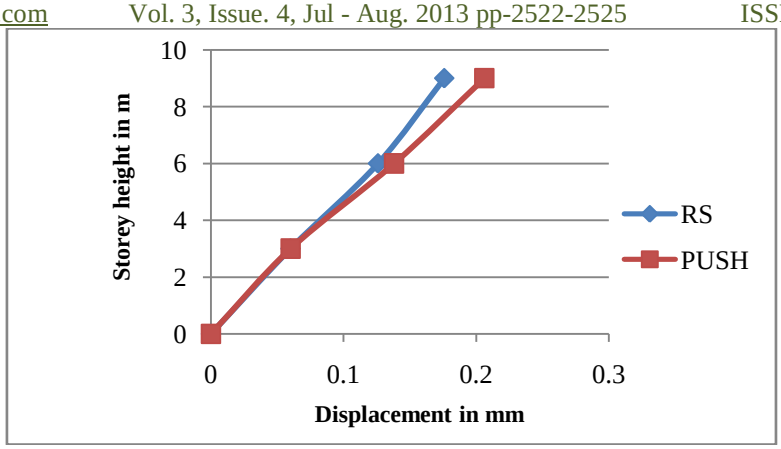

Figure 5 . The comparison of storey drift using response spectrum method and pushover analysis method for three storey building with plus shaped shear frame.

Figure. 6 illustrates the comparison of storey drift using response spectrum method and push over analysis method for three storey building with plus shaped shear frame .The percentage variation between the two methods of analysis for the above case is 43.76%.

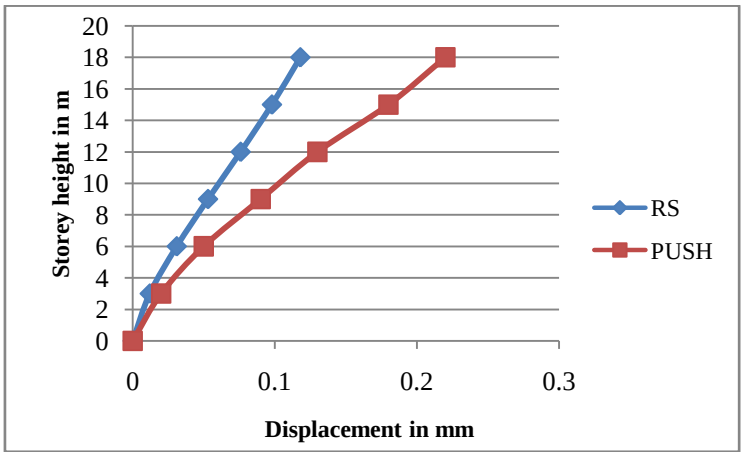

Figure 6. The comparison of storey drift using response spectrum method and pushover analysis method for six storey building with plus shaped shear frame

V. CONCLUSIONS

From the above studies it can be concluded that

1. Equivalent Static Method can be used effectively for symmetric buildings up to 20 m height. For higher and unsymmetrical buildings Response Spectrum Method should be used.
2. For important structures Push over Analysis should be performed as it predicts the structural response more accurately in comparison with other two methods since it incorporates p - Δ effects and material non linearity which is true in real structures.
3. From the above studies it is evident that Plus shaped shear wall can effectively resist the lateral forces coming on the structure.

REFERENCES

Journal papers:

[1] Romy Mohan and C Prabha , Dynamic Analysis of RCC Buildings with Shear Wall , *International Journal of Earth Sciences and Engineering ISSN 0974-5904, Volume 04, No 06 SPL, October 2011, pp 659-662.*

[2] Rahul Rana , Limin Jin and Atila Zekioglu, Pushover analysis of a 19 story concrete shear wall Building, *13th World Conference on Earthquake Engineering Vancouver, B.C., Canada August 1-6, 2004 Paper No. 133.*

Books:

[3] Chopra A. K, *Dynamics of structures theory and applications to earthquake engineering* (Prentice Hall, Englewood Cliffs, N.J. 1995).

Codes:

[4] ATC-40. "Seismic evaluation and retrofit of concrete buildings." Volume 1 and 2. Applied Technology Council, California, 1996.

[5] FEMA-273. "NEHRP guidelines for the seismic rehabilitation of buildings." Federal Emergency Management Agency, Washington DC, 1997.

[6] FEMA-356. "Prestandard and commentary for the seismic rehabilitation of buildings." Federal Emergency Management Agency, Washington DC, 2000.

[7] IS: 1893 (Part 1) 2002- Indian standard- "*Criteria for earthquake resistant design of structures"*, Bureau of Indian Standards, New Delhi.

International Journal of Modern Engineering Research (IJMER)
www.ijmer.com Vol. 3, Issue. 4, Jul - Aug. 2013 pp-2526-2529 ISSN: 2249-6645

Illustration Clamor Echelon Evaluation via Prime Piece Psychotherapy

C. Bala Saravanan, M. Rajesh Khanna, J. Aravind, R. Ramesh, M. Jeyalakshmi
Vel. Tech Multi Tech Dr. Rangarajan Dr. Sakunthala Engineering College, Chennai

Abstract: *The quandary of canopy clamor echelon evaluation arises in numerous illustration processing applications, such as demising, compression, and segmentation. In this paper, I intend an innovative clamor echelon estimation method on the basis of foremost constituent psychoanalysis of illustration blocks. I show that the clamor variance can be estimated as the negligible eigenvalue of the illustration block covariance matrix. Appraise with 13 existing methods, the proposed approach shows a good compromise betIen speed and accuracy. It is at least 15 times faster than methods with similar accuracy and it are at slightest two eras more precise than supplementary method. Manner does not presuppose the survival of homogeneous areas in the effort illustration and, hence, can fruitfully scrutinize illustrations contain only consistency.*

I. INTRODUCTION

Canopy clamor echelon assessment is an important illustration dispensation step, since the clamor echelon is not always notorious beforehand, but many illustration demising compression and segmentation algorithms take it as an input parameter; and their performance depends heavily on the accuracy of the clamor echelon estimate. The most widely used clamor model, which is assumed in this work as Ill, is signal-independent additive white Gaussian clamor. Clamor variance estimation algorithms Ire being developed over the last two decades; and most of them comprise one or several widespread stepladder.

a) Preclassification of homogeneous areas .These areas are the most suitable for clamor variance estimation, because the noisy illustration variance equals the clamor variance there.
b) Illustration filtering the process illustration is convolved with a high-pass filter (e.g. Palladian kernel); or the difference of the processed illustration and the rejoinder of a low-pass filter is computed. The filtering result contains the clamor as Ill as stuff edges, which can be recognized by an edge script the associate editor, harmonize the review of this manuscript and approving it for publication was Prof. Béatrice Pesquet-Popescu.detector and removed. The consequence of this procedure is assumed to contain only the clamor, which allows direct belief of the clamor variance.
c) c) Wavelet renovate The simplest assumption that the wavelet coefficients at the finest decomposition echelon (sub band HH1) correspond only to the clamor often leads to significant over estimated, because these wavelet coefficients are affected by illustration structures as Ill. In, it is assumed that only wavelet coefficients with the absolute value slighter than some doorsill are caused by the clamor, where the doorstep is found by an iterative course of action.

A. The recompense of the anticipated manner is:

1) Elevated computational efficiency.
2) Knack to process illustrations with textures, even if there are no homogeneous areas.
3) The alike or enhanced accuracy compared with the state of the sculpture.

B. Idea of the Method

Let us demonstrate the ability of illustration block PCA to estimate the clamor variance on a simple 1D example. Consider clamor-free signal (xk) = (2 + (−1)k) = (1, 3, 1, 3,...) and noisy signal (yk) = (xk + nk),where nk are realizations of a random variable with normal distribution N(0; 0.52).The processing of these signals using a sliding window, with the width equal to 2, results in two point sets: {xk}={(xk; xk+1)} for the clamor-free signal and {yk }={(yk; yk+1)}={(xk; xk+1)+(nk ; nk+1)} for the noisy signal. By construction, point's xk can have only two values: (1; 3) or (3; 1). Points yk are presented in Fig. 1.Applying PCA to point set {yk} gives new coordinate system (u1; u2) (also shown in Fig. 1), in which u1 is associated with **Fig. 1**. Points yk in original coordinate system (w1; w2) and new coordinate system (u1; u2) computed by PCA. Both the clamor-free signal and the clamor, and u2 is associated only with the clamor.

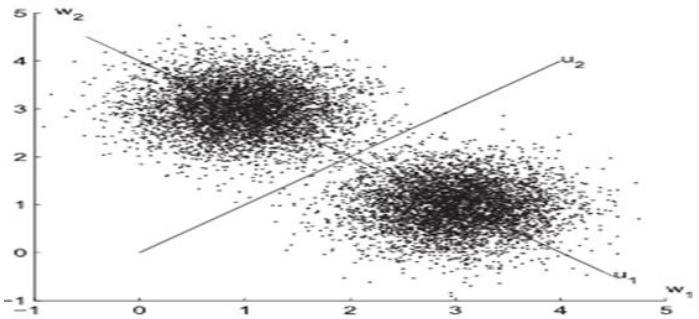

Fig- 1 Points *yk* in original coordinate system *(w1; w2)* and new coordinate system *(u1; u2)* computed by PCA

II. Illustration Block Model

Alike to the previous paragraph, let x be a clamor-free illustration of size S1 ×S2,where S1 is the number of columns and S2 is the number of rows, y = x + n be an illustration corrupted with signal-independent additive white Gaussian clamor n with zero mean. Clamor variance σ2 is unknown and should be estimated. Each of illustrations x, n, y contains N = (S1 − M1 + 1)(S2 −M2 + 1) blocks of size M1 × M2, whose left-top corner positions are taken from set {1,..., S1−M1+1}×{1,..., S2−M2 + 1}. These blocks can be rearranged into vectors with M = M1M2 elements and considered as realizations xi , ni ,yi , i = 1,..., N of random vectors X, N,and Y respectively.

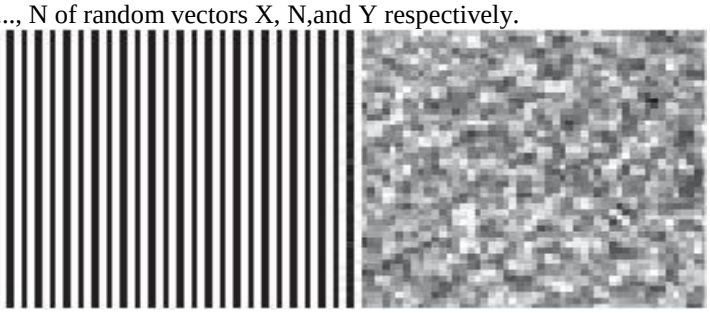

Fig - 2 Round markers and vertical bars are the mean values

III. Extraction of the Illustration Block Subset

As mentioned in the previous subsection, I need a strategy to extract a subset of illlustration blocks, which stases Assumption 1. Let di be the distances of xi to VM−m, i = 1,..., N.Assumption 1 holds, i.e. xi ∈ VM−m, i = 1,..., N, ifand only if di = 0, i = 1,..., N. Trying to satisfy this condition, it is reasonable to discard the blocks with the largest di from the total N illlustration blocks. Unfortunately, the values of di are not available in practice. Computation of the distances of yi to VM−m does not help, since a large distance of yi to VM−m can be caused by clamor. Several heuristics may be applied therefore in order to select blocks with largest di, e.g. to pick blocks with largest standard deviation, largest range, or largest entropy. I use the first strategy, since it is fast to compute and the results are the most accurate in most cases. This strategy is examined below.Let us consider the Spearman's rank correlation coefficient ρ betIen di and s(xi),where s(xi) is the sample standard deviation of elements of block xi , i = 1,..., N. I have computed ρ for the reference illlustrations from the TID2008 database.

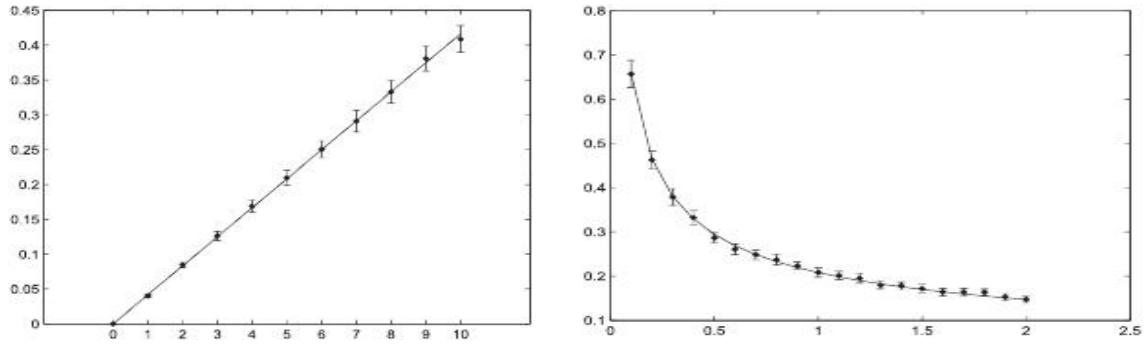

Fig - 3 Counterexample for selection of blocks with largest standard deviation

IV. Algorithm

Algorithm Estimate Clamor Variance

Takes the result of algorithm Get Upper Bound as the initial estimate and iteratively calls algorithm Get Next Estimate until convergence is reached. Parameter IMAX is the maximum number of iterations.

Algorithm Get Upper Bound computes a clamor variance

Upper bound. This algorithm is independent from illlustration block pyatykh et al.: illlustration clamor echelon estimation by principal component analysis.

V. EXPERIMENTS

I encompass evaluate the accuracy and the speed of our method on two databases: TID2008 and MeasTex the anticipated algorithm has been compared with several recent methods:

Manners which assume that the input illlustration has a sufficient amount of homogeneous areas:

a) Someplace Fisher's information is used in order to divide illlustration blocks into two groups: homogeneous Areas and textural areas.

b) To applies a Sobel edge detection operator in order to exclude the clamor-free illlustration content.

c) It can applies Palladian convolution and edge detection in order to and homogeneous.

d) To estimates the clamor standard deviation as the median absolute deviation of the wavelet coefficients at the finest decomposition echelon. The Daubechies wavelet of length 8 has been used in the experiments.

e) Someplace the clamor variance is estimated as the mode of the distribution of local variances.

f) Its divides the input illlustration into blocks and computes the block standard deviations.
g) To subtract low-frequency components detected by a Gaussian filter and edges detected by an edge detector from the input illlustration.

VI. Choice of the Parameters

I have tested our algorithm with different sets of the parameters; and I suggest the set presented in Table II. It has been used in all experiments in this section. Regarding block size M1 ×M2, there is a trade-off betIen the ability to handle complicated textures and the statistical significance of the result. In order to satisfy Assumption 1,I need to find correlations betIen pixels of the illlustration texture. Hence, the block size should be large enough, and, at least, be comparable to the size of the textural pattern.

VII. Clamor Echelon Inference Experiment with Tid2008

The TID2008 database contains 25 RGB illlustrations. 24 of them are real-world scenes and one illlustration is artificial. Each color constituent has been processed independently, i.e. the consequences for each clamor echelon have been obtained using 75 grayscale illlustrations. Noisy illlustrations with the clamor dissent 65 and 130 are included in the database; and I have additionally tested our method with the clamor variance 25 and 100. This catalog has been already applied for the evaluation of several other clamor echelon estimation methods Some illlustrations from the database are shown in Fig. 4.Though the reference illlustrations from TID2008 are painstaking as clamor-free illlustrations; they still contain a diminutive echelon of clamor.

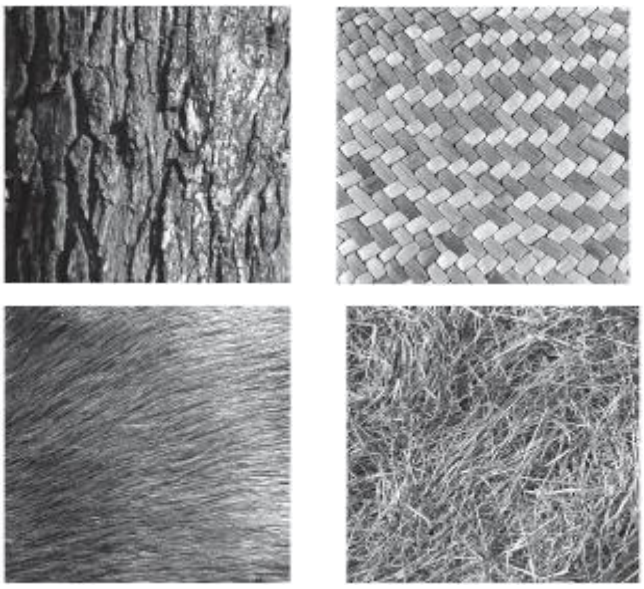

Fig - 4 Illlustrations from the TID2008 database

VIII. Clamor Echelon Estimation Experiments with Meastex

All illlustrations in the TID2008 database contain small or large identical area. Hoover, this is not the case for all illlustrations one can meet. For this reason, I have experienced our method on illlustrations containing only textures. I have selected the MeasTex texture database, which has been already used in many works on texture analysis. This database contains 236 real textures store as 512 × 512 grayscale illlustrations. Quite a lot of illlustrations from the catalog are shown in Fig. 5.The comparison fallout is presented .Compared with other methods, the accuracy of the projected manner.

Fig - 5. Images from the TID2008 database

IX. CONCLUSION

In this exertion, I have offered a new clamor echelon evaluation algorithm. The association with the several best state of the art methods shows that the correctness of the proposed approach is the highest in most cases. Among the methods with alike accuracy, our algorithm is forever more than 15 times faster. Since the proposed method does not require the existence of homogeneous areas in the input illlustration, it can also be applied to textures. Our experiment show that only stochastic textures, whose correlation properties are very close to those of white clamor, cannot be fruitfully processed. During our delousing experiments, I observed that privileged clamor echelon estimation accuracy leads to a higher delousing quality in most cases. It shows the magnitude of a careful selection of the clamor estimator in a delousing relevance.

REFERENCES

[1] Buades, B. Coll, and J. Morel, "On illlustration denoising methods," SIAM Multiscale Model. Simul., vol. 4, no. 2, pp. 490–530, 2005.
[2] K. Dabov, A. Foi, V. Katkovnik, and K. Egiazarian, "Illlustration denoising by sparse 3-D transform-domain collaborative filtering," IEEE Trans.Illlustration Process., vol. 16, no. 8, pp. 2080–2095, Aug. 2007.
[3] J. Walker, "Combined illlustration compressor and declamorr based on tree adapted wavelet shrinkage," Opt. Eng., vol. 41, no. 7, pp. 1520–1527, 2002.
[4] P. Rosin, "Thresholding for change detection," in Proc. 6th Int. Conf. Comput. Vis., 1998, pp. 274–279.
[5] M. Salmeri, A. Mencattini, E. Ricci, and A. Salsano, "Clamor estimation in digital illlustrations using fuzzy processing," in Proc. Int. Conf. Illlustration Process., vol. 1. 2001, pp. 517–520.

AUTHORS

C. BALA SARAVANAN received the M.Tech (I.T) from Sathyabama University in 2011. During 2009-2010, I stayed in orbit technologies as software engineer to develop health care automation tool.And I am doing (Ph.D) in VELTECH University and I am now working in VelTech MultiTech Dr.Rangarajan Dr.Sakunthala Engineering College as Assistant Professor and IBM TGMC Project Coordinator

M. RAJESH KHANNA received the M.E degree in computer science and engineering from B.S.A Crescent Engineering College in 2009. During 2009-2010, he stayed in orbit technologies as software engineer to develop health care automation tool. He is now working in VelTech MultiTech Dr.Rangarajan Dr.Sakunthala Engineering College as Assistant Professor and IBM TGMC Project Coordinator.

J.ARAVIND pursuing M.Tech(I.T) in VelTech MultiTech Dr.Rangarajan Dr.Sakunthala Multi Tech Engineering College

R.RAMESH pursuing M.Tech(I.T) in VelTech MultiTech Dr.Rangarajan Dr.Sakunthala Multi Tech Engineering College

M.JEYALAKSHMI pursuing M.Tech(I.T) in VelTech MultiTech Dr.Rangarajan Dr.Sakunthala Multi Tech Engineering College

International Journal of Modern Engineering Research (IJMER)
www.ijmer.com Vol. 3, Issue. 4, Jul - Aug. 2013 pp-2530-2536 ISSN: 2249-6645

Power System Stability Enhancement Using Static Synchronous Series Compensator (SSSC)

B. M. Naveen Kumar Reddy[1], Mr. G. V. Rajashekar[2], Dr. Himani Goyal[3]
[1]*M. Tech (PE), Dept. Of EEE, Aurora's Engineering College, Bhongir, A.P*
[2]*Associate Professor, Aurora's Engg. College, Bhongir, A.P*
[3]*Professor & HOD Dept. of EEE, Aurora Engg. College, Bhongir, A.P*

Abstract: *This paper investigates the problem of controlling and modulating power flow in a transmission line using a Synchronous Static Series Compensator (SSSC). The studies, which include detailed PWM techniques controlled for SSSC, are conducted and the control circuits are presented. In this study, a static synchronous series compensator (SSSC) is used to investigate the effect of this device in controlling active and reactive powers as well as damping power system oscillations in transient mode. The SSSC equipped with a source of energy in the DC link can supply or absorb the reactive and active power to or from the line.*

Simulations have been done in MATLAB/SIMULINK environment. Simulation results obtained for selected bus-2 in two machine power system shows the efficacy of this compensator as one of the FACTS devices member in controlling power flows, achieving the desired value for active and reactive powers, and damping oscillations appropriately.

Keywords: *static synchronous series compensator (SSSC), FACTS, Two machine power system, active and reactive powers.*

I. INTRODUCTION

Nowadays, the need for flexible and fast power flow control in the transmission system is anticipated to increase in the future in view of utility deregulation and power wheeling requirement. The utilities need to operate their power transmission system much more effectively, increasing their utilization degree. Reducing the effective reactance of lines by series compensation is a direct approach to increase transmission capability. However, power transfer capability of long transmission lines is limited by stability considerations. Because of the power electronic switching capabilities in terms of control and high speed, more advantages have been done in FACTS devices areas and presence of these devices in transient stability during transient faults resulting in improvement in power system stability [1].

This paper investigates the static synchronous series compensator (SSSC) FACTS controller performance in terms of stability improvements. A Static Synchronous Series Compensator (SSSC) is a member of FACTS family which is connected in series with a power system. It consists of a solid state voltage source converter (VSC) which generates a controllable alternating current voltage at fundamental frequency. When the injected voltage is kept in quadrature with the line current, it can emulate as inductive or capacitive reactance so as to influence the power flow through the transmission line [2,3]. While the primary purpose of a SSSC is to control power flow in steady state, it can also improve transient stability of a power system.

II. SSSC CONFIGURATION

The basic scheme of the SSSC is shown in Fig. 1. The compensator is equipped with a source of energy, which helps in supplying or absorbing active power to or from the transmission line along with the control of reactive power flow.

As the name suggests, SSSC is a series compensator. It is connected in series with the transmission line. Three phase series transformers are used to connect the compensator in series with the power system.

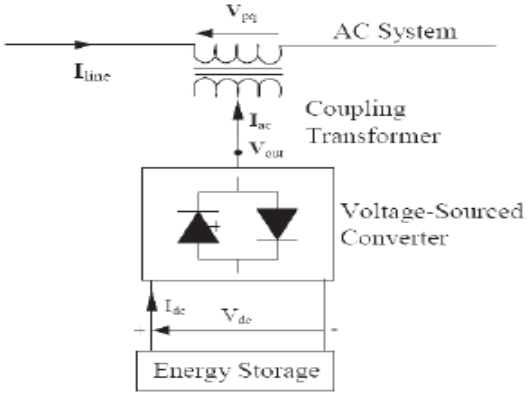

Figure 1. Static synchronous series capacitor

III. BASIC OPERATING PRINCIPLES OF THE SSSC

Fig.1 shows a functional model of the SSSC where the dc capacitor has been replaced by an energy storage device such as a high energy battery installation to allow active as well as reactive power exchanges with the ac system. The SSSC's output voltage and phase angle can be varied in a controlled manner to influence power flows in a transmission line. The phase displacement of the inserted voltage V_{pq}, with respect to the transmission line current *line I* , determines the exchange of real and reactive power with the ac system.

Fig. 2 shows the SSSC operation in four quadrants, again assuming an energy storage device connected at the SSSC's input terminals. The line current phasor I_{line} is used as a reference phasor while the injected SSSC voltage phasor is allowed to rotate around the center of the circle defined by the maximum inserted voltage V^{max}_{pq} .

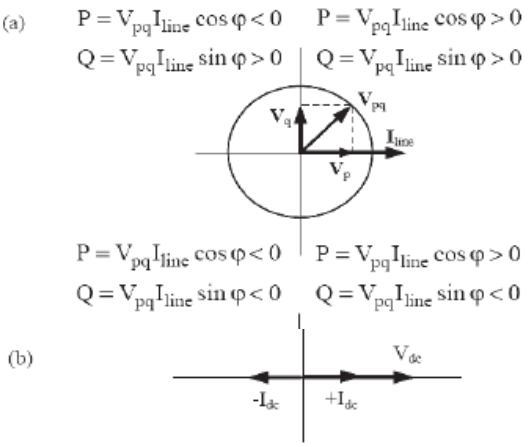

Fig 2. SSSC phasor diagram

Theoretically, SSSC operation in each of the four quadrants is possible, Theoretically, SSSC operation in each of the four quadrants is possible, but there are some limitations to the injected SSSC voltage due to operating constraints of practical power system. In capacitive mode, the injected SSSC voltage is made to lag the transmission line current by90° ; in this case, the SSSC operation is similar to the operation of a series capacitor with variable capacitance kXc, i.e., pq C line V = − jKX_cI_{line}, where k is a variable. By this action, the total transmission line reactance is reduced while the voltage across the impedance is increased, leading to increase in the line currents and transmitted power. This action is illustrated in Fig. 3. It is also possible to reverse the injected SSSC voltage by 180° , i.e., pq line −V = jKX_cI_{line} causing an increase in the transmission line reactance, which results in a decrease of the line current and transmitted power. While this equation for V_{pq} shows changes in the phasor magnitude and phase angle, it can be somewhat misleading, since it shows that the series injected voltage magnitude is directly proportional to the line current magnitude. In reality, this is not true; the inserted voltage magnitude is set by the SSSC control and is independent of the network impedance and, consequently, line current changes. It is assumed that the SSSC losses are zero and, therefore, the series injected voltage is in perfect quadrature with the line current, leading or lagging.

IV. CONTROL SYSTEM OF SSSC

SSSC is similar to the variable reactance because the injected voltage and current to the circuit by this device are changing depend upon to the system conditions and the loads entering/getting out. For responding to the dynamic and transient changes created in system, SSSC utilizes the series converter as shown in Fig. 3.

One side of the converter is connected to the AC system and the other side is connected to a capacitor and battery which in the system we assume DC source as battery. If a dynamic change in system will be occurred, SSSC circuit works such that according to the control circuit in Fig. 4 the energy of battery will be converted to the ac form by converter and then injecting this voltage to the circuit the changes will be damped appropriately.

To control the active and reactive powers of bus-2, the control circuit as shown in Fig. 3 is utilized. For controlling the powers, first, sampling from the voltage and current is One side of the converter is connected to the AC system and the other side is connected to a capacitor and battery which in the system we assume DC source as battery. If a dynamic change in system will be occurred, SSSC circuit works such that according to the control circuit in Fig. 4 the energy of battery will be converted to the ac form by converter and then injecting this voltage to the circuit the changes will be damped appropriately.

To control the active and reactive powers of bus-2, the control circuit as shown in Fig. 3 is utilized. For controlling the powers, first, sampling from the voltage and current is done and transformed to the dq0 values. Active and reactive powers of bus-2 are calculated using their voltage and current in dq0 references and compared with the determined reference and the produced error signal is given to the PI controllers. Adjusting parameters of the PI controllers, we are trying to achieve the zero signal error such that powers can follow the reference powers precisely. Then, the output of the controllers are transformed to the abc reference and given to the PWM.

V. TWO MACHINE POWER SYSTEM MODELINGSING

The dynamic performance of SSSC is presented by real time voltage and current waveforms. Using MATLAB software the system shown in Fig. 5 has been obtained. In the simulation one SSSC has been utilized to control the power flow in the 500 KV transmission systems. This system which has been made in ring mode consisting of 4 buses (B1 to B4) connected to each other through three phase transmission lines L1, L2-1, L2-2 and L3 with the length of 280, 150, 150 and 5 km respectively. System has been supplied by two power plants with the phase-to-phase voltage equal to 13.8 kv.

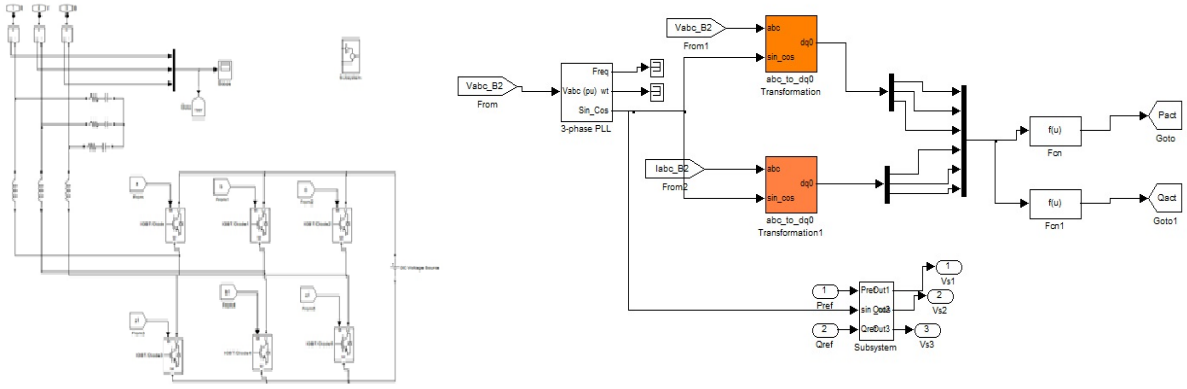

Figure 3. The convertor of SSSC

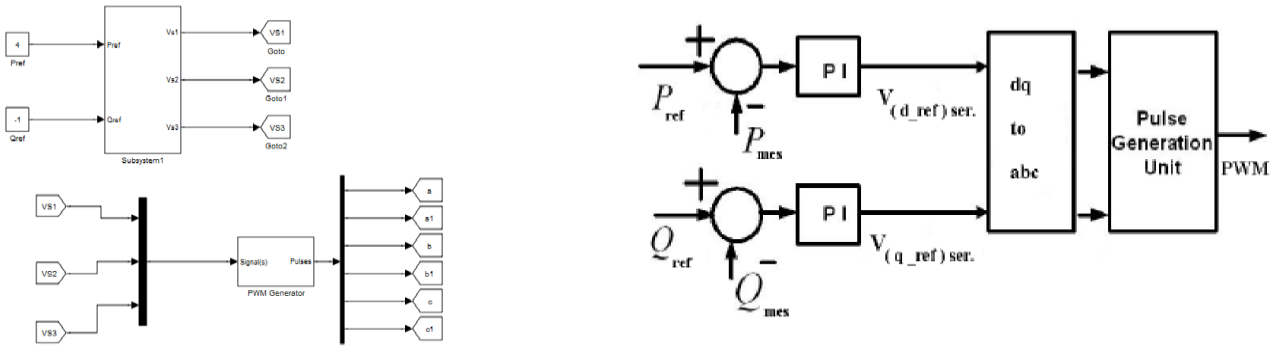

a) Simulated control signal generation using pwm generator circuit

b) Single line diagram

Figure 4. The control circuit of SSSC

Active and reactive powers injected by power plants 1 and 2 to the power system are presented in per unit by using base parameters Sb = 100MVA and
Vb=500KV, which active and reactive powers of power plants 1 and 2 are (24-j3.8) and (15.6-j0.5) in per unit, respectively.

VI. Simulation Results With MATLAB/SIMULINK

First, power system with two machines and four buses has been simulated in MATLAB environment, and then powers and voltages in all buses have been obtained. The results have been given in Table. Using obtained results bus-2 has been selected as a candidate bus to which the SSSC be installed. Therefore, the simulation results have been focused on bus-2.

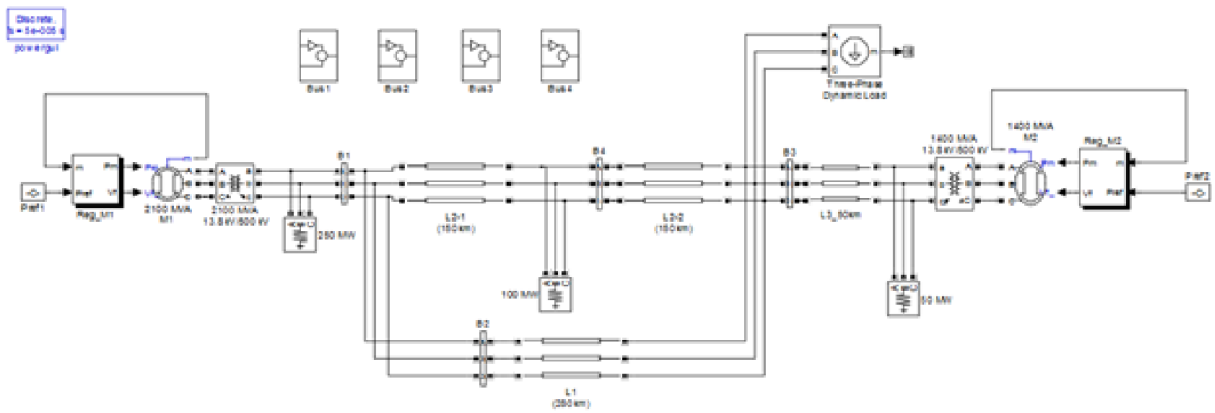

Figure 5. The configuration of two machine power system

TABLE I. OBTAINED RESULT FROM THE SIMULATIONS

Bus No.	Voltage	Current	Active Power	Reactive Power
1	1 pu	13.5 pu	20.06 pu	-3.77 pu
2	1 pu	6.7 pu	9.96 pu	1.82 pu
3	1 pu	10 pu	14.84 pu	-0.49 pu
4	1 pu	5.55 pu	8.45 pu	-.059 pu

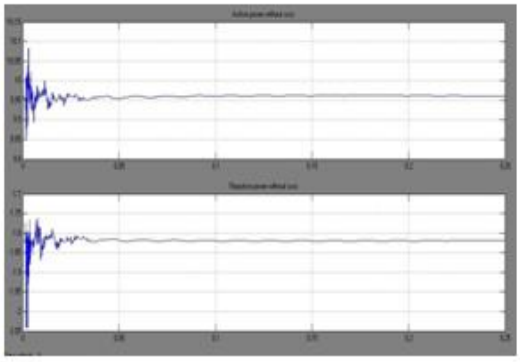

Figure 6. Active and reactive powers of bus-2 without the installation of SSSC

VII. CASE STUDIES

A. Bus-2 parameters without SSSC

Changes in current, voltage, active and reactive powers of bus-2 have been obtained in real time. According to the Figure. 6, at first, due to the large loads of the system active power of bus-2 got oscillations which keep continuing for 3 seconds. However, the controlling systems in power plants 1 and 2 such as governor, PSS and other stabilizing devices are used for damping these oscillations. As shown in Figure. 6, because of the abovementioned reasons reactive power of bus-2 got oscillations at first and then will be damped properly. Oscillations amplitude for active power is more than reactive power, and this is because the ohmic parts of loads of system are much more.

According to Figure. 7, after transient mode created at first in system, voltage and current waveforms of bus-2 got closer to sinusoidal waveforms. Voltage amplitude is 1 per unit, but, despite the drawn currents by loads in system, current amplitude is 6.7 pu.

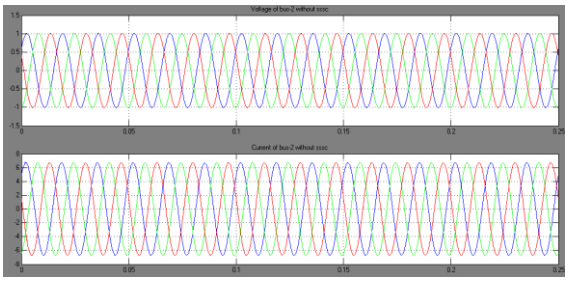

Figure. 7 Voltages and Currents of bus-2 without the installation of SSSC

B. Bus-2 parameters with SSSC

As shown in Figure.8, SSSC has been placed between bus-1 and bus-2 and the aim is achieving the following active and reactive powers:

P_{ref} = 4 pu ; Q_{ref} = -1 pu

The main role of SSSC is controlling the active and reactive powers; beside these SSSC could fairly improve the transient oscillations of system.

After the installation of SSSC, besides controlling the power flow in bus-2 we want to keep constant the voltage value in 1 per unit, hence the power flow is done in the presence of SSSC and the simulation results are as follows.

According to the Fig. 9, by installing the SSSC, active power damping time will be less than the mode without SSSC and it will be damped faster. Also as shown in Fig. 9, reactive power damping time will be decreased and system will follow the references value with acceptable error.

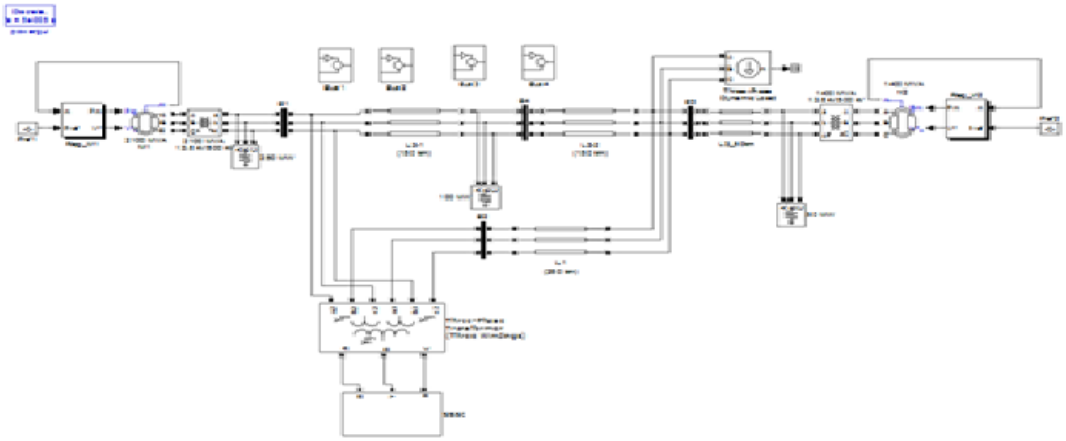

Figure 8. Two machines system with SSSC

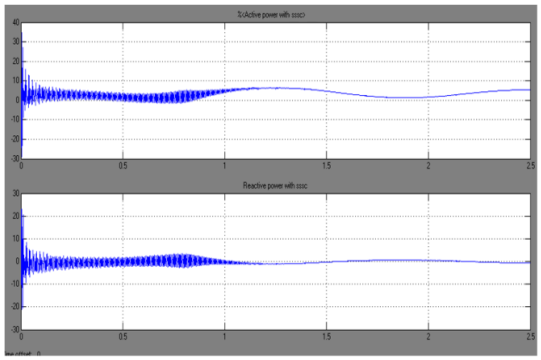

Figure 9. Active and reactive power of bus-2 in the presence of SSSC

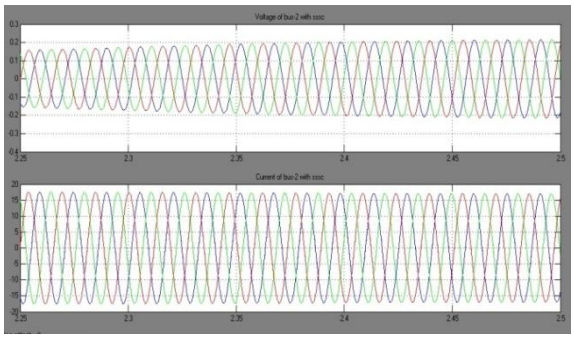

Figure. 10, Voltage and currents of bus-2 in the presence of SSSC

As shown in Fig. 10, Current of bus-2 in the presence of SSSC after transient mode will be in the form of sinusoidal form.

C. Bus-2 parameters with a fault without SSSC

In this section a three phase fault is applied to the power system, and observing the system performance without using SSSC.

Here, as shown in figure. 11, circuital arrangement having three phase faults is modeled using MATLAB/SIMULINK software. Figure 12 shows the active and reactive powers of bus-2

Figure 13 shows the voltage and currents of bus-2 for the system shown above. In this chapter, we conclude that the applied fault make disturbances in the system for a long time.

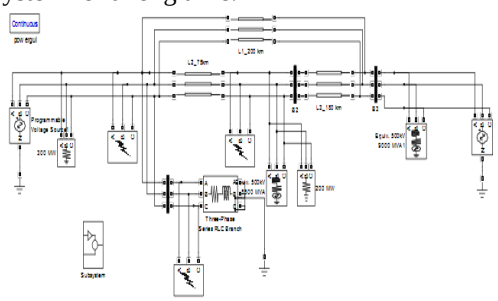

Figure. 11, Two machine system with a fault without SSSC

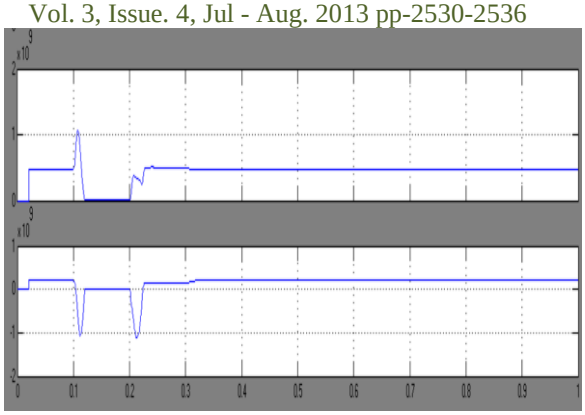

Figure. 12. Active and reactive powers of bus-2 with a fault without applying SSSC

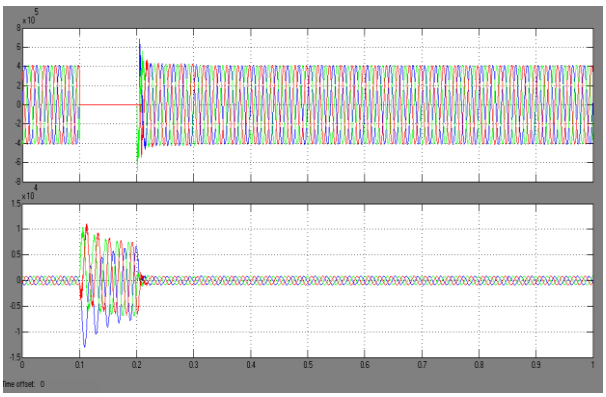

Figure. 13. Voltage and currents of bus-2 with a fault without applying SSSC

D. Bus-2 parameters with a fault with SSSC

To further test the proposed SSSC controller, a three phase fault is applied at Bus 2.also, in this simulation the transition times is set as follows: [0 1 1.5 2]; In Fig. 14, the simulation result shows that the power oscillation on the L1 line following the three-phase fault. Moreover the performed simulation indicates that the SSSC compensator is a very effective tool to damp power oscillation.

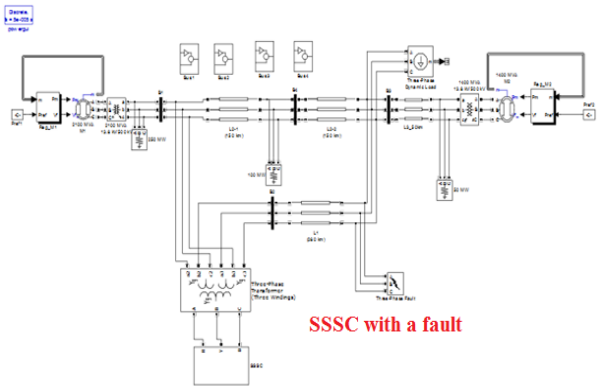

Figure. 14, Two machine system with a fault with SSSC

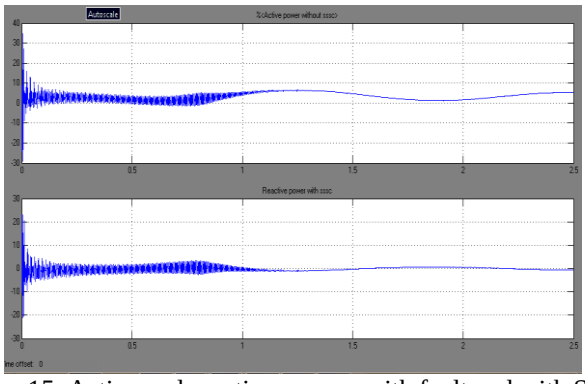

Figure. 15. Active and reactive powers with fault and with SSSC

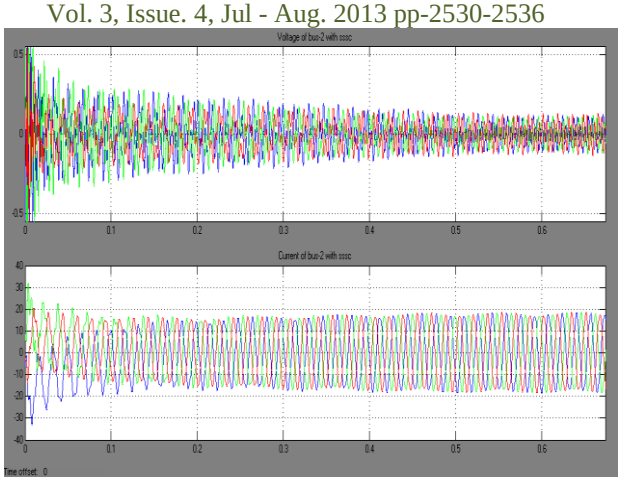

Figure. 16. Voltage and currents of bus 2 with fault and with SSSC

VIII. CONCLUSION

It has been found that the SSSC is capable of controlling the flow of power at a desired point on the transmission line. It is also observed that the SSSC injects a fast changing voltage in series with the line irrespective of the magnitude and phase of the line current.

This paper, the SSSC is used to damp power oscillation on a power grid following a three-phase fault Based on obtained simulation results the performance of the SSSC has been examined in a simple two-machine system simply on the selected bus-2, and applications of the SSSC will be extended in future to a complex and multi machine system to investigate the problems related to the various modes of power oscillation in the power systems.

REFERENCES

[1] Gyugyi, L. (1989). "Solid-state control of AC power transmission." *International Symposium on Electric Energy Conversion in Power System*, Capri, Italy, (paper No. T-IP.4).

[2] Sen, K.K. (1998). "SSSC-static synchronous series compensator: theory, modeling and publications." IEEE Trans. Power Delivery. Vol. 13, No.1, January, PP. 241-246.

[3] L. Gyugyi, 1994, "Dynamic Compensation of AC Transmission Line by Solid State Synchronous Voltage Sources," IEEE Transactions on Power Delivery, 9(22), pp. 904-911.

[4] Muhammad Harunur Rashid, "Power Electronics – Circuits, Devices, and Applications, "PRENTICE HALL, Englewood Cliffs, New Jersey.07632, 1988.

[5] Amany E L – Zonkoly, "Optimal sizing of SSSC Controllers to minimize transmission loss and a novel model of SSSC to study transient response, "Electric power Systems research 78 (2008) 1856 – 1864.

[6] B.N.Singh, A.Chandra, K.Al-Haddad and B.Singh, "Performance of sliding-mode and fuzzy controllers for a static synchronous series compensator, "IEE Proceedings onhe no. 19990072, IEE, 1999.

[7] F. Wang, "Design of SSSC Damping Controller to Improve Power System Oscillation Stability, "0-7803-5546-6/99/$10.00 © 1999 IEEE.

[8] A. Kazemi, M. Ladjevar DI and M.A.S. Masoum, "Optimal Selection of SSSC Based Damping Controller Parameters for Improving Power System Dynamic Stability Using Genetic Algorithm "Iranian Journal of Science & Technology, Transaction B, Engineering, Vol. 29, No. B1 Printed in the Islamic Republic of Iran, 2005 © Shiraz University.

[9] I. S. Jacobs and C. P. Bean, "Fine particles, thin films and exchange anisotropy," in Magnetism, vol. III, G. T. Rado and H. Suhl, Eds. New York: Academic, 1963, pp. 271–350.

BIOGRAPHY

B.M. Naveen Kumar Reddy has received his B.Tech degree fron Sindhura Engineering College, Ramagundam. He is post graduated in M.Tech(P.E) stream from Department of Electrical and Electronics Engineering from Aurora's Engg. College, Bhongir.

Presently he is working as an Assistant professor in Vidya Bharathi Institute of Technology, Hyderabad.

International Journal of Modern Engineering Research (IJMER)
www.ijmer.com Vol. 3, Issue. 4, Jul - Aug. 2013 pp-2537-2544 ISSN: 2249-6645

Productivity Improvement by Designing Storage Systems in a Manufacturing Industry

B. A. Magdum[1], Prof. Dr. M. Y. Khire[2]
[1](Mechanical Department, Walchand College of Engineering, An Autonomous Institute, Sangli, Maharashtra, India)
[2](Mechanical Department, Walchand College of Engineering, An Autonomous Institute, Sangli, Maharashtra, India)

ABSTRACT: *Productivity is crucial to the welfare of the industrial firm as well as for the economic progress of the country. High productivity refers to doing the work in a shortest possible time with least expenditure on inputs without sacrificing quality and with minimum wastage of resources. Originally, it was used only to rate the workers according to their skills. A system of measurement was then evolved to compare the improvement made in relation to the rate of output and in order to improve productivity. One way to improve productivity is to reduce the non-value added activities such as searching time reduction, idle time reduction, etc. Therefore, to emphasis on design of storage systems which reduces the searching time as a tool for improving productivity, a case study has been conducted on selected number of items of one of the leading pump manufacturing company from Western Maharashtra. Since it is impossible to devote equal attention to all items, it is desirable to concentrate on those items which are of highest value and most important. This paper deals with design of storage systems.*

Keywords: *Non-value added activities, Productivity.*

I. INTRODUCTION

Productivity is the quantitative relationship between what we produce and what we use as a resource to produce them, i.e. arithmetic ratio of amount produced (output) to the amount of resources (input). Productivity can be expressed as:

Productivity = Output / Input

This means to improve productivity, output (numerator) should be increased and input (denominator) should be decreased. The manufacturing industries mainly focus on production. To improve the productivity, it requires increasing production. [1]

The production can be increased by effective utilization of resources such as man, machine, material, money, etc. There should not be any delay in production. So that targeted production value can be achieved. Delay in production occurs due to time wasting in searching of required tool, material, etc. For that purpose, study has been carried out in the company and only those materials are selected which requires frequently during production. On the basis of collected data storage systems are designed and implemented on the shop floor. [2]

II. PRESENT SITUATION OF SHOP FLOOR

The Production division of the company is divided into different sections. In grinding section, grinding of line shaft, impeller shaft and column shaft as well as grinding of rubber sleeves, shaft sleeves, etc. is carried out. For grinding of these parts mandrels are required, but there was not any system for mandrels. They were dispersed anywhere on the shop floor.

In assembly section, hydro testing of pumps is carried out. In hydro testing all the bores of pumps i.e. suction bore, delivery bore, etc. are tightly closed with the help of pressure plates and through one bore which is kept open water is filled in pump. The pump is completely filled with water and maximum pressure limit for which pump sustains is recorded by using gauges. For that purpose pressure plates are required. Pressure plates are made up of high carbon steel plates. There are more than 250 pressure plates available. But they were not present at work station. Worker required searching of the required pressure plates.

Each time worker takes his vernier, micrometer, etc. Go on searching mandrel or pressure plate on shop floor. If the worker is permanent employee he knows where he will get the required mandrel or pressure plate. But the temporary worker faces many problems to get the required mandrel or pressure plate. He wastes much of his working time in searching the required mandrel or pressure plate.

III. DESIGN OF STORAGE SYSTEMS

3.1 DESIGN OF RACK SYSTEM FOR MANDRELS

When observed the present practice, it was noted that most of production time was wasted in searching required mandrel (about 2 to 3 hours out of 8 hours of production time). So to design the rack system for mandrels following steps are followed:

(1) Carry out the study of machines for which mandrels are required.

Following points are observed during study:

a. Component to be grinded
b. Drawing dimensions
c. Nominal mandrel diameter
d. Time to search required mandrel

e. Number of components to be machined.
f. Remarks.

(2) Searching all the mandrels dispersed on the shop floor.
(3) Measurement of dimensions of mandrels.
For designing the rack system important dimensions are:
a. Length (L) in mm.
b. Diameter (D) in mm.
(4) Find out the mandrels which are frequently required.
(5) Design the rack system for those mandrels.
Length and diameter of mandrels were measured and arranged in ascending order of first diameter and then length.

3.1.1 DIMENSIONS OF FREQUENTLY USED MANDRELS

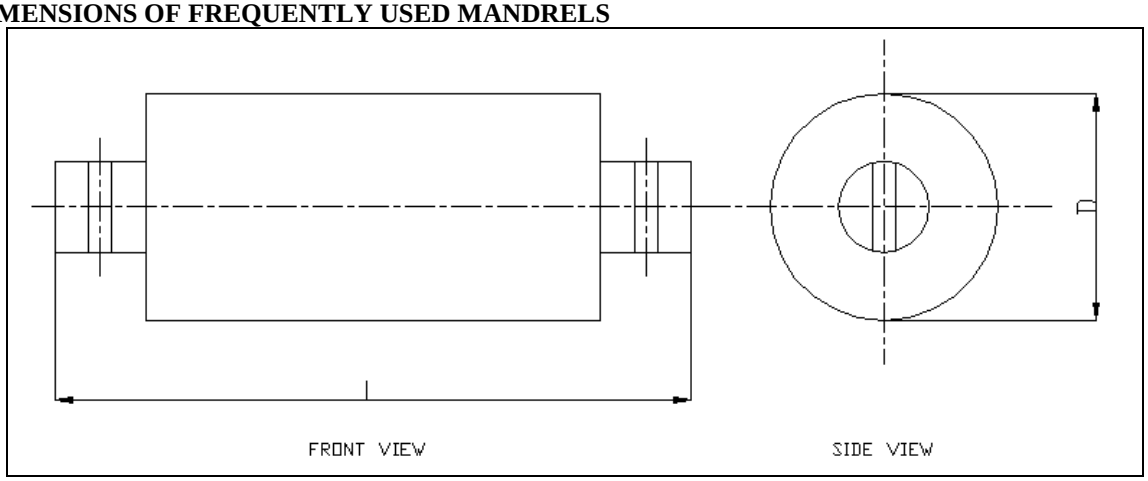

Fig.3.1.1: Mandrel

Table 3.1.1: Dimensions of frequently used mandrels

Sr.No.	Diameter (D)mm	Length (L)mm	Sr.No.	Diameter (D)mm	Length (L)mm
SET 1			SET 2		
1	120	630	**15**	140	865
2	120	710	**16**	140	910
3	123	820	**17**	141	575
4	125	670	**18**	143	600
5	125	740	**19**	145	793
6	130	810	**20**	145	920
7	130	810	**21**	146	720
8	131	920	**22**	150	860
9	132	570	**23**	150	900
10	132	780	**24**	152	620
11	134	820	**25**	155	750
12	135	720	**26**	155	900
13	139	796	**27**	156	1020
14	140	790	**28**	163	740

3.1.2 GIVEN CONDITIONS FOR RACK

(1) Maximum height of rack designed should be less than 1800mm.
(2) There should not be any complications while taking out mandrel from rack.
(3) There should be some cushioning for mandrels.
(4) All the mandrels should be stored in rack.
(5) Heavy weight mandrels should be at bottom of the rack and light weight mandrels should be at top.

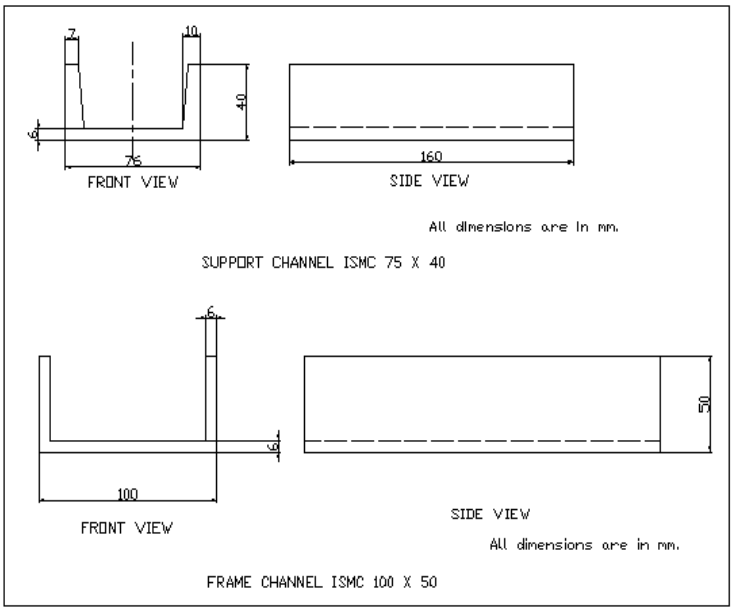

Fig.3.1.2 Frame channel ISMC 100 X 50 Selected for rack

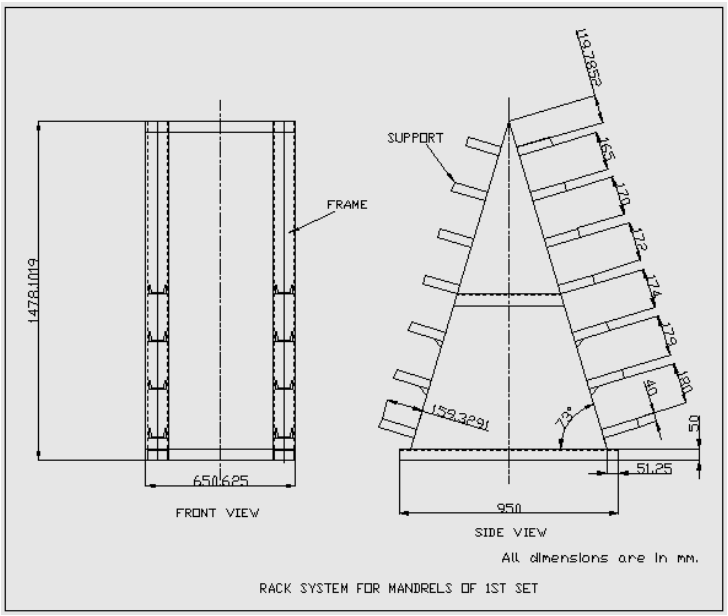

Fig.3.1.3: Rack system for mandrels of 1st set

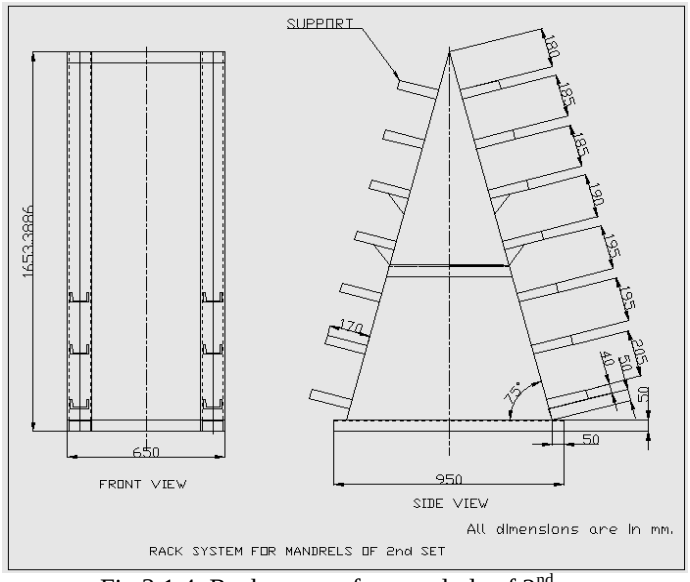

Fig.3.1.4: Rack system for mandrels of 2nd set

3.2 DESIGN OF STORAGE SYSTEM FOR PRESSURE PLATES

3.2.1 STEPS IN DESIGN OF STORAGE SYSTEM FOR PRESSURE PLATES

For designing the storage system for pressure plates following steps are followed:

(1) Creating database of pressure plates by physically measuring the dimensions of pressure plates.
For designing the storage system important dimensions are:
(a) Outer diameter (OD) in mm.
(b) Width (W) in mm.

(2) Design the storage system for those pressure plates.

3.2.2 PARAMETERS CONSIDERED FOR STORAGE SYSTEM OF PRESSURE PLATESs

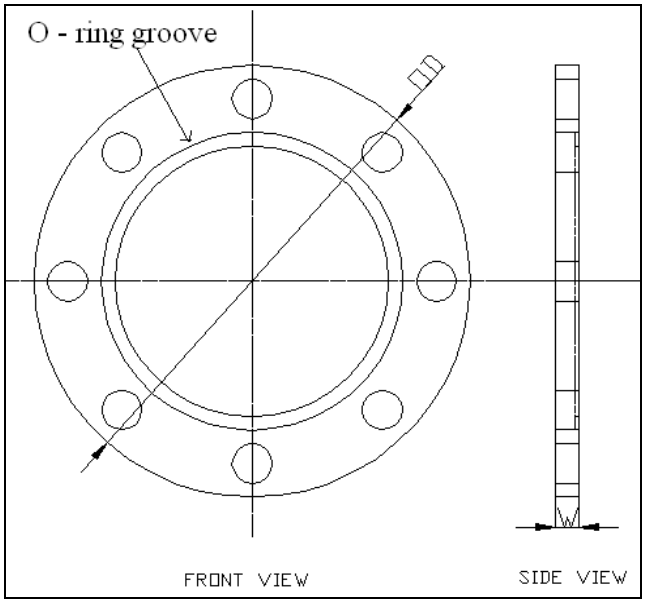

Fig.3.2.1: Pressure plate

The above Fig. 3.2.1 shows the important dimensions of pressure plate. Outer diameter and width of pressure plates are measured and arranged in ascending order of outer diameter and then width.

3.2.3 GIVEN CONDITIONS FOR STORAGE SYSTEM

(1) Maximum height of storage system designed should be less than 2100mm.
(2) There should not be any complications while taking out pressure plate from storage system.
(3) Maximum number of pressure plates should be stored in storage system.
(4) Heavy weight pressure plates should be at bottom of storage system and light weight pressure plates should be at top.

3.2.4 PRESSURE PLATES SELECTED FOR DESIGNING THE STORAGE SYSTEM

Out of all the pressure plates 30 number of pressure plates in the range of 740 mm to 805 mm outer diameter are selected for designing the storage system. Selected pressure plates are listed in Table 3.2.1.

Table 3.2.1: Pressure plates selected for designing the storage system

Sr. No.	Plate No.	Outer diameter (OD) in mm.	Width (W) in mm.
RACK 1			
1	174	740	47
2	6	740	105
3	244	750	45
4	271	750	60
5	21	750	64
6	239	750	100
7	170	753	50
8	19	780	120
9	177	780	131
10	267	785	40

RACK 2			
11	157	753	88
12	260	755	58
13	28	756	57
14	158	757	121
15	254	760	37
16	85	770	133
17	250	775	105
18	147	775	107
19	4	776	50
20	247	780	42
RACK 3			
21	278	785	42
22	249	785	55
23	269	785	70
24	188	785	86
25	231	790	100
26	7	790	126
27	24	795	58
28	143	795	98
29	167	800	125
30	11	805	41

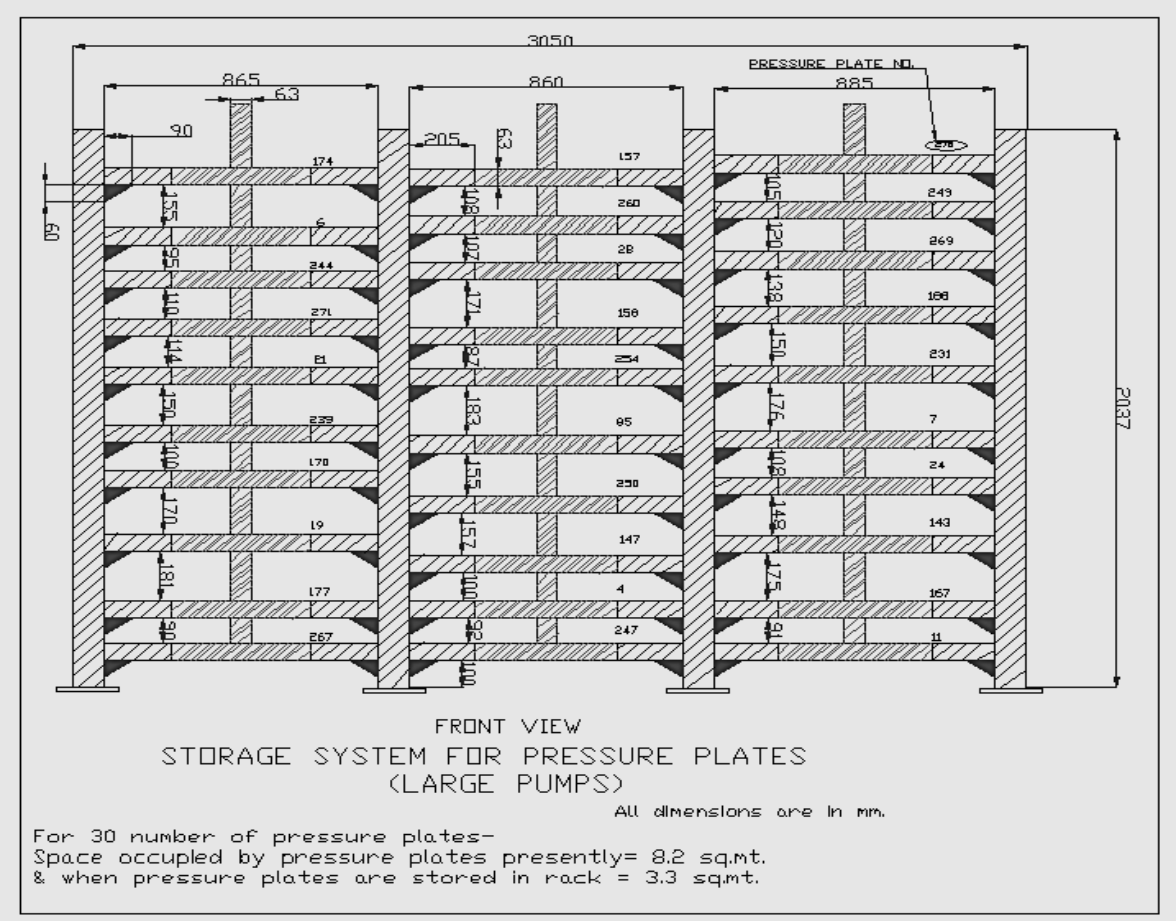

Fig.3.2.2: Front view of storage system for pressure plates

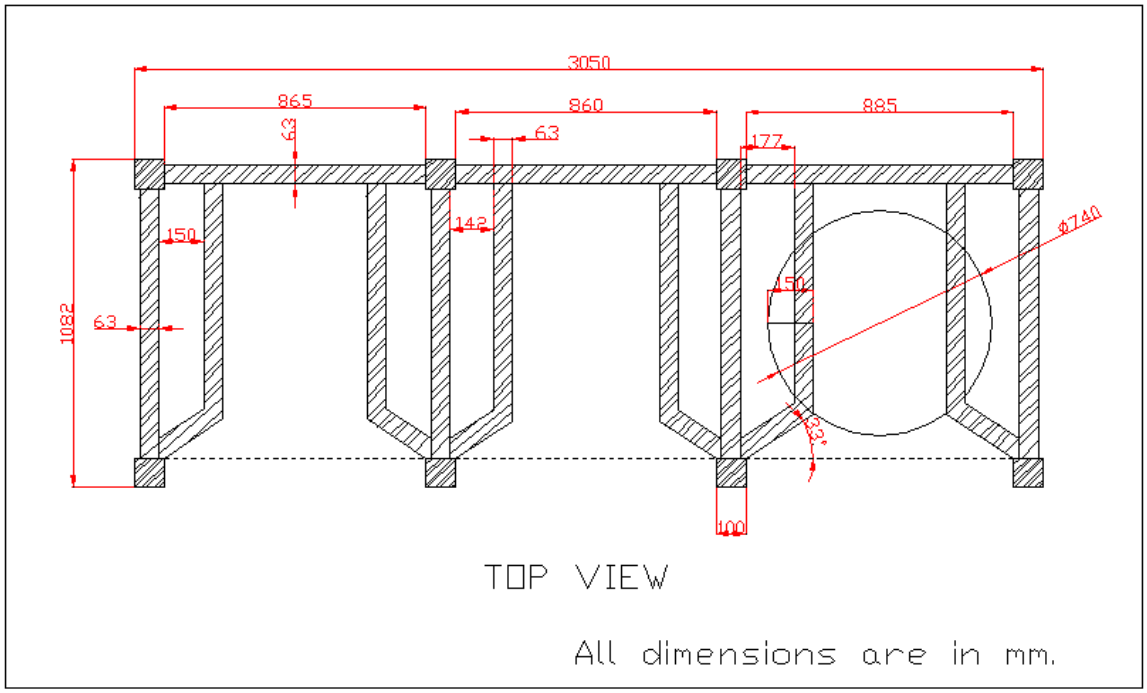

Fig.3.2.3: Top view of storage system for pressure plates

IV. COST SAVING, SPACE UTILIZATION AND PRODUCTIVITY IMPROVEMENT

4.1 PRODUCTION ENHANCEMENT IN GRINDING SECTION

Situation of grinding section before improvement was as given below.
Total time wasted in searching the required mandrel and carrying it up to the machine
= (Total production time – Total machining time) min.
= (420 – 180)
= 240 min.

Total time wasted in searching the required mandrel and carrying it up to the machine in terms of percentage of total production time
= (240 / 420) * 100
= 57.13 %
Average number of components ground by worker in a shift = 4

Situation of grinding section after improvement is as given below.
Number of components ground in a shift
= (Total production time) / (Average time required to grind the component)
= 420 / 45
= 9

Increase in production in comparison with the production before improvement is shown in Fig.4.1.

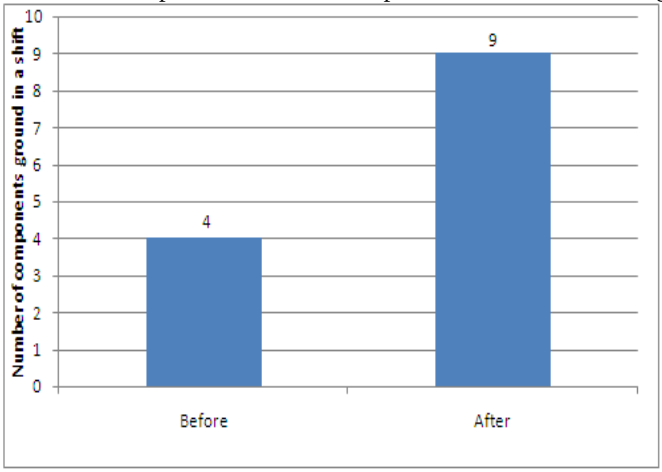

Fig.4.1: Number of components ground before and after improvement

4.2 COST SAVING IN MANUFACTURING OF STORAGE SYSTEM FOR PRESSURE PLATES

Weight of the storage system = 1250 kg
If storage system is given to vendor for manufacturing
Total cost = Material cost + Labour cost
= 55,000 Rs. + 10,000 Rs.
= 65,000 Rs.

If storage system is manufactured in house by using scrap material available only labour charges require paying.
Scrap material cost = 18 Rs. /Kg
Therefore,
Cost of scrap material = 18 x 1250 Rs.
= 22,500 Rs.
Total saving = Vendor's Total cost – (Scrap material cost + Labour cost)
= 65,000 – (22,500+10,000) Rs.
= 32,500 Rs.

The cost saved after manufacturing the storage system in house is compared with the vendor rate as shown in Fig.4.2.

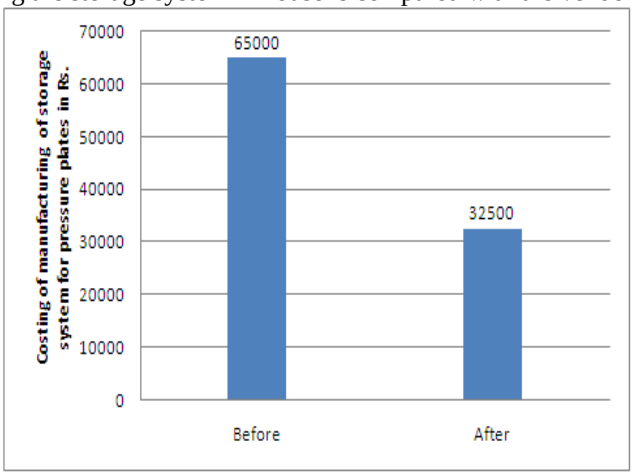

Fig.4.2: Cost saving in manufacturing of storage system for pressure plates

4.3 SPACE UTILIZATION

Before implementation of storage system, pressure plates were kept on shop floor. In that situation space occupied by 30 number of pressure plates was 8.2 m^2.
After implementation of storage system space require for 30 number pressure plates is 3.3 m^2.

V. CONCLUSION

The industry is successfully implementing storage systems and getting better results. The productivity of the industry is improved and quality of their products is enhanced.

The situation of mandrels and pressure plates are shown in Photo 5.1 to Photo 5.4.

Photo 5.1: Situation of mandrels before improvement

Photo 5.2: Improved situation of mandrels

Photo 5.3: Situation of pressure plates before improvement

Photo 5.4: Improved situation of pressure plates

The design of storage system gives following advantages

1. After implementing the designed storage systems required mandrels, pressure plates are found without any time loss i.e. searching time is reduced.
2. The storage systems are vertical as per workplace organization system.[3][4]
3. Easy accessibility because forklift driver can easily retrieve the pressure plate without anyone's help.
4. Almost 50 % of space is released.
5. Chances of accidents are reduced.
6. Storage system is manufactured by using in house scrap material which saved around 32,500 Rs

ACKNOWLEDGEMENT

On the submission of the paper report of "Productivity Improvement by Designing Storage Systems in a Manufacturing Industry" I would like to pay my a deep sense of gratitude that I express my sincere regards to my guide Prof. Dr. M. Y. Khire (Head of the Mechanical Department) for his invaluable guidance, constructive suggestions, encouragement and moral support at every stage of this work. He really boosted me in all the difficult and confusing situations.

I would be always grateful to my company guide where I carried out this work and company staff for their invaluable help. It was really difficult to complete this work without their involvement.

REFERENCES

[1] Goldratt, Eliyahu M., Cox. and Jeff, *The Goal: Excellence in Manufacturing* (Great Barrington: North River Press, 1984)
[2] Goldratt, Eliyahu M., Cox. and Jeff, *The Goal: A Process of Ongoing Improvement. (Revised edition.)* (Great Barrington: North River Press, 1986)
[3] Samuel, K. M. Ho, *Five S to Business Excellence* (Oshikawa: Kogan Page, 1993)
[4] Hirano, H., *Five Pillars of the Visual Workplace* (PHP Institute. Productivity Press, 1995)

International Journal of Modern Engineering Research (IJMER)
www.ijmer.com Vol. 3, Issue. 4, Jul - Aug. 2013 pp-2545-2552 ISSN: 2249-6645

Static Sustenance of Power System Stability Using FLC Based UPFC in SMIB Power System

L. Harini[1], Y. Hazarathaiah[2]
[1](M. Tech Student, S.K.T.R.M College of Engineering, Kondair-509125, Mahabubnagar, Andhra Pradesh)
[2](EEE Department, S.K.T.R.M College of Engineering, Kondair-509125, Mahabubnagar, Andhra Pradesh)

Abstract: *The unified power flow controller is the most versatile and complex power electronic equipment that has emerged as the indispensable equipment used to control the power flow ,to boost the transmission capacity and to optimize stability of the power system. Low frequency power system oscillations are inevitable characteristics of power systems and they greatly affect the transmission line transfer capability and power system stability. This paper present a control method for damping low frequency system oscillations using fuzzy logic controller installed in a single- machine infinite-bus power system. The UPFC uses two converters coupled through a common DC link to improve the dynamic performance of the system. System response with proportional UPFC controller and proportional fuzzy logic(using mamdani-type inference) based UPFC controller are compared at variable loading conditions through software simulation. The results of the simulation shows that the UPFC with fuzzy-based controller is effectively damping the Low frequency oscillations.*

Keywords: *Unified Power Flow Controller (UPFC), Fuzzy Logic Control (FLC), Transient stability, Flexible AC Transmission Systems (FACTS), Low frequency oscillations (LFO), Damping controller.*

I. INTRODUCTION

FACTS is an acronym which stands for Flexible AC Transmission System. FACTS is an evolving technology-based solution envisioned to help the utility industry to deal with changes in the power delivery business. These devices are used to control power flow and increase the stability of the system. They play a prominent role in the operation and control of power system. Among all the FACTS devices UPFC is more flexible and potent device which is widely in use [3]. The power flow through the transmission line is a function of line impedance, magnitude of sending and receiving end voltages, the phase angle between these voltages. By proper implementation of controllable components for these variables, it is possible to regulate the power flow through the transmission line [16]. Real and Reactive power can be controlled independently by using this. UPFC can also be used for voltage support and electromechanical oscillation damping [1]. For secure system maneuver damping of electromechanical oscillations due to sudden change in input mechanical power, faults is essential [17]. In this paper, the researches are based on single-machine infinite-bus system with UPFC. UPFC controller has the capacity not only to increase the transmission but also to improve the power system stability.

Flexible AC Transmission System (FACTS) involves the application of high power electronics to AC power transmission to achieve fast, reliable control of power transmission, reactive power control and enhancement of stability margins. The Unified Power Flow Controller (UPFC) was proposed for real-time control and dynamic compensation of AC transmission systems, providing the necessary functional flexibility required to solve the many problems facing the utility industry. The UPFC from the view point of conventional transmission compensation and control is an apparatus that can provide simultaneous, real time control of all or any combination of the basic power system parameters (Transmission voltage, Line impedance and Phase angle) which determine the transmission power. UPFC can control each parameter either selectively or simultaneously in appropriate combinations (control of real power and reactive power independently).

The main objective of this paper is to develop a fuzzy based power oscillation damping controller for the UPFC. For a better understanding of the performance of the controller, it is considered that the UPFC is connected with a Single Machine Infinite Bus (SMIB) system. A Simulink Model for Fuzzy logic controller based UPFC has been developed in MATLAB/SimPowerSystems environment in order to test the transient behavior of the system when it is connected with the fuzzy logic controller and proportional fuzzy logic controller.

II. UPFC SYSTEM

The basic block diagram of UPFC system used in the investigation of this paper is as shown in below figure 1.

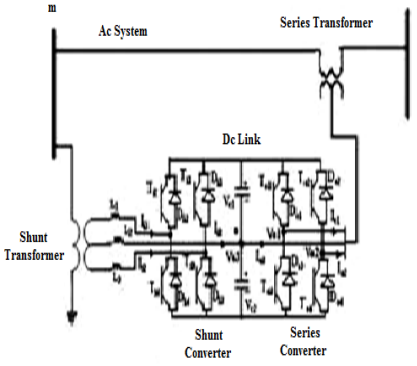

Fig. 1: Block Diagram of UPFC installed in a single-machine infinite-bus

It consists of two Voltage Source Converters (VSCs) coupled through a common dc link terminal. One VSC (series converter) is connected is shunt with the line through a coupling transformer and the other VSC (Shunt converter) is in series with the line through an interface transformer. DC voltage required for both the converters is provided by a common capacitor bank.

2.1 VSC AS SHUNT COMPENSATOR (STATCOM)

A STATCOM or Static Synchronous Compensator is a regulating device used on alternating current electricity transmission networks. It is based on a power electronics voltage-source converter and can act as either a source or sink of reactive AC power to an electricity network. If connected to a source of power it can also provide active AC power. A STATCOM works by rebuilding the incoming voltage waveforms by switching back and forth from reactive to capacitive load. If it is reactive, it will supply reactive AC power. If it is capacitive, it will absorb reactive AC power.

2.2 VSC AS SERIES COMPENSATOR (SSSC)

A series connected VSC injects a voltage in series with the line. Real and Reactive power exchange is controlled by the phase exchange is controlled by the phase displacement of the injected voltage w.r.t the line current. When it is in phase, only real power is exchanged and if it is in quadrature, reactive power is exchanged.

The series connected VSC is an extremely powerful tool for power flow control, as it is able to control both the transmission line impedance and phase angle. When restricted to fundamental frequency, it will not produce undesirable electrical resonance with transmission network. Also by suitable control it can damp SSR due to existing capacitive compensation by injecting non-fundamental voltage components of appropriate amplitude, frequencies and phase angles.

A static synchronous generator operated without an external electric energy source as a series compensator whose output voltage is in quadrature with, and controllable independently of, the line current for the purpose of increasing or decreasing the overall reactive voltage drop across the line and thereby controlling the transmitted electric power. The SSSC may include transiently rated energy storage or energy absorbing devices to enhance the dynamic behavior of the power system by additional temporary real power compensation, to increase or decrease momentarily, the overall real(resistive) voltage drop across the line.

III. PROPOSED UPFC WITH FUZZY CONTROLLER WITH MAT LAB MODELS.

The primary reason for choosing the fuzzy logic controller in this study is that the flexibility offered by it. In which the control strategy is represented by a set of rules and it doesn't require the exact set of equations to represent the system. This allows the design to change the basic characteristics of the controller with a minimal effort i.e., simply by redefining the rules. The block diagram of the fuzzy logic controller is shown in Fig. 2 and Fig. 3.

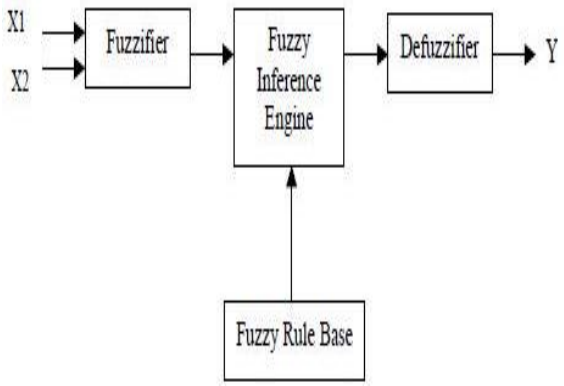

Fig. 2: Schematic diagram of Fuzzy Logic Controller

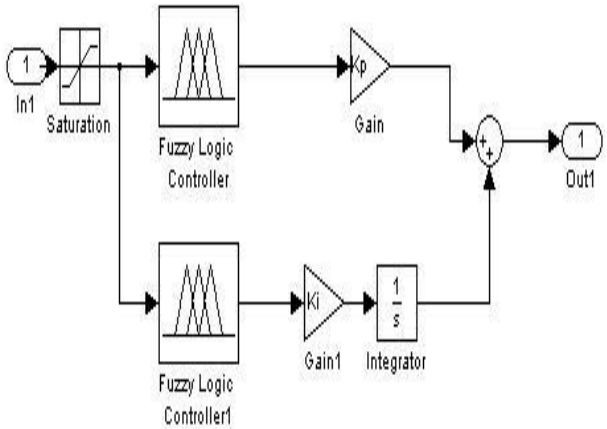

Fig. 3: Fuzzy Logic PI Controller in UPFC

As mentioned in the control strategy the stability and damping of the system is dependent on the electrical output power (Pe). In order to maintain the stability electrical output power (Pe) must be equal to that of the mechanical input power (Pm). Thus the two input variables chosen for the fuzzy logic controller are the deviation of Pe from Pm and its rate of change with respect to time. The rule base for the generic Fuzzy logic controller for UPFC is designated from the knowledge base of the system.

3.1. Membership Functions

The present design utilizes three types of membership functions (Γ, Ί ,&Δ). The input variables are partitioned into seven linguistic variables while the output variables are assigned form the any of the linguistic variables. The input and output membership functions with associated linguistic variables are shown in Fig. 3.

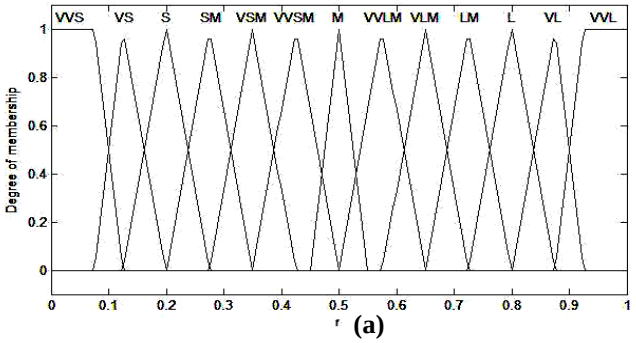

(a)

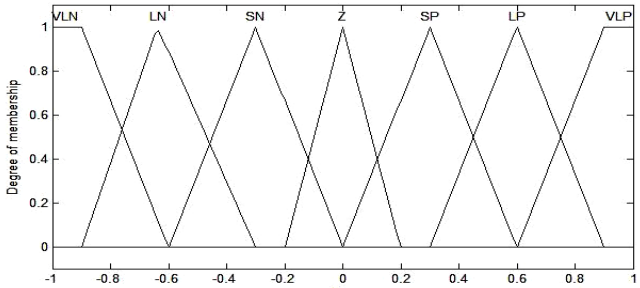

(b)

Fig 4: Input and output Membership function and linguistic Variables

3.2. Fuzzification

Fuzzification process convents the physical variables to fuzzy set variables. The crisp variables of the inputs are mapped into the fuzzy plane with the associated membership functions. It gives each input variable a membership function relating to the fuzzy set.

3.3. Fuzzy Rule Base

Each input variables are assigned to seven linguistics variables, therefore 49 rules are formulated. These rules are formulated with a simple IF-THEN structure. They map the inputs states into 49 output conditions. The fuzzy rules will take up the general form. The rule base can be represented by the fuzzy associative memory (FAM) table shown in Table 1.

Table 1: FAM table for UPFC Fuzzy Logic Controller

Pe/dPe	VLN	LN	SN	Z	SP	LP	VLP
VLN	VVS	VS	S	SM	VSM	VVSM	M
LN	VS	S	SM	VSM	VVSM	M	VVLM
SN	S	SM	VSM	VVSM	M	VVLM	VLM
Z	SM	VSM	VVSM	M	VVLM	VLM	LM
SP	VSM	VVSM	M	VVLM	VLM	LM	L
LP	VVSM	M	VVLM	VLM	LM	L	VL
VLP	M	VVLM	VLM	LM	L	VL	VVL

3.4. Fuzzy Inference Engine

The Fuzzy logic controller discussed in this paper incorporates Mamdani's implication method of inference. This implication has a simple min-max structure. It involves two phase of operations. In the first phase the two input variables are involved with min-operation, hence the antecedent pair in the rule structure are constructed by logical AND. Then all the rules are aggregated by using max operation.

3.5. Defuzzification

Defuzzification is the process by which fuzzy linguistic variables are converted to real control variables. Different defuzzification techniques have been introduced depending on the complexity of the system. The weighted average method is adopted in this study.

IV. MATLAB/Sim Power Systems Model

A Unified Power Flow Controller (UPFC) is used to control the power flow in a 230 kV transmission system. The UPFC located at the left end of the 50-km line L2, is used to control the active and reactive powers flowing through bus . It consists of two 100-MVA, three-level, thyristor based converters, one is connected in shunt with line and one connected in series with line. The shunt and series converters can exchange power through a DC bus. The series converter can inject a maximum of 10% of nominal line-to-ground voltage (28.87 kV) in series with line L2.

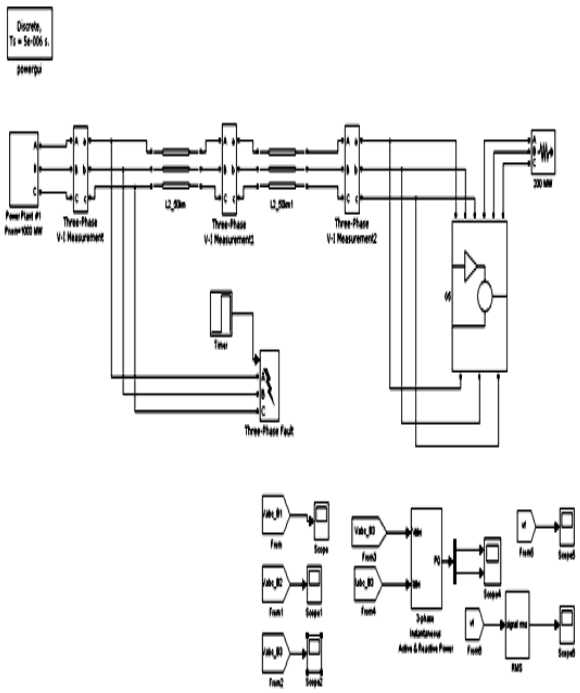

Fig. 5: MATLAB/Sim Power Systems Model of FLC based UPFC

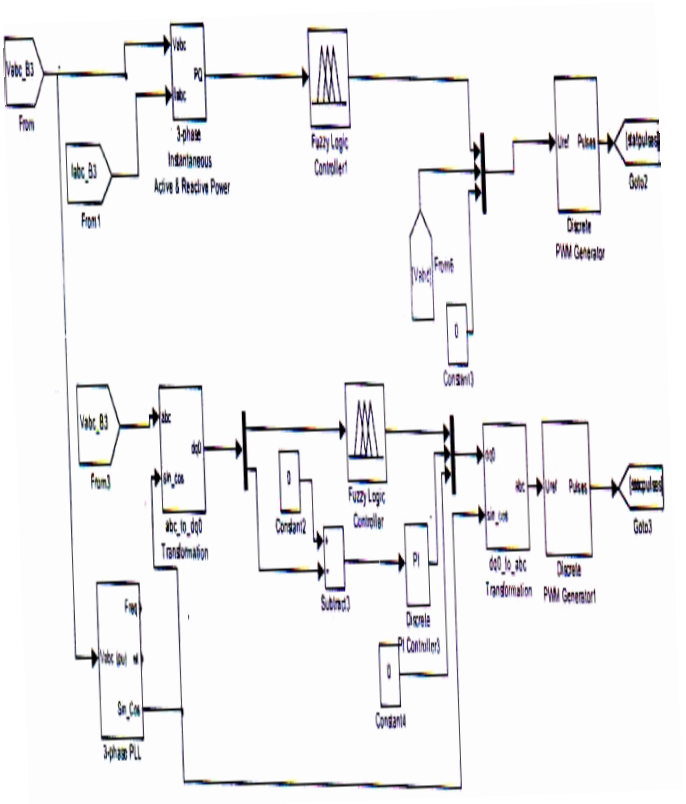

Fig. 6: MATLAB/Sim Power Systems Model of FLC

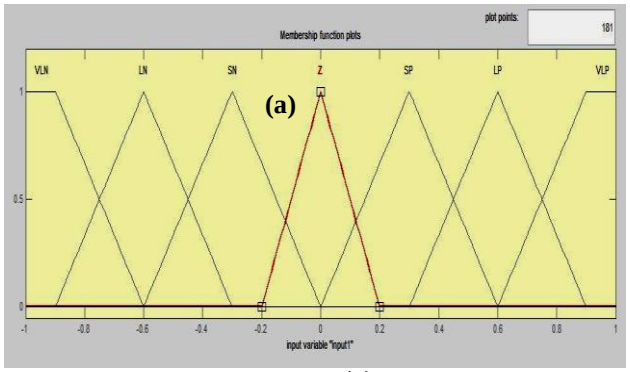

(a)

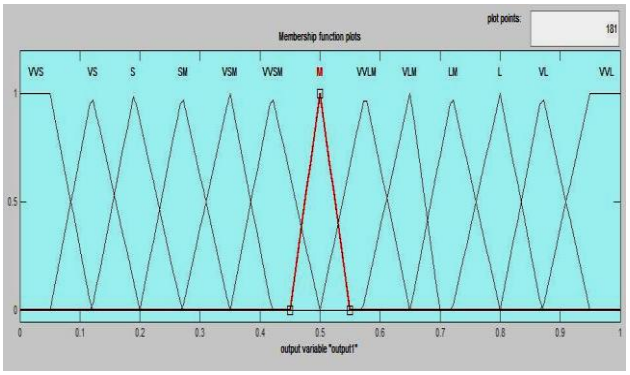

(b)

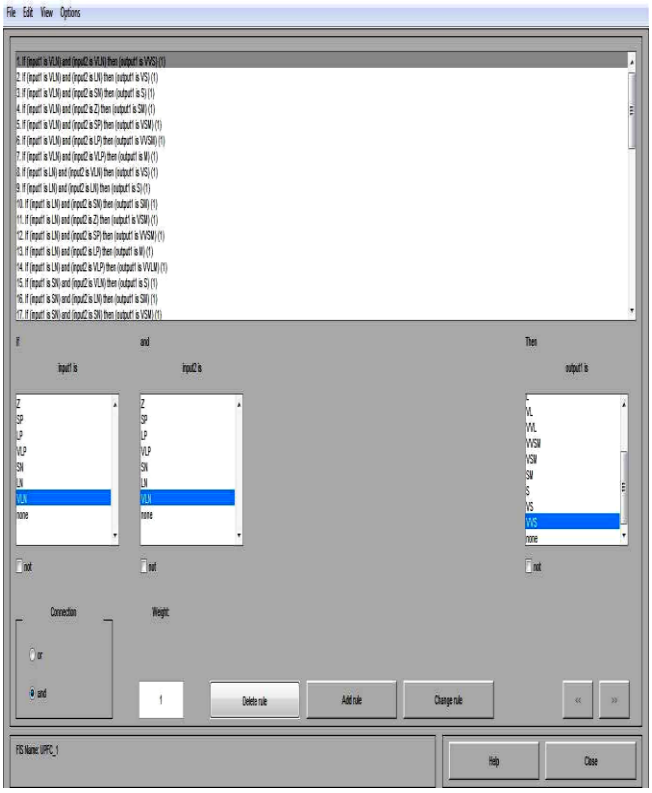

(c)

Fig. 7: MATLAB/Simulink Model of Fuzzy Membership Functions (a) Input Variable (b) Output Variable and (c) Fuzzy Rule Base

V. SIMULATION RESULTS

The simulation results shows that the UPFC with fuzzy based controller to damp the low frequency oscillation. The comparison of dynamic response of the system when it is used in UPFC mode With PI and Fuzzy Controller are shown in below figures. Fig 7 shows the active and reactive powers of the systems without transient fault. Fig 8 shows damping oscillations control with PI controller and fuzzy controller for three phase.

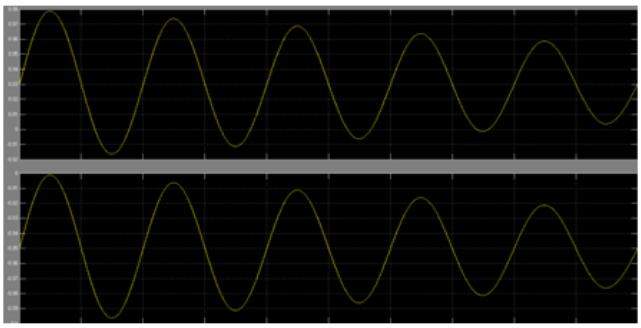

(a)

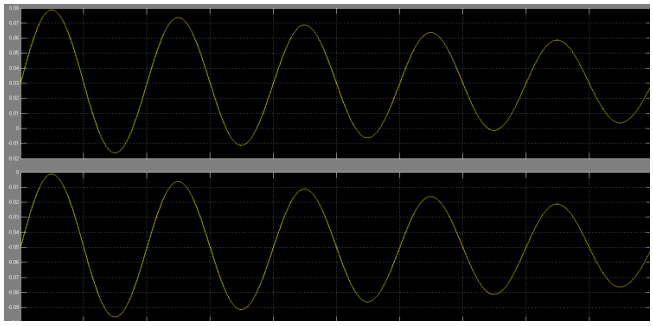

(b)

Fig. 8. Active Power and Reactive power control
(a) with PI Controller, (b) with Fuzzy based controller

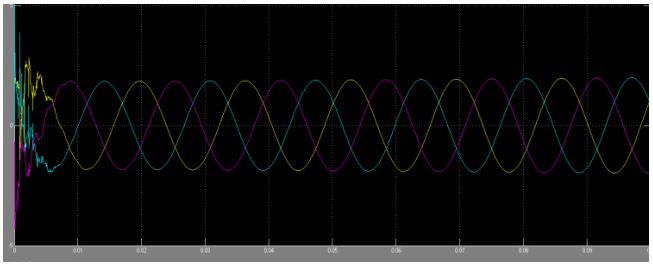

(a)

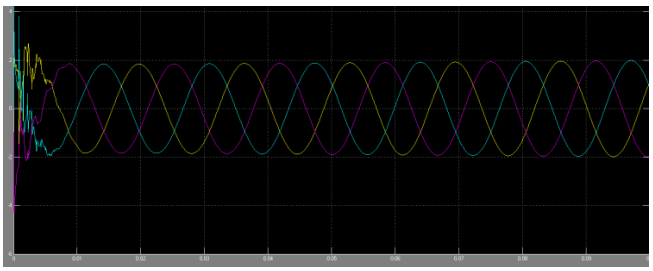

(b)

Fig.9 Damping oscillations control
(a) with PI controller, (b) with Fuzzy based controller
(Phase-B1)

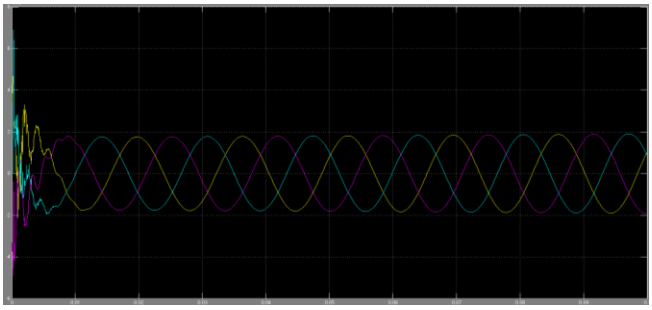

(a)

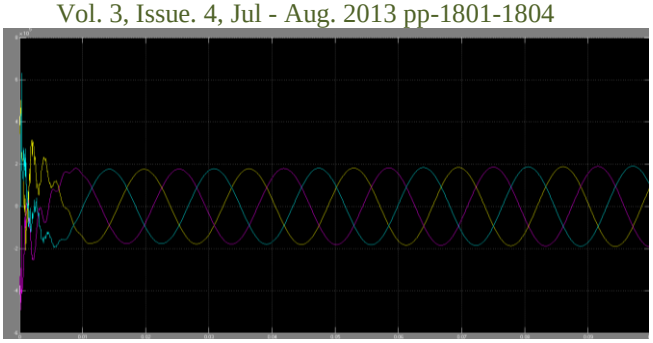

(b)

Fig.10 Damping oscillations control (a) with PI controller, (b) with Fuzzy based controller (Phase-B2)

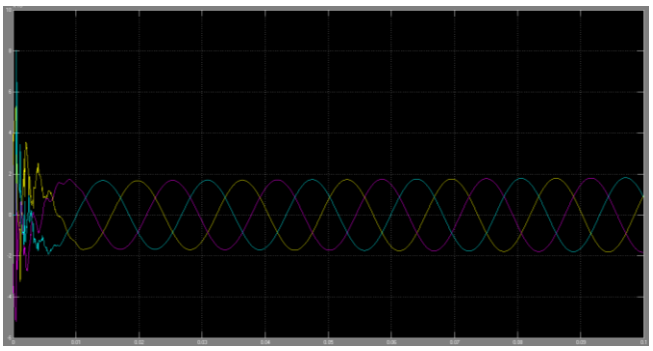

(a)

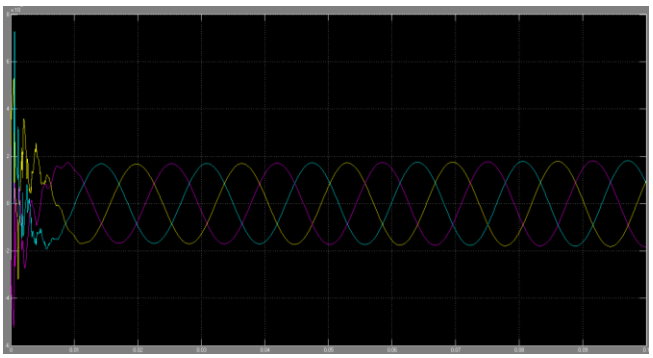

(b)

Fig.11 Damping oscillations control
(a) with PI controller, (b) with Fuzzy based controller
(Phase-B3)

VI. CONCLUSION

The substantial contribution of the study effort presented in this paper as follows:

A simple Fuzzy logic controller for a unified power flow controller (UPFC) in a single machine infinite bus (SMIB) system has been implemented using SimPowerSystems environment tool box in MATLAB Software. The dynamic behavior of the original SMIB system with UPFC devices is determined through the proposed model of the system. It was observed that the system performance is improved with the UPFC and it becomes easier to control with fuzzy logic.

Simulation results shows that Fuzzy based controller slightly increases the power flow control by increasing the damping rate and decreases the amplitude of low frequency oscillations. Results comparison between conventional PI controller and the proposed Fuzzy based controller for UPFC indicates that the proposed fuzzy based controller has less settling time and less overshoot when compared with the conventional PI controller.

REFERENCES

[1]. K.S. Smith, L. Ran and J. Penman. 'Dynamic Modeling of a Unified Power Flow Controller.' IEE Proceedings-C, Vol. 144, No. 1, January 1997, p. 7
[2]. H.F. Wang 'Damping Function of Unified Power Flow Controller.' IEE Proceedings-C, Vol. 146, No. 1, January 1999, p. 81.
[3]. Narain G. Hingorani, Laszlo Gyugyi. "Understanding FACTS concepts and Technology of Flexible AC Transmision Systems", IEEE Press, 1999.
[4]. R. Bakshai, G. Joos and H. Jin, "EMTP simulation of multi-pulse unified power flow controllers," proceedings of Canadian conference on electrical and computer engineering, May 1996, Vol.2.

[5]. A Nabavi-Niaki and M R Iravani.,"steady-state and dynamic model of Unified power flow controller (UPFC) for power system studies," IEEE Transactionson Power System , vol 11, no 4, November 1996, p 1937.
[6]. Hao ying, " Fuzzy Control and Modelling: Analytical Foundation and Applications, IEEE Press Series on Biomedical Engineering, Series Editor: Metin Akay, New york, 2000.
[7]. T Makombe and N Jenkins. "Investigation of a unified power Flow Controller," IEE Proceedings-C, vol 146, no 4, july 1999, p400.
[8]. H. F. Wang, F. J. Swift, "A Unified Model for the Analysis of FACTS devices in Damping power system Oscillations Part I: Single-machine Infinite bus power Systems," IEEE Transactions on power Delivery, Vol. 12, No. 2, April, 1997, pp. 941-946.
[9]. Mamdani, E.H. and S. Assilian, "An experiment in linguistic synthesis with a fuzzy logic controller," *International Journal of Man-Machine Studies*, Vol. 7, No. 1, pp. 1-13, 1975.
[10]. Sugeno, M., *Industrial applications of fuzzy control*, Elsevier Science Pub. Co., 1985.
[11]. A.M. Sharaf and Khaled Abo-Al-Ez, "A FACTS Based Dynamic Capacitor Scheme for Voltage Compensation and Power Quality Enhancement", *Proceedings of the IEEEISIE 2006 Conference*, Montreal, Quebec Canada, July 2006.
[12]. Y. L. Kang, G. B. Shrestha and T. T. Lie, "Application of an NLPID controller on a UPFC to improve transient stability of a power system," IEE Proc-Gener. Transm. Distrib.; Vol. 148. No. 6, November 2001.
[13]. M. Noroozian, L. Angquist, M. Ghandhari and G. Andersson, "use of UPFC for optimal power flow control," IEEE Transactions on power delivery, Vol. 12, No. 4, October 1997.
[14]. R. Mihalic, P. Zunko and D. Pouh, "Improvement of transient stability using unified power flow controller," IEEE Transactions on power delivery, Vol. 11, No. 1, January 1996.
[15]. Kundur. P, "Power system stability and control", EPRI Publications, Tata McGraw Hil Inc., New Delhi, 1994.
[16]. Gyugyi.L "Unified Power Flow Control Concept For Flexible Transmission Systems," IEE proceedings-C, vol. 139, No. 4, July 1992.s
[17]. Y Morioka and Y Nakach, et al. "Implementation of Unified Power Flow Controller and Verification for Transmission Capability Improvement," IEEETransactions on Power Systems, vol 14, no 2, May 1999, p 575.
[18] H. F. Wang, F. J. Swift, "A Unified Model for the Analysis of FACTS devices in Damping power system Oscillations Part II: Multi-machine power Systems," IEEE Transactions on power Delivery, Vol. 13, No. 4, October, 1998, pp. 1355-1362.

BIOGRAPHIES

L. Haini is born in 1987 in India. She is graduated from JNTU Hyderabad in 2009. Presently she is doing Post graduation in Electrical Power Systems Specialization at J.N.T.U.H, Hyderabad. Her main areas of interest include Electrical machines, Power systems, Power Electronics & FACTS.

Y. Hazarathaiah M.Tech, working as Assistant Professor in S.K.T.R.M College of Engineering, Affiliated to JNTUH, Approved by AICTE. New Delhi. He completed his M.Tech in 2012 from JNTU. He has seven years teaching experience in Electrical Engineering. He has done three Conferences and one Journal in Electrical Engineering.

International Journal of Modern Engineering Research (IJMER)
www.ijmer.com Vol. 3, Issue. 4, Jul - Aug. 2013 pp-2553-2562 ISSN: 2249-6645

An Efficient Security Way of Authentication and Pair wise Key Distribution with Mobile Sinks in Wireless Sensor Networks

P. Santhi[1], Md. Shakeel Ahmed[2], Sk. Mehertaj[3], T. Bharath Manohar[4]
[1,3]*M.Tech 2ndyr, Dept of CSE,PBRVITS(Affiliated to JNTU Anantapur), Kavali,Nellore.Andhra Pradesh.India.*
[2] *Assoc. Prof., Dept of CSE, PBRVITS(Affiliated to JNTU Anantapur), Kavali,Nellore.Andhra Pradesh.India.*
[4] *Asst. Professor, Dept of CSE, CMR College of Engineering &Technology, (Affiliated to JNTU Hyderabad)Hyderabad.Andhra Pradesh.India.*

Abstract: *Wireless sensor networks (WSN) are the emerging application in many industrial and missile sector. Mobile sinks (MSs) are vital in many wireless sensor network applications for efficient data accumulation, localized sensor reprogramming, and for distinguishing and revoking compromised sensors. However, in sensor networks that make use of the existing key pre-distribution schemes for pairwise key establishment and authentication between sensor nodes and mobile sinks, the employment of mobile sinks for data collection elevates a new security challenge: in the basic probabilistic and q-composite key predistribution schemes, an attacker can easily obtain a large number of keys by capturing a small fraction of nodes, and hence, can gain control of the network by deploying a replicated mobile sink preloaded with some compromised keys. The proposed work, three-tier framework permits the use of any pairwise key pre-distribution scheme as its basic component. The new framework requires two separate key pools, one for the mobile sink to access the network, and one for pairwise key establishment between the sensors. To further reduce the damages caused by stationary access node replication attacks, the authentication mechanism between the sensor and the stationary access node is strengthened in the proposed work. This framework has higher network resilience to a mobile sink replication attack as compared to the polynomial pool-based scheme.*

Keywords: *Wireless sensor networks (WSN), Mobile sinks (MSs) & replication attacks,Polynomial pool based scheme.*

I. INTRODUCTION

Recent advances in electronic technology have paved the way for the development of a new generation of wireless sensor networks (WSNs) consisting of a large number of low-power, low-cost sensor nodes that communicate wirelessly. Such sensor networks can be used in a wide range of applications, such as, military sensing and tracking, health monitoring, data acquisition in hazardous environments, and habitat monitoring.

In wireless sensor networks, the sensed data from sensor nodes are often need to be sent back to the base station for analysis. However, when the sensing field is too far from the base station, transmitting the data over long distances using multihop may weaken the security strength (e.g., some intermediate may modify the data passing by, capturing sensor nodes, launching a wormhole attack, a sybil attack, selective forwarding, sinkhole), and increasing the energy consumption at nodes near the base station, reducing the lifetime of the network. Therefore, mobile sinks (MSs) (or mobile soldiers, mobile sensor nodes) are essential components in the operation of many sensor network applications, including data collection in hazardous environments, localized reprogramming, oceanographic data collection, and military navigation.

II. MOTIVATION

In wireless sensor applications, sensor nodes transmit critical information over the network; therefore, security services, such as, authentication and pairwise key establishment between sensor nodes and mobile sinks, are important. However, the resource constraints of the sensors and their nature of communication over a wireless medium make data confidentiality and integrity a nontrivial task. Traditional schemes in ad hoc networks using asymmetric keys are expensive due of their storage and computation cost. These limitations make key predistribution schemes the tools of choice to provide low cost, secure communication between sensor nodes and mobile sinks.

The problem of authentication and pairwise key establishment in sensor networks with MSs is still not solved in the face of mobile sink replication attacks. For the basic probabilistic and q-composite key predistribution schemes, an attacker can easily obtain a large number of keys by capturing a small fraction of the network sensor nodes, making it possible for the attacker to take control of the entire network by deploying a replicated mobile sink, preloaded with some compromised keys to authenticate and then initiate data communication with any sensor node.

To address the above-mentioned problem, a general framework is developed that permits the use of any pairwise key predistribution scheme as its basic component, to provide authentication and pairwise key establishment between sensor nodes and MSs.

To make the three-tier security scheme more robust against a stationary access node replication attack, the authentication mechanism is strengthened between the stationary access nodes and sensor nodes using one-way hash chains algorithm in conjunction with the static polynomial pool-based scheme.

To facilitate the study of a new security technique, a general three-tier security framework is first cultivated for authentication and pair-wise key establishment, based on the polynomial pool-based key pre-distribution scheme.

A small fraction of the preselected sensor nodes, called the stationary access nodes, act as authentication access points to the network, to trigger the sensor nodes to transmit their aggregated data to mobile sinks. A mobile sink sends data request

messages to the sensor nodes via a stationary access node. These data request messages from the mobile sink will initiate the stationary access node to trigger sensor nodes, which transmit their data to the requested mobile sink. The scheme uses two separate polynomial pools: the mobile polynomial pool and the static polynomial pool.
Using two separate key pools and having few sensor nodes that carry keys from the mobile key pool will make it more difficult for the attacker to launch a mobile sink replication attack.

Advantages

- The proposed technique will substantially improve network resilience to mobile sink replication attacks compared to the single polynomial pool-based key pre-distribution approach, as an attacker would have to compromise many more sensor nodes to launch a successful mobile sink replication attack.
- For the attacker to launch a mobile sink replication attack on the sensor network by capturing only a few arbitrary sensor nodes.

III. III.LITERATURE SURVEY

The key management problem is an active research area in wireless sensor networks.

Eschenauer and Gilgor proposed a probabilistic key pre-distribution scheme to bootstrap the initial trust between the sensor nodes. The main idea was to let each sensor node randomly pick a set of keys from a key pool before deployment, so that any two sensor nodes had a certain probability of sharing at least one common key.

Chan et al. extended probabilistic key predistribution idea and developed two key predistribution schemes: the q-composite key predistribution scheme and the random pairwise keys scheme. The q-composite key predistribution scheme also used a key pool, but required two sensor nodes to compute a pairwise key from at least q predistributed keys that they shared. The random pairwise keys scheme randomly picked pairs of sensor nodes and assigned each pair a unique random key.

An enhanced scheme using the t-degree bivariate key polynomial was proposed by Liu et al.. They developed a general framework for pairwise key establishment using the polynomial-based key predistribution protocol and the probabilistic key distribution. Their scheme could tolerate no more than t compromised nodes, where the value of t was limited by the memory available in the sensor nodes.

LITERATURE REVIEW

Routing Security in Wireless Ad Hoc Networks
Hongmei Deng, Wei Li, and Dharma P. Agrawal, University of Cincinnati

A mobile ad hoc network consists of a collection of wireless mobile nodes that are capable of communicating with each other without the use of a network infrastructure or any centralized administration. MANET is an emerging research area with practical applications. However, wireless MANET is particularly vulnerable due to its fundamental characteristics, such as open medium, dynamic topology, distributed cooperation, and constrained capability. Routing plays an important role in the security of the entire network. In general, routing security in wireless MANETs appears to be a problem that is not trivial to solve. In this article we study the routing security issues of MANETs, and analyze in detail one type of attack — the “black hole” problem — that can easily be employed against the MANETs. We also propose a solution for the black hole problem for ad hoc on-demand distance vector routing protocol.

Directed Diffusion: A Scalable and Robust Communication Paradigm for Sensor Networks
Chalermek Intanagonwiwat; Ramesh Govindan; Deborah Estrin

Advances in processor, memory and radio technology will enable small and cheap nodes capable of sensing, communication and computation. Networks of such nodes can coordinate to perform distributed sensing of environmental phenomena. In this paper, we explore the directed diffusion paradigm for such coordination. Directed diffusion is data-centric in that all communication is for named data. All nodes in a directed diffusion-based network are application-aware. This enables diffusion to achieve energy savings by selecting empirically good paths and by caching and processing data in-network. We explore and evaluate the use of directed diffusion for a simple remote-surveillance sensor network.

Vital Signs Monitoring and Patient Tracking Over a Wireless Network
Tia Gao, Dan Greenspan, Matt Welsh, Radford R. Juang, and Alex Alm

Patients at a disaster scene can greatly benefit from technologies that continuously monitor their vital status and track their locations until they are admitted to the hospital. We have designed and developed a real-time patient monitoring system that integrates vital signs sensors, location sensors, ad-hoc networking, electronic patient records, and web portal technology to allow remote monitoring of patient status. This system shall facilitate communication between providers at the disaster scene, medical professionals at local hospitals, and specialists available for consultation from distant facilities.

Using Directional Antennas to Prevent Wormhole Attacks
Lingxuan Hu David Evans, Department of Computer Science, University of Virginia, Charlottesville, VA

Wormhole attacks enable an attacker with limited resources and no cryptographic material to wreak havoc on wireless networks. To date, no general defenses against wormhole attacks have been proposed. This paper presents an analysis of wormhole attacks and proposes a countermeasure using directional antennas. We present a cooperative protocol

whereby nodes share directional information to prevent wormhole endpoints from masquerading as false neighbors. Our defense greatly diminishes the threat of wormhole attacks and requires no location information or clock synchronization.

Data Dissemination with Ring-Based Index for Wireless Sensor Networks∗
Wensheng Zhang, Guohong Cao and Tom La Porta; Department of Computer Science and Engineering, The Pennsylvania State University

In current sensor networks, sensor nodes are capable of not only measuring real world phenomena, but also storing, processing and transferring these measurements. Many data dissemination techniques have been proposed for sensor networks. However, these techniques may not work well in a large scale sensor network where a huge amount of sensing data are generated, but only a small portion of them are queried. In this paper, we propose an index-based data dissemination scheme to address the problem. This scheme is based on the idea that sensing data are collected, processed and stored at the nodes close to the detecting nodes, and the location information of these storing nodes is pushed to some index nodes, which act as the rendezvous points for sinks and sources. We further extend the scheme with an adaptive ring-based index (ARI) technique, in which the index nodes for one event type form a ring surrounding the location which is determined by the event type, and the ring can be dynamically reconfigured for fault tolerance and load balance. Analysis and simulations are conducted to evaluate the performance of the proposed index-based scheme. The results show that the index-based scheme outperforms the external storage-based scheme, the DCS scheme, and the local storage-based schemes with flood-response style. The results also show that using ARI can tolerate clustering failures and achieve load balance.

IV. SYSTEM ANALYSIS

Network simulation is a technique where a program models the behavior of a network either by calculating the interaction between the different network entities (hosts/routers, data links, packets, etc) using mathematical formulas, or actually capturing and playing back observations from a production network. The behavior of the network and the various applications and services it supports can then be observed in a test lab; various attributes of the environment can also be modified in a controlled manner to assess how the network would behave under different conditions. When a simulation program is used in conjunction with live applications and services in order to observe end-to-end performance to the user desktop, this technique is also referred to as network emulation.

Motivation for Simulations

- Cheap -- does not require costly equipment
- Complex scenarios can be easily tested
- Results can be quickly obtained – more ideas can
- be tested in a smaller timeframe
- The real thing isn't yet available
- Controlled experimental conditions
- Repeatability helps aid debugging
- Disadvantages: Real systems too complex to model

Most of the commercial simulators are GUI driven, while some network simulators require input scripts or commands (network parameters). The network parameters describe the state of the network (node placement, existing links) and the events (data transmissions, link failures, etc). Important outputs of simulations are the trace files. Trace files can document every event that occurred in the simulation and are used for analysis. Certain simulators have added functionality of capturing this type of data directly from a functioning production environment, at various times of the day, week, or month, in order to reflect average, worst-case, and best-case conditions

Most network simulators use discrete event simulation, in which a list of pending "events" is stored, and those events are processed in order, with some events triggering future events -- such as the event of the arrival of a packet at one node triggering the event of the arrival of that packet at a downstream node.

Some network simulation problems, notably those relying on queuing theory, are well suited to Markov chain simulations, in which no list of future events is maintained and the simulation consists of transiting between different system "states" in a memory less fashion. Markov chain simulation is typically faster but less accurate and flexible than detailed discrete event simulation. Some simulations are cyclic based simulations and these are faster as compared to event based simulations.

Advantages of simulation

* Normal analytical techniques make use of extensive mathematical models which require assumptions and restrictions to be placed on the model. This can result in an avoidable inaccuracy in the output data. Simulations avoid placing restrictions on the system and also take random processes into account; in fact in some cases simulation is the only practical modeling technique applicable
* Analysts can study the relationships between components in detail and can simulate the projected consequences of multiple design options before having to implement the outcome in the real-world.
* It is possible to easily compare alternative designs so as to select the optimal system.

* The actual process of developing the simulation can itself provide valuable insights into the inner workings of the network which can in turn be used at a later stage.

Disadvantages of simulation

* Accurate simulation model development requires extensive resources.
* The simulation results are only as good as the model and as such are still only estimates / projected outcomes.
* Optimization can only be performed involving a few alternatives as the model is usually developed using a limited number of variables.
* Simulations cost a lot of money to build and are very expensive to make

Input data

Simulation models are generated from a set of data taken from a stochastic system. It is necessary to check that the data is statistically valid by fitting a statistical distribution and then testing the significance of such a fit. Further, as with any modelling process, the input data's accuracy must be checked and any outliers must be removed.

Output data

When a simulation has been completed, the data needs to be analysed. The simulation's output data will only produce a likely estimate of real-world events. Methods to increase the accuracy of output data include: repeatedly performing simulations and comparing results, dividing events into batches and processing them individually, and checking that the results of simulations conducted in adjacent time periods "connect" to produce a coherent holistic view of the system The main idea is to partly implement HTTP, FTP and TCP protocols.

Routing is the process of selecting paths in a network along which to send network traffic. Routing is performed for many kinds of networks, including the telephone network (Circuit switching) , electronic data networks (such as the Internet), and transportation networks. This article is concerned primarily with routing in electronic data networks using packet switching technology.

In packet switching networks, routing directs packet forwarding, the transit of logically addressed packets from their source toward their ultimate destination through intermediate nodes, typically hardware devices called routers, bridges, gateways, firewalls, or switches. General-purpose computers can also forward packets and perform routing, though they are not specialized hardware and may suffer from limited performance. The routing process usually directs forwarding on the basis of routing tables which maintain a record of the routes to various network destinations. Thus, constructing routing tables, which are held in the router's memory, is very important for efficient routing. Most routing algorithms use only one network path at a time, but multipath routing techniques enable the use of multiple alternative paths.

Routing, in a more narrow sense of the term, is often contrasted with bridging in its assumption that network addresses are structured and that similar addresses imply proximity within the network. Because structured addresses allow a single routing table entry to represent the route to a group of devices, structured addressing (routing, in the narrow sense) outperforms unstructured addressing (bridging) in large networks, and has become the dominant form of addressing on the Internet, though bridging is still widely used within localized environments.

Routing schemes differ in their delivery semantics:

- unicast delivers a message to a single specified node;
- broadcast delivers a message to all nodes in the network;
- multicast delivers a message to a group of nodes that have expressed interest in receiving the message;
- anycast delivers a message to any one out of a group of nodes, typically the one nearest to the source.

Path selection

Path selection involves applying a routing metric to multiple routes, in order to select (or predict) the best route.
In the case of computer networking, the metric is computed by a routing algorithm, and can cover such information as bandwidth, network delay, hop count, path cost, load, MTU, reliability, and communication cost (see e.g. this survey for a list of proposed routing metrics). The routing table stores only the best possible routes, while link-state or topological databases may store all other information as well.

Because a routing metric is specific to a given routing protocol, multi-protocol routers must use some external heuristic in order to select between routes learned from different routing protocols. Cisco's routers. A local network administrator, in special cases, can set up host-specific routes to a particular machine which provides more control over network usage, permits testing and better overall security. This can come in handy when required to debug network connections or routing tables.

As the Internet and IP networks become mission critical business tools, there has been increased interest in techniques and methods to monitor the routing posture of networks. Incorrect routing or routing issues cause undesirable performance degradation, flapping and/or downtime. Monitoring routing in a network is achieved using Route analytics tools and techniques.

Protocols: TCP, UDP, HTTP, Routing algorithms etc

- Traffic Models: CBR, VBR, Web etc
- Error Models: Uniform, bursty etc
- Radio propagation, Mobility models
- Energy Models

- Topology Generation tools
- Visualization tools
- Extensibility

Simulators help in easy verification of protocols in less time, money

- NS offers support for simulating a variety of
- protocol suites and scenarios
- Front end is oTCL, back end is C++
- NS is an on-going effort of research and development

V. SYSTEM DESIGN & ARCHITECTURE DIAGRAMS

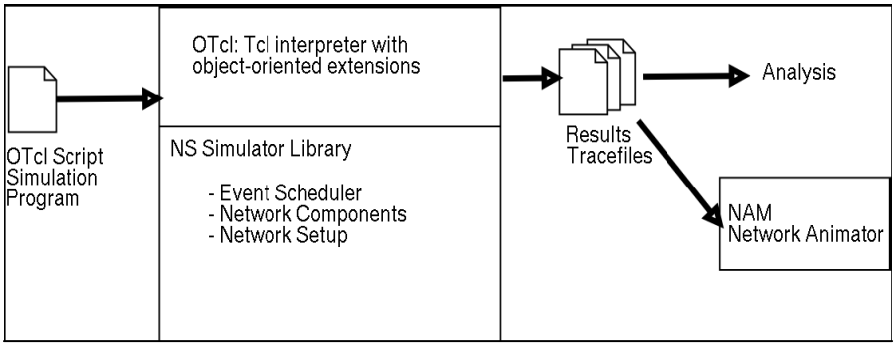

STRUCTURE OF NS2

MODULES

- ❖ Deployment of Nodes
- ❖ Data collection to Access points
- ❖ Data collection to sink
- ❖ Three tier security scheme

DEPLOYMENT OF NODES

We consider a wireless sensor network with N nodes. Let N denote the set of all nodes in the network. The communication among all n nodes is based on a tree topology with the sink as the root. The tree is formed in the initial phase as follows. The sink first broadcast a message with a hop counter. The nodes receiving the message will set the message sender as the parent node, increase the hop counter by one, and broadcast it to their neighbors. If a node receives multiple messages, it will select the one with the minimum hop counter to broadcast and set the sender of the message as its parent. Data are transferred along the edges in this communication tree. To transmit one data unit, the energy cost of the sender and receiver are etr and ere respectively, and etr is also relevant to the distance between the sender and receiver. To simplify the problem, we set the length of each tree edge to one unit, which means that sensor nodes have a fixed transmission range and the energy cost of transferring data is only proportional to the data size.

DATA COLLECTION TO ACCESS POINTS

In the wireless sensor network, we proposed a new security framework, a small fraction of the preselected sensor nodes, called the stationary access nodes, act as authentication access points to the network, to trigger the sensor nodes to transmit their aggregated data to mobile sinks. A mobile sink sends data request messages to the sensor nodes via a stationary access node. These data request messages from the mobile sink will initiate the stationary access node to trigger sensor nodes, which transmit their data to the requested mobile sink. The scheme uses two separate polynomial pools: the mobile polynomial pool and the static polynomial pool. The following figure, we represented a wireless sensor network, where node 1 and 2 are chosen as stationary access nodes. The sensor nodes sends data packet to stationary access nodes.

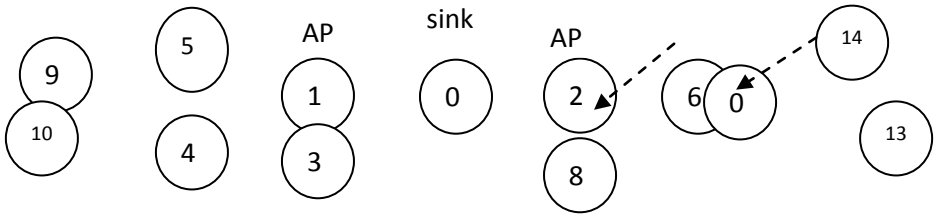

Fig: Data Collection to Access Nodes

DATA COLLECTION TO SINK

The stationary access nodes, collects data from mobile sensor nodes. These collected data packets sent to mobile sink from stationary access nodes. The scheme uses two separate polynomial pools: the mobile polynomial pool and the static polynomial pool. The following figure, we represented a wireless sensor network, where node 0 is the sink, node 1 and

2 are chosen as stationary access nodes. The sensor nodes sends data packet to stationary access nodes. Then the stationary access nodes send the collected data to sink

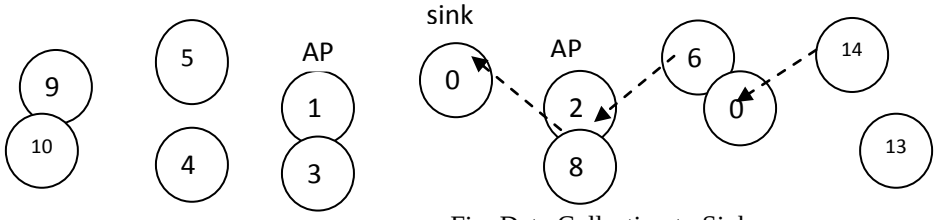

Fig: Data Collection to Sink

THREE TIER SECURITY SCHEME

Two separate polynomial pools are used. The mobile polynomial pool and the static polynomial pool are used. We use, MD5 algorithm for generating key pool for mobile sensor nodes and Sink separately. Polynomials from the mobile polynomial pool are used to establish the authentication between mobile sinks and stationary access nodes, which will enable these mobile sinks to access the sensor network for data gathering. Polynomials from the static polynomial pool are used to ascertain the authentication and keys setup between the sensor nodes and stationary access nodes. Thus, it is hard for an attacker to compromise at least a single polynomial from the mobile pool to gain access to the network for the sensor's data gathering.

UML DIAGRAMS:

USE CASE DIAGRAM:

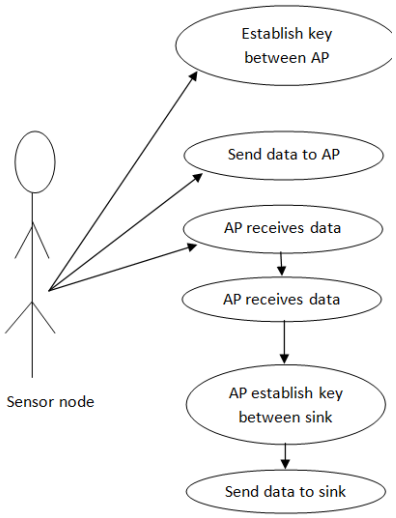

Fig: Use case diagram

ACTIVITY DIAGRAM:

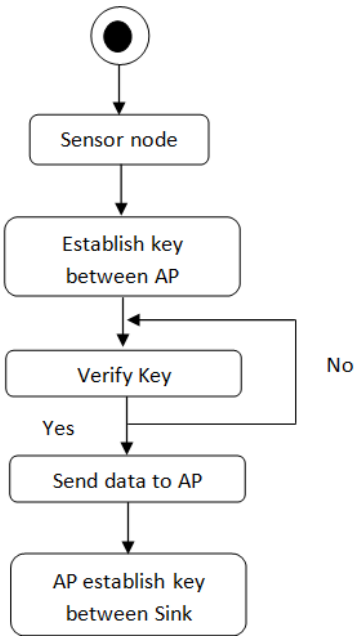

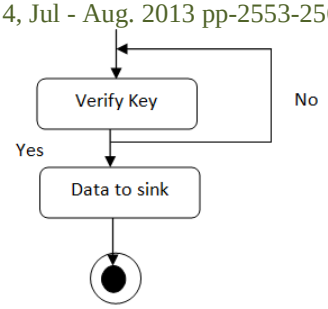

Fig: Activity Diagram

SEQUENCE DIAGRAM:

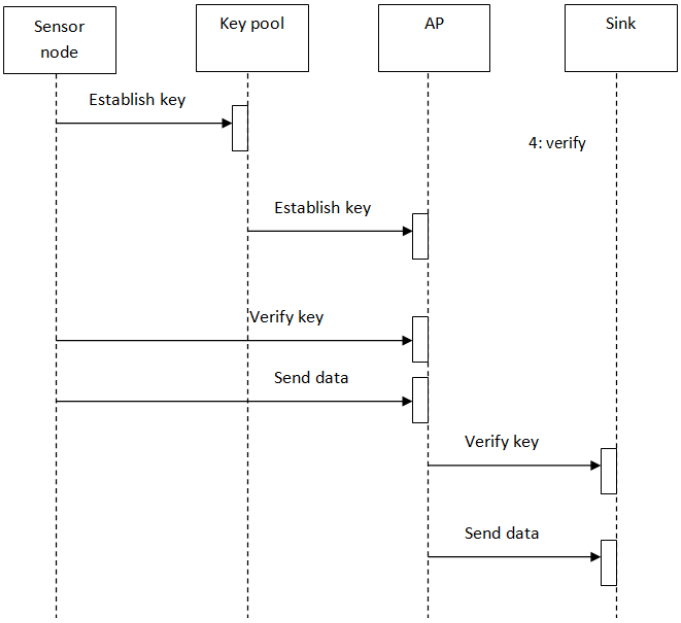

Fig: Sequence Diagram

COLLABORATION DIAGRAM:

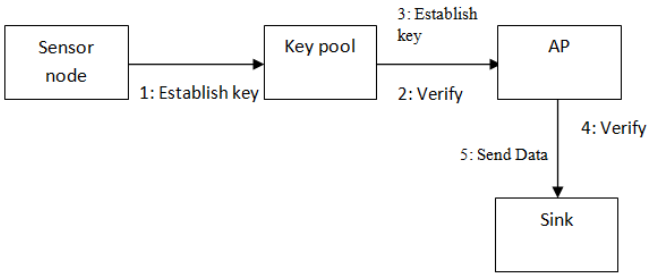

Fig: Collaboration Diagram

VI. EXPERIMENT & RESULT

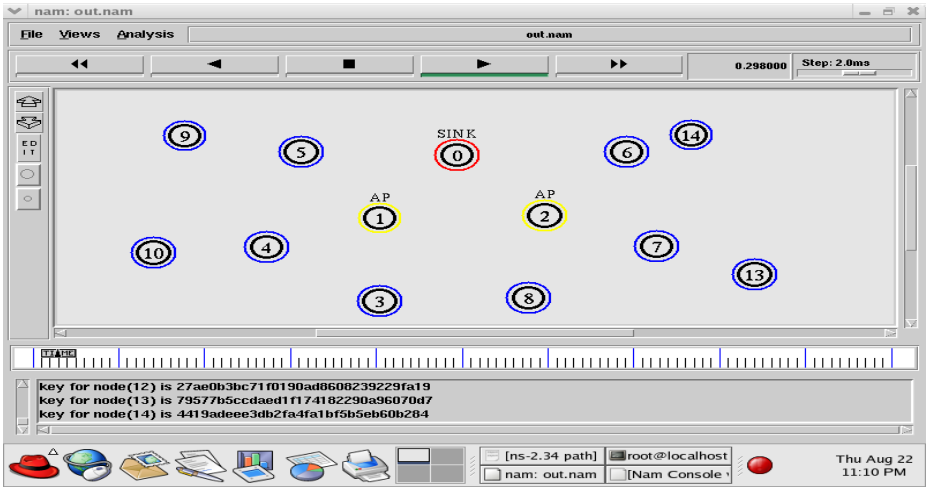

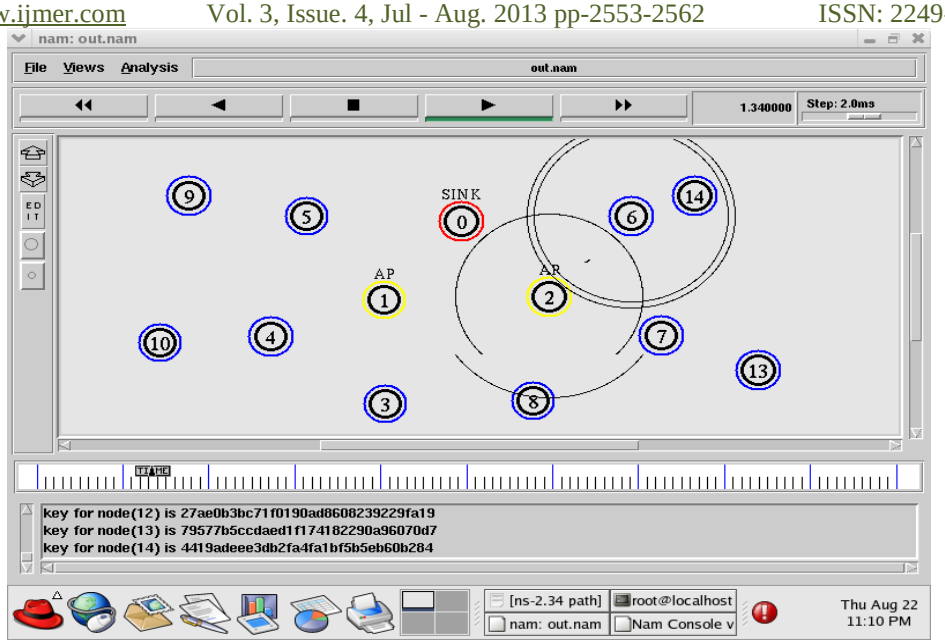
nam: out.nam
File Views Analysis
out.nam
1.340000
Step: 2.0ms
SINK
AP
AP
key for node(12) is 27ae0b3bc71f0190ad8608239229fa19
key for node(13) is 79577b5ccdaed1f174182290a96070d7
key for node(14) is 4419adeee3db2fa4fa1bf5b5eb60b284
[ns-2.34 path]
root@localhost
nam: out.nam
Nam Console v
Thu Aug 22
11:10 PM

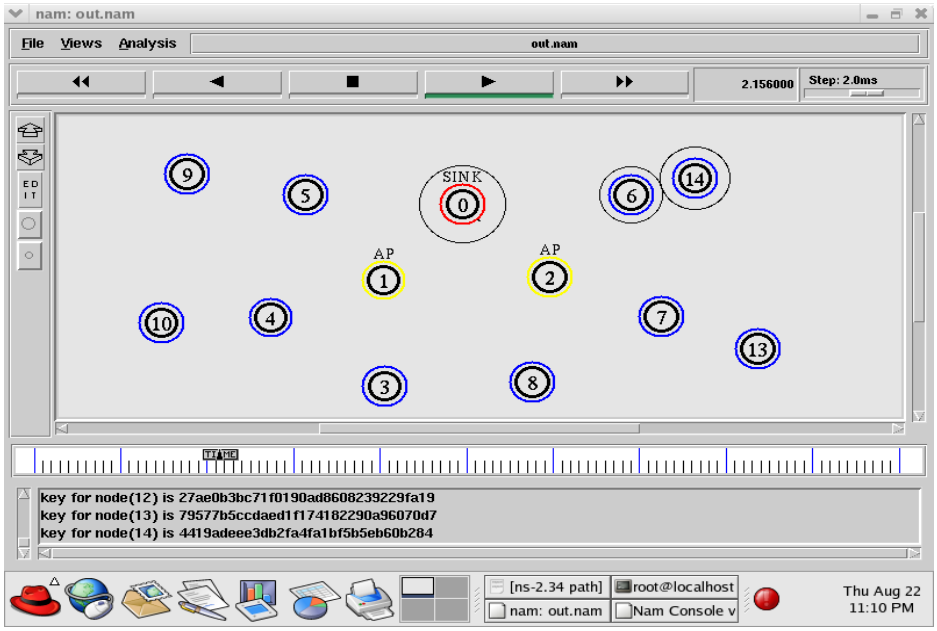
nam: out.nam
File Views Analysis
out.nam
2.156000
Step: 2.0ms
SINK
AP
AP
key for node(12) is 27ae0b3bc71f0190ad8608239229fa19
key for node(13) is 79577b5ccdaed1f174182290a96070d7
key for node(14) is 4419adeee3db2fa4fa1bf5b5eb60b284
[ns-2.34 path]
root@localhost
nam: out.nam
Nam Console v
Thu Aug 22
11:10 PM

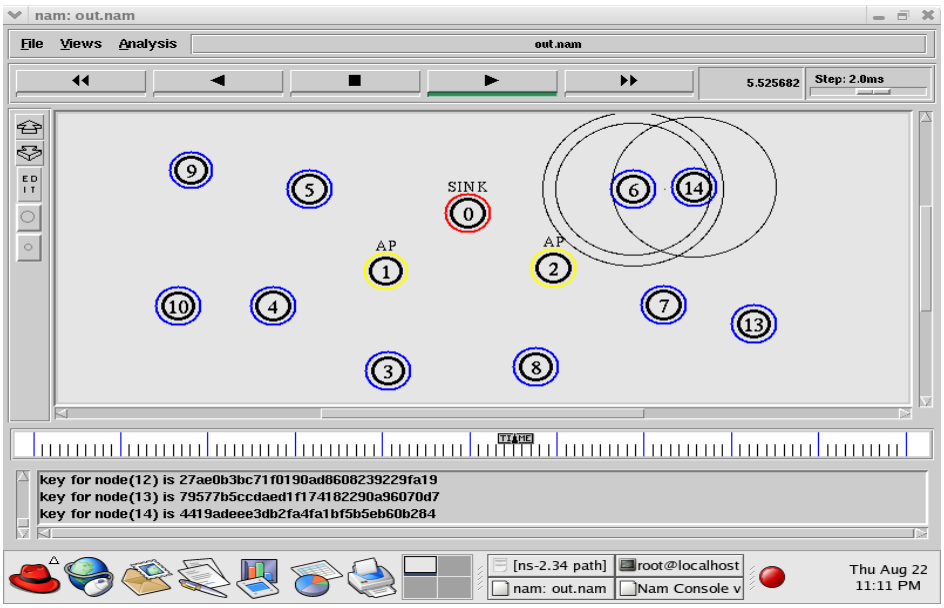
nam: out.nam
File Views Analysis
out.nam
5.525682
Step: 2.0ms
SINK
AP
AP
key for node(12) is 27ae0b3bc71f0190ad8608239229fa19
key for node(13) is 79577b5ccdaed1f174182290a96070d7
key for node(14) is 4419adeee3db2fa4fa1bf5b5eb60b284
[ns-2.34 path]
root@localhost
nam: out.nam
Nam Console v
Thu Aug 22
11:11 PM

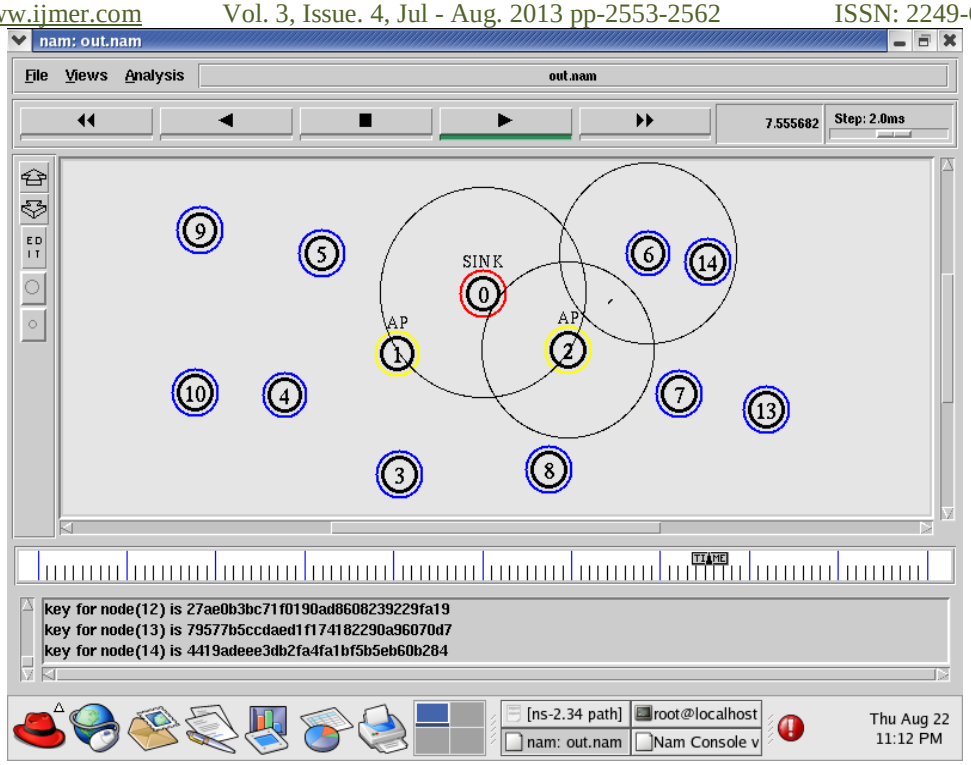

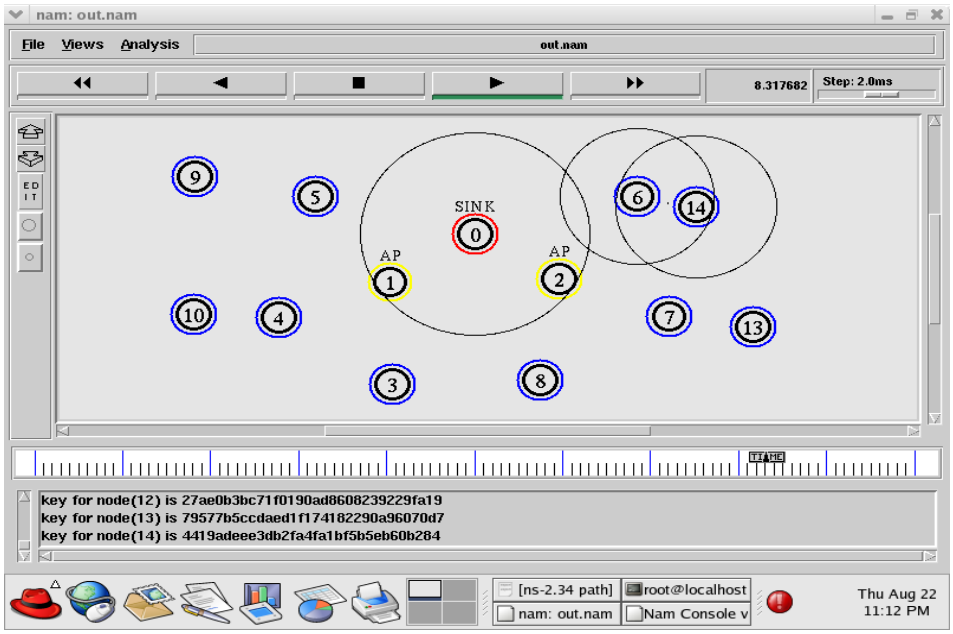

Screens Description:
Blue colour circles are Normal Sensor Nodes.
AP node is the Stationary Access Point, and Sink is the Mobile Sink,
Sensed Data Transmitted to the Base Station via Mobile Sink, in this Scheme we use Access Point (Stationary Access Points) in between Sensor Node and Mobile Sink.
Access Points acts as the Access Points to enter into the Sensor Network.
Ie., Sensor Node Sending Data to Mobile Sink through Access Point .
14-6-2-0
14-----is the Sensor Node
6----------Neighbour Node to 14(Indirect Path)
2- ---is the Access Node
0----- is the Mobile Sink

VII. CONCLUSION

Proposed a general three-tier security framework for authentication and pairwise key establishment between mobile sinks and sensor nodes. The proposed scheme, based on the polynomial pool-based key predistribution scheme substantially improved network resilience to mobile sink replication attacks compared to the single polynomial pool-based key

predistribution approach. Using two separate key pools and having few stationary access nodes carrying polynomials from the mobile pool in the network may hinder an attacker from gathering sensor data, by deploying a replicated mobile sink. The security performance of the proposed scheme is increased against stationary access node replication attack by strengthening the authentication mechanism between stationary access nodes and sensor nodes.

ACKNOWLEDGMENT

I would like to express my sincere thanks to my Guide and my Co-Authors for their consistence support and valuable suggestions.

REFERENCES

[1] T. Gao, D. Greenspan, M. Welesh, R.R. Juang, and A. Alm, "Vital Signs Monitoring and Patient Tracking over a Wireless Network," Proc. IEEE 27th Ann. Int'l Conf. Eng. Medicine and Biology Soc. (EMBS), Sept. 2005.
[2] L. Hu and D. Evans, "Using Directional Antenna to Prevent Wormhole Attacks," Proc. Network and Distributed System Security Symp., 2004.
[3] B.J. Culpepper and H.C. Tseng, "Sinkhole Intrusion Indicators in DSR MANETs," Proc. First Int'l Conf. Broadband Networks (Broad- Nets '04), pp. 681-688, Oct. 2004.
[4] A. Kansal, A. Somasundara, D. Jea, M. Srivastava, and D. Estrin, "Intelligent Fluid Infrastructure for Embedded Networks," Proc. Second ACM Int'l Conf. Mobile Systems, Applications, and Services (MobiSys '04), June 2004.
[5] Y. Tirta, Z. Li, Y. Lu, and S. Bagchi, "Efficient Collection of Sensor Data in Remote Fields Using Mobile Collectors," Proc. 13th Int'l Conf. Computer Comm. and Networks (ICCCN '04), Oct.2004.
[6] A. Rasheed and R. Mahapatra, "An Energy-Efficient Hybrid Data Collection Scheme in Wireless Sensor Networks," Proc. Third Int'l Conf. Intelligent Sensors, Sensor Networks and Information Processing, 2007.
[7] Amar Rasheed, Rabi N Mahapatra, "The Three Tier scheme in wireless sensor networks with mobile sinks", IEEE Trans. Parallel andDistributed Systems, vol 23, Issue 5, pp. 958-965, May.2012
[8] Y. Tirta, Z. Li, Y. Lu, and S. Bagchi, "Efficient Collection of Sensor Data in Remote Fields Using Mobile Collectors," Proc. 13th Int'l Conf.Computer Comm. And Networks (ICCN '04), Oct. 2004.
[9] W. Zhang, G. Cao, and T. La Porta, "Data Dissemination With Ring-Based Index for Wireless Sensor Networks," Proc. IEEE Int'l Conf. NetworkProtocols (ICNP), pp. 305-314, Nov. 2003.
[10] S. zhu, S. Setia, and S. Jajodia, "LEAP: Efficient Secuity Mechanisms for Large-scale Distributed sensor Networks," Proc. 10th ACM Conf.Computers and Comm. Security (CCS '03), pp. 62-72, Oct. 2003.
[11] A. Rasheed and R. Mahapatra, "An Efficient Key Distribution Scheme for Establishing Pairwise Keys with a Mobile Sink in Distributed Sensor Networks," Proc. IEEE 27th Int'l Performance Computing and Comm. Conf. (IPCCC '08), pp. 264-270, Dec 2008.
[12] A. Rasheed and R. Mahapatra, "A Key Pre-Distribution Scheme for heterogenouse Sensor Networks," Proc. Int'l Conf. Wireless Comm. AndMobile Computing Conf. (IWCMC '09), pp. 263-268, June 2009.

International Journal of Modern Engineering Research (IJMER)
www.ijmer.com Vol. 3, Issue. 4, Jul - Aug. 2013 pp-2563-2566 ISSN: 2249-6645

Narrating Fantasy in the Novel Pratimayum Rajakumariyum (The Statue and the Princes)

Sreedevi P.

Novelists sometimes have a strong persuasive intention on their readers and may use all the available resources of language to produce a powerful, emotional effect. Each writer takes the help of the medium of language to take his readers to a world which is familiar to him. Experience is the one which is not defined or varied, which at the same time can be a dream or reality, internal or external or social. A writer always leads a life which is far different from the one that live, if one goes into details.

According to Freud**:** The artist is one who is urged on by instinctive needs which are too clamorous: he longs to attain honour, power, riches, fame, and love of women, but he lacks the means of achieving these gratifications. So like any other, with an unsatisfied longing, he turns away from reality and transfer all his interests and his entire libido on to the creation of his wishes in the life of fantasy. (Freud, 314-315)

Padmarajan used the technique of this fantasy to narrate his novel *Pratimayum Rajakumariyum.* He also used the third-person objective perspective and tells a story without detailing any characters' thoughts, opinions, but instead gives an objective point of view. This point of view can be described as "the lens of a camera" that can only record the observable actions, but cannot visualize the thoughts going through the minds of the characters. The third-person objective is preferred in most pieces that are deliberately trying to take a neutral or unbiased view, as in newspaper articles. It is also called the third-person dramatic, because the narrator (like the audience of a drama) is neutral toward the plot — merely a commentating onlooker. Usually, his narrative is linear, with episodes. But in "Dimensions" he surprises us by charting a different path. Deliberately, he turns the story into a reflection on the art of writing a story itself, and wonders.

The living statue is one of the wonders at Fun Fort, the tourist place. In the Fun Fort there is a contest in which the winner would get free entry ticket worth thousand rupees to “Paradise on Island”, if he would stimulate any response in the statue. ‘The Paradise on Island’ can be called the next best attraction at the Fun Fort and it was a dream of Chuppan(the so called statue at the Fun Fort) to be there once. The princess Arundhati took this as a challenge.

She tried different ways to tempt the statue, but the statue fairly moved. Though Chuppan, the statue, wanted to move and accept his failure in front of the beautiful princess, his loyalty towards the owner made him act the other way. But this win over the beautiful princess put him down. The next day he even got punished by his boss (Dheerulal) for being late for the work. But Vairam(another member in Fun Fort) saved Chuppan from the punishments. By disguising himself as Govind Narayanan, Chuppan roamed around in the city with Vairam displaying their skills. Though people were watching their performance with amusement Govind’s mind was searching for the beautiful princess amidst the mob.

The princess who came to hear about the disappearance of Chuppan too did search for him. Between the activities of city, the princess spotted him. On the same night they met each other and left the city. Though they were busy among the amusements of the world the princess realized the dream of Govind to visit the ‘The Paradise on Island’. As the princess thought Chuppan was being lulled up with the thought of the island in his mind, she took him there. They met Dheerulal over there; the princess was ready to hand over Chuppan, to him on some conditions. To get Chuppan Dheerulal organized a dinner on the seventeenth floor of the guest house. There Chuppan stabbed Deerulal to death and leaped down from there. He stood up pushing the weeping princess aside who thought that Chuppan had passed away. He took three steps and stood like a statue, and still stands over there as a statue. This is the subject matter of the story. While entering, the novel reminds those words which describe the imaginary power of a writer as his greatest asset. The novel begins with the narration of the fun fort:

“This is an arid land; deep beneath the skies where a road stretches over it likes a ribbon evading the entire disturbance, carrying the Fun Fort at its one end and the outer world on the other end.”

The owner of Fun Fort is a Marvadi. The novel itself describes him as:

“The owner of the fun fort was one Marvadi, to be exact, just one Marvadi…Dheerulal Associates, Which means the Dheerulal family. The real owner is the present Dheerulal”. (*Prathimayum Rajakumariyum*, 11).

The Fun Fort of Dheerulal is said to be the narrative place in the novel, wherein he sells a lot of jokes. He drew in the leisure time and money of the people by providing entertainment for them. The English word ‘leisure’ appears to be derived from the Latin “licere” means ‘to be permitted” or ‘to be free’. Thus the word leisure is associated with a complexity of meaning in our language. Generally it is defined in terms ‘time left over after work’. (Anithakumari, 182)

The main attraction of leisure is to be free from responsibilities. Modern life is slipping to a tight schedule of time, where nobody finds time to do things they wish. All are in a rat race. Due to this busy life human relations become scattered and have no values. This miserable and painful human life is celebrated here. Here means the places which sell leisure and happiness which are creations of the upper society. The visitors might have had a lot to laugh over there, But the employees didn’t had much. The novel itself describes it like this:

“The 1500 employees of the fort did not really enjoy the fun in the part. Even though we may feel that there is something to laugh at…For them, as far as they were concerned this was not just fun, but a serious act.” (*Prathimayum Rajakumariyum*, 12)

Padmarajan emphasizes that even at times they felt bored. Bouvman presents life as an entertainment. But a poor homeless, Jobless person cannot consider life as merry making. His ideas are proved here. (Anithakumari, 184)

'In this new world, the entertainment is based on desires of gathering. But they fail to realize that they are inhumanly cheated by someone'. To take rest is part of entertainment. In this consumer world we can see how the free time of the people is also commercialized everywhere. In order to commercialize the free time of contemporary society, visually entertaining theme parks are constructed. It is in this kind of entertaining environment where this novel takes place. Padmarajan makes use of fantasy to create such an environment. What we get from this industry is the fantasy world created by them.

Here the author has worked out the theme of the novel *Prathimayum Rajakumariyum* from the fast evolving city culture, which is an integral part of globalization. In his earlier works the writer used to portray the life in the suburban villages. Later the scenes of fast moving city culture started to show up in his works, which naturally came with the exposure to the same.

The huss and buss of city life creates a disgustful life in the cities, Padmarajan recognized that all these were the necessities of a modern man. Even then no one was ready to step aside from the mechanical and confined life. Even villagers were not avoiding their journey into cites.

Radhalakshmi Padmarajan has this to say:

"Once they had been to a place known as Golden Beach in Chennai, where a person was standing like a statue to attract people coming over there. It was from that person, Padmarajan got inspired to write the novel *Prathimayum Rajakumariyum*." (Anithakumari, 183)

The background of the story is not a fantasy. Its a reality. But he narrated this novel to present the realities of modern world through unreal realms. He uses the technique of magical realism. Magic realism is a form which is widely used in Legendry literary works like Mahabharatha, Ramayana, Puranas and folktales in India. Padmarajan's works usually had a colour of his village and system. The typical Kerala Village is an undefined abode of myths and legends where riddles of vices and virtues exist. In which events are described realistically, but in a magical haze of strange local customs and beliefs.

The writer had a leap into the fantasy world in the novel. In the Fun Fort the statue was a reality. In this Context we should remember that a novelist is a person who looks upon his experiences through his Kaleidoscope. Here lies the importance of imagination. Reality and imagination merges together in a fantastic world created by the writer beyond place and time giving birth to a fantastic novel. Let us look how reality and imagination blends together in the novel *Prathimayum Rajakumariyum.*

In certain literary works there are human beings with super human qualities which are described as fantasy. This is different from the extra ordinary nature of the human beings found in myths and folktales. This comes under the category of characters that dwell in our surroundings either in the form of evil or divine. The same narrative fantasy is presented through Chuppan in *Prathimayum Rajakumariyum.*

"The fun fort was certainly a paradise for tourists. Every season was crowded with tourists. Birds, animals, plants groups of girls singing folk songs, shopping complex- all are present here. The murmuring statue of a gate keeper, a red turban on his head, a red crescent on his forehead, thick curled moustache red scapular resting on his shoulder. Silver bangles and diamond necklace- - with red silk around his waist. All these together make it a proud divine figure."

Here is a statue with all its masculine features in this story, the secret of this statue is unknown to others for its first year in Fun Fort. It is a tactic of Dheerulal.

"More than anyone else it is the owner himself to know the true degree of fineness of the main gate. That is a reason why he had played a trick to with hold every visitor who had come to this fort. He had a strong urge that even if the umpteen enjoyments remain in the mind, the memories of these amusements must last forever. And again come back to the fort. His calculations did not go wrong."

After a year he broke out the secret about the statue with great furore. The Statue once again attracted the attention of all the visitors who had been there for the last one year, as they came to know that it was not a statue that was standing over there, but a human being(Chuppan).

Chuppan lives in the fun fort and stands over there as a statue during the whole day, but disappears in the night to somewhere which is known to none. His deeds are super human. Thirst, hunger, weariness, aversion, love, sex which conquers ordinary man, does not seize Chuppan. With his supernatural mental ability he suppresses all his emotions. Even this suppression was mechanical. Therefore he discards this artificial world of the statue and celebrates aloud. When he reaches his own earth, there is the sight of Vairam following the statue; it is infact not the real face of the statue. Freedom to move was celebrated like a festival and the statue became restless. The speed and strength acquired by the motionless statue was amazing.

The freedom to move creates the fantasy. This novel is narrated through the eyes of Princess, Dheerulal, and Vairam. The statue is placed in the novel as Chuppan/ Statue/ Govind. For Dheerulal, the statue is mere Chuppan, for Vairam he is Govind Narayanan and for the princess he is the centre of her love.

The rich beautiful lady, Arundhathi's aim was to free the entity of the human in the statue. Even though she spends the money, beauty, pride, femininity, etc. for this, the mechanical mind of the statue maintained self control. But the temptations towards 'The Paradise on Island' tempted Chuppan inside the statue. For these Dheerulal is punished and imprisoned Chuppan, later he was rescued by Vairam. Arundhathi hears of Govindan, who performs amazing acts in cities. She doesn't feel any keen interest. But once unexpectedly she sees and recognizes him.

When the others fancy desires her, her fancy desires him, as her centre of love; she became aware of his libido in the state of the statue that stood in the wide spread sand bank. She was able to recognize the movements of the statue. She fell in love with him. Due to her love towards Govind she felt all his deeds are supernatural. The imaginary world of the love of the princess is mentioned by the statue in a brief conversation within the preface of this novel.

"The unconscious is the discourse of the other". What this means, essentially is that human passion is itself structured by the desire of other." (92)

Reading between the lines of '*Pratimayum Rajakumariyum'*, it is clear that the writer creates his other in this novel is to satisfy the needs of the other within him. In the study of *Pratimayum Rajakumariyum* done by Shaju.V.V, he creates an imaginary character called Mr. S, who did the interview with the Statue and the princess, who often tries to establish the desire of the unknown realms.

K.P Appan observes that "Where can such a story happen? And will not happen anywhere. Here what we find in that fiction becomes the alter ego of real life. But this is not a dream. This is a science of dream or a review of dream.
By placing a Philosophical doubt in the centre of the subject the novel is describing the theme. That's why Padmarajan writes like, as if he is trying to unlock the doors of an unknown world. This is the most valuable experience that the novel gives."

The Statue opens his mind in front of Mr. S. during the interview, 'you and the princess should not blame me for the values of male hegemony that you absorbed. I am not interested in putting on the dress of the hero. When some men touch the things under their authority, I don't interpret love as an authority. My subjectivity is not the problem here; the problem is your idea on it. There are many examples in history which shows the idolization of people who led an extra ordinary life. Let me say something simple. My stand facing the sea is also my rejection of your world.'
Princess' response to Mr.S, 'I am happy that you didn't present me as noble house wife, but I am also a woman who wishes subordination. I can't agree with the ideology you describe an ordinary woman.'

With this the Princess concludes the conversation with Mr. S like this, "I would rather expose myself to one, if someone whom I trust than you would pass through the story."

Shaju V.V, through his studies, point out the concept of the patriarchal society towards about the hero and the heroine. Throughout his studies he tries to portray the mental status of both the statue and the Princess and that of the readers. When the writer tries to create fantasy in the novel through its character blend with in artificial situations, the critic over here creates fantasy within fantasy, by examining the statue and the Princes created by the novelist. If examined closely we can spot the realism in the fantasy. The critic through his face to face encounter with the character breaks down the confined feelings that have been made by Patriarchy.
"Human desire, says Lacan, is expressed in language. Yet desire for Lacan is not pre-given; and it certainly does not just magically fit with language for its own particular ends."(19)

Likewise at times human desires come out through language. His wishes to be or not to be are expressed through this medium. On many occasions this way of seeing is practiced by the society.

Padmarajan has maintained a misogynist approach throughout the novel. Here the statue becomes a slave to her, and shows his back to the world. He can accurately objectify woman. This Ability conquered all his other abilities and rendered them unnatural. The days she spent with Govindhan made her realize that there is nothing beyond his ability and he could makes all her dreams come true. Many of his superhuman talents were displayed during the days he spent with the princess.

To fulfill his dream, to be at 'The Paradise on island', the princess brought him there. In his stories of sea voyage, at that moment he fought with Dheerulal at the sky castle building of that island. All these create the ultimate beauty of fantasy. The novelist presents Govind who stood like *Narasimha* incarnated in front of Dheerulal as a fantastic and callous figure. Govind woke up with a wild roar that he only made in the forest. She felt as if his sound was echoing all over the island and as his body was inflating up to burst in an attempt to grow to the skies……. He raised Dheerulal to the sky and slammed him on to the earth. Dheerulal's head got scattered by the demolishing power of that whip. At that time Govind behaves likes a Robot who lacks the control over its senses, like a revengeful wild animal. Then he tries to kill the princess like Dheerulal and he prepares to throw the princess down from the seventeenth floor. But when he saw her face in the light coming from outside, his mind urges for love, and gives her freedom. Before that moment of violence fades from the mind of the reader, he creates another fantasy. With a painful mourning Govind jumps down from the sixteenth floor. When the princess heard his mourning from eternity she fainted.

When the reader gets back to reality the narrator opens the door of fantasy again. Then what we get to see in the novel is the scene in which she comes down and hugs the body of Govind. To her surprise Govind turns his head towards her. When it became dusk she felt that peace had started enveloping him. Slowly parting his legs he stood up while she was pretending to be asleep. She noticed his gaze going beyond the horizon. He took three steps forward and stood motionless. In this way the riddle of fantasy goes on with the novel. Then the novelist takes him up from there and places him as a statue beyond the horizon.

He never moved at all from there as Arundhati's tears, cries, and appeal for forgiveness went in vain. According to K.P. Appan the role of the modern novelist is to create virtual characters that stand against reality into free imagination.

"The statue continues to stay there for a long time. It begins to rust, in the attack of the violent sea and persistent blow of salty wind. At the point where his eyes fixed, at the periphery of the promontory, mermaids would now and then raise their head above water to see him."

This can be observed in Padmarajan's works. Padmarajan's imagination is not experimental. It is a journey from reality to universal truth. Though imagination instead of clearing his doubts, he paves the way to enjoy autonomously.

From the beginning to the conclusion the real and the unreal are blended with the help of imagination. This helps the readers to rise from reality into an imaginary world. The writer discovers social truths around us. Certain truths are unfolded, that few lost are neutralized with the help of fantasy.Instead of being contented with the ordinary talents a writer using his imagination travels beyond universal truth.

Padmarajan occupies a unique place in Malayalam fictions. In terms of the theme and the narrative technique this novel has done justice to his genius. Reality and fantasy co-exist in the form of the fairy tale. Padmarajan has carefully presented modern man's materialistic approach. Modern mans desires do not rest completely in the natural balance of the universe. He discovers a void for himself and creates an artificial world of his own. In late 1960's, during the initial stage of Modernism, Padmarajan started writing novels. In 1990 through his work *Pratimayum Rajakumariyum* he became the creator of the electronic age in Malayalam fiction and paved way for part modern means of communication.

Bibliography

[1] Anithakumari, T. Padmarajan: Sahithyam, Cinema, Jeevitham. Cochin: Pranatha Books, 20007.
[2] Chullikkad, Balachandran. Balachandran Chullikkadinte kavithakal. Kottayam:D.C.books2000.
[3] Freud, Sigmund. Introductory Lectures on Psychoanalysis .London: Hogarth Press,1965.
[4] P.J, Pious and pradeep Pangad. Priyapetta Padmarajan. Pulikotin Publication, 1993.
[5] Padmarajan, P. Pratimayum Rajakumariyum. Kottayam: D. C. books, 1991.
[6] Padmarajante Thirakathakal. 4th edition.Kottayam: D.C Books, 1984.
[7] Itha Ividevare, Trissur:Current Books, 1997.
[8] Nakshatrangale Kaval, 4thedition. Trissur: Current Books, 1998.
[9] Padmarajante Kathakal. Kottayam: D.C. Books, 1998.
[10] Radhalakshmi, Padmarajan. Padmarajan Ende Gandharvan. Kozhikode: Matrubhumi Books, 2007.
[11] Sameeran, J.S. Padmarajan Gandharvano? Aparano? A journey through Padmarajan. Kayamkulam: Sree publications, 2001.

International Journal of Modern Engineering Research (IJMER)
www.ijmer.com Vol. 3, Issue. 4, Jul - Aug. 2013 pp-2567-2571 ISSN: 2249-6645

FPGA Based Wireless Jamming Networks

N. Radha Krishnaiah[1], Mrs. P. Brundavani[2]
M. Tech VLSI System Design, AITS, Rajampet, Kadapa(DT)
Assistant Professor, Dept: ECE, AITS, Rajampet, Kadapa (DT)

Abstract: *A mobile phone jammer is an instrument used to prevent cellular phones from receiving signals from base stations. When used, the jammer effectively disables cellular phones. These devices can be used in practically any location, but are found primarily in places where a phone call would be particularly disruptive because silence is expected. But the existing mobile phone jammers are having several defects so we are going to design a new mobile phone jammer using VLSI Technology which will be more efficient than existing jammers.*

Keywords: *Jammers, Mobile Jammer, FPGA, RF Transmitter, RF Receiver, LCD, Frequency Jamming.*

I. Introduction

A mobile phone jammer is an instrument used to prevent cellular phones from receiving signals from base stations. When used, the jammer effectively disables cellular phones. These devices can be used in practically any location, but are found primarily in places where a phone call would be particularly disruptive because silence is expected.

Mobile Jammers were originally developed for law enforcement and the military to interrupt communications by criminals and terrorists to foil the use of certain remotely detonated explosives. The civilian applications were apparent with growing public resentment over usage of mobile phones in public areas on the rise & reckless invasion of privacy. Over time many companies originally contracted todesign **mobile jammers** for government switched over to sell these devices to private entities. As with other radio jamming, **mobile jammers** block mobile phone use by sending out radio waves along the same frequencies that mobile phones use. This causes enough interference with the communication between mobile phones and communicating towers to render the phones unusable. Upon activating **mobile jammers**, all mobile phones will indicate **"NO NETWORK".** Incoming calls are blocked as if the mobile phone were off. When the **mobile jammers** are turned off, all mobile phones will automatically re-establish communications and provide full service. **Mobile jammer**'s effect can vary widely based on factors such as proximity to towers, indoor and outdoor settings, presence of buildings and landscape, even temperature and humidity play a role.

The choice of **mobile jammers** are based on the required range starting with the personal pocket mobile jammer that can be carried along with you to ensure undisrupted meeting with your client or a personal portable mobile jammer for your room or medium power mobile jammer or high power mobile jammer for your organisation to very high power military jammers to jam a large campuses.

Need & History of Jammers

The rapid proliferation of cell phones at the beginning of the 21st century to near ubiquitous status eventually raised problems, such as their potential use to invade privacy or contribute to academic cheating. In addition, public backlash was growing against the disruption cell phones introduced in daily life. While older analog cell phones often suffered from poor reception and could even be disconnected by simple interference such as high frequency noise, increasingly sophisticated digital phones have led to more elaborate counters. Cell phone jamming devices are an alternative to more expensive measures against cell phones, such as Faraday cages, which are mostly suitable as built in protection for structures. They were originally developed for law enforcement and the military to interrupt communications by criminals and terrorists. Some were also designed to foil the use of certain remotely detonated explosives. The civilian applications were apparent, so over time many companies originally contracted to design jammers for government use switched over to sell these devices to private entities. Since then, there has been a slow but steady increase in their purchase and use, especially in major metropolitan areas.

As with other radio jamming, cell phone jammers block cell phone use by sending out radio waves along the same frequencies that cellular phones use. This causes enough interference with the communication between cell phones and towers to render the phones unusable. On most retail phones, the network would simply appear out of range. Most cell phones use different bands to send and receive communications from towers (called frequency division duplexing, FDD). Jammers can work by either disrupting phone to tower frequencies or tower to phone frequencies. Smaller handheld models block all bands from 800 MHz to 1900 MHz within a 30-foot range (9 meters). Small devices tend to use the former method, while larger more expensive models may interfere directly with the tower. The radius of cell phone jammers can range from a dozen feet for pocket models to kilometers for more dedicated units. The TRJ-89 jammer can block cellular communications for a 5-mile (8 km) radius.

Less energy is required to disrupt signal from tower to mobile phone than the signal from mobile phone to the tower (also called base station), because the base station is located at larger distance from the jammer than the mobile phone and that is why the signal from the tower is not as strong.

Older jammers sometimes were limited to working on phones using only analog or older digital mobile phone standards. Newer models such as the double and triple band jammers can block all widely used systems (CDMA, iDEN, GSM, et al.) and are even very effective against newer phones which hop to different frequencies and systems when interfered with. As

the dominant network technology and frequencies used for mobile phones vary worldwide, some work only in specific regions such as Europe or North America. Some Cell Phone Jammers have been introduced to some State Prisons in the United States. Cell phones that have been sneaked into prison pose a security risk for guards and property owners living nearby.

Problems in Existing Jammers

Envisage a situation where you are essaying to dial 911 and cannot get through because someone has a cell phone jammer with him. Otherwise, you want to call the police to avoid a robbery in your building but the robber has a cell phone jammer with him. So, what could you do in such a dangerous situation? Jamming devices utilized with some thoughts may be much more useful than just a method of enjoyment. To remove these hazards a new efficient type of mobile jammer is proposed using FPGA. In this new design we are going to disable the keypad, MIC, speaker, will be only disabled by using the FPGA & we doing it using a 400MHz frequency which has an public license so there is no need of licensing.
Some of the Common Problems are listed below:

- The person didn't even get the notification of a call or message when he is in the jammer coverage area.
- The person cannot be contacted for some urgent information also.
- Nearly the mobile phone will be in Switch Off state.
- There will not be any notification that the user mobile has been jammed.

Proposed System Design

In most countries, it is illegal for private citizens to jam cell-phone transmission, but some countries are allowing businesses and government organizations to install jammers in areas where cell-phone use is seen as a public nuisance. In December 2004, France legalized cell-phone jammers in movie theaters, concert halls and other places with performances. France is finalizing technology that will let calls to emergency services go through. India has installed jammers in parliament and some prisons. It has been reported that universities in Italy have adopted the technology to prevent cheating. Students were taking photos of tests with their camera phones and sending them to classmates.

Alternatives to Cell Phone Jamming

While the law clearly prohibits using a device to actively disrupt a cell-phone signal, there are no rules against passive cell-phone blocking. That means using things like wallpaper or building materials embedded with metal fragments to prevent cell-phone signals from reaching inside or outside the room. Some buildings have designs that block radio signals by accident due to thick concrete walls or a steel skeleton. Companies are working on devices that **control a cell phone** but do not "jam the signal." One device sends incoming calls to voicemail and blocks outgoing calls. The argument is that the phone still works, so it is technically not being jammed. It is a legal gray area that has not been ruled on by the FCC as of April 2005.

Cell-phone alerters are available that indicate the presence of a cell-phone signal. These have been used in hospitals where cell-phone signals could interfere with sensitive medical equipment.

Block Diagram

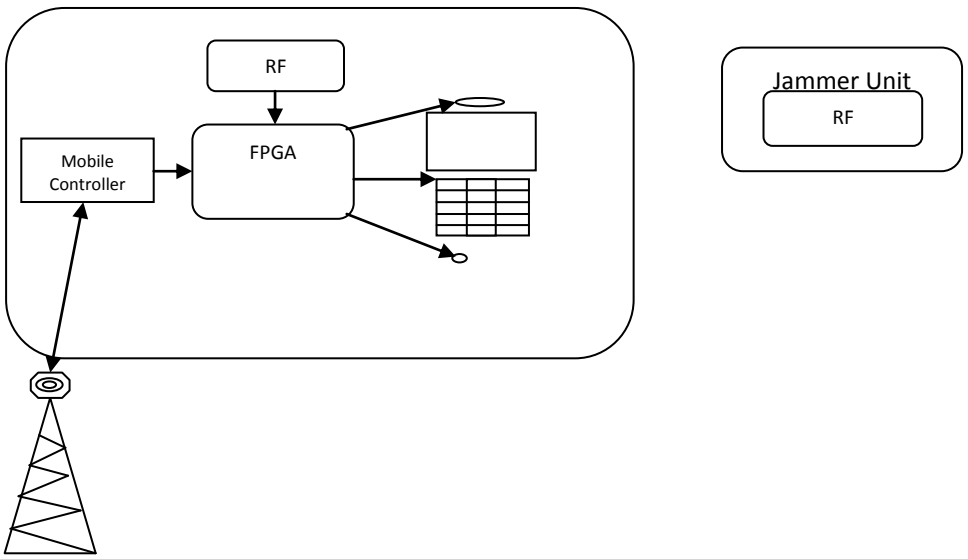

Figure 1: Mobile Jammer General Block Diagram

FPGA

A **Field-programmable Gate Array** (**FPGA**) is an integrated circuit designed to be configured by the customer or designer after manufacturing—hence "field-programmable". The FPGA configuration is generally specified using a hardware description language (HDL), similar to that used for an application-specific integrated circuit (ASIC) (circuit diagrams were previously used to specify the configuration, as they were for ASICs, but this is increasingly rare). FPGAs can be used to implement any logical function that an ASIC could perform. The ability to update the functionality after

shipping, partial re-configuration of the portion of the design[1] and the low non-recurring engineering costs relative to an ASIC design (notwithstanding the generally higher unit cost), offer advantages for many applications.

FPGA's contain programmable logic components called "logic blocks", and a hierarchy of reconfigurable interconnects that allow the blocks to be "wired together"—somewhat like many (changeable) logic gates that can be inter-wired in (many) different configurations. Logic blocks can be configured to perform complex combinational functions, or merely simple logic gates like AND and XOR. In most FPGAs, the logic blocks also include memory elements, which may be simple flip-flops or more complete blocks of memory.

In addition to digital functions, some FPGAs have analog features. The most common analog feature is programmable slew rate and drive strength on each output pin, allowing the engineer to set slow rates on lightly loaded pins that would otherwise ring unacceptably, and to set stronger, faster rates on heavily loaded pins on high-speed channels that would otherwise run too slow. Another relatively common analog feature is differential comparators on input pins designed to be connected to differential signaling channels. A few "mixed signal FPGAs" have integrated peripheral Analog-to-Digital Converters (ADCs) and Digital-to-Analog Converters (DACs) with analog signal conditioning blocks allowing them to operate as a system-on-a-chip. Such devices blur the line between an FPGA, which carries digital ones and zeros on its internal programmable interconnect fabric, and field-programmable analog array (FPAA), which carries analog values on its internal programmable interconnect fabric.

RF Encoder and Decoder

General Encoder and Decoder Operations

The Holtek HT-12E IC encodes 12-bits of information and serially transmits this data on receipt of a Transmit Enable, or a LOW signal on pin-14 /TE. Pin-17 the D_OUT pin of the HT-12E serially transmits whatever data is available on pins 10,11,12 and 13, or D0,D1,D2 and D3. Data is transmitted at a frequency selected by the external oscillator resistor.
By using the switches attached to the data pins on the HT-12E, as shown in the schematic, we can select the information in binary format to send to the receiver. The receiver section consists of the Ming RE-99 and the HT-12D decoder IC. The DATA_IN pin-14 of the HT-12D reads the 12-bit binary information sent by the HT-12E and then places this data on its output pins. Pins 10,11,12 and 13 are the data out pins of the HT-12D, D0,D1,D2 and D3. The HT-12D receives the 12-bit word and interprets the first 8-bits as address and the last 4-bits as data. Pins 1-8 of the HT-12E are the address pins. Using the address pins of the HT-12E, we can select different addresses for up to 256 receivers. The address is determined by setting pins 1-8 on the HT-12E to ground, or just leaving them open. The address selected on the HT-12E circuit must match the address selected on the HT-12D circuit (exactly), or the information will be ignored by the receiving circuit.

When the received addresses from the encoder matches the decoders, the Valid Transmission pin-17 of the HT-12D will go HIGH to indicate that a valid transmission has been received and the 4-bits of data are latched to the data output pins, 10-13. The transistor circuit shown in the schematic will use the VT, or valid transmission pin to light the LED. When the VT pin goes HIGH it turns on the 2N2222 transistor which in turn delivers power to the LED providing a visual indication of a valid transmission reception.

Controlling the Project with a FPGA

Using these RF transmitter & receiver circuits with a FPGA would be simple. We can simply replace the switches used for selecting data on the HT-12E with the output pins of the FPGA. Also we can use another output pin to select TE, or transmit enable on the HT-12E. By taking pin-14 LOW we cause the transmitter section to transmit the data on pins 10-13.
To receive information simply hook up the HT-12D output pins to the FPGA. The VT, or valid transmission pin of the HT-12D could signal the FPGA to grab the 4-bits of data from the data output pins. If you are using a FPGA with interrupt capabilities, use the VT pin to cause a jump to an interrupt vector and process the received data.
The HT-12D data output pins will LATCH and remain in this state until another valid transmission is received. **NOTE:** You will notice that in both schematics each of the Holtek chips have resistors attached to pins 15 and 16. These resistors must be the exact values shown in the schematic. These resistors set the internal oscillators of the HT-12E/HT-12D. It is recommended that you choose a 1% resistor for each of these resistors to ensure the correct circuit oscillation.

Range of Operation

The normal operating range using (only) the LOOP TRACE ANTENNA on the transmitter board is about 50 feet. By connecting a quarter wave antenna using 9.36 inches of 22 gauge wire to both circuits, you can extend this range to several hundred feet. Your actual range may vary due to your finished circuit design and environmental conditions. The transistors and diodes can be substituted with any common equivalent type. These will normally depend on the types and capacities of the particular loads you want to control and should be selected accordingly for your intended application.

RF Details

The TWS-434 and RWS-434 are extremely small, and are excellent for applications requiring short-range RF remote controls. The transmitter module is only 1/3 the size of a standard postage stamp, and can easily be placed inside a small plastic enclosure. TWS-434: The transmitter output is up to 8mW at 433.92MHz with a range of approximately 400 foot (open area) outdoors. Indoors, the range is approximately 200 foot, and will go through most walls.

Fig2: RF 434 Mhz Transmitter. Modulation: ASK

The TWS-434 transmitter accepts both linear and digital inputs, can operate from 1.5 to 12 Volts-DC, and makes building a miniature hand-held RF transmitter very easy. The TWS-434 is approximately the size of a standard postage stamp.

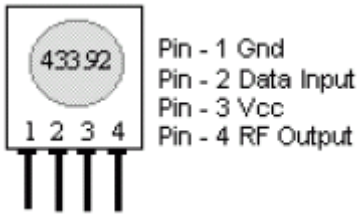

Fig 3: RF-434 Pin Diagram

LCD display

More FPGA devices are using 'smart LCD' displays to output visual information. The following discussion covers the connection of a 16x2 LCD display to a PIC FPGA. LCD displays designed around Hitachi's. LCD HD44780 module, are inexpensive, easy to use, and it is even possible to produce a readout using the 8x80 pixels of the display. Hitachi LCD display have a standard ASCII set of a characters plus Japanies, Greek and Mathematical symbols

For a 8-bit data bus, the display requires a +5 supply plus 11 I/O lines. For a 4_bit data bus it only requires the supply lines plus seven extra lines. When the LCD display is not enabled, data lines are tri-state which means they are in a state of high impedence and this means they do not interfere with the operation of the display is not being addressed.

Reading data from the LCD is done in the same way, but control line R/W has to be high. When we send a high to the LCD, it will reset and wait for instructions. Typical instructions sent to LCD display after a reset are: turning on a display, turning on a cursor and writing characters from left to right. When the LCD is initialized, it is ready to continue receiving data or instructions. If it receives character, it will write it on the display and move the cursor one space to the right. The Cursor marks the next location where a character will be written. When we want to write a string of characters, first we need to set up the starting address, and then send one character at a time. Characters that can be shown on the display are stored in data display (DD) RAM. The size of DDRAM is 80 bytes.

Fig 4(a)

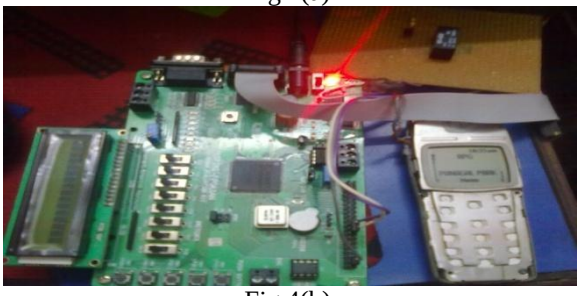

Fig 4(b)

Fig 4(a),4(b): Pictures of our Proposed Mobile jammer

II. Conclusions

Our Proposed Mobile Jammer is working perfectly without affecting the signals from the network. So that the user can able to get the notifications regarding Calls and messages (SMS, MMS). The notification about the calls will be given to the user. If there is any urgent call as we can get the notification we can go out from the coverage area and use our mobile as it is. No need of licensing. Implementation of our newly designed jammers is easy. As we are using a FPGA, our hardware can be modified whenever we want. Can be implemented where silence to be maintained. Future modifications are possible easily. Misuse of mobiles can be restricted. Thus our Mobile jammers can provide higher efficiency with lower misuses.

References

[1]. D. Adamy. *EW 101: A first course in electronic warfare*. Artech House Publishers, 2001.
[2]. I. Akyildiz, W. Lee, M. Vuran, and S. Mohanty. Next generation dynamic spectrum access cognitive radio wireless networks: A survey. *Computer Networks*, 50(13):2127–2159, 2006.
[3]. L. C. Baird, W. L. Bahn, M. D. Collins, M. C. Carlisle, and S. C. Butler. Keyless jam resistance. In *Proceedings of the 2007 IEEE Workshop on Information Assurance United States Military Academy*, 2007.
[4]. T. X. Brown, J. E. James, and A. Sethi. Jamming and sensing of encrypted wireless ad hoc networks. In *Proceedings of the ACM MobiHoc*, pages 120–130, 2006.
[5]. M. Cagalj, S. Capkun, and J.-P. Hubaux. Wormhole-based anti-jamming techniques in sensor networks. *IEEE Transactions on Mobile Computing*, 6(1):100–114, 2007.
[6]. A. Chan, X. Liu, G. Noubir, and B. Thapa. Control channel jamming: resilience and identification of traitors. In *Proceedings of ISIT*, 2007.
[7]. J. T. Chiang and Y.-C. Hu. Cross-layer jamming detection and mitigation in wireless broadcast networks. In *Proceedings of the MobiCom*, pages 346–349, 2007.

N. Radha Krishnaiah , born in Rajampet, A.P., India in 1989. He received B.Tech Degree in Electronics and Communication Engineering from J.N.T University Anantapur, India. Presently pursuing M.Tech (VLSI SYSTEM DESIGN) from Annamcharya Institute of Technology and Sciences, Rajampet, A.P., India. His research interests include VLSI, Embedded Systems

I did this project under the guidance of Mrs. P. Brundavani born in Proddatur, A.P., India in 1982. She received B.Tech Degree in Electronics and Communication Engineering from G Pullareddy Engineering College, Kurnool, A.P., India in 2004. Presently working as an associative professor in Annamacharya Institute of Technology and Sciences, Rajampet, India. She got her M.Tech from JNTU Anantapur, A.P., India. Her research area is in Digital IC Design, VLSI Technology, Testing and Testability, Microprocessor.

International Journal of Modern Engineering Research (IJMER)
www.ijmer.com Vol. 3, Issue. 4, Jul - Aug. 2013 pp-2572-2576 ISSN: 2249-6645

An Experimental Study to Predict Optimum Weld Bead Geometry through Effect of Control Parameters for Gas Metal Arc Welding Process in Low Caron Mild Steel

Arka Sen[1], Dr. Sudip Mukherjee[2]

[1]*Assistant Professor, Department of Mechanical Engineering, Surendranath Institute of Engineering & Management, Siliguri ,WestBengal, India*

[2] *Professor, Department of Mechanical Engineering, Jalpaiguri Government Engineering College, Jalpaiguri, West Bengal, India,*

Abstract: *Here in this work, an attempt has been made to find the interaction between control parameters and weld bead geometry for fillet welding in mild steel specimen using Gas Metal Arc Welding process. Accordingly control parameters have been adjusted to find the optimal bead geometry. Initially the equations involving control parameters and bead geometry were developed by multiple regression analysis method. These equations are then simulated in computer to find the effects of the control parameters on weld bead geometry. Finally optimization of weld bead parameters is done by obtaining a single set of control parameters from its four different best sets through computer simulation.*

Keywords: *Bead width, GMAW process, Left leg length, Re-informent height, Right leg length.*

I. INTRODUCTION

Nowadays Gas Metal Arc welding process (GMAW) has been the most commonly used welding technique throughout the industrial world. GMAW uses a welding torch, a electric power source, shielding gas & a wire pool with wire drive control. The welding process is very simple. GMAW process can be used to weld thicker metal plates with high productivity. The shielding gas is used to protect the weld pool from oxidation. The shielding gas used is either inert gas or carbon dioxide.

GMAW process is done in butt joints as well as fillet joints. The quality of weld is determined by the weld bead geometry characteristics (also referred as physical parameters in this study); i.e the weld bead width, weld bead penetration, weld re-inforcement height, weld left leg length , weld right leg length. This weld bead geometry characteristics is a function of input variables (also referred as control parameters in this study) which are welding current, welding voltage, welding speed, wire tip distance, weld joint position, wire diameter, shielding gas composition, gas flow rate, material composition and material thickness. These control parameters affect the quality of the weld.

Previously, various studies and analysis on butt weld for prediction of bead geometry have been performed but there is very little work done on describing the effects of control parameters on fillet weld bead geometry. This study has developed mathematical models to determine the effects of each control parameters on weld bead geometry and optimization of the control parameters to get the best weld bead geometry characteristics.

II. EXPERIMENTAL WORKS

The experimental research work for predicting the relationship between process parameters of welding & the weld bead geometry is done systematically by a defined process. For the purpose of the experimental work the gas metal arc welding process (GMAW) was conducted on mild steel plates.

2.1 Determination of experimental parameters.

Before conducting the welding experiment, three most important control parameters are identified which mostly determines the weld bead profile? These parameters are welding current, welding voltage & the welding speed. The operating range of each of the parameters is taken in accordance with the normal operating range for such kind of operation. The assigned control parameters are listed in the Table. 1

Table 1: Control factors & their levels

PARAMETERS	SYMBOL	LEVEL		
		LOW	MIDDLE	HIGH
WELDING CURRENT (Amp)	I	160	220	280
WELDING VOLTAGE (Volt)	V	20	22.5	27
WELDING SPEED (mm/sec)	S	1.97	3.57	5.17

2.2 Experimental procedure

The experimental procedure to measure bead geometry using input weld data was performed. In this experimental work, the FAIR WELD MIG 400A welding machine was used. The experimental material 25mm (2.5cm) thick 1018 Mild

(low carbon) steel plates cut into 150mm (15cm) length were fixed by the prepared jig. Table. 2 and Table. 3 show mechanical properties and chemical composition of base metal .Carbon-dioxide shielding gas was employed in the experiment.

Table 2: Mechanical properties of base metal

Ultimate Tensile Strength, Kpa	439885.514464
Yield Strength, Kpa	370248.465936
Elongation	15.00%
Rockwell Hardness	B71

Table 3: Chemical properties of base metal

Material	% Composition
Iron (Fe)	98.81 - 99.26%
Carbon (C)	0.18%
Manganese (Mn)	0.6 - 0.9%
Phosphorus (P)	0.04% max
Sulphur (S)	0.05% max

2.3 Conduct of the Experiment

From the Taguchi design of experiment, a conclusion is made that for three number of independent experimental parameters (i.e welding current, welding voltage & welding speed), with three different levels of each parameters (i.e. low level, mid level & high level), there has to be nine different observation sets. The physical parameters of the weld bead geometry to be measured are weld bead width, weld re-inforcement height, weld left leg length & weld right leg length.

The weld bead geometry is shown in Fig.1

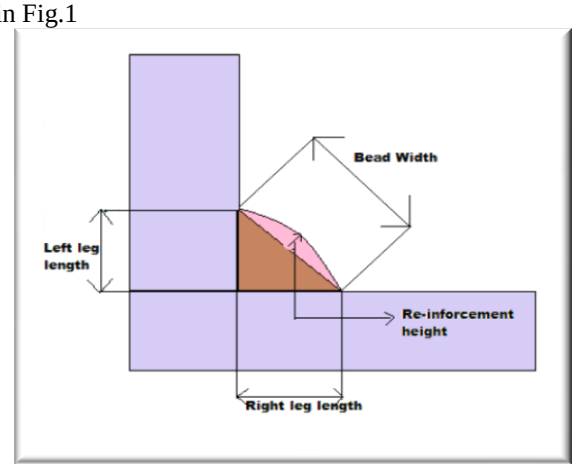

Fig.1: Weld bead geometry

Table. 4 shows the experimental results using the nine observation sets.

Table 4 : Measured experimental data

Experiment No	Welding Current (A)	Welding Voltage (V)	Welding Speed (sec/15cm)	Bead Width (mm)	Re-inforcement Height (mm)	Left Leg length (mm)	Right leg length (mm)
1	**160**	**21**	**76**	**10.2**	**0.5**	**7.4**	**7.4**
2	**180**	**20**	**58**	**10.1**	**0.7**	**6.3**	**5.8**
3	**190**	**21**	**65**	**10.4**	**0.9**	**8.6**	**8.1**
4	**200**	**23**	**52**	**11.1**	**1.2**	**8.0**	**8.4**
5	**210**	**24**	**76**	**10.1**	**1.5**	**7.1**	**7.2**
6	**220**	**22**	**74**	**12.1**	**1.5**	**9.0**	**8.6**
7	**240**	**22**	**55**	**10.5**	**0.9**	**7.1**	**8.4**
8	**250**	**26**	**35**	**11.0**	**1.3**	**7.6**	**7.2**
9	**280**	**27**	**29**	**12.5**	**1.1**	**9.1**	**8.6**

III. DEVELOPMENT OF MATHEMATICAL MODEL

From the experimental observations, multiple regression analysis was done to find the relationship between control parameters & physical parameters. The equations obtained are as follows:

Bead Width (BW) = 0.0123 + 0.0095 *I + 0.35005 * V + 0.00981 * S + 0.00092764* I^2 + 0.000561 * V^2 - 3.8726 * S^2 - 0.4 *I * V + 0.01329 *I*S +0.035 *V*S----------(1)

Re-inforcement height (RH) = -0.0035197 + 0.003848444 *I + 0.0017637334 *V +0.077151088 *S + 0.000048641* I^2 + 0.0000545898 *V^2 – 14.186 * S^2 + 0.0283 *I*V -0.000778671* I* S + 0.026906535 *V*S ----------(2)

Left leg length (LLL) = -0.044638867 + 0.281959034 * I + 2.840262884* V – 5.583572 * S + 0.00001485 * I^2 + 0.001725776 * V^2 + 527.541 * S^2 -14.07151286* I * V + 12.19315 *I*S+ 0.039817247 *V* S ----------(3)

Right leg length (RLL) = -0.0154 + 0.0900 * I + 0.8077 * V + 1.7139* S - 0.0002 * I^2 – 0.0004 * V^2 - 322.5063 * S^2 - 3.3705 * I * V + 0.0034 * I* S -0.0088 * V* S----------(4)

IV. EFFECT OF CONTROL PARAMETERS ON WELD BEAD GEOMETRY

It is observed that the control parameters have a definite effect on weld bead geometry and by the analysis of the graphs the best values of physical parameters are obtained. Keeping the two control parameters at their arithmetic means, the third control parameter is varied within its range to get the effect on physical parameters. The graph from Fig.2 to Fig. 13 illustrates the matter.

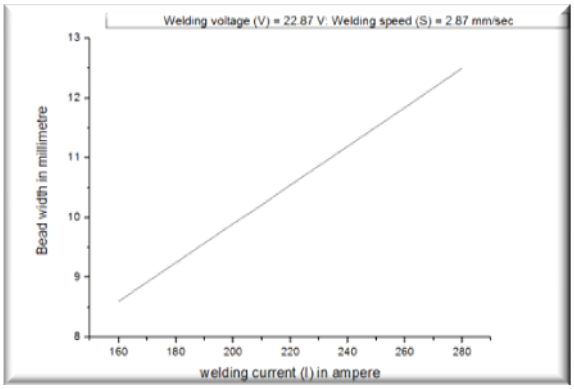

Fig.2: Variation of welding current with bead width

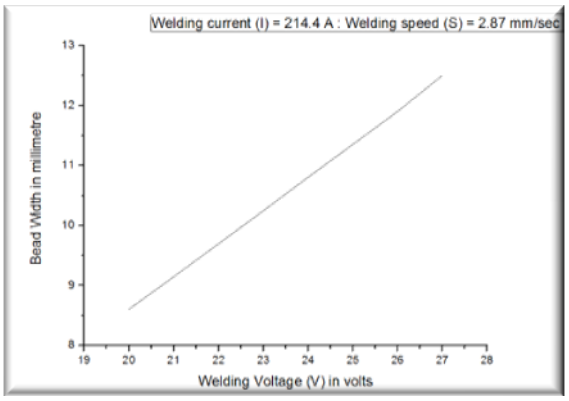

Fig.3: Variation of welding voltage with bead width

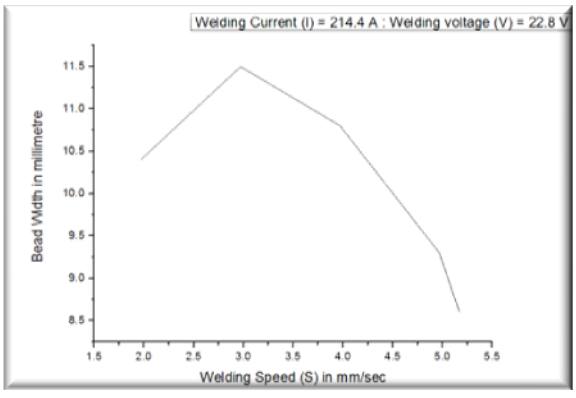

Fig.4: Variation of welding speed with bead width

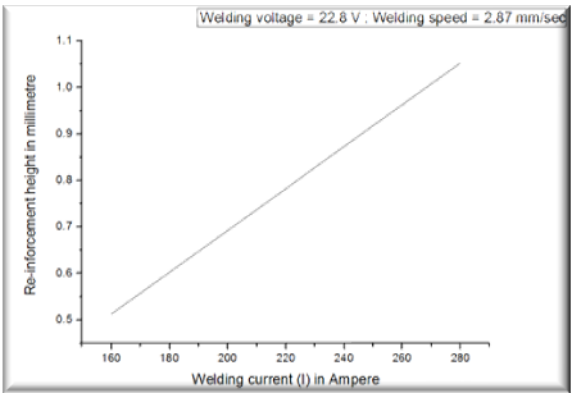

Fig.5: Variation of welding current with re-inforcement height

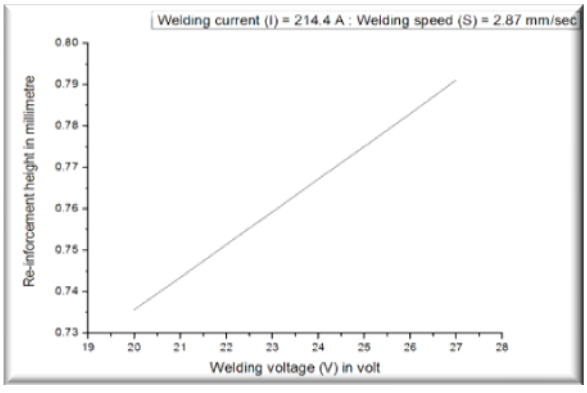

Fig.6: Variation of welding voltage with re-inforcement height

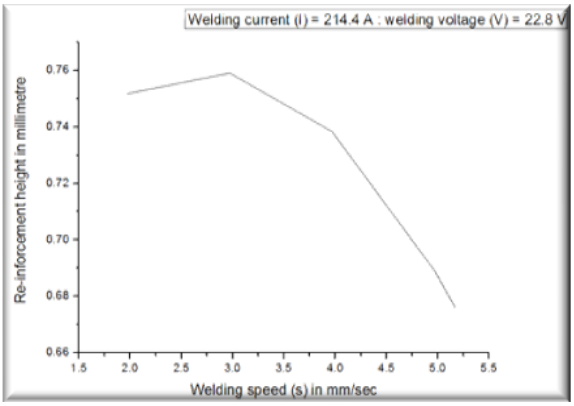

Fig.7: Variation of welding speed with re-inforcement height

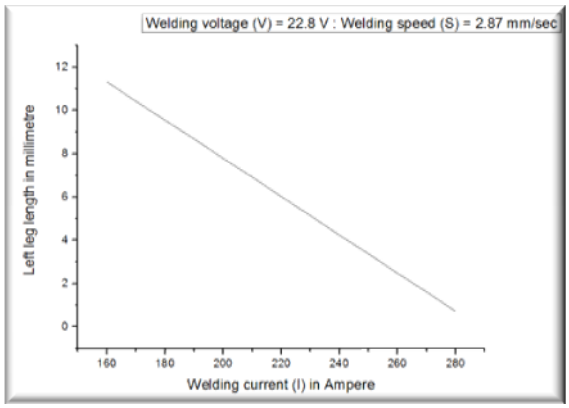

Fig.8: Variation of welding current with left leg length

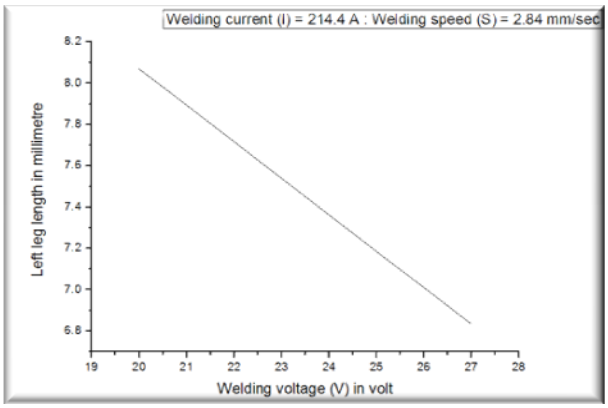

Fig.9: Variation of welding voltage with left leg length

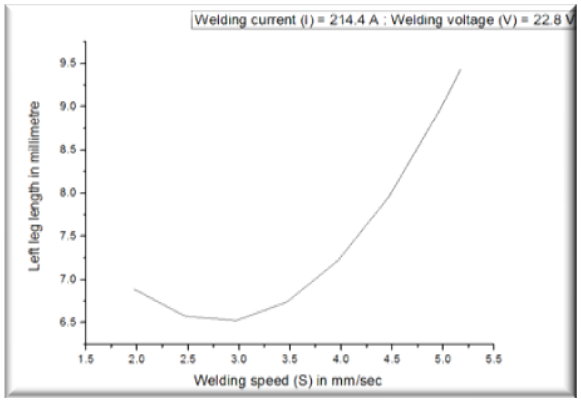

Fig.10: Variation of welding speed with left leg length

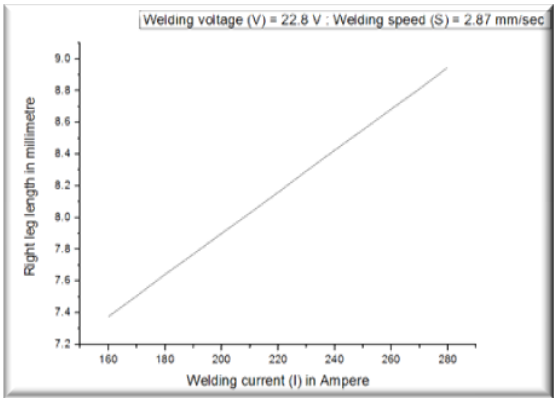

Fig.11: Variation of welding current with right leg length

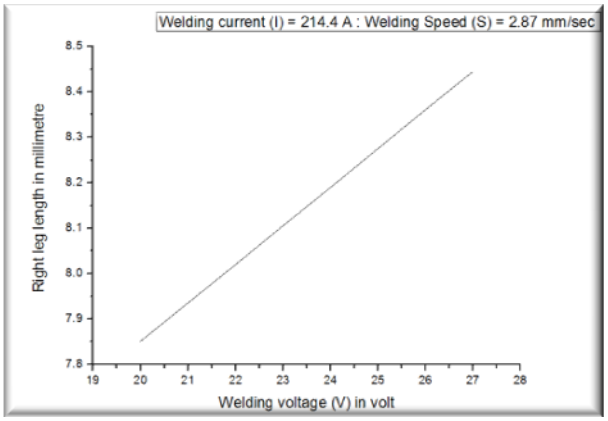

Fig.12: Variation of welding voltage with right leg length

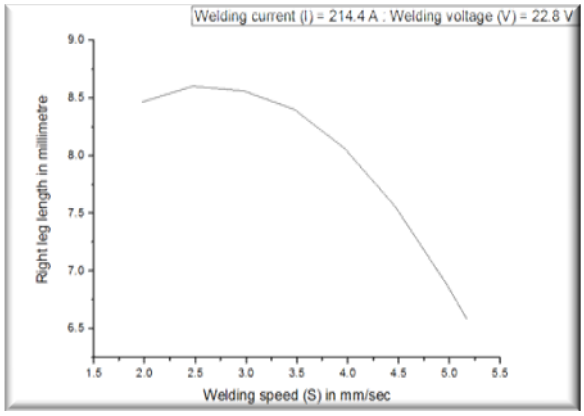

Fig.13: Variation of welding speed with right leg length

V. RESULTS & DISCUSSIONS

Based on the experimental results on gas metal arc fillet welding, regression analysis was done for predicting the weld bead geometry. From the graphs above, four different best sets of results for bead geometry profile is observed which are as follows:

a. The set of control parameters for maximum bead width are welding current (I) = 280 A, welding voltage (V) = 27 V, and welding speed (S) = 2.97 mm/sec and the corresponding bead width is 11.58 mm.
b. The set of control parameters for minimum re-inforcement height are welding current (I) = 160 A, welding voltage (V) = 20 V, and welding speed (S) = 5.17 mm/sec and the corresponding re-inforcement height is 0.408mm.
c. The set of values of control parameters for maximum left leg length are welding current (I) = 160 A, welding voltage (V) = 20 V, and welding speed (S) = 5.17 mm/sec and the corresponding left leg length is 8.05mm.
d. The set of control parameters for maximum right leg length are welding current (I) = 280 A, welding voltage (V) = 27 V, and welding speed (S) = 2.99 mm/sec and the corresponding right leg length is 8.35mm.

VI. OPTIMIZATION

In a welding process, best bead parameters are normally obtained by using different sets of control parameters as is shown in the results earlier. So practically it may not be possible to get the best bead parameters. Therefore it is necessary to develop a single set of control parameters which will provide optimum weld bead geometry.

From the four sets of control parameters providing the best bead parameters, it is seen that most of the control parameters are repeated twice. Therefore average from the four sets of control parameters are taken in a bid to find the optimum bead parameters which are:
Welding current (I) = 220 A
Welding voltage (V) = 23.5 V
Welding speed (S) = 4.075 mm/sec
These values are then varied by ±10% keeping the other two control parameters constant in order to find the optimum bead geometry which is found as follows:
Bead width = 10.08 mm
Re-inforcement height = 0.66 mm
Left leg length = 8.75 mm
Right leg length = 7.34 mm
And the corresponding control parameters are:
Welding current (I) = 198 A
Welding voltage (V) = 23.5 V
Welding speed (S) = 4.075 mm/sec

6.1 Comparison with best values:
The following Table.5 compares the best values of control parameters with their optimum values & their corresponding physical parameters. It is found that the optimum set of control parameters which gives the best values of physical parameters is very close to its corresponding best set of results.

Table 5: Comparison table of best values with optimum values

BEST VALUES			OPTIMUM VALUE		
		BEAD WIDTH			BEAD WIDTH
WELDING CURRENT	280 A	11.58 mm			10.08 mm
WELDING VOLTAGE	27 V				
WELDING SPEED	2.97 mm/sec				
		RE-INFORCEMENT HEIGHT			RE-INFORCEMENT
WELDING CURRENT	160 A	0.408 mm			0.66 mm
WELDING VOLTAGE	20 V		WELDING CURRENT (I)	198 A	
WELDING SPEED	5.17 mm/sec		WELDING VOLTAGE (V)	23.5 V	
			WELDING SPEED (S)	4.075 mm/sec	
		LEFT LEG LENGTH			LEFT LEG LENGTH
WELDING CURRENT	160 A	8.05 mm			8.75 mm
WELDING VOLTAGE	20 V				
WELDING SPEED	5.17 mm/sec				
		RIGHT LEG LENGTH			RIGHT LEG LENGTH
WELDING CURRENT	280 A	8.35 mm			7.34 mm
WELDING VOLTAGE	27 V				
WELDING SPEED	2.99 mm/sec				

VII. CONCLUSION

Hence from the experimental study, it can be concluded that a single set of control parameters can provide bead parameters which are considerably close to the best bead parameters obtained by four sets of control parameters. Therefore, it is much more practical to use a single set of control parameters which will provide optimum bead geometry.

REFERENCES

Journal papers:
[1] A New Approach for Predicting and Optimizing Weld Bead Geometry in GMAW by Farhad Kolahan, Mehdi Heidari, World Academy of Science, Engineering and Technology 2:2 2010
[2] Optimization of GMAW process parameters using Particle Swarm Optimization by Sreeraj, T Kannan, Subhashis Maji / Mechanica confab.
[3] Achieve to desired weld bead geometry for the vessel fillet joints in mobile robotic welding by M. Golestani Sehat, Kh. Farhangdoost Mechanical Engineering Department Ferdowsi University, mashhad, Iran; Published inTehran International Congress on Manufacturing Engineering (TICME2005) December 12-15, 2005, Tehran,Iran.
[4] Effect of Welding Parameters on Dilution and Weld Bead Geometry in Cladding by M.Nouri, A.Abdollah-zadehy and F.Malek Department of Materials Engineering, Tarbiat Modares University; J. Mater. Sci. Technol., Vol.23 No.6, 2007.
[5] Optimization of weld bead geometry in TIG welding process using grey relation analysis and taguchi method by Ugur Esme, Melih Bayramoglu, Yugut Kazancoglu, Sueda Ozgun: UDK 621.791.05 Original Scientific Article : ISSN 1580-2949, MTAEC9, 43(3)143(2009)

International Journal of Modern Engineering Research (IJMER)
www.ijmer.com Vol. 3, Issue. 4, Jul - Aug. 2013 pp-2577-2580 ISSN: 2249-6645

An Optimal Risk- Aware Mechanism for Countering Routing Attacks in MANETs

Shaik Silarbi[1], G. Sridevi[2]
[1]*M. Tech, Nimra College of Engineering & Technology, Vijayawada, A.P., India*
[2]*Assoc. Professor, Dept.of CSE, Nimra College of Engineering & Technology, Vijayawada, A.P., India*

***Abstract*:** *Mobile Ad Hoc Networks (MANET) are a distributed and self configuring wireless networks. MANETs does not have a predefined network infrastructure. Application of MANET is benefited in areas such as disaster relief, military services and mine site operations. Each node communicates with the other acting nodes as routers. The co-operation and trust between the nodes are depended for the proper functioning of MANET. Being the flexible network, MANET is exposed to various types of attacks especially the routing attacks. There are various methods introduced to mitigate such critical routing attacks. In this paper, we propose a risk-aware response mechanism to systematically cope with the routing attacks in MANET, proposing an adaptive time-wise isolation method. Our risk-aware approach is based on the extended Dempster-Shafer (D-S) evidence model. D-S theory has been adopted as a valuable tool for evaluating the reliability and security in information systems and by other engineering fields, where precise measurement is impossible to obtain or expert elicitation is required.*

Keywords: *D- S theory, MANET, Routing attack.*

I. INTRODUCTION

Mobile Ad Hoc Networks (MANET)[1] (Figure 1) is distributed and self configuring wireless network. MANETs does not have a predefined network infrastructure. Application of MANET is benefited in areas such as disaster relief, military services and mine site operations. Each node communicates with the other nodes acting as routers. The co-operation and trust between the nodes are depended for the proper functioning of MANET. Since the network topology in MANET changes unpredictably and rapidly it is highly vulnerable to various types of attacks. Attack prevention methods such as authentication and encryption, intrusion detection system, intrusion prevention can be used in defense for reducing certain attack possibilities. MANET is considered one of the most promising fields in both research and development of wireless networks. There exist many intrusion response mechanisms for the routing attacks. The existing techniques usually attempt to isolate the vulnerable nodes from the topology there by causing the partition of network topology.

Methods such as binary responses may result in the unexpected network partition, thereby causing additional damages to the network infrastructure, and naive fuzzy responses could lead to uncertainty in countering routing attacks in MANET. Several intrusion detection techniques have been introduced for detecting the vulnerable nodes and preventing the neighbor nodes compromised by the malicious nodes. Even though several mechanisms and routing protocols are introduced each of them has one or more vulnerabilities. Research on the MANETs and implementation has become a huge amount of task to be done. When a malicious node is being identified then the node has to be either repaired or another route has to be established. In most of the existing techniques the nodes when found slightly malicious is completely isolated from the entire network which will make splitting of the network and thereby causing communication problems between the nodes.

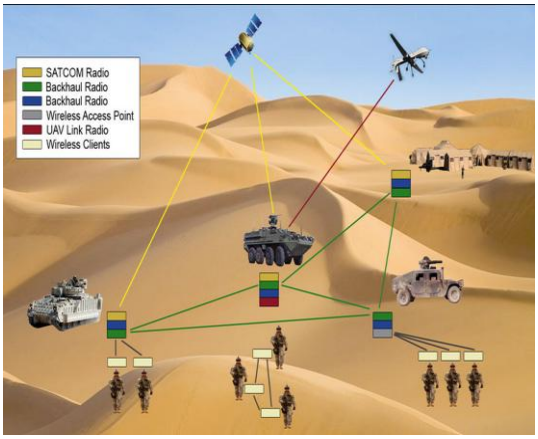

Figure 1: An Example MANET

II. RELATED WORK

In [2], the authors propose the ariadne protocol for preventing the attacks against the networks. An ad hoc network is a group of wireless mobile computers or nodes, in which individual nodes cooperate by forwarding packets for each other to allow nodes to communicate beyond direct wireless transmission range. Prior research in ad hoc networking has generally studied the routing problem in a non-adversarial setting, thereby assuming a trusted environment. Here routing attacks are

presented against routing in ad hoc networks, and the design and performance evaluation of a new secure on-demand ad hoc network routing protocol is presented i.e. called Ariadne. Ariadne [2] prevents compromised nodes or attackers from tampering with uncompromised routes consisting of uncompromised nodes, and also prevents a large number of types of Denial-of-Service (DOS) attacks.

In [3], the authors has presented the Secure Efficient Ad hoc Distance vector routing protocol (SEAD) mechanism to guard against the DoS attacks. An ad hoc network is a collection of wireless computers or nodes, communicating among themselves over possibly multi- hop paths, without the help of any infrastructure such as base stations or access points. In [4], the authors proposed a vector model for all security services rely to a great extent on some notion of trust. However, even today, there is no accepted technique or formalism for the specification of trust and for reasoning about trust. In [5], the authors developed an alternative methodology for the risk analysis of information systems security (ISS), an evidential reasoning approach under the Dempster-Shafer theory of belief functions. In [6], the authors has proposed the cooperative enforcement approach. Ad hoc networks rely on the co- operation of the nodes [6] participating in the network to forward packets for each other. A node may decide not to co- operate to save all its resources while still using the network to relay its traffic. If too many nodes exhibit this behaviour, the network performance degrades and cooperating nodes may find themselves unfairly loaded. If a node observes another node that not participating correctly, it reports this observation to other nodes who then take action to avoid being affected and potentially punish the bad node by refusing to forward its traffic.

III. PROPOSED WORK

A. Risk- aware Response Mechanism

In this section, we have a tendency to articulate an adjustive risk-aware response method supported quantitative risk estimation and risk tolerance. Rather than applying easy binary isolation of the malicious nodes, our approach adopts an isolation mechanism in a very temporal manner supported the danger price. We have a tendency to tend to perform risk assessment with the extended D-S proof theory introduced in for every routing attacks and corresponding countermeasures to make extra correct response picks illustrated in Figure 2.

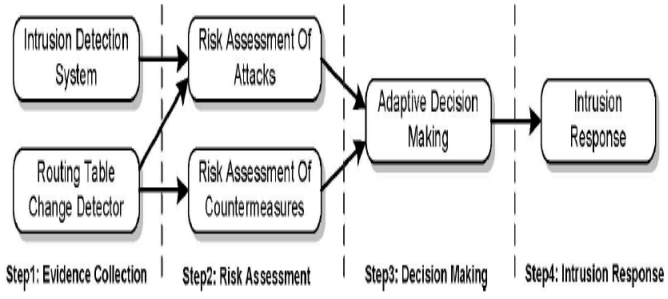

Figure 2: Risk-aware response mechanism

Evident Collection: In this step Intrusion Detection System (IDS) provides associate degree attack alert with a confidence price, and so the routing Table modification Detector (RTCD) runs to work out what percentage changes on routing table area unit caused by the attack.

Risk Evaluation: Alert confidence from IDS and therefore the routing table would be an additional thought-about as freelance evidences for risk calculation and combined with the extended D-S theory. Risk of countermeasures is calculated moreover throughout the risk assessment section, supported the danger of routing attacks and thus the chance of countermeasures, the whole risk of associate attack is also discovered.

Decision Creating: The accommodative decision module provides a flexible response decision making method, that takes risk estimation and risk tolerance into consideration, to control the temporary isolation level, a user can set fully totally different thresholds to satisfy her goal.

Intrusion Response: With the output from the risk assessment and decision-making module, the corresponding response actions, at the side of the routing table recovery and node isolation, administered to mitigate attack damages throughout a distributed manner.

B. Response to Routing attacks

In this approach, we use two different responses to deal with different attack methods: routing table recovery and the node isolation. Routing table recovery includes the local routing table recovery and global routing recovery. Local routing recovery is performed by the victim nodes that detect the attack and automatically recover its own routing table. Node isolation may be the most intuitive way to prevent further routing attacks from being launched by malicious nodes in MANET. To perform a node isolation response, the neighbors of the malicious nodes ignore the malicious node by neither forwarding packets through it nor accepting any network packets from it. Figure 3 shows an example scenario where nodes 2 to 0 are supposed to go through Nodes 3 and 5. Suppose a malicious node 1 advertises a fake link to node 0 and then it

would also cause all other nodes to update its routing table accordingly. As a result the data from Nodes 2 to 0 travels Node 1 rather than nodes 2 and 4 and Node 1 can manipulate and drop the traffic between Nodes 2 to 0.

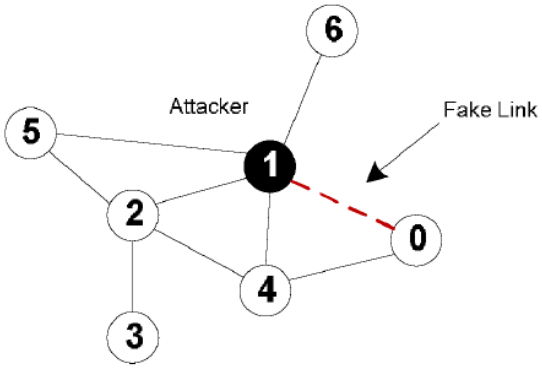

Figure 3: Example scenario

C. Risk Assessment

In risk assessment step, alert confidence from IDS and RTDC would be considered as different evidences and these two evidences combined using Dempster's rule of combination with the importance factors (DRCIF) algorithm. It provides entire risk of attack. Security state of the MANET can be classified into two categories. {Secure, Insecure} which means security state of MANET could be either secure or insecure. Risk of MANET could be represent by belief function called Bel{Insecure}. The algorithm for combination of the multiple evidences is constructed as follows:

Algorithm MUL-EDS-CMB
INPUT: Evidence pool Ep
OUTPUT: One evidence
1 |Ep|= sizeof(Ep);
2 While |Ep| > 1 do
3 Pick two evidences with the least IF in Ep, named E1 and E2;
4 Combine these two evidences,E= <m1 ⊕ m2, (IF1+ IF2)/2>;
5 Remove E1 and E2 from Ep;
6 Add E to Ep;
7 end
8 return the evidence in Ep

D. Adaptive Decision Making

ADM (Adaptive Decision Making) technique is used to provide a flexible response decision making method when it gets attack alert. Our adaptive decision making module is based on the quantitative risk estimation and risk tolerance, which is shown in Figure 4. The response level is additionally splitted into multiple bands. Each band is associated with an isolation degree, which presents a different time interval of the isolation action. The response action and the band boundaries are all determined in accordance with risk tolerance and can be changed when risk tolerance threshold changes. The upper risk tolerance threshold (UT) would be associated with the permanent isolation response. The lower risk tolerance threshold (LT) will remain each node intact. The band between the upper tolerance threshold and lower tolerance threshold is associated with a temporary isolation response, in which the isolation time "T" changes dynamically based on the different response level given by

$$i = \left\lceil \frac{Risk - LT}{UT - LT} \times n \right\rceil, \; Risk \in (LT, UT)$$

and

$$T = 100 \times i \; (milliseconds)$$

where "n" is the number of bands and i is the corresponding isolation band.

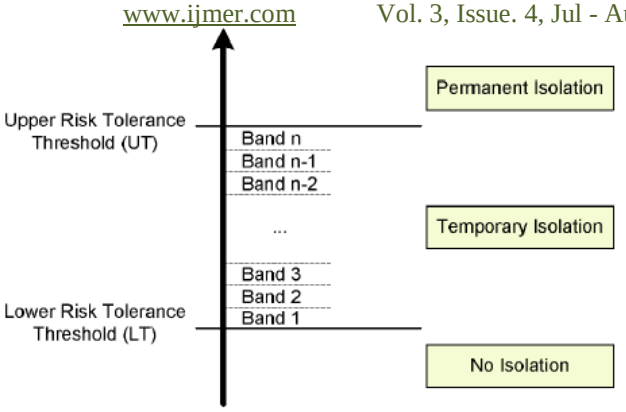

Figure 4: Adaptive decision making

IV. CONCLUSIONS

Mobile ad hoc network (MANET) is a collection of mobile nodes without the required intervention of any existing infrastructure or centralized access point such as a base station. MANET has the dynamic infrastructure hence it is highly vulnerable to various attacks. Several attacks are possible in MANET networks and among them the routing attack could cause the worst damage. There are several solutions available for mitigating such routing attacks. In this paper, we propose an adaptive risk-aware response mechanism with the extended D-S evidence model, considering damages caused by both attacks and their countermeasures. The adaptiveness of our method allows us to systematically cope with MANET routing attacks.

REFERENCES

[1] S. Wang, C. Tseng, K. Levitt, and M. Bishop, ―Cost-Sensitive Intrusion Responses for Mobile Ad Hoc Networks,‖ Proc. 10th Int'l Symp. Recent Advances in Intrusion Detection (RAIDf'07), pp. 127- 145, 2007.

[2] Hu, Y.C., Perrig, A. and Johnson, D.B. (2002), "Ariadne: A Secure On-Demand Routing Protocol for Ad Hoc Networks," Proceedings of 8th Annual International Conference on Mobile Computing and Networking (MobiCom'02), ACM Press, pp.12–23.

[3] Hu, Y.C., Perrig, A. and Johnson, D.B. (2002), "Secure Efficient Distance Vector Routing in Mobile Wireless Ad Hoc Networks," 4th IEEE Workshop Mobile Computing Systems and Applications (WMCSA'02), pp.3-13.

[4] Ray and Chakraborty, S. (2004). "A vector model of trust for developing trustworthy systems," European Symposium on Research in Computer Security, September, pp. 260–275.

[5] L. Sun, R. Srivastava, and T. Mock (2006), "An Information Systems Security Risk Assessment Model under the Dempster-Shafer Theory of Belief Functions," J. Management Information Systems, vol. 22, no. 4, pp. 109-142.

[6] Bansal, S. and Baker (2003), "Observation-Based Cooperation Enforcement in Ad Hoc Networks," Technical Report cs.NI/0307012, Stanford University, Vol.1, No.2, pp.1-10.

International Journal of Modern Engineering Research (IJMER)
www.ijmer.com Vol. 3, Issue. 4, Jul - Aug. 2013 pp-2581-2584 ISSN: 2249-6645

A Novel Method for Privacy Preserving Micro data Publishing using Slicing

Shaik Khasimbee[1], Syed Sadat Ali[2]
[1]*M. Tech, Nimra College of Engineering & Technology, Vijayawada, A.P., India.*
[2]*Assoc. Professor & Head, Dept.of CSE, Nimra College of Engineering & Technology, Vijayawada, A.P., India.*

***Abstract*:** *Data anonymization techniques for privacy-preserving data publishing have received a lot of attention in recent years. Microdata or detailed data contains information about a person, a household or an organization. Most popular anonymization techniques are: Generalization and Bucketization. Generalization transforms the Quasi-Identifiers (QI) in each bucket into "less specific but semantically consistent" values so that tuples in the same bucket cannot be distinguished by their QI- values. In bucketization, one separates the Sensitive Attributes (SAs) from the QIs by randomly permuting the SA values in each bucket. The process of Generalization loses considerable amount of information, especially for high-dimensional data. Where as Bucketization does not prevent membership disclosure and does not apply for data that do not have a clear separation between quasi- identifying attributes and sensitive attributes. To improve the current state of the art, in this paper, we propose a novel data anonymization technique called slicing. Slicing method preserves utility because it groups highly correlated attributes together, and preserves the correlations between such attributes. Slicing protects privacy because it breaks the associations between the uncorrelated attributes, which are infrequent and thus identifying.*

Keywords: *Bucketization, Generalization, Identifier, Slicing.*

I. INTRODUCTION

Data sharing has become common now- a- days and there is an exponential growth in the amount of information. Data mining is the process of extraction of large amount of hidden useful information from large databases. Privacy-preserving data mining (PPDM) deals with obtaining valid data mining results without underlying the data values. The problem of privacy preserving data publishing has received a lot of attention in recent years. Agencies and other organizations often need to publish micro data, e.g., census data, medical data, etc for research and other purposes. When releasing microdata, the association of quasi identifiers with sensitive attributes in the public records has long been recognized as a privacy risk. Microdata contains records each of which contains information about an individual entity, a household, such as a person, or an organization. Typically, microdata is stored in a table, and each record or row corresponds to one individual. Each record has a number of attributes or fields, which can be divided into the following three categories:

- **Identifier:** Identifiers are attributes or fields that clearly identify individuals. Examples include Social Security Number (SSN) and Name.
- **Quasi-Identifier:** Quasi-identifiers (QI) are attributes whose values when taken together can potentially identify an individual. Examples include Birthdate, Zip-code, and Gender. An adversary may already know the QI- values of some individuals in the data. This knowledge can be either from personal contact or from other publicly available databases (e.g., a voter registration list) that include both explicit identifiers and the quasi-identifiers.
- **Sensitive Attribute:** Sensitive attributes are the attributes whose values should not be associated with an individual by the adversary. Examples include Salary and Disease.

An example of microdata table is shown in Table 1.

Table 1: Micro data Example

Age	Sex	Zipcode	Disease
22	M	47906	dyspepsia
22	F	47906	flu
33	F	47905	flu
52	F	47905	bronchitis
54	M	47302	flu
60	M	47302	dyspepsia
60	M	47304	dyspepsia
64	F	47304	gastritis

II. ANONYMIZATION METHODS

A. Generalization

Generalization [1] [2] is the process of replacing a value with a "less-specific but semantically consistent" value. Tuple suppression removes the entire record from the table. Unlike traditional privacy protection techniques such as data swapping and adding noise, information in a k- anonymized table through generalization process remains truthful. For

example, through generalization, Table 2 is an anonymized version of the microdata table in Table 1. Typically, generalization process utilizes a value generalization hierarchy (VGH) for each attribute. In a VGH, the leaf nodes correspond to actual attribute values, and internal nodes represent less-specific values.

Table 2: Generalization

Age	Sex	Zipcode	Disease
[20-52]	*	4790*	dyspepsia
[20-52]	*	4790*	flu
[20-52]	*	4790*	flu
[20-52]	*	4790*	bronchitis
[54-64]	*	4730*	flu
[54-64]	*	4730*	dyspepsia
[54-64]	*	4730*	dyspepsia
[54-64]	*	4730*	gastritis

B. Bucketization

Another anonymization method is called. Bucketization. Bucketization is also known as anatomy or permutation-based anonymization [3][4]. The bucketization process first partitions tuples in the table into buckets and then separates the quasi-identifiers with the sensitive attribute by randomly permuting the sensitive attribute values in each bucket. The anonymized data consists of a set of buckets with the permuted sensitive attribute values. The main difference between generalization and bucketization methods lies in that bucketization does not generalize the QI attributes. When the adversary knows who are in the microdata table and their QI attribute values, the two anonymization techniques become equivalent. Table 3 gives the bucketization of data in Table 1.

Table 3: Bucketization

Age	Sex	Zipcode	Disease
22	M	47906	flu
22	F	47906	dyspepsia
33	F	47905	bronchitis
52	F	47905	flu
54	M	47302	gastritis
60	M	47302	flu
60	M	47304	dyspepsia
64	F	47304	dyspepsia

III. NEED OF SLICING

Generalization meyhod transforms the QI-values in each bucket into “less specific but semantically consistent” values so that tuples in the same bucket cannot be distinguished by their QI values. In bucketization, one separates the SAs from the QIs by randomly permuting the sensitive attributes values in each bucket. The anonymized data consists of a set of buckets with the permuted sensitive attribute values. It has been shown[5][6] that generalization for k-anonymity losses considerable amount of information, especially for high-dimensional data. This is due to the following three reasons: First, generalization for k-anonymity suffers from the curse of the dimensionality. Second, in order to perform the data analysis or data mining tasks on the generalized table, the data analyst has to make the uniform distribution assumption that every value in a generalized interval or set is equally possible, as no other distribution assumption can be justified. Third, because each attribute is generalized separately, then correlations between different attributes are lost.

While bucketization method [3][4] has better data utility than generalization, it has several limitations. First, bucketization method does not prevent membership disclosure [7]. Because bucketization method publishes the QI values in their original forms, an adversary can find out whether an individual has a record in the published data or not. As shown in [2], 87 percent of the individuals in the United States can be uniquely identified using only three attributes (Birthdate, Sex, and Zipcode). Second, bucketization method requires a clear separation between QIs and SAs. Third, by separating the sensitive attribute from the QI attributes, bucketization method breaks the attribute correlations between the QIs and the SAs.

Table 4: Slicing

(Age,Sex)	(Zipcode,Disease)
(22,M)	(47905,flu)
(22,F)	(47906,dysp.)
(33,F)	(47905,bron.)
(52,F)	(47906,flu)
(54,M)	(47304,gast.)
(60,M)	(47302,flu)
(60,M)	(47302,dysp.)
(64,F)	(47304,dysp.)

Slicing is the process of partitioning the dataset both vertically and horizontally. Vertical partitioning is done by grouping attributes into various columns based on the correlations among the attributes. Each column contains a subset of the attributes that are highly correlated. Horizontal partitioning is done by grouping the tuples into buckets. Finally, within each bucket, the values in each column are randomly permutated or sorted to break the linking between different columns. The basic idea of slicing method is to break the association cross columns, but to preserve the association within each column. This reduces the dimensionality of the data and preserves better utility than generalization and bucketization methods.

IV. SLICING ALGORITHM

The proposed algorithm consists of three phases: attribute partitioning, column generalization, and tuple partitioning.

A. Attribute Partitioning

Attribute portioning phase partitions attributes so that highly-correlated attributes are in the same column. This is good for both utility as well as privacy. In terms of data utility, grouping highly- correlated attributes preserves the correlations among those attributes. In terms of privacy, the association of uncorrelated attributes presents higher identification risks than that of the association of highly-correlated attributes because the association of uncorrelated attributes values is much less frequent and thus is more identifiable. Therefore, it is better to break the associations between the uncorrelated attributes, in order to protect privacy. In this phase, we first compute the correlations between a pairs of attributes and then cluster attributes based on their correlations.

B. Column Generalization

In the column generalization phase, tuples are generalized to satisfy some minimal frequency requirement. We want to point out that column generalization is not an indispensable phase in slicing algorithm. Bucketization method provides the same level of privacy protection as generalization, with respect to attribute disclosure. Although column generalization is not a required step, it can be useful in several aspects. First, column generalization phase may be required for identity/membership disclosure protection. Second, when column generalization phase is applied, to achieve the same level of privacy against attribute disclosure, bucket sizes can be smaller.

C. Tuple Partitioning

In the tuple partitioning phase, tuples are partitioned into various buckets. We modify theMondrian [8] algorithm for tuple partition phase. Unlike Mondrian k-anonymity, no generalization method is applied to the tuples; we use Mondrian for the purpose of partitioning the tuples into buckets. Algorithm 1 gives the description of the tuple-partition algorithm. The algorithm maintains two data structures: (1) a queue of buckets (Q) and (2) a set of sliced buckets (SB). Initially, "Q" contains only one bucket which includes all tuples and SB is empty (line 1). In each iteration (line 2 to line 7), the algorithm removes a bucket from "Q" and splits the bucket into two buckets. If the sliced table after the split satisfies ℓ-diversity (line 5), then this algorithm puts the two buckets at the end of the queue Q (for more splits, line 6). Otherwise, we cannot split the bucket anymore and then the algorithm puts the bucket into SB (line 7). When "Q" becomes empty, we have computed the sliced table. The set of sliced buckets is "SB" (line 8).

Algorithm 1: Tuple-partition(T, ℓ**)**
1. Q = {T}; SB = ∅.
2. while Q is not empty
3. remove the first bucket B from Q; Q = Q − {B}.
4. split B into two buckets B1 and B2, as in Mondrian.
5. if **diversity-check**(T, Q ∪ {B1,B2} ∪ SB, ℓ)
6. Q = Q ∪ {B1,B2}.
7. else SB = SB ∪ {B}.
8. return SB.

The main part of algorithm 1 is to check whether a sliced table satisfies ℓ-diversity (line 5). Algorithm 2 gives a brief description of the diversity-check algorithm.

Algorithm 2: Diversity-check(T, T^*, ℓ**)**
1. for each tuple t ∈ T, L[t] = ∅.
2. for each bucket B in T^*
3. record f(v) for each column value v in bucket B.
4. for each tuple t ∈ T
5. calculate p(t,B) and find D(t,B).
6. L[t] = L[t] ∪ {<p(t,B),D(t,B)>}.
7. for each tuple t ∈ T
8. calculate p(t, s) for each s based on L[t].
9. if p(t, s) ≥ 1/ℓ, return false.
10. return true.

Algorithm 2 first takes one scan of each bucket B (line 2 to line 3) to record the frequency f(v) of each column value v in bucket B. Then this algorithm takes one scan of each tuple t in the table T (line 4 to line 6) to find out all tuples that match B and record their matching probability p(t,B) and the distribution of the candidate sensitive values D(t,B), which are added to the list L[t] (line 6). The sliced table is ℓ-diverse iff for all the sensitive value s, $p(t, s) \leq 1/\ell$ (line 7 to line 10).

V. CONCLUSION

Data often contains personally identifiable information and therefore releasing such data may result in various privacy breaches. Several anonymization methods, like Generalization and Bucketization are designed for privacy preserving microdata publishing. Generalization loses considerable amount of information mainly for high dimensional data. Bucketization does not prevent membership disclosure and does not apply for data that do not have a clear separation between QI- attributes and SAs. In this paper we show how slicing method can be used for attribute disclosure protection. Slicing preserves better utility than generalization method and is more effective than bucketization method in workloads involving the sensitive attribute. It also demonstrates that how overlapping slicing is used to prevent the membership disclosure.

REFERENCES

[1] P. Samarati and L. Sweeney, "Protecting privacy when disclosing information: k-anonymity and its enforcement through generalization and suppression," 1998. Technical Report, SRI-CSL-98-04, SRI International.
[2] L. Sweeney, "k-Anonymity: A model for protecting privacy," International Journal on Uncertainty, Fuzziness and Knowledge-based Systems, vol. 10, no. 5, pp. 557– 570, 2002.
[3] X. Xiao and Y. Tao, "Anatomy: simple and effective privacy preservation," in Proceedings of the International Conference on Very Large Data Bases (VLDB), pp. 139–150, 2006.
[4] N. Koudas, D. Srivastava, T. Yu, and Q. Zhang, "Aggregate query answering on anonymized tables," in Proceedings of the International Conference on Data Engineering (ICDE), pp. 116–125, 2007.
[5] D. Kifer and J. Gehrke, "Injecting utility into anonymized datasets," in Proceedings of the ACM SIGMOD International Conference onManagement of Data (SIGMOD), pp. 217–228, 2006.
[6] C. Aggarwal, "On k-anonymity and the curse of dimensionality," in Proceedings of the International Conference on Very Large Data Bases (VLDB), pp. 901–909, 2005.
[7] M. E. Nergiz, M. Atzori, and C. Clifton, "Hiding the presence of individuals from shared databases," in Proceedings of the ACM SIGMOD International Conference on Management of Data (SIGMOD), pp. 665–676, 2007.
[8] K. LeFevre, D. DeWitt, and R. Ramakrishnan, "Mondrian multidimensional k- anonymity," in Proceedings of the International Conference on Data Engineering (ICDE), p. 25, 2006.

International Journal of Modern Engineering Research (IJMER)
www.ijmer.com Vol. 3, Issue. 4, Jul - Aug. 2013 pp-2585-2587 ISSN: 2249-6645

Optimal Converge cast Methods for Tree- Based WSNs

Mahammad Irfan Shaik[1], Sayeed Yasin[2]
[1]*M. Tech, Nimra College of Engineering & Technology, Vijayawada, A.P., India.*
[2]*Asst. Professor, Dept.of CSE, Nimra College of Engineering & Technology, Vijayawada, A.P., India*

Abstract: *A tree- based wireless sensor network (WSN) is a collection of sensors nodes, such as sink is the root of tree and leaves are the nodes. Data in such a topology flows from sensor nodes (leaves) to the sink (root) node of the tree. Collection of data from a set of sensors to an intermediate parent (sink) in a tree network is known as converge-casting. The delivery time and the data rate are application specific. As an example, in oil and gas refineries the sensor equipment and controllers need to collect data from all the sensors within a specific deadline for any kind of leakage or failures. Whereas applications like weather forecasting, under-water observations needs continuous and quick data delivery for analysis, for longer periods. In this paper our goal is on such applications focusing on fast data streaming from sensor to sink node. The two optimal approaches for data collection proposed in this paper are – aggregated-data convergecast where packets are aggregated at each hop, and raw-data convergecast where each data packet travel towards sink node individually. First method is most suitable where data is highly co-related and objective is to collect maximum sensor reading and second method is used where the reading of each sensor is equally important.*

Keywords: *Broadcast, Converge cast, Data collection, WSN.*

I. INTRODUCTION

Data collection from a set of sensors to a common sink over a tree-based network is a fundamental traffic pattern in wireless sensor networks (WSNs). This many-to-one communication paradigm in which data flows from many nodes to a single node is called as convergecast. One may view convergecast as opposite to multicast or broadcast in which data flows from a single node to a set of nodes in the network. The following figures shows a simple example that illustrates the characteristics of a typical broadcast and convergecast. In a broadcast, as shown in Figure 1, node s is the message source and nodes a, b, and c are expected recipients. Node "a" hears the message directly from s and forwards a copy to nodes b and c. In case of a convergecast, as shown in Figure 2, nodes a, b, and c each has a message destinedto the sink node s, and a serves as a relay for b and c.

Once data is collected at the sink node, it can either be recorded and stored for future analysis, or can be processed immediately to take certain actions depending on application requirements. In a sensor network, data collection can either be triggered by external sources, such as queries to get a snapshot view of the network, or events as and when they appear, or can be for the continuous periodic monitoring without any external triggering. In all cases, however, the many-to-one communication pattern is very common. Depending on application requirements, various objectives can be associated with data collection. For instance, in disaster early warning applications, such as forest fire detection [1] and gas/oil leaks [2], or structural damage identification [3], bursty traffic generated by events needs to be delivered to the sink as quickly and as reliably as possible to prevent catastrophes.

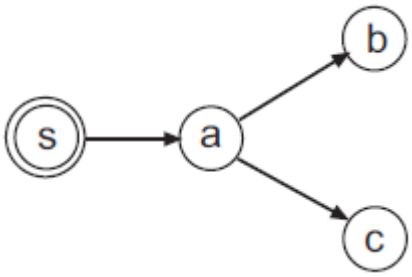

Figure 1: Broadcast

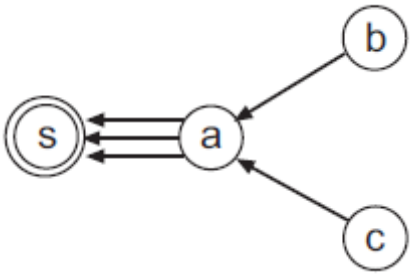

Figure 2: Convergecast

Particularly under regular, heavy traffic conditions, contention-free medium access control (MAC) protocols, such as Time Division Multiple Access (TDMA), where the nodes communicate on different time slots to prevent the conflicts, offer several advantages for data collection as compared to contention-based protocols [4]. They eliminate collisions, idle listening and overhearing, which are the main sources of energy consumption in wireless communications [5].

II. RELATED WORK

In [6], the authors discussed about the hypothetical limits of data collection capacity. Here the wireless sensor network is a TDMA based network. In the past, the data collection capacity is based on very large scale random networks, though most of the sensors are not deployed uniformly and the available sensors will not be as huge as in theory. In [7], the authors discuss about the improvement of communication performance by using multiple channels. The current multi-channel protocols are not suitable for sensor networks due to minimum number of available channels and unavoidable time errors found in such networks. Here a novel tree based multi channel scheme for data collection applications is constructed that allocates disjoint trees and exploits parallel transmissions among trees. In [8], the authors constructed a distributed scheduling algorithm for the tree networks that requires at most $\max(3n_k - 1, N)$ time slots for convergecast, where n_k represents the maximum number of nodes in any sub tree and N represents the number of nodes in network. The Distributed scheduling algorithm requires at most 3N time slots in any sensor network.

In [9], the authors address the problem of performing the operation of Data Aggregation enhanced Convergecast(DAC) in an energy and latency efficient manner. By assuming as all the nodes in the sensor network have a data item and there is an a priori known application dependent data compression factor, the total data is collected. In [10], the authors describes the contention free Time Division Multiple access scheduling based protocols for collecting data using tree based routing topologies. By using TDMA method, the nodes can communicate on different slots to prevent interference and conflicts. Consecutive time slots are grouped into non- overlapping frames. Hence the schedule for each time frame is repeated when data collection is periodic.

III. PROPOSED WORK

A. Periodic Aggregated Convergecast

Data aggregation is a commonly used technique in sensor networks that can eliminate redundancy and minimize the number of transmissions, thus saving energy and improving network lifetime. Aggregation can be performed in many ways, such as by suppressing duplicate messages; using data compression and various packets merging techniques; or taking advantage of the correlation in the sensor readings. Given the lower bound "$\Delta(T)$" on the schedule length in the absence of interfering links, we now present a time slot assignment scheme in Algorithm 1, called BFSTIMESLOTASSIGNMENT, that achieves this bound. In each iteration of the algorithm, an edge *e* is chosen in the Breadth First Search (BFS) order starting from any node, and is assigned the minimum time slot that is different from all its adjacent edges respecting interfering constraints. Note that, since we evaluate the performance of algorithm 1 also for the case when the interfering links are present, we check for the corresponding constraint in line 4; however, when interference is eliminated this check is always redundant. The algorithm 1 runs in $O(|ET|2)$ time and minimizes the schedule length when there are no interfering links. All the interfering links removed, and so the sensor network is scheduled in 3 time slots.

Algorithm 1 BFS-TIMESLOTASSIGNMENT

1. Let T = (V, ET)
2. while ET is not EMPTY do
3. Select edge (e) from ET using Breadth First Search Manner
4. Allocate minimum time slot *t* to the selected edge *e*
5. Move to next edge in ET.
6. end while

B. Raw Data Convergecast

In raw data convergecast, data of each sensor is equally important, therefore aggregation is not desirable. Each packet is individually scheduled to reach the sink node. The problem of minimizing the scheduling length for raw data convergecast is proved to be NP-complete problem. Figure 3, shows a basic tree structure where {s, 1, 4}, {s, 2, 5}, {s, 3, 6} are branches of tree and {1, 4}, {2, 5}, {3, 6} are sub-trees.

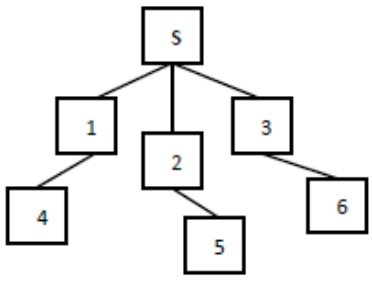

Figure 3: Tree Topology

We can deduce a local time slot allotment algorithm for each sensor node with an objective to schedule parallel transmissions and allow sink to collect data packets continuously. We assume that sink node knows the number of available nodes in each top sub-trees. Each sensor node maintains buffer and state of full or empty if it has data packet available or not. The algorithm for raw data convergecast slot allotment is shown in Algorithm 2.

Algorithm 2 LOCAL-TIMESLOTASSIGNMENT

1. Initialize node[buffer]=FULL
2. Pick a node (N)
3. If (N = Sink) then
Among available sub-tree, select one with largest
number of remaining packets (i).
4. Plan a link (root(i), S)
5. Else IF (N != Sink and node[buffer] = EMPTY)
then
6. Select a child (C) at random whose buffer is full
7. Plan a link (C, node)
8. C[buffer]= EMPTY
9. End If
10 End If

In Algorithm 2, lines 3-4 gives scheduling rules between sink and root node of sub trees. A top subtree is eligible to be elected for transmission if it has at least one packet to be transmitted. If none of the top- subtrees are eligible, the sink node does not receive any packet during that time slot. Inside each top-subtree, sensor nodes are scheduled according to the rules in lines 5-8. We define a subtree to be active if there are still packets left in the subtree that are to be relayed. If a node's buffer is empty and the subtree rooted at this node is active, then we schedule one of its children at random whose buffer is not empty.

IV. CONCLUSION

Wireless Sensor Networks (WSNs) consists of very small sensors. These sensors are wirelessly connected to each other for performing same task collectively such as monitoring weather conditions or specifically parameters like pressure, temperature, sound and vibrations etc. By using time division multiple access, the nodes communicate on different time slots in order to prevent conflicts. In order to improve the data collection, the capacity at each sensor node is adjusted whenever the packet moves from one sensor node to another sensor node. . An optimal convergecast method is proposed for transmitting the packets with minimum cost for long suited nodes.

REFERENCES

[1] Yu, L.,Wang, N., Meng, X.: Real-time forest fire detection with wireless sensor networks. In: WiCom, vol. 2, pp. 1214–1217 (2005)
[2] Dalbro, M., Eikeland, E., Veld, A.J.i., Gjessing, S., Lande, T.S., Riis, H.K., Sørsen, O.: Wireless sensor networks for off-shore oil and gas installations. In: SENSORCOMM '08, pp. 258–263 (2008)
[3] Chintalapudi, K., Fu, T., Paek, J., Kothari, N., Rangwala, S., Caffrey, J., Govindan, R., Johnson, E., Masri, S.: Monitoring civil structures with a wireless sensor network. IEEE Internet Computing 10(2), 26–34 (2006)
[4] Gandham, S., Zhang, Y., Huang, Q.: Distributed time-optimal scheduling for convergecast in wireless sensor networks. Computer Networks 52(3), 610–629 (2008)
[5] Demirkol, I., Ersoy, C., Alagoz, F.: Mac protocols for wireless sensor networks: a survey. IEEE Communications Magazine 44(4), 115–121 (2006)
[6] Siyuan Chen, Minsu Huang, Shaojie Tang, Yu Wang, "Capacity of Data Collection in Arbitrary Wireless Sensor Networks", IEEE Transaction on Parallel and Distributed Systems, Vol.23, No.1, January 2012.
[7] Yafeng Wu, John A. Stankovic, Tian He and Shan Lin, "Realistic and Efficient Multi – Channel Communications in Wireless Sensor Networks", University of Minnesota.
[8] Yiin Zhang b, Qingfeng Huang , Shashidhar Gandham, "Distributed time-optimal scheduling for convergecast in Wireless Sensor Networks", 7 November 2007.
[9] S.Upadhyayula, S.K.S.Gupta, "Spanning Tree based algorithms for low latency and energy efficient data aggregation enhanced convergecast,(DAC) in Wireless sensor Networks", Arizona state University, 22 April 2006.
[10] Ozlem Durmaz Incell, Amitabha Ghosh and Bhaskar Krishnamachari, "Scheduling Algorithms for Tree-Based Data Collection in Wireless Sensor Networks".

International Journal of Modern Engineering Research (IJMER)
www.ijmer.com Vol. 3, Issue. 4, Jul - Aug. 2013 pp-2588-2590 ISSN: 2249-6645

Novel Algorithms for Ranking and Suggesting True Popular Items

Shaik Jameer[1], Syed Sadat Ali[2]
[1]*M. Tech, Nimra College of Engineering & Technology, Vijayawada, A.P., India.*
[2]*Assoc. Professor & Head, Dept.of CSE, Nimra College of Engineering & Technology, Vijayawada, A.P., India.*

Abstract: *Ranking is the process of giving rank scores to the most popular item by taking user feedback. The most frequently occurring items are given the highest rank score. In practice, one may use prior information about the item popularity. For example, in the survey, the user may select the suggested item or they may also select the others. Suggestion is a list of items that are presented to the users. This is done based on the user's feedback. The users give their preference of items through feedback and use them in the ranking of items. In this paper, our aim is to propose novel algorithms for suggesting popular items to users in a way that enables learning of the users' true preference over items. The true preference refers to the preference over the items that would be observed from the users' selections over items without exposure to any suggestions.*

Keywords: *M2S, PROP, Ranking, Suggestions.*

I. INTRODUCTION

Ranking is the process of giving rank scores to the most popular item by taking user feedback. The most frequently occurring items are given the highest rank score. We focus on the ranking of items where the only available information is the observed selection of such items. In learning of the user's preference over items, one may leverage some side information about the items, but this is out of the scope of this paper. In practice, one may use prior information about the item popularity. For example, in the survey the user may select the suggested item or they may also select the others. If they selected the already suggested items they will become more popular and if he does not they may get out of the popular list.

Suggestion is the list of items presented to the users. This is made based on the feedback of the user. The users give their preference of items through feedback and use them in the ranking of items. The main goal of this paper is to learn the true popularity of items and suggest them to the user. Item mentioned here can be anything like documents, files, search query keywords etc. A more specific application of this system is that of tagging process where items are tags applied to the content e.g. photo (in fickr), web pages (in delicious) and video (in youtube) etc.. The users can choose the appropriate tags for the information object based on their preference. The previous tagging system is based on the history of tagging. Figure 1 shows an example user interface to enter tags for a web page, for example, tagging system in BBC. Suggested items and most popular items are also provided. Users can select those items from suggestion or popular sets or create own tag items.

Figure 1: An example tag entry user interface

Suggestion of items to the users becomes complicated process in the popularity of items. The user tends to select such items from the suggested list more frequently. It is because of (1) Bandwagon (the user conform the choice of other users) (2) least effort (selecting from the suggested list is easier than to think another alternative) (3) Conformance in vocabulary (no need to write whole word accurately or correctly). So the suggestion can skew the popularity over the items [1]. The item "news" becomes more popular if that item is suggested frequently. We see that suggesting popular items creates some problems in the popularity of the items list, then why we made such suggestion? There are many reasons; say it recalls what the candidate items are. In this paper, our aim is to prepare some algorithms for ranking and suggesting so that it

enables to learn the users' true preference over the items. The true preference is the user preference over the items without any exposure to any suggestions.

II. RELATED WORK

The problem studied in this paper relates to the broad area of some recommendation systems [2] in which the goal is to learn which items are preferred by the users based on the user's selection of items. Another related area is that of the voting systems. Specifically, our system could formally be seen as an instance of the approval voting [3] in that each user can select any set of candidates offered on a voting ballot. Our work is related to statistical learning problems of the multi-armed bandit type [4]). We consider a finite list of items. Each user is presented with an item that is selected by this user with unknown probability specific to this item.

An asymptotically optimal rule to decide which item to present was found in [4] and was further extended in [5] to allow presenting more than one item. In [6], the authors studied the entrenchment problem where the search engine result sets lock down to a set of popular URLs and proposed to intervene the results with randomly sampled URLs. In [7], the authors provide various statistical characterization results on the tagging in the social bookmarking application del.icio.us. In [8], the authors studied the effect of the tag suggestions on the users' choice of tags in MovieLens systems, which they instrumented for experiments. In [9], the authors provides an estimation procedure of the imitation rate defined in this paper and estimates for tagging of Web pages scenario.

III. PROPOSED WORK

A. Naïve Algorithm

Let us consider how the user selects the items. User selects an item from the entire list of items by sampling, using the true item popularity distribution *r*. Where

r= (r1, r2, ……., rc)

be the Users' true preference over the given set of items C and r called true popularity rank scores**.** Otherwise, user does get the same but confines his choice to items in the suggest set. The naive algorithm "TOP" which suggests a fixed number of the popular items, fails to determine the true popularity ranking of the items if the imitation probability in the user's choice model is adequately large. This can be explained in the Algorithm 1.

Algorithm 1: TOP (Top Popular)
Step 1: Init ci = 0 for each i item
Step 2: If item i is selected :
Step 3: ci ← ci +1
Step 4: S ← a set of s items with largest c values

Ranking process is made on the number of selection of items in the past. If an item "i" is selected then its count i.e., ci is incremented by one. Initially all the items count ci = 0 for each item "I". The suggestion set "S" contains s items.

B. Frequency Proportional Algorithm

Frequency proportional(PROP) is a randomized algorithm that for each user presents a suggestion set of items, sampled with probability proportional to the sum of the current rank scores of items. Also that this algorithm is computationally demanding when the number of items and suggestion set size s are non small; it requires sampling on a set of elements as shown in Algorithm 2.

Algorithm 2: PROP (Frequency Proportional)
Step 1: At the k- th item selsction
Step 2: Sample a set S of s items with probability

$$\propto \sum_{j \in S} \rho_j$$

C. Move- to- Set Algorithm

Move- to- Set(M2S) is a random iterative update rule of the suggestion set of items ,where the suggestion set is updated only when the user selects an item that is not in the suggestion set presented to the user. This algorithm suggests that the last used item for the suggestion set size of one item which is a recommendation rule used by many user interface designs. Due to the random eviction of the items from the suggestion set, M2S is different from suggesting the last distinct used items for the suggestion set size greater than one item although the rule prefers recently used items. As an aside, note that M2S algorithm relates to the self-organized sorting of items known as move-to-front heuristic as proposed in Algorithm 3.

Algorithm 3: M2S (Move- to- Set)
Step 1: At pth item selection
Step 2: If i item is selected and i is not in suggestion set, S
Step 3: Randomly remove an item from S
Step 4: Add i to S

D. Frequency M2S Algorithm

For each item, this algorithm keeps a counter of how many users selected this item over users that were not suggested this item. The rationale is not to update the counter for the items that were suggested and selected by users in order to mitigate the positive reinforcement due to exposure in the suggestion set. Furthermore, a selected item that was not suggested does not immediately qualify for the entry in the suggestion set (as with M2S), but only if its counter exceeds that of an item that is already in the suggestion set as in Algorithm 4. In addition, specific to FM2S is that the eviction of an item from the suggestion list is over a subset of items with smallest counter.

Algorithm 4: FM2S 9Frequency Move- to- Set)
Step 1: Init: Ni :=0 for each item i
Step 2: At pth item selection
Step 3: If i is selected and i not in S
Step 4: Ni ← Ni + 1
Step 5: If Ni greater than any N values of items in S
Step 6: Randomly remove one item from S
Step 7: Add i to S

Both M2S and FM2S learn true popularity ranking that are lightweight. Self tuning in that they do not require any special configuration parameters. FM2S algorithm confines to displaying only sufficiently popular items as the suggestion set can displayed as shown in the Figure 2.

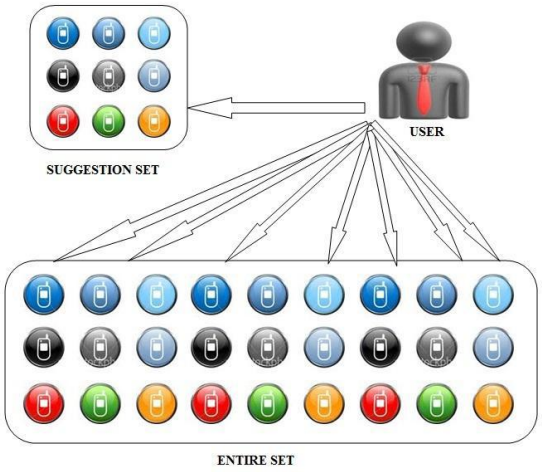

Figure 2: The Proposed Suggestion Set to the user.

IV. CONCLUSION

In this paper , to suggest the most popular items based on ranking process and popularity of items, we proposed the randomized algorithms like naive, PROP, M2S, FM2S.We assessed quality of suggestions which are measured by true popularity of suggested items, and we identified how limit the ranking of items are related to true popularity ranking. By learning the true popularity ranking of the items, the proposed objective of suggesting true popular items can be quickly achieved by using the proposed algorithms.

REFERENCES

[1] H.A. Simon, "Bandwagon and Underdog Effects and the Possibility of Election Predictions," Public Opinion Quarterly, vol. 18, pp. 245-253, 1954.
[2] R. Kumar, P. Rajagopalan, and A. Tomkins, "Recommendation Systems: A Probabilistic Analysis," Proc. 39th Ann. Symp. Foundations of Computer Science (FOCS), 1998.
[3] http://en.wikipedia.org/wiki/Approval_voting, 2009.
[4] T.L. Lai and H. Robbins, "Asymptotically Efficient Adaptive Allocation Rules," Advances in Applied Math., vol. 6, pp. 4-25, 1985.
[5] V. Anantharam, P. Varaiya, and J. Walrand, "Asymptotically Efficient Allocation Rules for the Multiarmed Bandit Problem with Multiple Plays—Part i: i.i.d. Rewards," IEEE Trans. Automatic Control, vol. 32, no. 11, pp. 968-976, Nov. 1987.
[6] S. Pandey, S. Roy, C. Olston, J. Cho, and S. Chakrabarti, "Shuffling Stacked Deck: The Case for Partially Randomized Ranking of Search Engine Results," Proc. 31st Int'l Conf. Very Large Data Bases (VLDB), 2005.
[7] S. Golder and B.A. Huberman, "The Structure of Collaborative Tagging Systems," J. Information Science, vol. 32, no. 2, pp. 198-208, 2006.
[8] S. Sen, S.K. Lam, A.-M. Rashid, D. Cosley, D. Frankowski, J. Osterhouse, F.M. Harper, and J. Riedl, "Tagging, Communities, Vocabulary, Evolution," Proc. 2006 20th Anniversary Conf. Computer Supported CooperativeWork (CSCW), 2006.
[9] F. Suchanek, M. Vojnovi_c, and D. Gunawardena, "Social Tagging: Meaning and Suggestions," Proc. 17th ACM Conf. Information and Knowledge Management (CIKM), Oct. 2008.